Lawrence Berkeley National Laboratory
Lawrence Berkeley National Laboratory

Title
ENERGY & ENVIRONMENT DIVISION. ANNUAL REPORT FY 1980

Permalink
https://escholarship.org/uc/item/8hj4j1w4

Author
Authors, Various

Publication Date
1981-07-01

Peer reviewed

eScholarship.org Powered by the California Digital Library
University of California

LBL-11990
UC-13

Energy & Environment Division

RECEIVED
LAWRENCE
BERKELEY LABORATORY
NOV 24 1981
LIBRARY AND
DOCUMENTS SECTION

Annual Report FY 1980

July, 1981

TWO-WEEK LOAN COPY

This is a Library Circulating Copy which may be borrowed for two weeks. For a personal retention copy, call Tech. Info. Division, Ext. 6782

Energy & Environment Division

Lawrence Berkeley Laboratory
University of California

LBL-11990

Prepared for the U.S. Department of Energy under Contract No. W-7405-ENG-48

LBL-11990

ENERGY & ENVIRONMENT DIVISION ANNUAL REPORT FY 1980

Elton J. Cairns
Head, Energy & Environment Division
and
Associate Director, LBL

Report Editor
Maya Osowitt

Energy & Environment Division
Lawrence Berkeley Laboratory
University of California
Berkeley, California 94720

This work was supported by the U.S. Department of Energy under Contract No. W-7405-ENG-48

LAWRENCE BERKELEY LABORATORY
UNIVERSITY OF CALIFORNIA
ENERGY & ENVIRONMENT DIVISION

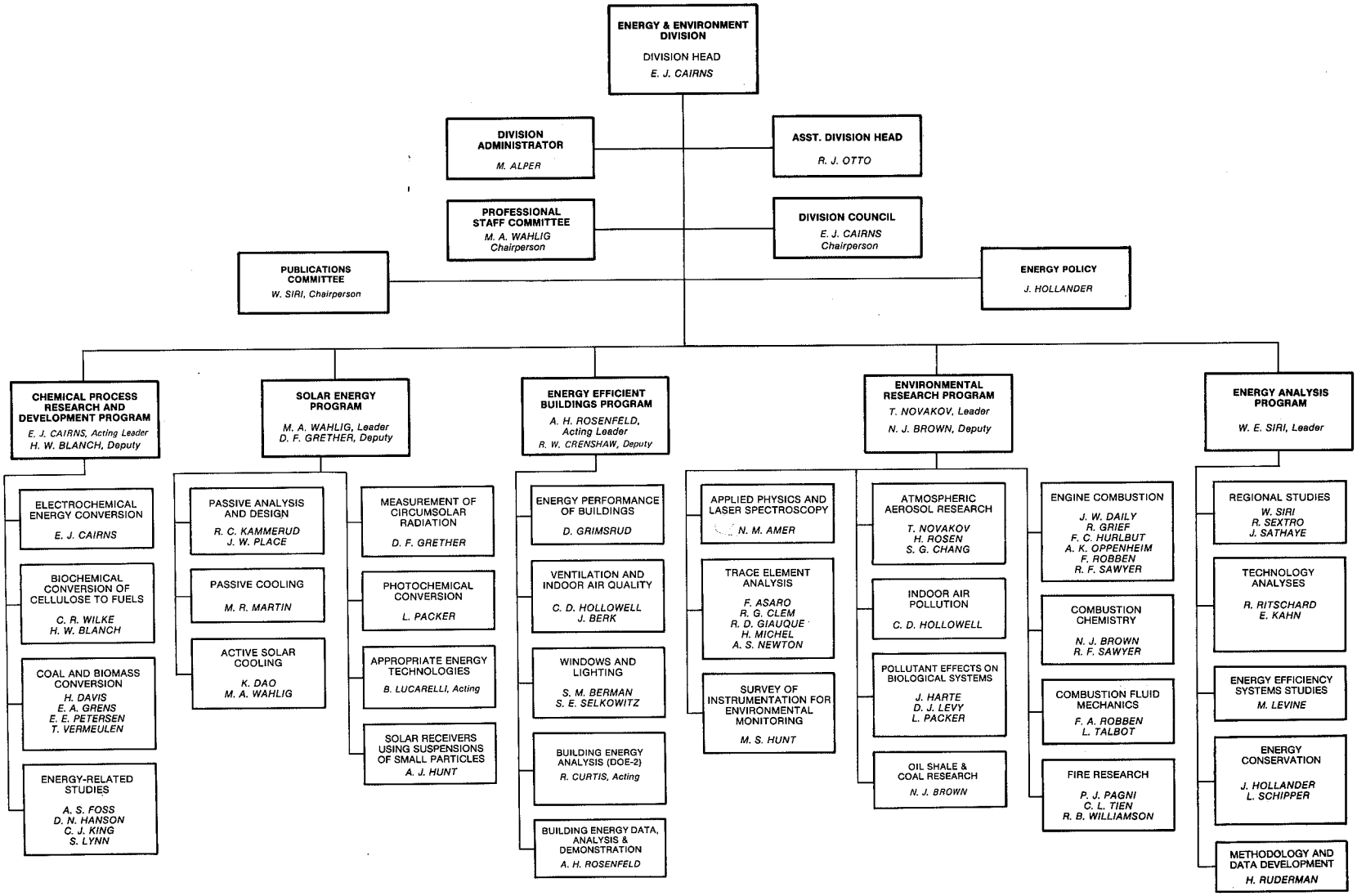

APRIL 1981

CONTENTS

ENERGY ANALYSIS PROGRAM

INTRODUCTION
R. Ritschard 1-1

TECHNOLOGY ASSESSMENTS

Biomass Energy Conversion in Hawaii
R. Ritschard and A. Ghirardi 1-2

Marine Kelp: Energy Resource in the Coastal Zone
R. Ritschard and K. Haven. 1-4

Economic Impacts of Energy Futures
J. Sathaye, H. Ruderman, and P. Chan 1-6

Organizational, Interface and Financial Barriers to the Commercial Development of Community Energy Systems
R. Schladale and R. Ritschard. 1-9

Commercialization of Solar Energy by Regulated Utilities
E. Kahn, P. Benenson, and B. Brown 1-11

Power System Reliability
D. Levy and E. Kahn. 1-15

Acid Mine Drainage Impacts on Groundwater
M. Henriquez and J. Sathaye. 1-18

Enhanced Oil Recovery
J. Sathaye and M. Milukas. 1-21

Geopressured Geothermal Resource of the Texas and Louisiana Gulf Coast: A Technology Characterization and Environmental Assessment
A. Usibelli, P. Deibler, and J. Sathaye. 1-23

REGIONAL STUDIES

Forecasting Energy Demand for Hawaii
H. Ruderman and P. Leung 1-26

Forecasting the Role of Renewables in Hawaii
J. Sathaye and H. Ruderman 1-28

Coastal Zone Assessment Program
R. Ritschard and K. Haven. 1-32

A Summary of Regional Impacts Associated with the Second National Energy Plan
R. Sextro, V. Berg, T. Chapman, M. El-Gasseir, P. Podvin, H. Ruderman, J. Sathaye, S. Schaffer, and K. Tsao. 1-35

Evaluating Land Use and Ecological Issues Associated with Future Energy Projections
V. Berg 1-38

Air Quality Constraints on Implementing the National Energy Plan in Federal Region IX
T. Chapman and R. Sextro 1-41

Water Availability and Quality Considerations Affecting Energy Futures in Federal Region IX
M. El Gasseir. 1-44

Urban and Community Impact Analysis
H. Ruderman, F. Fung, and R. Beran 1-46

ENERGY EFFICIENCY STUDIES

Building Energy Performance Standards for Residential Buildings
M. Levine, D. Goldstein, J. Ingersoll, and J. Mass 1-49

Determinants of Residential Energy Use
P. Craig, J. Cramer, K. Dake, T. Dietz
B. Hackett, D. Kowalezyk, M. Levine, and E. Vine 1-52

Life-Cycle Cost Analysis of Commercial Buildings
I. Turiel and M. Levine. 1-54

Implementing Building Energy Standards in California
R. Feinbaum. 1-56

Economic Benefits and Energy Savings of Appliance Efficiency Standards
J. McMahon and M. Levine 1-59

Life-Cycle Cost Analysis of Major Appliances
I. Turiel, H. Estrada, and M. Levine 1-62

A Comparison of Regional and National Energy Efficiency Standards for Room and Central Air Conditioners
I. Turiel. 1-67

New Data Applicable to the ORNL Residential Energy Demand Model
H. Herring 1-71

Assessment of Energy Demand Models
D. Freedman, T. Rothenberg, and R. Sutch 1-75

Energy Demand and Conservation in Kenya: Initial Appraisal
L. Schipper and J. Hollander 1-78

International Residential Energy Conservation
L. Schipper and A. Ketoff. 1-82

SOLAR ENERGY PROGRAM

INTRODUCTION 2-1

Small Particle Suspensions for Solar Thermal Collection
A. Hunt, P. Hull, J. Bouchez, C. Amkraut, and N. Pope 2-2

Passive Solar Analysis and Design
R. Kammerud, W. Place, B. Andersson, F. Bauman,
C. Bauer, W. Carroll, E. Ceballos, C. Conner, B. Curtis,
N. Friedman, A. Gadgil, A. Mertol, M. Nansteel,
D. Nawrocki, C. Polansky, J. Randolph, M. Tavana,
J. Thornton, T. Webster, and M. Wahlig 2-6

Nitinol Engine Development
R. Banks, W. Hubert, and M. Wahlig. 2-11

Appropriate Energy Technology
C. Case, B. Lucarelli, J. Kessel, H. Clark, J. Kay, and
J. Linse 2-13

Energy Conversion by Retinal Protein, Bacteriorhodopsin
L. Packer, A. Quintanilha, R. Mehlhorn, C. Carmeli,
P. Sullivan, P. Scherrer, N. Kamo, S. Tristram, J. Herz,
and A. Pfeiffhofer. 2-15

Experimental and Theoretical Evaluation of Control Strategies
for Active Solar Energy Systems
M. Warren, S. Schiller, M. Wahlig, G. Sadler, C. Vilmer,
and C. Weaver 2-20

Active Solar Cooling
K. Dao, M. Wahlig, A. Heitz, R. Glas, S. Mitina,
E. Molishever, B. Boyce, J. Rasson, and F. Salter 2-27

Passive Cooling
M. Martin, D. Elmer, P. Berdahl, F. Sakkal, M. Wahlig,
R. Fromberg, M. Kruskopf, and R. Sobolewsky 2-31

LBL Solar Demonstration Project
T. Webster. 2-35

Support for Commercial Solar Demonstration Program
F. Salter, S. Peters, and T. Webster. 2-36

Measurement and Analysis of Circumsolar Radiation
D. Grether, D. Evans, A. Hunt, M. Wahlig, and S. Kanzler. . . 2-37

CHEMICAL PROCESS RESEARCH AND DEVELOPMENT PROGRAM

INTRODUCTION 3-1

PRODUCTION OF SYNTHETIC FUELS

Process Development Studies on the Bioconversion of Cellulose
H. W. Blanch, C. R. Wilke, G. Dove, J. Perez, and A. F. Sciamanna 3-2

Enzymatic Conversion of Wood and Agricultural Residues to Sugars
C. R. Wilke, H. W. Blanch, K. Tangnu, D. Wiley, B. Long S. Rosenberg, J.-P. Riba, and L. Sindelar 3-7

Ethanol Production and Recovery from Biomass Sugars
C. R. Wilke, H. W. Blanch, B. Maiorella, K. Murphy, B. Vickroy, and H. Wong 3-10

The LBL Biomass Liquefaction Process
H. Davis, S. Ergun, C. Figueroa, C. Karatas, L. Schaleger, and N. Yaghoubzadeh 3-13

Chemistry of Biomass Liquefaction
H. Davis, D. Kloden, and L. Schaleger 3-15

The Solvolysis of Douglas Fir Wood in Acidified Organic Solvents
G. Yu, T. Vermeulen, and H. Davis 3-18

Selective Hydrogenation of Coal
E. Grens, T. Vermeulen, D. Bowyer, J. Edwards, F. Hershkowitz, J. Maienschein, C. Onu, and G. Zieminski. 3-20

PROCESSING TO ACHIEVE ENVIRONMENTAL COMPATIBILITY

Coal Desulfurization
T. Vermeulen, S. Ergun, S. Lynn, E. Petersen, L. Clary, G. Cremer, D. Mixon, and M. Smith 3-24

Kinetic Studies of Reactions Involved in the Interaction Between SO_2 and NO_x in Aqueous Solutions
S. G. Chang, S. Oblath, S. Gomiscek, R. Clem, and T. Novakov 3-27

Reactions of Sulfite and Nitrite Ions in Aqueous Solutions
S. G. Chang and D. Littlejohn 3-29

Absorption of NO by Fe^{+2}·NTA Solution
R. J. Demyanovich and S. Lynn 3-33

Processing of Condensate Waters from Coal Conversion
C. J. King, D. Mohr, J. Hill, P. Mackenzie, and J. MacGlashan 3-34

ELECTROCHEMICAL ENERGY STORAGE

Applied Battery and Electrochemical Research Program
E. J. Cairns and F. R. McLarnon 3-39

Battery Electrode Studies
E. J. Cairns, F. R. McLarnon, M. Katz, and J. Nichols. 3-40

ENERGY EFFICIENT BUILDINGS PROGRAM

INTRODUCTION
A. Rosenfeld, C. Hollowell, and S. Berman. 4-1

Energy Performance of Buildings (formerly Building Envelopes Program)
D. Grimsrud, A. Blomsterberg, W. Carroll, P. Condon, D. Dickerhoff, D. Krinkel, M. Modera, A. Rosenfeld, M. Sherman, B. Smith, and R. Sonderegger 4-2

BUILDING VENTILATION AND INDOOR AIR QUALITY PROGRAM

Introduction
C. Hollowell. 4-7

Combustion-Generated Pollutants
G. Traynor, M. Apte, and J. Girman. 4-7

Organic Contaminants
R. Miksch, K. Geisling, L. Jenks, H. Schmidt, M. Tashima, and D. Wolosin. 4-11

Radon: Emanation Studies, Indoor Measurements, and Control Strategies
A. Nero, M. Boegel, J. Ingersoll, W. Nazaroff, K. Revzan, and G. Zapalac 4-16

Field Monitoring of Indoor Air Quality
J. Berk, M. Breen, S. Brown, I. Ko, J. Koonce, B. Loo, J. Pepper, A. Robb, P. Strong, I. Turiel, and R. Young. 4-24

Mechanical Ventilation Systems using Air-to-Air Heat Exchangers
G. Roseme, W. Fisk, and F. Offerman 4-28

Energy-Efficient Windows Program
S. Selkowitz, S. Berman, R. Johnson, J. Klems, C. Lampert, M. Rubin, and R. Verderber 4-31

Energy-Efficient Lighting Program
S. Berman, R. Clear, J. Klems, F. Rubinstein, S. Selkowitz, and R. Verderber 4-40

DOE-2.1 Building Energy Analysis Group
R. Curtis, F. Buhl, S. Gates, J. Hirsch, M. Lokmanhekim, K. Olson, A. Rosenfeld, J. Rudy, and F. Winkelmann 4-45

Building Energy Data Compilation, Analysis, and Demonstration
A. Rosenfeld, H. Arin, P. Cleary, J. Costello, B. Dickenson, D. Goldstein, J. Harris, A. Meier, S. Meyers, B. O'Regan, L. Schipper, B. Shohl, and J. Wright. 4-50

ENVIRONMENTAL POLLUTANT STUDIES

ATMOSPHERIC AEROSOL PROJECT

INTRODUCTION
T. Novakov 5-1

Activated Carbon Catalyzed Oxidation of Aqueous S(IV) Species
R. Brodzinsky, S. Chang, S. Markowitz, and T. Novakov . . . 5-1

Oxidation of SO_2 by Wet Soot Particles: Application to Clouds, Fogs, and Plumes
W. Benner, R. Brodzinsky, and T. Novakov 5-5

Aqueous Reactions of Nitrite and Bisulfite
S. Oblath, S. Chang, S. Markowitz, and T. Novakov 5-7

The Importance of Soot Particles and Nitrous Acid in Oxidizing SO_2 in Atmospheric Aqueous Droplets
S. Chang, R. Toossi, and T. Novakov 5-10

Kinetics of the Reaction Between NH_2OH and SO_2 in Aqueous Solutions
S. Gomiscek, R. Clem, T. Novakov, and S. Chang 5-13

The Role of Fly Ash in the Catalytic Oxidation of SO_2
S. Cohen, S. Chang, S. Markowitz, and T. Novakov 5-15

Soot in the Arctic
H. Rosen, T. Novakov, and B. Bodhaine 5-19

An Intercomparison of the Integrating Plate and the Laser Transmission Methods for Determination of Aerosol Absorption Coefficients
M. Sadler, R. Charlson, H. Rosen, and T. Novakov 5-23

Determination of Black Carbon by Thermal Analysis
L. Gundel, R. Dod, and T. Novakov 5-26

A Model for the Progressive Combustion Analysis of Carbonaceous Aerosol Particles
A. Hansen and T. Novakov 5-30

Relation Between Concentrations of Polynuclear Aromatic Hydrocarbons and Black Carbon
L. Gundel, H. Rosen, and T. Novakov 5-32

Determination of Carbon in Atmospheric Aerosols by Deuteron-Induced Nuclear Reactions
M. Clemenson, T. Novakov, and S. Markowitz 5-35

Determination of Low-Z Elements Simultaneously by ^3He-Induced Nuclear Reactions
M. McKinney and S. Markowitz 5-38

MEMBRANE BIOENERGETICS RESEARCH

Membrane Oxidative Damage
L. Packer, A. Quintanilha, R. Mehlhorn, O. Augusto, J. Maguire, and K. Davies 5-40

LAKE ECOTOXICOLOGY RESEARCH

INTRODUCTION
J. Harte 5-43

Assessment of Optimum Microcosm Design for Pollution Impact Studies
J. Harte, D. Levy, J. Rees, and E. Saegebarth 5-43

Acid Precipitation Damage to Aquatic Ecosystems
J. Harte, K. Tonnessen, R. Schneider, G. Lockett, and J. Oldfather 5-47

COMBUSTION RESEARCH

INTRODUCTION 6-1

ENGINE COMBUSTION AND IGNITION STUDIES

Mechanism of Instabilities in Turbulent Combustion Leading to Flashback
J. Keller, L. Vaneveld, D. Korschelt, G. Hubbard, A. Ghoniem, J. Daily, and A. Oppenheim 6-2

Heat Transfer with Combustion
R. Greif, H. Heperkan, J. Woodard, S. Vosen, D. Wong, and J. Naccache 6-5

Engine Combustion Studies
R. Sawyer, J. Daily, A. Oppenheim, and H. Stewart 6-6

Ignition Studies
A. Oppenheim, F. Hurlbut, F. Robben, R. Peterson, P. Coico, and H. Stewart 6-8

COMBUSTION CHEMISTRY AND POLLUTANT FORMATION

Measurement of Nitrogeneous Pollutants in Combustion Environments
D. Lucas, N. Brown, and A. Newton 6-10

The Selective Reduction of NO by NH_3
D. Lucas, N. Brown, and R. Sawyer 6-12

Reduction of NO by Combustion Staging
N. Brown, J. Brunetto, D. Lucas, and R. Sawyer 6-14

Collision Dynamics Studies of HO_2 Dissociation
N. Brown and J. Miller 6-16

Statistical Theories of Unimolecular Reactions
N. Brown and Abdel Hafez 6-18

Combustion Diagnostics by Tunable Atomic Line Molecular Spectroscopy
E. Cuellar and N. Brown 6-20

Submicron Particulates from Pulverized Coal Combustion
J. Pennucci, R. Greif, G. Parsons, F. Robben, and P. Sherman 6-24

Surface Catalyzed Combustion
R. Schefer and F. Robben 6-26

COMBUSTION FLUID MECHANICS

Flame Propagation in Grid-Induced Turbulence
R. Bill, Jr., R. K. Cheng, I. Namer, T. Ng, F. Robben, and L. Talbot 6-28

Combustion in a Turbulent Boundary Layer
R. K. Cheng, R. Bill, Jr., T. Ng, F. Robben, and L. Talbot 6-30

Numerical Modeling of Turbulent Combustion
A. Ghoniem, A. Chorin, and A. Oppenheim 6-31

Vortex Interaction with a Premixed Laminar Flame
I. Namer, R. Bill, Jr., F. Robben, and L. Talbot 6-34

FIRE RESEARCH

Modeling of Burning and Extinction Characteristics of a Polymer Diffusion Flame and Comparison with Experiment
W. Pitz and R. Sawyer 6-37

Flame Radiation
C. Tien and S. Lee 6-40

Tests and Criteria for Fire Protection of Cable Penetrations
R. Williamson and F. Fisher 6-41

LASER SPECTROSCOPY AND TRACE ELEMENT ANALYSIS

INTRODUCTION 7-1

APPLIED PHYSICS AND LASER SPECTROSCOPY RESEARCH
N. Amer, N. Bergstrom, R. Gerlach, W. Jackson, R. Johnson, S. Kohn, M. Olmstead, C. Rosenblatt, D. Wake, and Z. Yasa 7-1

Laser Photoacoustic and Photothermal Measurements and Characterization 7-1

Amorphous Photovoltaic Semiconductors 7-8

Liquid Crystal Research 7-9

Novel Laser Systems 7-13

MICROPROCESSOR CONTROLLER ANODIC STRIPPING VOLTAMETER FOR TRACE METALS ANALYSIS IN WATER
R. Clem, F. Park, F. Kirsten, S. Phillips, and E. Binnall 7-16

THE SURVEY OF INSTRUMENTATION FOR ENVIRONMENTAL MONITORING
M. Quinby-Hunt, C. Case, R. McLaughlin, G. Morton, D. Murphy, A. Nero, and D. Mack 7-20

THE POSSIBLE CHRONDRITIC NATURE OF THE DANISH CRETACEOUS-TERTIARY BOUNDARY
F. Asaro, H. Michel, L. Alvarez, and W. Alvarez 7-22

IMPROVEMENT OF THE SENSITIVITY AND PRECISION OF NEUTRON ACTIVATION ANALYSIS OF SOME ELEMENTS IN PLANKTON AND PLANKTONIC FISH
F. Asaro, H. Michel, R. Flegal, and M. Quinby-Hunt 7-25

SOURCES OF SOME SECONDARILY WORKED OBSIDIAN ARTIFACTS FROM TIKAL, GUATEMALA
H. Moholy-Nagy, F. Asaro, and F. Stross 7-27

OIL SHALE AND COAL RESEARCH

OIL SHALE RESEARCH

INTRODUCTION
J. P. Fox. 8-1

CHARACTERIZATION STUDIES

Speciation of Inorganic and Organic Arsenic Compounds in Oil Shale Process Waters
R. H. Fish, J. P. Fox, J. Cantor, P. Babbitt, F. E. Brinckman, and K. L. Jewett 8-4

Identification of Carboxylic Acids in Oil Shale Process Waters
P. C. Babbitt, R. H. Fish, L. H. Joseph, and A. S. Newton 8-8

Characterization of Two Cores from the Naval Oil Shale Reserve Number 1
R. D. Giauque, J. P. Fox, and J. W. Smith. 8-13

PARTITIONING STUDIES

A Partitioning Model for Hg in Simulated In-situ Oil Shale Retorts
J. P. Fox 8-19

Partitioning of As, Cd, Hg, Pb, Sb, and Se During Simulated In-Situ Oil Shale Retorting
D. C. Girvin, A. T. Hodgson, G. J. Harris-Winston, and M. J. Pollard 8-24

On-Line Measurement of Trace Elements in Oil Shale Offgases by Zeeman Atomic Absorption Spectroscopy
D. C. Girvin and M. J. Pollard 8-28

Analytical Methods for Trace Elements in Oil Shale and Retorting Products
A. T. Hodgson, G. J. Harris-Winston, and R. G. Clem. 8-32

RETORT ABANDONMENT

Development of Low Cost Grouts from Spent Oil Shale
P. Persoff 8-36

The Prediction of the Penetration Distance of Spent Shale Grouts in an In-situ Retort
N. A. Thomsen and P. Persoff 8-39

Structural Requirements for the Abandonment of In-situ Retorts
J. L. Ratigan and R. E. Goodman 8-42

An Investigation of Dewatering for the Modified In-situ Oil Shale Retorting Process
M. Mehran, T. N. Narasimhan, and J. P. Fox 8-48

A Mathematical Model for Leaching of Organic Carbon from In-situ Retorted Oil Shale
W. G. Hall, R. E. Selleck, and J. F. Thomas 8-53

WASTEWATER TREATMENT STUDIES

Treatment of Wastewater from Modified In-situ Oil Shale Retorting
R. H. Sakaji, B. M. Jones, and C. G. Daughton 8-57

Raw and Spent Shale for the Treatment of Oil Shale Process Waters
R. H. Sakaji, B. M. Jones, and C. G. Daughton 8-62

Steam Stripping of Gas Condensate and Retort Water
F. Pearson, R. Selleck, V. Diyamandoghi,
Y. Nurdogan, and S. Wong 8-66

Analytical Problems in Monitoring Retort Water Treatment
C. G. Daughton, B. M. Jones, and R. H. Sakaji 8-70

COAL RESEARCH

Organic Compounds in Coal Slurry Pipeline Water
A. S. Newton, H. M. Villarreal, W. E. Walker,
and J. P. Fox 8-75

Water Quality and Hydrologic Effects of Coal Mining
J. P. Fox, M. J. Kland, F. H. Pearson,
and P. Persoff 8-78

APPENDIX

ENERGY AND ENVIRONMENT DIVISION PERSONNEL LISTING A-1

ENERGY ANALYSIS PROGRAM

INTRODUCTION

R. Ritschard

The Energy Analysis Program is concerned with energy impacts of many different kinds; these include impacts on regional and local economies and ecologies; on water availability and quality; on air quality; on land use; and on human health. These issues are studied from two perspectives.

The first perspective embraces the impacts of a specific technology, such as coal combustion, enhanced oil recovery, geothermal power, or solar energy and the economic, environmental, and institutional constraints on their use. Alternatively, this type of study focuses on a particular energy end use sector, e.g., agricultural, commercial, residential, or industrial, and addresses the impacts of, and constraints on, the use of alternative energy supplies to satisfy the demands of this sector.

The second perspective includes integrated assessments of regional and subregional impacts of alternative future energy supply systems and energy demand growth patterns. For these regional assessments, our energy analysts examine each major impact type for Federal Region IX (Arizona, California, Hawaii and Nevada), or for individual states, such as Hawaii.

The major integrated subprograms arise from national energy policy (contemplated or enacted) and from major energy research and development programs. In conjunction with the other national laboratories, LBL has participated in assessing national energy plans, energy supply technologies, and building energy performance standards. For the past several years, the Energy Analysis Program staff has taken a leadership role in analyzing the direct and secondary impacts on each economic sector as a result of the capital investment, direct employment, and material demands of each technology. During the past fiscal year, LBL accepted lead responsibility for conducting assessments of energy-related activities in the Pacific Coastal Zone (this includes the coastal areas of Alaska, California, Hawaii, Oregon, and Washington).

During FY 1980, a number of studies were conducted that are covered in the short reports that follow. The reports are grouped in three general categories although the analyses in many cases overlap each other.

Several energy technologies were described and assessed, including biomass energy systems in Hawaii; marine kelp conversion along the California coast; enhanced oil recovery; geopressured geothermal resource in the Gulf Coast region; acid mine drainage from increased use of coal; and other solar technologies. The assessments were on such topics as the direct and secondary economic impacts at the national and regional level; groundwater impacts; institutional constraints; and various environmental impacts.

The regional studies were made at several geographic levels including Federal Region IX, the Pacific Coastal Zone, and the State of Hawaii. The primary effort was to analyze the major environmental, socioeconomic, and institutional issues resulting from the Second National Energy Plan (NEP-2), from renewable energy resource development in Hawaii, and from energy-related activities in the coastal zone of the West Coast (of the U.S.).

A series of energy efficiency studies also have been undertaken. These studies evaluated energy performance standards for residential buildings; energy standards at the local and state levels; energy efficiency standards for appliances; and residential energy demand forecasting. In addition, two studies are included that address energy demand and conservation from an international perspective. The findings of all these assessments are intended primarily to aid decision-makers in formulating energy policy and energy research and development programs.

BIOMASS ENERGY CONVERSION IN HAWAII*†

R. Ritschard and A. Ghirardi

INTRODUCTION

Biomass is Hawaii's most productive natural energy resource in terms of the electricity generated from it. Further, it is the only indigenous resource that can be converted to liquid fuels to replace imported petroleum fuels. Direct combustion of bagasse (a fibrous sugar cane residue), wood chips, and macademia nut shells generates approximately 12% of the electricity now consumed in the state. Several studies have outlined a program of biomass energy use in Hawaii and have concluded that biomass can supply more than 15% of Hawaii's energy needs in the next two decades.

Fuels can be derived from several biomass resources: wastes, which include all organic materials that accumulate at specific locations and whose disposal carries an associated cost, e.g., municipal solid wastes (MSW), lumber mill wastes, and sewage sludge; residues, which are plant materials left in the field or forest after agricultural crops or timber are harvested; and energy crops, i.e., those crops specifically cultivated for their fuel content. Some recently proposed energy crops for Hawaii are aquatic plants (to be cultivated in land-based systems), ocean kelp, corn, sugar cane, and various tree crops, such as eucalyptus and giant koa haole.

Technologies that convert biomass to energy and that are believed to have the greatest potential in Hawaii for the near-term (before the year 2000) include direct combustion of wastes--such as bagasse, MSW, and pineapple trash--and the production of liquid fuels, especially ethanol from various feedstocks, e.g., cane juice, molasses, and pineapple. Biomass is the only renewable resource that will be suitable for conversion to liquid fuels before the turn of the century.

The most important factor in the use of biomass for energy is its availability as a resource. For Hawaii, four major biomass resources appear most available. These include (1) Hawaiian sugar industry resources (bagasse, cane juice, leafy trash, and molasses), (2) tree crops, (3) municipal solid wastes, and (4) algae. Of these, only the sugar industry products and trees are now available in sufficient quantities to supply a significant amount of Hawaii's future energy needs.

MAJOR FINDINGS

The biomass resources in Hawaii with the greatest potential to displace imported petroleum are outlined in this study. Emphasis is placed on conversion technologies that will meet the economic and technical constraints for the near-term (before the year 2000). Conversion technologies selected include direct combustion of wood chips and wastes (such as bagasse, MSW, and pineapple trash) and the production of liquid fuels, especially ethanol, from molasses.

Energy from aquatic biomass, i.e., kelp and other algae, will not be a viable energy source in Hawaii during the time period of this study. This is because system costs would be high and because advancements are required in feedstock cultivation, harvesting, and processing.

Direct combustion of municipal refuse, primarily on the island of Oahu, could supply up to 5% of the state's electricity demand in the year 2000. This electrical supply would consist of approximately 70 MW per year in the City and County of Honolulu and 10 MW on the other islands combined.

Bagasse, which is already a significant contributor to the electrical supply of Hawaii, will be an important source of biomass in the future. Currently, about 25 MW of electrical power are sold to the utility grid annually by the sugar industry, after supplying its own needs. With adequate financial incentives, sugar companies could expand this capacity by the 1990's so that they could sell up to 50 MW annually. However, various changes would need to be implemented in sugar plantations' growing, harvesting, and processing practices, including the drying and pelletizing of bagasse for more efficient storage and combustion.

Another sugar industry by-product, leafy cane trash, has some potential as a biomass feedstock. However, for cane trash to be available in quantities adequate to support a major conversion process, new harvesting techniques must be developed and used. If that proves feasible, an additional 11 trillion Btu's of energy would be available. The authors believe that the sugar mills will burn the cane trash rather than use it as a feedstock for the production of ethanol. Since the conversion of cellulosic products, such as cane trash, first requires either acid or enzymatic hydrolysis before fermentation to ethanol, it seems likely that combustion of this material is a more cost-effective use.

Tree crops are one of the more promising biomass resources available in Hawaii during the next two decades. Currently, some use is made of wood chips by direct combustion in sugar mill boilers.

---

* This work was supported by the Resource Applications Division, U.S. Department of Energy, under Contract No. W-7405-ENG-48.

† Condensed from R. Ritschard and A. Ghirardi, Biomass Energy Conversion in Hawaii, Lawrence Berkeley Laboratory report LBL-11902, 1980.

A successful wood biomass program will require that large acreage be planted in tree crops, such as eucalyptus and giant koa haole. Capital costs for an extensive tree farm in Hawaii have been estimated at $2500/acre. Although the conversion of wood to methanol and gasoline is an attractive alternative, the authors feel that the most cost-effective method of conversion is by the direct combustion of wood chips to produce electricity. The range of electrical capacity available in the year 2000 is estimated in this analysis to be between 150 MW (100,000 planted acres) to 480 MW (300,000 planted acres). The more probable level is about 320 MW, if 200,000 acres of eucalyptus and other tree crops are planted and harvested. The major uncertainty for any wood conversion process is the cost of conventional energy sources and the competing economic uses for wood, such as for lumber or paper pulp.

Other feedstocks, such as macadamia nut shells, pineapple trash, and hay, are available for direct combustion. The macadamia shells will probably continue to be used to a limited extent by the macadamia nut industry, but will not make an overall contribution to the state's energy needs. Combustion of pineapple trash, however, could contribute as much as 5 MW by the year 2000, especially for the County of Maui (Maui, Molokai, and Lanai). Hay is also available on the island of Molokai as a replacement for diesel fuel. This biomass resource could contribute about 2 MW of electricity annually by the late 1990's.

Finally, at today's prices, ethanol is not competitive with gasoline. The use of ethanol-gasoline blends has required government subsidies as well as by-product credits and will continue to do so in the near future. In Hawaii, molasses is the only feedstock likely to be available for production of alcohol over the next decade or so, barring a collapse of the international sugar market. If all molasses were used for production of ethanol, gasohol could displace 7-10% of the State's gasoline consumption (at 1978 levels), or some 20-30 million gallons per year. (See Fig. 1). As for leafy trash, wood, and other cellulosic materials, their use as boiler fuel will be their best contribution to displace imported liquid fuels in the state.

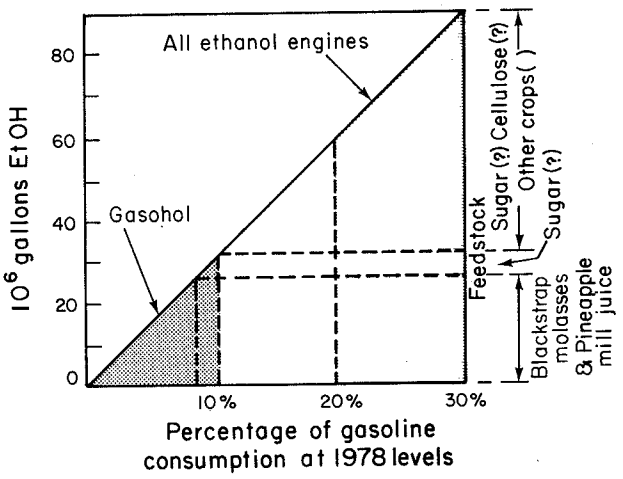

Fig. 1. Strategy for use of gasohol. (XBL 114-2334)

Several things stand in the way of fully utilizing biomass as an energy source for Hawaii. Some agricultural wastes and sugar industry products and by-products are currently more valuable as human and animal food than as energy sources. Molasses, for example, is now used to manufacture beverage ethanol, industrial alcohol, and animal feed and sells for between $70 and $100 a ton. At today's prices, the ethanol that would be made from molasses is not competitive with gasoline. Gasohol use to date has been supported by government subsidies, which are expected to continue. Gasoline would have to cost about $1.70 a gallon to make gasohol attractive or even competitive. In addition, tree crops, which are one of the most promising biomass resources available in Hawaii within the next 25 years, require substantial land areas. It would take a political decision to support the energy market for biomass or a drastic shift in existing market values to redirect existing biomass resources entirely into an energy-producing program. The technical problems that currently confront such a program are no greater than the economic and political barriers.

PLANNED ACTIVITIES IN FY 1981

This project was completed in FY 1980 and will not continue in FY 1981.

MARINE KELP: ENERGY RESOURCE IN THE COASTAL ZONE*†

R. Ritschard and K. Haven

INTRODUCTION

The assessment of energy-related impacts in the coastal zone has focused primarily on thermal power plants and outer continental shelf (OCS) petroleum development. However, there is a growing list of energy resources and conversion systems within the coastal environment that are currently being proposed. Marine biomass is one of the most recent entries on this list of coastal energy resources.

A marine biomass farm is one of the few biologically-based systems that has the potential to contribute large quantities of synthetic gaseous fuels to the nation's energy supply. This is especially true in that large surface areas are available on the ocean and large amounts of plant nutrients are available in the ocean waters. The California giant kelp (Macrocystis pyrifera), which is well established as a valuable coastal resource and a source of chemical products (algin), is a prime candidate for energy conversion, since it is efficient in converting sunlight into a fixed source of energy. In turn, kelp can be processed by anaerobic digestion or other procedures into methane. Furthermore, other by-products such as food, fertilizer, ethanol, and industrial material can be obtained.

This paper describes an ocean farm system that has been designed and used as an ocean test facility by the Energy from Marine Biomass Program, jointly sponsored by the Gas Research Institute and the Department of Energy and managed by the General Electric Company.[1] Figure 1 shows a generalized diagram of the marine biomass system used in this analysis.

The analysis of the ocean farm system includes a description of the types of impacts that might occur if large-scale operations begin, such as the production of environmental residuals, conflicts with the fishing and shipping industries, and other legal/institutional impacts. Finally, the relationship of the marine biomass concept and coastal zone management plans is discussed.

MAJOR FINDINGS

Environmental Impacts

The coastal regions of the United States are relatively rare, biologically important, and vulnerable to human perturbation. The coastal zone has been and will probably continue to be important in the industrial development of the nation. The placement of energy facilities along the coast,

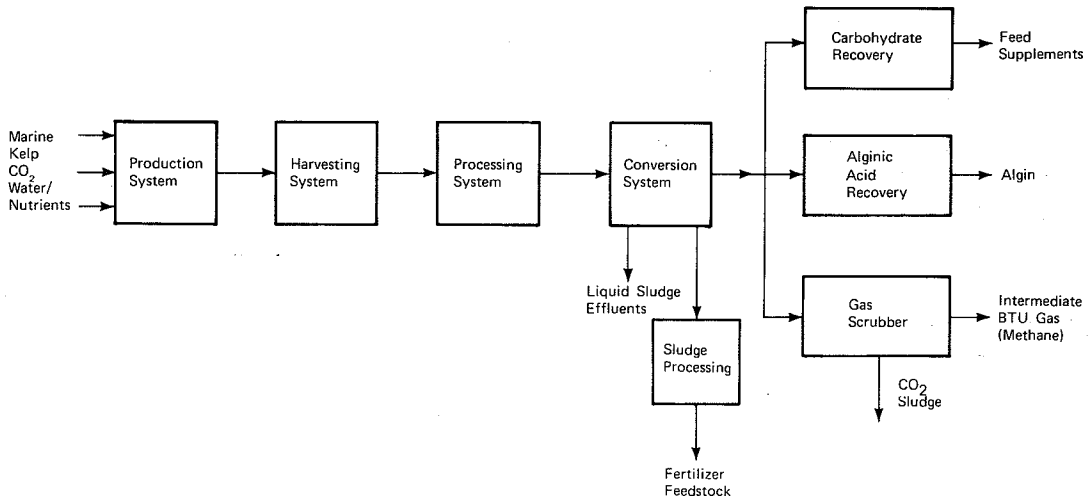

Fig. 1. Complete marine biomass system. (XBL 781-13495)

* This work was supported by the Regional Impacts Division, Office of Environment, U.S. Department of Energy, under contract No. W-7405-ENG-48.

† Condensed from R. Ritschard and K. Haven, "Marine Kelp: Energy Resource In the Coastal Zone." Coastal Zone 80, vol. 2, November 1980, pp. 967-979.

however, generates environmental impacts and creates conflicts in the use of our coastal resources.

Marine biomass has been suggested as an energy resource, since it has the potential to contribute significant quantities of gaseous fuels to the nation's energy supply. As part of another project, an ocean farm system, using the California kelp (Macrocystis pyrifera) has been designed and used as a test facility off the southern California shore.

Every energy conversion system has various impacts. Since there are no full-scale systems in operation, the data represent a compilation of potential impacts from bench-scale experiments, test farms, and from the conceptual plans for production, harvesting, and processing. The impacts of a massive open-ocean farm operation have not been explored. There is a potential for significant climatic modifications. The anticipated climatic changes stem from the massive artificial upwelling that will be required to stimulate kelp growth and maintain it at high rates. When large volumes of cold deep water, which are rich in nutrients and supersaturated with carbon dioxide, are brought to the ocean surface to fertilize the plants, events might occur that could lead to regional and global changes in climate. The culture and harvesting of seaweed over several thousand square miles of ocean surface could result in changes in albedo, air-sea exchanges of materials, and altered ocean surface roughness. The farm structures themselves will reduce or change the patterns of water circulation. These factors, which could change prevailing weather patterns and create additional fog banks, subsequently may have some effect on the productivity of the kelp beds.

A potential problem associated with the farm structure itself is the release of numerous chemicals into the ocean from the supports and synthetic lines used to hold the algae. Hruby (1978) noted the possibility of a slow release of toxic metals from the antifouling paints and organic chemicals used on the farm structures.[2] The seriousness of this chemical pollution problem is as yet unknown.

The upwelling system, which is designed to provide an abundance of nutrient rich water needed for kelp growth and development, could present several environmental problems. Included in this category are changes in the rate of productivity; alteration of salinity, temperature, dissolved oxygen, turbidity and nutrient levels; possible entrainment of marine organisms that cannot resist the vertical inflow velocities; and the potential air emissions related to the use of diesel-powered pumps.

Harvesting of the marine biomass system will be done with ships of Kelco Company design. These ships will create some environmental impact due to their emissions during normal operation. The Kelco ships burn diesel as a fuel, resulting in the production of particulates, nitrogen oxides, and hydrocarbons as primary air pollutants. These pollutants, however, will be diffused over a larger area than the kelp farm itself, since they are released as the ships travel to and from the farm.

The waste water generated from the shredder, presser, and digester during the processing phase will eventually be discharged into the sewer system. The composition of this effluent and the degree of pollution control that is necessary are unknown at this time. It is assumed, however, that the processing plant will conform to Environmental Protection Agency discharge permit standards regarding waste water effluents.

As a final step in the marine biomass system, the processed algae is fed into the anaerobic digester. The gas mixture from the digester must be passed through a scrubber to separate carbon dioxide, which is about 40 percent of the gas, from methane. The major environmental residual resulting from this stage of the process is sludge from the scrubber that must be collected for subsequent disposal. The composition of the sludge from the scrubber, as well as from other phases of processing/conversion, is also unknown. However, since marine algae will concentrate various heavy metals, the sludge may possibly contain considerable levels of heavy metals. If any of this sludge is to be used for fertilizer feedstock, it will require some detoxification.

The final concentration of heavy metals and other toxicants, and the biological oxygen demand and organic loading of the aqueous discharge, cannot be anticipated without specific measurements from a test, demonstration, or prototype facility. Until that information is available, only the potential environmental impacts can be identified.

Legal and Institutional Impacts

Algal farms, depending on their size and location, may have a negative impact on commercial shipping lanes. At a projected biomass yield of 50 dry-ash-free tons/acre-year, it has been estimated that about 55,000 mi.^{2} of ocean surface might be needed to supply the nation's current requirements for natural gas.[1] This area (approximately 235 mi. by 235 mi.), if concentrated offshore of the California coastline, might provide an additional hazard to ocean commerce.

In addition, such large marine biomass farms may adversely affect access to, and utilization of, coastal fishing locations. The potential exists for impacts on recreational and commercial fishing in the farm area. Since the kelp farms themselves will probably attract certain fish species, the further legal issue of trespassing on the marine farm and other liability questions arises.

Several institutional and legal issues are likely to accompany the research, development, and commercial phases of the open ocean system if they are located beyond the 12 mi. (territorial seas) or 200 mi. (high seas) limit. The current biological test farm is deployed about 4.5 mi. offshore from Laguna Beach in southern California. The prototype and commercial farms may be located as far as 20 mi. offshore. Not only will the international and domestic legal status have to be analyzed, but a regulatory framework will have to be established to guarantee the various uses of marine resources.

Legal questions include, but are not limited to, liability for: collisions between ships and the substrate or associated fixed structures; blockage of fishing rights and lanes; interference with shipping and navigation; residuals released from the farm structure; and the cold water plume's impact on coastal areas or fishing grounds.

Finally consideration is given to how the introduction of a new energy technology, such as marine biomass conversion, interacts with the coastal zone planning process. Major concerns with the offshore aspects of the ocean farm concept exist, including the overall lead regulatory authority; the question of federal consistency; and impact planning and mitigation by local coastal governments. Onshore activities will probably pose fewer problems, since the proposed facilities are not unlike those already sited in the coastal zone.

The conclusion is that the proponents of a biomass energy system should start early to promote a timely transfer of information between the various institutions (federal, state, and local) involved in coastal zone planning. The accurate prediction of environmental impacts and their mitigation, required by law, demands a fully-coordinated energy planning and coastal resource management process.

PLANNED ACTIVITIES IN FY 1981

This work was concluded in FY 1980 and will not continue in FY 1981.

REFERENCES

1. J. Leone, Marine Biomass Energy Project, (New Orleans, La.: Marine Technology Society, 1979.)

2. T. Hruby, "Environmental Impacts of Large Scale Aquatic Biomass Systems," in E. Ashare et al., Cost Analysis of Aquatic Biomass Systems (Cambridge, Mass., Dynatech R&D Company, 1978.)

ECONOMIC IMPACTS OF ENERGY FUTURES*

J. Sathaye, H. Ruderman, and P. Chan

INTRODUCTION

The Energy Analysis Program is the "lead laboratory" for national socioeconomic analysis under several programs sponsored by the Department of Energy's (DOE) Office of Environmental Assessment. In this role, we analyse the regional and national direct and indirect economic impacts, associated with energy scenarios formulated by DOE. Direct economic impacts include the capital, material, and equipment needed to construct, maintain, and operate the energy facilities required by the scenario. Indirect impacts include the secondary industrial output, income, and employment generated by the capital and manpower expenditures for new construction. During the past few years, we have developed a set of interconnected models to evaluate national and regional economic impacts. These were used in assessing the effects of accelerated coal utilization and an assessment of the President's first National Energy Plan (NEP). This work has been described in previous Annual Review articles.

ACCOMPLISHMENTS DURING FY 1980

During FY 1980, we continued to improve our analytic methodology for evaluating economic impacts and to apply this methodology in assessing specific scenarios. We have incorporated twenty additional solar technologies in the Energy Supply Planning Model. Our National Input-Output Model has been modified to take into account 1972-1977 price changes. The method for regionalizing indirect impacts has been completely revised. We analysed a total of four scenarios during the year--two for the Technology Assessment of Solar Energy (TASE) program and two for the Regional Issues Identification and Assessment (RIIA) program. In this report we will describe the change we made to the models, and we will discuss some of our analytical results for the four scenarios.

Methodology Improvements

The interlinkage of the models we use for calculating direct and indirect economic impacts is shown in Figure 1. The Energy Supply Planning Model (ESPM) is an adaptation of the original model formulated by the Bechtel Corporation.[1] It translates a scenario into a schedule of the number of facilities which have to be constructed and operated to meet the projected levels of energy supply. The capital costs and the annual manpower, equipment, and materials needed to construct, maintain, and operate the facilities are calculated. The original ESPM data base had information mainly on requirements for conventional technologies. We modified the data base to include data on twenty solar and other renewable technologies. The detailed requirements at the four-digit Standard Industrial Classification (SIC) level were determined at LBL and other national laboratories as part of the TASE program.

The input-output model of the U.S. economy is used to calculate secondary output, income, and employment. The I-O model was originally based on the 1967 national table constructed by the

* This work was supported by the Office of Environmental Assessment, Assistant Secretary for Environment, of the U.S. Department of Energy under Contract No. W-7405-ENG-48.

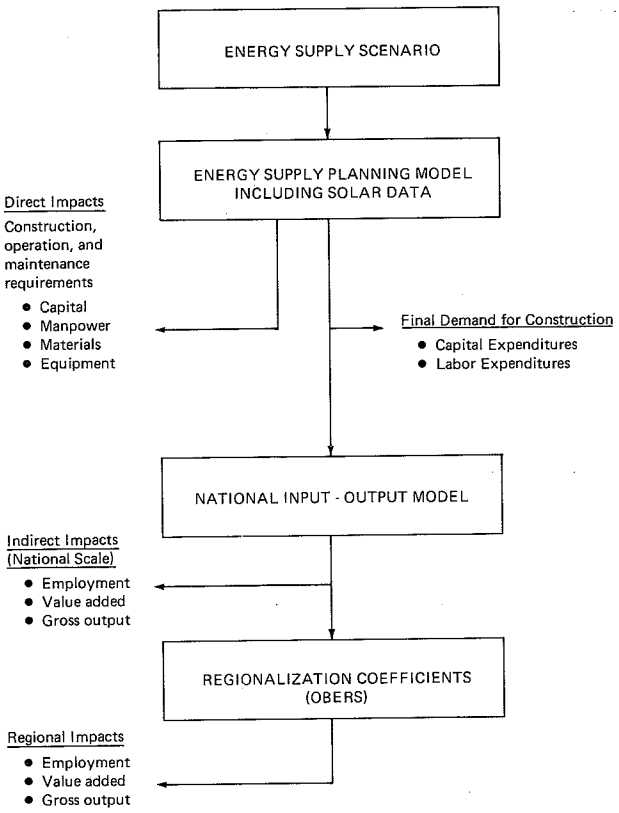

Fig. 1. Analytic methodology for estimating direct and indirect economic impacts.
(XBL 8012-2575)

Bureau of Economic Analysis[2] (BEA) and updated to 1972 at LBL. During 1980 we further updated the model to reflect 1977 prices. In addition we provided the model with income and employment coefficients that make use of the Bureau of Labor Statistics projections of changes in labor productivity.[3] We also began to update the 1972 BEA national table to 1977 in order to use this as the basis for our I-O model.

The third major improvement to our models was to revise the method we used to break down the indirect impacts from the national totals to the ten federal regions. The national impacts are calculated for about forty sectors of the economy. We used the interim revisions to the Office of Business Economics and Economic Research Service (OBERS) projections of earnings by state[4] to determine regionalization coefficients for each of these sectors. A report generator was written that prints tables of the regional output, income, and employment.

Analysis of Scenarios

The two scenarios[5] that we analysed for the TASE project assumed different levels of solar energy utilization by the year 2000. The low solar (TASE 6) scenario has six quads and the high solar (TASE 14) had fourteen quads of primary fuel replaced by solar. Our major objective was to compare the economic impacts of the two scenarios. Our results are shown in Tables 1 and 2.

Most solar and renewable technologies are capital and labor intensive. Market penetration by these technologies will therefore require considerably more capital investment than conventional technologies. Their labor requirements for both construction and operation will be correspondingly larger. During the period from 1975 to 2000, the TASE 14 scenario calls for 2.8 million more employee-years of maintenance and operation labor than the TASE 6 scenario. Projected investment over the period totals $330 billion higher. These differences will be most noticeable between 1990 and 2000 when the penetration by the new technologies will be highest. The South Atlantic, Midwest, and Southwest regions will experience far higher investment and employment from increased use of solar energy than the other regions.

Indirect employment associated with industries supplying goods and services for energy construction activities in the TASE 14 scenario than in the TASE 6 scenario. Average annual indirect employment in the high-solar case between 1991 and 2000 amounts to 1.95 million employee-years, compared to 1.40 million employee-years in the low case.

In the RIIA analysis, we compared the indirect economic impacts of NEP 2 high- and NEP 2 low-energy scenarios.[6] These scenarios specify the levels of primary energy demand and supply for each type of fuel. The analysis estimated the potential capital and labor requirements for the two scenarios. The indirect impacts are also estimated and regionalized.

The NEP 2 low-energy scenario calls for $934 billion of capital investment between 1975 and 2000, whereas the NEP 2 High scenario requires $1058 billion in the same period. For both scenarios, investment increases during the 1976 to 1990 period and then declines during the last decade. Construction labor requirements for the low and high scenarios are 6.9 million employee-years and 7.8 million employee-years respectively. The majority (82%) of this increase in labor requirements is concentrated in the Southwest, South Atlantic, North Central, and Midwest regions.

Labor requirements for operation and maintenance of facilities in the NEP 2 high scenario amount to 34.2 million employee-years over the 25-year period, compared to 33.2 million employee-years in the low scenario.

Average annual indirect employment amounts to 908,000 in the high scenario, as compared to 705,000 in the low scenario during the last decade. Total employment, which includes direct construction, operation and maintenance, and indirect employment, increases from 2.4 million to 2.9 million in the high scenario. In the low scenario it increases from 2.4 million to 2.6 million and then declines to 2.5 million. The Midwest and South Atlantic regions will experience the largest indirect employment in both scenarios (24 and 16% of the national total), followed by the West, New York and New Jersey, and the Mid-Atlantic regions.

Table 1. Average annual employment impacts - TASE 6.

Capital Investment (10^9 $)	1976-1985		1986-1990		1991-2000	
	Solar	Total	Solar	Total	Solar	Total
Manpower	1.3	10.9	3.7	15.1	5.2	16.7
Materials	1.0	8.1	4.3	12.2	6.2	13.9
Equipment	.3	11.1	1.5	14.6	3.3	16.7
Other		14.0.		16.2		17.0
Total	3.2	44.1	11.4	58.1	17.8	64.3
Employment (10^3 man-years)						
Direct construction	37	331	110	459	156	516
Direct operation	53	1112	101	1370	214	1825
Indirect	111	1169	336	1462	442	1405
Total	201	2612	547	3291	812	3746
Indirect Employment (per 10^6 $ Capital Investment)						
In materials, equipment and other costs	36.2	33.4	30.9	29.5	26.1	25.1
In manpower	43.1	43.3	38.9	38.1	32.9	32.9
Employment (per 10^6 Total Capital Investment)						
Direct	11.6	7.5	9.7	7.9	8.8	8.0
Indirect	38.4	35.1	33.0	31.7	27.6	27.1
Indirect/Direct	3.3	4.7	3.4	4.0	3.1	3.4

Table 2. Average annual employment impacts - TASE 14.

Capital Investment (10^9 $)	1976-1985		1986-1990		1991-2000	
	Solar	Total	Solar	Total	Solar	Total
Manpower	2.8	12.2	8.8	19.7	10.5	19.8
Materials	2.3	9.2	10.1	17.6	15.3	22.0
Equipment	0.8	11.4	5.1	17.6	11.5	22.2
Other	1.2	14.4	4.7	18.5	10.5	22.4
Total	7.1	47.2	28.7	73.4	47.8	86.4
Employment (10^3 man-years)						
Direct construction	82	369	264	597	397	689
Direct operation	80	1134	182	1432	437	1978
Indirect	244	1307	843	1916	1179	1954
Total	406	2810	1289	3945	2013	4621
Indirect Employment (per 10^6 $ Capital Investment						
In materials, equipment and other costs	39.1	33.7	30.7	29.8	25.6	25.2
In manpower	43.2	43.2	38.1	38.1	32.9	33.0
Employment (per 10^6 Total Capital Investment)						
Direct	11.5	7.8	9.2	8.1	8.3	8.0
Indirect	38.6	36.3	32.7	31.8	27.4	27.1
Indirect/Direct	3.4	4.7	3.6	3.9	3.3	3.4

PLANNED ACTIVITIES IN FY 1981

We are planning to perform an integrated analysis of the effects of energy development in the West. As part of this study, we will estimate the potential direct and indirect economic impacts, and we will continue updating the 1972 BEA national input-output table to 1977. Using this national table, we will contruct tables for California and other western states.

REFERENCES

1. Bechtel Corporation, "The Energy Supply Planning Model," vols. 1 and 2, San Francisco, Calif., August 1975.
2. U.S. Department of Commerce, "Input-Output Structure of the U.S. Economy: 1967," vol. 1-3, 1974.
3. U.S. Bureau of Labor Statistics, "Employment Projections for the 1980's," Bulletin 2030, 1979.
4. U.S. Bureau of Economic Analysis, "Population, Personal Income, and Earnings by State: Projections to 2000," October 1977.
5. U.S. Department of Energy, "Technology Assessment of Solar Energy Systems, Interim Report, Environmental and Socioeconomic Implications," (in preparation).
6. U.S. Department of Energy, Second National Energy Plan, April 1979.

ORGANIZATIONAL, INTERFACE AND FINANCIAL BARRIERS TO THE COMMERCIAL DEVELOPMENT OF COMMUNITY ENERGY SYSTEMS*†

R. Schladale and R. Ritschard

INTRODUCTION

At the present time, the United States is engaged in a vigorous search for new energy supplies. Community energy systems are small-scale technologies capable of providing new sources of supply. Most of these technologies are fully developed, but none has been commercialized to meet more than a fraction of a percent of U.S. energy demand. The purpose of this study is to identify the barriers that groups and individuals will face when attempting to commercialize community energy systems.

The energy systems studied were: municipal solid waste (MSW); small-scale wind; industrial cogeneration; and residential photovoltaics. The scope of the barriers was restricted to three general areas: (1) organization barriers, (2) interface barriers, and (3) finanical and investment barriers.

Organizational barriers stem from deficiencies in organizations that attempt to develop a community energy resource, and may consist of a lack of awareness of opportunities; a lack of familiarity with energy technology; an inability to finance a feasibility study; or other factors.

Interface barriers cover a broad range of problems that arise when an organization seeking to develop a community energy system must interact with other organizations whose institutional policies and procedures were developed to meet an earlier set of conditions, i.e., before the advent of community energy systems. Consequently, smooth interaction may be difficult, and current policies and procedures may have to be revised to facilitate the growth of the new systems.

Finally, financial and investment barriers stem from the fact that new energy systems--although technologically proven in laboratories and demonstration projects--have not been tested under actual commercial market conditions. Consequently, new energy systems are deemed risky and investors will either avoid making commitments to them, or will do so only after attaching a high risk premium to their interest rate.

MAJOR FINDINGS

The major conclusions of this institutional study are given below and are organized into three categories: organizational, interface, and financial barriers.

Organizational Barriers

With regard to organizational barriers, the following are especially important:

- Municipalities need financial assistance to cover prebonding costs in the development of an MSW facility. These costs may total several million dollars, an amount that few municipalities have at their immediate disposal.

* This work was supported by the Technology Assessment Division, Office of Environment, U.S. Department of Energy under Contract No. W-7405-ENG-48.

† Condensed from R. Schladale and R. Ritschard, Organizational, Interface and Financial Barriers to the Commercial Development of Community Energy Systems, Lawrence Berkeley Laboratory report LBL-11188, August 1980.

- Municipalities may also require state assistance to ensure an adequate fuel supply. The state should establish wastesheds for each MSW project.

- Better information, education, and assistance should be made available to industrial management in order to accelerate the development of cogeneration.

- Neither residential homeowners nor homebuilders are very likely to possess the knowledge or skills necessary to install a photovoltaic system. The development of standardized, mass-produced technologies might need to be subsidized by government. Direct involvement by electric utilities or some other brokerage firm might be necessary.

These barriers are neither new nor particularly dramatic, but may merit more attention than they have heretofore received.

Interface Barriers

The issues involved in the interfacing of community energy systems with electric utilities have received considerable attention since the passage of the Public Utilities Regulatory Policies Act of 1978. Much progress has been made in developing regulations and purchase prices that make the scale of energy and capacity to utilities an attractive proposition. The Federal Energy Regulatory Commission and a number of state public utility commissions have been very effective in this regard.

Many interfacing issues and regulations remain in a state of flux, and further refinements to various policies are possible. Most of the recently developed policies were structured with the "firm types" of community energy systems--cogeneration and MSW--in mind. The applicability of these regulations for non-firm systems, such as wind and photovoltaics, is uncertain, although different provisions will be required in some policies, such as those governing payment for capacity cost.

Among the issues to which attention will be paid in the immediate future are:

- How reliable a small power facility must be to receive capacity payments; during what periods must power be available; and how should capacity payments be made for non-firm power (at what rate, and under what regulations)?

- Are small facilities dispatchable to obtain maximum capacity payments from the utility?

- The level of control that the utility has over a private developer's plans for a new community energy system is an important issue. The question includes whether the utility can demand special system-protection equipment or other special facilities. If so, who will decide whether demands for such equipment are reasonable?

- There are possible difficulties for cogenerators in obtaining exemptions to the Power Plant and Industrial Fuel Use Act of 1978 in order to burn natural gas. An issue is whether the cogenerators should pay the same prices and hold the same priority for natural gas that electric utilities do.

- Who will pay for necessary emissions offsets for new cogeneration and MSW facilities?

The authors feel that each of these issues will ultimately be decided in a manner conducive to further commericalization of community energy systems. The regulatory process may be slower than some would wish, but little experience exists with interfacing technologies other than cogeneration. It would be unwise to impose regulatory changes whose effects could upset the smooth operation of the large utilities on which society relies. Moreover, rapid changes in the structure of the electricity industry might be unacceptable to politically powerful forces in state legislatures and Congress.

Financial Barriers

The central difficulties that developers of community energy systems face in obtaining sufficient investment capital are: (1) the perceived risk of the new technologies; and (2) their relatively high cost compared to the historical cost of conventional power generating facilities. The recent cost increases for fossil fuels have made community energy systems much more competitive, although in most cases fossil fuel power plants still produce cheaper power. However, over the long term, it is clear that fossil fuel supplies will diminish and rise in price. Thus, commercialization of alternatives must be accelerated now, and for this reason, various political bodies are willing to provide public subsidies to accomplish it.

Municipal Solid Wastes

The major financial barriers to the development of municipal solid waste plants are the need to offer higher interest rates to bondholders because of project risk and the possibility of unexpected costs stemming from new emissions control regulations. Federal or state governments could provide guarantees to bondholders, and thus reduce the project risk; or they could provide grants that would directly reduce the project cost. Either would make financing an MSW project more feasible, but neither option has yet been enacted anywhere.

Wind

The major financial barrier for wind developers is the lack of start-up capital. This problem may be overcome through loans from the Small Business Administration, but the analysis given previously suggests that the funds currently available may be inadequate for this purpose.

Industrial Cogeneration

Cogeneration has received less than maximum investment in the past because its return on investment was considered too low. Because fuel prices have doubled during the past year, this situation has changed. Cogeneration now offers attractive returns and no additional subsidies for it are proposed in this study. However, if tight credit should prevail in the future, the provision of low-interest loans in place of currently available tax credits might be useful.

Residential Photovoltaics

For photovoltaics, the central barrier is system cost. If rooftop photovoltaic systems are to become competitive, they will require substantial subsidies in the form of low-interest, extended-term loans, as well as tax credits. The cost per kilowatt-hour of photovoltaic electricity subsidized may run as much as thirty times the cost per kilowatt-hour of cogeneration subsidized, even assuming that the Department of Energy's 1985 goal of 50¢/watt for solar cells is achieved. Of course, an important reason for accepting high photovoltaic subsidies is that cogeneration potential--as well as that of virtually every other source--is limited.

Summary

Three general observations regarding community energy systems may be distilled from this study. First, although many barriers exist to the commercialization of the systems, few, if any, appear unresolvable. Perhaps most challenging will be the problem of expanding the use of cogeneration and municipal solid waste, while at the same time maintaining or improving ambient air quality. Second, the financial subsidies required to make community systems competitive are not extraordinary. Indeed, with the exception of photovoltaics, they should not amount to more than about 10% of the capital cost of the new systems, and mass production may elminate the need for subsidies altogether in the future. Third, the administrative and regulatory procedures required to make community energy systems viable appear to be taking shape in a positive and timely fashion.

PLANNED ACTIVITIES IN FY 1981

This work was concluded in FY 1980 and will not continue in FY 1981.

COMMERCIALIZATION OF SOLAR ENERGY BY REGULATED UTILITIES*

E. Kahn, P. Benenson, and B. Brown

INTRODUCTION

In this project, we examine the role of regulated public utilities as financial intermediaries in the commercialization of solar energy. First we analyze the effect of various economic incentives offered by utilities to consumers for solar investments. Second we employ utility financial flow analysis to study the financial impact on utilities of solar incentive programs.

These incentive proposals are needed because public utility rates, typically set below marginal cost, reduce the value of solar investment. Moreover, incentives may enable utilities to avoid unprofitable energy demand that can be served less expensively by solar technology. Residential water heating is one end use for which this may be possible. Instead of investing in high-cost new supply facilities, utilities and their customers may benefit by channelling funds into financial incentives for domestic solar water heating. This issue is treated more fully elsewhere.[1]

ACCOMPLISHMENTS DURING FY 1980

During FY 1980 a large collection of potential incentives was extracted from the California Public Utilities Commission hearing record on this subject. These incentives were organized into three generic categories: (1) cash payments or bill credits, (2) interest subsidies and favorable loan terms, and (3) direct utility investment. This categorization was made from the perspective of the potential solar adopter. Questions relating to the cost justification and allocation of these incentives are treated in less detail.

Analysis of Financial Incentives

The generic solar incentives can be compared by present-value methods. Payments spread out over time can be related to the present through the following definition of present value (PV)

$$PV = \sum \left[\frac{PMT_i}{(1+r)^i} \right]$$

where PMT_i = payment in period i

r = discount rate.

Since this valuation depends strongly on the discount rate, r, and since r will vary in different circumstances, a parametric approach is adopted.

* This work was supported by the Market Development Branch, Active Systems Division, Office of Solar Applications, U.S. Department of Energy under Contract No. W-7405-ENG-48.

The present value of bill credits or periodic payments is simple to calculate. A consumer decision to invest in solar water heating would result if the present value of the incentive plus the present value of the energy savings exceeded the cost.

Loan incentives are more complicated. One popular form of such incentives is a zero-interest loan with delayed repayment. The critical feature of this approach is that the future value of energy savings need only be greater than the present value of the loan principal for the investment to be economic. The major uncertainty in this approach is the number of years until repayment is required. In the programs adopted to date this has averaged between five and ten years. The value of delayed repayment, zero interest loans can be seen in Figure 1. The graph assumes that solar water heating displaces 3000 kWh/year of electricity. The price of that electricity, p, ranges from 5-7 cents/kWh and the number of years to repayment is represented by the variable n. For a given n and p, the value of savings depends upon a discount rate (x-axis). For example, where n = 7, p = $0.06/ kWh and the discount rate is 15% or more, then the future value is $2500 or more. If the loan obligation were $2500 or less, then the investment is economic.

Direct investment programs are more straightforward. The main issue in this case is cost justification, since the incentive is typically the most expensive of all.

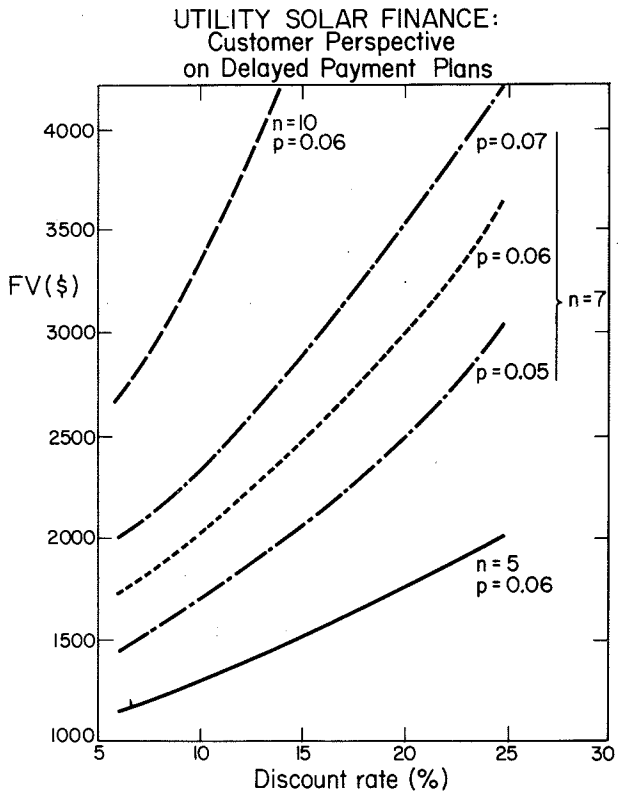

Fig. 1. Customer perspective on delayed payment plans. (XBL 803-424)

Utility Financial Impacts

Regulated public utilities face a variety of risks from their investment activity. These are reviewed in general and with regard to impacts from solar incentive programs. Particular attention is given to risk of competition, risk in the common equity market, risk in the bond market, interest-rate risk, inflation risk, and regulatory risk. Methods are developed to quantify the probability of negative utility cash flow. These methods are applied to recent financial data for a sample of utility companies. Various specifications of the basic model are compared to the corresponding bond ratings.

Analysis of Financial Simulation

The purpose of the simulation model is to estimate quantitatively the financial impacts of investments in conservation and solar energy on an electric or gas utility. The analysis is from the utility's viewpoint, and is microeconomic in scope; economy-wide parameters, such as energy demand, are assumed rather than internally determined. The analysis compares investments in conservation and solar energy with investments of corresponding magnitude in power plant construction. The calculations are made with a financial simulation model of a utility developed at the Environmental Defense Fund by Daniel Kirshner. The model is on the LBL computer system and is operated at LBL.

The model requires detailed inputs from the user regarding the present financial situation of the utility (e.g., average book life of the plant in the base year, amount of common and preferred stock, etc.). These data and the assumed investment plans are used to estimate the financial flows through the utility and to generate the balance sheet, income statement, sources and uses of funds, state and federal taxes, and other financial statistics for future years.

Such a computational model for estimating financial impacts is required because of the complexity of the regulatory and accounting options to which the utilities are exposed, such as normalization or flowthrough of accelerated depreciation and investment tax credits, construction work in progress in the rate base, and/or allowance for funds used during construction. The picture is complicated by several factors: (1) the maintenance of at least three sets of books by the utilities (one for stockholders, another for income taxes, and a third for regulatory purposes); (2) by the time in the asset life at which the impact is measured; and (3) by the fact that different construction projects often have different start and completion dates. The model accounts for these options and records the impacts according to the stockholder and regulatory sets of books. A schematic of the financial relationships that comprise the model is presented in Figure 2.

Some essential parameters are determined by market activity or by the regulatory process. Since this activity is beyond the model's scope, the assumption of their values introduces a static

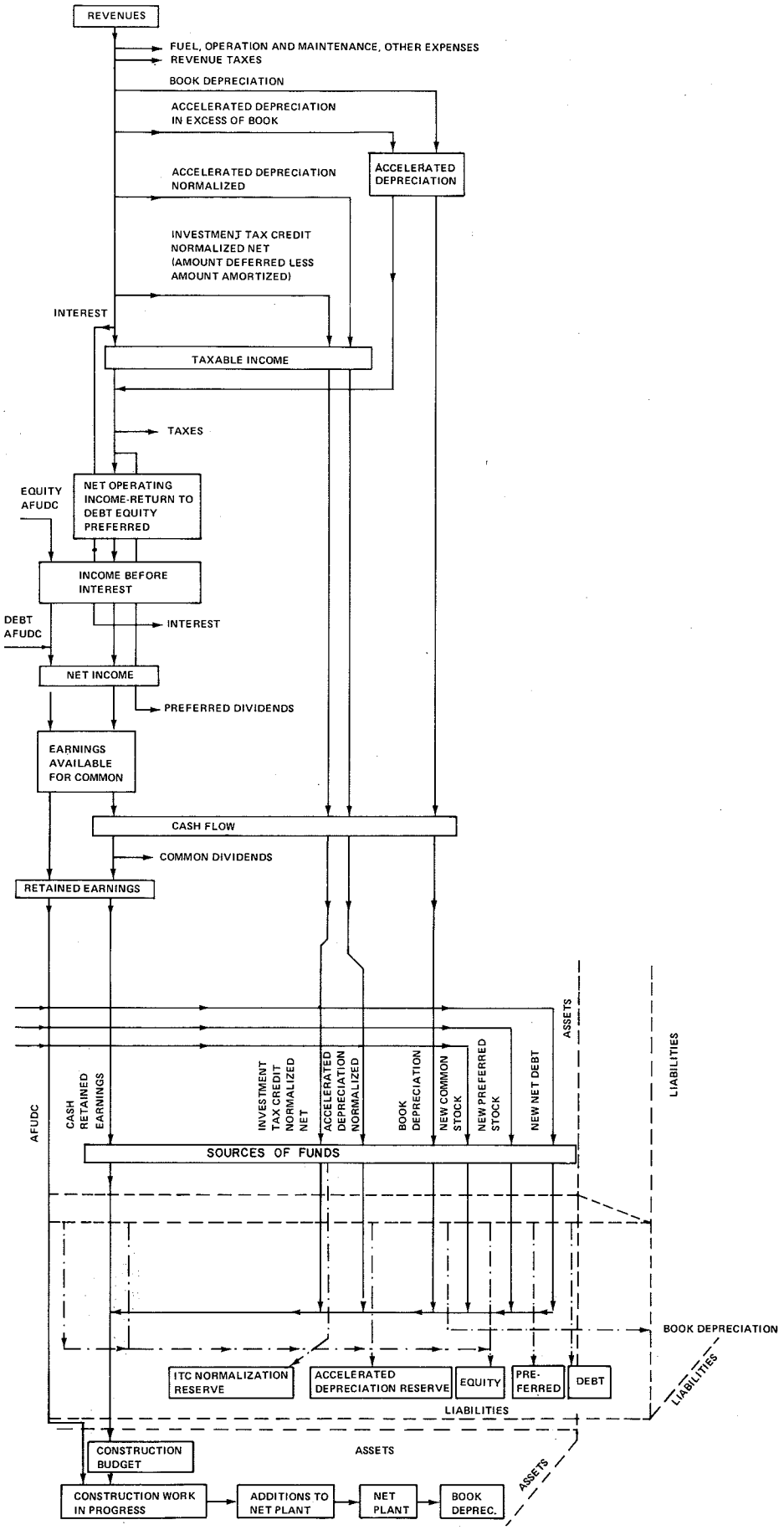

Fig. 2. Utility financial flows. (XBL 8010-4440)

treatment to what is determined dynamically in practice. Examples of such assumptions are electricity sales; the allowed rate of return on rate base and its equality with the realized rate; and the equality of fuel costs with fuel cost adjustments.

Two groups of cases are examined. The first, consisting of seven cases, begins with a base case of values approximating the present financial position of the Pacific Gas and Electric Company (PG&E). A general construction program of $1 billion per year, escalating at 10% per annum, is also assumed. The conservation cases differ from the base case by the addition of a ten-year, $100 million per year investment program in energy conservation equipment (construed broadly to include solar water heaters). They are depreciated in one case but not in another. In both, fuel costs are reduced to account for energy conservation. The power plant construction cases involve a substitution of the conservation expenditures by investments of equal amount and duration in power plant construction. The last two cases combine both investment programs with the power plant expenditures delayed to account for reduced energy demand from energy conservation. For this group of cases, the results show no major differences in financial variables examined. Ranking the cases is therefore difficult.

The second group, consisting of five cases, was designed to accentuate the differences between the impacts of the conservation and power plant investment paths. For the revised base case, the general construction expenditures were reduced to $500 million per year. The expenditures for conservation and power plant construction were increased to $200 million annually for ten years, and the conservation expenditures were depreciated.

A summary of the results for two of the five cases is presented in Table 1. Federal income tax is lower in the conservation case than in the power plant case because depreciation expenses can be claimed immediately, whereas for power plants they are delayed until the plant enters the rate base. The conservation case has a higher ratio of internal to total financing, a greater cash flow, and higher cash earnings per share. For many of the other impacts examined, there was little difference among the cases.

Table 1. Summary results of financial impacts from alternative investments.

Financial Category		Conservation $200 x 10^6/year (depreciated)	Power Plant $200 x 10^6/year
Federal income tax (10^6 $)	1980	17.00	31.00
	1983	28.00	63.00
	1986	90.00	57.00
	1989	163.00	129.00
	1992	293.00	331.00
	1995	406.00	454.00
	1998	522.00	619.00
Cash earnings per share ($)	1980	3.44	3.44
	1983	3.66	3.62
	1986	3.99	2.79
	1989	4.50	3.35
	1992	5.41	4.90
	1995	6.75	6.09
	1998	9.30	8.19
Cash flow (10^6 $)	1980	300.00	288.00
	1983	499.00	417.00
	1986	733.00	567.00
	1989	1015.00	918.00
	1992	1309.00	1354.00
	1995	1695.00	1757.00
	1998	2196.00	2310.00
Internal/total financing (%)	1980	22.80	29.10
	1983	34.00	34.20
	1986	43.10	15.20
	1989	50.60	41.70
	1992	61.80	59.10
	1995	63.80	63.00
	1998	66.00	67.20

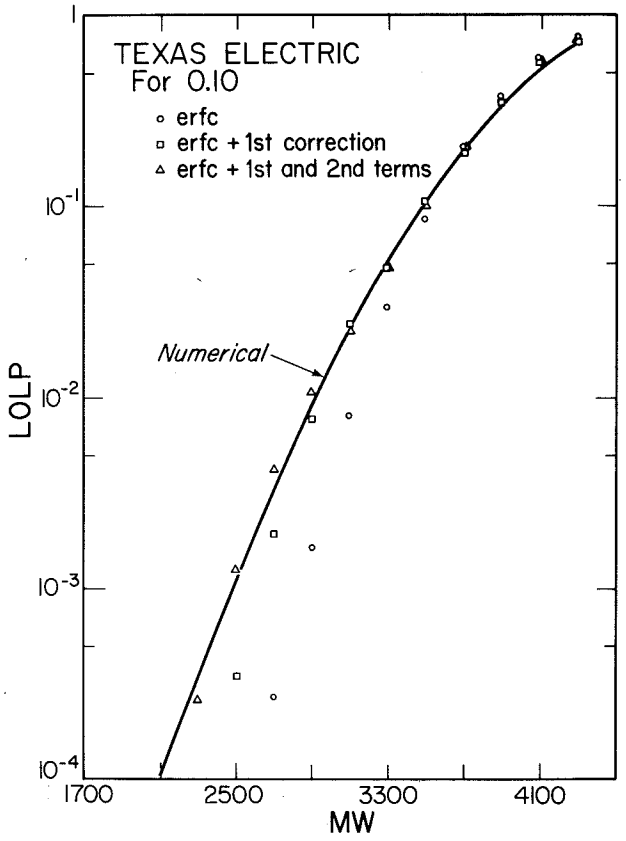

Fig. 1. LOLP plotted against generating capacity of Texas Electric System at FOR = 0.10. Edgeworth expansion error functions compared to numerical results. The acronym erfc stands for "the complementary error function." (XBL 803-432)

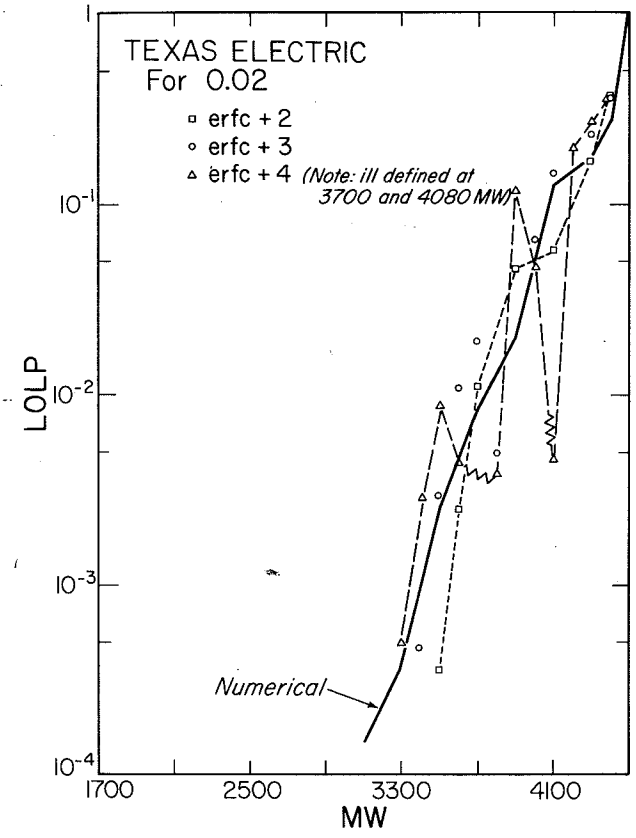

Fig. 2. Same as Fig. 1 except with FOR = 0.02. (XBL 803-431)

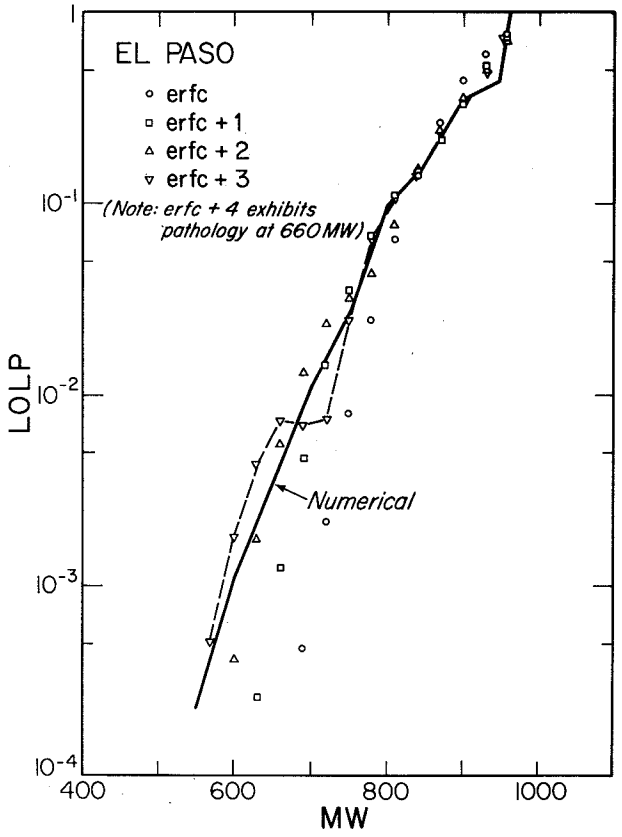

Fig. 3. LOLP plotted against capacity of El Paso Electric Co. system (based on Edison Electric Institute forced outage rates); Edgeworth expansion error functions compared to numerical results. (XBL 803-428)

study these results in a more general setting, the analytic properties of the Edgeworth series were examined more closely.

Analytic Results

Edgeworth-type expansions are usually appropriate when the underlying random variables take on continuous values.[9] This condition is violated in the case of most LOLP calculations where the generator's output characteristics are represented by probability distributions that limit the variables to discrete values only. Usually units are assumed to be either on or off in the two-state model. Where partial outages are considered, the standard model is again discrete rather than continuous. The underlying discrete probability distributions used to describe generators give rise to an aggregate probability distribution that is not continuous and that is referred to as a lattice-type probability distribution. In the limit of an infinite number of generators ($N \rightarrow \infty$), lattice as well as continuous probability distributions can be accurately described with the central-limit theorem.[9,10] In practice, the number of generators

The second group shows that the type of investment and the time path of expenditures can significantly impact a utility's financial situation. The conservation expenditures appear more advantageous because they can be depreciated and recovered more rapidly, but they must be of sufficient magnitude relative to the assets and expenditures of the utility to make an appreciable difference. These results are preliminary and await several modeling refinements and confirmation by industry personnel before they can be relied on for policy recommendations.

PLANNED ACTIVITIES FOR FY 1981

Financial simulation analysis of the solar incentives adopted by the California Public Utilities Commission will be conducted.[2] In addition, analysis of rate-making implications will be pursued. Utilities with large construction programs and/or in poor financial condition will also be studied.

REFERENCES

1. E. Kahn, P. Beneson, and B. Brown, Commercialization of Solar Energy by Regulated Utilities: Economic and Financial Risk Analysis, Lawrence Berkeley Laboratory report LBL-11398, October 1980.

2. California Public Utilities Commission, Decision No. 92251, September 10, 1980.

POWER SYSTEM RELIABILITY*

D. Levy and E. Kahn

INTRODUCTION

Numerical methods have historically been used to calculate reliability indices like loss-of-load probability (LOLP) for electric power generation systems.[1] For many purposes, however, numerical methods are a cumbersome means of computation. In capacity expansion models, for example, 20-year planning horizons are evaluated over a wide range of input assumptions. To reduce computational complexity and add conceptual perspective, several authors have studied analytic methods for approximating the numerical calculations. The most successful of these methods is an expansion based on the normal probability distribution, its moments and derivatives.[2-6] There are several variations on this approach, depending on the exact form of expansion used. Individual forms of the series are associated with Edgeworth and Gram-Charlier.[7]

The purpose of this research is to systematically investigate the accuracy of these methods with particular attention to power systems of 5000 MW and less. Two approaches are used: (1) a numerical approach with specific examples, and (2) an analytic approach in which underlying functional dependences are examined.

The most successful applications of the Edgeworth expansion and related approaches have been to large systems, typically in excess of 15,000 MW capacity. Even for systems of this size, if the average forced outage rate (FOR) is very low, the series can have disturbing properties and limited accuracy.[8] Since the method relies in part on central-limit theorem arguments, it can be expected to work well only when the number of random variables, i.e., generators, is large. Hence, there is reason to believe that the Edgeworth expansion will be less useful to approximate small systems than large ones.

ACCOMPLISHMENTS DURING FY 1980

Numerical Simulation Studies

Due to the substantial differences among electric utility systems it is important to examine particular configurations to test the accuracy of the Edgeworth approximation. To perform these tests, the Edgeworth series is written as a four-term expression, where each term has the opposite sign from the preceding term.[8] The standard numerical calculation of LOLP is compared to the analytic series. Typical results are shown in Figures 1-4 below.

Figure 1 shows a well-behaved case in which accuracy improves with additional terms and the approximation fits the numerical calculation well. In Figure 2 the same system is evaluated at a lower forced outage rate (FOR) for the individual generators in the system. Here oscillations and pathologies appear. At several points the series becomes ill-defined because the probability distribution takes on negative values. In Figures 3 and 4 the average forced outage rates for generators are based on data collected by Edison Electric Institute (EEI). Here the problems are not quite so extreme as in Figure 2. Accuracy, however, is limited in certain regions and does not necessarily improve with additional terms. Figure 3 is based on a very small system of less than 1000 MW and only 14 units. Figure 4 shows the effect of adding one large unit (1150 MW) to a system of just over 4000 MW. To

* This work was supported by the Solar Energy Research Institute through the Assistant Secretary for Conservation and Solar Energy, Office of Planning and Technology Transfer, U.S. Department of Energy under Contract No. W-7405-ENG-48.

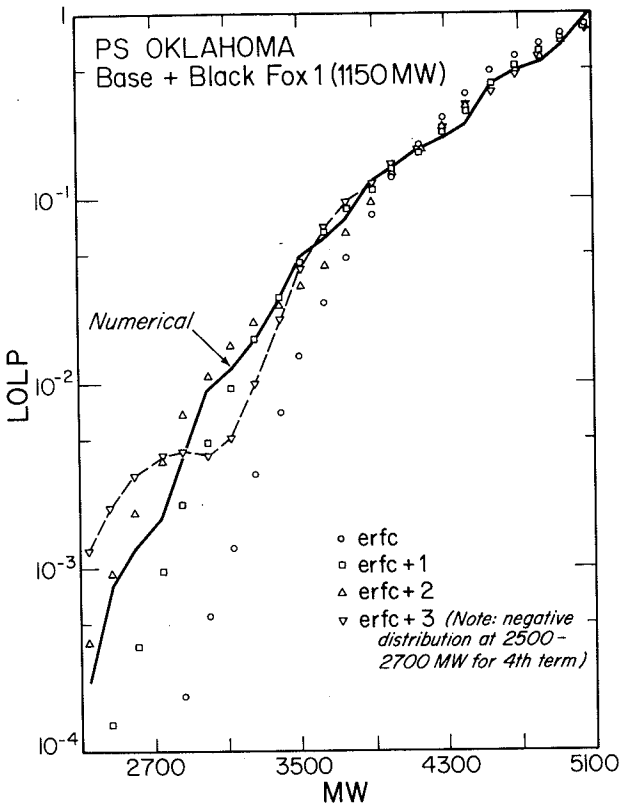

Fig. 4. LOLP plot for Public Service Co. of Oklahoma after addition of 1150 MW nuclear unit (based on Edison Electric Institute forced outage rates). (XBL 803-429)

(N), is finite so corrections to the central-limit theorem's normal distribution need to be considered. To calculate these corrections, most authors have used an Edgeworth series even though, as we have remarked, such expansions are inappropriate for lattice distributions and simple criteria, for their accuracy are lacking.

The essential problem with the Edgeworth expansion is that higher order terms, depending on higher moments of the underlying distribution function, can take on large values. For the case of small forced outage rates L_i and a finite number of generators N, each with capacity α_i, the following condition on the N + 1 unit will give the greatest accuracy:

$$\alpha_{N+1} = \sum_{i=1}^{N} \alpha_i^3 L_i \Big/ \sum_{i=1}^{N} \alpha_i^2 L_i \quad .$$

This expression will generalize to the case where forced outage rates are so low that convergence of the series will not occur. This condition is

$$\sum_{i=1}^{N} L_i < 1 \quad .$$

PLANNED ACTIVITIES FOR FY 1981

In FY 1981 several other approaches to analytic modeling of LOLP will be attempted. Based on the results of FY 1980 investigations, the new methods will take explicit account of the fundamentally discrete nature of the problem. One approach will use the Pearson-type system of frequency curves. In addition, new methods will take explicit account of load uncertainties in the LOLP calculation.

REFERENCES

1. R. Billinton, R. J. Ringlee, and A. J. Wood, Power System Reliability Calculations (Cambridge, Mass.: MIT Press, 1973).

2. E. Kahn, An Assessment of the Potential for Fuller Coordination of the California Electric Utilities, Lawrence Berkeley Laboratory report LBL-5941, January 1977.

3. E. Kahn, "Testimony before the New Jersey Board of Public Utilites," Docket 762-194, June 1977.

4. K. F. Schenk and N. Rau, "Analysis of Reliability Criteria for Generation Planning" (Ottawa, Canada: National Energy Board, 1977.)

5. J. P. Stremel and N. S. Rau, "The Cumulant Method of Calculating LOLP," Proceedings PICA Conference, Cleveland, Ohio, May 1979.

6. J. P. Stremel, R. T. Jenkins, R. A. Babb, and W. D. Bayless, "Production Costing Using the Cumulant Method of Representing the Equivalent Load Curve," IEEE Transactions on Power Apparatus and Systems (in press).

7. M. G. Kendall and A. Stuart, The Advanced Theory of Statistics, vol. 1 (New York: Hafner, 1977).

8. D. J. Levy and E. Kahn, Accuracy of the Edgeworth Expansion of LOLP Calculations in Small Power Systems, Lawrence Berkeley Laboratory report LBL-11324, July 1980.

9. C. G. Esseen, "Fourier Analysis of Distribution Functions, Acta Math., vol 77, 1945, pp. 1-125.

10. N. G. Gamkrelidze and Yu. V. Prokhorov, "On the Approximation of the Distribution of Sums of Lattice Random Variables when the Number of Summands is Small," Theory of Probability and Its Applications, vol. 15, 1970, pp. 144-147.

ACID MINE DRAINAGE IMPACTS ON GROUNDWATER *

M. Henriquez and J. Sathaye

INTRODUCTION

This study is one of the many technology assessment programs sponsored by the Technology Assessment Division within the Assistant Secretary for Environment. The study was conducted jointly with two other national laboratories, Argonne National Laboratory (ANL) and Oak Ridge National Laboratory (ORNL), which were responsible for analyzing the potential groundwater problems caused by acid mine wastes due to projected increases in coal mining activity.

Past experience has shown that rapid exploitation of coal resources results in long-term degradation of groundwater resources. The effects on the Appalachian region are well-documented. The adverse effects from unrestrained mining, such as acid mine drainage (AMD), and from unproductive reclaimed strip mine sites, are still felt decades after mining has ceased. Future major expansion of coal mining is expected in the Appalachian region as well as in the Western U.S.

In general, the new coal mining techniques are not expected to have significantly different impacts than those that occur with mining activity today, however, their magnitudes per ton of coal mined may be smaller because of improvements in mining techniques and because of soil alkalinity in the Western U.S. In this study, we have evaluated the relative magnitudes of the damages caused by acid wastes from both deep and surface mining in various U.S. regions.

The damage caused by acid mine waste can be both chemical and hydrological, depending on the various coal mining techniques and groundwater features. Furthermore, in many instances both types of damages are closely coupled, so that it is not possible to segregate their effects.

The magnitude of damage depends on coal mine characteristics and on groundwater characteristics. Mine geometry, relative transmissivity of spoil material, internal features, mine site, and type of operation all have an important role in determining the waste products generated from a coal mine. The extent to which the groundwater aquifers are affected will depend on the transmissivity and storage coefficient of each aquifer, the flow velocity, and the existing groundwater quality. The flow velocity is also influenced by the rate at which water is withdrawn from the system.

Acid mine wastes are formed when pyrite (FeS_2) oxidizes and dissolves in water to form sulfuric acid and ferric compounds. Pyrites and similar minerals are present in undisturbed coal seams. The process of coal mining exposes these compounds to air (oxygen); water movements through the exposed material then carry the oxidized pollutants to groundwater aquifers. For domestic or industrial users, AMD results in stains on laundry and in corrosion of pipes and engineering structures. Water containing AMD must be treated before use.

ACCOMPLISHMENTS DURING FY 1980

Methodology

The specific purpose of this study was to estimate the potential impacts on groundwater due to projected nationwide deep and surface coal mining activity. As noted earlier, the acid mine waste impacts are specific to the type and form of mining, to the coal seam, and to the groundwater aquifer underlying or surrounding the coal. With the limited time and data available to us, it was not possible to establish a mine-specific pollutant flow model for each U.S. coal mine.

We have established a methodology which in the aggregate accounts for all the variables that can affect aquifer pollution due to coal mining. The analysis is conducted for each of 21 water resources regions, which were delineated by their hydrological and geological characteristics. Data on aquifer parameters, such as storage coefficient, transmissivity, and soil permeability are available from several U.S. Geological Survey (USG) documents.[1] Projected levels of coal extraction by county were provided by the Futures Group[2] for 1980, 1985, 1990, 1995, and 2000, using base year information for 1975. Pollutant- (AMD) loading information was also provided for surface and deep mining by each coal region.[3]

These data, along with the average groundwater flow velocity (which is computed for each water resource region) are combined to form a comparative index. This index provides a guide to the relative severity of impacts among different regions of the country. The index value is directly proportional to flow velocity, permeability, coal mining rates, acid waste discharges, storage coefficients, and inversely proportional to aquifer transmissivity.

The index is primarily a comparative tool and is formulated so that it fits the base year data available from USGS. Aquifers for which we calculate a significant and related impact for a given year correspond to those aquifers in which AMD is recognized to be a major problem, on the basis of field measurements done by USGS. These areas are shown in the maps for 1975 (Figs. 1 and 2).

Results

The accompanying maps (Figs. 3 and 4) show the index values for the year 2000. Index values greater than 1000 correspond to counties where severe impacts may be expected because of increased coal mining activity. For all these counties, the

* This work was supported by the Technology Assessment Division, Office of Environment, U.S. Department of Energy under Contract No. W-7405-ENG-48.

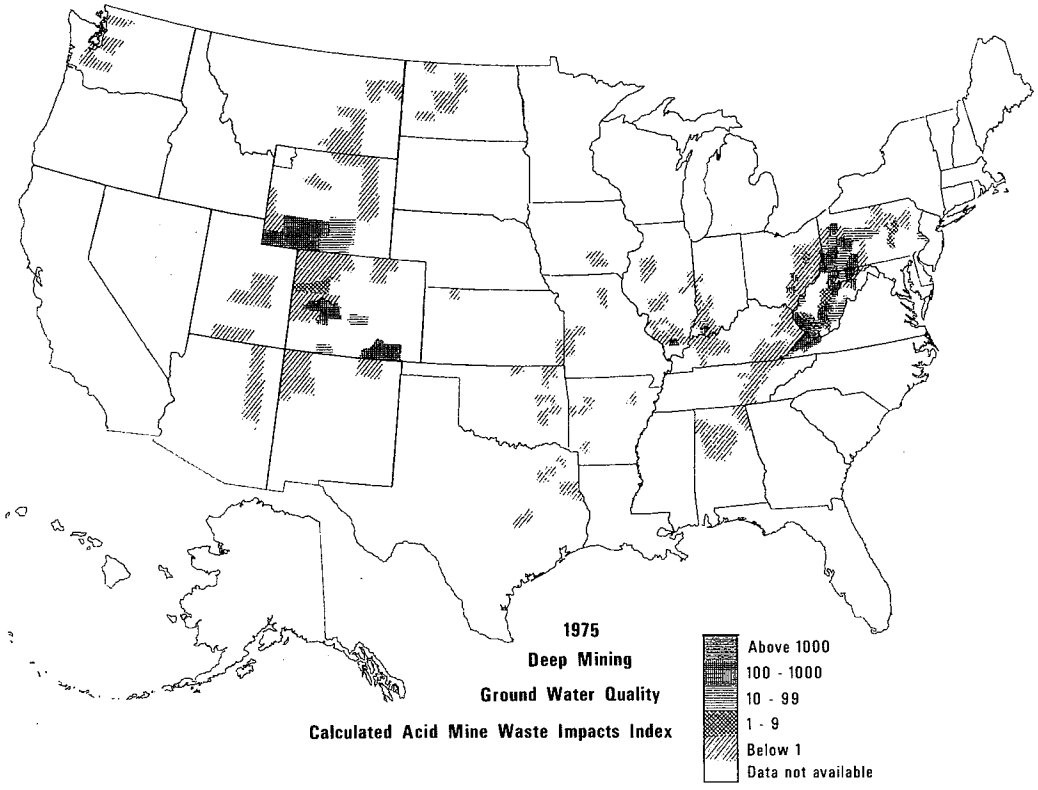

Fig. 1. 1975 calculated deep mining impacts. (XBL 8012-2441)

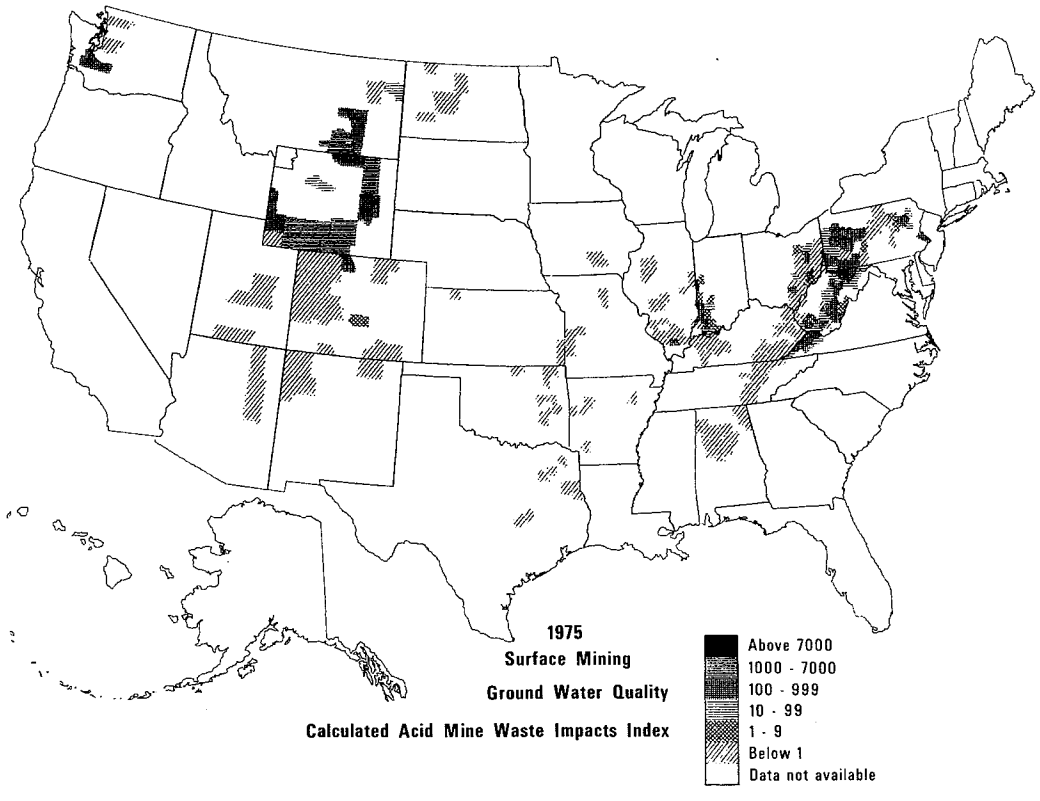

Fig. 2. 1975 calculated strip mining impacts. (XBL 8012-2442)

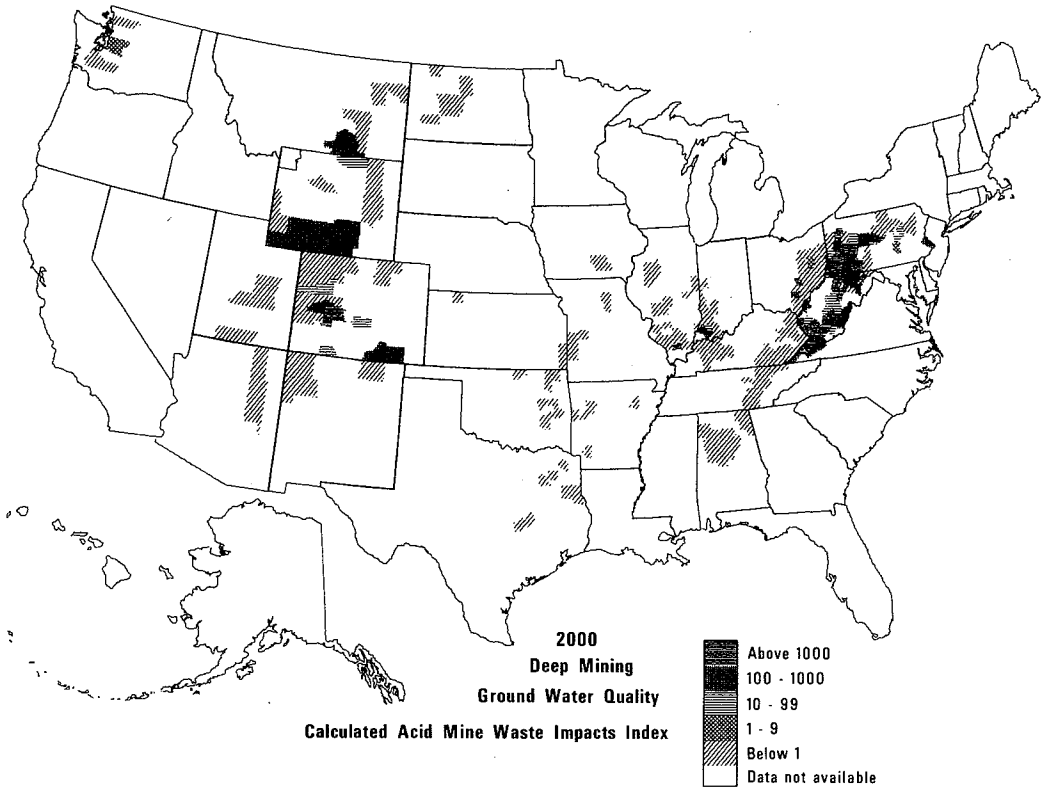

Fig. 3. 2000 calculated deep mining impacts. (XBL 8012-2443)

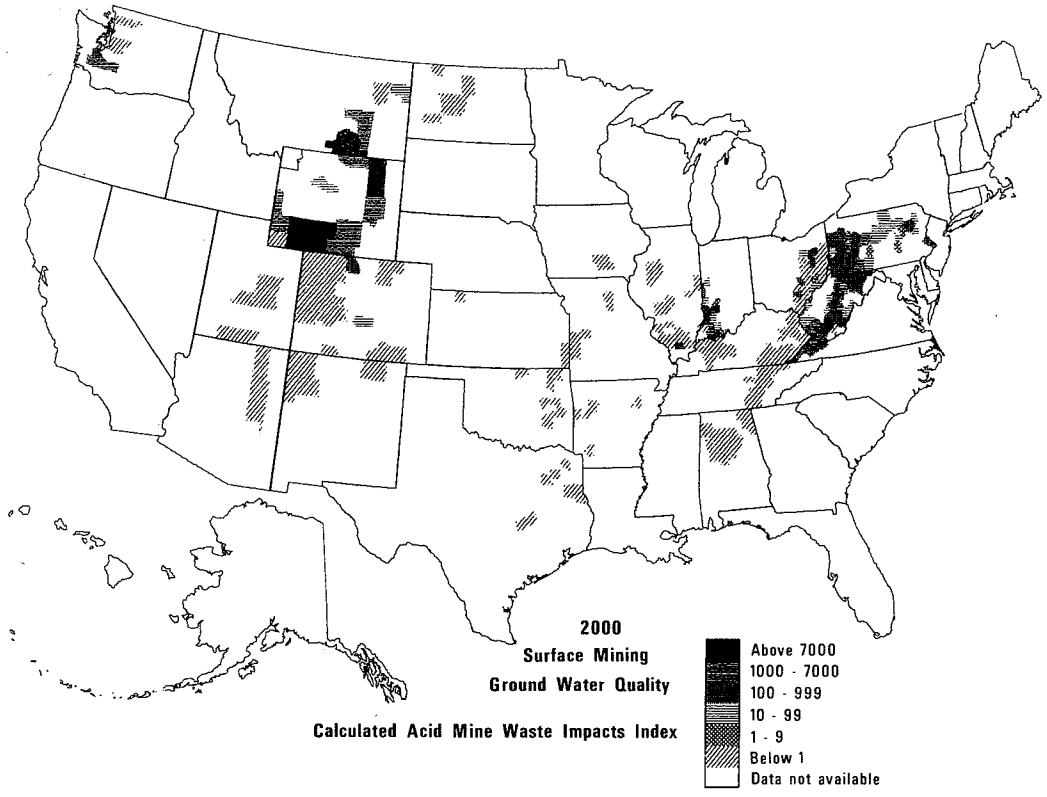

Fig. 4. 2001 calculated strip mining impacts. (XBL 8012-2444)

high level of coal mining activity is a more significant determinant of the environmental damage done than are the hydrological parameters. In other areas, where comparable amounts of AMD releases occur, e.g., the Ohio region and the Missouri region, different effects result due to the differences in groundwater hydrology.

The amount of potable water in the Ohio region is estimated at about 108,000 billion gallons in 1975, about 25% of Lake Ontario's liquid volume. Twenty-eight percent of the potable supply is in the Wabash and White subbasins, sites of high coal extraction. Acid mine drainage is a current problem in these basins along the Ohio-Pennsylvania border. The measured severity of the problem decreases further west. Groundwater systems in this area are highly permeable and are hydrologically connected to surface streams.

The Missouri basin has total aquifer storage of 150,000 billion cubic feet. Natural groundwater movement is in the direction of surface drainage, however, lateral movement in deep aquifers may be unrelated to surface drainage.

Table 1 shows the hydrological parameters for each basin. The AMD values used in our analysis are also shown. The 1975 index values for both surface and deep mines are roughly 60-80 for the Missouri region and 10-15 for the Ohio region. These values agree with reported USGS measurements regarding groundwater quality. The values are similarly dispersed for the year 2000.

Index values are proportionately higher for increased coal extraction forecast for 2000. Average values for the Missouri region are 250 for surface mining versus 30 for the Ohio region. This indicates that both regions will face an increase in damage due to coal mining although the level of impacts will still be lower in Ohio. The deep mining impacts do not increase very much in both regions. Index values (70 and 22) change little from 1975.

REFERENCES

1. Summary Appraisals of the Nations Groundwater Resources, U.S. Geological Service Publications Series 813A, 1974, Series 813I, 1975; Series 813S, 1979.

2. D. Canete, "Assessment of Increased Coal Production and Distribution," Futures Group Memorandum (unpublished), Washington, D.C., January 1980.

3. Mitre Corp., "Annual Environmental Analysis Report," vol. 1, Simulation Data Base for the Assistant Administration for Environment and Safety, (Washington, D.C.: MITRE Corp., 1977).

Table 1. Values of key parameters.

Region	Transmissivity (gallons per day)	Storage coefficient	Permeability (gallons/day/ft.^{2})	Velocity (ft.^{3}/sec)	AMD (tons/10^{12} Btu)	
					Surface	Deep
Missouri	1×10^6	0.080	20	33	6.9	67.7
Ohio	4×10^5	0.015	1500	433	6.9	67.7

ENHANCED OIL RECOVERY*

J. Sathaye and M. Milukas

INTRODUCTION

The environmental assessment of potential oil recovery by tertiary extraction methods is the primary objective of this study. This is a multilaboratory effort involving Brookhaven National Laboratory (BNL), Pacific Northwest Laboratory (PNL), and LBL, supported by the Technology Assessment Division of the Office of Environment. There are four basic methods of tertiary or enhanced oil recovery (EOR). These methods are steam flooding, fire flooding, gas injection, and chemical injection. These methods work by either reducing the oil viscosity or altering its surface tension, forces which tend to hold the oil in place.

Steam flooding, the first such technique to be applied, is the one EOR method to have reached the large-scale commercial use stage. Steam is injected into the reservoir, and the heat it carries lowers the oil's viscosity, thus improving recovery.

* This work was supported by the Technology Assessment Division, Office of the Environment, U.S. Department of Energy, under Contract no. W-7405-ENG-48.

Steam injection is carried out either as a cyclic process or on a continuous basis.

In fire flooding, a fraction of the oil in place is ignited while air is injected to maintain the combustion process. Water is injected sometimes, and it flashes to steam, helping to maintain a heat front which advances as the oil is removed from a production well.

Whereas thermal methods work primarily by lowering the viscosity of oil in place, chemical methods have as their main goal the reduction of interfacial tension between the oil in place and the sweeping fluid, which had been injected into the formation to decrease the oil's viscosity. This is accomplished with surfactants, polymers, and alkaline solutions.

The introduction of gases into an oil reservoir under high pressure has the desirable effect of vaporizing some of the hydrocarbons in the petroleum. This, in turn, acts favorably on the mobility of the reservoir fluids. Carbon dioxide is considered one of the most promising gases for use in this type of EOR operation.

EOR techniques at present account for about 4.5% of total daily U.S. oil production. Of the 385,000 bbl/day produced by EOR,[1] 296,000 or 77% are the result of steam applications. The next most promising techniques appear to be the gaseous methods with CO_2 floods the most important one. These gaseous applications resulted in another 75,000 bbl/day.

ACCOMPLISHMENTS DURING FY 1980

During FY 1980, a workshop was held on the environmental, economic, health, and safety aspects of EOR. The workshop was attended by experts in tertiary recovery from industry, government, public interest groups, consulting organizations, and academia.

A preliminary concern of the workshop participants was to agree on a reliable estimate of EOR production for the next twenty years. As with any new and rapidly developing technology, the issues and factors affecting production change rapidly. These are some major factors which could change current forecasts significantly:

- The development of EOR offshore and in Alaska is relatively unknown.
- The downhole steam generator technology could eliminate air pollution, thus removing one of the prime barriers to increasing oil recovery through steam injection.
- The windfall profits tax provides a tax incentive to EOR production for the next forty months; beyond that period, the industry representatives claim that the tax will hurt oil production from EOR.

Air pollution was an issue of major concern in one region: California. The boilers used to generate steam for injection in oil wells are a major source of sulfur oxide and nitrogen oxide emissions. Offsets for these emissions would have to be found under California law if these boilers are to continue to burn crude oil. The downhole steam generator would inject the steam and these gases into the oil wells, thus eliminating the need for air pollution control.

Groundwater pollution, often cited as the major concern about EOR, was downplayed as a major concern. In examining leakage of oil, other chemicals, and brine to groundwater, it is important to distinguish between pollutants due to tertiary recovery (which is the focus of this project), and those due to primary and secondary recovery. However, although there are no official records of groundwater contamination due to EOR, the hazard still exists and needs to be evaluated carefully.

Disposal of solid waste from scrubber sludge may be another major factor in restraining steam EOR production in California An appropriate hazardous waste-disposal site would have to be found to accept all the sludge with its heavy metals.

Shortage of trained manpower was cited as a major problem by industry representatives. Qualified engineers, technicians, and field personnel to work on EOR are in short supply and the problem was predicted to intensify with increased EOR activity.

PLANNED WORK FOR FY 1981

During FY 1981, we plan to concentrate on two major activities:

- Establishing a data base on EOR activities in various oil fields nationwide. This would include production levels, oil reservoir characteristics, and soil characteristics.
- Establishing a groundwater data base for areas where EOR activity is expected. Groundwater quality and proximity to water users can be estimated and monitored.

REFERENCE

1. S. Matheny, "EOR Methods Help Ultimate Recovery," Oil and Gas Journal, vol. 78, no. 13, March 31, 1980, p. 80.

GEOPRESSURED GEOTHERMAL RESOURCE OF THE TEXAS AND LOUISIANA GULF COAST: A TECHNOLOGY CHARACTERIZATION AND ENVIRONMENTAL ASSESSMENT*†

A. Usibelli, P. Deibler, and J. Sathaye

INTRODUCTION

This study examines two aspects of the Texas and Louisiana Gulf Coast geopressured geothermal resource: (1) the technological requirements for well drilling, well completion, and energy conversion, and (2) the environmental impacts of resource exploitation. The information contained in this study comes from the literature on geopressured geothermal research and from interviews and discussions with experts.

The technology characterization section of the report emphasizes those areas in which uncertainty exists and in which further research and development is needed. The environmental assessment section discusses all anticipated environmental impacts and focuses on the two largest potential problems: subsidence and brine disposal.

MAJOR FINDINGS

Technological Requirements

Nearly all aspects of geopressured well drilling and completion are similar or identical to techniques employed in conventional petroleum resource development. For those areas in which geopressured and conventional petroleum development vary, refinement of existing technique will be required. Experimentation will lead to use of the most appropriate mud and cement compositions. The greatest difficulty will be encountered in the development of monitoring devices adequate for extreme down-hole pressures. Accurate and safe drilling requires simultaneously obtaining information on a range of variables. In addition, in-situ sampling techniques require further basic and applied research in order to overcome current pressure limitations. A variety of completion methods, including both water well and petroleum well techniques, will be used experimentally in demonstrating resource feasibility. Additional experience will reduce the risk of blowouts and bad cementing, but as with conventional petroleum drilling, some risk will remain.

Energy embodied in the geopressured resource can be exploited in three different forms: the chemical energy of methane dissolved in the brine; the thermal energy in the form of geothermal heat; and the kinetic energy of high pressure fluids. The resource of major interest, however, is the methane contained in the extracted brines. Technologically, geopressured geothermal energy conversion is a hybrid of the conventional oil and gas and the geothermal electric industries. Development of major new techniques and technologies for geopressured resource development is not required. High brine flow rates coupled with the problems of erosion, scaling, and corrosion, however, will require refinement of both equipment and operating procedures. Disposal of brines into subsurface aquifers (2,000 to 5,000 feet deep) will not be technically difficult, although large volumes of spent brine at high pressure require careful management and monitoring of equipment.

Environmental Concerns

Surface subsidence resulting from geofluid withdrawal and the reinjection of spent brines into subsurface formations will be the two most difficult environmental aspects of resource development. In each case, the uncertainty is high. The severe adverse impacts of subsidence, or the inability to successfully reinject huge volumes of brine, may slow or halt commercial development of the resource.

The probability, magnitude, and rate of subsidence resulting from geopressured development is largely unknown. Experts disagree on the adequacy of current levels of theoretical knowledge for analyzing and predicting subsidence in the necessary site-specific manner. Some factors indicate a high potential for subsidence; others point to low potential. For instance, the extensive growth-faulting of the Gulf Coast may help limit the areal extent of subsidence. At the same time, the undercompacted sediments of geopressured reservoirs may enhance the probability of significant subsidence.

Geopressured rock testing is almost at a standstill until new samples can be obtained and data generated. Current simulation techniques cannot be refined until more data are available. Any analogy of geopressured subsidence with subsidence resulting from the extraction of geofluids (such as oil and gas, geothermal fluids, or groundwater), is far from precise. Its depth as well as its highly faulted sediments are unique features thought

---

* This study, conducted as part of a larger multilaboratory project to evaluate the technologies and environmental impacts of unconventional natural gas sources, was sponsored by the Technology Assessment Division within the Assistant Secretary for Environment's Office, U.S. DOE under Contract No. W-7405-ENG-48. Pacific Northwest Laboratory was responsible for evaluating tight sand, Devonian shale, and coal mine methane sources while LBL was responsible for the geopressured geothermal resource.

† Condensed from A. Usibelli, P. Deibler and J. Sathaye, The Geopressurized Geothermal Resource of the Texas and Louisiana Gulf Coast: A Technology Characterization and Environmental Assessment, Lawrence Berkeley Laboratory report LBL-11539, 1980.

to be determinants of subsidence. Efforts are now underway to standardize the nomenclature and testing procedures used by a variety of specialists from different disciplines. Increased emphasis will be placed on extensive testing of laboratory samples. The potential severity of geopressured subsidence in the low-lying Gulf Coast indicates that research should proceed in an unhurried but deliberate manner.

Spent brine is hot and chemically complex fluid that varies greatly in composition. Concentrations of heavy metals, organics, and trace elements frequently occur at levels far in excess of seawater concentrations and Environmental Protection Agency (EPA) toxicity standards. In an untreated form, discharge of this brine into terrestrial or aquatic ecosystems will cause major adverse biological impacts.

At present, reinjection of the waste brine into subsurface aquifers located above the producing formation is the only disposal method under serious consideration. Undesirable communication of the brine with adjacent fresh water formations, or with the ground surface, are risks that can be minimized with proper operating procedures. Control of reinjection pressures can aid in reducing the threat of environmental disruption resulting from fluid disposal. Surface disposal of brine to the Gulf of Mexico is more problematic. Disposal of hypersaline brines into the gulf from the Federal Strategic Petroleum Reserve (SPR) Program may provide useful data on dispersion patterns and possible impacts. Unfortunately, any disposal comparison is only partially realistic because of the different chemical and temperature characteristics of the two fluids. Brines probably cannot be dumped into the gulf except with intensive pretreatment.

Air quality, solid waste, noise, fault activation, and other environmental impacts have been mentioned in association with geopressured geothermal development. In each case either: the magnitude of the impact is small; the residuals are easily controlled; or, the probability of occurance is so small that impacts may be considered to be of second-order importance. Residual-monitoring programs should continue for existing and new test wells to enlarge the data base. Relative to subsidence and brine disposal, these impacts should not significantly affect resource development.

No geopressured wells have been drilled, or are planned, for the offshore Gulf Coast area. However, preliminary geological mapping of the offshore resource indicates several good prospect areas. But there are environmental, economic, legal, and institutional advantages and disadvantages to an offshore development strategy. From an environmental perspective, the impact of subsidence may be reduced through offshore development. Conversely, brine disposal may be more difficult unless adequate dispersion of brines can be achieved in the deep ocean areas beyond the outer continental shelf. Research is needed in certain areas to determine if an offshore development strategy should be pursued. The aim of this report is to discuss the pertinent issues and to indicate areas of research.

Recommendations

Technological

- Joint work on in-situ logging instruments for both geopressured and conventional geothermal wells should be encouraged.
- A range of well completion techniques should be tested in order to minimize drilling and completion risks.
- Full-scale testing of commercial production facilities--which include gas separators, hydraulic turbines, and geothermal electric units--should be conducted at the earliest possible time.

Environmental

- Funding for geopressured subsidence laboratory testing should be increased. The use of several laboratories, each with particular areas of expertise, should be encouraged.
- Communication between members of various disciplines working on subsidence research should be accelerated and research techniques and nomenclature should be standardized.
- Monitoring and analysis of the impacts of Gulf Coast disposal operations by the SPR should be closely scrutinized by researchers studying geopressured geothermal resources.
- Offshore brine disposal should be seriously studied as an option.
- The possibility of offshore development should be critically examined. A wide range of factors must be weighed in balancing the environmental, economic, legal and institutional advantages and disadvantages of such a strategy.

Table 1 is one of the study's environmental assessment matrices. The matrix is a qualitative summary of the subject areas considered in the environmental section. The assigned values attempt to balance diverse opinions expressed in the literature and the unpublished comments of researchers. Nonetheless, the choice of values often remains subjective. Because of the limitations of a ranking system with only three classifications, the correct characterization of a given aspect of resource development occasionally seemed to us to lie between two of the categories. However, this matrix may aid the reader in putting various aspects of geopressured development into perspective.

PLANNED ACTIVITIES IN FY 1981

Work may continue on this project in FY 1981.

Table 1. Summary of environmental assessment of geopressured geothermal extraction.

Impact Area	Analogy Oil/Gas	Analogy Geothermal	Analogy SPR*	Information Base	Experience Level	Research Basic	Research Applied	Magnitude	Mitigation	Uncertainty	Consensus
Subsidence											
Compaction	1	2	n.a.	2	3	x	x	n.a.	n.a.	2	2
Rock mechanics	2	2	n.a.	2	3	x	x	n.a.	n.a.	2	2
Shale dewatering	?	?	n.a.	2-3	3	x	x	n.a.	n.a.	1	3
Fault activation	2	2	n.a.	3	3	x	x	?	n.a.	1	2
Brine disposal											
Offshore-surface	2	3	2	3	3	x	x	1	3	1	2
Onshore-surface	2	2	3	2	3	n.a.	n.a.	1	3	3	1
Brine chemistry	2	2	2	2	n.a.		x	n.a.	n.a.	2	2
Subsurface injection	2	2	1-2	2	2	x	x	2	1	2	2
Fluid compatibility	2	2	2	2	2	x	x	3	2	2	2
Migration	2	2	2	2	2	x	x	2	1	2	2
Air quality	1-2	2	3	1	1			3	1	3	1
Land use	2	2	3	1	1			3	1	3	1
Solid waste	1	2	3	1	1			3	1	3	1
Occupational	1	2	2	2-3	1	x		3	1	3	1

Key to Environmental Assessment Matrix

Analogy
- 1-Direct
- 2-Partial
- 3-None

Information Base
- 1-Extensive
- 2-Moderate
- 3-None

Experience Level
- 1-High
- 2-Medium
- 3-Low

Research
- x-Research required
- blank-No research required

Magnitude
- 1-Major
- 2-Minor
- 3-Insignificant

Mitigation
- 1-Technology well developed
- 2-Technology partially developed
- 3-Technology poorly developed

Uncertainty
- 1-Major uncertainty about impacts
- 2-Medium uncertainty about impacts
- 3-Low uncertainty about impacts

Consensus
- 1-Major agreement among experts
- 2-Some areas of disagreement among experts
- 3-Wide range of expert opinion

n.a.-Not applicable
?-Uncertain
*-Strategic Petroleum Reserve

FORECASTING ENERGY DEMAND FOR HAWAII*

H. Ruderman and P. Leung†

INTRODUCTION

As part of the Hawaii Integrated Energy Assessment, we have developed a macroeconomic model of energy consumption in Hawaii. The Hawaii Energy Demand Forecasting Model (HEDFM) was designed to provide detailed forecasts of energy demand for the state's four counties. Demands for various types of energy were projected for each year until 2005 in Table 1. A summary of the forecasts made is given in Table 2. Combining the demand forecasts with supply scenarios furnished by other elements of the integrated assessment permits quantitative analyses of a range of possible energy futures for the state. In addition, the HEDFM provides empirical insights regarding the structure of energy demand in the state and its relationship to the local and world economies.

Work on developing the model was begun by the Hawaii Department of Planning and Economic Development (HDPED) during FY 1979. As a first step, HDPED compiled a data base of information on energy consumption and prices, as well as on economic and demographic variables. Using these data, they developed an initial version of the macroeconomic model. LBL's participation in this effort began toward the end of FY 1979.

ACCOMPLISHMENTS DURING FY 1980

The model and data base were transferred from HDPED to LBL early in FY 1980. We set up the model on the PDP 11/780 VAX computer system operated by the Computer Science and Applied Mathematics Department. This enabled us to take advantage of the interactive graphics capabilities of SEEDIS, the Socio-Economic Environmental Demographic Information System at LBL. An interface between the HEDFM and SEEDIS was written so that the demand forecasts could be displayed and plotted.

After the final version of the model was completed, we made five forecasts of energy demand under various assumptions of economic and demographic growth, energy prices, and conservation. The five cases were chosen to examine the sensitivity of the model to these assumptions and to provide a range of energy futures for the integrated assessment. Three of the futures were actually used in the assessment.

Table 1. Demand categories.

Residential Electricity Sales
Nonresidential Electricity Sales
Total Electricity Sales
Aviation Fuel Consumption
Diesel Fuel (Nonelectrical)
Residual Fuel (Nonelectrical)
Utility Gas Sales
Liquid Petroleum Gas (LPG)
Total Energy Consumption

Table 2. Regional dissaggregation for the HEDFM forecasts.

Regions for Forecasts
Honolulu County
Maui County
Hawaii County
Kaui County
State of Hawaii

Structure of the Model

The HEDFM forecasts energy use directly from explanatory demographic and economic variables. The model relates consumption in a given year to price, income, and the previous year's consumption. For most energy types, a set of log-linear equations is employed. The advantage of this form is that the coefficients of the explanatory variables provide estimates of the short- and long-run

* This work was supported by the Office of Conservation and Solar Energy and the Office of Resource Applications of the U.S. Department of Energy under Contract No. W-7405-ENG-48.

† Hawaii Department of Planning and Economic Development.

elasticities. The demand equations for each energy type are estimated using ordinary least-squares fitting of consumption data for 1963 to 1977.

The model for each fuel was estimated using several combinations of explanatory variables. The results were examined to confirm that the coefficients were of the proper sign and were statistically significant. They were also examined with respect to their suitability for forecasting. The pooled cross section-time series models gave the best results for electricity, gasoline, and diesel consumption. For residual fuel and LPG, a simple growth model was used for forecasting. The model for aviation fuel uses visitor arrivals and passenger load factors as the explanatory variables.

Forecasts

We examined three scenarios for energy demand in Hawaii. They differed in the future price of energy and in the level of energy conservation assumed. All three are based on the state's most likely projection of population and personnel income[1] and they assumed that the federally mandated automobile mileage standards will be implemented. The first case is a baseline projection assuming a 3%/yr escalation in world oil price above the general inflation rate. The second case, called the high price case, is based on a 10%/yr increase in oil price. The third case we called the savings case. In it, we modified the baseline forecasts by incorporating improved electrical appliance efficiencies.

Energy consumption in Hawaii during FY 1977 amounted to 200 x 10^{12} Btu. Of this total, approximately one-third was electricity, one-third aviation fuel, and the remainder primarily gasoline and other fuels for transportation. More than 80% of the energy and nearly all of the aviation fuel is consumed on Oahu. Except for a small amount of bagasse and hydropower, the energy comes from imported petroleum. During 1977, petroleum imports amounted to about 40 million barrels.

According to the baseline forecast, energy consumption is expected to increase to 354 trillion Btu in 2005. Reductions in consumption due to higher prices case would bring this total down to 244 x 10^{12} Btu, whereas improved efficiencies would reduce demand to 311 x 10^{12} Btu. These results are shown in Figure 1. The average growth rate in the baseline forecast is about 2.1%/yr. The largest growth will occur from 1985 to 1995. The savings case shows a similar behavior. The high price case, on the other hand, shows a growth in energy consumption of about 1%/yr until 1995 and then no growth thereafter.

The forecasts for total electricity sales in the state are shown in Figure 2. The baseline case shows an increase from 5.8 x 10^9 kWh in 1977 to 14.3 x 10^9 kWh in 2005. Most of this growth will occur in nonresidential sales. Residential sales will increase only by one-third because the large long-term price elasticity coupled with the forecasted price increases dampens demand growth. Savings from improved appliance efficiencies could amount to 3.8 x 10^9 kWh in 2005. This represents

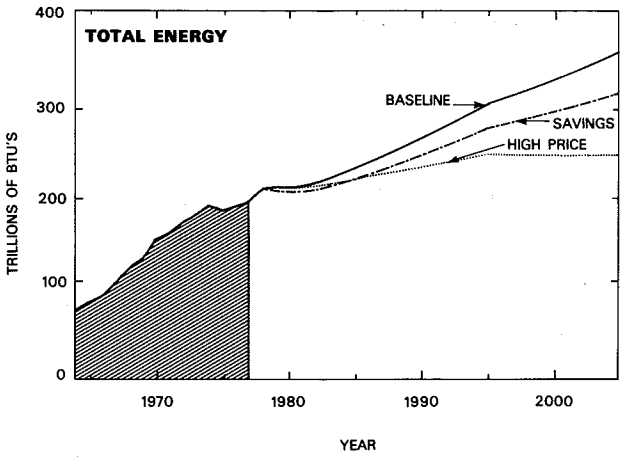

Fig. 1. Total energy consumption. (XBL 8012-2561)

a potential oil import reduction of about 7 x 10^6 bbl/yr. The high price case shows a leveling off and eventual decline in electricity consumption. By 2005, statewide consumption would be about 40% of the baseline forecast.

Our forecasts indicate that there will be a decline in the gasoline sales over the next twenty-five years. As shown in Figure 3, in the baseline and savings cases, gasoline sales will drop from 315 x 10^6 gal/yr to 155 x 10^6 gal/yr. Our results indicate that the currently mandated standards can reduce projected gasoline consumption by 60%. In the high price case, statewide sales in 2005 amount to 79 x 10^6 gal, about 75 x 10^6 below the baseline forecast or a quarter of the 1977 sales.

We made only one forecast for aviation fuel, using the state's projection that visitor arrivals would increase from 3.4 x 10^6 in 1977 to 8.2 x 10^6 in 2005, and we assumed that passenger load factors would gradually increase. Consumption nearly doubles during this period, reaching 860 x 10^6 gal by 2005.

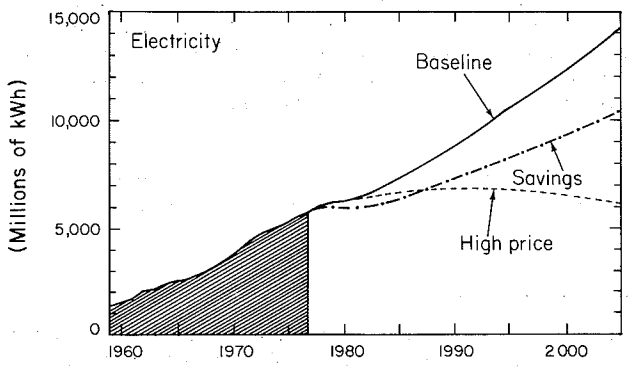

Fig. 2. Electricity sales. (XBL 8011-2338)

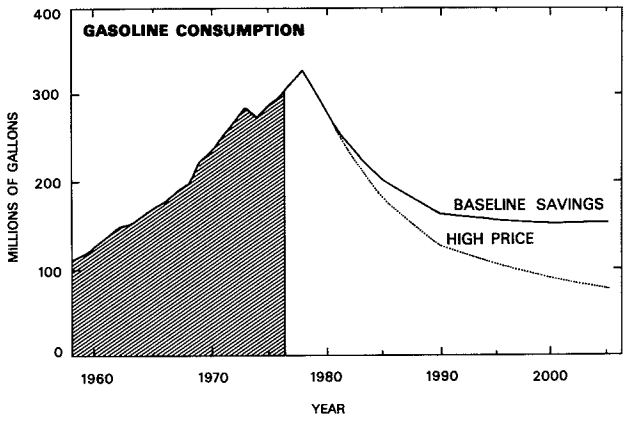

Fig. 3. Gasoline sales. (XBL 8012-2562)

The three demand forecasts described above do not take into account the impact of alternative energy technologies: The continuation of the current dependence on imported petroleum is assumed. Different energy supply scenarios will have different impacts on the economy in general which, in turn, will generate different energy demand patterns because of changes in the economic and demographic characteristics of the state.

PLANNED ACTIVITIES FOR FY 1981

Except for preparing a final report, work has been completed on the macroeconomic forecasting model. Towards the end of FY 1980, HDPED began gathering data and investigating methods for constructing an end-use model of energy demand in Hawaii. This type of model relates energy consumption to physical factors, such as the number of appliances in use and their unit energy consumption. End-use models tend to be more complex than macroeconomic models, and their data requirements are more extensive. However, an end-use model can provide better insight to the effects of policy decisions on energy consumption, because many of the factors that are affected by policy decisions can be incorporated in the model. During FY 1981 LBL will assist HDPED in constructing an end-use model of demand in the residential, commercial, and transportation sectors in Hawaii.

REFERENCES

1. Hawaii Department of Planning and Economic Development, "Long-Range Population and Economic Simulations and Projections for the State of Hawaii," Honolulu, Hawaii, 1977.

FORECASTING THE ROLE OF RENEWABLES IN HAWAII*

J. Sathaye and H. Ruderman

INTRODUCTION

Having no fossil fuel resources of its own, the State of Hawaii is almost totally dependent on external sources of energy. More than 90% of the state's energy is imported in the form of crude oil or petroleum products. The rest comes from hydroelectric plants and from burning bagasse at sugar mills. Hawaii is therefore extremely vulnerable to disruptions in the world oil market. Determining the extent to which oil can be replaced is the major purpose of the Hawaii Integrated Energy Assessment, a joint study by the Hawaii Department of Planning and Economic Development (HDPED) and the Lawrence Berkeley Laboratory (LBL). A complete description of the study and discussion of the results will be found in a forthcoming multivolume report.[1]

Each of the four counties in the state appears to have enough resources, such as ocean thermal, wind, solar, and geothermal energy, to supply nearly all its energy needs. The question arises, "To what extent should each of these resources be developed during the next 25 years to provide the state with a reliable and economic energy system?" To examine the role of renewables in supplying energy, we have constructed an integrated energy supply-demand model for the state. Using this model, we have examined three energy futures for Hawaii under different assumptions about prices and energy conservation. These are summarized in Table 1.

In this summary of our work we describe the methods developed for assessing a variety of energy futures. As an example of our results, we present the electricity demand forecast, generation mix, and prices in Honolulu County for the first energy future.

ACCOMPLISHMENTS DURING FY 1980

Methodology

The methods and data developed during FY 1980 for determining energy futures for Hawaii and their impacts on the state's economy are summarized in Figure 1. The Hawaii Energy Demand Forecasting Model provided energy demand projections for each of the counties by year up to 2005. We made three

* This work was supported by the Office of Conservation and Solar Energy and the Office of Resource Applications of the U.S. Department of Energy under Contract No. W-7405-ENG-48.

Table 1. Summary of Hawaii energy futures.

Future	Demographic Forecast*	World Oil Price Growth	Conservation
1.	"Most likely"	3%/yr.	Mandated automobile mileage standards.
2.	"Most likely"	10%/yr.	Mandated automobile mileage standards.
3.	"Most likely"	3%/yr.	Improved appliance efficiencies and mandated automobile mileage standards.

* From the Hawaii Macroeconomic Model Simulation, 1977. See Reference 2.

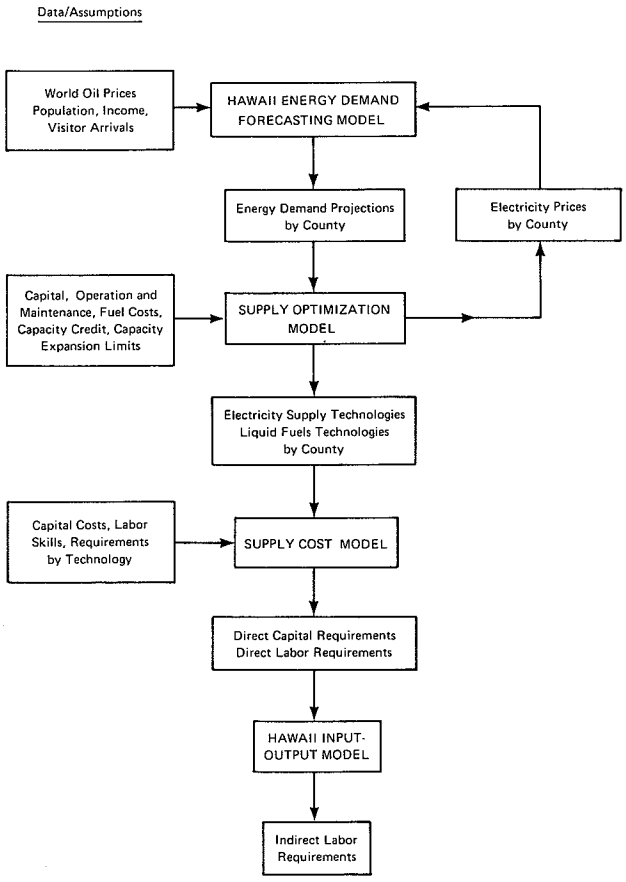

Fig. 1 Assessment methodology. (XBL 811-43)

forecasts which differed in their assumptions about energy prices and the level of energy conservation. The energy prices used in these forecasts are dependent on world oil prices. Demographic and economic projections were adopted from the state's forecasts.[2]

Because of the wide variety of technologies that will become available during the next 25 years, the projected electricity demands can be met in many ways. The technologies will differ in their costs, their reliability, their year of initial commercial availability, and in the amount of electricity they can ultimately supply. To facilitate the electricity supply-demand integration, the Supply Optimization Model was used to find the supply mix that meets the electricity demand and generating capacity demand at the lowest prices. In addition to determining the supply mix, the Supply Optimization Model also calculated the electricity prices for each county. In general, these prices were lower than those projected by the demand forecasting model. The new prices were fed back into the demand forecasting model, and a revised set of demand forecasts was obtained. We repeated this procedure until a consistent set of energy demands and prices was found.

The resulting supply scenarios were analysed for their direct and indirect economic impacts. Direct impacts include the materials, manpower, and equipment required to construct, operate, and maintain the new energy facilities. Indirect impacts include the income and employment in secondary industries within the state brought about by the expenditures on construction of the new facilities. We used the Supply Cost Model and our characterizations of renewable technologies to calculate the direct impacts in each county. The indirect impacts were estimated for the state as a whole using an input-output model of the state's economy.

Results

In this section we discuss our results for the County of Honolulu, of which Oahu Island is the principal part. Honolulu has about 80% of the state's population and accounts for more than 80% of its energy consumption. We present our projections of energy demand, the electricity generation mix, and electricity prices for the first future to illustrate the methods we developed to analyse the supply and demand options for the state. We are presently analysing the three supply-demand cases for the other counties. These results, along with the direct and indirect economic impacts in Honolulu County, will be published in Reference 1.

Energy Demand

Table 2 shows the energy demand on Oahu for the baseline case. The demand for electricity in Honolulu County will more than double during the next 25 years. Demand is heavily influenced by electricity prices, which will reach a plateau in 1955 as the fraction of electricity supplied by renewables becomes significant. Since electricity prices will no longer depend on ever-increasing oil prices, the demand for electricity will increase as prices decline or increase marginally.

The demand for imported petroleum will also reach a peak in 1995; then it will decline slightly in 2000 before increasing again in 2005. The non-electric portion of this demand will increase steadily; by 2005 it will be 40% higher than its present level. Oil required for electricity generation, however, will peak in 1990 and then decline to its lowest level by 2000. This decline is due to the rapid penetration of the renewables into the electricity supply mix after 1990. Although renewables will continue to increase their share after 2000, the use of oil will also increase because the maximum penetration by renewables is limited to a level insufficient to meet the increasing demand. Oil used for generation on Oahu will drop to 37% of renewables.

Supply Mix

Imported petroleum has been the predominant source of electricity in Hawaii for many years.

Table 2. Energy demand projections for Honolulu county baseline case with inter-island cable (trillions of Btu's).

	1980*	1985	1990	1995	2000	2005
Electricity						
Residual	57.1	60.9	65.3	54.6	23.2	37.8
Diesel	0.0	0.8	1.8	0.3	0.0	0.4
Oil total	57.1	61.7	67.1	54.9	23.2	38.2
Renewables at oil equivalent	1.4	4.5	9.9	38.8	91.2	104.1
Generation (10^6 KWh)	5,230	5,940	6,900	8,410	10,250	12,760
Liquid Fuels						
Gasoline†	25.7	17.8	14.0	13.2	12.6	12.5
Residual and diesel	18.9	21.3	24.2	27.6	30.9	34.7
LPG and utility gas	4.3	4.5	4.7	4.9	5.1	5.3
Subtotal	48.9	43.6	42.9	45.7	48.6	52.5
Aviation fuel	65.8	80.7	94.1	105.7	107.0	108.7
Total	114.7	124.3	137.0	151.4	155.6	161.2
Total oil demand	171.8	186.0	204.1	206.3	178.8	199.4
Oil demand without renewables	170.6	186.6	210.4	238.5	257.3	280.2
World oil price (1980 $/bbl)	30	35	40	47	54	63

* The figures for 1980 are estimates of demand, not actual consumption data.

† Alcohol could substitute for at least ten percent of gasoline consumption beyond 1990.

Bagasse combined with oil and hydropower have also contributed to the electricity supply, especially on the Neighbor Islands. Their contribution on Oahu has been relatively small. Figures 2 and 3 show the forecasts of generating capacity and the amount of electricity generated by each type of power plant for the next 25 years. The peak loads and reserve margins are indicated on the bars in Figure 3. The capacity demand includes a 20% reserve margin. We assumed that all the oil generating capacity available in 1980 will remain on line through 2005 to serve as a backup. The proposed 45 MWe of municipal solid waste (MSW) and 40 MWe of ocean thermal energy conversion (OTEC) plants have been included starting in 1985 and 1990, respectively. Additional generation from OTEC was included if it could compete favorably with the other technologies.

Oahu will continue to use its oil-fired power plants for baseload generation until about 1995. As OTEC and geothermal plants come on line for baseload, oil generation will mainly be used for intermediate and peaking loads. At the same time, wind and solar will also make major contributions. About 140 MWe of gas turbines will be built by 1990 to meet peaking loads. The largest capacity increments will occur between 1995 and 2000 when 830 MWe of new wind, solar thermal, OTEC, and geothermal plants will be constructed.

Electricity Prices

Electricity prices are related to the price of oil and to the cost of generating capacity. It is not surprising that, as the price of oil increases, so does the price of electricity. Electricity prices will increase rapidly until 1990. After this date, as lower-cost renewables become available, prices will decline or increase slightly. For Honolulu County, the average electricity price by 1990 will go from 86 mills/kWh to 109 mills/kWh, a 27% increase. During the subsequent 15 years, prices will increase by only 5%. The lower prices result in a larger demand than originally forecast assuming electricity would be generated primarily from oil.

PLANNED ACTIVITIES FOR FY 1981

During the first quarter of FY 1981, we will complete our analysis of the three energy futures for all four counties. We will examine some of the other options that are available to the state, such as the use of coal or biomass for generating electricity. The project should be completed during

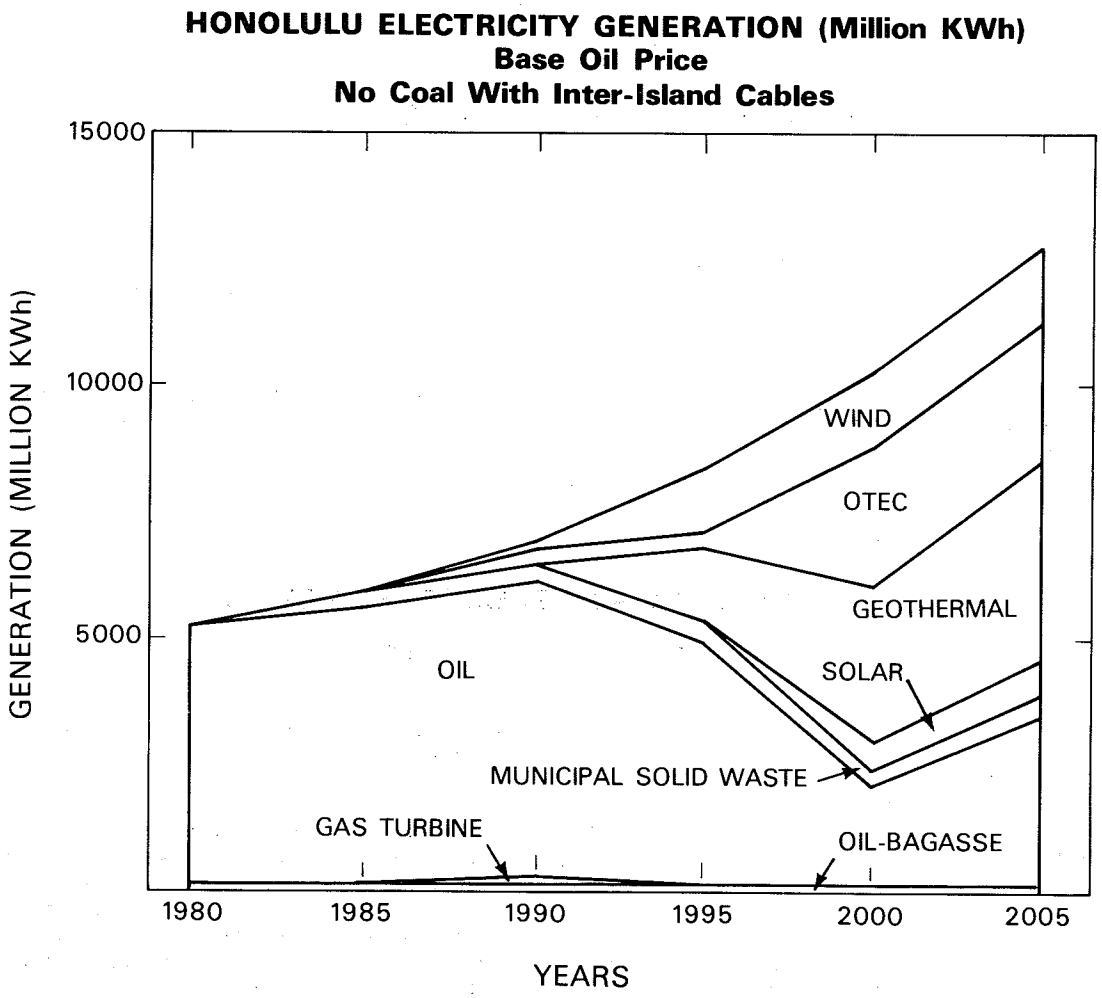

Fig. 2 Generating capacity in Honolulu County, Future 1. (XBL 8012-2557)

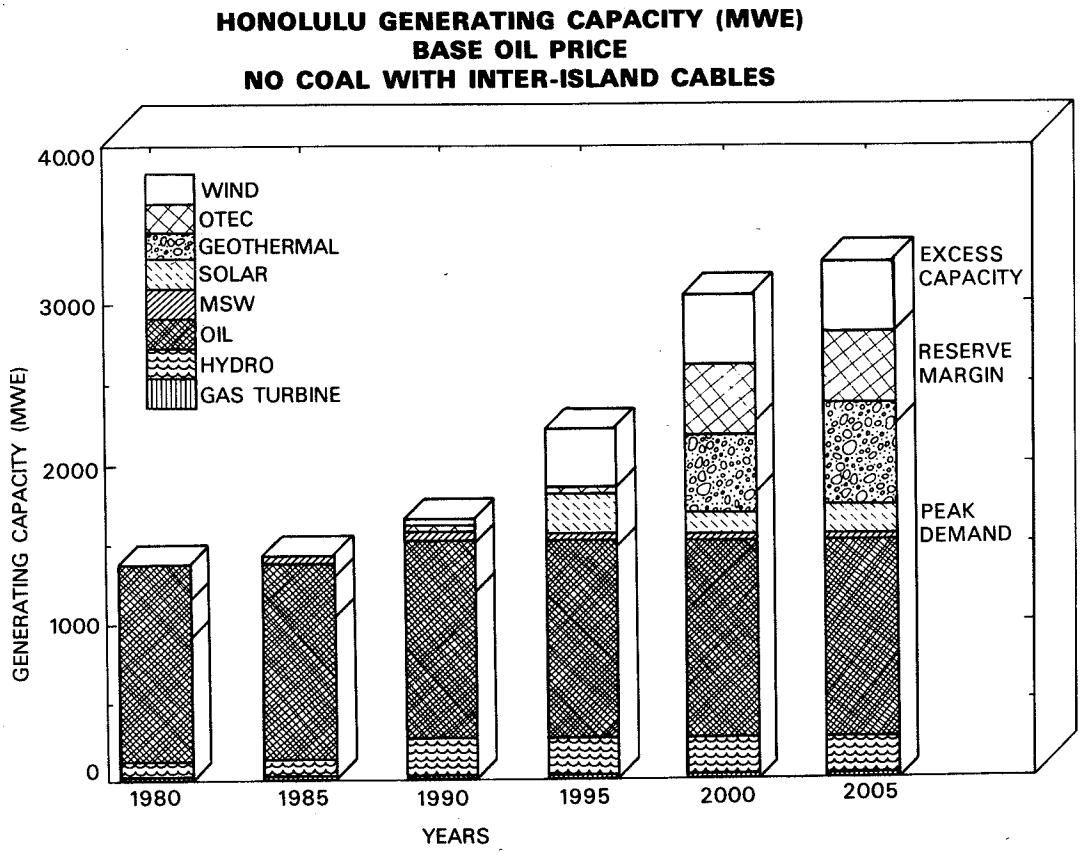

Fig. 3. Electricity generation in Honolulu County, Future 1. (XBL 8012-2559)

the second quarter with the publication of several volumes documenting our work.

REFERENCES

1. Hawaii Department of Planning and Economic Development and Lawrence Berkeley Laboratory, "Hawaii Integrated Energy Assessment," (unpublished), Honolulu, Hawaii, 1980.

2. Hawaii Department of Planning and Economic Development, "Long-Range Population and Economic Simulations and Projections for the State of Hawaii," (unpublished), Honolulu, Hawaii, 1977.

COASTAL ZONE ASSESSMENT PROGRAM*

R. Ritschard and K. Haven

INTRODUCTION

The coastal regions of the United States are rare, biologically important, and vulnerable to human perturbation. The coastal zone has been and will continue to be important in the nation's industrial development. The placement of energy facilities there generates environmental impacts and creates conflicts in the use of our coastal resources.

Since the coastal zone has been recognized by Congress and various coastal states as a geographic region of special concern, a set of state and federal institutions have been created specifically for coastal zone management. Other governmental regulatory agencies at the federal, state, and local level have been given topically specific authority for their coastal zone activities. While the number of agencies involved in

* This work was supported by the Regional Impacts Division, Office of Environmental Impacts, U.S. Department of Energy under contract No. W-7405-ENG-48.

the management and regulation of the coastal zone is vast, the involvement of each tends to have a single purpose. With the exception of outer continental shelf (OCS) oil and gas development, which is regulated by the Bureau of Land Management, U.S. Department of the Interior, energy development in the coastal zone is not the primary concern of any agency. Furthermore, these agencies tend to be regulators rather than planners; they have limited geographic jurisdictions; and they usually evaluate projects on a site-by-site basis.

Coastal energy activities are of great importance in the Pacific Coast region (Alaska, California, Hawaii, Oregon, and Washington). Nearly 90% of the region's electrical generating capacity (excluding hydroelectric), more than 50% of all regional oil production, and more than 80% of the region's refining capacity is located in the coastal zone. To date, the impacts of coastal facilities and activities have been evaluated on a site-specific basis, yet energy facilities in the coastal zone serve and affect an area far beyond the site. It is therefore imperative that the assessment of coastal energy development be conducted from a regional perspective and in an integrated fashion.

The Coastal Zone Assessment Program was initiated during FY 1980 to conduct integrated assessments of environmental, socioeconomic, and institutional impacts on the Pacific coastal zone as the result of energy development. The program emphasizes the cumulative effects of key energy and environmental impacts, identified and characterized by type and geographic area.

ACCOMPLISHMENTS DURING FY 1980

During FY 1980, the Energy Analysis Group at LBL, in conjunction with the Brookhaven National Laboratory, initiated a coastal zone assessment program. LBL's responsibility included the Pacific coastal region (Alaska, California, Hawaii, Oregon, and Washington).

The coastal zone has been recognized by Congress and by the various coastal states as having special significance to the economic and environmental well-being of the nation. Yet, there is no coastal-specific energy policy that considers both the development and implementation of a strong energy program and the attainment of the nation's environmental protection goals.

During the first year, the present and projected energy-related activities in the Pacific coastal region were addressed within the context of existing federal and state coastal management programs. Several regional energy supply issues in the coastal zone were identified: concentrated and dispersed facility siting; conversion to coal-fired power plants; OCS development; petroleum supply systems; siting of new technologies; and the cumulative impacts of energy activity.

The decision-making framework that has been created at the state and federal levels to protect the economic and environmental value of coastal resources was characterized. The major federal legislation is the Coastal Zone Management Act (1972) and its 1976 amendments. This act established the federal program that encourages the states to develop a planning process for coastal zone-related energy activities. Since state and local agencies are responsible for coastal planning, for implementing energy development in the coastal zone, and for bearing the environmental and socioeconomic impacts inherent in a particular energy activity, these agencies must be considered when federal energy plans are proposed.

An analysis of the interrelationships between federal, state, and local energy interests in the coastal zone indicated that two major roles are available to DOE's Office of Environment. The two roles are: (1) the analysis of the environmental impacts of various energy technologies and of proposed policies; and (2) the transfer of information from federal to regional, state, and local agencies that are responsible for coastal energy planning.

Within the first category, several new functions are proposed, including the identification of specific energy technologies and programs that may cause environmental impacts; and the integrative assessment of all energy-related activities within a large geographic area of the coastal zone, e.g., the Pacific Coast. The process of information transfer comprises the following proposed tasks: determine the regional, state, and local implications of federal energy supply scenarios; establish liaison with state and local agencies in order to define and clarify "national interest"; and act as a clearinghouse for energy and environmental data pertinent to the coastal zone.

The success of a well-coordinated national energy program that deals with the development of coastal energy resources while protecting the coastal environment will require better coordination between the federal, state, and local agencies involved. The authors feel that the Assistant Secretary for the Environment can play a critical part in this effort.

PLANNED ACTIVITIES FOR FY 1981

Several tasks are planned for FY 1981 in order to develop and apply a coastal assessment methodology to the Pacific Coast region. These activities include:

- Conduct of a regional coastal characterization that includes a detailed quantitative description of each component of the coastal energy technologies as they will be applied along the West Coast; identification of the most vulnerable estuarine systems; and selection of plausible siting patterns. Table 1 outlines the offshore and onshore requirements of various energy supply activities.

- Application of the coastal screening system to an appropriate scenario in order to establish residual loading patterns and to identify key coastal impact areas.

Table 1. Dependence of energy supply technologies on the coastal zone.

Energy Supply Activity	Offshore Requirements	Onshore Requirements
Offshore oil/gas production (pipeline)	Platform sites Gas treatment plant Pipeline to shore (oil and gas)	Platform fabrication yard Pipeline terminal and pumping plant Storage facilities Port support facility
Offshore oil/gas production (tanker)	Platform site Tanker loading bouy site On-site oil storage Gas treatment plant Gas pipeline to shore Tanker traffic lanes	Platform fabrication yard Tanker terminal Port storage facility Port support facility
Onshore oil/gas production		Well sites Pipelines Storage facility
Oil/gas processing	Tanker traffic lanes Barge traffic lanes Offshore terminals/ lightering sites	Pipelines Refinery Storage facilities Crude/product tanker terminals Product barge terminals
Liquefied natural gas	Offshore terminal (if selected over onshore terminal) Pipeline to shore Tanker traffic lanes	Regasification plant Tanker terminal Pipeline interties Storage facilities
Electric power plants	Tanker/barge lanes for waterborne fuel delivery and waterborne waste removal	Plant site Fuel delivery (waterborne); tanker/barge terminals Fuel delivery (rail); rail routes and terminals Fuel delivery (pipe); pipelines Onsite fuel storage Transmission lines Ash removal/disposal system
New technologies		
OTEC	Plant site Transission line	Platform fabrication yard Port support facility Cable intertie
Marine biomass	Farm site Harvest ship transit routes	Port support facility Farm fabrication plant Terminal for harvest ship Conversion plant Pipelines for gas supply
Wave energy	Plant site Maintenance ship travel Cable to shore	Fabrication plant Support base
Wind energy		Coastal plant sites Transmission lines

- Conduct of a detailed assessment of the environmental, socioeconomic, and institutional impacts resulting from the scenario's coastal energy activity and associated water quality impacts.

REFERENCE

1. R. Ritschard, K. Haven, and J. Cherniss, Energy in the Pacific Coastal Zone: Does D.O.E. Have a Role? Lawrence Berkeley Laboratory report LBL-11154, 1980.

A SUMMARY OF REGIONAL IMPACTS ASSOCIATED WITH THE SECOND NATIONAL ENERGY PLAN*†

R. Sextro, V. Berg, T. Chapman, M. El-Gasseir, P. Podvin, H. Ruderman, J. Sathaye, S. Schaffer, and K. Tsao

INTRODUCTION

The analysis of various national energy scenarios for potential regional environmental, socioeconomic, and institutional issues has been a continuing program within the Energy Analysis Program. Typically these assessments have had as a major objective the early identification of major impacts posed by national energy policies or strategies. This identification and assessment process is conducted at the state and local levels within each federal region, and therefore provides a "bottom-up" policy perspective for the U.S. Department of Energy.

This article summarizes the results of the Regional Issue Identification and Assessment project at LBL, which was based on an analysis of the President's Second National Energy Plan (NEP-II).[1] This project was conducted for the Regional Impacts Division, Office of Environmental Assessments of the Assistant Secretary for Environment, U.S. Department of Energy (DOE).

ACCOMPLISHMENTS DURING FY 1980

Scenario Discussion

The major assumptions of the scenarios based on the National Energy Plan are:

- Replacement cost pricing is achieved through gas and oil price deregulation;
- Increased coal use occurs with no federal coal-leasing barriers, and with federal policies designed to limit oil and natural gas use in utility and industrial boilers;
- Tax incentives are passed for new technologies, such as solar and oil shale, with these sources contributing 8 quads/yr and 2.5 quads/yr respectively by 2000;
- Nuclear power continues to be utilized, producing 17 quads/yr by 2000 (330 GW of installed capacity);
- GNP growth averages 3.5%/yr to 1985, then 2.9%/yr from 1985 to 2000;
- World oil prices move to $30/bbl by 1990, and $38/bbl by 2000 in the high oil price trajectory, and $17/bbl by 1990 and $21/bbl by 2000 in the low oil price case (1979 dollars).

This study focused primarily on the high world oil price scenario; the scenario based on low world oil prices was examined only where significant differences existed between the scenarios. Nationally, energy supply is expected to grow at almost 2%/yr. Overall reliance on natural gas and oil is projected to decrease slightly by the end of the century, while coal and nuclear are both expected to increase substantially during the same period. Alternative energy sources, particularly solar and geothermal, are expected to make a small contribution to the energy supply by 2000.

These national energy scenarios were disaggregated into regional supply and demand values for each of the ten federal regions. The scenario derived from the high world oil price case is shown in Table 1 for Federal Region IX. At the regional level, the overall growth rate in primary energy use is 1.5%/yr annually between 1975 and 2000. Aggregate natural gas use declines slightly, while oil use increases somewhat during this period. Coal use, however, increases dramatically as an industrial and utility boiler fuel, growing at nearly 7.5%/yr. Nevertheless, per capita energy use in the region is projected to decline during the last quarter of this century.

The increased emphasis on offshore oil and gas production is the most significant change in fossil fuel supply in the region. Imports of these two fuels increase somewhat to the middle of the time period, then decline to about the same level as the 1975 imports. Most of the increased coal use in Region IX is met by imports from other parts of the West as Region IX coal production expands only slightly.

The most substantial changes occur in the electricity sector, where sales are projected to increase by 3.5%/yr. Fuel use for electricity generation is shown in Table 2. The two sources with the largest changes are nuclear and geothermal, both growing by 10%/yr.

No major changes in technologies have been assumed in this study. New energy technologies, such as photovoltaics, fusion, the breeder or fluidized-bed combustion, have not been explicitly considered in the scenario. A regional siting pattern for supply and conversion facilities was assembled, based on utility, industry, or state agency plans in order to facilitate the assessment of impacts and issues arising from the scenario.

---

* This work was supported by the Office of Environmental Assessments, Assistant Secretary for Environment, U.S. Department of Energy under contract No. W-7405-ENG-48.

† Condensed from Lawrence Berkeley Laboratory report LBL-12024.

Table 1. Energy supply and use for Region IX based on NEP-2 (high world oil prices). (10^{12} Btu/year)

	1975[a]	1985	1990	2000
Regional production				
Coal	157	168	229	240
Crude oil	1870	2789	2815	2122
onshore	1413	2207	2026	1406
offshore	462	582	788	716
Natural gas	389	624	575	532
onshore	358	357	313	329
offshore	31	267	262	203
Hydro (electricity)[b]	490	496	550	550
Geothermal (electricity)[b]	33	181	295	421
Solar (electricity)[b]	0	0	5	150
Total regional supply	2939	4258	4469	4015
Fuel imports to Region IX				
Coal	34	273	544	1004
Oil	1400	1380	1231	1476
Natural gas	1689	1170	1261	1415
Nuclear (fuel)	64	363	598	1051
Total imports	3187	3186	3634	4940
Total supply	6126	7444	8103	8961
Regional energy consumption				
By end-use fuel type				
Coal	9	51	213	391
Oil	2638	2586	2466	2222
Natural gas	1750	1747	1798	1933
Electricity	601	871	1092	1433
Total	4998	5255	5569	5979
By end-use sector				
Residential	926	889	1000	1237
Commercial	576	576	605	682
Industrial	1146	1557	1790	1906
Transportation	2350	2235	2174	2154
Total	4998	5257	5570	5979

[a] Federal Energy Data System, 1975.

[b] 10,000 Btu/kWh.

Assessment Results

The scenario analysis was undertaken in two basic ways. Key issues that are critical to the regional implementation of the National Energy Plan were assessed. In addition, an analysis of the potential impacts was conducted. This section summarizes the study results for the Key Regional Issues. Detailed reports summarizing the air quality, water resource, ecology, and land use analyses are presented in companion articles in this annual report.

Key Regional Issues

Oil and Natural Gas Development

The scenario projects an increasing level of oil and natural gas production from Region IX sources, all of which would come from onshore and offshore California. With the exception of those areas with enhanced oil recovery (EOR) operations, production from existing onshore oil and gas fields is declining. Some of the areas with large EOR activity do not meet ambient air quality standards

Table 2. Fuel use for electricity production in Region IX (high world oil prices). (10^{12} Btu/year)

Fuel	1975[a]	1985	1990	2000
Coal	182	389	560	853
Oil	632	1583[c]	1580[c]	1376[c]
Gas	328	46	38	15
Nuclear	64	363	598	1051
Hydro[b]	490	496	550	550
Geothermal[b]	32	181	295	421
Solar[b]	0	0	5	150
Total	1728	3058	3626	4416

[a]Federal Energy Data System, 1975
[b]10,000 Btu/kWh.
[c]Includes some combined cycle plants.

for sulfur oxides. Hence, significant expansion of EOR operations in these areas will require the use of better emission controls.

Increased offshore oil and gas activity has considerable state and local opposition. One of the major issues is whether current outer continental shelf leasing plans are consistent with provisions of the federal Coastal Zone Management Act. The State of California also claims that the environmental review for the new leasing programs has been inadequate. Oil and gas development offshore will probably encounter a number of constraints; therefore the scenario projections regarding these resources may be optimistic.

Increased Coal Use

As can be noted from Tables 1 and 2, coal use is expected to increase rapidly in Region IX. In the industrial sector, much of this increase would take place in the industrialized metropolitan areas, most of which are nonattainment areas for one or more pollutants. At the same time, regional emissions from increased coal burning in this sector are estimated to increase 16 times for particulates and nearly 40 times for sulfur oxides. Required emission tradeoffs may therefore be difficult to obtain. In addition, the coal-handling infrastructure has not been developed in metropolitan areas of Region IX, unlike other industrialized areas of the country where industrial coal use has been established.

A number of new coal-fired power plants are projected by the scenario for the region. These plants should meet the federal New Source Performance Standards that have been adopted for most areas of the region. Many of the likely sites for these facilities are expected to be in rural or semirural areas where population impacts are reduced. However, in some cases the local area is in the nonattainment category; hence, emission offsets would still be required before the plant could be permitted. Most nonattainment areas do not have large local emission sources that can be used as tradeoffs for the proposed power plant.

Some states are considering the use of tighter controls on nitrogen oxide emissions. While this may increase plant costs, the lower resulting emissions may make finding emission offsets less difficult and it may reduce environmental impacts.

Nuclear Power

The scenario projects a nearly 13-fold increase in nuclear power by 2000. However, several states in the region have adopted legislation restricting development of new nuclear power plants until concerns regarding waste disposal, plant reliability, and overall emergency planning have been addressed. Similarly, public utility commissions throughout the region have expressed skepticism about utility financing of major capital intensive projects such as nuclear power plants. Costs for new nuclear plants have escalated considerably in the past several years.

In addition, the federal regulatory uncertainty following the accident at Three Mile Island has intensified state concerns. Emergency planning has become a major issue at plants currently in operation or under construction in the region. For all these reasons, the projected level of nuclear power development in the region is not likely to be attained.

Rural Development Impacts

Some energy developments proposed for Region IX will be located in rural areas because of the energy resource's location, as in the case of coal or geothermal energy deposits, some solar technologies, and onshore facilities needed for offshore oil and gas production. Other projects, such as coal or nuclear power plants, utilize rural sites as a means of reducing population impacts or risks. Changes in population and the resulting increase in demand for community services due to construction and operation of energy facilities are one of the main indicators of socioeconomic impact.

The extent to which communities are able to assimilate these changes depends on state and local tax laws, and on local economic conditions. Some communities in Region IX see energy development projects as a way of aiding the local economy and have encouraged such projects. In other cases, particularly following the passage of tax or local spending limitations, such as Propositions 13 and 4 in California, communities may not be able to raise or spend monies to cope with these impacts. Thus local socioeconomic impacts have become, and are likely to remain, important elements in the siting decision process, especially with regard to planning and implementing mitigation measures.

Financing Energy Development

Increasing marginal prices for new energy supplies and high interest and inflation rates have combined to make equity financing of new energy projects difficult and expensive for electrical utilities. The ratio of market price to book value of utilities' common stock has declined in the past few years. At the same time, the capital intensity

of the utility industry has increased. An accelerating construction and concomitant financing program will be required in order to meet the projected doubling of the region's electrical generating capacity. Since 80% of Region IX's electricity demand occurs in California, the utilities in that state will bear much of the financial burden of regional electrical energy expansion.

The ability to fund new projects will hinge on a number of factors, including rate regulation policies and the condition of external capital markets. Changes in utility rates generally have not kept pace with rapidly increasing costs, and concerns over fuel and technology choices and over environmental issues have become increasingly important in the regulatory process.

Overall, project financing is likely to be one of the major constraints to implementation of the NEP-II scenario. Several regional coal projects currently in the regulatory process have been delayed since traditional means of utility financing are apparently not capable of providing capital for simultaneous major projects.

PLANNED ACTIVITIES FOR FY 1981

A study of a larger number of western states has been initiated in cooperation with Los Alamos Scientific Laboratory. This study will develop a set of scenarios describing future energy, economic, and demographic growth in the region, and will provide an assessment of the environmental consequences.

REFERENCE

1. U.S. Department of Energy, National Energy Plan II, 0-294-651/BID (Washington, D.C.: Government Printing Office, 1979).

EVALUATING LAND USE AND ECOLOGICAL ISSUES ASSOCIATED WITH FUTURE ENERGY PROJECTIONS*

V. Berg

INTRODUCTION

Energy production and conversion require the use of land, often displacing an existing land use. Energy activities can also indirectly affect the use of larger areas of nearby land. Similarly, energy resource development can affect natural ecosystems either directly, through habitat disruption, or indirectly, as a result of residuals released into the environment.

Many of the residents of Federal Region IX have expressed concern about the possible land use implications and ecosystem disruption associated with energy development. This research is an assessment of some of the potential interactions between energy development patterns, land use, and natural ecosystems.

ACCOMPLISHMENTS DURING FY 1980

This report summarizes a study performed as part of the Regional Issues Identification and Assessment (RIIA) project, which is described elsewhere in this report.[1] The assessment was based on two oil price scenarios that were developed as part of the President's second National Energy Plan (NEP-II).

Direct Land Use

Table 1 lists the estimated land areas in Region IX directly affected by the energy activities in the NEP-II High World Oil Price scenario. The two types of electrical generation facilities with the largest capacity in the scenarios are nuclear and coal-fired power plants. These power sources occupy about 350 and 1200 acres per site, respectively. On a per-megawatt basis, direct land use for these power plants is among the lowest of the generation facilities studied.

Oil, combined cycle, and natural gas-fired power plants also occupy a relatively small area. Due to rising petroleum prices and policy decisions, no new facilities of these types are projected in the NEP-II scenario after 1986.

Geothermal, solar thermal electric conversion, and wind turbines require a large area of land per megawatt of capacity due to the dispersed nature of their energy sources. Not all the land area in their collecting fields is physically occupied by the facilities, but the entire land area was included in Table 1 because energy collection and conversion is the dominant land use in those areas.

The biomass facilities in the scenario were assumed to be fueled by municipal solid waste (MSW) and to be located in urban areas. They are the only energy technology in the scenario that is expected to result in a net decrease in land area used. This curious result occurs because the burning of MSW reduces the need for sanitary landfills, and this more than compensates for the land area physically occupied by the plant. The number of new residents expected in each county under the

* This work was supported by the Regional Impacts Division, Office of the Environment, U.S. Department of Energy under Contract No. W-7405-ENG-48.

Table 1. Land area needed for energy development under the RIIA High World Oil Price Scenario, 1976-2000. (Acres)

Technology	Ariz.	Calif.	Hawaii	Nev.	Total
Nuclear	386	2,180	0	0	2,566
Coal	6,960	5,330	0	3,655	15,945
Oil and combined cycle	102	947	157	0	1,206
Natural gas	0	0	0	0	0
Geothermal	0	25,574	1,786	7,824	35,184
Hydroelectric	1,230	7,906	0	0	9,136
Biomass (MSW)	0	-3,107	0	0	-3,107
Solar thermal	5,029	9,387	0	335	14,751
Wind	411	19,880	0	411	20,702
Subtotal	14,118	68,097	1,943	12,225	96,383
Surface mining	9,362	0	0	0	9,362
New residents (number)	2,430	10,779	0	19,460	32,669
New residents (acres)	307	1,362	0	2,460	4,129
Total acres	23,787	69,459	1,943	14,685	109,874

scenario was calculated by Argonne National Laboratory using the Social and Economic Assessment Model (SEAM).[2] These results were used to estimate the land area needed for homes, schools, water supply, etc.

Habitat Disruption

Table 1 shows a total of 109,874 acres directly affected by new energy facilities in Region IX. Much of this land use will displace native plants and animals from their habitats. In some cases, e.g., geothermal development, the most significant effect has been the physical removal of vegetation in the course of facility and road construction.

The hydroelectric development projects in the RIIA scenarios will probably change aquatic temperature regimes, oxygen content, water flow and siltation patterns, and salinity. These changes, in turn, may affect aquatic organisms at the reservoir site and for many miles downstream.

Threatened and Endangered Species

The problem of habitat destruction is especially critical for endangered species, whose habitat requirements are often extremely specific. Data on the number of endangered species in each county[3] were used to assess the relative constraints to facility siting in different counties. These data were adjusted statistically to eliminate bias due to the sizes of the counties.

California's coastal counties have more than their share of endangered species due to diverse topography; to a large number of native species; and to major climate changes during recent geologic history. The arid counties of Southern California have many endangered aquatic species, mostly limited to small areas with adequate water. Finally, urban counties contain more endangered species, possibly due to past conflicts with people or because rare species are more easily noticed and studied in those counties.

Indirect Effects on Nearby Land Uses

Most electrical generation technologies have some effects on land uses outside the power plant boundaries. The most striking example of this is nuclear power. Despite the safety assurances of nuclear power proponents, many members of the public believe nuclear power poses unacceptable risks.[4] This affects the desirability of some land uses for many miles around.

Because power sources such as geothermal and wind must be sited in the limited geographic area where they occur, conflicts with other land uses

usually cannot be avoided by changing the development site. Geothermal operations at The Geysers in Northern California have already conflicted with the quiet, rural lifestyle cherished by many local residents. Many potentially valuable wind resource areas cannot be developed because they are located on federal land with wilderness attributes.

The major off-site effect of coal use on other land and resource values results from visibility degradation in recreation areas. A third of the National Park managers in Region IX believe that visibility impairment is damaging to the parks' resources.[5] Visibility problems reduce the recreation experience of most park visitors, thus diminishing the value of an important western resource.

Air Pollutant Effects on Vegetation

Of all energy impacts on ecosystems, air pollutants may affect the widest geographic area. In Region IX in 1975, about 80% of the SO_2 emissions were produced by poorly-controlled nonferrous smelters. By the year 2000, the smelters are expected to greatly reduce their emissions. However, the NEP-II projection of a fourfold increase in utility and industrial coal and oil fuel use would leave SO_2 emissions in 2000 at about the same level as in 1975.

SO_2 damage to crops is expected to continue in the same areas as in 1975 (Fig. 1). The four counties in southeastern Arizona are affected under both the High and Low World Oil Price scenarios. The urban counties in California are only affected under the Low World Oil Price scenario. SO_2 damage to natural vegetation (Fig. 2) follows a similar pattern as for SO_2 damage to crops.

Figures 1 and 2 refer only to levels of SO_2 high enough to cause acute visible symptoms of injury. Synergistic effects with other pollutants and chronic low-level injury patterns may be more

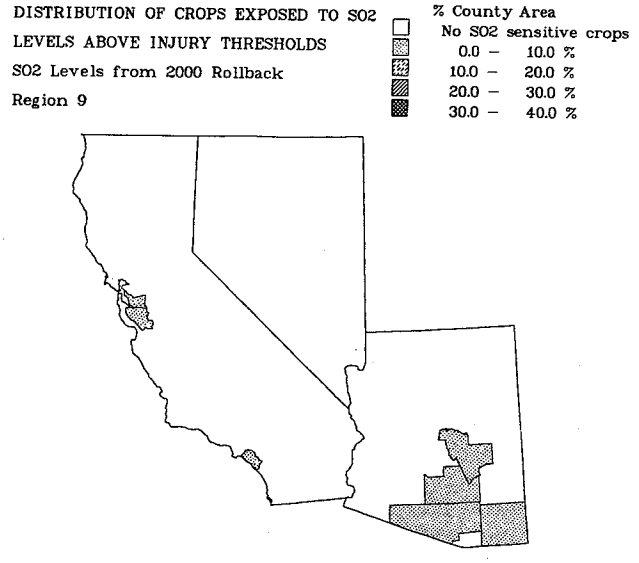

Fig. 1. Distribution of crops exposed to SO_2 levels above injury thresholds. NEP-II Low World Oil Price Scenario. (XBL 8011-3905)

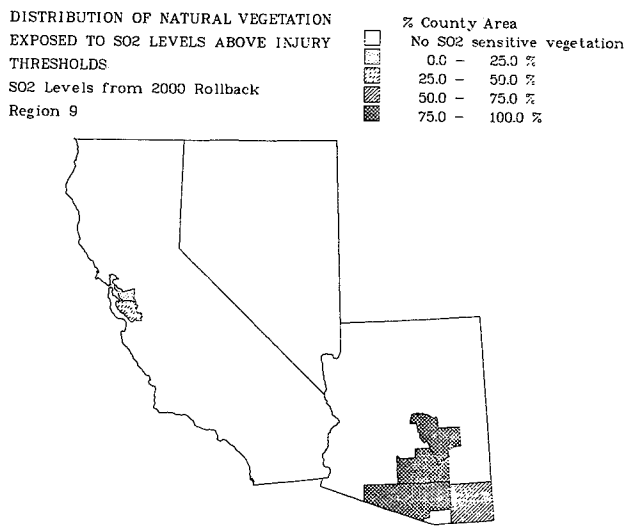

Fig. 2. Distribution of natural vegetation exposed to SO_2 levels above injury thresholds. NEP-II Low World Oil Price Scenario. (XBL 8011-3904)

widespread and significant, especially in natural communities where competition plays an important role.

Acid Rain

Acid precipitation has not been as extensively studied in Region IX as in some other areas, but it is receiving increased attention. The acidity of rainfall here is apparently increasing, and has been measured at values as acidic as pH 4.

The mountainous regions of the West tend to have shallow soils with low buffering capacity, so the full impact of acid deposition may be felt by aquatic organisms.

The desert areas of the West may not be severely affected by acid rain because the surface layer of many desert soils contains limestone, a good buffer. Where the soil surface is disturbed, as in surface mining, effects on aquatic ecosystems may be increased. This could be significant to the endangered aquatic species of the desert areas.[6]

PLANNED ACTIVITIES FOR FY 1981

A study of a larger number of western states has been initiated in cooperation with Los Alamos National Laboratory. This study will develop a set of scenarios describing future energy, economic, and demographic growth in the region, and will provide an assessment of the land use and ecological consequences.

REFERENCES

1. R. Sextro et al., "A Summary of Regional Impacts Associated with the Second National Energy Plan," Energy & Environment Division Annual Report 1980, Lawrence Berkeley Laboratory report-11972, 1980.

2. E.J. Stenehjem, Summary Description of SEAM: The Social and Economic Assessment Model, ANL/IAPE/TM/78-9 (Argonne, Ill.: Argonne National Laboratory, 1978).

3. J. Nagy and C.E. Calef, "ESUSA: U.S. Endangered Species Distribution File". BNL-51129 (Upton, N.Y.: Brookhaven National Laboratory Report, 1979).

4. B. Fischhoff et al; "How Safe is Safe Enough? A Psychometric Study of Attitudes Towards Technological Risks and Benefits," Policy Sciences, vol. 9, pp. 127-152, 1978.

5. National Park Service, Unpublished reports from managers of national parks and monuments in Region IX, National Park Service regional headquarters, San Francisco, Calif., 1979.

6. D. Nettleton, Western area liaison, National Cooperative Soil Survey Program, Soil Conservation Service, Lincoln, Nebr., personal communication, August 1980.

AIR QUALITY CONSTRAINTS ON IMPLEMENTING THE NATIONAL ENERGY PLAN IN FEDERAL REGION IX*

T. Chapman and R. Sextro

INTRODUCTION

This analysis is based in part on the changes in emissions of fine particulate matter (FPM) and sulfur oxides (SO_x) in Federal Region IX that would result from implementation of the National Energy Plan (NEP-II). While pointing out some assumptions to which outcomes are sensitive, the findings presented here should help elucidate the major constraints to the plan's achievement. This discussion focuses primarily on the high world oil price case (HWOP) for the NEP-II. Where significant differences arise, the assessment results from the low world oil price (LWOP) scenario will be included.

Air quality in Region IX ranges from pristine to highly polluted, and as a result of public awareness of the resource, vigorous local interests have long made air pollution control a primary political issue. Although basic research and enforcement are well-funded, most of the urban areas in this region, as in others, are nonattainment areas for one or more pollutants, usually oxidants.

New emissions sources in many of these areas will require emissions offsets if the new sources are to be permitted at all. At the other extreme, Region IX has 44 mandatory Prevention of Significant Deterioriation (PSD) Class I areas, and a number of additional areas under review for Class I status. Thus, siting in rural attainment areas may also be constrained by Class I concentration limits and/or visibility rules.

* This work was supported by the Regional Impacts Division, Office of the Environment, U.S. Department of Energy under Contract No. W-7405-ENG-48.

MAJOR FINDINGS

Particulates

Of total particulates, the FPM fraction has become the subject of closer scrutiny because of its potential for long-range transport (LRT) and visibility impairment, high respirability, and high chemical reactivity for these elements and compounds which are preferentially distributed in fly ash, and because of the greater difficulty in controlling its emission.[1]

The data aggregated in Table 1 for the region show an overall 27% increase in emissions from all sources between 1975 and 2000, and almost all areas in the region are predicted to experience degradation of air quality due to increases in fine particulate concentrations. Note that these data are for primary fine particulates (PFP) as opposed to sulfates, nitrates, and organic aerosols, which are secondary pollutants formed in atmospheric reactions.

FPM from industrial coal fuel-burning operations will increase by a factor of 15 while utility coal emissions increase tenfold. However, industrial and utility coal use together will account for only about 7% of total PFP emissions in the year 2000. At the same time some reductions in industrial process emissions are expected.

In spite of the activity in the utility and industrial sectors, it is the increased contribution from mobile sources that outweighs all others--apparently an artifact from assumed high diesel fuel market penetration. A gain of 65% over 1975 levels puts the transportation sector at 53% of the total emissions inventory by the year 2000. The increase in this sector alone could account for the 27% increase overall, and it is almost twice the increment from all fuel use in the utility sector.

Comparing the two scenarios, the emissions in the high world oil price case are predicted to

Table 1. Fine particulate emissions[a] in Region IX. (10^3 tons per year)

Sector	1975	1990		2000	
		HWOP[b]	LWOP[c]	HWOP	LWOP
Utility - coal	2.2	21.1	21.1	23.6	22.8
Utility - oil	13.7	38.2	37.0	30.5	25.7
Utility - gas and solar	0.2	0.6	0.5	1.3	1.3
Industry - coal	0.04	0.5	0.7	0.7	0.7
Industry - oil	5.7	14.2	26.7	1.9	40.0
Industry - gas	2.4	3.9	3.5	4.0	3.5
Residential/commercial - coal	0.0	0.0	0.0	0.0	0.0
Residential/commercial - oil	4.7	2.0	2.7	1.6	2.5
Residential/commercial - gas	5.6	4.9	4.9	5.9	5.8
Fuels - extraction, processes and distribution	36.2	34.3	37.1	25.8	35.4
Transportation	111.8	129.4	131.0	183.9	185.8
Industrial processes (SIC-32)	45.4	24.8	24.8	31.1	31.6
Industrial processes - other	46.7	34.0	34.5	38.1	39.1
Other	3.0	1.8	1.8	1.8	1.9
Total	277.7	309.7	326.3	350.1	395.6

[a] These data were derived by assuming a fixed ratio of fine to total particulates for a given source category. Fines are, by convention, particles of less than 2-3 microns in diameter.

[b] HWOP denotes high world oil price scenario.

[c] LWOP denotes low world oil price scenario.

be only 88% of those in the low world oil price scenario, primarily due to a net 67% reduction in industrial oil burning by 2000 under the former, as opposed to a 700% increase in that sector under the latter scenario.

Sulfur Oxides

SO_x problems in Region IX are highly localized when compared to other regions. The existing violations in Kern County, for example, result from insufficiently controlled emissions from enhanced oil recovery (EOR) operations there.[2] However, the major source of SO_x emissions in this region is nonferrous smelting in Arizona.[3]

In 1975, Greenlee County in Arizona experienced more than 100 days in violation of the SO_2 National Air Quality Standards (NAAQS) due to smelters upwind.[4] As indicated in Table 2, these sources are expected to be largely controlled by the end of the century; hence the predicted 75% decrease in emissions from these smelters drives the overall Regional SO_x emissions inventory down by 40%.

The decline in smelter emissions tends to mask significant upward trends in other sectors, including an 80% increase from utility oil burning, which at 21% of the total is the second largest sector by the year 2000. SO_x from mobile sources increase by 160%, or by a factor of 2.6 (again probably due to the assumption of very high diesel penetration,) but the increase fails to keep pace with utility coal-burning emissions that rise by a factor of 3.6. Industrial coal sulfur emissions are predicted to rise from a negligible amount in the base year to almost 10% of the total by 2000 under the HWOP scenario.

Utility Sector

Most states have adopted the federal New Source Performance Standards (NSPS) prescribed by the U.S. Environmental Protection Agency (EPA). With the exception of California, these rules typically apply uniformly throughout a state because local Air Pollution Control District's APCD's, although having primary responsibility for control of stationary sources, have not elected to promulgate tighter standards. Urban districts in Arizona (Phoenix and Tucson) and Nevada, (Las Vegas and Reno) and some special problem areas, e.g., Yuma and Pinal-Gila, Arizona also have more stringent emissions regulations which apply to utility plants.

In California, most APCD's have elected to set their own emissions standards; and some are only half to a third the level of federal NSPS. However, certain areas are being urged to relax the more stringent regulations, e.g., mass emission limits ("Rule 67" type), and process weight-based standards.[5] There are also fuel sulfur content rules which, in order to permit burning of coal or crude oil, must be eliminated or reworked so that tighter emission controls are seen as equivalent to prescribing low sulfur fuels.[6]

Table 2. SO_2 Emissions in Region IX. (10^3 tons per year)

Sector	1975	1990		2000	
		HWOP[a]	LWOP[b]	HWOP	LWOP
Utility - coal	42.6	125.9	125.9	155.1	145.4
Utility - oil	171.7	389.7	377.2	307.5	256.2
Utility - gas and solar	0.2	0.5	0.5	9.5	7.9
Industry - coal	3.4	81.6	114.9	140.8	64.3
Industry - oil	30.1	79.1	160.1	11.2	259.7
Industry - gas	0.2	0.3	0.2	0.3	0.2
Residential/commercial - coal	0.2	0.0	0.0	0.0	0.0
Residential/commercial - oil	19.6	7.3	10.11	5.5	9.2
Residential/commercial - gas	0.3	0.3	0.3	0.3	0.3
Fuels/extraction, processes and distribution	0.7	0.9	1.2	0.6	1.5
Transportation	57.3	104.6	105.8	149.5	150.9
Nonferrous Metals	1737.2	398.7	399.8	426.0	431.6
Other	359.6	321.6	345.3	258.8	340.3
Total	2423.0	1510.5	1641.4	1465.0	1667.6

[a] HWOP denotes high world oil price scenario.
[b] LWOP denotes low world oil price scenario.

Emissions offsets ("tradeoffs") policies are presently being decided on a case-by-case basis; among the unsettled issues are whether certain generic source categories are to be allowed as potential tradeoffs, and what tradeoff ratios should apply. Some jurisdictions have local new source review (NSR) rules that consider HC, NO_x, and SO_x as precursors to secondary particulate formation. Therefore, these rules require that these gaseous pollutants be offset in addition to primary particulates when siting in areas which are nonattainment for particulate matter. In fact, offsets are "far and away the most disputed issues in new power plant siting cases," according to the California Air Resources Board (CARB).[7] Preliminary regulations have been drafted which would permit "banking" of valuable potential offsets which might not otherwise be available and thus might delay progress toward attainment.[8]

One consequence of NSR rules has been to inhibit repowering and cogeneration at some existing facilities where Best Available Control Technology (BACT) and offset requirements render the project marginal or unsound from the applicant's economic standpoint. However, given that the demand would otherwise be met by a new plant, these alternative options--from a public welfare standpoint--are more efficient, cheaper, and usually have net air quality benefits over the conventional approach.[4]

Nevertheless, new plants of any type will burn cleaner than old plants, due in part to the federal and local NSPS but more as a result of the "technology-forcing" influence of NSR rules[9]. In addition, siting of new plants outside urban areas will further decrease direct population impacts of energy production. But while this option may avoid some local air quality regulations, low emissions tradeoff potential will constrain rural siting in some areas. In a recent decision regarding the siting of a coal-fired power plant, the California Energy Commission (CEC) and the California Air Resources Board (CARB) established the Japanese selective catalytic reduction process (SCR) as BACT for NO_x which in tests has achieved a 90% reduction in NO_x emissions.[10] If this determination is sustained in practice, capital and operating expenditures for NO_x control will increase and will probably be an issue between utilities and regulators in all new California plants; however, it will make siting in nonattainment areas more feasible, since the magnitude of the emissions to be offset will be reduced.

Prompted in part by the extensive geothermal development proposed for the state, California has promulgated an H_2S standard based primarily on the compound's nuisance potential. Although the Stretford scrubbing process has been proposed for control of H_2S in geothermal operations, BACT has not yet been determined. Much of the proposed geothermal development is in the areas with hot water resources rather than dry steam, and--depending on the technology chosen--H_2S control may be a factor in geothermal development.

From the air quality standpoint, the capacity goals set forth under NEP-II and sited as for the RIIA exercise do not appear severely constrained at this time. The uncertainty which will probably be most limiting is visibility--at least near Class I areas.

Industry

Unlike eastern industrial boilers, very few boilers in the region were designed to burn coal; therefore "coal conversion" will mean new furnaces--not retrofits--and must provide for all the activities that are ancillary to coal use, such as storage and handling of coal and wastes. It is true that tradeoffs are most easily obtained in small increments, but small boilers are typically less efficient and emit more pollution per unit heat input than large boilers. Although new fluidized bed combustion technologies promise versatile, clean, and efficient heat-transfer operations of varying scale and application, emissions regulations requiring state-of-the-art control equipment may disadvantage the smaller user as new systems will likely be manufactured to the specifications of large generic boilers.[1]

Predicted county-by-county industrial fuel use patterns exhibit significant increases in direct coal use. While the rate of coal use at the state or regional level may appear reasonable, especially when compared with other areas of the country, the feasibility of achieving the levels projected is much less certain than for the utility sector. Los Angeles, Orange and San Bernardino Counties in the South Coast Air Basin account for the bulk of the new coal use. By 2000, new coal in Los Angeles county alone, some 82 x 10^{12} Btu, will be larger than the total base year industrial energy use in Arizona and Nevada combined. Clearly, it is the projected distribution rather than the extent of coal penetration which is more uncertain.

REFERENCES

1. U.S. Congress, Office of Technology Assessment, The Direct Use of Coal, LOC 79-600071, GPO 052-00300664-2 (Washington, D.C.: U.S. Government Printing Office, 1979).

2. California Air Resources Board, Technical Services Division, Data Processing Branch, 1976 Emissions Inventory, Sacramento, Calif., 1979.

3. California Air Resources Board, Stationary Source Control Division, Issues Related to Power Plant Siting, Sacramento, Calif. September, 1980.

4. California Energy Commission, Constraints and Opportunities for Power Plant Siting: Technical Issues, Sacramento, Calif., November, 1979.

5. San Francisco Bay Area Air Quality Management District, "Draft Guidelines for Banking Emissions Reductions," San Francisco, Calif., January, 1980.

6. A. Thomas, "Air Quality as a Constraint to the Use of Coal in California," Proceedings of the Conference on Coal Use for California, Pasadena, Calif., May 9-11, 1978; JPL 78-56 (Pasadena, Calif.: California Institute of Technology, Jet Propulsion Laboratory, 1978).

7. California Air Resources Board, "Preliminary Air Quality Report on the California Coal Project," an appendix to Summary of Hearing Order on Southern California Edison's Notice of Intention to Seek Certification for the California Coal Project, California Energy Commission Docket No. 79-NOI-3, CEC P800-80-012, Sacramento, Calif., July, 1980.

8. Bay Area Air Quality Management District, Guideline for Banking Emissions Reductions, San Francisco, Calif., January 1980.

9. T. Austin, "Air Quality as a Constraint to the Use of Coal in California," Proceedings of the Conference on Coal Use for California, (Pasadena, Calif.: California Institute of Technology, May 1978).

10. California Air Resources Board, Preliminary Air Quality Report on the California Coal Project, Sacramento, Calif., May, 1980.

WATER AVAILABILITY AND QUALITY CONSIDERATIONS AFFECTING ENERGY FUTURES IN FEDERAL REGION IX*

M. El Gasseir

INTRODUCTION

This research is part of the Regional Issues Identification and Assessment (RIIA) project.[1] Specifically, we seek to identify and assess the water availability and water quality issues resulting from the implementation of certain national energy plans, represented by a set of two Department of Energy (DOE) scenarios based on the Second National Energy Plan (NEP-II). LBL's responsibility is limited to Federal Region IX, which consists of the states of Arizona, California, Hawaii, and Nevada.

This research has two long-term objectives. The first is to identify and evaluate the water-related issues and impacts of each energy scenario. The second objective is to establish and update a water and energy information base, so that the

* This work supported by the Regional Impacts Division, Office of the Environment, U.S. Department of Energy under contract No. W-7405-ENG-48.

RIIA process is improved as it progresses from one scenario to another. The lack of an adequate centralized information base and the complex nature of the "energy/water interface" have necessitated the adoption of the second objective, as well as a selective approach to the analysis of the energy and water issues.

ACCOMPLISHMENTS DURING FY 1980

The prospects for energy development as constrained by water resources in Region IX were investigated. The water situation in Region IX is characterized by these features:

- The natural water supply is more constrained than in most of the other regions.
- Water resources are already highly developed, leaving little opportunity for further flow regulation or diversion.
- Population growth has burdened an already strained water supply.
- Public awareness of the increasing water scarcity is growing. This situation was brought about by the following factors: the 1976-1977 drought; delays and cancellations in federal reservoir-construction activities; Indian lawsuits over the acquisition and use of water resources; intrastate rivalries with respect to flow diversion and interbasin transfers; and a common concern over the environmental impacts of water development projects.

Water Quality

A number of federal and state policies seek to eliminate the discharge of pollutants to navigable waters by 1985. Although uncertainties exist regarding how strictly the U.S. Environmental Protection Agency intends to implement Public Law 92-500 and subsequent amendments, the zero-discharge policies aimed at new point-sources will continue to be in effect at the state and local levels. The energy industry has generally demonstrated its willingness to abide by these policies in its development plans.

In Region IX, routine pollution of surface waters by new point-source facilities should no longer be an issue. Operating under zero-discharge conditions means the consumption, on-site, of all withdrawn water. This raises two kinds of problems:

1. Increased water consumption and its implications.
2. The generation of additional solid-waste loads and the attendant disposal requirements and problems, including possible contamination of groundwater resources underlying the solid-waste disposal sites and the containment of surface runoff from the disposal areas.

Since the passage of Public Law 92-500, considerable progress has been made in controlling pollution from point sources. In many areas, the major sources of water pollution belong to the nonpoint-source category. The contribution of energy activities to nonpoint-source pollution is almost exclusively confined to the urban areas where most of this pollution is associated with the transportation sector. Rain-out of air pollutants affects plant life as well as water quality and is a significant issue in parts of the U.S.

Electricity Generation

The only water-intensive energy facilities specified by the NEP-II scenarios for Region IX are steam-electric power plants. In 1975, the existing plants provided about 70% of the region's baseload capacity. Cooling accounts for essentially all of the consumptive water requirements of such a power plant. Most of the existing thermal generating capacity in Region IX is on the coast, and typically uses ocean or estuarine water for once-through cooling. However, there are no plans to use ocean water as a medium for disposing of excess heat from new power plants. The dominant sources of cooling water for existing inland power plants are groundwater and surface water from aqueducts as well as directly from rivers. Treated sewage effluent is becoming a significant source of cooling water.

Information obtained from utility companies indicates that the most commonly used device for cooling new plants is the evaporative mechanical draft tower. Typically, cooling effluents (the blowdown) wil be disposed of by evaporation in lined holding ponds. Some utilities plan to use part of the cooling effluents in other on-site uses. Few plans call for nonroutine small releases of treated effluents to nearby surface waters.

The electric-power cycle that is most water intensive and the least flexible with regard to siting and water availability is the extraction of heat from liquid-dominated geothermal fields. In some cases, nontraditional sources of cooling water, such as agricultural waste water, appear to be available. In other locations, the prospects of finding adequate sources of nontraditional cooling water are not encouraging. The technologies of wet and dry cooling--through which water consumption can be reduced significantly--may eventually provide the solution.

Nontraditional Sources of Cooling Water

A number of alternatives to the use of freshwater for cooling, such as treated urban waste water, agricultural drainage, and brackish groundwater, are being investigated. Treated waste water is already being used by utilities in California and Nevada. According to present utility plans, within ten years, a capacity of 6,257 MW will utilize this resource in Federal Region IX. The major advantages of using treated urban waste water are its relative availability, especially near the electricity demand centers; the moderate competition for its acquisition and use; and its adequate quality and reliability of supply. The major advantage agricultural drainage offers over treated urban waste water is its presence in areas relatively free of siting constraints relating to seismicity, public safety, or air quality. However,

until systems of collection and storage are constructed, agricultural drainage water will not be used for power-plant cooling. Brackish ground water is the least important of nontraditional sources of cooling water. The major problem is the lack of sufficient information on its availability for use as a coolant.

Water Availability

The availability of water for the steam-electric power plants projected to be built in the region was assessed. The results indicate:

- In Region IX, between the years 1990 and 2000, water consumption for power-plant cooling would increase five-fold. For a region where further water development is severely limited, the provision of more than 500 thousand gallons per day of freshwater for the purpose of cooling power plants is not likely to take place.
- The state with the lowest growth in cooling-water requirements is Arizona, due in part to an initially high level of water consumption by power plants.
- The average annual growth rates of cooling-water requirements for California, Hawaii, and Nevada are quite high (43%/yr, 65%/yr, and 49%/yr, respectively). In Nevada and to a lesser extent in California, the new requirements probably will not be satisfied largely through the consumption of freshwater.

By comparing the calculated consumptive water requirements with information on historic and projected water supply and demand, we concluded that in the following counties the impacts of the NEP-II scenario would be most significant:

- Arizona - Apache and Maricopa Counties,
- California - Butte, Imperial, Inyo, Lake, Merced, Mono, and San Bernardino Counties,
- Hawaii - Hawaii County,
- Nevada - Churchill, Eureka, Humboldt, Pershing, and Washoe Counties.

PLANNED ACTIVITIES FOR FY 1981

A study of a larger number of western states has been initiated in cooperation with Los Alamos Scientific Laboratory. This study will develop a set of scenarios describing future energy, economic, and demographic growth in the regions, and will provide an assessment of the water resource consequences.

REFERENCES

1. R. Sextro et al., "A Summary of Regional Impacts Associated with the Second National Energy Plan," Energy and Environment Division Annual Report 1980, Lawrence Berkeley Laboratory report LBL-12024, 1980.

URBAN AND COMMUNITY IMPACT ANALYSIS*

H. Ruderman, F. Fung, and R. Beran†

INTRODUCTION

The U.S. Department of Energy (DOE) is required to prepare an urban and community impact analyses for each proposed major policy and program initiative. The statement's purpose is to identify the likely effects of these programs and policy initiatives on cities, counties, and communities. The analysis is intended to insure that potentially adverse impacts of proposed federal activities will be identified during the decision-making process.

The DOE has promulgated criteria for determining whether proposed activities must undergo an urban and community impact analysis. These criteria are based in part on the anticipated social and economic impacts of the activity on the community and the nation. Impacts include both direct and indirect effects on employment, population, income, cost of living, and state and local government finances. Differential impacts on central cities, suburban areas, nonmetropolitan communities, areas with high and low unemployment, and minority and low-income communities are to be analyzed quantitatively wherever possible. The criteria require an evaluation of aggregate effects on the U.S. economy--in terms of employment, personal income, prices, and fiscal conditions--and on the economy's major industrial sectors.

In the work reported here, we used clustering methods to select typical regions of the country for the impact analysis. Communities and urban areas within these regions were then selected for further detailed analysis, which was performed at DOE and other national laboratories. The LBL phase of the analysis was begun and completed during FY 1980. A more detailed account of this work may be found in LBL-11084.[1]

* This work was supported by the Regional Assessments Division, Office of Technology Impacts of the U.S. Department of Energy under Contract No. W-7405-ENG-48.

† Department of Statistics, University of California, Berkeley.

ACCOMPLISHMENTS DURING FY 1980

Clustering analysis was performed on a set of 15 variables for each of the Bureau of Economic Affairs (BEA) regions of the country (see Table 1). These data summarize each region's demographic, economic, financial, and energy production characteristics.[2] Standard clustering methods[3,4] were used to group the regions into aggregates with similar characteristics. Careful attention was paid to using robust statistical techniques and validating the results. Six clusters were found

Table 1. Variables for clustering.

Extensive	Intensive
	Demographic
Area	n.a.
Population*	Population density*
n.a.	Percent nonwhite*
n.a.	Percent population change, 1970-1975*
	Urban - Rural
Urban land area	Percent urban land
Central city population	Percent population in central city*
Outlying area population	Percent population in outlying area*
Urban vehicle miles traveled	Per capita urban VMT
Rural vehicle miles traveled	Per capita rural VMT
Single-family dwellings	Percent single-family dwellings
	Employment
Civilian labor force	Labor participation rate*
Total employment	Unemployment rate*
	Personal Income
n.a.	Median household income
n.a.	Percent annual change 1969-1974
n.a.	Percent below poverty level*
n.a.	Percent above $15,000*
	Economic
Total retail sales	Per capita retail sales
Total wholesale sales	Per capita wholesale sales
Value added by manufacturers	Per capita value added
Electric generating capacity	Per capita capacity
Commercial landings and takeoffs	Per capita landings and takeoffs
	Energy Consumption
Residential and commercial	Per capita consumption
Industrial	Per capita industrial
Transportation	Per capita transportation
Coal	Per capita coal
Petroleum	Per capita petroleum
Natural gas	Per capita natural gas
Electricity	Per capita electricity
	Energy Production
Total coal	n.a.
Crude petroleum*	n.a.
Natural gas*	n.a.
Strippable coal reserves*	n.a.
Underground coal reserves*	n.a.
	Government Finance
Local government-- general expenditure	Per capita expenditure
Intergovernmental transfers	Per capita transfers
n.a.	Per capita debt*

*Used in final clustering
n.a.--not applicable.

which contain 161 of the 173 BEA regions that cover the country; the other 12 could not be classified. The six clusters exemplify a broad range of characteristics: There are distinct differences between the racial compositions, income levels, population growth rates, unemployment rates, and resources for energy development in different clusters.

Using density estimate techniques,[5] we selected several BEAs from each cluster which are representative of the cluster as a whole. These modal BEAs lie close to the maximum of the estimated density in the cluster. The six clusters and their modal BEAs are shown in Table 2. Five of the clusters are composed primarily of rural BEAs in which we expect the largest impacts of synfuels development. They are distinguished by differences in their economic and demographic characteristics as well as in their resources for energy production. Modal BEAs in each of the clusters contain fossil or biomass resources needed for producing synthetic fuels. These BEAs are suitable for studying the impacts of a variety of technologies in a single community, or the impacts of a single technology over a range of communities.

Table 2. Modal BEA regions.

Cluster	Code	Region	Density*
1	123	Lubbock, Tex.	0.461
1	125	Abilene, Tex.	0.416
1	110	Wichita, Kans.	0.367
1	88	Eau Claire, Wis.	0.315
1	86	Wausau, Wis.	0.308
1	92	Grand Forks, N.Dak.	0.286
1	124	Odessa, Tex.	0.279
2	76	South Bend, Ind.	0.926
2	75	Fort Wayne, Ind.	0.884
2	82	Rockford, Ill.	0.868
2	69	Lima, Ohio	0.770
2	105	Waterloo, Iowa	0.633
2	89	La Crosse, Wis.	0.614
2	78	Peoria, Ill.	0.609
3	54	Louisville, Ky.-Ind.	1.000
3	57	Springfield, Ill.	0.731
3	16	Harrisburg, Pa.	0.716
3	64	Columbus, Ohio	0.703
3	10	Erie, Pa.	0.657
4	119	Tulsa, Okla.	0.887
4	28	Greenville, N.C.	0.804
4	49	Nashville, Tenn.	0.770
4	137	Mobile, Ala.	0.719
4	20	Roanoke, Va.	0.697
4	25	Greensboro-Winston Salem, High Point, N.C.	0.696
5	107	Omaha, Nebr.; Iowa	0.923
5	70	Toledo, Ohio; Mich.	0.849
5	85	Appleton; Oshkosh, Wis.	0.844
5	60	Indianapolis, Ind.	0.797
5	62	Cincinatti, Ohio; Ky.; Ind.	0.733
5	21	Richmond, Va.	0.729
5	157	Portland, Oreg.; Wash.	0.681
6	147	Colorado Springs, Colo.	0.278
6	146	Albuquerque, N.Mex.	0.269
6	145	El Paso, Tex.	0.226
6	151	Salt lake City, Utah	0.207

*Density estimates show the relative compactness of the clusters.

A sensitivity analysis of the clusters to a variety of clustering methods indicated that the clusters that we found are not unique. Only two of the clusters are distinct; the other four appear to be compact regions in a single large diffuse cluster. The modal BEAs, however, tend to group together as the clustering method is changed. They are relatively stable compared to the clusters, and thus form a valid set of regions for impact analysis.

Because we are unable to find a unique set of clusters, we are limited in the extent to which we can generalize the impact analysis results. We believe that the results can be extended only to those BEAs that consistently cluster with the ones on which the analysis was done. For the data we used, the results are applicable to only 34 of the 173 BEA regions.

PLANNED ACTIVITIES IN FY 1981

This work was concluded in FY 1980 and will not continue in FY 1981.

REFERENCES

1. H. Ruderman, F. Fung, and R. J. Beran, Selection of Modal BEA Regions for Urban and Community Impact Analysis, Lawrence Berkeley Laboratory report LBL-11084, 1980.

2. Urban Systems Research and Engineering, Inc., Energy/Environment Data Study, Cambridge, Mass., May 1979.

3. J. A. Hartigan, Clustering Algorithms (New York: John Wiley & Sons, 1975).

4. B. Everitt, Cluster Analysis (Exeter, N. H.: Heinemann Educational Books, Ltd., 1977).

5. M. Rosenblatt, Ann. Stat., vol. 3, no. 1, 1975, pp. 1-14.

BUILDING ENERGY PERFORMANCE STANDARDS FOR RESIDENTIAL BUILDINGS*

M. Levine, D. Goldstein, J. Ingersoll, and J. Mass

INTRODUCTION

In August of 1976, Congress passed the Energy Conservation Standards for New Buildings Act.[1] This Act mandated the development, promulgation, implementation, and administration of energy performance standards for all new buildings constructed in the United States after 1981. In August 1979, the U.S. Department of Energy (DOE) released a Notice of Proposed Rulemaking pursuant to this legislation. The importance of the proposed Building Energy Performance Standards (BEPS) in the residential sector is underscored by the fact that their observance could accomplish the following:

- Reduce energy use for space conditioning by 30%-40% from current building practice (or 60%-70% from the energy use in an average house built before the OPEC oil embargo of 1973).
- Produce a net savings in life-cycle costs of more than $1,000 for an average new homeowner.

Lawrence Berkeley Laboratory has played a key role since 1979 in supporting the development of these standards. The largest portion of the LBL research effort has been devoted to single-family residential buildings, the subject of this article. The research on commercial buildings and on the implementation of BEPS is reported in separate articles in this volume.

METHOD OF APPROACH

The approach followed in the analysis of residential building energy performance standards includes the following phases:

1. Development of residential prototypes;
2. Selection of conservation measures to be evaluated;
3. Description of standard building operating conditions;
4. Development of economic data, projections, and assumptions;
5. Computer simulation of building energy requirements in different climatic regions;
6. Analysis of life-cycle costs of energy conservation measures;
7. Sensitivity analyses of building characteristics, operating conditions, conservation measures, and economic parameters; and
8. Analysis of impacts of alternative energy budget levels, in which the alternative budget levels are based on phases 1 through 7.

The basis of our analytic method is life-cycle cost analysis. The objective of achieving a minimum in life-cycle costs is a reasonable basis for establishing energy conservation policy, because it provides a rational framework for trading scarce energy resources for other resources (e.g., labor and capital) in achieving a particular goal (in this case, space conditioning in residential buildings).[2] The use of an economic approach to energy conservation--and the increasing public awareness of how economics can help resolve issues--can be greatly enhanced by a government decision to use life-cycle costing as a major element of its energy conservation policy. Details of the approach, assumptions, and data used to carry it out can be found in References 3, 4, 5, and 6.

RESULTS

Figure 1 provides a useful summary of the results of LBL's analysis of the impact of energy conservation measures in residential buildings.[7] The upper curve, labeled "U.S. Stock, Dole 1970," is an estimate of the fuel requirements for space heating the 1970 stock of houses in the United States. A typical gas-heated house in Chicago, constructed before 1970, consumed approximately 110×10^9 joules/100 m^2 in one year. The fourth curve from the top, labeled "HUD Current Practice (DOE-2)," is an estimate of the space-heating energy use of a typical house constructed in 1976. The results in this curve were obtained by simulating the energy performance of a typical new house on the DOE-2 computer model. A typical house in Chicago constructed in 1976 used about 65×10^9 joules/100 m^2 in one year.

The fifth curve from the top, labelled "LBL optimum: High Infiltration (DOE-2)," contains the results of the life-cycle cost analysis for gas-heated houses, with an infiltration rate of 0.6 air changes/hr. This curve corresponds to the energy use mandated by the proposed Building Energy Performance Standards. A typical house in Chicago would consume about 45×10^9 joules/m^2 for gas heating. This curve was established by choosing the minimum in life-cycle cost for only widely available energy conservation measures for the envelope of

* This work is supported by the Standards Branch, Buildings Division, Office of Buildings and Community Systems, U.S. Department of Energy under Contract No. W-7405-ENG-48.

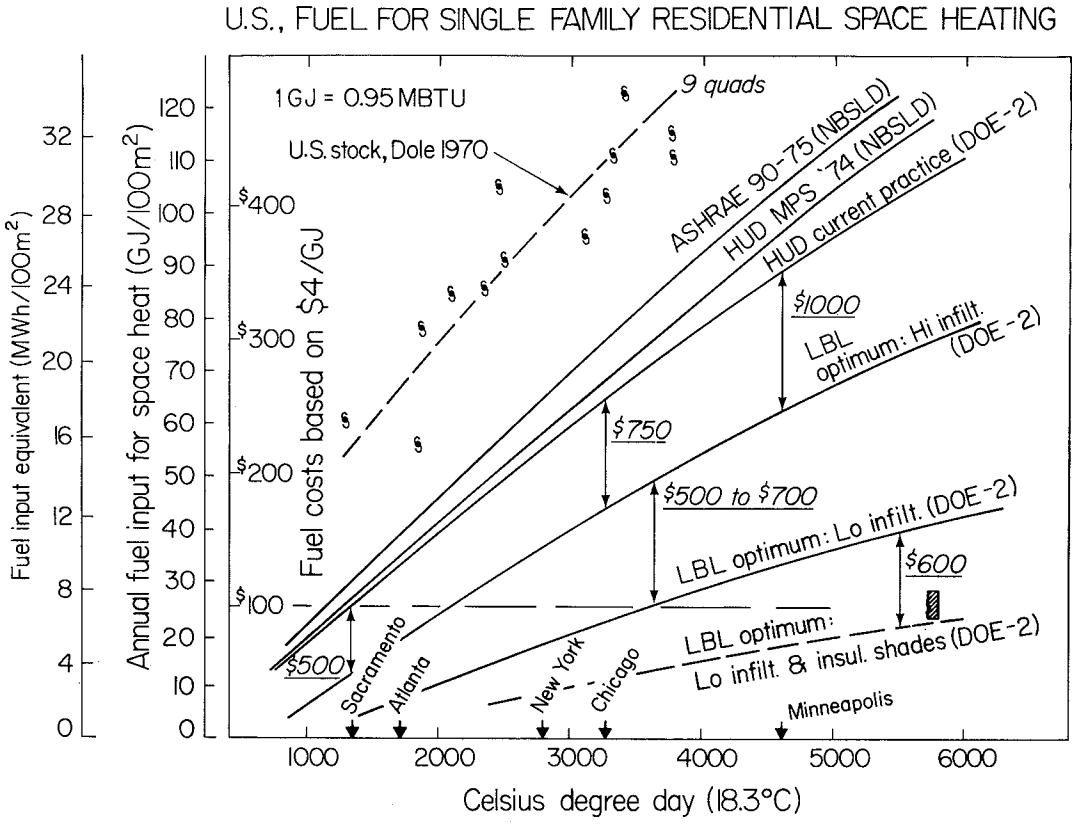

Fig. 1. Fuel use for single-family residential space heating. (XBL 795-1396)

the house. For Chicago, this corresponds to the use of R-38 ceiling insulation, R-27 wall insulation (i.e., insulated wall cavity and a sheet of insulating sheathing on the outside of the building), and triple glazing (or double glazing with a storm window). An important additional measure that could save substantial heating energy is the reduction of infiltration rates from 0.6 to 0.2 air changes per hour. For this case, the assumption is made that mechanical ventilation through a heat exchanger restores the outside air-exchange rate to 0.6 air changes per hour, to safeguard the quality of indoor air. (If the heat exchanger is 75% efficient, then the rate of heat loss by air infiltration would correspond to that of a house with 0.3 air changes per hour by natural ventilation). The energy use of a house with these measures is shown in the curve labelled "LBL optimum: Low Infiltration (DOE-2)." The annual gas-heating requirements of a Chicago house with low infiltration levels and conservation measures consistent with minimum life-cycle costs are about 22×10^9 joules/100m^2. Our estimates indicate that the construction of such an airtight house is cost-effective at the present time in most locations. The key barriers to such construction are (1) the availability of reliable residential heat exchangers, and (2) the lack of knowledge of the building industry and home buyers about the benefits of heat exchangers in saving energy and tight building construction and capital.

Other measures can further reduce the energy use in buildings. One example is shown in the bottom curve (Fig. 1), in which the conventional energy conservation measures used to derive the minimum in life-cycle costs and reductions in infiltration rates are combined with user-operated insulating shutters. Other user-operated devices or good energy management practices (such as setting the thermostat lower at night) can save energy. Passive solar techniques (direct gain, with increased glazing area on the south, and heavy mass in the building; attached greenhouses; and Trombe walls) can be combined with conventional energy conservation measures to achieve energy-use rates corresponding to those shown in the sixth and seventh curves, with a reduction in the requirements for conventional conservation measures and a reduction in air infiltration rates. Alternatively, conservation measures, infiltration reduction (with heat exchangers), user-operated energy management devices, and passive solar features can be combined to reduce space-heating energy requirements to low levels in almost all U.S. locations.

Figure 1 indicates that large energy savings can be accomplished by requiring all new houses to use all commonly available cost-effective energy conservation measures. BEPS can result in a substantial improvement in the thermal integrity of new houses in the U.S., and at the same time can save the consumer money. The magnitude of the

energy savings is great enough to make a major contribution toward reducing U.S. energy demand growth. (About 35% of the energy in the nation is consumed in buildings, and about half of this is consumed in residential buildings.)

If the levels in the proposed BEPS (based on LBL's analysis, shown in the fourth curve "LBL Optimum: High Infiltration") are in fact observed in new residential buildings, then

- A reduction of 30% to 40% (from current building practice) in the average energy use for residential space conditioning will be accomplished. This is a reduction of 60% to 70% from the energy use of an average existing house, built before the 1973 OPEC oil embargo.
- Simple payback on conservation investment will occur in one to four years for electric heat and three to ten years for gas heat;
- An increased investment of $0.50 to $1.00 per square foot for a new house will be required (i.e., an increased initial investment of 1.5% to 3%); and
- The new homeowner will achieve a net savings of $800 to $1500 over the term of the house mortgage, in addition to a higher selling price for the house.

If the list of conservation measures is expanded to include just one conservation technology (reduced air infiltration combined with mechanical venting through a heat exchanger), then

- A reduction of 50% to 60% in average energy use for residential space conditioning (from current building practice) can be accomplished. This is a reduction of 75% to 85% from the energy use of an average existing house;
- This requires an increased initial investment of $0.75 to $1.50 per square foot.
- The net savings is $1500 to $4000 to the new house owner, in addition to a higher selling price for the house.

PLANNED ACTIVITIES IN FY 1981

Four major activities are to continue through FY 1980 and 1981. They are described in the following paragraphs.

1. Analysis of Life-Cycle Cost Minima in 32 Cities

For the Notice of Proposed Rulemaking, only ten cities were analyzed to set the BEPS. This was an inadequate sample with respect to the weather variation throughout the nation. The analysis is therefore being extended to 32 cities. Additional prototypes are being evaluated. In the previous analysis, the DOE-2 computer model did not have the capability to evaluate the annual energy efficiency of heating and cooling equipment. This capability now exists and will permit an assessment of the effect of climate and building thermal performance on the efficiency of air conditioners, heat pumps, and furnaces. In past work, DOE-2 was not used to model the insulation in foundations. An approach has been developed to perform this simulation; results of this work will make it possible to specify cost-effective levels of insulation for residential buildings with different types of foundations.

2. Analysis of Weather Regions for Promulgation of the Standards.

LBL is involved in assessing the best ways to promulgate the standards. This is a complex task, in which the need for simplicity in implementing BEPS must be balanced by the need to obtain accurate and reproducible results consistent with appropriate benefits and costs for a given locale. Several proposals have been put forward:

1. Perform regression analyses on energy budgets against weather variables and promulgate energy budget levels resulting from this analysis. (This is the approach followed in the Notice of Proposed Rulemaking.);

2. Perform regression analyses of the energy budget levels against both weather variables and local energy prices;

3. Permit the local builder to perform his or her own life-cycle cost analysis, based on the energy performance results from the DOE-2 simulations and local energy prices; and

4. Divide the country into a small number of weather regions, assuming each location employs the same conservation measures, corresponding to the energy budget level proposed by DOE in its BEPS proposal.

All of these approaches have some difficulties. The first three approaches--to the extent that they provide information only on energy budget levels and not on the conservation measures to be used to meet BEPS--result in a regulation that does not communicate the information needed by the builder in selecting conservation measures. The fourth approach, to the extent that it provides only one acceptable set of conservation measures, is not in keeping with the performance nature of BEPS. Combining the fourth approach with one of the first ones can be made difficult by the large number of regions that could result, thereby reducing or eliminating the simplicity of the fourth approach. A full analysis of all these possibilities (including mixed approaches) will be undertaken.

3. Manual of Recommended Practice

A method of promulgating the standards in keeping with the need for simplicity (to communicate effectively with the local building code official and builder) is to present both a set of energy conservation measures that meet the standards and to provide, in simple form, necessary data to allow the builder a wide variety of alternative approaches. Such an approach is under development at LBL. The approach is termed "precalculated tradeoffs," because it relies on the results of

computer simulations of houses to assure that they meet the energy budget levels of the regulation. Some of the measures incorporated into the trade-offs include active solar water-heating systems; improvements in heating and cooling equipment efficiencies; redistribution of windows to the south face of the building to increase solar heat gain; other passive solar measures; changes in window area; reduction in air infiltration rates; dif- ferent shading devices for windows; alternative levels of wall, ceiling and floor insulation; different numbers of glazings; and other conservation approaches. To the extent possible, the presentation will be in terms of simple additions and subtractions that can be performed to represent any combination of energy conservation measures to be used.

4. Analysis of Market Behavior and Energy Conservation

Data are becoming available to characterize residential builders' energy conservation practices. Both cross-sectional and time-series data can provide insights into patterns of energy conservation investment over time and in different locations. A full set of data can reveal (1) the investment criteria of the decision-maker in the purchase of energy conservation (which may be expressed in terms of an implicit discount rate); (2) how these criteria have changed over time (revealing the market's responsiveness); and (3) how the decisions on energy conservation correspond with decisions in a perfectly functioning market. A quantitative analysis to evaluate these effects is underway, based on the computer simulations of residential energy use of houses constructed in the U.S. and on appropriate economic variables.

REFERENCES

1. U.S. Department of Energy, "Notice of Proposed Rulemaking for the Building Energy Performance Standards" (in press), Washington, D.C., 1979.

2. L. J. Schipper, J. Hollander, M. D. Levine, and P.P. Craig, "The National Energy Conservation Policy Act: An Evaluation," Natural Resources Journal (in press), 1979.

3. D. B. Goldstein, M. D. Levine, and J. Mass, Residential Energy Performance Standards: Methodology and Assumptions, Lawrence Berkeley Laboratory report LBL-9110 (in press) 1979.

4. M. D. Levine and D. B. Goldstein, "Building Microeconomics," Economic Analysis of Proposed Building Energy Performance Standards, PNL-3044 (Richland, Wash.: Pacific Northwest Laboratories, September, 1979).

5. M. D. Levine and D. B. Goldstein, "Appendices A" and Appendix I," Economic Analysis of Proposed Building Energy Performance Standards, PNL03044 (Richland, Wash.: Pacific Northwest Laboratories, September 1979).

6. M. D. Levine, D. B. Goldstein, M. Lokmanhekim, and A.H. Rosenfeld, Evaluation of Building Energy Performance Standards, Lawrence Berkeley Laboratory report LBL-9816, 1980.

7. A. H. Rosenfeld, W. G. Colborne, C. D. Hollowell, L. J. Schipper, B. Adamson, M. Cadiergues, G. Olive, B. Hidemark, G. S. Leighton, H. Ross, N. Milbank, and M. J. Uyttenbroech, Building Energy Use Compilation and Analysis (BECA): An International Comparison and Critical Review, Lawrence Berkeley Laboratory report LBL-8912, July 1979.

DETERMINANTS OF RESIDENTIAL ENERGY USE*

P. Craig, J. Cramer, K. Dake, T. Dietz
B. Hackett, D. Kowalezyk, M. Levine, and E. Vine

INTRODUCTION

Lawrence Berkeley Laboratory, in conjunction with a number of other cosponsoring organizations,[1] is investigating residential energy consumption in the City of Davis, California. Data from this project are being used as input to the DOE-2.1 energy-use model to validate the model's energy-use estimates for residential buildings. The project data will allow validation checks for projections of hourly and weekly electricity use, and monthly electricity and gas use. The project is also investigating a model of residential energy consumption that combines physical data on buildings, appliances, occupants' behavior, occupants' attitudes, demographics, and weather variables.

DATA COLLECTION

During the summer of 1980, 241 surveys were administered to a systematic random sample of Davis residents. The survey form consisted of two sections. The first section tallied information on the resident's lifestyle, demographics, energy-use attitudes, energy knowledge, and appliance-use behavior. The second section gathered information on the building, including type of wall construction; building orientation; wall, window, floor, and ceiling areas. The survey was administered by paid interviewers who received building audit

* This work is supported in part by the Systems Analysis Division, Office of Buildings and Community Systems, U.S. Department of Energy under Contract No. W-7405-ENG-48.

training by a Pacific Gas & Electric Company (PG&E) auditor.

The sampling area was defined by the boundaries of a PG&E circuit that serves approximately 2,000 customers. This circuit was selected because more than 95% of the circuit's load was residential with only a small (540) commercial customers' contribution. PG&E is recording electricity readings each half hour for the circuit. PG&E also has provided monthly billing information for the entire survey sample under the condition that their customer's billing information remain confidential. Weather data for the project is being provided by the University of California, Davis Campus Climatic Station, which is partially funded by a Department of Energy grant to gather detailed solar radiation data. Hourly data for all key weather variables have been supplied by the station for this project.

Since the primary goal of the project is to validate the DOE-2.1 energy model, detailed information on internal house temperatures along with infiltration rates were required. A subsample consisting of fifty houses was randomly selected from the larger sample to participate in a phase of the project that gathered continuous data on internal house temperatures. Also, weekly electric meter readings for the subsample were recorded for an eight-to-ten week period from mid-August through early October.

To characterize the infiltration rate of the houses, air pressurization measurements were taken with blower-door equipment made available by the LBL air-infiltration group. Air pressurization data was obtained for approximately 70% of the subsample.

ANALYSIS

The survey information along with the more detailed engineering data on the subsample houses will be used as inputs to the DOE-2.1 model. Prototypes for the DOE-2.1 analysis will be drawn from groups of houses that are statistically similar across a number of characteristics, such as floor area, window area, orientation, glazing area, and appliance ownership and use. Average building characteristics for these house groups will be used as DOE-2.1 inputs. These prototypes will be used to calculate electricity and gas demand over various time periods. Based on the hourly electricity profiles for the prototype houses and the number of housing types on the circuit, an hourly electricity demand curve will be synthesized by DOE-2.1 and compared to actual circuit data on an hourly, daily, weekly, and monthly basis. Gas use computations will be compared with actual monthly consumption.

The second component of the analysis is an attempt to combine engineering data with social science data to create a simple model of energy use for the residential circuit. For this type of analysis, the data are ordered according to their technical and behavioral characteristics. The model is based on the Twin Rivers, New Jersey experience and includes the following variables:

BENV = Occupant-mediated behavior of the building envelope, such as opening windows for night ventilation.

TENV = Technical characteristics of the building envelope, such as window, door, ceiling, and external wall area, and insulation levels.

AUI = An appliance use index containing the number and type of appliances present along with the number of house occupants.

T_a = Ambient temperature

T = Internal house temperature

Q = Energy consumption

PLANNED ACTIVITIES IN FY 1981

Data collection and preparation of the data for analysis have been the major activities since this project began in July 1980. Analysis of the data as described above will be the major effort in 1981.

REFERENCE

1. Kellog Public Research Program, University of California, Davis; Pacific Gas and Electric Company, San Francisco, Calif: Center for Environmental and Energy Policy Research, University of California, Davis; and the California Energy Commission, Sacramento, Calif.

LIFE-CYCLE COST ANALYSIS OF COMMERCIAL BUILDINGS*

I. Turiel and M. Levine

INTRODUCTION

In November of 1979, the Department of Energy (DOE) issued a notice of proposed rulemaking containing energy performance standards for new buildings.[1] The proposed standards consist of energy budget levels for different classifications of buildings in different climates, expressed as an annual rate of energy consumption per unit area.

The data base that was used to determine the energy budget levels consisted of 1,661 commercial, institutional, and high-rise apartment buildings constructed during 1975 and 1976. These buildings were analyzed for design energy performance using a shortened version of the building simulation computer program AXCESS. One hundred sixty-eight of the above buildings were redesigned to reduce design energy use; the average reduction was 40%. For these buildings, the energy budgets are based on the fraction of redesigned buildings that could achieve a specified level of design energy use. Economic considerations, such as life-cycle costs or simple payback periods for energy conservation investments, were not considered to be criteria for the development of energy budget levels for commercial buildings, as was the case for residential buildings.

PROJECT PURPOSE

The purpose of this project is to perform life-cycle cost analyses for office buildings to establish energy budget levels based on minimum life-cycle cost. Office buildings consume about 20% of the primary energy used by institutional and commercial buildings in the U.S.[2] Figure 1 shows average annual energy use per square foot for office and three other nonresidential building types as a function of end-use. The three largest end-uses are space heating, cooling, and lighting, although their relative magnitudes vary from one building to another and from one location to another.

PLANNED ACTIVITIES FOR FY 1981

The project is subdivided into four tasks as follows:

- Task 1. Perform an energy analysis of a typical office building using the DOE-2.1 building energy-use model.[3] Compare results obtained to the previous analysis with AXCESS and to actual energy use in building.

  We have chosen an electrically heated and cooled six-story office building in Denver, Colorado to commence our analysis, and we plan to look at the original building and the original building as modified by such design options as daylighting, deadband thermostats, natural gas space heating and increased insulation.

- Task 2. Determine the ability of a daylighting algorithm being developed by LBL's Windows and Lighting Group to properly model the reduction in lighting energy-use through the use of natural daylight in building perimeters.

- Task 3. Conduct a life-cycle cost analysis of the Denver office building, using results of Task 1 and the DOE-2.1 computer program (modified by the addition of the daylighting algorithm).

  To perform Task 3, a new life-cycle cost model (LCCM) will be developed which will incorporate such features as time-of-day electricity pricing, peak power charges, and potential changes in tax burden to encourage energy conservation. (The contractor who will develop the LCCM has yet to be chosen.) Initial cost data for various design changes must be developed to allow for computation of life-cycle costs. The objective of this task is to rank the energy-conserving strategies and combinations of strategies according to economic criteria, such as life-cycle cost, payback period, and benefit-to-cost ratio.

- Task 4. Perform climate sensitivity analyses for energy use and life-cycle cost with Denver office building.

  An energy and life-cycle cost analysis of the Denver office building will be performed for five other locations both with and without heating, ventilation, and air conditioning system (HVAC) sizing changes. Regional fuel and conservation costs will be used for this analysis. A determination will be made of the number of hours that comfort conditions are not met as HVAC systems of different size are utilized.

Upon conclusion of Task 4, recommendations will be made concerning further planned life-cycle cost work. Tasks 1-4 are expected to be essentially completed by the end of FY 1981. A more extensive analysis similar to Task 4 will be performed in FY 1982. The sensitivity of life-cycle cost results to variations in building parameters will be studied in FY 1982. Additionally, a complete life-cycle cost analysis will be performed for a prototypical office building in FY 1982. The prototypical building will incorporate design features common to office buildings designed and built in 1979 and

* This work is supported by Standards Branch, Office of Buildings and Community Systems, U.S. Department of Energy under Contract No. W-7405-ENG-48.

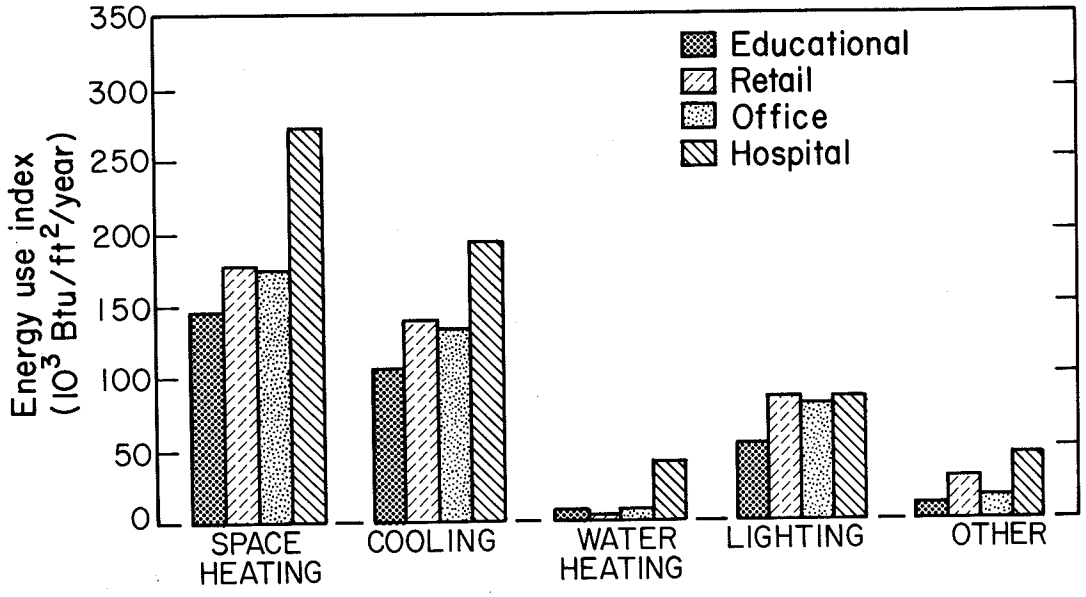

Fig. 1. Energy use indices for educational, retail, office, and hospital buildings, 1970. Data are from Oak Ridge National Laboratory's report, Commercial Energy Use, February 1978. Energy use is given in primary units. (XBL 7810-11637)

1980. Outputs from this project will be used in the Oak Ridge National Laboratory engineering-economic model of energy use for the commercial sector, which will provide estimates of the national impact of building energy performance standards on energy use.

PRELIMINARY RESULTS

The Denver office building, as originally designed and built in the 1975-1976 period, has been analyzed for annual energy consumption by end-use. The original building design is a six-story office building with the sixth floor cantilevered over the lower floors by approximately eight feet on each side of the building. The length of the building is oriented northeast to southwest, and the area is approximately 10^5 ft.^{2}. The glass area is approximately 25% of the total exterior wall surface. Glazing is recessed nine in. and is composed of two 3/16 in. sheets spaced 1/4 in. apart. Cooling and space heating are provided by a zoned, water-to-air unitary heat pump system with a circulating water loop. A 300 kW electric boiler provides back-up heat generation to maintain the water loop temperature above 60°F. The average lighting level is 2.6 W/ft^2.

Table 1 illustrates the results obtained at LBL from the use of two different building descriptions (1 and 2) assembled by two different architectural and engineering consulting firms. Also shown are the results of an energy analysis performed on the same building with the building simulation computer program known as AXCESS.[4] The input for that simulation is very similar to that in description 1 in Table 1. A 1976 weather tape was used for the AXCESS runs, and a 1971 weather tape was used for the DOE-2.0 runs; however, the energy required for space-conditioning for any one building description varies by only a few percent from year to year. This insensitivity of energy use to weather in office buildings is due to the fact that internal sources, such as lights and people, account for a large percentage of the cooling load and also satisfy some percentage of the heating load.

As can be seen in Table 1, the energy used for space conditioning as derived from the AXCESS simulation and from the first DOE-2.0 simulation is similar and accounts for approximately 44% of the total energy budget. Lighting accounts for about half of the total energy budget. Domestic hot water energy use has not yet been estimated.

Columns 2 and 3 summarize the results obtained from simulating the two different building descriptions on DOE-2.0. Description 2 results in 5% greater total energy use, but in much more significant differences for separate end-uses, particularly space heating. There are a number of differences in the two descriptions as regards important building parameters: For example, in description 2, there is no plenum and no use of layered materials to describe the external walls and roof. Differences in supply and outside air quantities and in infiltration schedules were remedied before the results shown in Table 1 were obtained.

Columns 3 and 4 illustrate the difference in results obtained when the same building input description is modeled on DOE-2.0 and DOE-2.1, an updated version of DOE-2.0. The total energy use is almost identical, however, large differences in end-use energy exist for space heating, cooling, and fans. A number of improvements have been made in the DOE-2.1 computer program as regards heat-pump operation and cooling-tower simulations that affect the results obtained.

Table 1. Annual site energy use (10^6 Btu).

End-Use	Building Description 1 AXCESS (column 1)	Building Description 1 DOE-2.0 (column 2)	Building Description 2 DOE-2.0 (column 3)	Building Description 2 DOE-2.1 (column 4)
Heating	┐	863	1257	1631
Cooling	2140[a]	555	652	690[a]
HVAC Auxiliary	┘	598	468	78[b]
Lighting	2612	2644	2584	2584
Elevators	94	94	94	94
Total	4846	4754	5055	5077

[a] For AXCESS 1, this figure is a composite of heating, cooling, and HVAC Auxiliary energy use.

[b] In DOE-2.1, cooling tower energy use is moved from HVAC Auxiliary to cooling as an end-use.

The effect of changes in various input parameters on a design energy budget is presently being investigated. Preliminary comparisons between two independent preparations of building input indicate that although total energy budget predicted by DOE-2.0 varies by only 5%, individual end-use components vary by as much as 45%. Similar results were obtained when DOE-2.0 and DOE-2.1 simulations were compared using the same input description.

REFERENCES

1. "Energy Performance Standards for New Buildings," Federal Register, vol. 44, no. 230, November 28, 1979, pp. 68120-68181.

2. Commercial Energy Use, A Disaggregation by Fuel, Building Type, and End Use, (Oak Ridge, Tenn.: Oak Ridge National Laboratory, February, 1978).

3. M. Lokmanhekim et al, DOE-2: A New State-of-the-Art Computer Program for the Energy Utilization Analysis of Buildings, Lawrence Berkeley Laboratory report LBL-8974, June 1979.

4. American Institute of Architects (AIA) Research Corporation, Life-Cycle Cost Study of Commercial Buildings, Final Report, Office of Conservation and Solar Energy, Office of Buildings and Community Systems, U.S. Department of Energy, Washington, D.C., December 1979.

IMPLEMENTING BUILDING ENERGY STANDARDS IN CALIFORNIA*

R. Feinbaum

INTRODUCTION

From the beginning, research for the Building Energy Performance Standards (BEPS) has focused on technical aspects of standards development. Sophisticated computer models, based on extensive engineering and economic analyses, have been used to set cost-effective levels of energy conservation in new residential construction. Projections of the amount of energy, or the millions of barrels of oil, the nation might save then follow from a comparison of past building practices with practices expected to result from the standards.

The potential oil savings are quite large (as much as 1.5×10^6 bbl/day by the year 2000). But unless standards are enforced, those savings are unlikely to occur, and projections of energy demand are likely to be lower than actual demand. Thus, enforcement is essential for an effective standards program. The BEPS Notice of Proposed Rulemaking (issued in November 1979) charges local building departments with the responsibility for enforcement of energy regulations through the normal building permit approval process. But, if the locals are unable, or unwilling, to enforce the standards, the U.S. Department of Energy (DOE) is supposed to do so.

Although the DOE is still developing the BEPS (working toward a new proposed rulemaking in August of 1981), the State of California has had standards in place for the past two years. In fact, the state is now in the process of updating its residential standards to "better the BEPS." Thus the California experience with energy standards may give important insights into the implementation and enforcement problems likely to arise in a national effort to regulate building designs for the purpose of lowering energy consumption.

ACCOMPLISHMENTS DURING FY 1980

LBL initiated a case study of California building standards in January 1980. At the outset, the study population included the entire spectrum of participants in the building process. We considered the California Energy Commission's (CEC) intentions and actions to be vital to understanding the impact

* This work is supported by the Standards Branch, Buildings Division, Office of Buildings and Community Systems, U.S. Department of Energy under Contract No. W-7405-ENG-48.

of California's Title 24 energy conservation regulations. We felt it was equally necessary to investigate the manner in which local building departments enforced the standards. (As with the BEPS, building officials were to see that the regulations were carried out.) The reactions of builders, architects, engineers also had to be discerned along with the attitudes of the "supporting actors"--realtors, financial institutions, utilities, and insurers--since they play an important role in the building community.

Much of the research has been focused on the energy commission's standards-setting process and the enforcement activities of the local building departments. Two basic techniques have been used. At the CEC, key staff and commissioners were interviewed; relevant documents were reviewed; and meetings of a task force (set up by the commission to investigate compliance) were monitored. A questionnaire was designed to use building officials' experiences and attitudes with respect to energy standards. The survey went to all 530 building departments in the state; the response rate of approximately 60% was especially good, given the survey's complexity and length. (About 30 minutes was required to complete it.) To supplement the information on the questionnaire, we interviewed selected local officials to understand better the role energy considerations have in building department activities.

The private sector's reactions have been explored with similar techniques. Interviews have been held with key figures in the building, architecture, utility, and banking fields. In addition, pilot studies have been completed with architects and builders. A questionnaire (comparable to the one given to building officials) was administered at a conference on energy-conserving design sponsored by the California Council of the American Institute of Architects. Slightly more than half of the 103 registered California architects responded. Representatives of 16 building firms were interviewed in depth concerning their experiences with state energy regulations. Interviewees were chosen from among various types of builders--large and small, custom and tract, innovative and conventional --to give a fuller picture of the industry's response to standards. In addition, magazines and newsletters read by builders and architects have been surveyed for the two years that the state's standards have been in effect.

Results

The major findings of the study may be placed in several categories; some findings relate to the standards themselves, some pertain to the Energy Commission's efforts to provide information and training; others related to enforcement at the local level, to acceptance by the private sector, and to reactions of the "supporting actors."

Standards

California's Title 24 standards have two sections, one dealing with residential buildings, the other with nonresidential buildings. Our primary mission has been to study reactions to the residential standards. Unlike the proposed BEPS, which is a performance standard, California's residential regulations are prescriptive in nature. Although trade-offs can be made, the vast majority of the state's homes are designed to conform to the component requirements, i.e., to a certain level of insulation, glass area, and furnace size. The nonresidential standards allow a performance approach with appropriate documentation. But building officials report that in only a small minority of the structures (2-10%) is an alternate approach to compliance with the regulations adopted.

The California Energy Commission has developed a procedure to certify local standards that differ from the state's. But only a few localities have tried to certify such standards. And those that have done so have usually mandated solar water heating or swimming pool heating, rather than to attempt sweeping revisions of the regulations.

Energy Commission Role

The Commission recognized the need to train building officials for effective enforcement. During the Spring, Summer, and Fall of 1978 (as the regulations were going into effect), CEC staff sponsored nearly 100 sessions to inform building departments and other interested parties about the regulations. Many officials felt that the sessions were helpful. But others criticized them as too heavily weighted towards theory; for trying to cover too much material in one session; for failure to answer specific questions; and for the convenors' lack of knowledge about local problems. CEC staff acknowledge many of these shortcomings. However, since the training program had to be put together hurriedly, the effort ought to be regarded as a qualified success.

CEC published a design manual to aid builders and local officials in complying with the regulations. But as Title 24 was to go into effect, the commission was sued by Building Code Action for alleged procedural violations and technical inaccuracies in the standards. A portion of the standards was stayed for nearly two years, until recently when the Court of Appeals ruled in the commission's favor. Since the manual was based on the original standards, portions of the manual have been incorrect for most of the time the regulations have been in effect. In addition, the commission itself made changes which were not quickly incorporated. Thus, the manual, which was to have been a main tool for compliance, lost most of its usefulness. Although the commission publishes a newsletter, the Blueprint, which notes changes in the standards, few people seem to integrate its (unofficial) interpretations with those of the manual.

CEC has never attempted to enforce the standards itself, even though the Warren-Alquist Act (the legislation which created the commission) gives it the power to do so in localities unable or unwilling to enforce the standards. Staff limitations have hampered any move in that direction. However in June of 1980, the commission appointed a task force to advise it on ways to gain greater compliance with the standards. One of the group's recently released recommendations is for development of a monitoring capability, but the suggestion has not been implemented.

Local Enforcement Efforts

Enforcement of energy standards varies throughout the state. Some departments check plans thoroughly, request redesigns for failure to comply with Title 24, and inspect for insulation installation. Other departments pay only minimal attention to energy conservation, accepting an architect's or engineer's stamp and certificates from insulation contractors in lieu of checking for compliance with the standards. Our questionnaire provides one measure of effort at the local level: the proportion of time departments spend in checking plans and inspection. About 25% of the building departments seem to be devoting a small proportion (less than 5%) of their time to energy conservation standards, while 20% seem to be treating enforcement more seriously (devoting 15% or more of their time to it).

A considerable number of building departments feel that they cannot adequately enforce energy standards because of a shortage of personnel. Shortly before Title 24 was to go into effect, Californians passed Proposition 13, which cut building department staffs. Although the energy commission authorized localities to raise fees to cover enforcement costs, most jurisdictions have been unable or unwilling to do so.

Few building officials can say whether buildings are in full compliance with Title 24. However, our questionnaire found that officals held several general impressions: Most of the official think that the standards are saving energy compared to the energy savings the market would have produced. And most believe that buildings in their areas just meet the standards; few builders provide more energy conservation than required or fail to include mandated features.

Local code officials generally feel "put upon" by higher levels of government. In California, not only have they recently been required to check for energy efficiency, but for seismic safety and for handicapped access as well. They see state and federal agencies mandating enforcement responsibilities without providing additional funds or staff so that the job can be done well. Building officials also worry about increased legal liability arising from their new responsibilities. No California department has been sued, but the possibility of legal action concerns many officials.

Private Sector Acceptance

Builders have gradually become resigned to energy standards. Most, however, still feel that the market will take care of energy conservation, given the expected price rises in the near future. Title 24 has not significantly changed residential design; basically, it has required added insulation and some limitation of glazing (as well as double-paned glass in some locations). Builders estimate that standards have raised the cost of a new home by 2-5%.

Architects generally dislike the state's prescriptive standards, and have been pushing for a performance approach to energy conservation. Engineers, by contrast, are more comfortable with a component approach, which allows trade-offs among design elements. The most innovative designers report the greatest amount of difficulty with current state standards. They sometimes find building officials reluctant to accept new ideas, and often are required to submit extensive calculations to satisfy Title 24 requirements.

Supporting Actors

There has been little action on the part of financial institutions to take account of energy costs in making loans for home purchases. Some banks and savings and loans institutions have financed active solar systems, and a few have backed builders of passive solar developments, but none have yet made a commitment to change loan qualification criteria to include the house's projected energy consumption.

The California Public Utilities Commission has urged the utilities to take major steps toward energy conservation. Some observers even feel that efforts by the utilities can play a greater role in saving energy in buildings than the CEC's standards. New programs tying "line extension credits" to conservation measures, and providing low- or even zero-interest loans to consumers for financing conservation measures are being readied for widespread use.

PLANNED ACTIVITIES FOR FY 1981

The California Energy Commission is currently in the process of up-dating its residential standards. Hearings should be held in December and January, with passage of new regulations likely to occur in the Spring of 1981. It is important to follow the revision process, and the new training efforts that will be employed, in order to compare the results with those of the previous efforts.

A number of innovative efforts are occurring throughout California. Several of these are of particular interest:

1. The city and county of Fresno's efforts to integrate land use and energy planning.

2. The effects of recently passed local solar-mandating ordinances in San Diego, Santa Barbara, and Santa Clara counties.

3. The reasons that builders' market advanced energy conservation homes.

We shall analyze these, and other innovative efforts, as a means of assessing policy options for energy savings beyond those provided in a standards program.

More systematic information will be collected --through questionnaires, and additional interviews, especially in Southern California--from builders and designers concerning their experiences with, and attitudes toward, state, and federal energy standards.

ECONOMIC BENEFITS AND ENERGY SAVINGS OF APPLIANCE EFFICIENCY STANDARDS*

J. McMahon and M. Levine

INTRODUCTION

The U.S. Department of Energy (DOE), working under the congressional mandate of the Energy Policy and Conservation Act, as amended,† has proposed a set of mandatory efficiency standards for eight types of consumer products. An appliance not meeting these performance standards cannot be sold in the United States. The residential appliances affected in the proposed rule are refrigerators and refrigerator/freezers, freezers, clothes dryers, water heaters, room air conditioners, kitchen ranges and ovens, central air conditioners, and furnaces. The mandated standards are supposed to achieve the maximum energy efficiency that is technologically feasible and economically justified.

ACCOMPLISHMENTS DURING FY 1980

A very large analytical effort was required to establish the technologically feasible engineering options, their cost, the appliances that consumers are likely to purchase in the absence of standards, and how appliance usage patterns may change. The effort was also designed to assess the effects of the standards as perceived by consumers in terms of equipment cost increases, fuel and dollar savings, and affects on the appliance manufacturers and their economic livelihood. Preliminary documents, published with the proposed rule, describe the analysis prior to the public comment period.[1-6] Subsequently, testimony from manufacturers, consumers, and interested parties has been obtained. Public comments and additional analysis will be incorporated in DOE's final recommendation of standards, to be published early in 1981.

One aspect of the analysis will be described here. The modeling of residential energy consumption to elucidate the proposed standards' economic and energy savings to the consumer involved the use of the Oak Ridge National Laboratory (ORNL) Residential Energy Demand Model.[7-11] This model was originally written by Eric Hirst and Janet Carney, and was subsequently modified at ORNL to include only those appliance types in the proposed regulation. The model has been used and further modified in the course of analysis at LBL.

ORNL Residential Energy Demand Model

Some key features of the ORNL model are that it details energy demand for the residential sector by treating each end-use separately, and that the efficiency of appliances can change over time in response to changing fuel prices. For each end-use (where appropriate), four "fuel types" are considered: electricity, gas, oil, and other. An additional level of detail is included (when supported by the data) by considering three housing types: single-family, multifamily, and mobile homes.

The essential inputs to the model include: initial estimates of energy consumption per unit; saturation of appliances in stock; new purchase market shares; thermal integrity of structures; elasticities of energy consumption to fuel price; engineering curves relating first cost to appliance efficiency; appliance lifetimes; initial capital cost of equipment; exogenous projections of housing stocks and new construction; anticipated fuel price increases; and income projection.

The most important calculations performed by the model, for each year of the projection period, include changes in efficiency of new appliances, thermal integrity of new structures, number of appliance installations, equipment costs, fuel costs, and energy consumption. Over the period, the present values of equipment, fuel, and total costs are calculated for each end-use.

One of the key elements of this analysis is the use of a life-cycle costing methodology[12] to determine the consumers' efficiency choice of appliance efficiency. It is assumed initially, based on historical evidence, that consumers have not minimized their life-cycle cost at a low discount rate when deciding which efficiency of a given appliance to purchase. The consumer's choice is modeled to move closer to a minimum life-cycle cost (at a reasonably low discount rate) as fuel prices increase. An alternative way of describing this is to say that the purchaser's implicit discount rate decreases as energy costs increase.

Energy Prices

Projections of energy prices are important because of their influence on the level of expected investment in energy conservation. The baseline is characterized throughout this analysis by two different sets of energy prices. The high price case assumes a 2.5% real annual escalation of electricity prices and 3.0% real annual increase of oil, gas and other fuel prices. The low price case assumes annual real price increases of 1.0% and 1.5%, respectively. Both energy price cases have the same initial prices for 1977.

Baseline Forecasts

The results of the energy demand forecasts are presented in Tables 1 and 2. In the high energy price case, primary energy demand increases from

* This work was supported by the Standards Branch, Consumer Products Division, Office of Buildings and Community Systems, U.S. Department of Energy under Contract No. W-7405-ENG-48.

† By the National Energy Conservation Policy Act.

Table 1. Baseline demand forecasts: Total residential energy use. (in 10^{15} Btu's)

Year	High Energy Price Case	Low Energy Price Case
1978	17.03	17.01
1980	17.97	18.02
1985	19.52	19.84
1990	20.74	21.55
1995	21.58	22.98
2000	22.22	24.29

Table 2. Percentage 1982-2005 energy demand by end use.

End Use	High Price Case Base (%)	Low Price Case Base (%)
Central space heater	39.8	39.5
Home space heater	12.5	12.5
Room air conditioner	2.0	2.1
Central air conditioner	5.2	5.3
Water heater	18.2	17.8
Refrigerator	10.0	10.5
Freezer	3.3	3.4
Range	6.0	5.9
Dryer	3.0	3.0

Table 3. Energy demand reduction resulting from the proposed standards.

	High Price Case	Low Price Case
Energy Savings By Fuel Type, 1982-2005 (in quads*)		
Electricity	10.0	17.1
Natural gas	3.0	6.0
Oil	0.6	1.1
Energy Savings by End Use, 1982-2005 (in quads)		
Central space heat	2.00	4.27
Room air conditioners	0.22	0.56
Central air conditioners	2.62	3.73
Water heaters	3.87	5.91
Refrigerators	3.64	7.56
Freezers	0.82	1.69
Ranges/ovens	0.26	0.82
Clothes dryers	0.32	0.59
Annual Energy Savings (quads per year)		
1985	0.01	0.04
1990	0.61	0.89
1995	0.79	1.34
2000	0.80	1.59
2005	0.68	1.65

*Includes both regulated and unregulated products.

18 quads* in 1980 to 22.2 quads in the year 2000 (an average growth of 1.1%/yr). In the low price case, 24.3 quads are consumed in 2000, representing an average growth of 1.5% per year. Table 2 indicates that the largest energy user in the residential sector is central space heating, representing 40% of the total primary energy consumed by the regulated products nationally. The next largest users are water heating, room space heaters, and refrigerators.

Energy Savings

Table 3 presents the reductions in primary energy demand estimated to be achieved by the Consumer Products Energy Performance Standards for the high and low price cases. These energy savings were obtained by subtracting the energy demand associated with the regulated consumer products in the standards case from that in the baseline case, with the price of energy the same in the two cases. These are the major findings of this analysis of energy savings:

- Measured at the building boundary, 46-49% of the energy savings is electricity; the remaining 51-54% of the savings is oil and natural gas;
- Measured in source energy units, 70-75% of the energy savings is electricity;
- The annual total energy savings in 1995 resulting from the Consumer Products Energy Performance Standards is equivalent to 0.4 to 0.8 million barrels of oil per day;
- Between 85 and 90% of the energy savings resulting from the standards is achieved by improving the energy efficiency of four end uses: water heating, refrigeration, central air conditioning, and central space heating.
- Measured as a percentage of total residential energy demand of the regulated products, the standards reduce residential

*1 quad = 10^{15} Btu and 1 kWh = 11,500 Btu.

energy demand by 5-8.4%; however, measured as a percentage of total residential energy demand growth, the standards are estimated to reduce growth after 1980 by 33-50% by the year 2000.

Reduction in Consumer Costs

The standards produce a net savings to the consumer of 15.2-19.3 billion dollars, excluding implementation and enforcement costs.* The savings on energy costs are estimated at 22-29 billion dollars; increased present cost of equipment is 7-10 billion dollars. The total economic savings are on net present value of equipment and energy costs of 950-1,100 billion dollars for the 1982 to 2005 period.

- The net present benefit to the consumer of the proposed standards is positive under the full range of sensitivity studies.
- The variables having the greatest impact on estimates of energy savings are the energy price escalation rates and the implicit discount rates that characterize the market response to higher energy prices.

PLANNED ACTIVITIES FOR FY 1981

The major tasks underway are incorporation in the model of public responses to the proposed rule and inclusion of newer user data and additional analyses. Subsequently, using the ORNL/LBL Model, new estimates will be made of energy consumption and economic and energy savings resulting from the final standards. Further research in data development and model improvements are recommended on the basis of the experience gained in this analytical effort.

REFERENCES

1. Department of Energy, Office of Conservation and Solar Energy, "Energy Conservation Program for Consumer Products," Federal Register, vol. 45, no. 127, June 30 1980, pp. 43976-44087.
2. J. McMahon and M. Levine, Economic Analysis of Proposed Consumer Product Energy Performance Standards, Lawrence Berkeley Laboratory report LBL-11359, December 1980 (in preparation).
3. J. McMahon, Consumer Discount Rates Implied in the ORNL Residential Energy Demand Modes, Lawrence Berkeley Laboratory report, August 1980 (in preparation).
4. U.S. Department of Energy, Technical Support Document No. 5, Engineering Analysis, Energy Efficiency Standards for Consumer Products, DOE/CS-0166, Conservation and Solar Energy, Office of Buildings and Community Systems, Washington, D.C., June 1980.
5. U.S. Department of Energy, Technical Support Document No. 4, Economic Analysis, Energy Efficiency Standards for Consumer Products, DOE/CS-0169, Conservation and Solar Energy, Office of Buildings and Community Systems, Washington, D.C., June 1980.
6. U.S. Department of Energy, Technical Support Document No. 1, Draft Regulatory Analysis, Energy Efficiency Standards for Consumer Products, DOE/CS-0172, Conservation and Solar Energy, Office of Buildings and Community Systems, Washington, D.C., June 1980.
7. E. Hirst et al., An Improved Engineering-Economic Model of Residential Energy Use, ORNL/CON-8 (Oak Ridge, Tenn.: Oak Ridge National Laboratory, April 1977).
8. E. Hirst et al., Residential Energy Use to the Year 2000, ORNL/CON-13 (Oak Ridge, Tenn.: Oak Ridge National Laboratory, September 1977).
9. E. Hirst and J. Carney, The ORNL Engineering-Economic Model of Residential Energy, ORNL/CON-24 (Oak Ridge, Tenn.: Oak Ridge National Laboratory, July 1978).
10. S. Thomas McCormick, User's Guide to the Oak Ridge National Laboratory Residential Energy Demand Model, Working Paper No. MIT-EL 79-042WP (Cambridge, Mass.: Massachusetts Institute of Technology Energy Laboratory, August 1979).
11. K. Hudson, The Oak Ridge National Laboratory Residential Energy Demand Model, Version 6, Lawrence Berkeley Laboratory, (in preparation).
12. I. Turiel, H. Estrada, and M. Levine, Life-Cycle Analysis of Major Appliances, Lawrence Berkeley Laboratory report LBL-11338, July 1980.

*All net present value estimates are obtained by discounting future costs and benefits at a 10% (real) discount rate basis of the experience gained in this analytical effort.

LIFE-CYCLE COST ANALYSIS OF MAJOR APPLIANCES*

I. Turiel, H. Estrada, and M. Levine

INTRODUCTION

The Energy Policy and Conservation Act (Public Law 94-163) as amended by the National Energy Conservation Policy Act (Public Law 95-619) established the Consumer Products Efficiency Standards Program and assigned the Department of Energy (DOE) the task of establishing mandatory minimum energy efficiency standards for 13 consumer products. In accordance with this requirement, DOE has proposed minimum energy efficiency standards for various classes of eight appliances: refrigerators and refrigerator-freezers, clothes dryers, water heaters, room air conditioners, ranges and ovens, central air conditioners, and furnaces.[1] The remaining five consumer products have been placed on a slower schedule with standards to be proposed at a later date.

DOE is required to set standards at a level that achieves the maximum improvement in energy efficiency that is technologically feasible and economically justified. One of the criteria on which this determination is based is the economic impact of the standards on consumers of the regulated products.

This paper provides a methodology for assessing the economic costs and benefits to the consumer who purchases appliances of varying initial costs and energy efficiency. The basis for the method of analysis is the use of life-cycle costing.[2]

The life-cycle cost of owning and operating an appliance is equal to the first cost or purchase price plus the operating and maintenance costs over the appliance's lifetime. The first cost may be paid when the product is purchased or the consumer may borrow money which is paid back with interest after the purchase is made. For the purpose of this analysis, it is assumed that the consumer makes a cash purchase of the appliance. The assumption is also made that the cost of maintenance over the appliance's lifetime is unchanged as the efficiency of a model is increased or decreased. Therefore, the maintenance cost is not included in the life-cycle cost calculation, as exclusion of maintenance costs has no effect on the differences in life-cycle costs among models of different efficiencies. In order to consider first cost and operating costs on a time equivalent basis, all future operating costs are discounted to present value.

A more energy efficient product is often more expensive than an otherwise identical product of low efficiency. However, the more energy efficient model uses less energy than a less efficient one and thus costs less to operate. If the more efficient model has lower total costs to the consumer over the life of the appliance, the consumer benefits, although a higher initial investment may cause an adverse impact over the short term.

This potential problem of higher first costs associated with lower life-cycle costs of more energy efficient products can be assessed in terms of a simple payback period. The simple payback period is the amount of time required for the consumer to recoup his or her additional investment in a more energy efficient product. For example, if the simple payback period is 11 months, then the extra costs of the purchase of a more efficient product are fully recovered in reduced energy bills during the first 11 months of operation of the product. This is equivalent to a return on investment of greater than 100% per year to the consumer. If, however, the simple payback period is 20 years, then the rate of return on the initial investment is small (unless energy prices escalate rapidly).

Because energy prices and appliance use patterns vary regionally, the imposition of national standards may result in an inequitable distribution of costs and benefits among regions. Since variations in energy consumption are most significant among space heating and cooling products, regional analyses will focus on gas-fired and oil-fired furnaces, central air conditioners, and room air conditioners.

METHODS AND ASSUMPTIONS

The total life-cycle cost (LCC) of an appliance is given by

$$LCC = IC + \sum_{i=1}^{N} (ENC)_i \times \frac{(PF)(1+f)^i}{(1+d)^i} \qquad (1)$$

where

IC = initial cost of appliance, in dollars,

ENC_i = energy consumption in year i, in million Btu's,

PF = fuel price in year 1, in dollars per million Btu's,

N = lifetime of appliance, in years

f = annual fuel escalation rate in constant dollars,

d = discount rate in constant dollars.

DOE is proposing two sets of energy performance standards for consumer products: one set applies in 1981 and a tighter set applies in 1986. The

* This work was supported by the Standards Branch, Consumer Products Division, Office of Buildings and Community Systems, U.S. Department of Energy under Contract No. W-7405-ENG-48.

life-cycle cost analysis applies only to the 1986 standards, because the tighter 1986 standards are intended to achieve substantial life-cycle cost savings to the consumer. The 1981 standards achieve much smaller life-cycle cost savings because of the relatively small energy efficiency improvements mandated by these near-term standards.

In the analysis as performed, yearly energy consumption (ENC_i) and the fuel escalation rate (f) are assumed to be constant over the appliance lifetime. Thus, equation (1) may be simplified to

$$LCC = IC + (ENC) \times (PF) \times (PWF) \qquad (2)$$

where

$$PWF = \sum_{i=1}^{N} \left(\frac{1+f}{1+d}\right)^i \qquad (3)$$

Table 1 shows the national average fuel prices and escalation rates used in the life-cycle cost calculations. Both a high and a low fuel price escalation rate are presented to illustrate the effects of differing price scenarios on life-cycle costs.* (These two price scenarios are used in the analysis to represent DOE's estimates of likely upper and lower bounds of fuel prices). Both the first cost and the fuel prices are expressed as 1985 prices measured in 1978 dollars: As such, the LCC results are expressed in constant 1978 dollars.† The fuel price escalation rates and the discount rate are expressed in real dollars, that is, as a rate above that of inflation. The discount rate was chosen to be 5%, real; sensitivity analyses for discount rates of 3% and 10% are discussed later. Table 2 presents the appliance lifetimes used in the LCC analysis.

There are two other very important inputs to the LCC computations: cost versus efficiency, and annual energy consumption for each class of appliance.

* The relative life-cycle costs and payback periods for products of differing energy efficiencies are not greatly changed between the two price scenarios. Only the high price case results are presented.

† At the time this article was written the authors expected the proposed standards to be effective in 1985. Therefore, the analysis was performed using 1985 fuel prices and a base case efficiency for each appliance projected to occur in 1985 without standards. Choosing 1985 as the year of purchase, yields results which are only a few percent different from those obtained if 1986 were the initial year of purchase. Throughout the remainder of this report, 1985 will be used as the year the standards become effective even though it now appears that January 1, 1986 is the correct date.

Table 1. Fuel prices and escalation rates.

	1985 fuel price in $/10^6 Btu (and 1978 $)	Annual escalation rate (percent)	
		High Case	Low Case
Electricity	15.70*	2.5	1.0
Gas	3.46	3.0	1.5
Oil	6.39	3.0	1.5

* Corresponds to 5.36¢/kWh at the building boundary.

Table 2. Appliance lifetimes (in years).

Central heater	20
Water heater	10
Ranges and ovens	14
Dryers (electric)	14*
Central air conditioners	14
Room air conditioners	10
Refrigerator	15
Freezer	20

* 11 for gas dryers.

Source: U.S. Department of Energy.[9]

Cost versus efficiency data were provided by Arthur D. Little, Inc. (ADL).[3] ADL began with a base case appliance which reflected 1978 sales-weighted energy efficiency data taken from an industry survey (DOE Form CS 179). Using engineering analysis and computer simulations, ADL estimated the efficiency improvements resulting from implementation of various design options. For the analysis, the design options considered were limited to those based on available technology, defined as those technologies presently implemented in units available in the marketplace, at least in limited quantities. Only those design options were considered which were represented by existing test procedures.

Figures 1 and 2 illustrate cost versus efficiency curves for automatic defrost top-mount refrigerators and split system central air conditioners, respectively. Also shown are the design options chosen for analysis. Points on the curves are generated by implementing combinations of design options. In Figure 2, the same design options (1, 2, 3) are used for each data point. In cases of this type, the design options were carried out to varying degrees. These design options are described in detail for each product type in Technical Support Document (TSD) No. 5, Engineering Analysis.[4]

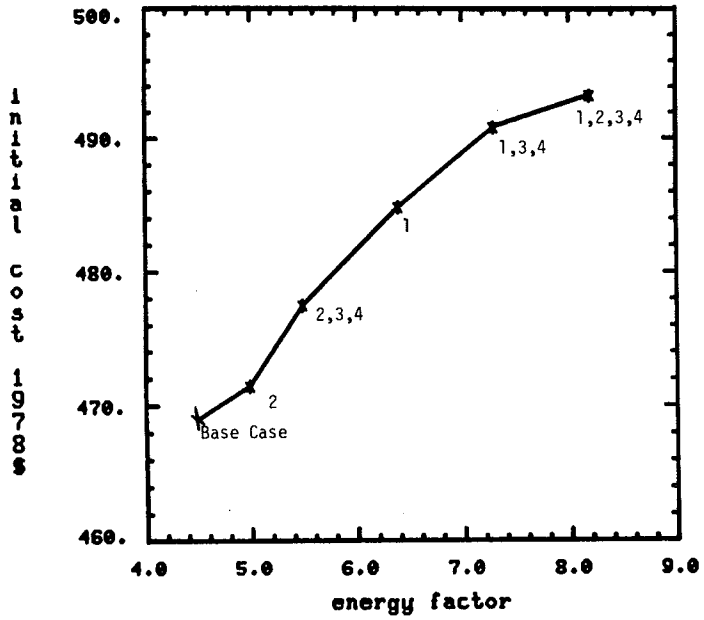

Fig. 1. Cost versus efficiency for automatic defrost, top-mount refrigerator. The design options are (1) foam insulation substitution; (2) high-efficiency compressor substitution; (3) double-door gasket in freezer; (4) place evaporator fan motor outside of cold space. (XBL 8010-12522)

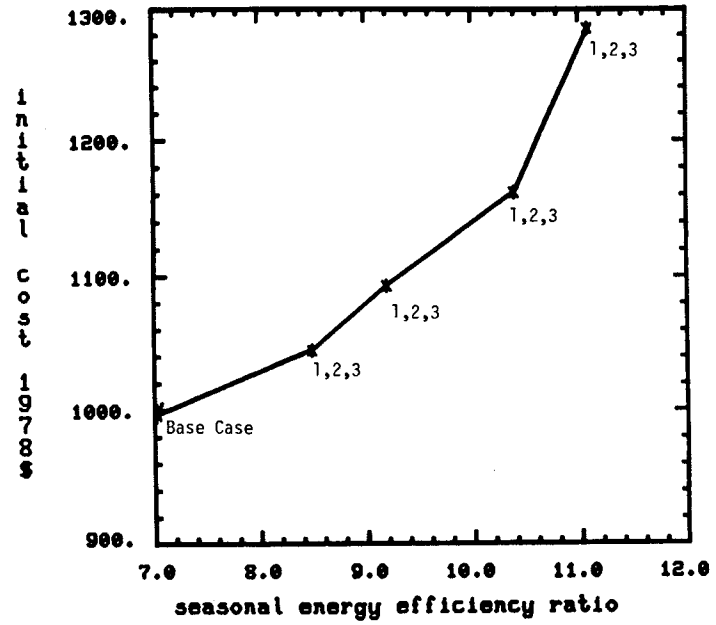

Fig. 2. Cost versus efficiency for central air conditioner, split-system. The design options are (1) increased condensor and evaporator heat-exchanger surface area; (2) decreased compressor size; and (3) different fan motor. In cases where the same design options are used for more than one data point, these options have been employed to varying degrees. For details see Reference 4. (XBL 8010-12523)

Average annual energy consumption per unit is composed of two factors, an energy (or efficiency) factor and a usage factor. In general for each appliance model:

$$\text{annual energy use per unit} \propto \frac{\text{usage factor}}{\text{energy factor}}$$

In some cases the annual energy consumption in the ADL data base is significantly different from that found by Oak Ridge National Laboratory (ORNL).[5] Table 3 compares values obtained from ORNL with data provided by ADL for the base case appliance.[6] The ORNL values were used in the LCC analysis because the ORNL estimates were from a broader, more complete data base.

The life-cycle cost analysis was performed on a national basis for all the covered products. In addition, the analysis was performed on a regional basis for the three products whose usage is highly dependent on weather: furnaces, central air conditioners, and room air conditioners. The regions, shown in Figure 3, were defined by DOE as follows:

Table 3. Annual energy use per unit.*

Consumer product	Fuel or energy source	ORNL†	ADL‡	ORNL/ ADL
Refrigerator	Electric	1740	1548.0	1.12
Freezer	Electric	1642.6	1170.5	1.40
Dryer	Electric	1114.8	1066.6	1.04
Dryer	Gas	7.0	4.2	1.67
Water heater	Electric	4599	6620	.69
Water heater	Gas	25.0	36.6	.68
Ranges/ovens	Electric	1246.1	407.0	3.06
Ranges/ovens	Gas	9.6	4.4	2.18
Air conditioners (room)§	Electric	1708.7	1238.2	1.38
Air conditioners (central)	Electric	3106.1	4373.7	.71
Central space heat	Gas	88.7	126.2	.70
Central space heat	Oil	141.8	118.7	1.19

* Energy use is in kWh for electric appliances and in 10^6 Btu for gas and oil appliances, respectively.

† 1977 values, weighted by housing units.

‡ A.D. Little values, weighted by 1978 sales.

§ 1708.7 kWh is the annual energy use per household. To obtain annual energy use per unit for room air conditioners, divide 1708.7 kWh by 1.45, the number of room air conditioners per household (among households having room air conditioners).

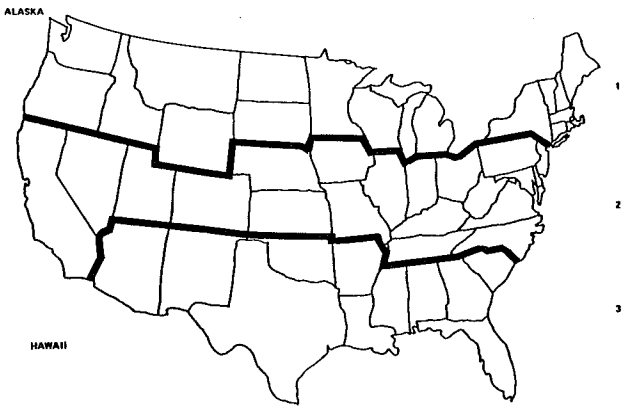

Fig. 3. Heating and cooling regions of the United States for purposes of analysis of appliance efficiency standards. Source: DOE (1980).
(XBL 8010-12524)

Region 1. > 2.500 heating-load hours
≤ 600 cooling-load hours

Region 2. > 1,750 ≤ 2,500 heating-load hours
> 600 ≤ 1,200 cooling-load hours

Region 3. ≤ 1,750 heating-load hours
> 1,200 cooling-load hours

RESULTS

Equations 2 and 3 have been used to calculate consumer life-costs for 32 classes of eight products covered by DOE's proposed regulation.[7] Figure 4, an LCC curve for an automatic defrost top-mount refrigerator/freezer is typical of most appliances studied. The LCC decreases continuously with increasing energy efficiency, i.e., the energy cost savings derived from the use of more efficient models of this class of refrigerator/freezer more than compensate for the extra initial cost of these models, when any model is compared to one of lower efficiency.

Figure 5, for a split-system central air conditioner, is illustrative of classes of appliances in which the minimum life-cycle cost does not occur for the highest efficiency model. There are four other cases [all room air conditioners (RAC), except those of capacity greater than 20,000 Btu/h, and gas clothes dryers] where the minimum in LCC occurs before the highest efficiency model. For appliances of this type, consumers do not benefit most by purchasing the highest efficiency model available.

Table 4 compares the proposed 1985 standards, the sales weighted energy factor (SWEF) in 1978, and the projected 1985 SWEF (in the absence of standards). The projected 1985 SWEF (baseline efficiency) was obtained by multiplying the 1978 SWEF by a factor equal to the improvement in energy efficiency predicted to occur between 1978 and 1985 (obtained from the ORNL residential energy use model).

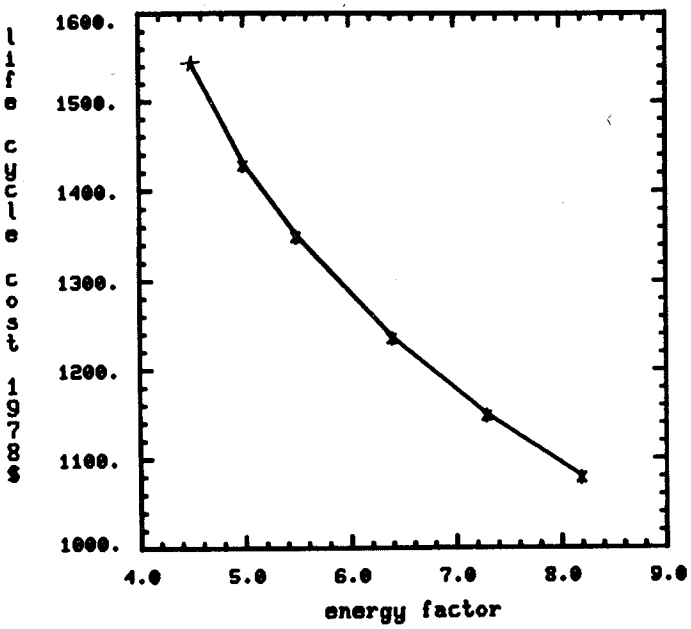

Fig. 4. Life-cycle costs of refrigerators (automatic defrost, top mount), evaluated at a 5% real discount rate and at DOE's high-energy price case (2.5% per year real electricity price escalation rate). (XBL 8010-12525)

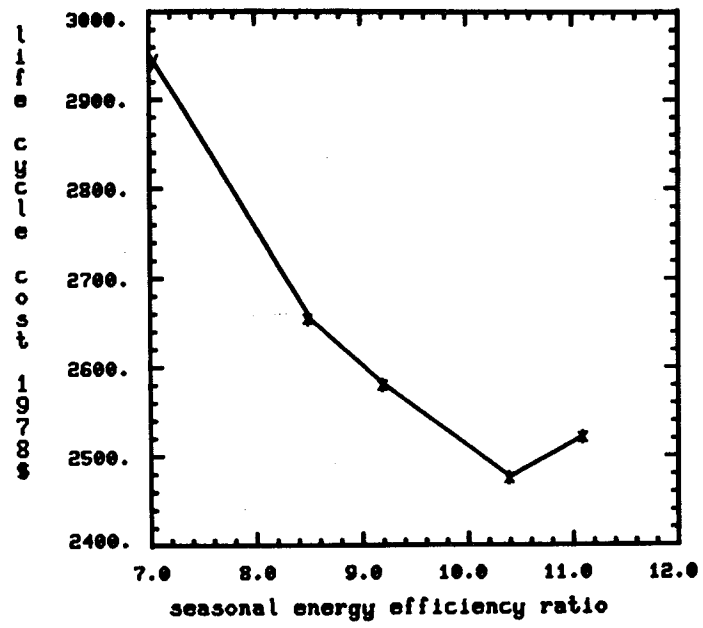

Fig. 5. Life-cycle costs of split-system, 30,000 Btu/h, central air conditioners evaluated at a 5% real discount rate and at DOE's high-energy price case (2.5% per year real electricity price escalation rate). (XBL 8010-12526)

Table 4. Compilation of proposed 1985 standards and base case energy efficiencies.

Product	DOE's Proposed 1985 Standard	SWEF (1978)	SWEF* (1985)
CAC			
Split	11.0	7.02	7.63
Single	10.5	6.90	7.50
RAC			
< 6,000 Btu	8.4	6.17	6.65
6,000 Btu to 20,000 Btu	9.5	7.25	7.80
>20,000 Btu	8.4	6.74	7.25
Through wall and reverse cycle	9.0	6.55	7.05
Furnaces			
Gas, indoor forced air	81	64.6	69.8
Gas, boiler	79	65.1	70.4
Gas, outdoor horizontal, nonweatherized	74	56.0	60.6
Gas, outdoor weatherized	76	68.0	73.4
Oil, forced indoor	80	75.25	79.6
Oil, boiler	82	75.8	80.2
Oil, outdoor forced air	78		
Water Heaters			
Gas	63	48.2	51.3
Electric	93	80.67	84.3
Clothes Dryers			
Electric standard	3.0	2.6	2.70
Electric compact, 120V	2.85	2.63	2.73
Electric compact, 240V	2.54	2.35	2.44
Gas	2.60	2.38	2.44
Ranges and Ovens			
Gas cook top	45.0	30.8	36.2
Gas oven	6.4	4.6	5.4
Gas oven, self-cleaning	6.0	4.8	5.6
Electric cook top	79	75.0	77.2
Electric oven	14.1	13.0	13.4
Electric oven, self-cleaning	13.6	12.6	13.0
Refrigerators			
Refrigerator, manual	17.2	7.11	8.3
Part. auto	11.6	5.35	6.24
Auto-top mount	8.2	4.73	5.52
Auto side-by-side	7.0	5.01	5.85
Auto side-by-side TTD	6.3	5.03	5.87
Freezers			
Manual chest	18.7	11.29	12.92
Manual upright	16.3	9.21	10.54
Auto, upright	9.6	6.36	7.28

* The projected 1985 sales weighted energy factor (SWEF) is obtained by multiplying the 1978 SWEF by the improvement in efficiency predicted by the ORNL residential energy use model.

SUMMARY AND CONCLUSION

On a national basis, the proposed 1985 standards are cost-effective with respect to the energy efficiency levels projected to occur in the absence of standards for all classes of products. The proposed 1985 standard produces higher life-cycle cost savings than a standard at a lower energy efficiency except for two cases, split-system central air conditioners and room air conditioners of 6,000 to 20,000 Btu/h capacity. However, in both cases, the life-cycle cost reduction achieved by the proposed standard is only slightly less (<1%) than that achieved at any lower trial level. In our view, this small increase in life-cycle cost for these two cases is justified by the resulting greater energy savings to the nation.

In two cases, the proposed efficiency standard is below the trial level where the life-cycle cost minimum occurs. These are (1) room air conditioners of capacity less than 6,000 Btu/h, where the proposed standard is at an energy efficiency ratio (EER)* of 8.4 and the LCC minimum is at 9.1, and (2) single-package central air conditioners, where the proposed standard is set at a seasonal energy efficiency rate (SEER) of 10.5 and the LCC minimum is at 10.7.

Data were not available to analyze the life-cycle costs of many advanced-technology options (including product redesigns) required to achieve higher levels of energy efficiency for most of the consumer products. As a result, no conclusions can be reached about the potential of many advanced-technology options for reducing life-cycle cost to the consumer. Advanced technologies that should be analyzed in the future include heat pump water heaters, integrated space and water heating appliances, and condensing furnaces.[8]

Simple payback periods are considerably less than the equipment service lifetime for all products evaluated (see Table 5). For the proposed standards, they range from several months for refrigerators and freezers to a maximum of 5.3 years for split-system central air conditioners. For most products, the payback period is less than 2 years.

The regional life-cycle cost analysis indicates that the distribution of costs and benefits from the proposed national standards varies significantly among the different regions for room and central air conditioners and for furnaces. For the product class with greatest variation, the split-system central air conditioner, the change in consumer life-cycle cost at the proposed standard ranges from an increase of $119 (8% of total LCC) in Region 1 to a decrease of $552 (15% of total LCC) in Region 3. For room air conditioners of capacity 6,000 to 20,000 Btu/h, the change in consumer life-cycle cost at the proposed standard ranges from an increase of 15 dollars (4%) in Region 1 to a decrease of 85 dollars in Region III.

* EER = the maximum rate at which heat is removed (in Btu/h) divided by the electric power input in watts.

Table 5. Appliance simple payback periods for national average energy use.

Product type	Payback period (years)
Refrigerator/freezers	0.5-0.8
Freezers	0.2-0.4
Clothes dryers	2.3-4.2
Water heaters	
Electric	0.7
Gas	0.9
Room air conditioners	1.5-4.5
Ranges and ovens	1.2-3.1
Central air conditioners	
Split-system	5.3
Single package	2.3
Furnaces	0.2-2.6

Simple payback periods are longer in Region 1 than those obtained in the national analysis for all classes of air conditioners. For two cases, the simple payback periods are greater than the average appliance lifetime.* These are split-system central air conditioners (22.1 years) and room air conditioners of capacity 6,000 to 20,000 Btu/h (15.2 years).

One potential method of redressing the inter-regional inequity in costs and benefits for air conditioners is to promulgate regional efficiency standards. This is a subject of continuing research, and no firm conclusions have been reached as yet.

*Simple payback period is greater than the appliance lifetime whenever there is an increase in life-cycle cost.

REFERENCES

1. "Energy Conservation Programs for Consumer Products," Federal Register, vol. 45, no. 127, Book 2, June 30, 1980.

2. R.J. Brown and R.R. Yanuck, Life Cycle Costing: A Practical Guide for Energy Managers, (Atlanta, Ga.: The Fairmont Press, 1980).

3. Arthur D. Little, Inc., Engineering and Manufacturing Analysis in Support of Federal Minimum Efficiency Standards, Cambridge, Mass.: February 21, 1980.

4. U.S. Department of Energy, Technical Support Document No. 5, Engineering Analysis, Energy Efficiency Standards for Consumer Products, Conservation and Solar Energy, Office of Buildings and Community Systems, Washington, D.C., June 1980.

5. D. O'Neal, Oak Ridge National Laboratory, personal communication, Oak Ridge, Tenn.

6. Arthur D. Little, Inc., op. cit.

7. I. Turiel, H. Estrada, and M. Levine, Life-Cycle Cost Analysis of Major Appliances, Lawrence Berkeley Laboratory report, LBL-11338, August, 1980.

8. Arthur D. Little, Inc., Study of Energy-Saving Options for Refrigerators and Water Heaters, May 1977; and S. Talbert, A. Putnam and D. DeWerth, "Efficiency Improvement Concepts for Residential Gas-Fired Furnaces and Water Heaters," ASHRAE Transactions, vol. 86, Part 2, June, 1980.

9. U.S. Department of Energy, Technical Support No. 4, Economic Analysis, Energy Efficiency Standards for Consumer Products, Conservation and Solar Energy, Office of Buildings and Community Systems, Washington, D.C., June, 1980.

A COMPARISON OF REGIONAL AND NATIONAL ENERGY EFFICIENCY STANDARDS FOR ROOM AND CENTRAL AIR CONDITIONERS*

I. Turiel

INTRODUCTION

In accordance with the Energy Policy and Conservation Act (Public Law 94-163), as amended by the National Energy Conservation Policy Act (Public Law 95-619), the Department of Energy (DOE) has proposed energy efficiency standards for eight consumer products.[1] One of the criteria on which these standards are based is the life-cycle cost (LCC) of owning and operating an appliance over its lifetime. In the long run the consumer benefits from the purchase of a product with the lowest life-cycle cost.

Because energy prices and appliance utilization patterns vary regionally, for some appliances,

* This work was supported by the Standards Branch Consumer Products Division, Office of Buildings and Community Systems, U.S. Department of Energy under Contract No. W-7405-ENG-48.

the imposition of national energy efficiency standards may result in an inequitable distribution of costs and benefits among various climatic regions. Since variations in energy consumption are most significant in space-heating and cooling products, this analysis of costs and benefits will focus on central and room air conditioners. Central space-heating equipment has not been analyzed in this comparative study since the total life-cycle cost (LCC) curve for all classes of space-heating equipment does not reach a true minimum in any climatic region (i.e., all presently available energy conservation measures are cost-effective in all regions).

Any inequity in distribution of consumer costs and benefits could be alleviated by promulgating efficiency standards on a regional basis. Three regions were selected along state boundaries for use in the regional analysis of the proposed standards for central and room air conditioners. The regions are shown in Figure 1 and are defined as follows:

Region 1. $>$ 2,500 heating-load hours
$\leq$ 600 cooling-load hours

Region 2. $>$ 1,750 $\leq$ 2,500 heating-load hours
$>$ 600 $\leq$ 1,200 cooling-load hours

Region 3. $\leq$ 1,750 heating-load hours
$>$ 1,200 cooling-load hours

The standards could be chosen so as to separately minimize life-cycle costs in each of the three regions, thereby eliminating any potential inequities. Figures 2 and 3 show LCC curves[2] for one class (half of yearly sales) of room air conditioners and one class (85% of yearly sales) of central air conditioners. In both cases, consumers in Region 1 would suffer an increase in LCC if they purchased air conditioners in 1986 whose efficiency was equal

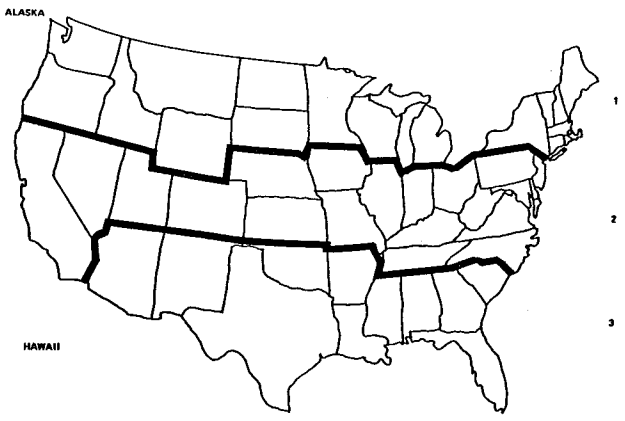

Fig. 1. Heating and cooling regions of the United States for purposes of analysis of appliance efficiency standards. Source: DOE (1980) (XBL 8010-12524)

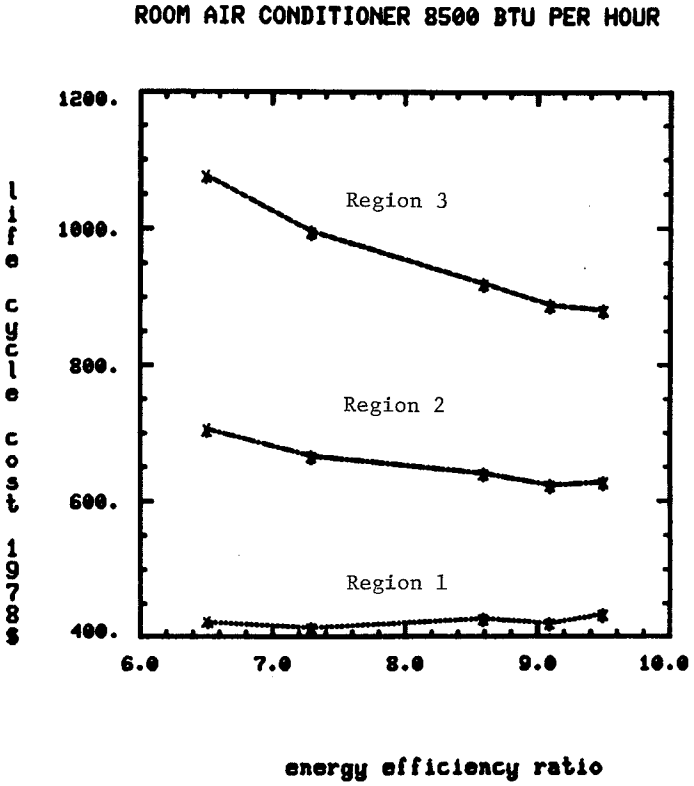

Fig. 2. Life-cycle cost as a function of energy efficiency for a room air conditioner with 8500 Btu/H capacity. (XBL 8010-12519)

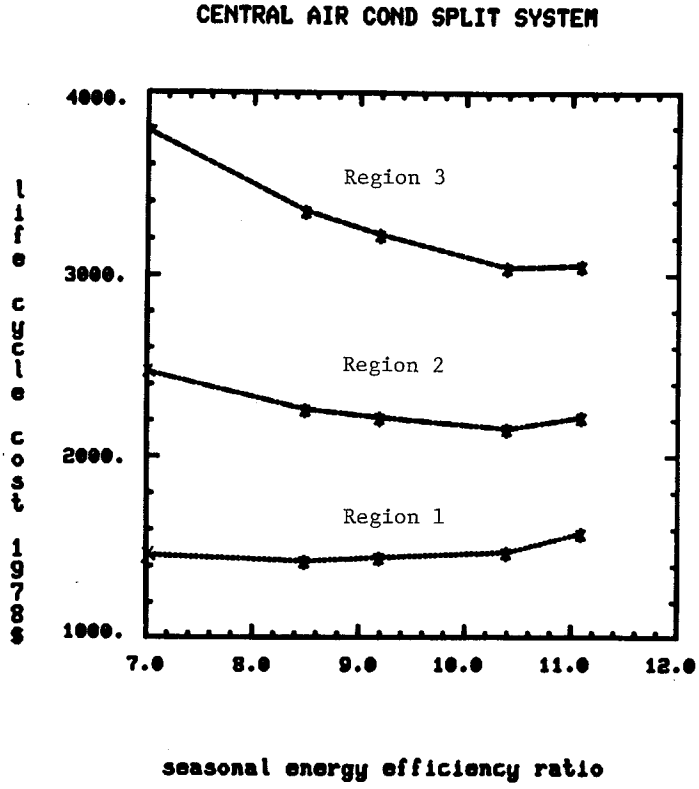

Fig. 3. Life-cycle cost as a function of energy efficiency for a split system central air conditioner with 30,000 Btu/H capacity. (XBL 8010-12520)

to the proposed 1986 standard rather than the projected 1986 energy efficiency in the absence of standards.

A study to determine the effect of regional and national energy efficiency standards on national energy consumption and total cost (appliance first cost plus operating cost) was carried out for central and room air conditioners. A discussion of the results obtained will follow a description of the methodology and assumptions.

METHODS AND ASSUMPTIONS

In order to evaluate the national economic and energy-use impacts of alternative standards, a simplified model of new appliance energy consumption was developed. In this energy use model, energy consumption of new appliances being purchased from 1982-2005 was calculated. National energy consumption is a function of appliance shipments, lifetime, energy efficiency, and annual energy use per base case (1978) unit.

Operating costs were determined by computing the product of energy use and fuel cost. The initial cost of new appliances was assumed to be paid in the year of purchase. A discount rate of 10%, real, was applied to fuel cost and appliance first cost to obtain the present value of each. High fuel price (2.5% real fuel price escalation rate for electricity) and low fuel price (1% escalation rate) scenarios were analyzed to bound the possible outcomes of alternative standards. The national average electricity price for the high and low fuel price scenarios in 1982 were $0.0498/kWh and $0.483/kWh respectively (in 1978 dollars).

Average appliance lifetimes were taken to be 10 years for room air conditioners (RAC's) and 14 years for central air conditioners (CAC's). In this simplified Energy Use Model, all appliances are assumed to have average lifetimes. For example, of 2.34 million CAC's purchased in 1982, all of them would still be in operation in 1995, and none of them would be in operation in 1996 or later. Appliance shipments were taken from the Oak Ridge National Laboratory (ORNL) Residential Energy Use Model predictions.[3]

As in the ORNL model, the relationships between initial appliance cost and energy efficiency are modeled with three-parameter equations as shown below:

$$\frac{C}{C_o} = \frac{B_3 + 1}{\left[\frac{E/E_o - B_1}{1 - B_1}\right]^{1/B_2}} - B_3$$

where

$\frac{C}{C_o}$ = initial cost relative to 1978 base case equipment cost

E = annual energy use (kWh/yr)

E_o = annual energy use for 1978 base case unit

B_1, B_2, B_3 = constants

The three parameters of the curves for each type of consumer product are given in Table 1. These parameters, describing the cost versus efficiency tradeoffs, are derived from engineering/economic analyses performed by Arthur D. Little, Inc. (ADL).[4] For central air conditioners, the energy consumption in any region, ENC(j), is given by the following equation:

$$ENC(j) = .71 \times ENCR(j) \times \left[\frac{6.87}{SEER\ (j)}\right]$$

where

ENCR(j) = base case energy consumption in region j

SEER(j) = seasonal energy efficiency ratio in region j.

The 0.71 in this equation normalizes the ADL energy use estimates to the ORNL values. The 6.87 in the equation is the SEER of an average central air conditioner sold in the base year.[5]

Regional energy use was obtained by weighting national energy use by a fraction equal to regional cooling load hours divided by national average cooling hours.[6,7]

In order to determine whether to establish a national standard or a regional standard for each product type, it is necessary to consider the following:

1. The reduction in fuel cost due to the implementation of a regional rather than a national standard.
2. The increase in equipment price due to the implementation of a regional rather than a national standard.
3. The inequity in distribution of costs and benefits to consumers in different regions under national standards.
4. The increase in first cost, certification, and enforcement costs due to the implementation of a regional rather than a national standard.
5. The energy savings achieved by each standard.

Table 1. Coefficients for cost versus energy efficiency curves for air conditioners.

	Year	B_1	B_2	B_3
Room air conditioners	(1982-1985)	.62	11.0	-.01
	(1986-2005)	.35	1.0	-.84
Central air conditioners	(1982-1985)	.57	5.7	-.40
	(1986-2005)	.46	1.05	-.88

The difference between items (1) and (2) is the net present benefit to all consumers in the nation purchasing the product of interest in the period 1982-2005. If this quantity is positive, then it should be compared to item (4). If (1)-(2) is greater than (4), then regional standards produce greater economic benefits to the nation than the proposed national standards.

RESULTS AND CONCLUSIONS

For central air conditioners, the potential energy use reduction resulting from promulgation of regional standards as compared to national standards is quite small (<5% increase). This result is due to the fact that the proposed national energy efficiency standards for central air conditioners (11.0 for split-system and 10.5 for single package) are almost as high as the maximum efficiencies (11.1) analyzed in the ADL cost book.[4] The potential energy savings derived from regional standards is much larger for room air conditioners.

As can be seen from Table 2, if the Regional Standard Scenario (8.7, 11.1, 11.1) is compared to the base case, 1.6 quads of primary energy are saved rather than only .8 quads when the Proposed National Standards are compared to the Base Case. While it is true that tighter National Standards (10.9) can produce the same energy savings (1.8 quads) as regional standards, the total cost to the nation is higher by 80 million dollars (for both the low and high fuel price cases) and the inequity in distribution of consumer costs and benefits among the three regions is significantly worsened.

Table 2. Total cost* and energy use for room air conditioner use in three DOE regions.

Scenario	Energy use‡	Region 1	Region 2	Region 3	Entire U.S.
Base case	6.43	1.834	7.175	6.917	19.594
Proposed national standards (7.44,9.0)	5.64	1.791	6.656	6.377	14.824
Tighter national standards† (7.44 10.9)	4.84	1.843	6.439	5.976	14.258
Regional standards (8.7,11.1, 11.1)	4.84	1.789	6.435	5.953	14.177

* Total cost includes first cost and operating cost and is expressed in billions of 1978 dollars.

† These tighter national standards are equivalent to the regional standards in energy use.

‡ Quads of primary energy.

There is a net present benefit, (1)-(2) > 0, for each of the three regions when national standards are instituted as compared to the no standards case. The net present benefit increases from 40 million dollars for Region 1 to approximately 530 million dollars for each of Regions 2 and 3. When Tighter National Standards (10.9) are compared to the Base Case, the net present benefit is negative in Region 1 by approximately 10 million dollars. Therefore, reducing national energy use to the same extent as the Regional Standards (8.7, 11.1, 11.1) by instituting Tighter National Standards (10.9), results in a net present cost, (1)-(2) < 0, in Region 1 of 10 million dollars whereas regional standards result in a net present benefit of 45 million dollars in Region 1. For the nation as a whole, the net present value is 80 million dollars greater for regional than for the equivalent national standards.

As stated earlier, it is necessary to estimate item (4), the increase in first cost, certification, and enforcement costs, and to compare the sum to the net present benefit of regional standards. If (4) is less than (1)-(2), (80 million dollars) then an economic argument for regional standards can be made. In this report, we do not attempt to quantify item (4) but only mention that increased first costs would result if manufacturers had to increase the number of product lines and models to meet standards in all capacity ranges for both regions (1 and regions 2 and 3, combined). In addition, distribution and storage costs may increase. We recommend that the potential additional costs (outlined above) of instituting regional standards be more precisely quantified by DOE. Table 3 summarizes the comparisons of various alternative standard scenarios to the base case (no standards). National net present benefit and national energy savings are shown for three alternatives and for a high and low fuel price scenario. In the low fuel price scenario, the base case energy consumption is greater than for the high fuel price scenario as consumers purchase less efficient (and lower cost) air conditioners when fuel prices are lower. The national energy savings for regional standards as compared to the

Table 3. National net present benefit and energy savings of alternative standards (relative to base case) room air conditioners.

Scenario	Net present benefit (billions 1978 $) high	low	Energy savings (in quads) high	low
Proposed national standards (7.44, 9.0)	4.77	1.28	.8	1.33
Regional standards (8.7,11.1,11.1)	5.42	1.69	1.6	2.13
Equivalent national standards (7.44, 10.9)	5.34	1.60	1.6	2.13

national standards is .80 quads (an increase from 1.33 to 2.13 quads).

Summarizing, for room air conditioners, regional standards (in the high and low fuel price scenarios) increase national energy savings by .80 quads relative to the base case and increase the net present benefit by 650 million dollars or 410 million dollars for the high and low fuel price scenarios respectively.

Two matters requiring additional attention are the expected time of availability for room air conditioners with higher efficiency (an average EER of 11.0 across all classes) and the magnitude of additional first cost, if any, caused by promulgation of regional standards rather than national standards.

REFERENCES

1. "Energy Conservation Programs for Consumer Products," Federal Register, vol. 45, no. 127 book 2, June 30, 1980.

2. I. Turiel, H. Estrada and M. Levine, Life Cycle Cost Analysis of Major Appliances, Lawrence Berkeley Laboratory, report LBL-11338, July, 1980 (to be published in Energy, The International Journal).

3. E. Hirst and J. Carney, The ORNL Engineering-Economy Model of Residential Energy Use, ORNL/CON-24 (Oak Ridge, Tenn.: Oak Ridge National Laboratory, July, 1978).

4. Arthur D. Little, Inc., Engineering and Manufacturing Analysis in Support of Federal Minimum Efficiency Standards, Cambridge, Mass., February 21, 1980.

5. U.S. Department of Energy, Technical Support Document No. 4, Economic Analysis, Energy Efficiency Standards for Consumer Products, Conservation and Solar Energy, Office of Buildings and Community Systems, Washington, D.C., June 1980.

6. I. Turiel et al., op. cit.

7. Science Applications, Inc., Regional Versus National Standards for Room Air Conditioners, Central Air Conditioners, Heat Pumps and Furnaces, La Jolla, Calif., November 30, 1979.

NEW DATA APPLICABLE TO THE ORNL RESIDENTIAL ENERGY DEMAND MODEL*

H. Herring

INTRODUCTION

The Oak Ridge National Laboratory (ORNL) Residential Energy Model has been widely used to forecast energy demand and to evaluate the impacts of federal energy conservation policies. The model has been criticized as inadequate in a number of areas. The objective of this work has been to make selected improvements in the model as a first step in a longer-term effort to substantially upgrade its accuracy, reliability, and sensitivity to a range of realistic input assumptions.

A model is only as good as its input data, and much of the input data to the model is poorly documented. Thus, one of our major objectives has been to improve the data inputs. These are major inputs to the model.

1. Appliance saturations by house type, both in the existing housing stock and in new homes.

2. The annual energy use of stock and new appliances.

3. The average lifetime of appliances, and hence the rate at which appliances are retired and are replaced by new ones.

4. The energy efficiency of stock and new applicances.

5. The price of fuels and their expected escalation rates.

6. The price of new appliances.

7. The thermal integrity of stock and new buildings.

ACCOMPLISHMENTS DURING FY 1980

Retirement Rates for Appliances

An important input to the ORNL Model is the rate of retirement of old appliances. Currently an exponential equation of the form

$$YKAP = 1 - e^{(-1/TEQ)}$$

is used, where TEQ is the average life of the appliance, and YKAP is the fraction retired each year. Thus the fraction surviving after n years is $(1-YKAP)^n$. Figures 1 and 2 show the retirement

* This work is supported by the Systems Analysis Division, Office of Buildings and Community Systems, U.S. Department of Energy under Contract No. W-7405-ENG-48.

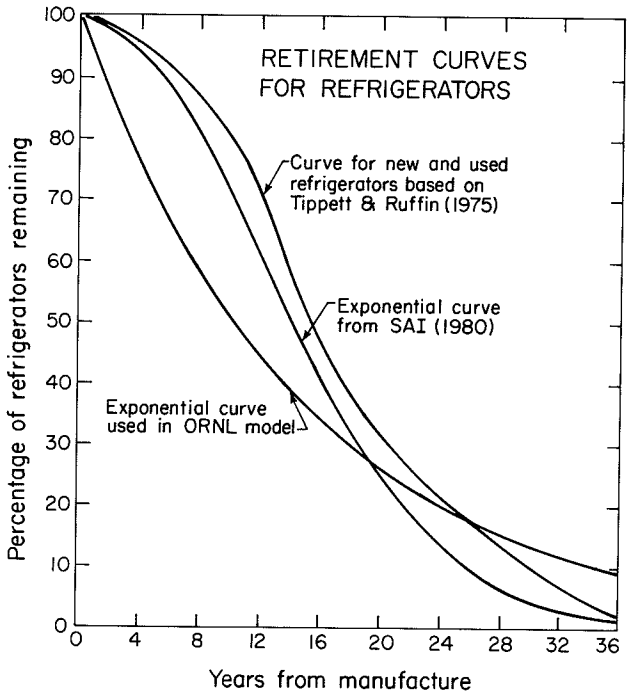

Fig. 1. Retirement curves for refrigerators. (XBL 8012-2467)

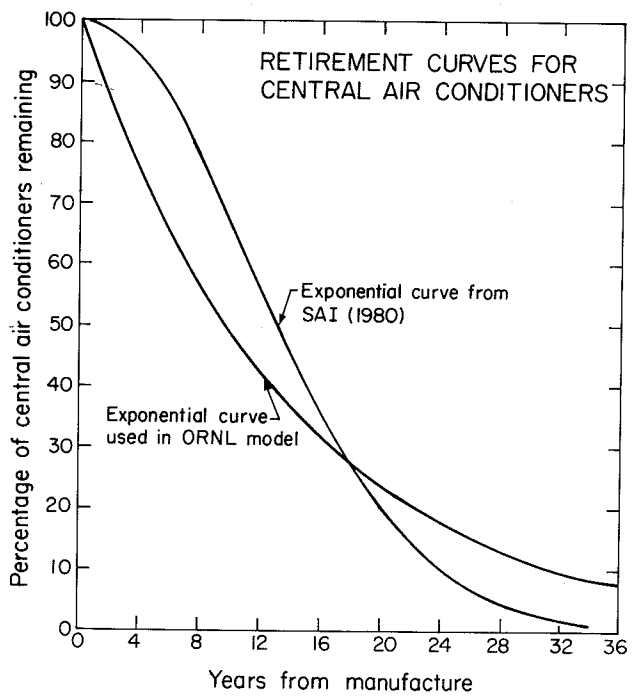

Fig. 2. Retirement curves for central air conditioners. (XBL 8012-2468)

rates for refrigerators and central air conditioners. The curve using the ORNL equation leads to a rapid decline in the early years of the appliance's life, and a slow decline in the later years.

Using the above exponential equation to specify retirement rates in the ORNL Model reduces energy demand growth more rapidly than should occur, as old, less efficient appliances are quickly replaced by new more efficient ones. A market survey in 1975 by Ruffin and Tippett of 11,696 households throughout the United States provided estimates of the service life expectancy of major appliances having one owner.[1] The data are for new and used appliances. To combine these data into the total life expectancy under all owners (as appliances are resold), one needs to know the rate at which appliances are sold according to their age. This was determined for refrigerators by analyzing the responses to a Market Facts, Inc. survey on appliance ownership and use.[2]

Figure 1 shows the retirement rates for refrigerators. The top curve is based on the work of Ruffin and Tippett, and combines their data for retirement rates for new and used refrigerators. This curve shows refrigerators have an average lifetime of 17.2 years. From their data on the average lifetime of new refrigerators (15.2 years) and of used refrigerators (7.4 years), one can calculate a resale rate of 26%.

The other two curves in Figure 1 are exponential curves based on a refrigerator lifetime of 15 years, which is currently used in the ORNL model. An alternative functional relationship can be used to better fit observed data:

$$N = N_o . e^{(-0.693\ t^2/T^2)}$$

where N is number of appliances remaining at t years, N_o is original number at t = 0, and T represents the time at which half of the original appliances have stopped operating. T is related to the average lifetime of all appliances, t_{ave}, by

$$t_{ave} = \frac{T}{2} . (\pi/\log 2)^{1/2} = 1.064\ T$$

This curve is fairly close to the modified Ruffin and Tippett curve and diverges most from it late in the appliance's life, when the numbers of refrigerators remaining in stock are small. Use of this curve, rather than the current ORNL curve, means that the energy consumed by appliances, is assumed to be greater in the near future as fewer older appliances have retired, and corresponds closer to empirical data than the current ORNL exponential equation.

Figure 2 shows retirement curves for central air conditioners. Unfortunately there are no

market survey data to provide information on retirement or resale rates, and the exponential curves shown are based on a 14-year lifetime, which is currently used in the ORNL Model.

Market surveys provide useful information on appliances ownership, use, and lifetimes. The National Interim Energy Consumption Survey (NIECS), conducted in 1977 and 1978, was particularly useful as actual fuel use was measured for 4081 surveyed households. By cross-tabulating fuel use by house type, house age, appliance ownership, central heating system, and other factors, much valuable information can be extracted which is directly relevant to the ORNL inputs

Total Residential Energy Use

Table 1 and 2 shows the energy consumption by fuel type. The houses in the survey have a wide range of fuel consumption rates, but the mean values for all three "fuels" (electricity, natural gas, and fuel oil/kerosene) are approximately equal. If the mean energy consumption is multiplied by the average fuel saturation, an average annual household energy consumption can be obtained, which is 213.8 million Btu of primary energy. This figure is 5.6% greater than that used in the ORNL model, and provides good support for this portion of the ORNL data base.

Household energy consumption can be cross-tabulated with house type, age, and region, but a good indicator of differing energy use is therms of energy consumed/ft^2 of household area/yr. Data from the ORNL Building Energy Use Data Book and other sources (ORNL/CON-28) give the average floor area of households by housing type and age.[3,4] Table 3 shows that the floor area for all house types has increased; for single-family homes the increase is by 21%; multifamily homes (which includes attached single family homes and apartments) increased by 6%; and mobile homes by 22%.

Table 4 shows energy consumption in terms of therms/ft^2/year. Although in absolute terms new homes use more energy than stock homes (built before 1976), new homes use less than older homes in terms of therms/ft^2/yr. The improvement in energy use varies according to whether electricity is measured in terms of primary energy use (11,500 Btu per kWh) or in terms of building boundary use (3,400 Btu/kWh). Overall electricity consumption has increased by 21% with the greatest increase being in multifamily homes with more than a 50% increase, while single-family homes have had a 32% increase; however, mobile homes show a 42% decrease in electricity use.

In primary energy terms, the total household energy use/ft^2 is greater than if it were measured

Table 1. Energy consumption in the residential sector by fuel type. (10^6 Btu Primary Energy)

	Electricity	Natural Gas	Fuel Oil/ Kerosene
Minimum	1.09	0.2	3.89
Maximum	832.2	599.2	442.3
Range	831.1	599.0	438.4
Median	85.8	111.9	113.2
Mean	111.8	119.0	124.4
Saturation (%)	100	63.1	21.6

Table 2. Average household energy consumption. (10^6 Btu)

Electricity	111.8
Natural gas	75.1
Fuel oil	26.9
Total	213.8

Table 3. Floor area of households (ft^2).

	Stock	New Homes
Single-family	1380	1672
Multifamily	845	895
Mobile homes	780	952
All	1194	1356

Table 4. Energy consumption per ft^2 primary energy units: therms/ft^2/year.

	Electricity	Natural Gas	Fuel Oil/ Kerosene	All Fuels
Stock				
Single-family	0.856	0.970	0.886	1.661
Multifamily	0.843	0.988	1.685	1.950
Mobile homes	1.678	1.777	0.771	2.194
All stock	0.888	0.973	1.029	1.736
New Homes				
Single-family	1.132	1.022	0.666	1.517
Multifamily	1.328	1.166	0.0	1.888
Mobile homes	0.977	0.899	0.634	1.601
All new homes	1.074	1.039	0.727	1.557

in building boundary units. Table 5 shows how new homes compare to stock homes in energy use. Mobile homes show the greatest decrease in energy use/ft^2, with single-family homes second and multi-family homes last. Energy use at the building boundary has decreased much more rapidly than primary energy. The reason for this is the switch away from natural gas and fuel oil for central space heating towards electricity.

Table 6 shows estimates of central space heating (CSH) fuel saturations by house type derived from the NIECS survey tape. There has been a dramatic switch from natural gas (55.4% of all CSH systems in older houses) to electricity 86.3% of all new CSH systems in 1978). The use of fuel oil has declined in all homes (from nearly 25% of the CSH systems), while electricity has almost doubled; it now provides a third of the fuel for CSH systems in new homes. The figures in parentheses are the values currently used in the ORNL model; they underestimate electricity CHS systems and overestimate fuel oil systems in older homes. The reverse is true for new homes, particularly for mobile homes where gas CSH systems are vastly underestimated.

Table 7 shows the saturations of fuels, for all end uses in homes.

Electricity use is practically universal in the United States: only one of the 4081 homes surveyed had no electricity. Gas is found less frequently in new single- and multifamily homes, but most often in mobile homes where it is the most common source of heating. Fuel oil has declined rapidly in popularity among new homes and was not used at all in the 46 new multifamily homes surveyed.

The fact that energy used/ft^2 has not declined as much as might be expected due to more stringent building insulation standards (for new homes than for old homes) probably results from the use of higher levels of space conditioning and a greater saturation of energy consuming appliances.

Mobile homes show the greatest decrease in energy use/ft^2, and are now about equal in energy use to single-family homes. This could be due to increased use of insulation measures compared to other housing types, and because of the shift away from electricity to natural gas.

Further analysis of the NIECS data will show fuel use and type for water heating and for cooking; regional fuel variations; saturations of appliances; and fuel use variations according to the presence (or absence of insulation).

Table 5. Comparison of new homes to stock energy use (therms/ft^2/yr).

	Primary Energy	Building Boundary Energy
Single-family	0.913	0.681
Multifamily	0.968	0.703
Mobile homes	0.730	0.554
All homes	0.897	0.721

Table 6. Central space heating fuel saturations by house type (%).

	Electricity		Natural Gas		Fuel Oil/ Kerosene		Other	
Stock								
Mobile homes	17.5	(12.3)	64.7	(39.5)	15.7	(22.2)	2.1	(25.9)
Single-family	16.8	(7.7)	60.8	(62.4)	20.7	(25.7)	1.7	(4.2)
Multifamily	17.1	(12.6)	55.4	(51.0)	26.2	(35.2)	1.3	(1.2)
All stock	16.9	(9.4)	59.4	(57.8)	22.0	(28.4)	1.7	(4.4)
New Homes								
Single-family	36.3	(42.1)	48.8	(48.6)	13.6	(6.9)	1.4	(2.3)
Multifamily (1978)	86.3	(58.0)	10.5	(33.4)	2.8	(8.0)	0.3	(6.0)
Multifamily (1976)	24.9	n.a.†	58.0	n.a.†	15.5	n.a.†	1.7	n.a.†
Mobile homes	10.9	(56.8)	69.1	(26.0)	18.0	(5.1)	1.9	(12.1)
All new homes	33.3	(48.1)	51.1	(42.5)	14.2	(7.2)	1.3	(2.2)

* Figures in brackets are those for 1977 CSH saturations, units, and existing units, from ORNL model.

† n.a. = not available.

Table 7. Saturation of fuels by house type (%).

	Electricity	Natural Gas	Fuel Oil/ Kerosene
Stock			
Single-family	100	62.5	22.4
Multifamily	100	77.1	20.5
Mobile homes	100	24.8	29.1
All stock	100	64.3	21.6
New Homes			
Single-family	100	32.0	8.7
Multifamily	100	48.0	0.0
Mobile homes	100	64.0	7.7
All new homes	100	42.0	6.4

Table 8. Number of cases in survey: house types.

	Stock	%	New Homes	%
Single-family	2568	66.3	114	58.2
Multifamily	1072	27.7	46	23.5
Mobile homes	234	6.0	36	18.3
Missing cases	11			
Total cases	4081			

PLANNED ACTIVITIES FOR FY 1981

The work will continue to analyze all data applicable to the projection of residential energy demand, in an effort to improve the quality of the ORNL energy demand model. The main emphases of the work will be on the following tasks:

- Continued use of the NIECS data base, and disaggregation of energy use among space conditioning and appliance uses.
- Gathering and analysis of data applicable to electric utility service areas.
- Improvement of regional energy use data bases applicable to ORNL model.
- Gathering and analyzing data to improve specific aspects of the ORNL model (e.g., retirement functions, demand elasticities, equipment saturation, fuel splitting ratio's).

REFERENCES

1. M.D. Ruffin and K.S. Tippett, "Service Life Expectancy of Household Appliances: New Estimates from the USDA," Home Economics Research Journal, vol. 3, no. 3, March 1975, pp. 159-170.
2. Market Facts, Inc., Appliance Survey, 1975 (Chicago, Ill.: MFI).
3. Oak Ridge National Laboratory, Buildings Energy Use Data Book, ORNL-5552 (Oak Ridge, Tenn.: Oak Ridge National Laboratory, December, 1979).
4. P.F. Hutchins and E. Hirst, Engineering Economic Analysis of Mobile Homes Thermal Performance, ORNL/CON-28 (Oak Ridge, Tenn.: Oak Ridge National Laboratory, October 1978).

ASSESSMENT OF ENERGY DEMAND MODELS*

D. Freedman, T. Rothenberg, and R. Sutch

INTRODUCTION

The main objective of this project is to describe and assess the midterm demand used in forecasting by the U.S. Energy Information Administration, to help users reach informed judgements about the probable accuracy of the forecasts. So far, the work has been largely qualitative. However, procedures are being developed to permit a quantitative assessment of some kinds of forecast uncertainty. These procedures may also facilitate the development of simpler and more robust forecasting models.

ACCOMPLISHMENTS DURING FY 1980

A major activity in FY 1980 was the assessment of the Regional Demand Forecasting Model[1] (RDFOR) and its data base, the Federal Energy Data System (FEDS).[2] This work can be summarized as follows:

An Overview of RDFOR

RDFOR forecasts what demand would be in a future year for each type of fuel, by consumption sector and geographical region, as a function of a vector of sector- and region-specific future prices. The demand surface has a constant matrix

* This work was supported by the Office of Analysis Oversight and Access, Office of Applied Analysis, Energy Information Administration, U.S. Department of Energy, Washington, D.C. under Contract No. W-7405-ENG-48.

of own- and cross-price elasticities. Thus, the demand surface can be defined by specifying one point on it, together with a matrix of elasticities. The model has three components:

1. A system of log-linear demand equations whose parameters have been estimated using econometric regression techniques from historical data;

2. A procedure which employs the demand equations to derive the matrix of own- and cross-price elasticities defining the shape of the forecasted demand surface.

3. Another procedure which employs the demand equations to derive the matrix of own- and cross-price elasticities defining the shape of the forecasted demand surface.

The demand model (1) is the structural heart of RDFOR. It consists of a system of equations which set the log of quantity of fuel "demanded" (i.e., apparent consumption) equal to a linear function of the log of price and other variables. This model is dynamic in the sense that it involves lagged independent variables and imposes a time-dependent structure on the stochastic disturbance terms over the fitting period.

RDFOR recognizes ten DOE regions, four consumption sectors (residential, commercial, industrial, transportation), and 13 types of fuel (coal, natural gas, electricity, gasoline, distillate oil, residual oil, etc.). Estimates of the parameters are made for each sector and region. The total fuel demanded in each sector and region is predicted first, as a function of the average price of energy for that sector and region and certain other explanatory variables (such as population and income). The total is then shared out to individual fuels, with the share for each fuel depending on the price of that fuel relative to the average price of energy. Prices are taken as exogenous by RDFOR.

Data

RDFOR is fitted to the FEDS data base. This source contains most of the annual data required by the model for the period 1960-78. Reviews of FEDS[2] come to the following conclusions. Much of the data in FEDS is synthetic: the numbers are the result of imputation rather than measurement. Allocations to consumption sectors are often questionable, and the price series quite unreliable. The consumption sectors are sometimes inconsistently defined, especially with reference to agriculture, transportation, and government. The problem is most acute in the definitions of the so-called "extended" sectors. The deficiencies in FEDS could have serious consequences for RDFOR: namely, errors in the data could cause large errors in estimates of the coefficients, and hence in the forecasts. Furthermore, use of synthetic data seriously compromises the validity of the standard statistical procedures used to measure precision in estimates.[3]

Logical Structure

RDFOR is used to predict demand almost 20 years in the future. It extrapolates from a past of energy abundance into a future of energy scarcity. Under these circumstances, the choice of functional form is critical. The equations chosen by the architects of RDFOR cannot be derived from economic theory, or from detailed knowledge of the fine structure of the energy market. At best, these equations can be described as reasonable guesses, or convenient approximations. However, many different equations would be equally reasonable, and would fit the data equally well. Each set of equations would produce a different set of coefficient estimates, and hence a different set of forecasts.

When a model is used to extrapolate, its technical assumptions may have a major impact on the results. This point is illustrated in Figure 1, for the trend of (computer-generated) data against time. The straight line and the exponential curve both track the data quite well during the fitting period (1960-1980). But by the year 2,000, the exponential curve has gone off the graph.

The results obtained from RDFOR seem to be quite sensitive to the choice of indices,[4,5] the level of aggregation, and the functional forms assumed for the demand equations.[3,6] Simulation studies can be used to investigate the sensitivity of a model to its technical assumptions. In preliminary experiments with RDFOR-like equations, dropping the lagged income and weather variables tripled the estimated long-run own-price elasticity. These equations were fitted using Btu-totals for quantities, and Btu-weighted averages on prices. Moving to divisia indices (as used in RDFOR) tripled the elasticity again. Technical assumptions matter.

The choices made in RDFOR are somewhat arbitrary. On balance, it seems that rising energy prices will probably lead to more substitution of labor, capital, and technology for energy than the model suggests. In part, this view is based on the rigidities in the equations. And in part, it is based on the fact that not much substitution occurred during the fitting period. The arbitrariness in the choice of functional forms for RDFOR constitutes a major source of uncertainty in forecasts derived from this model.

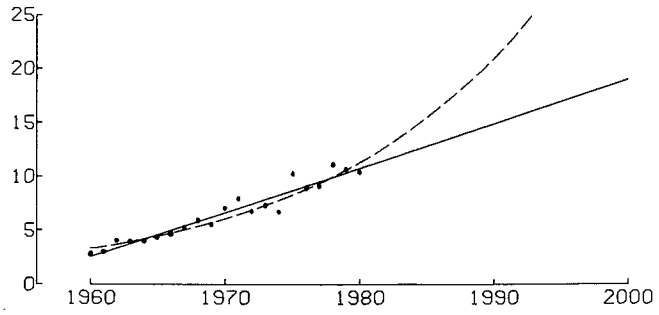

Fig. 1. In extrapolations, functional form matters.

Statistical Methods

The econometric and statistical methodology used in RDFOR is questionable. For example, the simultaneity of supply and demand is ignored; the constraints imposed on the coefficients are hard to justify; likewise, the assumptions on the stochastic disturbance terms seem arbitrary. These terms probably represent the effect of omitted variables and other specification errors. As such, strong correlations across fuels and across sectors may be expected. RDFOR ignores these correlations, and this may lead to serious errors in the estimates and in forecasts.

The strongest criticism of the methodology, however, is that RDFOR is over-fitted to the data. For example, the total industrial demand equation is fitted using generalized least squares, to account for interregional covariances. There are 10 regions and 17 years of data, from which are estimated 26 parameters, 10 variances, and 45 covariances.

RDFOR's many parameters allow it to track the historical data with artificial and misleading precision. As a result, small errors in the data, or small revisions to the data, are likely to have a disproportionate impact on the coefficient estimates. That is, the coefficient estimates are likely to be subject to large random errors. And unless the specification is exactly correct, which seems implausible, specification error can introduce large biases. This is illustrated in Figure 2. If the three points really follow the straight line, putting in an extra coefficient and fitting a parabola has very bad consequences. RDFOR seems to be doing exactly this sort of thing, in several hundred dimensions.

The statistical instability in RDFOR's structure was demonstrated in the simulation results described. The instability can also be seen by comparing the coefficients estimated in 1978 with the ones estimated in 1977. For example, in the total demand equation in the industrial sector, the long-run price elasticity estimated in 1978 was triple the one estimated in 1977, due to the addition of one data point and the revision of another.

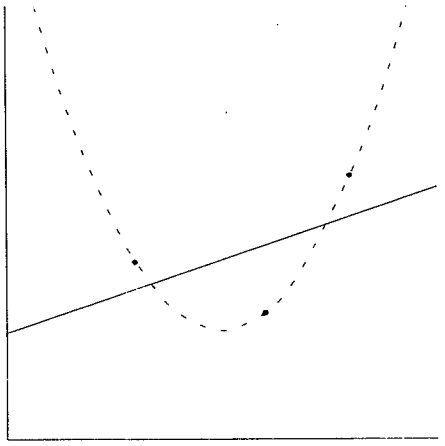

Fig 2. Over-fitting can cause serious bias.

PLANNED ACTIVITIES FOR FY 1981

In 1981, other demand models will be reviewed, including the Oak Ridge model of the residential sector.[7] Also, an effort will be made to develop some quantitative measures for the statistical uncertainty in the forecasts and the parameter estimates. The most promising technique is the "bootstrap," which is explained in detail elsewhere.[8,9,10] This technique involves stochastic simulation, to test the model against its own assumptions.

In brief, the model has been fitted to data by some statistical procedure, and there are residuals, or discrepancies between actual and fitted values. Some stochastic structure was imposed on these residuals, explicitly or implicitly, in the fitting. The key idea is to resample the residuals, preserving this stochastic structure.

Assuming the model and the estimated parameters to be right, the resampling generates "pseudo-data," both for the past and for the future. Now the model can be refitted to the pseudo-data for the past and used to "forecast" the pseudo-data for the future. In this artificial world, the error of forecast, and the errors in the parameter estimates, are directly observable. The Monte Carlo distribution of such errors can be used to approximate the distribution of the unobservable errors in the real parameter estimates and in the real forecasts. This gives a measure of the statistical uncertainty in the parameter estimates and the forecasts.

A variation on this idea can be used to compare two models, testing each one against the assumptions of the other. This involves generating the pseudo-data with one model; the second model is refitted to the pseudo-past, and used to predict the pseudo-future. Then the roles of the two models are interchanged. In this way, the bootstrap can be used to select forecasting equations which are relatively insensitive to specification error.

REFERENCES

1. D. Freedman, T. Rothenberg, and R. Sutch, The Demand for Energy in the Year 1990: An Assessment of the Regional Demand Forecasting Model, Lawrence Berkeley Laboratory report LBID-199, 1980.

2. D. Freedman, T. Rothenberg, and R. Sutch, An Assessment of the Federal Energy Data System, Lawrence Berkeley Laboratory report LBID-202, 1980.

3. D. Freedman, Some Pitfalls in Large Econometric Models (to appear in the University of Chicago Journal of Business), 1981.

4. J. Hausman, Project Independence Report: An Appraisal of U.S. Energy Needs up to 1985, Bell Journal of Economics, vol. 6, 1975, pp. 517-551.

5. H.D. Nguyen and R.W. Barnes, An Evaluation of the Midrange Energy Forecasting System, Technical Report (Oak Ridge, Tenn.: Oak Ridge National Laboratory, 1979).

6. D. Freedman, Are Energy Models Credible? (to appear in the proceedings of the National Bureau of Standards/Department of Energy conference on energy models,) 1981.

7. E. Hirst and J. Carney, The ORNL Engineering-Economic Model of Residential Energy Use, ORNL/CON-24 (Oak Ridge, Tenn.: Oak Ridge National Laboratory, 1978).

8. P. Bickel and D. Freedman, Some Asymptotic Theory for the Bootstrap, Technical report, (Berkeley, Calif.: Department of Statistics, University of California, 1980).

9. B. Efron, Bootstrap Methods: Another Look at the Jack-knife. Annals of Statistics, vol. 7, 1979, pp. 1-26.

10. D. Freedman, Bootstrapping Regression Models, Technical report (Berkeley, Calif.: Department of Statistics, University of California, 1980).

ENERGY DEMAND AND CONSERVATION IN KENYA: INITIAL APPRAISAL

ENERGY DEMAND AND CONSERVATION IN KENYA: INITIAL APPRAISAL*

L. Schipper† *and J. Hollander*†

INTRODUCTION

One of the most important factors in the growth in world oil consumption since 1972 has been the economic growth of the developing world. While a few nations account for most of the increase in oil use, all developing countries (LDCs) find that oil is an important ingredient in today's economic growth. Unfortunately, little is known of the nature of the demand for oil and other fuels traded commercially on world markets.

In this research, we take a detailed approach to accounting for energy end uses. We disaggregate important energy end uses according to various economic variables or physical activity levels (miles driven, tons produced, households) and into energy intensities (joules/mile, joules/ton, kWh/household).

To do this is to pay particular attention to the economic and demographic structure of the country: How many autos are there, and how far are they driven? How much steel is produced by individual plants and at what energy intensity? How many people visit a particular hotel in a particular year? In this way we can relate energy demands to specific economic activities that are often directly related to the degree of economic development in Kenya, particularly in the cities. This methodology arose in consideration of energy use in developed countries, such as in the study of the U.S. and Sweden published by Lawrence Berkeley Laboratory in 1976.[1] As in that study, the goal of the present work is to first account for energy flows, then to find examples of energy conservation in practice, and finally to make appropriate recommendations for further analysis and implementation of conservation in the modern sector of Kenya's economy.

Conservation in Developing Countries

Why should developing countries worry about energy efficiency and conservation? It is often contended that their per capita use among the people and institutions actually coupled to the market economy is so little that there is literally nothing to conserve. We found the opposite to be the case. Many factory managers and buildings experts were concerned about the cost of energy; government officials and oil company planners were worried about the cost to Kenya of importing increasing amounts of increasingly expensive oil. Ironically, the East African Oil Refinery (EAOR) was a profitable earner of export dollars before the oil embargo, since a large portion of the crude refined there was reexported, the profits paying for the net outflow of hard currency to buy all the crude. The oil embargo and subsequent price rise changed that situation.

The other important concern expressed in Kenya is over the commercial/noncommercial interface among energy supplies. Most world statistics only count commercially-sold energy, particularly that energy used in activities that are accounted for in the nominal GNP. Of course, there is intense competition among commercial and noncommercial

* This work is supported by the Beijer Institute, Stockholm; by the Lawrence Berkeley Laboratory under Contract W-7405-ENG-48; by Resources for the Future, Inc.; and by the Agency for International Development of the U.S. Department of State.

† Also associated with the Beijer Institute of Energy and Human Ecology, Stockholm.

energy sources--deforestation and high-cost charcoal may make commercial gas cylinders or solar cooking the only viable options for rural families who cook; low-cost commercially sold wood replaced oil (until recently) in one of the manufacturing firms we visited; bark could serve as a firing fuel for a paper mill we visited except that it proved to be cheaper in the past to debark trees where they were cut, by hand, and leave the residue behind. Oil is used instead to raise steam at the mill.

Much interaction and potential substitution exists among commercial and noncommercial or renewable energy sources. The problem is just that the average Kenyan, whether rural or urban, has little income with which to buy equipment that would make electric or gas cooking possible; has little choice in how efficient higher-cost wood is turned into charcoal; and must interact with a market economy that is more or less dependent on the inflow of commercial imported oil for its health. Better understanding of the efficiency of end-use energy in Kenya, and recognition of the many ways in which commercial and noncommercial energy sources, efficiently deployed, could complement each other, may be the key to Kenya's energy future. For as oil prices rise, internationally, Kenya, like the countries of the OECD, may find that as all other energy sources are also rising in cost, the most effective weapon against these costs remains energy conservation, the effective use of all forms of energy.

End Use Analysis

Industrial Energy Use

There exists no detailed surveys, by firm or product, of industrial energy use in Kenya. However, we found very quickly that the requisite data exist, given the relatively small number of firms listed in the Directory of Industries (1974 and 1977 editions). We did not have time to survey electricity and fuel use of each type of producer, but were able to sample data from individual firms, oil companies, and the East African Power and Light Company (EAPL). Finally, we conducted on-site interviews with engineers responsible for heat and power in more than a dozen important firms. Eventually we plan to completely classify energy use in Kenyan industries and measure energy intensities, and thereby the potential for increased energy efficiency in industry.

Table 1 gives an overview of energy intensities in key firms. For several years, data or

Table 1. Industrial energy intensities.

Type	Electricity (kWh)	Fuel (10^3 Btu)	Output Unit	Year	Notes (Oil Types)
Lorries	*	1850	Lorry	1978	--
	610	1690		1979	--
Tires	1.1	15.0	Pound	1975	Residual
	0.74	9.65		1978	--
	0.71	8.40		1979	--
Oil refining	11.5	1480	MTon	1973	Crude losses
	16	1480	MTon	1977	--
Cement					
1.	77.0	5000	MTon	1975	Residual
	81.2	5300	MTon	1977	--
	73.8	5200	MTon	1979	--
				1976	--
2.	105	3100	MTon	1977	--
				1979	--
				1976	--
3.	95	3600	MTon	1977	--
				1979	--
Paper	-	4500	MTon	1977/78	Purchase
	105	4170		1978/79	electri-
	196	3675		1979/80	city only
Hotel					
1.	16.1	130	Guest-day	1975	Distillate
	14.3	97	--	1979	(compared with 1975)
2.	35.5	290	--	1977	--
	23.7	240	--	1979	--

* Auto assembly electricity data omitted where meter was not functioning.

comparative figures from other parts of the world are given. The EAOR increased its size after 1973 but did not increase output. Consequently efficiency fell. A conservation program regained some of these losses. As output increases, the energy intensity will fall again. Given the rapid pace of growth of industry in Kenya, we expect to see new technologies in other industries that will allow output to increase considerably faster than energy use, particularly as energy prices rise.

Commercial Buildings

Commercial buildings include many kinds of enterprises; the most important for Kenya are public services (schools, hospitals), hotels and restaurants, office buildings (including governmental buildings), and stores. Some of these enterprises are described in Table 2. In the case of one major hotel, we found that overall electric power use per guest per year had decreased substantially from 1976 to 1979, in part due to the recent initiation of a conservation campaign. The drop in electricity use is dramatic, as indicated in the bottom of Table 1.

Homes

Commercial energy use in the residential sector is characterized by extreme concentration into a small fraction of all households. Complementing this situation is the relatively minor but growing use of kerosene for lighting and cooking and for somewhat greater use of cylinders. For cooking, the majority of Kenyans use charcoal as fuel for domestic purposes. This use may be as great as five times the sum of all commercial energy use. (Table 3)

We have been able to analyze electricity use further, using data from EAPL. The largest residential consumers register their electricity consumption for water heating on a special tariff (with an electronic signal interrupter). In 1976 there were 27,000 hot water customers, 51,000 regular residential customers (including the hot water), and 56,000 customers using very little electricity, most living in rural areas or in low-income estates. The designated income group for each housing tract, however, does not always reflect the incomes of the people who actually live there, due to subleasing. Similarly, data of wealthy households include use of energy in servants' quarters.

What is missing from this electricity use picture is the complementary use of fuels. While electric cooking probably dominates in those homes in the first row of the table, it is clearly absent in the case of small users, or for those for whom charcoal, kerosene, or in some cases gas is more important. One house we visited had switched from gas to charcoal, because the gas stove had exploded. We obtained an estimate of country-wide kerosene and liquid petroleum gas (LPG) consumption from Kenya Shell. This estimate includes sales of small lots of packaged kerosene and bulk kerosene sold for resale, as well as lots of small gas cylinders. We may have overestimated consumption of these two fuels in the residential sector since

Table 2. Provisional breakdown other electricity uses.

	Customers	Price/kWh (Kenyan cents)	Total Sector (10^6 kWh)	Remarks
Commercial				
Small[a]	20,000	55	132	1976
Large[b]	400	55	140	1976
Large industry	490	27.3	356	1976
Agriculture Nairobi (large estates)	50	40	13	--
Elsewhere	50			--
Nairobi Only				
Hotels	24	35	19.6	1977
	25	45	14.4	1978
(Coastal Region)	40	--	23.9	1978
Hospitals			15.7	1977
Offices, Banks (excluding government)	22	50	11.4	1977
	22	60	12.6	1978
(New customers only)	3	60	1.9	1978
Kenyatta Center	--	--	2.7	1977

[a] Mostly shops.
[b] Mostly large buildings, schools, some light manufacturing.
[c] Agriculture includes farms and estates.

Table 3. Residential energy, 1978.

Type	Customers	Price KC*	Use/Year (kWh)	Year
			Per Customer	
Regular electricity	51,000	33	3,000	--
Small users (electricity)	56,000	125	250	--
Hot water (electricity)	22,000	18	4,815	--
			Total Country	
Gas cylinders	--	--	90 GWh	1977
			103 GWH	1978
Cooking and lighting	--	--	405 GWh	1977
Oil	--	--	645 GWh	1978

*KC = Kenyan cents.

small stores or restaurants may use small quantities of these fuels as well.

The prospects for solar water-heating in Kenya are bright. We examined the records of one of the major assemblers and suppliers of solar water heaters. Based on an estimate that he has installed 2000 m^2 of collector thus far (with each m^2 providing about 9000 Btu/day of hot water), we find that installed residential and commercial hot-water systems save Kenya about 1.5×10^6 kWh/yr that would have been required in the form of electricity (more if required as gas or oil, for heating this water). Moreover, a great deal of this electricity would be under normal commercial tariff, in that the electricity is used in schools or hospitals. The total investment cost for these collectors has been approximately 3×10^6 Kenyan Schillings (KS). If normal tariff electricity cost 50 Kenyan cents (KC)/kWh in 1979, then the yearly savings to Kenya from this investment is approximately 750,000 KS.* The manufacturer we interviewed pointed out that business was booming, and provided us with the examples of new projects (a school, a hospital, and a condominium) that he expected to complete soon.

Conservation in Kenya

We noted at several sites that energy conservation programs were in progress. In every case, the person responsible cited higher prices for fuels and electricity as the primary motivation. As to our pessimism over the lack of interest on the part of some firms, it is well known from economic observations that the response to a price increase, be it steady or on-time, takes between a few and tens of years, to take effect. The reason is simply that the greatest changes in energy use take place with the least cost when new equipment is built. Thus the evidence we have seen so far indicates conservation is beginning to take place in Kenya. But we found many opportunities worth investigation. We noticed several buildings that could be retrofitted to reduce solar gain and hence air conditioning needs. We also note that homeowners can implement the following conservation measures: (1) add insulation to hot water heaters (in the U.S. some utilities now provide this as a service), (2) shade windows, (3) keep refrigerator coils clean, and (4) make a conscious effort to reduce the number of miles driven.

Since the beginning of 1979, energy prices have begun to rise in real terms in Kenya. Our visit in the summer of 1980 came after a severe drought had limited electricity use. We found interest in conservation more abundant than ever before, and some of the efforts of 1979 are reflected in the data in Table 1. In FY 1981 we will complete as many details as possible in the end-use balance for Kenya to identify more trends in conservation, and we will interview personnel at up to fifty factories and a dozen hotel organizations to chart the progress in conservation, as well as to investigate past and future possibilities for solar hot water heating in Kenya.

Foreign Trade and Embodied Energy

An extremely important source of energy often omitted from national data is the energy incorporated in imports and exports. A brief calculation

* This calculation assumes no standby losses for either system. We count only the hot water actually made available by solar systems. If all this were produced from the low cost interruptible tariff, the savings would be considerably less, on the order of 300,000/year. Either way, the rate of return is greater than 10%.

based on the known balance of nonenergy trade between Kenya and the rest of the world suggests that Kenya imports more energy embodied in goods and services that is exported. This is not at all surprising, but should be noted in any study looking at end uses of energy.

REFERENCE

1. L. Schipper and A.J. Lichtenberg, Efficient Energy Use and Well-Being: The Swedish Example, Science, vol. 194, no. 4269, 1976, pp. 1001-1020.

INTERNATIONAL RESIDENTIAL ENERGY CONSERVATION*

L. Schipper and A. Ketoff

INTRODUCTION

International comparisons of residential energy use have been hindered in the past by lack of data and common measuring systems. In this paper we report on ongoing efforts to disaggregate data on residential space comfort and appliance energy use for major member countries of the Organization For Economic Cooperation and Development (OECD). Indicators of residential energy consumption sector structure (i.e., dwelling size, number of appliances, incomes) and of intensity of energy use (i.e., energy use per degree day, etc.) are developed and compared for various countries. Comparisons among countries suggest that, in certain countries, much scope exists for energy conservation by reductions in energy intensity. At the same time, rising incomes in many countries allow greater use of heating, hot water, and appliances. Success in predicting future demand depends on our ability to separate the factors that have contributed to energy demand growth in the past, including greater efficiency, from those that will determine energy demand growth in the future.

Since FY 1979, LBL has been investigating residential energy use in major industrialized countries† in an effort to increase the Department of Energy's knowledge of the factors that shape worldwide demand for oil and other forms of energy. Since there has never been an international data base covering residential energy use, the LBL team began by collecting primary data on economic and demographic features of the major countries in the study.[1] At the same time, we examined the factors that seemed important a priori in shaping residential energy demand--factors that were usually overlooked in the cursory analyses of residential energy use or fuel consumption that have appeared in various placed during the past few years.[2] Our disaggregated approach follows the structure-intensity format used in Schipper and Lichtenberg:[3]

Energy use = Activity level x Energy/unit activity.

Data sources on structure are well known, though often unfamiliar to energy researchers. We found it necessary to study and extract much data from housing ministeries, censuses, utility surveys, and house-building companies. The latter are important because we try to capture not only the state of the building stock in a given year, but also the characteristics of each year's new stock.

Data sources for energy end use estimates have been varied. We encountered ten careful studies of historical demand by function in Germany, several from Japan (and the U.S.), but only one each from Italy, France, and Canada and virtually nothing of a historical nature from Sweden, where information is scattered through a score of unrelated studies. Not surprisingly, then, we turned to unofficial data sources, oil and gas companies, electric utilities, trade associations, housing and census bureaus, academic research groups, even professional societies. While we found studies that have attempted to reconstruct energy end use for at least one key year, we have not found systematic attempts in each country to analyze and understand the overall historical picture.

Our goal is to follow the evolution of space-heating, water-heating, cooking, and appliance energy use by fuel over the 1960-1980 period. Data have permitted partial success; for some countries primary data or analysis of the entire period were forthcoming, while for others little or no information was available. Our analysis of Italy[2,4,5] relied on our own reconstruction of many items of information, while our present effort towards completing the end-use data base[6] includes an effort to rebuild Swedish end-use data from original material[7]. Information from other countries came from sources too numerous to mention, but we have relied on primary data from energy companies, studies commissioned by governments or private institutions, and technical studies of aspects of energy consumption that can be generalized. Not surprisingly, we found little use for so-called official government data; such figures are usually too highly aggregated or poorly defined.

Residential Gas Use

At an early stage in our FY 1980 work we presented a detailed study of the use of gas in

* This work was supported by the Office of Applied Analysis, Energy Information Administration of the U.S. Department of Energy under Contract No. W-7405-ENG-48.

† Canada, England, France, Germany, Italy, Japan and Sweden.

households in several countries.[3] We focused on the physical factors that influence quantities of gas used, such as economic and lifestyle indicators, ownership of equipment, energy intensity of equipment use, gas prices, and conservation potentials. Detailed comparisons of gas use among countries and over time are possible.

We discuss the major uses for gas--cooking, and heating water, and since 1970, space-heating--and how they have evolved during the past two decades. We show the ownership of gas-using devices--the structural component of energy demand--and then examine the intensity of gas use on a per unit output basis. Changes in intensity are important signs of energy conservation. We summarize our findings in Table 1. Included herein are data on households and housing stock that comprised the bulk of our FY 1979 and early FY 1980 work.

While there are good indications that the intensity of gas use is falling, we have little systematic information on what people in each country may be doing to reduce heating gas use.

- For the U.S., the American Gas Association estimates that per household and degree day measures of heating-gas only, decreased 12% during the 1973-1978 period on average compared with 1967-1972, and by 16% in 1977. (The heating season begins in the fall of the year cited.)

- For Canada, Canadian Gas Association estimates an 8% drop in consumption in 1979 compared with 1972, corrected for weather but including all uses. Canada Shell finds a 10% drop in the weather-corrected heating gas consumption for single-family dwellings (SFD) only.

- For France, data from the Agence Pour Les Economies d'Energie show a slight increase from 1973-1977, though there was a clear decrease during the intervening years. Here the effect of rapidly growing central heating probably obscures the true conservation effect.

- For Germany, estimates were unavailable, but an enormous increase in gas central heating, from 1.2 million to 3.6 million dwellings from 1972-1979 was observed. While the centrally heated share of gas-heated dwellings increased from 56% (1972) to 74% (1977), the increase in heating-gas corrected for climate was much smaller, indicating that conservation offset much of the expected increase in gas use per dwelling due to central heat.

- Lifestyle differences that lead to differences in gas requirements for cooking and hot water should be studied. In particular, how much more or less gas per home might be demanded for these uses because of lifestyle changes?

- Technological differences in gas appliances for all uses should be compared from nation to nation. Are there hidden barriers to one country's adoption of another country's device, such as rules regarding venting, capacity or flues?

- Methods developed by LBL should be systematically applied to each country's conservation possibilities, both to compare technologies and costs and to see how large potentials in each country really are.

- Differences in energy-use patterns that have arisen since 1972 in each country should be examined closely, both at the macro level (as in the present work) and systematically at the micro level through metering, surveying, and interviewing. We will do this work in the near future.

The study of gas use established the feasibility of reconstructing historical facts of residential energy use using data still existent in archives of energy companies and government bureaus. This knowledge proved useful in our continuing effort to examine all residential fuels and uses.

Overall Residential End Uses

Working from an increasing supply of primary data from the countries under study, we completed our accounting of all fuel and electricity use and began analyzing end use by fuel types. Data on oil and electricity use were on a par with that which we had found on gas, while data on solid fuels were poor. By the end of FY 1980, the data base was substantially complete, and we began to prepare for the Energy Information Administration the completed tables of energy use by fuel of each country's energy use, and a comparison of indicators of energy use across time and countries.

For Italy and Sweden, we were forced to assemble country data from small bits of information scattered through the literature; there is little integrated historical analysis of end use for the period in question. In "reconstructing" residential energy use, we use estimates of unit consumption for appliances and other uses to allocate all energy forms over all end uses. Thus our balances for Sweden separately show cooking, hot water, and electric-only appliances, whereas so-called "official" data give "heat/hot water," sometimes disaggregated by fuel, and "appliance electricity." Gas, which played an important role in cities in the 1960's is all but ignored. Such reconstructions, we feel, show many important facets of energy consumption dynamics that are important to understanding the changes in energy use patterns over the past few years, particularly when the government has made large sums available to consumers for energy conservation projects. Lacking any official breakdowns, we were forced to make our own estimates for Sweden and Italy.

By contrast, integration of rich data from Germany was aided by the appearance of a report

Table 1. Residential gas end use breakdown: preliminary results.

Year	United Kingdom			Canada			Germany			France			Italy			Japan		
	1961	1972	1977	1960	1972	1977	1960	1972	1977	1962	1973	1977	1960	1972	1975	1965	1972	1977
Heating																		
Occupied dwellings (10^6)	15.9	18.9	20.3	4.6	6.5	7.2	16.2	22.0	24.2	14.6	16.9	18.3	12.8	15.5	16.1	20.9	29.4	32.0
Central heat (%)	8	37	51	67	81	84	14	48	57	20	44	58	–	41	43	4	–	12
Gas heat (%)	15[a]	34	55	16	34	37	1.6	12	17	8	15	21	5	18	23	14[f]	25[f]	38[f]
Natural gas and city gas (%)	–	–	51	15	33	36	1.3	9.5	16	8	15	21	5	17	22	–	–	–
LPG (%)	–	–	4	1	1	1	0.3	–	1	–	–	–	0	1	1	–	–	–
Gas central heat (%)	–	14	26	13	31	35	0.3	6	12	1	10	14	–	10	13	–	–	–
Gas/dwelling (GJ)	–	50	–	132	133	122	20	67	67	47	51	52	20	23	24	5	4	3
Gas/dwelling/degree day (MJ)[j]	–	21	–	29	27	27	6	18	20	19	23	26	9	9	11	4[g]	4[g]	4[g]
Total gas (PJ)	–	321	–	97	293	328	5	141	260	55	130	201	8	70	92	15	33	40
Hot Water																		
Gas share (%)	15[b]	26	38	18	30	34	11	18	–	17	23	30	–	12	13	–	125[h]	–
Gas/dwelling (GJ)[k]	–	7	–	37[d]	36[d]	37[d]	10	7	9	12	11	9	–	14	16	–	6[i]	–
Cooking																		
Gas share (%)	66	58	54[c]	20	13	9	40	29	25	43	42	40	80	90	94	0	98	–
Gas/dwelling (GJ)	–	7	–	d	d	d	2	2	–	8	6	5	4	5	5	–	4	–
Total Energy (all dwellings)																		
Total (PJ)	1484	1519	1586	734	1190	1297	1000	1845	1970	686	1523	1540	386	920	1018	526	931	1076
Gas (PJ)	140	479	701	142	369	405	54	185	321	72	273	353	–	167	250	136	347	439
Natural gas (PJ)	0	242	690	⎤	⎤	⎤	0	117	281	⎤	⎤	⎤	⎤	⎤	⎤	⎤	⎤	⎤
Natural gas and city gas (PJ)				136	355	393				38	205	289	–	130	209	96	207	257
City gas (PJ)	137	234	5	⎦	⎦	⎦	48	68	30	⎦	⎦	⎦	⎦	⎦	⎦	⎦	⎦	⎦
LPG (PJ)	3	3	6	6	14	12	6	20[e]	27[e]	34	68	64	–	37	41	40	140	182
Electricity (PJ)	138	313	309	80	199	289	46	200	271	23	108	175	34	90	106	78	218	287

MJ, GJ, and PJ refer to megajoules (10^6J), gigajoules (10^9J), and petajoule (10^{15}J) respectively.

[a]1964 figure.

[b]1966 figure.

[c]Gas also used for refrigeration in 3% of households.

[d]Cooking and water.

[e]LPG excluded from heating. Hot water also uncertain.

[f]Refers to gas stove saturation, including gas heat as secondary system.

[g]Degree Day base 14°C.

[h]Total saturation hot water plus bath water heaters.

[i]Average consumption of both appliances in h.

covering the period of interest by P. Sueding of the University of Koein. For Canada, the major part of the work was done by Canada Shell, to which we added refinements to make Canadian data compatible with that of other countries. Data for recent years from France and Japan was available from various sources, but data for earlier years from these countries and for the UK, where only one year had been carefully analyzed, were incomplete. While our data gathering is complete, we will attempt to make any worthwhile additions or corrections to our data base in FY 1981.

Following the scheme outlined above, we present in Table 2 summary data on residential energy use for all fuels for the countries we have studied. Note that not all countries' data sets are complete at this time; nevertheless the results we cite, based both on our surveying of existing studies and our derivations from other data show the pattern of residential energy use is changing in different countries. We use several summary indicators in this aggregated table:

- Space-heating per household, and per square meter (where possible) normalized to degree days;
- Water-heating and cooking, the two uses with the greatest substitution among fuels and electricity, per dwelling. The reader can derive the per capita values.
- Electric-specific appliances, that is, those that use primarily electricity for motors and very little for heat energy, on a per capita, per houselhold, and per unit of real disposable income basis.

Aside from space-heating, we warn readers against comparisons of energy uses across national boundaries until more is known about equipment, equipment use (e.g., quantities of hot water consumed) and other aspects of lifestyle that bear on energy use. Similarly, little is known about differences in consumer habits, preferences, or lifestyles that may influence consumer responses to changes in incomes and energy prices, the two parameters recognized as the most important determinants of energy use. Finally, many countries have developed differing approaches to conservation, both through research, and through programs of loans, grants, restrictions, or standards. Little quantitative information on the effects of these programs has been developed. Investigating these differences in detail as well as the approaches to conservation and their success, will comprise the bulk of our work in FY 1981.

Preliminary Findings

What does our historical analysis of residential energy use tell us? It is well known that space-heating dominates energy use in most countries. It appears, to the surprise of many, that structural changes, related to increases in income, as manifested in 20-40% increases in living space per capita, large increases in the penetration of modern heating systems, and even increase in the indoor temperatures in centrally-heated homes (in Sweden and Germany) account for much of the increase in space-heating use in most countries in Europe. There is evidence that building shells have become progressively tighter since 1945 in Sweden, and other countries have introduced building codes that should result in great decreases in the intensity of heating in the future. At the same time, the increase in central heating obscures gains made in the efficiency of heating, unless energy uses are carefully disaggregated.

Central heating penetration continues to increase. In 1980, only Sweden, Canada (and the U.S.) exhibit virtual saturation of central heating by any form. Germany is intermediate, France, Italy, and Great Britain are still growing markedly, while Japan remains without central heat. This means that there is still potential growth in heating demand in major countries. Table 2 gives indicators of both space-heating structure and intensity. In future work, we will present estimates of space heating disaggregated further by fuel and dwelling type.

Other Energy Uses

What about measures of activity levels besides those of space-heating? Structural data on appliances are very important for understanding the tremendous increase in electricity use seen during the 1960-1975 period. The dominant cause for this growth is the acquisition of appliances, much more so that the increased energy use or size of individual appliances. For example, data from France, Italy, Sweden, and Germany show little change in annual energy use for electric stoves and, in most cases, for refrigerators. On the other hand, many refrigerators in Europe do not contain large freezing compartments that freeze to -15°C. This feature, common in the U.S. or Canada, increases energy requirements for refrigeration.

In Table 3, we list the saturation of major appliances for most countries in our study. Growth rates for ownership of the major appliances fell typically in the 10-20%/yr. range through the early 1970s. Available information does not tell us all we would like to know about the characteristics of each appliance. Still, it is easy to see that the growth in stocks drives the growth in electricity consumption. And there appears no trend towards American-size refrigerators; American/Canadian levels of hot water consumption; or American-sized washers, dryers, dryers, TV, etc.

Here a difficulty for analysis of behavior and energy use is evident. In fact, it is very important to understand the characteristics and use patterns of major appliances. We suspect that the estimates of annual energy use do not carefully count both technical efficiency and usage patterns. That is, we really do not yet know the quantities and temperatures of hot water consumed by people in various countries. Yet a prescription for motivating consumers to save energy by changing hot-water use requires an understanding of how hot water is used, and where the big--and small--savings through behavior change may be. While today most countries' residential energy use is dominated by heating, the nonheating component in the U.S., Canada, and Sweden is large, and it is growing in other countries relative to heating. Therefore,

Table 2. Residential energy use breakdown: preliminary results.

Year	United Kingdom 1961	United Kingdom 1977	Canada 1960	Canada 1976	Germany 1960	Germany 1977	Sweden 1960[c]	Sweden 1977	France 1962	France 1977	Italy 1960	Italy 1975	Japan 1965	Japan 1977
Heating														
Occupied dwellings (10^6)	15.9	20.3	4.4	7.0	16.2	24.2	2.58	3.58	14.6	18.3	12.8	16.1	20.9	32.0
Persons/dwelling	3.0	2.8	3.9	3.1	3.5	2.6[q]	2.8	2.4[q]	3.2	2.9	3.9	3.5	4.5	3.4
Dwelling area (m^2)	-	80[q]	-	-	67.6	75.1[q]	73.2	81.8[q]	65	72	58	69	72.5	77.1
Single-family dwellings (%)	-	49	65	56[q]	48	45[q]	47	45	62	58	23	29	71	65
Central heat (%)	8	51	67	84	14	57	75	97	20	58	-	43	4	12
Fuel heat (%)	-	-	99	87	99(1)	89(4)	100	65(22)	20[d]	55[d]	71	90	67[h]	97[h]
Fuel/dwelling (GJ)	-	-	140	132	54	70	58	83	73[d]	89[d]	22	70	14	9
Fuel/dwelling/degree-day (MJ)	-	-	30	28	17	21	14	20	24[d]	33[d]	10	33	10[i]	8[i]
Electric heat (%)	0/65	11/72	0.5	13	0	7/33	0	13	0/-	3/4	-	6	16[j]	40[j]
Electricity/dwelling (GJ)	-/3	17/2	79	87	-	33/2	-	75	-	31/45	-	14	2	2
Electricity/dwelling/ degree-day	-/1	8/1	17	18	-	-	-	14	-	12/17	-	7	1[i]	2[i]
Total fuel (PJ)	-	927[q]	413	776	800	1485	226	300	514[e]	1177[e]	201	1019	197	305
Total electricity (PJ)	33	68	2	79	0	70	0	32	1[e]	33[e]	4	14	6	22
Hot Water														
Fuel share (%)	-	66[q]	34	46	28	61	75	87[o]	-	74	-	34	k	k
Fuel/dwelling (GJ)	-	18[q]	-	30	-	9[b]	-	22	-	12	-	16	k	k
Electric share (%)	35	66	47	51	19	39	-	13	11	28	9	42	k	k
Electricity/dwelling (GJ)	7	6	-	23	7	6	-	14	-	7	3	4	k	k
Total hot water/capita (GJ)	-	5.7	6.0	7.7	1.7	2.9	-	8.4	1.4	3.9	0.9	2.0	1.6	3.3
Cooking														
Fuel share (%)	74	63[p]	42[o]	12	89	29	32	2	95	90	94	99	k	k
Fuel/dwelling (GJ)	-	7[p]	-	7[a]	3.8	5.0	-	-	2.4	4.7	3.4	5	k	k
Electric share (%)	35	41[p]	58[o]	88	11	71	68	~98	5	10	6	1	k,l	k,l
Electricity/dwelling (GJ)	5	4[p]	-	3.6	2.5	1.7	2.2	3.1	3	3	3	3	k,l	k,l
Total cooking/capita (GJ)	-	2.1[q]	1.1	1.2	0.9	1.2	-	1.0	0.7	1.4	0.9	1.4	1.7	2.9
Appliances														
Use/dwelling (kWh)	750	1810	1100	4100	215	1535	970	3130	534	1418	220	670	940[m]	1853[m]
Use/dwelling (GJ)	3	7	4	15	1	6	4	11	2	5	1	2	3[m]	3[m]
Use/dollar disposable income (KWh)	0.3	0.2	0.2	0.5	0.02	0.1	0.2	0.4	0.09	0.14	0.1	0.2	0.2[n]	0.1[n]
Total Energy														
Total (PJ)	1484	1586	734	1297	1000	1970	-	379	686	1540	386[g]	1018	526	1076
Gas (PJ)	140	701	142	405	53	321	-	-	72	353	-	250	136	439
Natural gas (PJ)	0	690	⎤	⎤	0	281	-	-			-			
Natural gas and city gas (PJ)			136	393					38	289		209	207	257
City gas (PJ)	137	5	⎦	⎦	48	30	-	4						
LPG (PJ)	3	6	6	12	6	27	-	-	34	64	-	41	140	182
Oil (PJ)	73	147	416	571	111	1106	173	235	158	836	-	622	60	325
Coal (PJ)	⎤	344	⎤	⎤	⎤	28	20	0	⎤	147	-	⎤	66	20
	1132		14	780	172				433			40		
Wood (PJM)	⎦	65	⎦	⎦	⎦	26	10	-	⎦	25	-	⎦	42	5
Electricity (PJ)	138	309	80	289	46	271	26	78	23	175	34	106	78	287
District heat (PJ)	-	-	-	-	10	64	-	52	-	4	0	0	0	0
Electricity (TWH)	38	87	22	80	13	75	6	22	6	49	9.4	29	22	80

Notes to Table 2

"Occupant Dwelling" refers to households except when the number of households is greater than the number of dwellings, as is the case for Germany and Japan in the first year given. "Persons per dwelling" refers to only conventional dwellings from single detached dwellings (including farms) to multiple dwellings, but excludes persons in institutions, military barracks, etc. "Single-family dwelling" definitions vary among countries, but in Sweden, Germany, Italy, and France they include one-and two-family dwellings and row houses. In the United Kingdom, the totals are enlarged by great numbers of the latter. In Canada, row houses are excluded here. In Japan, the definitions do not generally correspond to those in Europe.

In "Heating," fuel heat includes all fuels except district heating. Only for Germany and Sweden, the figures for the district-heated share are given in parenthesis. For France, the figures refer only to central heating. "Electrical heat" refers only to central heating for Canada and Sweden. For the United Kingdom and Germany, the two figures presented show first central, then portable electric heating. For France, the second figure refers to all systems while the first is only central. For Italy and Japan, where central electric heat is insignificant, the figures refer to all systems.

In "Hot water," saturation may add to less than 100% as some homes have none, or more than 100%, because of multiple equipment. In the case of United Kingdom and Japan the totals refer to numbers of appliances per home. In each country a small percentage of homes have no hot water except for kettles.

"Appliances" excludes cooking where possible. We have extracted electric cooking from data from Canada (1000 kWh/yr), Sweden (about 600 kWh/dwelling in 1960, 800 kWh/dwelling in 1977) where sources gave only a total figure. We have also attempted to extract electric water-heating from Swedish data. As small electric heaters are often missed, there is a chance that some of this heating has been counted both under heating and also under appliances.

Fuel totals come from the International Institute of Environment and Development and from the Department of Energy, (United Kingdom); Statistics of Canada and Canada Shell (Canada); Deutsche Esso, BP, and various German reports (Germany); Agence pour les Economies d'Energie and CEREN (France); ENI, WAES-Montedison, and ENEL (Italy); Institute for Energy Economics (Japan). We have separated liquid petroleum gas (LPG) from oil totals in some countries and shown it under gas. Where solids or gases are only given in the aggregate, we give the aggregate figure on the intermediate line.

We give only district heat in those countries and years where it amounts to at least a few percent of total consumption. Dwellings in France, Sweden, and Germany had district heating. The Swedish/German figures for the number of dwellings are given in parenthesis in the breakdown of fuel-heated dwellings. Energy consumption is given in totals. In Germany, 10-12% of the district heating fuel total can be attributed to hot water; in Sweden the amount is about 18%.

MJ, GJ, and PJ refer to megajoules (10^6J), gigajoules (10^9J), and petajoules (10^{15}J), respectively.

[a]Gas cooking and water together. Our breakdown is shown, based on an Ontario estimate of gas used to heat water.

[b]Hot water uncertain.

[c]Demographic data 1960; energy 1963.

[d]Only central heating.

[e]Includes second homes.

[g]These data appear unobtainable. Estimate of total from WAES.

[h]Refers to homes with at least one fuel stove, plus part of the homes that have a gas stove (the other share of gas stoves being owned by homes already considered fuel heated, thus having at least one fuel stove).

[i]HDD base = 14 degree C.

[j]Only stoves, no kotatsu (small heaters for feet) considered.

[k]These data are available only for 1973. For that year, it is possible to know the amount of each fuel for each end use, but not the share.

[l]Electricity is almost not used for cooking tables, only for rice-cookers and microwave ovens.

[m]Includes some electric appliances for cooking (microwave rice cooker).

[n]"Disposable Income" not available, so we use "Private Income."

[o]1961 data.

[p]1972 data.

[q]1975 data.

Table 3. Saturation and yearly consumption: electric appliances in 1977.

	Cooking		Water Heater		Dish Washer		Clothes Washer		Refrigerator and Freezer	
	(%)	(kWh)	(%)	(kWh)	(%)	(kWh)	(%)	(kWh)	(%)	(kWh)
Canada	86	-	50	-	22	-	76	-	99/54	-
West Germany	71.3	600	39.0	1500	15.0	880	88.0	450	140	400/750
France	8.0	875	27.0	1700	12.0	900	72.3	300	91.6	410
Italy	1.2	910	41.0	1080	9.7	1200	75.0	550	97	222
Sweden	95.0	830	15.0[a]	2500[a]	17.0	370	50.0[b]	400[b]	160	660
United Kingdom	44.7	1970	66.1	1575	3.0	465	75.7	195	115	445

Source: Union des Producteurs et Distributeurs D'Electricite (UNIPEDE). German data from Verein der Deutschen Elektrizitaet Werken. Canadian data from Annual Household Surveys. Other Swedish data from Foerening foer Rationella Electricitet Anvaending.

[a]Swedish hot water estimated from central systems in centrally heated all-electric homes.

[b]Building-size appliances are not considered.

the consequences of a careful attempt to reduce nonheating energy use could be much greater in the future. As we suggest, however, that effort will depend greatly on intimate knowledge of how appliances are used.

Our preliminary assessment of available data suggests that the growth in nonheating energy use in residences has been propelled largely by structural growth, i.e., that of incomes. This finding, coupled with knowledge of the saturation of appliances, the characteristics of new models, and the fact that most new kinds of home appliances tend to be nonenergy intensive (i.e., involve little or no use of heat) suggests that future structural changes, i.e., the onset of ownership saturation, will retard the growth in the residential demand for energy, particularly electricity, in the future, relative to rising incomes. The slowdown in the growth of electric appliance energy use relative to income, which we observed in every country, is suggestive that this is taking place already. That is, consumers may not have made great changes in the way they use existing appliances, but the rate of increase in ownership/use of appliances is slowing. Indeed, examination of energy intensities based on heat, hot water or cooking per house or electric appliance electricity per income show marked retardation or cessation in the growth that was so prominent before 1972.

What about appliance energy intensity? As noted above, intensities are difficult to measure so we often settle for annual energy use, a quantity that combines lifestyle with intensity. We show some estimates of average annual electricity use per appliance for several countries (Table 3). We separate obligatory electrical uses--motors, lights--from low-temperature heat applications provided by appliances in Table 2. The data in Table 3 are only rough estimates. Nevertheless, they indicate some agreement among countries. High energy use for washers, for example, may be explained by the fact that some washers produce their own hot water electrically, while others, as is the case in the U.S., take hot water from central tanks. We found widespread use of "point of use" or "instant" water heaters using gas or electricity in Japan, England, France, Italy, and Germany, but we have found no careful study of the differences in efficiency coupled with differences in habits due to around this interesting technology. Thus we must refrain from any comments on intensity here.

Future Residential Energy Demand

Energy prices are now rising, often spectacularly. In Japan, for example, residential electricity prices hit ten U.S. cents/kWh in 1978: they are rising in every other country, though more slowly in Sweden and Canada than elsewhere. However, these prices often fell, in real or even in nominal terms, in nearly every country between 1960 and 1972. Subsidies of certain fuels (kerosene or gas in Japan, electricity in Italy) are disappearing if not already gone; all countries have felt the 1979/1980 OPEC price hikes and the increases in the cost of all forms of base load electric power. Only occasionally are there noticeable decreases in energy prices, not all of which are shown here (e.g., natural gas in England and oil and gas in resource-rich parts of Canada). What economists and engineers alike expect, therefore, is increased interest in technologies that use energy more economically in the home. These should be observable as data from 1979 and 1980 become available. Preliminary analysis suggests that 1978 energy intensities were somewhat lower than those before the oil embargo. The most

dramatic changes in consumption, however, arose after 1978. Examining the changes in consumption since 1973 will form an important part of our FY 1981 work.

CONCLUSIONS

What tentative conclusions do we read from these preliminary considerations? First, we repeat our observation that the rapid rise in fuel and particularly electricity use appears to be caused by rising incomes and increased ownership of energy-using devices. But these devices are saturating even as incomes continue to rise. Hence, we expect considerably less growth in energy use relative to incomes in the future.

Second, there appear to be several levels of energy/electricity use per household or per capita. Comparison across incomes suggests that electricity prices in particular, which seem to vary more than fuel prices, are extremely important determinants of consumption. New appliance costs are also important, but are at this time beyond our study scope. It is no surprise, however, that the Swedes and Canadians consume the most electricity for appliances in both an absolute sense and relative to income. These countries enjoy the lowest electricity prices.

A related conclusion from the data available to use so far is the clear departure from pre-1972 growth patterns. While space-heating use has decreased somewhat in all countries, particularly when the increase in central heating since the embargo is counted, appliance energy use and, in some countries, energy consumed for hot water and cooking has not grown as fast as before. Some of this change is coincidental to the embargo and arises because key uses, such as hot water or refrigerators, have approached saturation.

The prominence of Swedish (and to a certain extent Canadian) low heat losses is not clear from this comparison, because we have not disaggregated space-heating by dwelling type or age and presence or absence of central heating. Available data, however, appear to make this possible for some countries, and measurements of actual groups of homes are available to us from each country studied. But the levels of saturation of central heating in most countries are still growing, suggesting that here space-heating needs will continue to grow, though at a reduced rate. In the future, we hope to include in our survey data that show the space-heating needs of typical new centrally heated homes built before and after the institution of new building norms ushered in after the 1972 oil embargo.

Because the use of electricity for heating may arise out of deliberate government policy, we find it crucial to separate this use, which is growing in some countries, from other uses of electricity. In Sweden, electric heating comprises a major part of the growth in use between 1972 and 1979. Growth in electric heating has also been dramatic in France.

One issue that arises when aggregated data are examined is how to count the resource energy consumed by electric heat. Our scheme, which treats each kind of use and energy source separately, at least in the initial analysis, avoids that problem. In future work we will try to separate the components of growth in each energy source.

Now that most families have acquired the means to use energy for the most important amenities (cooking, hot water, and space-heating using electricity, gas, or liquid fuels; refrigeration, TV, washing devices, minor appliances) conservation need not be seen as a threat to the acquisition of appliances. The prospects for savings based on replacement of inefficient devices with new ones are somewhat bleak until the stock begins to be replaced. The time period for appliances is short; for houses it is very long. We find great room for improving efficiency, even "major appliances" in Europe that are small by U.S. standards.

Our work thus far leads us to certain important ideas about the interaction of consumer behavior and energy use. First, there is an enormous variation in energy use per family for a given end use, a variation too large to be explained only by technology. We suggest that behavior--the way people use hot water, their preference for frozen rather than fresh foods--plays a key role here. But much remains to be quantified.

PLANNED ACTIVITIES FOR FY 1981

In FY 1981 we will perform an econometric analysis of the factors that have influenced consumption during the period of rapid growth (through 1975) and subsequently.

REFERENCES

1. L. Schipper et al., International Residential Energy Use and Conservation Analysis: Structural and Economic Data Base, Lawrence Berkeley Laboratory report LBL-10960, May 1980.

2. L. Schipper, International Comparisons of Residential Energy Use, Proceedings Second International Conference on Energy Use Management, Los Angeles (New York: Plenum Press, 1979); Lawrence Berkeley Laboratory report LBL-9583, 1979.

3. L. Schipper and A. Lichtenberg, Efficient Energy Use and Well-Being: The Swedish Example, Science, vol. 194, no. 4269, December 3, 1976; Lawrence Berkeley Laboratory report LBL-4438.

4. L. Schipper and A. Ketoff, International Comparison of Residential Gas Use and Conservation, Proceedings First International Conference on Gas Technology, Institute for Gas Technology, Chicago, Ill., 1980; Lawrence Berkeley Laboratory report LBL-10896, June 1980.

5. L. Schipper, and A. Ketoff, International Comparisons of Residential Energy Use and Conservation: Data Base and Analysis, Presented at Conference on Energy Conservation and Con-

sumer Behavior, Banff, Alberta, Canada, September 1980 (to appear in the J. Consumer Research).

6. L. Schipper, A. Ketoff, and S. Meyers, Indicators of Residential Energy Use and Efficiency, (in preparation) Lawrence Berkeley Laboratory report LBL-11703, 1981.

7. L. Schipper, Reconstruction and Analysis of Residential Energy Use Data: The Case of Sweden 1960-1980, (in preparation) Lawrence Berkeley Laboratory report LBL-11702, 1981.

SOLAR ENERGY PROGRAM

INTRODUCTION

Solar energy has become a major alternative for supplying a substantial fraction of the nation's future energy needs. The U.S. Department of Energy (DOE) supports activities ranging from the demonstration of existing technology to research on future possibilities. At Lawrence Berkeley Laboratory (LBL), projects are in progress that span a wide range of activities, with the emphasis on research to extend the scientific basis for solar energy applications, and on preliminary development of new approaches to solar energy conversion.

To assess various solar applications, it is important to quantify the solar resource. Special instruments have been developed and are now in use to measure both direct solar radiation and circumsolar radiation, i.e., the radiation from near the sun resulting from the scattering of sunlight by small particles in the atmosphere. These measurements serve to predict the performance of solar designs that use focusing collectors employing mirrors or lenses to concentrate the sunlight.

Efforts have continued at a low level to assist DOE in demonstrating existing solar technology by providing the San Francisco Operations Office (SAN) with technical support for its management of commercial-building solar demonstration projects. Also, a hot water and space-heating system has been installed on an LBL building as part of the DOE facilities Solar Demonstration Program.

LBL continues to provide support for the DOE Appropriate Energy Technology grants program. Evaluations are made of the program's effectiveness by, for example, estimating the resulting potential energy savings. LBL also documents innovative features and improvements in economic feasibility as compared to existing conventional systems or applications.

In the near future, we expect that LBL research will have a substantial impact in the areas of solar heating and cooling. Conventional and new types of high-performance absorption air conditioners are being developed that are air-cooled and suitable for use with flat plate or higher-temperature collectors. Operation of the controls test facility and computer modeling of collector loop and building load dynamics are yielding quantitative evaluations of the performance of different control strategies for active solar-heating systems.

Research is continuing on "passive" approaches to solar heating and cooling, where careful considerations of architectural design, construction materials, and the environment are used to moderate a building's interior climate. Computer models of passive concepts are being developed and incorporated into building energy analysis computer programs which are in the public domain. The resulting passive analysis capabilities are used in systems studies leading to design tools and in the design of commercial buildings on a case study basis. The investigation of specific passive cooling methods is an ongoing project; for example, a process is being studied in which heat-storage material would be cooled by radiation to the night sky, and would then provide "coolness" to the building.

Laboratory personnel involved in the solar cooling, controls, and passive projects are also providing technical support to the Active Heating and Cooling Division and the Passive and Hybrid Division of DOE in developing program plans, evaluating proposals, and making technical reviews of projects at other institutions and in industry.

Low-grade heat is a widespread energy resource that could make a significant contribution to energy needs if economical methods can be developed for converting it to useful work. Investigations continued this year on the feasibility of using the "shape-memory" alloy, Nitinol, as a basis for constructing heat engines that could operate from energy sources, such as solar-heated water, industrial waste heat, geothermal brines, and ocean thermal gradients.

Several projects are investigating longer-term possibilities for utilizing solar energy. One project involves the development of a new type of solar thermal receiver that would be placed at the focus of a central receiver system or a parabolic dish. The conversion of the concentrated sunlight to thermal energy would be accomplished by the absorption of the light by a dispersion of very small particles suspended in a gas. Another project is exploring biological systems. In particular, we are investigating the possibility of developing a photovoltaic cell, based on a catalyst (bacteriorhodopsin) which converts light to electrical ion flow across the cell membrane of a particular bacteria.

SMALL PARTICLE SUSPENSIONS FOR SOLAR THERMAL COLLECTION *

A. Hunt, P. Hull, J. Bouchez, C. Amkraut, and N. Pope

INTRODUCTION

Concentrated sunlight provides an intense source of radiant energy that offers an alternative to fossil fuels for operating heat engines, providing high temperature industrial heat, and directly processing fuels and chemicals. Because sunlight originates from a radiating body at a considerably higher temperature than other familiar energy sources, solar radiation has quite different characteristics from those with which we gained our power conversion experience. Our work deals with a novel approach to power conversion that matches the characteristics of concentrated sunlight to the requirement of heating a gas.

The purpose of this work is to develop a new type of solar thermal receiver that is placed at the focus of a central tower or parabolic dish concentrator system. The principle of operation differs from other advanced receiver designs under development in that the radiant solar-to-thermal energy conversion is accomplished by a dispersion of ultrafine particles suspended in a gas to absorb radiant energy directly from concentrated sunlight.[1] The very large ratio of surface area to volume, which is a property of small particles, makes them ideally suited for this application.

The Small Particle Heat Exchange Receiver (SPHER) can be used to operate a gas turbine, supply industrial process heat, or provide radiant power directly to a particle suspension for thermal or photochemical reactions. SPHER's are suitable for a wide range of power applications and are easily adapted to hybrid solar/fossil operation. The advantages of this type of receiver are its simplicity, low pressure loss, light weight, high optical efficiency, lower chamber temperatures for a given output temperature, and lack of problems associated with heat exchanger lifetime.

An open-cycle heat engine utilizing SPHER operates by compressing ambient air and injecting a very small mass of carbon particles into a gas stream. The air and particle mixture enters a transparent heating chamber where the solar flux is concentrated. The particles absorb the radiation and, because of their very large surface area, quickly release the heat to the surrounding gas. After heating the gas, the particles oxidize. The heated gas then passes through an expansion turbine to provide power for the compressor and load before going to a regenerator and being exhausted.

An earlier analysis quantified the optical and physical processes of absorption and heating of the particles.[2] Related considerations investigated include particle production methods, window and chamber design, hybrid solar/fossil compatibility, as well as environmental and safety factors. Analyses confirmed that the operating parameters are flexible and suitable to a variety of solar thermal power applications. A small laboratory apparatus built earlier demonstrated the direct heating of a gas by a small particle suspension.

ACCOMPLISHMENTS DURING FY 1980

Considerable progress was made during FY 1980 to advance the SPHER concept toward the test and demonstration stage. The analytical work was expanded to study the optical properties of small particle suspensions as selective solar absorbers, to clarify the requirements for the particle generator, to study the receiver design, and to examine the operation of the system for a wide range of conditions. Investigation continued this year into a related concept, the Solar Engine (SOLGIN). This is a new design for a small, reciprocating, direct absorption engine for use with small scale point focus solar concentrators. In an effort to broaden the understanding of radiatively coupled small particle systems, an examination was started into considerations of direct radiant processing of chemical feedstocks in the form of particle suspensions.

The experimental work was concentrated on the generation and analysis of the ultrafine carbon particles that are the heart of the SPHER. A new particle generation technique utilizing the pyrolysis of hydrocarbon gas was developed and found to be superior to the flame generation technique. Laboratory measurements of the generator operation established its capability for supplying particles in the quantities and with the properties necessary to operate an experimental receiver. The receiver chamber is undergoing final design, and a solar simulator was constructed for laboratory testing.

Analytic Studies

The goal of this year's analytic studies of small-particle suspensions was to determine how the physical and optical properties of the particles affect the operation of direct absorption receivers. The efficiency of a suspension of absorbing particles in capturing sunlight and minimizing losses from radiation by the heated particles is dependent on the particle size, shape, and optical properties of the material comprising the particles.[3] The ratio of the amount of energy removed from a beam by absorption or scattering to the cross-sectional area of the particle is defined as the absorption efficiency, Q_{abs}, or scattering efficiency, Q_{sca}, respectively. To reduce the amount of light scattered back out of a receiver, the ratio Q_{sca}/Q_{abs} must be minimized. If the particles are very small and absorbing, this condition is met, and their interaction with light can be

* This work was supported by the Assistant Secretary for Conservation and Solar Energy, Office of Advanced Solar Thermal Technology, Solar Thermal Power Division of the U.S. Department of Energy under Contract number W-7405-ENG-48.

described by Rayleigh scattering theory. Under these conditions, Q_{abs} is proportional to the particle radius and Q_{sca} is proportional to the fourth power of the radius, so that the ratio of scattering to absorption is proportional to the cube of the radius. To maximize the optical efficiency of the receiver, the particle size is chosen to be less than 0.1 microns in diameter, resulting in scattering losses of less than about one percent.

The mass of particles, M_s, required to provide the necessary absorption in the chamber is an important quantity that can be calculated using Beer's law and neglecting multiple scattering (a reasonable assumption for small particles because the ratio of scattering to absorption is small). The mass of particles of density ρ and radius r required to reduce the intensity of a beam to I from I_o in a distance d is given by

$$M_s = \frac{4r\rho \ln (I/I_o)}{3Q_{abs}\, d} .$$

The general behavior of M_s as a function of particle size is shown in Figure 1. This figure illustrates that the required mass of particles to produce a given absorption reaches a constant value if the radius is small (as predicted by Rayleigh scattering theory). Large particles absorb an amount of light that is proportional to their cross-sectional area, leading to a roughly linear relationship between the required mass and the radius. The behavior in the intermediate region is shown as a dashed line because it depends heavily on the shape and optical properties of the particles. In fact, the experimental data for carbon particles (discussed later) indicates a strong minimum in the dashed region indicated by a bar in the figure.

Another dominant factor in determining the performance of a small particle suspension for a solar receiver is the dielectric response function $N^2 = (n+ik)^2 = \varepsilon_1 + i\varepsilon_2$ that describes the material from which the particles are made. The goal is to maximize the absorption efficiency in the visible part of the spectrum and to minimize it in the infrared part. The absorption efficiency for Rayleigh scattering may be written

$$Q_{abs} = 4x\,\mathrm{Im}\left\{\frac{N^2 - 1}{N^2 + 2}\right\}$$

where x is the ratio of the particle circumference to the wavelength of light. The absolute maximum of the function in the braces is unbounded and occurs at $\varepsilon_1 = -2$, $\varepsilon_2 = 0$. The closer the dielectric function approaches this point, the larger the Q_{abs} will become. This corresponds to a "resonant mode" for surface states in spherical particles, and materials that approach this condition can be used to maximize the absorption in the visible region of the spectrum. To minimize the value of Q_{abs} in the infrared, ε_1 and ε_2 should be as large as possible. Metals in the infrared have just this type of behavior. Carbon is an excellent choice of materials for solar absorber applications because of its high absorptance in the visible and its metal-like optical characteristics in the infrared.

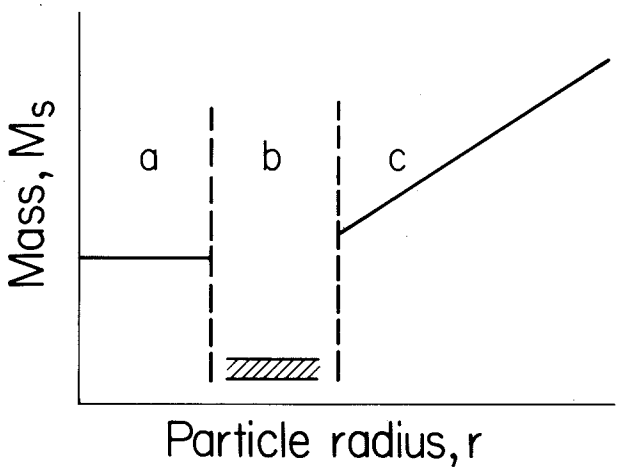

Fig. 1. Illustration of the dependence on particle size of the mass of particles required to produce a specified absorption. Region (a) is for the small particle limit (Rayleigh scattering); (b) is where the wavelength and particle size are comparable (Mie scattering); and (c) is the large particle limit (geometrical scattering). The hatched region indicates the area of the experimental results. (XBL 811-87)

The design of a realistic solar receiver must consider the confinement and flow of the particle suspension as well as the effect of the optics of the solar collection system. An important design guide for the chamber is that the overlap between the illuminated region and the particle suspension should be maximized. This overlap insures the maximum use of the particles as the absorber. Techniques were developed to analyze the required mass loading for cylindrical and conical receiver shapes. The analysis for a cylindrical shape is straightforward, but concentrating optical systems usually produce beams with considerable divergence. A conical-shaped receiver is a good approximation to this beam divergence. The analytical treatment is tractable because the decreases in beam intensity due to absorption and to geometry are separable. The results of this analysis offer the basis on which to design a chamber and to determine the requirements of the particle generator. Figure 2 illustrates the preliminary design of a receiver for laboratory testing.

The SPHER uses a transparent window to confine the suspension of absorbers. An analysis was performed to determine the efficiency of receivers using both one window and two windows in tandem.[4] To better understand the operation of windows in high-temperature environments, the analytic work was extended to study the thermodynamic stresses, sealing techniques, and cost for high-temperature windowed systems. The results confirmed that high silica materials can be used in practical, cost-effective windows for high-temperature operation.

A detailed analysis of the equilibrium properties of small particles in a radiant field was performed to investigate the effects of flux density, optical properties, and particle size. The analysis indicated that small particles can be used for radiant heat exchangers up to very high tem-

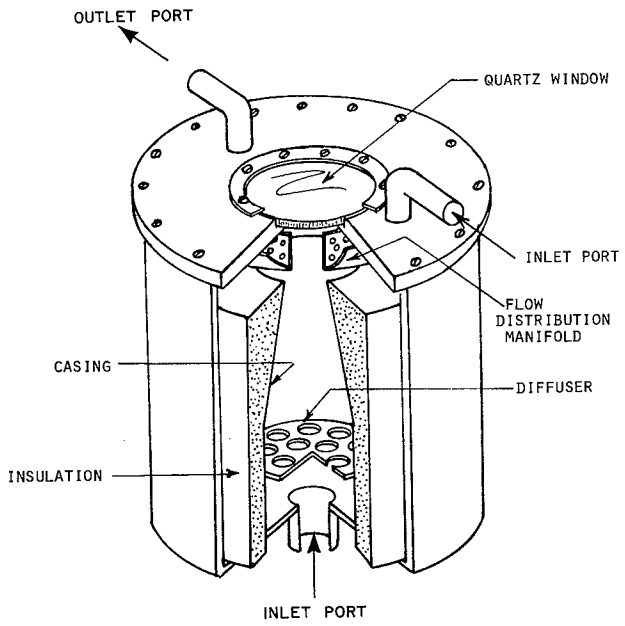

Fig. 2. Preliminary design of a small-particle heat exchange receiver.

(XBL 806-10317)

peratures (greater than 2000° C). This high-temperature capability is particularly important in processes such as the direct splitting of water into hydrogen and oxygen, the decomposition of carbon dioxide to produce carbon monoxide, and the oxidation of nitrogen to produce nitrates.

Solar Engine

Work has continued on the design and analysis of a new type of reciprocating solar engine that uses a small-particle suspension to absorb concentrated sunlight directly within the cylinders. The SOLGIN operates by drawing an air and particle mixture into the cylinder, compressing the mixture, opening an optical valve to allow concentrated sunlight to enter through a window in the top of the cylinder head, absorbing the solar flux with the particles, and converting the heat trapped by the air and particle mixture into mechanical energy with the downward stroke of the piston. SOLGIN differs from other gas-driven engines using solar energy in three main respects. First, the radiant flux is deposited directly in the working fluid inside the cylinder; second, the heat is directed to the appropriate cylinder by optically controlling the solar flux; third, the gas is heated during a significant portion of the compression stroke.

The thermodynamic efficiency of the engine was determined by use of an analytical model.[5] The efficiency depends on the compression ratio and the timing of the solar heating and is plotted in Figure 3 for a range of the parameters for a two-cylinder engine; the efficiency increases significantly for a larger number of cylinders. Efficiencies exceeding 50% can be obtained.

Experimental Work

Three different methods for producing carbon

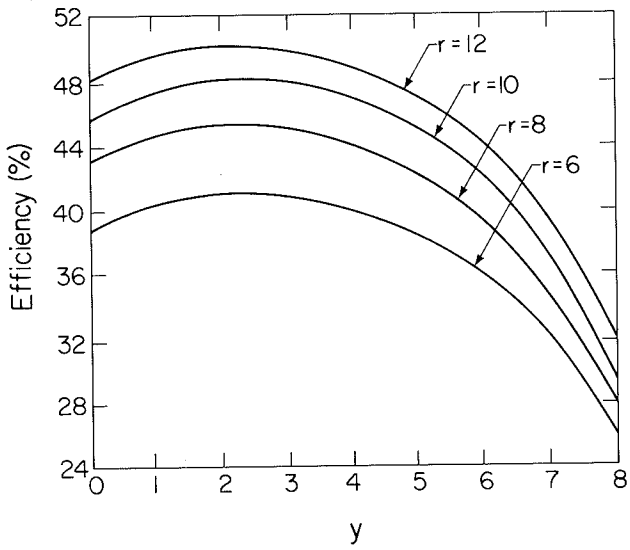

Fig. 3. The efficiency of the two-cylinder engine as a function of the timing of heat input. The variable y indicates the relative time for the onset of solar heating. When y = 0, the heating begins at the center of the compression stroke and when y = 8, the heat is added beginning at top dead center. r is the compression ratio.

(XBL 811-89)

particles suitable for high-temperature receiver applications were investigated experimentally. The methods included the use of a fuel-rich flame, the decomposition of carbon with a high intensity arc in argon, and the pyrolytic decomposition of acetylene gas. The optical absorption, particle density, and carbon production rates were determined experimentally. The size, shape, and state of agglomeration were studied with both scanning and transmission electron microscopy.[6]

A schematic diagram of the experimental apparatus for particle production and collection and for opacity and mass measurements is shown in Figure 4. The diagram shows the experimental setup used for producing particles from a fuel-rich flame. An extinction tube used with a He-Ne laser is used to determine the opacity of the gas-particle suspension. Nuclepore filters are used to collect the particles for weighing and scanning electron microscopy.

Opacity measurements of the particle suspensions showed consistent extinctions in excess of 95% for one-way light paths of 5 cm. The extinction and mass-loading measurements together indicated specific extinction coefficients of 15-20 m^2/gm. These results are extremely encouraging because they establish that the particles have four times greater absorption than the Rayleigh theory predicts, reducing the already very low requirement for particles. The higher absorption probably arises from two causes. An electron micrograph of a collected sample of carbon particles is shown in Figure 5. The median size of the smallest components is about 0.04 microns in diameter. Exact calculations for spherical particles this size give extinction coefficients about twice that predicted

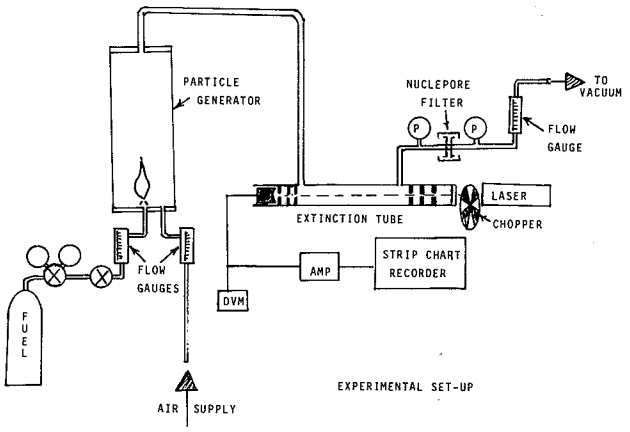

Fig. 4. Schematic diagram of the apparatus for the production and measurement of small-particle suspensions. (AMP stands for amplifier. DVM represents digital voltmeter. P's denote pressure gauges.)

(XBL 806-10318)

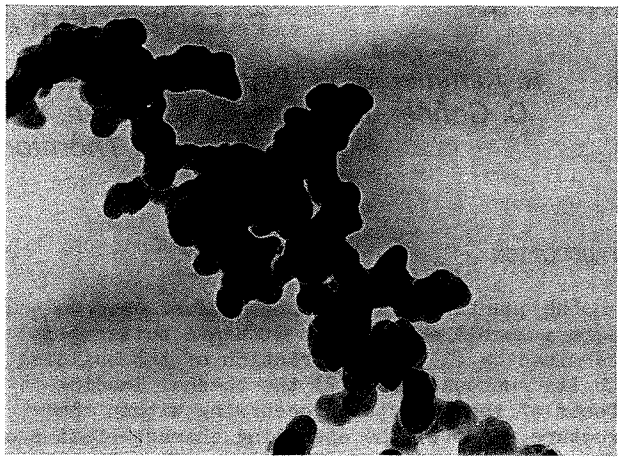

Fig. 5. Transmission electron micrograph of particles generated from the apparatus diagrammed in Fig. 4. The smallest particle diameter is approximately .05 microns.

(XBB 806-7255)

by Rayleigh theory. The second reason probably arises from the chain-like character of the agglomerates. Under some circumstances, a cylindrical particle can produce a larger mass normalized extinction than a spherical particle.

A particle generator based on the pyrolysis of acetylene was chosen for development for efficiency and stability reasons. At present a pyrolysis generator is being scaled up to operate with a 2 kW receiver chamber that is in the final design stage.

PLANNED ACTIVITIES FOR FY 1981

The main goal of the program in FY 1981 will be to build and test a complete SPHER receiver. The success of the work will rely on the continued experimental and analytical investigation of small-particle systems. The experimental program will concentrate on the continued development of the pyrolysis particle generator, including measurements of the yield and optical characteristics of the particles. A windowed receiver chamber will be constructed and mated with the particle generator. Instrumentation will be developed to measure the performance of the system. Laboratory tests of the receiver will be conducted with a small solar simulator. After successful laboratory results, we plan to test the complete receiver at a national solar thermal test facility.

The analytical program will continue with the investigation of the important features of direct absorption systems. Emphasis will be placed on studying the geometrical aspects of the interaction between the radiant flux and the particle suspension.

REFERENCES

1. A. J. Hunt, "Radiant Energy Collection and Conversion Apparatus," U.S. Department of Energy invention number S-50, 549. Patent application filed July 18, 1979 (pending).

2. A. J. Hunt, "A New Solar Thermal Receiver Utilizing a Small Particle Heat Exchanger," Proceedings of the 14th Intersociety Energy Conversion Engineering Conference, August 5-10, 1979, Boston, Mass.; Lawrence Berkeley Laboratory report LBL-8520, April 1979.

3. A. J. Hunt, "Optical Properties of Small Particle Suspensions for Solar Thermal Collection," Proceedings of the Optical Society of America Topical Meeting on the Optical Phenomena Peculiar to Matter of Small Dimensions, March 18-20, 1980, Tucson, Ariz.; Lawrence Berkeley Laboratory report LBL-10221, February 1980.

4. W. J. Fisk, D. E. Wroblewski, Jr., and A. J. Hunt, "Performance Analysis of a Windowed High Temperature Gas Receiver Using a Suspension of Ultrafine Carbon Particles as the Solar Absorber," Proceedings of the American Section of the International Solar Energy Society Meeting, June 2-6, 1980, Phoenix, Ariz.; Lawrence Berkeley Laboratory report LBL-10100, November 1979.

5. P. Hull and A. J. Hunt, "A Reciprocating Solar Heated Engine Utilizing Direct Absorption by Small Particles," submitted to the Journal of Solar Energy Engineering; Lawrence Berkeley Laboratory report LBL-10622 (in press).

6. A. J. Hunt, "Development of a New High Temperature Gas Receiver Utilizing Small Particles," Proceedings of the International Symposium on Solar Thermal Power and Energy Systems, June 15-20, 1980, Marseille, France; Lawrence Berkeley Laboratory report LBL-10148, November 1979.

PASSIVE SOLAR ANALYSIS AND DESIGN*

R. Kammerud, W. Place, B. Andersson, F. Bauman, C. Bauer, W. Carroll, E. Ceballos, C. Conner, B. Curtis, N. Friedman, A. Gadgil, A. Mertol, M. Nansteel, D. Nawrocki, M. Tavana, J. Thornton, T. Webster, and M. Wahlig

INTRODUCTION

The quantity of conventional fuel used to create a usable environment within a building is determined by (1) the interaction of the building with its surroundings, (2) the thermal loading effects of the activities occurring within the structure, and (3) the operating characteristics of the equipment used to convert conventional fuels to end-use energy. Significant reductions in the energy consumed in order to heat, cool, and light a structure can be realized by properly controlling the thermal coupling between the building and its environment and by appropriately managing the energy flows within the structure. To fully realize the benefits derived from these passive strategies, the collection, dissipation, storage, and distribution of thermal energy within the building's boundaries must be understood in terms of the design parameters of the structure and the environmental conditions under which the building is used. In this context, the specific objectives of the Passive Solar Analysis and Design Group at LBL are:

- to develop detailed, analytic descriptions for the collection, dissipation; storage, distribution, and management of thermal energy in buildings;
- to develop, analyze, and test innovative passive design concepts for application to specific building types and energy end uses; and
- to synthesize the results of the technical and design research in order to produce architectural and engineering design tools.

The focus of the program is the commercial building sector.

Long-range program directions have been selected based on an examination of existing energy use data for commercial buildings.[1] When disaggregated by building type and end-use category, the data provide the following information:

- The comparable magnitudes of heating, cooling, and lighting energy, and their obvious interactions within a specific building, indicate the need for a balanced program which addresses the three end uses from an integrated, rather than generic, systems standpoint.
- Because there is a strong interaction between the three dominant energy end uses, energy management is a key element in the passive design process.
- Both energy use intensity and growth rate imply the need for a programmatic focus on retail, wholesale, office, public, and educational building types for both new and retrofit applications of passive design principles.
- Although the growth rate of energy use in the hotel and motel category is relatively small, the energy intensity and total energy use in buildings of this type are large. This category of buildings, therefore, is an additional target for retrofit applications of passive design concepts.

To date, the LBL program has concentrated on the development testing and verification of public domain analysis tools necessary for exploring the application of passive concepts to commercial buildings, including (1) the development of thermal models for incorporation into BLAST† and (2) the development of stand-alone analysis capabilities for convective heat transfer under natural and forced conditions. This latter analytical tool is a critical element in the examination and characterization of energy management within passive and hybrid structures. A comprehensive tool for studying the thermal behavior of passive solar hot water heating systems has also been developed. The analysis technique is appropriate for conventional thermosiphons and for innovative systems, designed at LBL, that ensure positive protection from freezing.

In addition to the technical and design research activities, projects which synthesize the results of technical research with architectural design issues have been initiated. During development of passive analysis capabilities for commercial buildings, applications of developmental versions of BLAST to direct solar-gain residential buildings have been performed. These studies have examined:

- the effect of thermal mass on the heating and cooling loads of conventional and passive solar buildings;
- the interaction between thermally massive construction and common auxiliary system control strategies; and
- the impact on cooling load of direct-gain passive heating systems.

* This work was supported by the Assistant Secretary for Conservation and Solar Energy, Office of Solar Applications for Buildings, Research and Development Branch, Passive and Hybrid Division of the Office of Solar Applications for Buildings, U.S. Department of Energy under Contract No. W-7405-ENG-48.

† BLAST (Building Loads Analysis and System Thermodynamics) is copyrighted by the Construction Engineering Research Laboratory, U.S. Department of the Army, Champaign, Illinois.

Table 1. Passive analysis capabilities of BLAST.

Direct solar gain systems.
Thermocirculation systems and Trombe walls.
Roof pond systems.
Movable insulation.
Direct ventilative cooling.
Daylighting.
Building envelope and internal thermal mass.
Shading by attached or detached devices with complex geometries.
Simultaneous dynamic analysis of multizone buildings.
Variable convective heat transfer coefficients at all surfaces.
Environmental coupling through solar radiation, thermal radiation, and wind driven convection.
Mean radiant temperature and/or air temperature thermostat control.

Applications of BLAST in commercial building design projects have been a continuing part of the program; these case studies not only produce reliable technical input for the project design teams, but also provide direct feedback to LBL regarding the types of analysis capabilities that are needed by the private sector.

ACCOMPLISHMENTS DURING FY 1980

BLAST Development and Validation

Thermal models have been developed[2-5] and are being incorporated into BLAST-3.0, which is scheduled for release in early FY 1981. The major passive analysis features added to the program are listed in Table 1. In addition, standard features of the program allow users to specify the types of internal thermal loads (heat sources), their schedules, and the strength of their couplings to the internal space through radiation to exposed surfaces and convection and by evaporation to the ambient air. The program was originally written in order to provide user-oriented analysis capabilities for commercial buildings; it therefore includes dynamic simulation of mechanical systems and central energy plants. Program input consists of an English language description of (1) the building geometry, materials and construction; (2) mechanical systems and controls; (3) the internal loads, including lighting, occupancy, and equipment; and (4) hourly weather data. Output consists of (1) building loads; (2) the energy consumed by the central plant; and (3) the energy associated with the air handling system operation.

The daylighting algorithm which has been incorporated into BLAST-3.0 provides embryonic analysis capabilities that allow examination of the energy-consumption tradeoffs among heating, cooling, and lighting design strategies. Currently, the analysis requires input from daylighting experiments. In the longer term, a more independent daylighting analysis may be desirable. To provide input to the existing analysis capability and to examine future analysis needs, a daylighting project has been initiated. The project will include (1) experimental daylighting measurements in scale models under sky conditions and in an artificial sky dome facility; (2) tradeoffs between heating, cooling, and lighting loads based on building energy analysis using the daylighting measurements; and (3) synthesis of the results into design guidelines for specific classes of daylighting systems. The experimental work has begun and will provide input data to BLAST-3.0 for tradeoff analysis. The BLAST studies will provide the technical data on which the design tool development activities will be based.

The predictions of the BLAST thermal loads program have been compared to measurements performed in a small test room located at Los Alamos Scientific Laboratory. Comparisons were made between the measured and calculated air temperatures for three distinct weather periods.[6] The results of one of these comparisons are shown in Figure 1. In all cases, the predictions from BLAST were in excellent agreement with the measured data. The deviations were well within the limits implied by uncertainties in the test room construction and the properties of its construction materials.

The validation studies have been extended[7] to a full-scale high thermal mass test building located in an environmental chamber at the National Bureau of Standards. Whereas the test cell comparisons verify the ability of the program to account properly for solar excitation of an unconditioned structure, the data from the environmental chamber allows validation of the load calculation and of the excitation of thermal storage mass by direct ventilation cooling systems. To improve on existing validation data, a fully automated air infiltration measuring system has been developed. The system will be used to supplement the standard thermal measurements normally collected and compared to computer codes. The addition of infiltration data will remove one of the largest uncertainties in the validation process.

BLAST Applications

Two types of BLAST applications have been performed. In the first type, energy analyses of prototype direct solar gain systems have been performed in order to examine the sensitivities of the building heating and cooling loads to variations in design parameters and auxiliary system control strategies. The studies examined the effect on the annual thermal loads that result from varying the south-facing glazing area on a direct-gain residential building located in each of the 26 cities for which Typical Meteorological Year (TMY) weather data is available. In some types, the results were obtained for two variations of the building design:[4] in one case, all internal wall surfaces consisted of standard low-mass gypboard construction and, in the other case, the internal partition walls were assumed to be a 4-in. concrete construc-

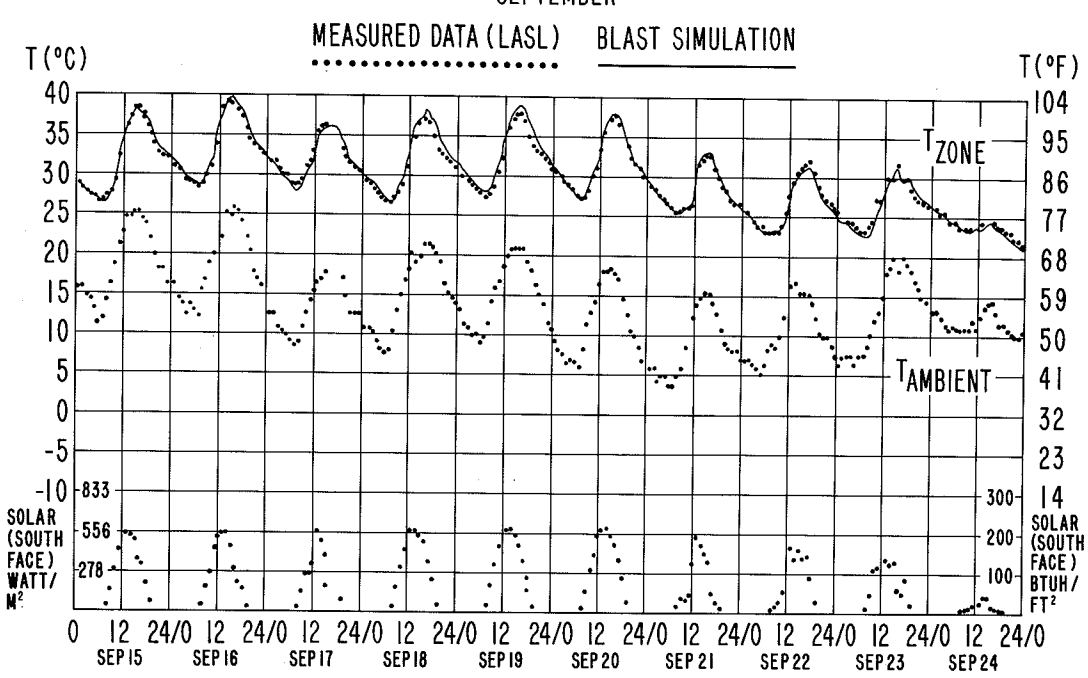

Fig. 1. Comparison of the interior air temperature predictions (F zone) of BLAST to measurement performed in a direct gain test room located in Los Alamos, N.M. The comparison is for a 10-day period in September and also shows the ambient temperature and the incident solar radiation.

(XBL 806-7121)

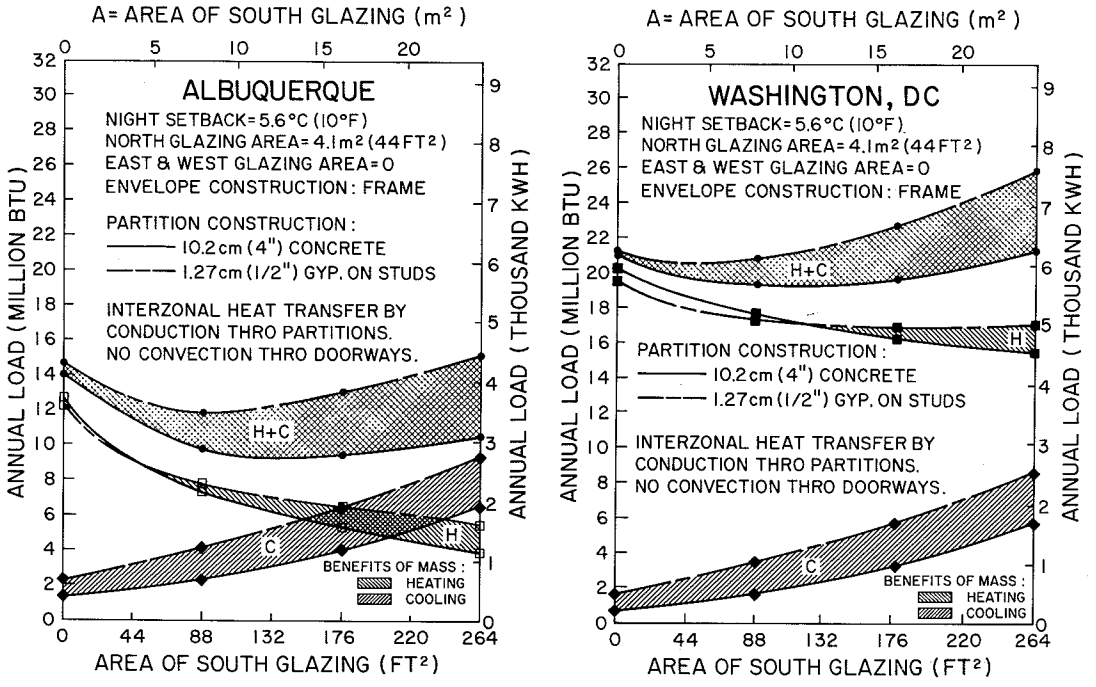

Fig. 2. Predicted annual auxiliary energy consumptions for heating and cooling a passive solar residential building located in Albuquerque, N. M. and in Washington, D. C., as a function of the area of south glazing. The calculations were performed using the building energy analysis computer program BLAST and were performed for a conventionally constructed building and for a variation which replaces the gypboard partition walls with concrete.

(XBL 804-6917A)

tion. Ventilation cooling was assumed throughout the year. Typical results from this study are shown for Washington, D.C. in Figure 2. We found that in most heating climates, as in Washington, D.C., that for south-facing glazing areas less than about 132 ft^2 (11% of the floor area) the heating benefits of south-facing glazing are dominant, but at larger glazing areas, the increase in cooling load which accompanies increased glazing area became more significant than the heating load reductions. A second striking feature of the study is also apparent in Figure 2: the importance of internal thermal mass in reducing the cooling load when forced ventilation is used. Although both building configurations included substantial mass in the insulated 4-in. concrete floor slab, the cooling performance is substantially improved by adding considerably more mass. Other important results include the observation that thermal mass can have a deleterious effect on the performance of buildings that incorporate night setback thermostat control strategies.

The second type of BLAST application has consisted of applying the program to commercial buildings during the design process. Extensive analyses have been performed on three projects during the schematic design phase. In one case, the results were used to determine the effectiveness of direct ventilation cooling and thermally massive construction on reducing cooling loads. In another case, a variety of passive heating and cooling strategies and energy conservation features were examined in order to define the scope of a retrofit project. In addition, several other DOE contractors and design firms in the private sector have been trained in the use of BLAST, and technical support has been provided for their independent applications of the program.

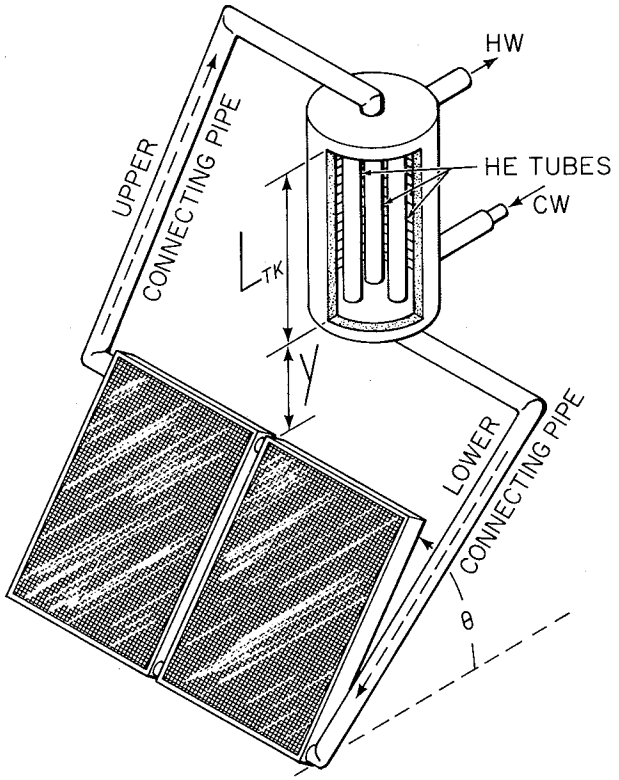

Fig. 3. Schematic representation of a thermosiphon hot water system which provides positive freeze protection. The system utilizes a primary loop filled with a nonfreezing liquid such as glycol to transfer thermal energy from the solar collector to a heat exchanger in the hot water storage tank.

(XBL 803-6909)

Natural Convection and Energy Management

A computerized numerical technique for studying natural and forced convection in room geometries has been developed.[9] The computer program has been validated[9-11] using data from the literature and from an experiment performed by LBL in conjunction with the Department of Mechanical Engineering at the University of California, Berkeley. The convection project includes the study of natural ventilation phenomena, energy management strategies, convective heat transfer coefficients, temperature stratification, and stack effect ventilation systems. Initial applications to residential scale systems have been performed in order to examine the validity of the common assumption in building energy analysis that convection coefficients are sensitive only to the direction of heat flow and not to temperature differences between building surfaces and the room air.[10,11] Initial results indicate that surface convection coefficients vary substantially from the standard assumptions and that this may be reflected in significant errors in heat transfer to and from thermal storage materials and in calculated thermal loads.

Toward the end of FY 1980, an analytic component was added to the convection research. Examinations of the numerical analysis results proved that some features of natural convection in an enclosure with a room geometry can be represented analytically. Efforts were therefore initiated to investigate the possibility of developing a hybrid convection analysis program which combines numerical techniques at the boundaries with analytic methods in the core, thereby providing far more efficient analysis and allows the convection studies to be extended to many more applications problems.

Domestic Hot Water and Process Heat

A passive solar hot water heating system that incorporates positive protection from freezing has been designed and thoroughly analyzed. A typical system configuration is shown schematically in Figure 3. The system utilizes a glycol-filled primary loop from the solar collector to a heat exchanger located in a conventional storage tank. This design eliminates the danger of freezing from mechanical malfunction and utilizes no parasitic power. A detailed simulation model[12,13] for the system has been developed and used to study performance as a function of climate, collector parameters, heat exchanger design, and hot water use profile.[14] The results of the analysis indicate that relatively simple heat exchangers consisting of straight tubes parallel to the axis of a cylindrical storage tank will provide system performance that is nearly equivalent to that for a standard

thermosiphon. An experiment is currently being set up to validate the analysis and parametrically examine the effectiveness of various heat exchanger configurations. If the concept is experimentally verified, one of the major barriers to widespread use of thermosiphons will be eliminated, and their regional applicability will be dramatically increased.

During FY 1980, simplified performance prediction techniques were explored. Based on detailed simulations, a correlation between system performance and system design parameters was identified. Assuming the correlations hold in future analyses and experiments, the simplified method will serve as a practical design tool for the engineering community.

PLANNED ACTIVITIES FOR FY 1981

Upon release of BLAST-3.0, thermal model development activities at LBL will focus on (1) further validation of existing capabilities using data from full-scale buildings where simultaneous measurements of thermal parameters and infiltration have been carried out, and (2) on development of algorithms that describe the thermal behavior of innovative passive solar building configurations. Examples include waffled concrete ceiling structures; thermodeck structural floor and ceiling elements coupled to ventilative and/or evaporative cooling systems; infrared reflective glazing materials; and optical shutter materials. In addition, further work will be devoted to energy management systems and to improvements in the representation of convection processes in BLAST. These activities will lead to a new version of BLAST in FY 1982.

Parametric studies of commercial buildings incorporating passive heating, cooling and/or lighting systems will begin on completion of BLAST-3.0 development. These studies will be directed initially at improving the ability of the designer to select basic design directions during the early phase of the design process. The initial studies will include:

- ventilative cooling strategies;
- daylighting tradeoffs with heating and cooling loads;
- comparisons of solar control glazing, shading, and summer movable insulation in controlling cooling loads; and
- thermal mass effects.

This type of study will be an ongoing part of the LBL program.

The convection analyses and experiments will be directed at:

- characterization of the natural ventilation potentials of commercial buildings utilizing stack effect systems such as atriums; and
- examination of, and algorithm development for, convective heat transfer within and between thermal zones.

In addition, the analysis capability will be applied to specific problems that arise in the analysis of passive systems and for which no acceptable algorithms currently exist. An example of this is the effect on thermocirculation system performance of inlet and outlet vent configurations.

Data collection from the hot water experiment will begin in early 1981. The data will be used for:

- validation of the thermosiphon simulation computer code; and
- comparison of different heat exchanger designs.

Later experiments will be oriented toward collection of a system performance data base to be used in the further identification of simplified correlative techniques for predicting system performance.

The daylighting experiments will continue during FY 1981 and daylighting designs will be examined. The results will be used to examine the tradeoffs of lighting with heating and cooling loads for various building types and climates.

REFERENCES

1. J. McMahon et al., A Review and Analysis of Commercial Building Energy Consumption Studies, Lawrence Berkeley Laboratory report LBL-10620 (to be published) 1981.
2. H. Akbari et al., Free Convective Laminar Flow Within the Trombe Wall Channel, Lawrence Berkeley Laboratory report LBL-7802, August 1978.
3. T. Borgers et al., Free Convective Turbulent Flow Within the Trombe Wall Channel, Lawrence Berkeley Laboratory report LBL-8323, April 1979.
4. M. Tavana et al., A Simulation Model for the Performance Analysis of Roof Pond Systems for Heating and Cooling, Lawrence Berkeley Laboratory report LBL-9292, June 1980.
5. M. Tavana et al., Roof Pond System Performance Sensitivities and Model Modifications, Lawrence Berkeley Laboratory report LBL-11381 (to be published), 1981.
6. B. Andersson et al., Verification of BLAST by Comparison with Direct-Gain Direct-Gain Test Cell Measurements, Lawrence Berkeley Laboratory report LBL-10619, November 1980.
7. F. Bauman, B. Andersson, W. Carroll, and R. Kammerud, Verification of BLAST by Comparison with Measurements of a Solar-Dominated Test Cell and a Thermally Massive Building, Lawrence Berkeley Laboratory report LBL-11387 (to be published) April 1981.
8. R. Kammerud et al., Human Comfort and Auxiliary Control Considerations in Passive Solar Structures, Lawrence Berkeley Laboratory report LBL-10034, April 1980.
9. A. Gadgil, On Convective Heat Transfer in Building Energy Analysis, Ph.D. dissertation, Department of Physics, University of California, Berkeley, 1980; Lawrence Berkeley Laboratory report LBL-10900, May 1980.

10. F. Bauman et al., Buoyancy Driven Convection in Rectangular Enclosures: Experimental Results and Numerical Calculations, Lawrence Berkeley Laboratory report LBL-10257, July 1980.

11. A. Gadgil et al., Natural Convection in Room Geometries, Lawrence Berkeley Laboratory report LBL-9297, October 1979 (longer version to be issued 1981).

12. A. Mertol, Heat Transfer and Fluid Flow in Thermosiphons, Ph.D. dissertation, Department of Mechanical Engineering, University of California, Berkeley, 1980; Lawrence Berkeley Laboratory report LBL-10939, April 1980.

13. A. Mertol et al., Detailed Loop Model (DLM) Analysis of Liquid Solar Thermosiphons with Heat Exchangers, Lawrence Berkeley Laboratory report LBL-10699, October 1980.

14. A. Mertol et al., Thermosiphon Water Heaters with Heat Exchangers, Lawrence Berkeley Laboratory report LBL-10033, June 1980.

NITINOL ENGINE DEVELOPMENT*

R. Banks, W. Hubert, and M. Wahlig

INTRODUCTION

Low-grade heat, in the form of thermal energy at temperatures below the boiling point of water, is a widespread energy resource that could make a significant contribution to worldwide energy needs if an economical technology can be developed for converting it to useful work. The Nitinol Engine Development project is investigating the feasibility of using the thermally activated shape-change phenomenon in certain intermetallic Shape Memory Alloys, particularly in the nickel-titanium compound "55-Nitinol," as the basis for thermal-to-mechanical energy conversion at temperatures available from such sources as industrial waste heat, low-temperature geothermal brines, solar-heated water, or the moderate-temperature differences of the ocean thermal gradient. An important advantage in using a solid rather than a fluid working medium in such applications is the possibility for eliminating the heat exchangers required by closed-cycle fluid systems, which often are a major cost and require frequent maintenance in conventional low-temperature energy conversion technologies.

A prototype Nitinol heat engine has been in operation at the Lawrence Berkeley Laboratory since August 1973. Several iterations of engine design since then have led to an improved understanding of the important practical considerations in applying this material to energy conversion in continuously cycling heat engines. These studies, as well as experimental and theoretical investigation of the material's thermodynamic and metallurgical properties, have confirmed that Nitinol engines for the recovery of thermal energy from low-grade or waste heat can be constructed; however, the question of economic feasibility is still unresolved.

* This work was supported by the Assistant Secretary for Energy Technology, Fossil Fuel Utilization Division of the U.S. Department of Energy under Contract No. W-7405-ENG-48.

ACCOMPLISHMENTS DURING FY 1980

During this past year, for the first time, we had available Nitinol wire specimens that had completed several million working cycles in uniaxial strain (linear tension) on the Tensile Fatigue Test Stand (shown in Fig. 1). Constructed at LBL during 1979, the stand continuously cycles Nitinol wires under controlled stress between baths of hot and cold water. Powered by the thermoelastic Shape Memory Effect (SME) response of the wires being cycled, the stand is a heat-engine. We believe this machine is the first device to exploit the SME of Nitinol wires in pure tension to achieve this many cumulative reproducible working cycles.

Single wires were taken from the power element of the Fatigue Test Stand at regular intervals, and their performance was evaluated on a high-resolution Laser-Beam Dilatometer. The dilatometer, developed during prior years of the project for characterizing the strain-temperature behavior of Nitinol wires in tension, heats and cools a specimen at slow and uniform rates so that changes in axial displacement (magnified by a factor of 200) may be precisely correlated with small changes in temperature over the material's complete thermal transformation range.

The dilatometer evaluations confirmed qualitative observations of the test stand's performance that Nitinol wires, whose properties have been stabilized by cycling in the test stand, exhibit improved thermomechanical characteristics in two important respects. The first improvement is an overall increase in potential displacement (length of "stroke") of the cycled material, as compared with that of reannealed but uncycled wire from the same stock. (Reannealing essentially restores the material to its initial condition.) The second improvement is a reduction in thermal hysteresis, the temperature difference required for the cooling and heating shape changes of the wire's thermoelastic response as a result of extended cycling on the test stand.

Dilatometer Measurements in Detail

The cyclical behavior of Nitinol wire that was reannealed but not engine-cycled can be compared with that of wires that had sustained 10^6 cycles and 5.3 x 10^6 cycles respectively on the Fatigue Test Stand in Figures 2, 3, and 4. On cooling, strain (elongation) occurs under a moderate uniform stress load of approximately 2.3 kpsi. The cooling path is shown as an unbroken line in computer-generated plots, in Figures 2-4, of data taken from the dilatometer. Shape-recovery (axial contraction), caused by reheating, is indicated by crosses.

In the uncycled wire, thermoelastic strain begins at a very moderate rate at about 25°C, with a more pronounced threshold occurring at 7.5°C.

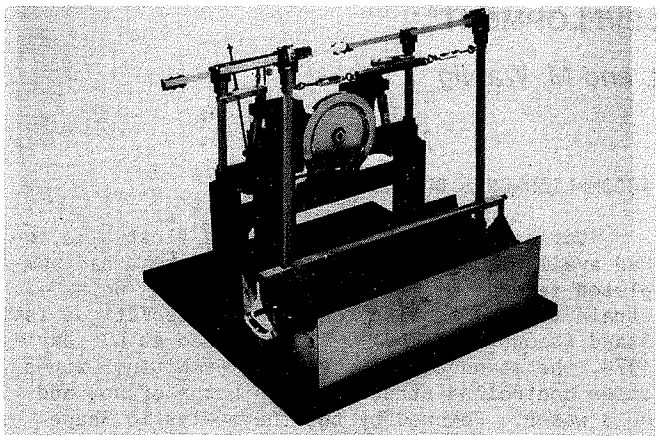

Fig. 1. Nitinol Tensile Fatigue Test Stand.
(CBB 809-11931)

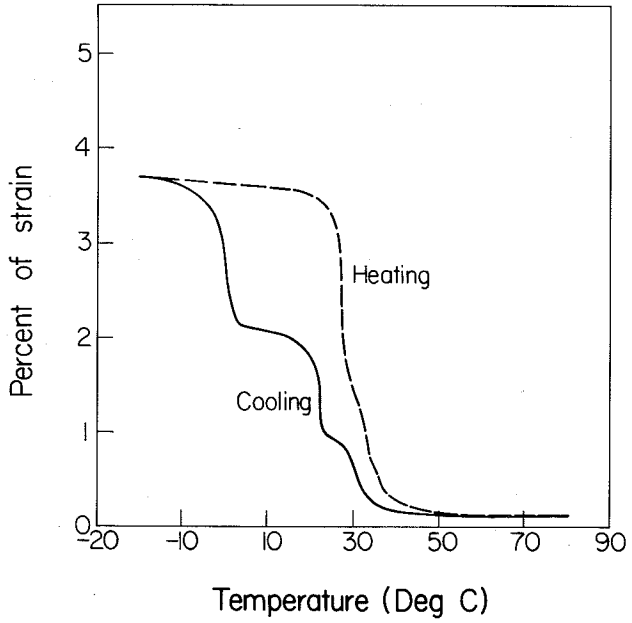

Fig. 2. Strain-Temperature Hysteresis Loop for Uncycled Nitinol Wire. Measurements were made at constant stress of 2.3 kpsi.
(XBL 811-85)

The major portion of strain in this specimen (and the maximum strain rate) occurs between the temperatures of +5° and -5°C, and displacement is essentially complete at the temperature of -20°C. On reheating, strain reversion (the shape recovery) begins at approximately 25°C and is essentially complete by 60°C. The distance between the active sections of the heating and cooling paths denotes the thermal hysteresis of the cycle, in this case about 30°C. Maximum strain in this specimen was approximately 1.3%.

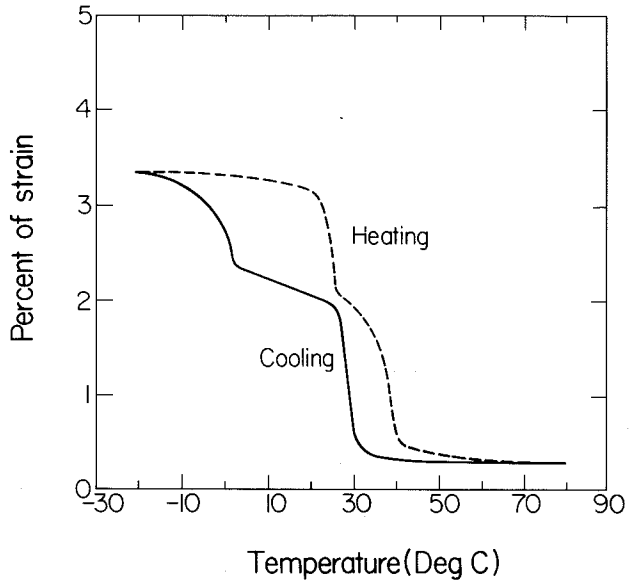

Fig. 3. Strain-Temperature Hysteresis Loop for Nitinol Wire that has undergone 1 x 10^6 cycles in the Fatigue Test Stand. Measurements were made at constant stress of 2.3 kpsi.
(XBL 811-88)

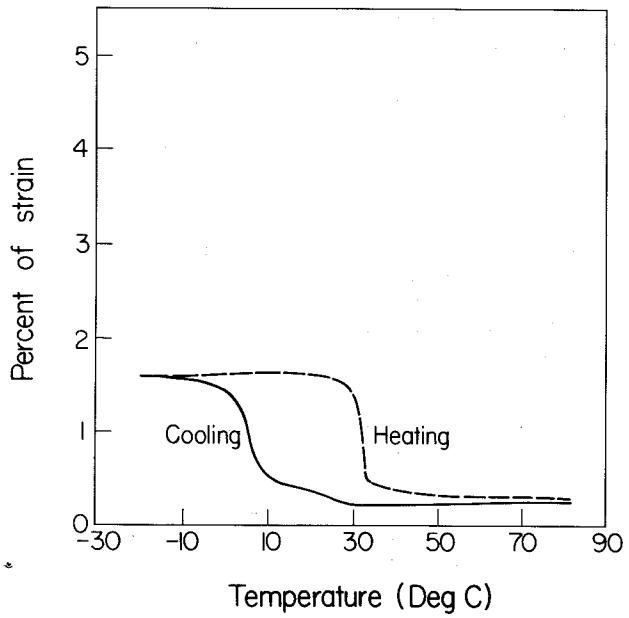

Fig. 4. Strain-Temperature Hysteresis Loop for Nitinol Wire that has undergone 5.3 x 10^6 cycles in the Fatigue Test Stand. Measurements were made at constant stress of 2.3 kpsi.
(XBL 811-91)

Wire taken from the Fatigue Test Stand after 10^6 working cycles was subjected to testing on the dilatometer (Fig. 3) under identical stress and temperature conditions as for the first sample previously described. Maximum strain in this specimen is approximately 3.5% for the complete thermal range of +80° to -20°C. However, in the thermal range defined by the operating temperatures of the test stand (+42° to -18°C), the wire had developed a novel pattern of thermoelastic behavior. Strain in this specimen begins at approximately 35°C (on cooling) followed by an elongation of about 0.75%, accomplished at the temperature of 20°C. This displacement is followed by a secondary strain threshold at ~20°C and rapidly increasing elongation to a total (local) strain of about 1.7% at the minimum (test stand) cycling temperature of 18°C. Because this subordinate or "working" strain-temperature cycle corresponds rigorously to the operating parameters of the test stand, some sort of microstructural accommodation in the material may have occurred which optimized its performance under actual working conditions. Thermal hysteresis for the working cycle was reduced to ≤10°C, according to the dilatometer measurements.

On further cooling (in the dilatometer) a third thermoelastic strain threshold appears, initiating a ternary strain-temperature cycle that preserves many of the features of the thermal hysteresis loop of the original uncycled specimen of Figure 2. This cycle occurs at temperatures never attained in the test stand's operating range of 0° to -20°C, and it is accounted for, presumably, by transformation and reversion of low-temperature crystal (martensite) variants unaffected--and therefore unoptimized--by microstructural accommodations occurring during the course of the first 10^6 working cycles.

The strain-temperature cycle for wire taken from the test stand after completion of 5.3×10^6 working cycles (Fig. 4) is qualitatively similar to that of the specimen tested at 10^6 cycles, although the consequences of the test conditions have become even more pronounced in the behavior of the more stabilized wire. The subordinate strain threshold observed at 20°C (on cooling) for the 10^6-cycle wire has now disappeared. Strain for the working cycle begins slightly above 30° and proceeds almost uniformly, reaching a local maximum of approximately 1.75% at 26°C, the temperature of the cold water bath at this stage of the cycle-testing schedule. The rate of elongation on cooling now exceeds the rate of contraction on heating, as indicated by the more nearly vertical slope of the unbroken line in the "working cycle" portion of the graph compared to the slope of the heating path opposite. Shape recovery on heating, for this "working cycle," also begins very close to the final (local) minimum temperature loop in this portion of the graph. At 5.3×10^6 cycles the area of the "unavailable" portion of the cycle--from 0° to -20°C--has become somewhat reduced, as has overall strain in the complete thermal transformation range. Displacement within the thermal extrema of the test stand operation, however, remains essentially unchanged.

Time and manpower constraints during this final period of the Nitinol Engine Development Project precluded correlating these changes in the macroscopic thermoelastic behavior of Nitinol wires from the test stand either with possible changes in the physical metallurgy of the material or with changes in the thermodynamic conversion efficiency of cycles employing these stabilized Nitinol materials. However, increased thermal sensitivity in these specimens does relate directly to systematic improvements in the observed operation of the Fatigue Test Stand (i.e., an increased cycling rate at reduced ΔT, under constant load). Therefore, it may be reasonable to assume that efficiency, as well as work output potential of the material, may be enhanced as the result of repetitive cycling under actual working conditions.

PLANNED ACTIVITIES FOR FY 1981

Support for this project was discontinued as of the end of FY 1980, and the project has been terminated.

APPROPRIATE ENERGY TECHNOLOGY*

C. Case, B. Lucarelli, J. Kessel, H. Clark, J. Kay, and J. Linse

INTRODUCTION

In 1977, the Energy Research and Development Administration (ERDA), now incorporated in the Department of Energy (DOE), established an appropriate technology small grants program. The purpose of the program is to fund projects that design, manufacture, and/or demonstrate small-scale energy technologies which conserve depletable fossil fuels or use renewable energy resources. DOE makes the grants available annually on a competitive basis to small businesses, individuals, nonprofit organizations, public agencies, and Indian tribes. The maximum grant award is $50,000.

To date, DOE has funded more than 1,100 projects nationwide for $19 million. The grants cover a complete spectrum of small-scale energy technolo-

* This work was supported by the Assistant Secretary for Conservation and Solar Energy, Office of Inventions and Small Scale Technology, Appropriate Technology Division of the U.S. Department of Energy under Contract No. W-7405-ENG-48.

gies, including solar active and passive systems, wind machines, biomass conversion systems, energy conservation devices, recycling methods, aquaculture systems, hydroelectric devices, and geothermal heating systems.

ACCOMPLISHMENTS DURING FY 1980

Since the program's start in 1977, LBL has assisted the DOE in establishing project review procedures and in evaluating the program's effectiveness. Our function has evolved from providing technical advice on a regional basis to conducting energy studies on a national level.

In the past, LBL provided DOE with technical support in three ways:

1. reviewing grant proposals for technical and economic merit;
2. monitoring projects in Arizona, Nevada, and the western Pacific; and
3. advising DOE on effective technical review procedures for the grants program.

As the program evolved, the regional DOE and state energy offices took over these functions. DOE then asked LBL to change the focus of its work and to conduct energy studies that determine the program's energy savings potential and the economic and technical feasibility of developing selected small-scale technologies and renewable energy resources. The next sections describe these studies, which are being completed in FY 1981.

Energy Impact Analysis

Because of the diverse array of technologies and end-use applications of DOE-funded appropriate technology projects, DOE has been unable to assess the program's energy savings potential, an assessment that is necessary for comparing the program with other DOE programs. To obtain this information, DOE asked LBL to assess the program's energy savings potential and cost-effectiveness.

We began our analysis in 1979, assessing the energy savings potential of 20 projects from Region IX.[1] We completed the analysis in 1979 and found that most of these projects could save a significant amount of energy either directly, from the original project, or indirectly, from demonstration and commercialization effects. However, the sample was small and specific only to Region IX; therefore, we could not extrapolate our findings to estimate the energy savings potential of the national grants program.

For our continuing analysis, we are evaluating a sample of 57 projects funded in FY 1979.[2] The 57 projects have been selected from eight of the ten federal regions and cover the full range of technology categories funded: wind, biomass, solar, geothermal, hydro, and conservation.

The analysis is being conducted in 4 steps:

1. evaluation of project energy savings;
2. assessment of economic feasibility;
3. estimation of replication potential; and
4. extrapolation of sample energy savings to estimate program energy savings.

For a project to have replication potential, the project must be cost-effective and the grantee must have a plan to market the device produced or to disseminate the results of the project. From the assessment of the 60 projects, we will attempt to estimate the energy savings potential of all projects funded in FY 1979.

Technology Assessment Study

We are also assessing the technical and economic feasibility of small wind energy systems in the U.S.[3] The analysis is being conducted from a sample of wind energy projects funded by the grants program in FY 1978. The projects apply wind systems in the agricultural, residential, and industrial sectors for pumping water, generating electricity, and heating water. Electric projects range in size from 1 to 35 kw. For this study, we are assessing each project for technical performance, economic feasibility, and physical infrastructure requirements. The end product will be a report which discusses near-term applications of small wind systems and the physical infrastructure requirements that can make feasible a larger array of small wind energy applications.

Biomass Energy Assessment

We have completed a comprehensive assessment of California's biomass and its energy potential.[4] The study estimates the amount of biomass in the form of agricultural, municipal, and forestry wastes produced in California in 1976 and then projects these estimates to 2025. The study considers the use of biomass for producing electricity, low-Btu gas, alcohol, and methane, with an emphasis on producing alcohol and methane as fuels for the transport sector.

In terms of economic feasibility, we found that the production of ethanol from feed grains and of methane from animal and human wastes are already cost-effective if the energy is used on site. By 1990, with moderate increases in energy prices, off-site energy use should be cost-effective. Methanol produced from wood will be a cost-effective technology by 1990 for large plants which consume 3,400 tons or more of wood per day. Overall, the state's biomass can meet only 20% of the projected demand for fuels in the state's transport sector even with a reasonable conservation effort. Moreover, the feasibility of producing methanol will be limited by a fragmented biomass fuels market and by the large size of methanol synthesis plants, which will require long-distance transport of biomass.

To conclude, the state's biomass can supply a significant fraction of the state's transportation energy demand, but because of the fragmented biomass market and high costs of biomass transport, small-scale applications of biomass technologies with on-site use of the energy will probably be the dominant use of biomass for the next 50 years.

PLANNED ACTIVITIES FOR FY 1981

In FY 1981, we will complete our analysis of program energy savings. In a third and final analysis, LBL will evaluate the energy savings potential and cost-effectiveness of 30 projects funded by DOE in FY 1980. This analysis plus the prior studies should provide DOE with the data needed for evaluating the grants program. We plan to expand our assessments of specific technologies in FY 1982. The following technologies will be considered:

- small-scale alcohol fermentation plants,
- anaerobic digesters,
- active solar systems, and
- wind energy systems (an expansion of the FY 1981 study).

For each technology assessment, we will document the technical innovations and cost-effectiveness of a large sample of projects and identify projects which have exceptional energy savings potential.

REFERENCES

1. F.B. Lucarelli, J. Morris, J.M. Kay, S. Rizer, C.W. Case, and H.R. Clark, The Energy Savings Potential of the Region IX Appropriate Energy Technology Grants Program: An Assessment of Twenty Projects, Lawrence Berkeley Laboratory report LBL-9715, October 1979.
2. F.B. Lucarelli, J. Kessel, J. Kay, and J. Linse, The DOE Small Grants Program and Its Energy Savings Potential, Lawrence Berkeley Laboratory report (in progress).
3. J. Kay, A Technical and Economic Assessment of 13 Small Wind Energy Projects, Masters thesis (in progress), University of California, Berkeley.
4. F. B. Lucarelli, Jr., California's Biomass and Its Energy Potential, Lawrence Berkeley Laboratory report LBL-10058, April 1980.

ENERGY CONVERSION BY RETINAL PROTEIN, BACTERIORHODOPSIN*

L. Packer, A. Quintanilha, R. Mehlhorn, C. Carmeli, P. Sullivan, P. Scherrer, N. Kamo, S. Tristram, J. Herz, and A. Pfeiffhofer

INTRODUCTION

Light generates a pH gradient and an electrical potential across the purple membrane of Halobacterium halobium. We are investigating the time-resolved changes in protonation of the side chains of specific amino acid residues and the correlation of these changes with photon absorption and the ensuing photoreaction cycle. Our aim is to determine the precise molecular description of the photocycle and of the time-dependent steps in the uptake, translocation, and release of protons by the retinal protein catalyst in this membrane, bacteriorhodopsin.

The photocycle is initiated by absorption of visible radiation (with an absolute maximum at 570 nm) by the all-trans retinal chromophore. The initial steps of the photocycle involve the isomerization of the chromophore to the 13-cis retinal. A deprotonated Schiff base forms with a $t_{1/2}$ of about 50 μmsec. Proton release occurs in this time range (illustrated in the upper half of Figure 1). Later, the deprotonated species decays ($t_{1/2}$ about 3-5 msec), restoring the original all-trans form of the chromophore. During this time, protons are taken up from the cytoplasmic surface of the protein. This process is shown in the bottom half of Figure 1. The deprotonated photointermediate is referred to as the M_{412} species.

To assess significant structural features of the lipid and the protein, which are important for proton movement, we have used chemical modification of amino acid side chains, spin labeling, and deuterium isotope effects on purple membranes. Purple membranes have also been reconstituted into liposomes before and after such treatment. The purpose of this step is to derive information relevant to the occurrence of proton movement at the cytoplasmic surface of the purple membrane. This information will help us understand the importance of the electrochemical potential developed across the closed vesicle membrane in the regulation of light energy conversion.

* This work was supported by the Assistant Secretary for Energy Research, Office of Basic Energy Sciences, Chemical Sciences Division of the U.S. Department of Energy under Contract No. W-7405-ENG-48.

ACCOMPLISHMENTS DURING FY 1980

Chemical Modification Studies

Modification of Positively Charged Amino Acids

PROTEIN CONFORMATION STATES OF BACTERIORHODOPSIN ASSOCIATED WITH PROTON TRANSLOCATION ACROSS THE PURPLE MEMBRANE

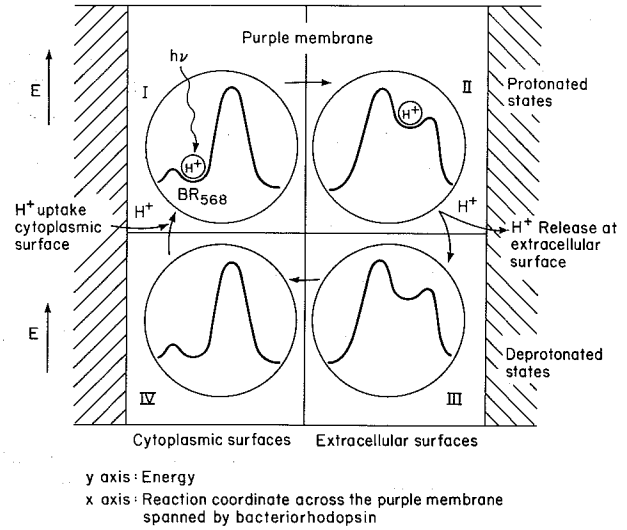

Fig. 1. Protein conformation states of bacteriorhodopsin associated with photon translocation across the purple membrane.

(XBL 8011-2373)

Lysine. Modification of up to 80% of the ε-amino groups of lysine, that is five of the six available lysine residues,[1] with imidoesters (methyl acetimidate, ethyl acetimidate and methyl butyrimidate) which introduce progressively more bulky groups onto the lysyl residues but leave the charge substantially unaltered, showed little effect on the rate of M_{412} formation and decay.[2] Similar results were obtained when the charge of the amino group was changed by the use of succinic or acetic anhydride, or pyridoxyl phosphate. These studies demonstrate that the ε-amino groups of lysine are probably not involved in a coordinated pathway of proton translocation by the protein.

However, lysine groups do play a structural role essential for activity. Using either dimethyl adipimidate (DMA) (8.3 Å) or glutaraldehyde (7.5 Å), bifunctional reagents which chemically cross-link lysyl residues, we found a very strong inhibition of M_{412} decay[3] and a decreased proton uptake in reconstituted liposomes. Cross-linking with longer chain bifunctional reagents (like dimethyl suberimidate (11.3 Å) of individual bacteriorhodopsin molecules to each other had no effect on activity. These effects suggest that intramolecular conformational changes and not protein-protein interactions in the membrane are essential for activity.

Arginine. With both 2,3-butanedione (BD) and phenylglyoxyl (PGO) treatments, similar effects were obtained for the modified purple membranes.[4] Modification of three of the seven arginine residues resulted in a 33- and 18-fold inhibition of the $t_{1/2}$ of the first and second phases of M_{412} decay, respectively, and a 19-fold increase in the amount of M_{412} stationary state when assayed at pH 8. These results indicate that the positive charges of the guanidinium groups of unmodified residues are essential for photocycling activity.

Modification of Negatively Charged Amino Acids

Glutamate and Aspartate. Water soluble carbodiimides cause the carboxyl groups of these amino acids to become either neutral or positive. These modifications slowed down the M_{412} decay; had no effect on its formation; and caused a large increase in its photostationary state.

In the presence of the added nucleophile, glycine methyl ester (GME), carbodiimide [1-ethyl-3-(3-dimethylaminopropyl) carbodiimide--EDC] treatment is expected to yield the amide adduct. With increasing concentrations of GME (1-250 mM), and in the presence of EDC, the degree of inhibition of M_{412} decay was partially decreased, suggesting that GME may be competing with a nucleophilic group on the protein. Evidence supporting this idea has come from double modification experiments. EDC-treated samples previously modified by ethyl acetimidate showed M_{412} decay kinetics similar to that observed in samples modified by EDC in the presence of high GME concentrations. The similarity suggests that EA-modified lysines have become unavailable for reaction with EDC, preventing the formation of intramolecular cross-links. Since EDC can only cross-link closely lying groups, we suspect that the ε-amino groups of lysine must be very close to the carboxyl groups.

Other important results of carbodiimide modification are the total disappearance of one of the photointermediates (O_{640}) in the photocycle and the inability to generate the acid stable form of the protein (with an absolute maximum at 605 nm). These results suggest that the protonation of one (or more) carboxyl residues is necessary for the generation of that photointermediate as well as for the acid stabilization of the protein.

Tyrosine. By investigating the time course of lactoperoxidase catalyzed iodination of purple membranes, we have been able to obtain evidence of an involvement of at least one tyrosyl residue in proton release and one or several tyrosyl residues involved in reprotonation.[5,6] Modification of one type of tyrosyl residue (localized on the cytoplasmic surface, according to modification studies done on intact cell envelope vesicles) markedly slows M_{412} decay but does not alter the optical and Raman spectral characteristics of the chromophore. Iodination of another tyrosyl residue alters the optical and Raman spectra of the chromophore and markedly stimulates M_{412} formation.

The modifications exhibit a strong effect on the pH-dependence of the photocycle, shifting the curve to lower pH values. This shifting suggests that the introduction of rather bulky groups onto the tyrosyl residues may alter the pK's and sterically effect their ability to take part in proton movements. What follows provides evidence for this explanation.

Deuterium Isotope Effects

In agreement with previous reports,[7] we find that the rise time of M_{412} is slowed by a factor of 4.7 in D_2O whereas the decay time is slowed by a factor of only 2.1. We have measured similar isotope effects for a number of chemically modified

Table 1. Kinetic parameters and isotope ratios for rise and decay of M_{412}.

Sample[c]	Rise[a] $t^H_{1/2}$	Rise[a] $t^D_{1/2}$	Rise[a] k^H_1/k^D_1	Decay[a] $t^H_{1/2}$	Decay[a] $t^D_{1/2}$	Decay[a] k^H_2/k^D_2
Control	0.069	0.33	4.76	3.65	7.7	2.11
EAC (Carboxyl)	0.099	0.42	4.24	90[b]	131[b]	1.45
I_2 (Tyrosine)	0.026	0.11	4.15	420[b]	1042	2.48
NBS (Tryptophan)	0.043	0.147	3.40	19.2	67.3[b]	3.5
DMA (Lysine)	0.072	0.35	4.86	33.0	46.2[b]	1.4
EA (Lysine)	0.062	0.32	4.9	10.8	27.4[b]	2.5
BD (Arginine)	0.096	0.49	5.1	359[b]	1055	2.9
PGO (Arginine)	0.142	0.71	5.0	355[b]	724[b]	2.0

[a] Half lives in milliseconds.

[b] Decay kinetics are biphasic, only slow phase given.

[c] Assay conditions: protein 0.15-0.30 mg/ml in 100 mM KCl and 5 mM phosphate; pH 7.5-8.0.

purple membranes. The similarity indicates that the basic mechanism remains similar in the modified samples (see Table 1). The activation parameters for the rates of rise and decay of M_{412} were determined from their temperature dependence.[8] For tyrosine modified samples, for example, the activation parameters are consistent with a decreased pK for a tyrosine residue (lowered E_a), an increased steric effect caused by iodine substitution (negative $S^\dagger$), and an overall decrease in the rate of reprotonation (increased $G^\dagger$) of the Schiff base. If the tyrosine residue is directly involved in the reprotonation of the Schiff base, the effect of its modification on the activation parameters is not surprising.

Light-Induced Surface Potential Changes of Purple Membranes

The positively charged paramagnetic amphiphile 4-(dodecyl dimethyl ammonium)-1-oxyl-2,2,6,6-tetramethyl piperidine bromide (CAT_{12}) partitions between the membrane and the aqueous phase. Therefore, CAT_{12} was useful in monitoring changes in surface potential associated with the release and uptake of protons from the purple membrane.[9] Using laser flash EPR and photolysis, we showed that the uptake and release of the CAT_{12} probe closely follows the kinetics of the rise and decay of the M_{412} intermediate.[10] This correlation indicated that the probe senses exposed negative charges at the surface from which protons are released. The number of light-induced surface charges per M_{412} in the photostationary state was calculated to be approximately 1. The value is more than 50% decreased for carboxyl and guanidinium group modification and for heavily modified tyrosine samples, suggesting that some of these groups may be located at the surface of the protein and may be involved in the uptake and release of protons from the aqueous environment.

Control of the Photocycle by the Transmembrane Potential Gradient

When reconstituted into liposomes, bacteriorhodopsin will generate light-induced electrochemical gradients across the lipid bilayer. Our reconstituted systems generate pH gradients of 0.6-1.0 and transmembrane electrical potentials of 60-80 mV.[11] The photostationary state of M_{412} at the same light intensity and protein concentration was much higher in the reconstituted system than in the isolated purple membranes. Valinomycin (0.5 μM) decreased the photostationary state of M_{412} by one order of magnitude in the reconstituted system but had no effect in isolated purple membranes. Nigericin (0.5 μM) had no effect on either system. Because we observed that, at the concentration used, Valinomycin collapses the transmembrane potential and Nigericin collapses the pH gradient, we assume that the electrical gradient was probably the major controlling factor on the kinetics of the photocycle.

Steady state, light-induced electrochemical gradients across bacteriorhodopsin containing liposomes showed a substantial slowdown of the M_{412} decay kinetics with virtually no effect on the rise kinetics. Again, Valinomycin, but not Nigericin, brought the decay kinetics of M_{412} to those measured in the absence of steady state illumination.

These responses suggest that within the protein, light may generate strong electric dipoles that could be very sensitive to the transmembrane electric potential gradients, which can be established across the bacterial membrane.

DISCUSSION

The sharp pH dependence seen in controls and the downward shift of the dependence in the rise and decay of the M_{412} species in tyrosine-modified purple membrane preparations suggests a direct involvement of reversible tyrosine protonation in the pathway of proton movement through bacteriorhodopsin (Fig. 2). Reversible dissociation of protons at both the outer and inner purple membrane surface would be expected to be pH- and pK-dependent, hence regulated by the electrochemical gradient. Since the pH gradients are small (≤ 1), pK effects on the photocycle are not to be expected, and indeed, we find that the main control parameter is the transmembrane potential.

Proton Uptake. Several structural requirements appear to be important for reprotonation of bacteriorhodopsin. Our results with modification of carboxyl and guanidinium groups suggest that a charge transfer complex essential for reprotonation may exist between the two types of groups. Moreover, the large changes in the entropy of activation for the M_{412} decay provides strong supporting evidence that interaction between these two types of groups is an essential structural feature involved in proton uptake and the photocycle's reprotonation phase. Furthermore, as judged by double modification experiments, an interaction between carboxyl groups and at least one amino group of lysine also appears to be important for reprotonation. The above structural requirements together with the inhibitory effects of bifunctional cross-linking reagents which restrain motion of intramolecular amino groups of lysine located within 8.3 Å of one another suggests that protein conformational changes are essential to proton uptake and M_{412} reprotonation. Tyrosine may also act as a donor for Schiff base reprotonation.

Proton Release. The specific groups involved in release of protons at the outer surface of the purple membrane probably include tyrosine residues; this conclusion is drawn from the observed effects of iodination and nitration[12] that shift the dissociation pK of the phenolic hydroxyl group of tyrosine residues. The pK shift may accelerate proton movement from this group on the tyrosine to a nearby basic group which may be water, OH-, a group on the lipid of the purple membrane, or a buffer anion. The acceleration would be expected to occur in the range where proton release is pH dependent. Based on the pronounced deuterium isotope effect on proton release as seen before and after iodination of tyrosine, it can also be argued that the tyrosine residues are involved in the early stages of the photocycle, i.e., those associated with the proton release.

Carboxyl groups may also play a role in the movement of protons; modification of these groups has inhibited the generation of one of the intermediates in the photocycle and the formation of an acid-stable species.

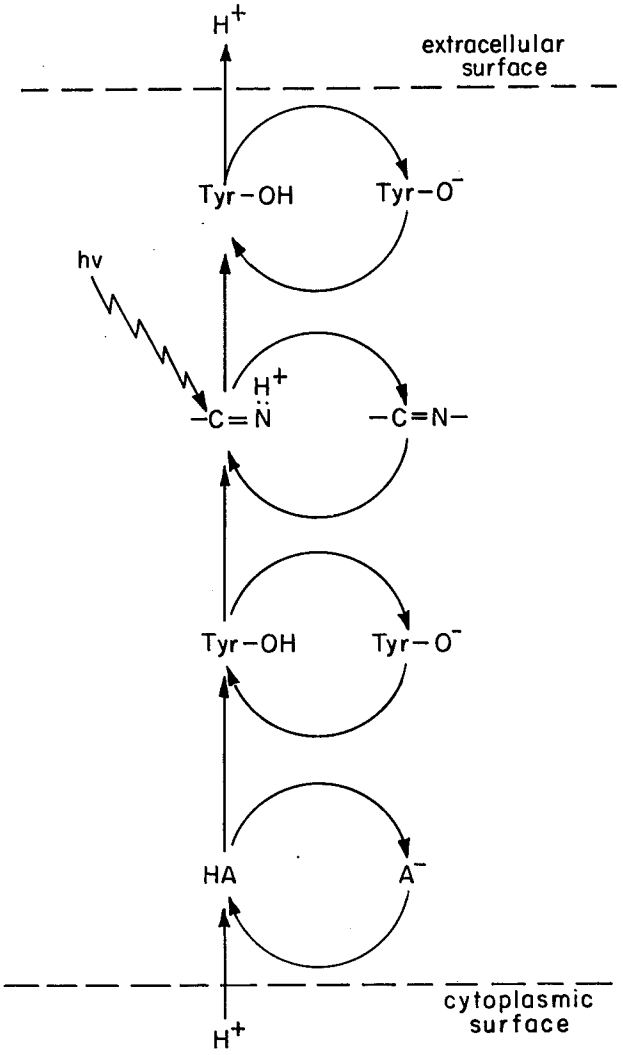

Fig. 2. A proposed pathway for uptake and release of protons by bacteriorhodopsin. We include on the pathway the reversible deprotonation of the tyrosine residues before and after the Schiff base. (XBL 805-5111)

Light-induced changes in the surface potential of the purple membrane suggest that protons are released from protonated groups at the surface, because these surface potential changes are closely coupled to the formation of the M_{412} species. Our experiments provide evidence that the groups involved may be carboxyl and tyrosyl residues.

PLANNED ACTIVITIES FOR FY 1981

Our studies of the molecular architecture of bacteriorhodopsin in relation to its energy conversion activity have been particularly fruitful in revealing that certain amino acid structural relationships and certain amino acid side chains play an essential role in the light-driven release and uptake of protons. We wish to arrive at a more fundamental understanding of the molecular basis for this activity.

Our research next year will take advantage of a spectacular new development: the discovery by Professor Y. Mukohata of Osaka, Japan of a mutant species of Halobacteria, which forms a "white membrane." The white membrane is an aggregate of protein and lipid molecules which can be recognized by electron microscopy as a patch in the plane of halobacterial membranes. This patch totally lacks retinal but apparently contains the apoprotein portion of bacteriorhodopsin, because a native purple membrane can be formed by the addition of all-trans retinal. Procedures have been developed for the isolation and purification of this patch, which is clearly the material par excellence for chemical modification studies designed to inform us about the importance of the protein structure and about different types of retinal analogues in the energy conversion process. We are the only laboratory in the U.S. that has been given this strain. Professor Mukohata, the discoverer, has spent three months on an NSF U.S.-Japan Cooperative Program, working with us to develop the methods of cultivating the organisms and preparing the white membranes. We intend to pursue studies using and comparing this material with native purple membranes.

Our research will also exploit the ability to modify groups in purple membranes in the dark and in the light. We have made some preliminary discoveries indicating that the ability to gain accessibility with external chemical modifying reagents to different groups differs in the dark and the light. Certain groups are available for reaction only in the light, such as the tyrosine groups, which are available for modification using nitration reagents. To better understand the protein conformational cycle driven by light energy absorbed by the retinal chromophore, we will perform chemical modifications in the white membrane and in regenerated purple membranes, both in the dark and during illumination, to determine the degree to which activity is affected after the specific modifications. These studies indicate the groups that become exposed and the part of the photocycle in which they will appear. Knowing the deuterium isotope effects, we ought to arrive at a better understanding of which groups play an essential role in the proton translocation, proton uptake and proton release process, all of which are aspects of the overall ability of this retinal protein system in bacterial membranes to generate a proton electrochemical gradient after absorption of a photon of 570 nm light.

REFERENCES

1. W. Stoeckenius and R. Lozier, "Light Energy Conversion in Halobacterium halobium," Journal of Supramolecular Structures, vol. 2, 1974, pp. 769-774.
2. T. Konishi, S. Tristram, and L. Packer, "The Effect of Crosslinking on Photocycling Activity of Bacteriorhodopsin," Photochemistry and Photobiology, vol. 29, 1979, pp. 353-358.
3. T. Konishi and L. Packer, "Light-Dark Conformational States in Bacteriorhodopsin," Biochemical Biophysical Research Communications, vol. 72, 1976, pp. 1437-1441.
4. L. Packer, S. Tristram, J. Herz, C. Russell, and C. Borders, "Chemical Modification of Purple Membranes: Role of Arginine and Carboxylic Acid Residues in Bacteriorhodopsin," Federation of European Biochemical Societies Letters, vol. 108, 1979, pp. 243-248.
5. P. Scherrer, C. Carmeli, P. Shieh, and L. Packer, "The Effect of Chemical Modification of Tyrosyl Residues on Proton Conductivity Mediated by Bacteriorhodopsin," Biophysical Journal, vol. 25, 1979, p. 207a.
6. P. Scherrer, L. Packer, S. Seltzer, and M. Lin, "Involvement of Tyrosine Residues in Bacteriorhodopsin Activity," submitted for publication.
7. R. Korenstein, W. Sherman, and R. Caplan, "Kinetic Isotope Effects in the Photochemical Cycle of Bacteriorhodopsin," Biophysics of Structure and Mechanism, vol. 2, 1976, pp. 267-276.
8. P. Sullivan, A. Quintanilha, S. Tristram, and L. Packer, "Isotope Effects and Activation Parameters for Chemically Modified Bacteriorhodopsin," Federation of European Biochemical Societies Letters, vol. 117, 1980, pp. 359-362.
9. C. Carmeli, A. Quintanilha, and L. Packer, "Light-Induced Surface Potential Changes in Purple Membranes and Bacteriorhodopsin Liposomes," in C. P. Lee et al., eds. Membrane Bioenergetics, (Reading, Mass: Addison Wesley Publishing Co., 1980) pp. 547-558.
10. C. Carmeli, A. Quintanilha, and L. Packer, "Surface Charge Changes in Purple Membranes and the Photoreaction Cycle of Bacteriorhodopsin," Procedures of the National Academy of Sciences (U.S.A.), vol. 77, 1980, pp. 4707-4711.
11. A. Quintanilha, "Control of the Photocycle in Bacteriorhodopsin by Electrochemical Gradients." Federation of European Biochemical Societies Letters, vol. 117, 1980, pp. 8-12.
12. M. Campos-Cavieres, T. Moore, and R. Perham, "Effect of Modification of the Tyrosine Residues of Bacteriorhodopsin with Tetranitromethane." Biochemical Journal, vol. 179, 1979, pp. 233-238.

EXPERIMENTAL AND THEORETICAL EVALUATION OF CONTROL STRATEGIES FOR ACTIVE SOLAR ENERGY SYSTEMS*

M. Warren, S. Schiller, M. Wahlig, G. Sadler, C. Vilmer, and C. Weaver

INTRODUCTION

Improved solar energy control systems will reduce the use of nonrenewable fuel sources for heating building spaces and domestic hot water. To accelerate this reduction, an experimental test facility has been constructed at LBL to test the system efficiency and cost effectiveness of alternative control strategies for collecting solar energy and delivering it to the building load. In parallel with this experimental effort, a computer analysis capability has been developed to study the dynamics of interactions between collector, load, and control system, and an investigation has been initiated into control-related reliability problems of installed solar-heating and solar-cooling systems. LBL has also provided technical support to DOE in the controls area, including program planning and monitoring of outside contractors.

ACCOMPLISHMENTS IN FY 1980

Experimental Test Facility.

The experimental test facility was constructed to evaluate the operation and performance of active hydronic solar energy system control strategies and equipment. The facility, shown in Figure 1, consists of a collector loop heat-input simulator, a storage tank, a load loop air channel with fan coil, an auxiliary heater, and associated pumps and valves. Only the apparent temperature of the collector and the load demand thermostat condition are simulated, enabling control strategy and equipment comparisons based on identical meteorological and load conditions. The facility is described in detail elsewhere.[1,2,3]

This year the experimental test facility was operated to simulate a specific residential solar-assisted heating system for several days, using both simulated weather and typical meteorological year (TMY) weather and insolation data for Madison, Wis. in January. The residential building loads and incident insolation are calculated using TRNSYS† and are used as inputs to drive the experimental system simulation. Early in the year a number of four-hour and one-day experiments were repeated to verify operation and energy balance of the collector loop and of the load loop separately. At the end of the year, a number of two-day experiments using TMY data were run.

Test Facility Improvements

Several improvements and modifications have been made to the test facility during FY 1980.

The storage tank was drained to a level of approximately 1,000 gal to accommodate a design solar fraction of 50% for Madison. Seven equally spaced thermocouples were installed in the storage tank to measure the temperature profile. Because of the finite number of thermocouples in the storage tank, the measured energy storage can vary typically ±5 MJ from hour to hour when there is a sharp gradient in the storage tank temperature. With the reduced storage tank volume, it was found that air was drawn into the collector and load loop piping causing minimal or no flow during start-up conditions. Several valves were moved and piping rearranged to correct the problem. Similar problems have been encountered in a number of installations, stressing the importance of correct placement of pumps and valves.

The test facility control software was rewritten to utilize hourly weather and building load data and quarter-hour insolation values, which can be inputed before an experiment. Another routine was written, in conjunction with the addition of some electronic hardware, to record the energy consumption from the electricity and gas meters. To predict more accurately the collector temperature, a simple one-node collector capacitance model was implemented for the stagnating collector simulation, thereby modeling more realistically the on/off cycling of the collector loop.

Experiments were conducted to determine system energy losses and the collector and load loop energy balances. Energy losses for each subsystem (storage tank, collector loop, and load loop) were determined observing the decay in storage tank temperature over several days with zero load or energy input.

Residential System Description

The building chosen for simulation, the weather data, and the residential heating load model are taken from the "Standard Assumptions and Methods" recommended by the Solar Energy Research Institute (SERI).[4] A typical, well-insulated 1,700 ft^2 single-story home located in Madison, Wis. was chosen for study. Meteorological data from TMY tapes combined with detailed building description determined the hourly heating requirements for the building for use in the test facility load loop. Hourly heating loads were calculated using the TRNSYS residential load model, TYPE 29. Quarter-

* This work has been supported by the Assistant Secretary for Conservation and Solar Energy, Office of Solar Applications for Buildings, Systems Development Branch, Active Heating and Cooling Division, U.S. Department of Energy under Contract No. W-7405-ENG-48.

† TRNSYS is a transient system simulation computer program developed at the University of Wisconsin and consists of a central algebraic and differential equation solver, a library of component models and associated input and output routines.

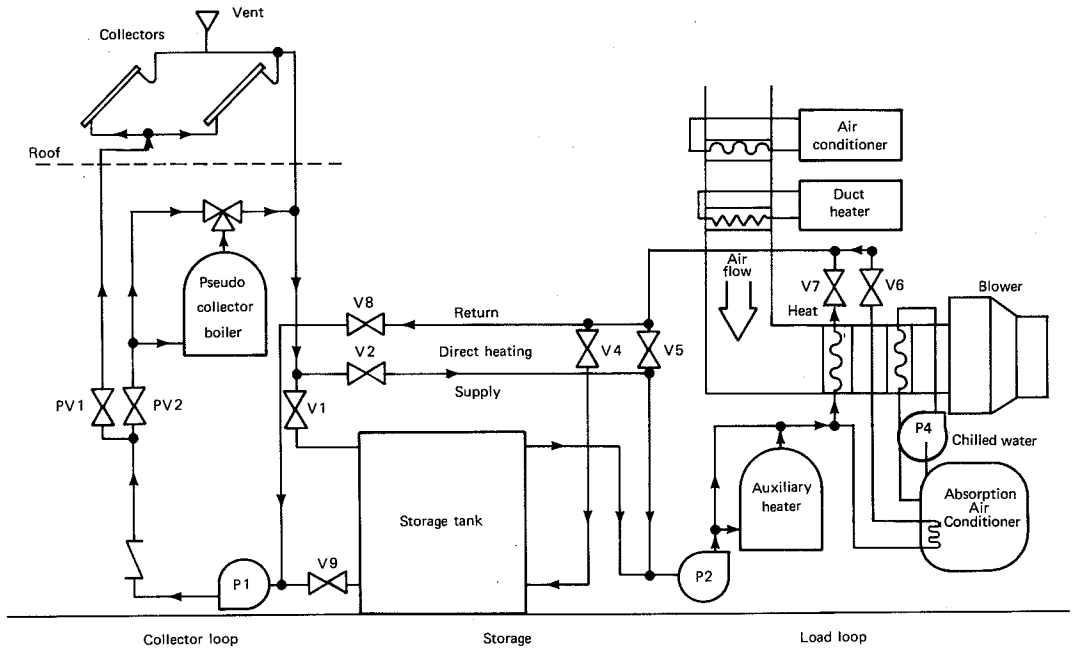

Fig. 1. Solar heating and cooling test facility. (XBL 794-1511)

hour insolation values incident in the plane of the collectors were calculated from TMY January data for Madison, Wis. using the TRNSYS solar radiation processor.

The components of the active solar system were sized using F-Chart 3.0. To provide a 50% annual solar heating fraction required a collector array of 50 m^2 and a water storage volume of about 3,800 liters (1000 gal).

The experimental procedure using the test facility is to test a particular control strategy during several "typical days" and then extrapolate results to determine long-term performance characteristics. The performance of a solar system during a particular day is dependent on the insolation, ambient temperature (which determines collector losses and building load), and the system's performance during the previous day. To evaluate the utilization of energy collected on a particular day, it is important to consider what the energy use is on the day following as well. Thus the minimum time required for a proper evaluation is two days, with the temperature of the storage tank on the first day indicative of the past day's operation.

The weather and insolation patterns for January in Madison were examined along with hourly storage tank temperatures predicted by TRNSYS for January to determine which days were appropriate for simulation. Based on the quantification of January days into categories, such as high amount of insolation, low ambient temperatures, and poor previous day, two pairs of days were chosen for detailed test facility simulation: a "bad-good" series (January 26-27) and a "good-bad" series (January 18-19).

Performance indicators recommended by Ward[5] are used for evaluating solar systems. These include collection efficiency, system thermal efficiency, solar coefficient of performance, system overall efficiency, and solar fraction. An additional performance indicator, storage tank temperature change, indicates the extent to which available solar energy is taken from, or added to, the storage tank over a given period.

Test Facility Results

Experiments were run using simulated meteorological and load inputs to evaluate experimental repeatability and to verify system energy balances. Experiments also compared two control strategies: a storage-coupled heating mode and a direct collector-to-load heating mode. In the more typical mode of operation, storage-coupled heating, collectors heat the storage tank and energy is drawn from storage to heat the load when energy is available and needed. With the direct-heating mode, the collectors can supply heat to the load without going through the storage tank. The direct-heat mode requires additional piping, valves, and control.

Tables 1 and 2 show results from test facility experiments. The quantities used in the tables are defined as follows: building load (QLOAD), auxiliary energy for load (QAUX), the natural gas usage (GAS), solar energy delivered to the load (QSOLAR-LOAD), insolation of the collector (QI), collected energy (QC), storage tank losses (SLOSS), load loop piping losses (LLOSS), collector loop piping losses (CLOSS), parasitic energy used (PARA), average storage tank temperature (T_{tank}), stored energy (QS), and change in stored energy (DQS).

Table 1 shows typical four-hour summaries of a 24-hour experiment for a cold January day in Madison with good insolation. The 24-hour system

Table 1. Typical four-hour summary results from a Direct Heating Test Facility Run. Simulation is of 18 January (TMY) in Madison, Wisc., a cold weather day with good insolation.

Time (hr)	T_{amb} (°C)	T_{tank}[QS] (°C) (MJ)	QLOAD (MJ)	SLOSS (MJ)	LLOSS (MJ)	QAUX (MJ)	QI (MJ)	QC (MJ)	CLOSS (MJ)	PARA (MJ)	GAS (MJ)
0	-5.4	31.5[209.6]	-	-	-	-	-	-	-	-	-
4	-8.8	30.7	86.9	2.9	4.7	72.2	0	0	0	4.5	176
8	-11.7	29.6	95.8	2.3	3.7	75.9	2.7	0	0	4.9	216
12	-9.8	36.6	83.1	3.6	5.8	45.5	416.0	191.1	4.6	7.8	89
16	-9.7	42.3	66.9	7.1	9.1	8.6	405.7	197.6	7.2	6.7	16
20	-14.1	37.5	85.8	6.7	8.7	11.7	6.6	0	0	3.0	16
24	-13.1	33.3[242.4]	99.4	4.8	6.5	34.1	0	0	0	4.0	81
Totals	-	+1.8[32.8]	517.9	27.4	38.5	248.0	831.0	388.7	11.8	30.9	594

Notes:

Qin = QC + QAUX - DQS = 388.7 + 248 - 32.8 = 603.9 MJ

Qout = CLOSS + LLOSS + SLOSS + QLOAD = 11.8 + 38.5 + 27.4 + 517.9 = 595.6 MJ

24-hour balance 2(Qin - Qout)/(Qin+Qout) = 8.3 MJ/599.8 MJ = 0.0138

QSOLAR-LOAD = QLOAD + LLOSS - QAUX = 517.9 + 38.5 - 248.0 = 308.4 MJ

Quantities in brackets represent storage energy QS and change in storage energy DQS.

energy balance is within 2%, indicating good accounting of energy flows in the collector and load loops and in the storage tank. This energy accounting is done minute by minute as the experiment progresses and is summarized on a floppy disk file after each thermostat cycle and at one- and four-hour intervals. A detailed record of the experiment is also printed out. Energy flow quantities are calculated from measured temperatures and flow rates. Energy losses are calculated from measured fluid and room temperatures and experimentally estimated loss coefficients. The parasitic and auxiliary gas consumption are measured with standard utility meters interfaced to the experiment instrumentation. The solar energy delivered to the load, QSOLAR-LOAD, includes the heat from the fan coil, QLOAD, less the auxiliary input, QAUX, and takes credit for heat lost from the load loop piping, LLOSS. The allocation of useful heating from the storage and load loop losses depends on the specific system layout.

Test days were run twice for each of two different control strategies: direct heating and storage-coupled heating. Table 2 shows the one-day energy balance totals for the different runs of the same day. The different runs show excellent agreement in the load demand, QLOAD, the total energy inputs to the system, Q_{in}, the total energy output from the system, Q_{out}, and the energy balance, ΔQ. The energy loss terms, SLOSS, LLOSS, and CLOSS also agree well from run to run. However, there is some variation from run to run in the auxiliary energy usage, QAUX, in the change in stored energy, DQS, and in the contribution to the load from solar, QSOLAR-LOAD. This variation is of the order of 25 MJ over the day and represents less than 5% of the total energy flow during the day, which was the accuracy goal for measuring energy flows in the test facility.

Comparison of Test Facility Results with TRNSYS

To assist in evaluating the results obtained from the test facility, TRNSYS simulations are conducted for the same test days. Typical simulation results are also shown on Table 2. The TRNSYS program's format allows the simulation of the test facility system using identical meteorological and load inputs as well as approximately the same component parameters and interconnections. The TRNSYS simulation was started on January 1 at 1 a.m., using TMY weather data, with a storage tank temperature of 20°C, and run continuously for the entire month. Initial average storage tank temperatures and time-dependent building loads, as determined by TRNSYS for a given period, were then used for the experiments.

The test facility operating strategy has an auxiliary boost mode where the auxiliary heater increases the temperature of the water to the fan coil as long as the return water temperature is not greater than the storage tank bottom temperature. Existing TRNSYS parallel and series auxiliary heating modes do not model this operation. The parallel mode draws the storage tank down to room temperature unrealistically, thus underestimating the auxiliary energy consumption. The series auxiliary heating mode of TRNSYS draws the storage tank temperature down until the storage can no longer satisfy the building heating requirements. It then switches to an auxiliary only mode. This more nearly approximates typical control action and is used to model the test facility. For identical conditions in Madison, the TRNSYS parallel auxiliary mode used only 9,424 MJ of auxiliary energy while the TRNSYS series auxiliary mode required 11,060 MJ of auxiliary energy to meet the January heating load.

Table 2. Comparison of Test Facility Runs with TRNSYS Simulation for January 18 in Madison, Wisc., a cold weather day with good insolation.

Quantity	Units	Run 7	Run 11	Run 8	Run 12	TRNSYS
Strategy	-	Direct	Direct	Storage	Storage	Series
Time	hr	0-24	0-24	0-24	0-24	408-432
$Tamb_{avg}$	°C	-10	-10	-10	-10	-10
Initial T_{tank}	°C	31.1	31.5	31.1	31.6	31.2
Final T_{tank}	°C	32.5	33.3	32.3	32.4	36.4
Change T_{tank}	°C	1.4	1.8	1.2	0.8	5.2
DQStank	MJ	24.7	32.8	21.0	14.6	94.7
SLOSS	MJ	27.6	27.4	27.4	25.6	35.4
QLOAD	MJ	517.8	517.9	517.9	517.3	514.6
LLOSS	MJ	38.6	38.5	36.0	32.1	24.2
QAUX	MJ	234.5	248.0	230.5	204.9	268.3
QI	MJ	831.0	831.0	832.1	831.5	831.4
QC_{th}	MJ	410.7	401.1	424.0	428.5	421.8
QC	MJ	390.7	388.7	386.8	412.5	421.9
CLOSS	MJ	12.4	11.8	11.8	11.2	15.6
PARA	MJ	32.7	30.9	33.4	31.9	-
Qin	MJ	600.5	603.9	596.3	602.8	595.5
Qout	MJ	596.4	595.6	593.1	586.2	589.8
Balance (ΔQ)	MJ	4.1	8.3	3.2	16.6	5.7
Balance (%)	-	0.7	1.4	0.5	2.8	0.97
QSOLAR-LOAD	MJ	321.9	308.4	323.4	344.5	270.5
Solar to load	%	62	60	62	67	53

Table 2 compares energy flows predicted by TRNSYS with the direct-heating and the storage-coupled heating modes run on the test facility. The solar energy collected, (QCth), as predicted by the test facility simulation Hottel-Whillier-Bliss collector model, agrees well with the TRNSYS simulation for clear days with good insolation, although in the direct-heating mode the collector loop tends to be on for a slightly shorter time. For both modes, the pseudocollector boiler system delivers slightly less energy (QC) than predicted. This may be due to a limitation in the boiler output control.

Differences between the TRNSYS simulation and the test facility direct and storage strategies are also indicated in Table 2 by the change in stored energy, the load loop piping losses, and the load handled by either solar or auxiliary energy. As expected, the test facility boost mode of operation increases the system performance slightly by using the stored solar energy at slightly lower temperatures.

The energy input to the system for the TRNSYS and test facility runs, Q_{in}, (energy from the collectors, from auxiliary, and from storage) agrees very well, as does the energy output, Q_{out} (energy to the load and all losses). The overall energy balance is quite good for all of the 24-hour runs.

Table 3. Comparison of two-day runs on test facility for direct heating and storage coupled heating modes for identical building load and meteorological conditions (January 18-19 in Madison, Wisc.). TRNSYS simulation results are also shown for comparison.

	Quantity	Direct Run 7	Direct Run 11	Storage Run 8	Storage Run 12	TRNSYS System 3
QC/QI	Collection efficiency	35.5	36.3	37.7	40.3	43.4
$\frac{QSOLAR-LOAD}{QI}$	Thermal efficiency	39.0	42.0	42.0	46.1	37.6
$\frac{QSOLAR-LOAD}{PARA}$	SCOP	7.3	8.3	7.4	8.8	-
$\frac{QSOLAR-LOAD}{QLOAD}$	Solar fraction	45.3	48.7	48.8	53.5	43.4
ΔT_{tank}	Storage temperature change (°C)	-4.8	-6.4	-5.4	-7.2	-1.0

The only significant discrepancy is the solar contribution to the load, which varied an average of about 10%. Parasitic energy for the control valves, pumps, and fans is not accounted for in the TRNSYS simulation.

Comparison of Storage Coupled and Direct Heating

A series of experiments were conducted using both direct heating and storage-coupled heating modes using real weather and insolation data for two January days in Madison. Table 3 indicates the difference in the performance between the two strategies for these two days through some performance indicators. Collection efficiency is the ratio of the energy collected by the collectors to the insolation on the collectors. Thermal efficiency is the ratio of solar energy utilized by the load to insolation incident on the collectors. Solar coefficient of performance is the ratio of the solar energy utilized by the load to the parasitic energy required to run the solar system. Solar fraction is the ratio of the solar energy utilized by the load to the total load. As indicated in the table, no significant difference exists between the control strategies for these days although the direct heating loop strategy does seem slightly better. Both modes of test facility operation utilize greater energy from storage than predicted by the TRNSYS simulation, as indicated by the storage tank temperature change. To determine long-term comparisons, more testing would be required.

Theoretical Studies to Support Experimental Program

Study Of Collector Loop Dynamics

During FY 1980, work was completed on modeling of collector loop dynamics,[6,7] and a report was prepared for publication.[8] Since the temperature drop encountered in the collector loop piping could affect the control set points, a set of curves were developed describing the predicted temperature drops to be expected in piping runs, as shown in Figure 2. These curves indicate that typical systems with properly insulated piping will have a minimal temperature drop across the piping runs and thus should not affect the control set points.

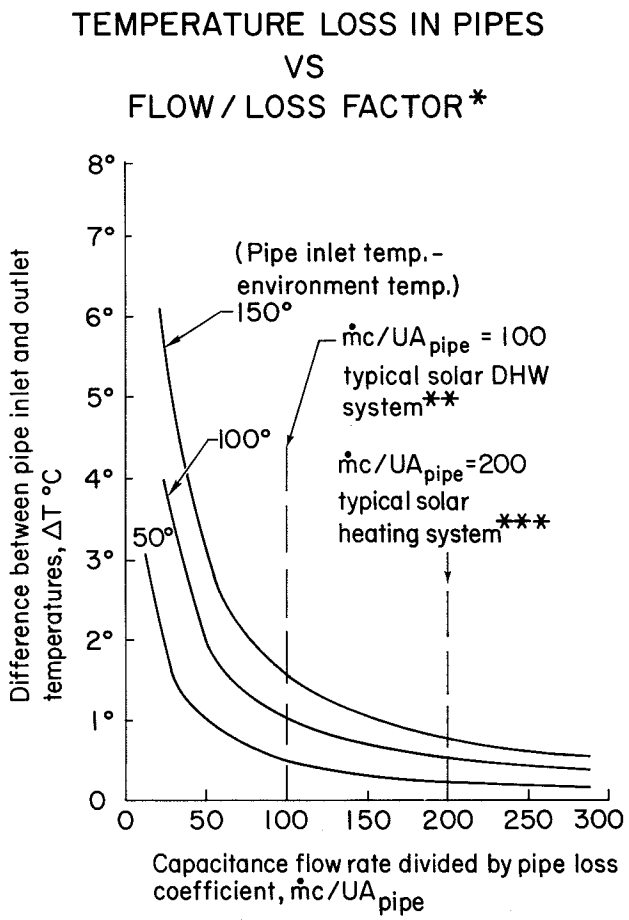

Fig. 2. Temperature loss in pipes versus flow/loss factor. * Temperature loss based on: $\dot{m}c\,(T_{in} - T_{out}) = U_{pipe}L_{pipe}[(T_{in} + T_{out})/2 - T_a]$, where U_{pipe} is the heat loss per unit length. U_{pipe} = 0.6 W/m-°C. $\dot{m}c/A_c$ = 90 W/m²-°C where A_c is the collector area.
** Typical hot water system:
A_c = 5 m²; L_{pipe} = 7.5 m. $\dot{m}c/U_{pipe}L_{pipe}$ = 100.
*** Typical heating system:
A_c = 50 m²; L_{pipe} = 37.5 m. $\dot{m}c/U_{pipe}L_{pipe}$ = 200.
(XBL 806-7161)

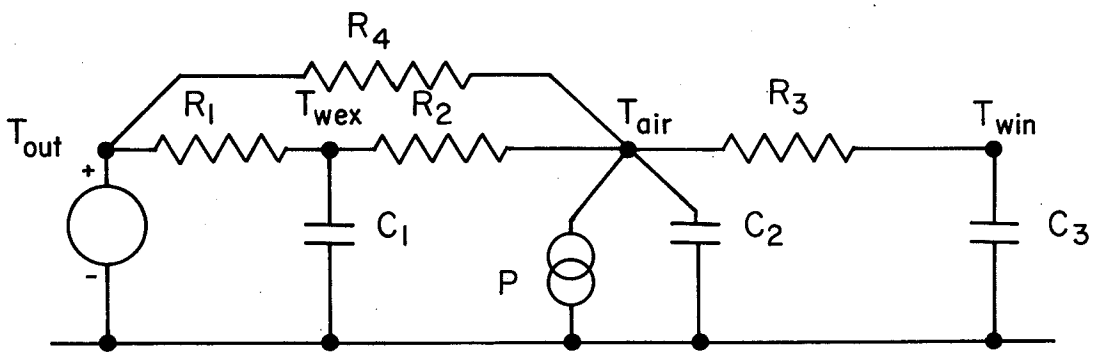

Fig. 3. The dynamic building model uses three resistance-capacitance nodes to represent the temperatures of the interior and exterior walls and room air. The heat input to the air is represented as a thermal current source, P.

(XBL 8011-2406)

Study Of Building Load Dynamics

A model of a residential building, a fan coil heat-delivery system, and a bimetal thermostat, developed previously[9] (to simulate the effects of heat input on room air dynamics) has been applied to examine the building thermal behavior in response to heat input from an active solar space-heating system.[10] The effects of the variable storage tank temperature, of outdoor temperatures, and of fan coil sizes on the cycling rate, on the on-time and off-time of a heating cycle, on room air temperature swing, and on offset of the average air temperature from the setpoint (droop) are determined by computer simulation. Heat input is provided directly to the air as, for example, when a heating fan coil is turned on. The three nodes shown in Figure 3 represent the temperature of the interior surface of the exterior wall, Twex(t); the temperature of the air in the space, Tair(t); and the temperature of the interior wall, Twin(t). The equations for the temperatures are determined from the resistance-capacitance network, using Kirchhoff analysis. The values of the thermal resistances R_1, R_2, R_3, and R_4 and the thermal capacitances C_1, C_2, and C_3 are typical of a well-insulated, single-zone building.

For given conditions of outdoor temperature, anticipation, and thermostat setpoints, the storage tank temperature has a direct effect on swing as shown in Figure 4. The droop, the offset of average room temperature from the setpoint, also depends on the amount of thermostat anticipation and on the heat-delivery duty cycle. The higher the storage tank temperature, the larger is the swing in room temperature and the smaller is the offset of the average air temperature from the setpoint (droop). Results indicate that to maintain room temperatures within comfort limits by minimizing both swing and droop, a hydronic solar space-heating system requires a control system that adjusts anticipation and setpoints in relation to the outdoor and the storage tank temperatures. This will require more than a simple on-off bimetal thermostat.

Reliability and Maintainability of Controls for Active Solar Energy Systems

Although a majority of the systems installed in this country effectively collect the sun's energy, systems that fail because of faulty controls have damaged the reputation of active solar energy systems. Low efficiency, improper operating modes, high auxiliary energy usage, and equipment damage can result from control or system failures caused by poor design and installation practices, defective components, and improper strategies. An

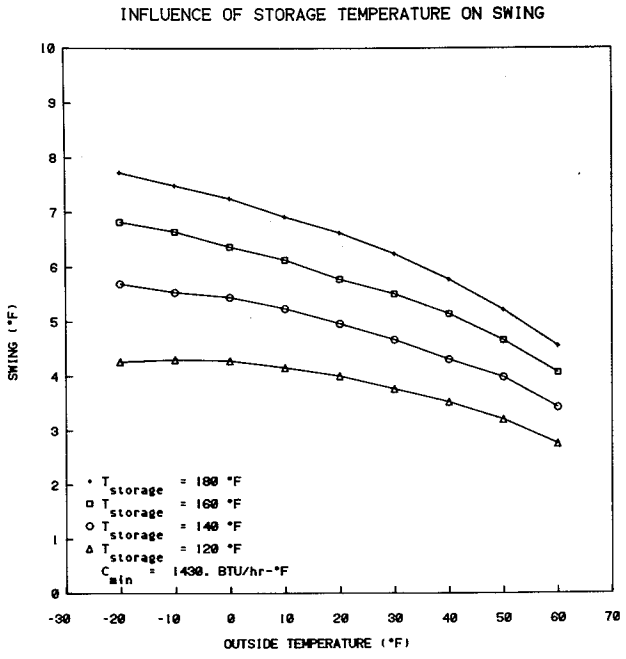

Fig. 4. Storage tank temperature influences room air temperature swing. As the storage tank temperature decreases, the swing decreases for a given outside temperature.

(XBL 8011-7564)

investigation of these failures has been initiated to determine what is needed to improve the effectiveness and reliability of solar control systems.

A preliminary review of the literature on the performance of solar control systems indicated several areas where further investigation can be very beneficial: freeze protection, fault-detection systems, effects of flow rates and set points on system performance, and the interaction of components as a system. Since failures of the freeze protection system can be both costly and destructive, an evaluation of freeze protection techniques is given the highest priority.

Technical Support Activities

This past year the laboratory has been actively involved in proposal review and contract monitoring for the Controls Element of the DOE solar heating and cooling Research and Development program. Activities have included coordination with the Solar Energy Research Institute, conducting project reviews, and reviewing the reports of DOE controls contractors. LBL served as host to a project review for the solar controls work at Drexel University and Middlebury College. We also prepared an overview of the controls program in collaboration with SERI.[11]

PLANNED ACTIVITIES FOR FY 1981

The experimental test facility work is being interrupted and probably terminated. The analysis capabilities are being transferred to provide needed assistance to the Active Solar Cooling program. The emphasis of the remaining controls work is on investigating and solving reliability and maintainability problems.

REFERENCES

1. M. L. Warren, S. R. Schiller, and M. Wahlig, "Experimental Test Facility for Evaluation of Controls and Control Strategies," Second Annual Systems Simulation and Economic Analysis Conference, January 23-25, 1980, San Diego, Calif.; Lawrence Berkeley Laboratory report LBL-10352, January 1980.

2. M. L. Warren, S. R. Schiller, and M. Wahlig, "Evaluation of Proportional and On/Off Control for Solar Collector Loops," Paper 162 (EM-2-3), Proceedings of the American Section of the International Solar Energy Society Annual Meeting, June 2-6, 1980, Phoenix, Ariz.; Lawrence Berkeley Laboratory report LBL-10716, June 1980.

3. M. L. Warren, S. R. Schiller, and M. Wahlig, "Controls for Solar Heating and Cooling," Proceedings of the Annual Department of Energy Active Solar Heating and Cooling Contractors' Meeting, March 26-28, 1980; Lawrence Berkeley Laboratory report LBL-10779. April 1980.

4. C. Leboeuf, "Standard Assumptions and Methods for Solar Heating and Cooling Systems Analysis," Solar Energy Research Institute Report SERI/TR-351-402, Golden, Colo., January 1980.

5. D. S. Ward, "Performance Evaluation Criteria," Proceedings of Operational Results Conference, November 27-30, 1979, Colorado Springs, Colo.

6. S. R. Schiller, M. L. Warren, and D. M. Auslander, "Comparison of Proportional and On/Off Collector Loop Control Strategies Using a Dynamic Collector Model," Second Annual Systems Simulation and Economics Analysis Conference, January 23-25, 1980, San Diego, Calif.; Lawrence Berkeley Laboratory report LBL-10347, January 1980.

7. S. R. Schiller, M. L. Warren, and M. Wahlig, Dynamic Modeling and Experimental Simulation of Active Solar Energy Systems, American Society of Mechanical Engineers report ASME-80-WA/Sol-14; Lawrence Berkeley Laboratory report LBL-10825, July 1980.

8. S. R. Schiller, M. L. Warren and D. M. Auslander, "Comparison of Proportional and On/off Solar Collector Loop Control Strategies Using a Dynamic Collector Model," Transactions of the American Society of Mechanical Engineers, Journal of Solar Energy Engineering, vol. 102, no. 4, November 1980, pp. 256-262; Lawrence Berkeley Laboratory report LBL-10315R, July 1980.

9. M. L. Warren, A. F. Sakkal, and S. R. Schiller, Predicting the Time Response of a Building Under Heat Input Conditions for Active Solar Heating Systems, Lawrence Berkeley Laboratory report LBL-10360, January 1980.

10. C. Vilmer, M. L. Warren, and D. Auslander, Interaction of Solar Space Heating System with the Thermal Behavior of a Building, Lawrence Berkeley Laboratory report LBL-11673, October 1980.

11. L. Groome and M. L. Warren, "Overview of the Solar Controls Program," Proceedings of the Annual Department of Energy (DOE) Active Solar Heating and Cooling Contractors' Meeting, March 26-28, 1980; Lawrence Berkeley Laboratory report LBL-10780. April 1980.

ACTIVE SOLAR COOLING*

K. Dao, M. Wahlig, A. Heitz, R. Glas, S. Mitina, E. Molishever, B. Boyce, J. Rasson, and F. Salter

INTRODUCTION

This project includes both inhouse research and development (R&D) activities and technical support activities for the active cooling program. The inhouse R&D activity includes the development of improved absorption-cycle systems for active solar cooling and heating applications. The objective is to achieve a significantly higher conversion efficiency than is possible using other cooling approaches. A secondary objective is to avoid the necessity for water cooling towers by using air-cooled condensers and absorbers.

The quest for higher conversion efficiencies is consistent with the overall national solar cooling program goal of achieving cost-effective solar cooling systems. The major cost component of a solar cooling system is the collectors; the collector area required to satisfy a given load can be reduced (lowering costs) as the efficiency of the chiller component is increased.

An absorption-cycle chiller is essentially a heat pump and, accordingly, can be used for heating as well as cooling as long as the refrigerant fluid does not freeze in the outdoor coil during heating applications. Thus an absorption chiller using the ammonia/water pair (ammonia as the refrigerant, water as the absorbent) can be used for heating as well as cooling, but one using the water/lithium bromide pair can be used only for cooling because the water in the outdoor coils would freeze in heating applications.

In accordance with these considerations, a phased plan has been devised to develop an advanced high-efficiency absorption chiller that is far beyond today's state-of-the-art. This is to be achieved through the design, fabrication, testing, and evaluation of a series of incrementally improved absorption chillers.

The first phase of this project consisted of the partial reconstruction for solar-powered operation of a conventional gas-fired ammonia/water absorption chiller. This phase was successfully completed some time ago,[1] and it demonstrated the capability of our analysis techniques to predict accurately the performance of single-effect, absorption-cycle chillers under operating conditions appropriate for solar-powered operation. (Single-effect cycles employ only one boiler.)

The second phase includes the design and fabrication of a single-effect ammonia/water absorption chiller that incorporates several unique design features: tube-in-tube heat exchangers for high effectiveness at reasonable cost and a pair of internally powered solution pumps for reduced parasitic power use. This chiller, which represents the starting point for the development of the higher efficiency units in subsequent phases, is currently in the test and evaluation stage.

The third phase of the project is the development of an advanced higher efficiency cycle, a double-effect regenerative cycle (which we call cycle 2R) that adds a unique second stage to the chiller developed in phase two. With the addition of this second stage, the overall chiller efficiency increases continuously as a function of the inlet temperature from the solar collectors. The basic concept of this 2R cycle was described some time ago.[2] Since then the design has been completed, and fabrication has started.

The fourth phase takes advantage of the experience gained in previous phases to develop a still higher efficiency chiller, yet one with less hardware and thus with the potential for lower cost. This chiller is based on a single-effect regenerative cycle (which we call cycle 1R). Although the basic concept has been described by our group previously,[3] this chiller is still in an early design stage. The success of the cycle 1R chiller depends on our experience gained from developing the cycle 2R chiller and on locating a refrigerant/absorbent fluid pair with suitable properties at the higher boiling temperatures where ammonia/water performance drops off.

The technical support activities provide assistance in the active solar cooling program area to the DOE San Francisco Operations Office (SAN) Conservation and Solar Division and to the DOE Headquarters (HQ) Active Heating and Cooling Division, Office of Solar Applications for Buildings. These activities include program planning, technical monitoring and evaluation of ongoing projects, including site visits and review of progress reports, coordination of review of unsolicited proposals, assistance in the preparation and evaluation of responses to program solicitations, and coordination of related activities by other organizations.

ACCOMPLISHMENTS DURING FY 1980

Absorption Air Conditioner Development

A major effort during FY 1980 has been the testing of the single-effect absorption chiller. Most of this effort has been expended on a single component: the solution circulation pump.

The development of the pump is critical to the viability of the single-effect chiller as a solar cooling machine. Conceived to operate at fairly low input temperatures (about 215°F), the single-effect chiller requires large circulation flow rates (of the order of two and one-half gallons of

* This work was supported by the Assistant Secretary for Conservation and Solar Energy, Office of Solar Applications for Buildings, Active Heating and Cooling Division of the U.S. Department of Energy under Contract W-7405-ENG-48.

ammonia-water solution per minute for a three-ton chiller). If a conventional electric diaphragm pump were used, the electric power required (about 3/4 hp) would render the chiller economically unacceptable. A piston circulation pump (called the recuperative pump) was therefore designed to recuperate 70% of the pumping power from the weak solution stream, thus reducing to 1/4 hp the external power required. A second piston pump (called the makeup pump), driven by high-pressure vapor, was designed to run in parallel with the first pump, thus eliminating altogether the requirement for any external electric power for pumping the strong solution.

We have had only limited success in developing these pumps during FY 1980. Extensive testing of the pumps using high-pressure air or nitrogen and water has shown that the pumps performed very well on the test bench. But when the pumps were connected to the chiller, mutual interactions prevented proper pump operation. The nature of the interactions is only partially understood. Pressure drops and water-hammer effects in the long lines of the chiller were some of the causes for interference with the switching of the pump valves. Valve redesign and proper choice for the location of the pilot pressure taps have eliminated these problems. Dirt in the chiller was another problem that caused valve sticking. This problem has not been eliminated yet because of difficulty in cleaning the chiller. Valve redesign using bellows may be the answer. Ammonia vapor absorption by the liquid ever present in the makeup pump switching lines may be the most difficult problem to overcome.

The status of the pumps' development as of the end of FY 1980 is: (1) the recuperative pump can be made to operate very reliably with the chiller; and (2) the success of the vapor makeup pump is in doubt, and a small electric makeup pump may be needed after all.

Considerable effort has also been spent during FY 1980 on continuing the development of the advanced cycle 2R and cycle 1R absorption chillers. For both of these cycles, higher efficiency (than the usual single-effect cycle) is predicated on a closer approach to the Carnot cycle by using the available heat input at the highest possible temperature and by rejecting heat at the lowest possible temperature. This requires that the design incorporate multipressure staged processes for boiling and for heat rejection. Since the absorption cycle must be a closed-loop flow circuit, the transition of a fluid element from the heat-input process to the heat-rejection process must be regenerative (or recuperative): i.e., the heat from a high-temperature fluid element going from the boiler to the absorber must be transferable to a fluid element going in the opposite direction.

The choice of the regenerative paths is what differentiates the cycle 2R from the cycle 1R design. Cycle 2R is simpler than cycle 1R (which is the reason 2R is being designed and fabricated first) but cycle 2R requires more heat-exchanger area. Thus the cycle 2R chiller will allow the basic multistage boiling and absorption processes to be studied without the complication of the complex regenerative path connections of the cycle 1R design.

The detailed design and all drawings for the cycle 2R chiller have been completed during FY 1980. Fabrication of parts has begun, and fabrication and assembly are expected to be completed by the end of FY 1981.

Work on the cycle 1R chiller during FY 1980 consisted of a first attempt to learn how to model the cycle and a detailed investigation of a method for selecting appropriate fluid pairs for a practical cycle 1R machine.

Detailed computer modeling of the 1R absorption cycle proved to be a formidable task. A straightforward approach was attempted during FY 1980; it consisted of writing out the equations (about 100) expressing conservation of mass, conservation of energy, thermodynamic properties (for ammonia/water mixtures), and heat-exchanger relationships, and then trying to solve this set of highly nonlinear equations. No solutions were found as the iterative scheme did not converge, even for a simpler version of this model.

A decision was made to learn techniques for solving these equations by first modeling the single-effect absorption chiller by this method. The solution technique led to a successful computer model for the single-effect chiller. The method for adopting this model to the 1R chiller remains for future investigation.

The other cycle 1R task during FY 1980--investigation of a method for selecting fluid pairs--has been quite fruitful. A solid foundation for a method for approximating the properties of binary mixtures has been achieved. The traditional method for calculation of mixture properties is based on setting up and solving an equilibrium equation for the fugacities of each of the components in the vapor and liquid states. However, the direct solution of the fugacity equation is impractical here because it requires complete and accurate knowledge of volumetric properties of vapor and liquid phases--information that is not generally available and is difficult to obtain experimentally.

A decision was made to devise an independent approach to approximate with sufficient accuracy the necessary properties of the binary fluid mixtures. An appropriate equation for this purpose turned out to be one that calculates the thermal efficiency of an ideal absorption power cycle. This cycle can be constructed by replacing the condenser and evaporator of a conventional single-effect absorption refrigeration cycle with an ideal isothermal turbine and by taking into account every possible heat and work recuperation.

The resulting basic equation for binary fluid mixtures is:

$$\left\{ (v_v - v_s)t - (\chi_v - \chi_s)\left[\frac{\partial(tv_s)}{\partial \chi_s}\right]_p \right\} \left(\frac{\partial p}{\partial t}\right)_{\chi_s}$$

$$= -h_v + h_s + (\chi_v - \chi_s)\left(\frac{\partial h_s}{\partial \chi_s}\right)_t \qquad (1)$$

where

t = 1/T = reciprocal of absolute temperature T

v = specific volume

h = specific enthalpies

p = system pressure

X = weight fraction of the more volatile component

All properties are saturated properties and the subscripts have the following referents:

v refers to the vapor phase, and

s refers to the liquid phase or the solution.

Note that the solution's heat of mixing is included in the enthalpy h_s.

There are many ways of approximating the individual terms of Equation (1). The choices depend on the available experimental data, on the accuracy required, and on judgment. A specific method for solving Equation (1) has been developed and adopted and will be reported in the near future.

Accordingly, a basic set of experimental data needed to determine the binary fluid properties [by using Equation (1)] for performance calculations of the 1R absorption cycle have been specified, along with the accuracy required for each parameter. A statement of work was written in FY 1980 to enable DOE to issue a Request for Proposal (RFP) soliciting the measurement of this basic set of data for a number of candidate fluid pairs. After review of the proposals received, DOE negotiated a contract with SRI International at the end of FY 1980. SRI will conduct a literature search and follow up with measurements of the as yet unmeasured parameters during FY 1981.

Technical Support Activities

The following program planning activities took place during FY 1980:

- Preparation of the first and second drafts of multiyear Program Element Plans for Rankine and Absorption Solar Cooling Systems.
- Writing of a "white paper" on solar cooling technologies, as input to the DOE's five-year planning exercise.
- Preparation of documents for DOE/HQ on solar cooling's potential to achieve eventual market penetration and on the DOE solar cooling program's role in accomplishing this.
- Participation in major planning meetings for the Active Solar Heating and Cooling Program at DOE/HQ and DOE/SAN.
- Organization of a meeting at LBL at which U.S. and Mexican participants prepared a draft proposal for a joint U.S.-Mexican project in solar refrigeration; discussions later with SERI, DOE/HQ, DOE/SAN and other organizations on implementation of this joint project.

The following are some of the major FY 1980 activities in technical monitoring and evaluation of solar cooling projects by outside (nonLBL) contractors:

- Conduction of, and participation in, 21 site visits and project reviews covering 14 different DOE contractors; review of seven final reports and phase reports; assistance to DOE/SAN in specifying the Statements of Work for follow-on efforts by several of these contractors.
- Initiation of a contract with SERI for LBL to provide technical monitoring of the five U.S.-Saudi (SOLERAS) solar cooling projects. During FY 1980, LBL staff participated in the project startup meetings, preliminary design reviews, and critical design reviews, in addition to continuing interactions with SERI and with the project contractors.
- Preparation and sending to DOE/SAN of monthly summary reports on all the DOE solar cooling projects; preparation and sending to DOE/HQ of several reports on solar cooling R&D program accomplishments and status.
- Accomplishment of preliminary activities in developing a methodology for comparative assessment of solar cooling technologies (e.g., absorption vs Rankine cooling) and projects.

During FY 1980 LBL carried out the review of nine unsolicited proposals. For each proposal, the comments of all the reviewers were summarized and sent to DOE along with a recommendation for action.

LBL assisted DOE/SAN in preparing and evaluating responses to an RFP on the Determination of Properties of Fluids for Solar Cooling Applications. LBL prepared the draft statement of work, secured reviewers for the technical evaluation committee, and conducted that committee's review of the proposals received in response to the RFP.

LBL staff were engaged in a number of coordination activities related to the solar cooling program during FY 1980:

- Participation in DOE Program Reviews, including
  - -Systems Development Division Review, in Reston, Va.
  - -Commercial Demonstration Program Review, in Norfolk, Va.
  - -Active Solar Heating and Cooling Contractors Meeting, in Nevada
  - -Passive Update Meeting, in Washington, D.C.
- Attendance at solar conferences:
  - -Operational Results Conference, in Colorado Springs, Colo.
  - -Systems Simulation and Economics Analysis

Conference, in San Diego, Calif.

-Annual International Solar Energy Society Meeting, in Phoenix, Ariz.

- Participation in the DOE active solar heating and cooling technical managers' coordination meeting in Nevada.
- Participation in the bimonthly review and coordination meetings associated with the cooling marketing study projects funded by DOE.
- Coordination with NASA/MSFC (Manned Space Flight Center in Huntsville, Ala.) on the status and future priorities of the solar cooling projects that they are managing for DOE.
- Coordination with Oak Ridge National Laboratory concerning the cooling projects (for which they are technical monitors) that make use of waste heat sources.
- Coordination with the Gas Research Institute on cooling and heat pump programs and projects of mutual interest, especially solar-powered cooling applications using gas auxiliary energy.
- Assistance to the American Samoa Energy Office with their plans for using large-scale solar cooling systems as a solution to one of their major energy problems, the scarcity and high-cost of diesel fuel.
- Coordination of the utilization of the LBL Building 71 Federal Buildings Solar Demonstration Project as a field test installation for a new 25-ton packaged absorption chiller recently developed as part of the DOE solar cooling R&D program.

PLANNED ACTIVITIES FOR FY 1981

Absorption Air Conditioner Development

The testing of the single-effect chiller will continue. Further improvement of the vapor pump will not be pursued; the chiller will be operated using an electric makeup pump for the remaining chiller tests. The testing is expected to be completed and the results published during FY 1981.

By September 1981, the fabrication of the 2R chiller should be completed. Testing is expected to begin by about December 1981, followed by testing and evaluation throughout the remainder of FY 1982.

The cycle analysis work on the cycle 1R chiller will continue during FY 1981 as we continue to reduce the theoretical cycle to a practical design. The required measurements of the properties of candidate fluids for the 1R cycle should be completed by SRI International by the end of FY 1981; we will work closely with them to insure the maximum utilization of the data measured during that project. The final 1R design and working drawings are expected to follow during FY 1982.

Technical Support Activities

Activities in FY 1981 will be similar to those carried out in FY 1980. Implementation of the new multiyear solar cooling program plan will be one of the major activities. Appreciable effort will be expended in developing the Statement of Work for a major program solicitation that will serve as the main vehicle for implementing the plan. We should progress a long way toward establishing realistic cost and performance goals for solar cooling systems, making use of new marketing analyses and system simulation capabilities. The joint U.S.-Mexican project should get underway, and preliminary negotiations will be conducted for a possible U.S.-Greek program in solar cooling. Technical monitoring and review of the DOE and SOLERAS solar cooling projects will continue. Unsolicited proposal reviews will be undertaken as received. LBL will continue to participate in DOE program reviews, in solar energy conferences, and in coordination activities with other organizations carrying out related programs.

REFERENCES

1. K. Dao, M. Simmons, R. Wolgast, M. Wahlig, Performance of an Experimental Solar-Driven Absorption Air Conditioner, Lawrence Berkeley Laboratory report LBL-5911, January 1977.
2. K. Dao, Conceptual Design of an Advanced Absorption Cycle: The Double-Effect Regenerative Absorption Refrigeration Cycle, Lawrence Berkeley Laboratory report LBL-8405, September 1978.
3. K. Dao, A New Absorption Cycle: The Single-Effect Regenerative Absorption Refrigeration Cycle, Lawrence Berkeley Laboratory report LBL-6879, February 1978.

PASSIVE COOLING*

M. Martin, D. Elmer, P. Berdahl, F. Sakkal,
M. Wahlig, R. Fromberg, M. Kruskopf, and R. Sobolewsky

INTRODUCTION

Passive or hybrid cooling occurs when thermal energy is rejected from a building to natural heat sinks in the environment. Such heat sinks include the atmosphere, the sky, and the ground. Cooling to the atmosphere occurs through ventilation and evaporative cooling; to the sky by infrared radiative cooling; and to the ground by conduction to the earth. Although air temperature reduction is the most obvious means for achieving comfort under overheated conditions, the comparable importance of humidity levels, mean radiant temperatures, and amount of air motion is well established. The primary objectives of this project are to evaluate the effectiveness of passive and hybrid cooling systems for displacing conventional fuels now used to power air conditioning and to develop systems that do this in an optimal manner.

The emphasis of the project to date has been on the assessment of the "resource" for comfort conditioning based on infrared radiative cooling. Infrared radiative cooling systems are composed of a radiator surface which is exposed to the sky, an (optional) infrared-transparent windscreen to reduce convective heat gain from the air, and a means for transporting heat from the building's interior to the radiator surface. The current work includes measurement of atmospheric infrared emission characteristics in order to identify geographical regions in which selective and nonselective radiators may be effective. This effort employs both atmospheric radiation models and experimental sky radiation measurements. Promising radiator surfaces and infrared-transparent windscreens will be experimentally evaluated at an outdoor test facility at LBL.

To predict accurately the net heat exchange between the sky and a surface of known infrared characteristics, knowledge is needed of the intensity of infrared radiation produced by the atmosphere as a function of both zenith angle and wavelength. Most published measurements in the literature pertaining to the spectral radiance of the sky were obtained on one or two nights or pertain to clear skies only. Therefore, to obtain data on which estimates of cooling system performance can be based, it was necessary to make our own measurements, during the day and night, over periods of months. During 1978 and 1979, a major effort was devoted to construction of four spectral infrared sky radiometers and the siting of these instruments at various locations in the southern United States. These radiometers were set up to measure the radiance of the zenith sky at half-hour intervals in six wavelength bands ranging from 8 to 22 μm. In 1979 the instruments were modified to perform measurements at several different zenith angles. Auxiliary measurements performed consist of total infrared sky radiance (using a pyrgeometer), air temperature, and dewpoint. Further details of the measurement system may be found in the 1978 and 1979 Annual Reports[1,2] and elsewhere.[3-6]

ACCOMPLISHMENTS DURING 1980

Data collection with the four spectral infrared sky radiometer systems continued during 1980. Two of these systems were moved to different southern cities to ensure the widest possible geographical coverage of the resulting data set. The continuing analysis of the spectral sky radiance data has led to improved characterization of sky radiance during clear sky conditions. Future analysis should lead to improved information for cloudy skies as well.

The LBL experimental test facility for evaluation of radiator cooling assemblies was completed, and the first tests were performed.

The Passive Solar Cooling Group assists U.S. Department of Energy management activities in the planning and execution of the National Passive Cooling Program. This included the development and evaluation of three solicitations (e.g., Requests for Proposals) for DOE in 1980, and technical monitoring responsibilities as new projects are funded. Coordination between these activities and the work at LBL is discussed in the following paragraphs.

Spectral Infrared Sky Measurements

During the Spring of 1980, the spectral sky radiometer systems in Gaithersburg, Md. and Tucson, Ariz. were moved to West Palm Beach, Fla., and Boulder City, Nev. The systems in San Antonio, Tex. and St. Louis, Mo. remained in place. The end of the summer data-acquisition period marks the end of the sky radiance measurement portion of this project. Although a substantial amount of data analysis remains to be performed, sufficient data has been collected to produce a thorough preliminary assessment of the resource for radiative cooling in the six cities in which measurements have been made.

Analysis of the Sky Radiance Data

One component of the spectral sky radiance analysis is the comparison of numerical calculations with radiometer measurements. A modified version of LOWTRAN 3B computer model[7,8] was used to compute sky radiance based on vertical profiles of temperature, humidity, and minor atmospheric constituents. These computed radiances are compared with measured values for clear sky conditions. In general the agreement with the computer model is

* This work was supported by the Assistant Secretary for Conservation and Solar Applications, Office of Solar Applications for Buildings, Passive and Hybrid Division of the U.S. Department of Energy under Contract No. W-7405-ENG-48.

very good.[9] In the center of the atmospheric window near a wavelength of 11 μm the agreement is excellent, but a measurable disagreement appears in the region of 8-10 μm. The maximum discrepancy, which corresponds to an observed radiance greater than predicted, is about 0.6 $W \cdot m^{-2} \cdot sr^{-1} \cdot \mu m^{-1}$ at a wavelength of 8.8 μm.[9] This error is about 15% of the clear sky radiance at this wavelength.

Another result of the data analysis is the development of a correlation to predict the total sky radiance for clear skies. The measurement of total (thermal) sky radiance S is made with an Eppley pyrgeometer operated in conjunction with each spectral infrared radiometer. The spectral radiometer is used to calibrate the pyrgeometer and to detect the presence of clouds. In place of the total sky radiance S, it is convenient to employ the sky emissivity defined by

$$\varepsilon_{sky} = S/(\sigma T_a^4), \qquad (1)$$

where σ is the Stefan-Boltzmann constant and T_a is the absolute air temperature near the ground. A correlation of 2,945 nighttime clear sky data points for ε_{sky} and the dewpoint temperature T_{dp} in degrees Celsius yields the relation:

$$\varepsilon_{sky} = 0.741 + 0.00624\ T_{dp}\ , \qquad (2)$$

$$-\ 20^{\circ}C \leq T_{dp} \leq 22^{\circ}C.$$

The standard (random) error in the use of Equation (2) is 0.031. The experimental (systematic) error is estimated to be 0.030. Figure 1 shows the correlation for each of the months of data used to form the overall correlation, as well as the overall correlation itself. No significant systematic difference exists between data sets from the various locations. Thus, the result given by Equation (2) may have rather general applicability.

Figure 2 shows a comparison of the derived correlation with relationships recommended by other researchers[10-12] as well as with calculations based on the LOWTRAN 3B computer model. From left to right, the crosses on this figure represent the following LOWTRAN model atmospheres: midlatitude winter, U.S. standard, midlatitude summer, and tropical. Because a sky emissivity of 1.00 corresponds to a zero resource for radiative cooling, this figure indicates how well the radiative cooling resource is known for clear skies.

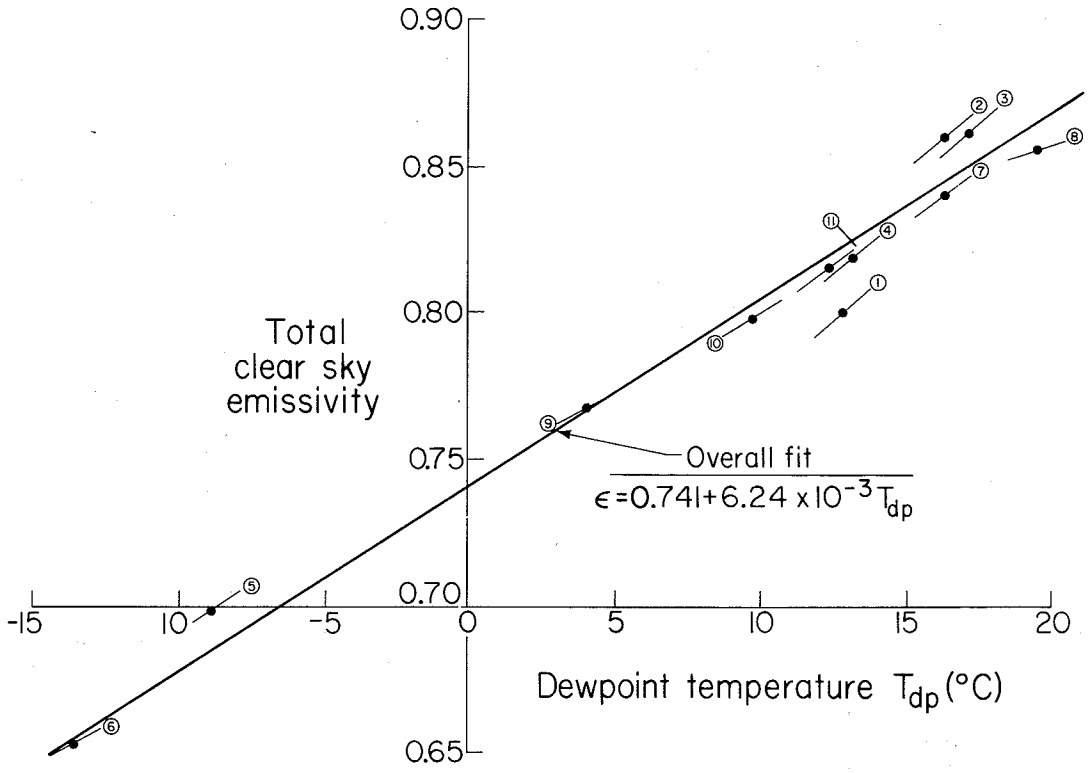

Fig 1. The measured emissivity of clear skies as a function of dewpoint temperature. The short line segments show the correlations obtained for various individual months: 1, 2, 3, and 4 represent June, July, August, and September, 1979 at Gaithersburg, Md.; 5 and 6 represent January, February, 1980 at Gaithersburg, Md.; 7 and 8 represent July, August, 1979 at St. Louis, Mo.; 9, 10 and 11 represent June, July, August, 1979 at Tucson, Ariz. The monthly fits are drawn centered at the average value of sky emissivity and dewpoint for the month concerned. The overall fit is a least-squares fit through the 2,945 individual measurements.

(XBL 8011-92)

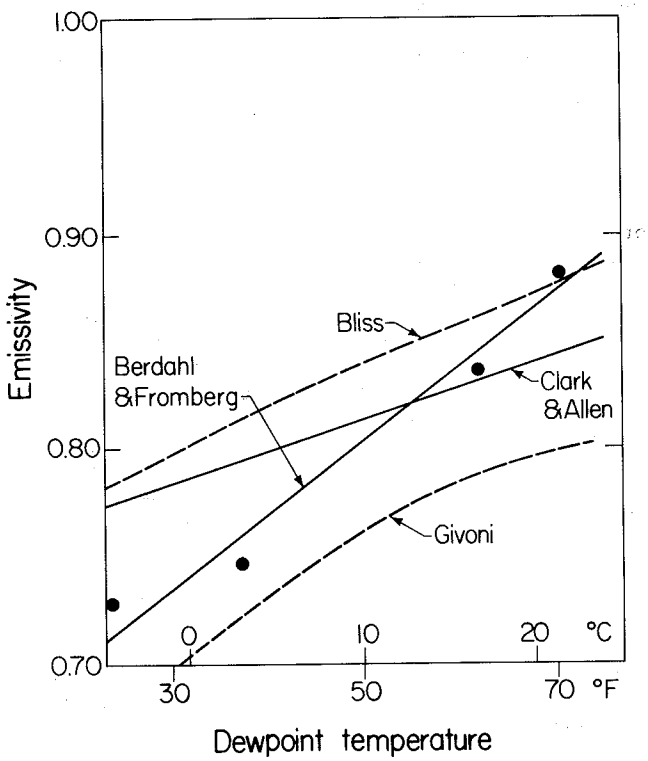

Fig 2. Relationships between the emissivity of clear skies and surface dewpoint temperatures as given by Berdahl and Fromberg and several other references.[10,11,12] The dots are results from the computer code LOWTRAN discussed in Reference 8.
(XBL 8011-90)

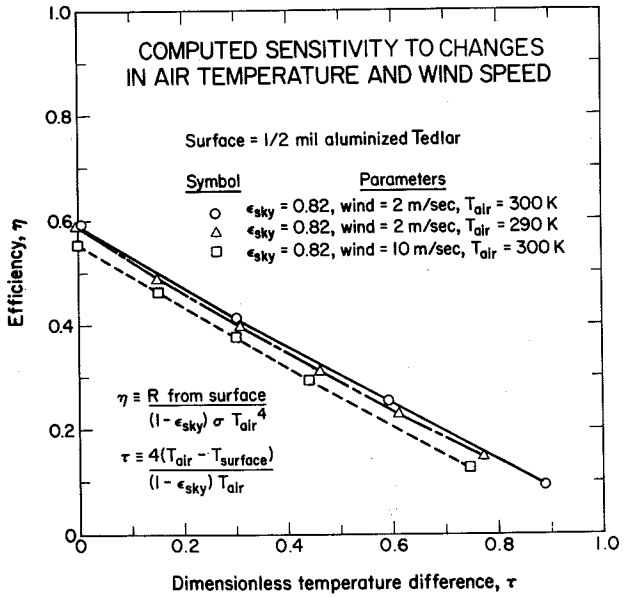

Fig 3. Computed efficiency versus dimensionless temperature difference curves for differing ambient conditions. The circles represent baseline conditions. The triangles show the effect of a decrease in air temperature. The squares show the effect of an increase in windspeed. The efficiency curve is not very sensitive to these changes.
(XBL 8012-2538)

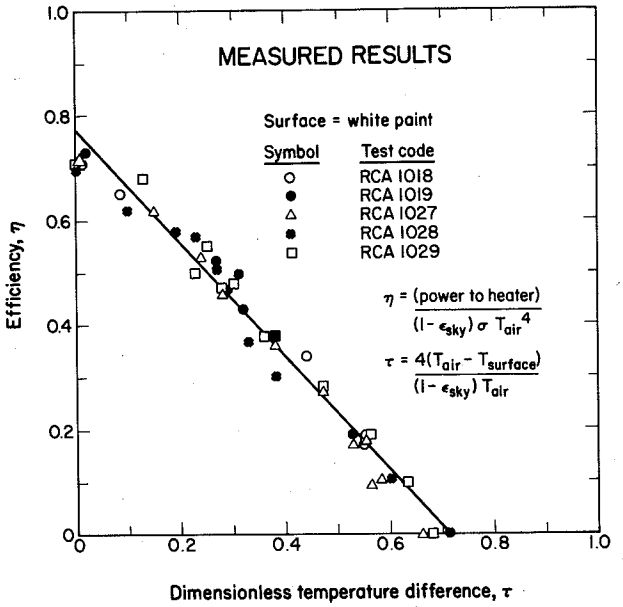

Fig 4. Measured efficiency versus dimensionless temperature difference for a white-painted radiator surface with 2 mil polyethylene glazing. Measurements were made at night with the panel facing directly upward. The solid line is a least-squares fit through the data points.
(XBL 8012-2543)

Test Facility for Radiative Cooling Assemblies

Systematic performance measurements were obtained for the first time with this new facility. Further description of the facility may be found in References 13 and 14. Both nonselective (white-painted) and selective (4 mil aluminized Tedlar) surfaces were tested, each glazed with a 2 mil sheet of polyethylene. The tests were designed to determine the amount of radiative cooling which can be produced by a given surface as a function of radiator temperature.

Analytical and numerical system modeling was performed in order to evaluate various radiative cooling assemblies. For glazed radiator surfaces, these models indicated that plots of efficiency η versus a dimensionless temperature difference τ are nearly independent of the detailed conditions of the test, such as sky emissivity, wind speed, air temperature, etc. The efficiency for radiative cooling η is defined as

$$\eta \equiv R/[(1-\varepsilon_{sky})]\sigma T_a^4 , \qquad (3)$$

where R is the radiative cooling rate in $W \cdot m^{-2}$. The denominator in this expression represents the maximum cooling permitted by the Second Law of Thermodynamics for any radiator with temperature less than or equal to the air temperature T_a. The dimensionless temperature difference τ is defined as

$$\tau \equiv 4(T_r-T_a)/[(1-\varepsilon_{sky})T_a], \qquad (4)$$

where T_r is the absolute radiator temperature.

Figure 3 shows a computer-generated plot of η versus τ for a typical radiator panel. Performance changes caused by variations in the ambient air temperature or wind speed are small. In the experiments the wind speed was typically less than 2 m/s.

Figure 4 shows the performance results for five sets of measurements on ordinary white painted surface with a 2 mil polyethylene glazing. A least squares fit to the data points characterizes the performance of this radiator panel.

Several criteria are important for obtaining good test results. First, the presence of dew on the windscreens must be detected and the corresponding data discarded because liquid water interferes with longwave infrared transfer. Second, the wind speed should be less than about 2 m/s to prevent motion of the thin polyethylene windscreen. Finally, the sky emissivity should be less than 0.85 to produce a sufficiently large cooling rate for the calculation of accurate efficiency values using Equation (3).

Programmatic Activities

The Passive Cooling Group supports the Department of Energy's Passive Cooling Program in several areas. Personnel participate in planning activities and preparation of solicitations. DOE issued three such documents during the Spring of 1980, resulting in the selection of nine proposals for funding early in 1981. The project staff also serve as technical monitors on all current DOE Passive Cooling Projects and and are responsible for the technical review of both solicited and unsolicited proposals.

PLANNED ACTIVITIES FOR FY 1981

Analysis of the spectral infrared sky radiance data will continue with the publication of two technical papers and one report during 1981. One technical paper will develop a method for estimating the total infrared sky radiance under cloudless conditions, based on air temperature and dewpoint. The report will present statistical summaries of all data collected from measurements at six locations. The second technical paper will treat the spectral and angular components of infrared radiation from cloudless skies in some detail, including comparisons with the LOWTRAN computer model. An additional technical paper (scheduled for FY 1982) will introduce a method for estimating the daily average spectral and angular distribution of sky radiation when only the daily average sky emissivity is known. The method envisaged is applicable for cloudy as well as clear skies.

Further work with the Experimental Test Facility for Radiative Cooling will be deferred until FY 1982, in order to accommodate some of the following activities.

A major systems analysis effort is to be undertaken to perform a comparative assessment of passive cooling technologies. One component of this effort will be the construction of simplified computer models of generic passive-cooling systems for various types of residential and commercial buildings in different parts of the U.S. The models will produce estimates of the projected energy impact of various passive cooling systems. These estimates will be used to formulate a Passive Cooling Area Plan to be used by DOE in planning the National Passive Cooling Program.

The other component of the systems analysis effort will consist of detailed computer modeling of existing passively cooled buildings. Computer models based on suitably modified existing programs (such as BLAST[16]) will be formulated. These models will be validated using data collected by two Passive Cooling Experimental Facilities (at Trinity University and the University of Arizona). Each Passive Cooling Experimental Facility presently consists of two well-instrumented experimental buildings specifically constructed to test a variety of passive cooling strategies. These facilities play a central role in the National Cooling Program, and will provide data for the validation of computer simulations to other research organizations. Comparison of experimental results with model calculations will enable both the validation of the computer models and the development of improved experimental procedures. The LBL role as DOE Technical Monitor for these projects assures close coordination between LBL and the Experimental Facilities.

REFERENCES

1. M. Martin et al., Passive Cooling, Lawrence Berkeley Laboratory report LBL-11175, 1979, pp. 3-30.
2. M. Martin et al., Radiative and Passive Cooling, Lawrence Berkeley Laboratory report LBL-8619, 1978, p. 58.
3. P. Berdahl and M. Martin, "Infrared Radiative Cooling," Proceedings of the 1979 International Congress of the International Solar Energy Society (Atlanta, Ga.: American Section of ISES, 1979).
4. P. Berdahl and M. Martin, "Spectral Measurements of Infrared Sky Radiance," Proceedings of the Third National Passive Solar Conference (San Jose, Calif.: American Section of ISES, 1979), p. 443.
5. P. Berdahl, "Routine Spectral Measurements of Infrared Radiation from the Atmosphere," Proceedings of the Second International Conference on Infrared Physics (Zurich, Switzerland: Eidgenossische Technische Hochschule, 1979), p. 406.
6. M. Martin and P. Berdahl, "Description of a Spectral Atmospheric Radiation Monitoring Network," Proceedings of the Third Conference on Atmospheric Radiation, Davis, Calif., 1978, p. 148.
7. J. Selby et al., Atmospheric Transmittance from 0.25 to 28.5 microns: Supplement LOWTRAN 3B, AFGL-TR-76-0258, AD A 040 701 (Hanscom Air Force Base, Mass.: Air Force Geophysics Laboratory); available from National Technical Information Service, Springfield, Va. 22151.
8. P. Berdahl and M. Martin, "The Resource for Radiative Cooling," Proceedings of the Second

National Passive Solar Conference, Philadelphia, American Section of ISES, vol. 2, 1978, p. 684.

9. P. Berdahl and M. Martin, "Spectral Radiance of the Clear Midlatitude-Summer Atmosphere, Proceedings of the 1980 International Radiation Symposium (Fort Collins, Colo.: Radiation Commission of the International Association of Meteorology and Atmospheric Physics, 1980), p. 167.

10. G. Clark and C. Allen, "The Estimation of Atmospheric Radiation for Clear and Cloudy Skies," Proceedings of the Second National Passive Solar Conference, American Section of ISES, vol. 2, 1978, p. 675.

11. R. Bliss, "Atmospheric Radiation Near the Surface of the Ground: A Summary for Engineers," Solar Energy, vol. 5, 1961, p. 103.

12. B. Givoni, "Passive Cooling of Buildings by Natural Processes," Energy and Buildings, vol. 2, 1979, p. 279.

13. F. Sakkal et al., "Experimental Test Facility for Selective Radiative Cooling Surfaces," Proceedings of the Fourth National Passive Solar Conference, (Kansas City, Mo.: American Section of ISES, 1979).

14. M. Kruskopf et al., Radiative Cooling Test Facility and Performance Evaluation off 4 Mil Aluminized Tedlar and White Paint Surfaces, Lawrence Berkeley Laboratory report (in preparation).

15. E. Clark and P. Berdahl, "Radiative Cooling: Resource and Applications," in The Passive Cooling Applications Handbook, issued at the Passive Cooling Workshop, Fifth National Passive Solar Conference, Amherst, Mass., 1980, p. 167; Lawrence Berkeley Laboratory publication Pub-375, 1980.

16. D. Hittle, "BLAST, The Building Loads Analysis and System Thermo-Dynamics Program," Users Manual, vol. 1, U.S. Army Construction Engineering Research Laboratory technical report CERL-TR-E-153, available from National Technical Information Service, Springfield, Va. 22151.

LBL SOLAR DEMONSTRATION PROJECT*

T. Webster

INTRODUCTION

The Building 90 solar demonstration project is one of eleven projects selected to be part of the FY 1977 Department of Energy Facilities Solar Demonstration Program, a pilot program for the Solar Federal Buildings Program recently authorized by The National Energy Act. The objectives of this pilot program are to establish procedures and techniques for assessing and implementing solar systems for federal facilities and to assist in reducing energy use within DOE facilities.

The LBL project was funded by the DOE Division of Solar Energy via the Construction, Planning and Support Division. LBL Plant Engineering was responsible for design and construction of the project with assistance provided by the LBL Solar Group. A detailed description of the building, solar systems, preliminary and final design considerations, construction problems, and final costs are contained in the 1977, 1978, and 1979 Energy and Environment Division Annual Reports.

ACCOMPLISHMENTS DURING FY 1980

The solar system was designed to operate in conjunction with a new building exhaust air-return system. Because of delays of about a year in installing the system (due to funding problems), the solar system was operated independently of the building. Water was circulated between the collector and storage but was not actively connected to the building heating system during 1980. This type of unloaded operation resulted in high operation temperatures and offered an opportunity for a thorough "shakedown" of the system. The return-air system installation will be completed in early 1981.

The following problems were identified and corrected during 1980:

- The freeze protection sensor/controller allowed circulation to start at 45-50° F instead of 35° F as designed; the controller was adjusted to the final setpoint by a trial and error process.
- Whenever the pump was activated for freeze protection, a thermosiphon action in the same direction as the pump flow caused warm water to continue circulating after the pump was turned off. This resulted in very high system losses. Motor-operated ball valves were installed at the circulation pumps to correct this problem.

* This work was supported by the the Assistant Secretary for Conservation and Solar Energy, Field Applications Branch, Office of Active Heating and Cooling, U.S. Department of Energy under Contract No. W-7405-ENG-48.

- The collector pump cycled excessively during morning startup; the ΔT controller was adjusted to reduce this cycling to a minimum.
- One pump relay failed and was replaced.

The instrumentation system was made fully operational in March 1980. Monthly advisory reports are being issued by Vitro Labs until the return-air system installation is complete. Data from these reports point out a number of interesting facts about the system operation. The following data are from the August report and are representative of system operating characteristics during the year.

- Average storage temperature for the month was 178° F. This high average temperature results from operating the system unloaded.
- Average collector array efficiency for the month was 19% (of total available insolation). This efficiency should improve for loaded operation.
- Because of the high operating temperature, the solar system provided 4% of the heating load in spite of not actually being activated. The system is designed so that the operating temperature is set by a three-way mixing valve (whose controls are not yet activated), and solar heat is provided whenever the heating system return water temperature is lower than the storage temperature. The storage was hot enough so that solar heat was provided even though the mixing valve was not set for a low operating temperature.
- Total system losses were 33% of collected energy. Storage and transmission losses were each about 12% with the remainder being startup, intentional heat dump, and unexplained losses.
- The maximum temperature of 190° F, necessary to activate the heat dump mode (i.e., to circulate hot fluid at night), was rarely achieved.
- The solar COP (collected energy divided by pump energy) was about 67.
- Domestic hot water use for the building was an average of only 40 gal per working day, considerably less than the expected one gal per day per person.
- Average daily incident solar radiation on the collector array was 1,721 Btu/S.F.-day versus the long-term average of 1,866 Btu/S.F.-day shown in the Solar Data Manual for Richmond, California.

PLANNED ACTIVITIES FOR FY 1981

After completion of the return-air system, the solar system will be activated, and formal monthly reports that will document the actual performance of the system will be issued by Vitro.

SUPPORT FOR COMMERCIAL SOLAR DEMONSTRATION PROGRAM*

F. Salter, S. Peters, and T. Webster

INTRODUCTION

The Solar Applications Group at LBL provides technical consulting and management services to support the Department of Energy's San Francisco Operations Office's (DOE/SAN) overall management of commercial-building solar demonstration projects and hotel/motel hot water solar projects located throughout the northwestern states and Hawaii. These projects are part of the National Solar Heating and Cooling Demonstration Program,[1] which has the primary objectives of stimulating a solar industry and promoting the use of solar energy as a means of reducing demand on conventional fuel supplies.

The group is currently involved in support for the projects in this program shown on Table 1.

ACCOMPLISHMENTS DURING FY 1980:

LBL was directed by DOE to terminate participation in the solar demonstration program by the end of FY 1980 and to restrict our activity level to one full-time employee during FY 1980. To carry out these instructions, we transferred a number of projects to DOE/SAN and to the Energy Technology Engineering Center (ETEC) during the course of the year. All but essentially completed projects were transferred by the end of FY 1980.

Table 1. Projects being assisted.

Projects	Program Solicitation	
1	NSF-1	Cycle I
4	DSE-76-2	Cycle II[2]
5	PON 4200	Cycle III[3]
3	PON 1450	Hotel/motel[4]

* This work was supported by the Assistant Secretary for Conservation and Solar Energy, Field Applications Branch, Office of Active Heating and Cooling, U.S. Department of Energy under contract No. W-7405-ENG-48.

As for the projects remaining with LBL, activities during FY 1980 included monthly reports, midconstruction and final project inspections, instrumentation checkouts on sites instrumented by Vitro Laboratories,† resolution of operation and instrumentation problems, review of participant Final Reports and Data Collection Reports, and refurbishment considerations on several projects.

PLANNED ACTIVITIES FOR FY 1981

LBL will continue technical consulting and management activities on the remaining complete or nearly complete projects until these projects are transferred to the Solar Energy Research Institute during the course of FY 1981.

† Vitro superseded IBM.

REFERENCES

1. U.S. Energy Research and Development Administration, National Program for Solar Heating and Cooling of Buildings, ERDA 76-6, Washington, D.C., November, 1976.
2. U.S. Energy Research and Development Administration, Commercial Integrated Projects for Use in Demonstrations for Solar Heating and Cooling, Program Opportunity Notice DSE-76-2, Washington, D.C., 1976.
3. U.S. Department of Energy, Commercial Integrated Projects for Use in Demonstrations of Solar Heating and Cooling, Program Opportunity Notice EG-78-N-01-4200, Washington, D.C., 1978.
4. U.S. Energy Research and Development Administration, Hot Water Initiative for Hotel/Motel Installations, Program Opportunity Notice EG-77-N-03-1450, Washington, D.C., 1976.

MEASUREMENT AND ANALYSIS OF CIRCUMSOLAR RADIATION*

D. Grether, D. Evans, A. Hunt, M. Wahlig, and S. Kanzler

INTRODUCTION

This project provides measurements and analyses of the solar and circumsolar radiation for application to solar energy systems that employ lenses or mirrors to concentrate the incident sunlight. Circumsolar radiation results from the scattering of direct sunlight through small angles by atmospheric aerosols (i.e., dust, water droplets or ice crystals in thin clouds, etc.). The solar energy system will typically collect all of the direct solar radiation (originating only from the disk of the sun) plus some fraction of the circumsolar radiation. The exact fraction depends on many factors but primarily on the receiver's angular size (i.e., its field-of-view). A knowledge of the circumsolar radiation is a factor in predicting or evaluating the performance of concentrating systems.

The project employs unique instrument systems (known as Circumsolar Telescopes) that were designed and fabricated at LBL. Each system has a "scanning telescope" mounted on a precision solar tracker. The telescope scans mechanically through an arc of 6° with the sun at the center of the arc. A digitization of the brightness of the sun or circumsolar radiation is taken every 1.5' of arc, with a complete scan taking one minute of time. One of the auxiliary instruments is a pyrheliometer, which has a fixed field of view (typically 5-6°) and is used to provide an estimate (called the "normal incidence" reading) of the direct solar radiation. The telescope and pyrheliometer have matched ten-position filter wheels: one open or "clear-filter" position, eight interference filters that divide the solar spectrum into eight intervals of roughly equal energy content, and one opaque filter to monitor detector noise. The data are recorded on magnetic tape, with one tape holding one week's worth of data per telescope.

The telescopes have been operated primarily at locations for which the instruments can play a dual role: (1) characterization of a region or climate, and (2) provision of site-specific data for proposed or actual concentrating solar energy systems. The data are used at LBL and other DOE-supported institutions (e.g., Sandia Laboratories and SERI) in considering the performance of concentrating systems.

A secondary project purpose is to relate the data to the atmospheric processes that attenuate the solar radiation available to terrestrial solar energy systems.

Details of the instrument system and examples of the measurements and summarized data have been given in previous annual reports. This present report is based primarily upon References 1 and 2.

ACCOMPLISHMENTS DURING FY 1980

Measurement Program

For the past several years, LBL had supported the operation of, and analyzed the data from, all four telescopes. This year, the budget was suffi-

* This work was supported by the Assistant Secretary for Conservation and Solar Energy, Office of Solar Applications for Buildings, Photovoltaic Energy Systems Division U.S. Department of Energy under Contract No. W-7405-ENG-48.

cient for LBL to support only two telescopes. Sandia National Laboratories in Albuquerque, N.M., agreed to operate one, but only in conjunction with tests at the Central Receiver Test Facility. LBL continued to support an instrument at the Advanced Components Test Facility at Atlanta, Ga. An instrument that had been upgraded at LBL during 1979 was installed in October, 1979 at the Jet Propulsion Laboratory Parabolic Dish Test Facility at Edwards, Calif. As well as providing specific data for the test facility, the telescope is providing climate characterization data for the Mojave desert area. The instrument that was located in nearby Barstow, Calif. for this latter purpose was returned to LBL. Barstow is the site of the 10 MWe Central Receiver Pilot Plant (Solar One) that is currently under construction.

A sunphotometer, on loan from the National Oceanographic and Atmospheric Administration, was mounted on the telescope installed at Edwards. The sunphotometer is used to estimate the turbidity of the atmosphere, a quantity that is related to the atmospheric scattering of sunlight by aerosols. The intent is to investigate possible correlations between turbidity values and circumsolar levels. The photometer, originally hand-held, was placed in an environmentally sealed and temperature-controlled housing, and the output was connected to the telescope's data-acquisition system.

Summary of Clear-Filter Data

Summaries of the clear-filter (nonwavelength selective) data through December, 1979 were prepared. The method for obtaining this type of summary is described in Reference 3. Sample results are shown in Figure 1 for the Mojave desert area. Displayed in Figure 1(a) is the monthly average circumsolar ratio, which is defined as the monthly total circumsolar radiation (from the edge of the sun out to 3^{o}) divided by the sum of the direct solar radiation (coming from the sun's disk) plus circumsolar radiation. This quantity is approximately the same as the fractional overestimate that a pyrheliometer would make in estimating the monthly total direct solar radiation. Figure 1(b) shows the ratio of the monthly total direct solar radiation to the extraterrestrial value (outside the earth's atmosphere). This quantity (similar to the commonly used K_T of Reference 4) compensates for the seasonal changes in day length and the varying earth-sun distance, and hence can be taken as an indicator of "cloudiness." The circumsolar ratio shows a distinct seasonal dependence with a winter peak of as much as 7% and summer minima of about 2%. A noticeable correlation also occurs with the total/extraterrestrial parameter; cloudy months tend to have high circumsolar levels. Comparable data from Albuquerque (not shown) do not have any obvious seasonal dependence. Rather, the circumsolar ratio shows a trend of increasing values from 2-3% in May and June, 1976, to 4-5% in February and March, 1977, and then, with considerable fluctuations, a relatively steady value thereafter.

Colored Filter Data

This year, a considerable effort was devoted to analyzing the colored-filter pyrheliometer data for application to wavelength selective systems, such as concentrating photovoltaic devices. As a tool in the analysis, the atmospheric transmission computer program LOWTRAN[5] was combined with an extraterrestrial solar spectrum.[6] The resulting Solar Spectral Model (SSM) provides a spectrum for any specified set of atmospheric conditions.

The first step in the analysis was to characterize the transmission function (transmission

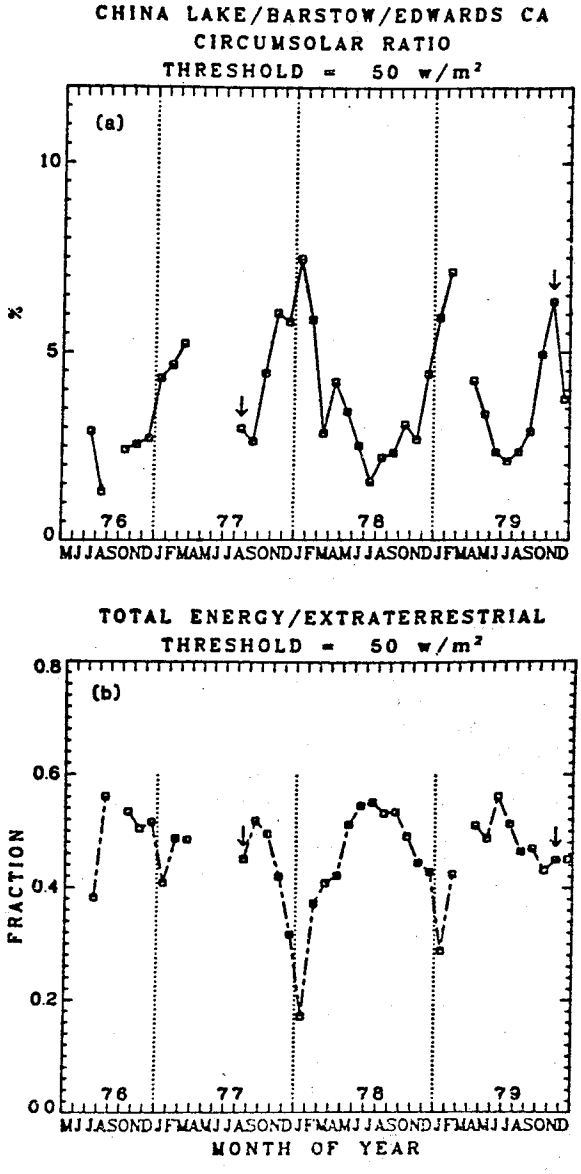

Fig. 1(a). The monthly value of the circumsolar ratio, as defined in the text, plotted from July, 1976 through December, 1979 for the Mojave desert area: China Lake, then Barstow, and finally Edwards, Calif. The small vertical arrows indicate the changes from one telescope location to the next.

Fig. 1(b). The corresponding value of the monthly total direct solar radiation divided by the extraterrestrial solar radiation.

versus wavelength and time) of each filter over an approximately three-year use period. The filters are of the interference type (multilayered dielectrics) and are known to be subject to degradation. Spectrophotometer measurements of the filters' transmission were made at LBL this year. Figure 2 displays the spectrophotometer measurement for a particular filter. Comparisons to similar measurements provided by the manufacturer when the filters were new suggested that many of the filters had changed in overall transmission. A method[1] was developed to track the change in transmission over time, using the colored-filter pyrheliometer readings for clear-sky conditions, when the atmosphere is relatively stable and the atmospheric attenuation processes are relatively well-understood. For each month of data, ratios of colored-filter to clear-filter pyrheliometer readings were extrapolated to zero air-mass, where the air-mass is a measure of the amount of atmosphere between the telescope and the sun. The extrapolated values are relatively independent of actual atmospheric conditions and the season of the year but quite sensitive to changes in filter characteristics. The analysis showed that most of the filters had undergone a slow but steady decrease in transmission over time, typically about 2%/yr. In contrast, one of the filters was observed to have experienced an abrupt reduction in transmission of about 17% during a particular month. To account for such effects, ad hoc "aging" factors were adapted, with a linear dependence being generally adequate to describe the data. The LBL spectrophotometer measurements together with the aging factors are then taken as specifying the filter transmission functions.

Given a knowledge of the filter transmission functions, the second step was to invert the pyrheliometer readings to obtain the spectral distribution of energy in the sunlight. As indicated by Figure 2, the transmission of any given filter has a complex dependence on wavelength. As a consequence, the inversion cannot be carried out exactly and an estimation method must be used. The method developed for estimating, described in detail in Reference 2, involves calculating an effective transmission over a nominal pass-band for each filter. The dotted rectangle in Figure 2 shows the nominal pass-band and an effective transmission value corresponding to the displayed filter transmission curve. The calculation uses an SSM spectrum to take into account, approximately, the shape (but not the magnitude) of the actual solar spectrum over the filter's wavelength region. The resulting effective transmission values have been shown to be insensitive to the details of the model. The energy content of the solar spectrum within the nominal pass-band is obtained by (i.e., the inversion is carried out by) dividing the pyrheliometer reading by the effective transmission.

Figure 3 displays in bar graph form the inverted values for two sequences of colored-filter, clear-sky pyrhelimeter readings. Superposed on the data is an SSM-modeled spectrum for nominal clear-sky conditions. For ease in comparison, the average of the modeled spectrum over each pass-band has been plotted as a solid square at the center of the band. The two data sequences and the

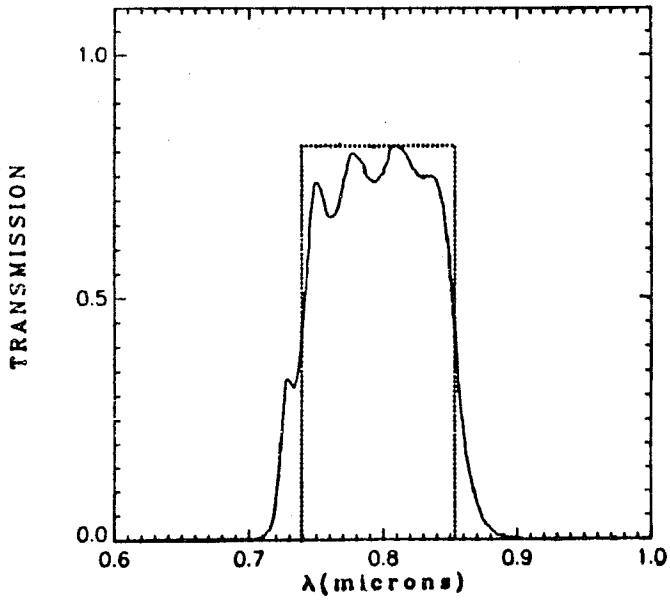

Fig. 2. The solid curve is the transmission versus wavelength, as determined on a spectrophotometer, for a particular colored filter. The dotted rectangle shows the nominal pass-band and an effective transmission for the filter.

modeled spectrum are for the same air mass value and have nearly the same clear-filter pyrheliometer readings (about 940 W/m^2). The variation in spectral composition of the data is noteworthy. One sequence is in quite good agreement with the model, and the other has a relative depletion in the 1.0 μ wavelength region; a portion of the spectrum that is particularly sensitive to photovoltaic applications.

PLANNED ACTIVITIES FOR FY 1981

For 1981, plans are to continue operating the instruments at Atlanta and in the Mojave desert area and to move a telescope to the site of Solar One by June, 1981. This latter telescope is to be interfaced to the data-acquisition system of Solar One so that the circumsolar radiation can be readily taken into account in evaluating the plant's performance. Plans call for the telescope currently at LBL to be rehabilitated, upgraded, and relocated.

Work will continue on the analysis of the clear-filter data with an increased emphasis on analyzing the systematic behavior of circumsolar radiation with respect to atmospheric conditions and their measurements. The goal is to develop a model of the circumsolar radiation so that estimates can be obtained for locations lacking actual measurements.

The effort on the colored-filter pyrheliometer data will be concluded using the data available to date, with summaries produced of the energy content of the solar spectrum for various locations, atmospheric conditions, seasons of the year, etc. Some attention will be given to the colored-filter scan data.

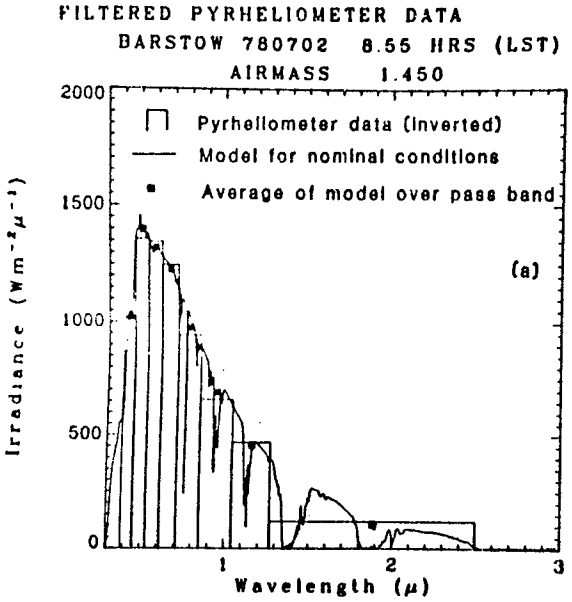

Fig. 3(a). Colored-filter pyrheliometer data for a particular date and time. The bar graph is for the actual data, inverted as described in the text. The solid curve is a modeled solar spectrum for nominal clear-sky conditions but for the same air-mass as the data. The solid squares are averages of the model over the pass-band of the filters and are included for comparison to the data.

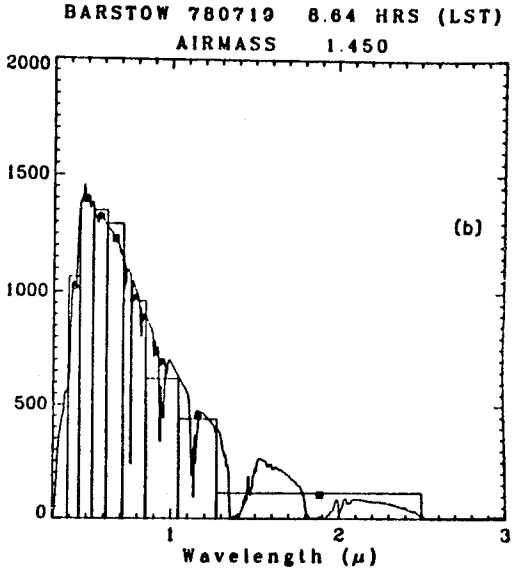

Fig. 3(b). Data for a second date but for the same air-mass value and essentially the same clear-filter pyrheliometer value as in 3(a).

If sufficient support is available, a new instrument will be designed as part of the FY 1981 program. The design would incorporate our knowledge of the character of circumsolar radiation as obtained with the current instruments and with a control system based on micro-processor devices. The instrument would be simpler to operate and maintain and would take fewer data points over a somewhat increased range of parameters. Actual construction would begin in FY 1982.

REFERENCES

1. D.F. Grether, D. Evans, A. Hunt, and M. Wahlig, "Measurement and Analysis of Circumsolar Radiation," Proceedings of the Annual DOE Insolation Resource Assessment Program Review, Davis, Calif., August 1980; Lawrence Berkeley Laboratory report LBL-11645, October 1980.

2. D.B. Evans, D.F. Grether, A.J. Hunt, and M. Wahlig, "The Spectral Character of Solar and Circumsolar Radiation," Proceedings of the Annual Meeting of the American Section of the International Solar Energy Society, Phoenix, Ariz., May 1980; Lawrence Berkeley Laboratory report LBL-10802, June 1980.

3. D. F. Grether, D. Evans, A. Hunt and M. Wahlig, "Application of Circumsolar Measurements to Concentrating Collectors," Proceedings of the 1979 International Congress of the International Solar Energy Society, Atlanta, Ga., June 1979; Lawrence Berkeley Laboratory report LBL-9412, June 1979.

4. B.Y.H. Liu and R.D. Jordan, "The Interrelationship and Characteristic Distribution of Direct, Diffuse, and Total Solar Radiation," Solar Energy, vol. 4, no. 3, 1960, p. 1.

5. J.E.A. Selby et al., Atmospheric Transmittance from 0.25 to 28.5 microns: Supplement Lowtran 3B, AFGL-TR-0258, AD A 040 701 (Hanscom Air Force Base, Mass.: Air Force Geophysics Laboratory, November 1976); available from National Technical Information Service.

6. M.P. Thekaekara, "The Total and Spectral Solar Irradiance and Its Possible Variations," Preprint X-912-75-155 (Greenbelt, Md.: Goddard Space Flight Center, June 1975).

CHEMICAL PROCESS RESEARCH AND DEVELOPMENT PROGRAM

INTRODUCTION

C. Judson King

The Chemical Process Research and Development Program deals with three principal application areas of chemistry: (1) production of synthetic fuels, (2) processing of effluent or recycled water and gas streams and/or feedstocks to achieve environmental compatibility, and (3) electrochemical energy storage. These projects have in common the use of principles of transport, thermodynamics, kinetics, separations and physical chemistry to improve fundamental mechanistic understanding and thereby to develop improved processing approaches.

Two of the larger projects pertain to different processes for the conversion of biomass--such as agricultural wastes, wood chips, newsprint--into fuels. The first of these projects consists of a study of enzymatic reactions that lead successively to sugars and then to ethanol. This product could be used as a fuel itself or could be blended with gasoline to make "gasohol." An important research target has been development of higher-capacity processing approaches that would significantly lower production costs. Another important research area has been the coupling of vacuum fermentation with vacuum distillation; this promises to bring about a major reduction in energy consumption. Still other studies are directed toward fundamental questions underlying these and related processing approaches.

The second biomass project concerns production of a fuel oil and a chemical feedstock by thermal, reductive conversion of biomass. Lawrence Berkeley Laboratory (LBL) has provided technical consultation and guidance to a Process Development Unit (PDU) of the Department of Energy (DOE) located at Albany, Oreg. A smaller, more flexible Process Engineering Unit (PEU) has been constructed in Berkeley, Calif. Recent research has dealt with means of pretreating biomass prior to liquefaction to improve properties such as pumpability in three ways: (1) by improving the means and understanding of homogenous catalysis for this process, (2) by solvolysis in acidified organic solvents, and (3) by chemical characterization of the product.

Another project relating to synthetic fuels deals with selective hydrogenation of coal using strong Lewis acid catalysts to achieve substantial conversion of coal to liquid at temperatures below those required for pyrolysis. This approach may require less severe process conditions, and it retains a large amount of coal's molecular structure and fuel value. At the same time, this project gives important insight into the mechanisms of homogeneous catalysis and solvation relating to coal liquefaction.

For environmental reasons, sulfur must somehow be removed from coal-burning systems, rather than being allowed to enter the atmosphere as SO_2 or SO_3. One approach is to remove sulfur from coal before coal combustion or further processing. A project is investigating oxidative acid-leaching as an improved means of sulfur removal. A by-product of this study is additional insight into the nature of sulfur bonding in coals.

A second approach for sulfur removal is flue-gas desulfurization. Under investigation are fundamental chemistry and transport mechanisms underlying reagent additive effects in flue-gas desulfurization processes based on scrubbing. This project is also working toward the development of a novel processing technique that will enable simultaneous removal of SO_2 and NO_x from flue gases.

Processes for coal conversion and manufacture of most other synthetic fuels generate large quantities of condensate water which have been in direct contact with the reacting mixture. These waters commonly have large loadings of ammonia, acid gases, and soluble organics. We are investigating novel separation methods that will allow the recycling of these condensate waters within fuels-conversion processes. Two areas of principal concern are (1) development of novel solvents that will enable a high degree of organics removal through extraction, and (2) combined stripping and extraction techniques that will substantially reduce the energy consumption for ammonia removal.

In the area of electrochemical energy storage, the division is involved in field management of the Applied Battery and Electrochemical Research Program supported by the Energy Storage Systems Division (STOR) of DOE. In addition, fundamental research is being carried out on mechanisms of redeposition and rearrangement of active material on battery electrodes during recharging processes. These studies are expected to lead to improved methods of reducing capacity loss during recharging, thereby eventually leading to longer service lifetimes for important battery systems that might be used for electric automobiles and large-scale energy storage.

PROCESS DEVELOPMENT STUDIES ON THE BIOCONVERSION OF CELLULOSES*

H. W. Blanch, C. R. Wilke, G. Dove, J. Perez, and A. F. Sciamanna

INTRODUCTION

The Department of Energy program has concentrated on the hydrolysis of cellulose and hemicellulose to sugars and on their subsequent fermentation to ethanol for use as a liquid fuel. A range of candidate cellulosic materials, mainly in the form of agricultural residues, forest-produced residues and whole tree biomass, have been analyzed and assessed for yields of sugar and ethanol under various processing conditions. Processing concepts under study include chemical (acid) pretreatment of these cellulosic materials to remove lignin and hemicellulose; enzymatic and chemical hydrolysis to produce hexose sugars; and production of ethanol by fermentation. Fundamental problems related to the development of optimal processing conditions have been studied under the auspices of the Basic Energy Sciences Division (BESD). More applied aspects and pilot plant studies are sponsored by the Solar Energy Research Institute (SERI).

Important basic problems include the kinetics of enzymatic hydrolysis of cellulose, the physical and chemical nature of the raw materials, production and recovery of the enzymes involved, and the development of new organisms for direct conversion of cellulose to ethanol.

Major developmental studies under the auspices of the Solar Energy Program include development of chemical treatment processes, studies on optimal cellulase production, enzymatic hydrolysis of hemicellulose and subsequent fermentation of the pentose sugars to ethanol, and optimization of a continuous-removal process for the ethanol fermentation using low pressure distillation. In all these studies, the economic impact of each process change is evaluated.

ACCOMPLISHMENTS DURING FY 1980

Support of SERI PDU Facilities of Gulf Oil Chemical Company

Currently the SERI program at LBL has undertaken various support functions for the Gulf Jayhawk Pilot Plant, Pittsburg, Kansas. These have included training of Gulf Laboratory personnel in analytical techniques, planning and monitoring of various pilot plant studies, and in interpretation of results. Studies to date have focused primarily on enzymatic hydrolysis of corn stover and the subsequent fermentation of the resulting sugars to ethanol. Additional work performed in conjunction with Gulf has been the analysis of corn stover from Nebraska, cotton gin trash from Mississippi, and Canadian aspen that was steam exploded by Iotech. These substrates were also enzymatically hydrolyzed at bench scale to establish the benchmark for the Process Demonstration unit (PDU).

The Fall 1979 corn stover crop grown in Nebraska was milled to approximately 0.5 to 2 mm particles, and was enzymatically hydrolyzed with cellulase enzyme derived from the Rutgers C-30 strain of Trichoderma reesei. There was obtained an approximate 40% conversion of the available carbohydrate to sugars. This result is much lower than observed for stover grown in Indiana and California in the Fall 1976, 1977, and 1978, respectively. With an acid pretreatment[1] followed by enzymatic hydrolysis, only a 55% carbohydrate conversion was obtained. It is unknown why the expected conversion of at least 80% was not obtained. The analysis[2] of this substrate, shown in Table 1, did not have an unusual composition. In fact, it is a little higher in carbohydrate content compared to those mentioned previously. The grower stated that no unusual herbicide, fungicide, bactericide was applied before, during, or after the growth cycle. Essentially the same results were obtained at the SERI/Gulf PDU for enzymatic hydrolysis of much larger batches (~110 lb) of this residue. Several tons of this Nebraska corn stover were used in the demonstration plant studies with no marked improvement in the conversion of the available carbohydrate.

While awaiting delivery of steam-explosive decompressed wood from Iotech Co. of Canada, work was started on cotton gin trash that was on hand at the Gulf Jayhawk plant. A sample of about 5 kg of 1975 harvest, Gulf cotton gin trash, grown in Indianola, Mississippi, was supplied to us. This was analyzed, and the results are shown in Table 2. This cotton gin trash is considerably higher in carbohydrate content compared to what is generated in California.[1] On enzymatic hydrolysis, a carbohydrate conversion of only 19% was obtained--nearly equal to what was obtained with the residue from California. Even though the residue from Mississippi contains about 2.5 times more carbohydrate, apparently the cellular carbohydrate is tightly bound or completely sheathed with lignin, thus preventing enzyme accessibility. Since this residue appears to be an unlikely candidate for economic conversion of the carbohydrate to fuel alcohol, no further studies were performed here.

* This work was supported by the Office of Energy Research in Basic Energy Sciences, Chemical Sciences Division of the U.S. Department of Energy under Contract No. W-7405-ENG-48 and by the Solar Energy Research Institute.

Table 1. Corn Stover* Zeamays-L. (Prairie Valley-76S) from Polk County, Nebr., Fall crop 1979; assay.†

Constituents of Sample	Percentage Composition
Carbohydrates (total)	61.6
glucan	40.7
mannan	0.36
galactan	1.2
xylan	18.0
arabinan	1.36
Sugar and/or equivalent (total)	69.9
glucose	45.2
mannose and/or fructose	0.4
galactose	1.3
xylose	20.4
arabinose	1.5
sucrose	1.1
Other constituents	
lignin	14.8
ash‡	5.1
azeotropic benzene/alcohol extractives	6.1
other acid insolubles (organic)	4.2
protein	4.4

*1 in. tub milled particles, courtesy of Charles Wosel and Mark Holscher, Gulf Oil Chemicals Co., Pittsburgh, Kans. 66762.

†2 mm Wiley-milled particles 0.25-0.35 mm fraction, 100% dry.

‡0.457 of the ash is acid insoluble; 0.543 of the ash is acid soluble.

Table 2. Cotton gin trash Gossypium Hirsutum-L. from Indianola, Miss., 1975 harvest*; assay.†

Constituents of Sample	Percentage Composition
Carbohydrates (total)	68.3
glucan	48.9
other hexosan‡	2.0
xylan	16.9
arabinan	0.5
Sugar equivalent	76.5
glucose	54.4
other hexose	2.2
xylose	19.3
arabinose	0.6
Other constituents	
lignin	20.7
ash	4.8
other acid insolubles	2.8
azeotropic benzene/alcohol extractives	4.2

*0.032 in. Hammer-milled particles, courtesy of Charles Wosel, Gulf Oil Chemicals, Pittsburgh, Kansas 66762.

†2 mm Wiley-milled particles, unsieved fraction, 100% dry.

‡includes mannan (mannose) and galactan (galactose).

A 100-lb batch hydrolysis done at Gulf resulted in essentially the same results.

Future work will be the analysis and hydrolysis of several types of recently received exploded wood. Results from preliminary enzymatic hydrolysis on one exploded wood sample shows a better than 90% carbohydrate conversion. This wood, exploded by Iotech, Canada, is presently being used in preliminary studies at Gulf for enzyme production as well as hydrolysis.

Enzymatic Hydrolysis of Agricultural Residues

The development of mutant strains of T. reesei has enhanced the potential for developing economically attractive processes that enzymatically hydrolyze biomass to produce glucose. During the past year, experiments were conducted to evaluate the hydrolysis of corn stover utilizing cellulase from T. reesei: Rutger's C-30, a new mutant strain. The strain is of interest because it is hyperproducing, catabolite repression-resistant, and capable of yielding significantly β-glucosidase activity.

Batch hydrolysis were conducted for a period of 24 to 48 h employing substrate concentrations ranging from 5 to 25 wt% and enzyme activities ranging from 2.6 to 9 International units (IU)/ml. Experiments were carried out in 600 ml Wide Mouth beakers containing 200 ml or substrate-enzyme mixture. The contents were stirred at approximately 150 rpm and were maintained at a constant temperature of 45°C and pH of 5.

Prior to hydrolysis, corn stover was milled to 2 mm and treated with sulfuric acid to hydrolyze hemicellulose. Following pretreatment,[2] the corn stover was neutralized and air dried. Treated corn stover typically contained 57-70% glucose equivalent by weight.

In experiments with substrate concentrations exceeding 10 wt%, stepwise addition of substrate was employed. After an initial solids loading of 5-10%, the reaction was allowed to proceed for 1/2 h at which point an increment of corn stover was added. Subsequent substrate increments enable 25% total substrate concentrations to be achieved in 2.5 h.

Hydrolysis conducted under the conditions described produce sugar streams ranging from 15-90 g/ℓ, containing 80-85% glucose. Figure 1 presents typical hydrolysis curves. Product concentrations increase both with increasing substrate

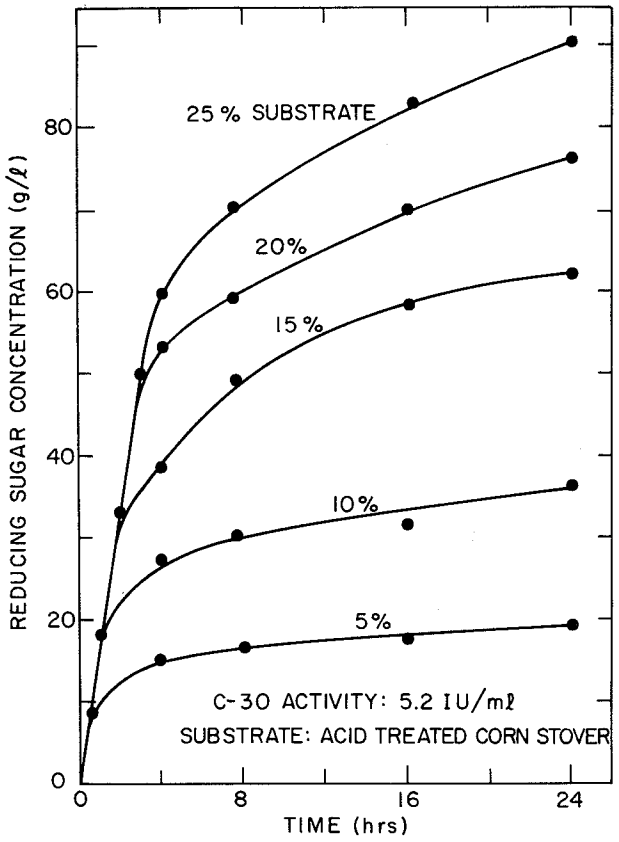

Fig. 1. Hydrolysis reducing sugar concentration versus time at various substrate loadings. (XBL 808-5703)

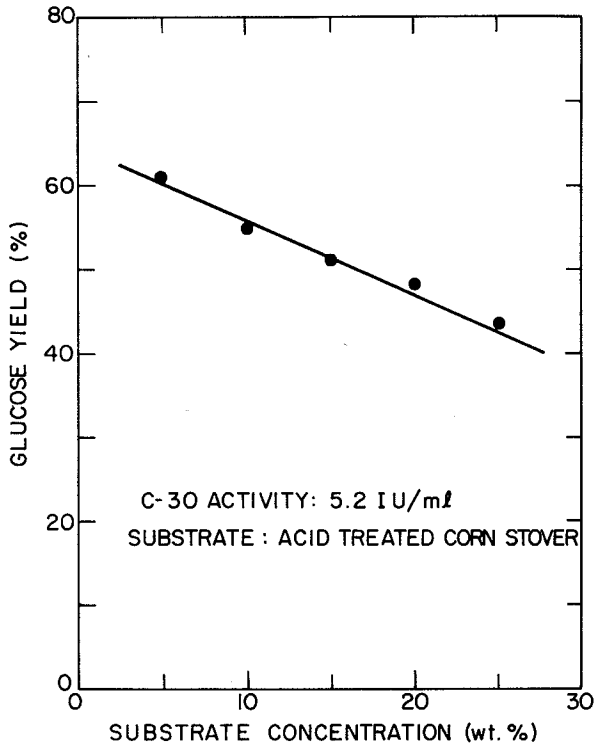

Fig. 2. Glucose yield at 24 hours versus substrate concentration. (XBL 808-5705)

concentration and time. The initial linear increase in sugar concentration is apparently due to the loading technique employed.

Glucose yields typically decrease with increasing substrate concentration for a given enzyme activity. Figure 2 projects typical yield data. To date, the highest glucose yield observed was 61% corresponding to 5% substrate and enzyme activities of 5 IU/ml or greater. In general, it was observed that increasing the enzyme activity at constant substrate concentration produced an increase of yield until a threshold was reached. Beyond this point, no further increase in yield was experienced. Further work is being carried out to characterize this observation.

Enzyme activity remaining in solution during hydrolysis was measured. Dissolved cellulase activity drops rapidly during the first few hours of hydrolysis and then levels to a slightly decreasing value. Figure 3 shows a typical curve of enzyme activity remaining in solution after 24 h of hydrolysis. Activity after 24 h is usually 85-30% of original, decreasing with increasing solids suspension. Activity after 24 h decreases with decreasing initial activity, but this loss is much less pronounced than concentration-related losses. Measurement of activity profiles of cellulase components during hydrolysis indicate that

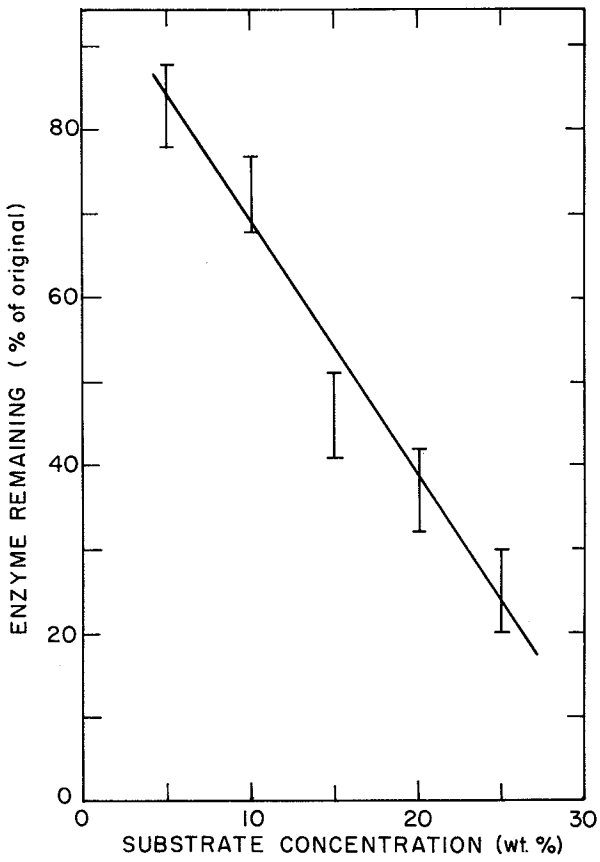

Fig. 3. Enzyme activity at 24 hours versus substrate concentration. (XBL 808-5706)

endo- and exo-glucanases parallel the behavior of the overall enzyme activity while β-glucosidase remains in solution to an appreciably greater extent.

Experiments are currently underway to investigate hydrolysis employing enzyme activities in the range of 0.5 to 2 IU ml. The incentive for this was provided by preliminary economic evaluations discussed in a later section. Preparations are being made to study enzymatic hydrolysis of steam-exploded corn stover.

Enzyme Recovery

A major economic obstacle in the conversion of cellulose to ethanol involves the loss of cellulolytic enzymes. The loss occurs primarily during the hydrolysis of cellulose to a sugar solution. The enzyme probably adsorbs onto the cellulosic residue, removing it from solution. Several approaches to cellulase recovery were analyzed: (1) isolation or immobilization of the enzyme; (2) modification of the enzyme to reduce its adsorption characteristics; and (3) modification of the substrate.

The third approach has been explored in some detail. A chemical may coat the entire substrate surface to prevent permanent adsorption, yet allow hydrolysis to occur. To observe their effects, the following salts were introduced into the hydrolysis: ammonium sulfate, ammonium oxalate, ammonium chloride, glycine and urea. Salt concentrations ranged from 6.0 M to saturated solutions. Preliminary conclusions suggest that the salts may be precipitating the enzyme reversibly ("salting out"). However, glycine may destroy the enzyme even at low concentrations.

Urea at 1 M concentration in the hydrolysis offers the most promising alternative, producing a recovery of 64%. Unfortunately, no economical method exists to remove the urea from an aqueous solution. Therefore, it must be recycled and work is being performed on exploring the feasibility of designing a cellulose to ethanol conversion scheme that employs a closed loop with total recycle of the urea. Urea is introduced into the hydrolysis, but must pass through the fermentation, distillation, and auxillary unit operations.

The effects of urea on the sugar fermentation in batch and continuous culture are being studied. A brief summary of results are given in Table 3.

The maximum growth rate and cell yield are adversely affected by urea. However, the ethanol productivity and conversion ratio of ethanol produced to glucose consumed do not decrease substantially over the range of urea concentrations explored thus far.

The efficiency of the distillation operation may be enhanced in the presence of urea. Acting as an azeotropic agent, urea distorts the ethanol-water equilibrium line and reduces the required number of separation stages. This advantage becomes significant at the pinch point at the top of the column.

Table 3. Effect of urea on enzyme growth rate and enzyme productivity.

Urea Concentration (M)	Maximum Growth Rate (h^{-1})	Ethanol Productivity* (g/ℓ-h)
0.000	0.450	4.7
0.125	0.375	4.6
0.250	0.341	4.7
0.500	0.171	-

*at a dilution rate of 0.25 h^{-1}.

A computer-generated equilibrium curve for ethanol and water only is being compiled now by other researchers in our group. This data may be very useful in predicting behavior of the urea system once some initial data are obtained with urea. This work may require six to sixteen months to complete, depending on the similarities of the two systems and the consistency of literature sources.

Process conditions in the hydrolysis have been changed dramatically in recent months. The substrate and enzyme concentrations have been increased by more than a factor of five, thereby increasing the exit sugar concentration. The effects of urea on enzyme recovery and sugar production at these conditions must be explored. The concentration of urea must be optimized over a range of combinations of substrate and enzyme to establish design parameters.

Process Economics

Preliminary economic evaluation of the Berkeley process (Figure 4) modified to include cellulase production from T. reesei Rut C-30 has been completed. Some hydrolysis results described earlier were utilized to estimate the cost of manufacturing glucose from corn stover at a rate of 214 tons per day of product.

From the limited data evaluated, a manufacturing cost of approximately 12¢/lb glucose was obtained. This constitutes 30% reduction over the cost of glucose obtained with processes of utilizing T. reesei strain QM-9414. Figures 5 and 6 give typical breakdowns of production cost by operation and by manufacturing component. For the cases presented, it can be seen that enzyme production is the dominant processing step and that, typically, capital-related factors predominate. Therefore, any subsequent improvements in cellulase production or increases in substrate yield brought about by improvements in substrate pretreatment are likely to make the largest cost reduction.

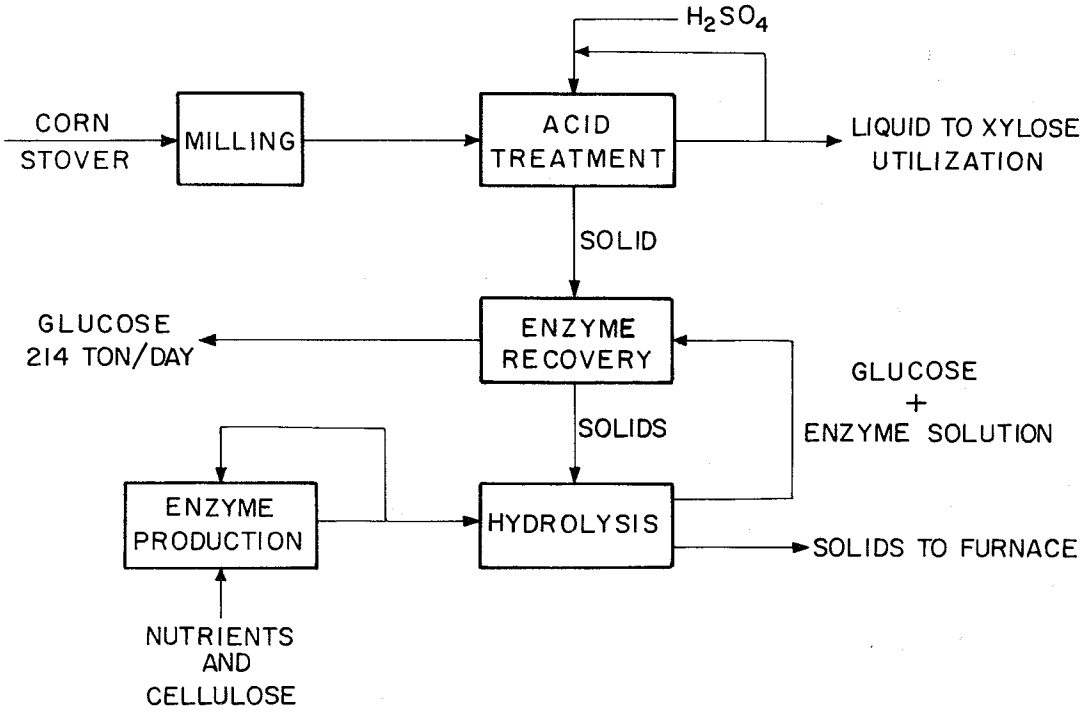

Fig. 4. Enzymatic hydrolysis process: block flow diagram. (XBL 808-5701)

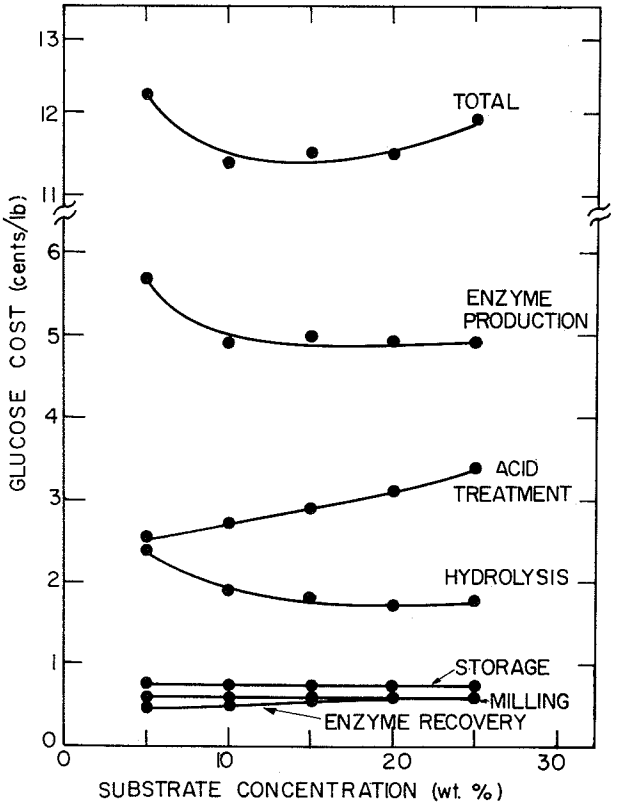

Fig. 5. Production cost by operation versus substrate concentration. (XBL 808-5710)

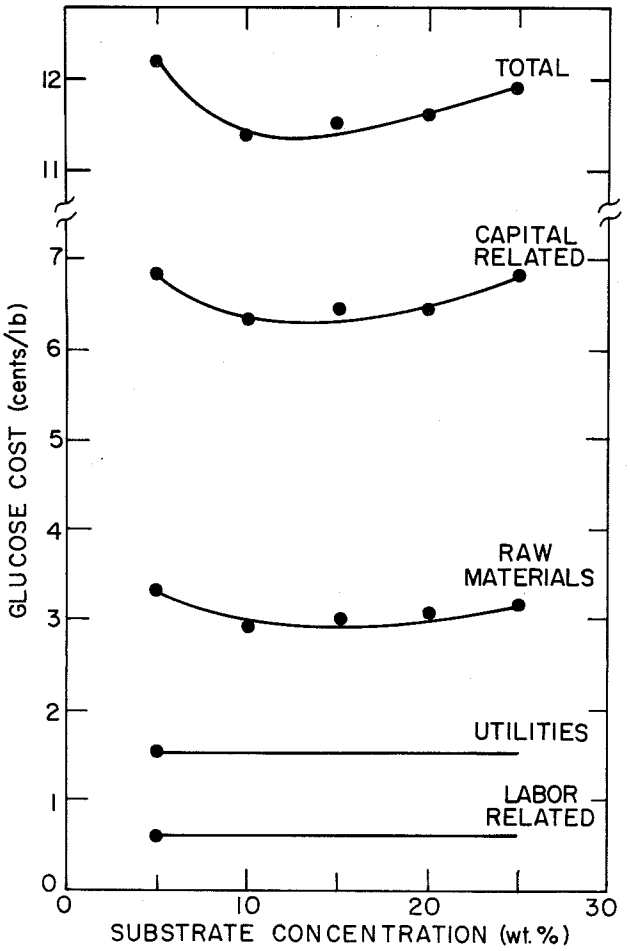

Fig. 6. Production cost by manufacturing component versus substrate concentration. (XBL 808-5709)

PLANNED ACTIVITIES FOR FY 1981

Some continued experimental work in connection with the SERI/GULF PDU is contemplated. If the program funding continues, then the predominant emphasis will be in directing modifications to the PDU for enzyme production from residues rather than from the considerably more expensive, manufactured cellulosic substrates.

Preparations are being made to study enzymatic hydrolysis of steam-explosive decompressed corn stover as a pretreatment rather than acid pretreatment.

In the fields of enzyme recovery, high concentrations of urea in the fermentor (up to 2.0 M) will be explored.

A computer program is being written to help evaluate the economics of the process with greater precision. When completed, the program will enable evaluation of the full range of hydrolysis data generated, and a closer approximation to the optimal processing conditions will be obtained. By evaluating process alternatives, the program should provide information useful in planning further experiments.

REFERENCES

1. A.F. Sciamanna, R.P. Freitas, and C.R. Wilke, Composition and Utilization of Cellulose for Chemicals from Agricultural Residues, Lawrence Berkeley Laboratory report LBL-5966, December 1977.

2. R. Freitas, B. Long, A. Sciamanna, and C.R. Wilke, Process for Analysis of Solids and Liquids from Cellulosic Sources, Lawrence Berkeley Laboratory report LBL-5967, December 1977.

ENZYMATIC CONVERSION OF WOOD AND AGRICULTURAL RESIDUES TO SUGARS*

C. R. Wilke, H. W. Blanch, K. Tangnu, D. Wiley, B. Long, S. Rosenberg, J.-P. Riba, and L. Sindelar

INTRODUCTION

This research effort encompasses three areas: cellulase production and kinetics, hemicellulose utilization, and organism development. The work's overall goal is the hydrolysis of cellulose and hemicellulose and the fermentation of the resulting sugars to ethanol and other useful neutral products.

In our process, cellulose is hydrolyzed using cellulase enzymes produced by the mold Trichoderma reesei. Two of the project aims are the optimization of enzyme production and purification of components of the cellulase complex. By knowing which member or members of the complex are restricting overall conversion, supplementation schemes can be devised.

Hemicelluloses can represent as much as a third of the total carbohydrate content of lignocellulosic materials. The major component of the hemicellulose polymer is the pentosan called xylan. The bacterium Bacillus macerans, which ferments xylose to ethanol and acetone, is being studied in order to maximize the production of these volatile neutral products and to minimize the production of unwanted products, mainly acetic acid.

Finally, we are developing new microorganisms for the direct fermentation of cellulose to ethanol without the preliminary separate enzymatic hydrolysis step.

ACCOMPLISHMENTS DURING FY 1980

Cellulase Production and Kinetics Research

Composition of Cellulase

A scheme for separating the components of the cellulase complex of enzymes obtained from batch cultures of T. reesei, Rutger's C-30 strain (Rut C-30), has been scaled up to obtain purified endoglucanase (EC 3.2.1.21), cellobiohydrolase (EC 3.2.1.91), and β-glucosidase (EC 3.2.1.4). While the latter is not a cellulase in that it acts on a soluble substrate, i.e. cellobiose, rather than insoluble cellulose and cello-oligomers, it is a necessary component of the complex of enzymes involved in the ultimate degradation of cellulose to glucose.

The scheme, which is shown in Figure 1, results in the preparation of these enzymes in gram amounts rather than the milligram quantities previously obtained from an analytic separation, and will be sufficient for a kinetic study of the separate activities. Description of the reactions catalyzed by the separate enzymes is essential to the development of a general mechanism for the overall rates of cellulose hydrolysis in the production of glucose from agricultural wastes, which is the impetus for this work.

*This work was supported by the Office of Energy Research in Basic Energy Science, Chemical Sciences Division of the U.S. Department of Energy under Contract No. W-7405-ENG-48 and by the Solar Energy Research Institute.

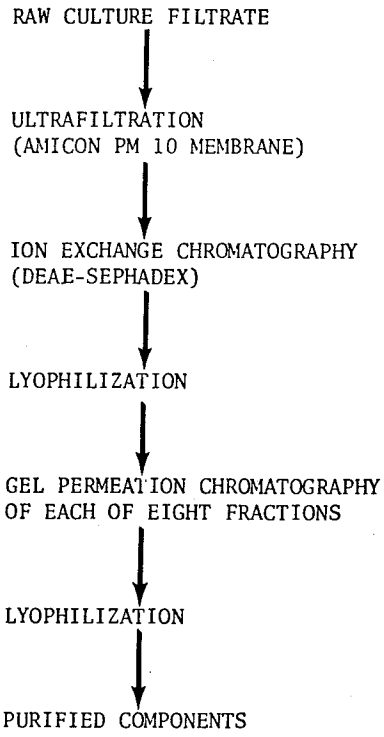

Fig. 1. Scheme for the preparation separation of cellulase components.

In the first step of the separation scheme, an ultrafiltration cell removes salts and other nonessential, low-molecular weight species, including a chromophore, from the raw culture filtrate. This enhances the separation obtained by elution with a salt gradient in the subsequent ion-exchange step. The latter results in the preparation of eight fractions, which are further purified by gel permeation chromatography after lyophilization and resuspension. Homogeneity is examined by sodium dodecyl sulfate-polyacrylamide gel electrophoresis, which indicates the requirement for an additional separation by cationic exchange for the first proteins eluted.

The preparation scheme results in the isolation of three major components: the principal cellobiohydrolase, endoglucanase, and β-glucosidase, which are listed in order of their prevalence in the cellulase complex, as well as minor components, showing each of these types of activities. Xylanase activity is presumed to be an auxillary activity of a principal component, and protease is assumed to be either irreversibly bound during the anion exchange, as expected of an acid protease, or present in such trace quantities as to be otherwise removed prior to the final purification steps.

The described separation scheme will be instrumental in the development of a kinetic model to be used in optimizing the hydrolysis of cellulosic materials.

Cellulase Production by Trichoderma Reesei

T. reesei QM-9414 and Rut C-30 were grown in batch and in a two-stage, single-stream continuous culture to produce cellulase, using cellulose as a carbon source.

Three cellulose concentrations (10, 25, and 50 g/ℓ) were tested to determine the maximum levels of cellulase activity obtainable in submerged culture. Temperature-pH profiling was tried in order to increase the cell mass to maximum levels, thereby enhancing fermentation at higher substrate concentrations.

For maximum production of cellulase by T. reesei QM-9414, the pH was allowed to decrease to 4 for the first day and to 2.8 for the second day. At the end of the second day, the pH was raised to 3.3 and controlled not to go below 3.3, while temperature was controlled at 28°C. With 50 g/ℓ and 25 g/ℓ substrate concentrations, filter paper activity of 6.1 and 4.3 International Units (IU)/ml, respectively, were obtained. There was not a substantial gain in filter paper activity with the increase in substrate concentration.

For production of cellulase and β-glucosidase by T. reesei Rut C-30, a pH of 5 and a temperature of 25°C were optimum. A higher temperature (31°C) for the initial fermentation time period (18 h) could substantially increase the β-glucosidase activity in the system. A pH of 6 can produce as much β-glucosidase in three days as can be obtained in eight days at a pH of four or five. With the help of environmental control, it is possible to produce enzyme mixtures with different ratios of FPA, C_1, C_x and β-glucosidase. Filter paper activities of 14.4 and 7.3 IU/ml were obtained using 50 g/ℓ and 25 g/ℓ of substrate, respectively.

Tween-80 concentration of 0.1% and 0.02% were optimized for T. reesei Qm-9414 and Rut C-30, respectively.

Two-stage continuous culture studies were carried out growing QM-9414 and Rut C-30 on a cellulose-containing medium in 14-liter stirred fermentors. Response to step changes in Tween-80 level, substrate concentration, dilution rate, pH and temperature was followed and steady-state values obtained.

For QM-9414 the first and second stages were operated in the pH range of 3.75-4.25 and 5.0, respectively. Decreasing the Tween-80 concentration by half (0.1%) increased the filter paper activity by 60% in the first stage of the fermentation. Increasing inlet substrate concentration from 1.75 to 2.5% did not increase the filter paper activity. Optimum dilution rates of 0.02 and 0.27 h^{-1} were found in the first and second stages, respectively. A fermentation temperature of 28°C optimized both stages.

For Rut C-30, the first and second stages were operated at a pH of 5.0. Tween-80 concentration of 0.02% and temperature 25°C were optimum for maximum cellulase production. Dilution rates of 0.02 and 0.04 h^{-1} optimized both the stages.

In the future, it would be advantageous to run two-stage fermentations with a cell recycle system.

Utilization of Hemicellulose Research

In our current bioconversion process, treatment of the cellulosic biomass substrate with hot, dilute sulfuric acid hydrolyzes the hemicellulose polymers yielding a solution rich in pentose sugars, the major component of which is D-xylose. Since as much as a third of the total carbohydrate of biomass may be in the form of hemicellulose, we have been examining methods for maximizing the fermentative conversion of D-xylose to ethanol. The organism we have been studying to effect this conversion is the bacterium Bacillus macerans. The major fermentation produced by this organism growing with D-xylose are ethanol, acetone, and acetic acid.

The current respective yields of ethanol, acetic acid, and acetone are 27, 23, and 1.5 g/g of xylose fermented. Theoretical considerations suggest that a balanced fermentation can occur without the production of acetic acid. Whether this can be achieved in practice will depend on the regulation of the enzymes of the biochemical pathways concerned. There is evidence from other systems that the concentrations of certain end products can affect the spectrum of fermentation products produced and their final concentrations. To investigate the regulation of fermentation pathways in B. macerans, it was first necessary to understand how various product concentrations would affect the organism's growth rate. These relations have been determined, and the results are shown in Figure 2. The maximum specific growth rate (μ_{max}) is approximately 0.2 h^{-1}, corresponding to a doubling time of about 3.5 h.

Organism Development Research

The goal of this research is the development of a biological process for the single-step conversion of cellulose to ethanol. To this end,

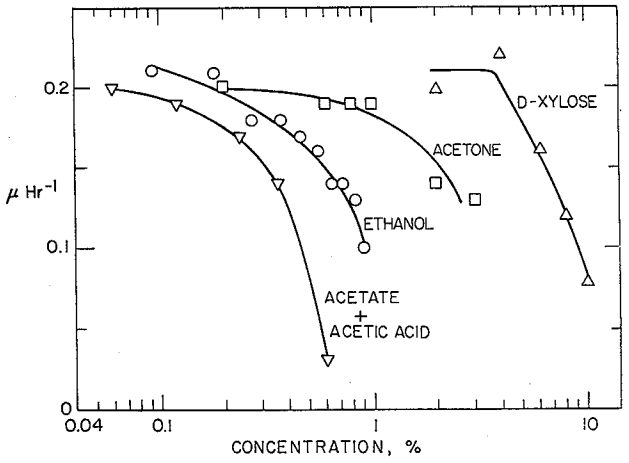

Fig. 2. Effect of substrate and fermentation product concentration of the growth rate of Bacillus macerans. (XBL 8011-13332)

we have tested a number of likely candidate microorganisms for ability to both degrade cellulose and to ferment glucose quantitatively to ethanol and CO_2.

Of 60 strains examined, 12 appeared able both to ferment glucose to ethanol and CO_2 and degrade cellulose. Of these 12, 6 showed especially good cellulose hydrolysis aerobically, and these were chosen for further detailed study. Cultures were grown with crystalline cellulose, ball-milled, crystalline cellulose, and phosphoric-acid swollen cellulose. Crystalline cellulose is most resistant to degradation, while swollen cellulose is least resistant. Strain A-106 grew faster on all three forms of cellulose and on this basis was selected for further study.

Physiological and nutritional studies reveal several important characteristics of this organism:

(1) Growth would occur on cellulose aerobically but not anaerobically.

(2) The organism would grow on glucose both aerobically and anaerobically, but anaerobic growth (fermentation) required the presence of a complex nutritional supplement, such as yeast extract, while aerobic growth could occur in an unsupplemented mineral medium.

(3) Fermentation of glucose can occur after net growth ceases.

(4) Approximately theoretical yields of ethanol (ca. 45%) are produced from glucose by this organism.

(5) Cellulose can be fermented if some oxygen is included in the culture initially. This lowers the yield of ethanol but allows the process to proceed.

During this period, we also developed a practical, small-scale culturing system that allows us to test the effects of many variables simultaneously rather than sequentially, as had been the case with our previous large-scale apparatus. This has greatly speeded up the pace of research.

PLANNED ACTIVITIES FOR FY 1981

Utilization of Hemicellulose Research

Now that we know what the growth inhibitory concentrations of the major products (and the substrate) are, we will repeat these experiments with various product concentrations and measure the concentrations of the various products produced. The resulting observations will allow us to model the regulation of the various fermentation pathways and potentially to skew the fermentation toward the production of neutral products.

Organism Development Research

Research for 1981 will be concentrated in two areas:

(1) Definition of the minimal nutrient requirements for complete fermentation of glucose. Fermentation of glucose may not be complete even in the presence of nutrients such as yeast extract unless at least a small amount of air (oxygen) is present. We need to determine what required nutrients are missing in order to eliminate the oxygen requirements and maximize ethanol productivity.

(2) Demonstration of cellulase production under anaerobic conditions. This is our major problem area. Currently cellulases are expressed aerobically but not anaerobically. We will conduct mutation-selection experiments in order to select mutant strains which produce high, unregulated levels of cellulase enzymes.

ETHANOL PRODUCTION AND RECOVERY FROM BIOMASS SUGARS*

C. R. Wilke, H. W. Blanch, B. Maiorella, K. Murphy, B. Vickroy, and H. Wong

INTRODUCTION

Ethanol is the logical intermediate product in the utilization of biomass for energy and chemical needs. Produced by fermentation of biomass sugars, ethanol can be used directly as a liquid fuel, or it can serve as a chemical feedstock of great flexibility. These uses help to reduce this country's dependence on imported petroleum only if the overall conversion uses much less energy than is recovered in the product. Hence the goal of this research is to improve ethanol production and recovery from biomass so that it can make as great a contribution as possible to reducing our imported petroleum requirements.

Research toward this objective is proceeding in four separate but inter-related projects. In the Flash Fermentation for Rapid Ethanol Production project, a process for continuous production and purification of ethanol from fermentation is being tested on a pilot-plant scale. The Alternative Ethanol Recovery work is developing other techniques for ethanol recovery which will consume less energy than traditional distillation. In the project on Novel Fermentor Development, the use of a hollow-fiber fermentor to achieve higher productivities than those of conventional fermentors is being investigated. The remaining project, Nutritional Requirements for Yeast Fermentation, is aimed at precise identification of the metabolic needs of the ethanol-producing yeast to allow specification of medium components for maximum ethanol productivity at minimum cost.

ACCOMPLISHMENTS DURING FY 1980

Flash Fermentation for Rapid Ethanol Production

A 5-liter volume flash-fermentation pilot plant has been assembled (Fig. 1).

The fermentative ethanol production rate is ordinarily limited by ethanol inhibition. Flash fermentation eliminates this problem by continually removing alcohol as it is produced. Fermentation beer is drawn by vacuum into an auxiliary isothermal vacuum flash vessel where it boils. Ethanol and water vapors are taken as flash vessel overhead products, condensed in a condenser train and collected in a dry ice-cooled collection vessel. The ratio of ethanol to water in this final product is fixed by the temperature and pressure of flash vessel operation. Ethanol-depleted beer is pumped back to the fermentor from the flash vessel. Fermentor ethanol concentration is thus maintained at a low level. A concentrated sugar feed (such as molasses) can rapidly be fermented to produce concentrated (ca. 30 wt%) ethanol vapor product.

In a shakedown run of the flashferm apparatus, a volumetric productivity of 36 g/ℓ-h was achieved in converting 350 g/ℓ glucose feed to 19.3 wt% ethanol product. This is more than ten times the volumetric productivity in simple batch fermentation, which yields a far more dilute product.

Alternative Ethanol Recovery Processes

The major emphasis in the work on alternatives to distillation as an ethanol recovery process has been in the area of solvent extraction. An extraction process could be very energy conserving and economical given a solvent which is highly selective for ethanol and easily regenerated. However, most solvents that are selective for ethanol in a dilute aqueous solution have a very low distribution coefficient (the ratio of weight or mole fraction of ethanol in the solvent phase to that in the aqueous phase).[1] Thus, studies have been done on ways of enhancing the distribution coefficient of selective solvents.

In one such method, an agent is added to the solvent to lower the activity of ethanol in the solvent phase. An example of this approach is the use of trioctyl phosphine oxide (TOPO) in organic solvents. Data from studies of this extractant system applied to acetic acid recovery

*This work was supported by the Office of Energy Research in Basic Energy Science, Chemical Sciences Division of the U.S. Department of Energy under Contract No. W-7405-ENG-48 and by the Solar Energy Research Institute.

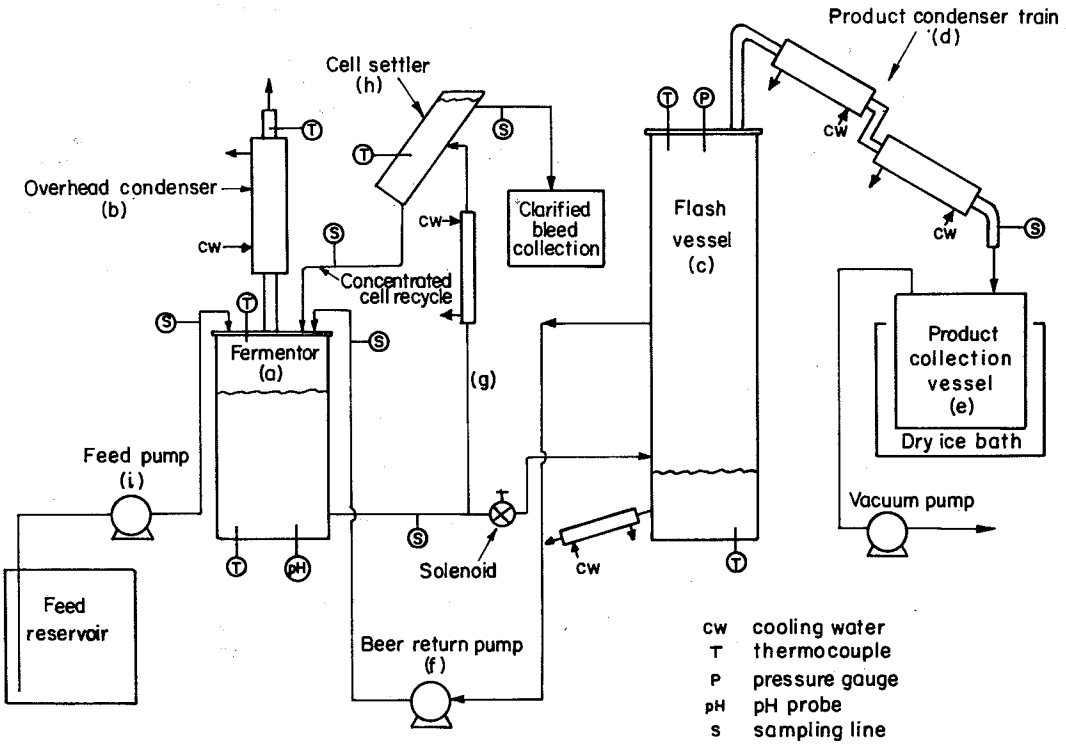

Fig. 1. Flash-ferm apparatus overview. (XBL 7912-5497)

suggested that it might be effective in enhancing the alcohol distribution coefficient.[2] Phase equilibrium experiments analyzed by gas chromatography showed the effect to be very small in the case of ethanol, however. Modifications of the idea, employing compounds with somewhat less hydrophobic character, such as tributyl phosphine oxide, are being tested.

Rather than lowering the activity of ethanol in the solvent phase, raising its acivity in the aqueous phase has also been studied as a means of improving ethanol distribution coefficients. This can be done by adding separating agents, such as sugars or salts, to the aqueous phase. A number of such compounds have been investigated by gas chromatographic analysis of batch-phase equilibrium experiments. While sugars show some enhancement of distribution coefficient, only at very high concentrations are they significant. Much more effective are some inorganic salts, including potassium phosphates and carbonate and ammonium sulfate. These salts will actually cause the formation of a separate liquid phase rich in ethanol (up to 90 wt%) when added to dilute aqueous ethanol solution. The use of such salting-out behavior depends, however, on economical recovery processes for the salt, which cannot be discarded because of its cost and possible environmental damage. Such processes are under continuing study.

Novel Fermentor Development

Equipment was built to study existing ultrafiltration (uf) modules for use as fermentors. A study of the flow pattern in the unit was made and a fermentation was attempted. Existing commercial units were unsatisfactory because of the large amount of fermentation gases that need to be vented. A new configuration to allow for easier gas-venting has now been made. In the new design, the fibers are spaced out to allow gas bubbles to rise; the shell side pressure can be regulated to control the volumetric rate of gas evolution; and the pathway for the gas to escape is less tortuous. Unfortunately, many problems in the construction of the fermentor have delayed the work.

Nutritional Requirements for Yeast Fermentation

A basic study of the nutrient requirements for yeast fermentation of sugars to ethanol is important because of the high cost contribution of the nutrients to the ethanol production cost and because of the major effects of media composition on ethanol and yeast productivities. Therefore, batch and continuous fermentations have been carried out to define the active components of the normally complex media used in yeast fermentation and to define their optimal ratios for balanced yeast growth.

It was shown that for low (10 g/ℓ) glucose concentrations, 88% of the complex component of the medium, yeast extract, could be replaced by synthetic vitamins and still increase both specific and total ethanol productivities. However, increasing the glucose concentrations to 100 g/ℓ and the other components in direct proportion led

to lower ethanol productivity with synthetic vitamins relative to yeast extract. Furthermore, total sugar utilization decreased for both media with higher glucose concentrations. Possible explanations currently being investigated are the effects of substrate inhibition, nonoptimal dissolved O_2 tension, and changes in the organism.

In particular, the effect of dissolved O_2 was studied intensively because previous reports showed important but contradictory results in the very low ranges of 0 to 10 ppb dissolved O_2. Unfortunately, the use of dissolved O_2 probes, chemical tests, and gas chromatography (with thermal conductivity detector) all lacked the sensitivity to measure this level of dissolved O_2. It has been reported that a gas chromatograph with a helium ionization detector has sufficient sensitivity, but it is expensive and difficult to operate.

Instead, attention was turned to determining the effects of higher measurable concentrations of dissolved O_2, which would be the range of practical importance. Control at the reported low optimal levels, because its range is so narrow, would be impractical for industrial applications. Preliminary results show that over a wide range of about 0 to 50% of air saturation, there is little or no effect due to dissolved O_2. However, carbon dioxide was inhibitory to yeast growth and ethanol production.

Also, an interesting change, which may be an adaptation, appeared to take place in the organism when an essentially anaerobic continuous culture was aerated vigorously. The cell yield was considerably greater than that expected from fermentative growth, indicating substantial aerobic or oxidative growth was occurring. However, the ethanol yield was much greater than that expected from aerobic growth, which is expected from the residual glucose level in the medium. Therefore, both fermentative and aerobic pathways were simultaneously being utilized, and the catabolite repression (glucose effect) must have been partially lifted. Measurement of O_2 uptake and CO_2 evolution are in progress to determine the relative extents of fermentative and oxidative growth as a function of aeration conditions. If this function can be determined, the ratio of cell mass to ethanol production can be controlled. A complicating factor in this study has been the stability of the possible adaptions.

PLANNED ACTIVITIES FOR FY 1981

Flash Fermentation for Rapid Ethanol Production research during the next calendar quarter will optimize operating conditions for the flashferm process, considering such variables as feed concentration, feed rate, and flash vessel temperature and pressure.

This work will be completed and a final report evaluating the flashferm process and comparing it with alternative fermentation schemes will be submitted by late August 1981.

Alternative Ethanol Recovery research will continue investigation of the promising aspects of FY 1980 work; plans for FY 1981 include study of two new concepts in extractive fermentation and economic analysis of process designs incorporating these features. The first of these is the use of inert gas stripping of ethanol fermentation beer followed by solvent absorption of the ethanol vapor. This concept avoids the formation of emulsions which have created problems with liquid-liquid extraction processes involving fermenter beers. It also, like the vacuferm and vacuflash processes, allows increased ethanol productivity by removing ethanol continuously, thus mitigating product inhibition. Preliminary calculations show that energy requirements for inert gas recirculation are very small.

The other new concept slated for study is a means of removing alcohol from the extractant stream without heating the entire stream (as would be necessary in a conventional distillation or stripping operation). This involves using the ability of certain salts to form alcoholate complexes analogous to hydrates. Recovery of ethanol from the solid ethanolates by evaporation has the potential for less energy consumption than conventional processes.

These ideas are to be evaluated using available data and the results of experimental determinations of solvent properties using the gas chromatographic system. Results will be used to determine parameters for a process design which will be evaluated for economic feasibility.

Novel Fermentor Development research will include a fermentation using the new fermenter design. If the gas problem is overcome, the system will then be modeled using a model similar to that cited by Schuler et al.[3] The effect of fermentation gases must be incorporated into this model. If gas venting still presents a serious problem, an alternate biosystem to study the unit may need to be found.

Nutritional Requirements for Yeast Fermentation research will determine the effects of dissolved O_2 and aeration, and then the cause of low cell and ethanol productivity with 100 g/ℓ glucose will be reexamined. If O_2 is not the problem, the effect of substrate inhibition by various minerals will be studied. Also, a mass balance will be obtained for the major elements so their quantitative requirements can be determined for a balanced medium.

REFERENCES

1. E. K. Pye and A. E. Humphrey, "Biological Production of Liquid Fuels from Biomass," Proceedings of Third Annual Biomass Energy Systems Conference, June 5-7, 1979 (Golden, Colo.: Solar Energy Research Institute, October 1979).

2. N. L. Ricker, J. N. Michaels, and C. J. King, "Solvent Properties of Organic Bases for Extraction of Acetic Acid from Water," Journal of Separation Proceedings Technology vol. no. 1, 1979, pp. 36-41.

3. I. A. Webster, M. L. Schuler, and P. R. Rony, "Whole-Cell Hollow-Fiber Reactor: Effectiveness Factors," Biotechnology and Bioengineering, vol. 21, 1979, pp. 1725-1748.

THE LBL BIOMASS LIQUEFACTION PROCESS*

H. Davis, S. Ergun, C. Figueroa, C. Karatas, L. Schaleger, and N. Yaghoubzadeh

INTRODUCTION

The major objective of this program is to provide a process for converting Douglas fir wood, and other sources of biomass, to a commercially usable fuel oil. Such a product could provide a storable fuel for peak-load power plant operation, transportation or power-plant fuel for a local area, and perhaps a raw material for particular chemicals.

A process development unit (PDU) is operated on a Department of Energy (DOE) contract at Albany, Oregon by Rust Engineering. The PDU was built in the mid-1970s, based on experiments at the Pittsburgh Energy Research Center (PERC), and it has been able to generate significant amounts of oil product from Douglas fir wood chips since late 1979. The PERC process, as used in the PDU, requires excessive recycle of product oil--10 parts or more of recycled oil to one part dry wood feed --and has other economic deficiencies. The LBL process was designed to correct these deficiencies.[1] Actually, the first substantial amounts of product in the PDU were made by an improvised version of the LBL process.[2] Two relatively successful PERC-mode runs were accomplished in June[3] and October 1980.

The basic principle of the LBL process is to replace the recycled oil, used in the PERC process with slurry wood flour for feeding to the reactor with water. Wood chips undergo mild hydrolysis (at 180°C, for 45 min in 0.075% H_2SO_4); this hydrolyzes hemicelluloses and leaves the chips weak and friable.

After neutralization with alkali, the wood chip-water mixture is passed through a paper industry-style "refiner" from which a stable slurry containing up to 30% or more dry solids is obtained. This is then heated to about 360°C with a CO/H_2 synthesis gas, held for an appropriate residence time, and cooled. The oil product is denser than water at low temperatures but can be recovered in a phase separator. A significant portion of the product (7 to 12% of the dry wood feed) remains dissolved in the aqueous product.

As of October 1, 1979, serious unresolved questions remained concerning the pumpability and stability of the aqueous wood slurry, optimum reaction time, initial pH and pressurizing atmosphere, behavior of recycle streams, and properties of the product. On October 1, 1980, some information is available but considerable effort is necessary before all the questions can be answered.

ACCOMPLISHMENTS DURING FY 1980

Slurry Preparation and Stability

Slurries of partially hydrolyzed wood have been made on a large scale in the PDU and have been pumped through tubing as small as .25 in. for extended periods in the PDU and at LBL.[1] Concentrations of dry solids >30% have been handled successfully. Storage in drums for several months makes no apparent difference in pumpability.[2] An actual run in the PDU, although it used only an 8% slurry, was reasonably successful and produced several drums of product, the first substantial amounts of wood oil available from the PDU. Concentrated slurries have also been preheated successfully in small tubing at LBL. Thus the process has been demonstrated in stages.

Continuous Experimental Unit

During 1980, a bench-scale continuous experimental unit (CEU) designed to feed about 1 liter/h of wood slurry was constructed at LBL.[1] First efforts to operate this in June and July 1980 revealed several deficiencies, and it was decided to rebuild the unit from August 1980 to the present. Safety features deemed necessary were added and instrumentation and controls were improved.[4] Mechanical completion was expected in late 1980 when initial testing could begin.[4] The CEU is an essential element in providing a link between laboratory batch experimentation and continuous pilot plant and commercial operation. Basic engineering variables, e.g., reaction time, temperature, initial pH, composition of reacting gases, etc., can be studied more readily than at the PDU and results are more relevant for commercial operation than batch work results.

A small colloid mill (equivalent to a refiner) has been rented and an autoclave suitable for prehydrolysis is on order. They will permit us to study the prehydrolysis step and the preparation of slurries of various concentrations for the CEU.

*This work was supported by the Assistant Secretary for Conservation and Solar Energy, Office of Solar Technology, Biomass Energy System Division of the U.S. Department of Energy under Contract No. W-7405-ENG-48.

A glass coil was used[5] to demonstrate the pumpability and stability of PDU wood slurry and to measure flow properties.

Batch Experimentation

During 1980, a series of factorial experiments was carried out in small "tubular bomb" reactors.[4,6] These experiments have many of the interpretation problems of batch experimentation in general in addition to a possibly serious deficiency in agitation. They have the advantage of availability of rapid heat-up and cooling (2.5 min to 360°C). The experiments are reported in some detail in the Biomass Group's fourth Quarterly Report.[4] Among the conclusions from the data are several which contradict the conventional wisdom on liquefaction.

- Synthesis gas, which may be H_2, CO, or mixtures thereof, and may include some CO_2, is essential to minimize char formation. Pressurizing with inert gas alone N_2 results in high char formation.
- At pHs near the neutral point, yields of acetone-soluble oils are higher and yields of char lower than when additional sodium carbonate is added. Sodium carbonate has been generally considered to catalyze the reduction of wood-oxygen by CO.
- At the usual reaction temperature of 360°C, yields of solubles are highest and yields of char lowest when heat-up rate is as high as possible and holding time at this temperature is very low.

This work must be checked in the continuous units. In particular, the apparent need for very short reaction times seems to contradict the results with the PERC process at the PDU, where liquid space times were of the order of two hours and the high recycle multiplied this by a large factor of the order of 20, without apparent serious effect on char formation. It is conceivable that the data are revealing the effect of agitation and gas-liquid contacting during heat-up and the subsequent slow reduction with CO and H_2.

Planned Activities for FY 1981

First order of business is the completion and testing of the CEU and an initial run under a set of standardized conditions. Once this is achieved, the CEU will be used to explore the effects of most of the pertinent process variables, particularly the variable which cannot properly be studied in batch equipment: reaction time. Studies of effects of slurry pH, gas composition, and reaction temperature will be guided by the results of batch experimentation. A serious effort will be made to obtain acceptable material balances. This has proven to be very difficult in the PDU, and data from batch autoclave work are skimpy. A flow-sheet of the CEU as it now stands is attached (Fig. 1).

A series of experiments in stirred autoclaves is planned to verify and extend the small tubular bomb results. The autoclaves are superior to the tubular bomb in at least two respects: stirring is possible and a material balance is possible. Also sizable amounts of products for chemical studies and for recycle experiments can be made. The relatively long heat-up times, however, are a serious drawback. Therefore, an effort to design and build slightly larger tubular bombs capable of agitation will be made. The larger amount of dry wood reacted in these (4-6 g versus 1-1.5 g) will also improve possibilities for a material balance.

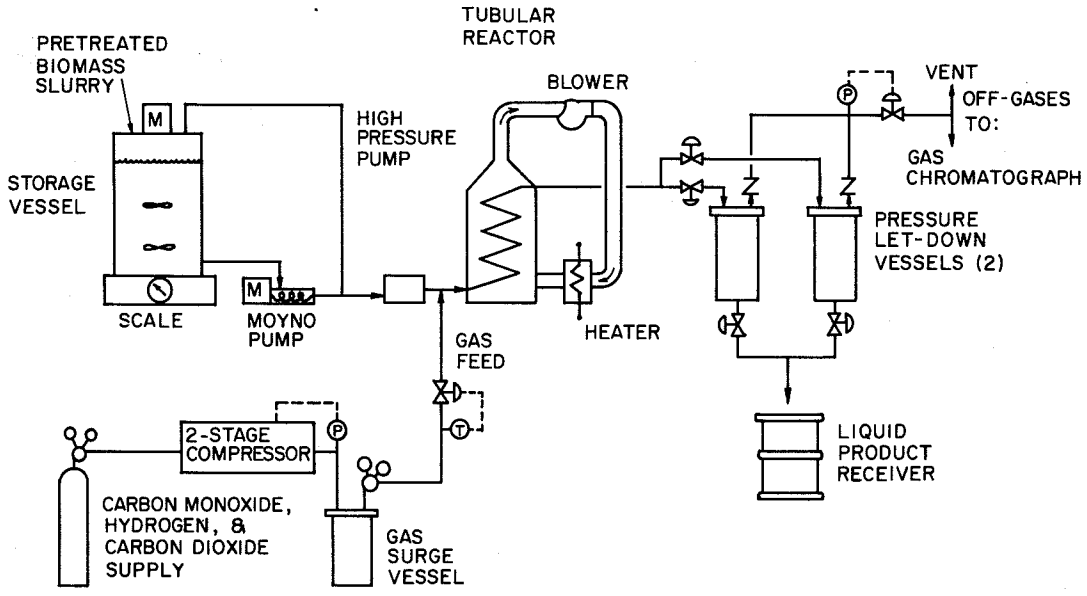

Fig. 1. LBL Process Evaluation Unit (PEU). (XBL 811-3585)

A most important effort involves the better characterization of product oils and a related effort to understand the mechanism of liquefaction. This effort employs the various methods of chromatography to effect group separations as well as individual product determinations. Samples obtained under various reaction conditions and from various feedstocks (including celluloses, hemicellulose components, and lignin) will be studied so that we can begin to understand some of the mechanisms of the many reactions which occur. This effort is discussed in a later section of this report.

While LBL no longer has monitoring responsibility for the Albany PDU operation, we have been requested to supply advice on equipment and operations and we plan to have engineers present when a definitive LBL test is made. At LBL's request, the following changes in the PDU equipment and flow sheet have been made preparatory to such an experiment:

- A direct-fired tubular preheater has been installed capable of heating 60 gal/h of feed slurry to 360°C with a total resident time of less than one min.
- A refiner has been rented so that slurry can be made on site.
- The PDU stirred-tank reactor has been repiped so that a lower product take-off, leaving about 50 to 60 gal of reactor volume, is available. This permits liquid space times of less than one h.
- Commercial phase separators for the product oil-aqueous layer separation were ordered.
- The older vertical, scraped-wall preheater has been bypassed, but can be reinstalled as a standpipe reactor (~17 gal capacity) with the scraper removed.

Neither the stirred-tank nor the standpipe constitutes the reactor we would prefer. This should be tubular-really an extension of the preheater to allow an appropriate time at temperature. As of October 1, 1980, however, we were hopeful that one or both of these available reactor systems would work. Judging from the batch experimentation work discussed above, we would get the least amount of charry residue and the largest amount of product (if not the best quality) by stopping reaction after the tubular preheater.

REFERENCES

1. S. Ergun, Cl. Figueroa, C. Karatas, L. Schaleger, M. Seth, J. Wrathall and N. Yaghoubzadeh, Catalytic Biomass Liquefaction, Lawrence Berkeley Laboratory report, LBL-10667, February, 1980.
2. Operations of the Biomass Liquefaction Facility, Albany, Oregon Quarterly Report, July-September 1979, Rust Engineering Co., November 5, 1979. Prepared under DOE Contract ET-78-C-06-1092.
3. Operation of the Biomass Liquefaction Facility, Albany, Oregon, (Technical Progress Report) April -June 1980, Rust Engineering Co., August 7, 1980. Prepared under DOE Contract DE-AC01-78-ET-23032.
4. H. Davis, R. Djafar, S. Ergun, C. Figueroa, C. Karatas, L. Schaleger, M. Seth, J. Wrathall, N. Yaghoubzadeh and G. Yu, Catalytic Biomass Liquefaction, Quarterly Report, July-September, 1980, Lawrence Berkeley Laboratory internal document LBID-34.
5. J. Wrathall and S. Ergun, Hydrolyzed Wood Slurry Flow Modeling, Lawrence Berkeley Laboratory report LBL-10090, November, 1979.
6. H. Davis, R. Djafar, S. Ergun, C. Figueroa, C. Karatas, L. Schaleger, M. Seth, J. Wrathall, N. Yaghoubzadeh and G. Yu, Catalytic Biomass Liquefaction Quarterly Report, April-June 1980, Lawrence Berkeley Laboratory internal document LBID-272.

CHEMISTRY OF BIOMASS LIQUEFACTION*

H. Davis, D. Kloden, and L. Schaleger

INTRODUCTION

The liquefaction of wood, municipal waste, and other forms of biomass has been studied for many years. The present efforts stem from work done by H. Appel, I. Wender and others at the U.S. Bureau of Mines' Bruceton Station, (later known as PERC and referred to now as PETC) in the 1960s and early 1970s. It was found that treatment of biomass materials in an autoclave at temperatures of 300-400°C under pressures of water vapor and CO gave an oil-like product. The product was definitely not hydrocarbon. It contained up to 15% O_2, including substantial amounts of carbonyl and phenolic hydroxyl groups. Its heating value was therefore considerably lower than that of a petroleum fuel oil. Still, it burned, and was substantially free of sulfur, nitrogen, and ash, making it a desirable nonpolluting fuel. A process development unit (PDU) was therefore designed and construction

*This work was supported by the Assistant Secretary for Conservation and Solar Energy, Office of Solar Technology, Biomass System Division of the U.S. Department of Energy under Contract No. W-7405-ENG-48.

on it at Albany, Oregon in 1974. It operates on Douglas fir wood chips, and was designed both to scale-up the process and to convert it from a batch to a continuous process.

Over the years various efforts have been made to deduce the stoichiometry and mechanism (or mechanisms) of the conversion and the chemical make-up of the product. At all levels of operation, tests with good material balances have been lacking. There has been argument as to the role of CO or of the CO-H_2 mixtures usually substituted for it. Catalysts have been tested, supported, then abandoned. The original U.S. Bureau of Mines' work indicated that an alkaline system--achieved by adding Na_2CO_3--was necessary for CO to be effective. Even this is questioned today.

Nuclear magnetic resonance (NMR) analysis and physical properties of the oil from wood chips show it to be highly aromatic. This suggests that much of the oil product comes from the lignin portion of wood (~32% in Douglas fir) rather than from the aliphatic polysacharide portions. Experiments with cellulose, sugars, and lignin feeds bolster this conclusion.

The temperatures at which liquefaction takes place (the PDU operates at 360°C) are in a range where pyrolysis readily occurs. Large amounts of CO_2 and water are formed. The liquefaction is therefore a controlled pyrolysis accompanied by a reduction reaction.

Characterization of the reaction and the product oil has been inhibited by the wide variety of reaction conditions and feed stock tried in batch experiments. The present existence of two reasonably well identified processes (PERC and LBL), both operable in the PDU and both leading to reasonably consistent products, makes a renewed effort on characterization attractive.

Accomplishments During FY 1980

Stoichiometry

The lack of good material balances and the variety of processing conditions has left the stoichiometry of the process somewhat uncertain. The best material balances for the PDU to date were obtained in test run 8,[1] using the PERC process. An analysis of the data[2] shows that several classes of reactions definitely occur, and that the stoichiometry can be described at least semi-quantitatively. From 100 lb of dry wood approximately 0.6 lb-mol of CO_2 and 0.5 lb-mol water were formed essentially by pyrolysis, while about 0.6 mol CO reacted to further reduce O_2 in the product oil and, of course, form an additional 0.6 mol CO_2. There is no net usage of H_2. In fact, the reaction medium, the reactor, or both, catalyze the water-gas shift reaction. Additional CO reacts with water to form H_2 and CO_2.

Material balance closure demands that roughly 45 lb of the wood be accounted for as CO_2 + H_2O (plus a trace of methane) and roughly 55 lb as liquids or solid product. However, the PDU run showed only 41% oil yield plus 4% char residue. Thus our forced balance requires an additional 10%. A portion of this is probably material dissolved in the aqueous effluent or volatiles lost overhead. The rest simply indicates the limits of our current ability to obtain (and to calculate) a material balance.

The LBL process differs from PERC in a fundamental way: the feed to the process is an aqueous slurry of partially hydrolyzed wood, as opposed to a slurry of wood flour in recycled product. Since in the PERC process as carried out in the PDU, the feed is 90% recycled oil, the overall residence time in the reactor is many hours (as opposed to about one hour for LBL). The presence of larger excesses of water and the absence of recycled oil may also have secondary effects on the process chemistry. Also, the portion of overall product dissolved in the larger aqueous effluent will be greater in the LBL process.

Nevertheless, the same general processes must occur. Apparently, to obtain a product, other than char, with less than about 10-15% O_2 some reduction by synthesis gas must occur. (See Table 1.) We suggest the following as a resonable goal for either process:

$$\text{100 lb dry wood + 0.6 mol CO} \xrightarrow[\text{4000 psig } H_2O,\ H_2,\ CO]{360^\circ}$$

$$\text{0.5 mol } CO_2 + \text{0.5 mol } H_2O + \text{55 lb nonvapor product.}$$

The above requires about 430 ft^3 of synthesis gas per 100 lb of dry wood. The "nonvapor product" includes an amount of water solubles dependent on process and process conditions. It also includes solid char residue, that must, however, be minor if the process is to be acceptable.

Characterization of Products

The gross product of liquefaction has been characterized largely by elemental analysis, by simple physical properties, such as density and viscosity, and occasionally by distillation (typically 60 to 70% is vaporizable in a laboratory vacuum still). Numerous individual compounds have been identified in the lower boiling fractions.

Table 1. Product analysis.

Wood (wt%)		Nonvapor Product (wt%)	
C	53.2	C	83.9
H	5.6	H	8.3
O	40.5	O	7.5
N	0.13	N	0.1
Others	0.6	Others	0.2
Total	100.0	Total	100.0

These are largely cyclic ketones, phenols, and cyclic ethers, with few if any hydrocarbons (other than those in the PERC product, which may have come from the initial anthracene oil). Alkaline extractions have indicated 10 to 40% acidic components (primarily phenols), depending on the process and the treatment method.

A list of compounds identified by steam distillation of an LBL process product oil is reproduced as Table 2, from the LBL fourth Quarterly Report.[3] Somewhat similar materials have been extracted from aqueous effluent or from other oil products.

While the majority of the compounds identified in Table 2 are aliphatic and of low molecular weight, the more typical compounds must be quite different. Distillation curves and gel permeation chromatography show the average molecular weight to be about 300 or more. Physical properties, H:C ratio and NMR studies show that well over 50% of C atoms are aromatic--probably 90% of the compounds are aromatic. The identification of any very high percentage of these as individual compounds is a difficult, nearly impossible task and not a very rewarding one. Accurate and well-characterized methods of dividing the product by functional type and by molecular weight range have long been needed.

PLANNED ACTIVITIES FOR FY 1981

With the addition of a graduate chemist and a chemical technician to our staff, we hope to make real progress in the development of rapid type-analyses. Equipment available includes gas chromatography, gas chromatography plus mass spectrometry, high precision liquid chromatography, gel permeation chromatography, and the usual techniques of solvent extraction.

The objective is twofold: first to know what the product is and second to be able to follow changes in the product as the process changes. There are many ways, of course, in which such a product might be characterized. At this point, we would be well-satisfied if a given sample could be divided into four or five fractions according to molecular weight and if each of these (except perhaps the heaviest) could be separated into four or five fractions according to polarity. Within each fraction, gross properties would be known. These include elemental analysis, average molecular weight, molecular weight distribution, viscosity, and density. Types of compounds concentrated in each fraction would be known at least semiquantitatively, e.g., aromatic and aliphatic hydrocarbons, phenols (mono and dihydric), methoxy phenols, ethers, cyclic ethers, and ketones. Estimates of aromaticity, ring structure, and degree of ring

Table 2. Major components of steam distillate of TR-7 oil.*†

No.‡	c	Time(s)	Mass	Probable Identity	Type§
1		429	84	cyclopentanone	CK-S
2*		446	98	cyclohexanone	CK-S
3		486	98	3-methylcyclopentanone	CK-S
4		694	112	cycloheptanone (tentative)	CK-S
5		853	110	dimethyl-2-cyclopentenone isomer	CK-S
6*		941	96	2-methyl-2-cyclopentenone	CK-U
7		1114	124	dimethyl-2-cyclopentenone	CK-U
8*		1173	110	dimethyl-2-cyclopentenone isomer	CK-U
9		1246	110	dimethyl-2-cyclopentenone isomer	CK-U
10		1302	124	trimethyl-2-cyclopentenone isomer	CK-U
11*		1412	-	(computer omission)	-
12		1467	-	(computer omission)	-
13		1498	138	alkyl cyclohexenone (tentative)	CK-U
14		1527	138	alkyl cylcohexenone (tentative)	CK-U
15*		2184	124	guaiacol	MP
16		2389	138	4-methylguaiacol (creosol)	MP
17*		2477	136	$C_9H_{12}O$ (alkyl phenol)	P
18		2548	152	4-ethylguaiacol	MP
19		2630	122	C2 phenol isomer	P
20		2639	150	alkyl phenol	P
21		2709	166	4-n-propylguaiacol	MP
22		2817	122	ethylphenol isomer	P

*Obtained from Albany Drum #5 (sample TR-7 - 190 LBL Process).

†GC conditions: OV-225 SCOT column; 50°C for 3 min, then 30/min to 250°C and hold.

‡The six most abundant components are starred.

§CK-S; cyclic ketone, saturated; CK-U: cyclic ketone, unsaturated; MP; methoxyphenol; P: phenol.

substitution would be available. Compounds present in significant percentages would be identified and measured.

Comparison with the slow international progress in defining properties of coal products suggests that this is only partly achievable by a small group. Not all of it is necessary for following the reaction or finding uses for the products. But we should at least be able to follow the concentration of major product types like phenols, acids, and furans as they are affected by process variables. We should also be able to follow changes in molecular weight, boiling range, and aromaticity. In FY 1981 we hope to achieve a goal somewhere between this minimum and the ultimate: a truly well-identified product.

REFERENCES

1. Operation of the Biomass Liquefaction Facility, Albany, Oregon, Technical Progress Report, April-June 1980, Rust Engineering Co. August 7, 1980. Prepared under DOE Contract DE-AC01-78-ET-23032.

2. H. Davis, Stoichiometry of Wood Liquefaction, Lawrence Berkeley Laboratory report LBL-11776, October 1980.

3. H. Davis, R. Djafar, S. Ergun, C. Figueroa, C. Karatas, L. Schaleger, M. Seth, J. Wrathall, N. Yaghoubzadeh and G. Yu, Catalytic Biomass Liquefaction, Quarterly Report, July-September, 1980, Lawrence Berkeley Laboratory internal document LBID 314, 1980.

THE SOLVOLYSIS OF DOUGLAS FIR WOOD IN ACIDIFIED ORGANIC SOLVENTS*

G. Yu, T. Vermeulen, and H. Davis

INTRODUCTION

There are two major engineering and economic problems of wood liquefaction. These arise from the difficulty of feeding the substrate into a reaction system (the "front end" problem) and the need for a reaction temperature near the critical temperature of water, and consequently for a high operating pressure. The front end problem is currently met by feeding a liquid and biomass slurry. This is wood flour-recycle product oil in the PERC process and prehydrolyzed wood-water in the LBL process.

The objective of the present work was to find an alternate method of liquefying wood to solve the front-end problem by producing a material easily fed into a liquefaction reactor that might yield an interesting product, thereby totally bypassing the present liquefaction reaction system.

This report summarizes work done mainly during FY 1980 by G. Yu as part of work on his doctoral thesis under Professor T. Vermeulen of the Department of Chemical Engineering at the University of California, Berkeley, and carried out in the laboratories of the LBL Coal and Biomass Group.

ACCOMPLISHMENTS DURING FY 1980

Solvolysis Process

Based on wood chemistry concepts, a process capable of solubilizing more than 95% of wood under some mild conditions has been developed. Unlike the PERC and LBL processes, no H_2 or CO is required. The product is a soft, black, bitumen-like solid at room temperature and melts readily at 140°C. Its heating value is estimated to be roughly 11,000 Btu/lb.

The process concept is based on two well-known reactions, lignin alcoholysis and cellulose hydrolysis. The former involves solubilization of lignin using alcohol under conditions such as 5-24 reaction time at 40-120°C. It is apparently a very slow and low-yield process. Cellulose hydrolysis, however, requires hydrolyzing cellulose to glucose in an aqueous acidic medium. In both cases, either carbohydrate or lignin is left as a solid residue. A combination of acid and alcohol, however, could conceivably enable both the lignin and cellulose to depolymerize and be solubilized. Essential ingredients of the process are, therefore, an alcohol (or phenol) and dilute strong acid.

Table 1 depicts some results of our process feasibility and process solvents evaluation study. The solvents can either be derived from cellulose or from lignin. The results showed that alcohols with a small amount of acid added are good media for solubilizing wood. An estimated reaction temperature of 250°C is needed to define a high degree of solubilization in an acceptable time. Analysis of reactor off-gas showed that the synthesis gas used to pressurize the reactor did not participate in the reaction. We made our trials, therefore, with acidified alcohols (or phenols) under an initial condition of 1 atm N_2. At reaction temperature, the atmosphere consists largely of the vapors of solvent and water from the wet alcohol feed.

Effects of Product Variables

Figures 1 and 2 illustrate effects of process variables such as temperature and time on the degree of wood solubilization. In both cases, opti-

*This work was supported by the Assistant Secretary for Conservation and Solar Energy, Office of Solar Technology, Biomass System Division of the U.S. Department of Energy under Contract No. W-7405-ENG-48.

Table 1. Preliminary process feasibility and solvents evaluation study.

Solvent*	Unreacted Wood (%)
methanol†	47.81
methanol	27.82
ethanol†	39.25
ethanol	25.30
propanol	19.43
butanol	16.52
pentanol	18.77
hexanol	13.80
ethylene glycol	15.29
glycerol	26.67
cyclohexanol	6.60
phenol	4.18
catechol	1.02
cresol	4.33
guaiacol	4.78
water‡	42.64
water	45.73

*Process condition: solvent = 50% alcohol: 50% water (pH 2.5); solvent: wood = 4:1; gas = 400 initial psig CO:H_2(1:1); and temperature:time = 250°C for 1 h.

†pH 2.0 @ 180°C.

‡pH ∿ 7.0.

mum conditions exist for maximum solubilization. In the case illustrated, i.e., 0.1% H_2SO_4 at 250°C, maximum solubilization occurs after about 0.5 h.

Not surprisingly, some solvent is incorporated into the wood. This incorporation may be considered a stabilization step which prevents depolymerized species from repolymerizing. Table 2 shows the result of our solvent incorporation study. Excessive incorporation obviously adds greatly to cost and has a negative effect on equipment size and process energy recovery. Recovery of solvent will be necessary unless we can use a solvent intended as a fuel anyway and incorporated to only a modest degree. Various types of hydrolysis have been suggested as recovery steps. "Gasohol," alcohol and wood, or coal liquefaction products are examples of possible solvents which, being themselves fuels, could be left in the product.

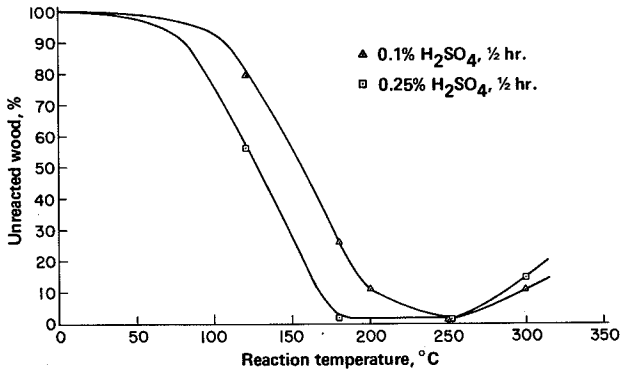

Fig. 1. Degree of solubilization by phenol as a function of reaction temperature and acid concentration. (XBL 809-1874)

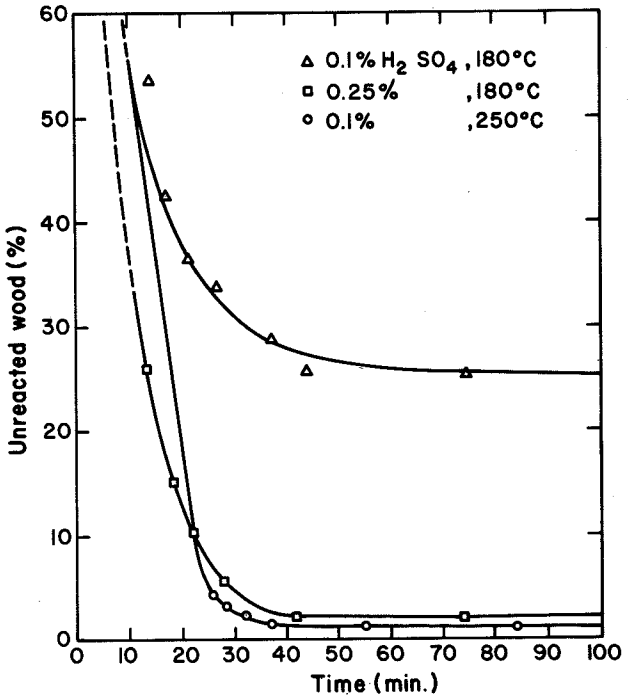

Fig. 2. Degree of solubilization by phenol as a function of time and acid concentration. (XBL 809-1859)

Table 2. Solvent incorporation study.

Solvent*	Solvent Incorporated (%) Based on Initial Solvent	Based on Initial Dry Wood	Water Produced (%) Based on Initial Dry Wood
butanol†	2.32	10.18	9.96
ethylene glycol	2.23	9.82	12.38
cyclohexanol	2.87	12.60	11.14
phenol	17.56	77.14	23.30

*Process condition: solvent:wood = 4:1; speed of stirring = 140 rpm; 0.1% H_2SO_4 @ 250°C for 0.5 h.

†0.25% H_2SO_4 @ 180°C for 1 h.

The product, after recovery of the unincorporated process solvent, is a soft bitumen-like material at room temperature. It melts and starts flowing at around 140°C. Elemental analysis of the product shows a reduction of 25 to 50% of the O_2 compared to original wood. Since almost no CO_2 is formed, this reduction must be achieved through formation of water. Table 3 depicts a comparison between our solvolytic oil and other materials.

Planned Activities for FY 1981

At present, the solvolysis must be considered primarily as a source of information for subsequent work. As part of a liquefaction process, it constitutes the front end, i.e., a method by which wood, or other biomass material may be put into a form suitable for feeding into a reactor. There the solubilized product may be further reacted--perhaps in tubular or stirred reactors in the presence of CO and H_2 as in present liquefaction processes. Other possibilities include the passage of the product as a solution across a catalyst giving reduction under relatively mild conditions.

Table 3. Comparison between solvolytic oil and other materials.

	Wood	Solvolytic "Oil"	Lignite	Subbituminous Coal -- Wyodak
N	0.13	0.15	0.93	0.92
S	0.05	0.06	0.55	1.20
Ash	0.50	0.58	16.90	14.09
H/C	1.27	0.78	0.89	0.96
O/C	0.57	0.28	0.24	0.19

We expect that the program for FY 1981 will include assessing the usefulness of the solvolysis step and gaining a better understanding of the kinetics and mechanism of this very complex reaction, or mix of reactions. Only limited experimental work required to clear up identified problems is planned until specific possibilities for using results are identified. Answers to certain questions, including those below, are very worthwhile obtaining:

- Can a recycled product-oil with a high expected phenolic hydroxyl content be used as the "solvent"? If so, solvolysis could be a viable front-end step.
- Are there specific catalytic reactions we could easily carry out in parallel or in sequence with solvolysis?
- Do alcohols simpler than butanol, cyclohex and phenol work well at supercritical pressures?

SELECTIVE HYDROGENATION OF COAL*

E. Grens, T. Vermeulen, D. Bowyer, J. Edwards, F. Hershkowitz, J. Maienschein, C. Onu, and G. Zieminski

INTRODUCTION

Coal liquefaction processes currently under development involve thermal decomposition (pyrolysis) of the coal in an organic liquid medium followed by hydrogenation of the initial pyrolysis products, often with the aid of heterogeneous catalysts. The thermal degradation reactions are not selective and do not take advantage of reactive bond types in the coal structure. They produce a wide range of products, including light hydrocarbon gases and refractory char. The former contribute to high H_2 consumption while the latter require special processing (e.g., gasification) for their utilization. The coal pyrolysis is required because reactions of coal with available solvent media are far too slow below pyrolysis temperatures, and solid catalysts can not promote the reaction of the solid coal material.

This project's aim is to convert coal to liquid products by using homogeneous catalysts that can promote selective scission of certain linkages in the coal structure below coal pyrolysis temperature. These linkages join conjugated hydroaromatic groups in the coal, and include aliphatic and O_2 (ether) bridges. The catalysts are dissolved in, or constitute, a liquid reaction medium, which has access to the extensive interior pore surfaces in the coal.

Included in this research program are studies of the interaction of organic solvent media with coals, the effects of homogeneous catalysts in promoting reactions at moderate temperatures, and the use of inorganic, Lewis-acid type melts as catalytic media for coal conversion. The action

* This work was supported by the Office of Energy Research, Basic Energy Sciences, Chemical Sciences Division of the U. S. Department of Energy under Contract No. W-7405-ENG-48.

of the catalytic treatments on model chemical compounds containing certain types of bond structures found in coal is examined to elucidate the mechanisms of coal decomposition. Transport processes for coal reaction products and dissolved H_2 gas are considered to determine the extent to which these processes may limit conversion rates. Since 1978 the major effort has been directed to the use of mixed organic-inorganic treatment media, in particular $ZnCl_2$ melts in combination with hydroaromatic solvents (e.g., tetralin) or with alcohols (e.g., methanol). This type of coal treatment was found to be much more effective than treatment with either organic or inorganic media separately, doubling or tripling conversions compared to those obtained with treatment in a single medium under the same temperature conditions.

ACCOMPLISHMENTS DURING FY 1980

The major project activities during FY 1980 included studies of the kinetics of coal/organic solvent interactions, investigation of coal conversion in both $ZnCl_2$/tetralin and $ZnCl_2$/methanol treatment media, and model compound studies to test proposed reaction mechanisms. Product analyses and characterization, with emphasis on hexane-soluble products ("oils"), were conducted to provide insight into the behavior of the conversion process.

Interaction of Coal with Organic Solvents

(by E. Grens and G. Zieminski)

Investigation of the dissolution rate of coal in hydroaromatic organic solvents was continued in a specially designed apparatus having a time resolution of about 30 s. These experiments examined the interaction of Wyodak subbituminous coal with tetralin in the temperature range of 200-300°C, and they arose from previous investigations of the action on coal of a number of organic solvents.[1] The dissolution rates observed indicate that at least two distinct classes of soluble material are involved: one dissolves almost instantaneously (if exposed at sufficiently small particle size) and is apparently associated with exinite macerals in the coal; the second dissolves much more slowly, at least partly under pore diffusion control, and exhibits an activation energy on the order of 10 kcal/gmol for the dissolution reaction. The effect of coal particle size was examined to help clarify the rate-controlling mechanism, but this effect was, to a degree, obscured by the considerable comminution of the coal particles that occurs with solvent contact. This suggests that reported solubilities of coals in given solvents, and of temperature effects on these solubilities, reflect the rate phenomena involved and the contact times chosen. At 250°C, contacts of more than 200 h may be required to approach equilibrium.

Coal Conversion in Zinc Chloride/Tetralin Mixtures

(by E. Grens, J. Edwards, and F. Hershkowitz)

Our recent investigations of coal conversion in mixed organic-inorganic media have been primarily on one two-phase system, $ZnCl_2$/tetralin, and one single-phase system, $ZnCl_2/CH_3OH$.[2] The treatments of coal in $ZnCl_2$/tetralin have so far involved essentially equal weights of subbituminous coal and organic solvent in the presence of excess $ZnCl_2$ melt. During FY 1980 these studies concentrated on the effects of treatment temperatures and on the yields and properties of the hexane-soluble fraction of the products.[3]

The yields of oils, as well as of asphaltenes (toluene solubles) and total conversion (cumulative pyridine solubles) increase significantly with increasing temperature below the initial pyrolysis temperature of the coal (325°C) as shown in Figure 1. The relatively greater increase of the oils, and corresponding decrease in preasphaltene yield (soluble in pyridine but not toluene) is important, since oils are desirable products while preasphaltenes offer severe difficulties for downstream processing. Examination of conversion rates indicates that reaction times of about 30 min are appropriate at 325°C while times up to 60 min may be required at 250-300°C. Experiments in which asphaltenes and preasphaltenes were separated from oils for continued treatment have demonstrated the effectiveness of this approach to further increase oil yields and offer the possibility of use of higher temperatures for this subsequent processing without exposing the oils, or initial coal, to undesired pyrolysis conditions.

Characterization of oil products by proton nuclear magnetic resonance (NMR) and gel-permeation chromatography (GPC), as well as elemental analysis, leads to a structure for a representation "oil molecule," with a molecular weight of about 500, composed of two linked four-ring hydroaromatic clusters. This "oil molecule" has a formula $C_{40}H_{38}$, with 37% of the H atoms and 70% of the C atoms being involved in aromatic structures. This is a less aromatic material than that produced by most liquefaction processes operating at higher temperatures.

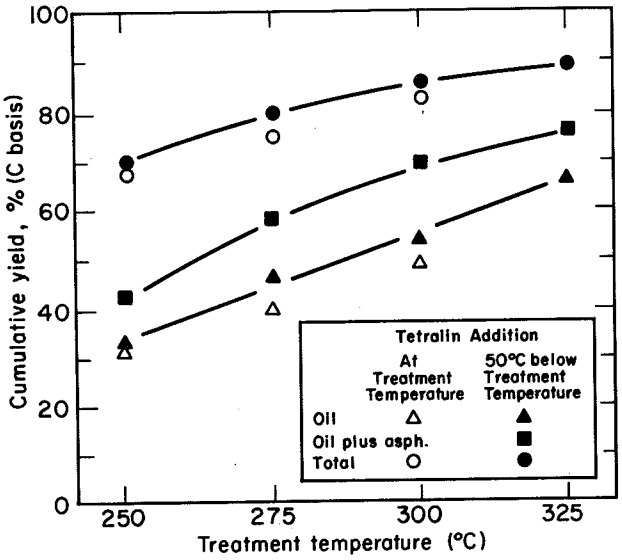

Fig. 1. Effect of treatment temperature on the conversion of coal to soluble products. Treatment of 50 g Wyodak coal for 60 min with 273 g $ZnCl_2$, 27 g H_2O, 50 g tetralin, and 3.5 MPa total pressure. (XBL 811-3584)

Coal Conversion in a Zinc Chloride/Methonal Melt

(by T. Vermeulen, C. Onu, and D. Bowyer)

When CH_3OH addition is used in $ZnCl_2$ treatment of subbituminous coal, to depress the freezing point of the melt and act with the $ZnCl_2$ so that it can be used without a recycle solvent (e.g., tetralin), relatively high conversions to solvent-soluble products are obtained. Total conversion levels approaching 90% at 250°C, 95% or better at 275°C, and nominally 100% at 300°C have been reported previously.[4]

Further experiments have been conducted to determine the effect of temperature staging on the yield of oils, which preferably would be very high. Addition of 1.5 to 3.0 wt% of metallic Zn to the melt increases the oil content of the product by 10% or more. (It is likely, also, to diminish corrosion by the $ZnCl_2$ in cases where corrosion is a problem.) Results are shown in Table 1.

The following conclusions can be drawn from the tabulated data and from earlier experiments:

1. Heating at 300°C for 30 min, alone, is not significantly better than at 275°C. However, less time (e.g., 20 min) at 300°C might also produce the same result.

2. Oils production at 325°C is clearly better than at 300°C, suggesting the onset of another kind of bond-breaking. However, total conversion is slightly reduced. The preasphaltene fraction (pyridine-soluble but toluene-insoluble) from 325°C operation began to melt at 200°C, with nearly 30% melted by 400°C; whereas the 300°C product did not show any melting below 400°C (the limit of the test). In GPC, the 325°C preasphaltene shows a lower average molecular weight, with fewer aromatic fused rings and consequent reduced ultraviolet absorption.

3. In last year's report, it was noted that a short step at 340°C diminished the oils production. It also raised the mean melting point of the oils fraction from ∿60°C to ∿90°C, indicating a deterioration in quality.

To improve the understanding of $ZnCl_2/CH_3OH$ catalysis, and to assess its potential for converting materials with intermediate levels of coalification (such as peat and lignite), the solubilization of wood, as chips or flour, and of wood-derived lignin and cellulose, has also been examined in the $ZnCl_2$-CH_3OH catalytic medium. Experiments at 250°C for 40-60 min show a carbon recovery of 79% for cellulose and 90% for both wood flour and chips. Under treatment, wood changes markedly in form and O_2 content before solubilization begins, as shown by both scanning electron microscopy and elemental

Table 1. Effect of temperature staging in treatment of 50 g Wyodak coal at 55 bars hydrogen, with 3% Zn and 14% CH_3OH (relative to 250 g $ZnCl_2$).

Run	Temp. (°C)	Time (min)	Extractibles Oil.	Asphaltene	Caf (%) Preasphaltene	Atomic H:C
51	275	30	32	15	54	0.99
77	300	30	33	17	50	1.04
72	325	30	46	14	37	1.08
73	275 300 325	15 15 30	54	10	36	1.19
82	275 300	15 30	35	18	45	1.10
81[a]	250 275 300 325	10 10 10 10	39	13	48	1.20
86[b]	250 275 300 325	10 10 10 10	41	12	47	1.25

[a] 18% CH_3OH

[b] 24% CH_3OH. Results similar to Run 78 at 14% CH_3OH (reported previously) except for 1.06 HC determined in Run 78.

analyses. Subsequently, the bulk of the wood is converted rapidly to preasphaltenes, with asphaltenes and oils being formed and additional oxygen being removed as the reaction progresses.

Model Compound Studies

(by E. Grens and T. Maienschein)

A number of pure organic compounds, chosen to contain bond types similar to those that are thought to be affected during coal conversion, have been subjected to $ZnCl_2$ catalysis under conditions similar to those used in coal treatment.[6] In these experiments a nonreactive solvent (dodecane) containing a small amount of the compound of interest was contacted with excess $ZnCl_2$ melt (with 10% water) at 175-275°C and (usually) 1.4 MPa H_2 pressure for times up to 60 min. To facilitate identification of initial reaction products, excess aromatic substrates (benzene or ethylbenzene) were often added to provide location for alkylation by carbonium ions (or radicals) formed; this prevented polymerization of the model compounds to "tars."

The two principal classes of model compounds investigated were those having aromatic groups (i.e., phenyl and naphthyl) joined by aliphatic bridges and those having aromatic groups joined by ether linkages, either directly or removed by a methylene group from the ring (e.g., benzyl). These classes are representative of aliphatic and ether linkages in coals.

At 250°C only aliphatic bridges consisting of a single methylene group are cleaved, with a rate constant of about .02 min^{-1} for diphenylmethane. Bridges of length 0, 2, or 3 are not affected. Polarization of one of the aromatic groups by addition of an OH substituent greatly increases the reaction rate; 4-hydroxydiphenylmethane has a rate constant of about 0.6 min^{-1} at 250°C. Aromatic ethers, with the exception of diphenyl ether, are cleaved quite rapidly at 250°C. Phenylbenzyl ether has a rate constant of about 1 min^{-1}, and hydroxy substitution again increases this rate.

Examination of reaction products by gas chromatography indicates that the $ZnCl_2$ promotes cleavage of aliphatic bridges preferably adjacent to the least polarized aromatic group, and that the resulting carbonium ions alkylate the available aromatic centers. With aromatic ethers the cleavage occurs between the O and any methylene groups in the bridge, with the resulting carbonium ion again alkylating an aromatic substrate.

These model-compound results are good evidence that $ZnCl_2$ catalysis of coal liquefaction can act through cleavage of both aliphatic and ether linkages in the coal. In subbituminous coals the ether links, which are expected to often involve also a two-carbon aliphatic chain, are very likely the location of much of the initial decomposition.

PLANNED ACTIVITIES FOR FY 1981

The results achieved thus far in this program have demonstrated the possibility of homogeneously-catalyzed coal liquefaction processes, operating below the pyrolysis temperature of the coal and giving high yields of "oils," with corresponding low productions of light gases, refractory char, and tar. Much additional work is still required to determine processing conditions and sequences for best yields and to develop continuous coal treatment and catalyst recovery processing techniques.

The support of this work by the Office of Basic Energy Sciences has not been extended to cover these future activities, and their accomplishment will depend on other sources of funding.

REFERENCES

1. E. A. Grens, G. P. Dorighi, and D. Lindsay, The Effects of Solvents on Sub-bituminous Coal Below its Pyrolysis Temperature, Lawrence Berkeley Laboratory report LBL-10333, 1979.

2. E. A. Grens, F. Hershkowitz, R. R. Holten, J. H. Shinn, and T. Vermeulen, Industrial and Engineering Chemistry, Process Design and Development, vol. 19, 1980, p. 396.

3. F. Hershkowitz and E. A. Grens, Low Temperature Coal Liquefaction by Zinc Chloride and Tetralin, Lawrence Berkeley Laboratory report LBL-11325, 1980.

4. C. O. Onu and T. Vermeulen, Zinc Chloride Catalysis in Coal and Biomass Liquefaction at Prepyrolysis Temperatures, Lawrence Berkeley Laboratory report LBL-11769, 1980.

5. P. J. Joyce and T. Vermeulen, Multiphase Reactor Modeling for Zinc Chloride Catalyzed Coal Liquefaction, Lawrence Berkeley Laboratory report LBL-9870, 1980.

6. J. L. Maienschein and E. A. Grens, The Effect of Zinc Chloride on Organic Solvents and Compounds Modeling Certain Bonds in Coal, Lawrence Berkeley Laboratory report LBL-11395, 1980.

PROCESSING TO ACHIEVE ENVIRONMENTAL COMPATIBILITY

COAL DESULFURIZATION*

T. Vermeulen, S. Ergun, S. Lynn, E. Petersen,
L. Clary, G. Cremer, D. Mixon, and M. Smith

INTRODUCTION

Coal is most economically used directly as boiler fuel. Its S content is converted during combustion to SO_2, which is discharged in the stack gases. Environmental constraints make it necessary to limit the S content of the effluent gas by imposing chemical treatment to remove S either from the entering coal or the exiting gases.

In previous years this problem was investigated on a broad scale, first with support from the Office of Basic Energy Sciences, and in 1979 under the auspices of the Office of Fossil Energy in the Division of Coal Mining and Preparation.

ACCOMPLISHMENTS DURING FY 1980

Coal Alkalinization Prior to Combustion

(by E. Petersen and M. Smith)

Earlier studies at LBL suggested that impregnation of sulfur-bearing coal with alkaline compounds could cause trapping of SO_x produced during combustion, thus eliminating the need for stack-gas cleaning. Experiments during the past year have involved impregnation, followed by drying and controlled combustion. Combustion at a nominal 800-1000°C gives substantially cleaner stack gas than at 1200°C. Without alkali, 25% of the total initial S (inorganic plus organic) is retained by the solid. With 15% of added Na_2CO_3 (about 1.5 times the stoichiometric requirement), 90% of total S is retained at 800-1000°C.

Such use of Na_2CO_3 would tend to be more expensive than stack-gas cleaning, and would thus be desirable only in special cases. The possibility arises that seawater or other saline brines, alone or with accessory use of CO_2 and CaO from $CaCO_3$, might be used economically to impregnate coal with $Mg(HCO_3)_2$. This prospect will be investigated further.

Oxidation of Organic Sulfur[1]

(by S. Lynn, and L. Clary)

Model-compound experiments were run in order to test their conversion under pyrite-oxidation conditions. Dibutyl sulfide reacts rapidly, and diphenyl sulfide slowly (15% per hour), under these conditions; dibenzothiophene is refracting except in the presence of VO^{2+} (which corrodes stainless steel and actively oxidizes the carbon of coal). The products were mainly sulfoxides and sulfones, with scant evidence of S-C bond breaking. Aqueous $ZnCl_2$, or $FeCl_3$ at 200°C was found ineffective for hydrolytic decomposition of sulfones, other than dibutyl sulfone.

Although pyrite-oxidation treatments do not remove organic S from coal, the results just cited suggest that S compounds in coal are somewhat altered. Exploratory extractions with liquid SO_2 at 150°C gave ambivalent results, sometimes yielding a modest reduction and sometimes an increase. The use of two or more reaction steps in series is now viewed as essential and is believed to constitute a promising approach.

Pyrite Oxidation in Coal[2]

(by T. Vermeulen, S. Ergun, S. Lynn, G. Cremer, and D. Mixon)

S removal from coal has been investigated with the use of an aqueous oxidizing medium comprising $Fe_2(SO_4)_3$, O_2, and H_2SO_4. This mixture markedly reduces water consumption and waste disposal; the by-products of coal treatment can be recovered in marketable form. About 90% conversion of pyrite, entirely to sulfate, is obtained in treatment at 130-150°C for 1 h at 30 atm O_2 pressure. Conversion is higher for more finely powdered coal (Table 1). Illinois No. 6 coal was mainly studied using four different samples; two other high-sulfur coal (three samples) showed similar behavior.

Reaction-kinetics analysis was made for both pyrite in coal and bulk FeS_2. Although the effects of O_2 and Fe^{3+} are not entirely separate, the rate depends primarily on Fe^{3+} concentration at low pressures of O_2, and becomes first-order in O_2 pressure at elevated pressures (Table 2). The rate is nearly constant as H_2SO_4 concentration increases (Table 3), decreases somewhat as ferric sulfate concentration increases, and increases somewhat with temperature (Table 4). It is possible that Fe^{+++} is more effective in a partial oxidation to elemental S and that O_2 is more effective in completing the oxidation. Although a standard reaction time of one h was selected because of initially conversion low rates, an almost equal degree of pyrite removal at the optimum temperature and pressure apparently could be obtained in 30-40 min (with less C oxidation in proportion to the residence time).

A proposed process layout is shown in Figure 1. After conventional crushing and grinding to minus

*This work was supported by the Lawrence Berkeley Laboratory's Director's Office under Contract No. W-7405-ENG-48 with the U.S. Department of Energy.

Table 1. Effect of particle size on pyrite removal (1 h, 150°C, 420 psi O_2).

Sample Number	1	2	5	7	3	4	6
Tyler screen range	-20+35		-20		-100+150		-100
Effective average mesh size	25		50		125		175
Pyrite removed (%)	--	64*	77	73	84	80	91

*Estimated.

Table 2. Effect of oxygen pressure on pyrite removal (150°C, 1 h, various treating solutions).

Mesh	-20+35			-100+150	
Psi	150	200	280	280	400
Removal (%)	21	43	56	75	83

Table 3. Effect of acid strength on pyrite removal [-100+150 mesh, 1 h, 12 wt % $Fe_2(SO_4)_3$].

Strength (wt %)	5	15	25
Sample 3 (150°C)	76%	-	84%
Sample 4 (130°C)	80%	80%	75%

Table 4. Effect of temperature on removal (420 psi O_2, 1 h).

Coal Sample	Mesh Size	Treating Solution	Temperature (°C)	Removal (%)
4*	-100+150	25/12	100	62
4*			110	67
4*			120	70
4*			130	75
4*			140	80
4*		5/12	150	76
3*		25/12	150	84
6+	-100		100	60
6+			150	91

*Illinois No. 6.

+Bevier.

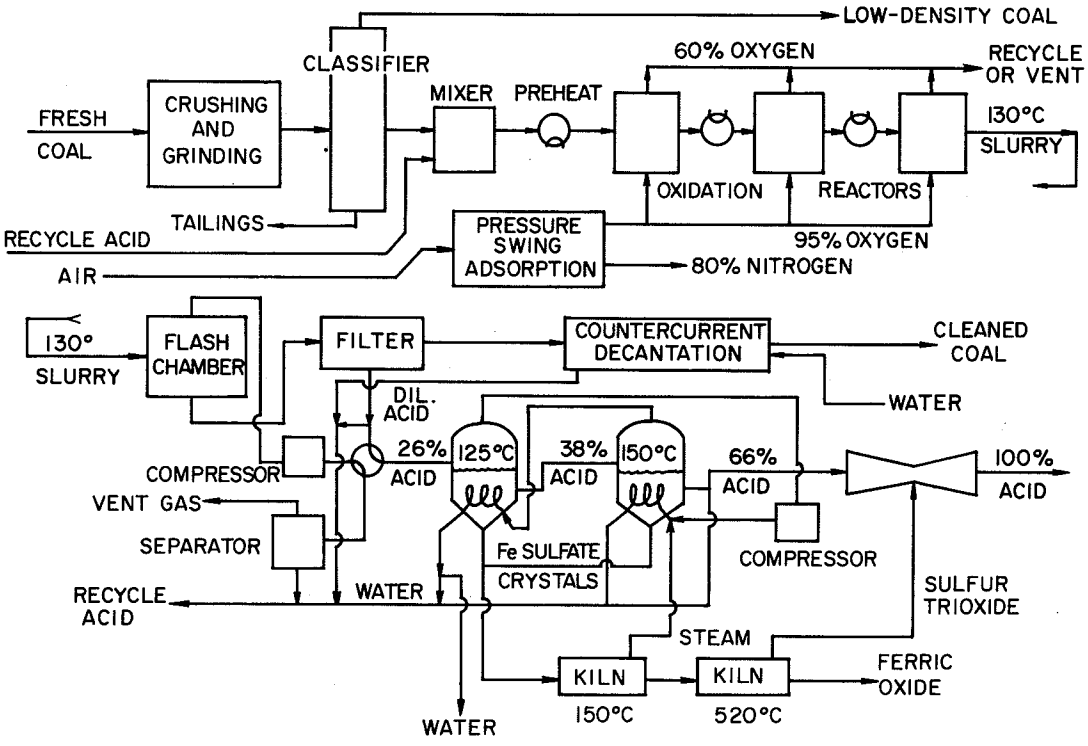

Fig. 1. Proposed flowsheet for chemical desulfurization of coal by the acidic iron sulfate process. (XBL 811-3587)

100 mesh, hydraulic classification of the sized fractions would be used to separate low-, medium-, and high-density materials. Only medium-density material would be subjected to chemical cleaning, the low-density material being adequately low in S content and the high-density material being considered unusable. The prepared feed would be blended into recycle acid in a 1:2 volume ratio, passed through a slurry pump, and fed in series to a bank of autoclaves (at 130°C and 40 atm abs). Ninety-five percent O_2 would be prepared by pressure-swing adsorption through molecular sieves. The off-gases would be withdrawn at 60% O_2. The treated slurry would then enter a flash tank where its pressure would be reduced to atmospheric, and from there it would pass to a rotary filter for removing the acid. The coal would be washed with minimum amounts of water by counter-current decantation, and the wash water would be returned to the process.

The acid fed to the reactors would contain 25% H_2SO_4 and 15% $Fe_2(SO_4)_3$, and the product acid liquor from the filters would contain about 26% and 20%, respectively. About two-thirds of this acid would be recycled directly. The other one-third would go to double-effect evaporation and crystallization, actuated by vapor compression of steam from the first effect. The acid strength leaving the first effect would be 38%, the temperature in that effect would be about 130°C, and the iron sulfate concentration would be about 22%. The second effect, at 150°C, would discharge 66% acid with 2% of iron sulfate. About 85% of this product acid would be returned to the process, diluted with condensate and with wash liquor from the decantation to restore it to feed composition.

$Fe_2(SO_4)_3$ crystallized from the evaporators would be washed, drained dry, and fed to two kilns in series. The first, at 150°C, would discharge chemically bound water, the off-gases being cooled to condense out water and then conveyed to vent-gas disposal. The second kiln, at 520°C, would discharge gaseous SO_3 and solid $Fe_2(SO_4)_3$ in marketable form. The relatively small stream of 66% acid diverted from the process after evaporation would pass first to a chilling crystallizer to lower its temperature to 50°C and reduce its $Fe_2(SO_4)_3$ content to 0.2%. It would then enter a venturi-mixer unit fed with SO_3 produced from the $Fe_2(SO_4)_3$ so as to bring the acid product to a concentration level of 96-98% H_2SO_4.

With suitable management of the water and reaction-product flows, coal nearly free of inorganic sulfur would be provided, along with H_2SO_4 and $Fe_2(SO_4)_3$ as marketable by-products.

PLANNED ACTIVITIES FOR FY 1981

These studies will be continued on a reduced scale, with special attention given to Coal Alkalinization Prior to Combustion. The entire program will be reactivated and extended if the opportunity arises.

REFERENCES

1. L. R. Clary, T. Vermeulen, and S. Lynn, Use of Ferric Sulfate - Acid Media for Desulfurization of Model Compounds of Coal, Lawrence Berkeley Laboratory report LBL-11992, 1980.

2. D. A. Mixon and T. Vermeulen, Oxydesulfurization of Coal by Acidic Iron Sulfate Solutions, Lawrence Berkeley Laboratory report LBL-9963-Revised, 1981.

KINETIC STUDIES OF REACTIONS INVOLVED IN THE INTERACTION BETWEEN SO_2 AND NO_x IN AQUEOUS SOLUTIONS*

S. G. Chang, S. Oblath, S. Gomiseck, R. Clem, and T. Novakov

INTRODUCTION

Many concurrent and consecutive reactions[1-6] can take place as a result of interaction between SO_2 and NO_x in aqueous solutions. Although the kinetics of many of these reactions have been studied, the results of previous work by other scientists showed conflicting conclusions[7-9] on some reactions, while the kinetics of some other reactions[6] have not been well characterized yet. We have investigated the kinetics of reactions between nitrite and bisulfite, and hydroxylamine and bisulfite as part of an effort to acquire a fundamental understanding of the chemical interaction between SO_2 and NO_x in aqueous solutions and to develop and investigate the potential of chemical additives for lime/limestone flue gas desulfurization (FGD) scrubbers to upgrade performance in environmental control of SO_2 and NO_x.

ACCOMPLISHMENTS DURING FY 1980

Reactions of Nitrite and Bisulfite

We studied the nitrite and bisulfite reaction over the pH range of 4.5 to 7 and found two concurrent processes for the formation of hydroxylamine disulfonate. These two processes can be expressed mathematically by the following equation.

$$-\frac{d[NO_2^-]}{dt} = k_1[H]^+ [NO]_2^- [HSO]_3^- + k_2[NO]_2^- [HSO]_3^{-2} .$$

An additional process independent of bisulfite ion concentration was proposed by Seel and Knorre[9] and by Yamamoto and Kaneda.[8]

We have recently carried out experiments to determine the presence or absence of this pathway at lower reactant concentrations by employing various buffer reagents. Nitrite concentrations (initially 0.5 to 10 mM) were monitored by visible spectrophotometry. Bisulfite ion concentration was between 5 and 40 mM. The pH was maintained by using oxalate, tartrate, or phthalate buffers with an ionic strength of 0.2M.

Results of our experiments indicated that there is no process occurring that is independent of bisulfite concentration. A process independent of bisulfite ion concentration observed by other scientists might be attributed to the employment of acetate buffer, a medium believed to catalyze the formation of NO^+ in nitrous acid/nitrite solution.

We have also performed a kinetic study of this reaction at low pH (<3) and found the formation of nitrous oxide in addition to hydroxlamine disulfonate. It appears that nitrosulfonic acid, an intermediate resulting from the reaction between nitrous acid and bisulfite, can undergo either further sulfonation to produce hydroxylamine disulfonate or hydrolysis to form sulfuric acid and nitrous oxide. The ratio of the amounts of sulfite to nitrite consumed will be two if the former reaction takes place, whereas this ratio is expected to be one if the latter reaction occurs. By determining this stoichiometric ratio as a function of pH or bisulfite concentration, we have found that the ratio of the rate constant of sulfonation to that for hydrolysis is 1.7 ± 0.5. The value of each individual rate constant cannot be determined under the experimental conditions and analytical techniques employed because the rate-controlling step is the formation of the nitrosulfonic acid.

If sulfonation of nitrosulfonic acid takes place in wet flue gas scrubbers, then at least 2 mol of SO_2 are needed to remove 1 mol of NO. However, if the hydrolysis reaction takes place, only 1 mol of SO_2 is needed.

Reactions of Hydroxylamine and Bisulfite

Hydroxylamine, one of the species produced as a result of reaction between NO_x and SO_2 in aqueous solution, can undergo further reaction[10-12]

*This work was supported by the Assistant Secretary for Fossil Energy through the Morgantown Energy Technology Center of the U.S. Department of Energy under Contract No. 80MC14002 and by the Biomedical and Environmental Research Division of the U.S. Department of Energy under Contract No. W-7405-ENG-48.

with SO_2 to form either sulfamic acid or ammonium bisulfate. We have performed kinetic studies of this reaction as a function of temperature by monitoring the concentration of total hydroxylamine with a PAR differential polarograph.

The reaction follows the rate law

$$-\frac{d[\text{total hydroxylamine}]}{dt} = k_{obs}[\text{total hydroxylamine}][\text{total sulfite}].$$

The rate of reaction was found to be independent of the ionic strength of the solution. The rate constant k_{obs} in l/mol-sec was determined at two temperatures: 7.67×10^{-3} at 35°C and 1.48×10^{-3} at 22°C. Sisler and Audrieth[10] and Fraser[12] suggested that formation of both sulfamic acid and ammonium bisulfate involves attack by the $SO_2 \cdot H_2O$ on the NH_2OH. The reaction can therefore be expressed as

$$NH_2OH + SO_2.H_2O \xrightarrow{k_a} NH_2HSO_3 + H_2O \quad . \qquad (1)$$
$$\xrightarrow{k_b} NH_4HSO_4$$

The rate law can be written as

$$-\frac{d[\text{total hydroxylamine}]}{dt} = (k_a + k_b)[NH_2OH][SO_2 \cdot H_2O] \quad . \qquad (2)$$

To evaluate the rate constant and activation energy of both reactions using our experimental measurements, Equation 1 is expressed in terms of the concentration of reaction species NH_2OH and $SO_2 \cdot H_2O$. Because [total hydroxylamine] = $[NH_2OH] + [NH_3OH^+]$ and [total sulfite] = $[SO_2^{=}.H_2O] + [HSO_3^-] + [SO_3^{=}]$, Equation 1 can be rewritten as

$$-\frac{d[\text{total hydroxylamine}]}{dt} = k_{obs}\left\{1 + \frac{[H^+]}{K_n}\right\}\left\{1 + \frac{K_1}{[H^+]} + \frac{K_1K_2}{[H^+]^2}\right\} \cdot [NH_2OH]\,[SO_2 \cdot H_2O], \qquad (3)$$

where K_n, K_1, and K_2 are respectively the acid dissociation constant for hydroxylamine and the first and second dissociation constants for sulfurous acid.

By comparing Equations 2 and 3, we obtain the following relationship:

$$k_a + k_b = k_{obs}\left\{1 + \frac{[H^+]}{K_n}\right\}\left\{1 + \frac{K_1}{[H^+]} + \frac{K_1K_2}{[H^+]^2}\right\}$$

The ratio k_a/k_b can be obtained by the corresponding ratio of the products $[NH_2HSO_3]/[NH_4HSO_4]$; this ratio was determined by Fraser[12] at several temperatures. The following values of k_a/k_b were obtained from interpolation of Fraser's results: 9 at 22°C and 19 at 35°C. By applying the transition-state theory, the enthalpy and entropy of activitation for the formation of both sulfamic acid and ammonium bisulfate can be calculated as shown in Table 1. The results of this study are in fairly good agreement with those of Fraser.

PLANNED ACTIVITIES FOR FY 1981

The kinetics of the following reactions will be investigated:

1. Production of hyponitrous acid and sulfates from the reaction of hydroxylamine monosulfonate with nitrite.
2. Reactions of ferrous and nonferrous chelates with NO to form nitrosyl metal chelate complexes.

Table 1. The enthalpy and entropy of activation for the formation of sulfamic acid and ammonium bisulfate by the reaction of NH_2OH with $SO_2 \cdot H_2O$.

	Sulfamic Acid		Ammonium Bisulfate	
	ΔH_a^+ (kcal/mol)	ΔS_a^+ (e.u.)*	ΔH_b^+ (kcal/mol)	ΔS_b^+ (e.u.)*
Fraser	10.9	-16	1	-56
This work	13.4	- 6.1	3.0	-45.8

*e.u. = entropy unit.

REFERENCES

1. W. Duecker and J. West, eds., The Manufacture of Sulfuric Acid, American Chemical Society Monograph Series No. 144, 1959.

2. F. Raschig, Schwefel und Stickstoffstudien, (Berlin, Germany: Verlag Chemie, 1924).

3. W. Latimer and J.H. Hildebrand, Reference Book of Inorganic Chemistry (New York, NY: MacMillan, 1951) p.208.

4. S.B. Oblath, S. Markowitz, and S. G. Chang, Kinetics of the Formation of Hydroxylamine Disulfonate by Reaction of Nitrite with Sulfites, Lawrence Berkeley Laboratory report LBL-10504, 1980; accepted for publication in Journal of Physical Chemistry, 1980.

5. S. G. Chang, R. Toosi, and T. Novakov, The Importance of Soot Particles and Nitrous Acid in Oxidizing SO_2 in Atmospheric Aqueous Droplets, Lawrence Berkeley Laboratory report LBL-11380, 1980; accepted for publication in Atmospheric Environment, 1980.

6. S. G. Chang, Reactions of Sulfite and Nitrite Ions in Aqueous Solutions, Lawrence Berkeley Laboratory report LBL-11800, 1980.

7. V. F. Seel and E. Degener, Zeitschrift fuer Anorganische und Allgemeine Chemie, vol. 284, 1956, p. 101.

8. S. Yamamoto and T. Kaneda, Nippon Kagaku Zasshi, vol. 80, 1959, p. 1908.

9. V. F. Seel and H. Knorre, Zeitschrift fuer Anorganische und Allgemeine Chemie, vol. 313, 1961, p. 70.

10. H. H. Sisler and L. F. Audrieth, Journal of American Chemical Society, vol. 61, 1939, p. 3389.

11. D. S. Brackman and W. C. E. Higginson, Journal of Chemical Society of London, 1953, p. 3896.

12. R. T. M. Fraser, Journal of Chemical Society of London, 1965, p. 1747.

REACTIONS OF SULFITE AND NITRITE IONS IN AQUEOUS SOLUTIONS*†

S. G. Chang and D. Littlejohn

INTRODUCTION

Lime/limestone scrubbers represent the current generation of technology for power plant flue gas desulfurization (FGD). The important chemical reactions that take place after dissolution of flue gas in an aqueous lime and limestone slurry must be identified so that a scrubber with better performance and reliability can be constructed. Because power plant flue gas contains hundreds of ppm of both SO_2 and NO_x, it is essential to understand the chemistry between SO_2 and NO_x in aqueous solutions. This scientific understanding could also aid the development of a wet simultaneous desulfurization and denitrification process based on the addition of reagents and additives to the existing lime or limestone FGD scrubbers.

We have reviewed the literature[1-5] and found that many concurrent and consecutive chemical reactions can occur as a result of the interaction between NO_x and SO_2 in liquid water. Nitrous (III) and nitric (IV) acids are produced in the aqueous phase after NO_x are absorbed into liquid water, and sulfite/bisulfite ions (IV) are formed if SO_2 dissolves in water. We have examined the kinetic studies of reactions that can take place as a result of interactions between sulfite/bisulfite and nitrite ions and calculated the concentration profile of species produced in this system as a function of reaction time.

ACCOMPLISHMENTS DURING FY 1980

Review of Previous Kinetic Studies

Nitrous acid and sulfite react to form nitrosulfonic acid, which then continues along one or more of three reaction paths:

1. Further sulfonation to produce hydroxylamine disulfonate and amine trisulfonate. These can hydrolyze to form sulfuric acid and reduced N species. The latter can undergo further reaction with bisulfite and nitrite.

2. Hydrolysis to form sulfuric acid and hyponitrous acid. The latter decomposes to produce nitrous oxide.

3. Reaction with nitrous acid to yield sulfuric acid and nitric oxide. The extent to which these three different paths will contribute to the system depends on the

*This work was supported by the Morgantown Energy Technology Center under Contract No. 80 MC 14002 through an agreement with the Assistant Secretary for Fossil Energy, U. S. Department of Energy, under Contract No. W-7405-ENG-48.

†Condensed from S. G. Chang, Reactions of Sulfite and Nitrite Ions in Aqueous Solutions, Lawrence Berkeley Laboratory report LBL-11800, 1980.

pH, temperature, and concentration of nitrite and sulfite species. A summary of reactions that can take place as a result of interaction between sulfite and nitrite ions is shown in the following reaction scheme:

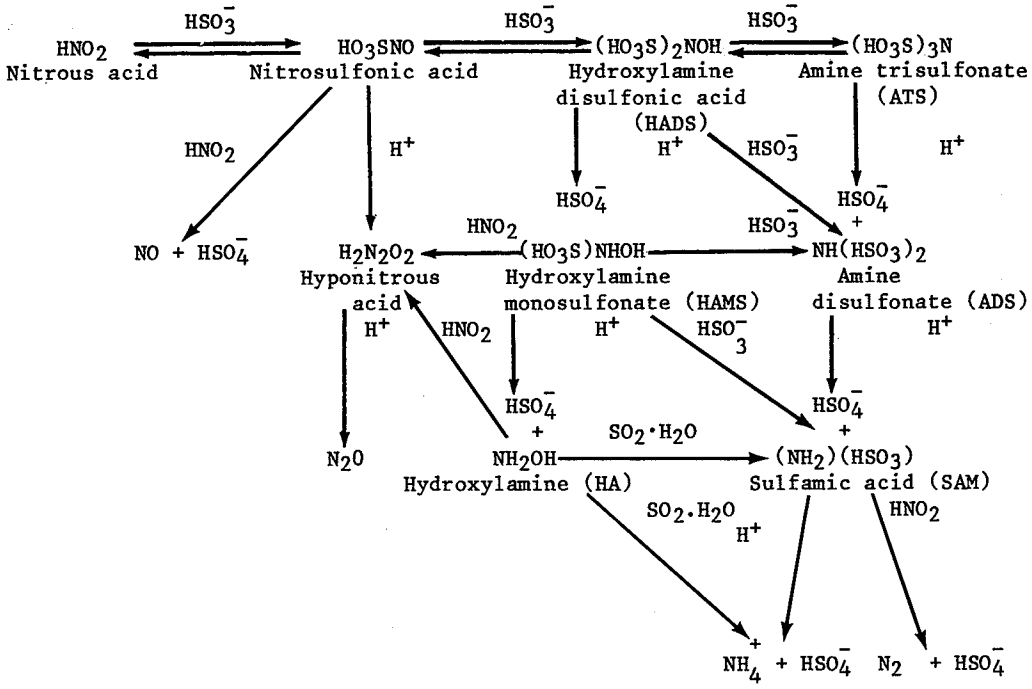

The kinetic information on the reactions involved in this system has been obtained (Table 1).

Chemical Kinetics Modeling

Table 1 lists elementary reactions considered and rate constants used. The following assumptions were made in this calculation:

1. Gas dissolution and liberation rates are much larger than chemical reaction rates.
2. Any reaction involving HNO_3, NO(aqueous [aq.]), NO_2(aq.), N_2O_3(aq.), and N_2O_4(aq.) is neglected.
3. The equilibrium is maintained all the time for the following reaction pairs: 3, 4; 10, 11; 12, 13; 14, 15; and 16, 17. The rate constants of these ten reactions were adjusted to satisfy the equilibrium condition.
4. Oxidation of NO to NO_2 (both in gas phase and aqueous solution) is discounted.
5. The pH of the solution was assumed to be constant throughout the reaction.

Figures 1-4 and 5-6 show the time-resolved concentrations of species in a batch reactor at various pH's, temperatures, and initial partial pressures of SO_2 and NO_x for the first 2 and 24 hours respectively. The gas-to-liquid ratio (G/L) is 75. Figure 1 (at P_{SO_2} = 1000, P_{NO} 450, and P_{NO_2} = 50 ppm, pH = 5, and T = 328K) demonstrated that the removal efficiency of NO is only about 10% although NO_2 can be almost completely removed because NO alone cannot be converted into HNO_2. The major product is HADS within the initial 1.5h;

Table 1. Some reduced nitrogen species identified in a few flue gas wet simultaneous desulfurization and denitrification processes.

Process	Additives	Reduced Nitrogen Species Identification
Asahi	Na_2SO_3, Fe^{+2}(EDTA*)	$NH(SO_3Na)_2$, N_2
Chisso	$(NH_4)_2SO_3$, Fe^{+2}(PCC†)	$NH(SO_3NH_4)_2$, $NH_2(SO_3NH_4)$ $(NH_4)_2SO_4$
Chiyoda	O_3	N_2O, N_2
Ishikawajima Harima	O_3	$Ca(NH_2SO_3)_2$, N_2
Mitsubishi	O_3	$Ca[NH(SO_3)_2]$, $Ca[NOH(SO_3)_2]$ NH_2OH, N_2O, N_2

*Ethylenediaminetetraacetic acid.

†Proprietary chelating compound.

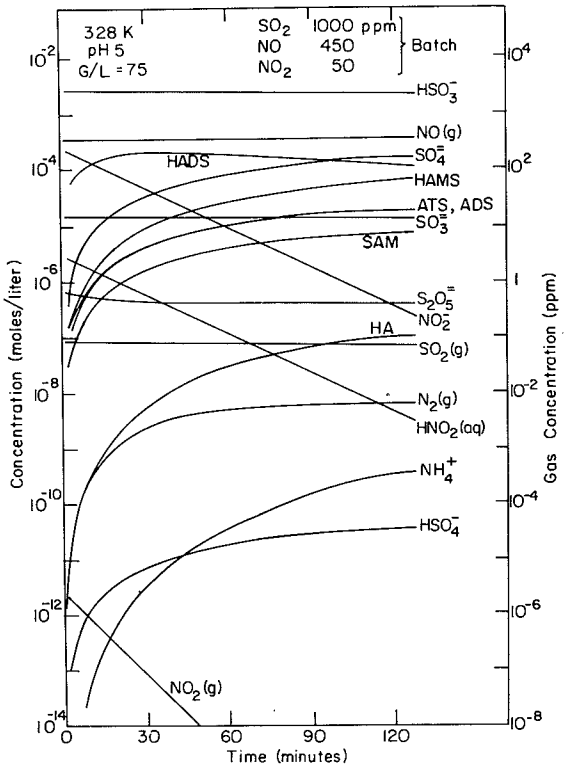

Fig. 1. The concentration profile of species as a function of reaction time in a batch reactor (ph = 5 and temp = 328K) at the following initial condition: $P_{SO_2} = 1000$, $P_{NO} = 450$, and $P_{NO_2} = 50$ ppm. The gas to liquid ratio, G/L is 75. (XBL 8011-6246)

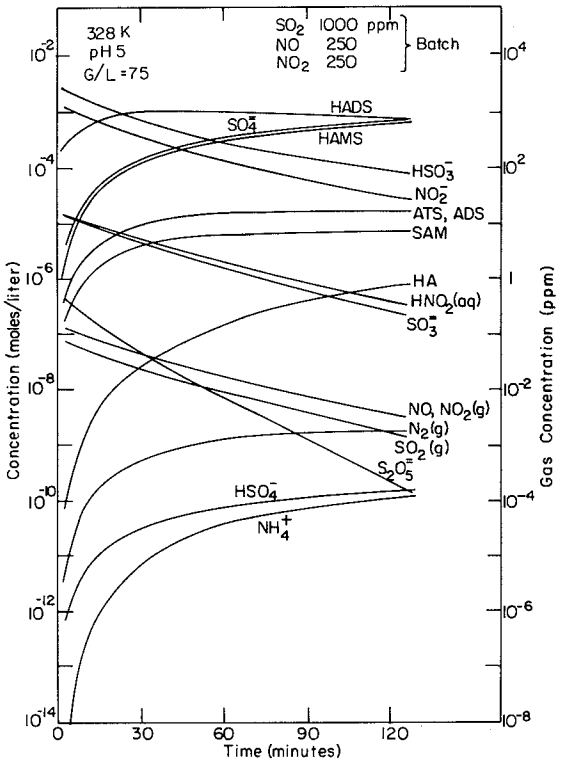

Fig. 2. The concentration profile of species as a function of reaction time in a batch reactor (pH = 5 and temp = 328K) at the following initial condition: $P_{SO_2} = 1000$, $P_{NO} = P_{NO_2} = 250$ ppm. The gas to liquid ratio, G/L is 75. (XBL 8011-6247)

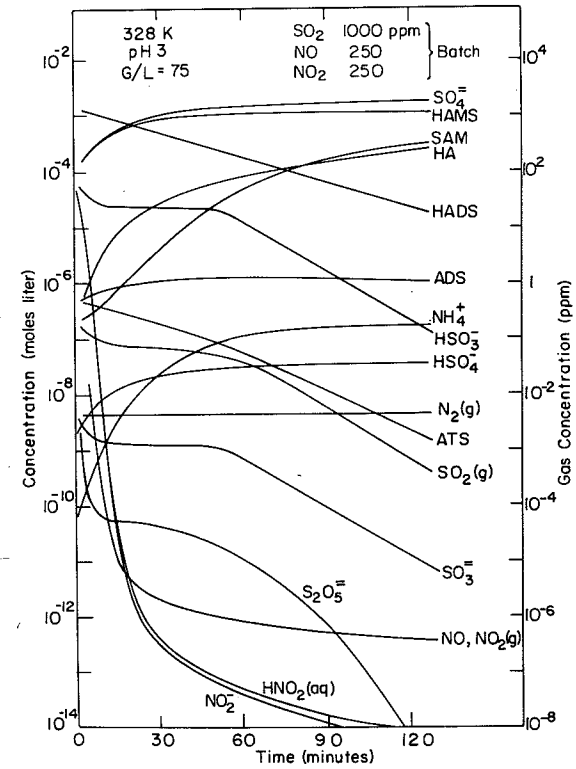

Fig. 3. The concentration profile of species as a function of reaction time in a batch reactor (pH = 3 and temp = 328K) at the following initial condition: $P_{SO_2} = 1000$, $P_{NO} = P_{NO_2} = 250$ ppm. The gas to liquid ratio, G/L is 75. (XBL 8011-6245)

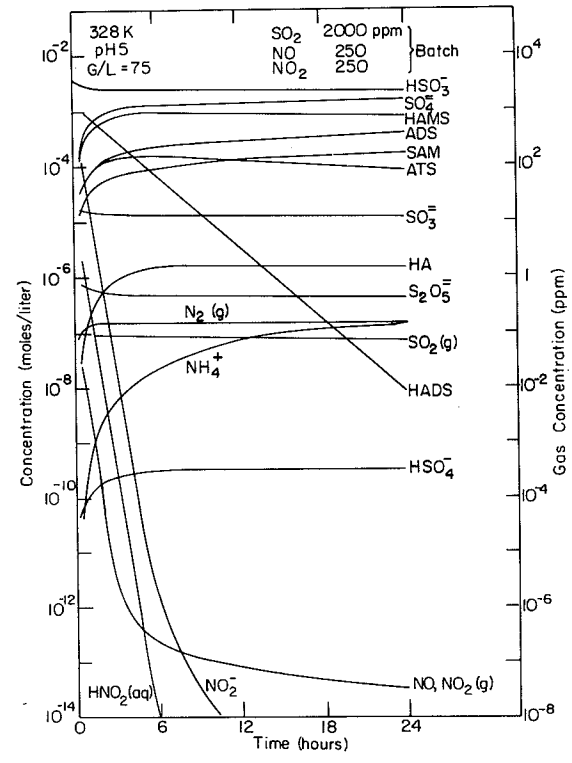

Fig. 4. The concentration profile of species as a function of reaction time in a batch reactor (pH = 5 and temp = 328K) at the following initial condition: $P_{SO_2} = 2000$, $P_{NO} = P_{NO_2} = 250$ ppm. The gas to liquid ratio, G/L is 75. (XBL 8011-6250)

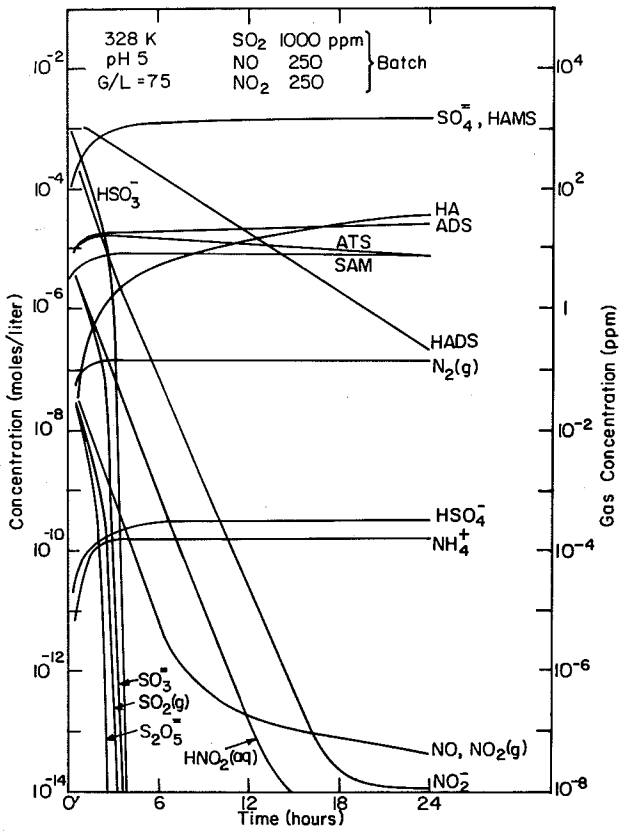

Fig. 5. The concentration profile of species as a function of reaction time in a batch reactor (pH = 5 and temp = 328K) at the following initial condition: P_{SO_2} = 1000, P_{NO} = P_{NO_2} = 250 ppm. The gas to liquid ratio, G/L is 75. (XBL 8011-6253)

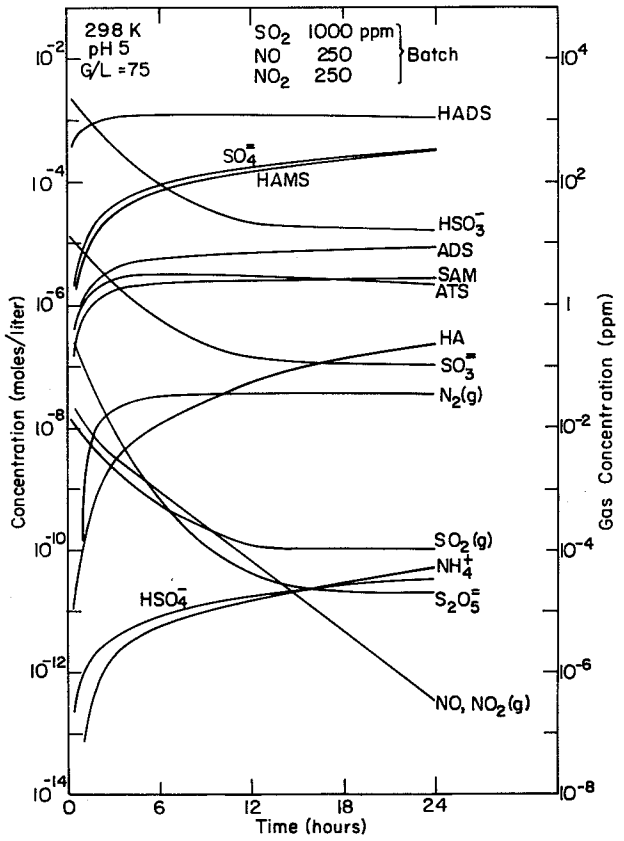

Fig. 6. The concentration profile of species as a function of reaction time in a batch reactor (pH = 5 and temp = 298K) at the following initial condition: P_{SO_2} = 1000, P_{NO} = P_{NO_2} = 250 ppm. The gas to liquid ratio, G/L is 75. (XBL 8011-6252)

the concentrations of HAMS and sulfate increase while that of HADS decreases as the reaction time continues. If the reaction is allowed to continue, the final products will be NH_4^+, N_2, and sulfate. Because we disregard the reaction of HAMS and HA with HNO_2 and the hydrolysis of nitrosulfonic acid, no N_2O is formed.

The effect of the oxidation of NO to NO_2 on the reaction is illustrated in Figure 2 (P_{SO_2} = 1000, P_{NO} = P_{NO_2} = 250 ppm, pH = 5, and T = 328K). The result indicates enormous improvement in NO_x removal efficiency. The concentration of HADS, HAMS, ATS, and other species is larger (compared to Figure 1) because of the larger concentration of nitrite/nitrous acid in the solution. By the same token, HSO_3^- is consumed at a larger rate.

The effect of the pH of the solution on the reaction is shown in Figure 3 (P_{SO_2} = 1000, P_{NO} = P_{NO_2} = 250 ppm, pH = 3, and T = 328K. The reactions are faster at a lower pH (between pH 5 and 3), and NO_x is reduced at a larger rate. The concentration of HAMS is larger than HADS after about 20 min. Similarly, larger concentrations of HA, SAM, N_2, and NH_4^+ are observed at a given time because the hydrolysis reaction is acid catalyzed, and therefore low pH conditions would favor the formation of hydrolysis products.

If the concentration of SO_2 is increased while that of NO_x is held constant, i.e., at larger SO_2/NO_x ratios as in Figure 4 (P_{SO_2} = 2000, P_{NO} = P_{NO_2} = 250 ppm, pH = 5, and T = 328K), the production rates of ATS, ADS, and SAM increase because this larger SO_2/NO_x ratio favors sulfonation reactions. It is interesting to note that the NH_4^+/N_2 ratio increases with the increase in the SO_2/NO_x ratio because the rate of formation of N_2 is only slightly affected by the change in the SO_2/NO_x ratio. (The effect due to the increase in SAM concentration is offset by that due to the decrease in HNO_2 concentration.) However, the rate of formation of NH_4^+ increases as the concentration of SAM increases at a constant pH.

The effect of temperature is demonstrated in Figure 5 (P_{SO_2} = 1000, P_{NO} = P_{NO_2} = 250 ppm, pH = 5, and T = 328K) and Figure 6 (P_{SO_2} = 1000, P_{NO} = P_{NO_2} = 250 ppm, pH = 5, and T = 298K. The results indicate that the overall reaction rate increases at higher temperatures.

Table 1 shows that some reduced N species identical to those discussed in this paper have been identified in a few flue gas wet simultaneous desulfurization and denitrification process[6] based on both oxidation-absorption-reduction and absorption-reduction principles.

Further exploration of reagent/additives to promote the absorption of relatively insoluble NO in aqueous solution and investigation of the kinetics of reactions subsequently involved in the system could permit the simultaneous removal of NO_x in lime/limestone FGD scrubbers without requiring major capital investment.

PLANNED ACTIVITIES FOR FY 1981

The formation of N_2O by the reaction of hydroxylamine monosulfonate and hydroxylamine with nitrite ion will be included in the calculation. The effect of HNO_3, NO, NO_2 and metal ions in the solution will be considered.

REFERENCES

1. W. Duecker and J. West, eds., The Manufacture of Sulfuric Acid, American Chemical Society Monograph Series No. 144, 1959.
2. F. Raschig, Schwefel und Stickstoffstudien, (Berlin, Germany: Verlag Chemie, 1924).
3. W. Latimer and J. H. Hildebrand, Reference Book of Inorganic Chemistry (New York, N.Y.: MacMillan, 1951, p. 208.
4. S. B. Oblath, S. Markowitz, and S. G. Chang, Kinetics of the Formation of Hydroxylamine Disulfonate by Reaction of Nitrite with Sulfites, Lawrence Berkeley Laboratory report LBL-10504, 1980; accepted for publication in Journal of Physical Chemistry, 1980.
5. S. G. Chang, T. Toossi, and T. Novakov, The Importance of Soot Particles and Nitrous Acid in Oxidizing SO_2 in Atmospheric Aqueous Droplets, Lawrence Berkeley Laboratory report LBL-11380, 1980; accepted for publication in Atmospheric Environment, 1980.
6. L. H. Yaverbaum, Nitrogen Oxides Control and Removal Recent Developments, (Park Ridge, N.J.: Noyes Data Corporation, 1979).

ABSORPTION OF NO BY FE^{+2}·NTA SOLUTION*

R. J. Demyanovich and S. Lynn

INTRODUCTION

As cited in the previous section, work in Japan has shown ferrous ion complexed with ethylenediaminetetraacetic acid (EDTA) to be an effective absorbent for NO. Nitrilotriacetic acid (NTA) is less expensive than EDTA and has been shown in previous work to be effective as a buffer for absorbing SO_2,[1] as a catalyst for the reaction between O_2 and ferrous ion,[2] and as a chelating agent for both Fe^{+2} and Fe^{+3}. The present work is investigating the absorption of NO and SO_2 by Fe^{+2}·NTA solutions.

The need for the presence of a chelating agent results from the finding, reported in the previous section, that NO is not readily absorbed by a sulfite or hydroxide solution unless an equimolar quantity of NO_2 is also present. Since 90% or more of the NO_x in a typical flue gas is in the form of NO, this has led some Japanese workers to advocate the introduction of ozone to promote oxidation of part of the NO to NO_2. Others have advocated the use of Fe^{+2}·EDTA to allow absorption of NO. In none of the latter cases was the fate of the NO after absorption discussed.

ACCOMPLISHMENTS DURING FY 1980

Semiquantitative experiments have shown that a solution that is 0.10 M in $FeSO_4$ and 0.11 M in NTA absorbs pure NO rapidly and quantitatively until a limit of 1 NO per Fe^{+2} is reached. Subsequent sparging of the solution with O_2 produces darkening, indicating oxidation of Fe^{+2} to Fe^{+3}, but no NO is released by the solution. The rate of absorption of NO and the relative quantity of NO absorbed are greater in the presence of NTA than in its absence.

PLANNED ACTIVITIES FOR FY 1981

The investigation of the chemistry of this system will be continued. Of particular interest are the following: the fate of the NO after absorption; the reactions, if any, between absorbed NO and SO_2 in the presence of Fe^{+2}, Fe^{+3}, and NTA; and the stability of NTA in this reactive medium in the 50°-60°C temperature range of aqueous scrubbing.

The mass-transfer characteristics of this system will be studied to determine the rate-limiting step under conditions of interest to scrubber operation.

REFERENCES

1. H. Hernandez Orozco, Oxidative Absorption of SO_2 from Simulated Flue Gas, M. S. thesis, Department of Chemical Engineering, University of California, Berkeley, 1978.
2. B. J-L. Dubs, Background Chemistry of an H_2S Absorption Process, M. S. thesis, Department of Chemical Engineering, University of California, Berkeley, 1976.

*This work was supported by the Assistant Secretary for Fossil Energy through the Morgantown Energy Technology Center of the U.S. Department of Energy under Contract No. W-7405-ENG-48.

PROCESSING OF CONDENSATE WATERS FROM COAL CONVERSION*

C. J. King, D. Mohr, J. Hill, P. Mackenzie, and J. MacGlashan

INTRODUCTION

Coal-gasification and coal-liquefaction processes produce large volumes of condensate water, formed from reactor effluents as they are cooled. This water typically contains large quantities of ammonia, neutralized by near-equivalent quantities of dissolved acidic gases (CO_2, H_2S). It also contains substantial amounts of dissolved polar organics, reflected by a high chemical oxygen demand (COD). There can also be dissolved nonvolatile salts and lower concentrations of other problem substances, such as polynuclear aromatics, N and S compounds, and cyanides. Condensate waters from other synthetic fuel processes, such as shale retorting and pyrolysis of biomass, have similar characteristics.

Conventional biological treatment (1) has given nonreproducible results for these waters, (2) is subject to upsets from high or varying feed concentrations, and (3) removes about 60 to 70% of the COD at best. Biological treatment is also a destructive process and so does not allow recovery of chemicals such as phenol in unchanged form. The purpose of this project is therefore toward developing solely physicochemical processing methods that will enable recycle of the process condensate waters as cooling-tower make-up. This leads toward process configurations which will build up large concentrations of contaminants in condensate waters before the water is processed, as opposed to the dilution of these waters which is sometimes practiced for biological treatment. A typical physicochemical processing scheme might involve solvent extraction and stripping, followed by carbon adsorption or ozonation, as necessary to provide sufficiently complete removal of problem organics.

Our work to date has focused on four different areas--analysis of individual constituents of typical condensate waters, extraction with novel solvents which will allow more complete COD removal, interpretation of rates of stripping NH_3, CO_2, and H_2S from samples of real condensate waters, and innovative combinations of extractions and stripping which can substantially decrease the energy consumption required for removal and recovery of ammonia.

Our initial results relating to extractability of phenols by different conventional solvents, the effects of pH and temperature on extractability, and means for recovering residual dissolved solvent from extraction processes are described in the FY 1979 report and in a recently prepared summary.[1]

ACCOMPLISHMENTS DURING FY 1980

Sampling and Analysis of Condensate Waters

Samples of condensate waters were obtained from the Ft. Lewis, Washington Solvent Refined Coal (SRC) liquefaction plant. These were adjusted to different pH values for different portions immediately on arrival and were stored cold in the dark. Analyses of this water and of synthetic solutions of different phenols show that the polyhydric phenols had probably largely degraded before the sample was received. The polyhydrics are subject to rapid free-radical polymerization on contact with O_2 or light, as is evidenced by darkening of the solution. The process configuration of the Ft. Lewis plant collects condensate water in an open tank. There is no simple way to obtain a sample of water that has not already been thoroughly exposed to O_2.

Samples of condensate water were then obtained from the slagging-bed gasifier plant at the Grand Forks Energy Technology Center (GFETC). This water had not been exposed to air, and was sampled and stored under N_2 and in the dark, with different portions changed to different pH values. Most of our subsequent work has been carried out with this water, which does appear to be stable over time.

A gradient-solvent high-performance liquid chromatography (HPLC) technique (methanol/water gradient with C-18 μBondapak column) has been developed to analyze different organic solutes in condensate waters both qualitatively and quantitatively. We have modified the standard COD titration procedure to remove interferences from thiosulfate and sulfide. Components reliably identified in the GFETC gasifier condensate water are shown in Table 1 and account for about two-thirds of the total measured COD. These components are largely phenol and nonalkylated and slightly alkylated mono- and polyhydric phenols. Nearly all of the remaining COD apparently is organic and much of it is composed of highly polar substances. We are pursuing identification and quantification of the components that are important contributors to the remainder of the COD. Techniques being employed are HPLC with a methanol/water gradient, a more polar column and preconcentration of portions of HPLC effluent, followed by combined gas chromatographic and mass spectrometric (GC/MS) analysis.

A striking difference between the SRC and GFETC waters concerns the dihydric phenol isomers --pyrocatechol (1,2), resorcinol (1,3), and hydroquinone (1,4). In the condensate water from the SRC process, the amount of resorcinol is large

*This work was supported by the Assistant Secretary for Environment, Office of Environmental Compliance and Overview, Division of Environmental Control Technology, U. S. Department of Energy under Contract No. W-7405-ENG-48.

Table 1. Substances identified in GFETC slagging-bed gasifier condensate water.

Compound	Concentration (ppm)
phenol	4430
cresols	2640
pyrocatechol	990
dimethyl cresols	400*
resorcinol	70
hydroquinone	20
acetophenone	15
2-naphthol	20

*Approximate.

(3,200 ppm), and equal to the concentration of phenol itself. In the GFETC gasifier water, the concentration of pyrocatechol is much larger than those of the other two isomers. Other published analyses for dihydric phenols in gasification and liquefaction condensate waters are sparse, but those few that have been published support the same strong directional difference in the isomeric distribution of the dihydric phenols between gasification condensates and liquefaction condensates.

Extraction of Condensate Waters

We have carried out extraction studies in which removals of both individual identified components and overall COD are monitored, with the aim of evaluating the effectiveness of different solvents as well as obtaining useful information on the chemical characteristics of as yet unidentified constituents.

Table 2 shows results obtained for extractions of GFETC gasifier condensate with methyl isobutyl ketone (MIBK), which was shown in our earlier work[1,2] to be much more effective than the more conventionally used diisopropyl ether (DIPE). For measurements of residual COD after extraction, the aqueous raffinate was first stripped extensively with N_2 to remove volatile, dissolved MIBK solvent. The removal of MIBK was confirmed gas-chromatographically. About 76% of the COD is removed with a single-stage extraction, including essentially all of the COD associated with those components identified in Table 1. Little additional COD is removed by a second extraction at system pH, indicating that the residual COD is associated with components that are very poorly extracted by MIBK. About 30% of the remaining COD is removed by a second extraction at low pH, indicating that the substances thus removed have characteristics of moderate to moderately strong acids.

As shown in the 1979 report and in the following section, we have found that trioctyl phosphine oxide (TOPO) is a very effective extractant for phenolics, including polyhydric phenols. It is a much stronger Lewis base than MIBK, is available commercially at about $8/lb, and is now being used extensively in the hydrometallurgical industry.

Table 2 shows results of extractions with a mixed solvent composed of 25% wet weight (w/w) TOPO in MIBK, the MIBK diluent being used to dissolve TOPO and form a solvating medium for reaction complexes. A significantly greater fraction of the COD is removed at system pH than for extraction with MIBK alone. Again, the vanishingly small additional removal in a second extraction indicates that the components giving the remaining COD are poorly extracted by TOPO/MIBK at system pH. A second extraction at low pH removed about 50% of the remaining COD, indicating again that these additional substances have moderate to moderately strong acid character, or at least are transformed at low pH into a form more attracted by the Lewis base.

Table 2 also shows results for successive extractions by MIBK and then methylene chloride (CH_2Cl_2). Since CH_2Cl_2 is a Lewis acid, the additional COD removed by extraction into it is a measure of the amount of COD with a basic character. Only a small percentage of the COD remaining after MIBK extraction appears to have this basic property, even when the pH is raised to 12.

The results shown in Table 2 are encouraging with regard to the likely ultimate success of extraction processes for bulk COD removal.

Raffinates from these extractions are being examined further by the analytical methods indicated above, as a supplemental approach for identifying the principal constituents contributing to the COD not already identified in Table 1.

Extraction of Phenol with TOPO/DIBK

In earlier work,[3,4] we observed that pyrogallol (1,2,3-trihydroxybenzene) exhibits a very high equilibrium distribution coefficient (K_D = weight fraction in solvent phase/weight fraction in aqueous phase, at equilibrium) of the order of 100 when extracted from water into a solvent mixture of 25% w/w TOPO in diisobutyl ketone (DIBK). We have carried out more extensive measurements of extraction of phenol itself from water into TOPO/DIBK.

Table 3 reports a series of measurements in which the phase ratio, and thereby the stoichiometric ratio of TOPO to phenol, was varied for a solvent of fixed initial composition. From these results it can be seen that TOPO is a very strong extractant for phenol and that the values of K_D found are at least qualitatively consistent with the Law of Mass Action.

Stripping of NH_3, CO_2, and H_2S from Condensate Waters

A batch, one-stage stripping apparatus was used to follow removals of NH_3, CO_2, and H_2S from samples of condensate water as N_2 was sparged through at ambient temperature.[5] The pH and concentrations of the three solutes in the remaining solution were monitored using a pH meter and specific-ion electrodes, respectively. Partial pressures of the solutes in the effluent gas were determined by means of an acid/base chemical-absorption train.

Table 2. COD removals by extractions of GFETC gasification condensate water.*

Conditions	% Removal of COD†	Number of Measurements Used in Finding Average
1. Extraction with methyl isobutyl ketone (MIBK)		
One extraction, without pH adjustment	76.1 ± 0.6	3
Two successive extractions, without pH adjustment	77.7 ± 0.4	2
One extraction without pH adjustment, followed by one extraction at pH < 2	83.6 ± 1.1	2
2. Extraction with 25% (w/w) trioctylphosphine oxide (TOPO) in MIBK		
One extraction, without pH adjustment	81.4 ± 0.2	3
Two successive extractions, without pH adjustment	81.4 ± 0.1	2
One extraction without pH adjustment, followed by one extraction at pH < 2	90.5 ± 0.1	3
3. Extraction with MIBK, followed by extraction with methylene chloride (CH_2Cl_2)		
Two successive extractions with MIBK, followed by one extraction with CH_2Cl_2, all without pH adjustment	79.5	1
Two successive extractions with MIBK, without pH adjustment, followed by one extraction with CH_2Cl_2 at pH = 12	80.3	1

*Equal volumes of aqueous and solvent phases used in all extractions.

†Initial COD = 30,200 ppm; raffinate stripped thoroughly for removal of residual volatile solvent.

Table 3. Extraction of phenol from water into TOPO/DIBK*

Solvent/Feed (vol./vol.)	Temperature (°C)	Mols TOPO/Mols Phenol (Stoichiometric Ratio) Total Feed	Extract	K_D
1.00	20.6	10.2	10.2	474
0.50	21.8	5.1	5.1	406
0.25	22.0	2.55	2.56	332
0.125	22.2	1.28	1.34	208
0.0625	23.8	0.64	0.78	86
0.0400	24.5	0.40	0.64	56

*Solvent composition: 25% w/w TOPO in DIBK; each result is the average of 2-3 separate measurements; feed phenol concentration = 4900 ppm w/w.

Figure 1 shows observed results for N_2 stripping of condensate water from the Ft. Lewis, Wash. SRC coal-liquefaction plant. A general result is that H_2S is removed more readily than CO_2 and NH_3. Also shown in Figure 1 are the partial pressures predicted from the prevailing solution compositions using the theoretical model of Edwards et al.,[6] which allows for activity coefficients and Henry's Law constants of the three solutes in solution, neglecting any effects from other solutes. It can be seen that the theoretical prediction matches the experimental results well up to the point where H_2S has been fully removed. Subsequently the pH drops to a lower value than predicted, and the NH_3 and CO_2 partial pressures become concomitantly lower and higher, respectively, than the predictions. Apparently additional anions were formed by an oxidation mechanism after H_2S was removed, causing the observed trends. The observed results late in the stripping process can be rationalized[5] by adding a certain constant amount of nonvolatile strong-acid anions to the model of Edwards et al.

We have made similar measurements for a sample of Omega 9 retort water from in-situ retorting of oil shale. Here the results can be rationalized by allowing for an excess of nonvolatile strong-base cations (e.g., Na^+) in the theoretical model.[5]

Combined Stripping and Extraction

Steam requirements for stripping ammonia from condensate waters tend to be very large (e.g., boil-up of 10 to 15% of the total water). This

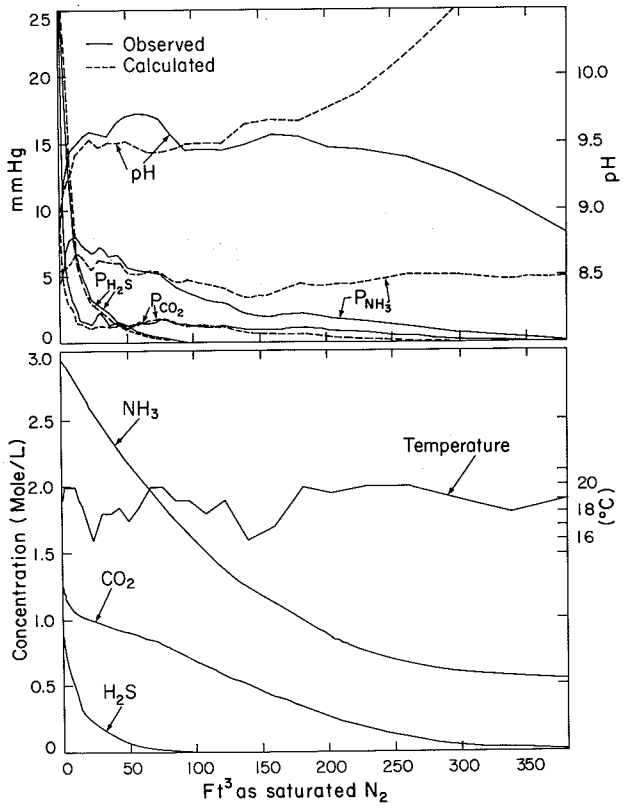

Fig. 1. Experimental results for stripping of SRC condensate water, and comparison with model of Edwards et al.[6] (XBL 806-1211)

results from the simultaneous presence of acid gases (CO_2, H_2S) in solution with the basic ammonia. The water thereby acquires a pH (typically 8.5 to 9.0) where all these species are ionized to a large extent, and the volatility of the ammonia is considerably suppressed below what it would be in the absence of the acid gases. Similarly, the volatilities of the acid gases are also considerably suppressed compared to what they would be in the absence of the ammonia. The presence of large concentrations of multiple volatile species also complicates isolation of ammonia as a salable product.

We are exploring a novel approach whereby two separation processes are combined to function simultaneously, with one serving to remove and isolate the ammonia and the other serving to remove the acid gases. This concept follows from a suggestion originally made by Cahn et al.[7] in the context of liquid-membrane processes. In our work, we are combining extraction with stripping, i.e., we are trying to achieve the goal of removing ammonia (or acid gases) by extraction while removing acid gases (or ammonia) by stripping. Removal of the one solute by extraction should increase the volatility of the other, thereby reducing the steam requirement for stripping.

As an example, for a condensate water initially containing 8,500 ppm NH_3 and 12,000 ppm CO_2, with other solutes contributing negligibly to the pH, selective extraction of 25% of the NH_3 should increase the partial pressure of CO_2 by 250%, while selective extraction of 25% of the CO_2 should increase the partial pressure of NH_3 by 60%. The percentage increases are less at lower NH_3 and CO_2 concentrations, but it is the behavior at the highest (feed) concentration that should set the steam requirement, since the pinch on an operating diagram usually occurs at the feed end of the column.[8] Thus extraction of 25% of the ammonia at the feed end could reduce stripping steam requirements to about 30% of those without extraction.

In work through FY 1980, we have explored the Lewis bases tributyl phosphate, TOPO, Alamine 336 (tertiary amine), Adogen 283 (secondary amine), and dimethylaniline as possible selective extractants for CO_2, without particularly encouraging results. We are exploring neodecanoic acid, ethylhexanoic acid, and di-2-ethylhexyl phosphoric acid (D2EHPA) as selective extractants for ammonia, and have found very encouraging results for D2EHPA. These results have so far been difficult to quantify, however, because of complications due to a washable acid impurity in the D2EHPA, which we are now removing before use of D2EHPA. This impurity would not be a complication in a practical process. We have also experienced a phase-settling problem with D2EHPA, and we are taking steps to understand and overcome this. D2EHPA is a commonly used extractant in commercial hydrometallurgical processing.

PLANNED ACTIVITIES FOR FY 1981

We are continuing investigations by HPLC and GC/MS to identify the most important remaining constituents composing the COD in condensate waters. This work will be coupled with extractions using

various chemically specific solvents in order to generate information on the chemical classes of unidentified components. We shall continue to emphasize GFETC gasifier condensate water, with additional samples of it and other condensate waters obtained as warranted.

Experimental studies are continuing with MIBK, TOPO, and other candidate solvents to monitor removal of COD as related to removals of specific chemical constituents in condensate waters. These measurements will be followed by conceptual design calculations to assess the relative attractiveness of these and other candidate solvents. In the case of TOPO, different diluents and different methods of regeneration will be considered. Other factors, such as rate of extraction and settling properties, will be evaluated and measured as needed.

Measurements are also continuing on the extraction of specific phenols (phenol, resorcinol, pyrogallol, etc.) from aqueous solution under controlled conditions using TOPO/diluent solvent mixtures. These measurements are directed toward a fuller understanding of the chemical-equilibrium factors at work, and should aid in the identification of attractive solvent compositions and operating conditions. Similar studies will be made as needed with other extractants effective for compounds found or expected to be at substantial concentrations in condensate waters.

An immediate goal in our studies related to combined stripping and extraction for removal and isolation of ammonia is quantitative understanding of the effectiveness of selective extraction of ammonia by D2EHPA with various diluents. We are also exploring ways of enhancing the settling characteristics of this system. Other potentially selective solvents for H_2S or NH_3 are being investigated. This work is guided by design concepts of how the simultaneous stripping-extraction approach could be used most effectively in practice. In this, we are open to the possibility that the extraction portion of this step could also be effective toward the goal of bulk COD reduction.

We are also investigating other general design approaches through which the energy consumption of extraction and/or stripping processes for condensate waters could be reduced.

REFERENCES

1. D. C. Greminger, G. P. Burns, S. Lynn, D. N. Hanson, and C. J. King, Solvent Extraction of Phenols from Water, Lawrence Berkeley Laboratory report LBL-10480, February 1980.

2. D. C. Greminger and C. J. King, Extraction of Phenols from Coal Conversion Process Condensate Waters, Lawrence Berkeley Laboratory report LBL-9177, June 1979.

3. C. J. King, "Removal and Recovery of Carboxylic Acids and Phenols from Dilute Aqueous Streams," Proceedings of the International Conference on Solvent Extraction, Paper No. 80-66 (Liege, Belgium: University of Liege), September 1980.

4. Energy and Environment Division Annual Report 1979, Lawrence Berkeley Laboratory report LBL-11650, October 1980.

5. J. D. Hill and C. J. King, Stripping of Process Condensates from Solid Fuel Conversion, Lawrence Berkeley Laboratory report LBL-11031, December 1980.

6. T. J. Edwards, G. Maurer, J. S. Newman, and J. M. Prausnitz, AIChE Journal vol. 24, 1978, p. 966.

7. R. P. Cahn, N. N. Li, and R. M. Minday, Environmental Science and Technology, vol. 12, 1978, p. 1051.

8. F. H. Verhoff and M. K. Choi, Sour Water Stripping of Coal Gasification Waste Water, Morgantown Energy Technology Center report METC/CR-79/23, May 1979.

APPLIED BATTERY AND ELECTROCHEMICAL RESEARCH PROGRAM*†

E. J. Cairns and F. R. McLarnon

INTRODUCTION

Lawrence Berkeley Laboratory (LBL) has lead mission responsibility for management of the Applied Battery and Electrochemical Research Program, which is supported by the Office of Advanced Conservation Technologies of the Department of Energy (DOE). This program provides the applied research base which supports all of DOE's Electrochemical Systems missions, and the general objective of the program is to help provide electrochemical systems that can satisfy economic, performance, and schedule requirements. The specific goal of the project is to identify the most promising electrochemical technologies and transfer them to industry and/or another DOE program for further development and scaling-up.

The general problem areas which the program deals with include the identification of new electrochemical couples for advanced batteries; the determination of technical feasibility of the new couples; improvements in components of batteries under development by other Electrochemical Systems projects funded by DOE; and the establishment of engineering principles applicable to batteries and electrochemical processes. Major emphasis is given to applied research which will lead to superior technical performance and lower life-cycle costs. The program is divided into three major research areas: Exploratory Battery Research and Development, Engineering-Science Research and Materials Research.

ACCOMPLISHMENTS DURING FY 1980

Both the Implementation Plan and Program Charter for the Applied Battery and Electrochemical Research Program were approved by DOE. LBL placed 25 subcontracts in FY 1980 and conducted a vigorous in-house research program.‡

The Exploratory Battery Research and Development area includes studies of new electrochemical couples or of new approaches to known battery systems. High-temperature systems under investigation include Ca/molten salt/FeS_2, Li/LiI·Al_2O_3/TiS_2, and Na/β"-Al_2O_3/SCl_3^-NaCl-$AlCl_3$. Ambient temperature systems being studied are $LiSO_2$/CZn/NaOH/$Fe(CN)_6^{\equiv}$. New electrode/electrolyte formulations for Zn/KOH/NiOOH and Li/organic electrolyte/TiS_2 cells are being investigated, and a status study of ambient temperature secondary Li batteries was conducted.

Projects grouped under Engineering-Science Research include morphological and optical studies of battery electrodes in $Pb/H_2SO_4/PbO_2$, Zn/KOH/NiOOH, and metal/air cells; and a thermal management study of the high-temperature Li/molten salt/FeS battery. Improvements in alkaline (Zn/NiOOH and Fe/NiOOH) battery performance are being sought by investigating the effect of temperature on electrode kinetics, measurements of thermodynamic efficiencies, and detailed studies of electrode restructuring phenomena.

The Materials Research effort seeks to identify, characterize, and improve the materials and components to be used in batteries and electrochemical processes. Basic investigations of new materials for battery components have led to the discovery of a novel all-solid electrode structure for possible use as negative electrodes in molten salt cells. New ternary Li-transition metal oxides have been identified as possible positive electrode reactants for use in similar systems. Projects aimed at developing improved separators for high-temperature Na/S and Li/S cells are focusing on such materials as β"-alumina, nasicon, conducting glasses, and novel superionic conductors. New polymeric separators are being studied for use in ambient-temperature Li/TiS_2 cells, and composition profiles in molten-salt electrolytes are being analyzed.

PLANNED ACTIVITIES FOR FY 1981

New projects will include studies of novel photoelectrochemical cells, new ambient-temperature Li batteries and dendritic growth in Zn/halogen cells.

---

*This work was supported by the Assistant Secretary for Conservation and Solar Energy, Office of Advanced Conservation Technologies, Division of Energy Storage Systems of the U.S. Department of Energy under Contract No. W-7405-ENG-48.

†The LBL participants in the program are: E. J. Cairns and F. R. McLarnon of the Energy and Environment Division, and L. C. DeJonghe, J. W. Evans, R. H. Muller, J. S. Newman, P. N. Ross, and C. W. Tobias of the Materials and Molecular Research Division.

‡"Development of Electrochemical Synthesis and Energy Storage" is described in both the 1980 Materials and Molecular Research Division Annual Report and elsewhere in this report (under "Battery Electrode Studies").

BATTERY ELECTRODE STUDIES*

E. J. Cairns, F. R. McLarnon, M. Katz, and J. Nichols

INTRODUCTION

This project's purpose is to study the behavior of electrodes used in secondary batteries and to investigate practical means for improving their performance and lifetime. Systems of current interest include ambient-temperature rechargeable cells with zinc electrodes (Zn/NiOOH, Zn/AgO, Zn/Cl_2, Zn/Br_2, Zn/Air, and Zn/$Fe(CN)_6^{\equiv}$) and rechargeable molten salt cells (Li-Al/FeS, Li-Al/FeS_2, Li-Si/FeS, Li-Si/FeS_2, and Na/β-Al_2O_3/NaCl-$AlCl_3$-SCl_4). The approach used in this investigation is to study the life- and performance-limiting phenomena under realistic cell operating conditions. Further background information can be found elsewhere.[1-3]

ACCOMPLISHMENTS DURING FY 1980

Investigations have focused on the zinc electrode, which exhibits satisfactory performance in rechargeable alkaline cells (Zn/NiOOH, Zn/AgO) but has an inadequate cycle life. The short lifetime and continual capacity loss of the zinc electrode are closely related to a phenomenon known as shape change,[4-6] the redistribution of active material over the electrode's face as the cell is cycled.

Computer-Control of Electrode Performance Experiments

(by M. Katz, E. Cairns, and F. McLarnon)

Cycle-life performance testing of battery electrodes requires continuous control and/or monitoring of a variety of cell parameters (electrode overpotential, cell current, cell voltage, temperature). Design of a suitable control system must take into consideration several possibly conflicting requirements: the system should be capable of continuously cycling up to 50 cells simultaneously and independently. It must be reliable, accurate, cost-effective, and flexible enough to permit a wide variety of cell charge and discharge regimes. It also must be suitable for convenient data reduction, storage, and display.

An appropriate computer-controlled test system has been designed, constructed, and partially tested. The system configuration is shown in Figure 1. The core of the system is a microcomputer (DEC LSI 11/23) with 128K of RAM and two hard memory disks (RL01), each with five megabytes of storage. The CPU is provided with a 16-bit I/O card and a four-channel D/A card. Two prototype current controllers were constructed to permit operation of eight independent cells from a single power supply.

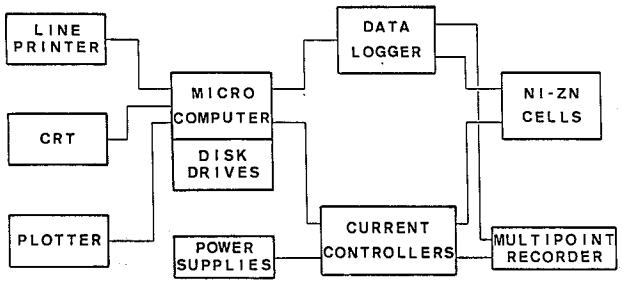

Fig. 1. Test system. Microcomputer: DEC LSI 11/23, RL01 Disk drives. Line printer: LA-120. Data logger: Fluke 2240B. (Other components are being designed and specified.) (XBL 811-7880)

Zinc Electrode Research

(by J. Nichols, E. Cairns, and F. McLarnon)

Researchers have recognized[2,4-7] that reduced solubility of zinc species in alkaline electrolyte would reduce shape change and thereby improve the lifetime of Zn/NiOOH and Zn/AgO cells. The focus of this project is to identify candidate electrolytes and characterize the effect of lowered zinc solubility on the cycle-life performance of Zn/NiOOH cells.

A tri-electrode cell (Fig. 2) was designed, constructed and tested. A 2.6 A-hr zinc electrode is sandwiched between two 1.3 A-hr NiOOH electrodes. Vacuum-table methods were employed to construct teflon-bonded zinc electrodes, and the nickel electrodes were generously supplied by battery manufacturers.[8] Analytical techniques[9] for the determination of zinc, hydroxide, and carbonate concentrations are being adapted to selected battery electrolytes.

PLANNED ACTIVITIES FOR FY 1981

The computer-controlled electrode testing system will be completely implemented, and cycle-life testing of Zn/NiOOH cells will be initiated. Work on rechargeable molten-salt cells will begin.

*This work was supported by the Assistant Secretary for Conservation and Solar Energy, Office of Advanced Conservation Technologies, Division of Energy Storage Systems of the U.S. Department of Energy under Contract No. W-7405-ENG-48.

†This project is part of a larger effort, "Electrochemical Synthesis and Energy Storage," which is reported in the Materials and Molecular Research Division 1980 Annual Report.

REFERENCES

1. Chemical Process Research and Development Program, Energy and Environment Division Annual

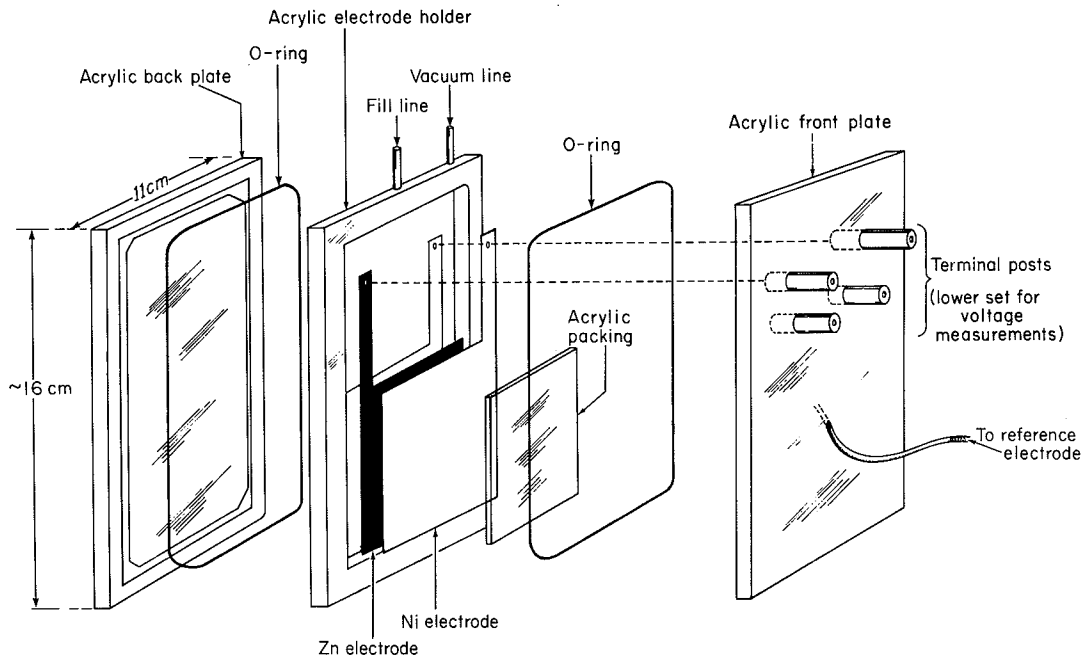

Fig. 2. Test cell. (XBL 811-31)

Report 1979, Lawrence Berkeley Laboratory Report LBL-10319, 1980, pp. 438-439.

2. J. McBreen and E. J. Cairns, "The Zinc Electrode," in H. Gerisher and C. W. Tobias (eds.), Advances in Electrochemistry and Electrochemical Engineering (New York: Wiley-Interscience, 1978), pp. 273-352.

3. E. J. Cairns, "Rechargeable Molten Salt Cells", Extended Abstract No. 641, 158th Meeting of the Electrochemical Society, Hollywood, Fla., Fall 1980 (Princeton, N.J.: Electrochemical Society, 1980).

4. J. McBreen, Journal of the Electrochemical Society, vol. 119, 1972, p. 1620.

5. K. W. Choi, D. N. Bennion, and J. Newman, Journal of the Electrochemical Society, vol. 123, 1976, p. 1616.

6. K. W. Choi, D. Hamby, D. N. Bennion, and J. Newman, Journal of the Electrochemical Society, vol. 123, 1976, p. 1628.

7. R. F. Thornton and E. J. Carlson, Journal of the Electrochemical Society, vol. 127, 1980, 1448.

8. Eagle-Picher Company and General Electric Company.

9. D. Otterson, Technical Report NASA TN D-8007 (Cleveland, Ohio: Lewis Research Center, 1975).

ENERGY EFFICIENT BUILDINGS PROGRAM

INTRODUCTION

A. Rosenfeld, C. Hollowell, and S. Berman

About 38% of United States energy resources is consumed by the building sector. In contrast, the energy consumed as gasoline represents only 18% of our energy use. With the scarcity of fuel and the attendant rise in fuel prices, it has been necessary to make radical design changes in automobiles and buildings to enhance their efficiency, at the lowest possible cost, without compromising their previous level of service. For automobiles, Congress mandated a factor-of-two improvement in efficiency and, for buildings, research has shown that present resource energy use can be similarly reduced by 50% through careful retrofitting. In the case of new construction, houses and commercial buildings are already being designed to use only half the energy of their pre-1975 counterparts, but our research findings suggest that to minimize life-cycle cost, we should--and can--further reduce this figure to 10% in the case of residences, and to 20% in the case of commercial buildings.

The aim of the Energy Efficient Buildings Program is to conduct theoretical and experimental research on various aspects of building technology that will permit such gains in energy efficiency without decreasing occupants' comfort or adversely affecting indoor air quality. To accomplish this goal, we have developed five major research groups whose activities are regularly reported in technical and scientific journals, presented at international conferences, and disseminated in the form of Lawrence Berkeley Laboratory (LBL) reports.

A brief overview of the scope and objectives of each group follows.

Energy Performance of Buildings

Formerly called the "Building Envelopes Program," this group has changed its name to "Energy Performance of Buildings" to more accurately reflect the focus of its work. Essentially, the energy performance of a building is assessed by regarding the building as a system. In this framework, the parameters tested are its air infiltration rates, thermal characteristics of its structural elements, and the behavior of the interface between dissimilar materials. From an analysis of overall performance, we are able to recommend cost-effective solutions for reducing infiltration and thermal losses, either by retrofitting (existing buildings) or improving design features (new construction). This research is conducted in the laboratory and in the field, and tests are made on our research house as well as with computer models.

Building Ventilation and Indoor Air Quality

One of the more obvious means of improving the energy efficiency of a building is to reduce air infiltration/ventilation. Lowering this air-exchange rate, however, can seal in indoor-generated pollutants and allow them to build up to potentially harmful levels. In this program, our goal is to furnish a scientific basis for setting energy-efficient ventilation standards and developing system designs that promote energy efficiency while taking into account the comfort, health, and safety of building occupants. Project activities in support of this goal include (1) development of new methodologies for measuring indoor air quality parameters, (2) laboratory studies of organic and radioactive emissions from building materials, soil, water, and natural gas that may affect indoor air quality and (3) field monitoring of indoor air quality in different types of buildings (e.g., schools, office buildings, residences) under a variety of ventilation conditions. Integrally related to this work is the investigation of prevention and control strategies for indoor air pollution that do not sacrifice energy efficiency. In this connection, we perform laboratory and field tests of various ventilation systems, including those that incorporate air-to-air heat exchangers--devices which can provide the necessary level of ventilation while recovering a substantial portion of the energy that would normally be lost.

Building Energy Analysis Group

The Building Energy Analysis group is responsible for developing, improving, and documenting the computer program, DOE-2, which has been designated as the national program for calculating building energy performance standards. DOE-2 can also be used by architects and engineers as a means of designing buildings to improve their energy efficiency and minimize their life-cycle costs. DOE-2 is systematically updated to incorporate the latest energy-conserving design features (e.g., passive and active solar, thermal storage, natural ventilation, daylighting, and evaporative cooling).

Energy Efficient Windows and Lighting

The Windows and Lighting group is developing a technical basis for understanding the energy-related performance characteristics of windows and lighting systems and, with industry, is working to develop and promote energy-efficient products that are cost-effective to end-users. A primary consideration in the Windows section of our group is to assure that daylight is provided to the building's interior with minimum thermal loss in cool weather and minimum thermal gain in hot weather. To this end, considerable research activity has centered on developing and testing optical coatings for windows as well as evaluating a number of insulating window treatments. Our testing capabilities are being expanded with the addition of an outdoor window testing facility.

The Lighting section is concentrating on developing energy-efficient lighting systems (lamps, ballasts, fixtures, and controls) to provide lighting designers with an array of options for meeting occupant needs. Energy-efficient,

high-frequency, solid-state ballasts for fluorescent lights are being field-tested in several buildings. Preliminary results are confirming that installation of these devices can effect a 25% savings over conventional core ballasts.

Building Energy Data, Analysis and Demonstration

The Building Energy Data, Analysis, and Demonstration group compiles and evaluates data on end-uses of energy and on the costs and performance of energy-efficient technical measures, both from direct field measurements and from secondary sources. Using these data, we prepare estimates of "least-cost technical potentials" for improving energy efficiency in new and existing homes and commercial buildings--often as a cooperative effort with utilities or state agencies. Individual conservation (or solar) measures can be catalogued in order of increasing unit-cost-of-conserved-energy ($/MBtu or ¢/kWh) with careful attention paid to the interactions among conservation and solar measures that affect certain end-uses (notably heating, cooling, and water heating). Using this technique, we create, in effect, a "supply curve of conserved energy," comparable to the supply curves for other market commodities that show the expected levels of production as a function of unit price. The national energy savings that might be effected as a result of our research is discussed in detail in the BEDAD section of the text that follows.

More Energy-Efficient Buildings Research Reported in Other Chapters

Other closely related research on energy efficient buildings and appliances is carried on in other programs within the Energy and Environment Division, and is reported in other chapters of this division's Annual Report.

Specifically, the Energy Analysis chapter, printed separately as LBL-11972, covers 11 studies related to building energy performance standards and labels, appliance energy performance, rating systems for auditors and appraisers, and energy and peak power modeling.

Further, the Solar chapter, LBL-11984 covers the work of the Passive Solar Analysis and Design group.

ENERGY PERFORMANCE OF BUILDINGS*

D. Grimsrud, A. Blomsterberg, W. Carroll, P. Condon, D. Dickerhoff, D. Krinkel, M. Modera, A. Rosenfeld, M. Sherman, B. Smith, and R. Sonderegger

INTRODUCTION

The design of an energy-efficient building begins with a tightly built and well-insulated thermal envelope (exterior walls, windows, etc.) and then adds efficient equipment for heating, cooling, hot water, and other energy needs. Formerly called the Building Envelopes Program when our activities focussed on investigations of air infiltration and wall thermal performance, we have now expanded our activity to encompass a broader range of building energy concerns--ergo, our new designation as "Energy Performance of Buildings." Our objective is to provide fundamental information on the energy performance of buildings as a basis for the eventual establishment of energy-conserving guidelines and standards governing the design and construction of new buildings as well as retrofit strategies for existing buildings. Our two primary research areas of air infiltration and wall thermal performance are conducted in the field, in the laboratory, in our research house, and on computer models. A third effort this year has been the development of an instrumented residential energy audit, which will be field-validated in FY 1981.

* This program was supported by the Assistant Secretary for Conservation and Solar Energy, Office of Buildings and Community Systems, Buildings Division of the U.S. Department of Energy under Contract No. W-7405-ENG-48.

Air Infiltration

Air infiltration typically accounts for one-third of the annual space heating load of residential buildings in the United States. This energy loss can be reduced in new construction by changes in design and construction techniques, and to some degree in existing structures, by careful repair and maintenance. An important goal of our work in this area, which deals with measuring, modeling, and reducing air infiltration, is to provide design guidelines for architects and engineers, and to develop construction quality standards for air leakage in U.S. buildings. A breakthrough this year was the development of a new model that identifies a single parameter--the "effective leakage area" obtained from fan pressurization--for scaling infiltration rates in different types of buildings. This parameter is a powerful design tool for architects and builders in reducing air infiltration in new construction. In addition, we are demonstrating techniques to reduce air leakage in existing buildings.

Walls

The information currently available on the thermal performance characteristics of building walls is based on theoretical analysis and laboratory tests. Where actual measurements have been made in buildings, the thermal resistance of the walls is often 20% to 30% less than that predicted

by laboratory measurements and standard calculations. Ultimately, recommendations for energy conservation standards should be based on accurate measurements of building walls rather than on unverified inferences from laboratory measurements and computer models. Even though a wall may be well designed, differences in construction methods and aging of materials can produce substantial variations in thermal performance. Accordingly, the purpose of our research is to develop techniques for field (or in situ) measurements of the thermal performance of walls. We need to understand what data must be collected to adequately characterize a wall, and how this data can be reduced to uniquely describe the thermal performance of any wall.

Computerized Instrumented Residential Audit (CIRA)

In 1978 Congress passed the National Energy Conservation Policy Act, a part of which, the Residential Conservation Service, required major public utility companies and fuel-oil dealers to provide a house energy audit to customers who request it. States have two options in complying: either they submit a plan for DOE approval, or DOE will mandate its own audit (developed by Oak Ridge National Laboratory (ORNL) and Solar Energy Research Institute (SERI)). In accordance with RCS regulation, this audit is site- and house-specific, considers both conservation and solar measures in its recommendations, and will give the homeowner a cost-benefit analysis of its recommendations.

In addition to the basic ORNL/SERI audit, DOE commissioned LBL to develop a more sophisticated, state-of-the-art residential audit. This audit, the Computerized Instrumented Residential Audit (CIRA) uses a portable microcomputer for evaluating retrofits based on information collected during the audit. In addition, several simple retrofits are completed at the time of the audit, with an expected initial energy savings of 10-15%.

The instrumented audit requires an initial screening of utility bills and weather data to obtain an "energy signature" for the house. Two auditors then make a four-hour visit to the house where they measure air leakage with a blower door that pressurizes or depressurizes the house, and identify leaks, plugging the easy ones as they go and noting the more difficult ones to repair later. They measure furnace efficiency, check water and air temperature settings, insulate the water heater, change the air filter on the furnace, calibrate the thermostat and, with the permission of the homeowner, install a low-flow showerhead and reset the water-heater thermostat.

At the conclusion of the physical inspection, all necessary data are fed to the microcomputer. The auditor then confers with the homeowner on a suitable retrofit package. The computer will scan a master list of possible retrofits stored on a disc that contains conservation measures such as insulation, storm and double-pane windows, insulating shutters, caulking and weatherstripping, furnace retrofits, and active and passive solar systems for space and water heating. Savings and costs of each retrofit are then calculated on a life-cycle basis, and an economically optimal retrofit package is assembled on a minimal total life-cycle cost. The computer will give optimized retrofit packages for several budgets, along with total costs and savings of each package. All cost estimates take into account the possibility that homeowners may wish to do the retrofits themselves. At the conclusion of the visit, the auditor leaves detailed information on the suggested retrofits with the homeowner.[1]

ACCOMPLISHMENTS DURING FY 1980

Air Infiltration

MITU: For model validation work, we have been taking measurements in occupied houses over a relatively long period of time. Because these procedures necessarily inconvenience occupants, we sought and found a solution in the MITU--a mobile infiltration test unit that simulates a house and can be moved to different locations to study the effect of different micro-climates on air infiltration rates (see Figures 1 and 2). The test unit was designed and built to simultaneously monitor air infiltration, surface pressures, and weather data for extended periods of time. By moving the MITU to different locations, we can study the effect of the leakage area and its distribution, and local terrain and shielding on infiltration rates. The data from MITU will be used to test a predictive model of air infiltration discussed below. A complete description of the MITU facility including preliminary results is available.[2]

Data Base: The Infiltration Data Base was developed to provide support for the Air Infiltration Centre, an organization sponsored by the International Energy Agency (IEA). The data base is set up to help researchers perform literature searches and to test predictive models of infiltration. Its four subfiles contain information on infiltration researchers, published articles, test locations, and numerical infiltration data from field measurements. The data base user's manual is a complete tutorial on accessing and using the file.[3]

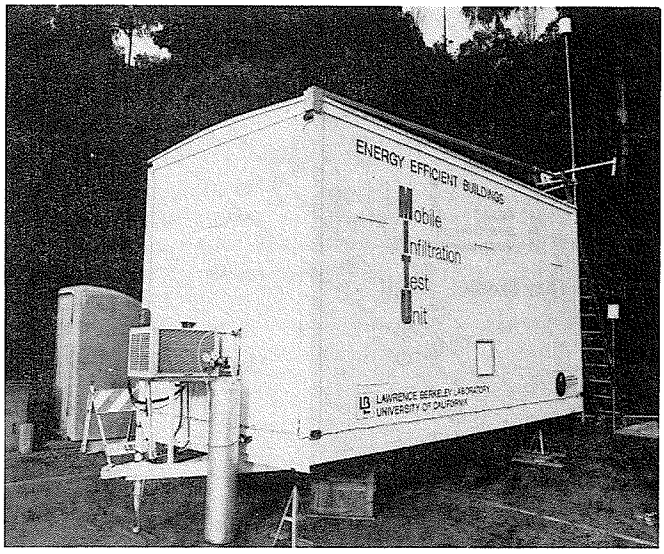

Fig. 1. The Mobile Infiltration Test Unit (MITU). (CBB 8011-13932)

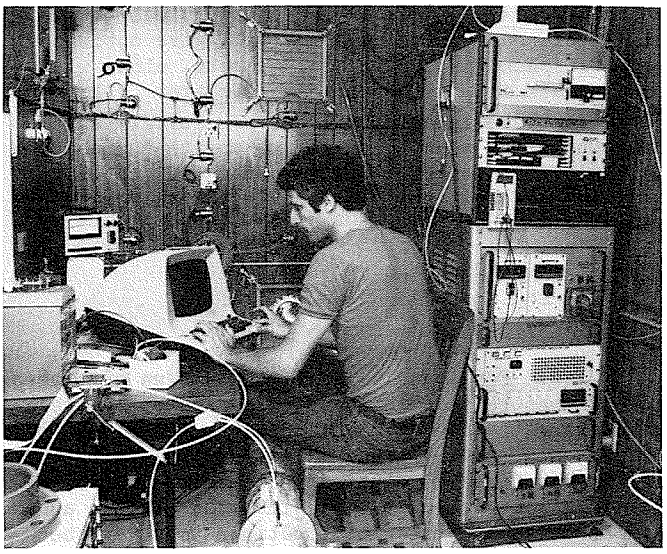

Fig. 2. The MITU interior. (CBB 809-11263)

Models: Unlike conduction losses which can be modeled by means of a single parameter--thermal resistance--infiltration losses have had no equivalent quantity. We have developed a model that uses the effective leakage area for characterizing infiltration losses. Equivalent leakage area is determined from a fan pressurization test of the structure. In addition to this parameter, the model uses the height of the structure, the inside-outside temperature difference, the terrain class, the shielding class, and wind speed to determine infiltration rates. The model can predict the impact of retrofits or other changes in the building envelope on air infiltration using measurable performance changes effected in a few parameters. Figure 3 shows the correlation between predicted and measured infiltration in fifteen houses.[4,5]

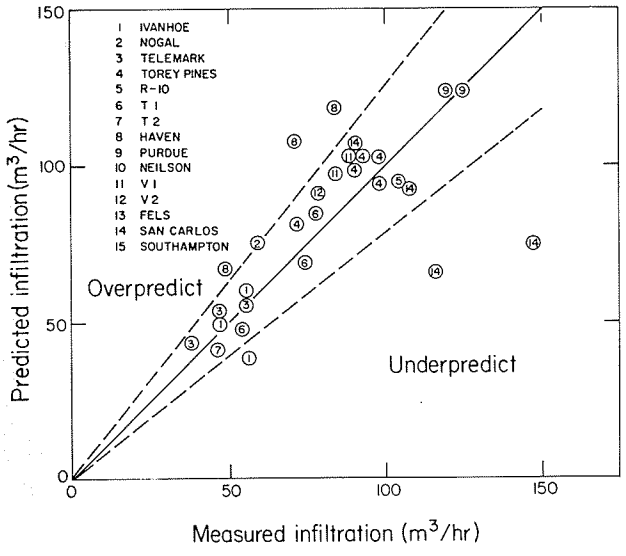

Fig. 3. Predicted vs Measured Infiltration. (XBL 805-907)

AC Pressurization: A technique for examining the low-pressure leakage function of a residence using an oscillating pressure source was developed and tested. The advantage of this method is that it simulates the low-pressure range where natural infiltration occurs, and is independent of weather interactions. We found that even at the low-pressures characteristic of natural infiltration the leakage structure of the house showed flow behavior typical of an inviscid fluid.[6]

Average Infiltration Monitor: The Average Infiltration Monitor (AIM), a portable device capable of taking long-term average infiltration measurements, was designed and prototypes were tested. Essentially a suitcase crammed with sample pumps and injectors that operate unattended over a month-long period, AIM will be used in occupied houses and enable us to monitor long-term average infiltration including the effects of occupant behavior, such as opening windows and doors.[7]

Field Studies: A major part of the program this year has been our work with several state utilities and local builders in setting up air leakage measurements in houses. Houses in Washington and New York state were pressurized for air leakage measurements and later retrofitted to reduce the air leakage. In the Washington houses where the initial retrofits were performed by the Bonneville Power Authority, adding storm windows and doors alone resulted in a 15% reduction in air infiltration. The houses in Rochester, New York were standard tract homes where the builder, Ryan Homes, had added features for greater energy efficiency. Air leakage measurements were also taken in eight houses in Atlanta, Georgia to assess the effect of infiltration on the air conditioning load in a hot-humid climate.[8,9]

Collaborative Activities: Our group was active this year in contributing infiltration-related work to national projects. For the Residential Conservation Service (RCS) Model Audit, we developed a simplified infiltration algorithm, and for the ASHRAE Handbook of Fundamentals, we submitted a revised chapter on infiltration which is to be incorporated in the next edition of the text.

Construction Quality Standard: A preliminary draft of a framework for a construction quality standard for air leakage in residential buildings was prepared and circulated to professional groups for discussion and review.[10] The draft proposes using the newly developed infiltration model to develop a verifiable standard for ventilation in new buildings. Included in the report is a survey of the average infiltration during the heating season of 219 houses throughout North America. The infiltration of these houses averages 0.67 ach with a standard deviation of 0.48 ach.

Walls

The key element in our walls testing project is the Envelope Thermal Test Unit (ETTU).[11,12] Designed to measure the steady-state and dynamic thermal response of building walls, the prototype ETTU and the new passive ETTU-2 are capable of taking field measurements. The work this year has

centered around building and debugging these units. The computer program to drive the system heaters and log the data has been written. The data acquisition system that interfaces with the general-purpose microprocessor system has also been completed.[13] Preliminary measurements of steady-state R-values of a test sample using ETTU agreed with ASHRAE Handbook values.

Through working on the ASTM C16-30 (Task Group on Characterization of Wall Performance), plans were made with the Portland Cement Association for conducting runs comparing the performance of ETTU with their guarded hot-box.

Computerized Instrumented Residential Audit (CIRA)

Five essential tasks have been detailed in developing our energy audit:

- software development,
- system documentation,
- auditor's resource package,
- homeowner's information package,
- audit validation.

Earlier this year we assembled and tested field instrumentation and built the prototype microprocessor system for the audit. Software development has consisted of the microprocessor-based algorithms that optimize the mix of conservation, solar, and wind options for a given house. These algorithms include recent advances in building science from other national laboratories, e.g., LASL passive solar methodology, F-chart active solar methodology, BNL boiler and furnace performance data, LBL infiltration modeling, etc.

Fireplace Testing

While no new testing of fireplaces took place in FY'80, data analysis, including economic considerations, was undertaken. Both a technical report on the measurements and analysis and a report for homeowners were published.[14,15]

PLANNED ACTIVITIES FOR FY 1981

Air Infiltration

Continued development and validation of measurement techniques and infiltration modeling will be a major part of the program in the coming year. Both AIM and MITU are scheduled for field measurements around the country. The infiltration model will be extended to include the effects of flues and chimneys, local shielding, and occupant ventilation. The model will be coded for use in the DOE-2 residential package.

Several tasks are planned for developing air leakage design guidelines for architects and engineers. Among these is an examination of the effectiveness and cost-benefits of air leakage retrofits. A popular description of the infiltration model, together with tables of normalized air infiltration values for different regions of the U.S. and component leakage areas are part of the package for designers.

A new undertaking will be to extend the AC pressurization technique to multichamber buildings without using large-capacity fans. We plan to begin measurements with a multi-chamber infiltration system in an apartment complex.

Walls

Four main activities are planned for the coming year:

- Initial field measurements of walls in our research house using ETTU;
- Field survey of thermal performance of typical residential wall construction;
- Activity in ASTM C-16.30 task group on in-situ measurement of wall performance;
- Collaboration with Portland Cement Association in completing development of data reduction techniques for laboratory hot-boxes.

The ETTU work will significantly advance our capabilities for measuring wall performance. Through our contacts with ASTM C-16.30 and the Portland Cement Association, our work will have immediate application to ongoing wall testing programs at the Cold Regions Laboratory of the U.S. Army, Owens-Corning Fiberglas Corp., DCS Corp., the University of New Mexico, and Oak Ridge National Laboratory.

CIRA

Tasks in the coming year involve completing the software development, writing the program documentation, preparing a resource package for both the auditor and the homeowner and, finally, validating the entire audit. Validation will consist of actual field testing and comparisons of projected energy savings with DOE 2.1 computer simulations.

REFERENCES

1. R. C. Sonderegger, D. T. Grimsrud, "Energy Audits of Existing Residential Buildings In-Situ with a Microprocessor," Proceedings of the International Congress on Building Energy Management, Portugal, May 1980.
2. M. P. Modera et al., The Mobile Infiltration Test Unit--Its Design and Capabilities: Preliminary Experimental Results, Lawrence Berkeley Laboratory report LBL-10706 (to be published in 1981).
3. D. T Grimsrud et al., The LBL Infiltration Data Base: A User's Manual, Lawrence Berkeley Laboratory report LBL-10778 (to be published in 1981).
4. M. H. Sherman, D. T. Grimsrud, "Infiltration-Pressurization Correlation: Simplified Physical Modeling," ASHRAE Trans., vol. 86 no. II, 1980, pp. 778-807; Lawrence Berkeley Laboratory report LBL-10163, March 1980.
5. M. H. Sherman, D. T. Grimsrud, The Measurement of Infiltration using Fan Pressurization and Weather Data, Lawrence Berkeley Laboratory

report LBL-10852 (to be published in Proceedings of the First International Air Infiltration Centre Conference, London, 1980).

6. M. H. Sherman, D. T. Grimsrud, R. C. Sonderegger, The Low Pressure Leakage Function of a Building, Lawrence Berkeley Laboratory report LBL-9162, November 1979 (to be published in Proceedings of ASHRAE-DOE Conf. on Thermal Performance of Exterior Envelopes of Buildings, Orlando, Fla., 1979).

7. M. H. Sherman, D. T. Grimsrud, P. E. Condon, and B. V. Smith, Air Infiltration Measurement Techniques, Lawrence Berkeley Laboratory report LBL-10705, April 1980 (to be published in Proceedings of the First International Energy Agency Symposium of the Air Infiltration Centre, Windsor, England, 1980).

8. D. L. Krinkel, D. J. Dickerhoff, J. J. Casey, and D. T. Grimsrud, Pressurization Test Results: BPA Energy Conservation Study, Lawrence Berkeley Laboratory report LBL-10996, December, 1980.

9. D. J. Dickerhoff, D. T. Grimsrud, B. B. Shohl, Infiltration and Air Conditioning: A Case Study, Lawrence Berkeley Laboratory report LBL-11674, February, 1981.

10. D. T. Grimsrud et al., A Framework for a Construction Quality Standard for Air Leakage in Residential Buildings, Lawrence Berkeley Laboratory report LBL-9416 (to be published in 1981).

11. P. E. Condon, W. L. Carroll, Measurement and Analysis of in situ Dynamic Thermal Performance of Building Envelopes using Heat Flow Meter Arrays, Lawrence Berkeley Laboratory report LBL-9821, June 1980 (to be published in Proceedings of ASHRAE-DOE Conf. on Thermal Performance of Exterior Envelopes of Buildings, Orlando, Fla., 1979).

12. P. E. Condon, W. L. Carroll, R. C. Sonderegger, A New Measurement Strategy for in situ Testing of Wall Thermal Performance, Lawrence Berkeley Laboratory report LBL-8822, June 1980 (to be published in Proceedings of ASHRAE-DOE Conf. on Thermal Performance of Exterior Envelopes of Buildings, Orlando, Fla., 1979).

13. B. V. Smith, P. E. Condon, The LBL-EPB Data Acquisition System: Its Description and Construction, Lawrence Berkeley Laboratory report LBL-11739 (to be published in 1981).

14. M. P. Modera, R. C. Sonderegger, Determination of In-Situ Performance of Fireplaces, Lawrence Berkeley Laboratory report LBL-10701, August 1980.

15. R. C. Diamond, What About Fireplaces?, Lawrence Berkeley Laboratory Publication, Pub. #313, September 1980.

BUILDING VENTILATION AND INDOOR AIR QUALITY

INTRODUCTION

C. Hollowell

The Building Ventilation and Indoor Air Quality (BVIAQ) program is a major component of Lawrence Berkeley Laboratory's Energy Efficient Buildings Program. Funded by the Department of Energy's (DOE) Office of Buildings and Community Systems and the Office of Health and Environmental Research, The BVIAQ program is part of a coordinated effort to respond to the need for conserving the nation's energy while maintaining the health and comfort of building occupants. The overall objective of the BVIAQ program is to conduct in-depth research and development on existing and proposed ventilation requirements in order to provide recommendations for the establishment of energy-efficient ventilation standards and ventilation designs for residential, institutional, and commercial buildings. LBL is also providing technical and management support to DOE for other related ventilation projects.

BVIAQ program activities for FY 1980 represent a continuation of the following tasks:

1. laboratory studies of indoor combustion emissions, organic contaminants, and radon;
2. field monitoring of indoor air quality in buildings;
3. indoor air quality health-risk assessment studies;
4. demonstration and assessment of residential mechanical ventilation systems incorporating air-to-air heat exchangers;
5. completion of subcontract activities consisting of:
   - assessment of ventilation requirements for odor control in buildings;
   - assessment of hospital ventilation standards;
   - study of automatic variable ventilation control systems based on air quality detection in institutional and commercial buildings.
6. completion and implementation of a ventilation/indoor air quality data base.

A description of the work accomplished and projected by our group is presented by program in the next five articles.

COMBUSTION-GENERATED POLLUTANTS*

G. Traynor, M. Apte, and J. Girman

INTRODUCTION

Field and laboratory measurements carried out thus far have indicated clearly that combustion-generated indoor air pollutants can have a significant impact on human health. We have demonstrated that levels of gaseous air pollutants (CO, CO_2, NO, NO_2 and formaldehyde) and respirable particulate carbon compounds are elevated in indoor environments where gas appliances are used--in the case of CO, NO_2 and formaldehyde, approaching or exceeding existing (and recommended) ambient air-quality standards and, in the case of respirable particulate mass, comparable to those typical of a very smoggy day.[1-4] In energy-efficient structures where the reduction of infiltration tends to inhibit the escape of indoor-generated pollutants, the health risk may be more serious.

While our previous studies have concentrated on emissions from gas stoves,[1-4] there are many other indoor sources of combustion pollutants. Two important sources are portable kerosene heaters, which have become very popular recently, and side-stream smoke from cigarettes. Our research activity for FY 1980 focussed on these two pollutant sources.

ACCOMPLISHMENTS DURING FY 1980

Kerosene Heater

A portable kerosene heater (convective type) was operated under two ventilation rates in an environmental chamber with a volume of 27 m^3, the size of a small bedroom. The manufacturer's rated output for this heater was 2,300 kcal/hr, but actually it consumed 830 kcal/hr based on a kerosene heat production value of 8800 kcal/1.

The heater was operated at the low ventilation rate of 0.33 air changes per hour (ach) using no mechanical ventilation and at the high ventilation

* This work was supported by the Assistant Secretary for Environment, Office of Health and Environmental Research, Human Health and Assessments Division of the U.S. Department of Energy under Contract No. W-7405-ENG-48.

rate of 1.6 ach using mechanical ventilation. Figures 1 and 2 show the respective NO, NO_2, and CO_2 concentrations at low and high ventilation rates. Most striking are the NO_2 levels: At the low ventilation rate, the NO_2 concentration reached 1.24 ppm above background after 30 minutes, while at the high ventilation rate the NO_2 level reached 0.89 ppm over background after the same time period. These values should be compared to recommended and proposed short-term (usually peak one-hour average) outdoor NO_2 standards that range from 0.1 ppm to 0.5 ppm.[5]

High levels of CO_2 were also observed, but only very small amounts of CO and particulates. The workplace standard promulgated by the Occupational Safety and Health Administration (OSHA) for CO_2 is 5000 ppm averaged over eight hours.[6] After 30 minutes of heater use at the low ventilation rate, this value was exceeded and, at high ventilation, this value was approached. CO levels peaked at 2.2 ppm at the low ventilation rate, and particulate emissions were undetectable.

Sidestream Tobacco Smoke

Particulate emissions contained in the sidestream smoke of one cigarette smoked by a volunteer situated inside the chamber were measured. The volunteer, who was asked to smoke at his usual pace, was a student, and chose to study while he smoked--his typical pattern. The chamber was maintained at a low ventilation rate (0.30 ach) during the entire experiment. The particulates released into the chamber from the sidestream smoke were size-fractionated and weighed using a ten-stage piezoelectric cascade impactor (QCM Cascade Impactor, California Measurements, Inc., Sierra Madre, California). As is evident from Figure 3, very high levels of particulates were measured: during the smoking period, total particulate levels increased 390 $\mu g/m^3$ over background. Ninety-six per cent of this increase is attributable to particulates under 0.4 ± 0.1 µg in diameter--a size range that has a high probability of penetrating the pulmonary region of the lung. The short-term (24-hour average) outdoor air quality standard set by the U.S. Environmental Protection Agency is 260 $\mu g/m^3$; the equivalent California standard is 100 $\mu g/m^3$.

In a similar experiment, this time using an automatic smoking machine, CO, NO, NO_2, and particulates from the non-inhaled fraction of tobacco smoke were measured. (The non-inhaled fraction is different from sidestream smoke in that it does not contain the smoke exhaled by the smoker.) Particulate emissions were essentially the same as in the previous experiment. CO levels in the chamber peaked at 2.7 ppm above background as compared to the outdoor one-hour standard of 35 ppm while NO and NO_2 levels peaked at 0.08 ppm and 0.09 ppm, respectively. NO and NO_2 measurements were made with a Thermo-Electron chemiluminescent analyzer which is subject to a substantial positive interference from hydrogen cyanide; therefore the NO and NO_2 measurements may not be accurate.[7]

Pollutant Emission Rates

Pollutant emission rates from the kerosene heater and sidestream smoke were calculated, and

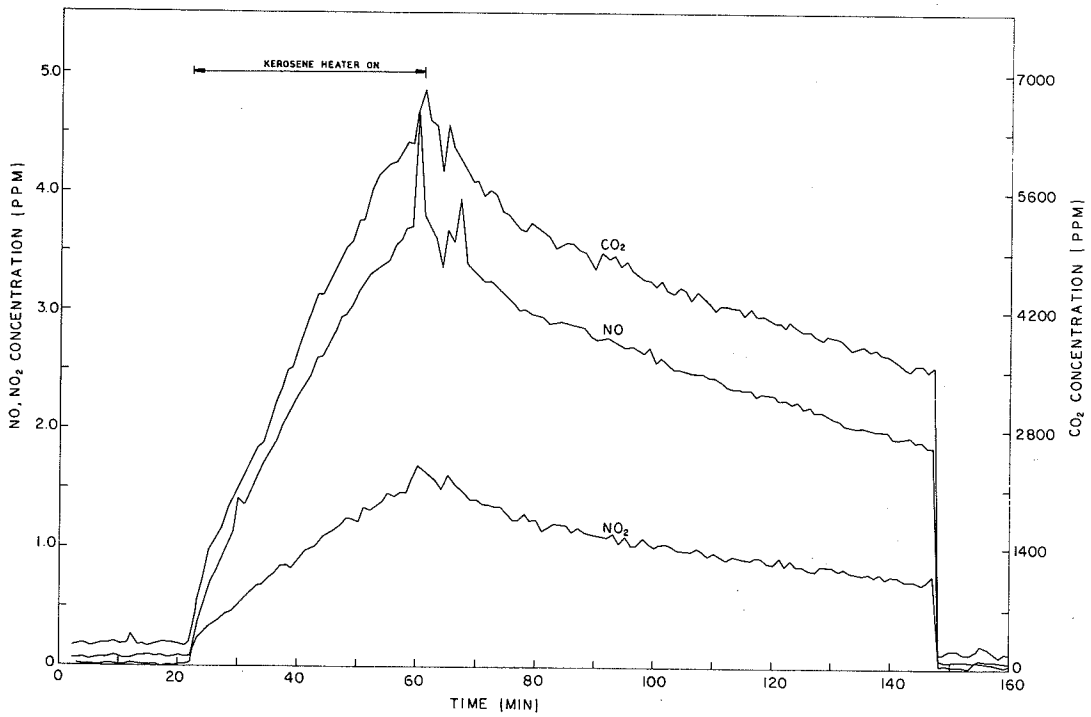

Fig. 1. NO, NO_2 and CO_2 emissions from a portable convective kerosene heater operated for 39 min. CO levels peaked at 2.2 ppm and particulate emissions were negligible. Tests were conducted in a 27 m^3 environmental chamber under a ventilation rate of 0.33 air changes per hour. (XBL 8010-12781)

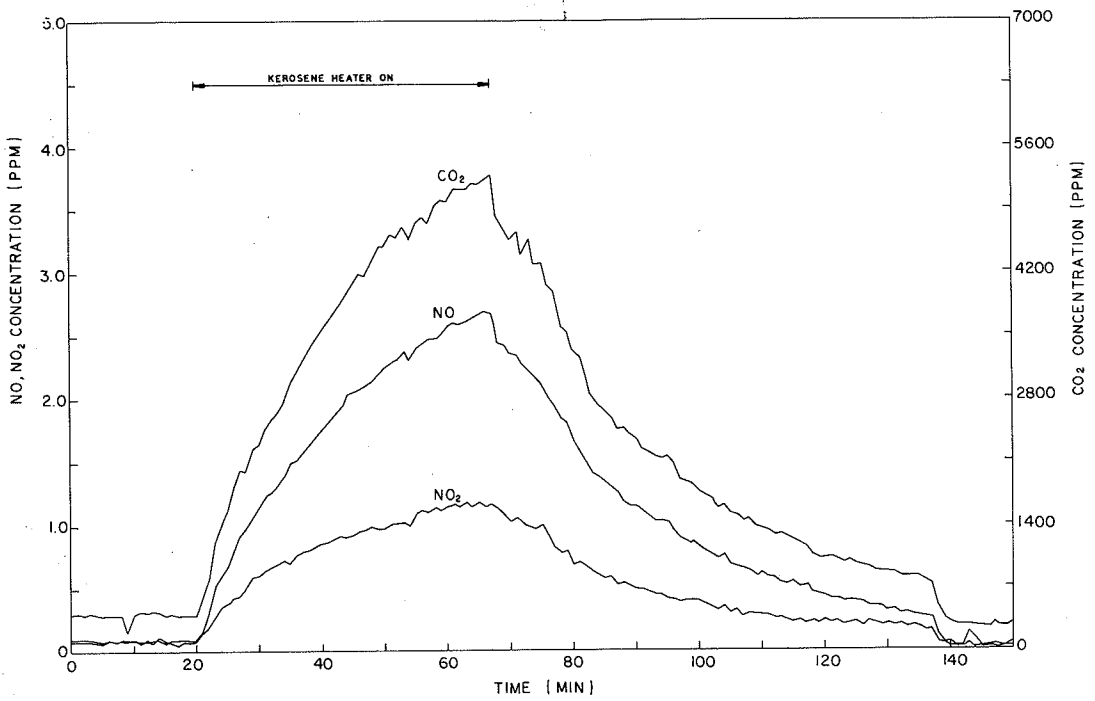

Fig. 2. NO, NO_2 and CO_2 emissions from a portable convective kerosene heater operated for 46 min. CO levels peaked at 1 ppm and particulate emissions were negligible. Tests were conducted in a 27 m^3 environmental chamber under a ventilation rate of 1.60 air changes per hour. (XBL 8012-12888)

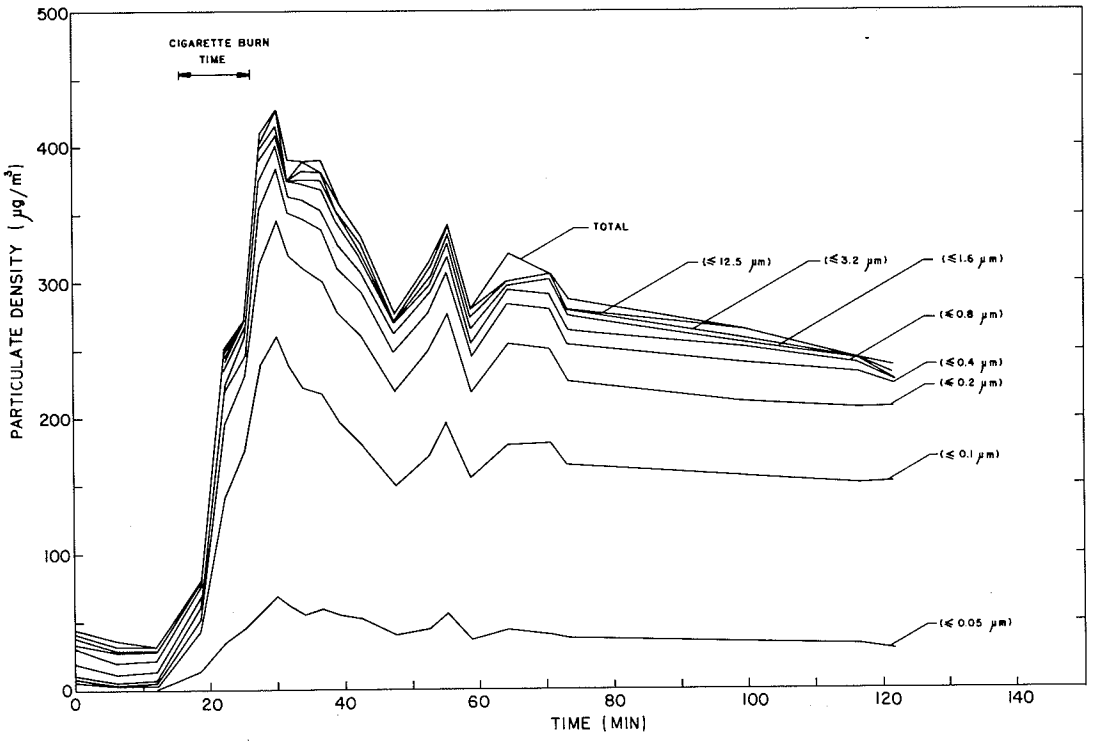

Fig. 3. Size-segregated particulate emissions from one cigarette smoked by a volunteer. The test was conducted in a 27 m^3 chamber under a ventilation rate of 0.30 air changes per hour. (XBL 8012-12887)

the results are summarized in Table 1. Multiplying the pollutant emission rate by the source consumption rate yields the actual mass of pollutant emitted into the room. The kerosene heater we used consumes 830 kcal/hr. One king-size cigarette combusts approximately 600 mg of tobacco in ten minutes. Emission rates combined with source consumption rates are useful for making approximations of pollutant concentrations under conditions other than the ones we tested.

PLANNED ACTIVITIES FOR FY 1981

Our research plans for FY 1981 are to complete the analysis of gas stove-generated pollution data collected at an experimental research house. The data include the pollution profiles of CO, CO_2, NO, and NO_2 throughout the house under various conditions of ventilation and stove use. We intend to add the following activities to our project for 1981: (1) We will use data already collected at a research house as a basis for testing, evaluating, and improving various models of indoor air quality in residences. (Several models published by others were either not tested in residences or yielded inadequate predictions of indoor air pollution levels.[8,9,10]) (2) We intend to further characterize particulate and gaseous emissions from other indoor combustion sources. (3) We will attempt to develop a comprehensive passive-monitoring package to determine one-week average pollution levels in various building types. Such a system would allow us to conduct extensive field studies at minimal cost for instrumentation and personnel. Field studies would have the dual goals of testing a wide variety of building types (using different ventilation schemes) and determining actual site-specific pollutant levels to which occupants are exposed.

REFERENCES

1. C. D. Hollowell, R. J. Budnitz, G. D. Case, and G. W. Traynor, Generation of Gaseous and Particulate Sources: I. Field Measurements 8/75-10/75, Lawrence Berkeley Laboratory report LBL-4416, January 1976.
2. C. D. Hollowell, R. J. Budnitz, and G. W. Traynor, "Combustion-Generated Indoor Air Pollution," Proceedings of The Fourth International Clean Air Congress, Tokyo, Japan, May 16-20, 1977, pp. 684-7, Japanese Union of Air Pollution Prevention Associations, Tokyo, Japan, 1977.
3. G. W. Traynor, D. W. Anthon, and C. D. Hollowell, Indoor Air Quality: Gas Stove Emissions, Energy and Environment Division Annual Report, 1978, Lawrence Berkeley Laboratory report LBL-8619, 1978.
4. G. W. Traynor, "Gas Stove Emissions," Energy and Environment Division Annual Report, 1979, Lawrence Berkeley Laboratory report LBL-11650, 1980.
5. C. D. Hollowell, J. V. Berk, and G. W. Traynor, Impact of Reduced Infiltration and Ventilation on Indoor Air Quality in Residential Buildings, Lawrence Berkeley Laboratory report LBL-8470, November 1978.
6. National Institute for Occupational Safety and Health [NIOSH], Summary of NIOSH Recommendations for Occupational Health Standards, NIOSH, 4676 Columbia Parkway, Cincinatti, Ohio 45226, October 1978.
7. R. A. Jenkins and B. E. Gill, "Determination of Oxides of Nitrogen (NO_x) in Cigarette Smoke by Chemiluminescent Analysis," Analytical Chemistry, vol. 52, no. 6, May 1980.

Table 1. Pollutant emission rates.

Pollutant	Kerosene Heater[a] (µg/kcal)	Sidestream Cigarette Smoke[b] (µg/mg)	Conversion Factors[c] 100 µg/m^3 equivalent (ppm)
CO	d	130[e]	0.086
CO_2	630,000	d	0.055
NO	270	f	0.080
NO_2	210	f	0.052
Particulates	d	18	n/a

[a] Expressed as microgram of pollutant emitted per kilocalorie of kerosene burned.

[b] Expressed as microgram of sidestream pollutant emitted per milligram of tobacco burned.

[c] Calculated at a pressure of 1 atm and a temperature of 20 °C.

[d] Observed concentrations were too close to background levels to calculate an emission rate.

[e] Does not include exhaled fraction.

[f] Subject to positive hydrogen cyanide interference.

8. F. H., Shair, and K. L. Heitner, "Theoretical Model for Relating Indoor Pollutant Concentrations to those Outside," Environmental Science and Technology, May 1974.

9. Ishizu Yoshiaki, "General Equation for Estimation of Indoor Pollution," Environmental Science and Technology, October 1980.

10. A. J. Moschandreas, and J. W. C. Stark, The GEOMET Indoor/Outdoor Air Pollution Model, EPA contract #68-02-2294, U.S. Environmental Protection Agency, Environmental Research Center, Research Triangle Park, N. C. 27711, February 1978.

ORGANIC CONTAMINANTS*

R. Miksch, K. Geisling, L. Jenks, H. Schmidt, M. Tashima, and D. Wolosin

INTRODUCTION

The Organic Contaminants Project of the Building Ventilation and Indoor Air Quality Group has been conducting a diversified research effort involving basic research in the laboratory and analysis of field samples. Two main areas of activity have been established, one focusing on formaldehyde and the other on various organics present in indoor air. Formaldehyde can be emitted from common building materials that contain formaldehyde resins, such as plywood, particleboard and foam insulation. Work in this area has included extensive field measurements in energy-efficient and retrofitted homes, assessment of analytical methods used to measure formaldehyde, and the development of primary formaldehyde sources, passive monitors and filter techniques. For other organic contaminants in indoor air, techniques have been developed for collecting and analyzing a wide range of compounds found in buildings. Organic compounds are emitted from such materials as paints and adhesives, household cleaning products, office furnishings, building materials, combustion sources, and people.

ACCOMPLISHMENTS DURING FY 1980

Development of Methods of Analysis

During the past year, extensive effort was devoted to developing a more satisfactory thermal desorption device for analyzing samples collected on the porous polymer Tenax. A new thermal desorption system, designed and built at LBL, was completed in the Fall of 1980. Specific design improvements include a new oven which accommodates smaller sample tubes and does not desorb compounds on the outside of the tube. This change reduces the background and facilitates field sampling. Another improvement was the construction of a new cryogenic trap that is resistively heated and has a "buffer zone" of capillary tubing to handle flashback; this modification enhances chromatographic behavior and eliminates ghost peaks that have been a problem with commercially available devices used previously. The operating parameters of this system are now being optimized. Problems with the breakage of Tenax cartridges and the loss of sample integrity during shipping and handling have been resolved.

Two approaches have been taken to quantify the results of air sampling with Tenax. One method of generating standards involves using an automatic sampling device and a gas chromatograph to load trace quantities of standards directly onto Tenax cartridges. This technique has been tested and appears to be very promising. The other approach involves the use of an electrobalance, which forms the core of a rigorous quantification system based on permeation and diffusion.

Methods of analysis have also been improved for formaldehyde research. Specifically, we have developed a modified pararosaniline technique for more precisely determining formaldehyde in aqueous solution. Unlike earlier methods, this method eliminates the need for a hazardous mercury reagent. The optimization of reagent concentrations, the effect of varying temperature, and potentially interfering compounds were also studied. Comparative data on the analysis of aqueous formaldehyde solutions indicate that the modified pararosaniline method is more sensitive, more reproducible, and easier to use than the widely accepted chromotropic acid method. Results of two of the experiments are presented in Figures 1 and 2. The procedures are described in a report submitted to Analytic Chemistry.[1]

A new gas generation system for low levels of gaseous formaldehyde in air has been developed this year and is now being validated. The system shows promise of providing primary formaldehyde sources; it is based on the catalytic decomposition of trioxane to formaldehyde. Trioxane vapor released from a diffusion tube is passed over a phosphoric-acid-coated carborundum catalyst. The amount of formaldehyde formed may be calculated directly from the weight loss of trioxane, based on initial data showing a 100% conversion of trioxane to formaldehyde.

A passive monitoring system is being developed for the sampling of low levels of formaldehyde in ambient air. The passive monitors are prepared by

* This work was supported by the Assistant Secretary for Conservation and Solar Energy, Office of Buildings and Community Systems, Buildings Division of the U.S. Department of Energy under Contract No. W-7405-ENG-48.

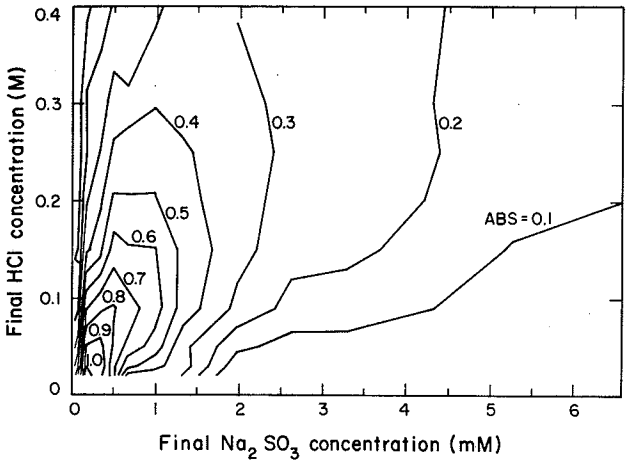

Fig. 1. Net absorbance as a function of the final hydrochloric acid and sodium sulfite concentrations. Hydrochloric acid, sodium sulfite, and pararosaniline are the key reagents in the analysis of aqueous formaldehyde solution by the pararosaniline method. All analyses were performed on a solution of 1.0 μg mL^{-1} (33 μm) formaldehyde. Data shown were obtained by linear interpolation from the data given in Table 1. (XBL 806-1151)

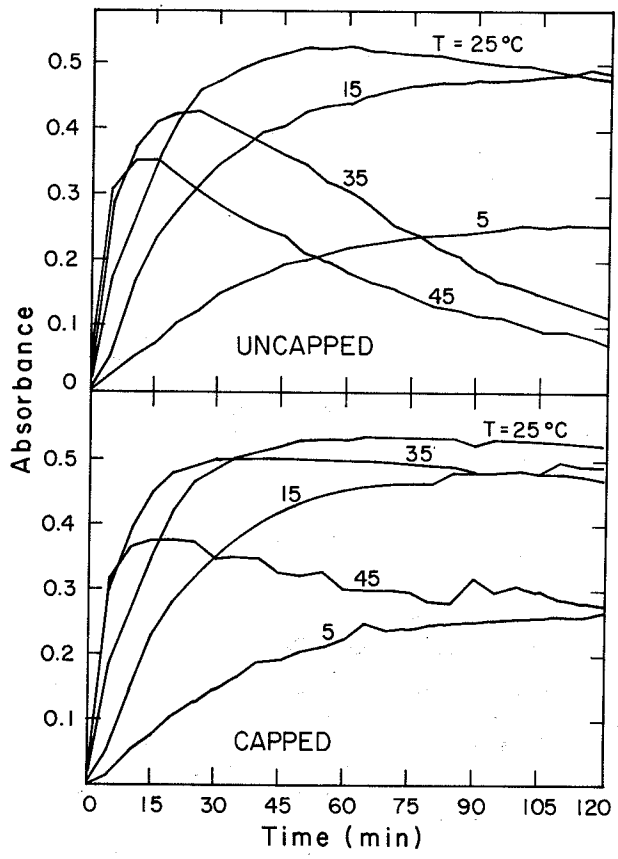

Fig. 2. Net absorbance as a function of development time at various temperatures: a) with cuvettes and b) with cuvettes uncapped. Since the sodium sulfite will equilibrate with the atmosphere while the color of the solution is being developed, the absorbance can be maximized by capping the cuvettes containing the sample solution. The optimized reagent concentrations were used. (XBL 806-1154)

treating glass fiber filters with sodium bisulfite and placing them in glass vials. In the process of establishing a calibration curve for the passive monitors, their collection efficiencies are being tested for reliability and reproducibility.

Field Monitoring of Organic Contaminants

Various field sites were sampled for organic contaminants using Tenax and the unmodified desorption system.[2] Four of these sites were offices at LBL where indoor air quality complaints had been registered; all of these sites were typical modern office settings with partitions, carpeting, and synthetic furniture. In all cases, the organic compounds found indoors were absent or present in substantially lower quantities outdoors. A comparative set of chromatograms is shown in Figure 3. The results of these analyses are presented in Table 1. The most interesting site sampled this year was a new office building in Marin County, where an unusually high number of complaints had been registered with the company nurse following occupation of the building. Although the complaints varied widely, irritation of the respiratory tract and allergic reactions were most commonly cited. The potential health hazard from the organic compounds found in these samples cannot be assessed at this time. No single compound was

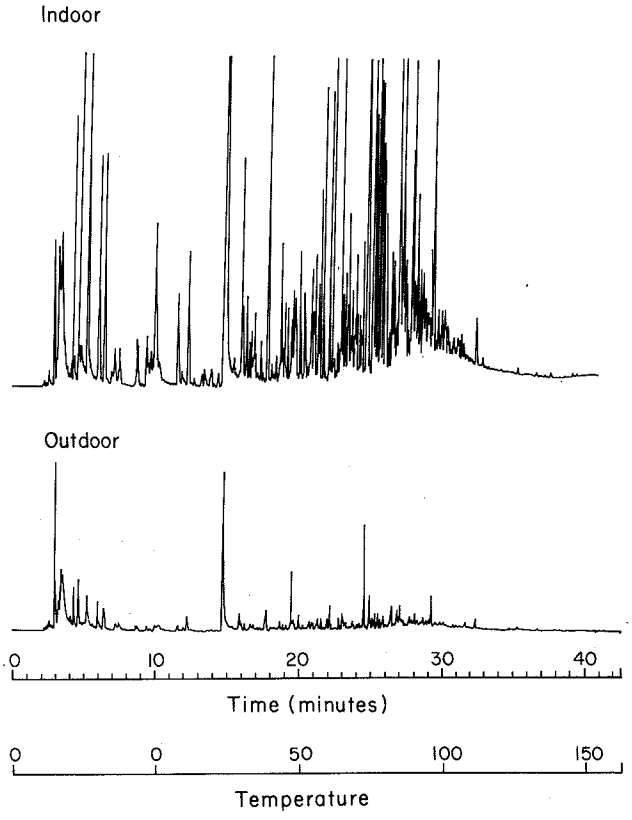

Fig. 3. A comparison of chromatograms of samples taken inside Rm. 3145, Building 90 and outside Building 90. (XBL 808-1727)

Table 1. Organics detected in LBL offices.

	LBL 67C	LBL 90H	LBL 90-3145		OSHA Permissible Exposure Limit (ppm)
Hydrocarbons					
n-hexane	x	x	x		500
n-heptane			x		500
n-octane			x	x	500
n-nonane			x	x	
n-undecane			x	x	
2-methylpentane	x	x			
3-methylpentane		x			
2,5-dimethylheptane			x		
methylcyclopentane	x	x	x		
ethylcyclohexane			x	x	
methylcyclohexane			x	x	500
pentamethylheptane			x	x	
Aromatics					
benzene		x	x		1
xylenes	x				100
toluene		x	x	x	200
Halogenated Hydrocarbons					
trichloroethane	x	x	x	x	350
trichloroethylene	x		x	x	100
tetrachloroethylene			x	x	100
Miscellaneous					
hexanal		x			
methylethylketone	x				200

found to be present in great enough concentration to be singled out as a health hazard by existing criteria. On the other hand, existing criteria were established under conditions of the workplace environment where unusually high exposures to a single compound are routinely encountered.

During the summer, a study was made of organic compounds emitted in trace quantities from common building materials. The materials analyzed included caulking compounds, two rugs, two linoleums, and several mastics and glues. Samples were collected via headspace analysis using a glass vacuum apparatus with liquid nitrogen cold traps. The small-volume liquid samples collected were identified by means of gas-chromatography/mass-spectroscopy. The results of the study are presented in Table 2. The major emissions were aliphatic hydrocarbons, but other emissions included alkyl benzenes, higher aromatics (naphthalenes), ketones, and some phenols and glycols. A few samples contained toluene or methyl ketone; only traces of chlorinated hydrocarbons were found.

In the Fall, the same apparatus was used to qualitatively analyze samples of building materials and office furniture from the office building in Marin County where air samples had been analyzed in September. Many of the compounds emitted by the building materials were found to correspond to those identified in the air samples.

The EEB Mobile Laboratory (described in "Field Monitoring") continues to be used for measuring formaldehyde and total aldehydes in the field. Sites in Minnesota, Wisconsin, Oregon, and New Jersey were studied for two-week periods. Formaldehyde levels at all of the sites were below the level at which significant health effects are expected to occur. Initial analysis of the data indicates that while no obvious correlation exists between ventilation rate and formaldehyde levels at these low concentrations, formaldehyde levels may be related to temperature and relative humidity.

Table 2. Organic contaminants identified in headspace vapor over selected building materials.

Building Material[a]	Description	Major Organic Contaminants[b]	Organic Contaminants of Interest[c]	Remarks
carpet #1	nylon (?) fiber, jute backing	3-phenylcyclohexene, aliphatic hydrocarbons	3-phenylcyclohexene	3-phenylcyclohexene derived from alcohol?
carpet #2	polypropylene fiber, foam backing, self-stick	trimethylcyclohexane, aliphated hydrocarbons	traces of alkylbenzene	
carpet #3	synthetic fiber, thin composition backing	n-octane, n-nonane aliphatic hydrocarbons	none	
carpet #4	nylon fiber, jute backing	3-phenylcyclohexene, decane, dichlorobenzene, styrene, aliphatic hydrocarbons	3-phenylcyclohexene, dichlorobenzene, styrene, small amounts of alkyt-benzenes, traces of napthalene, 1- and 2-methylnapthalene, nonanal, analog of butylated hydroxytoluene (BHT)	3-phenylcyclohexene derived from alcohol? Dichlorobenzene from air deodorizer
carpet #5	acrylic fiber, foam backing	Heavy oxygenated compound, aliphatic hydrocarbons	heavy oxygenated compound, small amounts of phenol, biphenyl, napthalene, 1- and 2-methylnapthalene	Heavy oxygenated compound clearly largest component emitted, unknown.
linoleum #1	vinyl, self-stick	dimethylcyclohexane, n-octane, aliphatic hydrocarbons	none	
linoleum #2	vinyl asbestos, self-stick	octane isomers, nonane	small amounts of toluene, xylene, propyl-benzene, trace of trichloroethylene	
linoleum #3	vinyl	acetone, methyl ethyl ketone (MEK), toluene, butyl acetate, aliphatic hydrocarbon background	acetone, MEK, toluene, butylacetate, small amounts of dimethyl-dioxane, trichloroethylene, benzaldehyde, 2-(2-ethoxy-ethoxy) ethanol (Carbitol)	
linoleum #4	vinyl asbestos	toluene	toluene, small amounts of benzaldehyde, acetophenone, benzylalcohol, butyl benzyl ether, alkylbenzenes	

acoustic ceiling tile	pulp faced by vinyl acrylic latex coating	butyl acetate, aliphatic hydrocarbon background	butyl acetate	water was major emission
acoustical tile/ tileboard cement	mastic	aliphatic hydrocarbons	xylene, ethylbenzene toluene, traces of benzene, napthalene, alkylbenzenes, butylated hydroxytoluene (BHT)	allowed to dry 24 hrs before vapor collected
contact cement	liquid	trimethylcyclohexane, methyl ethyl ketone (MEK), aliphatic hydrocarbons	none	allowed to dry 24 hrs before vapor collected
linoleum cement	mastic	denatured alcohol (ethanol, methanol)	methyl isobutyl ketone (MIBK)	allowed to dry 24 hrs before vapor collected
ceramic tile cement	mastic	hexane, aliphatic hydrocarbons	small amounts of alkylbenzenes, trace of trichloroethane	allowed to dry 24 hrs before vapor collected
caulk #1	"Phenoseal"	butylacetate, 2-(2 ethoxy-ethoxy) ethanol (carbitol)	butylacetate, carbitol small amount of butyl propyl ether	water was major emission, allowed to dry 24 hrs before vapor collection
caulk #2	vinyl acrylic latex caulk	ethylene glycol	ethylene glycol	allowed to dry 24 hrs before vapor collection
caulk #3	butyl caulk	octane, octene, nonane, aliphatic hydrocarbons	octene, small amounts of alkylbenzenes	allowed to dry 24 hrs before vapor collection

[a] Samples were purchased in local hardware stores, obtained from local building sites, or supplied by interested consumers.

[b] "Major" is defined as one of the five largest peaks. "Aliphatic hydrocarbons" is used in place of a detailed description of the components of petroleum-derived solvent constituents.

[c] Organic contaminants of interest are defined as those compounds that possess functional groups that enhance chemical reactivity. "Trace amounts" applies to compounds that were approaching the limit of detection, while "small amounts" refers to compounds that were clearly present but did not form one of the five largest peaks (see previous footnote).

PLANNED ACTIVITIES FOR FY 1981

Planned activities for FY 1981 include laboratory and field validation of formaldehyde passive monitors, continued field measurement of formaldehyde, and continued optimization of the solid-solvent organic contaminant sampling apparatus.

REFERENCES

1. R. R. Miksch, D. W. Anthon, L. Z. Fanning, C. D. Hollowell, K. Revzan and J. Glanville, "A Modified Pararosaniline Method for the Determination of Formaldehyde in Air," to be published as Lawrence Berkeley Laboratory report LBL-9785.

2. H. E. Schmidt, C. D. Hollowell, R. R. Miksch and A. S. Newton, Trace Organics in Offices, Lawrence Berkeley Laboratory report LBL-11378, December 1980.

RADON: EMANATION STUDIES, INDOOR MEASUREMENTS, AND CONTROL STRATEGIES*

A. Nero, M. Boegel, J. Ingersoll, W. Nazaroff, K. Revzan, and G. Zapalac

INTRODUCTION

When energy-conserving features designed to reduce infiltration are effected in buildings, the levels of radon, as well as other indoor air contaminants, can increase. The main objective of this project is to determine the extent to which radon and its daughters are present in indoor air and to study radon sources and source strengths. In addition, an important aspect of our research is to evaluate control strategies in the light of existing data on health risk factors, so that the formulation of national programs promoting energy conservation in buildings can consider the potential health impact of indoor concentrations of radon and its daughters.

Radon 222 is a chemically inert gas, occurring from decay of radium 226 that is naturally present in the earth's crust. Radon can migrate from its site of formation, and the potential for radon gas emissions into the interior space of buildings depends on the presence of radium in the soil under and around the structure or in the materials used to construct the building, as well as on transport of radon from more distant radium deposits that occurs, for example, via underground water supplies.

The indoor daughter levels associated with a given radon source strength depend, at a minimum, on the rate at which indoor air is exchanged for outdoor air, the internal air circulation rate and pattern, and the indoor particulate concentration. As a result, understanding sources and concentrations of indoor radon and its daughters requires study both of sources--which we know vary from one building to another and one geographical region to another--and of radon daughter behavior. Correspondingly, control techniques can be based on either prevention of radon entry into the interior space or on removal of radon or its daughters from indoor air.

The recognition that radon exposure poses a health risk, generally, and that energy-conservation measures may exacerbate present risks to building occupants has made such studies a research priority. The health hazards of radon result from its four short-lived daughters (^{218}Po, ^{214}Pb, ^{214}Bi, and ^{214}Po) all of which have half-lives of less than 30 minutes and two of which (the polonium isotopes) are alpha emitters. These daughters can be inhaled into the lower respiratory tract, and exposure to high levels over prolonged periods (as was historically the case for uranium miners) can increase the incidence of lung cancer. The risk factors associated with low-level exposures are not directly known; however, if factors derived from the high-exposure data are applied to the lower indoor exposures, the estimated risk appears to be significant.

Our investigations have focussed primarily on the following activities:

1. measuring the rate of radon emanation from commonly-used building materials;
2. monitoring radon and daughter levels in conventional and energy-efficient residential buildings;
3. developing appropriate monitors for detecting radon and radon daughters; and
4. evaluating control techniques and strategies effective in limiting indoor concentrations.

ACCOMPLISHMENTS DURING FY 1980

One major project this year was to examine samples of building materials commonly used in the

* This work was supported by the Assistant Secretary for Conservation and Solar Energy, Office of Buildings of Community Systems, Buildings Division, and the Assistant Secretary for Environment, Office of Health and Environmental Research, Human Health and Assessments Division of the U.S. Department of Energy under Contract No. W-7405-ENG-48.

United States, emphasizing concrete, to determine their contribution to radon concentrations observed indoors. Our principal measurement technique employs gamma detection using a heavily shielded sodium iodide system. Measurement of gamma rays from ^{214}Bi and ^{208}Tl from a sample in a sealed container indicates concentrations of the ^{238}U and ^{232}Th decay chains, respectively. Subsequent measurement with the container open, allowing radon (the parent of ^{214}Bi) to escape, yields the radon emanation rate. (In both cases, ^{40}K is measured from its own gamma ray.) An alternative technique, developed by our group[1,2] measures radon emanation directly by sealing the sample in a container for one to three days and then transferring the radon collected to a scintillation cell for counting. This technique is effective even for low emanation rates.

The results of our survey of ordinary concrete from ten U.S. metropolitan areas are shown in Table 1, which gives emanation rates per unit mass and elemental concentrations. The mean rate for the ten sample groups ranges from 0.4 to 1.2 pCi kg^{-1} h^{-1}. As seen in Table 2, a group of concretes containing fly ash also fell within this range, while samples containing phosphate slag fell below. Gypsum, brick and wood were toward the bottom of this range or lower, as were solar rock bed samples with high uranium content and a radon escape-to-production ratio of 4%.[3]

The materials examined appear to contribute only a small portion of the radon levels ordinarily found in U.S. homes. For 0.2 m thick concrete, 1 pCi kg^{-1} h^{-1} corresponds to an emanation rate per unit area of approximately 0.05 pCi m^{-2} s^{-1}, which would contribute 0.1 pCi/l to the indoor radon concentration in a house having an air exchange rate of one per hour and an emanating-surface-to-interior-volume ratio of 0.5 m^2 per m^3.

We have also been engaged in other concrete-related studies. A few measurements of radionuclide concentrations in and radon emanation from concrete components have been performed,[3] but more extensive studies are required to determine the contribution of these components to the radon emanation rate from concrete, since the reactions that take place in the formation of concrete can influence the extent to which radon is free to move through the cured material. We have made a few measurements of components of ordinary concrete, and have also examined a selection of fly-ash samples, supplied by the U.S. Environmental Protection Agency, as a prelude to further study of fly-ash concretes. A more substantial effort has been devoted to developing a technique for measuring diffusion parameters for radon in concrete. (A few samples have already been measured by this technique.[4]) Knowledge of these diffusion parameters is important not only for understanding the emanation of radon originating in the concrete itself, but also for characterizing the transport of radon from other sources through concrete building components. The latter is necessary for us to evaluate the extent to which radon from soil and rock underlying buildings affects indoor concentrations of radon.

Indoor Concentrations of Radon and its Daughters

During FY 1980, we completed a review of available information on indoor radon and daughters.[5] This review, as expected, indicates that the range of indoor radon concentrations is very large. Perhaps more importantly, it emphasizes the fact (established primarily by LBL work) that in U.S. housing the major influence on indoor radon concentrations is the source strength rather than the air exchange rate, a crucial conclusion for formulating strategies for energy conservation and indoor air quality control.

LBL has conducted surveys in both energy-efficient and conventional houses, measuring radon, infiltration rate and, in most cases, radon daughters. Radon and its daughters are measured using grab samples, and the infiltration rate is measured by a tracer gas technique. Occupants are asked to close windows and doors for the night prior to measurements to assure a degree of correspondence between the observed radon concentrations and infiltration rates and thereby yield the radon source strength. These surveys indicate the range of source strengths and concentrations in houses and provide a basis for more intensive research characterizing indoor exposures and the influence of energy-conservation and control measures.

Two of these surveys, one in energy-efficient and one in conventional houses, were conducted largely in FY 1979,[1] with subsequent analysis of results in FY 1980. The "energy-efficient" houses surveyed in the United States and Canada were typically demonstration or research houses, privately-owned residences built to assure low infiltration rates, or passive solar houses with rock-bed heat storage.[6] Measured radon concentrations and infiltration rates in these houses are shown in Figure 1. If the radon source strengths were the same for all these houses, and if the outdoor radon concentrations were low, the points would be on a straight line. Source strengths were found to differ by more than a factor of 10, however, even in this small number of houses.

The second 1979 survey group, 26 conventional houses in the San Francisco Bay Area, was examined in a similar manner.[1] Radon concentrations in these houses ranged from 0.4 to 0.8 pCi/l, typically much lower than those obtained in our energy-efficient sample. Measured infiltration rates ranged from 0.02 to 1.2 air changes per hour (ach) with 80% in the range of 0.1 to 0.6. (These infiltration rates are thought to be lower than typical for these houses because of mild weather conditions at the time of measurement.)

A third group of houses was surveyed during 1980. These were conventional houses in the vicinity of the single energy-efficient house in Maryland that showed the highest radon concentration in our earlier survey. The purposes of this survey were to examine the efficacy of random sampling for characterizing indoor concentrations of an entire community and to determine whether the high radon levels measured in the energy-efficient house

Table 1. Emanation rates and radionuclide concentrations in ordinary concrete.

Origin of Material	No. of Samples	Emanation Rate per Mass ($pCikg^{-1}h^{-1}$) Range	Mean	S.D.	Elemental Concentrations (mean) U (ppm)	Th (ppm)	K (%)	Average Escape-to-Production Ratio (%)
Albuquerque, NM	12	0.70-1.95	1.22	0.35	2.5	6.0	1.5	22
Kansas City, MO	12	0.40-0.65	0.53	0.07	1.0	2.0	0.7	25
Philadelphia, PA	7	0.35-0.55	0.42	0.08	0.6	1.5	0.7	17
Salt Lake City, UT	9	0.50-0.75	0.64	0.08	2.0	4.0	0.6	14
San Francisco - Oakland, CA	21	0.65-1.10	0.83	0.12	1.5	3.0	0.6	24
Austin, TX	8	0.60-0.92	0.73	0.12	1.3	1.5	0.8	24
San Antonio, TX	8	0.27-0.72	0.46	0.14	3.0	7.5	1.5	8
Chicago, IL	12	0.25-1.39	0.66	0.36	1.5	2.0	0.5	25
St. Paul - Minneapolis, MN	5	0.54-0.75	0.62	0.09	1.5	4.0	1.5	19
Knoxville, TN	6	0.46-0.78	0.59	0.12	1.0	1.2	0.5	23

Table 2. Emanation rates and radionuclide concentrations in miscellaneous materials.

Material (Origin)	No. of Samples	Emanation Rate per Mass ($pCikg^{-1}h^{-1}$) (Mean)	Elemental Concentrations (means) U (ppm)	Th (ppm)	K (%)	Average Escape-to-Production Ratio (%)
Fly-ash Concrete (4%) Knoxville, Tenn.	8	1.01	1.5	2.6	0.7	25
Phosphate Slag Concrete (20%) Savannah, Ga.	1	0.23	0.6	2.2	0.6	14
Gypsum four locations in the U.S. and one in Baja Calif.	12	0.61	1.0	0.5	0.2	28
Rock (Solar storage) N. Mex.	9	0.50	4.5	13.0	3.0	4
Red Brick Calif.	6	0.10	3.6	10.4	1.7	1
Adobe Brick N. Mex.	2	0.35	2.5	6.7	1.9	6
Wood Western states	2	0.02	--	--	--	--
Soil San Jose, Calif.	2	2.1	3.2	11.2	1.6	25
Soil Mt. Airy, Md.	2	2.1	3.3	15.1	2.2	25

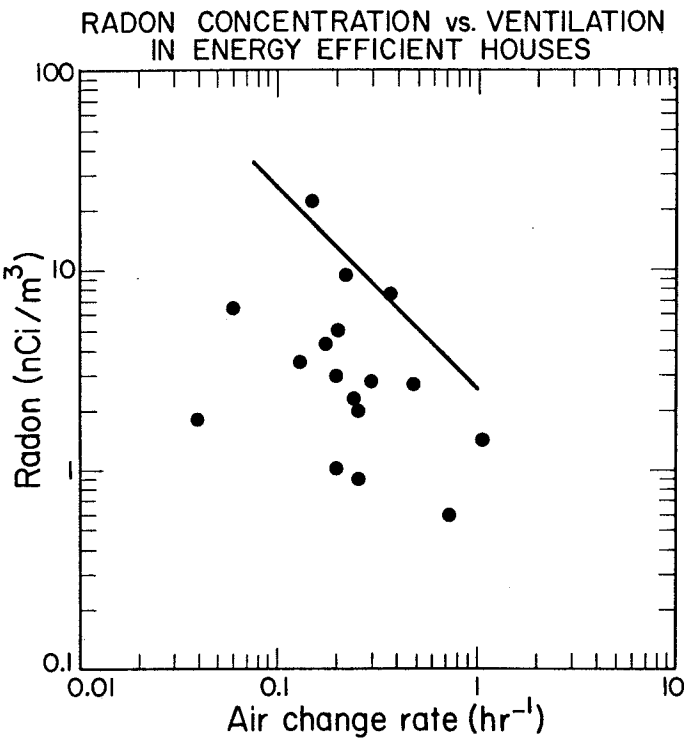

Fig. 1. Radon concentrations and ventilation rates in energy-efficient houses. Results are from grab samples of radon and concurrent ventilation rate measurements. The line indicates results from a house in which the ventilation rate was varied using mechanical ventilation with air-to-air heat exchange. (XBL 801-38A)

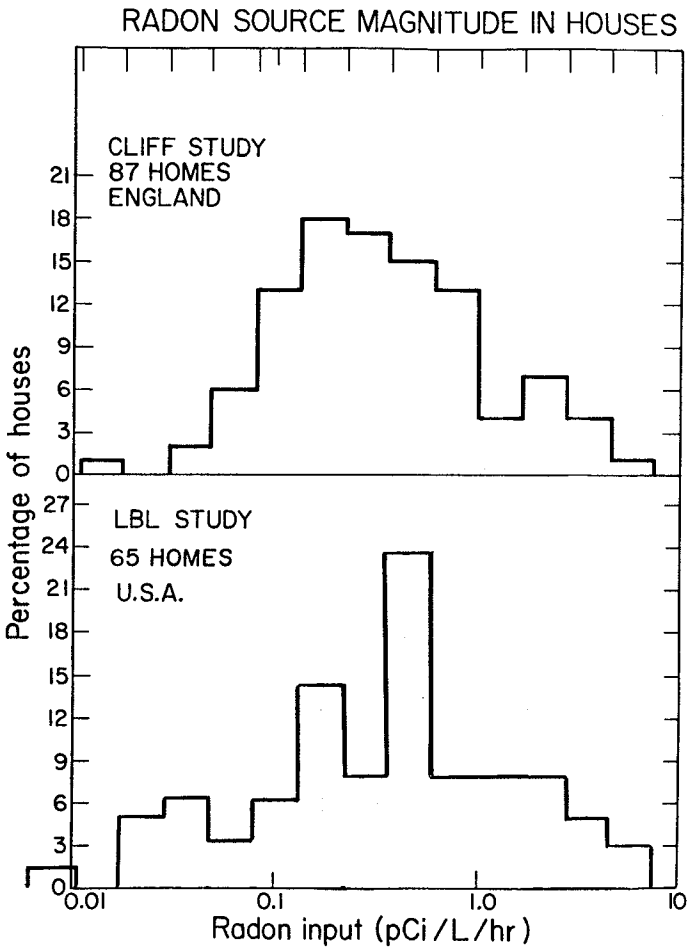

Fig. 2. Frequency distribution of radon source strengths in houses. The radon input per unit interior volume can be calculated from measured values of indoor radon concentration and air exchange rate. The upper distribution shows results obtained in England (Ref. 7). The lower distribution shows results based on measurements in three LBL surveys, including both conventional and energy-efficient houses. (XBL 803-419A)

extend throughout or beyond the community. Preliminary results indicate that the source strengths and indoor radon concentrations in this particular area are, indeed, atypically high.

The combined data from these surveys provide us with a unique view of radon source strengths in U.S. housing. The two surveys of conventional housing in the San Francisco area and in the Maryland area indicate differences in indoor source strength of more than a factor of 100. Moreover, our survey of energy-efficient houses gives source magnitudes within the same range. A preliminary compilation of our data is given in Figure 2, which also shows comparable results from England.[7]

CONTROL TECHNIQUES AND STRATEGIES

Of the available techniques for controlling indoor radon and daughter concentrations, those we investigated are designed to directly affect the airborne concentration rather than reduce the source strength. In particular, we have investigated the effect of mechanical ventilation systems incorporating air-to-air heat exchangers on indoor concentrations of radon. Such systems can control indoor pollutants other than radon and its daughters, are applicable to existing as well as new structures, and avoid much of the energy loss ordinarily associated with mechanical ventilation in heating and cooling seasons.

For our initial tests, we selected the Maryland house mentioned above. Using a mechanical ventilation system with air-to-air heat exchange to vary the air exchange rate, we measured both radon and radon daughter concentrations for a two-week period. The line shown in Figure 1 represents the equilibrium radon concentration. Individual daughter concentrations yielded the potential alpha energy concentrations (PAEC) shown in Figure 3.[8]

These measurements indicate a very complex behavior of individual daughter concentrations (and even PAEC), with an as yet ill-defined dependence on particulate concentrations. This complexity, also observed in our laboratory measurements, cannot as yet be understood in terms of existing models for indoor concentrations of radon and its daughters. Its explanation awaits more comprehensive measurements in controlled conditions and more complete modeling of the behavior of indoor radon daughters and particulates.

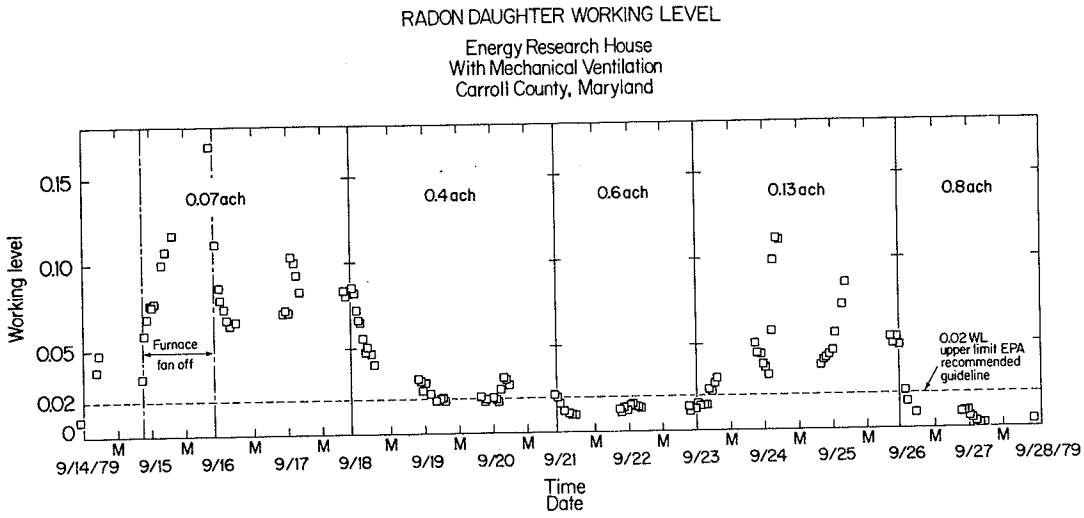

Fig. 3. Variation of potential alpha energy concentration (PAEC) with time. Five ventilation rates were examined using mechanical ventilation with air-to-air exchange during a two-week test period. (The indicated EPA guideline for average PAEC applies to houses on land reclaimed from phosphate mining.) (XBL 7910-4484)

In addition to the energy-efficient Maryland house, we have also begun to study the effectiveness of ventilation with air-to-air heat exchangers for radon control in a number of recently built conventional houses. As discussed in the section, "Mechanical Ventilation with Air-to-Air Heat Exchangers," these houses were selected as having relatively low infiltration rates, i.e., 0.6 ach or less.

We have begun to assess the potential use of mechanical ventilation and other control measures for limiting radon exposures in conventional and energy-efficient houses. As indicated by findings to date, present exposure rates vary substantially among geographic areas and from house to house in the same area. A significant percentage of the population receives exposures in the "occupational" range, that is, in the vicinity of 1 Working Level Month (WLM) per year or higher. National programs implementing ordinary tightening measures--those that reduce existing infiltration rates (typically 0.5 to 1 ach) by about 25%--will not increase this incidence greatly. (Independently of programmatic decisions to employ infiltration-reducing measures, however, it appears that some remedial action is required in cases where radon exposures are found to be high.) On the other hand, in new, very tightly constructed houses where infiltration rates are being reduced to as low as 0.1 ach, ventilation or air-cleaning systems appear to be required to control the levels of indoor-generated pollutants, including radon. Strategies to control radon exposures could have two complementary goals: to assure that virtually no exposures exceed a designated limit, as yet undetermined; and to design buildings to assure an acceptably low average exposure, also to be determined. Development of such limits requires substantial work characterizing indoor daughter concentrations. (See reference 9 for discussion of these issues.)

INSTRUMENTATION DEVELOPMENT

We have devoted substantial efforts to developing and evaluating instrumentation, primarily for measuring airborne radon and daughter concentrations, but also for source monitoring. Particular attention has been given to alpha spectroscopic methods for both field monitoring and laboratory measurement of radon daughter concentrations. We have analyzed two-count procedures used to measure individual daughters, adjusting the timing of the counting intervals to maximize precision.[10] Results of this analysis, shown in Figure 4, compare favorably with other techniques employing total measurement time in the vicinity of 40 minutes. An instrument with parameters chosen on the basis of this analysis yielded the results shown in Figure 3. An automated instrument using a two-count spectroscopic procedure is being fabricated for use in experiments studying radon daughter behavior. In addition, we have analyzed the suitability of rapid single-count spectroscopic methods for field measurements of PAEC. This analysis indicates that a single-count procedure taking a total of 11 minutes yields the PAEC with statistical uncertainty less than 20%, and with methodological error due to assumptions about equilibrium conditions ordinarily less than 20%.

In cooperation with the air-to-air heat exchanger project, we have also designed and fabricated an automatic system, the "Aardvark", for field measurement of indoor radon concentration. The Aardvark uses a continuous radon monitor previously described[1] and measures infiltration rate by means of tracer gas techniques and infrared analysis[12] (see Table 3 for approximate parameters). A more complete system incorporating an automatic spectroscopic daughter monitor of the kind mentioned above is under development for use in a "radon research house."

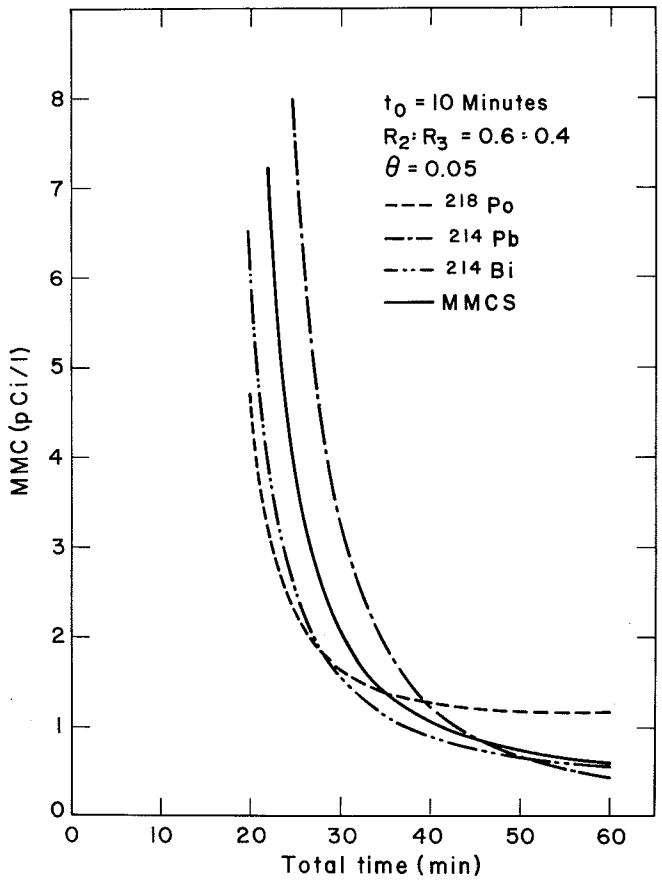

Fig. 4. Minimum measurable concentrations of radon daughters as a function of total measurement for optimized alpha-spectroscopic technique. The solid line (MMCS) is a weighted average of the individual daughter concentrations. (XBL 803-465A)

Table 3. Features of the Aardvark instrumentation system.

Computer controlled
Ventilation
-Tracer gas (SF_6) decay
-Measurement every 1.5 hours
-Automatic analyzer calibration
Radon
-Continuous radon monitor (after Thomas)
-Average measurement every 3 hours
-Precision: 50% uncertainty @ 0.25 pCi/l
Temperature
-Seven points: indoor (2), outdoor (1), heat exchanger airstreams (4)
-Recorded each 1/2 hour
Furnace activity
-Continuously monitored for change in state (on/off)

We have also engaged in testing and refining integrating radon monitors for our field program, including those based on thermoluminescent and track etch detection. The passive environmental radon monitor, PERM,[1] has been modified and tested to determine the effect of various features on its sensitivity and stability. In addition, we have conducted chamber studies to measure the sensitivity of track etch detectors and are examining their usefulness by pairing such detectors with other measurement devices in our field studies.

A new development this year has been the design and fabrication of a prototype radon "sniffer" to be used in houses for identifying places at which radon enters the structure. In preliminary tests, the prototype performed as designed, and more detailed laboratory and field testing is continuing. If such devices can be used to measure soil gas concentrations, we may be able to determine time correlations between radon source behavior and indoor concentrations.

PLANNED ACTIVITIES FOR FY 1981

The major projects already initiated will continue during 1981. We will conduct laboratory and field (in situ) studies of radon sources, including building materials and soils. Field projects will also use the radon "sniffer" to observe entry of radon into homes.

Monitoring of radon, radon daughters, and infiltration rates in conventional and energy-efficient buildings will be continued, both to determine the range and distribution of source strengths and concentrations and to correlate these parameters with structural and operational features of buildings. Cooperative efforts with organizations such as commercial home builders and utility companies will continue, as will our joint undertakings with the air-to-air heat exchanger project and the combustion pollutants group.

In our instrumentation development and evaluation work, we will continue to give attention to passive and active field radon monitors, field and laboratory radon daughter monitors, and source-monitoring techniques.

Several fundamental topics must be addressed more vigorously than heretofore if we are to characterize indoor radon and its daughters successfully, i.e.:

1. geographic distribution of radon sources and strengths;
2. radon transport into structures;
3. behavior of daughters indoors (including the effect of removal processes);
4. sensitivity of measurement techniques under various environmental conditions.

With additional support from DOE/Environment, we can undertake such studies in FY 1981. The first two of these research areas will receive modest emphasis as part of our program of source studies.

A much more intensive effort will be devoted to studies of radon daughter behavior in a "radon

research house." This facility, now being established in an off-campus University of California building, consists of a three-room area that is being refurbished to permit control of infiltration rate over the range typical of U.S. housing. A gas-fired hot-air heating-ventilation system that can accommodate potentially interesting air-cleaning devices is now being installed. The research house is being instrumented for automatic remote measurement of air exchange rate, radon concentration, individual daughter concentrations, temperature, and wind, as well as for measurement of particulate concentration, particle size distribution, and humidity. The instrumentation package will also permit study of air transport between rooms, using tracer-gas techniques.

The studies of radon and daughter behavior in this research house will serve as a basis for indoor radon modeling and for testing or evaluating control techniques. Although some of our effort in FY 1981 will be expended on such modeling and testing, more substantial resources must be devoted to acquiring an adequate understanding of the research areas listed above.

Finally, the radon research house, as well as other LBL facilities, will serve as sites for evaluating field monitoring instrumentation. During FY 1981, LBL will initiate a routine program of interlaboratory comparisons of radon monitoring instrumentation.

REFERENCES

1. J. V. Berk, M. L. Boegel, J. G. Ingersoll, W. W. Nazaroff, B. D. Stitt, and G. H. Zapalac, "Radon Measurements and Emanation Studies," Energy and Environment Division Annual Report, 1979 Lawrence Berkeley Laboratory report LBL-11650, December 1979.
2. J. G. Ingersoll, B. D. Stitt, and G. H. Zapalac, Method for Measuring the Exhalation of Radon from Building Materials, Lawrence Berkeley Laboratory report LBL-10631 (to be published in 1981).
3. J. G. Ingersoll, B. D. Stitt, and G. H. Zapalac, A Survey of Radionuclide Contents and Radon Emanation Rates in Building Materials Used in the United States, Lawrence Berkeley Laboratory report LBL-11771 (to be published in 1981).
4. G. H. Zapalac, A Time-Dependent Method for Measuring the Diffusion of Radon 222 in Concrete, Lawrence Berkeley Laboratory report LBL-11870 (to be published in 1981).
5. A. V. Nero, Airborne Radionuclides and Radiation in Buildings, chapter for report of the U.S. National Academy of Sciences Committee on Indoor Pollutants (to be published in Spring, 1981).
6. C. D. Hollowell, J. V. Berk, M. L. Boegel, J. G. Ingersoll, D. L. Krinkel, and W. W. Nazaroff, Radon in Energy-Efficient Houses, Lawrence Berkeley Laboratory report LBL-9560, March 1980.
7. K. D. Cliff, Assessment of Airborne Radon Daughter Concentrations in Dwellings in Great Britain, Physics in Medicine Biology, vol. 23, 1978, pp. 696-711,
8. W. W. Nazaroff, M. L. Boegel, C. D. Hollowell, and G. D. Roseme, The Use of Mechanical Ventilation with Heat Recovery for Controlling Radon and Radon-Daughter Concentrations, Lawrence Berkeley Laboratory report LBL-10222, March 1980, (to be published in Atmospheric Environment).
9. A. V. Nero, Indoor Radiation Exposures for Radon and Its Daughters: A View of the Issue, Lawrence Berkeley Laboratory report LBL-10525 (to be published in 1981).
10. W. W. Nazaroff, A Residential Radon Daughter Monitor Based on Alpha Spectroscopy, (M.S. thesis), Lawrence Berkeley Laboratory report LBL-10768, May 1980.
11. W. W. Nazaroff, A. V. Nero, and K. L. Revzan, Alpha Spectroscopic Techniques for Field Measurement of Radon Daughters, presented at the Second Special Symposium on Natural Radiation Environment, Bombay, India, Jan. 19-23, 1981 (proceedings to be published).
12. M. H. Sherman, D. T. Grimsrud, P. E. Condon, and B. V. Smith, Air Infiltration Measurement Techniques, Lawrence Berkeley Laboratory report LBL-10705, April 1980.

FIELD MONITORING OF INDOOR AIR QUALITY*

J. Berk, M. Breen, S. Brown, I. Ko, J. Koonce,
B. Loo, J. Pepper, A. Robb, P. Strong, I. Turiel, and R. Young

INTRODUCTION

One of the primary considerations involved in setting energy-efficient ventilation standards is their effect on indoor air quality. In support of the various laboratory research projects ongoing in the BVIAQ group, this project conducts on-site measurements of numerous parameters of indoor air quality in a variety of building types, including structures that have been weatherized and otherwise retrofit and new construction specifically designed for energy-efficient performance. By manipulating ventilation rates and measuring such comfort parameters as moisture, odor, and humidity as well as the levels of indoor-generated pollutants (see Table 1), we hope to ascertain what level of ventilation is required to assure a comfortable and safe indoor environment without compromising energy-conservation goals. It is important that any ventilation standards recommended on a wide scale differentiate the needs of various categories of buildings based on structural factors specific to the building, the source strengths of the indoor pollutants encountered, the relative hazards of the pollutants present, and the way the building is used by the occupants. (Schools and hospitals, for example, have different needs from those of residences, and occupant behavior and activity affects the air quality in houses.) Much of our work is accomplished in the Energy Efficient Buildings (EEB) Mobile Laboratory, an instrumented facility that can be stationed at a field site for extended periods of time. The capabilities of the mobile laboratory and the field sampling sites visited this year are described below.

EEB Mobile Laboratory

Since its construction in 1978, the EEB Mobile Laboratory has been used extensively in our field monitoring projects. As shown in Figure 1, the unit is positioned outside a building whose air quality is to be monitored. Air sampling lines are installed at several sites within the structure under study and terminate inside the laboratory where the air monitoring instrumentation is located. As a general practice, we sample the outdoor air in order to determine what fraction of the pollution indoors originates outside. For indoor sampling, we select three sites to account for the spatial distribution of pollutant sources and incomplete mixing of the interior air, both of which can cause variations in the pollutant concentration from one room to another. Air is sampled sequentially from these four locations with a microprocessor-controlled sampling and data logging system.

* This work was supported by the Assistant Secretary for Conservation and Solar Energy, Office of Buildings and Community Systems, Buildings Division of the U.S. Department of Energy under Contract No. W-7405-ENG-48.

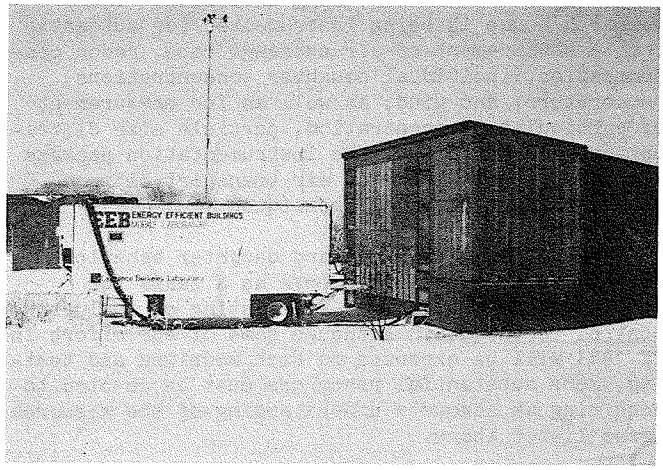

Fig. 1. The EEB Mobile Laboratory.
(CBB 806-7077)

The total exposure to occupants is determined not only by the respective pollutant concentrations in the rooms occupied, but also by the time spent in these rooms, for the concentration of any single pollutant may vary widely over the course of time. Figure 2 shows the concentration of nitrogen dioxide over a 24-hour period in the kitchen of a Wisconsin farmhouse. Nitrogen dioxide is a product of combustion; in this house, propane cooking, cigarette smoking and a woodburning stove constituted the combustion sources that we see reflected in the peaks.

Table 1 lists the various parameters that can be measured by the mobile laboratory, and the relevant method or instrumentation it uses. Most of the gaseous pollutants, as well as air exchange rates and comfort and meteorological parameters can be measured on a continuous basis, as indicated. Several of the pollutants, however, because of their physical and chemical properties or low concentrations, must be measured on a time-integrated basis. Often these measurements must be made directly at the sampling site rather than in the mobile laboratory. For example, radon measurements are made in the structure under study for a one-week period using a portable battery-operated device which records the alpha decays from decaying radon atoms.[1] Formaldehyde and total aldehydes are collected over periods up to 24 hours using temperature- and flow-controlled gas bubblers.[2] Other organic contaminants are collected over periods of hours using the porous polymer Tenax-GC as an adsorption medium. This collection system is still under development (see Organics). Inhalable particulates are divided according to size and collected on teflon filters, typically for 24-hour periods.[3] Most of these collection devices were

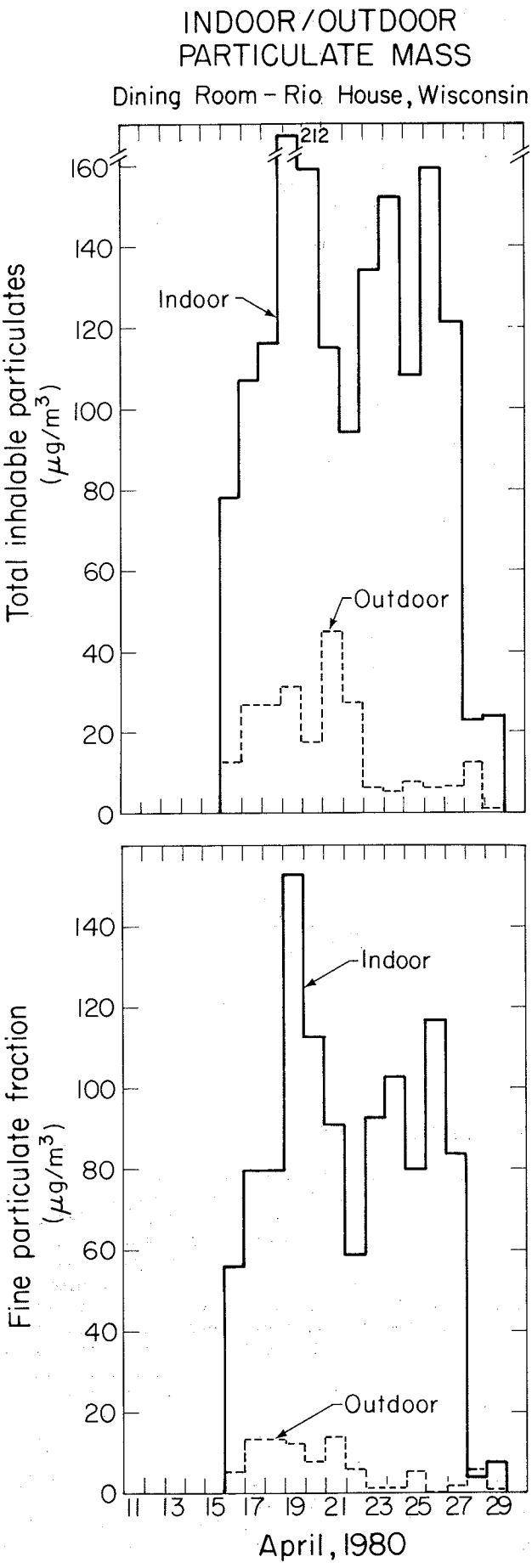

developed at LBL and all require subsequent laboratory analyses to determine composition and concentrations.

ACCOMPLISHMENTS DURING 1980

During the sampling year, which began in the summer of 1979 and continued into 1980, we used the EEB Mobile Laboratory to monitor the Minimum Energy Dwelling, MED-II, in Mission Viejo, California, the Oakland Gardens Elementary School in Bayside, New York, the Fridley Jr. High School in Fridley, Minnesota, two highly energy-efficient houses in Northfield, Minnesota and in Dundas, Minnesota, and a retrofitted residence in Rio, Wisconsin.

Oakland Gardens Elementary School

Air quality was monitored in two classrooms, a corridor, and outdoors for a period of seven weeks, and odors measurements (sensory perception, odor acceptability and chemical composition) were made by an LBL subcontractor, The Research Corporation of New England (TRC), for a two-week period. Ventilation of the classrooms was controlled by a system that exhausted air through ducts under negative pressure to exhaust fans located on the roof. Outdoor air entered through cracks around the windows. We restricted the exhaust flow by various means in order to monitor indoor air quality under different ventilation conditions. The three rates selected ranged from a high of approximately 14.8 m^3/h (8.8 cfm) per occupant to a low of approximately 4.4 m^3/h (2.9 cfm) per occupant, with one intermediate rate of approximately 8.2 m^3/h (4.9 cfm) per occupant.

In terms of pollutants, the only problems encountered were high levels of particulates in the hallway (but not in the individual classrooms) and an elevation in nitrogen dioxide levels (both indoors and outdoors) close to or slightly exceeding EPA ambient air quality standards. TRC findings showed a decrease in odor acceptability in one of the classrooms at the lowest ventilation rate. The small number of panelists used and the large uncertainty margin inherent in odor measurements make these data difficult to evaluate. We concluded that ventilation rates could be safely reduced to the intermediate level of 8.4 m^3/h (5 cfm) per occupant (one-half the level recommended by ASHRAE) without any adverse effects on health, safety, and comfort of the occupants.

Fridley Jr. High School

The study at Fridley Junior High School was a demonstration project jointly conducted by LBL and its subcontractor, Honeywell Inc. The purpose of this study was to determine the feasibility of operating a variable ventilation control system based on CO_2 levels which serve as an indication of

Fig. 2. Total inhalable particulate mass (<15 μ) and fine particle fraction (<2.5 μ) at a Wisconsin farmhouse. Occupants refrained from cigarette smoking for the final two days of the study. (XBL 808-1592)

Table 1. Instrumentation used in the EEB Mobile Laboratory.

Purpose	Method/Instrument	Manufacturer/Model
Continuous monitoring of the following parameters:		
Gases:		
CO_2	NDIR	Horiba PIR 2000
CO	NDIR	Bendix 8501-5CA
SO_2	UV fluorescence	Thermo Electron 43
NO, NO_x	Chemiluminescence	Thermo Electron 14D
O_3	UV absorption	Dasibi 1003-AH
Indoor temperature & moisture:		
Dry-bulb temperature	Thermistor	Yellow Springs 701
Relative humidity	Lithium chloride hygrometer	Yellow Springs 91 HC
Outdoor meteorology:		
Dry-bulb temperature	Thermistor	MRI 915-2
Relative humidity	Lithium chloride hygrometer	MRI 915-2
Wind speed	Generator	MRI 1074-2
Wind direction	Potentiometer	MRI 1074-2
Solar radiation	Spectral pyranometer	Eppley PSP
Infiltration	Automated controlled-flow measurement or tracer gas decay/IR absorption	LBL/Wilkes
Time-averaged monitoring of the following parameters:		
Gases:		
Radon	Electrostatic collection/ thermoluminescence	LBL
Formaldehyde/total aldehydes	Absorption (gas bubblers)/ colorimetry	LBL
Selected organic compounds	Tenax GC adsorption tubes/ GC analysis	LBL
Inhalable particulates (fine & coarse fractions)	Virtual impaction/ filtration	LBL
Data acquisition:		
	Microprocessor	Intel System 80/20-4
	Multiplexer A/D	Burr Brown Micromux Receiver MM6016 AA Remote MM6401
	Floppy disk drive	ICOM FD3712-56/20-19
	Modem	Vadic VA-317S

occupancy; that is changes in occupancy levels are reflected in fluctuations in carbon dioxide concentration which is monitored by a sensing device that, in turn, regulates the ventilation rate accordingly. Such a control system, because it responds to actual occupancy conditions rather than having an arbitrarily fixed rate, promises significant energy savings. The study was restricted to the music wing of the school which contained a band room, two chorus rooms, and many practice rooms. Outdoor air entered the rooms by natural infiltration and through the ventilation system's CO_2-controlled outside air damper. The operating set point at which the outside air damper began to open was set at 3,000 ppm; at 5,000 ppm, the lowest existing standard for CO_2 concentration, the damper opened fully. During the test period, the occupancy level was low enough that infiltration alone was sufficient to keep the CO_2 levels below 3,000 ppm; thus the energy savings were significant.

Energy Efficient Houses

Table 2 summarizes the indoor air quality data collected at five energy-efficient houses throughout the 1979-80 year. The house in Carroll County, Maryland was an energy-efficient research house which, in addition to other energy-conserving features, had a plastic vapor barrier to minimize infiltration; this house had electric appliances and was occupied by LBL field personnel during the sampling period. The house in Mission Viejo, California was built by a large home building company as a model home incorporating several energy-conserving features. It has natural gas appliances and was occupied by a family of three during the sampling period. Both houses in Minnesota were owner-designed and include many energy-conservation features. Because of the very low air exchange rates achieved in these latter houses, indoor moisture problems arose. To circumvent these and other

Table 2. Indoor air quality measurements in five energy-efficient occupied houses.

	Carroll County, Md.	Mission Viejo, Calif.	Northfield, Minn.		Dundas, Minn.		Rio, Wisc.
			HX off	HX on	HX off	HX on	
Infiltration rate (ach)	0.15[a]	0.4	0.1	0.3	0.1	0.3	0.3
CO (ppm)	1.2	1.4	0.5	0.4	0.7	0.4	2.2
CO_2 (ppm)	598	689	1175	722	1316	478	1125
NO_2 (ppb)	9	41	15	16	19	20	77
NO (ppb)	5	44	5	2	70	5	72
SO_2 (ppb)	3.2	0.9	1.0	1.7	---	---	9.0
O_3 (ppb)	4.3	15.6	1.7	1.7	9.0	9.3	15.0
Particulates--fine ($\mu g/m^3$)	7.8	32.6	6.8	6.8	19.5	8.0	92.4[b] 6.0[c]
Particulates--total ($\mu g/m^3$)	9.9	48.9	14.8	13.8	27.9	14.6	129.6[b] 23.5[c]
Formaldehyde (ppb)	98	214	69	73	80	64	53
Total aldehydes (ppb)	150	227	99	91	122	163	81

[a] All values represent average concentrations during the monitoring period.

[b] Smoking.

[c] No smoking.

possible indoor air quality problems, we recommended the installation of air-to-air heat exchangers in both houses, and air quality measurements were taken with and without the heat exchangers operating (0.3 and 0.1 air changes per hour, respectively). Both houses had electric cooking appliances. The Northfield house was occupied by a family of five and the Dundas house was occupied by a family of two. The Rio, Wisconsin farmhouse had been retrofitted (storm windows, weatherstripping, and a vapor barrier on the interior walls). It was occupied by a family of five, one of whom was a cigarette smoker, and propane cooking appliances were used. The house was heated with a woodburning stove which was located in the basement.

As indicated in the table, the infiltration rates in these houses is considerably less than the national average. No significant carbon monoxide problems were observed in any of the houses. (Such problems are usually associated with unvented or improperly tuned gas appliances or cracks in the heat exchanger surrounding the combustion chamber which can cause combustion gases to enter the ventilation system.) Carbon dioxide levels remained low and were expected to remain low unless a large number of people were present. In the two Minnesota houses where air-to-air heat exchangers had been installed in the basement, it is clear that these devices were effective in reducing the concentrations of pollutants originating in this area. The high levels of nitric oxide in the Dundas house before the heat exchanger was turned on were associated with the operation of a basement oil-burning furnace, and the dramatic reduction effected by the heat exchanger was because its exhaust inlet was adjacent to the furnace.

Very high levels of particulates were measured in the Rio, Wisconsin house. As is evident in Table 2 and in Figure 2 (which shows the levels of total inhalable and fine particulates measured for a two-week period in the dining room of this house) the difference in particulate levels between smoking and non-smoking periods is dramatic. Although this house differed from the others in using propane combustion appliances and a woodburning stove, the data clearly confirm that the significant rise in particulates was attributable to cigarette smoke.

PLANNED ACTIVITIES FOR 1981

In FY 1981, we will conduct intensive field monitoring at additional sites, as described below:

- Detailed indoor air quality measurements will be taken at two houses in Medford, Oregon that are being retrofitted as part of a weatherization program sponsored by the Pacific Power and Light Company, in an energy-efficient earth-sheltered house in Minnesota, and in a house undergoing extensive retrofit as part of the "house doctor" program conducted by Princeton University.
- Air leakage measurements will be taken in approximately six other houses involved in the PP&L weatherization program.
- Heat exchanger performance will be evaluated in several energy-efficient houses in Rochester, New York. Parameters to be tested are: their effectiveness in improving indoor air quality, their performance in cold weather, including potential freeze-up and leakage problems, and their cost-effectiveness in saving energy.

REFERENCES

1. M. L. Boegel, W. W. Nazaroff, and J. G. Ingersoll, Instructions for Operating LBL Passive Environmental Radon Monitor (PERM), Lawrence Berkeley Laboratory report LBID-073, 1979.
2. C. Lin, R. N. Anaclerio, D. W. Anthon, L. Z. Fanning, and C. D. Hollowell, Indoor/Outdoor Measurements of Formaldehyde and Total Aldehydes, Lawrence Berkeley report LBL-9397, 1979.
3. B. W. Loo, R. S. Adachi, C. P. Cork, F. S. Goulding, J. M. Jaklevic, D. A. Landis, and W. L. Searles, A Second Generation Dichotomous Sampler for Large-scale Monitoring of Airborne Particulate Matter, Lawrence Berkeley Laboratory report LBL-8725, 1979.

MECHANICAL VENTILATION SYSTEMS USING AIR-TO-AIR HEAT EXCHANGERS*

G. Roseme, W. Fisk, and F. Offerman

INTRODUCTION

One of the primary means of reducing energy consumption in buildings is to reduce infiltration, the uncontrolled leakage of air into and out of buildings. When the infiltration rate in houses is lowered through various weatherization measures, the levels of indoor-generated air pollutants (e.g., odors, chemical contaminants, moisture, formaldehyde, and radon gas) can build up and degrade indoor air quality. One possible method to resolve the problem without compromising energy efficiency is to use a mechanical ventilation system with an air-to-air heat exchanger. A research program to investigate the pollutant control capability and energy performance of these systems is underway at Lawrence Berkeley Laboratory.

The essential feature of the heat exchanger is that it brings the incoming and exhaust air into close proximity in its "core" where heat is exchanged between the two air streams. Such devices are commercially available in a number of different configurations. Figure 1 illustrates a fully ducted installation in the attic of a house, and Figure 2 depicts the principle of operation.

Three tasks have been delineated to accomplish the goals of this project:

1. Analytical and experimental (laboratory) evaluation of air-to-air heat exchanger performance;
2. Installation and testing of various heat exchanger/ventilation systems in occupied homes;
3. Economic analyses of heat exchanger/ventilation systems in different climate zones of the U.S.

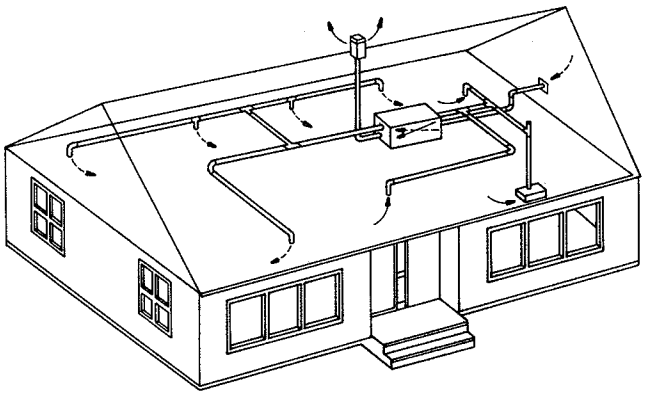

Fig. 1. Attic installation of a residential heat exchanger. (XBL 812-8054)

* The work was supported by the Assistant Secretary for Conservation and Solar Energy, Office of Buildings and Community Systems, Buildings Division of the U.S. Department of Energy under Contract No. W-7405-ENG-48.

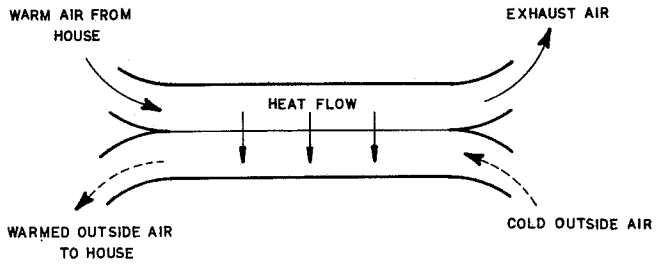

Fig. 2. Principle of thermal transfer in a heat exchanger. (XBL 813-8790)

ACCOMPLISHMENTS DURING FY 1980

Laboratory Testing

The experimental evaluation of air-to-air heat exchangers at our test facility was initiated early in 1980. Five commercially available residential size heat exchangers have been tested for thermal performance versus flow rate. In two of these heat exchangers, the performance of the fan system was also measured using a newly constructed Fan Performance Test System. The results of this testing program are detailed in an LBL report entitled The Performance of Residential Air-to-Air Heat Exchangers: Test Results and Methods.[1] Heat exchanger "effectiveness" is the ratio of actual heat transfer within a heat exchanger to the maximum level that is theoretically possible. Figure 3 is a graph showing the measured effectiveness versus flow rate for these heat exchangers.

Cross-leakage between the airstreams within a heat exchanger can affect both the thermal performance of the unit and its ability to remove indoor contaminants. A cross-leakage test system that uses a tracer gas to measure the rate of leakage between heat exchanger airstreams was constructed during 1980. Cross-leakage tests have been completed for two heat exchangers. One heat exchanger showed very high cross leakage rates (up to 30% of the airstream flow rates) when the airstream pressures were highly imbalanced. The leakage in the second heat exchanger was only a few percent of the airstream flow rates.

Field Testing

A field testing project to evaluate the use of mechanical ventilation with heat recovery for controlling indoor radon and formaldehyde concentrations was conducted by LBL with the National Association of Home Builders Research Foundation Inc., and Geomet Corporation as subcontractors. For this study, two air-to-air heat exchangers were installed in a home built by the Home Builders Association that had elevated indoor concentrations of radon and formaldehyde. Formaldehyde and radon concentrations versus ventilation rate were measured for a two-week period. The natural infiltra-

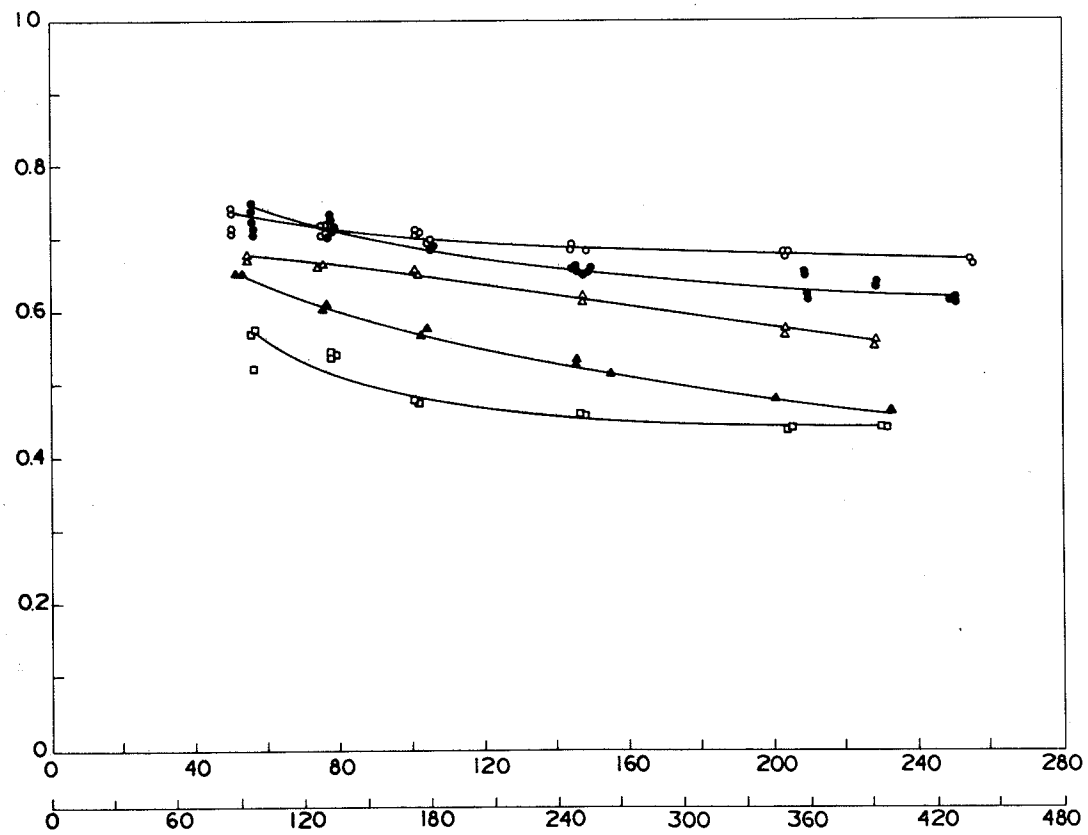

Fig. 3. Effectiveness versus flow rate for five models of residential air-to-air heat exchangers. (XBL 8011-12106)

tion rate of the home with the doors and windows closed was found to vary between 0.1 and 0.25 air changes per hour (ach) depending on outside weather conditions. When the air exchange rate was increased to 0.6 ach by mechanical ventilation, the radon concentrations in the home were reduced from very high levels to a level below EPA guidelines (established for homes built in Florida on land reclaimed from phosphate mining). The findings from this study are detailed in an LBL report entitled The Use of Mechanical Ventilation with Heat Recovery for Controlling Radon and Radon Daughter Concentrations.[2]

Another field study initiated this year is a joint project with the New York State Energy Research and Development Administration, Rochester Gas and Electric Company and the Rochester Institute of Technology. Thus far, approximately 60 homes built by two commercial builders in the Rochester area have been tested for air-tightness using a blower door designed by LBL. We have selected nine of these homes for a study of indoor air quality, and the energy efficiency and pollutant reduction capability of mechanical ventilation systems with heat exchangers. In seven of the homes, a small computer-controlled ventilation monitoring system, called the AARDVARK, will be used. Figure 4 is a photograph of the AARDVARK, which measures average ventilation rate every 1.5 hours and average radon concentration every three hours. The AARDVARK, pictured in Figure 4, also monitors the furnace on and off times; these data will be used to determine the energy consumed by the home heating system. In addition, the system monitors the thermostat setting, the outside temperature,

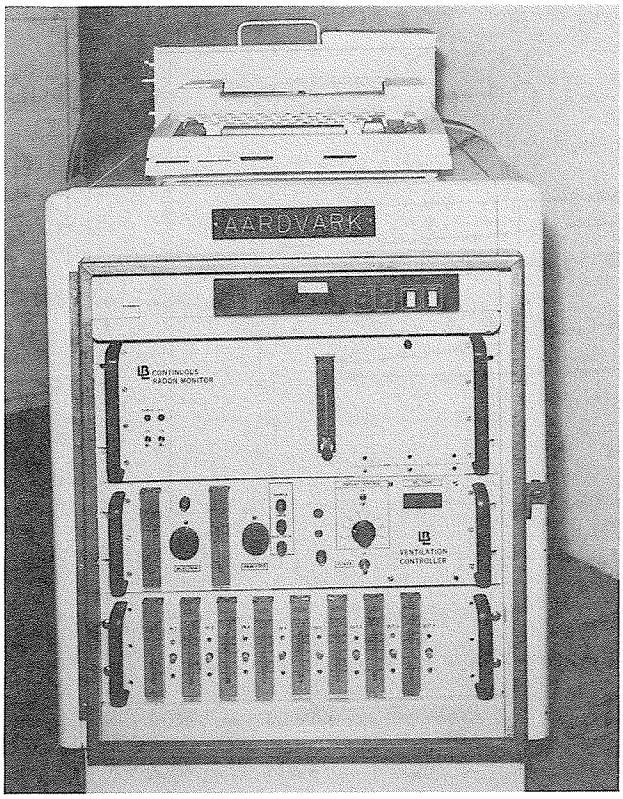

Fig. 4. AARDVARK--automatic infiltration and radon monitor. (BBC 800-12102)

the four temperatures at the inlets and outlets of the heat exchanger, and one other interior temperature. Studies will be conducted in each home for one week without mechanical ventilation and one week with mechanical ventilation. Average daily formaldehyde concentration and average weekly nitrogen dioxide concentration are also being measured in these homes. In the remaining two homes in the study, indoor pollutant levels and ventilation rate will be measured by the EEB Mobile Laboratory (see Field Monitoring).

Economic Analyses

An economic analysis of the residential use of mechanical ventilation systems with heat exchangers was made in FY 1980 and is presented in an LBL report entitled Residential Ventilation with Heat Recovery: Improving Indoor Air Quality and Saving Energy.[3] The analysis indicates that these systems can be cost-effective in most geographical areas of the country if the initial cost of the heat exchanger including installation is in the range of approximately $400 to $500. In cold climates, a higher initial cost remains cost-effective.

PLANNED ACTIVITIES FOR FY 1981

In addition to the continuing field program in Rochester N.Y., field studies of installed air-to-air heat exchangers will be undertaken in central Washington state (in a joint project with Bonneville Power Administration) and in Minneapolis, Minnesota. In the Washington project, six occupied homes will receive a one-day "house doctor" retrofit and an additional six will receive two-day "super retrofits" to reduce air infiltration. Heat exchangers will be installed in each of the twelve homes. Indoor air quality measurements will be made prior to the retrofit and after retrofit, with and without the heat exchanger operating. The focus of the Minneapolis study, which involves only one home, is to assess the performance of a heat exchanger in a cold climate. Heat exchanger effectiveness and airstream flow rates will be monitored, and visual inspections will be made for freezing within the heat exchanger core. The data obtained from the field studies and laboratory tests will be used to reassess the economics of employing air-to-air heat exchangers in homes.

REFERENCES

1. W. J. Fisk, G. D. Roseme, and C. D. Hollowell, Performance of Residential Air-to-Air Heat Exchangers: Test Results and Methods, Lawrence Berkeley Laboratory report LBL-11993, September 1980.

2. W. W. Nazaroff, M. L. Boegel, C. D. Hollowell, and G. D. Roseme, The Use of Mechanical Ventilation with Heat Recovery for Controlling Radon and Radon-Daughter Concentrations, Lawrence Berkeley Laboratory report LBL-10222, March 1980.

3. G. D. Roseme, J. V. Berk, M. L. Boegel, H. I. Halsey, C. D. Hollowell, A. H. Rosenfeld, I. Turiel, Residential Ventilation with Heat Recovery: Improving Indoor Air Quality and Saving Energy, Lawrence Berkeley Laboratory report LBL-9749, May 1980.

ENERGY-EFFICIENT WINDOWS PROGRAM*

S. Selkowitz, S. Berman, R. Johnson,
J. Klems, C. Lampert, M. Rubin, and R. Verderber

INTRODUCTION

Approximately 20% of the annual energy consumption in the United States is used for space conditioning of residential and commercial buildings, and about 25% of that figure is required to offset heat loss and heat gain through windows. In other words, 5% of our national energy consumption, 3.5 quads annually, or the equivalent of 1.7 million barrels of oil per day, is tied to the thermal performance of windows.

An important aim of the Windows and Daylighting Program is to develop a sound technical base for predicting the net energy performance of windows and skylights, including both their thermal and daylighting aspects. This capability will be used to generate guidelines for optimal design and retrofit strategies in residential and commercial buildings, and to assist development of effective new materials and designs. Of critical importance to our program is that both design professionals and the public recognize, accept, and use this information. To that purpose we have implemented a broadly based program that encompasses research and development projects, field demonstrations, market studies, and information dissemination activities. While most of the program is conducted at LBL, portions are performed under subcontract, with LBL maintaining technical management responsibility.

ACCOMPLISHMENTS DURING FY 1980

Our work is organized into four major areas: (1) Window Performance: Analysis and Testing; (2) Fenestration Systems: Research, Development, and Demonstration; (3) Daylighting; and (4) Program Planning and Support.

Window Performance: Analysis and Testing

Analytical Modeling

The ability to accurately model all aspects of the energy-related performance of windows is a prerequisite to optimizing energy-efficient design strategies and product selection. Analytical models are required at several performance levels: for component materials and assemblies, for isolated window systems, and for windows or skylights studied in the context of a surrounding building. In addition, while some models are needed to predict single performance variables such as conductance, air leakage, or solar transmittance, the primary goal is to create models that predict net energy performance over time.

A number of improvements have been made to our window heat-transfer program, THERM. It can model a window that is composed of an arbitrary number of layers, such as glass panes or plastic films. The effects of plastic substrates that are semi-transparent to long-wave infrared radiation can now be properly modeled. Any layer may have a thin-film coating (heat mirror, solar-control film, optical shutter, anti-reflection coating), and the space between may contain a gas having a low thermal conductance. Extensive parametric studies of heat-transfer rates of windows having transparent heat mirrors and gas fills were performed this year. Figure 1 shows the effects of heat-mirror coating position and emissivity on the overall thermal conductance of single, double, and triple glazing. A significant new result from these studies was the discovery that if a plastic film coated with a heat mirror is mounted in the air space of a double-glazed window, asymmetric mounting of the plastic film provides lower heat-transfer rates than does a film located in the center. The effect is most significant for small air spaces.

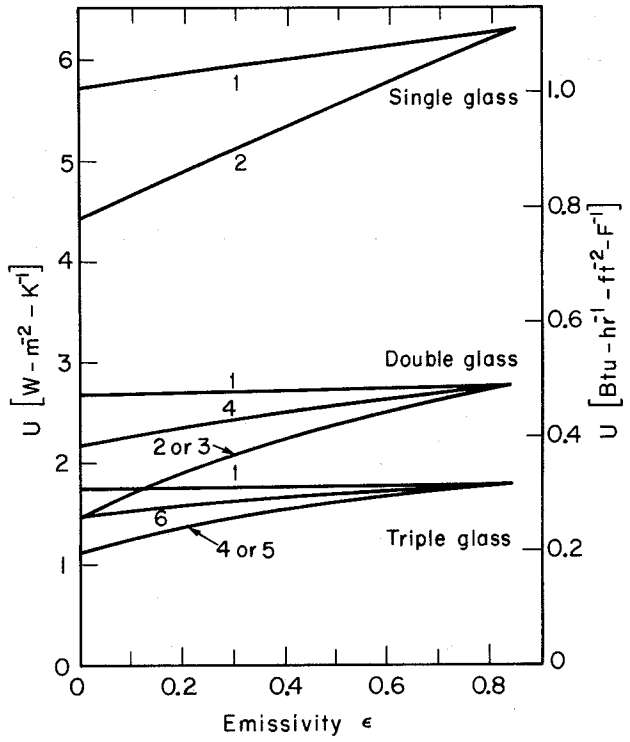

Fig. 1. U-value vs. emissivity for single, double, and triple glazing with low-emissivity coatings on several different surfaces. Surfaces are numbered consecutively starting from the outside surface. (XBL 807-3489)

* This work was supported by the Assistant Secretary for Conservation and Solar Energy, Office of Buildings and Community Systems, Buildings Division of the U.S. Department of Energy under Contract No. W-7405-ENG-48.

The detailed window model may be coupled with another newly developed program that simulates hour-by-hour weather conditions in a given city and employs a simplified thermal model of the building. With this program, the yearly energy loss or gain attributable to the glazed area can be predicted. This program has been tested with ordinary multiple-pane glass windows and with windows that incorporate heat mirrors.

New algorithms and data were developed this year to expand the capabilities of the DOE-2 Building Energy Analysis program. The public-domain version was modified to allow use of triple glazing with clear or with heat-absorbing glass types. Other energy-conserving windows, such as heat mirrors, solar-control films, and gas fills, are being added to our development version of DOE-2. A standard set of input data has been compiled to test the sensitivity of window energy consumption to climatic factors and building construction. These results will allow us to make specific recommendations about the use of new energy-efficient window designs for residential and commercial buildings in different parts of the country.

A study of the effect of movable insulation on heating loads in a residence in Minneapolis was extended to include results of changes in the standard house operating schedule and the incorporation of new sun-control options for three diverse climates. The trends and patterns observed were similar to the Minnesota case, although the magnitude of the savings was greatly reduced. These results further reinforce the finding that insulating options beyond R5 offer only marginal improvements in most cases. Preliminary studies of fixed and operable shading devices and daylighting strategies in commercial buildings were also undertaken.

Parametric studies of the type described above are important for helping specifiers and producers of products choose from a bewildering array of new products. In September 1980 we published an updated listing of commercially available window-insulating products. The list nearly doubled during a nine-month period and continues to grow. For each product, it includes calculated and measured thermal-performance data in a consistent format to assist building designers in making intelligent decisions regarding window-insulating products.

Performance Testing

In 1977, we established a Building Technology Laboratory in the College of Environmental Design of the University of California, Berkeley, to support our research and development activities, to provide independent testing and evaluation of materials and products submitted by subcontractors, and to permit evaluation of new products being introduced to the market. Testing facilities include a calibrated hotbox (shown in Figure 2), which is now being used to test the thermal performance of windows and associated energy-conserving accessories. A sample of devices now on the market or prototypes of devices soon to be on the market was tested to establish a baseline against which future improvements in window performance can be compared. Sample results are shown in Figure 3.

The heat-loss and heat-gain rates of windows can be improved with the use of thin-film coatings on glazing materials. To fully characterize glazing material performance, we have added capabilities for measuring a range of optical properties of glazing materials and coatings. Infiltration tests on windows are also being made in our laboratory.

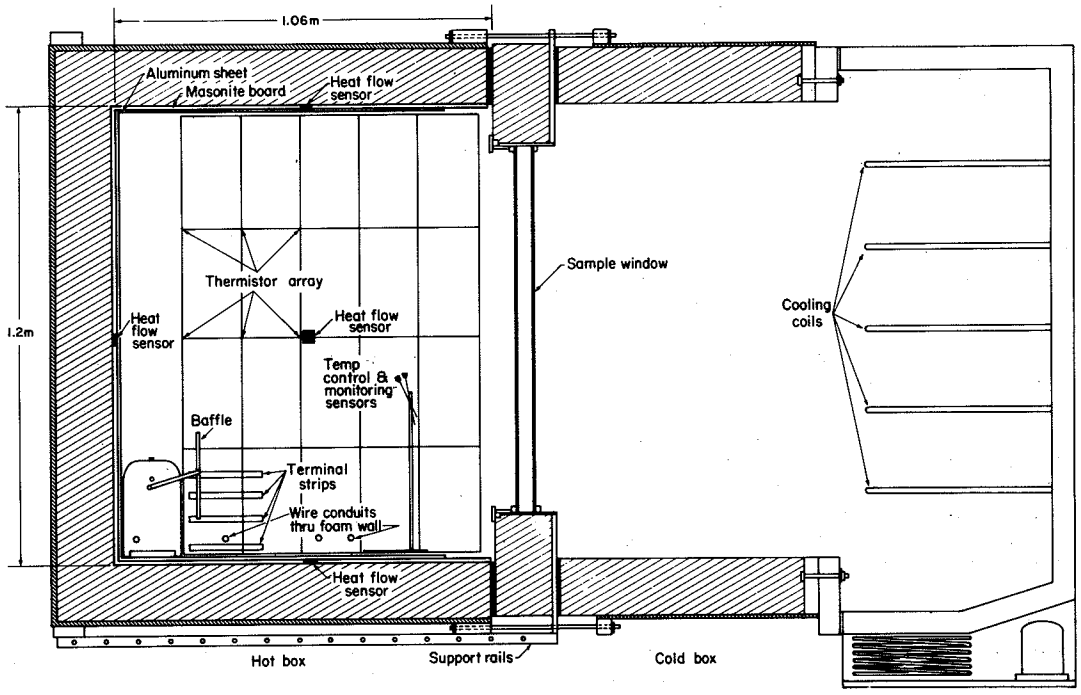

Fig. 2. Section through calibrated hotbox showing hot and cold box chambers and sample window. (XBL 799-2921A)

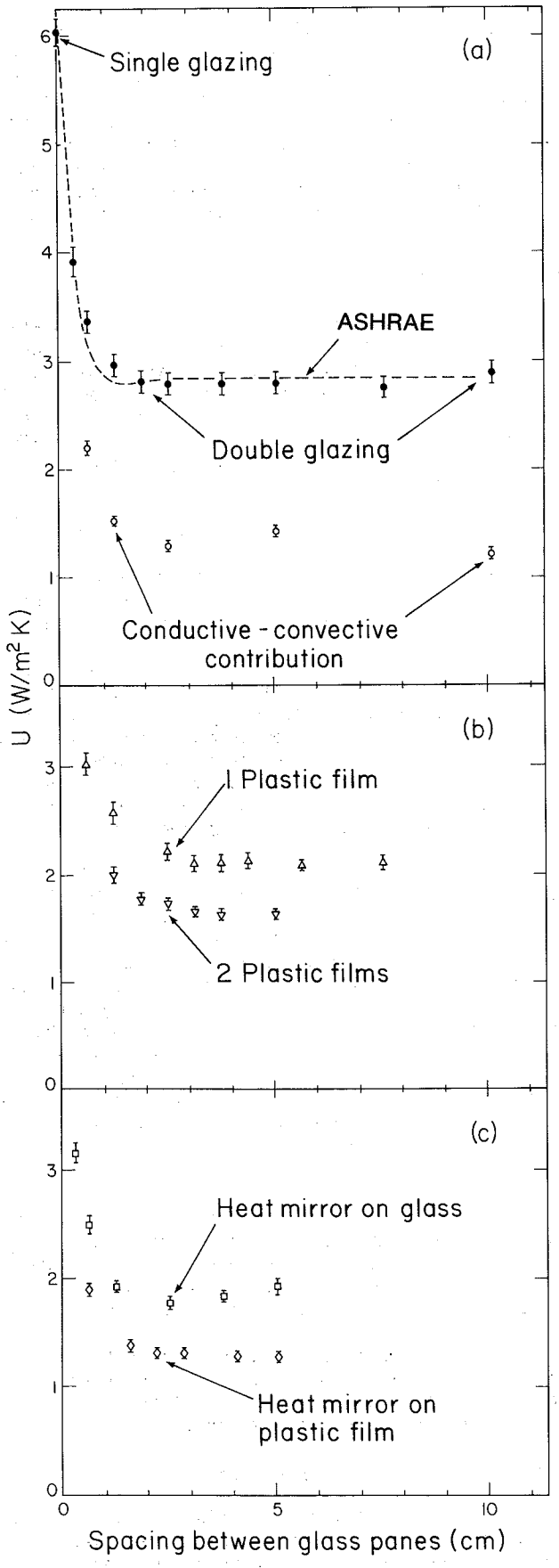

The single piece of information most relevant to assessing the benefit to be derived from a window or window improvement is its net energy performance under actual conditions of use in buildings. This is a dynamic property, essential for predicting the performance of managed window systems (i.e., windows that have thermal/optical properties that can be manually or automatically changed by building occupants). The laboratory testing facilities described above, however, are designed primarily to conduct steady-state measurements of static materials and devices. No experimental methodology currently exists for measuring the net performance of windows in situ. Accordingly, in 1980 we continued design studies on our Mobile Window Thermal Test (MoWiTT) facility, being developed to permit the study of combined solar, infiltrative, conductive/convective, and radiative heat transfers through a window as a function of window type and orientation and changing weather conditions throughout the day (see Figure 4). Design, scheduling, and cost estimates for the MoWiTT facility have been completed, and construction is planned for 1981. Development of software for its control and data-acquisition systems is in progress. The thermal properties of each of the four test chambers in the MoWiTT facility can be altered by varying wall insulation level, thermal mass, and air-leakage rate, thus allowing us to simulate a wide range of building conditions. Winter testing will be conducted in a cold, mountainous location and summer testing in a near-desert area. From these experimental results, we will be able to validate or modify our analytical models and to rank the performances of various window-management strategies.

An outgrowth of work on the MoWiTT facility has been the development of a new heat-flow meter concept. Instead of the usual method of measuring the temperature difference across a known thermal resistance using a deposited thermopile, this heat-flow meter uses resistance thermometry to measure the temperature difference (see Figure 5).

This innovation has produced a heat-flow meter that is more sensitive than the commercial variety and one that can be made economically in sizes large enough to cover entire walls. This heat-flow meter will be an integral part of the MoWiTT facility.

Fig. 3. Sample thermal transmittance vs. glass spacing for prototype windows. [a]Ordinary double glazing (solid points) and double glazing with aluminum foil on inside of both glass panes (open circles). [b]Double glazing with one (triangles) or two (inverted triangles) plastic films. [c]Double glazing with heat-mirror coating on plastic film, where the plastic film is mounted on the surface of one glass pane (squares) or suspended between panes (diamonds). (XBL 799-2917A)

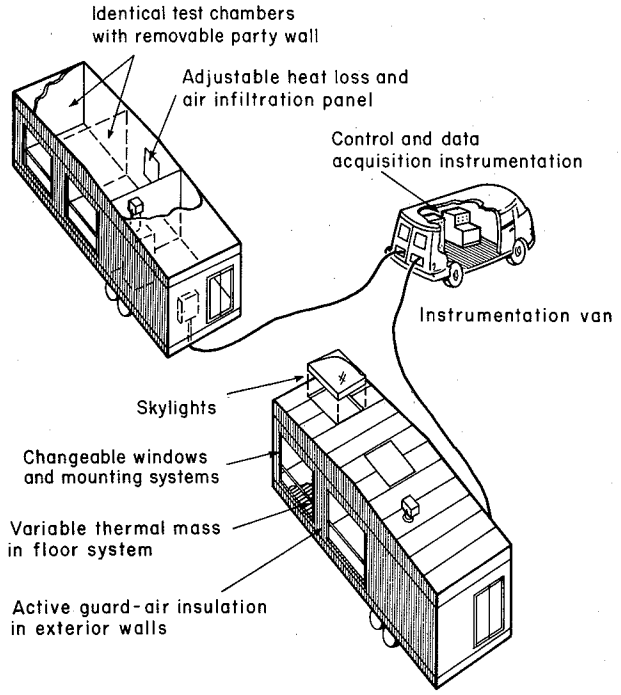

Fig. 4. Schematic view of Mobile Window Thermal Test (MoWiTT) facility. (XBL 811-30)

Fenestration Systems: Research, Development, and Demonstration

To provide real energy savings, window innovations developed by inventors in both the private and public sectors must find their way to the market and then to building installations in significant numbers. The transition from laboratory prototype to local building supply store is not a simple one. A variety of activities are needed to help establish the energy-saving potentials of new and existing window products. Demonstrations and field tests of products frequently lead us back to the laboratory to re-investigate thermal performance characteristics and the properties and durabilities of various materials. Several demonstration projects undertaken this year are described below.

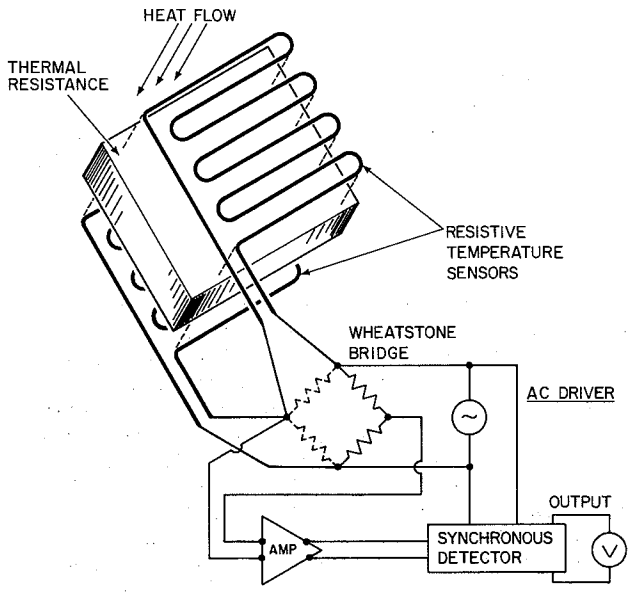

Fig. 5. Schematic view of heat-flow meter design based upon resistance thermometry. (XBL 8011-2627)

Transparent Heat Mirrors

A transparent heat mirror is an optical coating that is applied to a glass or plastic glazing material to transmit the full solar spectrum and reflect long-wave infrared radiation emitted by room temperature surfaces. By reducing the radiative component of thermal losses, the heat-transfer coefficient of a single- or double-glazed window is greatly reduced.

In prior years our program has supported several heat-mirror development projects. Several potential manufacturers are now at the point of introducing heat mirrors on both glass and plastic substrates. The coated-plastic substrate would be incorporated into a window unit either by being glued to glass or by being stretched across the air space in a double-glazed unit, creating an additional air space and, thus, even better insulating values. In 1980 several new computer programs were developed at LBL to provide thermal performance values for many different window configurations that incorporate heat-mirror coatings (see Window Performance: Analysis and Testing section).

For both the manufacturer and the ultimate buyer, the durability of heat-mirror coatings is an essential attribute. Poor resistance to corrosive and abrasive forces characterized many of the coatings first developed and still remains a significant obstacle to widespread and rapid commercialization. In 1980 we examined some of the generic failure mechanisms of coatings by means of sophisticated coating analysis equipment available at LBL, by visual inspections of the coating structure using a scanning electron microscope, and by chemical analysis of corrosion sites. A typical result from the scanning electron microscope is shown in Figure 6.

To prove to the architectural and engineering community that heat-mirror coatings will save energy without creating adverse effects, we conduct and support demonstrations of windows incorporating heat mirrors in new and existing buildings. In 1980 we identified and specified windows incorporating appropriate heat-mirror coatings for several demonstration projects. We expect to expand this type of activity in 1981 and to assist in analyzing and interpreting results.

High-Performance Sun-Control Systems

Although conventional Venetian blinds are reasonably successful in reducing solar heat gain through windows, their performance could be improved considerably. Stevens Institute of Technology, Hoboken (NJ), completed an experimental program to determine the shading coefficients of

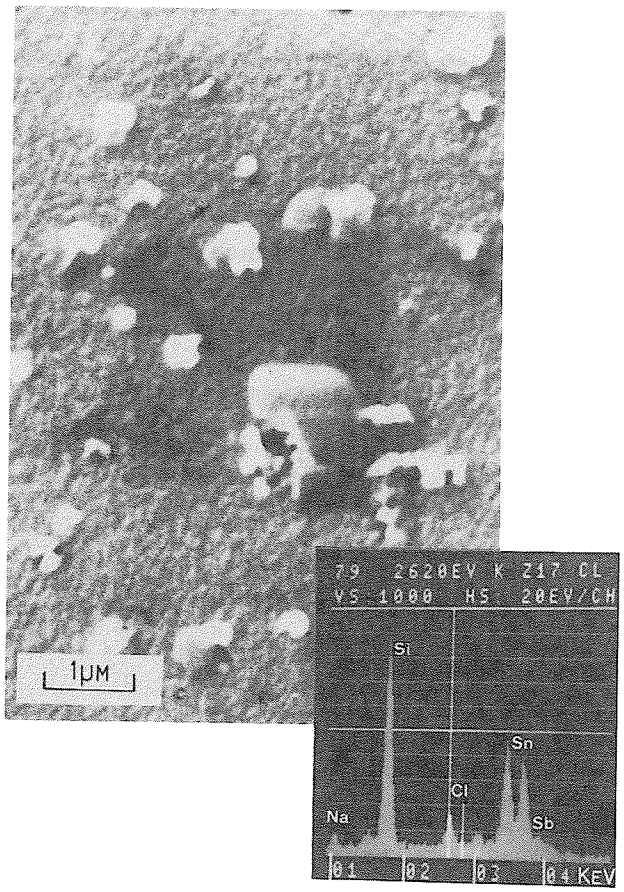

Fig. 6. Scanning electron micrograph of a degraded SnO_2:Sb heat-mirror on window glass. EDAX analysis revealed that surface particles were high in sodium and chlorine. This salt formation can be traced back to diffusive chemical reactions during deposition. (XBB 801-544)

many different types of venetian blinds using an indoor hotbox with an artifical sun. Results of extensive testing were used to generate tables that give the shading coefficients for various combinations of slat tilt, reflectivity, and solar-incidence angle. Although it was expected that some of the blinds with highly reflective surfaces would have shading coefficients as low as 0.2, none having shading coefficients below 0.4 were measured. Newer blinds having experimental coatings are expected to meet the lower value.

Optical Shutter Materials

Thin-film coatings having sun-control properties that can be changed by sunlight, temperature, or an applied voltage represent a long-term development goal of our program. In 1980 we completed an extensive literature search and review of electrochromic materials that might have potential as optical shutters for windows.

Movable Insulation Systems

Movable window insulating systems have attracted much interest, but there is uncertainty surrounding the real savings that can be achieved through their use. One such device, developed by the Insulating Shade Company of Branford (CT), consists of multiple layers of aluminized plastic that separate when the shade is pulled down. The air spaces thereby created are bounded by reflective surfaces, which create a high thermal resistance. Two hundred of the shades were installed in a university dormitory. Building energy consumption was monitored and occupant use patterns studied. Test results demonstrate that, properly managed, movable window insulation reduces building energy consumption. A detailed technical report will be issued on our results.

Selective-Reflectance Coatings

Reflective and/or tinted glass is widely used in many commercial buildings to reduce solar impact and, thus, the energy required for air conditioning. This glazing, however, also reduces the amount of daylight entering interior spaces and thus potentially increases the use of electric lighting. An optical coating that selectively reflects short-wave infrared rays (which account for approximately one-half of the sun's radiation) but transmits visible light could, ideally, reduce cooling loads by 50% without reducing available illumination. Under subcontract, Kinetic Coatings, Inc. of Burlington (MA), has used novel ion-beam sputtering techniques to produce such a coating that is durable and weather-resistant and can be applied to the outside of a window.

Now in the last phase of their subcontract program, Kinetic Coatings has demonstrated that coatings of high quality and good uniformity can be deposited on a thin plastic substrate in a roll-coating process. Coatings tailored to four building applications (residential, new and retrofit; commercial, new and retrofit) were produced and tested in 1980.

As noted earlier, durability of window coatings is a critical issue, for coated plastic glued directly to existing windows must withstand UV exposure, thermal cycling, abrasion, atmospheric pollutants, and cleaning agents. In previous years a wide range of selective-reflectance coatings and protective layers were produced and tested for both optical performance and weatherability. Multilayer metal-dielectric coatings deposited on polyester and polypropylene substrates have shown excellent durability in exposure tests conducted to date.

Because coating durability has been the key uncertainty restricting the development of successful energy-conserving products, we developed a materials science analysis and test capability in 1980. We can now examine the physical structure of coated samples by transmission and scanning electron microscopic techniques, and analyze the chemical composition of film defects by auger spectroscopy and EDAX techniques. Figure 7 shows the type of data generated by this analysis.

Air-Flow Window Systems

Another category of high-performance window systems are those known as air-flow windows. In these systems a stream of air flowing between the

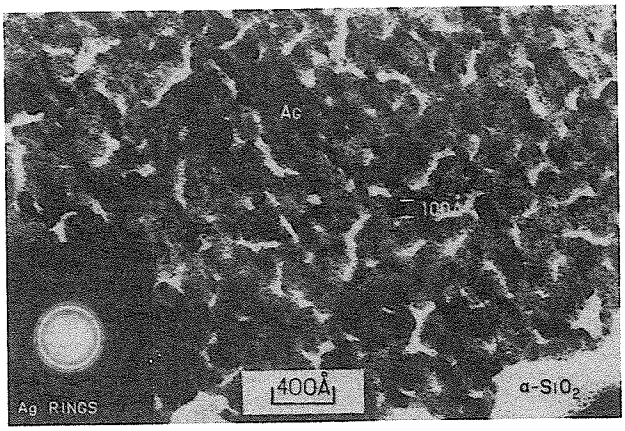

Fig. 7. Transmission electron micrograph (bright field at 100 kv) of an Si_2O_2/Ag heat mirror. The polyester substrate was removed for this investigation. Diffraction information reveals very fine silver crystallites along with amorphous SiO_2. (XBB 801-543)

panes of multiple-glazed windows acts as a heat-transfer fluid. Solar gain can be either collected or rejected as required, and daylighting can be fully utilized throughout the year. A design approach that has been used in Europe for many years involves integrating the window into the heating, ventilating, and air-conditioning (HVAC) system and exhausting room air through the glazing cavity. Venetian blinds in the glazing cavity can be adjusted to allow optimum daylight penetration, to control the glare of direct sunlight, and to function as solar absorbers. By means of the air flow, solar gain is either rejected to the outside or distributed through the HVAC system as required (Fig. 8).

Under subcontract, windows from two manufacturers, one domestic and one European, were tested during 1980 in a full-size test building at the University of Utah. Each window was tested separately and in side-by-side comparison with a high-quality conventional window. Performance data were taken during the full range of local weather conditions. These data are presently being analyzed.

Although the first cost for such windows is higher than for conventional windows, the prospect for widespread commercialization is attractive. The window package fits within currently accepted architectural vocabulary, utilizes conventional components having well established reliability, and offers multifunctional control of energy performance.

Another approach being investigated is one developed at the Environmental Research Laboratory (ERL) of the University of Arizona. Their window system, designed primarily for residential application, combines existing commercially available components to achieve control of energy flows, and relies on gravity-induced draft for heating, and on overpressurization of the building by an evaporative cooler for cooling. ERL has completed summer

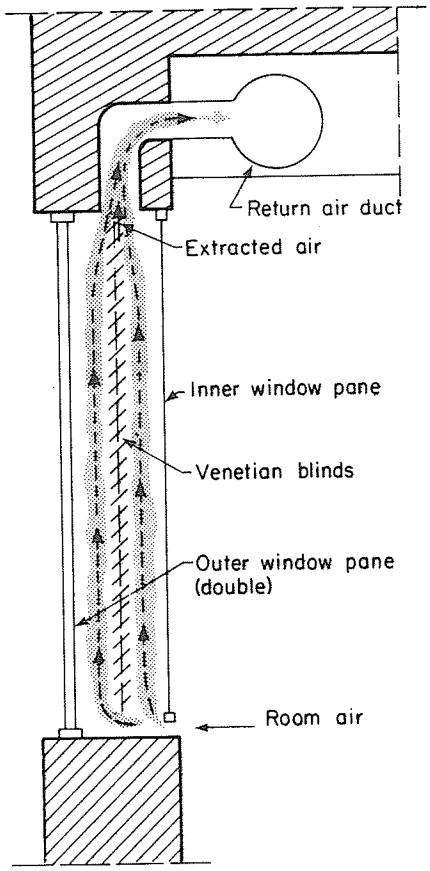

Fig. 8. Schematic cross-sections for air-flow window system. (XBL 7912-13366)

and winter testing and has written computer simulation codes. The computer codes have been validated against the test data. Performance data are being correlated with ASHRAE solar heat-gain tables in order to provide a design tool having widespread applicability.

Preliminary results of performance tests on these air-flow windows are promising. Industry interest has been growing because of the multifunction control options, and it is expected that U.S.-made units will be commercially available in 1981.

Daylighting

Windows and skylights provide daylight in buildings, thus reducing both electric lighting use and peak-power requirements. In addition, because natural lighting has always been valued by architects and building occupants, daylighting studies represent an area where good architectural design and significant energy savings are mutually supportive goals.

Studies of potential annual energy savings from maximum use of daylight in buildings require data on daylight availability (including the frequency and intensity of daylight). No source for such data currently exists for most of the United States. In 1979 the Pacific Gas & Electric Company

building in San Francisco was instrumented to collect and record the amount of solar and visible radiation available at all building surfaces. An array of thirteen pyranometers and photometers was installed to feed readings to a data-acquisition system at fifteen-minute intervals (see Figure 9). Preliminary results from the first year of monitoring suggest strong linear correlations between illumination and insolation -- a finding that encourages us to believe that daylight availability data can be generated from existing measurements of solar radiation. Figure 10 illustrates one technique for analyzing and displaying the data. Daylight illumination on a vertical east-facing surface is shown as a set of contour lines for all hours of the day throughout the year. A generalized method for developing illumination availability data from insolation is now being developed based upon data collected in 1979 and 1980.

Accurate and efficient daylighting design methods must be conveyed to building designers if they are to successfully incorporate daylighting designs in buildings. Several approaches are in progress as part of the overall LBL program in this area: Under subcontract, Renssallear Polytechnic Institute in New York began development in 1979 of a computer program to predict daylight illumination in interior spaces. A working version of the program that can compute illumination for non-rectangular geometries and can treat several types of window-shading devices was completed in 1980. Additional modeling capabilities are now being added. A team at the University of Washington has developed a graphic design method that employs transparent overlays for daylight predictions. This method, meant to be used by architects at an early stage in the design process, was tested before an audience of professional designers in 1980. Several parallel modeling efforts were completed at LBL. A technique for predicting daylight

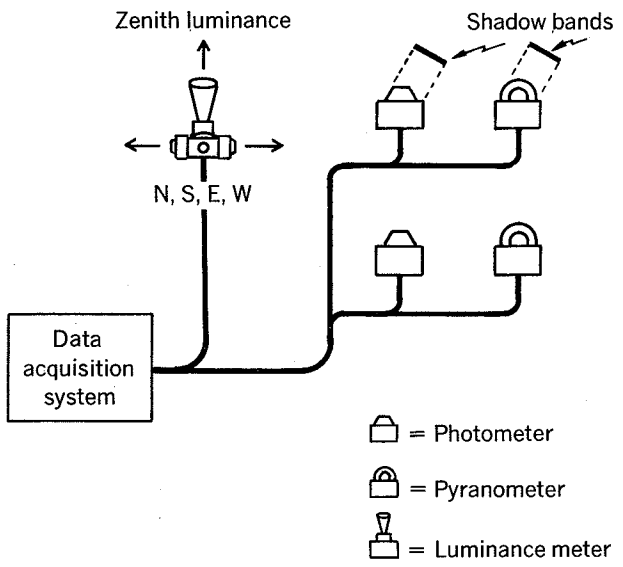

Fig. 9. Schematic of photometric and radiosensor array on rooftop for determining insolation/illumination correlations.
(XBL 796-10182)

illumination from clear and overcast skies was completed in 1979, and, while relatively accurate, it requires repetitive calculations. In 1980 this model was adapted for use with a programmable hand calculator.

An effort to incorporate daylighting analysis capabilities into a building energy analysis program (DOE-2) continued in 1980. Although the ultimate goal is to incorporate a daylighting algorithm within DOE-2, a simplified approach was developed and completed in 1980. The program calculates the average hourly effect that daylight will have on building lighting schedules. Results are presented in the form of extensive tables that become input parameters for DOE-2.

The 24-foot-diameter artificial sky dome, designed and built on the U.C. campus in 1979 to facilitate model studies for daylighting, became operational in 1980 with the simulation of luminance distributions for an overcast sky. We are now installing improved lighting controls in the dome in order to simulate luminance distributions for clear skies. Sky luminance distributions are reproduced on the underside of the hemisphere; light levels are then measured in a scale-model building under the artificial sky. From these measurements, we will be able to predict daylighting illumination patterns in real buildings. The artificial sky already has been used for research and teaching purposes, as well as by architects working on daylighting features for new office buildings (Fig. 11).

To test the combined effects of sky and direct sun, without collimation or horizon errors, four scale models, 3 feet by 5 feet each, were fabricated and mounted on the roof of our building. These test cells incorporate a tilting base so that the sun's incident angle can be varied over a wide range.

Although direct energy savings from daylighting are the main interest of building owners, significant potential savings might also accrue from savings on peak-power demands. For example, a computer simulation study of energy/peak power relationships in a 31-story office building was undertaken in 1980 for two climate conditions. Preliminary results indicate that savings on the cost of time-of-day utility pricing as well as peak-demand charges can equal or exceed the direct energy savings from daylighting in some buildings. This finding suggests that the economic benefits to building owners of employing daylighting strategies can be even greater than those predicted from an analysis of direct energy savings. Such peak-power reductions, if properly utilized by utilities, might also assist their own management efforts.

Because direct sunlight is the only natural light source having sufficient intensity and collimation to illuminate interior spaces deep in a building, various design approaches have been studied to exploit beam daylighting in buildings. During the past four years we have examined the feasibility of mounting reflective and refractive devices in windows to take advantage of direct sunlight. Limited computer simulation and model studies have been conducted; however, additional study

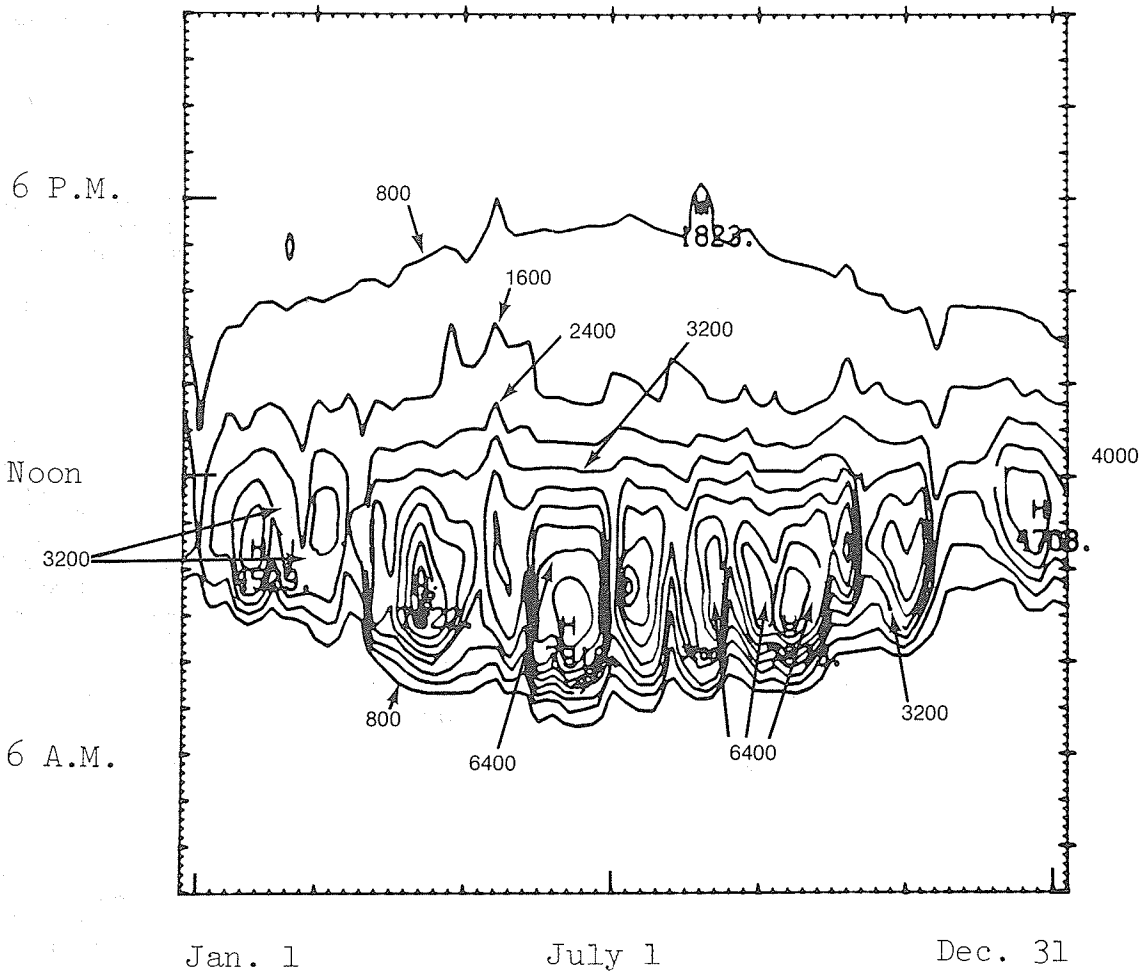

Fig. 10. Vertical illuminance on an east-facing surface as measured during 1979 at the PG&E building in San Francisco. Interval between contour lines is 800 footcandles. (XBL 813-8789)

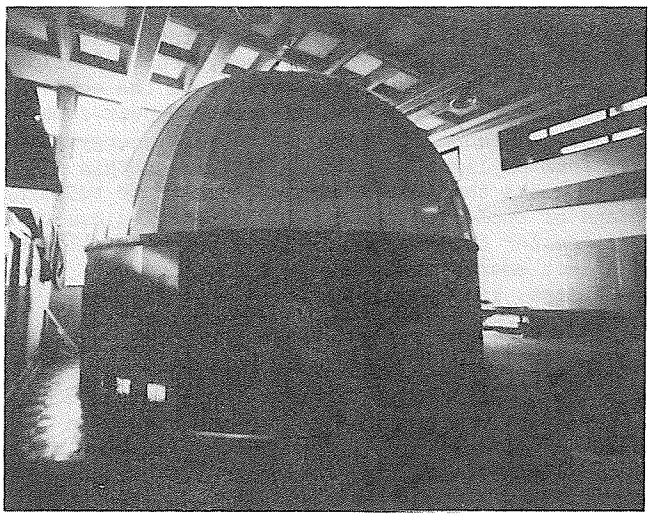

Fig. 11. Exterior view of 24-foot-diameter hemispherical sky simulator for daylighting studies. (CBB 803-2837)

is needed if we are to validate their technical feasibility and cost-effectiveness.

Out of our belief that daylighting techniques would be more widely used by architects and builders if technically accurate information was more accessible to them, we have collaborated with the U.C. College of Environmental Design to develop a comprehensive educational program on daylighting. A draft of our Daylighting Resource Package, aimed at educators and building designers and prepared in collaboration with the Illuminating Engineering Society, several universities, and daylighting experts throughout the country, has been produced. The first draft was discussed in June 1980 at a week-long workshop in Berkeley attended by 35 university educators and 15 other experts and observers. During the next two years, the resource package will be refined, expanded, and disseminated widely.

Program Planning and Support

An early draft of a program plan for the Windows and Daylighting program was completed and, after revision, will be circulated for public comment and review. In addition to identifying the research and development required to achieve the full energy-conservation potential of windows and skylights, the plan will help define the links between this program and related DOE Conservation and Solar programs. Technical and non-technical information on energy-conserving window designs derived from this research program will be transmitted to architects, engineers, manufacturers, inventors, suppliers, code officials, and researchers via a new publication, Windows for Energy-Efficient Buildings. This brochure reports on the latest developments, patents, new materials and products, legislation, etc., of concern and interest to this audience. The first issue was published in 1979 and a second in 1980. Circulation now exceeds 6000. In the process of generating material for this publication, extensive product files, patent files, bibliographies, and related informational resources have been compiled and readied for putting into computer data bases. This capability will enable us to make fast and extensive searches.

Another important aspect of our program is to participate in national and international research programs. In 1980, LBL staff represented DOE at an International Energy Agency (IEA) meeting in Delft, Holland, on the Energy Performance of Windows. The participating countries agreed to share research results and to embark on collaborative research efforts.

PLANNED ACTIVITIES FOR FY 1981

Window Performance: Analysis and Performance Testing

Additional modifications will be made to the window computer model THERM to permit calculation of heating and cooling loads resulting from new materials systems and window designs for both residential and commercial buildings. An intercomparison between THERM (a sophisticated window model coupled with a simplified building algorithm) and DOE-2 (a sophisticated building model with relatively simple window algorithms) will be completed. We will begin analyzing results from extensive parametric modeling of the performance of various window-insulating and shading devices, with the complementary goals of developing more detailed insights into subtleties of performance and creating procedures to simplify and communicate results to architects and engineers.

Studies of window system performance in the calibrated hotbox will be continued. Window system prototypes incorporating new state-of-the-art coatings and glazing materials will be tested. The primary performance-testing effort will focus on the final design and construction of the first unit of the MoWiTT facility so that it may be calibrated in the field in late 1981.

Fenestration Systems: Research, Development, and Demonstration

It is expected that the first commercially available windows incorporating heat mirrors and other selective-reflectance coatings will reach the market in 1981. We will continue to test and model the net performance of these products in an effort to develop guidelines for their optimal utilization. Data from several demonstration projects will be reviewed and analyzed. Coating durability, a central problem area, will be investigated in our materials science program, a limited effort will be undertaken to identify new heat-mirror materials having improved coating properties, and thin-film/substrate interactions will be studied. Additional tests of candidate materials for optical shutters will also be conducted.

Test data collected in 1980 on the performance characteristics of air-flow windows will be analyzed, and performance characteristics will be compared to those of other heat-collecting window designs.

Daylighting

A complete summary of daylighting availability data based upon analysis of three full years of data from our San Francisco site will be completed in 1981. A recommended correlation between radiation and illumination data will be developed.

The simulation capability of our artificial sky will be completed in 1981, and improvements will be made in modeling variable ground reflectances. Plans will be completed to add a sun simulator, although construction will not begin until 1982. As the facility's capabilities are improved, we plan to perform an extensive series of tests comparing results from the indoor simulator, from outdoor tests, and from the computer modeling studies as a means of defining the inherent limitations and constraints of all model-testing studies.

In the area of daylighting computations, the large computer model will be completed and used for parametric modeling studies of various fenestration and building designs. The simplified method for adding daylighting capabilities to DOE-2 will be replaced with a more powerful and flexible model that operates within the hourly calculations of DOE-2. A working version will be completed in 1981, and plans for improving the modeling capabilities will be completed in 1982.

Initial studies of the energy savings attributable to daylighting will be expanded to include the effects of daylighting and lighting controls on a building's peak-power loads. An analysis of prior work on glare from windows and its impact on the potential savings from daylighting will also be undertaken.

A second draft of the Daylighting Resource Package will be completed and distributed for review and comment. Work on a daylighting directory and bibliographic data bases will continue.

Program Planning and Support

A draft of the program plan for Windows and Daylighting will be circulated for public review and comment. Development of bibliographic and product data bases will be continued. Another issue of Windows for Energy-Efficient Buildings, this one centered on daylighting, will be published. We will continue collaborative studies of window performance with other international research groups.

REFERENCES

See publications list at the end of this chapter.

ENERGY-EFFICIENT LIGHTING PROGRAM*

S. Berman, R. Clear, J. Klems, F. Rubinstein, S. Selkowitz, and R. Verderber

INTRODUCTION

The Lawrence Berkeley Laboratory has managed the National Lighting Program for the Department of Energy for the past four years. The goal of this program is to bring about a 50% reduction in our nation's energy consumption for lighting by the mid-1990s. We plan to achieve this goal by accelerating the introduction of cost-effective energy-efficient lighting products, designs, and procedures that will enhance the comfortable performance of visual tasks as well as productivity.

Compared to other energy-efficient retrofit potentials, improved lighting will have a more rapid market penetration because the replacement rate of lighting sources and systems is high. We estimate that if energy-efficient lighting products begin to enter the market during the next couple of years, the nation's annual energy consumption for lighting can be reduced by more than 200 billion kilowatt-hours by 1995. This energy savings is equivalent to 381 million barrels of oil annually, or more than 1 million barrels of oil equivalent per day--an amount greater than could be produced by the proposed synfuel program.

The energy-efficient lighting program focuses on two major tasks. The first is the development, testing, and demonstration of energy-efficient light sources and equipment including (1) solid-state fluorescent ballasts; (2) switching and lighting controls; and (3) energy-efficient light bulbs. The second area concerns the science of illumination and illuminating systems, including (1) the physics of light sources and equipment; (2) visibility, illumination, and performance; and (3) health and environmental effects of illumination.

Each of the above projects, with accomplishments realized in 1980 and the activities planned for 1981, is described below.

ACCOMPLISHMENTS DURING FY 1980

Solid-State Fluorescent Ballasts

This project has been concerned with operating fluorescent (low-pressure gas-discharge) lamps at high frequency to improve their efficiency. In the first stage of the program, we evaluated electronic ballast designs in a controlled laboratory environment. Our results showed that electronically ballasted lighting systems were 20% to 25% more efficient than standard systems and improved regulation, eliminated flicker, and could dim gas-discharge lamps.[1] In the next stage, we examined the performance of these electronically ballasted systems in a real environment (the Pacific Gas and Electric Company headquarters in San Francisco) where more than 700 ballasts had been installed on two floors. Although the results of this demonstration identified several reparable design flaws, they clearly indicated that electronic ballasts are a viable energy-efficient alternative to core-coil ballasts, as evidenced by the fact that, after three years, the electronic ballasts are still in operation in the PG&E building. The positive results that have emerged from these studies[2,3,4] have served as a basis for the advanced circuit designs that represent the final stage of commercialization.

In 1980 the electronic ballast systems were assessed for total performance; that is, we considered all of the improved attributes of the electronically ballasted system -- the tighter system control brought about by improved voltage regulation, the regulation of light output, and the ability to dim lamps, in addition to the 25% "intrinsic" improvement in system efficiency. Among our findings, now being compiled for publication as an LBL report,[4] we demonstrated that total energy savings can be as high as 40-70%.

Another significant accomplishment during 1980 was the demonstration of electronic ballasts in the Veteran's Administration Hospital in Long Beach, California. This demonstration was designed to determine whether the radio frequency interference (RFI) radiated and/or conducted by electronic ballasts adversely affected any of the sensitive examining or monitoring equipment in a hospital. We replaced standard ballasts with electronic ballasts near a CAT scanner, diagnostic equipment, and in a

* This work was supported by the Assistant Secretary for Conservation and Solar Energy, Office of Buildings and Community Systems, Consumer Products Division of the U.S. Department of Energy under Contract No. W-7405-ENG-48.

coronary ward. We monitored the equipment both before and after the replacement. The data are now in the final stages of analysis,[5] but a preliminary review shows that the electronically ballasted system is as safe regarding RFI as is a standard core-coil ballasted system.

High-Pressure Sodium (HPS) Ballasts

A project to develop electronic ballasts for high-pressure sodium lamps was begun in 1980. Three subcontracts were initiated for the development of circuits to operate 150-watt, 200-watt, and 400-watt HPS lamps at high frequency. In the initial phase, we assessed the performance of the subcontractors' electronic ballast systems in a controlled laboratory environment and compared their performance with that of the same HPS lamp operated with a high-quality core-coil ballast.[6] The results, presented in Table 1, show that both 120- and 277-voltage input electronic ballasts can be designed, and that electronic ballasts can improve the efficiency of both the ballast and the lamp by as much as 15%. In addition, efficient electronic ballasts can be designed to have high power factors. For HPS lamps used in an area that has rotating machinery, the percent flicker was improved to the extent that stroboscopic effects from lamps operated at high frequency were eliminated.

Besides the improvement in intrinsic efficiency, approximately 15%, the electronically ballasted HPS lamps also save energy because of the constant wattage that the electronic ballast supplies to the lamp throughout its life. The total energy savings amounts to approximately 26%. Standard ballasts supply excess power to the lamps due to the reduction of the arc impedance that occurs as the sodium migrates. The average excess, both of light and of energy consumed, is approximately 20% to 30%. Furthermore, as an HPS lamp ages, the voltage applied must be increased to keep the lamp from being extinguished. For testing purposes, we simulated this characteristic by heating the lamp and plotting lamp power versus lamp voltage for both core-coil and electronically ballasted lamps (see Figure 1). This evidence again supports our assertion that the real energy savings from electronic ballasts can be greater than that gained by the intrinsic efficiency of the system, and that the 26% savings should be considered in determining payback or life-cycle costs on the design change.

Switching and Lighting Controls

Strategies and Techniques

The primary goal of the lighting-control project is to evaluate the energy savings realizable by employing different lighting-control strategies. Given this information and the cost of an automatic control system, one can calculate the expected payback, or return, on investing in such strategies.[7]

To evaluate all the desired strategies (daylighting, tuning, scheduling, and load shedding) and techniques (local and group controls; step and continuous dimming), two demonstration sites were required. We selected General Electric and Honeywell as subcontractors, and requested that they install their prototype systems on one floor of the World Trade Center office building in New York (G.E.) and in the Pacific Gas and Electric building in San Francisco (Honeywell). Both of these installations became functional in 1980, and

Table 1. Performance testing of high-pressure sodium (HPS) solid-state ballasts.

	150-Watt hps		200-Watt hps		400-Watt hps	
	Core-Coil	Electronic	Core-Coil	Electronic	Core-Coil	Electronic
Input						
voltage (volts)	120	120	277	277	240	277
power (watts)	189	187	282	230	447	438
power factor	0.48	0.93	1.00	0.95	0.97	0.78
Output						
voltage (volts)	54.4	52.5	116	93	96	96
power (watts)	149	154	215	198	376	324
light (lux)	3500	3840	9440	9160	18,330	19,070
Efficiency						
ballast	0.788	0.824 (+4%)[a]	0.76	0.86 (+12%)	0.84	0.74 (-14%)
lamp (lux/w)	23.5	24.9 (+6%)	43.9	46.3 (+5%)	48.8	58.8 (+17%)
system (lux/w)	18.5	20.5 (+10%)	33.5	39.8 (+16%)	41.0	43.5 (+6%)

[a] Figures in parentheses indicate the percentage change in efficiency from core-coil to electronic ballast system.

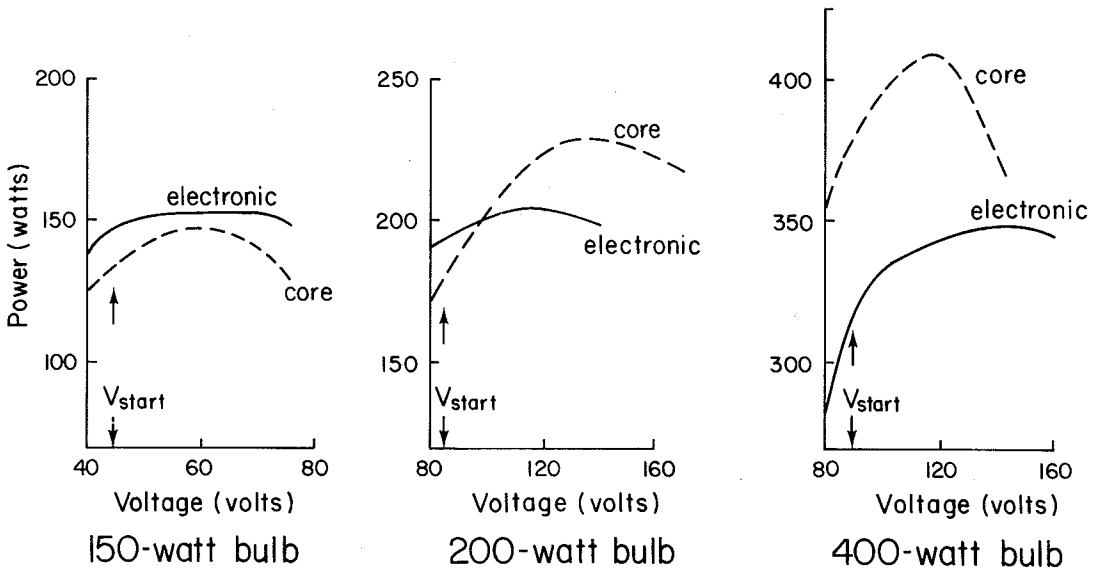

Fig. 1. Comparison of power voltage curves for core-coil and electronically ballasted high-pressure sodium lamps (150-watt, 200-watt, and 400-watt). Electronically ballasted lamps maintained constant wattage outputs that were consistently closer to design levels. (XBL 8011-2625A)

were tested in place prior to initiating performance experiments. Near the end of the year, data were obtained which confirmed our estimates of the energy savings that can be realized through automatic controls.

The General Electric system used a microprocessor to control the switching of each fixture; that is, to turn it on or off separately. Figure 2 shows the power usage for one day's operation using this tuning and scheduling strategy. The tuning (de-lamping) turns off fixtures in aisles and in work areas where a full light level is not required. The scheduling strategy lowers light levels to 1/6 in the evening for the cleaning crews, who do not require the high light levels used in the daytime.

The initial daily energy use was 2256 kWh. Tuning reduced the daily use to 1561 kWh. The scheduling strategy reduced the daily usage to 1020 kWh. At an energy cost of $0.10 per kWh (the cost of electric energy in New York City), the savings is $123.60 per day, or more than $32,136 per year for a single floor.

The Honeywell system used a computer to control the light level of a large group of lamps, each of which can be dimmed continously over a large range of light levels. Figure 3 plots the power usage for a single day at the PG&E building in San Francisco. A photocell senses the light level of the outer zones of the building and, when specified light levels are exceeded because of the contribution of daylight, the light supplied is electrically reduced to maintain the prescribed level of illumination.

For the day these data were obtained, the energy use in the offices in the outer zone decreased from 201 kWh to 147 kWh, or 27%. At a cost of $0.05 per kWh (the cost of electric energy in the San Francisco area), the savings could be more than $702 per year.

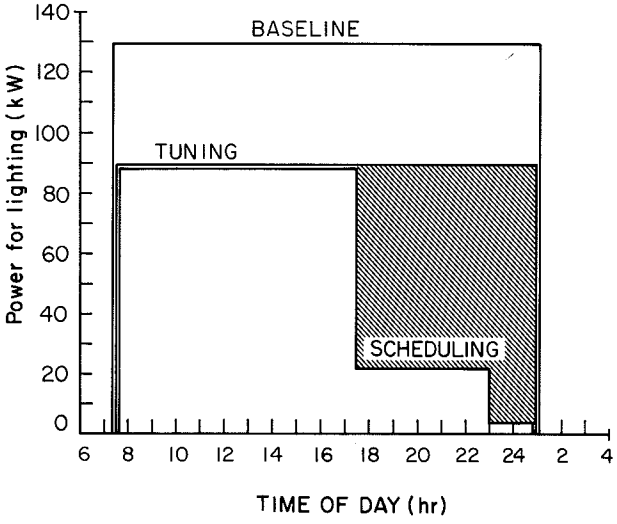

Fig. 2. Results of two approaches to reducing electrical energy consumption on one floor of the World Trade Center, New York. The tuning technique, which adjusts the light level of fixtures to the needs of the task in each area, decreased the baseline or normal energy use by 40 kilowatts per hour. Usage was further reduced at night by the scheduling technique, which lowered light levels to 1/6 daytime use. (XBL 8011-2351)

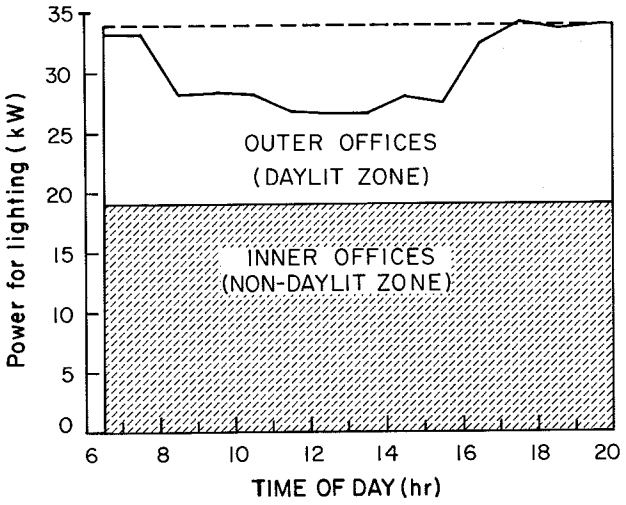

Fig. 3. The daylighting strategy used to reduce electrical consumption in the PG&E building, San Francisco reduced the energy consumption for perimeter offices by 27% but had no effect on the lighting energy required for interior offices (shaded area). (XBL 8011-2350)

Energy Efficient Light Bulbs (EELB)

The objective of our EELB project is to develop energy-efficient light sources that can be used in incandescent sockets (Edison sockets), and that will approach efficacies of 40 to 50 lumens per watt (as compared with the 17 lumens per watt characteristic of a 100-watt incandesecent bulb).[8,9] The national energy consumption for incandescent light is about 180 billion kWh annually. The potential savings associated with replacing 50% of the incandescent lamps (17 lumens/watt) with energy-efficient lamps (45 lumens/watt) is approximately 60 billion kWh, which is equivalent to more than 100 million barrels of oil--the amount needed annually to generate this electrical energy.

Near the end of FY 1980 we signed contracts to have four companies develop their EELBs. Among the objectives we specified for each contractor was the identification of any major technical barriers to production.

Physics, Visibility, and Health

Physics and Engineering Lighting Laboratory

In 1976, a small laboratory facility, designed primarily to measure the relative performances of electronic ballasts and the relative light outputs of light sources, was set up in conjunction with the Windows Laboratory at the College of Environmental Design in Wurster Hall on the University of California campus at Berkeley. Since then, our program has expanded to include involvement in standards committees, e.g., American National Standards Institute (ANSI), which requested LBL staff to propose specifications and testing procedures for high-frequency lighting systems, as well as to perform life testing for new energy-efficient lighting products. In addition to the above activities, we required greater in-house technical competence when we began the EELB program. The laboratory is now responsible for in-depth analysis of the generation of visible light from low-and high-pressure gas discharge, including plasma effects at high frequencies and radio frequency interference (RFI). Because of these added responsibilities, a larger Physics and Engineering Lighting Laboratory was designed in FY 1980 and is now located in Building 46 on the LBL site. The new laboratory includes an area for testing lighting systems (maintained at 25 $\pm$ 1°C in order to obtain absolute measures of light output under controlled conditions), as well as a general laboratory area and a lamp-life testing area. The necessary equipment--high-frequency wattmeters, a seven-foot integrating sphere, a spectral-radiometer, and standard certified NBS light sources--has been purchased to provide absolute measurements of light output from light sources as well as to measure the spectral distribution of the visible radiation.

The first project for the new laboratory, undertaken in 1980, was a fundamental study of the H_g isotope mixture in a discharge in order to determine the effect of optimizing the isotope mixture for the generation of the 253.7 nanometer line. Lamps generally use the isotope mixture of naturally occurring H_g. We expect that the efficacy of the low-pressure gas discharge can be increased 5% to 10% by enriching the natural mixture with H_g 196. This improvement will substantially increase the total light output of compact fluorescent lamps.

Visibility and Productivity Laboratory

The connection between visibility in commercial/industrial buildings, as determined by lighting codes and/or design practices, and the productivity of the work force has become an important issue because of the rapidly escalating price and scarcity of electricity and the coincident loss of much of the nation's competitive position in person-hours per dollar of value added. Target light levels used under existing standards allow for a broad comfort/safety margin--a reasonable practice when energy prices and availability were not in question. Disagreement about how much visibility is needed to assure efficient operation and comfort has, in fact, resulted in several different standards, and resolving these differences to arrive at a "best" standard is hampered by lack of information about the relationship between visibility and worker productivity. A review of field studies in this area shows contradictory results.

Because statistically validated data on the relationship between productivity and visibility are critical to determining cost-effective lighting levels, LBL and the University of California School of Optometry developed a joint program in 1980 to examine, in a laboratory setting, the effects of physical lighting parameters such as intensity, spectrum, distribution, and polarization on performance and productivity, using subjects whose visual capabilities are known (e.g., age, corrected or uncorrected 20-20 vision, etc.). To date, the group has published a critical review of the basis

for the Equivalent Sphere Illumination concept of quantifying the quality of illumination.[10] In addition, a paper has been presented at the national Illuminating Engineering Society Conference at Dallas, Texas on the cost-effectiveness of visibility design procedures.[11]

PLANNED ACTIVITIES FOR FY 1981

Solid-State Fluorescent Ballasts

In the next phase of this project, we will examine some advanced electronic ballast designs from which we anticipate further improvements in efficiency. We will also evaluate the reliability of these ballasts when voltage surges occur, as they do commonly in real situations.

Switching and Lighting Controls

Further studies are needed to optimize lighting layout designs. One aim is to provide daylighting designers with a way to determine the best position for the sensing photocells. We will obtain this information for areas facing north, south, east, and west, in different parts of the country, and for different types of building spaces. By the end of the next fiscal year, we expect to have developed design techniques that more effectively use natural illumination.

Energy-Efficient Light Bulbs (EELB)

Four viable energy-efficient light bulbs--the compact fluorescent lamp, the coated filament lamp, the magnetic-arc spreading fluorescent lamp, and the electrodeless fluorescent lamp--will be studied in FY1981. While all these designs are more efficient than an incandescent lamp, each has limitations that hinder commercialization. In the first phase of this program, each participating manufacturer will deliver ten laboratory prototypes to LBL for our evaluation of any design or performance shortcomings.

Although the compact fluorescent lamp requires no major changes, its application is currently limited to lower output lamps (less than 1500 lumens). We will study highly efficient phosphors and electronic ballasts, and gas fill with optimized Hg isotope mixtures to achieve light outputs of up to 2200 lumens (equivalent to a 150-watt 3-way lamp).

The coated filament lamp has not been assessed for life, efficacy, or quality control. In addition to determining the ultimate obtainable efficacy of this lamp, we will seek to determine how uniform a coating is required for reliable performance and whether that degree of uniformity can be manufactured commercially.

The electrodeless fluorescent lamp operates at 13 MHz and emits RFI, which can disturb radio and television receivers or computers and other sensitive electronic devices. Our task here is to develop a low-cost electronic ballast system for this lamp and to determine ways of minimizing RFI.

Health Effects Related to Environmental Artificial Lighting

Artificial lighting is now ubiquitous in the living/working environment. Although assertions of potentially harmful effects of artificial lighting on both health and performance have been circulated (especially in the lay community--e.g., Health and Light by John Ott and The Zapping of America by Paul Brodeur), no hard data exist in this area. We are initiating a new project to address the questions of reduced performance and health effects from artificial lights. We will begin by addressing three questions:

1. Are there populations whose eyes are sensitive to artificial lighting, especially in association with other environmental factors?
2. Do certain artificial lighting sources induce fatigue and increase the "work error" rate?
3. Do certain artificial lighting sources act as physiological "stressors" for certain individuals?

Until now, there has been a lack of coherence in the various protocols used by qualified investigators spanning the disciplines of engineering, biochemistry, psychometry, behavioral sciences, and neurophysiology, all of which are involved in any reasonably complete investigation of the human effects of artificial light. To address the potential long-term health effects from artificial lighting, as well as to identify potential environmental hazards of new products before they are introduced into the market, LBL is collaborating with the faculty of the University of California's School of Medicine in San Francisco where test facilities are currently being developed. We hope, in this collaborative effort, to verify, statistically, any aspects of artificial lighting that present hazards to fundamental biochemical and neurophysiological mechanisms.

REFERENCES

1. Stevens Luminoptics Corporation, Energy Efficient Fluorescent Ballasts, Lawrence Berkeley Laboratory report LBL-7852, June 1978.
2. R. R. Verderber, S. Selkowitz, and S. Berman, Energy Efficiency and Performance of Solid-State Ballasts, Lawrence Berkeley Laboratory report LBL-7828, June 1978. Also published in Lighting Design & Application, vol. 9, no. 4, April 1979, pp. 23-28.
3. R. R. Verderber, D. Cooper, and D. Ross, Testing of Energy Conservation of Electronic Ballasts for Fluorescent Lighting: Review of Recent Results and Recommendations for Design Goals, Lawrence Berkeley Laboratory report LBL 8315, October 1978.
4. R. R. Verderber, The "Real" Energy Savings with Electronic Ballasts, Lawrence Berkeley Laboratory report LBL 10707, March 1980. Also published in Electrical Consultant, November - December 1980.

5. R. R. Verderber, A. Arthur, O. Morse, and F. Rubinstein, Energy Savings and Safety of Solid-State Ballasts in a Hospital Environment, Lawrence Berkeley Laboratory report (in preparation).

6. G. Felper, High Intensity Discharge 400-Watt Sodium Ballast-- Phase I Final Report (Data-Power), Lawrence Berkeley Laboratory report LBL-11254, June 1980.

7. F. Rubinstein and R. R. Verderber, Report on Lighting Controls: Survey of the Potential Market, Lawrence Berkeley report LBL-11209 (in preparation).

8. R. R. Verderber and O. Morse, Cost Effectiveness of Long Life Lamps and Energy Buttons, Lawrence Berkeley Laboratory report LBL-10789, April 1980.

9. T. Kohler, Electronic Screw-in Ballast and Improved Circline Lamp--Phase I Final Report (EETech), Lawrence Berkeley Laboratory report LBL-11255, September 1980.

10. R. Richardson and S. Berman, Equivalent Sphere Illuminaton and Visibility Levels, Lawrence Berkeley Laboratory report LBL-9492, August 1980.

11. R. Clear and S. Berman, Cost Effectiveness of Visiblity-Based Design Procedures for General Office Lighting, Lawrence Berkeley Laboratory report LBL-10514, August 1980.

DOE-2.1 BUILDING ENERGY ANALYSIS GROUP*

R. Curtis, F. Buhl, S. Gates, J. Hirsch,
M. Lokmanhekim, K. Olson, A. Rosenfeld, J. Rudy, and F. Winkelmann

INTRODUCTION

The purpose of this project has been to create, test, document and maintain a user-oriented, public domain, computer program that will enable architects and engineers to perform design studies of whole-building energy use under actual weather conditions. The development of this program, which in its successive public generations has been known as Cal-ERDA, DOE-1.4, DOE-2.0A, and, finally, DOE-2.1, has been guided by several objectives: (1) that the description of the building by the user be in quasi-English so that the input can be read and understood easily by non-computer scientists; (2) that, when available, the calculations be based upon well-established algorithms, i.e., the calculational procedures used should be acceptable to the engineering community; (3) that it permit simulation of commonly available heating, ventilation, and air-conditioning (HVAC) equipment; (4) that the computer costs of the program be minimal; and (5) that the predicted energy use of a building be acceptably close to measured values.

These objectives require compromises to be made. Higher accuracy, for example, can be purchased only at the cost of more detailed and time-consuming algorithms and more complex demands upon the user for data about the building being modeled. Considerable experience and user feedback has culminated in a program which has received much acceptance, and DOE-2.1 has been named by the Department of Energy as the standard evaluation technique (SET) of the Congressionally mandated Building Energy Performance Standards (BEPS).

Details of the development and structure of the DOE-2.1 program are available in past Annual Reports[1,2] and other published materials.[3-8]

ACCOMPLISHMENTS DURING FY 1980

The major accomplishment of FY 80 was the completion of the DOE-2.1 edition of the program, including its accompanying documentation.[9-12] LBL was assisted in this work by the WX-4 Group at Los Alamos Scientific Laboratory (LASL), which was responsible for developing and testing the active solar simulator (known as CBS, for the Component Based Simulator) and for producing the DOE-2.1 Reference Manual. In addition, the DOE-2.1 User Coordination Office at LBL, charged with coordinating user services at commercial computer service bureaus, universities, and national laboratories, has published the first of a periodic journal, entitled "DOE-2 USER NEWS", which serves to keep the user community informed about the latest developments and uses of the program. We have also carried out the first of several training sessions designed to train trainers of DOE-2.1 users.

Among the additions and improvements that distinguish DOE-2.1 from its predecessor (DOE-2.0A) are its ability to create and to store custom weighting factors, its restructured simulation of the HVAC systems, and its integration of the active solar simulator.

Custom Weighting Factors and Thermal Balance Loads

DOE-2.1 has been substantially improved over DOE-2.0A by adding two new techniques to calculate

* This work was funded by the Office of Buildings and Community Systems, Architectural and Engineering Systems Branch, Buildings Division, U.S. Department of Energy under Contract No. W-7405-ENG-48.

heating and cooling loads. The development of both techniques was stimulated by the inadequacy of the technique used in DOE-2.0A to predict energy use in buildings with high thermal mass where solar heat gain is an important component of the loads. In the "Custom Weighting Factor" method, which is now documented and available in DOE-2.1, a fast-executing transfer function approach is used. The second new method, called "Modified Thermal Balance" and now being tested, is a more accurate, but also a more time-consuming, technique. The user will ultimately be able to choose the technique best suited to the application at hand.

Custom Weighting Factors

In this approach the heat gain from lights, solar radiation, people, equipment, and conduction through the envelope are calculated for each hour. Part of each of these gains will appear immediately as a load on the HVAC system; the rest will be stored as heat in the walls, the floor, the furniture, and other mass in the building and will be released over time to the room air. The time delays involved in this process are accounted for by the weighting factors. Mathematically, the cooling load in hour t in Btu/hr due to the i^{th} source (Q_t^i) is given by:

$$Q_t^i = V_0 q_t^i + V_1 q_{t-1}^i + V_2 q_{t-2}^i + W_1 Q_{t-1}^i + W_2 Q_{t-2}^i,$$

where

q_{t-j}^i = the heat gain in hour t-j (Btu/hr)

Q_{t-j}^i = the cooling load in hour t-j (Btu/hr)

V_j, W_j = the weighting factors

i = the index for the source of heat gain (lights, solar, etc.)

The net load for a particular hour is the sum of the Q_t^i over all of the sources. A similar transfer function relationship relates the cooling loads to the actual space temperatures and the heat extraction rates for that hour and previous hours.

In earlier versions of the program "ASHRAE Weighting Factors" were used. These were calculated about 15 years ago by the National Research Council of Canada for buildings of very simple geometry and were adapted by the American Society of Heating, Refrigerating, and Air-Conditioning Engineers (ASHRAE).[13] Studies by Los Alamos Scientific Laboratory (LASL) showed that the ASHRAE weighting factors lead to inaccurate results for buildings where direct gain is important. Figure 1 shows temperature measurements for the LASL direct-gain test cell as well as the predictions yielded by using the ASHRAE weighting factors. There is a 7°F space temperature difference at the peaks between the predicted and the measured data.

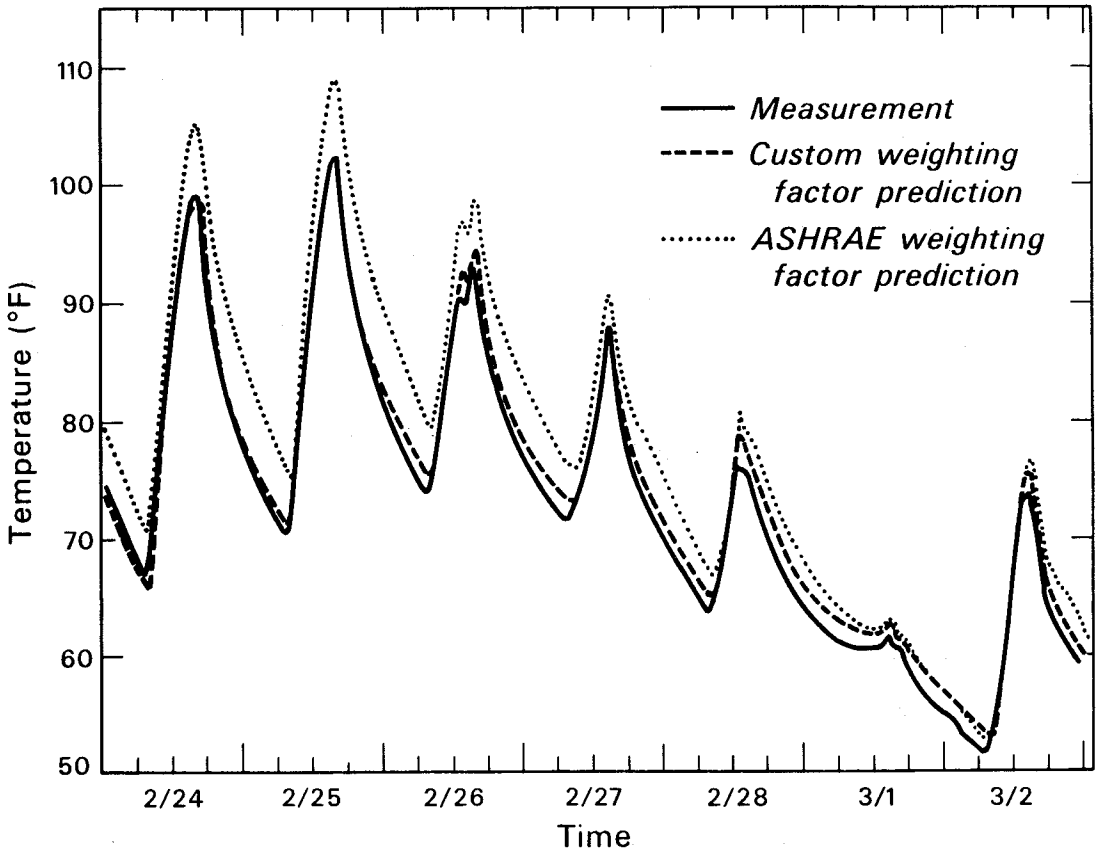

Fig. 1. LASL test cell measurement comparison with DOE-2.1 predictions.
(XBL 812-270)

A technique for calculating weighting factors specifically for the space configuration under consideration was developed[14] and incorporated into DOE-2.1. In this technique a detailed thermal balance calculation is made initially to find the cooling load profile produced by a unit impulse of heat gain from each of the sources listed above. Equation (1) is applied to these profiles, and the weighting factors are extracted by solving the resulting equations simultaneously. When these "Custom Weighting Factors" are applied to the LASL test cell (Figure 1), the agreement with measured data is vastly improved.

Modified Thermal Balance (MTB)

The Modified Thermal Balance technique does not treat the various heat gains separately. Instead, the heat balance equations at the inside surfaces of the space are solved simultaneously each hour. For calculating cooling loads, the room air temperature is held fixed, and, similarly to the weighting factor approach, the actual variation of the space temperatures is treated through transfer functions. It is felt that the MTB technique may be more accurate in certain situations than the weighting factor approach. For example, it would allow moveable insulation to be placed over windows at night. The weighting factor technique does not permit the room transfer functions to be functions of time, as is necessary when the conductance of the windows varies with time. The MTB approach also computes the inside surface temperature as a function of time. If these temperatures vary widely, the convective, and even the radiative, heat transfer coefficients can vary enough to cause significant changes in the building conditions. Human comfort strongly depends upon the inside surface temperatures, and, yet, the weighting factor approach provides no information in this regard. Further studies will be made of the differences among the weighting factor, the MTB, and the full thermal balance techniques to determine what situations require the more complex, and therefore more time-consuming, techniques, if sufficient accuracy is to be maintained.

Restructured HVAC Systems

The SYSTEMS and PLANT sub-programs of DOE-2.0A were designed to estimate the energy consumption of the HVAC equipment of large buildings. Many modeling assumptions were based on the philosophy that the most important considerations should be those that have a significant impact upon the energy consumption values integrated over time. The program made no attempt to simulate the performance of the equipment components on an hour-by-hour basis but, rather, to predict overall energy use. This philosophy was supported by the fact that, in the past, the larger HVAC equipment was systematically oversized and tightly controlled. For modeling such systems, it was not necessary to take into account performance parameters that depend on inside or outside environmental variables.

As DOE-2.0A gained popularity, the user community wanted to extend the use of the program to small commercial and residential buildings. At the same time the engineering community, in an effort to conserve energy, was moving away from recommending oversized systems and constant, year-round control points. These shifts prompted us to make substantial changes in the algorithms of both SYSTEMS and PLANT. The new algorithms tend to be more concerned with modeling hourly performance of actual equipment than rather merely estimating the integrated daily or annual energy consumption. This new philosophy permitted the introduction of several new equipment simulations into DOE-2.1.

In the SYSTEMS program the most significant changes address the details of the air moisture levels and the cooling coil simulation. The DOE-2.0A program assumed that the sensible capacity of the equipment was constant throughout the entire simulation period. It also assumed that the air moisture level exiting from the cooling coil was a constant fraction of the saturation level at the exit temperature. The newest version of DOE-2.1 more realistically calculates the capacity of each piece of equipment on an hourly basis. This approach allows a strong coupling between the envelope and the equipment by solving simultaneously the equations describing the action of the equipment and the equations describing the space temperature swings within the hourly time step. In addition, we developed a moisture exchange model for cooling coils that simulates the condensation that takes place on the coil surface by calculating the time-dependent surface temperature and the degree of air "contact" with the surface, based upon free-stream conditions of flow rate, and drybulb and wetbulb temperatures. Such a calculation yields an hourly steady-state simulation of the moisture condensation on the coil surfaces in association with the latent space gains due to people, equipment, infiltration and ventilation.

With these new capabilities for performance simulation, it became possible to extend the number of types of equipment simulations to include those appropriate for residential and small commercial buildings. These additional system types include direct expansion, air-cooled cooling systems, as well as water- and air-source heat pumps. Specifically, the new equipment for SYSTEMS includes: packaged rooftop units for single-zone, multizone, and variable air volume applications; packaged terminal air conditioners for window-mounted or through-the-wall applications; central forced air furnace and split-system direct-expansion cooling for residential applications. The residential simulation also permits the evaluation of the efficacy of using operable windows in place of mechanical cooling. The original simulations for chilled and hot water equipment were also upgraded to allow more accurate tracking of hourly performance. (See Table 1.)

Simulation algorithms for the PLANT program were also redesigned to track more accurately the performance of the equipment and to be consistent with the algorithms in SYSTEMS. The treatment of the chilled and hot water supply loops has been modified in DOE-2.1 to take into account the variation of loop temperature. Similarly, the temperature of the condenser water is now allowed to vary. The cooling tower simulation was upgraded as experimental performance data became available. New performance parameters for the chillers were introduced to permit more exact simulation, and an

Table 1. Equipment simulations in DOE-2.1

Systems	Plant
Single Zone	Steam Boiler (fossil fuel)
Packaged Single Zone*	Steam Boiler (electric)
Multizone	Hot Water Boiler (fossil fuel)*
Packaged Multizone*	Hot Water Boiler (electric)*
Dual Duct Fan	Furnace (fossil fuel)*
Ceiling Induction	Furnace (electric)*
Unit Heater	Domestic Hot Water Heater (fossil fuel)*
Unit Ventilator	Domestic Hot Water Heater (electric)*
Floor Panel Heating	Open Centrifugal Chiller
Two-Pipe Fan Coil	Open Reciprocal Chiller
Four-Pipe Fan Coil	Hermetic Centrifugal Chiller
Two-Pipe Induction	Hermetic Reciprocal Chiller*
Four-Pipe Induction	Single-Stage Absorption Chiller
Variable Air Volume	Two-Stage Absorption Chiller
Packaged Variable Air Volume*	Solar-Assisted Absorption Chiller*
Reheat Fan	Double-Bundle Chiller
Unitary Heat Pump	Cooling Tower
Heating and Ventilating	Ceramic Cooling Tower
Ceiling Bypass	Steam Turbine Generator
Residential*	Gas Tubine Generator
Packaged Terminal Air-Conditioner*	Diesel Generator
	Hot Water Storage Tank
	Cold Water Storage Tank

* New equipment in DOE-2.1

improved optimization algorithm was developed to allow efficient operation of a multiple chiller plant.

Like the new additions in SYSTEMS, new PLANT equipment was introduced in DOE-2.1 for smaller installations. These include: electric and fossil fuel hot water boilers, electric and fossil fuel domestic hot water heaters, open and hermetic reciprocal chillers, and electric and fossil fuel furnaces.

Component Based Systems (CBS)

A major addition to the program is an active solar system simulator, called "CBS" for Component Based Systems. This code was adapted and expanded by the WX-4 group at LASL from the TRANSYS program developed at the University of Wisconsin, and was integrated into the PLANT portion of DOE-2.1 with the assistance of our group at LBL. This program offers the user four pre-assembled solar systems (both liquid and air systems for commercial and residential buildings) that are modified for specific applications through the use of keywords, like the rest of DOE-2.1. In addition, the user can assemble his or her own system by connecting together individual components: collectors, pipes or ducts, heat exchangers, hot water storage tanks or rock beds, pumps or fans, and their associated controls. Through either approach the user can simulate the collection of solar energy to satisfy space heating and/or cooling loads or process loads.

In an example used to introduce this program to the user[3] a solar system was simulated to provide a solar assist to the domestic hot water heater in a small commercial building in Sacramento, California. The domestic hot water heater had a heating capacity of 12,800 Btu/hr and a demand schedule for weekdays as given in Figure 2. The demand schedule during weekends and holidays was assumed to be the same as the demand at night during the week. The natural gas consumed annually by the heater dropped from 131.9 therms without solar assist to 76.0 therms with solar assist, an annual savings of 42%. On the other hand the fuel consumption of 131.9 therms produced 72 therms of hot water for an efficiency of 55%, while the fuel consumption of 76.0 therms produced only 31 therms of hot water for a conversion efficiency of only 41%. These values illustrate an important problem that is involved with making

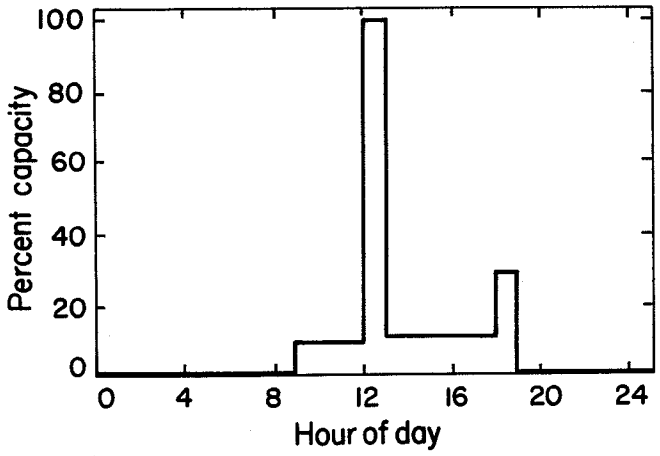

Fig. 2. Domestic hot water hourly profile.
(XBL 816-972)

solar retrofits to non-solar systems. Unless the back-up equipment to the solar system is altered to perform at higher efficiency at lower loads, an overall reduction in energy conversion efficiency can occur.

PLANNED ACTIVITIES FOR FY 1981

Future plans for the program lead in two separate directions. On the one hand, the existing program will be maintained and supported and its documentation will be clarified and supplemented as areas of confusion are uncovered. Several additions will be made to the existing program to supplement its capabilities. These include: (1) expanded output report capability; (2) a daylighting simulation in collaboration with the Windows and Lighting Group at LBL; (3) an expanded user-library capability; (4) the thermal balance LOAD program alternative; (5) improved economic calculations; (5) expanded energy cost alternatives; (6) simulation of evaporative coolers; (7) improved infiltration algorithm; (8) simulation of thermal storage devices; and (9) metric input and output options. The program will also be converted so that it will run on IBM, Honeywell, UNIVAC, and Digital Equipment Corporation computers.

The other direction for FY 81 activity is exploratory; i.e., we will probe the development of a building energy use analysis program that can be easily adapted to new developments in the building and conservation sciences.

REFERENCES

1. Energy & Environment Division Annual Report, FY 1978, Lawrence Berkeley Laboratory report LBL-11650.
2. Energy & Environment Division Annual Report, FY 1979, Lawrence Berkeley Laboratory report LBL-11990.
3. S. C. Diamond and B. D. Hunn, The DOE-2 Verification Project: Phase I Results, Los Alamos Scientific Laboratory publication LA-UR-80-357.
4. M. D. Levine, D. B. Goldstein, M. Lokmanhekim, and A. H. Rosenfeld, Evaluation of Residential Building Energy Performance Standards, Lawrence Berkeley Laboratory report LBL-9816, December 1979.
5. M. Lokmanhekim, F. C. Winkelmann, and W. F. Buhl, Thermal Load Analysis of the Avonbank Building Using DOE-2.1 (Parametric Studies), Lawrence Berkeley Laboratory pub. GR-30, May 1979.
6. N. M. Schnurr, J. F. Kerrisk, J. E. Moore, B. D. Hunn, and Z. O. Cumali, Applications of DOE-2 to Direct-Gain Passive Solar Systems: Implementation of a Weighting Factor Calculative Technique, Los Alamos Scientific Laboratory report LA-UR-79-2227.
7. M. A. Roschke, B. D. Hunn and S. C. Diamond, A Component Based Simulator for Solar Systems, Los Alamos Scientific Laboratory pub. LA-UR-78-1494.
8. W. L. Carroll, Annual Heating and Cooling Requirements and Design Day Performance for a Residential Model in Six Climates: A Comparison of NBSLD, BLAST 2 and DOE-2.1, Lawrence Berkeley Laboratory report LBL-9270, June 1980.
9. Building Energy Analysis Group, DOE-2 Users Guide, Version 2.1. Lawrence Berkeley Laboratory report LBL-8689 Rev. 1, May 1980.
10. Building Energy Analysis Group, DOE-2 BDL Summary, Version 2.1, Lawrence Berkeley Laboratory report LBL-8688 Rev. 1, May 1980.
11. Building Energy Analysis Group, DOE-2 Sample Run Book, Version 2.1, Lawrence Berkeley Laboratory report LBL-8688 Rev. 1, May 1980.
12. Group WX-4, Program Support, Los Alamos Scientific Laboratory, DOE-2 Reference Manual (Part 1, Part 2), Version 2.1, Lawrence Berkeley Laboratory report, LBL-8688 Rev. 1, LA-7689-M Ver.2.1, May 1980.
13. 1977 ASHRAE Handbook Of Fundamentals, (New York, N. Y.: American Society of Heating, Refrigerating, and Air-Conditioning Engineers, Inc.).
14. Z. O. Cumali et al., Final Report -- Passive Solar Calculation Methods, (Oakland, Calif.: Computer Consultants Bureau/Cumali Associates), June 15, 1979.

BUILDING ENERGY DATA COMPILATION, ANALYSIS, AND DEMONSTRATION*

A. Rosenfeld, H. Arin, P. Cleary, J. Costello, B. Dickenson, D. Goldstein, J. Harris, A. Meier, S. Meyers, B. O'Regan, L. Schipper, B. Shohl, and J. Wright

INTRODUCTION

The Building Energy Data Compilation, Analysis and Demonstration group is responsible for compiling, analyzing, and demonstrating the research of the Energy-Efficient Buildings program and integrating it with building science research nationally and internationally. We organize our research by technology (windows, thermal storage, and infiltration) or professional specialty (indoor air quality, building performance modelling, etc.); but we and our clients tend to organize our questions by building type (homes, schools, etc.) or operation requirements (design and retrofit) which, of course cut across all of our research fields. Accordingly, the BEDAD group in addition to responding to questions from utilities, planners, governmental groups, and even our own research directors, reformulates and publishes some of our findings in an aggregated form, which is more useful to building industry and policy professionals.

ACCOMPLISHMENTS DURING FY 1980

During the past year, BEDAD continued to develop and refine a technology data base on the cost and performance of conservation measures in new and retrofitted houses and residential appliances, and began to compile data on commercial buildings and equipment. Using these data, along with the results of DOE-2 runs and other analyses made in support of BEPS (Building Energy Performance Standards), we completed a major study of technical and economic potentials for conservation and solar use in California residences. A similar study of conservation and solar potentials in all U.S. buildings (residential and commercial) between now and the year 2000 was also conducted and preliminary results have been reviewed. Both studies have generated a great deal of interest among utilities, government agencies, and the building industry, and were used extensively as background material for a Summer Study on Energy Efficient Buildings, sponsored last August in Santa Cruz by the American Council for an Energy Efficient Economy, the Solar Energy Research Institute, (SERI) and DOE. Finally, in 1980 we initiated with the Pacific Gas and Electric Company a joint project to (1) demonstrate "house doctor" audit/retrofit techniques, (2) train an initial core group of utility and private industry house doctors, and (3) measure resultant energy savings and cost-effectiveness in a sample of 26 northern California homes. Results to date from each of these projects are summarized below.

*This work is supported mainly by the Assistant Secretary for conservation and Solar Energy, Office of Buildings and Community Systems, Buildings Division, U. S. Department of Energy under Contract No. W-7405-ENG-48, and by the Solar Energy Research Institute. We also thank the California Policy Seminar for partial support.

Reports

Building Energy Use Compilation and Analysis (BECA). BECA is a series of publications providing an international comparison and critical review of building standards and the energy use of typical buildings as well as cost-effective, low-energy buildings. Its findings are published as a review consisting of three parts which are to be updated and republished regularly. Part A, Single-Family Residences, was submitted to Energy and Buildings, in January 1981; Part B, Retrofitting of Residences, is in progress, as is Part C, Commercial Buildings.

BECA-A: Single-Family Residences

In BECA-A, the potential for energy conservation in space heating of new residential buildings is characterized using results from computer analysis and from a survey of low-energy houses. Simulations of the energy requirements of a prototypical house in the United States at different levels of conservation have shown that minimum life-cycle cost can be achieved with much higher levels of conservation than those presently employed. Measurements taken in actual houses indicate that very low energy requirements for space heating--comparable to those now used for domestic water heating--can be achieved in new houses by adding insulation, reducing infiltration, and using solar-design principles. We conclude that building standards should be made more stringent to hasten the adoption of cost-effective conservation measures.

Figure 1, taken from BECA-A, plots ten cost-effective low-energy homes comparing them with proposed standards and with current building practice.

BECA-B: Residential Retrofit

Parallel to our work on energy use in new homes, we have begun to compile and evaluate data on the characteristics, energy performance, and associated costs of retrofits to existing structures. The data collected thus far are summarized in Figure 2, which shows the percentage of energy saved as a function of contractor cost. The entries shown on Figure 2 range from individual values for single homes to averages for a large number of retrofitted homes (nearly one million, in the case of the Canadian "CHIP" homes). All but two of the data points are derived from actual metering of homes, and soon all points will be based on meter readings or utility billing records.

The exponential decay curve drawn on Figure 2 is our estimate of the "frontier" curve for space heating requirements after retrofit vs. the cost of the retrofit. The curve starts down with an initial slope of 8% fuel savings per $100 invested (cost of conserved fuel oil at 10¢/gal) and passes

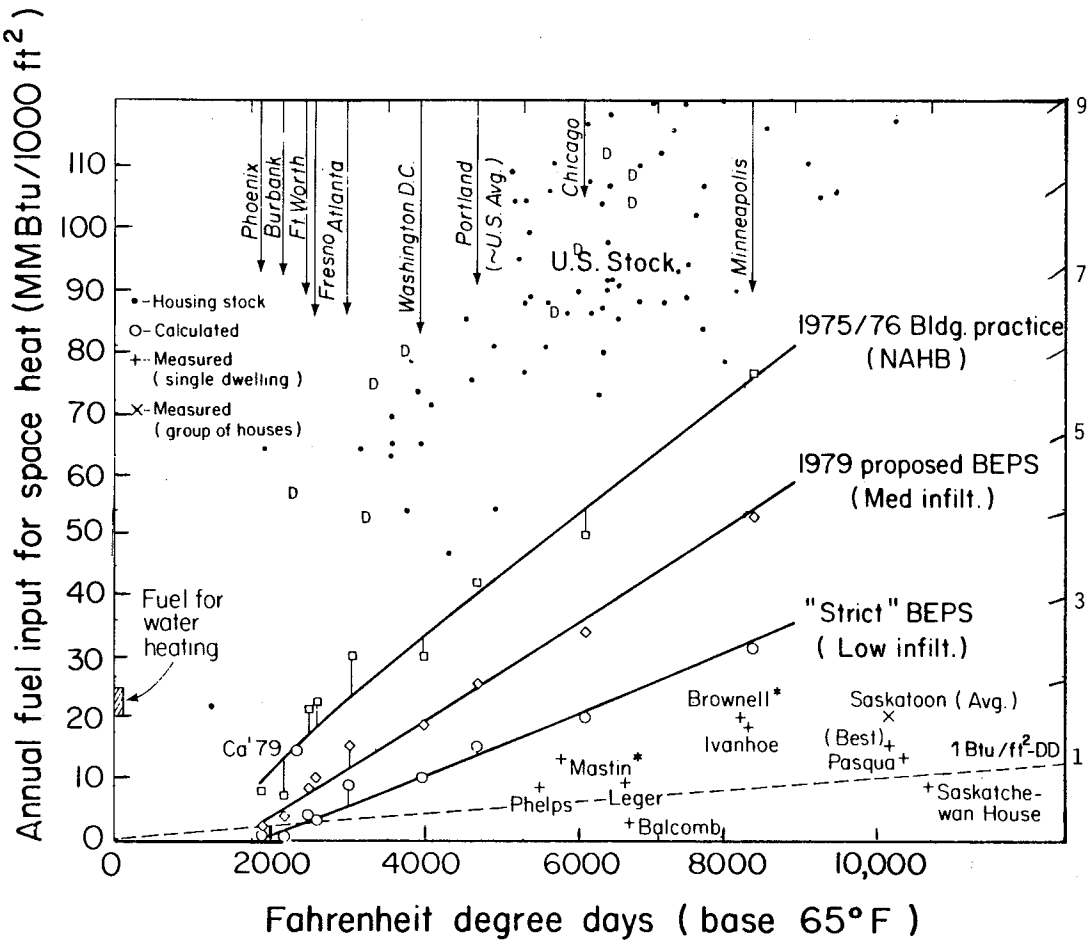

Fig. 1. Annual fuel input for space heating of single-family U.S. homes. Black dots are actual gas sendout to residential customers for space heat for calendar year 1978. The 1979 proposed BEPS (Building Energy Performance Standards) leaves infiltration at current practice levels of 0.6 air changes/hour (ach); strict BEPS reduces infiltration to 0.2 ach but restores 0.4 ach with mechanical ventilation through a heat exchanger. Approximate extra costs for conservation above 1975/76 practice; BEPS, $1,000; tight BEPS, $1,500; better-than-BEPS houses, several hundred to several thousand dollars.[3] (XBL 809-1904E)

close to 50% savings for $2500 (40¢/gal). Even 40¢/gal is considerably cheaper than the price of $1.20/gal, the cost of fuel in New England during the winter of 1980-81, or the tailblock rate for natural gas in northern California of 60¢/therm or the equivalent of 80¢/gal.

In the course of 1981, we plan to continue adding to and refining the data on residential retrofits, especially as new information sources become available from demonstration projects (like our "House Doctor" demonstration, described below) and the nationwide Residential Conservation Service programs. These data will be published as Part B of the "BECA" series, and then regularly updated in future years.

BECA-C: Commercial Buildings

We plan to issue our first edition of BECA-C in April 1981. Figures 3 and 4 display some of the data compiled and estimated for commercial buildings to date. In Figure 3, long-range trends in the energy efficiency potential for newly built office structures in the U.S. are compared with trends in the efficiency potential for new passenger cars over the same 40-year time-frame. What is perhaps most striking about both sides of Figure 3 is the sudden improvement in efficiency of both new automobiles and new commercial buildings beginning in the mid-1970's. We anticipate that efficiency levels for both autos and office buildings will continue to improve over the next decade in response to rising energy costs, the spread of technical innovations, competition from imported cars, and direct incentives or government regulations.

Figure 4 presents several examples of possible retrofits in office, commercial, and university buildings at costs of conserved energy ranging from $.20 to $1.22 per MBtu and indicates similar opportunities for improving the operation and maintenance of non-residential buildings.

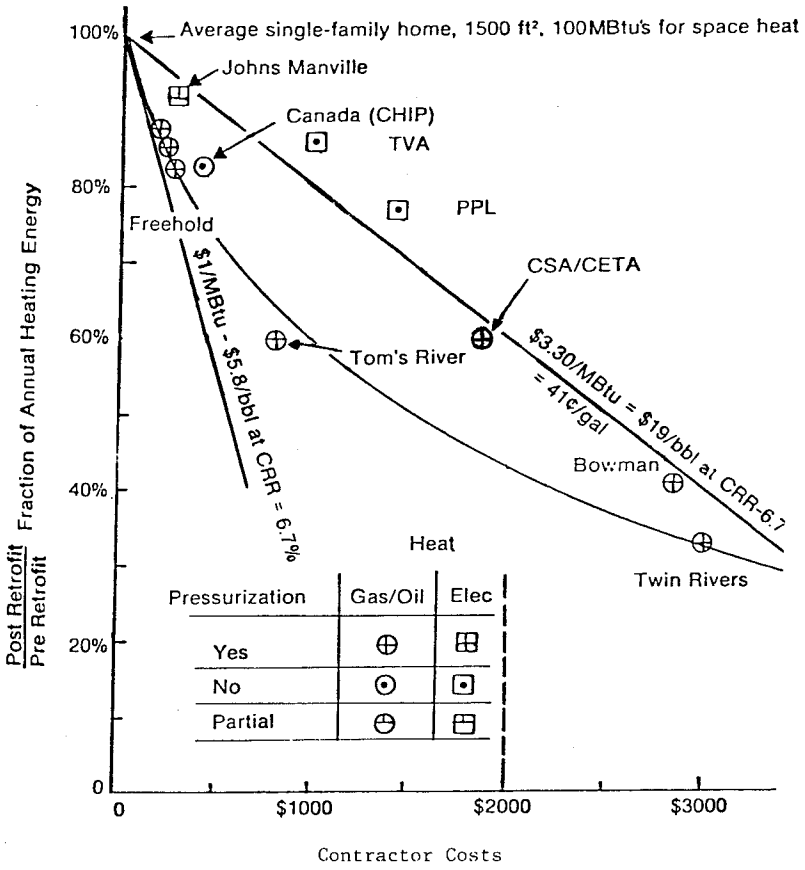

Fig. 2. "Frontier" curve for measured single-family home retrofits. The upper and lower edges of the wedge represent costs of conserved energy of $3.30/MBtu and $1/MBtu, respectively. All points represent measured data except for the CHIP (Canadian Home Insulation Program) sample of 700,000 homes. (XBL 813-8793)

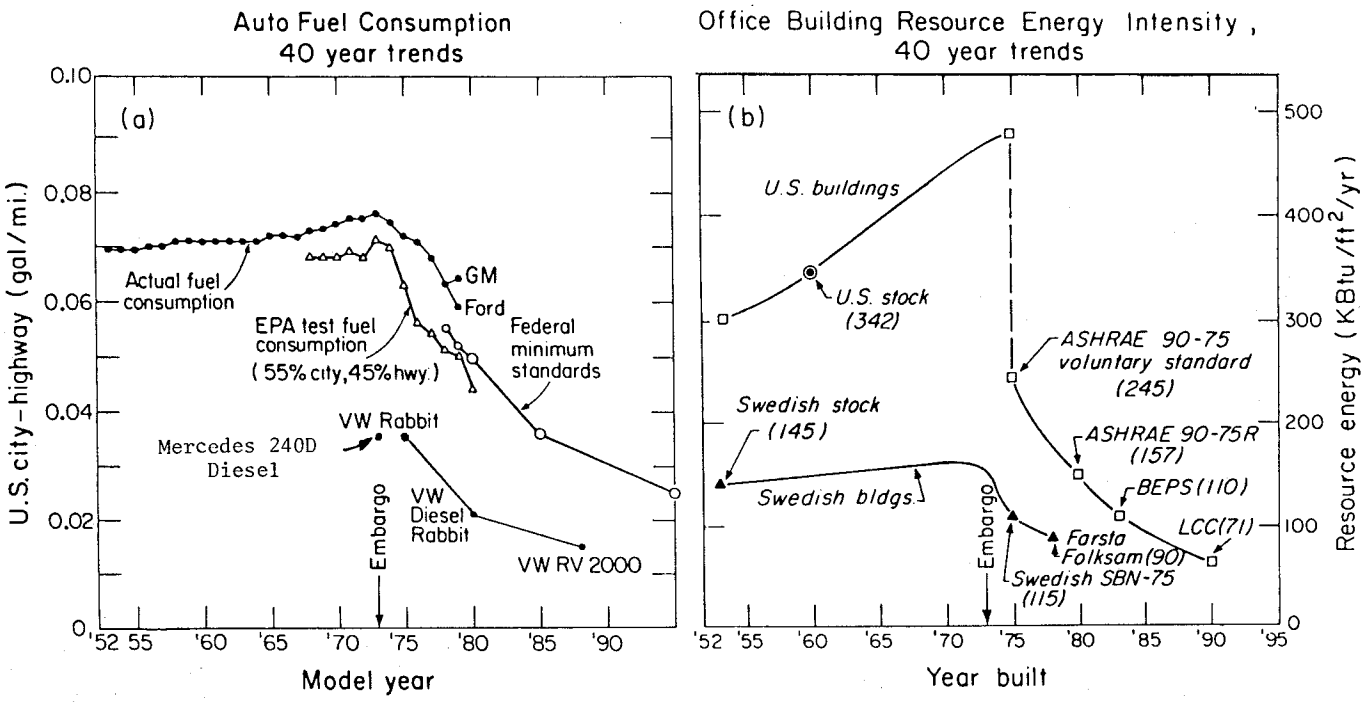

Fig. 3. Horsepower Race: Forty-year trends in energy use for automobiles vs. office buildings (measurements vs. calculations).4,5 (XBL 809-1847A)

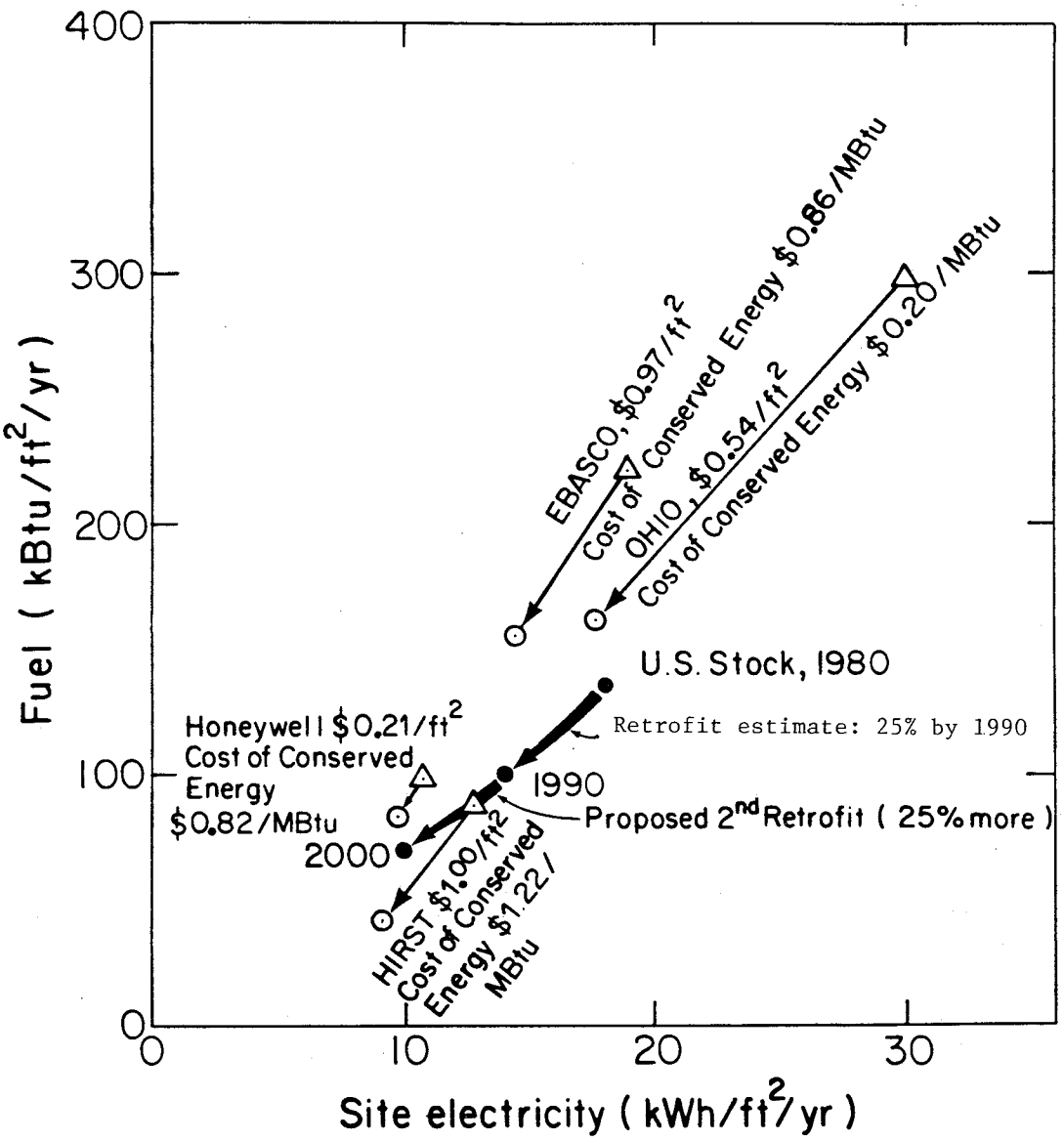

Fig. 4. Possible retrofits in offices (Hirst), commercial buildings and hospitals (EBASCO), and a university (Ohio State). For comparison, a proposed retrofit sequence is included. For details, see LBL-11300. (XBL 809-1845)

The next two sections show how the data compiled through "BECA," along with other sources, have been used both at the state and national levels to develop estimates of maximum cost-justified technical potentials for improving the energy efficiency of buildings.

California Residential Conservation Potential

The work described here was supported by the California Policy seminar and has been published as an LBL report.[1] In order to show the potentials for energy conservation in California's residential sector, we have developed "supply curves of conserved energy" in which individual conservation measures are ranked in order of increasing cost-per-unit of energy saved. Unit costs are measured in constant dollars on the vertical axis, and cumulative annual energy savings on the horizontal axis. In this way, conserved energy is put on a par with other new sources of energy, such as synthetic fuels. A computer program, CPS 1.0, was created to perform the energy accounting.

Figure 5 shows a supply curve of conserved electricity for California residences, as of 1980. Table 1 is a key to the curve, listing the name of each measure and the statewide annual energy savings expected from it. To estimate the available "reserves" of conserved energy, one must choose a suitable cost of conventionally supplied energy for comparison. The measures that are cost-effective are those for which the cost of conserved energy is less than the price of conventional fuels or electricity. For our supply curves, energy savings are always expressed as technically feasible, economically justified potentials--not necessarily as forecasts of a future that is likely to be achieved.

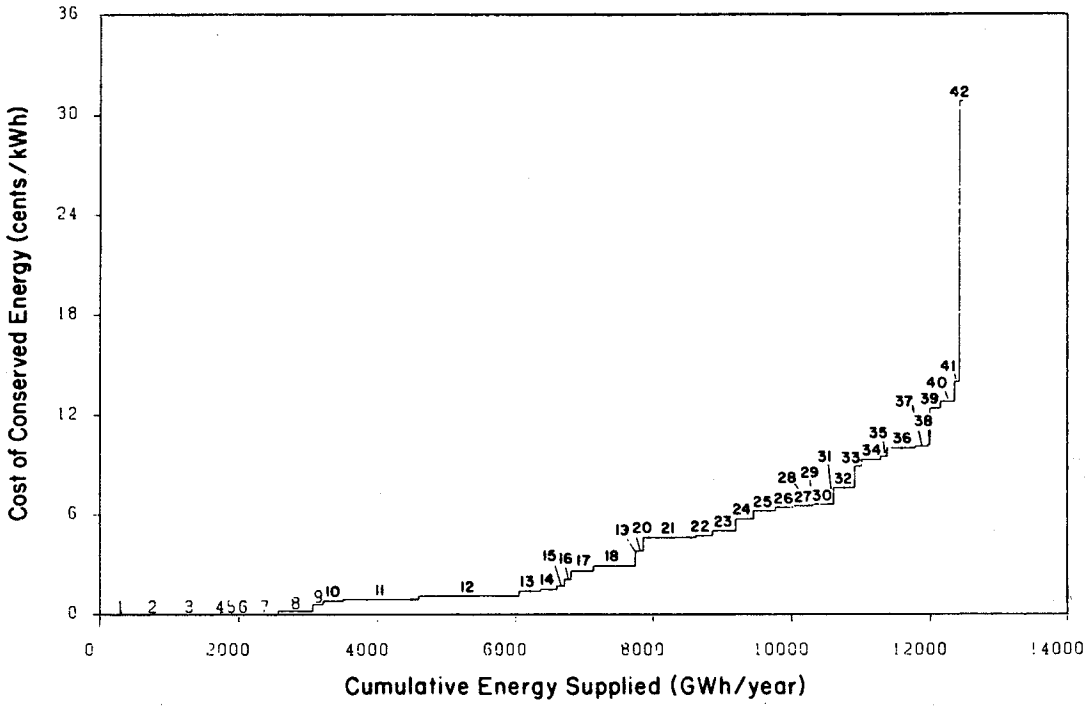

Fig. 5. The grand electricity conservation supply curve for California's residential sector. The total residential use in California in 1978 was 49,000 GWh. Conservation measures with costs up to 6 cents/kWh will save roughly 20% of current use. See Table 1 for a guide to the conservation measures involved. Note that 1000 GWh = 1 billion kWh. (XBL 813-8792)

The current tailblock price for residential electricity in California is roughly 8 cents/kWh. About 22% of California's current residential electrical use could be saved at costs of conserved electricity below 8 cents/kWh. A similar conservation supply curve for natural gas (not shown) indicates that roughly 34% of current residential use could be saved at costs of conserved energy below $7/MBtu.

Conservation supply curves can also be generated for single end-uses, such as water heating or refrigeration. In these cases, the thermodynamic limits to the reserve of conserved energy can also be displayed.

Technical Potentials for Energy-Efficient U.S. Buildings by the Year 2000

This work was supported by the Solar Energy Research Institute (SERI) and is detailed in an LBL report[2] as well as in a book to be published by the University of California Press.

Looking at energy use in U.S. residences and commercial buildings from a perspective of conservation and solar technical potentials leads to a very different picture for the year 2000 than do even the "low-growth" energy-demand forecasts that have recently become conventional wisdom in technical and policy circles. Recent demand forecasts by the Energy Information Agency at DOE anticipate that today's annual energy use of about 27 quads will probably grow to about 32 quads by the year 2000, or an average annual growth rate well under 1%. (Actually, fuel use, now about 13 quads, is expected by EIA to shrink to about 10 quads, with increased electricity consumption making up the difference.)

In contrast to this conventional outlook based on demand, our analysis suggests that it is technically feasible and economically cost-justified (even with current technology and at today's average energy prices) to dramatically reverse the expected 4-quad increase in energy demand in buildings. By the year 2000, the U.S. building stock could use as little as 16 quads--two-thirds of today's consumption levels -- despite the addition of more than 40 million new housing units and 20 billion new square feet of commercial space (see Table 2). This would be the result if virtually all existing buildings were retrofitted over the next two decades with cost-effective measures now commercially available, and if the efficiency of new buildings and newly-manufactured appliances and equipment were designed to minimize life-cycle costs.

The difference between a conventional demand forecast for the year 2000 and our "least-cost potentials" outlook is significant in absolute as well as percentage terms. By the year 2000, the difference in annual energy consumption for the buildings sector alone is greater than today's total imports of foreign oil (most of which go to sectors other than buildings, particularly industry and transportation).

A major capital investment in improved building and appliance efficiency would be required to

Table 1. Supply table for the electricity supply curve (Fig. 5). The time horizon is 10 years; the discount rate is 5%. For comparison, note that in 1978 the California residential sector used 49,600 GWh; thus conservation estimates out to a marginal cost of 6.4¢/kWh (Col. 1), which save 10,000 GWh (Col. 4), save about 20% of residential electricity, or the output of two standard generating plants.

	Conservation Measure[a]	Cost of Conserved Energy[b] (cents/kWh)		Energy Supplied (GWh/y)[c]		Total Dollars Invested
		Marginal	Average	Per Measure	Total	(millions)
1	Solid-state color TV	0	0	599.1	599	0
2	Solid-state black-and-white TV	0	0	322.3	921	0
3	CEC standard refrigerator	0	0	728.0	1,649	0
4	CEC standard room A/C	0	0	152.1	1,802	0
5	CEC standard central A/C	0	0	168.0	1,970	0
6	Water heater temp. setback	0	0	186.2	2,156	0
7	Cold-water laundry	0	0	407.4	2,563	0
8	Low-flow showerhead	0.2	0	496.6	3,060	8
9	Night setback of 10 °F	0.6	0.1	153.1	3,213	20
10	Savings on pool filter from cover	0.8	0.1	287.0	3,500	24
11	Most efficient refrigerator	0.9	0.3	1092.0	4,592	102
12	Refrigerator package "A"	1.1	0.5	1466.4	6,058	227
13	Most efficient freezer	1.4	0.5	305.8	6,364	259
14	Water heater insulation blanket	1.5	0.6	240.6	6,605	275
15	3-way bulb to GE Halarc	1.7	0.6	110.6	6,715	283
16	Sealed attic bypasses	2.1	0.6	92.5	6,808	307
17	Freezer package	2.6	0.7	327.6	7,135	373
18	Kitchen fluorescent lights	2.9	0.9	608.9	7,744	511
19	R-19 ceiling insulation	3.7	0.9	9.9	7,754	515
20	Diversion of electric clothes dryer vent	3.8	0.9	105.4	7,860	546
21	Gas clothes dryer	4.6	1.3	766.7	8,626	821
22	Exterior fluorescent lights	4.7	1.4	239.0	8,865	909
23	100 W bulb to fluorescent (1)[d]	5.0	1.5	334.5	9,200	1,039
24	Storm windows	5.7	1.6	258.4	9,458	1,224
25	Central A/C wall insulation	6.2	1.7	308.7	9,767	1,462
26	Most efficient central A/C	6.4	1.9	252.0	10,019	1,630
27	Manual refrig. improvement	6.5	2.0	208.0	10,227	1,734
28	Most efficient electric dryer	6.5	2.0	62.0	10,289	1,765
29	Fireplace damper	6.5	2.0	13.4	10,302	1,772
30	100 W bulb to fluorescent (2)[d]	6.6	2.1	290.3	10,593	1,920
31	R-11 insulation in walls	7.4	2.1	8.8	10,601	1,928
32	3-way bulb to fluorescent	7.6	2.3	305.3	10,907	2,108
33	Caulking	8.9	2.3	102.1	11,009	2,178
34	Gas range	9.3	2.5	274.2	11,283	2,374
35	Window shading for central A/C	9.5	2.6	94.5	11,377	2,443
36	Refrigerator package "B"	10.0	2.8	405.6	11,783	2,755
37	100 W bulb to fluorescent (3)[d]	10.1	2.9	191.2	11,974	2,904
38	Most efficient room A/C	10.2	2.9	24.3	11,999	2,926
39	75 W bulb to fluorescent	12.4	3.1	155.8	12,154	3,074
40	Weatherization (apartments)	12.8	3.2	204.0	12,358	3,346
41	Additional R-19 in ceiling	14.0	3.3	68.9	12,427	3,466
42	Weatherstripping	30.8	3.4	47.9	12,475	3,530

[a] The conservation measures are listed in the order they appear in the supply curve, i.e., according to cost of conserved energy.

[b] in 1979 dollars.

[c] Note that 1 Terawatt-hour (TWh) = 1 billion kWh, and 1 gigawatt-hour (GWh) = 1 million kWh.

[d] Residential lamps are divided into three groups according to annual hours of use: (1) = average of 800 hr, (2) = 600 hr, and (3) = 400 hr.

Table 2. Summary of energy consumption in the residential and commercial sectors of U.S.: 1980 vs 2000.

	Year 1980			Year 2000								
				Baseline			Conservation Measures to Current Cost of Oil and Electricity			Conservation and Solar Measures to Curent Cost of Oil and Electricity		
	Fuel (Q)	Elec. (Q resource)	Total	Fuel (Q)	Elec. (Q resource)	Total	Fuel (Q)	Elec. (Q resource)	Total	Fuel (Q)	Elec. (Q resource)	Total
A) Residential												
Existing residences space heating and cooling	7.04	2.65	9.69	5.50	1.98	7.48	1.95	0.88	2.83	1.37	0.66	2.03
New residences space heating and cooling	---	---	---	1.59	1.96	3.55	0.74	0.92	1.66	0.54	0.81	1.35
Water heating	1.29	1.00	2.29	1.46	2.11	3.57	0.75	1.26	2.01	0.55	0.92	1.47
Appliances	0.47	4.16	4.63	0.68	6.67	7.35	0.43	4.13	4.56	0.43	4.13	4.56
Residential total	8.80	7.81	16.61	9.23	12.72	21.95	3.87	7.19	11.06	2.89	6.52	9.41
B) Commercial												
Existing buildings	4.8	5.6	10.4				1.6	2.4	4.0			
New buildings				3.2	10.1	13.3	0.2	3.1	3.3			
Commercial Total	4.8	5.6	10.4	3.2	10.1	13.3	1.8	5.5	7.3			
C) Total (Residential and Commercial)	13.6	13.4	27.0	12.4	22.8	35.2	5.6	12.7	18.3			

Note: The conservation and solar technology potential is based on conservation measures with a cost less than 7.5 $/million Btu or 5.7 cents per kWh. The additional savings for all measures with a higher cost is 0.70 quads.

achieve this technical potential of $450 billion cumulatively over the next 20 years (in undiscounted 1980 dollars). But the direct economic returns to such investments would be even greater, due to reduced needs to import high-priced oil and to construct costly new power plants and other energy facilities. For example, the conservation and solar measures we analyze can save energy at an average cost of about $10 per barrel-of-oil-equivalent--an attractive investment by any criterion.

We based these estimates on a detailed, end-use analysis of energy waste and inefficiency in today's buildings and appliances, and the opportunities for improved efficiency in new additions to the stock. For purposes of the analysis, we accepted (without necessarily agreeing with) all of the EIA projections of stocks, appliance saturations, and fuel choice, but adjusted the assumed building and equipment efficiency levels to minimize overall life-cycle costs. For the residential sector, individual conservation and solar measures were ranked in order of cost-effectiveness (cost per unit of conserved energy), as with the California residential analysis. The result was once again a series of "supply curves of conserved energy," illustrated in Figures 6A and 6B. End-use data were not available in sufficient detail for the various categories of commercial buildings to permit us to compile conservation supply curves for that sector; this task will be part of our continuing efforts in 1981 and 1982.

A statement of technical potentials is not the same as a forecast of what is actually expected to occur through the workings of the market or the effects of public policies. Achieving most or all of this technical potential will require a massive effort to retrofit the existing building stock, improve building operation and maintenance practices, and introduce the best available energy-efficient technologies in new construction and new appliance manufacture.

"House Doctor" Demonstration, Training, and Retrofit Monitoring Project

Researchers at LBL are currently conducting a cooperative project with Pacific Gas and Electric Company (PG&E) to determine the energy savings resulting from "house doctor" retrofitting of single-family residences in Walnut Creek, CA. The standard house-doctor visit is designed to increase the effectiveness of residential audits by including instrumentation and ~2 person-days of retrofitting. House doctoring also has potential as a contractor type business similar to, or combined with, insulation installation.

The procedure emphasizes use of a "blower door," a device which can both pressurize and depressurize a house to facilitate the measurement of infiltration levels and permit quick identification of air leaks. An infrared scanner is used in conjunction with the blower door to detect leaks in the attic and to check the quality of wall insulation.

From the audit portion of the visit, a series of recommendations are made to the homeowner, as in other audit procedures. The principal feature of the retrofit portion is that the auditor, at the time of the visit, will implement simple energy-saving measures while the house is pressurized. The convenience to homeowners is that the work is not only done immediately (and correctly) but also at low materials cost.

Thirty houses were included in our study. Ten of the houses were "active controls" which received house-doctor audits only (no retrofit). Ten received a standard house-doctor visit, and ten received an "extended retrofit," which is a house-doctor visit plus additional retrofit to be performed by contractors. In our experiment, the house-doctor audit is essentially the PG&E Enercom computerized audit with the addition of an infiltration measurement and a few extra items on the audit form/prescription. Our retrofits included installation of electronic ignition devices on the furnace--not always considered part of house doctoring. The contractor retrofits will be installed in Spring 1981, selected on the basis of economic attractiveness from a list that includes: increased insulation in attics, walls, and floors; installation of storm windows; taping and insulating furnace ducts; further house-doctor-type leak plugging; and replacement of incandescent with fluorescent light fixtures.

The energy use of each house will be monitored for at least one year after the retrofitting occurs. Consumption by furnace, water heater, pool heater (if any), and air conditioner will be recorded weekly. A regression of energy use with respect to temperature data from a nearby site, done before and after the retrofits, will allow calculation of energy savings in an average year.

Several useful materials have been developed as part of this project. One is a comprehensive House Doctor Manual which describes the on-site audit and retrofit procedure. Another is a complete list of the equipment, tools, and retrofit materials needed for a house-doctor visit. In addition, a curriculum for training house doctors was developed and used in a two-week intensive training course for seven PG&E "weatherization specialists." These trained PG&E house doctors completed the twenty partial retrofits and thirty audits during November and early December of FY 1980.

Various members of the public were invited to observe a series of retrofit demonstrations in October. This program was designed so that the observers could get a first-hand idea of the kind of retrofit procedure that becomes possible when the various instruments mentioned above are used. The houses were house-doctored by two members of our LBL staff, while a third explained the procedure to the observers.

The preliminary results from this project are summarized in Tables 3 and 4. The average reduction in infiltration (as calculated from the blower-door measurements) is 30%, with a range from 14% to 65%. The average infiltration rate for the 16 houses included in the preliminary calculations is 0.75 air changes per hour (ach) before, and 0.52 ach after house doctoring. We estimate the costs

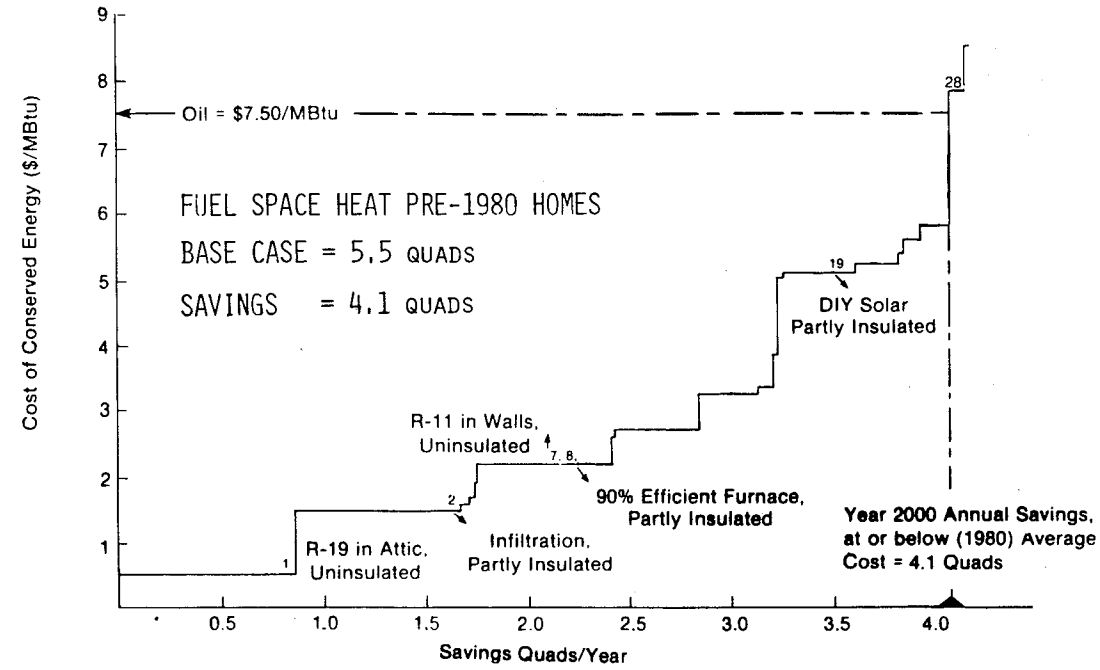

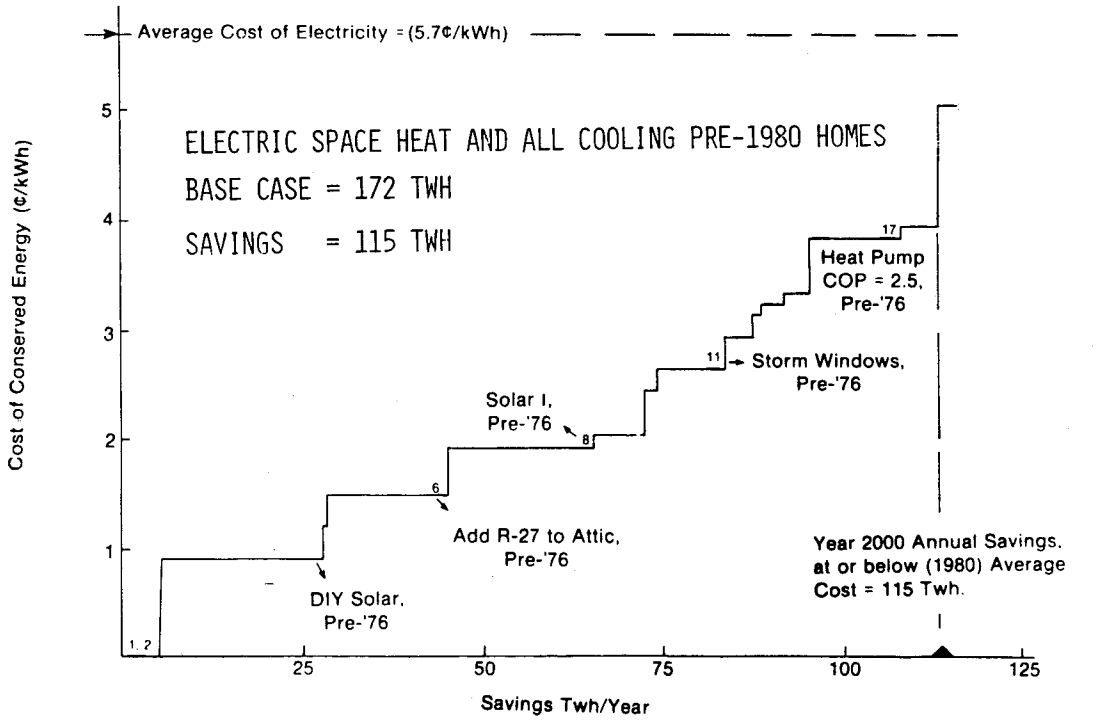

Fig. 6A, 6B. Supply curves for space heat and cooling for pre-1980 homes surviving in 2000. Note that 1 TWh = 1 billion kWh. For details, see LBL-11300.

(XBL 813-8791)

Table 3. Infiltration reduction from house-doctor retrofits.

House	Year Constructed	Volume (m^3)	Leakage Area (cm^3)		Heating Season Average Air changes/hour		Infiltration Reduction (%)
			Before	After	Before	After	
A2	1969	430	1421	1081	.62	.47	24
A3	1955	350	1499	1282	.78	.67	14
A5	1965	370	1325	789	.68	.40	41
A6	1956	350	1126	951	.62	.52	16
A7	1969	600	1638	1319	.52	.42	19
A9	1966	420	1148	944	.68	.56	18
A10	1960	340	2010	1510	1.12	.84	25
B1	1965	490	2091	1606	1.06	.82	23
B2	1970	520	1916	1297	.70	.47	33
B4	1969	640	2712	950	1.06	.37	65
B5	1970	510	1761	1106	.67	.42	37
B6	1960	440	1437	1049	.62	.45	27
B7	1969	640	1462	1127	.57	.44	23
B8	1969	600	3164	1827	.99	.57	42
B9	1965	480	2148	1458	.85	.58	32
B10	1969	770	1230	881	.40	.28	30
Average	--	497	1756	1199	.75	.52	29

(including labor, materials, and overhead) of a standard house-doctor visit at $365, (or $556 including the cost of IID installation). This yields a cost of conserved energy, over the useful lifetime of the retrofits, of $0.22/therm.

By finding and fixing leaks which are undetectable in current (uninstrumented) audits, house doctoring not only cuts energy waste but can make other conservation measures more effective. For example, if an attic is insulated before leaks are identified and patched, two serious problems arise: some leaks will be hidden by the insulation and harder to find and fix, and (2) loss of heat through these undetected leaks will undermine the benefits of insulation (in energy and dollar savings) and discourage homeowners from investing in energy-efficient strategies. Because of the relatively low materials cost and moderate labor intensity, this audit procedure may be well suited for use by small contractors and community groups.

New homes

Use of the blower door as a diagnostic tool during construction of new homes will probably turn out to be even more effective than its use in occupied houses.

Homes at time of sale

A house-doctor visit at the time of sale is probably a good investment for the future owner. If the house is doctored while it is empty (of furniture, rugs, and material stored in the attic), far more work can be done in one day. Preliminary results indicate that house doctor techniques can save energy at costs below the current fuel prices, and far below the price of new energy supplies. As prices rise and the importance of conservation grows, the importance of testing and refining these techniques will likewise increase.

Table 4. Savings and cost of conserved energy (CCE) for house-doctored homes of Table 3, before final contractor retrofit.

House No.	Therms/year saved by infiltration Reduction[a]	Total therms/year saved[b]	Estimated Cost[c] ($)	Cost of Conserved Energy[d] ($/therm)
A2	41	121	526	.29
A3	28	108	526	.33
A5	70	189	556	.20
A6	24	143	556	.26
A7	45	125	526	.26
A9	32	112	526	.32
A10	62	101	365	.24
B1	77	77	336	.29
B2	71	151	526	.23
B4	269	349	526	.10
B5	89	208	556	.18
B6	44	44	336	.51
B7	53	172	556	.22
B8	151	190	365	.13
B9	78	158	526	.22
B10	55	94	365	.26
Average	74	146	480	.22

[a]Calculated from leakage area measurements. Assumes 65°F heating degree day base and 20% reduction in furnace steady-state efficiency due to cycling and duct losses.

[b]Includes calculated savings from water heater and/or intermittent ignition device (IID) in houses where these were installed.

[c]Includes labor, materials, and 50% overhead. For a typical visit including infiltration reduction and water heater insulation labor costs are $155 and materials costs are $75. Additional costs for IID installation are $67 (labor) and $60 (materials).

[d]CCE calculated on the basis of an amortization period equal to expected useful life of the retrofits (20 years). Real interest rate assumed to be 3%.

PLANNED ACTIVITIES FOR FY 1981

BECA-A (Compilation of New Homes)

We plan to enlarge our data bank of efficient, cost-effective homes from ten to several hundred.

BECA-B (Residential Retrofit)

We will continue to add to and refine the data of Fig. 2, and submit our report for publication during the year.

BECA-C (Commercial Buildings)

We plan to greatly increase our rate of data collection, probably by agreement with Energy Users News, and to publish a regular update in Energy Users News and other trade journals. BECA-C will be submitted for publication.

Technical Potentials for Energy-Efficient U.S. Buildings

We plan to complete this work, incorporate reviewers' comments, and offer it to commercial publishers.

House Doctoring.

We shall continue our collaboration with PG&E, submetering and monitoring the savings in both heating and cooling loads. We shall further collaborate with PG&E and community groups to train more house doctors.

REFERENCES

1. J. Wright, A. Meier, M. Maulhardt, A. H. Rosenfeld, Supplying Energy through Greater Efficiency, The Potential for Conservation in California's Residential Sector, Lawrence Berkeley Laboratory report LBL-10738, January 1981 (to be published by The University of California Press).
2. A. H. Rosenfeld, P. Cleary, D. B. Goldstein, J. Harris, J. Wright (LBL), P. Claridge, K. Gawell, H. Kelly (SERI), Technical Potentials and Policy Recommendations for Conservation and Renewable Resources: A Least Cost Scenario, 1980-2000, Lawrence Berkeley Laboratory report LBL-11300 (to be published).
3. A. H. Rosenfeld et al., BECA-A: Building Energy Use Compilation and Analysis, Lawrence Berkeley Laboratory report LBL-8912 (submitted to Energy and Buildings, 1980).
4. Society of Automotive Engineering Transactions, No. 750957; C. L. Gray, Jr. and F. von Hippel, "The Fuel Economy of Light Vehicles," Scientific American, vol. 244, no. 5, May 1981; F. von Hippel, U.S. Transportation Energy Demand, Draft Report (Princeton, N.J.: Princeton Center for Energy & Environmental Studies), July 1980.
5. A. Rosenfeld et al., Energy Efficient Buildings: Technical Potentials and Policy Recommendations for Conservation and Renewable Resources: A Least-Cost Scenario, Draft Report, Lawrence Berkeley Laboratory report LBL-11300, July 1980.

ENVIRONMENTAL POLLUTANT STUDIES

ATMOSPHERIC AEROSOL PROJECT

INTRODUCTION

T. Novakov

The principal research interest of the Atmospheric Aerosol Research group is in determining the role of primary particles in atmospheric chemistry and physics. Specifically, we are interested in heterogeneous atmospheric chemical reactions that involve primary particles, such as soot and fly ash, and gaseous species, and in the effects of primary particles on visibility and climate. This research entails laboratory studies complemented by selective field sampling and experiments. All our studies rely on analytical chemistry and other measurement sciences. We are therefore actively developing methods for chemical characterization of aerosol particles and for determining their optical properties.

In the field of atmospheric chemistry, we have primarily focused on the formation of sulfates by aqueous reactions catalyzed by solid particles and dissolved metal ions. In addition, the role of the oxides of nitrogen in SO_2 oxidation was also studied.

During recent years, we have definitely established that black graphitic carbon is a major constituent of the carbonaceous fraction of urban aerosol particles. During the past year, measurements were extended to the Arctic region, where a substantial concentration of these particles was determined. The impacts of these highly absorbing species on climate have not yet been assessed, but preliminary studies indicate that they could be very important, especially over regions with a high surface albedo, such as the polar ice caps.

In methods development, we have been working on determining aerosol absorption coefficients, developing thermal analysis methods (combined with optical measurements and solvent extraction procedures) to study carbonaceous and nitrogenous species, and further developing deuteron and ^3He-induced activation analysis for determination of low-Z elements in aerosol particles.

ACTIVATED CARBON CATALYZED OXIDATION OF AQUEOUS S(IV) SPECIES*

R. Brodzinsky, S. Chang, S. Markowitz, and T. Novakov

INTRODUCTION

The formation of acid rains is a source of major interest and concern. Acid rain is caused by nitric and sulfuric acids that are formed by the oxidation of nitrogen oxides (NO_x) and sulfur dioxide (SO_2). The precipitation's increased acidity as much as pH ~3 in parts of New England and Europe instead of the "normal" of pH ~5.6) has had many deleterious effects. Many lakes have become too acidic to sustain aquatic life; most fish cannot live in water with a pH <4.5.[1] The acidity also affects plant life, both by attacking the vegetation's leaves and branches and by leaching nutrients from the soil. Acidity also has its effects on buildings and statues. Many older structures, especially those constructed of sandstone or marble, are literally dissolving.

Many mechanisms are known for the oxidation of SO_2.[2] We have been studying the catalytic effects of carbonaceous soot particles and activated carbons on this reaction.[3] Carbonaceous particles in aqueous suspension were found to be efficient catalysts for the oxidation of aqueous sulfur (IV) [S(IV)] species.

Those studies' kinetic results showed that the reaction followed a Langmuir adsorption isotherm for its rate dependence on dissolved O_2 and the product of two adsorption isotherms for S(IV). The rate of reaction is linearly dependent on the concentration of carbon particles in the solution. (Note: Hydrated sulfur dioxide ($SO_2 \cdot H_2O$) is also known as "sulfurous acid" (H_2SO_3), but this molecule has never been observed. Within this work the symbol S(IV) and the formula H_2SO_3 are used to signify all the S(IV)-containing species in solution ($SO_2 \cdot H_2O$, HSO_3^-, and SO_3^{2-}). The symbol C_x signifies the carbonaceous particle surface, while the term "carbon" refers to the particles of activated carbon or soot and not the element C.)

We propose a possible four-step reaction mechanism which consists of the adsorption of a dissolved O_2 molecule onto the carbon surface,

*This work was supported by the Assistant Secretary for Environment, Office of Health and Environmental Research, Division of Biomedical and Environmental Research of the U.S. Department of Energy under Contract No. W-7405-ENG-48 and by the National Science Foundation under Contract No. ATM 80-13707.

followed by the adsorption of 2 S(IV) molecules or ions. These are oxidized on the surface to sulfate, which desorbs from the surface, regenerating the catalytically active site.

We have extended this research to other activated carbons and to soot collected in a highway tunnel.

ACCOMPLISHMENTS DURING FY 1980

The following experimental methods were used. A known amount of S(IV) was added to the basic reaction system, consisting of a flask in which carbonaceous particles were suspended in deionized water. Three different commercially available activated carbons were used: Nuchar C-190 and Nuchar S-N, manufactured by the West Virginia Pulp and Paper Co. (Wesvaco), and EM Reagents, Aktivkohle, manufactured by E. Merck.

The Aktivkohle is a 30-50 mesh activated carbon for use in gas chromatography. It was ground in an agate ball mill for 15 h to produce a powder of ~200 mesh. The two Nuchars are decolorizing carbons of 200-400 mesh. The manufacture of C-190 was discontinued in 1978. The activated carbons were washed three times with boiling water to remove water soluble sulfates and nitrates that were adsorbed on the surface, and then the carbons were dried. Elemental analysis and physical properties of the activated carbons are shown in Table 1.

Automotive soot was collected in the ventilation duct above the Caldecott Tunnel, a 1.5-mile highway tunnel on California Route 24 beneath the Berkeley hills between Oakland and Orinda. A ventilation tunnel above the roadway is coated with automotive soot. This soot was scraped from the walls with a plastic scraper into a large plastic bucket. It was then washed three times with boiling water and dried. The water wash removed the

Table 1. Elemental analysis of carbons (w%).

Element	C-190	SN	Aktivkohle	Tunnel	Method
C	74.7	77.7	88.1	14.2	Combustion
H	0.9	1.56	1.60	1.75	
N	0.1	0.23	1.17	0.30	
Ca	0.221	b.d.	0.025	1.98	XRF
S	0.116	0.07	0.39	1.15	
Si	>0.111	b.d.	b.d.	>10.1	
Fe	0.117	0.011	0.018	2.83	
K	0.091	b.d.	b.d.	b.d.	
Al	>0.055	b.d.	b.d.	>4.05	
Ti	0.016	0.0017	b.d.	0.122	
Mn	0.013	0.0012	b.d.	0.022	
Cr	0.002	0.0011	b.d.	0.014	
Cu	0.002	0.0007	b.d.	0.018	
Zn	0.002	0.0006	0.117	0.122	
Sr	0.002	b.d.	b.d.	0.086	
Ni	0.001	b.d.	0.002	0.108	
Cl	0.001	b.d.	0.001	0.101	
As	0.0004	b.d.	b.d.	b.d.	
Br	0.0004	b.d.	0.001	0.007	
Rb	0.0004	b.d.	b.d.	b.d.	
Zr	0.0004	b.d.	b.d.	b.d.	
Pb	0.0004	b.d.	0.007	5.06	
Ga	0.0001	b.d.	b.d.	b.d.	
Ba	b.d.	b.d.	b.d.	0.158	
O	23.6	20.4	8.57	<57.8	Difference
Surface area (m^2/g)	550	1150	1130	6	
Activation temperature (°C)	650	650	300		
pH (1g/ℓ)	5.4	7.2	6.2	5.0	
Made from	coal	coal	peat		

b.d. = below detection limits.
XRF = X-ray fluorescence technique.

water soluble organics, as well as the inorganics, which had adsorbed onto the soot surface. The composition and physical properties of the tunnel soot are shown in Table 1.

The dependence of the reaction rate on S(IV) concentration for the four different carbons is shown in Figure 1. Oxygen- and temperature-dependence data for the activated carbons are shown in Figures 2 and 3 respectively. Table 2 summarizes the coefficients for the experimentally seen rate law for the activated carbons. Oxygen and temperature studies were not performed on the tunnel soot. Within the experimental rate law for the tunnel soot,

$$k = Ae^{-Ea/RT} \frac{\gamma[O_2]^2}{1+\gamma[O_2]} = 1.97 \times 10^{-7} \text{ mol/g·s}$$

$\alpha = 6.36 \times 10^6$ l^2/mol^2

$\beta = 9.93 \times 10^2$ l/mol

Ea = activation energy

R = gas constant

T = temperature

γ = adsorption constant

Our proposed mechanism for this reaction is:

$$C_x + O_2(aq) \underset{k_{-1}}{\overset{k_1}{\rightleftarrows}} C_x \cdot O_2 \qquad (1)$$

$$C_x \cdot O_2 + S(IV) \underset{k_{-2}}{\overset{k_2}{\rightleftarrows}} C_x \cdot O_2 \cdot S(IV) \qquad (2)$$

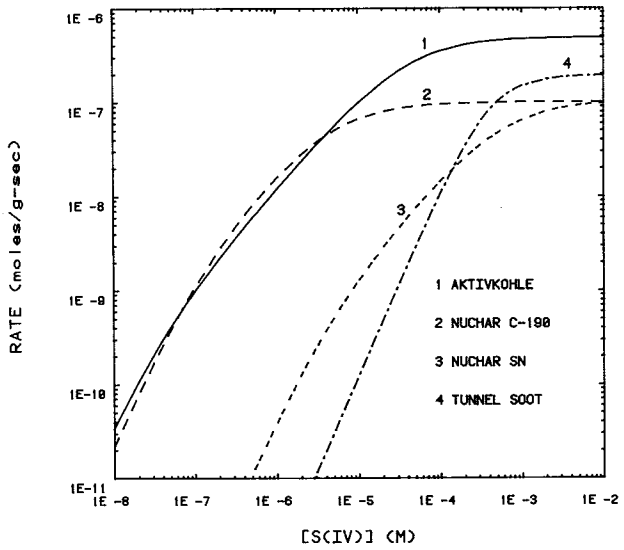

Fig. 1. Normalized rate of reaction versus total S(IV) concentration for various activated carbons and tunnel soot. (XBL 8010-12601)

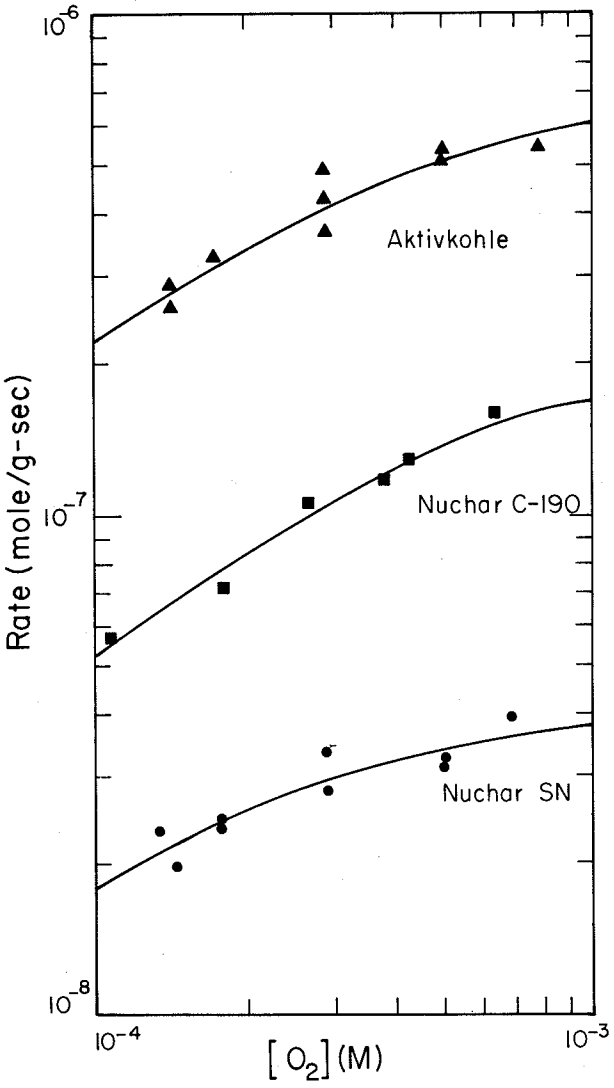

Fig. 2. Normalized rate of reaction versus dissolved oxygen concentration. [S(IV)] = 5 x 10^{-4} M. (XBL 8010-2279)

$$C_x \cdot O_2 \cdot S(IV) + S(IV) \underset{k_{-3}}{\overset{k_3}{\rightleftarrows}} C_x \cdot O_2 \cdot S^2(IV) \qquad (3)$$

$$C_x \cdot O_2 \cdot S^2(IV) \overset{k_4}{\rightarrow} C_x + 2S(VI) \qquad (4)$$

with

$$\frac{d[S(VI)]}{dt} = 2k_4[C_x]\left(\frac{K_1[O_2]}{1 + K_1[O_2]}\right)\left(\frac{K_2[S(IV)]}{1 + K_2[S(IV)]}\right)$$

$$\left(\frac{K_3[S(IV)]}{1 + K_3[S(IV)]}\right)$$

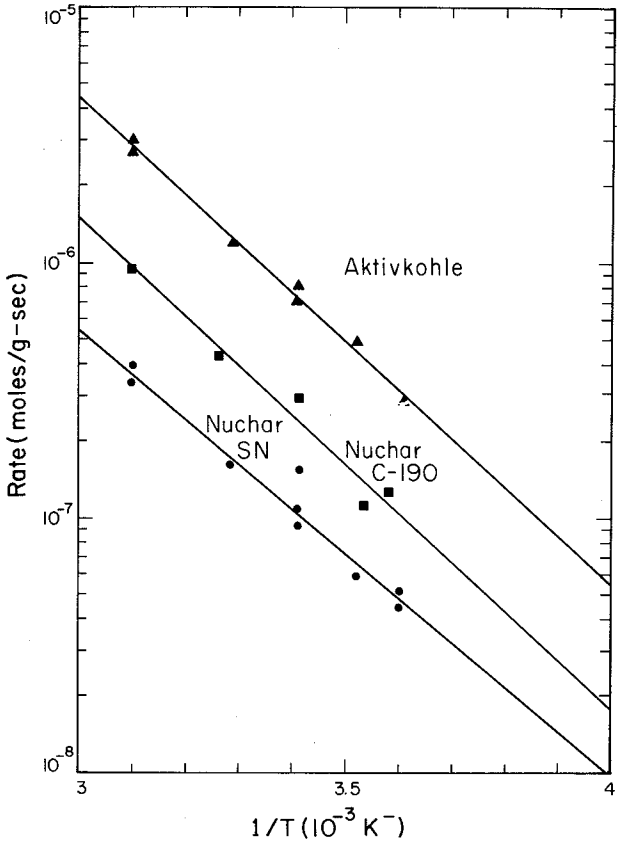

Fig. 3. Normalized rate of reaction versus 1/T (Arrhenius plot). (XBL 8010-2280)

where $K_1 = k_1/k_{-1}$, $K_2 = k_2/k_{-2}$ and $K_3 = k_3/k_{-3}$. Multiplication of the S(IV) terms yields the experimentally seen expression where $K_2K_3 = \alpha$, $K_2 + K_3 = \beta$ and $K_1 = \gamma$.

PLANNED ACTIVITIES FOR FY 1981

Work is currently in progress to determine the catalytic activity of true ambient aerosols. The results of these experiments will be of immeasurable help in determining the contribution of the carbon-catalyzed oxidation of SO_2 to the formation of atmospheric sulfates and acid rain.

REFERENCES

1. S. West, "Acid from Heaven," Science News, vol. 117, 1980, p. 76.

2. D. Möller, "Kinetic Model of Atmospheric SO_2 Oxidation," Atmospheric Environment, vol. 14, 1980. p. 1067.

3. R. Brodzinsky, S. G. Chang, S. S. Markowitz, and T. Novakov, "Kinetics and Mechanism for the Catalytic Oxidation of Sulfur Dioxide on Activated Carbon in Aqueous Suspension," Journal of Physical Chemistry, vol. 84, 1980, p. 3354.

Table 2. Summary of kinetic data for S(IV) oxidation on activated carbons.*

	Activated-Carbons		
	C-190	SN	Aktivkohle
A (mole/g-sec)	0.874	0.158	2.47
E_a (kcal/mole)	8.8	8.1	8.8
γ (ℓ/mole)	2.10×10^3	7.43×10^3	4.37×10^3
α (ℓ^2/mole^2)	2.40×10^{12}	4.92×10^8	9.52×10^{11}
β (ℓ/mole)	1.22×10^7	2.96×10^5	3.74×10^7
r^2 (oxygen)	0.978	0.851	0.925
r^2 (Arrhenius)	0.961	0.952	0.993

*

$$\frac{d[SO_4^{2-}]}{dt} = Ae^{-E_a/RT}\,[C_x]\left\{\frac{[O_2]}{1+[O_2]}\right\}\left\{\frac{\alpha[S(IV)]^2}{1+\beta[S(IV)]+\alpha[S(IV)]^2}\right\}$$

$\sigma_A^2 = \pm 10\%$

$\sigma_E^2 = \pm 5\%$

$\sigma_\alpha^2 = \sigma_\beta^2 = \sigma_\gamma^2 = \pm 3\%$

OXIDATION OF SO_2 BY WET SOOT PARTICLES: APPLICATION TO CLOUDS, FOGS, AND PLUMES*

W. Benner, R. Brodzinsky, and T. Novakov

INTRODUCTION

Concentrations of $SO_4^=$ and H^+ ions in acid rain are strongly correlated, and therefore the formation of atmospheric $SO_4^=$ is thought to be related to the formation of acid rain.[1] We are constantly revising our understanding of the chemical and physical processes that introduce sulfate into the atmosphere. Our recent studies have been directed towards sulfate formation pathways which involve liquid water. Work in our laboratory[2] has shown that aqueous suspensions of diesel, propane, and natural gas soot particles and several activated carbons oxidize SO_2 to SO_4. The work reported here is an extension of these earlier findings and focuses on the oxidation of SO_2 by dispersed water droplets that contain soot particles.

In laboratory studies, the exposure of dispersed wet soot particles to SO_2 simulates reactions which could occur in clouds, fogs, and plumes. Such dispersed droplet studies would also supply information that could be introduced into computer models to evaluate the relative importance of the soot-fog-SO_2 mechanisms for sulfate formation in the atmosphere. To meet our experimental objectives, we constructed a fog chamber in which stable fogs could be exposed to pollutant gases. The fog chamber work presented in this paper is not intended as a rigorous kinetic study; these experiments were conducted to show that SO_2 can be oxidized in droplets that contain soot particles.

ACCOMPLISHMENTS DURING FY 1980

Particles of Nuchar-SN, pre-extracted to remove SO_4, were resuspended by nebulization, and the resultant mist was passed over heated water and subsequently cooled to cause the nebulized particles to grow into larger droplets (Fig. 1). These droplets were exposed to SO_2 and introduced into the bottom of the fog chamber. The fog droplets were forced upwards through the chamber at a velocity which permitted an approximately 30-min reaction time between droplets and SO_2. A prefired quartz fiber filter and a Fluoropore (0.5-μm pore) filter were used simultaneously to collect samples from the top of the chamber. The filter holders and tubing leading to the filters were heated to decrease the relative humidity of the air stream to at least 30%, and reactions involving liquid water were thereby prevented. After collection of the sample, the Fluoropore filter was extracted in water and analyzed for SO_4 using ion chromatography. A portion of the quartz filter was analyzed for total carbon by combustion analysis.

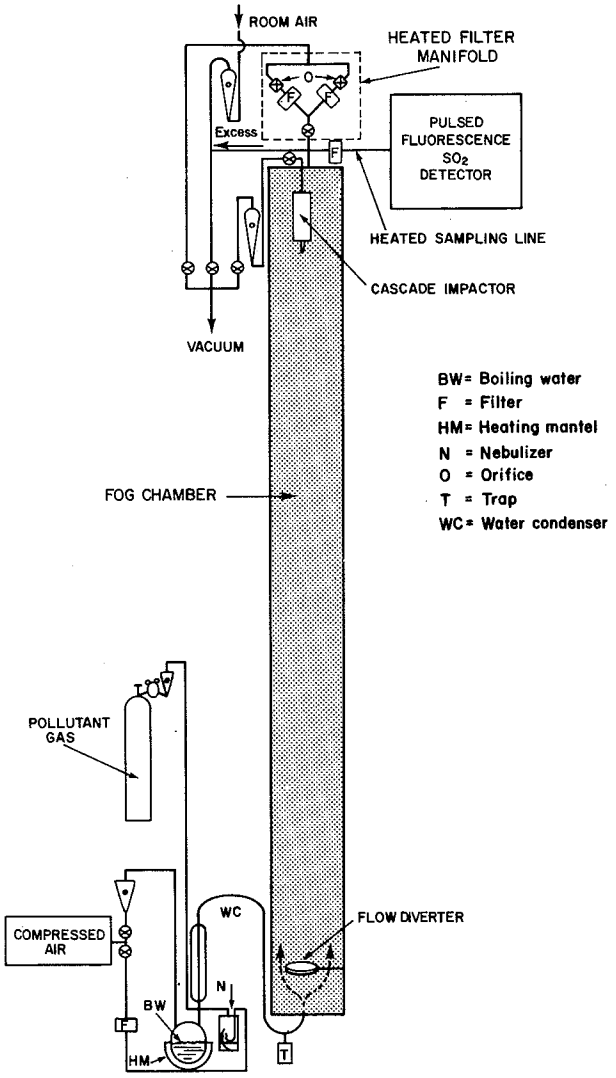

Fig. 1. Laboratory fog chamber and associated equipment. (XBL 804-4124)

When pure water droplets were exposed to SO_2 in the fog chamber, the rate of SO_4 formation ($\mu g\ SO_4/m^3 \cdot h$) equals 4.06 (ppm SO_2).0007 (Fig. 2). If the droplets contained Nuchar-SN particles, the rate of SO_4 formation was found to be significantly faster than for pure water droplets. For example, wet soot particles exposed to 0.007 ppm SO_2 produced SO_4 faster than pure water droplets exposed to 222 ppm SO_2. The data for SO_4 formation by wet soot particles is plotted with open circles in Figure 2. When the soot-droplet data in Figure 2

*This work was supported by the Department of Energy under Contract No. W-7405-ENG-48 through the Environmental Protection Agency under Contract No. 79-D-X-0533.

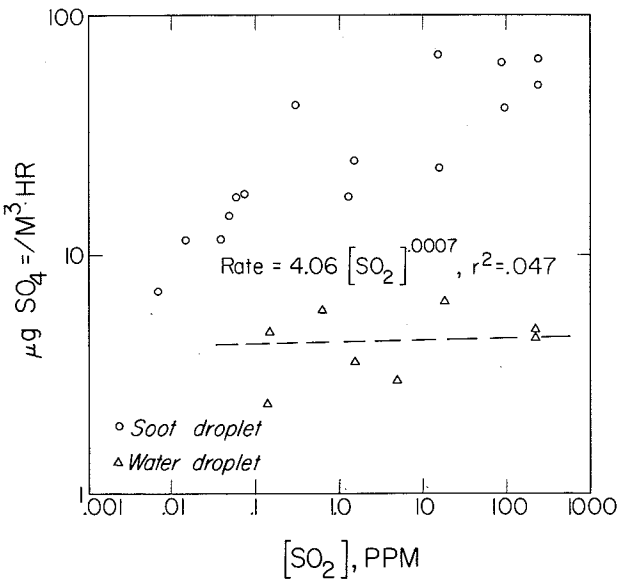

Fig. 2. Production of SO_4 in fog droplets versus SO_2. (XBL 809-1861)

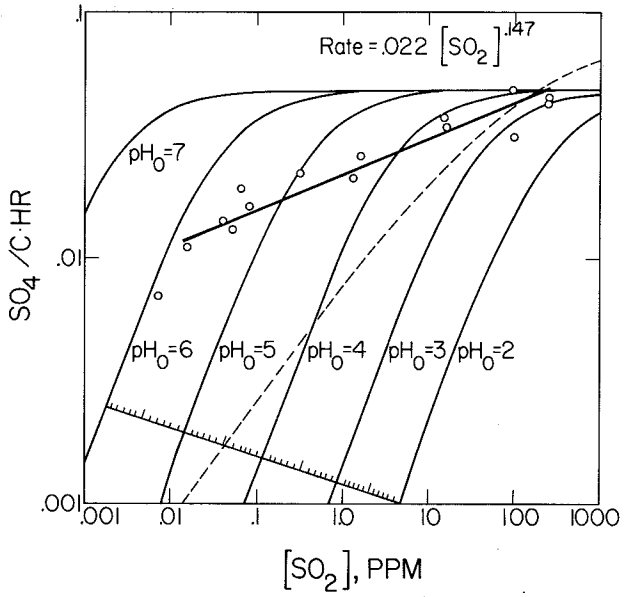

Fig. 3. The normalized rate of SO_4 formation in wet soot droplets vs. SO_2. The open circles and the solid line drawn through the circles were obtained from fog chamber data. The family of curves labelled pH_0 = 2 through pH_0 = 7 was calculated from Equation 1. pH_0 is the pH of droplets in equilibrium with SO_2 and CO_2 before the start of the reaction. The dashed line shows the rate for SO_4 formation (Eq. 1) for wet soot droplets whose pH before exposure to SO_2 and 320 ppm CO_2 is determined by SO_2-CO_2-H_2O equilibria. The dashed line is juxtaposed on pH coordinates created by the family of curves labelled pH_0 = 2 through pH_0 = 7. (XBL 809-1860)

are normalized to [C], the carbon-normalized rate of SO_4 formation can be plotted as shown in Figure 3 (open circles). The equation which best fits the carbon-normalized soot droplet data is $SO_4^{2-}/C \cdot h = 0.222(SO_2)^{.147}$.

In Figure 3, a family of curves is presented which shows the rate of SO_4 formation, normalized to C, as a function of $[SO_2]$ for various initial $[H^+]$'s. This family of curves was calculated from the following rate expression:[3]

$$\frac{d[S(IV)]}{dt} = k(C) \quad \frac{[S(IV)]^2}{1 + \beta[S(IV)] + \alpha[S(IV)]^2} \qquad (1)$$

where [C] = soot concentration in droplet, (g/ℓ)

$$[S(IV)] = [SO_2 \cdot H_2O] + [HSO_3^-] + [SO_3^=]$$

$$\alpha = 4.915 \times 10^8 \ l^2/mol^2$$

$$\beta = 2.956 \times 10^5 \ l/mol$$

$$k = 1.336 \times 10^{-7} \ mol/g \cdot s$$

The family of curves in Figure 3 indicates a pH effect on sulfate formation, but pH only becomes a factor when soot suspensions are exposed to SO_2. The pH effect is related to the absorption of SO_2 by the droplet. For example, two droplets, one of which has an initial pH of 3 and the other a pH of 5, are equilibrated with 1 ppm SO_2. The droplet with the lower initial pH will have a lower equilibrium [S(IV)] and the oxidation rate will be similarly slower. The family of curves was calculated assuming that the droplet had a specified initial pH and equilibrated with SO_2 and 320 ppm CO_2 to produce a certain equilibrium [S(IV)] before the oxidation started. The resultant [S(IV)] was then used to calculate the reaction rate using Equation 1.

The dashed line in Figure 3 shows the S(IV) oxidation rate expected for wet soot particles in equilibrium with SO_2. This curve was calculated assuming that the soot droplet initially had a pH of 7 and was then equilibrated with SO_2 and 320 ppm CO_2 to produce a certain equilibrium [S(IV)] and equilibrium pH before oxidation started. The resulting [S(IV)] was used to calculate the reaction rate using Equation 1. It was also assumed in the calculation that the soot possessed no pH-altering species.

The difference between the fog chamber data and the dashed line in Figure 3 is due to the alkaline nature of Nuchar-SN. The release of alkaline species into the droplet from the Nuchar-SN neutralized some of the absorbed $SO_2 \cdot H_2O$ and/or HSO_3^-, and thus the equilibrium [S(IV)] was larger than that predicted by Henry's Law for pure water and SO_2. This neutralization increased the oxidation rate because it brought more $SO_2 \cdot H_2O$ and HSO_3 into the droplet. The magnitude of the difference between the fog chamber data line and the dashed line depends on the $[SO_2]$. At low $[SO_2]$, the alkaline species on the soot particles attract into solution more $SO_2 \cdot H_2O$ or HSO_3^- than would be expected for pure water, and thus these alkaline species strongly influence the resultant [S(IV)]. At high $[SO_2]$, the dissolved SO_2 becomes the dominant factor

for controlling the resultant [S(IV)]. Therefore, at high [SO_2], the fog chamber data line and the dashed line in Figure 3 coincide.

Data presented here show that dispersed wet soot particles (Nuchar-SN being a type of soot) can oxidize SO_2 to sulfate. This indicates that the SO_2 oxidation mechanism (Eq. 1) can be applied to the troposphere. These data also confirm predictions made by others in our laboratory[4] which indicated that the oxidation of SO_2 by wet soot particles is an important tropospheric source of particulate sulfate.

PLANNED ACTIVITIES FOR FY 1981

The fog chamber experiments will be continued to include other types of wet soot particles.

REFERENCES

1. G. E. Likens, R. F. Wright, J. N. Galloway, and T. J. Butler, "Acid Rain," Scientific American, vol. 241, 1979, p. 43.

2. R. Brodzinsky, S. G. Chang, S. S. Markowitz, and T. Novakov, "Kinetics and Mechanism for the Catalytic Oxidation of Sulfur Dioxide on Carbon in Aqueous Suspensions," Journal of Physical Chemistry, vol. 84, 1980, p. 3354.

3. R. Brodzinsky, Catalytic Oxidation of S(IV) on Activated Carbon in Aqueous Suspension: Kinetics and Mechanism, Ph.D. dissertation, University of California, Berkeley, 1981.

4. R. Toossi, T. Novakov, and S. G. Chang, "Relative Importance of Various Sulfate Production Mechanisms in Aqueous Droplets," in Atmospheric Aerosol Research Annual Report 1977-78, Lawrence Berkeley Laboratory report LBL-8696, 1978.

AQUEOUS REACTIONS OF NITRITE AND BISULFITE*

S. Oblath, S. Chang, S. Markowitz, and T. Novakov

INTRODUCTION

In studies of particulate sulfate formation, it is important to know what role the oxides of nitrogen (NO_x) will play, as they are both abundant pollutants. This question may be of even greater importance with respect to aerosol droplets, as both SO_2 and NO_x are soluble gases. Homogeneous reactions involving the two gases have been studied for a number of years.[1] More recently studies have been undertaken to determine the effect of NO_x on heterogeneous sulfate formation.[2,3]

Several years ago we began a study to investigate the reactions of nitrite (NO_2^-) and bisulfite (HSO_3^-) as a first step toward understanding the $NO_x/SO_2/H_2O$ system. Nitrite is known to react with bisulfite over a wide range of conditions. Previous work by other scientists[4-6] reported conflicting results and left several questions unanswered. The experiments which we performed have clarified many of these questions and are reported in a recent publication.[7]

*This work was supported by the Assistant Secretary for Environment, Office of Health and Environmental Research, Division of Biomedical and Environmental Research Division of the U.S. Department of Energy under Contract No. W-7405-ENG-48, and the Morgantown Energy Research Center under Contract No. AA 050515.

All the known aqueous reactions of nitrite with bisulfite begin with the formation of hydroxylamine disulfonate (HADS). The results of our previous work may be summarized by the following rate expression:

$$\text{Rate} = K_A[H^+][NO_2^-][HSO_3^-] + k_B[NO_2^-][HSO_3^-]^2 \quad .$$

This rate law is valid over the pH range of 4.5 to 7. Work has been progressing during the past year to answer several remaining questions pertaining to the formation of HADS: (1) Is a process independent of bisulfite concentration really present, as noted in the literature; (2) What role will carbon particles have in this reaction; and (3) What effect will extremely low reactant concentrations (or high acidity) have on the products or rate of the nitrite-bisulfite reaction.

ACCOMPLISHMENTS DURING FY 1980

Bisulfite Independent Pathway

A HADS formation pathway that is independent of bisulfite ion concentration is of importance to atmospheric chemists as the rate is not affected when the SO_2 concentration is lowered to ambient levels. Previous researchers had identified a process of this type.[4,6] We have carried out experiments to determine the presence or absence of this pathway by addition of $NaNO_2$ to buffered solutions of bisulfite ion under pseudo-first-order conditions. Nitrite concentrations (initially 0.5

to 10 mM) were monitored by visible spectrophotometry as in our previous work. Bisulfite ion concentration was between 5 and 40 mM. The pH was maintained by using oxalate, tartrate, or phthalate buffers of an ionic strength of 0.2 M.

Results of these experiments are shown in Figure 1. The zero intercepts show that there is no process occurring which is independent of bisulfite concentration. The buffers that were used overlap in their pH ranges, and tests in different buffers show no evidence of inhibitory or catalytic effect. Tests carried out at differing buffer concentrations (ionic strength maintained at 0.2 M) again show no inhibiting effect of the buffer. Previous work was carried out in acetate buffers, a medium believed to stabilize NO^+ formation. (NO^+ is the predicted intermediate for a bisulfite independent pathway.) Although NO^+ may be formed, the rate in the absence of acetate is too slow to be important at pH's accessible to ambient aerosol droplets.

Effect of Carbon

Since aerosol droplets are often formed around carbonaceous particles, it is important to understand the effects of carbon on this set of reactions. A finely ground activated carbon (Nuchar SN) was used at a concentration of approximately 0.1% by weight. This is about what would be expected in a wet aerosol. Reaction conditions were the same as in the previous study, except that aliquots of the solution were filtered before the nitrite was measured. Blank runs (no carbon present) showed that filtering had no effect on the results. A sulfite-bisulfite buffer was used, which insures pseudo-first-order conditions. The results with and without carbon agree well, which indicates Nuchar SN has no effect on the reaction. After long reaction times, the runs with carbon proceed more slowly. This is consistent with the oxidation of HSO_3^- on the Nuchar[8] and the breakdown of pseudo-first-order conditions.

Effect of Low Concentration or High Acidity on the Reaction

Prior to determining the rate of HADS formation at lower pH's, we determined the stoichiometry by determining the changes in concentrations of bisulfite (by iodometry) and nitrite (by spectrophotometry). The initial HSO_3^- concentration was always greater than twice that of NO_2^- to insure that HADS could form. The pH was measured at the start of each experiment. The results are shown in Figures 2 and 3. As one goes to pH less than 3, the stoichiometric ratio ($\Delta S/\Delta N$) ratio begins to decrease from 2 to 1, and some other product is being formed. The same trend is seen if one maintains a constant pH and lowers the bisulfite concentration. This indicates that some intermediate is reacting to form another product, most likely N_2O.

To test this hypothesis, several trials were carried out in a flask sealed with a rubber septum. The gas above the solution was then analyzed using gas chromatography with a Porapak Q column and a thermal conductivity detector. Typical results (Fig. 4) indicate that N_2O is the product when $\Delta S/\Delta N = <2$.

In going to very low (micromolar) concentrations, the competition for the intermediate becomes very important because the pH of the droplet will remain roughly constant while the bisulfite ion concentration drops. The studies at high acidity allow us to estimate the relative magnitude of the rate constants and thus determine the branching ratio under different conditions. To do this, we assume a system as follows:

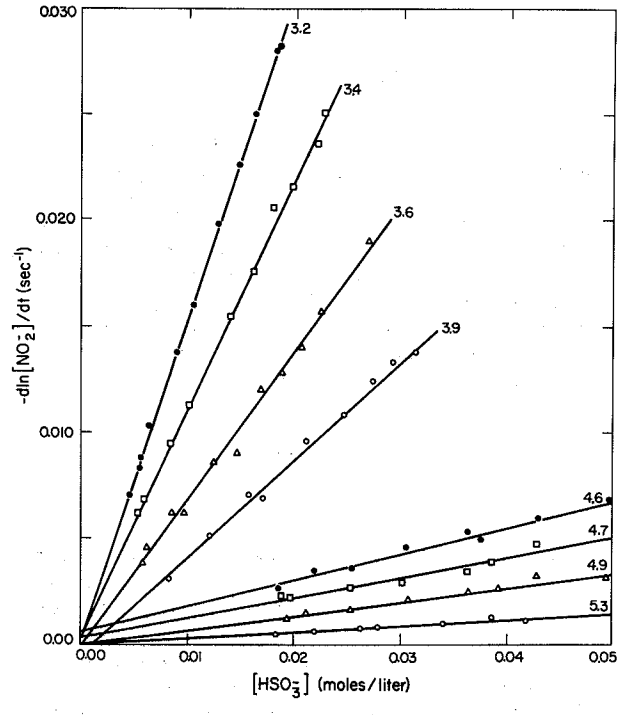

Fig. 1. Experimental rates as a function of bisulfite ion concentrations. Numbers indicate the pH for each set of reactions. (XBL 8011-2377)

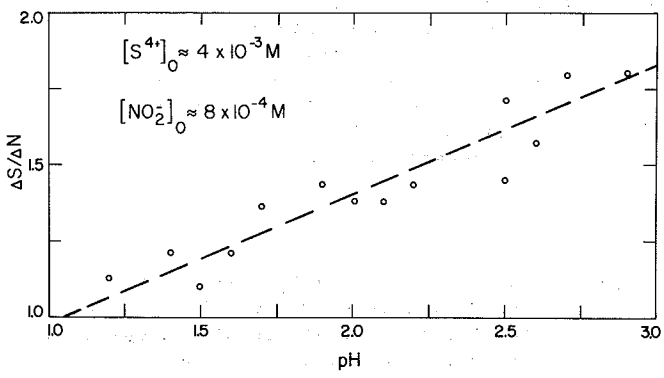

Fig. 2. Stoichiometric ratio at various pH's. (XBL 8011-2381)

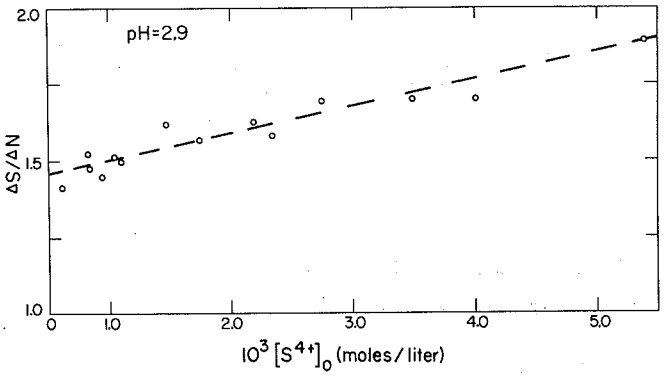

Fig. 3. Stoichiometric ratio at various bisulfite ion concentrations at a fixed acidity.
(XBL 8011-2380)

$$HONO + HSO_3^- \xrightarrow{} \text{intermediate} \xrightarrow[1]{HSO_3^-} HADS$$

$$\text{intermediate} \xrightarrow{2\ H^+} NOH \text{ (or } N_2O)$$

The value of $\Delta S/\Delta N$ is related to the amount of products formed and is therefore related to the ratio $k_1[HSO_3^-]/k_2[H^+]$. By taking the data presented in Figures 2 and 3, we have determined the ratio k_1/k_2 to be 1.7 ± 0.5. Therefore, whenever the H^+ ion concentration is much greater than that of bisulfite ion, the major product will be N_2O, with SO_4 being the fate of the SO_2. Under typical ambient conditions, N_2O will most likely be the N-containing product which is formed. The rate limiting step should remain the same as that for HADS formation.

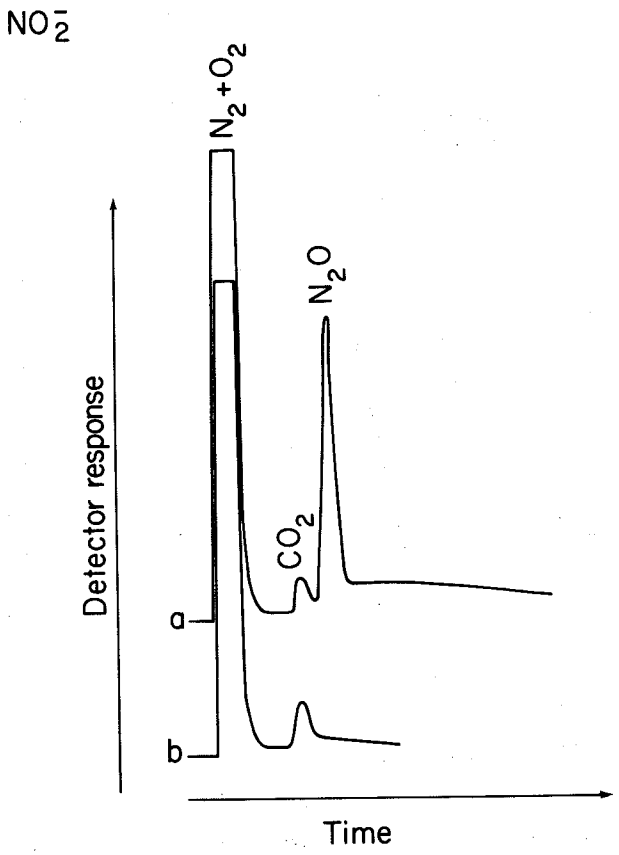

Fig. 4. Chromatogram of gaseous products. Curve a for $\Delta S/\Delta N = 1.4$; curve b for $\Delta S/\Delta N = 2$.
(XBL 8011-2382)

Conclusions

The work which has been described here will enable the modeling of one set of reactions of NO_x and SO_2 under a wide range of conditions. The fates of both the N and S have been determined. The kinetics of this system indicates a strong dependence on reactant concentrations. The increase in rate with increase in acidity will counter the effect of decreasing solubility of the gases with increasing acidity.

PLANNED ACTIVITIES FOR FY 1981

Future work will include an investigation of reactions of HADS with NO_2^- and hydroxylamine monosulfonate with NO_2^-. This will allow us to determine the fate of N and S over a more complete range of conditions than is currently possible.

REFERENCES

1. J. G. Calvert, F. Su, J. W. Bottenhiem, and O. P. Strausz, "Mechanism of the Homogeneous Oxidation of Sulfur Dioxide the Troposphere," Atmospheric Environment, vol. 12, 1978, p. 197.

2. L. G. Britton and A. G. Clarke, "Heterogeneous Reactions of Sulphur Dioxide and SO_2/NO_2 Mixtures with a Carbon Soot Aerosol," Atmospheric Environment, vol. 14, 1980, p. 829.

3. W. R. Cofer, III, D. R. Schryer, and R. S. Rogowski, "The Enhanced Oxidation of SO_2 by NO_2 on Carbon Particulates," Atmospheric Environment, vol. 14, 1980, p. 571.

4. V. F. Seel and E. Degener, "Kinetik und Chemismus der Raschigschen Hydroxylamin-Synthese," Zeitschrift für Anorganische und Allegemeine Chemie, vol. 284, 1956, p. 100.

5. V. F. Seel and H. Knorre, "Die Umsetzung von Nitrit mit Hydrogensulfit in Hydrogensulfit-Sulfit-Pufferlösungen," Zeitschrift für Anorganische und Allegemeine Chemie, vol. 313, 1961, p. 70.

6. S. Yamamoto and T. Kaneda, "Kinetics of Formation of Hydroxylaminedisulfonate and Nitrilosulfonate by Raschig's Hydroxylamine Process," Nippon Kagaku Zasshi, vol. 80, 1959, p. 1098.

7. S. B. Oblath, S. S. Markowitz, T. Novakov, and S. G. Chang, "Kinetics of the Formation of Hydroxylamine Disulfonate by Reaction of Nitrite with Sulfites," Journal of Physical Chemistry, vol. 85, 1981, p. 1017.

8. R. Brodzinsky, S. G. Chang, S. S. Markowitz, and T. Novakov, "Kinetics and Mechanism for the Catalytic Oxidation of Sulfur Dioxide on Carbon in Aqueous Solutions," Journal of Physical Chemistry, vol. 84, 1980, p. 3354.

THE IMPORTANCE OF SOOT PARTICLES AND NITROUS ACID OXIDIZING SO_2 IN ATMOSPHERIC AQUEOUS DROPLETS*

S. Chang, R. Toossi, and T. Novakov

INTRODUCTION

Sulfuric and nitric acids make a major contribution to the acidity of rain water. These acids are produced primarily from the oxidation of SO_2 and NO_x by homogeneous and/or heterogeneous processes in the atmosphere. The dominant mechanisms responsible for this transformation have not yet been established. In our laboratory we found two previously unrecognized reaction pathways which involve water droplets and could be important processes in the genesis of acid rain and sulfate aerosols: (1) oxidation of SO_2 in water droplets containing soot particles[1,2] and (2) oxidation of SO_2 by HNO_2 in water droplets.[3] Here we discuss the impact of these two systems on atmospheric sulfate aerosol formation.

ACCOMPLISHMENTS DURING FY 1980

For the oxidation of SO_2 in water droplets containing soot particles, the reaction rate law can be expressed by the following equation:

$$\frac{d[S(VI)]}{dt} = k[C_x]\, O_2^{0.69} f[S(IV)], \qquad (1)$$

$$\text{where } f[S(IV)] = \left\{ \frac{\alpha [S(IV)]^2}{1 + \beta[S(IV)] + \alpha[S(IV)]^2} \right\},$$

$[C_x]$ = grams of carbon particles/l,

$[O_2]$ = moles of dissolved oxygen/l, and

$[S(IV)]$ = total moles of S(IV)/l.

The dependence of the rate of formation of sulfate on the partial pressure of SO_2 (P_{SO_2}) in the atmosphere can be obtained from Equation 1.

Because the effect of P_{SO_2} on the rate is contained in f[S(IV)], we illustrate the relationship of f[S(IV)] with P_{SO_2} and pH of the aqueous droplets as shown in Figures 1 and 2. The f[S(IV)], or the rate of production of sulfate (because the rate is linearly proportional to f[S(IV)]), decreases as the pH decreases at a given P_{SO_2}. The magnitude of f[S(IV)]'s changing per unit pH change is much larger at a lower P_{SO_2}. Also f[S(IV)] (or the rate) depends only slightly on P_{SO_2} under most atmospheric conditions when P_{SO_2} is between 1 and 10 ppb and the pH ranges between 5 and 6. The f[S(IV)] increases only 10% and 100% respectively at pH of 6 and 5 when P_{SO_2} increases from 1 to 10 ppb. However, f[S(IV)] depends strongly on P_{SO_2} when the pH is low.

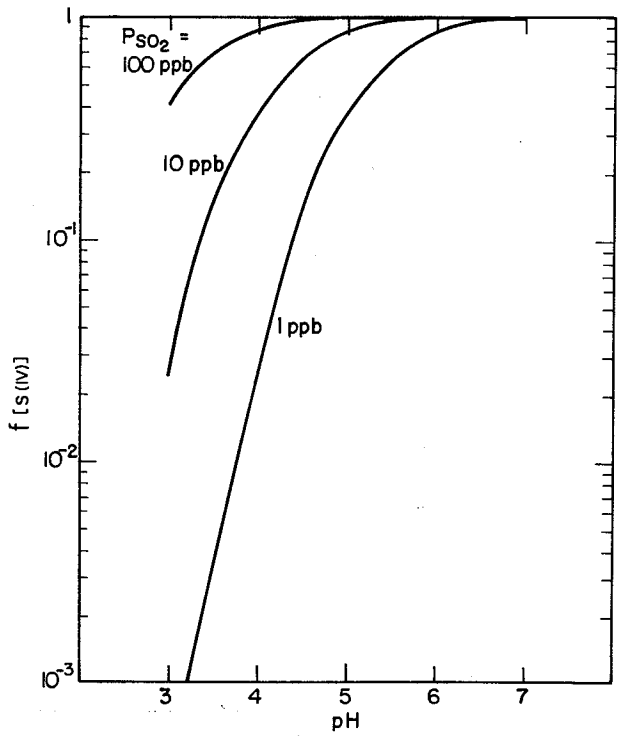

Fig. 1. The effect of the pH of aqueous droplets on f[S(IV)] is a function of S(IV) on which the aqueous oxidation rate of sulfites on soot particles depends. (XBL 808-5732)

*This work was supported by the Assistant Secretary for Environment, Office of Health and Environmental Research, Division of Biomedical and Environmental Research of the U.S. Department of Energy under Contract No. W-7405-ENG-48.

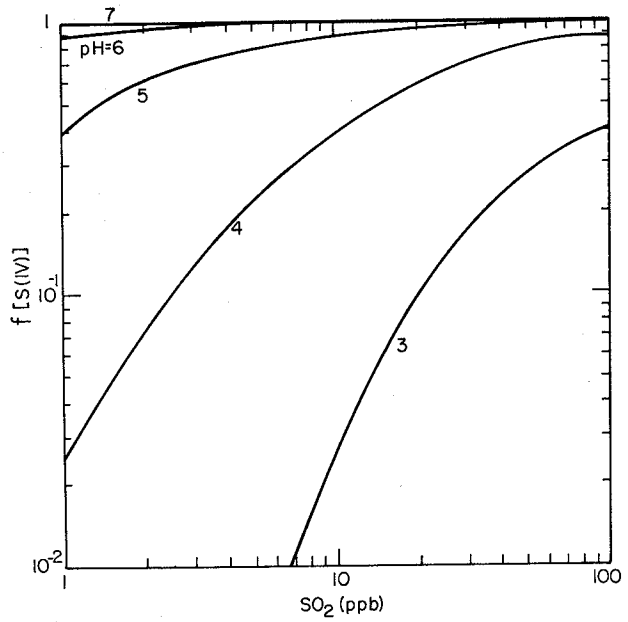

Fig. 2. The effect of partial pressure of SO_2 on f[S(IV)] at pH of 7, 6, 5, 4, and 3. The f[S(IV)] is a function of S(IV) on which the aqueous oxidation rate of sulfites on soot particles depends. (XBL 808-5733)

In the oxidation of SO_2 by HNO_2 in water droplets, many concurrent and consecutive chemical reactions can occur as a result of the interaction between the nitrous acid and the sulfurous acid.[4-6] Hydroxylamine disulfonate (HADS) is the first stable product under most atmospheric conditions:

$$HNO_2 + 2HSO_3^- \rightarrow HNO(SO_3)_2^{-2} + H_2O \ .$$

The formation kinetic of HADS has been found to consist of three concurrent processes. The reaction rate law can be expressed as:

$$\frac{d[HADS]}{dt} = k_0[H^+]^2[NO_2^-] + k_I[H^+][NO_2^-](HSO_3^-) + k_{II}[NO_2^-][HSO_3^-]^2, \quad (2)$$

where $k_0 \approx 8\times10^5$ l^2/mol-s (at 295K),

$k_I = 3.7\times10^{12}\ e^{-6100/T}$ l^2/mol^2-s, and

$k_{II} = 9.0\times10^{-4}\ e^{2.1(\mu)^{1/2}}$ l^2/mol^2-s,

T = temperature in Kelvin, and

μ = ionic strength in mol/l).

We tentatively assumed that this rate law will still hold in an atmosphere where concentrations of both nitrite and sulfite are several orders of magnitude lower than the concentrations used when this rate equation was derived.

HADS can undergo further reaction, either hydrolysis or sulfonation. Hydrolysis of HADS[7] produces hydroxylamine monosulfonate (HAMS) and sulfates. Sulfonation of HADS[8,9] yields amine trisulfonate. The major fraction of HADS undergoes hydrolysis under most atmospheric conditions.

HAMS can either undergo further hydrolysis to form hydroxylamine and sulfates or react with nitrous acid to produce nitrous oxide and sulfates. Although a complete rate law has not been determined for both reactions, the kinetic studies[7,10] indicate that the reaction with nitrous acid is much more important than the hydrolysis. Therefore, it appears that the reaction between SO_2 and HNO_2 in atmospheric water droplets will first produce HADS, which undergoes acid-catalyzed hydrolysis to form HAMS and sulfate. HAMS then reacts with nitrous acid and finally becomes nitrous oxide and sulfate. The total stoichiometric equation can be expressed as

$$2HNO_2 + 2HSO_3^- \rightarrow N_2O \uparrow + 2HSO_4^- + H_2O.$$

If the reaction is at steady-state condition, then 1 mol of sulfate will be produced for every mole of SO_2 or HNO_2 consumed, assuming that the reaction rate between HAMS and nitrous acid is very large.

Comparison of Sulfate Production Mechanisms

We have carried out a box-type calculation to compare the relative importance of sulfate production mechanisms by soot particles and nitrous acid with other mechanisms involving liquid water. The following initial conditions were used in the calculation: liquid water, 0.05 g/m^3; SO_2, 0.01 ppm; O_3, 0.05 ppm; NH_3, 5 ppb; and CO_2, 0.000311 atm. Concentrations of particulate Fe and Mn of 250 ng/m^3 and 20 ng/m^3 respectively were assumed. However, only 0.13% of the total iron and 0.25% of the Mn are water soluble, according to Gordon et al.[11] The concentrations of soot and HNO_2 were taken as 10 $\mu g/m^3$ and 8 ppb respectively. The latter corresponds to 25 ppb of NO and 50 ppb of NO_2 at equilibrium conditions.[12]

The results of this calculation, shown in Figure 3, indicate that O_3, soot, and HNO_2 can be important mechanisms for sulfate aerosol formation. In general the O_3 mechanism is more important under high pH and/or photoactivity conditions when the concentration of O_3 is high, whereas both soot and HNO_2 processes are more important when the lifetime of fog or clouds is long[13] and the pH of the droplets is low. Both soot and HNO_2 processes can be dominant processes close to sources and in heavily polluted urban areas, where the concentrations of soot and NO/NO_2 are high and the pH of aqueous droplets is low.

PLANNED ACTIVITIES FOR FY 1981

We will calculate the concentration profile of all important species produced in NO_x/SO_2/liquid/H_2O systems as a function of reaction time.

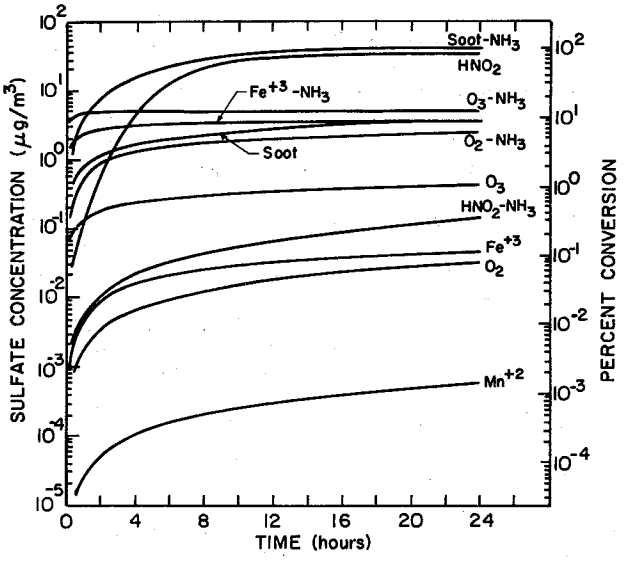

Fig. 3. Comparison of the relative importance of various sulfate production mechanisms involving liquid water based on a box-type calculation. (XBL 808-5735)

REFERENCES

1. S. G. Chang, R. Brodzinsky, R. Toossi, S. S. Markowitz, and T. Novakov, "Catalytic Oxidation of SO_2 on Carbon in Aqueous Suspensions," Proceedings, Conference on Carbonaceous Particles in the Atmosphere, Lawrence Berkeley Laboratory report LBL-9037, 1979, p. 122.

2. R. Brodzinsky, S. G. Chang, S. S. Markowitz, and T. Novakov, "Kinetics and Mechanism for the Catalytic Oxidation of Sulfur Dioxide on Carbon in Aqueous Suspensions," Journal of Physical Chemistry, vol. 84, 1980, p. 3354.

3. S. B. Oblath, S. S. Markowitz, T. Novakov, and S. G. Chang, "Kinetics of the Formation of Hydroxylamine Disulfonate by Reaction of Nitrite with Sulfites," Journal of Physical Chemistry, vol. 85, 1981, p. 1017.

4. F. Raschig, Schwefel und Stickstoffstudien (Berlin: Verlag Chemie, 1924).

5. W. Latimer and J. H. Hildebrand, Reference Book of Inorganic Chemistry (New York: Macmillan, 1951), p. 208.

6. W. Duecker and J. West, eds., The Manufacture of Sulfuric Acid, American Chemical Society, Washington, D.C., Monograph Series No. 144, 1959.

7. S. Naiditch and D. M. Yost, "The Rate and Mechanisms of the Hydrolysis of Hydroxylamine Disulfonate Ion," Journal of American Chemical Society, vol. 63, 1941, p. 2123.

8. S. Yamamoto and T. Kaneda, "Kinetics of Formation of Hydroxylamine Disulfonate and Nitrilosulfonate by Raschig's Hydroxylamine Process," Nippon Kagaku Zasshi, vol. 80, 1959, p. 1098.

9. V. S. Seel and H. Knorre, "Die Umsetzung von Nitrit mit Hydrogensulfit in Hydrogensulfit-sulfit-pufferlosungen," Zeitschrift für Anorganische und Allegemeine Chemie, vol. 313, 1961, p. 70.

10. V. F. Seel and H. Pauschmann, "Zum Kinetic der Umsetzung von Hydroxylaminemonosulfonat mit Nitrit," Zeitschrift für Naturforschung, vol. 17b, 1962, p. 347.

11. G. E. Gordon, D. D. Davis, G. W. Israel, H. E. Landsberg, and T. C. O'Haver, Atmospheric Impact of Major Sources and Consumers of Energy, NSF/RA/E-75/189 (1975). Available from NTIS as PB 262 574.

12. S. E. Schwartz and W. H. White, Equilibrium Solubility of the Nitrogen Oxides and Oxyacids in Aqueous Solution, Brookhaven National Laboratory Report BNL27102, Long Island, N.Y., 1980.

13. R. Toossi, S. G. Chang, and T. Novakov, "Lifetime of Liquid Water Drops in Ambient Air: Consideration of the Effects of Surfactants and Chemical Reactions," in Atmospheric Aerosol Research Annual Report 1977-78, Lawrence Berkeley Laboratory report LBL-8696, 1979, p. 149.

KINETICS OF THE REACTION BETWEEN NH_2OH AND SO_2 IN AQUEOUS SOLUTIONS*

S. Gomiscek, R. Clem, T. Novakov, and S. Chang

INTRODUCTION

Hydroxylamine, one of the species produced as a result of interaction between NO_x and SO_2 in aqueous solution can undergo further reaction[1-3] with SO_2 to form either sulfamic acid or ammonium bisulfate. We have investigated the kinetics of this latter reaction as part of an effort to understand the importance of the interaction of NO_x with SO_2 in atmospheric aqueous droplets in terms of acid rain and sulfate aerosol formation.

ACCOMPLISHMENTS DURING FY 1980

The reaction mixture was prepared by aliquoting to a 100-ml volumetric flask in the following sequence: hydroxylamine stock solution, buffer solution, and finally sodium bisulfite. The flask was quickly made to volume with the distilled water after the last addition and mixed; then the first polarographic determination of the hydroxylamine concentration was made. Subsequent measurements were made after the appropriate time intervals to monitor the time rate of hydroxylamine disappearance. For some of the work the solutions were thermostatted.

The first set of experiments determined the reaction order with respect to total hydroxylamine. An excess of bisulfite was used, and the solution was buffered at pH 5 in these runs. Figure 1 shows a semilog plot of total hydroxylamine concentration versus time for several initial concentrations. Parallel lines indicate a first order dependence on hydroxylamine.

The dependence of the reaction on total sulfite was determined by varying the excess sulfite concentration for a fixed hydroxylamine concentration at pH 5. Because the hydroxylamine is first order as determined above, one can write the rate law as

$$\frac{-d[\text{total hydroxylamine}]}{dt} = k_{obs}[\text{total hydroxylamine}]\cdot[\text{total sulfite}]^n,$$

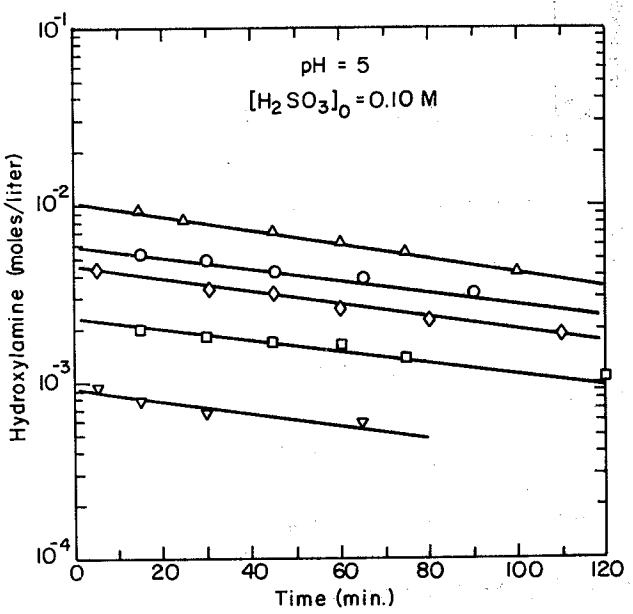

Fig. 1. Loss of hydroxylamine as a function of time. Straight lines indicate first order dependence. $[H_2SO_3]$ indicates total sulfite, (S(IV) concentration. (XBL 809-5897)

in which one can define

$$Q = -\frac{d \ln[\text{total hydroxylamine}]}{dt} = k_{obs}[\text{total sulfite}]^n.$$

A log-log plot of Q versus [total sulfite] should give a straight line with the slope equal to the order of the reaction with respect to total sulfite. Figure 2 shows that the slope is 0.94, which is regarded as first order dependence. Therefore, the reaction follows the rate law

$$-\frac{d[\text{total hydroxylamine}]}{dt} = k_{obs}[\text{total hydroxylamine}]\cdot[\text{total sulfite}].$$

The rate of reaction was found to be independent of the ionic strength of the solution. The rate constant k_{obs} in 1/mol-s was determined at two temperatures: 7.67×10^{-3} at 35°C and 1.48×10^{-3} at 22°C. Sisler and Audrieth[1] and Fraser[3] suggested that formation of both sulfamic acid and ammonium bisulfate involves attack by the $SO_2 \cdot H_2O$ on the NH_2OH. The reaction can therefore be expressed as

*This work was supported by the Assistant Secretary for Environment, Office of Health and Environmental Research, Division of Biomedical and Environmental Research, U.S. Department of Energy under Contract No. W-7405-ENG-48 and by the Morgantown Energy Research Center under Contract No. AA 050515.

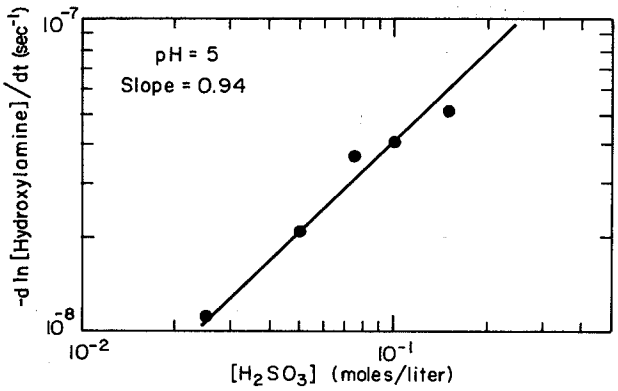

Fig. 2. Dependence of the rate on total sulfite concentration. The slope is the order of the reaction with respect to sulfite. (XBL 809-5898)

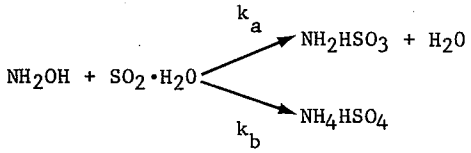

The rate law can be written as

$$-\frac{d[\text{total hydroxylamine}]}{dt} = (k_a + k_b)[NH_2OH][SO_2 \cdot H_2O]. \quad (2)$$

To evaluate the rate constant and activation energy of both reactions using our experimental measurements, Equation (1) is expressed in terms of the concentration of reaction species NH_2OH and $SO_2 \cdot H_2O$. Because [total hydroxylamine] = $[NH_2OH] + [NH_3OH^+]$ and [total sulfite] = $[SO_2 \cdot H_2O] + [HSO_3^-] + [SO_3^=]$, Equation (1) can be written as

$$-\frac{d[\text{total hydroxylamine}]}{dt} = k_{obs}\left(1 + \frac{[H^+]}{K_n}\right)\left(1 + \frac{K_1}{[H^+]} + \frac{K_1K_2}{[H^+]^2}\right) \cdot [NH_2OH][SO_2 \cdot H_2O]. \quad (3)$$

where K_n, K_1, and K_2 are respectively the acid dissociation constant for hydroxylamine and the first and second dissociation constants for sulfurous acid.

By comparing Equations (3) and (4), we obtain the following relationship:

$$k_a + k_b = k_{obs}\left(1 + \frac{[H^+]}{K_n}\right)\left(1 + \frac{K_1}{[H^+]} + \frac{K_1K_2}{[H^+]^2}\right). \quad (4)$$

The ratio k_a/k_b can be obtained by the corresponding ratio of the products $[NH_2HSO_3] / [NH_4HSO_4]$; this ratio was determined by Fraser[3] at several temperatures. The following values, obtained from the interpolation of Fraser's result were used: 9 at 22°C and 19 at 35°C. By applying the transition-state theory,[4] the enthalpy and entropy of activation for the formation of both sulfamic acid and ammonium bisulfate can be calculated as shown in Table 1. The results of this study are in fairly good agreement with those of Fraser.

PLANNED ACTIVITIES FOR FY 1981

We will study the kinetics of other reactions involved in the interaction of NO_x and SO_2 in aqueous solution.

REFERENCES

1. H. H. Sisler and L. F. Audrieth, "The Preparation of Sulfamic Acid by the Hydroxylamine-Sulfur Dioxide Reaction," Journal of the American Chemical Society, vol. 61, 1939, p. 3389.

2. D. S. Brackman and W. C. E. Higginson, "The Reaction Between Hydroxylamine and Sodium Sulphite in Solution in Dilute Acid," Journal of the Chemical Society, London, 1953, p. 3896.

3. R. T. M. Fraser, "The Hydroxylamine-Sulphur Dioxide Reaction," Journal of the Chemical Society, London, 1965, p. 1747.

4. S. W. Benson, The Foundations of Chemical Kinetics, New York: McGraw-Hill, 1960.

Table 1. The enthalpy and entropy of activation for the formation of sulfamic acid and ammonium bisulfate by the reaction of NH_2OH with $SO_2 \cdot H_2O$.

	Sulfamic acid		Ammonium bisulfate	
	$\Delta Ha^{\ddagger}$ (kcal/mol)	$\Delta S_a^{\ddagger}$ (e.u.)*	$\Delta H_b^{\ddagger}$ (kcal/mol)	$\Delta S_b^{\ddagger}$ (e.u.)
Fraser	10.9	-16	1	-56
This work	13.4	- 6.1	3.0	-45.8

*e.u. = entropy units.

THE ROLE OF FLY ASH IN THE CATALYTIC OXIDATION OF SO_2*

S. Cohen, S. Chang, S. Markowitz, and T. Novakov

INTRODUCTION

The catalytic behavior of fly ash in the oxidation of S(IV) in aqueous systems has been reported.[1,2] Prior work has considered the potential of fly ash as a scrubber medium,[1-3] and has suggested that fly ash may function in promoting acid rain formation in droplets.[4] Although several properties of the ash--surface characteristics, metal oxide content, trace metal dissolution--have been proposed to account for its catalytic role, no systematic investigation of the nature of the catalysis has been made. It is important to distinguish between surface and homogeneous catalysis. For example, the presence of chelating agents in wet scrubbers containing fly ash should inhibit catalysis by leached metals.[1,5]

In this study the oxidation of S(IV) in slurries of fly ash has been examined after different ash pretreatment and under varying experimental conditions. Our evidence indicates that dissolved iron is a prime factor in fly-ash-catalyzed oxidation of SO_2.

ACCOMPLISHMENTS DURING FY 1980

Materials and Methods

Mallinckrodt or Baker reagent-grade chemicals were used without further purification. The fly ash types were National Bureau of Standards (NBS) Standard Reference Material 1433a, and four lot samples, referred to as A-D, were used. A is from the TVA Shawnee Power Plant; B is from the Duke Power Steam Plant; C is from the Jim Bridger Plant in Wyoming; and D is an untreated ash sample obtained from Lawrence Livermore Laboratory.

Reactions were monitored by three different methods:

1. in open-air Erlenmeyer flasks agitated with a magnetic stirrer, and with S(IV) loss being monitored by idometry;
2. the reaction was set up as above, except that SO_3^{2-} loss and SO_4^{2-} appearance monitored by ion chromatography; and
3. in a closed system--allowing no diffusion of O_2 into solution during the course of the reaction--with O_2 decay from initially saturated solutions being monitored with a Clark-type O_2 electrode.

The initial S(IV) concentration in the reactions studied varied from 9.0×10^{-4} to 1.5×10^{-2} M. The pH varied from 2.5 to 3.9 by using appropriate mixtures of $H_2O \cdot SO_2$ and $Na_2S_2O_5$. The fly ash concentration was varied from 0.10% to 0.36% by weight. Although reproducibility was at times inadequate, most rates reported are the average of 2-3 runs agreeing within 10%.

Leaching experiments are described elsewhere.[7]

Equipment and Materials

Elemental and chemical compositions of fly ash were characterized by ion chromatography and atomic absorption (AA). AA work was performed on a Perkin-Elmer Model 360 atomic absorption instrument in an air-acetylene or N_2O-acetylene flame. The ion chromatograph used was a Dionex System 14 equipped with precolumn and, where necessary, a concentrator column. A 0.22-μm pore size Millipore filter was used to filter solutions for leachate analysis and reaction aliquots. This pore size was chosen as the maximum size which appears to trap all ash particles to which metals might adsorb.[7]

Role of Surface in Catalysis

To determine the relative importance of surface-mediated or solution-phase reactions, a reaction slurry was filtered after the reaction was partially complete. Loss of sulfite was monitored in the filtrate; and as can be seen in Figure 1, the reaction rate is not affected by removing particulate matter.

Because the catalysis is apparently due to trace metals which can be leached from the ash, an attempt was made to remove such species from the ash surface by leaching with different solvents. Leaching with deionized water or strongly basic solution did not affect the ash reactivity. However, an acid wash in 0.02 N acid completely deactivated the ash. Metals commonly implicated in SO_2 oxidation--Cu, Fe, Mn, Co, V--could be removed by an acid wash, depending on chemical state, so it is not surprising that washing with acid deactivates the fly ash.

Leaching experiments were carried out using a variety of solvents. In Table 1 an attempt has been made to correlate Fe and Mn concentrations with ash reactivity. These are the only two catalysts present in high enough concentration to account for the observed rates. Fe concentration shows a good correlation with reaction rates (Table 1). The fact that the reaction reaches its maximum rate within 3-4 min of initiation indicates that the species responsible for the catalysis is rapidly leached from the ash and is therefore found on the surface, rather than in the aluminosilicate matrix. V, Co, Cu, and Mn are present to some

*This work was supported by the Assistant Secretary for Environment, Office of Health and Environmental Research, Division of Biomedical and Environmental Research of the U.S. Department of Energy under Contract No. W-7405-ENG-48 and by the Morgantown Energy Research Center under Contract No. AA 050515.

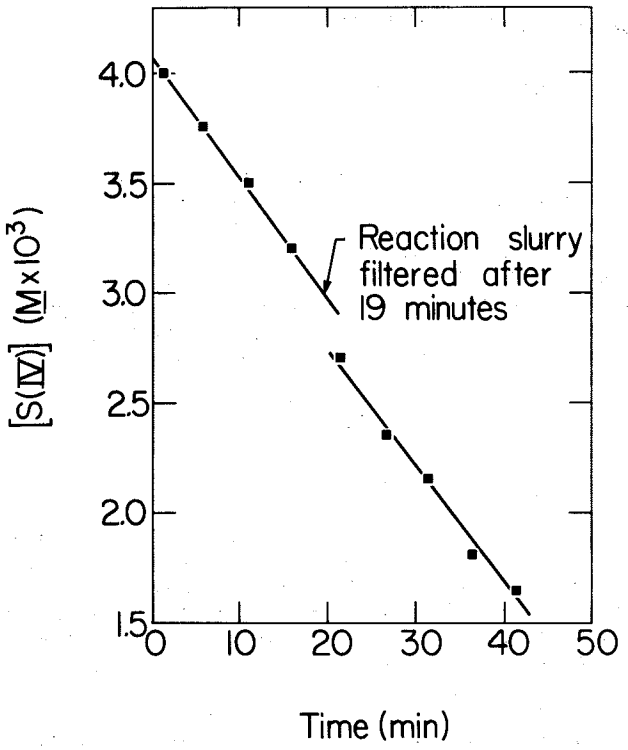

Fig. 1. Comparison of rate of [S(IV)] oxidation before and after filtering reaction slurry. Initial pH = 2.9, ["D" fly ash] = 0.18%.
(XBL 809-1927)

degree on the ash surface, whereas Fe is predominantly matrix-associated.[8] Since significant concentrations of Fe are present in stirred reaction slurries, we believe that the small quantity of Fe which is surface-associated--perhaps as a ferrous or ferric salt--is catalytically important.

By augmenting the catalyst concentration, we hoped to increase the reaction rate. Stirring reaction slurries for long time periods to increase the Mn and Fe concentrations by as much as twofold did not always increase the reaction rate. Graefe et al.[1] also observed this phenomenon. In addition, there was no simple relation between fly ash concentration and reaction rate: Although increasing the ash content in reaction slurries generally accelerated the reaction, the rate dependence on fly ash concentration was not monotonically increasing and not reproducible with varying reaction conditions. Equilibrium control of metal dissolution could be responsible for this behavior. This would be independent of kinetic control of the leaching described in the preceding paragraph. Chemical kinetic saturation is another possibility. Hudson found a zero order dependence on Fe concentration for [Fe] > 1 ppm.[9]

pH Studies

It is important to know the pH dependence of the reaction for at least two reasons: The two opposing factors which are controlled by pH are (1) metal dissolution (favored at lower pH), and (2) fraction of SO_3^{2-} and HSO_3^- present relative to the total concentration of S(IV) species (increases with increasing pH). Many studies implicate $SO_3^{=}$ as the reactive species in catalytic oxidation of S(IV).[11,12] The U-shaped curve in Figure 2 is thus qualitatively what is expected for homogeneous catalysis by metals leached from the ash.

Comparison With Known Rates

Attempts were made to correlate reaction rates observed here with values in the literature for metal-assisted S(IV) oxidation.[11-16] Initial rates of the fly ash reaction were compared to initial rates calculated from the referenced equations. For each case, the concentration of metal catalyst used was the maximum found in a fly

Table 1. Comparison of rates with metal concentrations.

Ash type	[Metal] in $NH_2OH \cdot HCl$ Extract[a]		[Metal] in Filtered Reaction Slurry[a]		Reaction Rate[b]	
	[Mn]	[Fe]	[Mn]	[Fe]	Reaction in Untreated Ash	In NH_2OH HCl Extracted Ash
NBS	0.071	1.8	<0.01	-	1.92×10^{-5}	-
A	0.64	12.5	0.05	1.9	12.0×10^{-5}	1.0×10^{-5}
B	1.71	5.0	0.19	1.2	3.6×10^{-5}	1.3×10^{-5}
C	0.59	7.2	0.07	1.5	8.0×10^{-5}	6.0×10^{-5}
D	0.83	3.4	0.11	-	6.8×10^{-5}	1.4×10^{-5}

[a]All metal concentrations are in μg/ml.

[b]Initial rate = d[S(IV)]/dt (mol/l min).

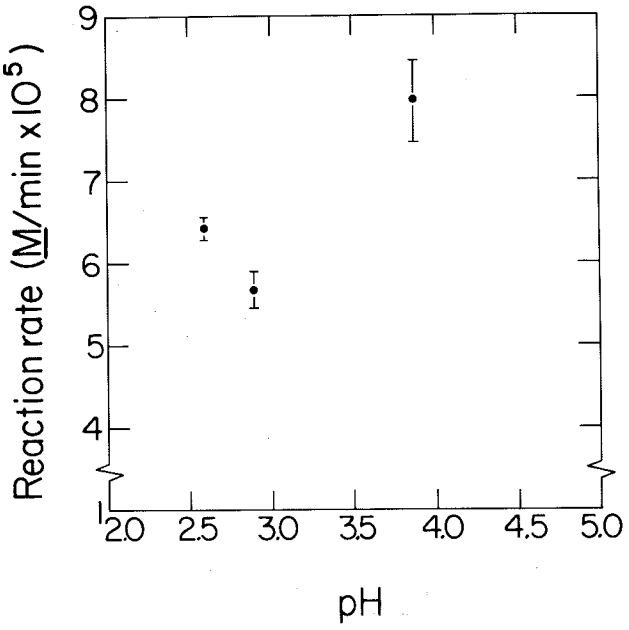

Fig. 2. pH dependence of fly ash (type D) reaction rate. pH variation during reaction = ± 0.05. $[S(IV)]_0 = 9 \times 10^{-3}$ M, [fly ash] = 0.12%, T = 22°C. (XBL 809-1928)

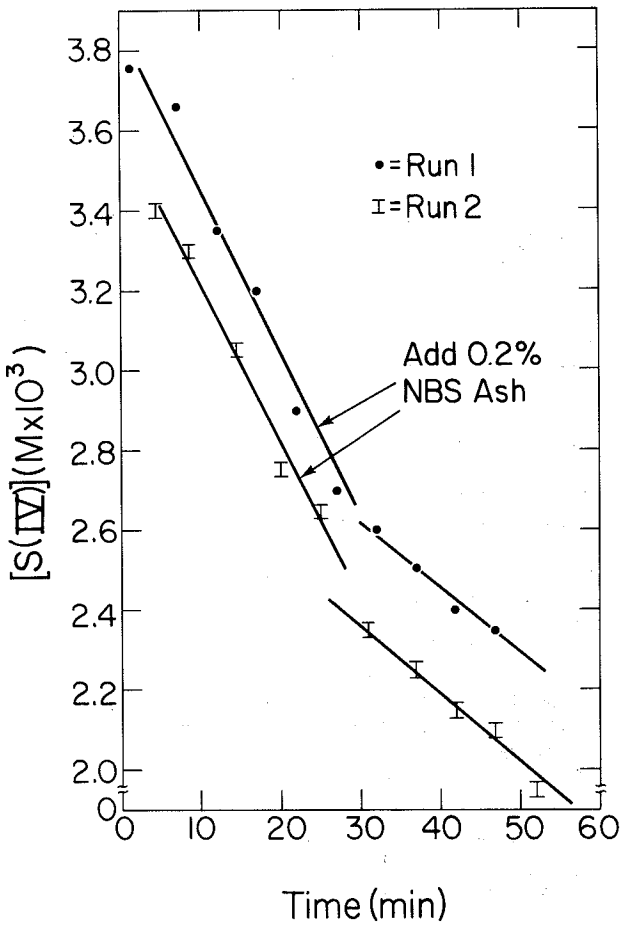

Fig 3. Demonstration of rate inhibition by NBS ash. Initial pH = 2.9 ± 0.1, ["D" fly ash] = 0.15%. (XBL 809-1926)

ash solution. As expected, Mn is not present in high enough concentration to account for the observed rate, whereas Fe is. Because of the complexity of the system, this result serves only to support the empirical evidence presented above.

Inhibition

Other complications exist. The presence of inorganic arsenite and SO_4^{2-} from the ash could inhibit the reaction.[10,18] Several organic compounds also inhibit the oxidation.[9,19] It was suspected that the NBS ash could be unreactive because of the presence of inhibitor in addition to the lack of catalyst. X-ray fluorescence and combustion data show the NBS ash contains more C and As than active ash type D. Inspection of Figure 3 shows that the NBS ash does indeed serve as an inhibitor. Extracting the NBS ash in base to remove suspected inhibitors arsenite and cyanide does not, however, render this ash more catalytically active. In addition, neither soxhlet extraction using methanol nor combustion to remove all organic matter causes a significant rate increase.

CONCLUSION

Fly ash is not a uniform substance. Compositional inhomogeneities are to be expected even within one sample lot. For this reason, a thorough rate study of fly-ash-catalyzed SO_2 oxidation could serve little purpose. The goal of this study has been to isolate fly ash components essential to SO_2 oxidation. Evidence presented here discounts the importance of the ash surface in this catalysis. Filtering the reaction slurry leaves the rate unchanged. Also, leaching under relatively mild conditions which should not change surface morphology renders the ash catalytically inactive. Unimportance of the ash surface is not surprising considering the low surface area (1-30 m^2/gm) of most fly ash. In addition, it appears that Fe plays a more important role than Mn in the oxidation. Since Mn is more soluble than Fe at pH levels found in droplets and wet scrubbers, this result is important.

PLANNED ACTIVITIES FOR FY 1981

The synergistic effect of metal ions in fly ash on the catalytic oxidation of SO_2 will be investigated.

REFERENCES

1. A. F. Graefe et al., Report to National Air Pollution Control Administration, NTIS #PB 196781, 1970.

2. P. Marrier and H. P. Dibbs, "The Catalytic Conversion of SO_2 to SO_3 by Fly Ash and the Capture of SO_3 by CaO and MgO," Thermochimica Acta, vol. 8, 1974, p. 155.

3. G. E. Gordon, D. D. Davis, G. W. Israel, H. E. Landsberg, and T. C. O'Haver, "Atmospheric Impact of Major Sources and Consumers of Energy," National Science Foundation Report NSF/RA/E-75/189 (NTIS #PB 262574), 1975.

4. J. B. Green, Potential of Humic Acid as Stack Gas Scrubbing Media for Removal of Sulfur Dioxide and Fly Ash, Ph.D. dissertation, University of Maryland, 1977.

5. H. Head and S. C. Wang, EPA Alkali Scrubbing Test Facility Advanced Program, Basic Report, vol. 1, 1979.

6. S. Cohen et al., "Surface Characterization of Fly Ash," Atmospheric Aerosol Research Annual Report FY 80, Lawrence Berkeley Laboratory report LBL-10735, 1980, p. 37.

7. G. L. Fischer et al., "Filtration Studies with Neutron Activated Coal Fly Ash," Environmental Science and Technology, vol. 13, 1979, p. 689.

8. L. D. Hansen and G. L. Fisher, "Elemental Distribution in Coal Fly Ash Particles," Environmental Science and Technology, vol. 14, 1980, p. 1111.

9. J. L. Hudson, Sulfur Dioxide Oxidation in Scrubber Systems, Environmental Protection Agency report EPA-600/7-80-083, 1980.

10. M. J. Matteson, W. Stober, and H. Luther, "Kinetics of the Oxidation of Sulfur Dioxide by Aerosols of Manganese Sulfate," Industrial and Engineering Chemical Fundamentals, vol. 8, 1969, p. 677.

11. H. Bassett and W. G. Parker, "The Oxidation of Sulphurous Acid," Journal of American Chemical Society, 1951, p. 1540.

12. L. A. Barrie and H. W. Georgii, "An Experimental Investigation of the Absorption of Sulphur Dioxide by Water Drops Containing Heavy Metal Ions," Atmospheric Environment, vol. 10, 1976, p. 743.

13. E. C. Fuller and R. H. Crist, "The Rate of Oxidation of Sulfite by Oxygen," Journal of American Chemical Society, vol. 63, 1941, p. 1644.

14. P. Brimblecombe and D. J. Spending, "The Catalytic Oxidation of Micromolar Aqueous Sulfur Dioxide - I," Atmospheric Environment, vol. 8, 1974, p. 937.

15. D. R. Coughanowr and F. E. Krause, "The Reaction of SO_2 and O_2 in Aqueous Solutions of $MnSO_4$," Industrial and Engineering Chemical Fundamentals, vol. 4, 1965, p. 61.

16. D. G. Karraker, "The Kinetics of the Reaction between Sulfurous Acid and Ferric Ion," Journal of Physical Chemistry, vol. 67, 1963, p. 871.

17. P.N. Dasgupta, private communication, August 1980.

18. L. C. Schroeter, Sulfur Dioxide: Application in Foods, Beverages, and Pharmaceuticals (Oxford: Pergamon Press, 1966), p. 56.

19. H. L. Backstrom, "The Chain-Reaction Theory of Negative Catalysis," Journal of Physical Chemistry, vol. 49, 1927, p. 1460.

SOOT IN THE ARCTIC*

H. Rosen, T. Novakov, and B. Bodhaine†

INTRODUCTION

Recent studies in the Arctic[1,2] show the presence of large aerosol concentrations that significantly affect optical transfer through the atmosphere and lead to the phenomenon of Arctic haze, which was first reported by Mitchell.[3] In particular, the observation of substantial concentrations of particulate sulfur and vanadium at the National Oceanographic and Atmospheric Administration and Geophysical Monitoring for Climatic Change sampling station near Barrow, Alaska, has attracted considerable attention.[1,2] Questions have been raised as to the anthropogenic character, sources, and climatic impacts of these aerosols. In order to gain a better understanding of these issues, a study of the physical and chemical properties of the carbonaceous aerosol at Barrow was initiated in October, 1979.

Recent studies of the urban aerosol indicate the presence of substantial graphitic carbon concentrations. These graphitic species--identified by a variety of modern analytical techniques (e.g., Raman spectroscopy,[4] photoacoustic spectroscopy,[5] thermal analysis[6])--are very effective absorbers of visible radiation and are responsible for the high optical absorption coefficients which have recently been observed in urban air.[7,8] The impacts of these highly absorbing particles on a regional or global scale have not been assessed so far, but they could be important, especially over regions with a high surface albedo like the polar icecaps. Furthermore, graphitic carbon can only be produced from combustion processes, and therefore it can offer a very attractive and convenient tracer for anthropogenic activity.

ACCOMPLISHMENTS DURING FY 1980

An aerosol sampler was constructed to collect parallel 47-mm quartz fiber and Millipore filter samples at a flow rate of ~1.5 cfm. The sampler had two chambers--a lower chamber which contained the pumps and an upper chamber for collecting the aerosol samples. The upper chamber was warmed by several thermostatically controlled heat lamps, while temperature control in the lower chamber was achieved by using a thermostatically controlled fan and heat lamps. The exhaust of the pumps was vented below the sampling platform. To minimize local contamination, the aerosol sampler was controlled by a wind sensor built by the University of Rhode Island group.[1] This allowed samples to be collected only when the wind was from the clean air sector at Barrow, between 0° N and 130° SE. Results obtained with and without the wind controller suggest that there is no significant influence from local sources. Approximately 50 filter pairs have been collected at sampling time intervals ranging from 2 days to 1 week. The quartz filters were used to determine the total carbon content of the aerosol by a combustion method,[9] and the Millipore substrate was used to determine the optical absorption coefficient of the aerosol by the LBL laser transmission method described elsewhere.[4,5,8] The absorption coefficients reported here are consistent with the optical constants of graphitic carbon and are expected to have an accuracy of better than a factor of two. The Millipore substrate was also analyzed by the X-ray fluorescence technique to determine the concentration of elements with $Z > 11$. The quartz blanks had a carbon loading of $< 0.5\ \mu g/cm^2$, while typical filter deposits corresponded to $15\ \mu g/cm^2$. Selected filters have been analyzed by Raman spectroscopy, thermal analysis, and solvent extraction techniques. The results of these analyses are described below.

Raman spectroscopy is a highly selective method of analysis which has been used to identify large concentrations of graphitic carbon in urban particulates.[4] This technique has been applied to the analysis of several samples collected at Barrow. The experimental arrangement and methods are described elsewhere.[4] The results are shown in Figure 1, in which the spectrum of an Arctic sample collected in December 1979 is compared to that of urban particulates, various source emissions, and carbon black. All these spectra show the presence of two intense Raman modes located at 1350 cm^{-1} and 1600 cm^{-1}, which have been identified as due to phonons propagating within graphitic planes.[10] This result shows that graphitic structures similar to carbon black and due to combustion processes are present in the Arctic aerosol. Furthermore, the high intensity in these modes indicates that, just as in urban samples, the graphitic structures represent a major component of the aerosol.

The filters collected at Barrow from Fall through late Spring have a grey or black appearance similar to that found for urban particulates. For the urban samples, this optically absorbing component has been identified as graphitic carbon.[4] Preliminary measurements on a limited number of samples show that the optically absorbing species in the Arctic has a $1/\lambda$ wavelength dependence, is

*This work was supported by the Assistant Secretary for Environment, Office of Health and Environmental Research, Division of Biomedical and Environmental Research of the U.S. Department of Energy under Contract No. W-7405-ENG-48 and by the National Science Foundation under Contract No. ATM 80-13707 and by the Air Resources Laboratory of the National Oceanographic and Atmospheric Administration.

†Geophysical Monitoring for Climatic Change Program of the Air Resources Laboratory, National Oceanographic and Atmospheric Administration, Boulder, Colo.

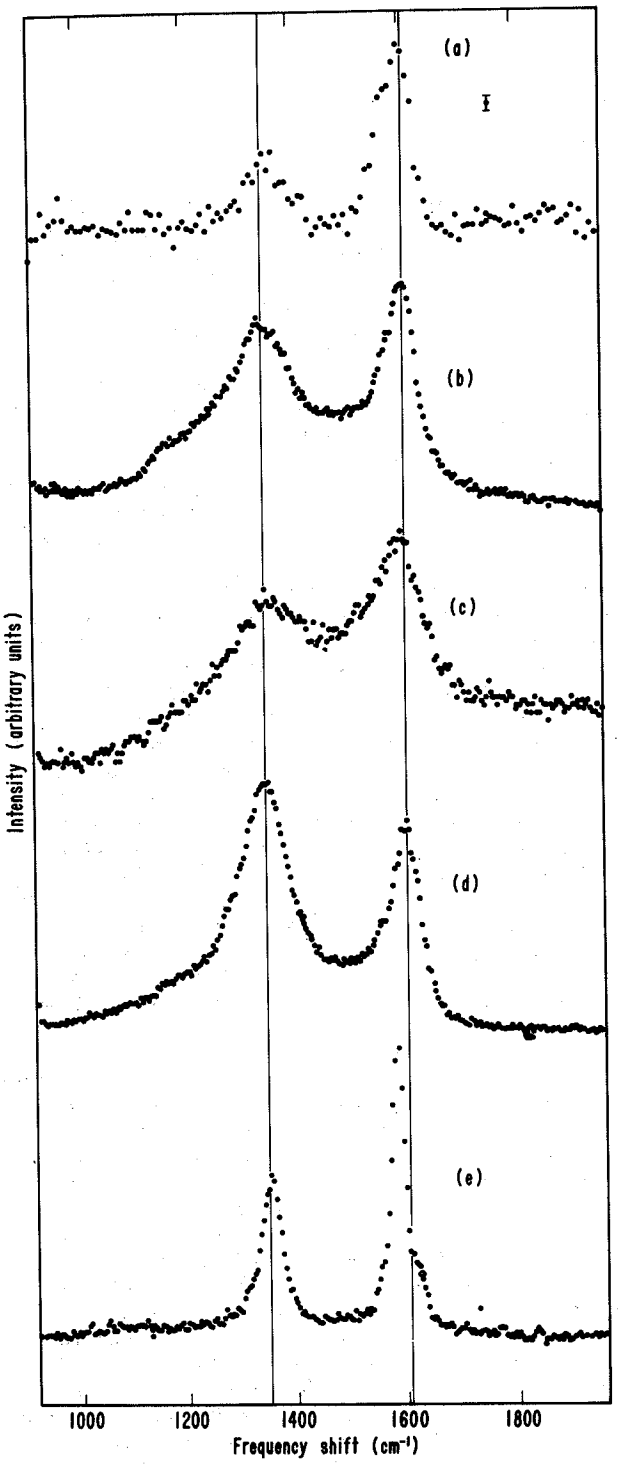

Fig. 1. Raman spectrum of an Arctic sample compared to those of urban particulates for various source emissions, carbon black, and polycrystalline graphite. (XBL 767-3091A)

insoluble in a wide range of solvents, and has a high temperature stability with an oxidation threshold of approximately 500°C. These results are consistent with the properties of graphitic carbon and strongly suggest that indeed the optically absorbing species at Barrow is graphitic in nature.

The seasonal variation of the optical absorptivity (or graphitic carbon concentration) of the Barrow aerosol is shown in Figure 2. The absorption coefficient changes by more than an order of magnitude from mid-October to early January and remains at a relatively high level throughout most of February, March, and April. It decreases substantially in May. The magnitude of the absorption coefficient during the Winter and Spring is comparable to that found in urban environments (Table 1) (i.e., the peak values in February are only about a factor of ten less than the average absorption coefficients in New York City and a factor of three less than those found in Berkeley, Calif., and Denver, Colo.). This absorption coefficient is large enough to produce significant optical effects. For example, an absorption coefficient of 5×10^{-6} m^{-1} extended over a path length of 10 km would produce an optical thickness of .05. This would be a large perturbation on the transfer of optical radiation through the atmosphere when the sun's irradiance is at a high level, as it is during part of these pollution episodes. In order to assess the importance of these effects, more detailed measurements of the seasonal variation in the optical properties (visible and infrared) and the vertical and horizontal extent of the aerosols need to be determined.

The pollution episodes observed at Barrow are not a local phenomenon but appear to be areawide with similar seasonal variations occurring at widely spaced sites across the Arctic.[11,12] This is illustrated in Figure 3, in which a comparison of the monthly variations in the blackness of the filter deposits collected at Barrow and Mould Bay, Canada, are shown. (The samples from Mould Bay were provided by Dr. L. A. Barrie and Dr. P. Hoff of the Canadian Atmospheric Environment Service.) These sampling stations are widely separated, yet the initial onset and duration of the episodes observed at these two sites are almost identical.

Using the optical constants of graphitic carbon determined from our urban studies,[13] we can make an estimate of the graphitic carbon

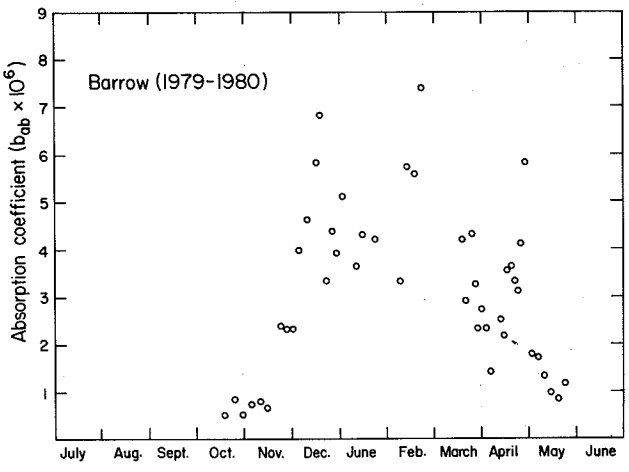

Fig. 2. Seasonal variations in the optical absorption coefficient in m^{-1} at Barrow from October 1979 to May 1980. (XBL 8010-4418)

Table 1. A comparison of absorption coefficients, carbon concentrations, and graphitic carbon concentrations at Barrow, Alaska, and various urban locations.

Site	Date	Number of Samples	Average Absorption Coefficient x 10^5 (M^{-1})	Average Total Carbon ($\mu g/m^3$)	Average Graphitic Carbon as Percent of Total Carbon[a]
Barrow, Alaska	12/79-4/80	33	.4	1.2	24
Argonne, Illinois	1/79-3/80	438	2.8	8.1	22
Gaithersburg, Maryland	1/79-3/80	381	2.1	6.1	22
Denver, Colorado	11/78-5/79	141	2.4	9.8	16
Anaheim, California	8/77-1/80	852	4.9	16.6	19
Fremont, California	7/77-3/80	924	3.4	12.0	18
Berkeley, California	6/77-4/80	998	2.1	6.7	20
New York, New York	11/78-4/80	439	6.4	15.2	27

[a]Calculated from optical constants in Reference 13.

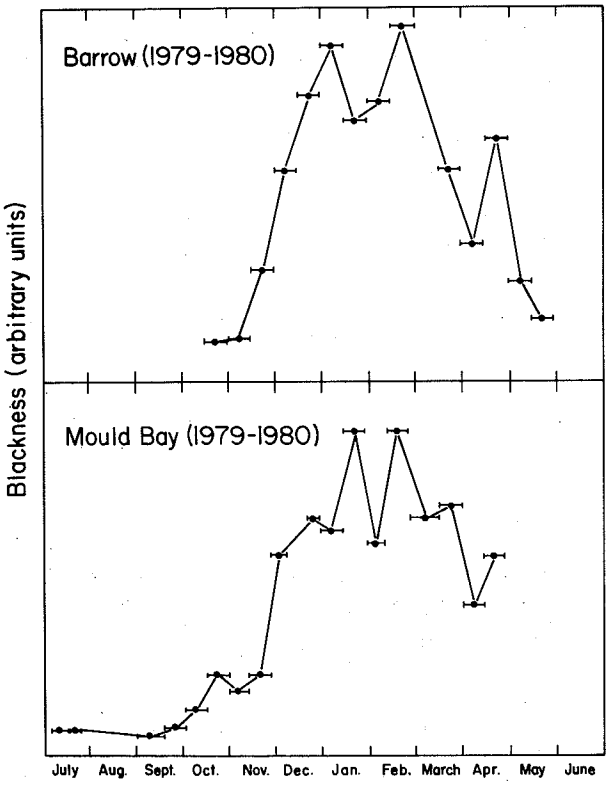

Fig. 3. A comparison between the seasonal variation in the blackness of filter deposits collected at Barrow, Alaska, and Mould Bay, Canada, in 1979 and 1980. Mould Bay samples were provided by L. A. Barrie and P. Hoff of the Canadian Atmospheric Environment Service.
(XBL 8010-4420)

concentration at Barrow. These results are shown in Figure 4, where we plot the graphitic carbon concentration as a fraction of the total carbon content of the aerosol for various periods of time during the year. The results shown a strong enrichment of the graphitic fraction of the carbonaceous aerosol from early to late winter. The concentration of graphitic carbon in late February is almost 40% of the carbonaceous mass. It is remarkable that this percentage is higher than that found in urban centers like New York City and Los Angeles.[14] After its peak in February, the fraction of graphitic carbon seems to level off to a value which is more typical of those found in urban environments. The interpretation of these interesting features in terms of transport, atmospheric chemistry, and deposition processes is complicated and will have to await more detailed analyses and further measurements.

In summary, these observations indicate that large graphitic concentrations can develop at remote locations. If one ignores the possible contribution of natural burning processes (e.g., forest fires), which is expected to be small during these times of year in the northern hemisphere, this component can be attributed directly to the burning of fossil fuels. The source and the climatic effects of these highly absorbing species are uncertain and will have to await more systematic measurements and careful modelling.

PLANNED ACTIVITIES FOR FY 1981

The project will continue to explore the sources and climatic impact of carbonaceous aerosols in the Arctic region.

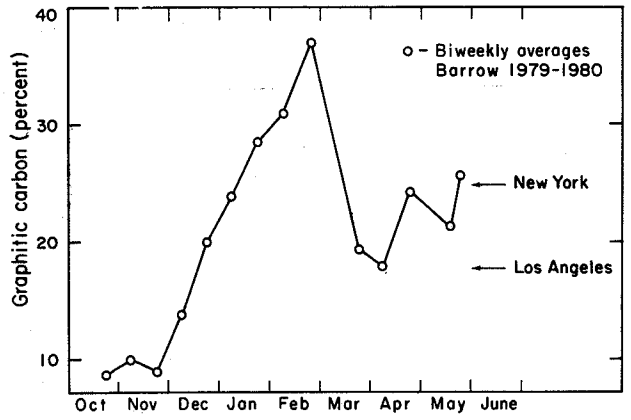

Fig. 4. Seasonal variation of graphitic carbon as a percentage of the total carbon content of the aerosol at Barrow from October 1979 to May 1980. These values are compared to the average values obtained in New York City and Los Angeles. (XBL 809-2013)

ACKNOWLEDGMENTS

The authors would like to acknowledge stimulating and helpful discussions with Lester Machta, National Oceanographic and Atmospheric Administration, and with Michael MacCracken, Lawrence Livermore Laboratory.

REFERENCES

1. K. A. Rahn and R. J. McCaffrey, "On the Origin and Transport of the Winter Arctic Aerosol," Proceedings, Conference on Aerosols: Anthropogenic and Natural - Sources and Transport (New York City: New York Academy of Sciences, January 9-12, 1979, in press).

2. G. E. Shaw and K. Stamnes, "Arctic Haze: Perturbation of the Polar Radiation Budget," Proceedings, Conference on Aerosols: Anthropogenic and Natural - Sources and Transport (New York City, New York Academy of Sciences: January 9-12, 1979, in press).

3. M. Mitchell, "Visual Range in the Polar Regions with Particular Reference to the Alaskan Arctic," Journal of Atmospheric Terrestrial Physics, Special Supplement, 1956, pp. 195-211.

4. H. Rosen, A. D. A. Hansen, L. Gundel, and T. Novakov, "Identification of the Optically Absorbing Component in Urban Aerosols," Applied Optics, vol. 17, 1978, p. 3859.

5. Z. Yasa, N. M. Amer, H. Rosen, A. D. A. Hansen, and T. Novakov, "Photoacoustic Investigation of Urban Aerosol Particles," Applied Optics, vol. 18, 1979, p. 2528.

6. R. Dod et al., "Application of Thermal Analysis to the Characterization of Nitrogenous Aerosol Species," Energy and Environment Division Annual Report, 1979, Lawrence Berkeley Laboratory report, LBL-10735, 1980.

7. R. E. Weiss, A. P. Waggoner, R. Charlson, D. L. Thorsell, J. S. Hall, and L. A. Riley, "Studies of the Optical, Physical, and Chemical Properties of Light Absorbing Aerosols," Proceedings, Conference on Carbonaceous Particles in the Atmosphere, Lawrence Berkeley Laboratory report LBL-9037, 1979, p. 257.

8. M. Sadler, R. J. Charlson, H. Rosen, and T. Novakov, An Intercomparison of the Integrating Plate and the Laser Transmission Methods for Determination of Aerosol Absorption Coefficients, Lawrence Berkeley Laboratory report LBL-11176, 1980.

9. P. K. Mueller, R. W. Mosley, and L. B. Pierce, "Carbonate and Non-carbonate Carbon in Atmospheric Particulates," Second International Clean Air Congress, Proceedings (New York Academic Press, 1971).

10. F. Tuinstra and J. L. Koenig, "Raman Spectrum of Graphite," Journal of Chemical Physics, vol. 53, 1970, p. 1126.

11. L. A. Barrie et al., "The Influence of Mid-Latitudinal Pollution Sources in the Haze in the Canadian Arctic," Atmospheric Environment (in press).

12. B. Ottar et al., "The Transfer of Airborne Pollutants to the Arctic Region," Atmospheric Environment (in press).

13. A. D. A. Hansen et al., "The Use of an Optical Attenuation Technique to Estimate the Carbonaceous Component of Urban Aerosols,' Energy and Environment Division Annual Report, 1979, Lawrence Berkeley Laboratory report LBL-10735, 1980, p. 16.

14. H. Rosen, A. D. A. Hansen, R. L. Dod, and T. Novakov, "Soot in Urban Atmospheres: Determination by an Optical Absorption Technique," Science, vol. 208, 1980, p. 741.

AN INTERCOMPARISON OF THE INTEGRATING PLATE AND THE LASER TRANSMISSION METHODS FOR DETERMINATION OF AEROSOL ABSORPTION COEFFICIENTS*

M. Sadler,† R. Charlson,† H. Rosen, and T. Novakov

INTRODUCTION

Recent studies of atmospheric aerosol particles indicate the presence of a large, optically absorbing component which can cause both visibility degradation and climatic effects. The nature of this absorbing species has been investigated in the past by solvent extraction, heat treatment, and wavelength dependence studies.[1,2] These investigations led to the conjecture that it could be a graphite-like material. More recently, the Raman scattering technique has been applied to identify this component in urban aerosols on a microscopic level as "graphitic" carbon.[1]

The fact that aerosol particles absorb light is evident from the usual grey or black appearance of filter samples collected from even rural locations. However, the absolute measurement of the component of extinction due to absorption, σ_{ap}, has posed significant challenges. Here we define the extinction coefficient, σ_{ext}, and its components with the Beer-Lambert law. For light of intensity I passing through an atmospheric path of length dx:

$$\frac{dI}{I} = -\sigma_{ext}dx = -(\sigma_{scatter} + \sigma_{absorption})\ dx$$

and

$$\sigma_{absorption} = \sigma_{absorption\ by\ particles} +$$

$$\sigma_{absorption\ by\ gases} = \sigma_{ap} + \sigma_{ag}.$$

Not only is the measurement of σ_{ap} difficult, it is also extremely hard to make aerosols of known absorption coefficient for testing, calibration, and validation of methods.

Historically, one of the earliest measurements was performed by Waldram,[3] who measured the total extinction and its scattering component, arriving at the absorption component by subtraction. He found a relatively large percentage of extinction to be caused by particle absorption--typically half in an industrial area of England. However, this result has often been discounted as being atypical, and the assumption is usually that $\sigma_{ext} \cong \sigma_{scat}$.

There are fundamentally two general approaches in use for assessing light absorption by particles. One set of methods aims at establishing the absorption coefficient in the atmosphere, σ_{ap}; the other set of methods determines the imaginary refractive index of the bulk material of which the particles are formed. These approaches can be connected via Mie calculations if size distribution and the distribution of absorbing material with size are known.

In addition to the difference method of Waldram,[3] the integrating plate method,[4] the laser transmission method, and the multipass transmissometer[5] are examples of the first of these approaches; the integrating sphere,[6] the Kubelka-Monk method,[7] and inversion of angular scattering data have been used to estimate the imaginary refractive index of the material of which the particles are formed.

Two of these methods (the integrating plate and laser transmission) have been extensively used because of their practicality. This paper will compare the absorption coefficients determined by these two methods at a wide range of sites. Furthermore, these absorption coefficients will be correlated to the total carbon content of the aerosol. These measurements should provide an independent test of the strong correlation found by previous investigators[8,9] at urban locations, as well as to extend this type of observation to rural areas.

ACCOMPLISHMENTS DURING FY 1980

Five sampling sites in the western part of Washington state were used in this study, from a highly congested site in a highway tunnel to a very remote site on a western foothill in the Olympic Mountains. By sampling such diverse aerosol conditions, the range of absorption coefficients of the air samples was nearly four orders of magnitude, from $\sim 10^{-7}$ m^{-1} to 10^{-3} m^{-1}, with the total carbon concentration ranging from about 5 $\mu g/m^3$ (Mt. Octopus) to nearly 90 $\mu g/m^3$ (highway tunnel). The sites are shown in Figure 1.

The results of these comparisons are shown graphically in Figures 2 and 3. In Figure 2, a plot of absorption coefficients is shown, as determined by the Integrating Plate Method (IPM)

*This work was supported by the Assistant Secretary for Environment, Office of Health and Environmental Research, Division of Biomedical and Environmental Research of the U.S. Department of Energy under Contract No. W-7405-ENG-48 and by the National Science Foundation under Contract No. ATM 80-13707.

†Department of Civil Engineering, University of Washington, Seattle, Washington.

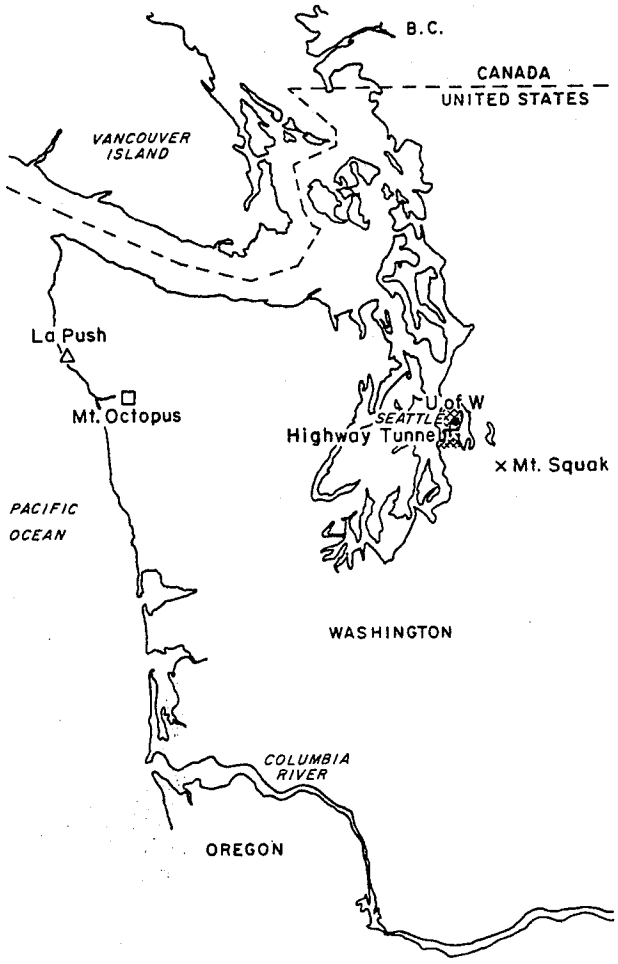

Fig. 1. Sampling sites. (XBL 811-7714)

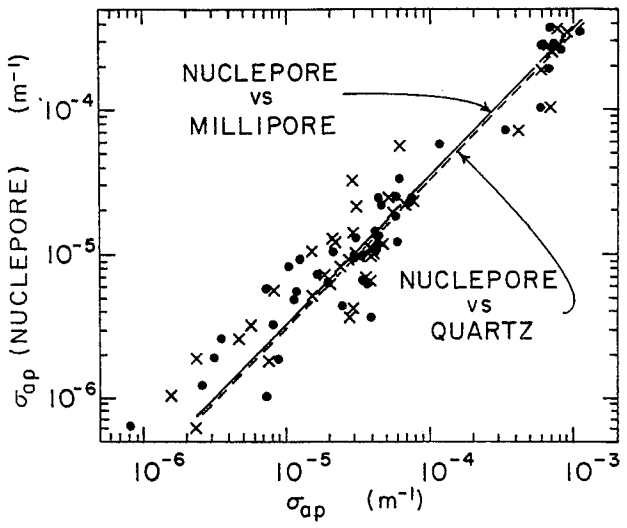

Fig. 2. Light absorption coefficient, $\sigma_{ap}(m^{-1})$, determined on Millipore (X) and quartz (0) filters. (XBL 811-7713)

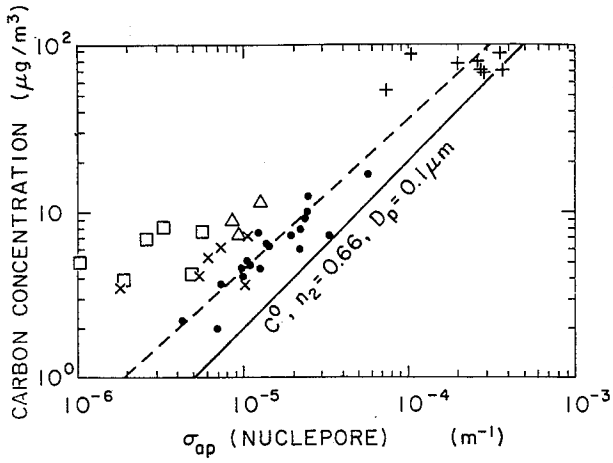

Fig. 3. Light absorption coefficient, $\sigma_{ap}(m^{-1})$ determined by the IPM versus total carbon concentration in $\mu g/m^3$. For site notation, see Figure 1. (XBL 811-7712)

using a Nuclepore substrate and the Laser Transmission Method (LTM) using a Millipore substrate. Also shown in the figure are absorption coefficients determined at the University of Washington on quartz fiber filters. A total of 44 filters of each type were used in this comparison. The correlation coefficient between the two measurements is 0.95, with the absorption coefficient determined by the LTM being greater by a factor of approximately 2.5 than the one determined by the IPM.

Figure 3 presents the plot of the concentration of total carbon ($\mu g/m^3$) versus the absorption coefficient from Nuclepore filters. The correlation found between these two variables was 0.90. Also shown in this figure is a value of σ_{ap} for monodisperse graphite particles (n_2 = 0.66, D_p = 0.1 μm), estimated as a function of mass concentration from Faxfog and Roessler.[10]

Three points emerged as the main conclusions of this study. First, the light absorption coefficients determined by these two methods are comparable and highly correlated. The reason for the higher indicated absorption coefficient using the LTM could be due to several factors, including (1) penetration effects in the Millipore substrate, which could lead to enhanced absorption due to multiple scattering effects within the filter medium itself; (2) possible pile-up at the holes or loss of particles in the holes of the Nuclepore substrate; (3) differences in the collection efficiency of the two substrates. Studies are under way in both of our laboratories to assess the magnitude of these effects. However, the differences found between these two techniques are small in comparison with the large uncertainties reported in the literature for the magnitude of the absorbing component of aerosol particles. These differences are also small compared to the range of more than three orders of magnitude observed in the value of σ_{ap}.

Second, and at least as important, a high degree of correlation is found between the absorption coefficients, σ_{ap}, and the carbon-loading

with the ratio of $[C]/\sigma_{ap}$ being similar at the highway tunnel, the University of Washington, and Mt. Squak. This correlation has been observed in the past[8,9] in many urban locations and for various source emissions, but this work represents the first verification of this important result by an independent absorption technique. Both these results are quite independent of site and are correspondingly independent to a high degree of the concentrations of carbonaceous material or level of σ_{ap}. The higher value of $[C]/\sigma_{ap}$ for the remote sites on the Olympic peninsula may be an indication of a very small natural background of non-light-absorbing carbon compounds. Such a background evidently might have values of total carbon of the order one to a few $\mu g/m^3$. The results also indicate that light-absorbing aerosols are ubiquitous in the atmosphere, even in such remote locations as our coastal sites. The fact that the ratio of $[C]/\sigma_{ap}$ is nearly the same in rural areas as in an urban area might imply that the light-absorbing carbonaceous materials in our rural samples were derived from an urban source. This suggestion is of course highly tentative and requires further measurements for resolution.

Third, we include in Figure 3 a comparison of the observed C concentration/σ_{ap} relationship to a calculation from the Mie formalism for pure graphite particles. Uncertainties of a factor of two or so exist in the imaginary refractive index for graphitic carbon, with 0.66 appearing as a typical value.[11] This calculated relationship is close to the observed values, which is consistent with the suggestion of Novakov[12] and Rosen et al.[9] that soot (which contains a graphitic and an organic component) is a major fraction of the carbonaceous aerosol in urban areas.

REFERENCES

1. H. Rosen, A. D. A. Hansen, L. Gundel, and T. Novakov, "Identification of the Optically Absorbing Component of Urban Aerosols," Applied Optics, vol. 17, 1978, p. 3859.

2. R. Weiss, R. J. Charlson, A. P. Waggoner, M. B. Baker, D. Covert, D. Thorsell, and S. Yeun, "Application of Directly Measured Aerosol Radiative Properties to Climate Models," Atmospheric Aerosols: Their Optical Properties and Effects; A Topical Meeting on Atmospheric Aerosols, National Aeronautics and Space Administration Report NASA CP-2004.

3. J. M. Waldram, "Measurement of the Photometric Properties of the Upper Atmosphere," Transactions of Illuminating Engineering Society London IU, 147, 1945.

4. C. I. Lin, M. B. Baker, and R. J. Charlson, "Absorption Coefficient of Atmospheric Aerosol: A Method of Measurement," Applied Optics, vol. 12, 1973, p. 6.

5. H. E. Gerber, "Absorption of 632.8 nm Radiation by Maritime Aerosols Near Europe," Journal of Atmospheric Sciences, vol. 36, 1979, p. 2502.

6. K. Fisher, "Mass Absorption Coefficient of Natural Aerosol Particles in the .4-2.4 μm Wavelength Interval, Beitr. zur Physik der Atmos. vol. 46, 1973, p. 89.

7. J. D. Lindberg, and L. S. Laude, "Measurement of the Absorption Coefficient of Atmospheric Dust," Applied Optics, vol. 13, 1974, p. 1923.

8. A. D. A. Hansen, H. Rosen, R. L. Dod, and T. Novakov, "Optical Characterization of Ambient and Source Particulates," Proceedings, Conference on Carbonaceous Particles in the Atmosphere, Lawrence Berkeley Laboratory report LBL-9037, p. 116.

9. H. Rosen, A. D. A. Hansen, R. L. Dod, and T. Novakov, "Soot in Urban Atmospheres: Determination by an Optical Absorption Technique," Science, vol. 208, 1980, p. 741.

10. F. R. Faxfog and D. M. Roessler, "Carbon Aerosol Visibility vs. Particle Size Distribution," Applied Optics, vol. 17, 1979, p. 2612.

11. D. M. Roessler and F. R. Faxfog, "Optical Properties of Agglomerated Acetylene Smoke Particles at .5145 μm and 10.6 μm Wavelength," Journal of Optical Society of America, vol. 70, 1980, p. 230.

12. T. Novakov, "Chemical Characterization of Atmospheric Pollution Particulates by Photoelectron Spectroscopy," Proceedings, Second Joint Conference on Sensing of Environmental Pollutants (Pittsburgh, Pa. Instrument Society of America, 1973), p. 197.

DETERMINATION OF BLACK CARBON BY THERMAL ANALYSIS*

L. Gundel, R. Dod, and T. Novakov

INTRODUCTION

Aerosol particulate material collected from ambient air and combustion sources always contains carbonaceous particles which are black or grey when collected on filters.[1] The absorption of visible light by these carbonaceous aerosols is predominantly due to the presence of carbon, which has optical properties similar to graphitic or elemental carbon and to activated carbon.[2,3] The term "black carbon" is used in this paper to refer to the optically absorbing carbonaceous component of ambient and source aerosols. Black carbon is implicated in visibility reduction,[4,5] and it could have effects on the tropospheric energy balance which could lead to regional and global climate modifications.[4,5]

Previous work at Lawrence Berkeley Laboratory (LBL) has shown that attenuation of visible light as it passes through ambient or source-particulate-loaded filters is related to concentrations of black carbon.[1,6] Attenuation measurements show that black carbon appears as a constant fraction of the total carbon contained in daily filter samples collected for two years at various urban sites throughout the United States.[6] Selective solvent extraction studies have shown that black carbon is nonextractable,[1] as expected for elemental carbon. In order to measure concentrations of black carbon on filters by optical attenuation, a direct determination of black carbon is necessary.

One method of identifying black carbon is optico-thermal analysis,[7] a combustion thermal analysis in which both the product CO_2 concentration and the optical transmission of the material are continuously monitored. This method yields simultaneous measurement of the amount of particulate carbon burned and of the change in light transmission through the filter sample as temperature-programmed combustion proceeds. For some types of samples, primarily those collected directly from combustion sources, the black carbon can be unambiguously identified and quantified from the thermogram, as shown in Figure 1a. Differentiation of black carbon from organic carbon in thermograms of ambient particulate samples may be more difficult, as illustrated in Figure 1b. Thermograms of ambient samples sometimes show carbonization, as indicated by a decrease in light transmission during thermal analysis. An example of this is shown in Figure 1c, where production of black carbon during analysis compounds the difficulty of isolating the original black carbon. Removal of soluble organic material by selective solvent extraction before thermal analysis leads to thermograms in which isolation of the black carbon peak is straightforward.[8]

ACCOMPLISHMENTS DURING FY 1980

Experimental Methods

Determination of black carbon in urban ambient and source particulate material has been accomplished by complementary use of optico-thermal analysis (as described above) and selective solvent extraction. The selective solvent extraction technique is based on the work of Appel et al.,[9,10] in which a filter sample is subjected to soxhlet extraction in benzene, followed by extraction in a methanol-chloroform mixture (1:2, v:v). This procedure removes most of the nonblack organic carbon but leaves the optical attenuation unchanged to within 10%. Optico-thermal analysis is performed on untreated particulate carbon samples and on portions of the same material after solvent extraction. For each extracted sample the amount of black carbon is determined by measuring the area under the CO_2 peak, which corresponds to the decrease in blackness, as shown by increased light transmission. Since the gas flow through the apparatus is constant, as is the temperature ramp, this area is proportional to the total mass of black carbon. Optical attenuation, ATN, is defined as

$$ATN = 100 \ln I_0/I, \qquad (1)$$

where I and I_0 represent the intensity of light transmitted through the filter before combustion and after removal of the black carbon by combustion, respectively. Optical attenuation values may depend on the type of filter substrate and on measurement technique.

Black Carbon in Ambient and Combustion Source Particulate Matter

Figure 2 shows thermograms of ambient particulate carbon collected near LBL and near the Eastshore Freeway in Berkeley, Calif. during the same 24-hour period. The patterns for the untreated samples are typical for urban particulate matter. The freeway particulate carbon thermogram shows enrichment in high temperature carbon. Total carbon and ATN are also higher for the freeway sample. After extraction, thermograms for both samples show a simpler structure. The black carbon peaks have been indicated by shading in the figure. Note that some nonblack carbon remains after extraction and that black carbon accounts for only part of the high temperature peak of the untreated sample collected at LBL (Fig. 2a).

*This work was supported by the Assistant Secretary for Environment, Office of Health and Environmental Research, Division of Biomedical and Environmental Research of the U.S. Department of Energy under Contract No. W-7405-ENG-48 and by the National Science Foundation under Contract No. ATM 80-13707.

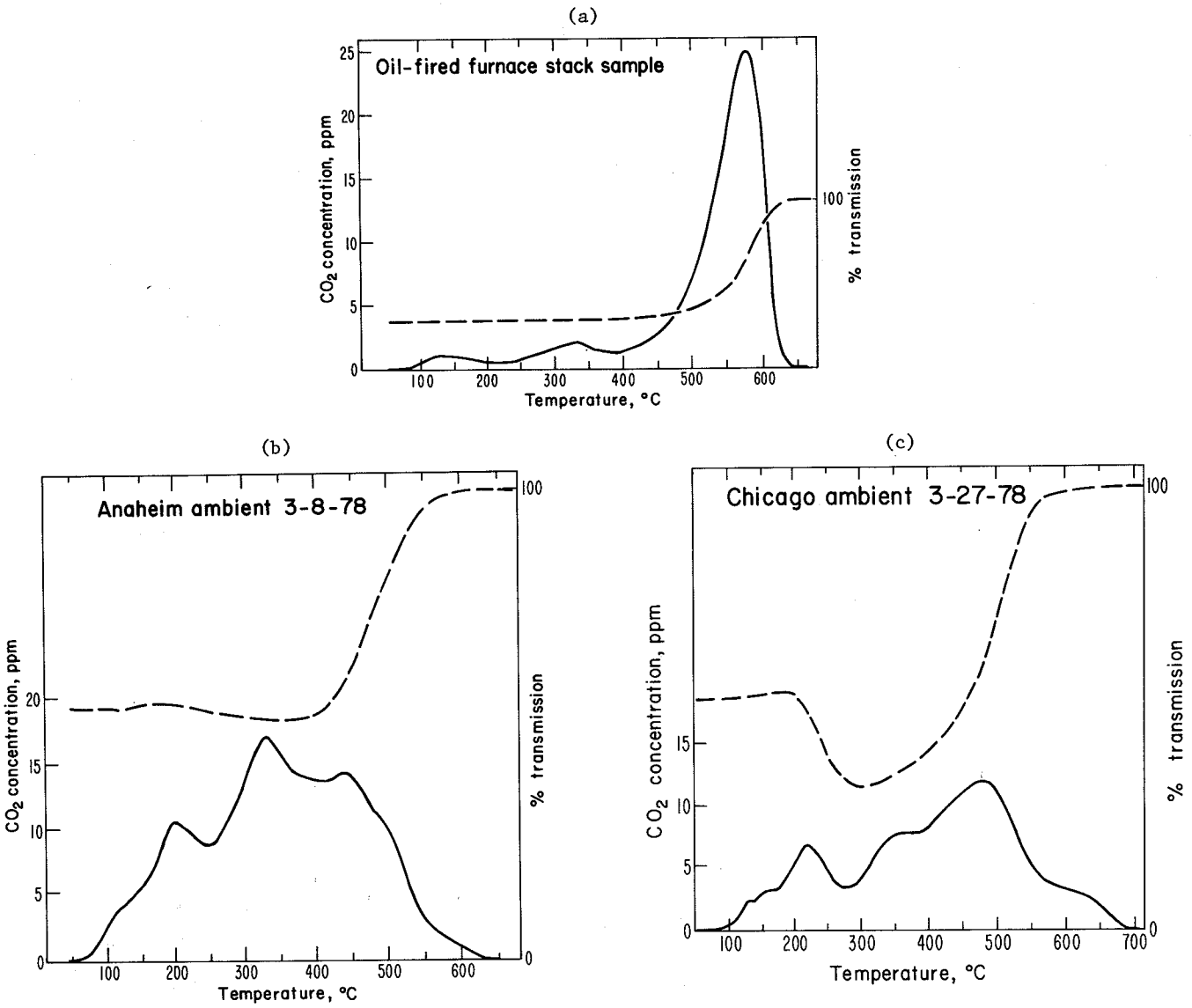

Fig. 1. Thermograms of particulate carbon collected from (a) oil-fired furnace; (b) Anaheim, Calif.; (c) Chicago, Ill. [(a) XBL 791-157; (b) XBL 791-159; (c) XBL 791-161]

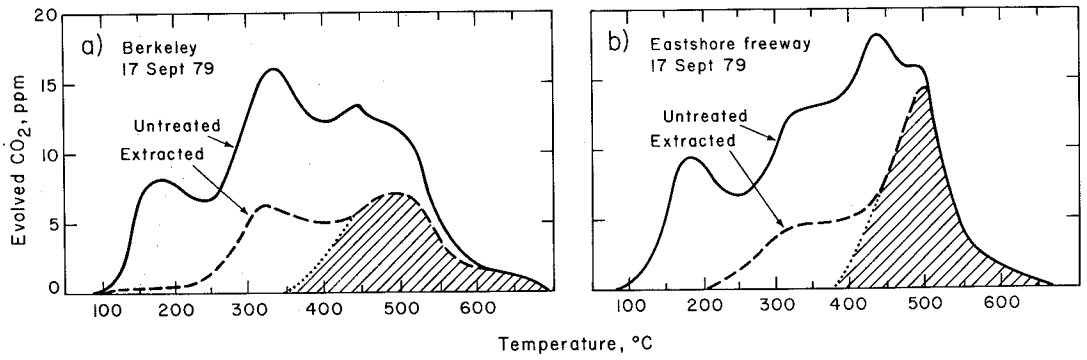

Fig. 2. Thermograms of particulate carbon collected in Berkeley, Calif. and near a major highway for untreated and sequentially extracted filter samples. The shaded area represents the black carbon. (XBL 811-40)

Thermograms for typical combustion sources are shown in Figure 3. Particulate carbon from the natural gas and propane samples is dominated by black carbon, as shown by comparison of their thermograms before and after extraction. Particulate carbon samples collected in a parking garage and in the Caldecott tunnel contain large amounts of organic as well as black carbon. Although the combustion characteristics of the black carbon in these source samples may be changed by extraction to produce temperature shifts, for example, the amount of carbon represented by the high temperature peak can be ascribed to black carbon in both extracted and unextracted samples.

The Relationship Between Optical Attenuation and Black Carbon Concentration

Figures 4 and 5 show the relationship between optical attenuation and concentration of black carbon for urban and combustion source particulate carbon respectively, as measured by optico-thermal analysis. In each case the line is a linear least squares fit to the data. The slopes of the fitted lines are 18.9 for ambient and 19.1 for source particulate matter, expressed in units of optical density/$\mu g\text{-}cm^{-2}$. Correlation coefficients are 0.98 and 0.99, respectively. Within experimental error, the slopes are identical. This indicates that the black carbon produced by these sources has the same optical properties as black carbon present in urban particulate matter. This agreement with the results of other work at LBL[2,6] supports the validity of measurement of concentrations of black carbon and ATN by optico-thermal analysis of preextracted filter samples.

The results presented here show that we now have a method for determination of the specific attentuation[2,6] σ of black carbon, where

$$\sigma = ATN/[C] \qquad (2)$$

σ has the value 19 optical density units/$\mu g\ cm^{-2}$ black carbon, when ATN and concentration of black carbon are measured by the method described here.

Planned Activities for FY 1981

We will determine the relationship between ATN as measured by this method and ATN as measured using the standard LBL technique.[1] We will participate in a study sponsored by General Motors Research Laboratories to compare methods used by various laboratories to measure black carbon concentrations in carbonaceous particulate matter.

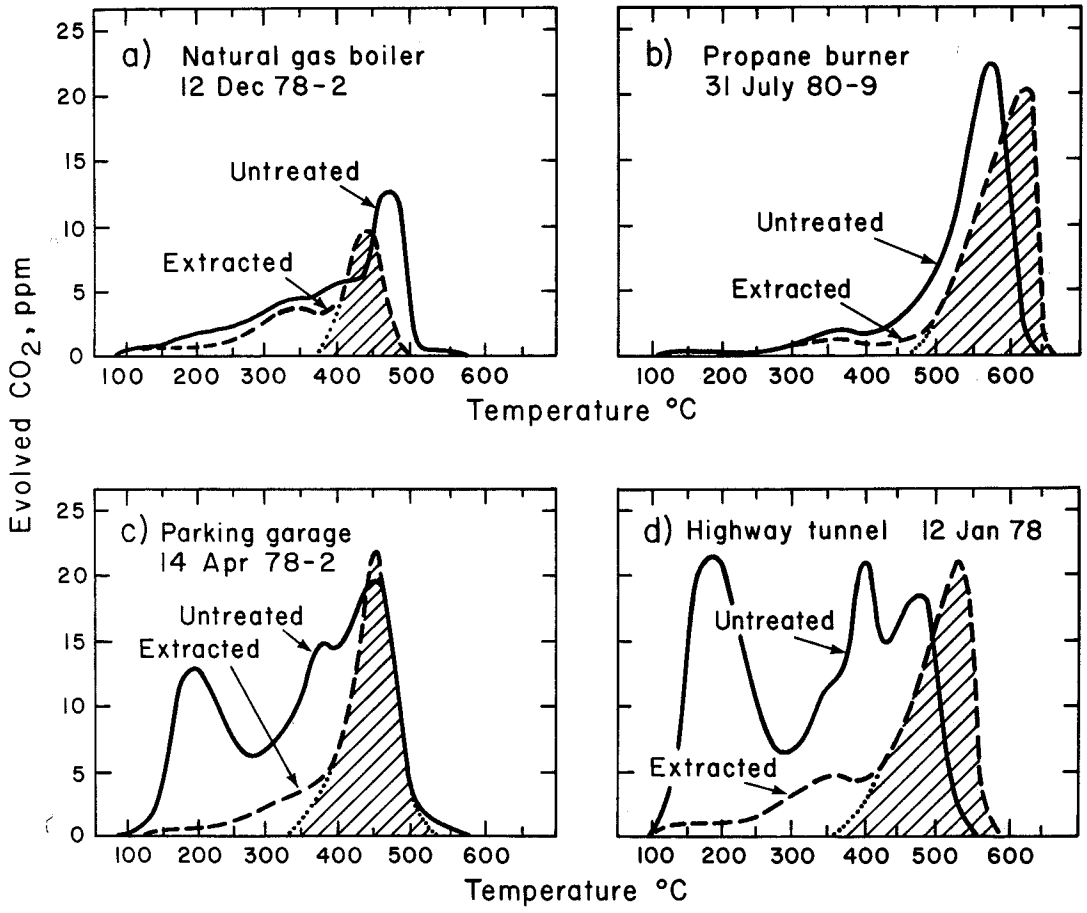

Fig. 3. Thermograms for combustion-source-generated particulate carbon for untreated and solvent extracted filter samples. The shaded area represents the black carbon. (XBL 811-39)

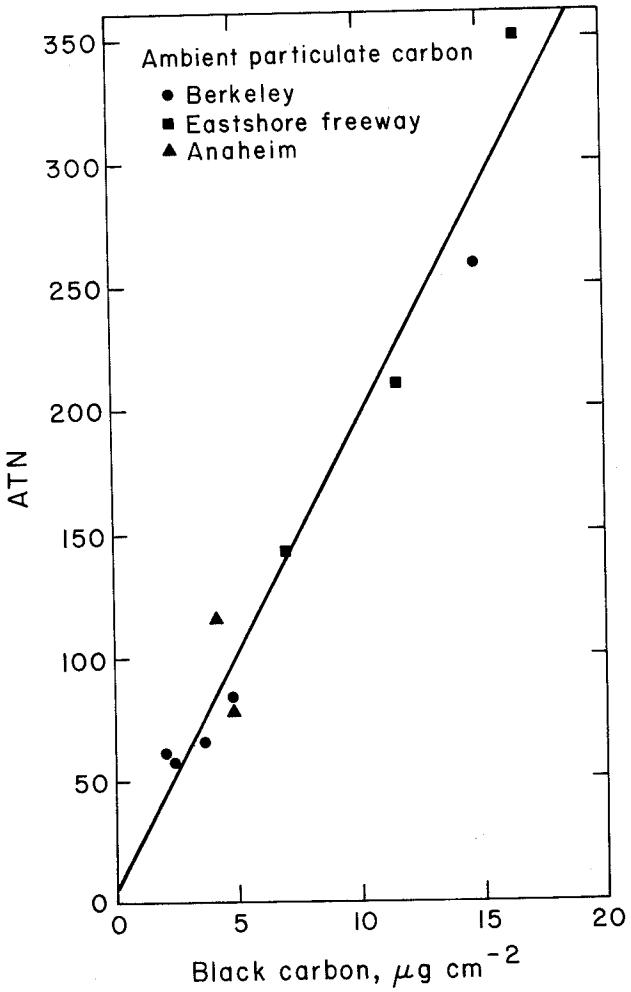

Fig. 4. Results of optico-thermal analysis for ambient particulate carbon: ATN versus amount of black carbon for samples collected in Berkeley (●), near a major highway (■), and in Anaheim, Calif. (▲). The amount of black carbon is determined from the area of the optically absorbing peak in the thermogram of the extracted filter sample. (XBL 811-37)

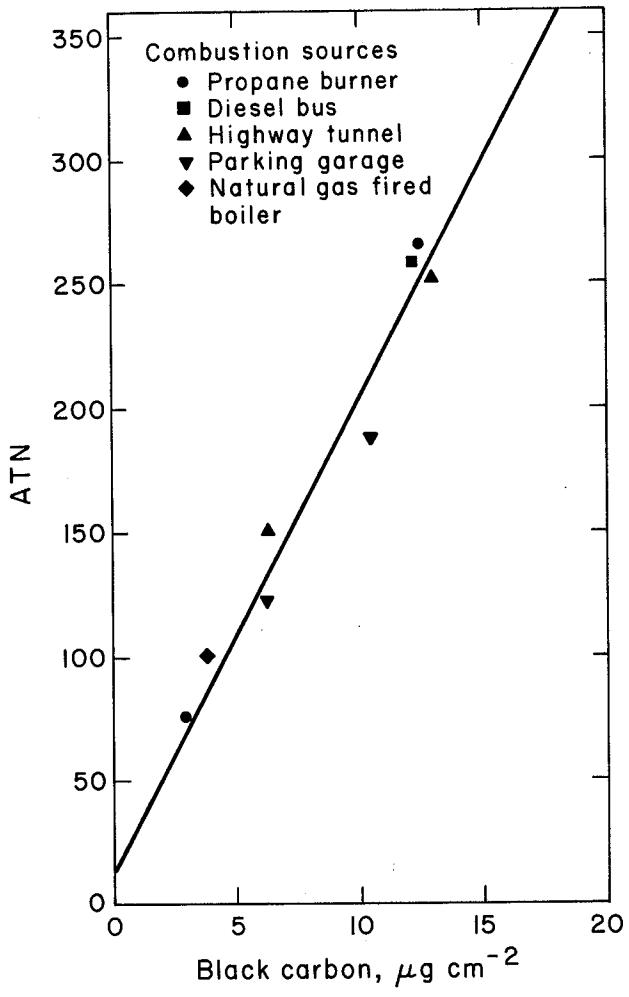

Fig. 5. Results of optico-thermal analysis for combustion-source generated particulate carbon: ATN versus amount of black carbon for a propane burner (●), a diesel bus, idling (■), a highway tunnel (▲), a parking garage (▼), and a natural gas fired boiler (◆). (XBL 811-38)

Further work is in progress to determine what particulate sample properties affect the combustion temperature of black carbon.

REFERENCES

1. H. Rosen, A. D. A. Hansen, L. Gundel, and T. Novakov, "Identification of the Optically Absorbing Component in Urban Aerosols," Applied Optics, vol. 17, 1978, p. 3859.

2. H. Rosen and T. Novakov, "Raman Scattering and the Characterization of Atmospheric Aerosol Particles," Nature, vol. 266, 1977, p. 708.

3. Z. Yasa, N. M. Amer, H. Rosen, and A. D. A. Hansen, "A Photoacoustic Investigation of Urban Aerosol Particles," Applied Optics, vol. 18, 1979, p. 2528.

4. R. E. Weiss, A. P. Waggoner, R. J. Charlson, D. L. Thorsell, J. S. Hall, and L. A. Riley, "Studies of the Optical, Physical, and Chemical Properties of Light Absorbing Aerosols," Proceedings, Conference on Carbonaceous Particles in the Atmosphere, Lawrence Berkeley Laboratory report LBL-9037, 1979.

5. H. Rosen, T. Novakov, and B. A. Bodhaine, Soot in the Arctic, Lawrence Berkeley Laboratory report LBL-11648, 1980.

6. A. D. A. Hansen et al., "The Use of an Optical Attenuation Technique to Estimate the Carbonaceous Component of Urban Aerosols," Atmospheric Aerosol Research FY 1979, Lawrence Berkeley Laboratory Report LBL-10735, 1980, p. 16.

7. R. L. Dod, H. Rosen, and T. Novakov, "Optico-Thermal Analysis of the Carbonaceous Fraction of Aerosol Particles," Atmospheric Aerosol Research Annual Report, 1977-78, Lawrence Berkeley Laboratory report LBL-8696, 1979, p. 2.

8. L. Gundel, R. Dod, and T. Novakov, "Application of Selective Solvent Extraction and Thermal Analysis to Ambient and Source Enriched Aerosols," Atmospheric Aerosol Research FY 1979, Lawrence Berkeley Laboratory report LBL-10735, 1980, p. 27.

9. B. R. Appel, E. M. Hoffer, E. L. Kothny, S. M. Wall, M. Haik, and R. L. Knights, "Analysis of Carbonaceous Material in Southern California Atmospheric Aerosols," Environmental Science and Technology, vol. 13, 1979, p. 98.

10. L. A. Gundel, G. E. Mason, and T. Novakov, "Characterization of Source and Ambient Particulate Samples by Solvent Extraction," Atmospheric Aerosol Research Annual Report, 1977-78, Lawrence Berkeley Laboratory report LBL-8696, 1979, p. 63.

A MODEL FOR THE PROGRESSIVE COMBUSTION ANALYSIS OF CARBONACEOUS AEROSOL PARTICLES*

A. Hansen and T. Novakov

INTRODUCTION

The analysis of aerosol particles by progressive thermal decomposition was first reported by Malissa et al.[1] and has subsequently been developed into a powerful method for the qualitative and quantitative analysis of carbonaceous and nitrogenous aerosols.[2,3] This paper presents a model for the combustion process that may be fit to the data to yield further information on the nature of the carbonaceous species.

ACCOMPLISHMENTS DURING FY 1980

The analytical method subjects the sample to a steadily increasing temperature in an atmosphere of pure oxygen. The evolved gas is passed over an oxidizing catalyst, and the CO_2 concentration is recorded. The technique is similar to that of the flash desorption spectrometer[4] used in studies of surface bonding. Most ambient samples yield complex traces of carbon evolution versus temperature due to the presence of many different classes of compounds. However, certain samples may be chosen or selectively pretreated so that the "thermogram" shows a single set of distinct characteristics, suggesting a process of combustion at elevated temperatures. Figure 1a shows this trace for a diesel exhaust sample; when displayed as an Arrhenius plot (Fig. 1b), it is clear that the trace is characteristic of a thermally activated process, with a slope corresponding to an activation energy of 26.9 kcal/mol. Other samples may show different slopes or maxima (see Fig. 1c for aerosol collected from an oil-fired furnace). The model has been designed to interpret these traces in terms of underlying physical and chemical characteristics.

Considering the combustion of a homogeneous single component material, we write the rate of reaction of a carbon atom exposed to oxygen at time t, temperature T(t) as

$$P(T) = C \cdot T^{\alpha} \cdot \exp(-E_a/T), \qquad (1)$$

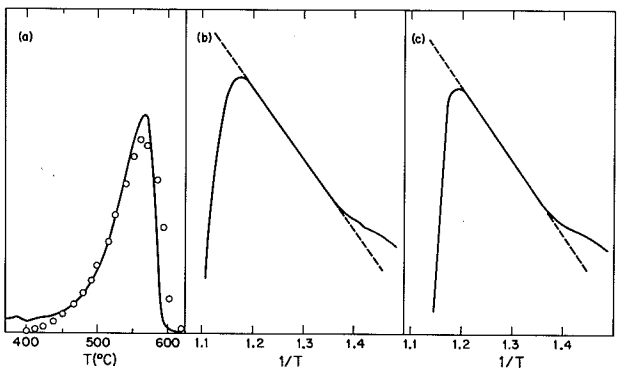

Fig. 1. Experimental data and fit: (a) Evolved CO_2 versus temperature for diesel exhaust particulate sample. Solid curve indicates experimental data; circles indicate best fit to Equation (3) with parameters E_a = 26.9 kcal/mol, rate constant C = 6.0 x 10^5 sec^{-1}, and three-dimensional combustion geometry. (b) Arrhenius plot of Figure 1(a): $\log(CO_2)$ versus inverse temperature. Dashed line slope corresponds to activation energy of 26.9 kcal/mol. (c) Arrhenius plot of data from oil-fired furnace stack sample. Dashed line slope corresponds to activation energy of 25.9 kcal/mol. (XBL 811-7672)

*This work was supported by the Assistant Secretary for Environment, Office of Health and Environmental Research, Division of Biomedical and Environmental Research of the U. S. Department of Energy under Contract No. W-7405-ENG-48 and by the National Science Foundation under Contract No. ATM 80-13707.

where E_a is the activation energy (in degrees K), C is the rate constant, and the exponent α represents the temperature dependence of the rate of collision of oxygen molecules with the carbon atom. If there are n such atoms, all equally exposed, their rate of removal from the sample is

$$-\frac{dn}{dt} = nP(T). \qquad (2)$$

Since the temperature T is a function of time t, this equation does not have a simple analytic solution, and discrete-step numerical methods must be used.

Other work has shown that the carbon species responsible for high-temperature (~500°C) thermogram traces may be in the form of graphitic microcrystallites of dimension ~30Å.[5] This could result in the exclusion from combustion of the atoms interior to the reacting surfaces or plane edges. Equation (2) is then modified to become

$$-\frac{d}{dt}(\log n) = B\, n^{\beta} P(T), \qquad (3)$$

where the constant B depends on geometry and packing fraction, and the exponent β is zero if all atoms are exposed, (-1/2) for two-dimensional combustion from the edges of graphitic planes, or (-1/3) for combustion from the outer surface of a sphere.

The presence of carbon in i different forms will produce a net yield of

$$\frac{dN}{dt} = \sum_i \frac{dn_i}{dt}$$

if the components are noninteracting. However, for the case of internally mixed particles, it is plausible that the combustion of an atom j may increase the probability of combustion of a neighboring atom i--an effect similar to ignition. This is modelled by increasing the combustion probability of the atom i by $[P_i(T + \tau_{ij}) - P_i(T)]$ for each atom of component j that burns with probability $P_j(T)$. The fraction of these is (n_j/N) and so Equation (3) becomes

$$-\frac{d}{dt}(\log n_i) = BN^{\beta}\left\{P_i(T) + \sum_j (n_j/N)[P_i(T + \tau_{ij}) - P_i(T)]\cdot P_j(T)\right\} \qquad (4)$$

The matrix elements τ_{ij} represent the coupling of combustion energy among neighboring atoms; diagonal elements represent intraspecies self-ignition.

For single component combustion, the effect of τ_{11} is to sharpen the trace (Fig. 2a); for a two-component mixture the off-diagonal elements result in a reduction of the higher temperature peak (Fig. 2b). With simplifying assumptions,

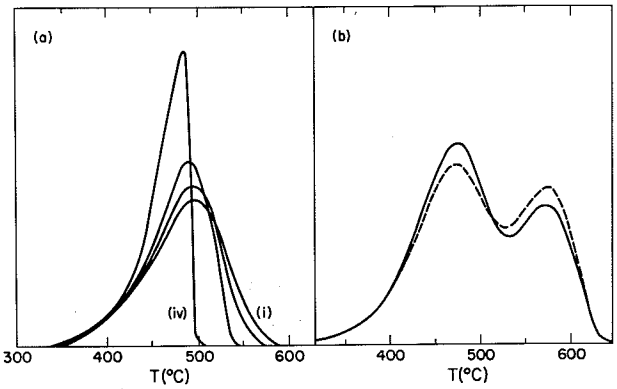

Fig. 2. Simulated curves calculated from Equation (4), illustrating intercomponent coupling. (a) Single component. Activation energy 28 kcal/mol, rate constant 2 x 10^6 sec^{-1}. Curves (i) - (iv) show the progression of coupling temperatures τ_{11} = 0, 100, 150, 200K. (b) Two components. Activation energies 27 and 31 kcal/mol, equal quantities, and equal rate constants 2 x 10^6 sec^{-1}. Dashed curve indicates no coupling. Solid curve indicates all τ_{ij} = 150K. (XBL 811-7673)

Equation (4) may be fit to experimental data to yield best values of the parameters.

In conclusion, we have shown that a progressive combustion model can account for experimental data from the analysis of carbonaceous aerosol particles and can yield reasonable parameters when fit to those data. We wish to thank Dr. R. Schefer of the Combustion Research Group (LBL) for helpful discussions.

PLANNED ACTIVITIES FOR FY 1981

Future work will be aimed at improving the fitting capability so that the full form of Equation (4) may be used to extract morphological and ignition-coupling information from experimental data.

REFERENCES

1. H. Malissa, H. Puxbaum, and E. Pell, "Zur Simultanen Relativkonduktometrischen Kohlenstoff und Schwefelbestimmung in Stäuben," Zeitschrift für Analytische Chemie, vol. 282, 1976, p. 109.

2. R. L. Dod, H. Rosen, and T. Novakov, "Optico-Thermal Analysis of the Carbonaceous Fraction of Aerosol Particles," Atmospheric Aerosol Research Annual Report, 1977-78, Lawrence Berkeley Laboratory report LBL-8696, 1978, p. 2.

3. R. L. Dod et al., "Application of Thermal Analysis to the Characterization of Nitrogenous Aerosol Species," Atmospheric Aerosol Research Report FY 1979, Lawrence Berkeley Laboratory report LBL-10735, 1980, p. 35.

4. H. D. Hagstrum, "Instrumentation and Experimental Procedure for Studies of Electron Ejection by Ions and Ionization by Electron Impact," Review of Scientific Instruments, vol. 24, 1953, p. 1122.

5. H. Rosen, A. D. A. Hansen, L. Gundel, and T. Novakov, "Identification of the Optically Absorbing Component in Urban Aerosols," Applied Optics, vol. 17, 1978, p. 3859.

RELATION BETWEEN CONCENTRATIONS OF POLYNUCLEAR AROMATIC HYDROCARBONS AND BLACK CARBON*

L. Gundel, H. Rosen, and T. Novakov

INTRODUCTION

We have developed an optical attenuation technique[1] to measure the black carbon content in particulate material. In addition to the black carbon, particulate organic carbon in ambient aerosols also contains primary organics, directly produced from combustion sources.[2] This primary organic carbon together with black carbon is defined as "soot." We have studied the relationship between the black carbon concentration and one class of primary organic compounds, polynuclear aromatic hydrocarbons (PAH) in urban carbonaceous particles. These compounds and their oxidized derivatives may constitute the health hazard associated with ambient and source carbonaceous particles.[3-5]

ACCOMPLISHMENTS DURING FY 1980

Experimental Methods

The samples used in this study were selected from loaded (47-mm diameter) quartz filters collected as part of the Lawrence Berkeley Laboratory sampling program during the summer of 1980.[6] Optical attenuation (ATN) measurements were made on Millipore cellulose acetate filters collected simultaneously. ATN is defined as equal to 100 ln I_0/I, where I_0 and I are the intensities of light transmitted through blank and loaded filters, respectively. ATN has units of optical density per 10^6 m air.

For determination of PAH concentrations on each filter sample, one section (1.94 cm^2) of the quartz filter was extracted in 0.400 ml peroxide-free spectral quality tetrahydrofuran by sonication at 25°C for 15 min.[7] A 50-µl aliquot of the extract was injected onto a liquid chromatographic column, which had been chosen for its selectivity for separation of PAH compounds[8] (VYDAC 201TP, 10-µm particle size, 25-cm length, 0.46 cm i.d.). The hydraulic system was purchased from Waters, Inc. A mixture of acetonitrile and tetrahydrofuran (19:1, v:v) in water was used as the mobile phase at a flow rate of 3.0 ml min^{-1}. Composition of the acetonitrile-tetrahydrofuran mixture varied from 70-98% in 30 min using Waters' gradient #9. The separated PAH compounds were detected with a Schoeffel Model SF970 fluorescence detector with excitation wavelength set at 280 nm. All fluorescence at wavelengths $\geq$ 389 nm was recorded as the sample eluted from the column. PAH standard compounds were supplied by Pfaltz and Bauer, Aldrich Chemical Co., and Nanogens, Inc. Peak heights were used for measurement of concentrations of PAH in the extracts of ambient particulate loaded filters.

Identification of PAH compounds from retention times of fluorescent peaks in chromatograms of ambient extracts was accomplished by comparison to retention times of PAH standards. The fluorescence ratio technique[9] was used to confirm the assignments. Identification by this technique requires that the ratios of peak intensities for several wavelength combinations of excitation, λ_{ex}, and emission, λ_{em}, match for an extract peak and a known PAH peak with the same retention time.

Results

Figure 1 shows chromatograms for a mixture of PAH compounds and for a typical filter extract. The major fluorescent compounds have been identified as benzo(b)fluoranthene, benzo(k)fluoranthene, benzo(a)pyrene, benzo(ghi)perylene, and indeno(1,2,3-cd)pyrene. Some PAH compounds which fluoresce weakly under the same conditions were not detected: chrysene, benzo(e)pyrene, perylene, and dibenz(a,h)anthracene. The PAH compounds found in this study have been detected in urban particulate matter collected in other cities and in particulate samples[11] from combustion sources.

Figure 2 shows concentrations of benzo(a)pyrene (BaP), indeno(1,2,3-cd)pyrene (IcdP), and benzo(ghi)perylene (BghiP) plotted versus optical attenuation, ATN. The lines are linear least squares fits for the data. The benzofluoranthenes, BbF and BkF, show similar trends. The concentrations of these PAHs correlated with ATN as indicated in Table 1. Degradation of these PAH compounds by processes such as photo-oxidation or

*This work was supported by the Assistant Secretary for Environment, Office of Health and Environmental Research, Division of Biomedical and Environmental Research of the U.S. Department of Energy under Contract No. W-7405-ENG-48 and by the National Science Foundation under Contract No. ATM 80-13707.

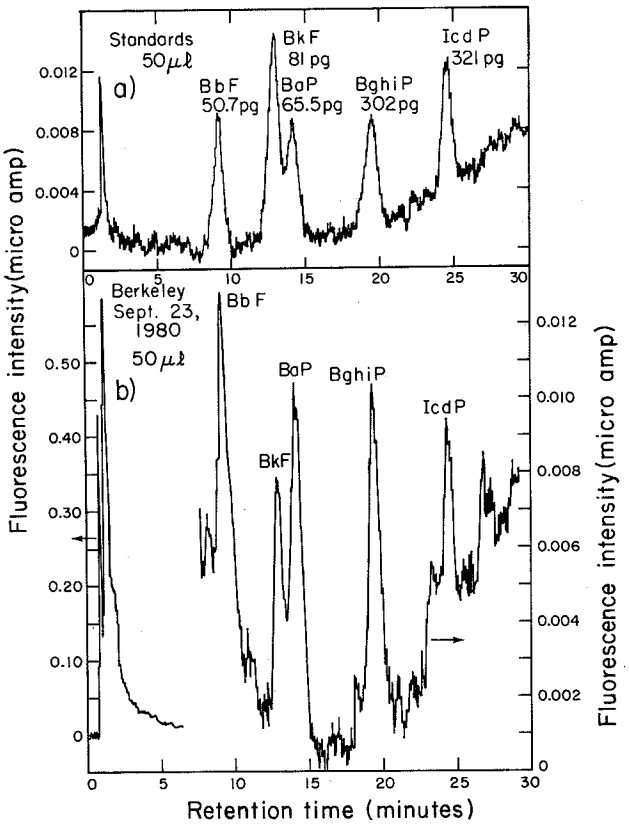

Fig. 1. Fluorescence chromatograms for (a) Mixture of PAH standard compounds. BbF = benzo(b)-fluoranthene; BkF = benzo(k)fluoranthene; BaP = benzo(a)pyrene; BghiP = benzo(ghi)perylene; IcdP = indeno(1,2,3-cd) pyrene; (b) Tetrahydrofuran extract of ambient carbonaceous particles.
(XBL 8101-42)

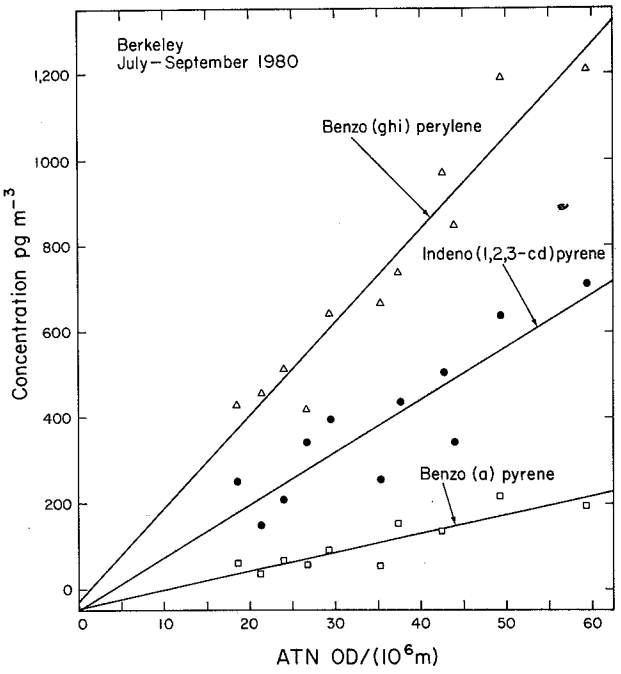

Fig. 2. The relationship between concentrations of three polynuclear aromatic hydrocarbons and optical attenuation ATN, a measure of black carbon concentration. (XBL 8101-41)

Table 1. PAH concentrations, total carbon, and attenuation data for carbonaceous particles collected in Berkeley, Calif., July-September 1980.

	Average [PAH]	[PAH] versus ATN		
	(pg m^{-3})	Slope	Intercept	r
Benzo(b)fluoranthene (BbF)	82 ± 29	1.76	20.0	0.76
Benzo(k)fluoranthene (BkF)	82 ± 28	1.66	23.0	0.76
Benzo(a)pyrene (BaP)	106 ± 65	3.82	-34.2	0.75
Benzo(ghi)perylene (BghiP)	730 ± 290	21.8	-35.1	0.96
Indeno(1,2,3-cd)pyrene (IcdP)	380 ± 180	12.3	-48.6	0.88
		[C] versus ATN		
	Average Values	Slope	Intercept	r
Total carbon (μg m^{-3})	7.3 ± 2.1	5.64	-7.30	0.93
ATN (o.d. 10^{-6} m^{-1})	35 ± 13	--	--	--

reaction with pollutant gases[12] may account for some of the scatter observed. BghiP shows the largest correlation coefficient (r - 0.96) and BaP, the smallest (r - 0.75). These values are consistent with the observation that BghiP is less susceptible to degradation than is BaP.[13] The average correlation coefficient relating [PAH] to total carbon (r = 0.78) is close to the average correlation coefficient relating [PAH] to ATN (r = 0.82).

Conclusion

The preliminary results presented here establish a linear relationship between concentration of several polynuclear aromatic hydrocarbons and optical attenuation as measured on filter samples of carbonaceous particles collected in Berkeley, Calif., during the summer of 1980. Since ATN measures the amount of black carbon, our results show that concentrations of PAH's are proportional to black carbon concentrations. Measurement of ATN may provide a fast and simple method to estimate concentrations of PAH compounds in particulate matter collected in Berkeley.

The authors thank A. Hansen for providing optical attenuation and total carbon concentration data.

PLANNED ACTIVITIES FOR FY 1981

Future work is to include measurement of PAH concentrations and ATN for carbonaceous particles collected in other cities that are part of the LBL sampling network. Concentrations of oxidized derivatives of PAH compounds will be measured to determine what relationship may exist between their concentrations and the blackness of urban carbonaceous particles.

REFERENCES

1. H. Rosen, A. D. A. Hansen, L. Gundel, and T. Novakov, "Identification of the Optically Absorbing Component in Urban Aerosols," Applied Optics, vol. 17, 1978, p. 3859.

2. D. Schuetzle, D. Cronn, A. L. Crittenden, and R. J. Charlson, "Molecular Composition of Secondary Aerosol and its Possible Origin," Environmental Science and Technology, vol. 9, 1975, p. 838.

3. Y. Y. Wang, S. M. Rappoport, R. F. Sawyer, R. E. Talcott and E. Wei, "Direct Acting Mutagens in Automobile Exhaust," Cancer Letters, vol. 5, 1978, no. 39.

4. J. N. Pitts, Jr., D. Grosjean, and T. Mischke, "Mutagenic Activity of Airborne Particulate Organic Pollutants," Toxicology Letters, vol. 1, 1977, p. 65.

5. D. Schuetzle, F. S-C. Lee, T. J. Prateer, and S. B. Tejada, "The Identification of Poly-Nuclear Aromatic Hydrocarbon Derivatives in Mutagenic Fractions of Diesel Particulate Extracts," International Journal of Environmental and Analytical Chemistry, (in press).

6. A. D. A. Hansen et al., "The Use of an Optical Attenuation Technique to Estimate the Carbonaceous Component of Urban Aerosols," Atmospheric Aerosol Research FY 1979, Lawrence Berkeley Laboratory report LBL-10735, 1980, p. 16.

7. C. Golden and E. Sawicki, "Ultrasonic Extraction of Total Particulate Aromatic Hydrocarbons (TpAh) From Airborne Particles at Room Temperature," International Journal of Environmental and Analytical Chemistry, vol. 4, 1975, p. 9.

8. K. Ogan and E. Katz, "Retention Characteristics of Several Bonded-Phase Liquid Chromatography Columns for some Polycyclic Aromatic Hydrocarbons," Journal of Chromatography, vol. 188, 1980, p. 115.

9. B. S. Das and G. H. Thomas, "Fluorescence Detection in HPLC Determinations of Polycyclic Aromatic Hydrocarbons," Analytical Chemistry, vol. 50, 1978, p. 967.

10. For a summary, see Ontario Ministry of the Environment, Polynuclear Aromatic Hydrocarbons, Air Resources Branch, ARB-TDA Report Number 57-79, 1979, p. 146.

11. J. M. Daisey, M. A. Leyko, and T. J. Kneip, "Source Identification and Allocation of Polynuclear Aromatic Hydrocarbon Compounds in the New York City Aerosol," Polynuclear Aromatic Hydrocarbons, P. W. Jones and P. Lever (Ann Arbor, Mich.: Ann Arbor Science, 1979), p. 201.

12. J. N. Pitts, Jr., K. A. Van Cauwenberghe, D. Grosjean, J. P. Schmid, D. R. Fitz, W. L. Belser, G. B. Knudson, P. M. Hynds, "Atmospheric Reactions of Polycyclic Aromatic Hydrocarbons: Facile Formation of Mutagenic Nitro Derivatives," Science, vol. 202, 1978, p. 515.

13. M. N. Iscoe, "Photochemical Changes in Thin Layer Chromatograms of Polycyclic Aromatic Hydrocarbons," Analytical Chemistry, vol. 36, 1964, p. 2505.

DETERMINATION OF CARBON IN ATMOSPHERIC AEROSOLS BY DEUTERON-INDUCED NUCLEAR REACTIONS*

M. Clemenson, T. Novakov, and S. Markowitz

INTRODUCTION

Nuclear reactions induced by 7.6-MeV deuterons are used to determine total carbon in atmospheric aerosols. The $^{12}C(d,n)^{13}N$ reaction produced the radionuclide ^{13}N, a 10.0-min positron emitter which is detected by its 0.511-MeV annihilation radiation. The detection system is a Ge(Li) γ-ray spectrometer. The method is nondestructive of the sample, permitting the sample to be studied by additional methods. Comparison of carbon found by deuteron activation analysis with that found by independent but destructive combustion methods shows a standard deviation of 10% for 15 samples analyzed over a wide range of carbon contents. The detection limit is estimated to be 0.5 $\mu g/cm^2$, corresponding to a carbon concentration of 0.2% in a sample of total thickness 250 $\mu g/cm^2$.

ACCOMPLISHMENTS DURING FY 1980

Carbon has been found to be a major elemental constituent of urban particulate pollution.[1,2] The determination of the carbon's origin in terms of primary and secondary components is a difficult problem, to which a solution is necessary if meaningful control strategies are to be implemented. Some work has been done, but much more work is required.[3-5] Of important analytical concern is the nondestructive determination of the total carbon content of atmospheric aerosol samples. The common method of carbon determination in atmospheric aerosol samples is by combustion analysis. This method, however, is destructive of the sample, and thus does not allow other analyses to be performed on the same sample. A new method for the nondestructive determination of carbon and other low-Z elements in atmospheric aerosols has been developed by Macias and coworkers.[6] Their method involves the in-beam measurement of γ rays from the inelastic scattering of 7-MeV protons accelerated in a cyclotron. This type of analysis, however, does require lengthy use of accelerator time. Another method for the nondestructive determination of carbon has been developed by Gordon and coworkers.[7] This involves the measurement of prompt γ rays following neutron capture by using an external beam port of the National Bureau of Standards (NBS) research reactor as the neutron source. Relatively large samples (~1 g), however, and long irradiation periods (~20 hr) are required. A new activation-analysis method that uses only a short amount (2 min) of beam time for the determination of carbon in atmospheric aerosols will be described here. This method has already been used to determine nitrogen in aerosols, and future work will center on the development of a method for the determination of oxygen in aerosols.[8] General principles of charged-particle activation have been given by Markowitz and Mahony.[9]

The absolute excitation function for the $^{12}C(d,n)^{13}N$ reaction is shown in Figure 1. A comparison of results from the destructive combustion method with our deuteron activation method is given in Table 1. The ratio of "activation" to combustion" carbon found averages 1.01 with a standard deviation of ±10%. A typical aerosol γ-ray spectrum is given in Figure 2. The decay of the 10-min ^{13}N activity is displayed in Figure 3.

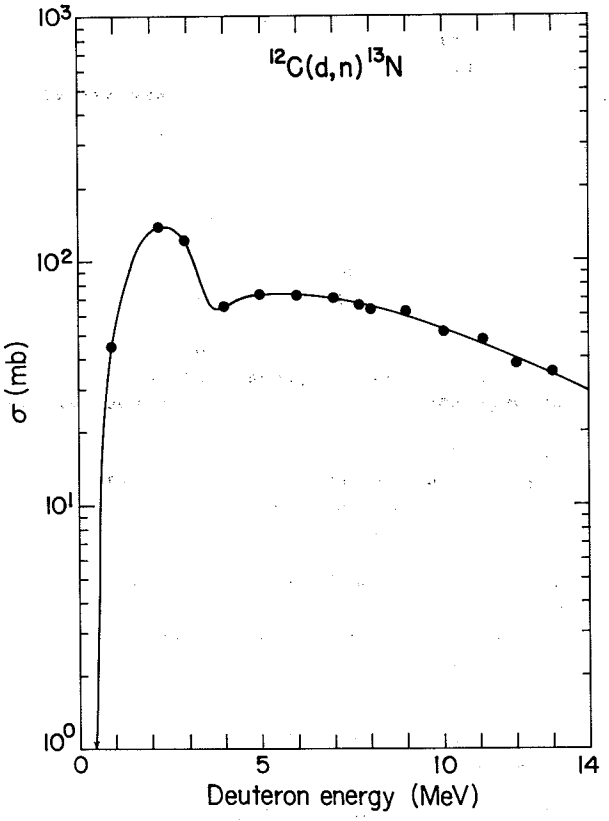

Fig. 1. Excitation function for the $^{12}C(d,n)^{13}N$ reaction. (XBL 797-2331)

*This work was supported by the Assistant Secretary for Environment, Office of Health and Environmental Research, Division of Biomedical and Environmental Research of the U.S. Department of Energy under Contract No. W-7405-ENG-48 and by the National Science Foundation under Contract No. ATM 80-13707.

Table 1. Comparison of methods for carbon determination in atmospheric aerosols.

Sample	Material	C Found ($\mu g/cm^2$) Deuteron Activation	C Found ($\mu g/cm^2$) Combustion	Ratio Activation/ Combination
AO-1	ammonium oxalate	218	210	1.04
AO-2	ammonium oxalate	268	224	1.20
AO-3	ammonium oxalate	131	122	1.07
AO-4	ammonium oxalate	74	62	1.19
AO-5	ammonium oxalate	109	113	0.96
AA-1	aerosol	84	85	0.99
AA-2	aerosol	100	99	1.01
AA-3	aerosol	106	111	0.95
AA-4	aerosol	76	76	1.00
AA-5	aerosol	103	100	1.03
AA-6	aerosol	93	93	1.00
AA-7	aerosol	5.2	4.8	1.08
AA-8	aerosol	0.6	0.7	0.86
AA-9	aerosol	57	62	0.92
AA-10	aerosol	28	32	0.88
				$\bar{R} = 1.01 \pm 0.10$

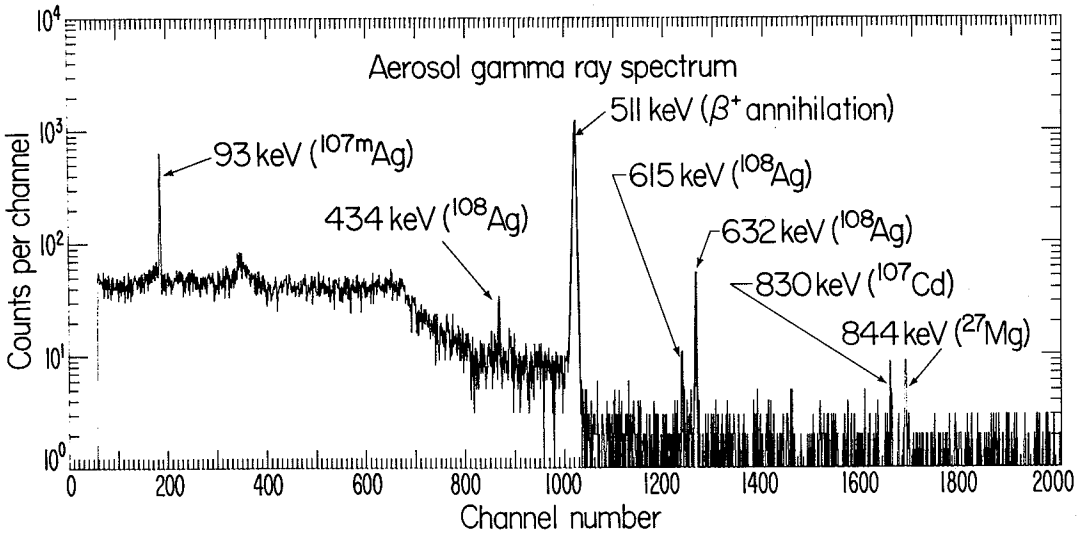

Fig. 2. The region from 0 to 1 MeV in the gamma ray spectrum of an aerosol sample following deuteron irradiation. (XBL 797-2335)

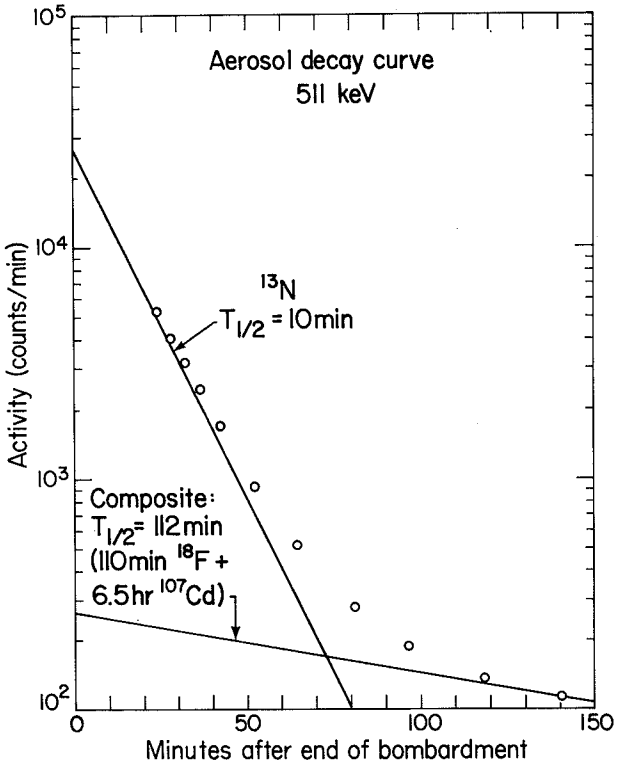

Fig. 3. Decay of the 0.511-MeV annihilation radiation activity following deuteron irradiation of an atmospheric aerosol sample. (XBL 797-2332)

PLANNED ACTIVITIES FOR FY 1981

Nuclear reaction work for the chemical analysis of atmospheric aerosols will continue.

REFERENCES

1. H. Malissa, "Some Analytical Approaches to the Chemical Characterization of Carbonaceous Particulates," Proceedings, Conference on Carbonaceous Particles in the Atmosphere, Lawrence Berkeley Laboratory report LBL-9037, 1979, p. 3.

2. Atmospheric Aerosol Research Annual Report, 1977-78, Lawrence Berkeley Laboratory report LBL-8696, 1978.

3. D. Grosjean, "Secondary Organic Aerosols and Mechanisms of Formation," Proceedings, Conference on Carbonaceous Particles in the Atmosphere, Lawrence Berkeley Laboratory report LBL-9037, 1979, p. 107.

4. R. L. Dod, H. Rosen, and T. Novakov, "Optico-Thermal Analysis of the Carbonaceous Fraction of Aerosol Particles," Atmospheric Aerosol Research Annual Report, 1977-78, Lawrence Berkeley Laboratory report LBL-8696, 1978, p. 2.

5. H. Rosen and T. Novakov, "Raman Scattering and the Characterization of Atmospheric Aerosol Particles," Nature, vol. 266, 1977, p. 708.

6. E. S. Macias, C. D. Radcliffe, C. W. Lewis, and C. R. Sawicki, "Proton Induced Gamma-Ray Analysis of Atmospheric Aerosols for Carbon, Nitrogen, and Sulfur Composition," Analytical Chemistry, vol. 50, 1978, p. 1120.

7. M. P. Failey, D. L. Anderson, W. H. Zoller, G. E. Gordon, and R. M. Lindstrom, "Neutron Capture Prompt Gamma-Ray Activation Analysis for Multielement Determination in Complex Samples," Analytical Chemistry, vol. 51, 1979, p. 2209.

8. M. Clemenson, T. Novakov, and S. S. Markowitz, "Determination of Nitrogen in Atmospheric Aerosols by Proton Activation Analysis," Analytical Chemistry, vol. 51, 1979, p. 572.

9. S. S. Markowitz and J. D. Mahony, "Activation Analysis for Oxygen and other Elements by Helium-3 Induced Nuclear Reactions," Analytical Chemistry, vol. 34, 1962, p. 329.

DETERMINATION OF LOW-Z ELEMENTS SIMULTANEOUSLY BY ^{3}HE-INDUCED NUCLEAR WASTES*

M. McKinney and S. Markowitz

INTRODUCTION

This work is a continuation of the work of Clemenson et al.[1,2] for developing rapid nondestructive techniques for determining carbon, nitrogen, and oxygen in atmospheric aerosols. X-ray fluorescence or neutron activation analysis can then be used to determine nearly all the higher Z elements. Combustion analysis could be used for these elements, but it is not sufficiently sensitive and the sample is destroyed.

Nondestructive techniques have been developed for determining these elements by Macias et al.,[3] Failey et al.,[4] and Gladney et al.;[5] these methods, however, require lengthy use of accelerator or reactor time and the latter method requires large samples. Previously Clemenson et al.[1,2] developed methods of determining carbon, nitrogen, and oxygen separately by activation analysis using different charged particles in different experiments. We want to develop a method for simultaneously determining carbon, nitrogen, and oxygen in atmospheric aerosols by irradiating the sample with a single particle.

ACCOMPLISHMENTS DURING FY 1980

The experiments are carried out using the stacked-foil technique. The standards and samples are irradiated with 20-MeV ^{3}He particles; the energy of the beam is degraded by placing aluminum foils of the desired thickness before the standard and between the standard and sample. The range-energy tables of Williamson, Boujot, and Picard[6] are used to calculate the required thickness. Mylar, a known polyester, is the standard.

The samples were irradiated for 0.5 min at 0.5 μA beam intensity; they were analyzed by detecting the 511-keV positron annihilation radiation using an Ortec Ge(Li) detector coupled to a Canberra Multichannel analyzer and printer. After 10 min, the decay curve is dominated by the $^{12}C(^3He,^4He)^{11}C$ and $^{16}O(^3He,p)^{18}F$ reaction products with half-lives of 20.4 min and 110 min respectively. By analysis of the decay curve using the CLSQ computer code,[7] we can determine the contributions to the activity from carbon and oxygen. The amounts of carbon and oxygen present were determined by the "relative" method of activation analysis. The end-of-bombardment activities of carbon and oxygen in the aerosol samples were compared with the activities from the known amounts of carbon and oxygen in the -.0005-in. Mylar standard, from which the amounts of carbon and oxygen can be calculated. A typical decay curve of the sample is shown in Figure 1.

The aerosols were collected on a silver membrane filter in parallel with a quartz filter with the use of a vacuum pump. The aerosols collected on the quartz filters were analyzed using the combustion technique. Knowing the relative flow rates through the two filters permits us to compare the amounts of carbon in atmospheric aerosols determined by these techniques (see Table 1). No other satisfactory method exists for determining these small amounts of oxygen. Untreated silver filters give a blank value of 5 μg/cm^2 of carbon. With 8-10 MeV ^{3}He particles, no other interfering reactions are observed on the silver or aluminum; and the spectrum consists only of the 511-keV annihilation radiation and its Compton background.

PLANNED ACTIVITIES FOR FY 1981

In future experiments, we propose to make use of the $^{14}N(^3He, d)^{15}O$ reaction to simultaneously analyze for the nitrogen. The ^{15}O has only a 2-min. half-life, so it will be necessary to develop rapid methods of dismantling, mounting, and counting the samples at the 88-in. cyclotron instead of in our counting room.

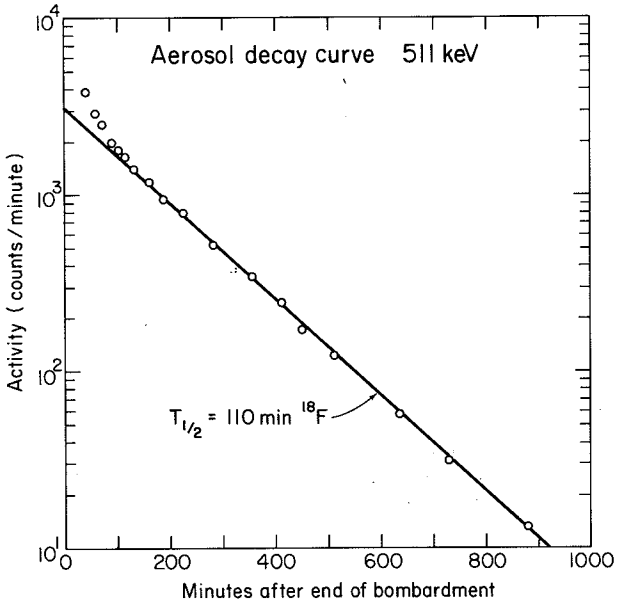

Fig. 1. Decay of the 0.511-MeV annihilation radiation following ^{3}He irradiation of an atmospheric aerosol sample. (XBL 7910-4325)

*This work was supported by the Assistant Secretary for Environment, Office of Health and Environmental Research, Division of Biomedical and Environmental Research of the U.S. Department of Energy under Contract No. W-7405-ENG-48 and by the National Science Foundation under Contract No. ATM 80-13707.

Table 1. Comparison of Carbon Analyses in Aerosols.

Aerosol	Combustion ($\mu g/cm^2$)	^3He activation ($\mu g/cm^2$)
1	30.6	27
2	12.0	14
3	40.0	39
4	50.0	54
5	56.0	40

REFERENCES

1. M. Clemenson, T. Novakov, and S. S. Markowitz, "Determination of Nitrogen in Atmospheric Aerosols by Proton Activation Analysis," Analytical Chemistry, vol. 51, 1979, p. 572.

2. M. Clemenson, T. Novakov, and S. S. Markowitz, "Determination of Carbon in Atmospheric Aerosols by Deuteron Activation Analysis," Analytical Chemistry, vol. 52, 1980, p. 1758.

3. E. S. Macias, C. D. Radcliffe, C. W. Lewis, and G. R. Sawicki, "Proton Induced γ-ray Analysis of Atmospheric Aerosols for Carbon, Nitrogen, and Sulfur Composition," Analytical Chemistry, vol. 50, 1978, p. 1120.

4. M. P. Failey, D. L. Anderson, W. H. Zoller, G. E. Gordon, and R. M. Lindstrom, "Neutron Capture Prompt γ-ray Activation Analysis for Multielement Determination in Complex Samples," Analytical Chemistry, vol. 51, 1979, p. 2209.

5. E. S. Gladney, D. B. Curtis, and E. Jurney, "Simultaneous Determination of Nitrogen, Carbon, and Hydrogen by Thermal Neutron Prompt γ-ray Spectrometry," Analytical Chimica Acta, vol. 110, 1979, p. 339.

6. L. F. Williamson, J. P. Boujot, and J. Picard, "Tables of Range and Stopping Power of Chemical Elements for Changed Particles," J. Centre d'Etudes Nucleaires de Saclay Rapport CEA-R 3042, Paris, Documentation Francaise 1966.

7. J. B. Cumming, Applications of Computers to Nuclear and Radiochemistry, N.A.S.-N.R.C. Pub. NAS-NS 3107, 1963.

MEMBRANE OXIDATIVE DAMAGE*

L. Packer, A. Quintanilha, R. Mehlhorn, O. Augusto, J. Maguire, and K. Davies

INTRODUCTION

Our studies have focused on the effects of environmental factors and pollution on mammalian cellular membranes. Our previous report[1-3] showed how sensitive to oxygen are isolated mitochondria, whole cells (hepatocytes and bacteria), model membranes, and enzymes.

Our working hypothesis has been that reactive species of oxygen, sometimes generated by endogenous cellular photosensitizers (flavins and hemes) in the presence of visible light, would react with cellular components thereby altering their structure and function. We have extended our work to studies of microsomal enzymes, particularly the very important drug metabolizing components NADPH-cytochrome-P_{450}-reductase and cytochrome P_{450}. The differential photosensitivity of the microsomal enzymes and the anaerobic component of the photoinactivation of NADPH reductase have enabled us to clarify different mechanisms of photodamage.

The use of a variety of different spin probes and their photomediated reduction and/or destruction has been a powerful tool in implicating free-radical intermediates in the mechanisms of photooxidative damage to biological membranes.

Free iron has been evaluated for its prooxidant effects; even at very low concentrations (μM), we have found that it will promote the auto-oxidation of epinephrine (a neural transmitter) and the formation of hydroxyl radicals (OH•) via the Fenton reaction.[2]

ACCOMPLISHMENTS DURING FY 1980

Microsomal Studies

We have been particularly interested in the mechanisms of initiation and of cellular damage by visible light ($\lambda > 400$ nm) through endogenous chromophores, in particular flavin coenzymes,[4-6] and the propagation of this damage by oxygen radicals.

The electron transport system in microsomes plays a vital role in xenobiotic metabolism, fatty acid desaturation and carcinogenesis, and contains both heme and flavin chromophores. The effect of visible light on microsomal electron transport components is shown[7] in Figure 1. There is a preferential inactivation of the NADPH-cytochrome-P_{450}-reductase and cytochrome P_{450}. In addition to protein inactivation, visible light also induces lipid peroxidation. Externally added flavin (FMN) increases both cytochrome P_{450} inactivation and lipid peroxidation. It is interesting that the reductase inactivation is not strictly oxygen-dependent since, to fully protect the enzyme, both anaerobiosis and a photoreductant, ethylene diamine tetra-acetic acid (EDTA) are required. The NADPH-reductase contains the photosensitive flavin cofactors, FMN and FAD. Following inactivation under anaerobic conditions, we have found that the NADPH-reductase can be largely reactivated by addition of FMN (but not FAD) suggesting that inactivation may be due to photomediated loss of FMN.

On the other hand, cytochrome P_{450} destruction appears to depend only on lipid peroxidation: Both processes are oxygen dependent, and are inhibited approximately to the same extent by antioxidants and radical scavengers. After FMN is lost and the NADPH-reductase is inactivated during anaerobic photosensitization, and the preparation

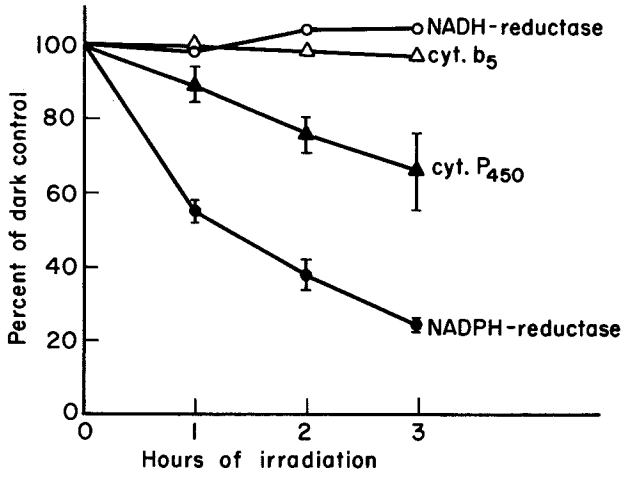

Fig. 1. Effect of visible light on microsomal electron transport activities. Data points are the average of results obtained with microsomes from two different rats; for clarity, the deviations are not shown for cytochrome b_5 and NADH-cytochrome b_5 reductase. Initial activities for the two preparations were: NADPH-cytochrome P_{450} reductase 100 and 96 nmol/min/mg; NADH-cytochrome b_5 reductase 1.7 and 3.0 μmol/min/mg, cytochrome P_{450} 0.8 and 0.7 nmol/min/mg;cytochrome b_5 0.5 and 0.4 nmol/mg. (XBL 806-3442)

*This work was supported by the Assistant Secretary for Environment, Office of Health and Environmental Research, Division of Life Sciences of the U.S. Department of Energy under Contract No. W-7405-ENG-48.

is further illuminated in the presence of air, we found that the extent of lipid peroxidation and cytochrome P_{450} destruction is a function of the NADPH-reductase activity left in the preparation. This suggests that lipid peroxidation and cytochrome P_{450} destruction are induced by the light excited flavin (FMN?) of the NADPH-reductase.

The greater photochemical reactivity of FMN as compared to FAD[8] could explain both the preferential inactivation of NADPH-reductase (NADH-reductase contains only FAD) as well as the selective destruction of FMN during illumination. Since it is known that cytochrome P_{450} reacts and is destroyed by hydroperoxides, whereas cytochrome b_5 is unaffected,[9] this may explain the differential inactivation of the microsomal cytochromes by visible light/0_2.

Photosensitized Nitroxide Spin Loss

Changes in the electron spin resonance (ESR) signal of nitroxide-free radicals were used to monitor very rapid light-induced free-radical reactions in inner mitochondrial membrane preparations.[10] After preincubation in the dark at 37°C for 2 h, illumination (at λ > 400 nm) of membranes in the presence of nitroxide probes (Fig. 2) showed that (a) oxidized probes are reduced and destroyed, and (b) reduced probes are oxidized and destroyed. The action spectrum of spin loss was shown to be similar to the absorption spectrum of FMN and was stimulated by the addition of exogenous flavin. However, in an aerobic model system containing buffer, FMN and oxidized nitroxide illumination has no effect on the ESR signal of the probe, whereas the reduced nitroxide is rapidly oxidized. Centrifugation experiments showed that flavines were released from the membrane during incubation

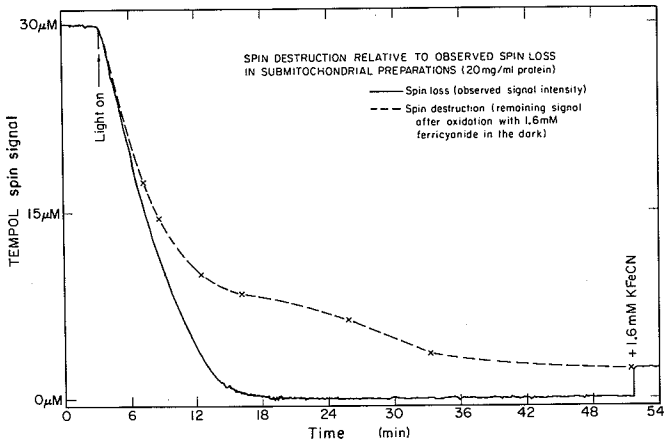

Fig. 2. Light dependent destruction, reduction and oxidation of TEMPOL and TOLH. 2 ml of SMP's were illuminated in 25 ml flasks in air and aliquots were withdrawn at the indicated times and examined either directly by ESR (spin loss) or after 2 min. of treatment with 1.6 mM of potassium ferricyanide (spin destruction). Buffer: 30 mM potassium phosphate, pH 7.4. Light intensity: 41 mW/cm^2. SMP's were preincubated in the dark at 37° C for 2 h.
(XBL 773-3219)

and that the light-induced free radicals were generated in the aqueous environment of the membranes.

An interesting finding was that in the presence of 10 μM exogenous FMN, light causes the mitochondrial membrane to consume oxygen, suggesting the production of lipid peroxides. Positively charged spin probes exhibit considerably smaller light-induced spin-loss rates than either uncharged or negatively charged probes. An amphiphilic positively charged spin probe (CAT_{10}) was used to demonstrate that there is an irreversible rapid increase in negative surface charge[11] of the membranes during illumination.

Our experiments with exogenous flavins show the existence of a dark activation phenomenon other than flavin release. A "factor" is released from the membranes which may serve as the primary cofactor for spin destruction. The identification of this "factor", which is obviously important in free radical production and membrane damage, is presently under study.

Pro-oxidant Effects of Iron

Hydroxyl radical (OH•) production via the Fenton reaction[2] and epinephrine auto-oxidation can be propagated by catalytic amounts of iron. The role of iron in *in vivo* oxidative damage is of great relevance in many hydroxyl-radical investigations. In human iron toxicity studies, marked intracellular increases in the accumulation of hemosiderin and a lipofuscin-like pigment were observed[12], indicating an increase in the complex processes of damage that occur in the cell.

We have followed the rate of OH• generation via the Fenton reaction using bound iron as a catalyst.[13] The radical was trapped by 5,5' dimethyl-1-pyrroline-N-oxide (DMPO). Figure 3 shows that 10 μM Fe added as Fe^{+3}-EDTA gave rise to a substantial DMPO•OH signal. Even at 0.5 μM, iron was still effective. Ferritin (the chief form of storage of iron *in vivo*), even at a concentration equivalent to 100 μM, Fe did not give any signal; Transferrin (which serves as the main avenue of iron transport in the serum), with a bound iron concentration of 50 μM, also did not give any detectable signal. These results suggest that neither Ferritin nor Transferrin are able to propagate the Fenton reaction.

Epinephrine auto-oxidizes to adrenochrome rapidly at pH 10. Trace amounts of Fe^{+3}-EDTA were found to substantially increase the rate of auto-oxidation. However, neither Ferritin nor Transferrin had any effect on these rates. These results suggest that there are great differences in the catalytic capacity of iron when it is physiologically bound to proteins as compared to when it is chelated to EDTA (or DTPA, diethylene triamine penta-acetic acid).

PLANNED ACTIVITIES FOR FY 1981

Airborne pollutants generated by energy-related technologies pose a risk to human health. During exercise, pulmonary ventilation in animals and man increases exponentially in response to workload,

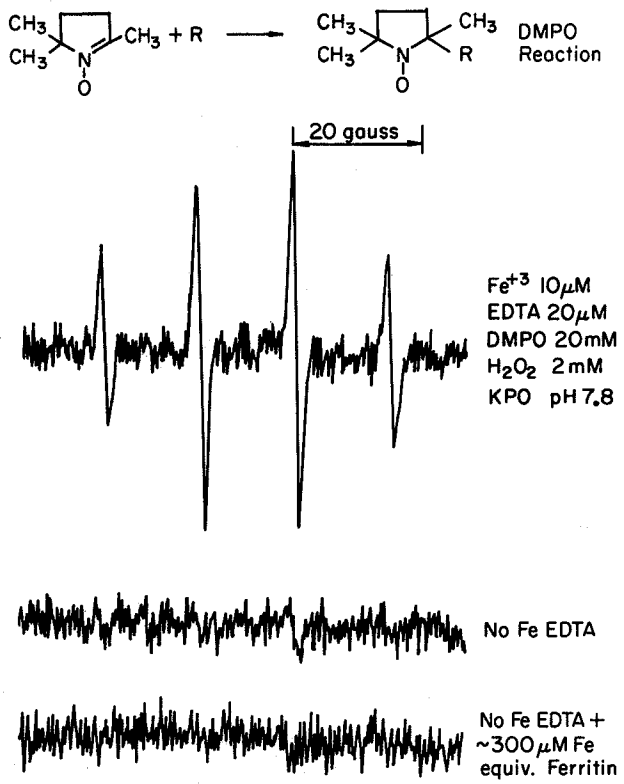

Fig. 3. Comparison of DMPO-OH signals by the reaction of differently bound forms of Fe and H_2O_2. (XBL 811-3586)

and the upper respiratory tract becomes less effective in removing pollutants.

In vivo tests will be made to measure the metabolic responses to exercise in man and small animals; the results will be correlated with biochemical and biophysical studies of whole organs, cells and subcellular parameters of animals. In vitro studies of lipid peroxidation will be correlated with in vivo activity through respiratory pentane production at rest and during exercise. The effects of different dietary levels of the anti-oxidant vitamin E will be investigated. Calorimetric systems will be used to monitor the effects of high ambient oxygen, argon, carbon monoxide, SO_2 and NO_x concentrations (and mixtures) on work capacity, endurance, oxygen consumption, and pentane production. Acute and chronic effects of exposure to these gases will be evaluated.

Our approach will lead to investigations of both basic research and applied research questions at the whole-animal level. Selected results will be verified with human subjects using noninvasive techniques. These studies will have special significance in the areas of membrane bioenergetics, exercise biochemistry, muscle and respiratory physiology, and environmental medicine.

REFERENCES

1. L. Packer, R. J. Mehlhorn, A. T. Quintanilha, B. Aggarwal, and J. J. Maguire, "Visible Light and Ozone Damage to Mammalian Membranes," Energy & Environment Division Annual Report 1977, Lawrence Berkeley Laboratory report LBL-6877, 1977, pp. 142-146.

2. L. Packer, A. T. Quintanilha, R. J. Mehlhorn, E. W. Kellogg, III, and J. J. Maguire, "Visible Light and Ozone Damage to Mammalian Cells and Membranes," Energy & Environment Division Annual Report 1978, Lawrence Berkeley Laboratory report LBL-8619, 1978, pp. 166-170.

3. L. Packer, A. Quintanilha, E. Kellogg, III, R. J. Mehlhorn, M. Nova, L. Cheng, and J. Maguire, "Membrane Oxidative Damage," Lawrence Berkeley Laboratory report LBL-11650, Energy and Environment Division Annual Report 1979, October 1980, pp. 7-5-7-7.

4. B. B. Aggarwal, A. T. Quintanilha, R. Cammack and L. Packer, "Damage to Mitochondrial Electron Transport and Energy Coupling by Visible Light", Biochimica et Biophysica Acta, vol. 502, no. 367, 1978.

5. L. Y. L. Cheng and L. Packer, "Photodamage to Hepatocytes by Visible Light" FEBS Letters, vol. 97, 1979, pp. 124-128.

6. L. Packer and E. W. Kellogg III, "Photooxidative Damage to Mammalian Cells and Proteins by Visible Light" American Chemical Society Symposium, vol. 123, 1980, pp. 83-93.

7. O. Augusto and L. Packer, "Photodamage to Microsomal Electron Transport Systems by Visible Light" (submitted to Photochemical Photobiology).

8. D. B. McCormick, "Interactions of Flavins with Amino Acid Residues: Assessments from Spectral and Photochemical Studies," Photochemical Photobiology, vol. 26, 1979, pp. 169-182.

9. E. G. Hrycay and P. J. O'Brien, "The Peroxidase Nature of Cytochrome P-420 Utilizing a Lipid Peroxide Substrate" Archives of Biochemistry and Biophysics, vol. 147, 1971, pp. 28-35.

10. R. J. Mehlhorn and L. Packer, "Photosensitized Nitroxide Spin Loss by Released Flavins in Mitochondrial Membranes" (in preparation).

11. R. J. Mehlhorn and L. Packer, "Membrane Surface Potential Measurements with Amphiphilic Spin Labels," Methods in Enzymology, vol. LVI, 1979, pp. 515-526.

12. T. H. Bothwell and C. A. Finch, eds., Chapter 9, Iron Metabolism, (Boston, Mass.: Little Brown and Co., 1962).

13. J. J. Maguire, E. W. Kellogg III, and L. Packer, "Evaluation of Pro-Oxidant Effects of Bound Iron" (in preparation).

LAKE ECOTOXICOLOGY RESEARCH

INTRODUCTION

J. Harte

The primary goal of the lake ecotoxicology projects is to develop and apply experimental methods for understanding and predicting effects of toxic substances on lake ecosystems. Both field and laboratory investigations comprise the research. Field studies focus mainly on mechanisms of acid precipitation damage in lakes on the western slopes of the California Sierra Nevada and the high Colorado Rockies. Laboratory work is focused on developing, validating, and applying innovative ecosystem-effects test systems. These test systems, involving laboratory ecosystems called "microcosms," are designed to allow more rapid, cheap, and statistically reliable prediction than field tests permit and to allow testing of more complex ecosystem-level effects than is possible with the single-species laboratory bioassays traditionally used.

The laboratory and field studies are tightly coupled in two ways. First, comparisons of the chemical and biological behavior of real lakes with microcosms allow us to assess the realism of microcosms, an essential step if these test systems are to provide an experimental basis for regulatory activity. Second, by adding simulated acid rain to lake microcosms, we are able to learn more about mechanisms of acid rain damage to natural lakes than could be learned from field investigations alone.

Theoretical modeling and policy analysis are a secondary, but not unimportant component of these projects. Mathematical models of the phenomena observed in the microcosms assist in the planning of experiments and in the extraction of useful damage indices from the raw data obtained from microcosm perturbation experiments. A nontraditional approach to statistical analysis of the often rapidly-time-varying biological parameters in microcosms and lakes has been developed by us and is now in use to provide measures of the realism and replicability of microcosms. Finally, policy implications of our work--particularly the freshwater constraints on energy development in the western United States--are addressed by us in publications and conference presentations.

ASSESSMENT OF OPTIMUM MICROCOSM DESIGN FOR POLLUTION IMPACT STUDIES*

J. Harte, D. Levy, J. Rees, and E. Saegebarth

INTRODUCTION

Laboratory microcosms may play an important role as experimental tools for examining ecological impacts resulting from human activities. The major advantage of microcosm studies over field research is that the former allow a greater opportunity for manipulation and control. In addition, the expense and environmental risk from microcosm investigations are relatively small compared to the risk from field studies of toxic substance effects. Microcosms also potentially offer greater realism than that provided by studies of impacts on single species.[1,2] Studies carried out with freshwater lake microcosms during a four-year period in our laboratory have been directed mainly toward developing and evaluating microcosms as toxicological testing systems.

Microcosms can be a useful tool for impact evaluation only to the extent that: (1) identically initiated systems replicate well, (2) the systems' biological and chemical behaviors, under both undisturbed and disturbed (with toxicant present) conditions, are similar to that of natural systems, (3) the attainment of (1) and (2) does not result in excessive complexity or cost. The degree to which the inherent drawbacks of microcosms reduce their usefulness, in the above sense, will depend on the manner in which microcosms are used. The specific objective of our research has been to investigate some of the major options for freshwater lake microcosm design and operation, emphasizing the ways in which the choices among these options influence the system's usefulness.

ACCOMPLISHMENTS DURING FY 1980

The major activity in FY 1980 was the completion of a two-year study of the realism and replicability of freshwater lake microcosms.[3] Only the upper pelagic zones (or water columns) of the lakes were modeled in these experiments--no sediments were included in the microcosms. Two local lakes (Briones and Lafayette Reservoirs)

*This work was supported by the Department of Energy under Contract W-7405-ENG-48 through the Energy Analysis and Environment Division of the Electric Power Research Institute under Contract No. RP 1224-1.

were used in this study. In three separate tests, replicate microcosms were initiated with water from these lakes, and the subsequent behavior of the lakes and microcosms was compared over three-month periods.

A number of different microcosm configurations were studied. The size of the microcosm containers (4 ℓ - 200 ℓ); the method of algal surface-growth prevention; and the degree of water mixing and aeration were the most important design and operating parameters explored. In addition, the microcosm-lake comparisons (or "tracking" studies) were carried out at various seasons, allowing us to determine the influence of natural seasonal factors, such as the washing of watershed nutrients into the lakes by winter rain, on the chemical and biological differences between the lakes and the microcosms.

Our most important findings were:

1. In microcosms greater than 15 l in volume, chemical and biological behavior is quite independent of microcosm volume if surface growth of algae on the inner walls of the microcosm containers is prevented by pouring the tank contents into a clean container at weekly intervals.

2. The amount of water agitation can influence the chemical and biological behavior of the microcosms; the optimum level of water mixing needs to be determined.

3. The week-by-week concentrations of chemical nutrients replicated well in all but the smallest microcosms and tracked (mimicked) the lake adequately except during periods when nutrient inputs to the lake from the surrounding watershed were high.

4. The patterns of phytoplankton succession in the microcosms adequately tracked those in the lake for up to 2 mo (a period adequate for many ecotoxicological tests) only when the physical conditions of the lake matched well those in the laboratory microcosm. Specifically, these lake conditions were: little runoff from the surrounding watershed, little water temperatures difference between lake and microcosms, and a well-defined, isolated epilimnion (upper part of the water column during the period when the lake water is thermally stratified).

During the late fall and winter in California, when the conditions listed in item 4 do not hold, diatom populations in the microcosms crashed within a month after initiation of the microcosms, while the diatom populations in the lake either bloomed or remained roughly constant. The lake behavior was probably due to replenishment in the upper water column of silica, an important limiting factor in diatom growth. Other factors that may have caused a discrepancy between the diatom populations in the lakes and in the microcosms were differences in water temperatures and zooplankton population densities. At the time of these experiments, our laboratory facility was incapable of bringing the microcosm water temperature down to winter-time levels. A new, improved microcosm cooling system now in operation permits matching in the laboratory of winter-time temperatures in the lakes. Figures 1 and 2 illustrate examples of excellent and poor tracking of lake diatom populations by the microcosms.

In order to compare the behavior of microcosms and lakes, appropriate statistical measures of "tracking" were needed. To illustrate the problem, consider a typical case in which three microcosms are set up in replicate using lake water. During the several months after initiation, weekly measurements of chemical and biological parameters in the lake and the microcosms are made. A suitable measure of tracking would involve a comparison between the replicate systems and the lake. One possible, and often used, procedure would be to average the microcosms over the three replicates and compare the average with the lake. Such a comparison could be made week-by-week or over time-averaged measurements. Because of measurements errors, and because of differences between

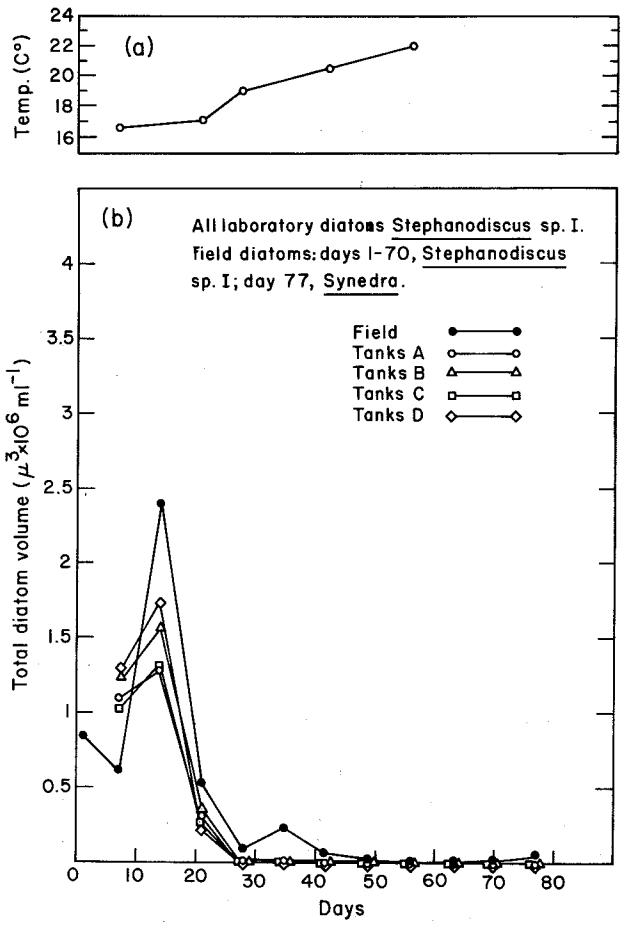

Fig. 1. Experiment 3. (a) Field temperature and (b) diatom populations for field and laboratory microcosms. Diatoms in both field and laboratory are all Stephanodiscus. Each point of the field data represents the mean of two samples. Each point of laboratory data represents the mean of three triplicate laboratory microcosms. (XBL 8012-2570)

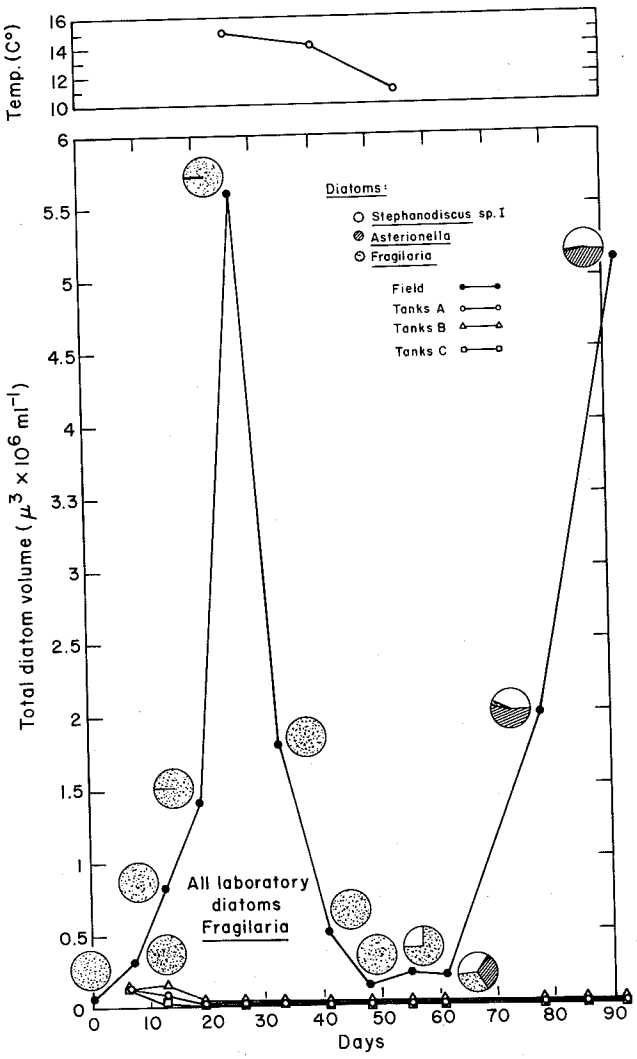

Fig. 2. (a) Field temperature and (b) diatom populations for field and laboratory microcosms. Each point of laboratory data represents the mean of three triplicate laboratory microcosms. All laboratory diatoms are Stephanodiscus. The circles above each field data point represent relative abundances of the designated diatom species. (XBL 8012-2573)

the replicate systems, there are standard deviations associated with each system's parameters. The difference between the lake and the averaged microcosms would have to be compared with microcosm and lake standard deviations in order to judge the statistical significance of the results.

In previous applications of this procedure, it had been assumed that each of the replicate microcosms are in fact the same system, with the same true mean values of each parameter. Differences among them are ascribed, in effect, to measurement error only. If that assumption is not made, and instead each of the three replicate system's true mean is taken to be its measured mean, then statistical significance tests can give quite different results. This is particularly true if, as is the case with most of our chemical and biological measurements, the measurement errors are strongly dependent on the mean values of the parameters. The result of our assumption is that the significance test for tracking is more stringent. That is, a situation that would have been deemed good tracking with the previous assumption might be considered poor tracking with ours. The previous procedure has been in widespread use, in many contexts in biology, because it is simpler to carry out. Nevertheless, our revised procedure is more appropriate to the conditions of the experiments.[4]

Our experimental results over the past two years have demonstrated that lake microcosms are inappropriate for certain types of toxicological testing. In particular, long-term tests, extending beyond several months, cannot be carried out because lake microcosms do not function similarly to natural lakes for such extended periods. Moreover, experiments involving macrofauna, such as fish, cannot be carried out in laboratory-sized systems (up to 1000 liters) without distorting the behavior of the system by the presence of the macrofauna. A type of test that is particularly appropriate to microcosms is a determination of the effects of a toxic substance on the rate of decomposition of organic matter and the related production rate of inorganic nutrients. Such nutrient cycling processes in lakes generally take place by the microorganisms' action on detritus. Because of the great importance of these processes to ecosystems' overall health and productivity; because the microorganisms and their chemical environment can be represented realistically in microcosms; and because nutrient regeneration processes take place relatively rapidly on the time scale of lake dynamics, we have begun exploring a possible microcosm test protocol for determining effects of toxicants on nutrient recyling rates in lakes.

Work carried out in FY 1979 demonstrated that additions of lake detritus to lake microcosms, followed by measurements of the nitrogen budget on a daily basis for a week or two provided considerable information about the population biology of the microorganisms responsible for the decomposition and nutrient regeneration activity.[5] This year, attention was focused on constructing a mathematical model of the microorganism-detritus-nutrient system to yield results consistent with the wealth of experimental information available from the detritus-addition studies. The goal of this modeling effort is to learn how to extract from the detritus-addition experiments useful indices characterizing the health of the nutrient cycling function in the system. This will allow development of a test procedure, involving simultaneous additions to lake microcosms of detritus and toxic substances, for determining the damage to the nutrient cycling function caused by the toxicant.

The results to date have been encouraging. A relatively simple mathematical model has been constructed that is capable of fitting the complex behavior seen in the experiments.[6] Moreover, a wide class of models based on assumptions that are plausible but different than ones reflected in the successful model, have been shown to be inadequate. With this model, we are now able to extract from the experimental results the needed damage indices.

Two experimental advances in lake decomposition research took place in FY 1980. In order to perform the detritus-addition experiments, large amounts of concentrated dissolved lake-water organic matter need to be obtained. Off-the-shelf organic chemicals are inadequate for the purpose as they lack the biochemical diversity characteristic of real lake detritus. After pursuing a number of dead ends, we found a suitable approach based on successive freeze concentrations of lake water.[7]

The second advance was a method of "fingerprinting" lake organic matter. Adapting an approach developed by the Atmospheric Aerosol Research group, we took a number of carbon and nitrogen thermographs of water samples from local lakes and from pure algal cultures. Information obtained from thermography is intermediate in complexity between simple total C and N analysis and a complete gas chromatography analysis of organic constituents. Our preliminary studies (using only about a dozen tests to date) suggest that thermography may provide a characteristic fingerprint that differs from one type of alga to another and that varies with the amount of decomposition of an algal sample. A more intensive effort to develop this technique for ecological materials is warranted.

In FY 1980, heightened national concern over effects of toxic substances in the environment led the National Academy of Sciences to convene an 11-member Panel on Ecotoxicology; J. Harte was appointed as one of the members. Its task was to make recommendations to the Environmental Protection Agency (EPA) on how best to implement the ecologically relevant sections of the Federal Toxic Substance Control Act. A major part of the year-long effort was devoted to evaluating the role of microcosms as test systems for toxicant pathways, fate, and effects studies. The panel's final report is in preparation.[8] Three reports written by members of the LBL lake ecotoxicology group will also appear as appendices to the report.[9,10,11] In conjunction with this National Academy effort, Oak Ridge National Laboratory (ORNL) conducted a review of prior work in the area of microcosms; D. Levy assisted in that review process.

Expected Progress in FY 1981

The major focus of research in FY 1981 will be on extensions of aquatic microcosms to include lake sediments. Our lake microcosms to date have been models of the pelagic zone, or water column, of lakes. Because of the importance of lake sediments as a source of nutrients to the pelagic zone at certain times of year, as a sink of pollutants, and as a site in which pollutants can be transformed or can enter the aquatic food chain via benthic organisms, it is vital to have the capability of modeling the sediment zone as well as the overlying water. Doing so is not a trivial task. Microcosms are considerably shallower than real lakes, and therefore if sediments are simply placed along the bottom of a microcosm they will exert an exaggerated influence on the overlying water. The approach we will follow is similar to one that has been shown to work for marine estuarine microcosms at EPA's Naragansett Bay laboratory in Rhode Island.[12] The basic idea is to place the sediments in small chambers, with portals carefully adjusted to provide a level of flushing that will allow oxygen levels in the microcosm sediments to match those in the lake sediments.

During FY 1981, experimental studies of benthic lake microcosms will begin. Two types of microcosms will be studied. In one, water and sediments from a shallow cove in Briones Reservoir will be placed in microcosms. In the second, a deep-water site will be chosen and sediments plus water from the hypolimnion (the stratified layer of lake water overlying the sediment) will be placed in microcosms. The replicability of these systems and the degree to which they can be designed and operated to track the lake will be investigated.

Of particular interest in these studies will be the degree to which the chemical composition of the water within and immediately overlying the sediments is the same in the microcosms and the lake. If benthic microcosms are to be of use in ecotoxicology, it is essential that oxygen levels in the chemically active benthic zone match well those in natural systems. For this reason, we will design benthic chambers to house the sediments in such a manner as to allow adjustments of the oxygen levels. This will be accomplished by means of the portals mentioned. A related variable to be adjusted so as to maximize the microcosms' realism is the degree of water-mixing in the microcosms. Our past work has shown that this variable can influence biological behavior in the microcosms;[3] in FY 1981, research to determine an optimum level of water mixing will commence. Optimality will again be determined by the twin criteria of realism and replicability.

Among the variables of interest in these planned benthic studies is the diatom population. Because sediments are a source of silica, we hypothesize that the diatom populations will behave more realistically in the benthic systems than in our pelagic microcosms tested previously.

In these tracking studies, Briones Reservoir will again be the source of microcosm water and the system against which microcosms will be compared to assess their realism. Research to characterize the chemical and biological parameters of Briones will continue in FY 1981. The major focus will be to determine the degree of spatial (horizontal and vertical) and temporal (diurnal and seasonal) variation in chemical concentrations and species composition. This information is needed in order to design a lake-monitoring schedule that will minimize expended effort and yet will be sufficiently thorough so as to provide an accurate characterization of the significant ecological processes in the lake. Moreover, this information will assist in selecting the best method for initiating the microcosms--for example, choosing between stocking the microcosms with a depth-integrated sample from a particular stratified layer or working with water from only one depth.

In FY 1981, further study of detrital thermographs will be undertaken. The major effort here will be to determine the degree to which different lakes, and the same lake at different times of the year, yield characteristically different thermographs of their dissolved and suspended detrital matter. In related work, using our freeze-concentration method for preparing detritus, additional decomposition experiments will be carried out. Our recently-developed mathematical model, while consistent with the previously-measured phenomena, makes several detailed predictions, which we will test in FY 1981.

REFERENCES

1. M. Dudzik, J. Harte, A. Jassby, E. Lapan, D. Levy, and J. Rees, "Some Considerations in the Design and Aquatic Microcosms for Plankton Studies." International Journal of Environmental Studies, vol. 13, 1979, pp. 125-130.

2. J. Harte, D. Levy, J. Rees, and E. Saegebarth, "Making Microcosms an Effective Assessment Tool," Microcosms in Ecological Research, J. P. Giesy, ed. (in Press).

3. J. Harte, D. Levy, J. Rees, and E. Saegebarth, "Assessment of Optimum Aquatic Microcosms Design for Pollution Impact Studies," a report to the Electric Power Research Institute (Palo Alto, Calif: Electric Power Research Institute, 1980).

4. D. Levy, "Appropriate Statistical Methods for Ecological Microcosm Investigations" (in preparation).

5. J. Harte and D. Levy, "Investigation of the Responses of Lake Waters to Detritus Additions," Energy and Environment Division, Lawrence Berkeley Laboratory, Berkeley, Calif., 1979 (to be submitted for publication).

6. J. Harte, "Modeling the Response of Lake Water to Organic-Matter Loading" (in preparation).

7. R. Schneider, "A Method for Concentrating Freshwater Lake Detritus for Microcosm Research," Energy and Resources Group Research Report, University of California, Berkeley (in preparation).

8. J. Cairns, M. Alexander, K. Cummins, W. T. Edmondson, C. Goldman, J. Harte, R. Hartung, A. Isensee, R. Levins, J. F. McCormick, T. Peterle, J. Zar, Testing Effects of Chemicals on Ecosystems. A Report by the Committee to Review Methods in Ecotoxicology, National Academy of Sciences - National Research Council, Commission on Natural Resources, Washington, D. C., 1980.

9. P. Gleick, "Lakes and Microcosms: Extending Microcosm Data to Aquatic Ecosystems," (to appear as an appendix to reference 8).

10. R. Schneider, "Classes of Ecotoxicological Tests: Their Advantages and Disadvantages for Regulation," (to appear as an appendix to reference 8).

11. J. Harte, "Optimum Microcosms for Lake Ecotoxicology," (to appear as an appendix to reference 8).

12. K. T. Perez et al., "The Importance of Physical and Biotic Scaling in Experimental Simulation of a Coastal Marine Ecosystem." Helgolander wiss Meeresuuters, 30, 1977, pp. 144-162.

ACID PRECIPITATION DAMAGE TO AQUATIC ECOSYSTEMS*

J. Harte, K. Tonnessen, R. Schneider, G. Lockett, and J. Oldfather

INTRODUCTION

Present evidence suggests that high-elevation aquatic ecosystems are particularly vulnerable to human disruption. In the Eastern United States, acidic rain and snowmelt have lowered the pH of water bodies at the higher elevations in the Adirondack Mountains. This has resulted in loss of certain species of fish,[1] leaching of metals from soils, suspension of metals from sediments,[2] and altered rates of decomposition activity.[3]

Research on artificially acidified water bodies (streams and microcosms) indicates significant export of nutrients and biomass from acidified regions[4] and mobilization of metals from sediments.[5,6] Alterations of plankton populations have also been observed under acidic conditions. In addition to acid precipitation, trace metals and hydrocarbons released during coal combustion can affect aquatic systems, including the possibility of their biomagnification within aquatic foodchains.[7] Despite the accumulating evidence for acid precipitation damage to certain aquatic ecosystems, present understanding of the mechanisms of transport and effect are far from adequate.

Two research efforts to study acid precipitation effects in high-elevation aquatic ecosystems

*This work was supported by the Department of Energy under Contract No. W-7405-ENG-48 through the California Policy Seminar.

are underway at Lawrence Berkeley Laboratory (LBL). One goal of this research is to establish baseline conditions against which changes can be detected should they occur. A second and related goal is to develop from the pattern of such changes and from associated laboratory studies an increased understanding of the mechanisms and progression of acidification and its impacts on high-elevation aquatic ecosystems.

ACCOMPLISHMENTS IN FY 1980

Acid Precipitation Effects in the Sierra Nevada

Field and laboratory research on the potential for acid-precipitation damage to aquatic systems of the Sierra Nevada, California was carried out by K. Tonnessen and J. Oldfather. Twenty lakes on the Sierra's western slope were characterized during the 1980 field season with reference to pH, temperature, alkalinity, trace metal concentrations, phytoplankton populations and sediment composition. None of the lakes sampled had a pH less than 6.0, although alkalinities were low. Some of the lakes sampled were found to have high iron levels in the water column.

These field analyses formed the basis for selecting Mosquito Lake (8500 ft) as one of the three lakes to be modeled in the laboratory using microcosm systems.

Twelve 18-l systems using water taken from Mosquito Lake were established in a room with controlled light (10 h light: 14 h dark) and controlled temperature (8° C). Six replicate tanks (three with sediment, three without sediment) were treated with sufficient HNO_3 to reduce the system pH to 4. Six control tanks, with and without sediment, were left untreated. During a 6-week period, changes in pH, metals, and phytoplankton and zooplankton species were monitored weekly.

Analysis of data from previous microcosm experiments was completed and the results presented at a national meeting of the American Water Resources Association in Minneapolis, Minn. in October 1980[6] and at the International Symposium on the Ecological Effects of Acid Precipitation, Sandefjord, Norway, March 1980.[8]

Acid Precipitation Research on Colorado Alpine Aquatic Ecosystems

Three researchers from the LBL aquatic ecology group designed and initiated a research program to investigate acid precipitation impacts on Colorado alpine aquatic ecosystems. The scope of the research is to monitor a number of meteorological, chemical, and biological variables that characterize a selected alpine watershed over a period of up to twenty years. The site selected is the Mexican Cut/Galena Mountain Research Preserve, a hydrologically self-contained watershed spanning the elevations from 3200 to 3800 m (approx.) on the Rocky Mountains' western slope. The watershed contains a lake of about 30,000 m^2 situated above timberline; a series of ponds below timberline in a subalpine forest of Englemann spruce and alpine fir; and a drainage creek (see Fig. 1). The Preserve is located approximately 25 km southwest of Aspen, Colo. and 15 km north of Crested Butte, Colo.

Measurements made during the summer of 1980 showed rain pH to be 4.0 - 4.6 with 4.2 the most common value. Snow core pH measurements were 5.6 - 5.9. However, these measurements were taken in mid-June after considerable snow melting had occurred, and good evidence exists that the majority of the ions are released during the early part of the melt.[3] It would appear from our measurements, therefore, that acid stresses are occurring on the western slope of the Rockies. Data of other investigators on the eastern slope of the Rockies show similar results.[10]

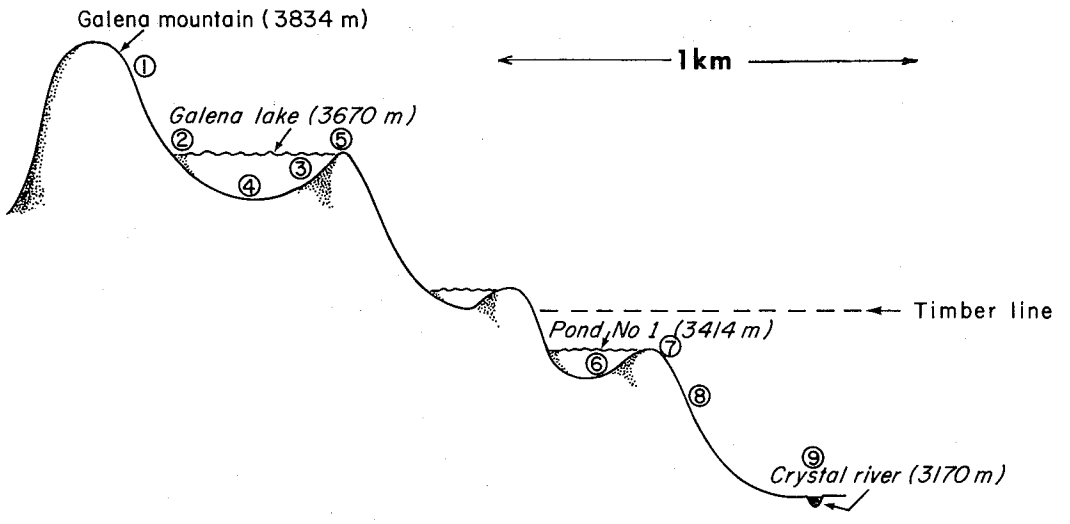

Fig. 1. Cross section of the Galena/Mexican Cut watershed showing research sites. (XBL 8012-2567)

pH measurements in the surface waters gave values ranging from 5.6 at the higher elevations (snow-melt) to more than 7 at the lower elevations (see Fig. 2). During 1980 we began to characterize the buffering capacity of the watershed. As measured by alkalinity, the buffering capacity ranged from a low of <30 microequivalents/l in Galena Lake to over 200 in the ponds (see Fig. 3). The low values above timberline indicate that those water bodies are especially vulnerable to acid loading. The higher values at the lower elevations are caused by more extensive soil development in the forest and by increasing organic content of the water. The bedrock is primarily metamorphosed quartzite, siltstone, and shale; these minerals are quite resistant to weathering and provide little buffering capacity.

Water and snow samples from various sites were collected for metals analyses, which are now underway. These measurements are a regular part of the monitoring effort to determine if there exist significant airborne metals deposition, soil leaching, and/or sediment mobilization.

Populations of salamanders have proven to be useful indicators of acid precipitation damage in aquatic systems of the northeast U.S.[11] Large populations of Ambystoma tigrinum (tiger salamander) inhabit a number of the ponds in the Preserve. During the summer of 1980, a salamander census in Pond #1 conducted three times at about weekly intervals yielded a population of 230 ± 20 individuals.

In summary, during 1980 a research program into acid precipitation impacts was designed; analytical methods were selected and tested; field and base laboratories were established; sampling strategies were chosen, and preliminary data were collected.

PLANNED ACTIVITIES FOR FY 1981

Acid Precipitation Effects in the Sierra Nevada

Acid-precipitation effects research will continue in both the laboratory and the field. Two additional Sierra lake microcosm experiments will

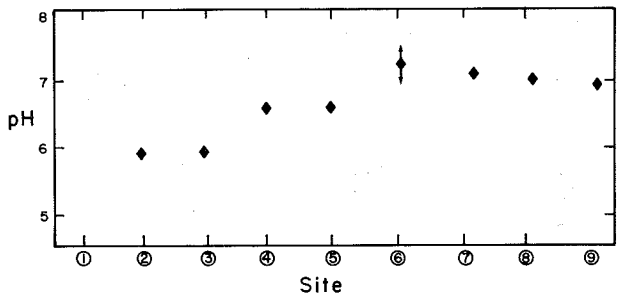

Fig. 2. Results of pH measurements at the nine sites (see Fig. 2) during the summer of 1980. The ♦'s represent averages over weekly measurements, but except for site-6, the variation from week to week was insignificant.
(XBL 8012-2565)

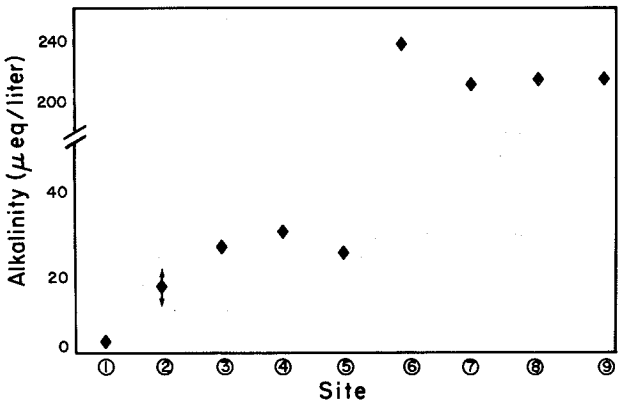

Fig. 3. Results of alkalinity measurements at the nine sites (see Figure 2) during the summer of 1980. The ♦'s represent averages over weekly measurements, but except for site 2, the variation from week to week was insignificant.
(XBL 8012-2564)

be carried out in 18-l systems, with and without sediments. Sediment composition, determined by neutron activation analysis, will be an important consideration in the selection of sensitive western slope lakes. Metals resuspension from lake sediments will be monitored following system acidification. The impact of pH and metals concentration changes on the biological populations will be monitored.

Additional western slope lakes will be sampled in 1981, with emphasis being placed on sampling during the spring melt period. In other regions of North America and in Scandinavia, the low pH of runoff water during this period has proven to be a crucial factor in lake acidification process. Sampling in the western Sierra will indicate whether a similar situation exists in the western U.S.

A cooperative effort in acid precipitation field research in the Sierra will be established with Dr. John Melack of the University of California at Santa Barbara. The extent of the acid precipitation problem in California will be explored at the California Symposium on Acid Precipitation to be held January 14-15, 1981. A report on the activities of the LBL Group will be presented at this symposium.

Acid Precipitation Research on Colorado Alpine Aquatic Ecosystems

Meteorological sampling stations will be set up to measure precipitation volumes and to collect samples for ion and metals analysis. Snowpack and spring snowmelt will be similarly analyzed. Regular monitoring of pH, alkalinity, and metals concentration in surface waters will occur. Further characterization of the buffering capacities and metals content of watershed soils and of lake and stream sediments will be made. Attempts will be made to understand the relative contributions of mineral, organic, and carbonic acids to the total buffering capacity of the water bodies.

Nutrient export rates in the forms of inorganic nitrogen (NO_3 + NO_2, NH_3) and total phosphorous concentrations will be measured in the drainage creek. These measurements will indicate whether significant downstream export of nutrients from the watershed is occurring, a phenomenon observed in artificially acidified water bodies.[4] A series of microcosm experiments will be performed to determine changes in the mineralization potential of the Galena water column. Standard additions of organic substrates will be made to lakewater aliquots, and the evolution of inorganic nutrients will be measured. If evolution of inorganic nutrients decreases with time, this will be an indication that lake decomposition processes are being affected, as reported elsewhere.[3]

Population counts of salamanders in Pond #1 will be made on a biweekly basis. Monitoring of lake and pond phytoplankton and zooplankton and of stream insects will be done by other members of our research team. Further refinements of field methods will be undertaken.

A Model of Watershed Acidification

A watershed subjected to continuing acid precipitation will neutralize the acids as long as sufficient alkalinity, or buffering capacity, is present in the lake and stream waters, the watershed soils, and the lake sediments. As the buffering capacity is gradually overwhelmed by acids flowing through the system, a threshold is reached at which a sudden, large drop in the pH of the water bodies takes place. Developing the ability to predict the time to reach threshold is an important task in acid precipitation research. The approach of the system to the threshold is not well understood. Even at relatively well-studied sites, experimental information is incomplete regarding some of the critical steps in the buffering process (such as the rate of deposition of atmospheric alkaline materials, or the influence of lake sediments on the buffering of the overlying water column). However, even with an adequate data base, predicting the time to reach threshold would not be simple because of the diversity of both competing and reinforcing processes. Needed is a reliable mathematical model capable of describing the linkages among these processes. The development of such a model, incorporating only empirically accessible rate parameters and variables, will be carried out in FY 1981. During the summer of 1981, baseline values for the model components will be measured at the Galena/Mexican Cut watershed; in subsequent years, model predictions will be confronted with experimental measurement.

REFERENCES

1. C. L. Schofield, "Lake Acidification in the Adirondack Mountains of New York: Causes and Consequences," in L. S. Dochinger and T. A. Seliga, eds. Proceedings of the First International Symposium on Acid Precipitation and the Forest Ecosystem, United States Department of Agriculture Forest Service Technical Report NI-23, 1976.

2. C. S. Cronan and C. L. Schofield. "Aluminum Leaching Response to Acid Precipitation: Effects on High Elevation Watersheds in the Northeast," Science, vol. 204, pp. 304-306.

3. F. H. Braekke, Impact of Acid Precipitation on Forest and Freshwater Ecosystems in Norway, Research Report 6, 1432 AAS-NLH, SNSF Project, Norway, 1976, (Available from SNSF Project, Box 61, 1432 As-NLH, Norway.)

4. R. J. Hall, and G. E. Likens, "Chemical Export in an Acid-Stressed Stream" (submitted to Science, 1980).

5. A. O. Davis, J. N. Galloway, and D. K. Nordstrom. "Lake Acidification: Its Effect on Lead Mobility in the Sediment of Two Adirondack Lakes," Limnology and Oceanography (in press), 1980.

6. K. Tonnessen and J. Harte, "The Potential for Acid Precipitation Damage to Aquatic Ecosystems of the Sierra Nevada, California," abstract of paper presented at Annual Meeting of the American Water Resources Association, October 12-16, 1980.

7. Office of Technology Assessment (OTA), The Direct Use of Coal, prepared for U.S. House of Representatives Committee on Science and Technology, U.S. Government Printing Office, Washington, D.C., 1979.

8. K. Tonnessen and J. Harte, "The Potential for Acid Precipitation Damage to Aquatic Ecosystems of the Sierra Nevada, California (USA)," Proceedings of the International Conference on the Ecological Impact of Acid Precipitation, Sandefjord, Norway, March 11-14, 1980 (in press), (December 1980).

9. W. M. Lewis, Jr., and M. C. Grant, "Changes in the Output of Ions from a Watershed as a Result of the Acidification of Precipitation," Ecology, vol. 60, no. 6, 1979, pp. 1093-1097.

10. F. H. Pough, "Acid Precipitation and Embryonic Mortality of Spotted Salamanders, Ambystoma Maculatum," Science, vol. 192, pp. 68-70.

COMBUSTION RESEARCH

INTRODUCTION

Combustion processes are an essential part of the utilization of more than 90% of the energy consumed in the United States, play important roles in the extraction and processing of fossil energy, are responsible for most of our air pollution, and are at the center of the field of fire safety. The art of combustion has been highly developed during the past hundred years, producing through trial and error a variety of combustion devices that convert chemical energy into thermal and mechanical energy. Traditional design methods can no longer meet the often competing demands of high efficiency, low pollutant emissions, and alternative fuels utilization. Combustion science is able to provide the fundamental understanding of combustion processes essential for the application of theory to the analysis and design of advanced combustion systems.

Combustion research at the Lawrence Berkeley Laboratory focuses on the study of the chemical and physical processes which are important in combustion. Two areas of application dominate; the control of combustion processes to allow the utilization of new fuels while limiting pollutant formation and the reduction of fire hazards accompanying energy generation and utilization technologies. Principal program areas are the interaction of fluid-mechanical turbulence and combustion, the development and application of new physical and chemical diagnostic techniques for combustion research, pollutant formation and destruction processes, theoretical and computational modeling of combustion processes, combustion processes in engines, fire science, and fire safety.

The research team consists of research scientists at the Lawrence Berkeley Laboratory, faculty and graduate students of the Departments of Mechanical and Civil Engineering at the University of California at Berkeley, visitors from throughout the United States and the world, and a supporting technical, clerical, and administrative staff.

A major component of the research program is the training of combustion scientists and engineers at all levels. The graduate program in combustion at the University of California at Berkeley is one of the largest and most diversified in the world. Laboratory facilities are located at the Lawrence Berkeley Laboratory, on the campus of the University of California, and at the Richmond Field Station. Cooperative research is conducted by Lawrence Berkeley Laboratory scientists with investigators at the Lawrence Livermore National Laboratory and at the Sandia National Laboratory Combustion Research Facility.

ENGINE COMBUSTION AND IGNITION STUDIES

MECHANISM OF INSTABILITIES IN TURBULENT COMBUSTION LEADING TO FLASHBACK*

J. Keller, L. Vaneveld, D. Korschelt,
G. Hubbard, A. Ghoniem, J. Daily, and A. Oppenheim

INTRODUCTION

In conventional combustors for gas turbines, the flame front is established at the stoichiometric contour in the primary zone.[1,2] This produces optimum conditions for the generation of pollutants. The best remedy for this state of affairs is offered by "lean, premixed/prevaporized combustors".[3,4] Such systems require the use of a premixing chamber while combustion is stabilized by a bluff body flame holder.[5] Their operation is handicapped by potentially harmful combustion instabilities.[6,7] At the lean limit, they cause blow-off; at the rich, they lead to flashback. The purpose of our studies is to explore the mechanism of the instabilities associated with the rich limit, under highly turbulent flow conditions.

ACCOMPLISHMENTS DURING FY 1980

The experiments were performed using our combustion tunnel depicted in Figure 1, p. 6-33, Energy and Environment Division Annual Report FY 1979. In this tunnel, the flame was stabilized by a streamlined contraction culminating in a rearward facing step. Propane/air mixtures were employed as the working substance, instabilities were triggered by a sudden increase in the flow rate of fuel, and observations were made using high speed schlieren cinematography combined with pressure measurements. As the rich limit was thus approached, we were able to identify three modes of instabilities called, for lack of better names, (1) humming, (2) buzzing, and (3) chucking.

In comparison to the flow field associated with stable combustion which was described in the 1979 Annual Report, the characteristic features of these instabilities are presented here in Figures 1, 2, and 3, all pertaining to the same inlet flow velocity of 13.3 m/sec as in Figure 1b of the 1979 Annual Report. The first was obtained when the pressure in the test section was maintained at a minimum level; the second, when it was slightly increased (about 10 mm of water) by closing a butterfly valve in the exhaust duct; the third was established when the equivalence ratio was at a flashback limit.

We attribute the mechanism of these instabilities to the interaction between the set of trailing vortices in the mixing region behind the edge of the step and the set of recirculation vortices formed behind its base. Salient features of this process are depicted schematically in Figure 4.

Shown in the sketch at the top of Figure 4 is the trailing vortex pattern associated with stable combustion. Here, the flame front delineates the outer edges of the mixing layer at the contour of the interface between the burned gases and the fresh charge. In the next photograph below, not detectable by schlieren optics, is the recirculation vortex, A, that is, as a rule, established behind the step irrespective of whether the flow field is associated with combustion or not. This gives rise to a counter-rotating vortex, B.

When more burned gases are produced in the presence of combustion, both of these vortices grow, as shown in the second sketch. The growing recirculation vortex of the burned gases causes vortex A to be pushed downstream, as shown in the third sketch, while vortex B increases in size. As a consequence of the counter clockwise circulation of this vortex, it must give rise to vortices C and D, as required by compatibility with the flow of the fresh charge. When vortex B becomes larger, as shown in the fourth sketch, vortex C may be forced upstream, causing a flow reversal on top of the step, tripping the boundary layer, and pushing the flame upstream. This, in our opinion, is the characteristic feature of turbulent flashback we observed. The flame front is attached at its upstream edge to the boundary layer; but, behind this edge, it is lifted from the wall by the action of vortex C.

As vortex B grows still further, it is convected downstream, while vortex C pairs with vortex D to form a new vortex A' and, concomitantly, a new corner vortex B', as shown in the fifth sketch. Finally vortex A' grows to a size comparable to that of Vortex A, and B' to B, as in the second sketch. At the same time, vortex B is convected further downstream and, as illustrated in the sixth sketch, the combined action of vortex A' and B causes the flame to acquire a practically vertical orientation, extending across the full height of the combustor.

* This work was supported by the Director of the Office of Energy Research, Office of Basic Energy Sciences, Engineering, Mathematics, and Geosciences Division of the U.S. Department of Energy under Contract No. W-7405-ENG-48 and by the U.S. National Aeronautics and Space Administration under Grant No. NSG 3227 through the Engineering Office of Research Services, University of California, Berkeley.

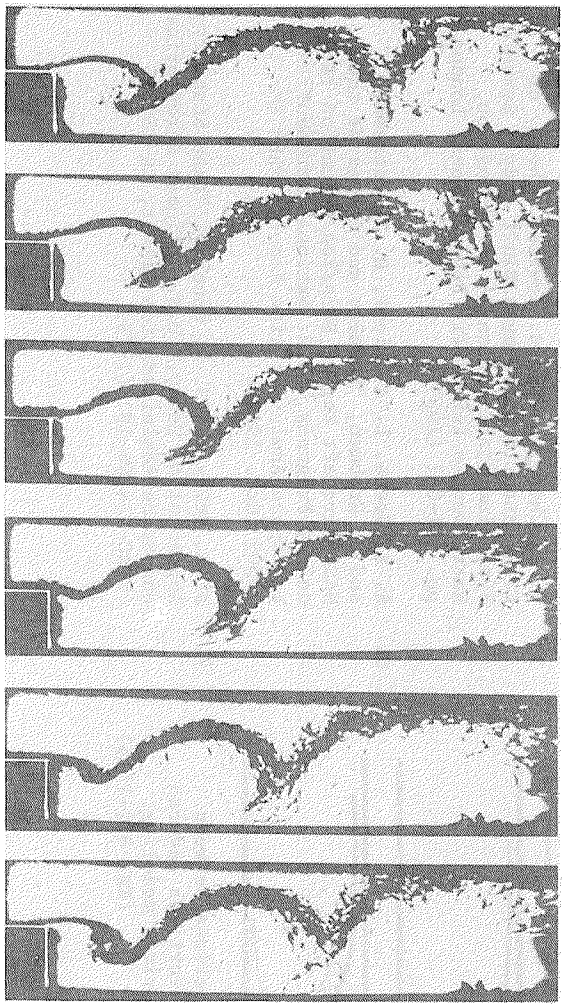

Fig. 1. Cinematographic schlieren record of humming. Equivalence ratio: 0.86. Time interval between frames: 1 msec. (XBB 811-13)

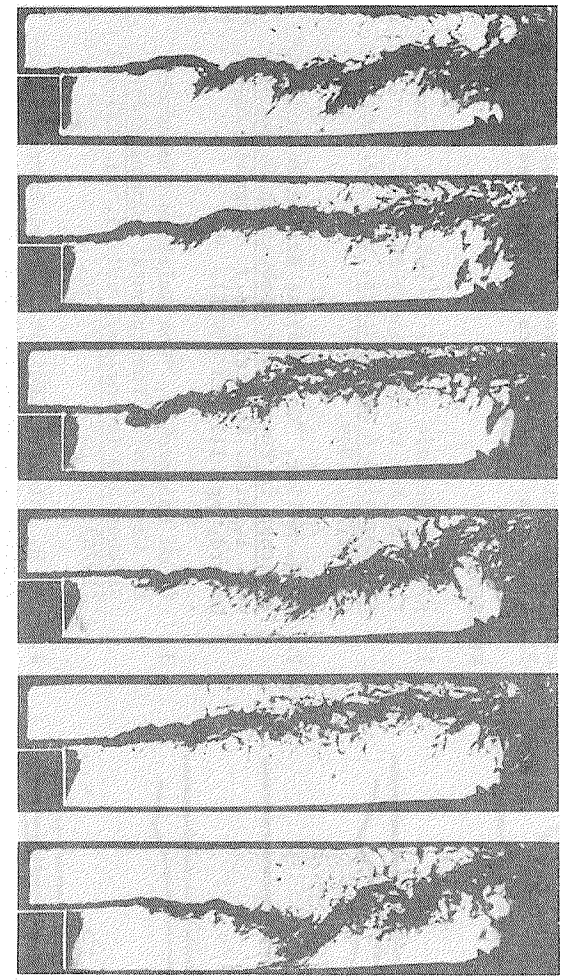

Fig. 2. Cinematographic schlieren record of buzzing. Equivalence ratio: 0.80. Time sequence of frames: 0, 8, 14, 22, 36, 48 msec. (XBB 811-14)

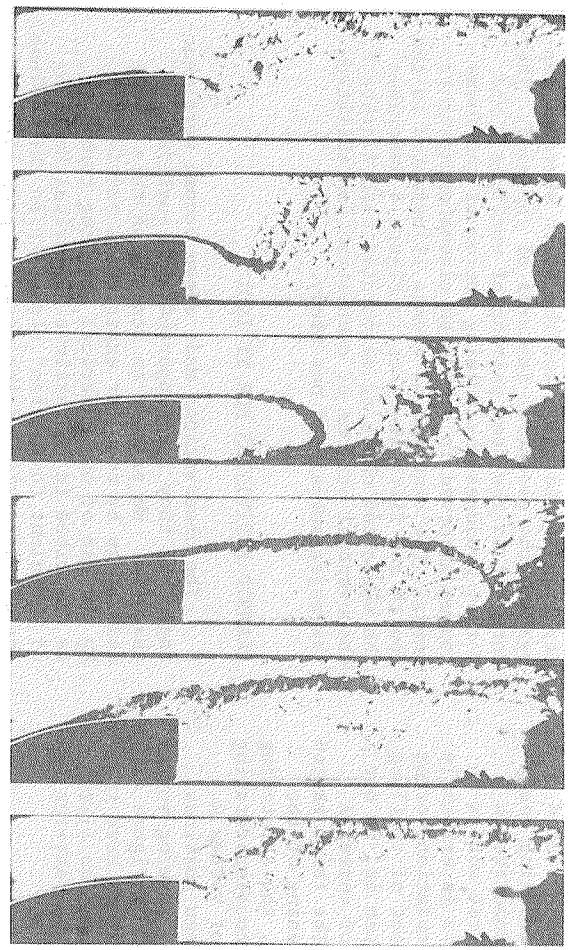

Fig. 3. Cinematographic schlieren record of chucking. Equivalence ratio: 0.85. Time interval between frames: 4 msec. (XBB 811-15)

The first sketch in Figure 4 was deduced from the results of the numerical modeling analysis for stable combustion. The second sketch illustrates the formation of the first vortex in humming displayed in Figure 1. This is evidently caused by the pairing of the recirculation vortex A with the first component of the set of trailing vortices. The next vortex downstream is, in our opinion, the result of the growth of vortex A in the course of its convection. The third sketch describes the reason for the flattening of the flame observed in buzzing (Fig. 2), the stretching due to the combined action of the counter-rotating vortices A and B. The convection of vortex B downstream ushers the pairing between vortices C and D, a relatively rapid process forming vortex A' as it appears in the last sketch of Figure 4. The occurrence of this process does not have to be associated with the propagation of the flame upstream. Thus the repetition of the patterns depicted in the third and the sixth sketches represents the essential features of chucking. Therefore, it is the fast pairing of vortices C and D that produces the pulsing motion of the flame tongue observed in schlieren cinematographic records. The sequence of events illustrated in the fourth and fifth sketches in Figure 4 describes the augmented chucking associated with flashback, the eventual outcome of combustion instabilities -- the major subject of our study.

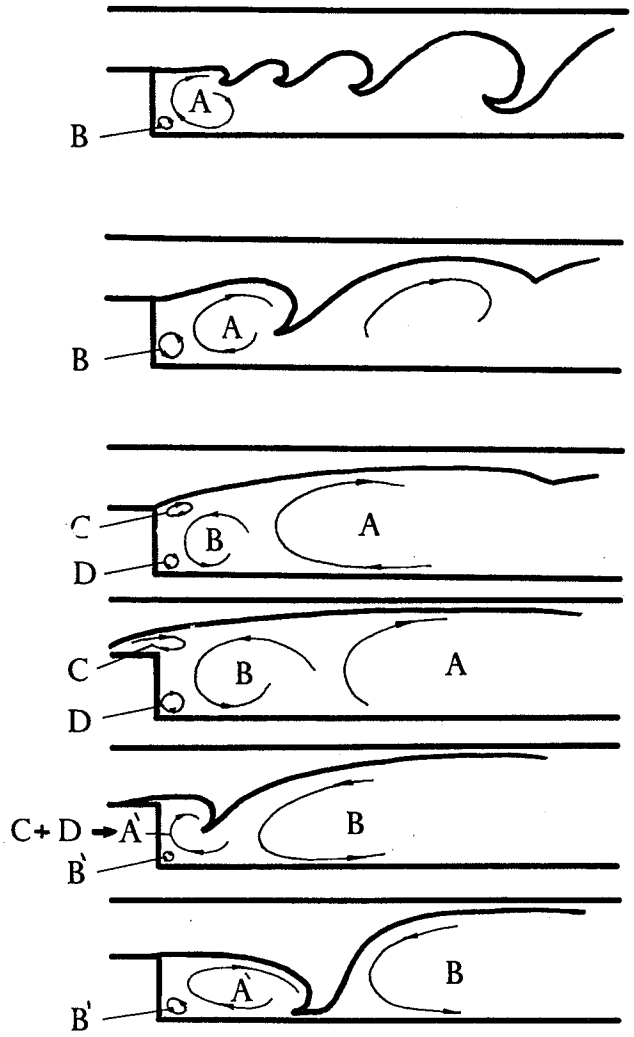

Fig. 4. Sketches of the interactions between the recirculation and trailing vortices deduced from schlieren records and numerical modeling analysis. (XBL 811-7515)

PLANNED ACTIVITIES FOR FY 1981

The observations made above become more meaningful if they are supported by a qualitative analysis. We propose to accomplish this at the next stage by computer experiments carried out by the use of our numerical modeling technique, as described in the article "Numerical Modeling of Turbulent Combustion" elsewhere in this volume. The clarification of the detailed properties of the flow field obtained in this manner should assist designing future combustion tunnel experiments, as well as expanding our studies to include other geometrical configurations of bluff body flame holders in combustors for premixed gases.

REFERENCES

1. A. K. Oppenheim and F. J. Weinberg, "Combustion R&D Key to Our Energy Future," Astronautics & Aeronautics, vol. 12, no. 11, pp. 22-31, (Nov. 1974).

2. A. M. Mellor, "Gas Turbine Engine Pollution," Progress in Energy and Combustion Science, vol. 1, N. A. Chigier, ed.: Pergamon Press, Oxford, pp. 111-133 (1976).

3. L. J. Spadaccini, "Low Emission Combustors for Gas Turbine Powerplants," Combustion Science and Technology, vol. 9, pp. 133-136 (1974).

4. A. H. Lefebvre (Editor), "Lean Premixed/Prevaporized Combustion," U.S. National Aeronautics and Space Administration Report, NASA CP-2016 (Jan. 1977).

5. S. I. Cheng, and A. A. Kovitz, "Theory of Flame Stabilization by a Bluff Body," Seventh Symposium (International) on Combustion, Butterworths Scientific Publications, London, pp. 681-691 (1959).

6. R. E. Jones, L. A. Diehl, D. A. Petrash, and J. Grobman, "Results and Status of the NASA Aircraft Engine Emission Reduction Technology Programs," U.S. National Aeronautics and Space Administration Report, NASA TM-79009 (Oct. 1978).

7. J. B. McVey and J. B. Kennedy, "Lean Stability Augmentation Study," U.S. National Aeronautics and Space Administration Report, CR-159536 (UTRC-914104-18) (1979).

HEAT TRANSFER WITH COMBUSTION*

R. Greif, H. Heperkan, J. Woodard, S. Vosen, D. Wong, and J. Naccache

INTRODUCTION

One of the major goals of this research has been the experimental and theoretical determination of the temporal variation of the heat flux during compression and combustion processes. This is of considerable practical importance and is also of fundamental interest. With respect to internal combustion engines, heat transfer processes are critical to: quenching of wall reactions which cause high hydrocarbon emissions, the loss of energy which results in decreased efficiency, and the durability of engine components.

Measurements have been made in a single pulse, compression expansion apparatus that was built by Oppenheim, et al.[1] to study reciprocating engine processes under well-controlled laboratory conditions which simulate the operation of a spark-ignition engine. Completed studies in the apparatus include the experimental and theoretical determination of the unsteady wall heat transfer in non-reacting gases during piston compression.[2,3]

Measurements in the presence of reacting gases have been made in a shock tube and in a constant volume combustion chamber.[4] These studies are of general interest and provide an introduction to the study of more general phenomena concerning combustion during piston compression.

ACCOMPLISHMENTS DURING FY 1980

Measurements to determine heat transfer during combustion were made previously in non-reacting gases with a thin film resistance thermometer. The resistance thermometer, consisting of a thin platinum film on an insulted backing, is connected as the active element in a dc bridge. An increase in surface temperature causes a change in resistance of the platinum film. The measured variation of the resistance as a function of time yields the desired wall temperature variation.

Using these measurements, the temporal variation of the wall heat flux may be obtained when the resistance thermometer is mounted flush with the wall. The result is derived by solving the conduction equation in the solid wall (insulated backing), subject to the measured variable surface temperature. The heat flux is expressed as a Duhamel integral in terms of the variable surface temperature and the wall properties. The validity of this measurement and analysis has been demonstrated in our previous publications.[2,3]

An alternative, independent approach for determining of the wall heat flux is the solution of the conservation equations in the gas to obtain a heat flux based on the gas properties. Good agreement has been obtained for the two heat fluxes in the following experiments: (a) during piston compression in the single pulse apparatus, and (b) during shock wave compression in a shock tube.

When reactions occur, the gas dynamic and transport phenomena are complex. For this condition, the measured heat flux is used to determine fundamental results concerning combustion phenomena. These measurements have been made in a shock tube where a mixture of hydrogen, oxygen and argon was ignited due to shock wave heating. New results include the temperature distribution in the gas at different times (Fig. 1). The wall location corresponds to the zero value of the abscissca with ignition commencing at 20 μsec.[4] Another important result is the location of the combustion zone as a function of time. The analysis shows that the zone moves toward the wall and then remains, for a considerable time, at a fixed, quenching distance from the wall.[4]

Another study with reacting gases has been initiated in a constant volume chamber with a methane air mixture. Experiments were performed in a steel explosion vessel that was fitted with optical glass windows suitable for schlieren photography. The mixture was ignited by a spark and the flame that formed propagated toward the wall which contained a resistance thermometer. In preliminary measurements, the temporal variation of the wall heat flux was obtained and photographs were also taken of the advancing flame front.

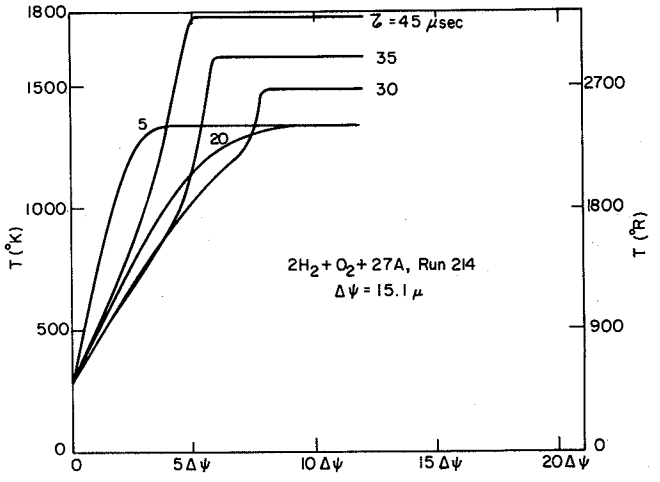

Fig. 1. Gas temperature distribution.
(XBL 806-10302)

* This work was supported by the Assistant Secretary for Conservation and Solar Energy, Office of Transportation Programs, Transportation and Energy Conservation Division of the U.S. Department of Energy under Contract No. W-7405-ENG-48.

PLANNED ACTIVITIES FOR FY 1981

Experiments in the constant volume chamber and analysis of the fluid flow and energy transport associated with the advancing flame front will be continued. This work follows as a natural outgrowth of previous shock tube studies. In addition, studies will be made in the two single pulse compression expansion facilities. In particular, experiments and analyses of the roll-up vortex, piston expansion, and combustion phenomena will comprise this part of the research.

REFERENCES

1. A. K. Oppenheim, R. K. Cheng, K. Teichman, O. I. Smith, R. F. Sawyer, K. Hom, and H. E. Stewart, "A Cinematographic Study of Combustion in an Enclosure Fitted with a Reciprocating Piston," in Stratified Charge Engines, Institution of Mechanical Engineers Conference Publications 1976-11, pp. 127-135 (1976).

2. M. Nikanjam and R. Greif, "Heat Transfer During Piston Compression," Transactions of the ASME, J. of Heat Transfer, vol. 100, p. 527 (1978), and Lawrence Berkeley Laboratory Report LBL-7338.

3. R. Greif, T. Namba, and M. Nikanjam, "Heat Transfer During Piston Compression Including Side Wall and Convection Effects," International J. of Heat and Mass Transfer, vol. 22, pp. 901-908 (1979).

4. H. A. Heperkan, "An Experimental and Theoretical Study of Heat Transfer with Combustion," Ph.D. Dissertation, University of California, Berkeley (1980) and Lawrence Berkeley Laboratory Report LBL-10868.

ENGINE COMBUSTION STUDIES*

R. Sawyer, J. Daily, A. Oppenheim, and H. Stewart

INTRODUCTION

Development of efficient and environmentally benign internal combustion engines depends to a large extent on the attainment of their reliable operation, using premixed, lean mixtures. Studies of lean combustion processes pertaining to this objective have been conducted in our laboratory by the use of a single-pulse, compression-expansion machine. This unique facility, which we developed, features a square piston between two windows, permitting an unobstructed optical access to the entire chamber where combustion takes place, under conditions similar to those existing in reciprocating piston engines.

In the initial version of the machine, the piston was pneumatically driven and hydraulically controlled. This version had a number of drawbacks, the most important being the difference of the piston trajectory from that of a reciprocating piston engine.

Nonetheless, the pneumatically operated prototype has been used successfully to investigate piston induced flow fields, valve generated turbulence, ignition processes, flame structure and propagation, bulk and wall quenching, and time-resolved heat transfer phenomena.

On the basis of experience gained, an improved version of the machine has been designed and constructed. Its major features are:

1. The piston is driven by a crankshaft, and its motion is controlled by a fast acting clutch-brake mechanism, permitting one, two, three, or four stroke operation.

2. The cross-section of the combustion chamber is larger and has the same area as a standard CFR laboratory test engine.

3. The head is provided with conventionally operated overhead intake and exhaust valves.

ACCOMPLISHMENTS DURING FY 1980

The crankshaft operated compression-expansion machine has been assembled and provided with controls and a computerized data processing system, as schematically described in Figure 1. Basically, the computer has the capability to control the operation of the machine and the acquisition and reduction of data. However, at this stage, these facilities have not yet been put into operating condition, and the cylinder head, fitted with solenoid actuated valves indicated in Figure 1, is not yet available.

PLANNED ACTIVITIES FOR FY 1981

Initially, we intend to use the apparatus for the study of the local consumption of fuel by making time resolved measurements of methane concentration, using absorption at 3.39 μ m with an

* This work was supported by the Assistant Secretary for Conservation and Solar Energy, Office of Transportation Programs, Transportation Energy Conservation Division of the U.S. Department of Energy under Contract No W-7405-ENG-48.

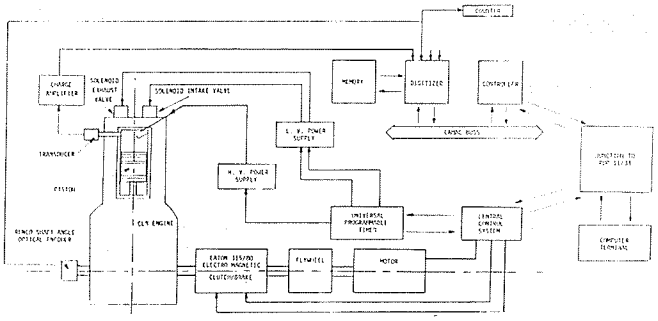

Fig. 1. Schematic diagram of the crank-operated compression-expansion machine with a computerized control and data processing system. (XBL 811-7563)

Ne-He laser as the light source. Figure 2 shows the test section of the apparatus with the laser system in place. The optical arrangement of the method is depicted on the photograph by the light beam that has been traced with the use of the alignment laser.

Upon the completion of this preliminary investigation, we plan to use the machine for a comparative study of ignition systems, with particular attention given at first to plasma jet ignition in comparison to a conventional spark plug. At the same time, work will be in progress on the introduction of computer monitored operation of the apparatus and data processing system.

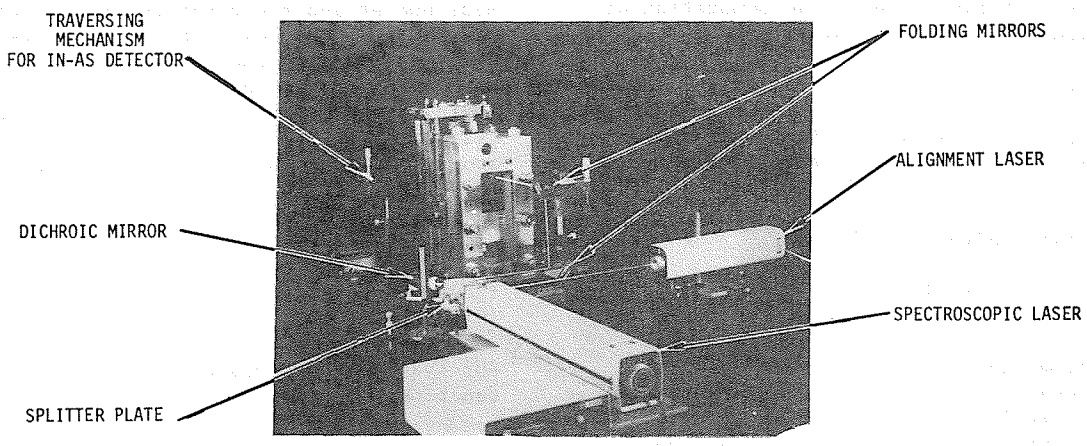

Fig. 2. Test section of the crank-operated compression-expansion machine with laser instrumentation for time-resolved measurement of methane concentration by absorption at 3.39 μm.
(XBB 811-438)

IGNITION STUDIES*

A. Oppenheim, F. Hurlbut, F. Robben, R. Peterson, P. Coico, and H. Stewart

INTRODUCTION

It had become increasingly apparent that work on the fundamental science of combustion processes in lean mixtures, specifically work on lean mixture ignition processes, would be greatly advanced through the methods of direct molecular beam mass sampling. It was envisioned that a suitable system to accommodate the simultaneous coordination of optically based diagnostic observations would include high speed schlieren photography, emission and absorption spectroscopy, and laser fluorescence. Accordingly, our objective has been development of a system for time-resolved mass analysis which would lend itself easily to the accommodation of the peripheral instrumentation.

Funding for this program of study became effective at the end of 1978, and preliminary design was initiated by January of 1979. Fabrication of primary elements of the vacuum shell and support frame was completed in FY'79.

ACCOMPLISHMENTS DURING FY 1980

Major effort was devoted to the continuing construction and development of the molecular beam system. Construction and installation of the essential elements of the vacuum shell and its instrumentation were accomplished during the winter of 1979. In April 1980, the system was placed under evacuation by diffusion pumps. By May, following final minor modifications, a system base pressure of 5×10^{-7} Torr was reached. Preliminary tests in June verified that all regions of the beam system were at design pressures or lower, under the design beam load.

During the spring of 1980, installation of the mass spectrometer[1] and related system components was started. By late June, preliminary tests of molecular beam and mass spectrometer functions were made to determine acceptable mass resolution and signal sensitivity.

We selected the CAMAC design approach for function control and instrumentation housing to serve the substantial number of controlled mechanical and electronic system elements eventually required. A resident dedicated computer will be used to control essential functions, including the precise timing of events and the recording and analysis of data. A standard Engineering MIK-11 computer, housed in the CAMAC "crate", would serve for system function sequencing, data acquisition, and preliminary processing. The LBL Real Time Measurements Group acquired and assembled the basic system and provided it with essential operating programs. It was delivered to the main system by May 1980 and was then combined with a fast ATD converter. Subsequently, in early June, during a check of computer system function, the pressure history of methane-air ignition was digitized and recorded. Entirely satisfactory agreement was observed between the digitized record and oscilloscope photographs.[2] Two other electronic components essential to computer controlled system operation were received by the close of FY'80: the precision (16 bit) DTA converter for setting spectrometer mass number and the clock controller for operations sequencing. The remainder of FY'80 was occupied with continued system development, including installation of the molecular beam modulator, the timing signal system, and the back-to-air back-fill system, as well as refinements to the calibration source and associated pressure instrumentation.

System Overview

The cross-section of the molecular beam apparatus is displayed in Figure 1. Shown in Figure 2 is a functional schematic diagram of the associated control system. The apparatus consists of several sub-systems which may be identified according to function:

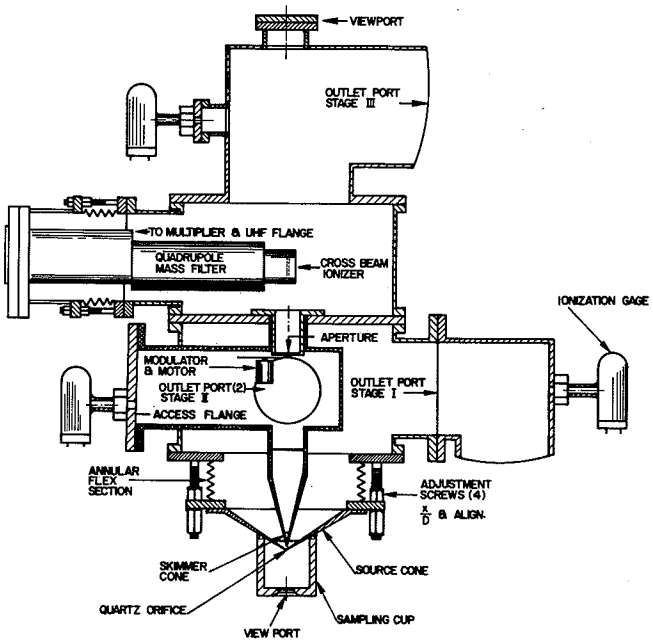

Fig. 1. Cross-section of the molecular beam shell. (XBL 811 7513)

* This work was supported by Director, Office of Energy Research, Office of Basic Energy Sciences, Engineering, Mathematics, and Geosciences Division of the U.S. Department of Energy under Contract No. W-7405-ENG-48.

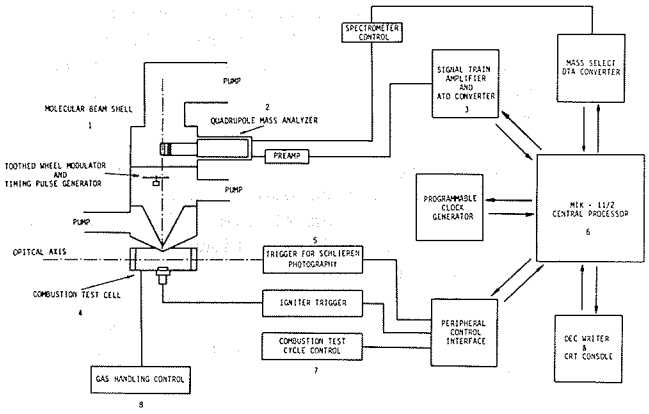

Fig. 2. Functional schematic diagram of molecular beam mass sampling system. (XBL 811 7514)

1. Molecular beam, consisting of the sampling source, skimmer, modulator with timing signal generator, associated vacuum pumps, gauges, and controls.

2. Quadrupole mass analyzer, consisting of ionizer, analyzer, particle detector, R. F. power supply, High-Q head, ionizer control, and quadrupole control.

3. Signal train, consisting of *preamplifier, *voltage amplifiers, and fast ATD converter.

4. **Test cell and igniter.

5. *Flash schlieren (optic axis only shown).

6. Central processor, consisting of MIK-II mini-computer with DEC writer and scope monitor, *clock controller, *mass select DTA converter, and **peripheral control interface.

7. **Cycle controller for combustion test cell and igniter.

8. **Combustion cell, calibration gas supply, and metering system, including calibration source cell.

Items marked with an asterisk (*) are under development while those marked with two asterisks (**) are yet to be designed or acquired. In addition (not shown), a synchronous detector and waveform educator have been installed to assist with the initial calibration.

General views of the apparatus are shown in Figures 3 and 4. In Figure 3, spectrometer components and the MIK-11 computer are on the right; vacuum control and monitoring components are on the left, and the molecular beam shell is at the upper center. Figure 4 is a side view of the molecular beam shell, showing the outer end of the spectrometer at upper left center and lower center, depicting the clear optical path past the sampling path.

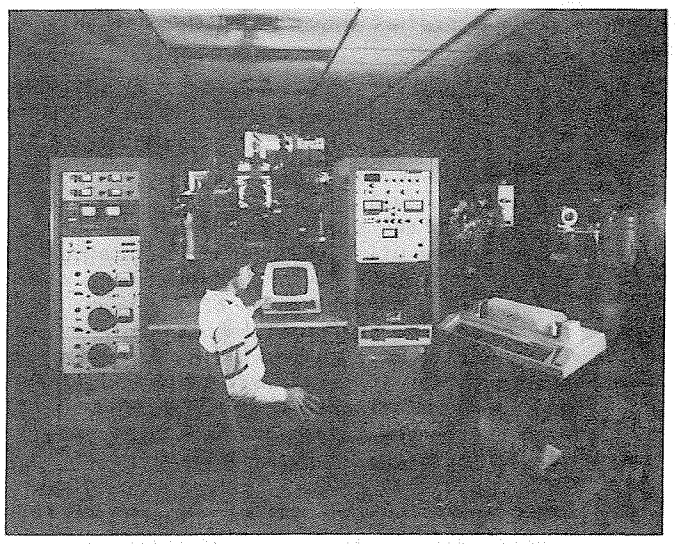

Fig. 3. General view of molecular beam mass sampling system. (CBB 803 3319)

PLANNED ACTIVITIES FOR FY 1981 and FY 1982

For the next year we will be engaged in experimental work designed to give needed information on system function and, in its later phases, on system performance with respect to time-resolved analysis

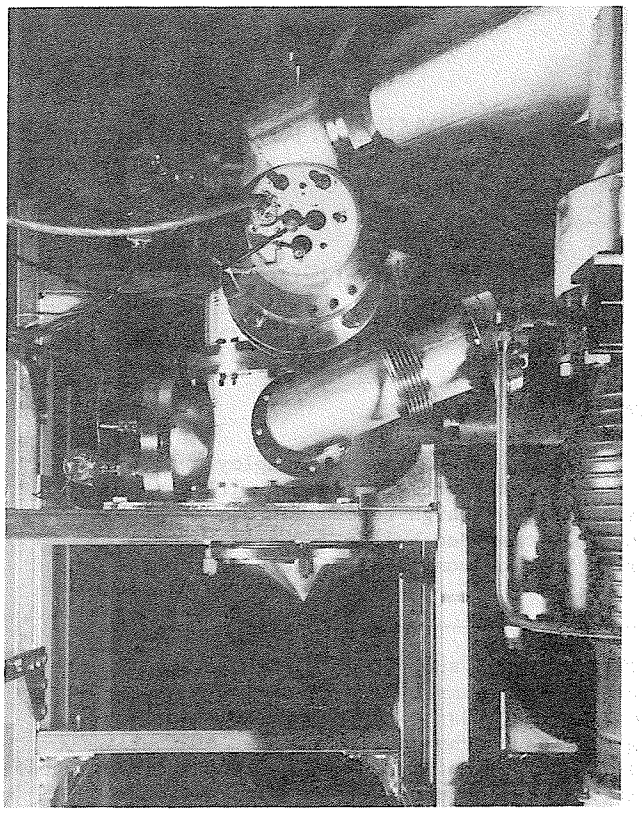

Fig. 4. Side view of molecular beam system showing sampling cone. (CBB 803 3317)

of active radical production. The program of this work will be:

1. A series of time resolution, calibration experiments for various permanent gases will be performed using the disc modulator with narrow slots. This will be used to demonstrate full system functional capability. At the same time, beam intensity measurements will give needed information on system sensitivity. This will enable a detailed rationalization of the beam performance of this instrument. Information developed in these studies is essential to the next phases of the program and for completion of a system documentation report now in preparation. Estimated completion date: January 1981.

2. Detection of active radicals will be first demonstrated in studies of hydrogen peroxide (H_2O_2), using flash photolysis. This method for the production of radicals was actively studied in the 1950's[3] complementing the time-history information obtained by absorption and emission spectroscopy.[4] Because of the relative simplicity of the chemical system, it is expected that quantitative calibration can be achieved. At the same time, useful new information concerning rate constants in this system can be derived. Estimated completion date: end of FY'81.

3. We envision next the studies of transient thermal ignition of H_2 and of other gases at the surfaces of catalytic and non-catalytic ribbons. This work will also produce spectrometer-calibration information and new rate-constant information. Completion date: mid- to end-FY'82.

4. The foregoing work will, to a degree, be coincident with development and preliminary experimentation studies of plasma and combustion jets and jet-stimulated ignition. Although the broad scope of this work makes a detailed projection inadvisable at this time, we expect some portion of the work on plasma jets to be completed by the end of FY'82.

REFERENCES

1. Extra Nuclear Laboratories, Inc.

2. R. Peterson "Application of Analog-to-Digital Converter to Data Gathering" ME249 Project Report.

3. R. G. W. Norrish, "The Study of Combustion by Photochemical Methods" Tenth Symposium (International) on Combustion, pp. 1-18, The Combustion Institute (1965).

4. C. Birkby and E. Hutton, "Gaseous Explosions Initiated by Flash Photolysis - An Investigation of Radical Ion Formation," Thirteenth Symposium (International) on Combustion, pp. 767-775, The Combustion Institute (1971).

COMBUSTION CHEMISTRY AND POLLUTANT FORMATION

MEASUREMENT OF NITROGENEOUS POLLUTANTS IN COMBUSTION ENVIRONMENTS*

D. Lucas, N. Brown, and A. Newton

INTRODUCTION

Combustion systems that employ synthetic or fossil fuels are often faced with problems associated with high concentrations of chemically bound nitrogen and sulfur. The assessment of health and environmental effects of combustion generated pollutants and research into pollution control techniques are handicapped by a lack of analytical techniques that can accurately determine the types and amounts of nitrogen and sulfur compounds present in post-combustion environments.

Research in this area has been directed to the detection and measurement of nitrogenous species, with emphasis on ammonia measuring techniques. Ammonia measurements are of particular interest because some NO control technology employs NH_3 to selectively reduce NO in post-combustion gases.

Ammonia concentrations in combustion systems are currently measured by a variety of techniques.[1] We have developed a technique, based on the sodium phenolate method, that can accurately and reproducibly measure NH_3 in combustion exhausts over a wide range of concentrations and combustion conditions.[2]

* This work was supported by the Assistant Secretary for Environment, Office of Environmental Compliance, Division of Environmental Safety and Engineering of the U.S. Department of Energy under Contract No. W-7405-ENG-48; by the Morgantown Energy Research Center of the U.S. Department of Energy under Contract No. PR-14037; and by the California Air Resources Board under contracts No. A6-196-30 and No. A8-146-31.

We have compared two of the more commonly used methods with our technique to determine what errors and interferences arise from their application to combustion research.

All of the sampling was done in a laboratory combustion tunnel fired with light fuel oils which could be doped with prototype fuel nitrogen compounds. Identical uncooled-quartz sampling probes and Teflon transfer lines were used in all systems to eliminate differences due to probe effects.

ACCOMPLISHMENTS DURING FY 1980

The sodium phenolate method was developed specifically to measure NH_3 in combustion exhaust gases. The collection system consists of glass U-tubes in series, the tubes filled with phosphoric acid coated glass beads. The sampling manifold is designed to eliminate the problem of water and/or ammonia condensation elsewhere in the system. Measurements indicate that recovery of NH_3 is in excess of 95% in the first tube. After collection, the ammonia is transferred to a flask by washing. Here it is chlorinated and subsequently reacted with sodium phenolate to form an indophenol dye. The optical density of the dye is measured at its absorption maximum, 632 mm. Numerous tests confirm that the NH_3 is quantitatively collected, transferred, and converted to the dye, and that only low molecular weight primary amines could possibly interfere in the analysis. Using this method, absolute errors to sample combustion exhausts are estimated to be less than 10%. While the method gives excellent results, it may not gain widespread use because of its low sampling rate and relatively long analysis time. It is particularly useful as a reliable standard to determine if other methods yield consistent results.

Perhaps the most convenient way of measuring NH_3 is to oxidize it to NO in a catalytic converter, followed by NO detection in a chemiluminescent analyzer. This method suffers mainly in that most NO analyzers are not equipped to handle the high concentrations of water vapor present in combustion exhausts, and there is interference from any nitrogenous species that can be oxidized to NO in the converter. Condensation of water anywhere in the system can lead to large errors because of the high solubility of NH_3. In addition, NH_3 can be adsorbed on many surfaces. To avoid these problems, a TECO Model 12 chemiluminescent analyzer was modified to eliminate condensation. The conversion efficiency of NH_3 to NO over a stainless steel catalyst was measured as a function of both temperature and NH_3 concentration; the results are presented in Figures 1 and 2. Table 1 is a comparison of NH_3 concentrations measured by the sodium phenolate and the NO_x method for a variety of combustion conditions. The NH_3 concentrations measured by the chemiluminescent method have been corrected for the vapor concentration. Corrections for CO_2, H_2O, and O_2 quenching of NO* are estimated to be less than 5% for the conditions studied. In lean combustion systems, the NO method can be successfully used to measure NH_3 concentrations as long as other nitrogenous species such as NO_2 or HCN are not present in large amounts. The accuracy of this method is estimated to be $\pm$10%, the same as for the sodium phenolate method. It

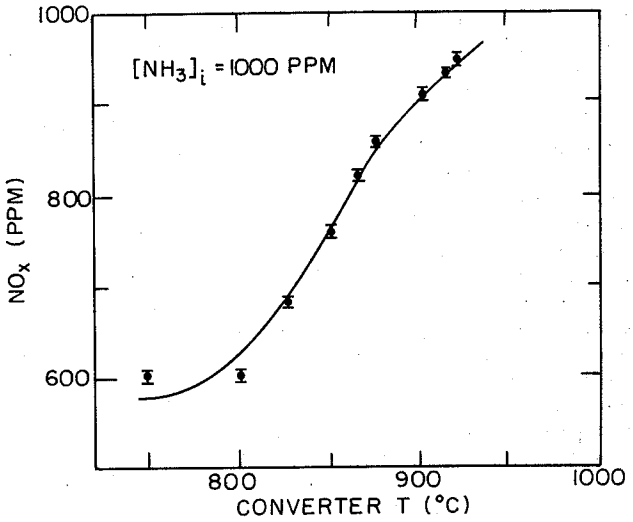

Fig. 1. NH_3 to NO conversion efficiency as a function of temperature of a stainless steel catalyst. (XBL 8012-13386)

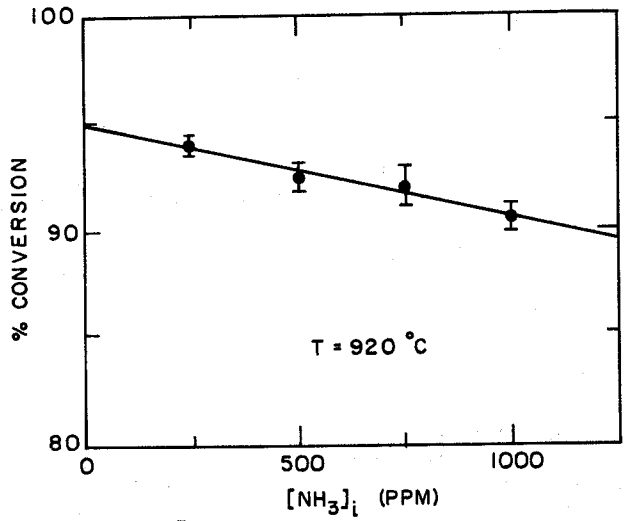

Fig. 2. NH_3 to NO conversion efficiency as a function of NH_3 concentration. (XBL 8012-13383)

Table 1. NH_3 Measurements.

			NH_3 (ppm)	
T(K)	ϕ	NO (ppm)	NO_x Method	Phenolate Method
1100	.83	320	677	653
1169	.95	117	318	352
1229	.78	29	340	362
1233	.74	265	27	32
		31	249	274
1235	.73	350	8	12
		49	2	1

should be noted that low (less than 0.1%) concentrations of fuel sulfur did not poison the catalyst.

The third method of analysis employs a specific ion electrode, which uses a hydrophobic gas-permeable membrane to separate the sample from an internal solution. Dissolved ammonia diffuses across the membrane where it can react with the internal solution: $NH_3 + H_2O \leftrightarrows NH_4^+ + OH^-$. The electrode is sensitive internally to the OH^- concentration, which is proportional to the NH_3 concentration in the sample. Ammonia is often collected by bubbling exhaust gases through a weak solution of sulfuric acid. The NH_3 can be collected quantitatively, but the CO_2 that dissolves in the solution can lead to a 20% absolute error in the electrode potential. This is due to two factors: the CO_2 acts as an acid, altering the pH of the solution and the effect of the dissolved species (including HCO_3^- and $CO_3^=$) which changes the ionic strength of the solution, which in turn effects the partial pressure of NH_3. Although this interference may be well known to electrochemists, it has not been characterized for combustion applications. The collection technique developed for the sodium phenolate method works well for the ion analysis and is especially attractive due to the small liquid volumes employed, which reduces the CO_2 interference problem. With no CO_2 interference, the electrode works as well as the sodium phenolate method. However, it suffers from a larger amine interference and is also somewhat plagued by an arduous analytical procedure.

PLANNED ACTIVITIES FOR FY 1981

Techniques for measuring NH_3 in the presence of other nitrogenous species and rich combustion environments will be examined. Hydrogen cyanide detection in combustion exhaust will be measured by at least three techniques: gas chromatography, cyanide specific ion electrodes, and Kitagawa - type gas detectors. Analytical procedures for measuring sulfur compounds in post-combustion environments will also be characterized.

REFERENCES

1. Examples of the techniques used are direct neutralization, infrared analysis using conventional spectrometers and laser diodes, UV absorption, and Nessler tubes.

2. D. Lucas, A. S. Newton, and N. J. Brown, "The Measurement of NH_3 in Combustion Environments." In preparation.

THE SELECTIVE REDUCTION OF NO BY NH_3*

D. Lucas, N. Brown, and R. Sawyer

INTRODUCTION

Photochemical smog, nitrogen dioxide and other potentially harmful nitrogenous species in the atmosphere can be significantly reduced by controlling nitrogen oxide emissions from combustion sources. Different control processes to achieve a reduction in nitrogen oxide emissions are under consideration, including combustion modification and/or staging and the use of low nitrogen content fuels. Other processes, rather than limiting the formation of NO during combustion, allow NO to form and selectively eliminate it through chemical reactions in the post-combustion gases. Our research is concerned with characterizing the selective, homogeneous reaction of NO with NH_3 in the post-combustion environment of prototype oil fuels. The selective reduction was first described by Lyon and Longwell.[1] This approach appears promising because it can be used in a variety of combustion systems and is not dependent upon the formation mechanism of NO.

The reduction of NO by NH_3 is being studied in a laboratory scale combustion tunnel which allows good control over a range of experimental conditions. The tunnel is approximately 3.5 m long, with an internal diameter of 5 cm over most of its length. It consists of three major parts: a combustion section, an ammonia injection region, and a reactor region where the selective reduction occurs. Complete, stable, and reproducible burning of a fuel/oil/air mixture is accomplished in the first section. The fuel, a light diesel oil with a hydrogen/carbon ratio of 1.85, is injected through a high pressure atomizing nozzle into a metered air stream. Rapid mixing and combustion stabilization is accomplished with baffles and blockage disks. Fuel nitrogen is simulated by admixing NO to the air supply or by mixing small amounts of pyridine with the fuel oil. The temperature of the products of combustion exiting this section is controlled by water cooling of the combustor walls, and achieves a specified value T* immediately prior to the ammonia injectors. A mixture of NH_3 and N_2 is introduced through four symmetrically placed quartz injectors and admixed rapidly with the products of combustion. Composition and temperature profiles in both the axial and radial directions are measured in the reactor section. Samples are withdrawn for analysis through quartz sampling probes at four locations downstream of the ammonia injection.

* This work was supported by the U.S. Department of Energy under Contract No. W-7405-ENG-48 and by the California Air Resources Board under Contracts No. A8-146-31 and No. A6-196-30.

Conditions are such that uniform radial composition profiles are obtained quickly, with the NH_3 - NO reaction essentially complete (>95%) by the final probe station. The survival of NO is determined as a function of equivalence ratio, the source and initial concentration of NO, the temperature at the ammonia injection, and the amount of NH_3 added to the combustion gases. Concentrations of CO, CO_2, NO_x, NH_3, HCN, H_2O, and O_2 are measured by a variety of techniques, including continuous gas analyzers, wet chemical methods, and gas chromatographs. The NH_3 concentration remaining after 95% or greater reduction is termed ammonia breakthrough.

ACCOMPLISHMENTS DURING FY 1980

Nitric oxide reduction by NH_3 addition has been studied at three equivalence ratios (ϕ = 0.78, 0.83, and 0.95) as a function of temperature and the amount of added NH_3 ($\beta = [NH_3]_i/[NO]_1$). Figure 1 shows the NO reduction and NH_3 breakthrough measured at a fixed temperature and equivalence ratio. This behavior is observed over the entire range of conditions studied. As more ammonia is injected, more NO reduction occurs, even at β values greater than 4.0. As expected, the ammonia breakthrough increases with increasing β. These results are consistent with previous investigations[2,3,4], despite their use of different fuels and NO sources. No significant difference in the NO reduction was observed when pyridine was burned as the source of NO, rather than directly injecting NO gas into the air supply.

Determination of the temperature at which maximum NO reduction occurs at a fixed equivalence ratio is shown in Figure 2. At a constant ϕ, the

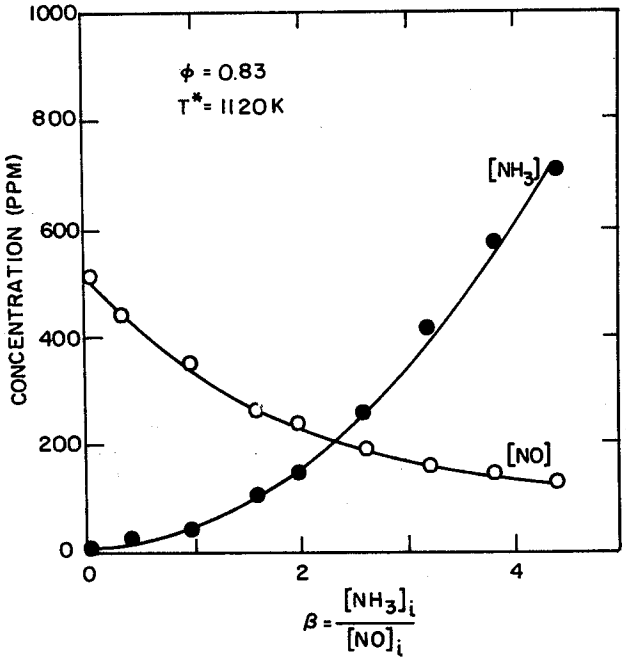

Fig. 1. Nitric oxide and ammonia concentrations as a function of β at a constant temperature equivalence ratio and ammonia injection temperature.
(XBL 8012-13387)

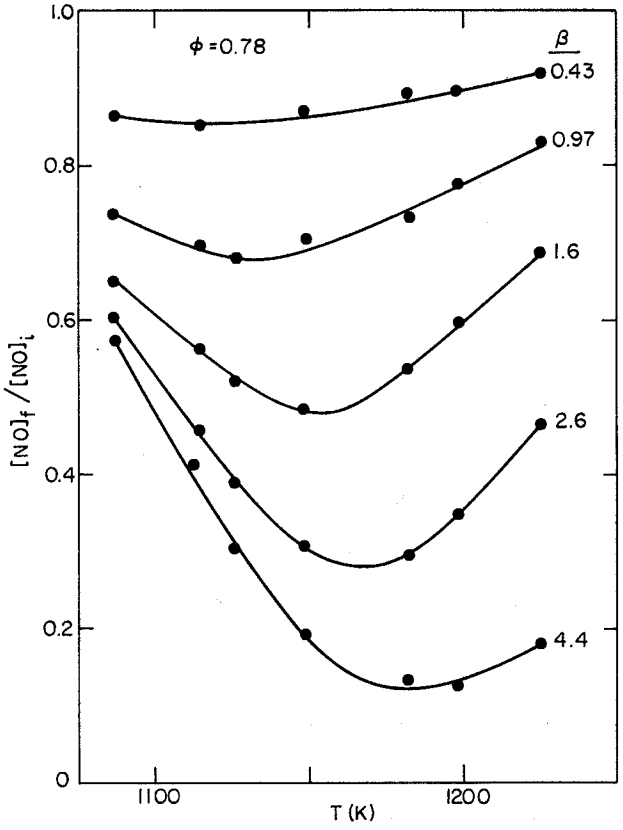

Fig. 2. The NO survival, $(NO)_f/(NO)_i$, as a function of β. The equivalence ratio is 0.78.
(XBL 8012-13384)

temperature for optimum NO reduction increases with increasing β. The relationship between the optimal reduction temperature and β changes when the equivalence ratio is altered, becoming more pronounced at lower levels of ϕ. Additional data also indicate that at a fixed β value, the optimum temperatures increases with ϕ. Our studies indicate that the temperature for maximum NO reduction varies rather significantly from about 1120 K to 1200 K for conditions investigated.

Ammonia breakthrough measurements are presented in Figure 3. It appears that the temperature and the relative amount of NH_3 injected are the only factors that determine the concentration of NH_3 which remains after reaction. The problem of ammonia breakthrough can thus be minimized by operating at conditions of high NH_3 injection temperature and low β values. It should be noted that the importance of the ammonia breakthrough in terms of health and environmental effects has not been established.

Numerous attempts were made to detect and quantify the presence of other "odd nitrogen" species, including NO_2, HCN, and higher amines. With no NH_3 addition, up to 2 parts per million of a nitrogenous compound, presumed to be NO_2, capable of being converted to NO in a stainless steel catalytic converter at 920 C, was observed when the fuel oil was doped with pyridine. However, no HCN or amines were detected by other independent methods at any of the conditions used

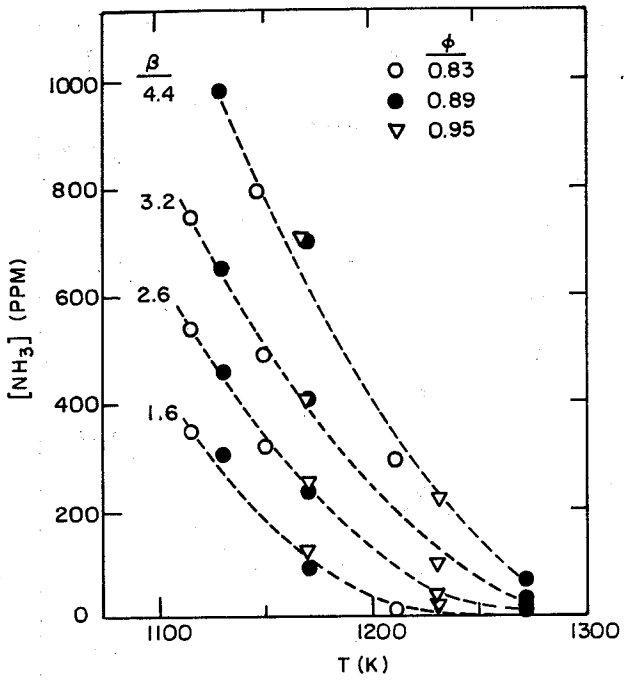

Fig. 3. Ammonia breakthrough measurements as a function of the ammonia injection temperature. (XBL 8012-13385)

in this study. A conservative upper limit of a few parts per million can be set for the total concentration of odd nitrogen species other than NH_3 and NO.

In practical applications, utilization of the selective reduction of NO by NH_3 requires monitoring temperature, excess oxygen, NO, and NH_3 to insure maximum reduction. The trade-off which exists in terms of nitric oxide emissions and ammonia breakthrough necessitates the development of techniques that reliably measure NH_3 in combustion exhaust environments. Another possible alternative is to remove the remaining NH_3 from the exhaust gases, either catalytically or through homogeneous reactions.

PLANNED ACTIVITIES FOR FY 1981

Current research centers on the role of sulfur compounds in the selective reduction of NO. Thiophene and pyridine doped fuel oil will be used as a prototype fuel that contains high concentrations of both fuel nitrogen and fuel sulfur. Analysis of SO_2 in the product gases with a fluorescent detector will help determine if synergistic effects between sulfur and nitrogen compounds are important in the NO reduction process.

REFERENCES

1. R. K. Lyon and J. P. Longwell, "Selective Non-Catalytic Reduction of NO_x with NH_3," EPRI NO_x Control Technology Seminar, San Francisco, California (1976).

2. T. S. Eitzen, N. J. Brown, A. S. Newton, A. K. Gordon, and K. S. Basden, "Characterization of NO_x Removal Through Ammonia Addition," Western States Section, The Combustion Institute Paper No. 79-22 (1979). Also Lawrence Berkeley Laboratory Report LBL-8849 (1979).

3. N. J. Brown, R. F. Sawyer, and T. S. Eitzen, "Characterization Studies of the Selective Reduction of NO by NH_3." Final report submitted to the State of California Air Resources Board. Lawrence Berkeley Laboratory Report LBL-10254 (1979).

4. L. J. Muzio, J. K. Arrand, and D. P. Teixeira, "Gas Phase Decomposition of Nitric Oxide in Combustion Products," Sixteenth Symposium (International) on Combustion, The Combustion Institute, Pittsburgh, 199-208 (1977).

REDUCTION OF NO BY COMBUSTION STAGING*

N. Brown, J. Brunetto, D. Lucas, and R. Sawyer

Combustion sources of the mobile and stationary types are largely responsible for the emissions of the nitrogen oxides, NO and NO_2, into the atmosphere. Two mechanistic paths are responsible for NO production during combustion of lean and near stoichiometric mixtures; one involves the oxidation of atmospheric nitrogen (thermal NO), and the other results in NO production from the oxidation of nitrogen chemically bound to fuel molecules (fuel NO). In the combustion of fuels with nitrogen content in excess of 1% by weight, the two mechanisms contribute equally to NO production. Many coals, coal-derived fuels, and shale oil have nitrogen concentrations in excess of 1%. Reductions of NO emissions from the combustion of high nitrogen content fuels are more difficult to achieve because the fuel and thermal NO formation mechanisms, which operate simultaneously, depend differently on experimental variables (e.g., temperature and residence time).

Staged combustion is an abatement technique that appears capable of achieving significant reductions of NO while also minimizing emissions of criteria and non-criteria pollutants. Staged

* This work was supported by the Assistant Secretary for Fossil Fuels, Office of Utilization of the U.S. Department of Energy under Contract No. W-7405-ENG-48 and by the Morgantown Energy Technical Center of the U.S. Department of Energy under Contract No. PR-14037.

combustion divides the overall combustion process into two or more stages to prevent the formation of noxious pollutants. Experimental variables which differentiate one type of staging from another are: (1) the number of stages, (2) equivalence ratio of each stage, (3) residence time associated with each, (4) fuel properties, and (5) nitrogen content.

Our current research program uses innovative and characterizing staging methods suitable for achieving NO reductions during the combustion of fossil fuels with a significant nitrogen content. The program uses two different kinds of laboratory scale combustion experiments. Staged combustion has been investigated in a combustion tunnel suitable for studying turbulent combustion under a variety of experimental conditions. A fluidized bed combustion facility, under construction, will also be used in staging studies. Additional research effort concerns development of analytical techniques suitable for quantifying pollutant emissions under various experimental conditions. This research is described elsewhere in this report.

ACCOMPLISHMENTS DURING FY 1980

The combustion tunnel used in this research is a turbulent flow reactor capable of supporting three combustion stages. This tunnel, modified during FY80 to achieve complete, stable, reproducible burning of liquid fuel sprays, is illustrated schematically in Figure 1. A pressurized liquid fuel delivery system and a nozzle assembly were installed, and a larger combustion section was added to provide a longer residence time in the first stage. The upstream air supply and exhaust sections are packed with steel wool to eliminate accoustic feedback. Fuel/air mixing is achieved by proper positioning of slotted and perforated disks upstream of the flame. Wrapping the primary combustion section with copper cooling coils provides temperature control in the second and third stages. Radial and axial composition and temperature profile measurements indicate that combustion is steady state and reproducible from day to day. Axial temperature gradients in the second stage are approximately one Kelvin per centimeter.

Nitric oxide reduction has been investigated as a function of first and second stage equivalence ratios and temperature. The first stage is fueled by diesel oil admixed with 7% by volume pyridine; the equivalence ratio of this stage varies between 0.73 and 0.87. Nitric oxide levels in the absence of staging are between 540 and 600 ppm, which corresponds to 50% conversion of the fuel nitrogen to nitric oxide. The second stage fuel, propane, is introduced into the first stage exhaust through four symmetrically oriented quartz injectors. The oxygen concentration, calculated after the first stage has been completed, is used with the added propane concentration to determine the equivalence ratio for the second stage. The first and second stage equivalence ratios are both on the lean side of stoichiometric, and the net equivalence ratio is increased by propane addition. For propane addition, reduction of NO is achieved under certain experimental conditions. Illustrative results are shown in Figure 2. NO reduction is the ratio of final NO concentration with propane addition, $[NO]_f$, to NO concentration without propane addition, $[NO]_i$. This is plotted as a function of second stage equivalence ratio, ϕ_2, for two values of the first stage equivalence ratio, ϕ_i. The reduction in NO achieves an optimum value at a second stage equivalence ratio of 0.4. The reduction of NO by two stage combustion is sensitive to the temperature of the second stage and to the equivalence ratio of both stages.

A major portion of our research effort has been devoted to the design and construction of a fluidized bed combustor. The most basic configuration of a fluidized bed combustor consists of a column into which a porous distributor plate has been fitted with bed material placed above the distributor plate. Fluidizing material, injected into the column below the plate, is forced to flow through the plate and bed. For relatively low flow rates, the viscous forces on the bed particle are overcome by gravitational forces. As the fluid velocity increases, a velocity termed the minimum fluidizing velocity is achieved whereby the two opposite forces on the bed particles are exactly balanced. At velocities in excess of the fluidization velocity, the bed expands and bed particles are free to move relative to one another.

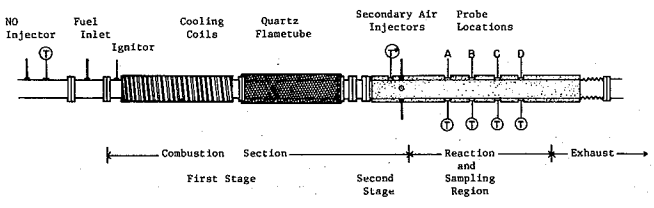

Fig. 1. Schematic diagram of combustion tunnel used for staging studies. (XBL 812-8257)

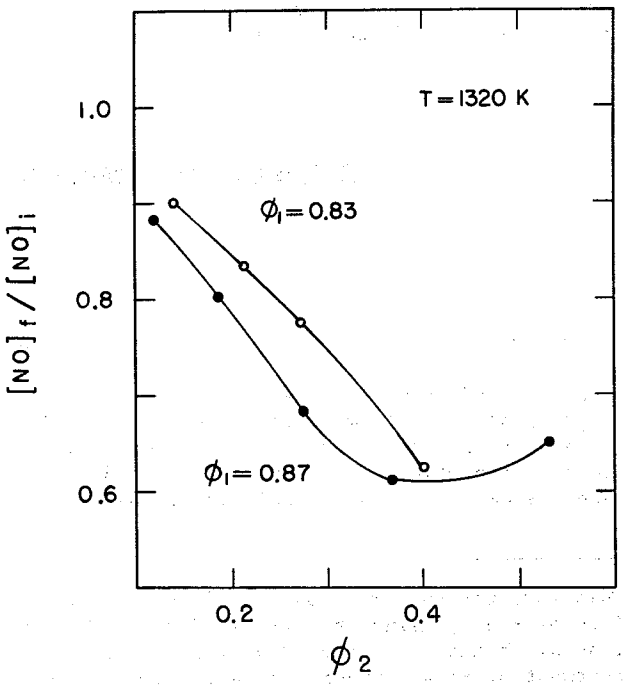

Fig. 2. Nitric oxide reduction as a function of second stage equivalence ratio ϕ_2, for first stage equivalence ratios 0.83 and 0.87. (XBL 812-8265)

Fluidized beds have characteristics which are extremely desirable in combustor design. Three of these (uniform bed temperature, low combustion temperature, and high heat transfer rates) are caused by vigorous mixing in the bed. These characteristics, which render fluidized beds remarkably insensitive to fuel properties, have great potential for reducing pollutant formation during combustion.

A multi-purpose experimental facility has been designed for the study of combustion staging in fluidized and spouted beds. Major design objectives for the facility are: (1) operation in a single, two, or three stage configuration; (2) operation in either a fluidized or spouted mode; (3) access for the insertion of temperature, pressure, and sampling probes; (4) optical access for visual observation and photographic studies, and (5) a simple two-dimensional flow geometry to ease data analysis. Assembly of the laboratory full-scale fluidized bed combustor has been initiated. A plexiglass model of one of the staged fluidized bed reaction sections was constructed and used to obtain cold flow characterization for the various fluidized modes; these are shown in Figure 3, where bed depth is plotted as a function of superficial velocity. The bed can be operated in packed, spouted, bubbling, and fluidized states.

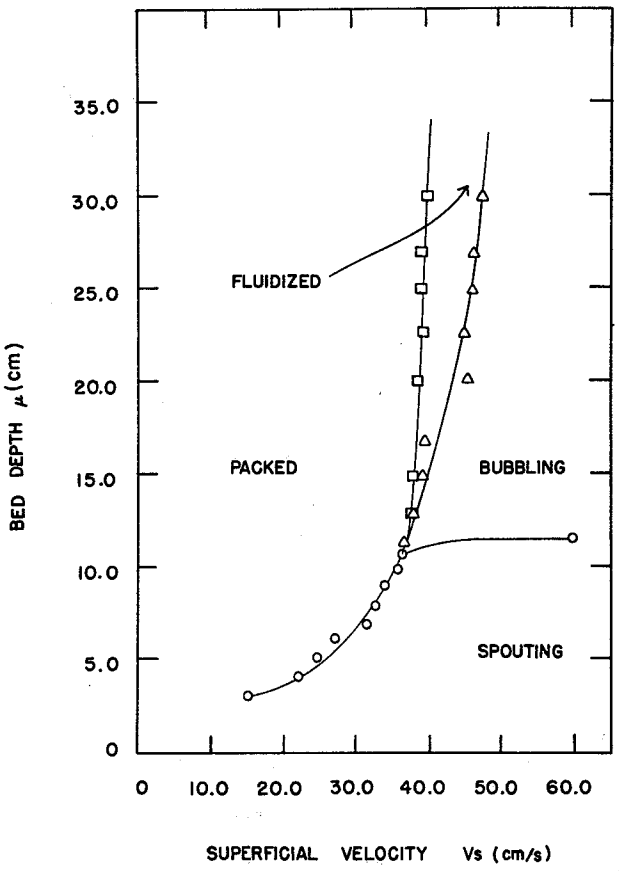

Fig. 3. Bed depth (cm) as a function of superficial velocity (cm/s) for cold flow characterization experiments. (XBL 812-8264)

PLANNED ACTIVITIES FOR FY 1981

Two types of staged combustion experiments (lean/lean and rich/lean) will be performed in the tunnel for two stages. The net equivalence ratio will be less than one (fuel lean). Propane will be mixed with variable amounts of simple nitrogen and sulfur compounds to simulate fuel nitrogen and fuel sulfur. The following compounds will be routinely measured: O_2, CO, NO, CO_2, SO_2, HCN, NH_3, and unburned hydrocarbons. Construction of the fluidized bed combustor will be finished, and characterization studies of cold and hot flow will be completed, using propane and propane doped fuels. Modelling studies of zero dimensional kinetics will be undertaken for nitric oxide reduction by staged combustion.

COLLISION DYNAMICS STUDIES OF HO_2 DISSOCIATION*

N. Brown and J. Miller†

INTRODUCTION

A detailed understanding of the kinetics of the hydrogen/oxygen flame system over a range of temperatures and densities typical of combustion systems is important. Reactions of the hydrogen/oxygen system play a unique role in combustion chemistry because they are sub-reactions in all hydrocarbon oxidation schemes. The specific chemistry of the radical species HO_2, which is formed as an intermediate during oxidation, is important in understanding: (1) ignition limits, (2) chain-branching, (3) heat release, and (4) radical shuffling mechanisms in combustion systems.

Our current research is concerned with investigating unimolecular reactions important to combustion processes. We are specifically interested in acquiring a better understanding of intramolecular energy transfer that dominates high pressure limit kinetics and is important in determining fall-off behavior. The existence of a realistic potential energy surface for the HO_2 molecule has provided us with a rather unique opportunity

* This work was supported by the Director of the Office of Energy Research, Office of Basic Energy Sciences, Chemical Sciences Division of the U.S. Department of Energy under Contract No. W-7405-ENG-48.

† Combustion Research Facility, Sandia National Laboratory, Livermore, CA

to investigate the statistical nature of intramolecular energy transfer in HO_2 for molecular energies in excess of the OH bond dissociation energy. This is important because advanced theories describe unimolecular reactions such as the RRKM[1] and adiabatic channel model[2] theories. These theories are based primarily on statistical approximations, and their success as a predictive tool depends greatly on the validity of these approximations.

ACCOMPLISHMENTS DURING FY 1980

Classical dynamics calculations were performed to investigate the dissociation reaction $HO_2 \rightarrow H + O_2$ at a fixed total energy in excess of that required to break the OH bond. The potential energy surface used to investigate HO_2 dissociation by intramolecular energy transfer is the analytical representation of the $^2A''$ state of HO_2 given by Melius and Blint[3] in their initial calculations. The $^2A''$ correlates with $H(^2S)$ and $O_2(^3\Sigma g)$ and is 17 kcal/mol below $HO_2(^2A')$. This surface has been used by Miller[4] to compute the thermal rate coefficient of the $H + O_2 \rightarrow OH + O$ reaction; the calculated results agree well with experiment results. Initial conditions for trajectory calculations were determined by Monte Carlo sampling the twelve dimensional phase space of the excited (above threshold) HO_2 molecule. A sampling technique used is similar to the Bunker[5] orthant sampling method and is suitable for averaging over sample sizes smaller than the number of orthants (2^{12}).

Dissociation times are defined as the time required to cross a 2.1 kcal/mol energy barrier in the exit channel separating $H + O_2$ from HO_2 on the surface. Fifty picoseconds are allocated for dissociation of each trajectory and those which did not dissociate in this time are deemed non-reactive. At the end of each reactive trajectory, the energy and angular momentum distributions in the products are determined. Final state attributes of several trajectories at a fixed total energy are histogrammed to verify whether the reaction was statistical.

Several interesting results emerge from our calculations. Figure 1 illustrates the distribution of reaction times for a sample of 355 trajectories at a total energy of 55 kcal/mol (approximately 10 kcal/mol above threshold). Also shown is a curve indicative of a random lifetime distribution:

$$\rho(t) = ke^{-kt}$$

where

$$\rho(t) = \frac{N}{N_0 \Delta t} \quad .$$

The rate coefficient and time are designated by k and t, respectively. The number of lifetimes, N, in each category is normalized by $N_0\Delta t$ where N_0 is the total number of trajectories and Δt is the lifetime interval width. Two features of Figure 1 indicate non-statistical, non-RRKM behavior. First,

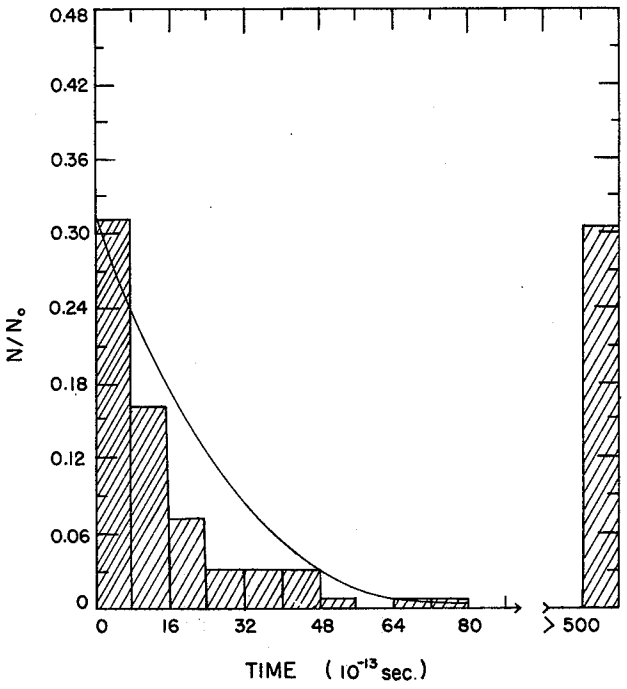

Fig. 1. Distribution of reaction times at a total energy of 55 kcal/mol. Solid curve represents random time distribution, histogram indicates calculated results. (XBL 814-9402)

only two-thirds of the trajectories are reactive in a fifty-picosecond time interval. Second, there are too few reactions at short reaction times and thus departures from the random distribution. This intrinsic non-RRKM behavior occurs when transitions between two or more vibrational states are slower than transitions leading to products. This is often the case when two vibrations have markedly different vibrational frequencies and is a manifestation of a light/heavy atom effect. It is possible that these long lived vibrational states may be characterized by quasi-periodic motion that persists over times of the order 10^{-10} sec and whose periodicity is energy dependent.

The distribution of final relative translational energy of the products H and O_2 is plotted in Figure 2 for reactive trajectories at 55 kcl/mol. This distribution is also markedly different from one predicted by an RRKM theory, which is a decaying exponential. Departures from non-RRKM translation energy distributions often indicate exit channel coupling effects. All reactive trajectories have final relative translational energies in excess of 2 kcal/mol; this indicates that energy requisite for surmounting the 2 kcal/mol energy barrier is released to the translational degrees of freedom and not to the internal energy of the O_2 molecule.

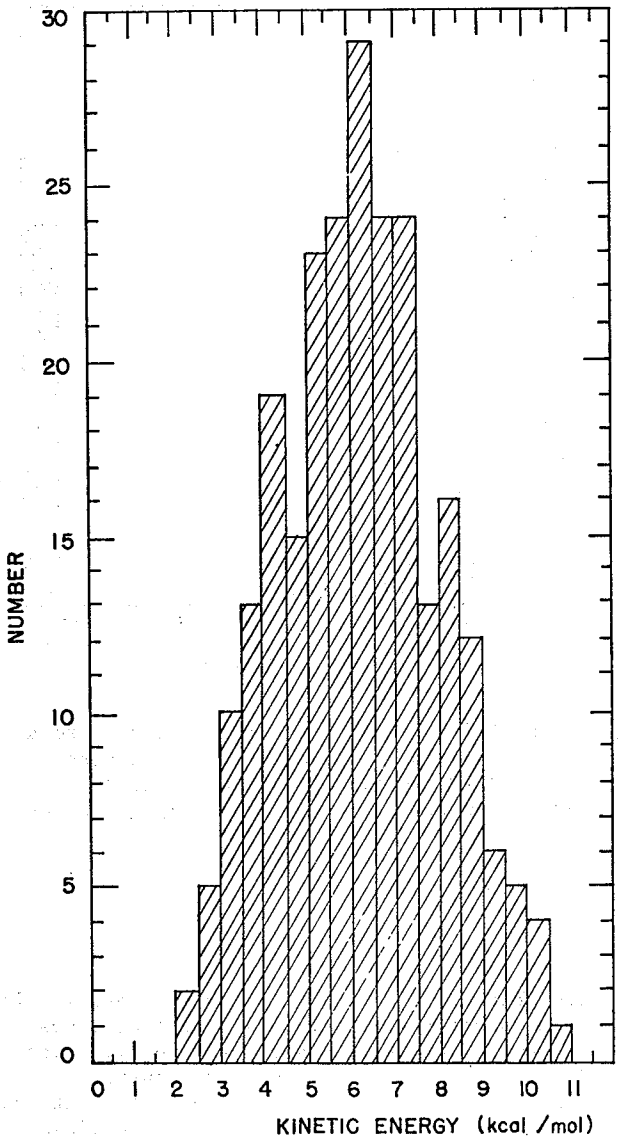

Fig. 2. Distribution of final relative translational energy for reactive trajectories at 55 kcal/mol. (XBL 812-8262)

PLANNED ACTIVITIES FOR FY 1981

Various techniques used to sample the 12 dimensional phase space will be compared, and criteria for determining whether or not sampling is representative will be developed. The effect of angular momentum on the reactivity of HO_2 will be investigated in detail. The fixed energy will be varied to provide additional reaction paths which, in turn, will be characterized. The most exciting aspect of our new work will also involve an in depth study of the non-reactive trajectories and a determination of their quasi-periodic nature. We will also study the dissociation of DO_2. Direct comparison of results obtained from dynamics studies will be compared with the results from statistical theories, whenever possible.

REFERENCES

1. R. A. Marcus, "Unimolecular Dissociations and Free Radical Recombination Reactions," J. Chem. Phys., vol. 20, p. 359 (1952).

2. M. Quack and J. Troe, "II Adiabatic Channel Model," Ber. Bunsenges. Phys. Chem., vol. 78, p. 240 (1974).

3. C. F. Melius and R. J. Blint, "Potential Energy Surface of the HO_2 Molecular System," Chem. Phys. Lett. vol. 64, p. 183 (1979).

4. J. A. Miller, "Collision Dynamics and the Thermal Rate Coefficient for the Reaction $H + O_2 \quad OH + O$," accepted for publication J. Chem. Phys. (1981).

5. D. L. Bunker, "Monte Carlo Calculations. IV Further Studies of Unimolecular Dissociation," J. Chem. Phys., vol. 40, p. 1946 (1964).

STATISTICAL THEORIES OF UNIMOLECULAR REACTIONS*

N. Brown and Abdel Hafez

INTRODUCTION

Recombination, dissociation, and isomerization reactions are classified as unimolecular reactions; these are important at various stages of combustion processes. The kinetics of unimolecular reactions are second order at low pressure where the reaction is rate-limited by the intermolecular transfer of energy. At the so-called high pressure limit, kinetics are first order and are limited by the rate of intramolecular energy transfer. The pressure associated with the high pressure limit is inversely related to molecular complexity and becomes higher as temperature increases. Kinetics in pressure regimes between the two limits, the so called fall-off regime, are influenced by both intermolecular and intramolecular energy transfer.

* This work was supported by the Director of the Office of Energy Research, Office of Basic Energy Sciences, Chemical Sciences Division of the U.S. Department of Energy under Contract No. W-7405-ENG-48.

There have been numerous attempts to describe unimolecular reactions theoretically; the most notable of these is the RRKM[1] theory. Although RRKM theory is often quite satisfactory for the prediction of rate coefficients for certain types of reactions, it is particularly poor for determining rate coefficients for simple bond fission reactions. Because these reactions lack a maximum in the electronic potential energy surface in the region of configuration space between reactants and products, it is difficult to describe the fixed activated complex which is implicitly assumed in RRKM theory. The RRKM theory is also deficient in its treatment of angular momentum effects. A more recent theory, the so-called phase space theory of Pechukas and Light [2], provides an improved treatment of angular momentum coupling but often overestimates rate coefficients. Reasons for the latter difficulty are not known although they are probably related to the loose transition state assumption.

Our current research is concerned with the improvement and application of statistical theories to the study of dissociation and recombination reactions of triatomic molecules: HO_2, H_2O, H_2S, SO_2, and $C\ell NO$. We compute the rate coefficients k (E,J) as a function of energy, E, and total angular momentum, J. This is appropriate for describing dissociation kinetics at the high pressure limit and is a major ingredient of the unimolecular rate coefficient in the intermediate fall-off regime. The number of states of the activated (energized above threshold) molecule and the density of states of the reactant molecule are determined and their ratio is proportional to k (E,J).

We are presently using the adiabatic channel model of Quack and Troe[3] and our own modification of the adiabatic channel theory. Adiabatic theories of reaction are characterized by the existence of so-called good quantum numbers which remain unchanged during the course of reaction. In triatomic dissociation reactions, the vibrational degree of freedom, termed the symmetric stretch, is considered adiabatic. Quantum numbers associated with the transition from bending vibration to hindered rotation to free rotation of the fragments which occurs during reaction are not good quantum numbers, and the degrees of freedom associated with these are termed diabatic. One degree of freedom is selected as a reaction co-ordinate, and the energy associated with the other degrees of freedom depends parametrically on the value of the reaction co-ordinate. We then compute the energy levels or channels of the energized molecules as a function of reaction co-ordinate and consistent with conservation constraints and adiabaticity. The energy terms in the energy channel expressions are of the following types: electronic, ro-vibrational, centrifugal energy, and zero point energy terms. The channel energies depend on the reaction coordinate through an exponential interpolation formula which connects reactant and product energy levels. A channel is open at a given energy, E, if the maximum energy of the channel is less than E. The number of open channels, W (E,J), is computed by determining channel maxima for those states of fixed, total-angular momenta and comparing the channel maxima with the total energy to determine whether the channels are open. The rate coefficient k (E,J) is computed according to

$$k(E,J) = \frac{W(E,J)}{h\,\rho(E,J)}$$

where h is Plancks constant and $\rho(E,J)$ is the density of states of the reactant molecule. The thermal rate coefficient k(T) is obtained by averaging k(E,J) over energy and angular momentum distributions.

ACCOMPLISHMENTS DURING FY 1980

We have successfully computed micro-canonical and canonical rate coefficients for reactions of triatomic molecules which dissociate into radical fragments. The rate coefficients, k(E,J), for the reaction $C\ell NO \rightarrow C\ell + NO$ is plotted in Figure 1 as a function of total energy above threshold ($E - V_o^\infty$) for three values of total angular momentum. It is interesting to note that the dependence of the rate coefficient on total angular momentum changes with energy. An Arrhenius plot of a thermally averaged rate coefficient for the same reaction is shown in Figure 2. These results agree with those of Quack and Troe[3]. A new expression for the evaluation of channel energies has been determined which, hopefully, will better describe triatomic molecule dissociation reactions.

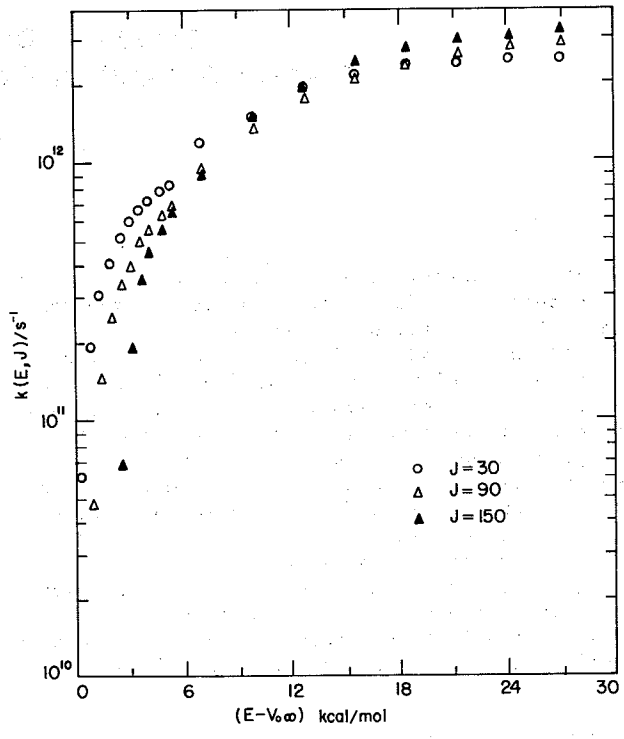

Fig. 1. Rate Coefficient k(E,J) in units of reciprocal seconds for the reaction $C\ell NO \rightarrow C\ell + NO$ as a function of energy above threshold, ($E - V_o$) in (kcal/mol) for three values of total angular momentum. (XBL 812-8261)

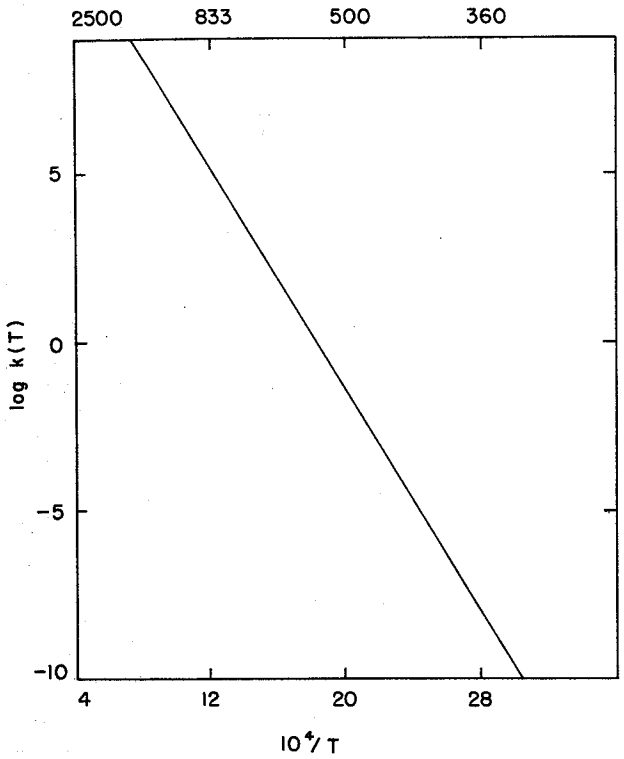

Fig. 2. Arrhenius plot of thermal rate coefficient (s^{-1}) for the reaction $C_2NO \rightarrow C_2 + NO$. Temperature, T, is in degrees Kelvin. (XBL 812-8260)

PLANNED ACTIVITIES FOR FY 1981

Revised and regular adiabatic channel model calculations will be performed to determine microcanonical and canonical rate coefficients for HO_2, H_2O, H_2S, and SO_2. Sensitivity of computed results to energy level expressions and parameter dependence will be examined in detail. Adiabatic channel model results will be compared with experiment and with a minimum number of states calculation which properly describes angular momentum coupling.

REFERENCES

1. R. A. Marcus, "Unimolecular Dissociations and Free Radical Recombination Reactions," J. Chem. Phys., vol. 20, p. 359 (1952).

2. P. Pechukas and J. C. Light, "On Detailed Balancing and Statistical Theories of Chemical Kinetics," J. Chem. Phys., vol. 42, p. 3281 (1965).

3. M. Quack and J. Troe, "II Adiabatic Channel Model," Ber. Bunsenges. Phys. Chem., vol. 78, p. 240 (1974).

COMBUSTION DIAGNOSTICS BY TUNABLE ATOMIC LINE MOLECULAR SPECTROSCOPY*

E. Cuellar and N. Brown

INTRODUCTION

The characterization of emissions produced in the combustion of fossil fuels plays an important role in the utilization of energy resources. A detailed understanding of the chemistry of the combustion of sulfur containing fuels is of great importance, because sulfur, in the form of organic and inorganic compounds, can account for a significant proportion of the fuel mass. Corrosion in power plants due to sulfuric acid, atmospheric pollution by oxides of sulfur, and acid rain represent enormous problems which can seriously limit the full utilization of fossil fuels. Although much is known about the combustion chemistry of sulfur containing compounds[1], a basic mechanistic understanding of all of the decomposition and combustion reactions of even relatively simple molecules, such as H_2S or CS_2, is not yet available. Furthermore, the combustion kinetics of organic sulfur compounds, such as heterocyclic rings, is virtually unknown.

The principal sulfur containing product formed in the combustion of sulfur compounds is sulfur dioxide (SO_2). In addition to SO_2, numerous other sulfur containing species, e.g., SH, S_2, SO, H_2S are present in flames in significant proportions. Their identification and measurement is clearly of great importance if a detailed kinetic understanding of sulfur chemistry is to be obtained.

We present here results obtained with a new optical technique for measuring concentrations of species such as might be present in a combustion environment. This technique, called Tunable Atomic Line Molecular Spectroscopy (TALMS), is a line of sight, incoherent absorption technique which is highly sensitive and selective. TALMS is based on the Zeeman effect, which permits magnetic tuning of an atomic line into resonance with a molecular absorption[2]. Atomic absorption spectroscopy based on the Zeeman effect has been used in the analytical determination of numerous atomic species[3] and

* This research was supported by the Assistant Secretary for Environment, Office of Environmental Compliance and Overview, Environmental Safety and Engineering Division of the U.S. Department of Energy under Contract No. W-7405-ENG-48.

was recently extended to the detection of small molecules which exhibit sharp rotational electronic structure, e.g., NO (Reference 4) and SO_2 (Reference 5). We have applied this technique to the detection and measurement of S_2 formed in the equilibrium vapor of elemental sulfur and from the thermal decomposition of H_2S.

RESEARCH METHODS

A detailed description of the application of the Zeeman effect to atomic absorption spectroscopy has appeared elsewhere[6] and will be reviewed only briefly here. In the presence of an external magnetic field, atomic energy states which give rise to spectral lines may be split into new states by the Zeeman effect. Transitions between these new states produce an emission pattern with components which are not shifted (or shifted slightly) from the zero-field value ν_o of the transition (the π components), and components which are shifted symmetrically to lower and higher energies about ν_o (the $\sigma\pm$ components). Besides differing in frequency, the π and $\sigma\pm$ components also differ in their polarization.

The splitting of spectral lines produced by the magnetic field and the polarization of these lines form the basis for the detection of molecules by TALMS. By varying the strength of the magnetic field, one of the Zeeman components of the atomic emission line is tuned into exact coincidence with a sharp vibrational-rotational transition in the electronic absorption spectrum of the molecule to be detected; the other component is shifted off resonance. The matching component indicates the extent of absorption by the molecule of interest plus any background absorption due to other species present. The unmatched Zeeman component indicates background absorption only. A differential measurement of the absorption of the matched and unmatched components provides a quantitative measurement of the molecule to be detected.

Detection of S_2 and Magnetic Field Dependence

The electronic spectrum of S_2 has been extensively studied both in absorption and emission[7]. Particular attention has been devoted to the $B^3\Sigma_u^- \leftarrow X^3\Sigma_g^-$ system, extending from 2500 to 7000 Å and containing hundreds of bands which are resolved into rotational electronic transitions. The emission spectrum of chromium was selected as a good candidate for the detection of S_2, principally because there are several intense atomic lines around 3000 Å,[8] and the emission spectrum was easy to excite in a reasonably stable manner. Furthermore, SO_2, which is the principal sulfur-containing product in the combustion of sulfur compounds, absorbs in the region of 3000 Å; and selection of an atomic transition in this region would test the ability to detect S_2 in the presence of SO_2.

Several different cathode materials were used to produce the emission spectrum of chromium. Best results were obtained by spot welding several turns of nichrome tape (Tophet C, 16% Cr, 60% Ni, and 24% Fe) to the tip of the cathode, thus exciting the emission spectra of Ni, Cr, and Fe simultaneously. In this manner, relatively stable discharges could be obtained over a period of 2 to 4 hours.

Figure 1 shows the differential absorption signal obtained due to the matching of the atomic emission lines with individual S_2 molecular absorptions. The lower trace represents a section of the emission spectrum, while the upper trace, recorded simultaneously, is the output of the lock-in amplifier. The dotted lines between the two curves show that several atomic emission lines, each split into its own Zeeman pattern by the external magnetic field, give rise to differential absorption signals corresponding to a match of the Zeeman components of each line with a molecular absorption of S_2. Although any one of the matching lines (from Fe or Cr) could be used to detect S_2, we selected the Cr (I) line at 3018 Å because of its higher relative intensity. This Cr (I) emission line was assigned to the transition $^5D_3 \leftarrow {}^5F_4{}^0$ at 3017.57 Å (33,129.6 cm^{-1} vac.)[9].

The dependence of the differential absorption signal caused by S_2 on the strength of the external magnetic field is shown in Figure 2. As the field is increased from 2.5 kG, the signal decreases and passes through zero at about 8 kG. Increasing the field strength further results in differential absorption signals opposite in sign to those obtained at lower fields. This change in

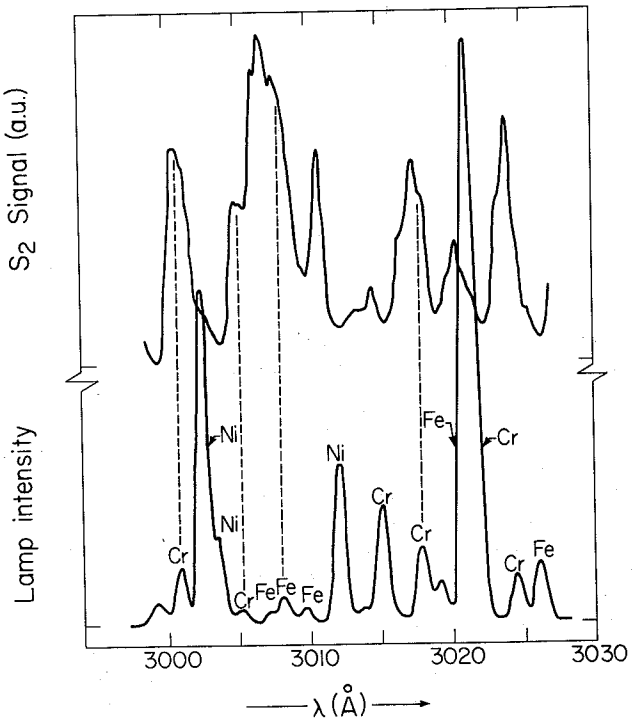

Fig. 1. The lower trace is a scan of the emission spectrum of nichrome tape. The upper trace monitors the differential absorption signals due to matching of the Zeeman split atomic emission lines with different molecular absorptions of S_2 (see text). Care must be taken to distinguish true differential absorption signals from excursions of the lock-in amplifier when the light intensity is near zero. (XBL-809-2034)

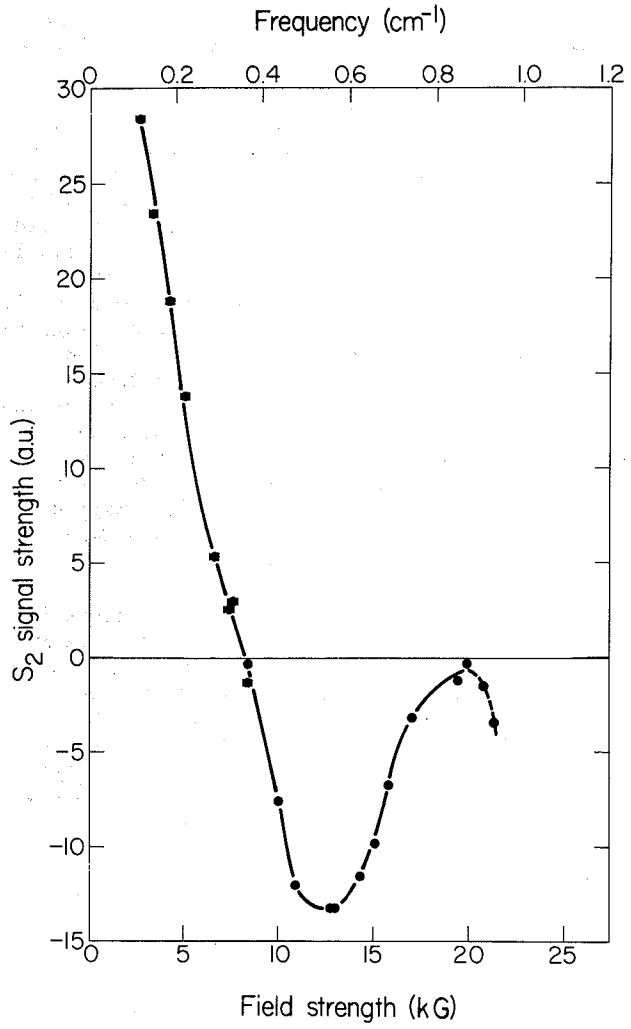

Fig. 2. Differential absorption signal due to S_2 as a function of the strength of the external magnetic field. $\Delta V_s = 0.0438\ cm^{-1}/kG$.
(XBL 809-2038)

polarity implies that at lower field strengths, one of the circularly polarized Zeeman components of the Cr (I) line, $\sigma+$ or $\sigma-$, is in resonance with a molecular absorption of S_2, while, at higher fields, this component falls off resonance while the other σ component tunes into a different absorption of S_2. Furthermore, the increasing positive signals observed at the lowest field strengths, where the separation between the + and - components is small, suggest that the center of the S_2 absorption which results in this positive signal is very close in frequency to the frequency of the zero field transition of the Cr (I) atomic line at 3018 Å. To interpret further the dependence of the S_2 absorption signals on the magnetic field strength, it is necessary to examine the spectroscopy of the $B^3\Sigma_u^- - X^3\Sigma_g^-$ system of S_2 in more detail.

Triplet Splitting of S_2

Frequencies for electronic transitions between individual rotational states within each vibrational manifold of S_2 were calculated using spectroscopic constants given by Huber and Herzberg [10]. As a first approximation, the finer details (due to electronic spin) of the rotational electronic structure of $^3\Sigma$ states were ignored and the rotational ladder within each vibrational level was considered to consist of single rotational levels for each value of K, the quantum number for total rotational levels for each value of K, the quantum number for total rotational angular momentum excluding spin. From this initial calculation, the frequency of the Cr (I) transition at 33,129.6 cm^{-1} could overlap with a low K line in the v', v" = 7, 2 band or with a high K (K ~ 60) line in the (4,0) band. Because S_2 is a homonuclear diatomic molecule and the nuclear spin of the ^{32}S nucleus is zero, even numbered K states are missing in the $X^3\Sigma_g^-$ state, and odd numbered K states are missing in the $B^3\Sigma_u^-$ state.

The rotation of the nuclei couples with the motions of the electrons (including spin) in a manner which increases the complexity of the energy level diagram of S_2. This coupling, plus the interaction between spins, splits each level given by the quantum number K into three levels, F_1, F_2, and F_3, with J = K + 1, K, and K - 1, respectively, where J is the total angular momentum, including spin.

The resulting energy level diagram for a value of K" = 13 in the (7,2) band of S_2 is shown in Figure 3. The transitions allowed for these

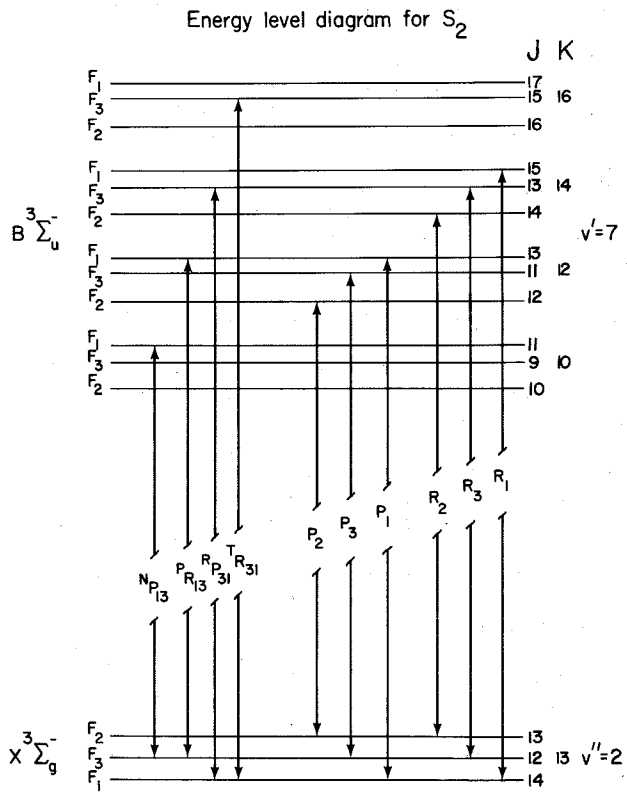

Fig. 3. Triplet splitting of the rotational levels of S_2. The v" = 2 level is normal while the v' = 7 level is inverted. The six main branches ($\Delta K = \Delta J$) and four satellite branches ($\Delta K \neq \Delta J$) are shown for K" = 13. The Cr (I) emission overlaps the $P_3(13)$ line. (XBL 809-2024)

triplet split states are also shown. There are six main branches which have $\Delta K = \Delta J$. These are indicated by $R_i(K)$ and $P_i(K)$, where i indexes the F_i levels involved. There are also four weaker satellite branches for which $\Delta K \neq \Delta J$: $^{T}R_{31}$, $^{N}P_{13}$, $^{R}P_{31}$, and $^{P}R_{13}$.

Frequencies for the six main branches and four satellite branches were calculated for K" = 1 to 60 using the expressions for F_1, F_2, and F_3.[11] Details of this calculation can be found in Reference [6]. The interpretation of the magnetic field dependence (Fig. 2) is shown in Figure 4. The Cr (I) atomic emission line at 3017.57Å (33,129.6 cm $^{-1}$ vac.) is nearly resonant with the P_3 (13) branch of S_2, calculated at 33,129.7 cm^{-1}. At a field strength of 2 kG, the differential absorption is dominated by the σ- component, resulting in the large positive signal observed in Figure 2. As the field increases, the σ- and σ+ components spread apart and begin to overlap two other branches of S_2, R_2 (13) and R_1 (21), at 33,129.3 and 33,130.0 cm^{-1} respectively. At ~8 kG, the σ- and σ+ components overlap these two branches approximately equally, and, therefore, there is no differential absorption signal. Both of the σ components are attenuated equally by different S_2 absorptions. As the field increases to 13 kG, the σ- component moves off resonance from the

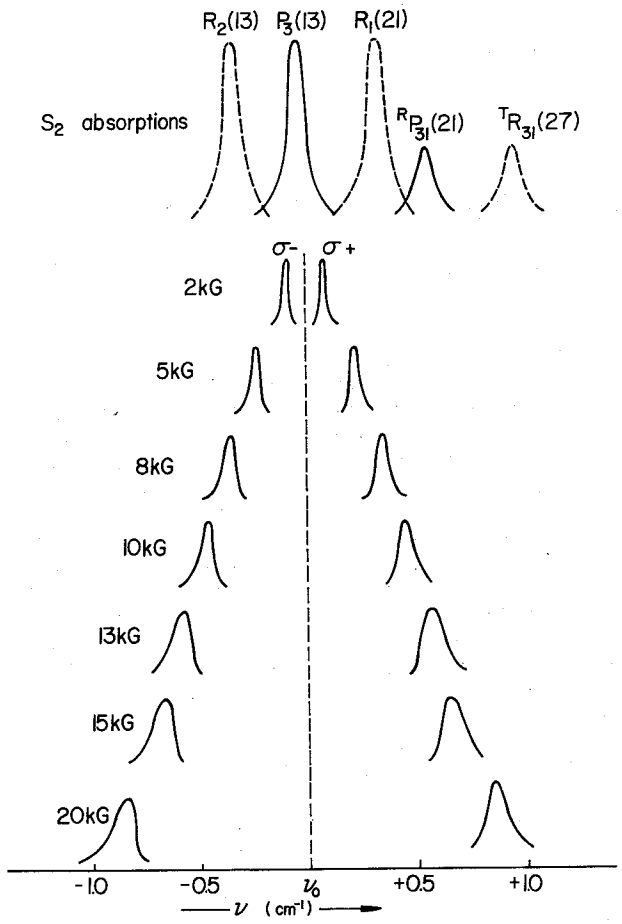

Fig. 4. Interpretation of the differential absorption signal for S_2 as a function of increasing magnetic field. (XBL 809-2031)

R_2(13) branch while σ+ overlaps the satellite branch $^{R}P_{3_1}$(21) at 33,130.2 cm^{-1}, resulting in a negative absorption signal. The roles of σ- and σ+, as monitors of S_2 and of background are reversed. Therefore, the polarity of the observed S_2 differential absorption signal is also reversed. As the field is increased further to 20 kG, the low frequency σ- component remains off resonance with any of the rotational branches of S_2 (the next branch is calculated to be $^{N}P_{13}$ (9) at 33,127.9 cm^{-1}), while σ_+ begins to overlap $T_{R_{31}}$ (27) at 33,130 cm^{-1}. This overlap results again in an increasing negative differential absorption signal.

CONCLUSIONS

The technique of TALMS has been applied to the detection of the molecule S_2. An atomic transition in the emission spectrum of Cr (I) at 3017.57Å was found to be resonant with a rotational electronic absorption of S_2. By scanning the magnetic field from 0-20 kGauss, it is possible to map out several discrete absorptions of S_2 belonging to the v' = 7 ← v" = 2 band in the $B^3\Sigma_u^- \leftarrow X^3\Sigma_g^-$ system. These absorptions are identified as branches arising from the triplet splitting of the rotational states of S_2. It is interesting that rotational analyses for (v',v") bands of S_2 generally resolve only the main P and R branches, even with the use of high dispersion (~0.008 Å/mm) vacuum spectrographs. The weaker satellite branches have been detected only in fluorescence experiments, where a particular v', J' level is selected for excitation. It is remarkable that very high resolution, better than 6 x 10^4, is possible using the TALMS technique.

PLANNED ACTIVITIES FOR FY 1981

A major effort in FY81 will be devoted to the application of the TALMS technique to the measurement of NO and NO_2 in a CH_4 - air flat flame burner. The flat flame burner has been characterized, and the thermal NO produced can be compared with the results obtained using a chemiluminescent analyzer. A thorough study of the problem of third body quenching in the chemiluminescent analyzer will be conducted.

We will continue our efforts to develop techniques for detecting and measuring small molecules such as NH_3 and SO_2, in combustion environments. An atomic emission line in the spectrum of arsenic was recently found to be nearly resonant with an electronic transition of NH_3[12]. A weak differential absorption signal was observed using the TALMS technique, and further work will be required to improve the detection capability. SO_2 has been detected using a Zn line at 213.8 nm[5]. We propose to compare this optical technique with the conventional probe measurements of SO_2 using a commercial pulsed fluorescence SO_2 analyzer. A very significant problem associated with these SO_2 analyzers is the necessity to remove water from the sample gas and to make large corrections for third body quenching.

REFERENCES

1. C. F. Cullis and M. F. R. Mulcahy, "The Kinetics of Combustion of Gaseous Sulphur

Compounds," Comb. and Flame, vol. 18, p. 225 (1972).

2. H. Koizumi, T. Hadeishi, and R. D. McLaughlin, "Detection of Small Molecules by Magnetically Tuned Frequency-Modulated Atomic Line Sources," Appl. Phys. Lett. vol. 34, p. 382 (1979).

3. See for example T. Hadeishi and R. D. McLaughlin, "Hyperfine Zeeman Effect Atomic Absorption Spectrometry for Mercury," Science (London), vol. 174, p. 404 (1971); H. Koizumi and K. Yasuda, "An Application of the Zeeman Effect to Atomic Absorption Spectrometry: A New Method for Background Correction," Spectrochim. Acta Part B, vol. 31B, p. 237 (1976); H. Koizumi and K. Yasuda, "A Novel Method for Atomic Absorption Spectroscopy based on the Analyte Zeeman Effect," Spectrochim. Acta B, vol. 31, p. 523 (1977); Hideaki Koizumi and Kazuo Yasuda, "Determination of Lead, Cadmium, and Zinc Using the Zeeman Effect in Atomic Absorption Spectrometry," Anal. Chem., vol. 48, p. 1178 (1976).

4. H. Koizumi, T. Hadeishi, and R. D. McLaughlin, "A New Technique for the Determination of Isotopic Species Using Zeeman Scanning of an Atomic Line," Appl. Phys. Lett., vol. 34, p. 277 (1979); H. Koizumi, Tetsuo Hadeishi, and R. D. McLaughlin, "Nitric Oxide Determination by a Zeeman-Tuned Frequency-Modulated Atomic Line Source," Anal. Chem., vol. 52, p. 500 (1980).

5. H. Koizumi, T. Hadeishi, and R. D. McLaughlin, "Determination of SO_2 by a Zeeman Shifted Atomic Line," Anal. Chem. (to be published).

6. E. Cuellar, Detection of S_2 by Tunable Atomic Line Molecular Spectroscopy, Lawrence Berkeley Laboratory Report LBL-11323 (1980).

7. R. F. Barrow and R. P. du Parcq, in Elemental Sulfur (Beat Meyer, ed.), John Wiley and Sons, New York (1965), and references cited therein.

8. J. Reader and C. H. Corliss, "Line Spectra of the Elements," Handbook of Chemistry and Physics, 60th edition, CRC Press, Boca Raton, Florida (1979-1980).

9. J. Sugar and C. H. Corliss, "Energy Levels of Chromium, Cr I through Cr XXIV," J. Phys. Chem. Ref. Data, vol. 6, p. 317 (1977).

10. K. P. Huber and G. Herzberg, Molecular Spectra and Molecular Structure IV. Constants of Diatomic Molecules, Van Nostrand Reinhold Co., New York (1979).

11. G. Herzberg, Molecular Spectra and Molecular Structure I. Spectra of Diatomic Molecules, Van Nostrand Reinhold Co., New York (1950).

12. E. Cuellar, unpublished results.

SUBMICRON PARTICULATES FROM PULVERIZED COAL COMBUSTION*

J. Pennucci, R. Greif, G. Parsons, F. Robben, and P. Sherman

INTRODUCTION

During the combustion of pulverized coal, the bulk of the mineral matter is converted to fly ash. A fraction of the mineral matter may be vaporized and subsequently condense, either on existing particles or by forming new particles by the process of homogeneous nucleation.[1] The latter process results in a large number of particles in the size range 0.005 to 0.1 microns diameter; the size of typical ash particles is from 2-50 microns. Because of their small size, the submicron particles do not contribute substantially to the total mass of fly ash and may be overlooked. However, they can be a significant fraction of the total number of particles produced.

The submicron particles are most easily ingested into the lungs and may be a significant health hazard. Further, there is evidence that certain toxic trace elements are concentrated in the submicron particles, creating a greater health hazard than their prevalence would indicate.[2] Electrostatic precipitators and other cleanup devices effectively remove large particles, but their efficiency decreases for small particles, enabling them to pass into the atmosphere. Because the mineral matter in the coal is necessarily converted to ash during combustion, it is preferable that the ash particles be large to reduce their health hazard and to ease their removal from the stack gases.

This work consists of an experimental study of the effect of heat transfer and combustion parameters on the number and size distribution of particles in the submicron range and includes consideration of practical methods for control of the particles. The parameters studied are the flame temperature, cooling rate, and oxygen concentration in the fuel lean range. Peak temperatures have been varied from 1900 K to 2500 K. By changing the thermal resistance of the burner chimney

* This work was supported by the Assistant Secretary for Environment, Office of Environmental Research and Development, Environmental and Safety Engineering Division of the U.S. Department of Energy under Contract No. W-7405-ENG-48.

wall, cooling rates of 4000 KS^{-1} and 7000 KS^{-1} were obtained during the primary cooling period.

ACCOMPLISHMENTS DURING FY 1980

Details of the burner geometry are shown in Figure 1. The pulverized coal is entrained in a small amount of air and carried from the hopper to the burner. At the exit of the burner tube, the flame is stabilized by a ceramic flame holder. The chimney is used to prevent the burning mixture from mixing with the cool ambient air and to control the rate at which the flow is cooled. At the downstream end of the chimney, secondary air was injected to rapidly cool the products. The particle sampler was located 20 cm downstream of the chimney exit.

The particle sampler eliminates most of the large particles and collects the submicron particles on a carbon film surface. A transmission electron microscope is used to obtain photographs of the particles with resolution down to about 0.01 microns. The number of particles in various size ranges were manually determined.

The variation of the particle size and distribution with combustion and temperature is shown in Figure 2. The observed distributions appear to be a combination of two somewhat independent size ranges and physical effects. The number of particles in the range 0.01 to 0.02 microns was highly dependent on the cooling rate in the chimney, while particles in the range 0.02 to 0.05 microns do not appear to be dependent on the cooling rate. The effect of increasing peak temperature (higher methane concentration) was to increase the number of particles, particularly the larger ones, and shift the distribution toward the larger size ranges.

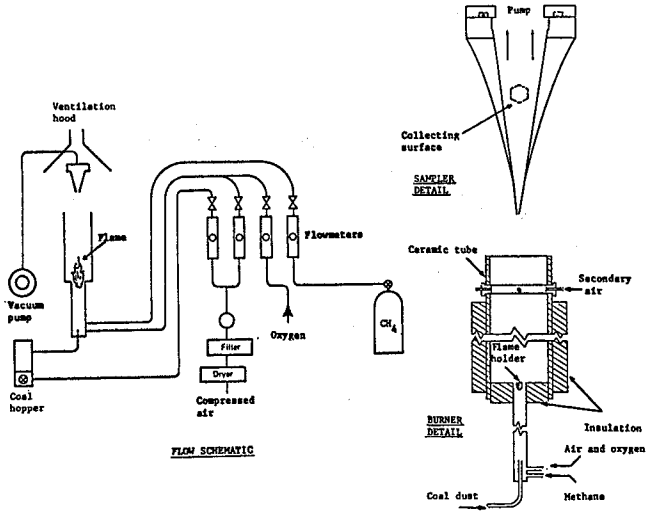

Fig. 1. Experimental apparatus. (XBL 811-7658)

Detailed presentation and results of these experiments is available.[3] In particular, the above mentioned result is believed to be caused by competition between homogeneous nucleation of new, small particles and condensation of the vapor on existing particles. With the higher cooling-rate uninsulated chimney, the temperature drops below the condensation point of the remaining vaporized ash; and most of the vapor condenses on pre-existing particles in the range 0.02 microns and larger. The rapid quench which accompanies the air injection at the end of the chimney does not result in any additional condensation. With the lower cooling rate, the vaporized ash remains in vapor form throughout the chimney and undergoes homogeneous nucleation during the rapid quench accompanying the air injection. In this case, we find a

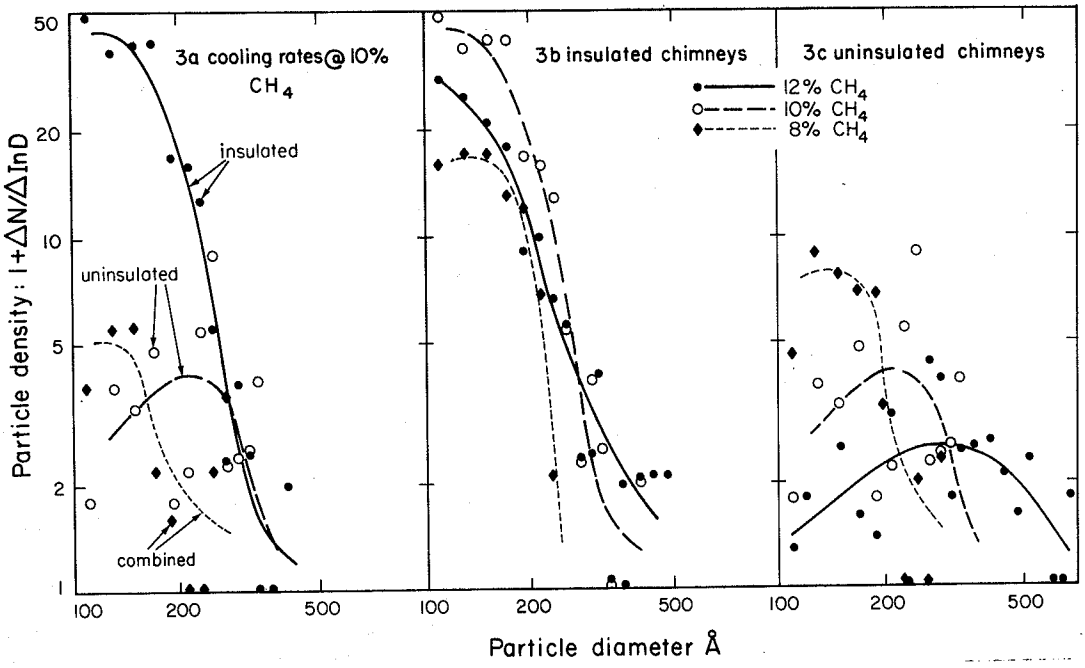

Fig. 2. Histograms of partial density versus diameter for different flame temperatures (percent methane) and cooling rates. (XBL 8012-2553)

much larger number of particles with sizes less than 0.02 microns.

Particles in the size range 0.02 to 0.05 microns may have been formed by homogeneous nucleation of another ash constituent, with a higher condensation temperature, immediately after the combustion region of the original coal particles. Their size would be dependent on the vapor characteristics and the rate of cooling, and a range 0.02 to 0.05 microns is reasonable.

These results are indications of the competition between homogeneous and heterogeneous nucleation which has been discussed in various models of pulverized coal fly-ash formation. The results indicate that it may be possible to control the smallest particles by varying the cooling rates in the post flame region.

PLANNED ACTIVITIES IN FY 1981

Investigation is planned to determine if certain toxic trace metals in coal are concentrated in the submicron portion of the fly-ash. For this purpose, an effective particle separator, probably of the impactor type, must be used to collect a sufficient sample of submicron particles to permit an x-ray fluorescence analysis of the atomic composition to be made. Initial measurements, using an LBL-developed sampler with two size fractions divided at 2 microns, has been successful. A suitable sampler will be obtained and similar studies on the particle size distribution will be conducted. Field test measurements on a large coal-fired steam boiler, using the same test equipment, would be very useful for comparison with the laboratory studies.

REFERENCES

1. R. C. Flagan and S. K. Friedlander, "Particle Formation in Pulverized Coal Combustion - A Review," Symposium on Aerosol Sciences, 82nd National Meeting, AICHE (1976).

2. R. D. Smith, "Laboratory Studies of Submicron Particles from Coal Combustion," Eighteenth Symposium (International) on Combustion, Waterloo, Canada (August 1980), to be published.

3. J. Pennucci, R. Greif, F. Robben and P. Sherman, Parametric Study of Submicron Particulates from Pulverized Coal Combustion, Lawrence Berkeley Laboratory Report LBL-12113 (January 1981).

SURFACE CATALYZED COMBUSTION*

R. Schefer and F. Robben

INTRODUCTION

Catalyzed combustion has been proposed as a method for promoting efficient burning of a variety of conventional and future alternative fuels with minimum pollutant formation. While preliminary tests have been quite promising, a number of aspects of catalyzed combustion are either not well understood or the necessary data are lacking. Necessary steps for the development of an optimum catalyst design will be: (1) to develop a greater understanding of the role of the catalyst in the combustion process, and (2) to determine high-temperature catalytic surface reaction mechanisms and reaction rates. It is the goal of the present study to provide some of the necessary understanding and data for catalytic combustor design.

Previous work has provided a detailed study of the combustion characteristics of lean H_2/air mixtures flowing over platinum catalytic and quartz (SiO_2) noncatalytic surfaces.[1] Regions were identified in which only surface reaction was present and others, at higher equivalence ratios and surface temperatures, in which both surface reaction and stable gas phase boundary layer combustion occurred simultaneously. Ignition temperatures were determined for surface reaction and gas phase reaction as a function of equivalence ratio, surface temperature, and surface reactivity (catalytic vs. noncatalytic). Surface energy release rates were measured and from these measurements models were developed for the high temperature surface oxidation of H_2.[2] Based on these models and known gas phase kinetic data for H_2/air reactions, a numerical computational scheme was developed for modeling H_2/air combustion in the presence of a catalytic surface and the effect of catalytic surface reactions on gas-phase combustion was investigated.[3]

ACCOMPLISHMENTS DURING FY 1980

During FY 1980, the combustion of lean C_3H_8/air and C_2H_6/air mixtures were studied extensively over platinum catalytic and quartz (SiO_2) noncatalytic surfaces, using Rayleigh scattering for boundary layer temperature measurements.[4] Based on the experimentally measured temperature profiles, gas phase ignition temperatures were determined over a range of operating conditions. Typical results for C_3H_8 are shown in Figure 1 where the surface temperature required for gas phase ignition is plotted as a function of equivalence ratio.

* This work was supported by Assistant Secretary for Conservation and Solar Energy, Office of Transportation Programs, Transportation Conservation Division of the U.S. Department of Energy under Contract No. W-7405-ENG-48.

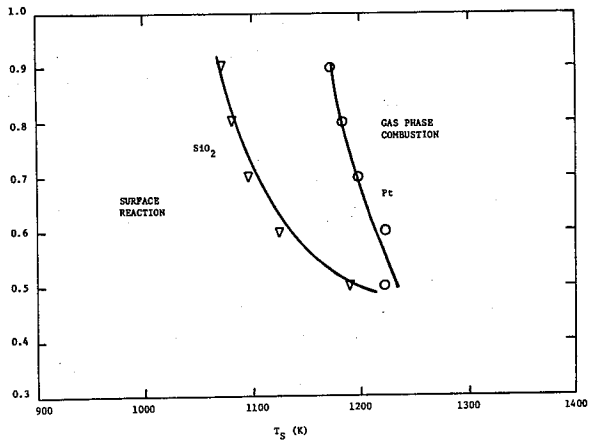

Fig. 1. Gas phase ignition temperatures for C_3H_8 combustion. U = 1.5 m/s. (XBL 812-8068)

It can be seen that, for both surfaces, the gas phase ignition temperature increases with decreasing equivalence ratio. At lower surface temperatures, i.e., higher equivalence ratios, the ignition temperature for the SiO_2 surface is approximately 100 K less than for the platinum. As the surface temperature increases, the ignition temperature for the SiO_2 surface approaches that of the platinum. This behavior is consistent with an increase in the catalytic activity of the quartz surface at higher temperatures. Numerical calculations for H_2/air mixtures flowing over a catalytic surface have shown that reactions at the surface, particularly surface oxidation of the fuel and radical recombination, result in a suppression of gas phase reactions in the boundary layer. Thus, at high equivalence ratios where a lower surface temperature is required for gas phase ignition, the noncatalytic nature of the quartz surface results in approximately a 100 K lower gas phase ignition temperature. At higher surface-ignition temperatures, where the catalytic activity of the quartz surface approaches that of the platinum, the gas phase ignition temperatures become comparable. Similar results were found using H_2/air and C_2H_6/air reactant mixtures.

Surface reaction ignition temperatures were also determined for C_3H_8/air and C_2H_6/air mixtures on a platinum surface. Ignition temperatures were found to be 470 K and 700 K, respectively, and were only a weak function of equivalence ratio. Based on experimentally measured values of surface heat release rates, surface oxidation rates were calculated for C_3H_8. This agreed well with a rate constant of the form $K_s = 1.1 \times 10^7 [C_3H_8]$ exp (-17000/RT) kg moles/m^2s. It was also found that, for temperatures less than approximately 670 K, CO is the primary oxidation product and that, for temperatures greater than 870 K, complete oxidation to CO_2 occurs.

A laser excited fluorescence technique was used to measure the OH radical concentration during combustion of H_2/air mixtures in the boundary layer of a heated platinum catalytic surface.[5] The technique consisted of exciting the OH molecule to the $A^2\Sigma$ (v= 0) excited state from a specific rotational level in the $X^2\Pi$(v=o) ground state, using a narrow bandwidth pulse dye laser and monitoring the resulting band fluorescence at 32380 cm^{-1}. Relative OH concentration profiles were determined from the above fluorescence measurements, and absolute concentrations were determined from the integrated absorption spectra centered at 32380.99 cm^{-1}.

The measured OH concentration profiles using this technique are shown in Figure 2. These concentration profiles are highly nonequilibrium in character. For the hydrogen-air mixture (ϕ = 0.2) at the plate temperature of 1170 K, an OH concentration of 1.5×10^{13} (molecules/cc) would be expected at equilibrium. Near the leading edge (X = 5 mm), the peak OH concentration exceeds this equilibrium condition by a factor of 200, with a correspondingly high concentration near the plate surface. Proceeding further downstream, the peak OH concentration decreases slowly, being only a factor of two lower at X = 50 mm. than that closest to the leading edge. The decrease in the OH concentration nearest the plate surface with distance from the leading edge is the result of fuel depletion and recombination reactions. Near the free stream edge of the OH profile, the concentration drops very fast as the recombination reactions compete with the chain branching reactions of the H_2/O_2 system.

PLANNED ACTIVITIES FOR FY 1981

During FY 1981, work will continue on determining gas phase and surface ignition characteristics of conventional hydrocarbon and future alternative fuel/air mixtures flowing over a catalytic surface. From this additional data, it will be possible to determine with greater certainty the precise role of the catalyst and to determine both reaction mechanisms and kinetic constants for surface and gas-phase reactions. Catalyst operation under fuel-rich conditions will also be investigated, with emphasis on soot-formation characteristics in the presence of a high-temperature catalyst.

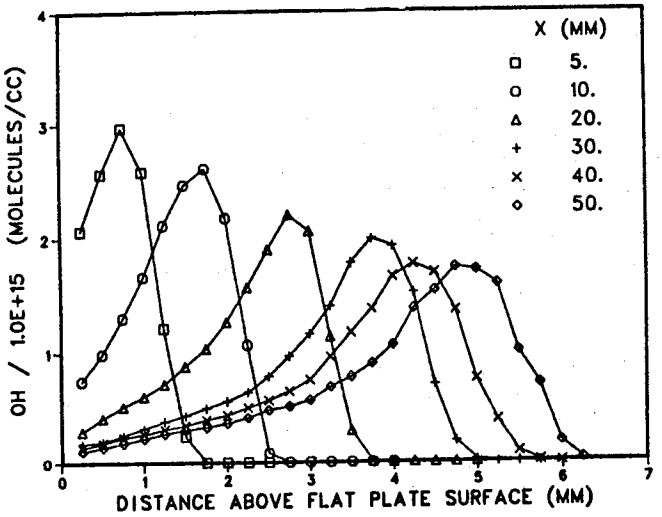

Fig. 2. OH concentration profiles for flow over a heated platinum surface. (XBL 812-8067)

REFERENCES

1. R. W. Schefer, F. Robben, and R. K. Cheng, "Catalyzed Combustion of H_2/Air Mixtures in a Flat Plate Boundary Layer: I. Experimental Results." Combustion and Flame, vol. 38, pp. 51-63 (1980).

2. R. W. Schefer, R. Cheng, F. Robben, and N. Brown, "Catalyzed Combustion of H_2/Air Mixtures on a Heated Platinum Plate." Western States Section/The Combustion Institute, Boulder, CO (1978).

3. R. W. Schefer, "Catalyzed Combustion of H_2/Air Mixtures in a Flat Plate Boundary Layer. II. Numerical Results." Combustion and Flame, to be published.

4. R. W. Schefer and F. Robben, "Catalyzed Combustion of Lean Fuel/Air Mixtures." Proceedings of the Fourth Workshop on Catalytic Combustion (1980).

5. R. J. Cattolica and R. W. Schefer, "Laser Fluorescence Measurements of the OH Concentration in Boundary Layer Combustion." Eastern States Section/The Combustion Institute, Princeton, NH (1980).

COMBUSTION FLUID MECHANICS

FLAME PROPAGATION IN GRID—INDUCED TURBULENCE*

R. Bill, Jr., R. K. Cheng, I. Namer, T. Ng, F. Robben, and L. Talbot

INTRODUCTION

The increase in flame propagation speed and volumetric heat release rate in a premixed turbulent flame relative to a laminar flame is important in designing combustion systems with optimum size and power characteristics. Although considerable attention has been given to the study of turbulent flame propagation, difficulties were encountered in obtaining measurements in the flame zone and, as a result, only gross properties of the flame have been studied. The effect of different turbulence scales and intensity on flame propagation was inferred by measuring the mean turbulent burning velocity. Questions concerning the effect of combustion on mean streamlines, turbulent kinetic energy, and turbulent length scales remained unanswered. Theoretical and numerical modes of turbulent flame propagation have focused attention on these problems. However, little data is available to guide theorists in their choice of proper models in turbulent combustion.

The objective of this program is to characterize the statistical nature of turbulent flame propagation by studying the change in scale and intensity of density and velocity fluctuations through the flame zone. This will be used to verify the assumptions of current and developing theoretical and numerical premixed flame models and to compare with the results of these models. The flame propagation is studied in low intensity grid-induced isotropic turbulence using laser diagnostics such as Rayleigh scattering and Laser Doppler Velocimetry (LDV).

ACCOMPLISHMENTS DURING FY 1980

Profiles were obtained of mean and fluctuation intensities of the streamwise component of velocity and the density through a v-shaped, premixed C_2H_4-air flame at several free stream velocities and mixture ratios.[1] The probability density function (pdf) and spectral density distribution at locations inside the flame were obtained. The experimental conditions covered flow velocities from 2.5 to 7.0 m/s and equivalence ratios from 0.55 to 0.75. Typical velocity root-mean-square (rms) fluctuation level was 4% of the free stream velocity.

Mean density and rms density fluctuation profiles through a flame are shown in Figure 1. The flame zone is characterized by the s-shaped mean density distribution. The density fluctuations shown are primarily due to the movement of the flame sheet across the measurement volume. The maximum intensity of 33% is typical for all results. The thickness of the flame zone at this location, 7.5 cm downstream from the grid, is about 4 mm and is found to increase at locations further downstream. Mean streamwise velocity profiles and corresponding rms fluctuation profiles are shown in Figures 2 and 3. The location of the flame zone at each axial location is indicated by the increase in velocity due to heat release. The locations of the peak rms velocity fluctuation are found to correlate well with the locations of peak density fluctuation. Behind the flame, the turbulence intensity decreased to approximately one-half of the level upstream of the flame. Thus, a substantial decrease in turbulent kinetic energy occurs. This is consistent with the result of numerical models.

* This work was supported by the U.S. Air Force Office of Scientific Research under Contract No. F44620-76-C-0083 through the Office of Research Service of the University of California, Berkeley. Additional facility and equipment support was provided by the Director of the Office of Energy Research, Office of Basic Energy Sciences, Chemical Sciences Division of the U.S. Department of Energy under Contract No. W-7405-ENG-48.

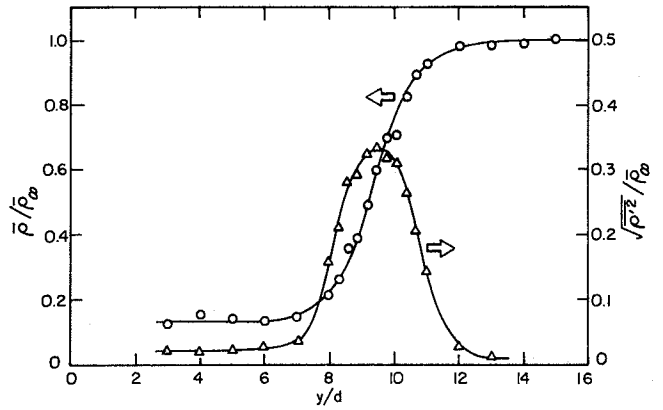

Fig. 1. Mean and rms intensity profiles of density. U_∞ = 6.84 m/s, ϕ = 0.75, d = 1.0 mm, x = 7-5 cm.
(XBL 809-5938)

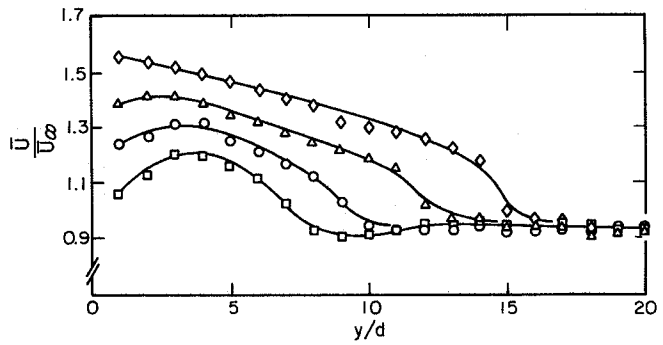

Fig. 2. Mean velocity profiles through a flame. U = 6.84 m/s; ϕ = 0.75; d = 1.0 mm, □; x = 7.0 cm, O; x = 7-5 cm, △; x = 8.0 cm, ◇; x = 8.5 cm.
(XBL 802-368)

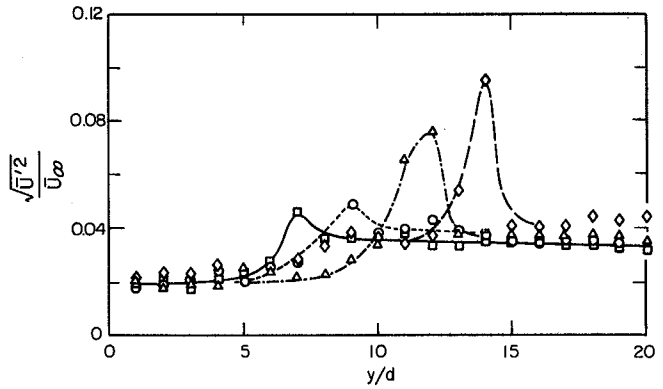

Fig. 3. Turbulence intensity profiles conditions. U_∞ = 6.84 m/s; ϕ = 0.75, d = 1.0 mm, □; x = 7.0 cm, O; x = 7-5 cm, △; x = 8.0 cm, ◇; x = 8.5 cm.
(XBL 802-370)

To verify the assumption of the Bray-Moss-Libby model[2] that the gas consists simply of burnt products and unburnt reactants, pdf's of density were computed at locations[3] inside the flame zone (Fig. 4). These pdf's show that the intermediate state between burnt product and unburnt reactants constitutes as much as 30% of the gas in the flame. A comparison of statistics for fluctuation intensity and skewness with results predicted by this model indicate that the model overpredicts these statistical moments.[3]

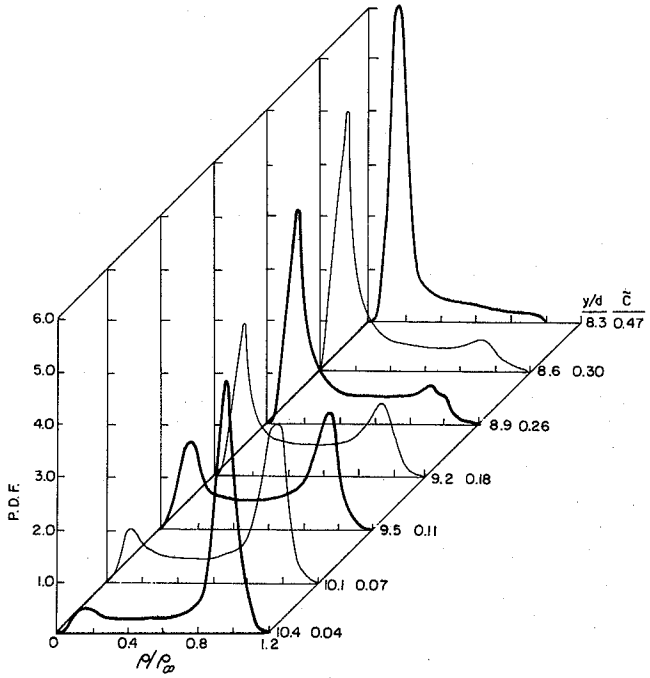

Fig. 4. Evolution of pdf's through a flame. U_∞ = 6.84 m/s, ϕ = 0.75, x = 7-5 cm.
(XBL 807-5565)

PLANNED ACTIVITIES FOR FY 1981

Diagnostic techniques for measuring spatial correlation of density fluctuation will be developed. This will involve obtaining Rayleigh scattering from two measurement points. These results will provide insight into the scale and intensity of the flame front movement to properly interpret the Reynolds stress and other velocity measurements inside the flame.

REFERENCES

1. R. G. Bill, Jr., I. Namer, L. Talbot, R. K. Cheng, F. Robben, "Flame Propagation in Grid Induced Turbulence," to appear in Combustion and Flame, 1981.

2. K. N. C. Bray and P. Libby, "Interaction Effects in Turbulent Premixed Flames," Phys. of Fluids, vol. 19, p. 1687 (1976).

3. R. G. Bill, Jr., I. Namer, L. Talbot, and F. Robben, "Density Fluctuations in Turbulent Flames" submitted for publication in Combustion and Flame, to be published.

COMBUSTION IN A TURBULENT BOUNDARY LAYER*

R. K. Cheng, R. Bill, Jr., T. Ng, F. Robben and L. Talbot

INTRODUCTION

Although turbulent combustion occurs in most practical combustor configurations, the interaction between fluid mechanical turbulence and combustion heat release is not well understood due, in part, to the lack of sufficient experimental data on turbulence in combustion environments to develop an analytical description of the process. With the advancement of laser diagnostics in recent years, it is now possible to obtain time- and space-resolved measurements of turbulent parameters in combustion. The objective of this program is to study premixed turbulent combustion in a well-defined configuration, in this case a heated turbulent boundary layer. This study will contribute to the experimental data base necessary for development of theoretical and phenomenological models of turbulent combustion.

Using a heated wall turbulent boundary layer to study combustion has some advantages over more conventional combustion systems, such as flames. By adjusting wall temperature and mixture ratios, combustion heat release can take place throughout the boundary layer, permitting an alternate means for studying the combustion-turbulence interaction. Characteristic features of H_2-air combustion in a heated boundary layer near transition have been studied in a small (2.5 cm square) channel.[1] This facility was built as the prototype of a larger (10 cm square) wind tunnel for the study of combustion in a fully-developed turbulent boundary layer.

ACCOMPLISHMENTS DURING FY 1980

Experiments in the 10 cm square channel have been carried out in the heated turbulent boundary with and without H_2-air combustion. This wind tunnel is driven by a centrifugal fan and is mounted on a 3-axis stepping-motor-controlled traverse mechanism. In the present experiment, the boundary layer develops in an unheated section 0.5 m in length before entering the heated bottom wall section 0.25 m in length. The heated wall consists of nine electrically heated Kanthal strips stretched over ceramic blocks.

The heated wall flow without combustion was studied in detail by the use of Rayleigh scattering and Laser Doppler Velocimetry (LDV). The diagnostics are interfaced with a computer-controlled data acquisition system based on a PDP 11/10 computer. Using a CDC 7600 computer, data analysis was made by transferring the raw data on magnetic tape. Density, velocity and Reynolds stress profiles as well as probability density functions and spectral density distributions were obtained at each measurement point.[2]

Typical experimental conditions were free stream velocity of 20 m/s and wall temperature of 1000 K. In the unheated case, both the velocity and Reynolds stress profiles were in reasonably good agreement with hot-wire data reported in the literature. In the heated wall case, the temperature profiles obtained from density measurements followed a power law. However, no similarity was found between the mean temperature and velocity profiles, in contrast to the similarity found in a slightly heated wall ($\Delta T \approx 20$ K) turbulent boundary layer.[3] Shown in Figure 1 are mean and fluctuation profiles obtained at various axial stations along the heated wall section. In all, the velocity fluctuations were found to be increased slightly by wall heating. Comparison of the Reynolds stress profiles obtained with and without wall heating (Fig. 2) demonstrated that the Reynolds stress near the wall was reduced by heat transfer from the wall.

The experiments involving H_2-air combustion in the boundary layer were studied using high-speed laser schlieren cinematography to determine the conditions at which various modes of boundary layer combustion would occur. These movies have shown that the turbulence structures were not altered by lean H_2-air combustion and that large scale coherent turbulent structures were not apparent in this turbulent boundary layer.

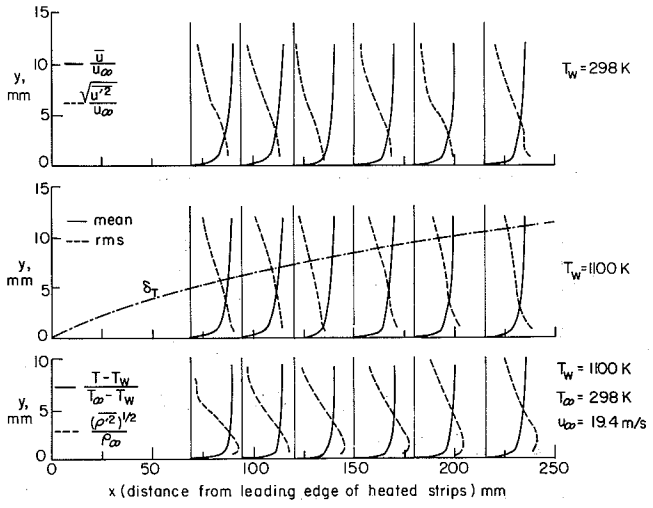

Fig. 1. Comparison of mean and fluctuation profiles of velocity and density profiles in heated and non-heated turbulent boundary layer. S_T = thermal boundary layer thickness based on ρ/ρ_∞ = .99. (XBL 8011-6364)

* This work was supported by the Director of the Energy Research, Office of Basic Energy Sciences, Chemical Sciences Division of the U.S. Department of Energy under Contract No. W-7405-ENG-48.

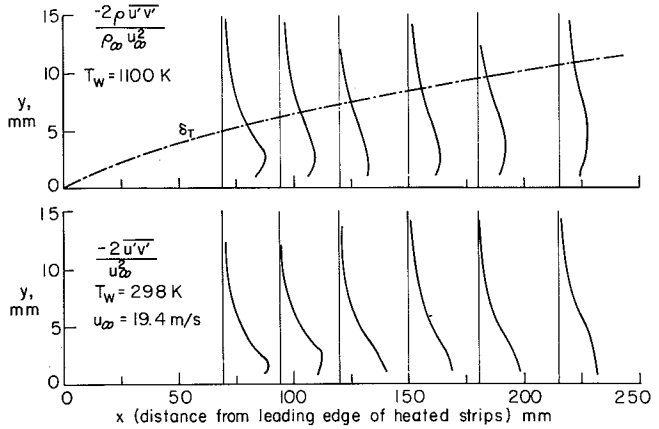

Fig. 2. Comparison of Reynolds stress

$$(-\overline{2u'v'}/u_\infty 2)\ (\rho/\rho_\infty)$$

profiles in heated and non-heated turbulent boundary layers. (XBL 8011-6363)

PLANNED ACTIVITIES FOR FY 1981

Completion of the data analysis will provide a comprehensive description of the turbulent flow field in the heated boundary layer. Detailed measurements of C_2H_4-air combustion in the heated boundary layer will be made. Comparison of these data will make possible the study of the effect of combustion on the turbulence parameters.

In addition to measurements using existing diagnostic tools, more advanced laser diagnostic techniques will also be developed to obtain cross-correlations between fluctuation parameters. These will include combined Rayleigh and LDV to measure the cross-correlation between velocity and density and a two component LDV system to measure instantaneous Reynolds stress. These quantities are important for the study of turbulent kinetic energy exchange in combustion regions.

REFERENCES

1. R. K. Cheng, R. G. Bill, Jr., and F. Robben, "Experimental Study of Combustion in a Turbulent Boundary Layer" to appear in 18th (International) Symposium on Combustion, The Combustion Institute (1980).

2. R. K. Cheng and T. T. Ng, "Measurement of Density and Reynolds Stress in a Heated Wall Turbulent Boundary Layer," Bulletin of the American Physical Society, vol. 25, no. 9, p. 1019 (1980).

3. W. C. Reynolds, W. M. Kays and S. J. Kline "Heat Transfer in the Turbulent Incompressible Boundary Layer, I - Constant Wall Temperature," U.S. National Aeronautics and Space Administration Report, NASA Memorandum 12-1-58W, 1958.

NUMERICAL MODELING OF TURBULENT COMBUSTION*

A. Ghoniem, A. Chorin, and A. Oppenheim

INTRODUCTION

Combustors in all practical power plants are operated under turbulent flow conditions. Good understanding of the mechanism of such flows is important in developing proper means for the control of the combustion process, an essential requirement for the attainment of clean exhaust and efficient performance. Of particular significance is the numerical modeling technique we developed, as described in the 1979 Annual Report (p. 6-38ff), based on the random vortex method (RVM) due to Chorin.[1]

This method was designed to develop a satisfactory approximation to the solution of the equations describing the flow without the use of finite differencing, a conventional technique that inherently obscures the mechanism of turbulence. In RVM, essential features of the flow field are mimicked by the action of vortex elements modeling the essential ingredients of turbulence, the elementary eddies. Their random walks express the effects of diffusion, while compliance with the tangential boundary condition at the walls is assured by creation of vorticity in the proper amount. A potential flow solution is used at the same time, using the principle of fractional steps to guarantee that the normal boundary condition is satisfied.

The RVM keeps track of the position and strength of all the vortex elements constituting the flow field and is thus essentially grid-less. It is therefore devoid of the smoothing, intrinsic to the finite difference technique, and unaffected by the numerical diffusion it introduces. Above all, RVM does not involve any averaging whatsoever. On the contrary, instead of damping the disturbances, it actually introduces a certain amount of randomness, or numerical noise, simulating the mechanism of local perturbations in a way similar to the one which occurs in real flow.

* This work was supported by the Director of the Office of Energy Research, Office of Basic Energy Sciences, Division of Chemical Sciences of the U.S. Department of Energy under Contract No. W-7405-ENG-48, and by the U.S. National Aeronautics and Space Administration under Grant No. NSG 3227 through the Engineering Office of Research Service, University at California, Berkeley.

ACCOMPLISHMENTS DURING FY 1980

In 1979, we obtained results modeling the turbulent flow in a two-dimensional combustion tunnel with the flame stabilized behind a rear-facing step (1979 Annual Report, p. 6-38ff). We have now included the exothermic effects of combustion adding a new algorithm for handling flame propagation to the vortex dynamics. The structure of the full computational scheme describing the two algorithms and their interrelationship is shown in Figure 1. It should be noted that, whereas vortex dynamics refers to a solenoidal field associated with vorticity generation, flame propagation involves an irrotational field, the exothermic effects of combustion being expressed in terms of potential volumetric sources. Thus, according to our model, the only way combustion can affect turbulence is by augmenting the velocity vector field which, in turn, gives rise to new vortex elements caused by the no-slip condition at the walls, as indicated at the left upper corner of Figure 1.

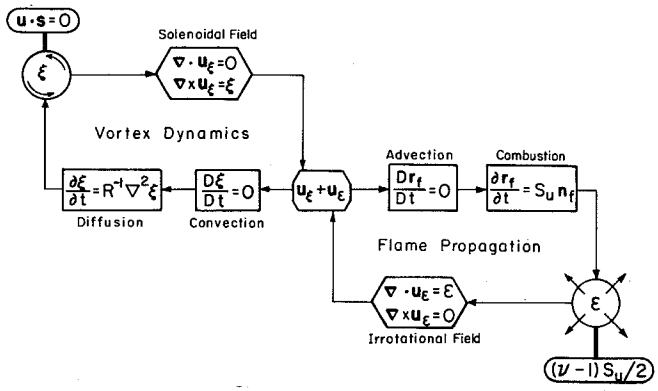

Fig. 1. Structure of the computational scheme. (CBB 802-2190)

Our studies were reviewed at the 18th Combustion Symposium[2] and described in an LBL Report.[3] Pertinent results of these studies are presented in Figure 2 which illustrates two sequential series

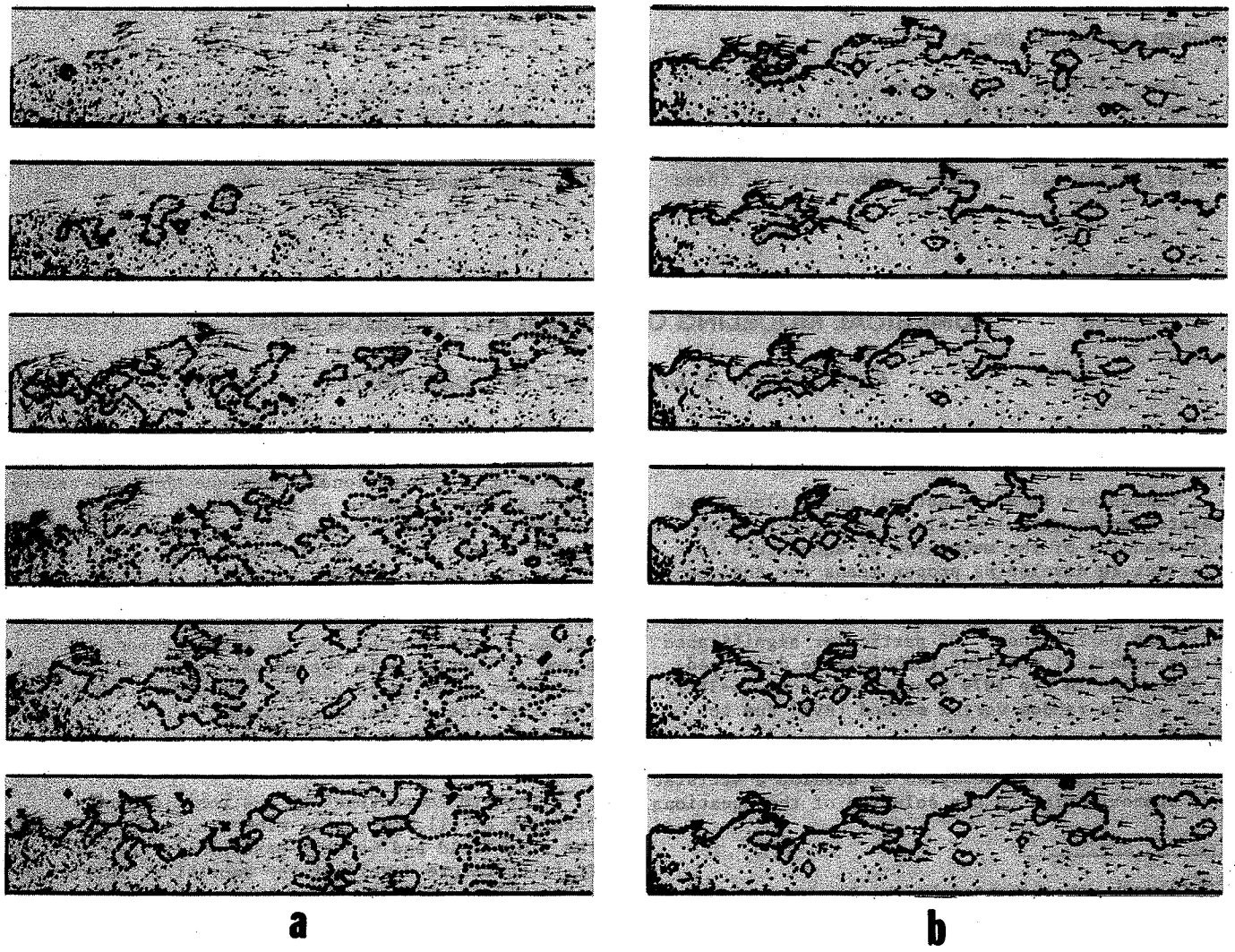

Fig. 2. Sequential series of computer plots displaying vortex velocity fields and flame fronts in turbulent combustion behind a step at Reynolds number of 10^4, while the ratio of the normal flame velocity to the flow velocity at inlet is 0.02. (a) Ignition in a fully developed turbulent flow at a point situated at the level of the step one step height downstream. (b) Fully established turbulent combustion in the flow field behind the step. (CBB 802-2190)

of computer outputs depicting the variation of the velocity fields and flame fronts. The series are expressed in terms of velocity vectors represented, as usual, by line segments providing information on their magnitude and direction. However, instead of being furnished with conventional arrowheads, the vectors are attached at their origin to small circles denoting the locations of the vortex elements to which they pertain. The flame front is depicted by closely spaced series of dots forming distinct contours.

The sequence in Figure 2a depicts the process of ignition in a turbulent flow field which has been already established in the combustion tunnel behind a rear-facing step. The combustible medium to which it pertains is a lean propane/air mixture, whose normal flame speed is 12 cm/sec, flowing at a velocity of 6 m/sec (corresponding to the Reynolds Number of 10^4). The sequence at the left bottom corner of Figure 2b displays the combustion field following ignition initiated at the moment when the medium was set in motion. In both cases, the effects of the turbulent flow field are quite remarkable if one realizes that it was capable of stabilizing the combustion process under conditions where the normal burning velocity was only 2% of the average velocity of flow. The relative ease with which a continuous flame front was established in the latter case demonstrates the importance of proper timing and location of the ignition source.

PLANNED ACTIVITIES FOR FY 1981

Using the method we developed, it is our intention now to examine the properties of turbulent flow fields under the geometrical conditions modeling the essential features of bluff body flame holders with and without combustion. Of particular interest in this respect are: the mean velocity profiles, the Reynolds stresses, and the pressure profiles--quantities which can be compared with available experimental data.[4]

We also intend to apply our numerical modeling analysis to the study of the unstable behavior of flow behind a step. Of special significance here is the effect of enriching the fuel/air mixture, leading to various modes of instabilities that have been identified recently in an experimental program of research completed.[5]

The RVM will be applied, moreover, to the analysis of combustion in jets, the major subject of our studies on ignition described elsewhere in this Annual Report.[6] This should be particularly helpful in assessing the effects of distributed ignition centers that can be achieved by the use of active radicals.

Finally we will be working on the development of novel random element methods, using RVM as the basis, to model heat transfer processes, so that their effects in combustion systems could be included.

REFERENCES

1. A. J. Chorin, "Numerical Studies of Slightly Viscous Flow," J. Fluid Mech., vol. 57, pp. 785-796 (1973).

2. A. F. Ghoniem, A. J. Chorin, and A. K. Oppenheim, "Numerical Modeling of Turbulent Combustion in Premixed Gases," Eighteenth Symposium (International) on Combustion, The Combustion Institute, in press (1981).

3. A. F. Ghoniem, A. J. Chorin, and A. K. Oppenheim, "Numerical Modeling of Turbulent Flow in a Combustion Tunnel," Lawrence Berkeley Laboratory, LBL-11520 (1980).

4. R. W. Pitz and J. W. Daily, "Experimental Study of Combustion in a Turbulent Free Shear Layer Formed at a Rearward Facing Step," AIAA 19th Aerospace Sciences Meeting, St. Louis, Mo. (January 1981).

5. J. O. Keller, L. Vaneveld, D. Korschelt, G. L. Hubbard, A. F. Ghoniem, J. W. Daily, and A. K. Oppenheim, "Mechanism of Instabilities in Turbulent Combustion Leading to Flashback," AIAA 19th Aerospace Sciences Meeting, St. Louis, Mo. (January 1981).

6. A. Oppenheim, F. Hurlbut, F. Robben, R. Peterson, P. Coico, and H. Stewart, "Ignition Studies," Lawrence Berkeley Laboratory, Energy and Environment Division Annual Report FY-1980, LBL-11650.

VORTEX INTERACTION WITH A PREMIXED LAMINAR FLAME*

I. Namer,† R. Bill, Jr.,†† F. Robben, and L. Talbot

INTRODUCTION

As part of a research program on premixed turbulent flame propagation, the interaction of an otherwise laminar flame front with the vortices produced in the wake of a single rod (the so-called Kármán vortex street) has been studied. The goal of this work is to provide greater insight into turbulent flame propagation under conditions where the wrinkled laminar flame model should apply. Measurements have been made of velocity, using laser Doppler anemometry, and density, using Rayleigh scattering; and mean turbulence levels, probability density functions, and power spectra have been obtained. In addition, the regularity of the vortex street has allowed the use of phase-locked signal averaging to obtain the instantaneous velocity fields from a time averaged ensemble of reasonably repeatable vortices. A complete description of this experiment and the results obtained has been prepared[1] and a previous report on some preliminary work is also available.[2]

ACCOMPLISHMENTS DURING FY 1980

Measurements were made in a small open jet wind tunnel which produced a 50mm diameter jet of premixed ethylene and air. A sheet flame was stabilized on a small rod, and a larger upstream rod produced the vortex street, shown schematically in Figure 1. The fuel-air jet was surrounded coaxially by an air jet of the same velocity, which served to reduce the turbulence level at the fuel jet boundary and thus to minimize the flowfield and flame front fluctuations originating in the jet boundary region of the flame.

A one-watt argon-ion laser was the source for both the LDA and Rayleigh measurements. The Laser Doppler Anemometry (LDA) was a dual beam, real fringe type, using a Thermal Systems, Inc. (TSI) tracker to produce a voltage proportional to the velocity of each validated particle. The intensity of the Rayleigh scattered light was measured at right angles to the laser beam using about f/2.4

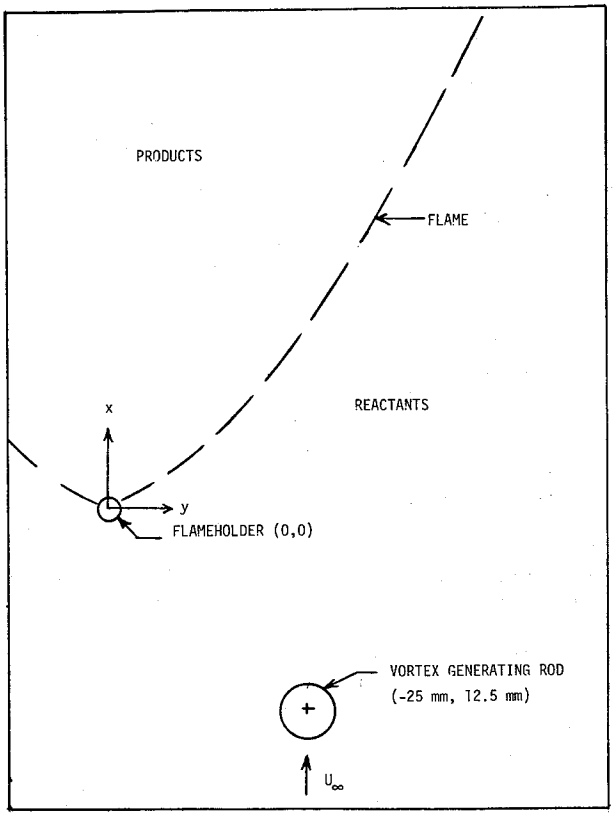

Fig. 1. Schematic diagram of flame holder, flame location, vortex generating rod, and undisturbed flow direction. (XBL 805-9543)

optics, a filter, and an RCA type 931A photomultiplier. The results were recorded by a PDP-11 computer and stored on magnetic tape for final data reduction on a large (CDC 7600) computer.

Flowfield surveys of velocity and density were made for three vortex shedding Reynolds numbers, Re_D, of 73, 110, and 500, Phase-locked flowfield surveys were made only for Re_D = 73 and 110. For reference, the frequency of vortex pair generation for the 2.0 mm rod, with a free stream flowfield of 55 m/s, was 30 Hz.

The mean and rms fluctuation of the x-component of the flow velocity is shown in Figure 2; two y-profiles taken at the same axial (x) location, but with 2.0 and 3.0 diameter vortex generating rods, are shown. Figure 3 shows a contour plot of the mean velocity (x component only). The flame front is identified as the region of sharp rise in velocity; the minimum upstream of the flame is caused by the wake of the vortex-generating rod. This minimum is deflected outward by the flame, as can be seen from the figure.

The phase-locked measurements are representative of the conditions at a certain time (phase

* This work was supported by the U.S. Air Force Office of Scientific Research under Contract No. F44620-76-C-0083 through the Campus Research Office of the University of California, Berkeley. Additional facility and equipment support was provided by the Director of the Office of Energy Research, Office of Basic Energy Sciences, Chemical Sciences Division of the U.S. Department of Energy under Contract No. W-7405-ENG-48.

† Present address: Department of Mechanical Engineering, Drexel University, Philadelphia, PA

†† Present address: Department of Mechanical Engineering, Columbia University, New York, NY

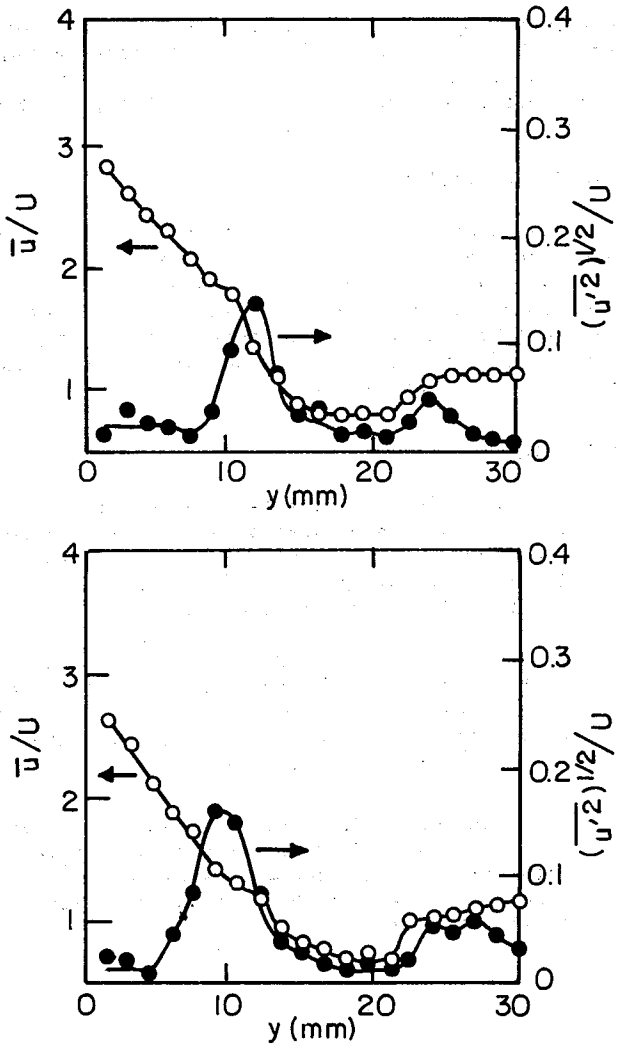

Fig. 2. Mean and rms fluctuation profiles of the x-component of the velocity, taken at a given axial location through the flame front and the vortex wake of the rod. The two figures are for (a) 2.0 mm and (b) 3.0 mm vortex generating rod. (XBL 808-5624)

angle) in the position of the vortex generated by the rod. The position of the vortex is obtained by a hot-wire sensor located in the wake region of the vortex-generating rod, upstream of the flame front. A constant velocity contour plot example at a given phase angle is shown in Figure 4, which can be considered to be an instantaneous "snapshot" of the velocity. Here, it is seen that the flame front is highly distorted by the wake. Further, vortices generated by the rod can be seen to be present upstream of the flame front but cannot be identified downstream of the flame in the burned gases. These measurements indicate that the turbulence level of the flow is drastically reduced by the flame, so much so that there do not appear to be identifiable vortex structures in the burned gas. This may be simply due to the combination of the flow dilatation and increased viscous dissipation in the burned gases. However, a more subtle interaction of the flame front with the vortex structure may serve to further reduce the overall vortex strength.

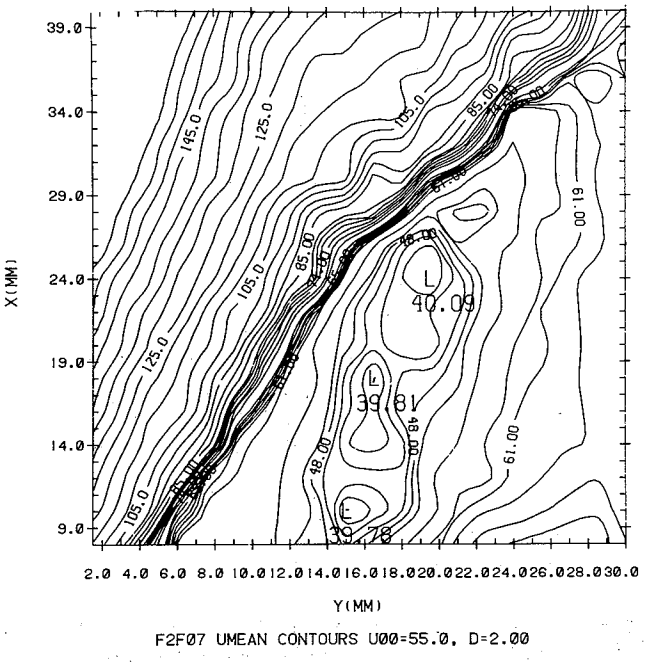

Fig. 3. Constant mean axial velocity contours for the flame in the wake of a 2.0 mm vortex generating rod. (XBL 812-8258)

One of the more interesting results of the density measurements is shown in Figure 5. This is a 3-D plot of the evolution of the probability density function of the gas density through the turbulent flame front. The horizontal axis is the ratio of the measured gas density to the unburned gas

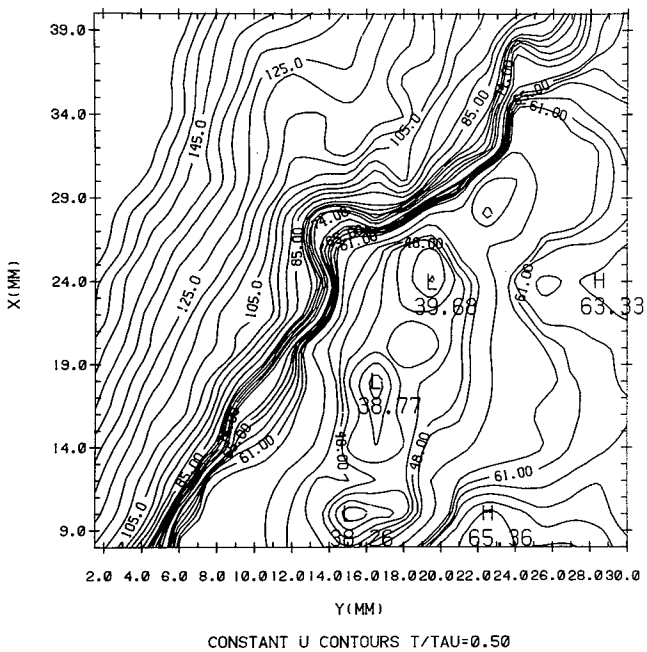

Fig. 4. Constant "instantaneous" axial velocity contours, at a given phase angle in the vortex generating cycle, for a flame in the wake of a 2.0 mm vortex generating rod. (XBL 812-8259)

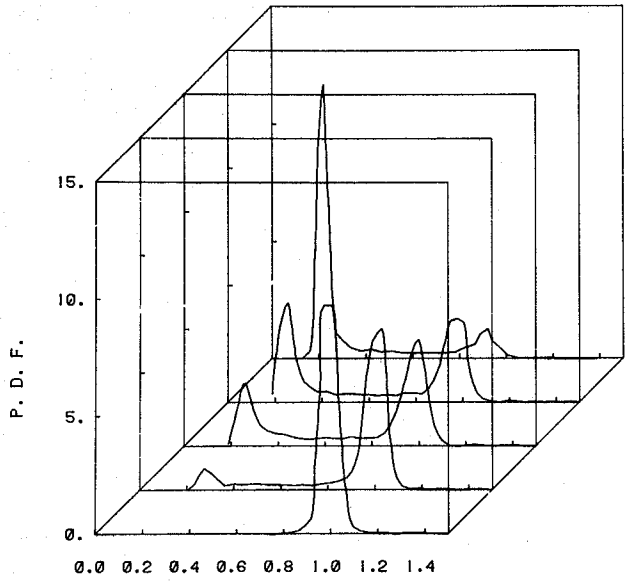

Fig. 5. Evolution of the probability density function (pdf) of the gas density as a function of position ($\tilde{c}$) through the fluctuating flame in the wake of a 2.0 mm vortex generating rod.

(XBL 808-11109)

density; the cold, unburned gas is located at 1.0 while the hot, burned gas is at 0.25. The position through the flame front is represented by $\tilde{c}$, a reaction progress variable. It can be seen that, at any point within the flame front, the gas tends to be either completely burned or unburned, with not much in between (a so-called bimodal distribution). Thus, the flame is fairly well represented by a thin fluctuating sheet, which can be highly contorted as indicated in Figure 4.

PLANNED ACTIVITIES FOR FY 1981

The experimental portion of this research has been completed and additional work is not presently planned. Numerical computations simulating a two-dimensional vortex interacting with a flame have been made[3] and further refinement of these computations is continuing. Further analysis of the experimental results is planned.

REFERENCES

1. I. Namer, "An Experimental Investigation of the Interaction between a Kármán Vortex Street and a Premixed Laminar Flame," University of California, College of Engineering Report FM-80-2, Ph.D. Thesis (1980).

2. I. Namer, Y. Agrawal, R. K. Cheng, F. Robben, R. Schefer, and L. Talbot, "Interaction of a Plane Flame Front with the Wake of a Cylinder," University of California, College of Engineering Report FM-77-3 (Oct. 1977).

3. I. Karasalo, A. J. Chorin, I. Namer, F. Robben, and L. Talbot, "Numerical Simulation of the Interaction of a Flame with a Kármán Vortex Street," Lawrence Berkeley Laboratory Report, LBL-10679 (1980).

MODELING OF BURNING AND EXTINCTION CHARACTERISTICS OF A POLYMER DIFFUSION FLAME AND COMPARISON WITH EXPERIMENT*

W. Pitz and R. Sawyer

INTRODUCTION

The importance and contribution of the inherrent flammability of polymeric materials to problems of fire safety is well recognized. This study was undertaken to provide a better understanding and interpretation of previous experimental investigations of polymer flammability. The structure of opposed flow diffusion flames have been measured by several investigators using both gaseous[1,2] and solid[3,4,5] fuels. The opposed flow diffusion flame is a convenient geometry for the study of the flammability of polymers because it allows both steady, diffusion controlled burning and extinction to be observed under well-controlled laboratory conditions. Conveniently available experimental parameters include fuel composition, oxidizer composition, and oxidizer blowing rate. Reported experiments generally have not included the variation of pressure or temperature. Radiation effects, which are important in fires, remain to be well-characterized in laboratory studies of opposed flow diffusion flames where radiation generally is of minor importance.

ACCOMPLISHMENTS DURING FY 1980

Reacting flow in a stagnation point boundary layer was modelled with the objective of examining its properties near extinction, Figure 1. Axisymmetric geometry, laminar-flow, and steady-state combustion were considered to conform to an existing diffusion flame burner[5]. Variation of fluid properties with both temperature and composition was included. The specific heats of the three species considered (fuel, oxygen and products) were chosen to be those of ethylene, oxygen, and nitrogen respectively, and approximated as cubic functions of temperature. The effective viscosity was obtained from the individual, temperature-dependent viscosities using Wilke's mixture rule[6]. The Prandtl number was fixed at 0.7, which is a good approximation for the reactants and products considered. The Lewis number was assumed to be 1.

Finite reaction rate chemistry was incorporated with a one-step reaction and Arrhenius rate expression. Three species were considered: fuel, oxygen and products. The reaction rate was of order one with respect to both fuel and oxygen.

The boundary conditions for the N_2/O_2 flow were an ambient temperature of 294K and a pressure of 1 atm. The polymer burning rate was calculated from the enthalpy gradient at the fuel surface and the effective latent heat. The latent heat was extracted from the mass transfer B number, previously reported by Holve and Sawyer,[7] based on their experimental observation of the combustion poly (ethylene) in an opposed flow diffusion flame, $B = 3.48Y_{O}^{\infty}-0.18$, where Y_{O}^{∞} is the oxygen mass fraction in the ambient N_2/O_2 flow. The fuel surface temperature was specified at 800K. The oxygen concentration at the fuel surface was set at zero. The fuel surface mass fraction, Y_{fw}, results from species and energy balances,

$$Y_{fw} = (B - Y_{O}^{\infty}/s)/(1 + B) \qquad (1)$$

where s is the stoichiometric ratio, mass fuel consumed per mass of oxygen.

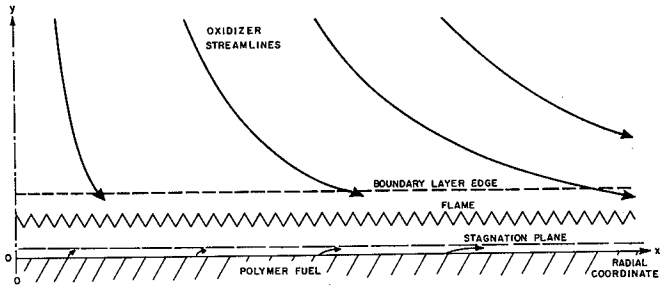

Fig. 1. Description of a reacting, stagnation-point flow. (XBL 811-5106)

Solutions to the boundary layer equations were found by using GENMIX,[8] which solves the finite difference equations in implicit form. The flame structure was found for both finite and infinite reaction rate cases for an oxygen mole fraction, X_{O}^{∞}, of 0.232 as shown in Figures 2 and 3. If only a solid curve appears on the profiles, the finite and infinite reaction-rate curves are super-imposed for this graph size. For an infinite reaction rate, the oxygen and fuel concentrations go to zero at the maximum temperature location, which will be designated the flame. When the reaction rate is finite, some of the fuel and oxygen survive and are transferred through the flame. Transfer of molecular oxygen through the flame was also found experimentally, as shown by the experimental points in Figure 2.

The velocity profiles for the finite and infinite reaction rate are identical on the graphic scale presented. The variable u/u_{max} is plotted because it is independent of radial location. The

* This work was supported through the U.S. National Bureau of Standards under Contract No. 805180 through the U.S. Department of Energy under Contract No. W-7405-ENG-48 .

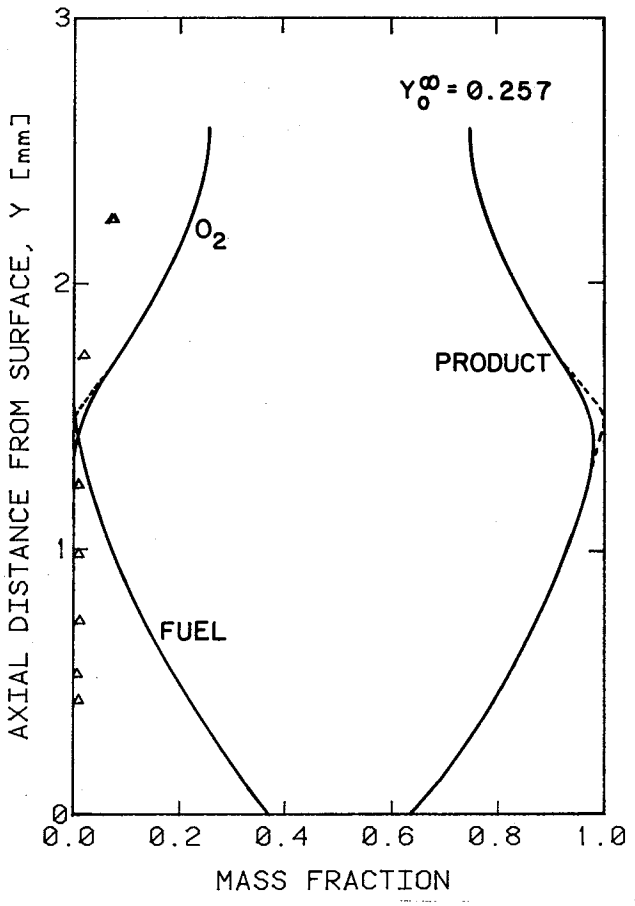

Fig. 2. Calculated species profiles for finite (——) and infinite (---) reaction rates. Measured oxygen profile (Δ). (XBL 811-5110)

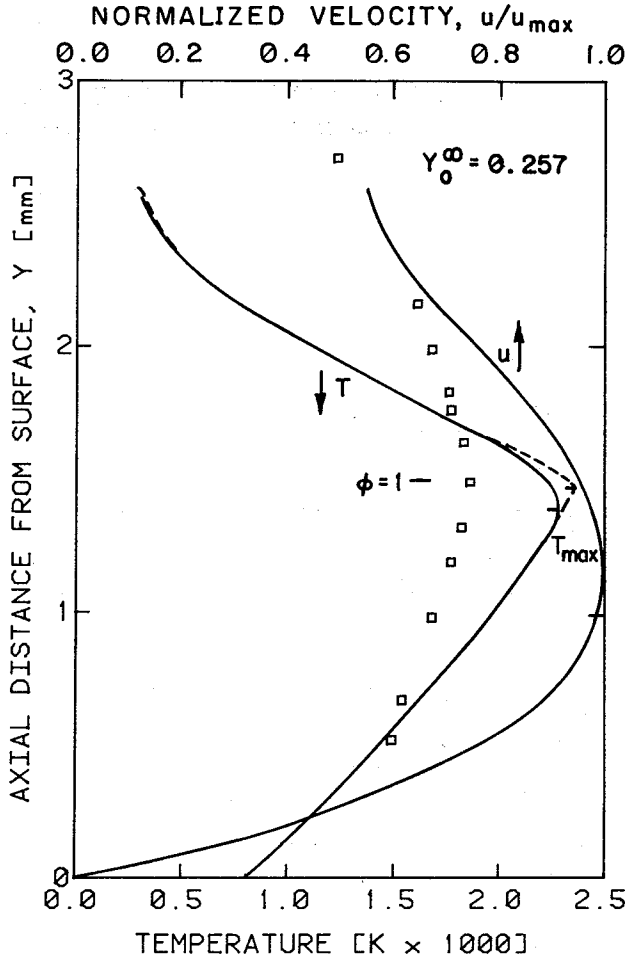

Fig. 3. Calculated temperature profiles for finite (——) and infinite (---) reaction rates. Measured temperature profile (□). Calculated velocity profile. (XBL 811-5109)

location of u_{max} is between the flame and fuel surface for the following reasons. Since the viscosity is temperature dependent, it is maximum at the flame. As indicated in Figure 1, the streamlines pass through the flame convecting the flow into this lower viscosity region where the maximum velocity is attained.

Calculated flame stand-off distances for finite and infinite reaction rates and measured stand-off distances are shown in Figure 4. All stand-off distances presented decrease with decreasing ambient oxygen mole fraction, $X_{O}\infty$. When $X_{O}\infty$ is lowered, the flame temperature is reduced, which decreases temperature gradient at the surface and, thereby, the fuel blowing rate. The fuel mass fraction at the surface is also decreased since the B number is lowered (eq. 1). Both of these effects reduce the flame stand-off distance. It is crucial to include finite rate flame chemistry when predicting flame stand-off distances near extinction (Fig. 4). When $X_{O}\infty$ is increased, the flame condition moves out of the extinction regime, and the flame stand-off distance predictions are the same for both finite and infinite rate cases. If the flame is near extinction, the net fluid motion through the flame and towards the surface becomes important. The reactants are convected for significant distance before they are fully reacted and the maximum temperature is reached.

Overall reaction-rate parameters were extracted from extinction data. Extinction measurements in the opposed flow apparatus were performed for poly(ethylene) burning in N_2/O_2 mixtures (Fig. 5). The values of the reaction-rate parameters were iterated until the calculated extinction curve approximated the least squares fit of the data. The resultant activation energy, E_A, and pre-exponential coefficient, K, are defined by the following Arrhenius expression,

$$\dot{m}_f = K\, p^2\, Y_f\, Y_O\, \exp\,(-E_A/RT)$$

where E_A is 31 ± 3 kcal/gmole, K is 5.4×10^{-2} $kg/(Pa)^2m^3s$, $\dot{m}_f$ is the mass consumption rate of fuel per unit volume in kg/Pa^2m^3s, p is the pressure in Pa, Y_f and Y_O are the fuel and oxygen mass fractions, R is the gas constant, and T is the temperature in K.

PLANNED ACTIVITIES FOR FY 1981

Measurements of inhibition characteristics and the final report of this study will be accomplished and this research will then be concluded.

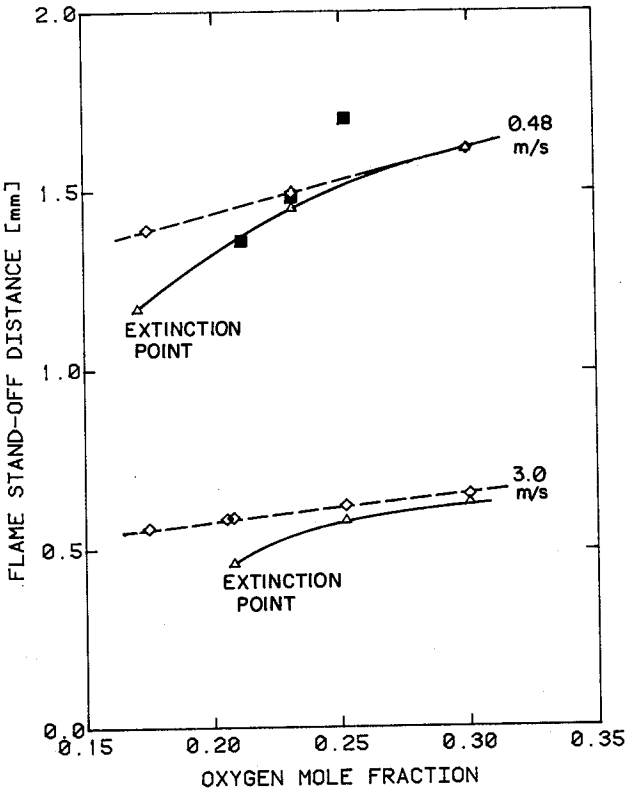

Fig. 4. Flame stand-off distance calculated for finite (——) and infinite (---) reaction-rate and measured by experiment (□). (XBL 811-5111)

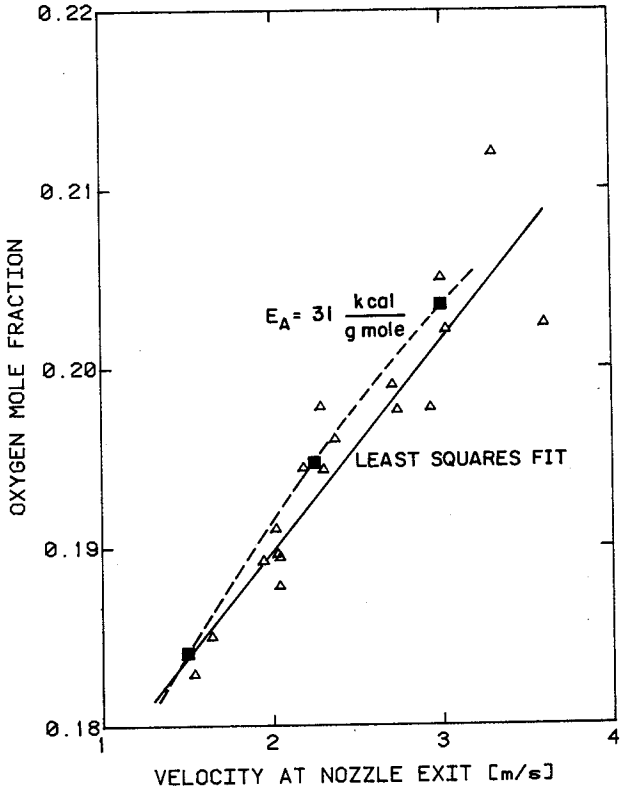

Fig. 5. Measured extinction conditions for PE burning in N_2/O_2 mixtures (△) and calculated extinction conditions (□). (XBL 811-5113)

REFERENCES

1. T. P. Pandya and F. J. Weinberg: Proc. Roy Soc. A., vol. 279, p. 544 (1965).

2. H. Tsuji and I. Yamaoka: Twelfth Symposium (International) on Combustion, The Combustion Institute, p. 997 (1969).

3. J. R. Richard, C. Vovelle, and R. Delbourgo: Fifteenth Symposium (International) on Combustion, The Combustion Institute, p. 205 (1975).

4. K. Seshadri and F. A. Williams: J. Polymer Sci.: Polymer Che. Ed., vol. 16, p. 1755 (1978).

5. W. J. Pitz, N. J. Brown and R. F. Sawyer: Eighteenth Symposium (International) on Combustion, The Combustion Institute, 1981.

6. C. R. Wilke: J. Chem. Phys., vol. 18, p. 517 (1950).

7. D. J. Holve and R. F. Sawyer: Fifteenth Symposium (International) on Combustion, The Combustion Institute, p. 351 (1975).

8. D. B. Spalding: GENMIX: A General Computer Program for Two-Dimensional Parabolic Phenomena, Pergamon Press (1977).

FLAME RADIATION*

C. Tien and S. Lee

INTRODUCTION

Thermal radiation from flames has long been recognized as an important factor in many physical systems, such as fires and combustors. The combustion products from flames of hydrocarbon fuels generally consist of several gas constituents plus numerous unburnt solid particulates called soot. Soot particles in flames contribute significantly to the infrared radiation, as well as the luminosity of flames. To estimate the radiative contribution of soot to flames, detailed soot information must be known.

Soot particles are characterized by optical properties, composition (hydrogen/carbon ratio), size distributions, and shapes. By assuming the soot is spherical, other properties, as well as radiative heat transfer analyses, have been explored in several previous investigations.[1-5]

In the past, research progress was concerned primarily with the physical and specific analytical basis of infrared radiation from flames. The fundamental aspects of soot characteristics, such as soot optical properties, composition, shapes, and measurements of soot volume fraction for various flames, were determined.

ACCOMPLISHMENTS DURING FY 1980

Research during the past year was focused on obtaining the various characteristics of soot and determining their effect on soot radiation and heat transfer. These are discussed below.

Soot Optical Properties and the Effect of Composition

A dispersion model has been established for the optical constants of soot in hydrocarbon flames on the basis of a more rigorous consideration of the electronic band structure and the dispersion constants.[6] The dispersion constants of hydrocarbon soot have been determined from this model in conjunction with the in-situ flame transmission data in the visible and infrared ranges, thus truly reflecting soot in flames. It is shown that the soot optical properties are rather insensitive to temperature changes at elevated temperatures, but the room temperature values representative of soot in smoke do exhibit appreciable deviation.

On the experimental side, transmission experiments were performed to obtain the spectral extinction coefficients and volume fractions of soot from various flames. Agreement between the experimental and predicted results is excellent. The results also indicate that the soot optical properties are relatively independent of the fuel hydrogen/carbon ratio.

Soot Particle Shape

The radiative heat transfer characteristics of a sooty medium may vary greatly because of soot conglomeration. Information on the number of various conglomerated shapes is required for the exact calculation of flame and smoke radiation. The complexities and uncertainties involved in accounting for all particle shapes present a formidable problem and may not justify any detailed or elaborate computation for practical applications. Therefore, radiation from different particle shapes was investigated recently[7] to develop a better understanding of the effect of soot conglomeration on soot radiation.

Radiative Heat Transfer with Particulate Scattering

The resistance-network representation for radiative heat transfer is developed for a planar absorbing-scattering medium on the basis of the two-flux model and the linear anisotropic scattering model.[8] Particular attention is given to the scattering effect caused by particulates such as flame soot or smoke particles. Limiting relations for various regimes are derived and the physical significance of the resistances are discussed. An illustrative example is presented for thermal radiation from a smoke layer. Extension to two-phase dispersed systems is also demonstrated.

REFERENCES

1. R. O. Buckius and C. L. Tien, "Infrared Flame Radiation," International Journal of Heat and Mass Transfer, vol. 20, pp. 93-106 (1977).

2. W. W. Yuen and C. L. Tien, "A Simple Calculation Scheme for the Luminous-Flame Emissivity," Proceedings of the 16th International Combustion Symposium, pp. 1481-1487 (1977).

3. G. L. Hubbard and C. L. Tien, "Infrared Mean Absorption Coefficients for Luminous Flames and Smoke," Journal of Heat Transfer, vol. 100, pp. 235-239 (1978).

4. W. W. Yuen and C. L. Tien, "Approximate Solutions of Radiative Transfer in One-Dimensional Non-Planar Systems," Journal of Quantitative Spectroscopy and Radiative Transfer, vol. 19, pp. 533-549 (1978).

5. W. W. Yuen and C. L. Tien, "A Successive Approximation Approach to Problems in Radiative Transfer with a Differential Formulation," Journal of Heat Transfer, vol. 102 (1980).

* This work was supported by the Center for Fire Research of the U.S. National Bureau of Standards under Contract No. NB80NAGE1653 through the U.S. Department of Energy under Contract No. W-7405-ENG-48.

6. S. C. Lee and C. L. Tien, "Optical Constants of Soot in Hydrocarbon Flames," Proceedings of the 18th International Combustion Symposium (1980).

7. S. C. Lee and C. L. Tien, "Thermal Radiation of Spherical and Cylindrical Soot Particles," Paper presented at the Western States Section/ The Combustion Institute, Paper No. 80-54, Fall Meeting, Los Angeles, CA., October 20-21, 1980.

8. T. W. Tong and C. L. Tien, "Network Representation of Radiative Heat Transfer with Particulate Scattering," Journal of Quantitative Spectroscopy and Radiative Transfer, vol. 24, pp. 491-503 (1980).

TESTS AND CRITERIA FOR FIRE PROTECTION OF CABLE PENETRATIONS*

R. Williamson and F. Fisher

INTRODUCTION

The spread of fire in nuclear reactors depends critically on the barrier qualities of the cable penetrations of fire resistant walls and floor/ceiling assemblies. The ASTM E-119 Fire Endurance Test Method has been used to qualify the unpenetrated walls and floor/ceiling assemblies; but, if such assemblies contain cable penetrations, special attention is required. This is the focus of this project.

The actual fire conditions represented by the E-119 test method, termed "post-flashover," are conditions in which fire fully involves a compartment. Post-flashover fires are characterized by a positive pressure differential between the upper half of the fire compartment and the unexposed face of the wall and floor/ceiling assemblies which make up its boundaries. The initial portion of this post-flashover period is also characterized by excess amounts of fuel which have been pyrolized by the fire within the compartment. The positive pressure and excess pyrolyzate are clearly proven by the flames which commonly are observed to emerge from the doors and windows of both actual and laboratory post-flashover building fires.

The ASTM E-119 Standard does not specify either the pressure differential or the presence of excess fuel at the surface of the test assembly. One of the objectives of this project has been to establish the effects of varying furnace pressure on cable penetrations performance in the ASTM E-119 fire test. Another objective has been to investigate the modes of failure for these cable penetrations and to explore the possibility of new pass/fail criteria.

Experiments were conducted during 1979 which clearly showed that positive pressure and excess pyrolyzates play a vital role in the spread of fire through cable penetrations. If there is a path through the penetration opening, flames always appear on the unexposed face when there is a positive pressure differential and there are excess pyrolyzates in the furnace.

ACCOMPLISHMENTS DURING FY 1980

A draft fire test proposal for positive pressure and excess pyrolyzates was written and circulated to the appropriate Task Group and Subcommittee in the American Society for Testing and Materials where both fire protection and nuclear engineers participated. There has been an extensive debate on these measures, and it now appears (as of January 1981) that the non-nuclear interests on the ASTM committee have dominated the issue and that the penetration test standard will not call for either positive pressure or excess pyrolyzates, although the former will be an option.

Experimental fire tests were conducted during 1980 to establish the best methods of regulating pressure and providing excess pyrolyzates during the ASTM E-119 test.[1] It was found that the pressure was relatively easy to regulate using dampers on the furnace stacks, but the excess pyrolyzates were much more difficult to control. Part of the problem is that, with both positive pressure and excess pyrolyzates, the Standard E-119 time-temperature curve is very difficult to maintain. In some experiments, we had a runaway fire with a much greater "severity" than the relatively benign E-119 fire.

The net results of the circulation of draft fire test standards through the ASTM, in conjunction with the experimental difficulties, has lead to the realization that it is not sufficient to add additional requirements to the ASTM E-119 Test Method in order to evaluate cable penetrations; it will be much better to develop an entirely new fire test standard.

Another accomplishment during 1980 has been the development of a probabilistic network for fire spread. A paper entitled "Using Fire Tests for Quantitative Risk Analysis" was presented at the ASTM Symposium on "Risk Analysis" at Hilton Head, S.C., June, 1980, describing the use of fire tests.

* This work was supported by the U.S. Nuclear Regulatory Commission through Sandia Laboratories, Albuquerque, New Mexico under Contract No. 46-6967 through the U.S. Department of Energy under Contract No. W-7405-ENG-48.

In the course of preparing this paper, a new and potentially revolutionary approach to fire protection was discovered. This is the subject of a proposal for new research as follows:

"Quantitative Fire Risk Analysis
Utilizing Probabilistic Methods"

The application of networks to solve fire protection problems has led to a new method of quantitative analysis. If the networks for fire spread, smoke development, and evacuation of occupants are converted to probabilistic networks, such as those used in communications engineering, these networks can be solved simultaneously to quantify a range of fires which could occur in a given building. The possible fires, their expected potential for injury to occupants, and their potential for property damage would be explicitly presented. The research project has two principal objectives: first, the development of probabilistic networks for fire and smoke spread and the movement of people, and emphasis in designing these for simultaneous solution; second, there would be an experimental program to develop the methods of gathering the physical data to quantify the probabilistic networks.

This proposed research project is oriented toward the environmental health and safety of buildings. The recent tragic fire in the MGM Grand Hotel in Las Vegas, where 84 persons died, shows the continuing problem of unwanted fire. This research project is focused on a new and powerful method of analyzing the fire safety of buildings. It has potential application in many areas of special interest to DOE, such as conservation, solar power, and nuclear power. The use of new materials and new building designs requires a careful analysis for fire safety before a disastrous fire emphasizes the problem. Support of this new research will be sought from various potential sponsors.

PLANNED ACTIVITIES FOR FY 1981

A special floor fire-test furnace, constructed for another project, will be used to perform experiments on cable penetration assemblies, with specific pressure and excess pyrolyzates on the fire side of the test specimen. The emphasis in the research will be to investigate the experimental methods required to subject cable penetrations to the range of potential fires which they might face under actual fire conditions.

REFERENCE

1. Annual Book of ASTM Standards, American Society for Testing and Materials, Philadelphia, PA.

LASER SPECTROSCOPY AND TRACE ELEMENT ANALYSIS

INTRODUCTION

Energy production and utilization result in the emission of pollutants that are potentially harmful to man and to other forms of life. It is desirable to provide means to measure these pollutants, to understand their fate, and to assess their effects on health and other biological activities such as agriculture.

In order to control these pollutants, adequate methods are required for monitoring the level of various substances often present at low concentrations. The Energy and Environment Division Applied Research in Laser Spectroscopy & Analytical Techniques Program is directed toward meeting these needs. Emphasis is on the development of physical methods, as opposed to conventional chemical analysis techniques. The advantages, now widely recognized, include ultra-high sensitivity coupled with minimal sample preparation. In some instances physical methods provide multi-parameter measurements which often provide the only means of achieving the sensitivity necessary for the detection of trace contaminants.

APPLIED PHYSICS AND LASER SPECTROSCOPY RESEARCH

N. Amer, N. Bergstrom, R. Gerlach, W. Jackson, R. Johnson, S. Kohn, M. Olmstead, C. Rosenblatt,† D. Wake, and Z. Yasa*

OVERVIEW

The research philosophy of our group is to apply the knowledge of advanced laser spectroscopy and condensed matter physics to energy and environmental problems. Because of the narrow linewidth and tunability of lasers, unsurpassed sensitivity and specificity can be achieved in detecting trace contaminants of the environment. The advanced state of condensed matter physics makes it possible to apply such knowledge to energy production and to test novel methods for energy conversion such as photovoltaic solar cells, superionic electrical energy storage devices, and the recovery and extraction of oil from abandoned wells and oil shales with lyotropic liquid-crystal emulsifiers.

---

*Group Leader

†Present Address: National Magnet Laboratory, M.I.T., Cambridge, Mass.

‡This work was supported by the Assistant Secretary for Environment, Office of Health and Environmental Research, Pollutant Characterization and Safety Research Division of the U.S. Department of Energy under Contract No. W-7405-ENG-48.

§Complete version of this report is given in LBL-11541 and will be published in Applied Optics, April 15, 1981.

LASER PHOTOACOUSTIC AND PHOTOTHERMAL MEASUREMENTS AND CHARACTERIZATION‡

Laser photoacoustic and photothermal spectroscopies provide a powerful tool for the detection of trace contaminants in air and water, as well as a means for investigating the fundamental properties of gaseous, liquid, or solid phases of matter. One of our goals in this project is to develop ultrasensitive, multiparameter, elemental and molecular detectors for the characterization of pollutants released in the process of energy production and utilization. Another aim is to maintain a state of the art capability in photoacoustic and photothermal detections by fully understanding the physics of these techniques. Concurrent with these efforts, we are actively developing new or modified laser systems compatible with our particular needs. Below, we report our results for FY 1980.

PHOTOTHERMAL DEFLECTION SPECTROSCOPY AND DETECTION: THEORY§

Before proceeding with the theoretical treatment of photothermal deflection spectroscopy (PDS), a brief physical description of PDS is in order. The absorption of the optically exciting beam (pump beam) causes a corresponding change in the index of refraction of the optically heated region. The absorption also causes an index-of-refraction gradient in a thin layer adjacent to the sample surface. By probing the gradient of the varying index of refraction with a second beam

(probe beam), one can relate its deflection to the optical absorption of the sample. This is in contrast with probing thermally induced changes in optical path lengths, as in interferometric techniques, or probing the curvature of the index of refraction, as in thermal lensing (TL). As can be seen from the above description, one has two choices in performing PDS: (1) collinear photothermal deflection, where the gradient of the index of refraction is both created and probed within the sample (Fig. 1), or (2) transverse photothermal deflection, where the probing of the gradient of the index of refraction is accomplished in the thin layer adjacent to the sample--an approach most suited for opaque samples and for materials of poor optical quality (Fig. 1).

The calculation of the expected beam deflection for PDS can be divided into two parts. One first finds the temperature distribution in the sample and then solves for the optical beam propagation through an inhomogeneous medium. Below, we give the solutions for the probe beam deflection for various experimental configurations.

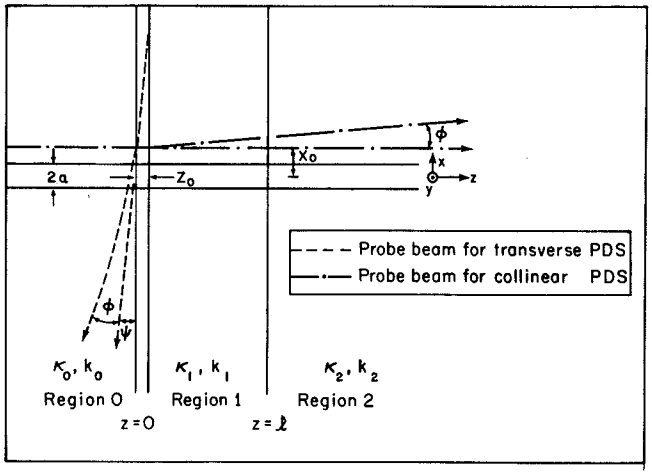

Fig. 1. Geometry for theory. The heat deposited diffuses into Region 0 and Region 2 as well as radially. For transverse PDS, the probe beam may be displaced along the y axis by a distance y_o. (XBL 8012-2089)

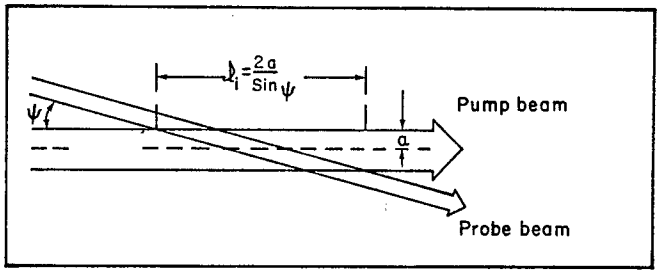

Fig. 2. Effective intersection length for collinear PDS. (XBL 8010-2083)

Solution for Beam Deflection

Collinear PDS. For collinear PDS, the beam is deflected by the temperature gradient in all three regions. For simplicity, we assume that the probe beam travels parallel to the pump beam axis and is deflected only in Regions 1 and 2. However, the interaction length is restricted to be consistant with an angle between the pump and probe beams (see Fig. 2).

The deflection in this case is given by:

$$\phi = \frac{-e^{i\omega t}}{2n_o}\frac{\partial n}{\partial T}\left[\int_o^{\ell} dz \int_o^{\infty} \delta^2\, d\delta J_1(\delta x_o)\, \Gamma(\delta)\, e^{-\alpha z} + A(\delta)\, e^{-\beta_1 z} + B(\delta)\, e^{\beta_1 z} + \right.$$

$$\left. \int_o^{\ell_i} dz \int_o^{\infty} \delta^2 J_1(\delta x_o)\, d\delta D(\delta)\, e^{-\beta 2(z-\ell)}\right] + \text{c.c.}\quad \ell_i > \ell \qquad (1)$$

where $\ell_i = 2a/\sin\psi$ is the length of interaction of the two beams, x_o is the displacement between the beams, and ψ is the angle of their intersection. If the beams overlap in Region 1 only, then

$$\phi = -\frac{1}{2n_o}\frac{\partial n}{\partial T} e^{i\omega t} \int_o^{\ell_i} dz \int_o^{\infty} \delta^2\, d\delta J_1(\delta x_o)\left[\Gamma(\delta)\, e^{-\alpha z} + A(\delta)\, e^{-\beta_1 z} B(\delta)\, e^{\beta_1 z}\right] + \text{c.c.}\quad \ell_i < \ell \qquad (2)$$

Transverse PDS. For transverse PDS, the probe beam propagates completely within Region 0. The probe beam path (Fig. 1) is the deflection in this case and is given by

$$\phi = \frac{1}{2}\frac{e^{i\omega t}}{n_o}\frac{\partial n}{\partial T}\int_{\infty}^{-z_o/(\tan\psi)} dz \int_{o}^{\infty} \delta J_o\left(\delta\sqrt{y_o^2 + x^2}\right)\beta_o E(\delta)\, e^{\left[(\tan\psi)x + z_o\right]\beta_o} + c.c. \qquad (3)$$

SENSITIVE IN-SITU TRACE GAS DETECTION BY PHOTOTHERMAL DEFLECTION SPECTROSCOPY†

This work presents an approach to photothermal deflection spectroscopy where the refractive index gradient is both created and optically detected within the medium of interest (in this case a gas). Such an approach proved to be sensitive and suited for the in-situ detection of trace gases since it obviates enclosing the sample in some container in order to perform the detection.

Using diffraction theory, we have recently shown that, for modulation of the pump beam at low frequency, the amplitude ϕ of the probe beam deflection is given by

$$\phi = (dn/dT)(P/\kappa\pi^2 x_o)\left[1-\exp(-\alpha\ell)\right]\left[1-\exp(-x_o^2/a^2)\right] \qquad (1)$$

where dn/dT is the temperature coefficient of refractive index, P is the amplitude of the incident laser power modulation, κ is the thermal conductivity of the gas, x_o is the distance between the intensity maxima of the pump and probe beams, α is the optical absorption coefficient, ℓ is the interaction length of the pump and probe beams, and a is the radius of the pump beam at 1/e intensity. Thus, for small $\alpha\ell(\lesssim 2)$ the amplitude of the deflection is proportional to $\alpha\ell$ and to the power. Furthermore, ϕ exhibits a maximum near $x_o/a \sim 1$ defining the optimal separation between the pump and probe beams.

To investigate the sensitivity of photothermal deflection spectroscopy for the detection of small absorption in gases, we chose to determine the minimal detectable concentration of ethylene at a signal to noise ratio (S/N) of unity. We also tested the in-situ capability of this detection scheme by measuring the absorption spectrum of laboratory air (without any sample cell or enclosure) in the 9-11 μm region of the infrared.

The experimental arrangement is shown in Figure 3. To determine the sensitivity and obtain a calibration of the apparatus, we initially employed a calibrated mixture of ethylene in nitrogen and other lower-concentration mixtures obtained by dilution of the calibration mixture in a 20 cm long cell. In Figure 4, we plot signal from the photodiode as a function of ethylene concentration. As can be seen, the detected signal is a linear function of the concentration over four orders of magnitude. No coherent background signal was detected when the cell was filled only with nitrogen.

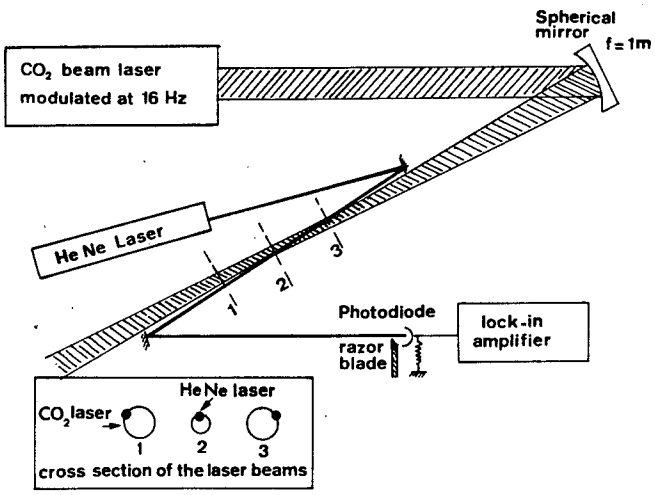

Fig. 3. Schematic of experimental equipment. (XBL 813-8370)

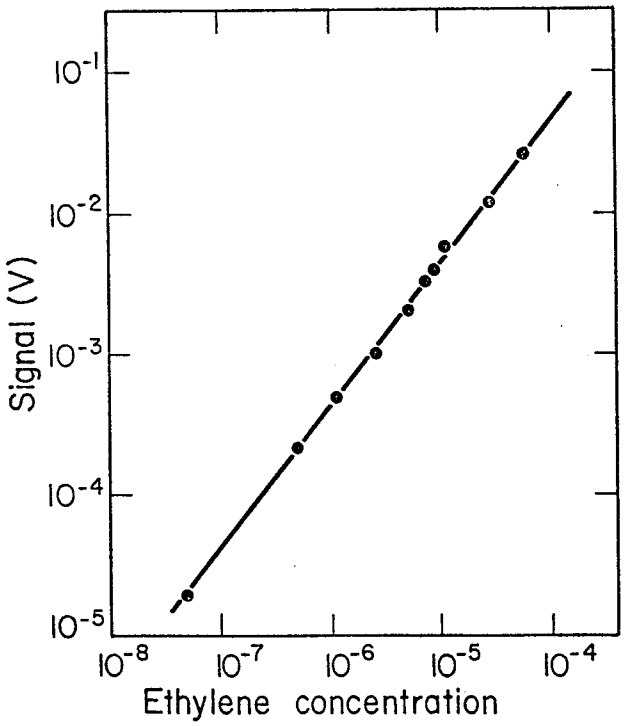

Fig. 4. Thermal deflection signal versus ethylene concentration in nitrogen (molar fraction). (XBL 813-8371)

†Complete version of this work appeared in Applied Physics Lett., vol. 37, no. 519 (1980).

From these results, we compute a minimum detectivity (S/N=1) of 5 ppb, i.e., a minimum absorption coefficient detection of $\sim 10^{-7}$ cm^{-1}.

We also measured, in situ, the absorption spectrum of laboratory air using the various lines of the R branches of the 9.4 μm and 10.4 μm bands of CO_2 lasers. Tables 1 and 2 compare our results with published data. Although the dominant contribution to the absorption in the 9.4 μm region can be interpreted as due to water vapor, other unidentified gases appear to contribute significant absorption in the 10 μm region.

Table 1. Observed signal for laboratory air in the 9.4 μm band of the $C^{12}O_2^{16}$ laser.

Laser line	Frequency (cm^{-1})	Experimental absorption coefficient[a] (10^{-6} cm^{-1})	Abs. coeff. of water vapor (10^{-6} cm^{-1})
R(10)	1071.884	2.9	0.35
R(12)	1073.278	1.5	0.44
R(14)	1074.646	2.3	1.48
R(16)	1075.988	1.45	0.57
R(18)	1077.303	1.35	0.43
R(20)	1078.591	1.2	0.40
R(22)	1079.852	1.51	0.40
R(24)	1081.087	1.65	0.39
R(26)	1082.296	1.2	0.36
R(28)	1083.479	1.3	0.38
R(30)	1084.635	2.6	1.40
R(32)	1085.765	3.0	0.58

[a]Data were normalized to published data for the R(20) line of the 10.4 μm band.

Table 2. Observed signal for laboratory air in the 10.4 μm band of the $C^{12}O_2^{16}$ laser.

Laser line	Frequency (cm^{-1})	Experimental absorption coefficient[a] (10^{-6} cm^{-1})	Abs. coeff. of water vapor (10^{-6} cm^{-1})
R(8)	967.707	0.55	0.41
R(10)	969.139	0.65	0.34
R(12)	970.547	1.5	0.97
R(14)	971.930	1	0.92
R(16)	973.289	1.1	0.78
R(18)	974.622	0.75	0.61
R(20)	975.930	5.5	5.49
R(22)	977.214	0.85	0.84
R(24)	978.472	0.65	0.50
R(26)	979.705	0.68	0.49
R(28)	980.913	0.68	0.40
R(30)	982.096	1	0.46
R(32)	982.252	0.95	0.40

[a]Data were normalized to published data for the R(20) line of the 10.4 μm band.

Our detection limits were set by the following factors:

- Fluctuations in the pointing stability of the probe beam were estimated to be two orders of magnitude above the photon noise. This limitation can be alleviated, for example, by the inclusion of an intracavity iris to force the laser to oscillate on the fundamental transverse mode.
- In the case of experiments requiring long beam paths, air turbulence can be a limiting factor when the pump beam is modulated at low frequencies. Introduction of a Fabry-Perot interferometer as close as possible to the interaction region should overcome this problem. Another simple solution is to have the two laser beams intercept each other inside an open ended tube.
- Electronic noise was a limiting factor only when a position-sensing detector was used.
- With adequate isolation, mechanical vibrations do not set the detection limit.

In conclusion, we have shown that photothermal deflection spectroscopy provides a simple means for the measurement of very weak absorptions in gas phase samples. We have also demonstrated its feasibility for in-situ measurements, i.e., in the absence of a sample container, thus eliminating the problems associated with sampling techniques. This technique also eliminates the background signal associated with scattering and with the heating of the sample cell windows which one encounters in photoacoustic spectroscopy.

SENSITIVE PHOTOTHERMAL DEFLECTION SPECTROSCOPY OF CONDENSED MEDIA[†]

When an intensity modulated beam of electromagnetic radiation (pump beam) is incident on an absorbing medium, heating will ensue. Concomitant with this time-dependent change in the medium temperature is a corresponding modulated index of refraction gradient which can be employed to deflect a probe beam intersecting the pump beam within the sample and/or substrate. The deflection can be as small as 10^{-9} - 10^{-10} radians, which is well within the detectivity levels of available position sensors. The amplitude of the deflection is related to the optical absorption in a straightforward manner.

Using diffraction theory, we have derived general expressions for the deflection of a laser beam by an absorbing medium on a given substrate. A very brief description of this theory is given on page 1. Neglecting the effects of the substrate and considering the case where the thermal diffusion length of the medium is much smaller than the Gaussian pump beam radius (the case of high frequency modulation and/or low thermal con-

[†]Complete version of this work appeared in Optics Lett. vol. 5, no. 377 (1980).

ducting medium), the deflection angle ϕ is given by

$$\phi = (dn/dT)(P/\omega\rho c\pi^2 a^2)\left[1-\exp(-\alpha\ell)\right]\left[-2x_o/a^2)\exp(-x_o^2/a^2)\right] \qquad (1)$$

where dn/dT is the temperature coefficient of the index of refraction of the medium, P is the incident laser power, ω is the angular modulation frequency of the pump beam, ρc is the heat capacity per unit volume, a is the radius of the pump beam at 1/e intensity, x_o is the separation between the intensity maxima of the pump and probe beams, α is the optical absorption coefficient, and is the optical path length in the absorbing medium. Thus, for small $\alpha\ell$ ($\lesssim 2$) the deflection amplitude is proportional to the optical absorption and to the power, while inversely proportional to the modulation frequency. Furthermore, ϕ exhibits a maximum near $x_o/a \sim 1$ defining the optical separation between the pump and probe beams.

On the other hand, in the case where the thermal diffusion length is much larger than the pump beam radius, ϕ is given by

$$\phi = (dn/dT)(P/\kappa\pi^2 x_o)\left[1-\exp(-\alpha\ell)\right]\left[1-\exp(-x_o^2/a^2)\right] \qquad (2)$$

where κ is the thermal conductivity of the medium. Note that in this case, ϕ is independent of ω. The experimental arrangement is shown in Figure 5.

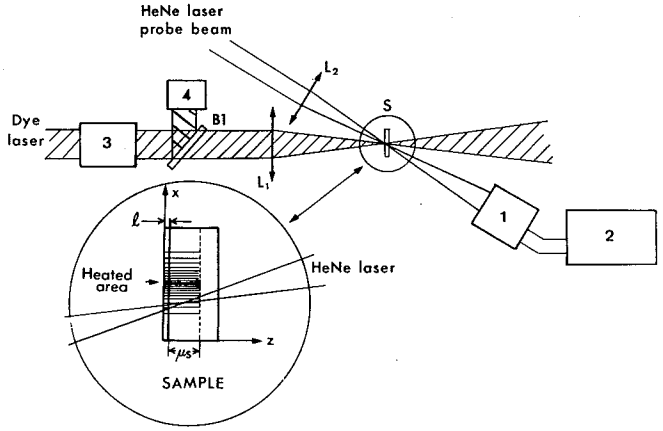

Fig. 5. Schematic of experimental equipment.
1 - Position sensor
2 - Lock-in amplifier
3 - Modulator
4 - Power meter
L_1 - 12-cm focal length lens
L_2 - 6-cm focal length lens
B_1 - Beam splitter

(XBL 806-1128)

In Figure 6, we present the amplitude of the deflection as a function of the distance from the center of the optically heated region. The results are given for low (5 Hz) and high (5 kHz) modulation frequencies. As predicted by Equations (1) and (2), the optically heated region is much larger than the waist of the pump beam at low frequency. On the other hand, at high modulation frequency, the pump beam waist and the heated region are of comparable dimensions.

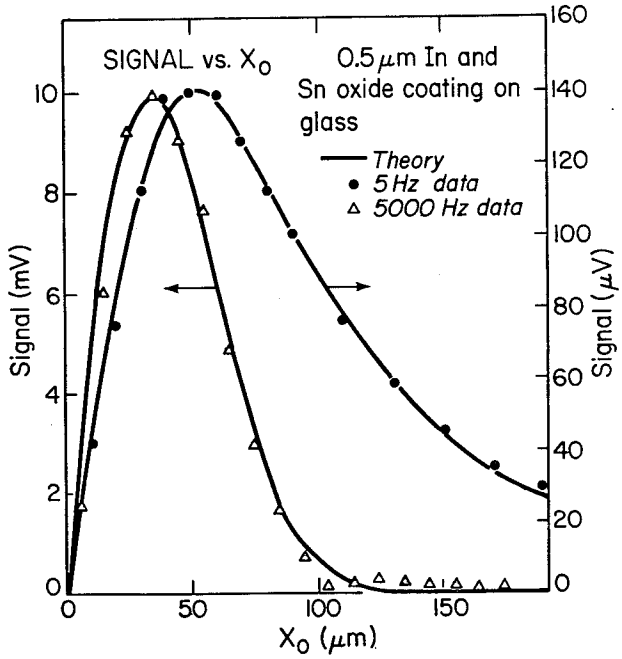

Fig. 6. Thermal deflection signal vs. the separation between the pump beam and the probe beam. The solid lines are the results of the theory.
(XBL 804-577)

To deduce the minimum detectable absorption coefficient, we compared the wavelength dependence of the photothermal deflection with the absorbance of the film when measured with a Cary 17 spectrophotometer. The film consisted of a 0.5μ thick mixture of 80% indium oxide and 20% tin oxide and was deposited on a glass substrate. At the maximum absorption, we found that for an average power of 100 mW and a time constant of 3 seconds, the noise equivalent signal was $\alpha\ell \sim 2 \times 10^{-7}$. This implies a minimum detectable absorbed power of 8×10^{-8} W/Hz$^{1/2}$. Using the value of the absorption measured by the Cary spectrophotometer, we derived a calibration relating absorption coefficients to the measured voltage output of the position sensor. Similar sensitivities were achieved with a 2μ film of CdS deposited on a glass substrate.

We have also measured the absorption spectra of bulk liquid samples. In this case, the optically heated medium is directly probed with the He - Ne laser. In Figure 7-a, we present the absorption spectrum of the 6th harmonic of the C-H stretching excitation of neat benzene, filtered through 0.22 millipore filter. Using a Cary 17 spectrophotometer, the calibration factor for the absolute absorption was determined from a long-

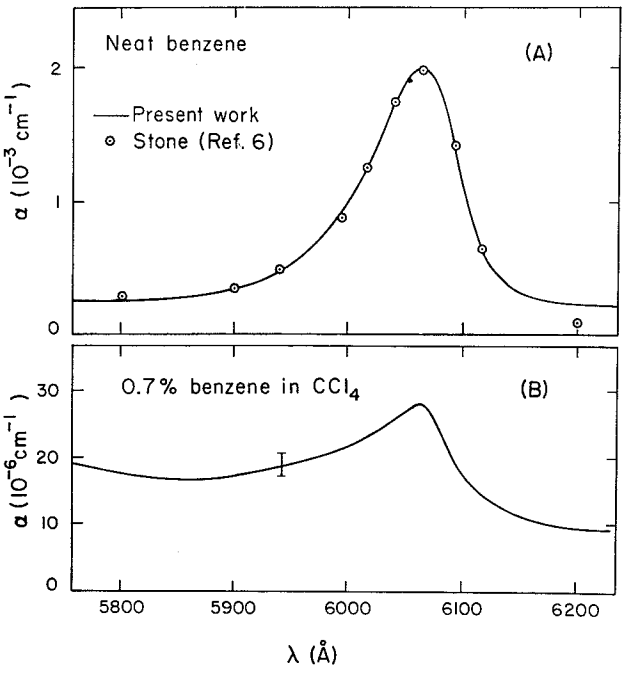

Fig. 7. a. The absorption spectrum of the 6th harmonic of the C-H stretching excitation of neat benzene. ℓ = 0.5 mm. Beam power = 60 mW.

b. The absorption of 0.7% benzene in CCl_4. ℓ = 0.5 mm. Beam power = 60 mW. Lock-in amplifier time constant = 0.3 seconds. Bar represents typical errors of $\pm$ 2×10^{-6} cm^{-1}.

(XBL 806-1127)

optical-path absorption measurement at the peak of this absorption band. As can be seen from the figure, both the line shape and strength of the absorption agree well with published results. To determine the minimum detectable absorption coefficient, we diluted the benzene (0.7%) in carbon tetrachloride (see Fig. 7-b). The noise equivalent absorption was 2×10^{-6} cm^{-1} for a pump beam of 60 mW and a 0.3 second time constant. Hence, our noise equivalent absorption is 1.5×10^{-7} cm^{-1} $W/Hz^{1/2}$. Since the optical path length ℓ was only 0.5 mm, this demonstrates that $\alpha\ell$ values of 10^{-8} are measurable by this technique. The increased detectivity in the case of liquids is due to their typically larger dn/dT values when compared with those of solids.

To check for saturation of the signal, we measured the absorption of a 0.5 mm didymium glass in the 5900 Å region. We found, as predicted by our theory, that the deflection amplitude depends linearly on α for $\alpha\ell \simeq 1-\exp(-\alpha\ell)$, beyond which signal saturation sets in.

Factors setting the limits of our sensitivity were:

- In the case of low frequency modulation, the pointing stability of the probe laser was the limiting factor. This limitation can be alleviated, for example, by the insertion of an intracavity iris to force the laser to oscillate on the fundamental transverse mode. At high frequency modulation, the limits were set by the stability of the probe laser and by the electronic noise of the position sensor.

- Care must be taken to avoid overlapping the two beams on the window of the liquid cell, otherwise a significant background signal is observed.

- With reasonable isolation, mechanical vibration was not a limiting factor.

In conclusion, we have described in this summary a simple photothermally based method for the determination of very small absorption coefficients in thin films and coatings, in highly transparent solids, and in liquids. Extension of this method to the investigation of nonlinear absorption phenomena is planned.

A NEW APPROACH TO PHOTOACOUSTIC RAMAN SPECTROSCOPY

In photoacoustic Raman spectroscopy[1] (PARS) two laser beams, one of which is tunable, pass collinearly through a gas sample enclosed in a spectrophone. One of the beams, referred to as the pump beam, can excite the molecules of the medium to virtual excited-electronic states. If the other beam, referred to as the Stokes beam, is tuned such that the frequency difference between the two lasers equals the frequency of a Raman-active vibrational mode of the molecules, it can produce stimulated Raman emission. The net result is a transfer of energy from the pump beam to the Stokes beam and a change in the vibrational state of the molecules involved in the Raman process. This vibrational energy is transferred to translational energy by collisions, and the resultant heating of the gas produces a pressure change which is detected with a microphone, as in ordinary photoacoustic spectroscopy. PARS has several attractive features distinguishing it from other coherent Raman processes: it has no threshold; it requires no phase matching; and, unlike coherent anti-Stokes Raman Scattering (CARS), the PARS signal is linearly proportional to the intensities of both the pump and the Stokes beams and also to the concentration of scattering molecules. Like CARS, it can be performed with light in the visible part of the spectrum where dye lasers serve as convenient sources of tunable coherent light, and it allows access to vibrational modes that are not infrared-active.

Among the problems encountered in PARS are the usual spurious background signal due to window heating (observed in ordinary photoacoustic spectroscopy) and the possibility of interference due to linear absorption of one of the laser beams due to (non-virtual) electronic transitions or vibrational overtones.

We propose to demonstrate some new techniques for PARS that alleviate the problems described above. A pulsed dye laser and a cw Kr^+ ion laser will provide the pump and Stokes beams, respectively. A spectrophone having a high Q acoustical resonance and designed to produce minimal back-

ground signal will be used.[2] An oscillator will be tuned to the acoustical resonant frequency of the spectrophone and used as a reference for a lock-in amplifier. The oscillator output will also be divided down to a subharmonic at which the dye laser is capable of firings.[3] If energy is being absorbed from the dye laser beam, then each pulse will produce ringing of the acoustical cavity. Since the dye laser is pulsed at a subharmonic of the cavity resonance, each pulse will reinforce the ringing left over from the previous pulse, which is still large due to the high Q, and a high pressure amplitude will develop at the resonant frequency of the spectrophone. This pressure amplitude will be detected by the microphone and lock-in amplifier. The signal thus detected could be due to the Raman process or could equally well be due to linear absorption of the dye laser beam or to window heating. The test of whether it is a Raman signal is whether it disappears when the ion laser beam is absent. Therefore, the ion laser beam is modulated at a low frequency which is used as a reference for a second lock-in. The output from the first, or high-frequency, lock-in is fed to the second lock-in, which picks out that portion of the output which is modulated at the ion laser chopping frequency. Since it is unlikely that the chopping of the ion laser beam will affect the linear absorption of the dye laser beam by the molecules or the windows, it can be concluded that this signal is due solely to the nonlinear interaction of the two laser beams caused by the Raman effect.

REFERENCES

1. J. J. Barrett and M. J. Berry, Appl. Phys. Lett. vol. 34, no. 144 (1979).

2. R. Gerlach and N. M. Amer, Appl. Phys. vol. 23, no. 319 (1980).

3. C. F. Dewey and J. H. Flint, Paper No. WC3, OSA Topical Meeting on Photoacoustic Spectroscopy, Ames, Iowa, Aug. 1-3, 1979.

DUMPING MECHANISMS IN ACOUSTICALLY RESONANT GASEOUS PHOTOACOUSTIC DETECTION

Photoacoustics has become important recently, largely because of the development of lasers. Resonant gaseous photoacoustics is important as a technique for the analysis of gases. An absorption spectrum can easily be obtained, or very small quantities of impurities can be readily detected.

One major unresolved question is, "What are the damping mechanisms that dominate the standing sound waves in a resonant photoacoustic cell?" It is vital that this be answered if the signal of resonant spectraphone (photoacoustic cell) is to be fully understood.

There are two categories of energy loss: volumetric losses and surface losses. Volumetric losses consist of what are called Stokes-Kirchhoff losses, radiation, diffusion effects, and molecular relaxational effects. Of these, only the molecular relaxational effects are significant. Surface losses are: (1) wave reflection losses due to the compliance of the walls, (2) scattering losses due to irregularities, (3) dissipation at the microphone, and (4) viscous and thermal losses at the cell boundaries. Each of these losses can be minimized by suitable construction of the cell.

The loss mechanisms can be experimentally verified by determining the Q of the cavity for a particular resonance.

$$Q = 2\pi \frac{\text{Total Energy in Cavity}}{\text{Energy Loss/Cycle}}$$

$$= \text{fm,n,p}/\Delta f\,1/2 \text{ power}$$

where f is the resonance frequency.

The experiment is set up to accurately measure this Q for various pure "buffer gases" (i.e., optically transparent) mixed with 50 ppm of C_2H_4, the absorbing gas.

A CO_2 laser beam is opto-electronically modulated and travels axially down the center of a hollow stainless steel cavity filled with 50 ppm of ethylene in some pure buffer gas. The walls of the cavity were carefully polished to $\leq 1\mu$ and kept free of obstructions. The miniature microphone is mounted flush with the cylinder wall. The Q is measured by slowly scanning through a resonance. The data obtained is fitted, using a nonlinear least squares routine.

All the noble gases through Xenon have been investigated extensively at pressures from 10 torr to 1 atm. The final fitted Q's have little scatter and can be explained, considering only the viscous and thermal dissipation at the cell boundaires.

The diatomic and polyatomic gases investigated to date are H_2, N_2, CO_2, N_2O and SF_6. Concurrently, the theoretical work needed to explain the damping for these gases is in progress. However, the molecular relaxational model, in addition to viscous and thermal wall losses, adequately explains the damping in H_2 and is expected to be largely successful in the other gases.

Through this work, a tractable theory of damping in resonant gaseous photoacoustics will be achieved. This is important for the general knowledge of physics and of great practical importance in the field of photoacoustics.

A PROPOSAL FOR A NEW PHOTOTHERMAL DEFLECTION METHOD FOR PROBING SOLID SURFACES

In designing experimental apparatus to make photothermal measurements on solid surfaces in an ultra-high vacuum environment, there are numerous technological problems. Two of these problems are: (1) how to detect the PAS signal, and (2) how to make the experiment more surface specific.

One of the best known techniques for making optical measurements on solid surfaces is attuated total reflection (ATR) spectroscopy. This technique is illustrated in Figure 8. A glass prism is placed near the sample surface with a small gap ($\sim$.1-1 μm) separating them. If an optical

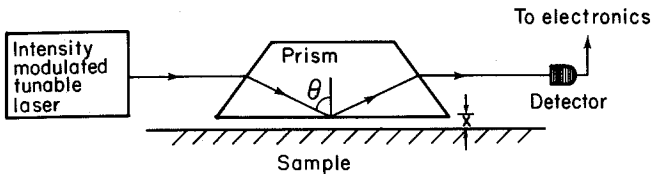

Fig. 8. Schematic of proposed experimental arrangement.

(XBL 812-162)

beam enters the prism as shown (Fig. 8), it would normally be totally reflected on the bottom surface of the prism. However, the presence of the sample surface close to the prism allows energy from the light beam to be coupled into the sample. An exact solution of Maxwell's equations for the coupled energy is straight forward. The amount of energy coupled into the sample, I, is

$$I \propto e^{-\alpha x} \qquad (1)$$

where x is the gap width and $\alpha = \frac{4\pi}{\lambda}\sqrt{h^2 \sin^2\theta - 1}$

where λ is the wavelength of the light, n is the index of refraction of the glass prism.

This technique not only makes any optical measurement more sensitive to the sample surface, it also can be used to detect the photothermal signal. Energy absorbed by the sample from an exciting beam of light, chopped at a frequency Ω, will generate acoustic phonons and thermal expansion. These will both cause the gap width, x, to be modulated at the chopping frequency, Ω. If a probe beam from a He - Ne laser is then passed through the prism in the ATR geometry, its transmitted intensity will be modulated at Ω. The calculation of the modulation of the transmission of the probe beam is straight forward. Because the gap width enters the equation exponentially, this can be a very sensitive technique for measuring small fluctuations of the gap. For the case of a silicon sample with a gap of 0.1 μm,

$$\frac{dT}{dx} \sim 5 \cdot 10^{-4} \ (1/\text{Å})$$

where T is the He Ne transmission. With phase sensitive detection, it should be possible to detect motions of 1Å or less.

AMORPHOUS PHOTOVOLTAIC SEMICONDUCTORS*

Amorphous photovoltaic semiconductors, such as hydrogenated amorphous silicon, hold promise for meeting DOE cost and efficiency guidelines for thin film solar cells prior to 1990. In order to achieve the higher conversion efficiencies required, it is necessary to better characterize the unique optical and transport properties of these materials. Photoacoustic and photothermal spectroscopies can be used to elucidate the optical and electronic properties of a-Si:H. Of particular interest is the investigation of the opti cal properties near the so-called bandgap. By combining luminescence studies, a full and accurate characterization of the de-excitation of these photo-excited amorphous semiconductors can be achieved.

Experiments investigating the optical properties of hydrogenated amorphous silicon are currently underway. The experiments are designed to yield new information on the details of the optical absorption, the nature of the bandgap, and the electronic properties which determine the photoconductivity.

OPTICAL PROPERTIES OF HYDROGENATED AMORPHOUS SILICON (a-Si:H)

Hydrogenated amorphous silicon is of great interest as a representative of a new class of disordered solids which can be doped and have a small density of states within the bandgap and a low intrinsic conductivity. Despite the interest in the physics of a-Si:H and its great potential for photovoltaic and vidicon applications, much of the important physics remains poorly understood. In particular, the density of states within the bandgap is not well measured, the mobility of the carriers as a function of excitation energy is unknown, and several competing models for the recombination of excited carriers remain experimentally untested.

One model for the carrier recombination is an electron that deforms the lattice and becomes trapped near a hole. The hole and the electron recombine radiatively, emitting sub-bandgap radiation (peaked at 1.3 eV). At higher temperatures, such as room temperatures, a non-radiative channel for de-excitation dominates the radiative channel. The alternative model proposes the existence of a "bump" in the density of states below the conduction band edge. At low temperatures, the electron is trapped in the sub-conduction band states and recombines radiatively with a hole. At higher temperatures, the sub-conduction band states are ionized to the conduction band, and the electron recombines non-radiatively.

N. Mott and W. Anderson have predicted that the mobility of the carriers as function of excitation energy predicted will exhibit a sharp decrease to zero due to the disorder of the material and the decreasing density of states within the gap. Renormalization theories also predict an abrupt decrease of the mobility as the excitation energy becomes smaller than the bandgap. This decrease has not been observed in a-SI:H; and, in fact, some workers believe that the mobility does not show a decrease until far into the gap.

Finally, the effect of the preparation conditions on the density of states, optical properties, and the mobility are not well characterized. It is known that the concentration of hydrogen within the film, the deposition rate, the substrate temperature, and the film thermal history affect the

*This work was supported by the Assistant Secretary for Conservation and Solar Energy, Office of Solar Energy, Photovoltaic Energy Systems Division, U.S. Department of Energy under Contract No. W-7405-ENG-48.

bandgap as well as the mobility of the carriers. Exactly how these parameters affect the film awaits further understanding of the carrier transport and recombination mechanisms.

We have begun a series of measurements of the absorption of the films at and below the bandgap using photothermal deflection techniques. This is an ideal technique because the films cannot be thickened, and the subgap absorption is small. We have succeeded in measuring an $\alpha\ell$ of 5×10^{-4} at photon energies of 0.6 eV.

Because the absorption is proportional to the joint density of states, if the matrix elements are energy independent, the "bump" in the density of states predicted by one of the recombination models should give rise to a shoulder in the absorption spectra below the absorption edge. The model, which hypothesizes that electron deforms the lattice, predicts no such "shoulder." Therefore, we should be able to decide between the two models. Additionally, by comparing the observed absorption to that predicted by various models for the density of states, we may be able to eliminate some models.

If we compare the absorption data with photoconductivity data, we can measure the mobility-lifetime product as a function of excitation energy. Finally, by performing such experiments for samples prepared under different deposition conditions, we may shed some light on the connection between the deposition parameters and the properties of the films.

INVESTIGATION OF CARRIER DRIFT MOBILITY BY PHOTOTHERMAL DEFLECTION SPECTROSCOPY

Reported values of the drift mobility of the carriers in hydrogenated amorphous silicon have varied by as much as two orders of magnitude, due in part to the indirect nature of the techniques employed. We initiated a set of experiments which employ a very different technique and which, in principle, should yield a more direct determination. Briefly, electrodes are deposited on a hydrogenated amorphous Si film which is then placed in a fluid (in this case, CCl_4). An alternating electric field would spatially modulate a conduction band population in the film. A chopped Ar^+ laser beam generates the conduction band population. The heat of recombination flows from the location of the carrier population into the film and the surrounding fluid, producing a local gradient in the index of refraction, n, which follows the field. A second, sub-bandgap probe laser beam will then be deflected by the gradient of the index of refraction that is synchronous both with the Ar^+ laser beam, which creates the gradient, and the electric field, which spatially displaces the gradient. The deflection is detected with a position sensor placed some distance from the film. A two lock-in detection scheme discriminates in favor of deflections arising from both sources together.

From independent measurement of τ, the carrier movement, $l = \mu E \tau$ yields the mobility. This experiment, which was begun in the summer of 1980, is continuing.

LIQUID CRYSTAL RESEARCH*

The liquid-crystalline state of matter is characterized by a spontaneous anisotropic order and by fluidity. The anisotropic order leads to anisotropy in the physical properties of the medium, and the fluidity makes it easily susceptible to external perturbations in the form of electric or magnetic fields, temperature, or pressure. In addition, we have demonstrated that certain gaseous organic pollutants change the liquid-crystalline structure. This change, which is readily detectable, is the basis for an inexpensive and sensitive (10^{-6}) personal dosimeter for some organic pollutants. Once their physical properties are well understood, the class of liquid crystals known as lyotropics offers the potential for employing such a material for the efficient recovery of oil from abandoned wells and from oil shale.

PHYSICAL PROPERTIES OF LIQUID-CRYSTALLINE MONOLAYERS

Lyotropic liquid-crystalline monolayers are interesting for several reasons. First, not unlike other 2-d systems but unlike one-dimensional systems, these monolayers exhibit a variety of phases; many of these phases are similar to those observed in three dimensions. Also, these 2-d systems may have important technological applications in such diverse fields as oil recovery, catalysis, electronics, and liquid crystal displays. Additionally, 2-d systems are interesting in their own right and are not yet well characterized, either experimentally or theoretically. Furthermore, they are of unique biological importance.

The particular 2-d system we are investigating consists of a high-purity monolayer of amphiphillic lecithin molecules at a water-aliphatic hydrocarbon liquid interface. This system exhibits interesting phase behavior at temperatures slightly above room temperature because the submonolayer is compressed toward a close-packed state. To date, most work on this type of system has been conducted on air-water interfaces where complex motion of the "tails" obscures the results. The oil-water interface used places the tails in their natural milieu.

We have chosen to investigate this system using the non-perturbing technique of light scattering. Scattering from the monolayer molecules themselves is very small. However, the presence of the monolayer causes reduction of the interfacial tension and greatly alters the behavior of small wavelength capillary waves at the liquid-monolayer-liquid interface. In thermal equilibrium, r.m.s. fluctuations of the interface are on the order of a few angstroms. These fluctuations consist of the superposition of a large number of traveling wave frequencies, ω, and wavelengths,

*This work was supported by the Assistant Secretary for Environment, Office of Health and Environmental Research, Pollutant Characterization and Safety Research Division of the U.S. Department of Energy under Contract No. W-7405-ENG-48.

q. Any given wave of fixed q will act somewhat like a moving diffraction grating and will cause part of the laser beam to be scattered into an angle determined by q with frequency shifts of $\pm \omega$. Thus, the scattering is caused by a change in index of refraction between the two bulk liquids. Typical values are $q \sim 350\ cm^{-1}$ and $\omega \sim 6 \times 10^4\ sec^{-1}$. In this experiment, the laser beam enters and leaves the upper non-polar liquid through a coupling prism at right angles to the beam (Fig. 9). A small fraction of this beam is scattered, relative to the reflected beam, into angles $\lesssim 1$ degree. Some light is also elastically scattered into small angles by the liquids and optical components. The beam then leaves the system by a path similar to that by which it entered. Next, a precision small angle rotation is made on the beam, causing the main beam to go off axis and allowing light scattered by the negative of this angle to enter a small pinhole and finally a photomultiplier. Here, the elastically and inelastically scattered light beats together on the photocathode, generating a photocurrent containing the difference or ripple frequency. A real-time digital autocorrelator and microcomputer determines the frequency and the damping coefficient from the time correlation function.

To obtain the interfacial tension from ω and q, an accurate hydrodynamic theory of the fluctuation-driven ripples is needed. As an illustration, the dispersion relation for harmonic waves on the clear surface of a single liquid is

$$\omega^2 = \gamma q^3/\rho + g\,q$$

where γ (T) = surface tension at a given temperature

ρ = liquid mass density (3-d)

g = acceleration due to gravity

Since we investigate only very small q values, we may ignore the gravity term and a measurement of ρ, w, and q will give the surface tension in this simple case. The actual experimental situation is complicated by a second liquid, bulk (3-d) liquid shear viscosities, the visco-elastic constants of the 2-d monolayer, and the fact that not all waves are harmonic. Therefore, we have extended the anharmonic theory of fluctuation-driven ripples of a single fluid to our system. The predicted power spectra can be fit to the Fourier transformer of the measured time correlation function. To be discussed later is the fact that hydrodynamics also give the form of the power spectra for "longitudinal" waves in which the monolayer molecules move in the plane of its interface. A schematic of experimental equipment is shown in Figure 10.

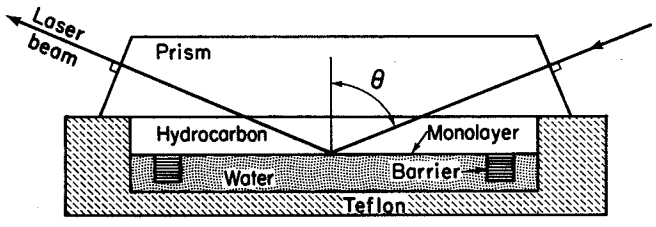

Fig. 9. Details of the scattering configuration (side view). (XBL 812-160)

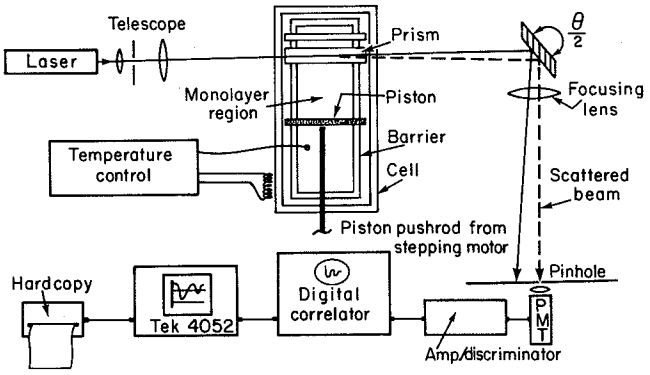

Fig. 10. Schematic of experimental equipment (top view). (XBL 812-161)

Measurements already obtained show three interesting regions along a 2-d isotherm. At low concentrations, there seems to be a single fluid-like phase and, at high concentration, a much more rigid solid-like phase. Between these two phases is an intermediate region where the isotherm has a very slight or zero slope. This region, which begins by a rather abrupt change in slope from the fluid-like region, seems to smoothly enter the solid-like region. These results are preliminary in nature.

There are several theoretical models for these 2-d phases. Models specifically dealing with amphiphillic monnolayer usually treat the transition region as being the result of the "melting" of the molecules' hydrocarbon tails to a more random state. One would predict a first order phase transition with a coexistence region for this type of model. A general theory of two stage melting in two dimensions, recently developed by Halperin and Nelson, predicts a solid with algebraic decay of translational order and long range orientational order. At high temperatures, an unbending of dislocations could allow the system to enter a "hexatic liquid crystal" phase with a reduction in both types of order. Even higher temperatures would result in an isotropic 2-d fluid with exponential decay of all order.

The Halperin-Nelson theory makes dramatic predictions for the dynamic properties of such a system. The 2-d shear viscosity behavior would provide a clear test of this model if it could be determined accurately. Our light scattering measurement provides some sensitivity to the 2-d viscosity of the monolayer. Much greater sensitivity would be provided by scattering due to the "longitudinal" waves mentioned earlier. This is a possible direction for future work. At present, we are concentrating on clean, unambiguous data on the equilibrium properties of the system. These measurements should give us the 2-d phase diagram which is badly needed. Once this is accomplished, accurate measurements of dynamic properties, such as viscosity and mass diffusion, can be attempted.

OPTICAL DETERMINATION OF SMECTIC LAYER SPACING IN FREELY SUSPENDED LIQUID-CRYSTALLINE FILMS†

The accurate determination of smectic layer spacing is of technological interest. Complex methods exist for accomplishing this task. We have employed a simple optical approach to deduce the layer spacing of smectic A thin films ($2 \leq N \leq 15$). Since these freely suspended films are much thinner than optical wavelengths, one can make use of optical interference effects to measure smectic layer spacings. In the case of a light beam incident on a thin uniform[1] slab of material, the reflectivity coefficients for electric fields in ($R_\parallel$) and perpendicular to ($R_\perp$) the plane of incidence are given by[2]

$$R_\parallel = \frac{(n_\parallel^2 \cos^2 i - \cos^2 r_\parallel)^2 \sin^2 a_\parallel}{4n_\parallel^2 \cos^2 i \cos^2 r_\parallel + (n_\parallel^2 \cos^2 i - \cos^2 r_\parallel)^2 \sin^2 a_\parallel} \qquad (1)$$

$$R_\perp = \frac{(\cos^2 i - n_\perp^2 \cos^2 r_\perp)^2 \sin^2 a_\perp}{4n_\perp^2 \cos^2 i \cos^2 r_\perp + (\cos^2 i - n_\perp^2 \cos^2 r_\perp)^2 \sin^2 a_\perp} \qquad (2)$$

where: i = angle of incidence

$r_\parallel$ ($r_\perp$) = angle of refraction for the parallel (perpendicular) mode

$n_\parallel$ ($n_\perp$) = index of refraction for the parallel (perpendicular) mode

$a_\parallel = n_\parallel k h \cos r_\parallel$

$a_\perp = n_\perp k h \cos r_\perp$

k = wavevector of light

h = thickness of film

The smectic A phase is birefringent and the optic axis lies perpendicular to the plane of the film and therefore in the plane of incidence (see Fig. 11). Therefore, $n_\perp$ is independent of i and is equal to n_o, the ordinary component of the refractive index. However, for light polarized in the plane of incidence (parallel mode), $n_\parallel$ is given by the usual formulae

$$n_\parallel = \left[\frac{\sin^2 r_\parallel}{n_\varepsilon^2} + \frac{\cos^2 r_\parallel}{n_o^2}\right]^{-1/2} \qquad (3)$$

and $\sin r_\parallel = \dfrac{\sin i}{n_\parallel}$, (4)

which easily simplify to yield a transcendental equation in the variable $n_\parallel$. Here n_ε is the extraordinary component of the refractive index. In principle, three independent measurements of $R_\parallel$ at three different angles i would yield n_o, n_ε, and the film thickness h. Such a measurement, in addition to yielding the film thickness, and hence layer spacing for a film of N layers, would provide useful information about the density of the film, through the symmetric component of the dielectric tensor. It would also provide information about the orientational order through the asymmetric component of the dielectric tensor. Nevertheless, small errors in such quantities as $R_\parallel$ and uncertainties in i strongly propagate in this technique, creating errors in the quantities of interest sufficiently large to render this measurement meaningless.

We have consequently opted for a somewhat less ambitious, though nevertheless interesting,

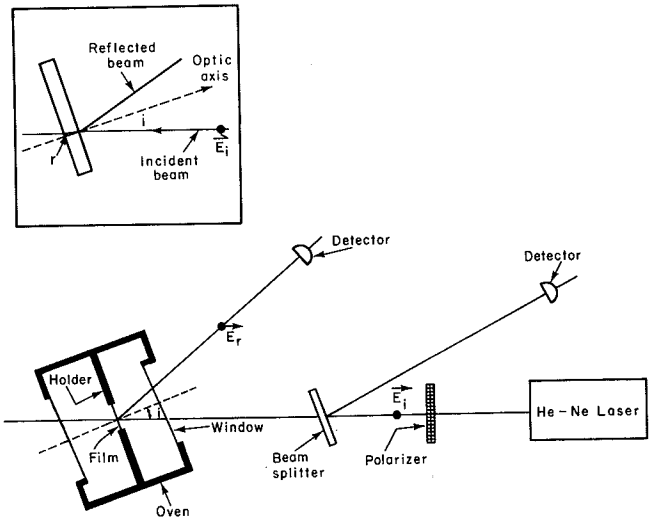

Fig. 11. Schematic of experimental arrangement. (XBL 7910-4520)

†Complete version of this work appeared in Appl. Phys. Lett. vol. 36, 432 (1980).

measurement. One measurement of $R_{\parallel}$ at a given angle yields a surface in (h, n_o, n_e) space [Eq. (1)]; on the other hand, a measurement of $R_{\perp}$ at some angle i yields a line h vs. n_o. Therefore, although we cannot extract absolute values of h and n_o, we can nevertheless gain some insight as to their behavior in thin films.

Three materials are investigated: octyloxy cyanobiphenyl (80CB) butyloxybenzylidene octylaniline (40.8), and cyanobenzylidine octyloxyaniline (CBOOA). The experimental arrangement is shown in Figure 11.

Thirty to forty films are drawn at a given temperature for each material studied. The measured reflectivities are quantized, developing well-defined values corresponding to the number, N, of smectic layers; the scatter in data around any given value of $R_{\perp}$ is generally less than 1%. For very thin films (N 15), Equation 2 reduces to $R_{\perp} \propto h^2$. Assuming that $h = a_o N$, where a_o is a constant layer spacing, one can associate a value of N with each $R_{\perp}$ such that $R_{\perp} \propto a_o^2 N^2$. We also assume that the index of refraction n_o is constant and independent of film thickness. Therefore, from Equation (2), we calculate a film thickness for each measured $R_{\perp}$ and N. In Figure 12a, we plot h vs. N, assuming $n_o = 1.50$, the bulk value for 80CB at T = 67.3°C. Performing a least squares fit to the function $h = a_o N + b$, we obtain $a = 31.1 \pm 0.2$, $b = -1.4$, and an rms error of 2.2. The very small negative intercept is characteristic of all our results. Although it may arise from real physical effects, such as slightly thinned outer layers because of the asymmetric environment near the surface, it can also be due to a changing value of n_o, which is a function of N.

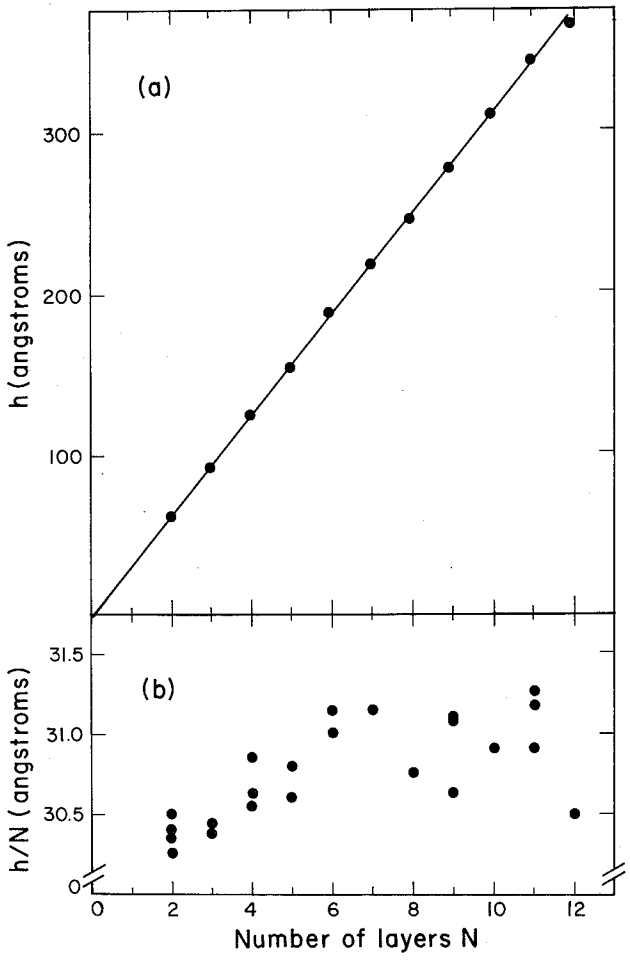

Fig. 12. (a) Film thickness vs. N in 80CB at 65.5° C, assuming n = 1.50. Line is least squares fit to dta points. Error° bars are approximately ± 1%.

(b) h/N vs. N for some material. (XBL 7910-4522)

In Figures 13a, b, and c, we plot layer spacing vs n_o for the materials 80CB, 40.8 and CBOOA respectively. We have assumed that n_o is constant as a function of N and, therefore, that the layer spacing shown is the slope of the h vs. N line (Fig. 12a). If one assumes, however, that n_o is N-dependent (Fig. 12b) and that a_o is simply h/N, values of a_o would be reduced by 0.1 to 0.2 Å in thicker films from those reported in Fig. 13, for a constant n_o. In thinner films, the correction would be slightly greater. Since the error bars for a_o are ± 0.5 Å, these corrections fall within experimental error.

We have also investigated the temperature dependence of the layer spacing. For 80CB and 40.8 there appears to be no systematic temperature-dependent behavior of h vs. N_o in the films. In CBOOA, however, there appears to be a weak but systematic increase in a_o as a function of temperature. The data shown in Figure 13c are for T = 82.3° C. Assuming a fixed n_o, a_o decreases by approximately 0.2 Å at T = 74.5° C and increases from that shown by 0.2 Å at T = 85.3° C. It is interesting to note that this is the first reported case of a smectic A film existing at temperatures which would normally be nematic in bulk.

In Figure 13, asterisks show the approximate bulk behavior in the smectic A phase at T = 64° C for 80CB, T = 60° C in 40.8, and T = 80° C in CBOOA. Although the bulk data lie very close to the a_o vs. n_o lines, the measured values of a_o are consistently smaller than their corresponding bulk values, assuming n_o is identical in film and bulk. Such an effect might arise from an asymmetric surface potential or the smeared-out nature of the film's surface. However, one can also view the data from the standpoint of a_o being the same in both bulk and films, with n_o in films being smaller than in bulk. Such an effect can arise from a decreased density in films because films tend to maintain the chemical potential of the bulk reservoir in the presence of a surface tension.

REFERENCES

1. Molecular times are much faster than detector response times; the detector therefore integrates over thermal motions, resulting in a uniformly appearing slab, except perhaps near the surfaces.

2. M. Born and E. Wolf, Principles of Optics, Pergamon Press, Oxford (1975).

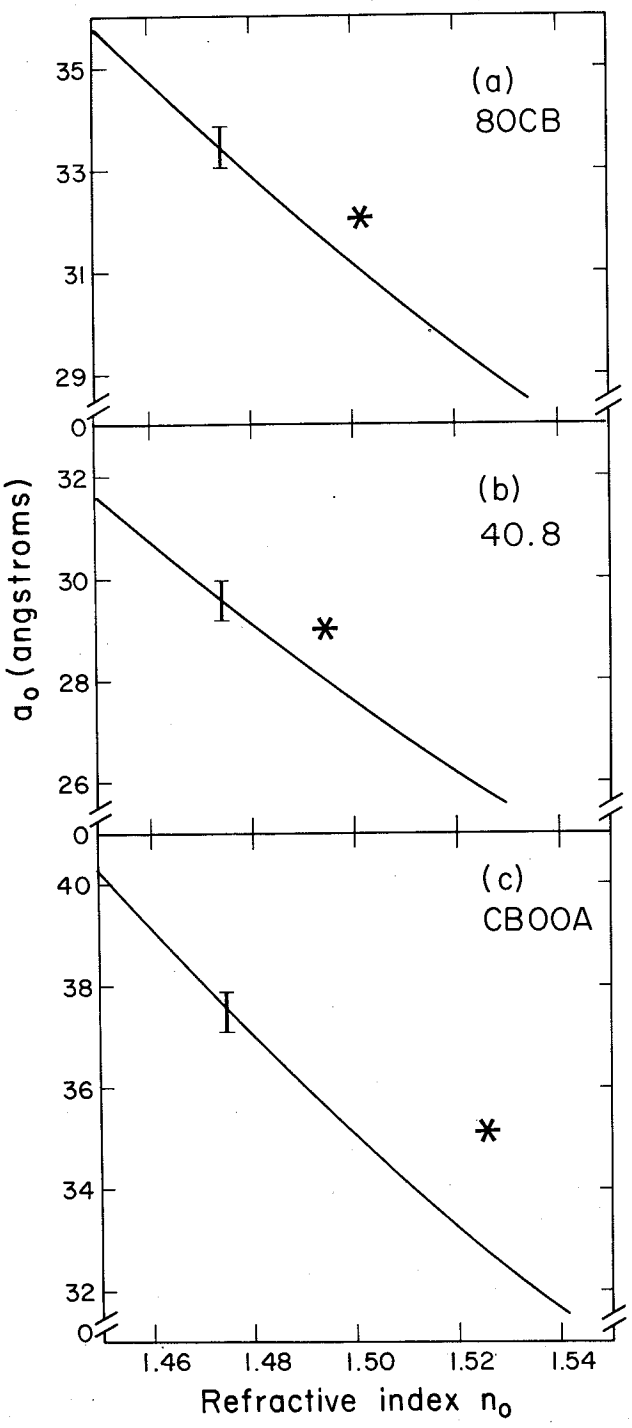

Fig 13. Layer spacing obtained in Fig. 12 vs. ordinary refractive index, n_o, for three materials. Error bars are as shown. Asterisks represent bulk data, where values of a_o are obtained from x-ray experiments. (XBL 7913-4521)

NOVEL LASER SYSTEMS*

Our research activities encountered experimental conditions which require the development of novel approaches to laser technology. An example of such a case is the simple waveguide CO_2/N_2O laser described in the 1978 Annual Report and which has been published in Reviews of Scientific Instruments. During FY 1980, we conceived a novel method for obtaining ultrashort pulses from cw dye lasers. This summary briefly describes this laser and a method for monitoring such ultrashort pulses in "real-time".

RECIPROCAL PASSIVE MODE-LOCKING OF A CW DYE LASER AND THE ION PUMP LASER†

With the advent of synchronous pumping, mode-locked cw dye lasers have become an important tool for performing time-resolved spectroscopy. In such a scheme, an acousto-optically mode-locked cw ion laser (pulse width of $\sim$ 100 pSec) externally pumps a dye laser whose cavity length is matched to the cavity length of the pump laser. When the lengths of the two cavities are optimally matched to within a few μm, picosecond pulses are generated. Such pulses have considerably higher average power and wider tuning range than those obtained from cw-pumped passively mode-locked dye laser systems.

We present here preliminary results of the reciprocal passive mode-locking of the 5145 Å line of an Ar^+ laser by an intracavity Rhodamine 6G (R6G) dye laser. This mode-locked line, in turn, synchronously mode-locks the dye-laser-generating, tunable, ultrashort pulses of duration and average power comparable to those obtained from synchronously mode-locked systems. Our approach, therefore, eliminates the need for actively mode-locking the pump laser with an acousto-optic modulator driven by the amplified output of a stable oscillator. Furthermore, we observe that the pulse width appears not to be too critically dependent on the mismatch of the two cavities.

Fig. (14) shows a schematic of this mode-locking arrangement. The Ar^+ laser cavity is extended, in a folded configuration, to include the broadband high reflecting mirrors, M_1 and M_2 (10 cm radius of curvature R). The dye jet stream is placed at the focus of the mirrors at Brewster's angle. The cavity is completed through prism P and a flat high reflecting mirror M_3. The dye laser beam, which has M_1, M_2, and P in common with the argon beam, is dispersed by the prism P and propagates to a partially transmitting end mirror M_5 ($R = \infty$, transmission T=3%).

In this intracavity pumped configuration, R6G acts as a saturable absorber of the 5145 Å line. However, its relaxation time, $\sim$ 6 n Sec, is not short enough to induce mode-locking. When M_5 is misaligned such that R6G is not lasing, it is observed that the Ar^+ intracavity intensity is strongly modulated but not completely mode-locked. On the other hand, when M_5 is aligned to allow R6G to lase, short-pulsed operation of the 5145 Å

*This work was supported by the Assistant Secretary for Environment, Office of Health and Environmental Research, Pollutant Characterization and Safety Research Division of the U.S. Department of Energy under Contract No. W-7405-ENG-48.

†Complete version accepted for publication in Optics Lett., vol. 6 no. 67 (1981).

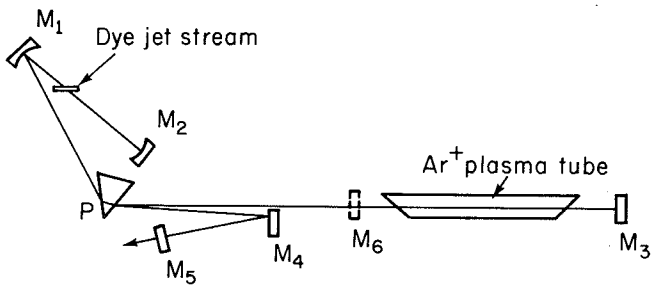

Fig. 14. Reciprocal mode-locking scheme. M_1 and M_2: broadband high reflectors (r = 10 cm). M_3: R6G high reflector (R = ∞). M_4: Ar^+ broadband high reflector (R = ∞). M_5: R6G partial transmitter (R = ∞). M_6: Ar^+ output coupler (removed after initial alignment, see text). (XBL 8010-2264)

line is obtained, as coarsely monitored with a fast photodiode and a sampling oscilloscope. This occurs when the cavity length of the dye laser is optimally adjusted by the translation of M_5 with a differential micrometer to a position approximately equal to, or one-half of, the cavity length of the Ar^+ laser. The passive mode-locking of the Ar^+ laser is the result of the effective shortening of the relaxation time of the saturated dye absorption, caused by the formation of a dye laser pulse at the trailing edge of the Ar^+ laser pulse. This stimulates a rapid depletion of the excited S_1 state of the dye. The dye laser pulses, in turn, will also be ultrashort, being synchronously pumped by the mode-locked Ar^+ laser pulses.

A typical autocorrelation trace of pulses at λ = 5700 Å is shown in Fig. (15). Assuming a $sech^2$ pulse shape, the measured pulse-width is 11 pSec. Similar pulses were observed over a wavelength range of 5650 Å- 5950 Å, with a typical average power output of $\sim$ 80 mW. In general, the pulses have amplitude substructure as evidenced by the 3 : 2 : 1 contrast ratio. The typical FWHM bandwidth of such pulses was $\lesssim$ 4 Å. Shorter pulses, without substructure, were also observed with a 3 : 1 contrast ratio, but these pulses are not easily reproduced, even after the introduction of an iris in the dye laser cavity.

Although the presently generated pulse widths are somewhat longer than those obtained from conventional synchronously-pumped mode-locked dye lasers, our approach has several advantages. First, the active mode-locking of the pump laser is eliminated. Second, our preliminary results indicate that the optimum pulse duration may not be critically dependent on the cavity mismatch parameter. Finally, because mode-locking was achieved at small values of linear cavity losses, cavity dumping techniques can be readily incorporated into this system.

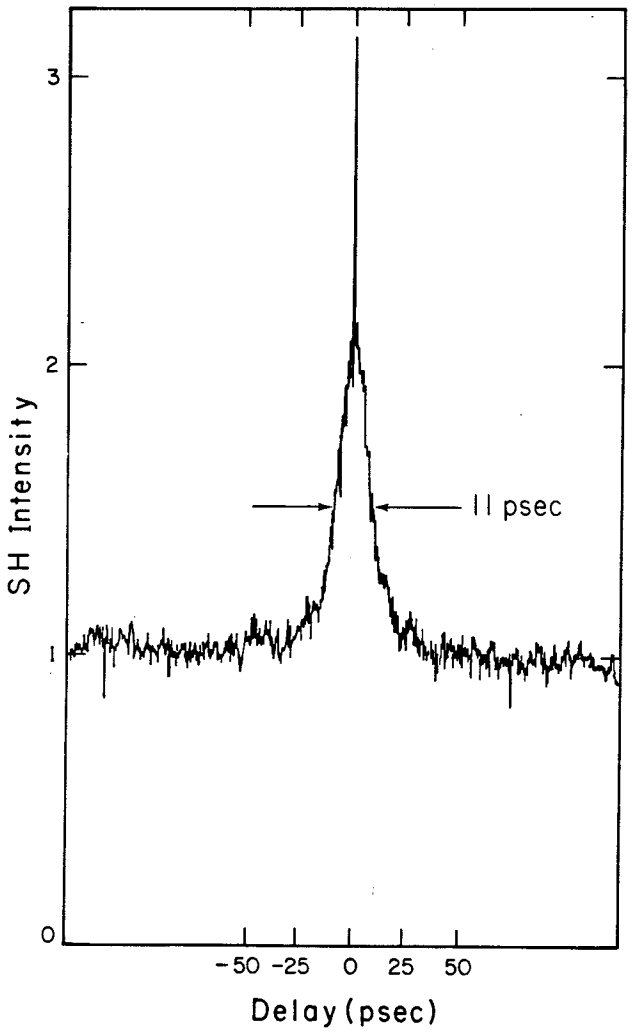

Fig. 15. Intensity autocorrelation trace (with background, $sech^2$ pulse shape) of a typical dye pulse. (XBL 8010-2267)

A SCHEME FOR CONTINUOUS MONITORING OF PICOSECOND LASER PULSES IN REAL-TIME†

Although the standard method for measuring the width of the pulses produced by these laser systems is the well known second harmonic (SHG) autocorrelation technique, useful autocorrelation traces require minutes to obtain. It is therefore desirable to devise methods which enable the continuous monitoring of the temporal characteristics of these pulses in "real time". One approach involves the rapid introduction of a periodically varying time delay in one arm of the Michelson interferometer (MI) used in conventional second harmonic generation autocorrelators.

This summary describes a simple yet precise method for the introduction of a periodic time delay to a train of picosecond laser pulses. It enables the high resolution display of the auto-

†Complete version of this work appeared in Optics Comm. vol. 36, p. 406 (1981).

correlation function of picosecond pulses continuously on an oscilloscope. This method is highly linear over a wide scanning range ($\geq$ 150 psec) and is dispersion-free.

The rapid introduction of a linear periodic time delay is achieved by incorporating in one arm of the Michelson interferometer a pair of parallel mirrors mounted on the two ends of a shaft rotating at a constant angular frequency f (Fig. 16). Thus, after being equally split by the beam splitter, one half of the incoming train of picosecond pulses is incident on mirror M_1 and is reflected to mirror M_2, from which it is transmitted in a direction parallel to that of the original direction. Following a rotation of the shaft by an angle θ, this beam traverses a different path (i.e., is delayed) and is transmitted with a certain displacement while remaining parallel to the direction of incidence. The transmitted beam is normally incident on a stationary mirror M_3, from which it is retroreflected, retracing the incident beam in the opposite direction.

In the other arm of the MI, a stationary mirror M_4 (mounted on a translation stage) retroreflects the other half of the incoming train of pulses; and the two reflected beams from mirrors M_3 and M_4 are recombined collinearly at the beam splitter. The combined beam is focused onto an angle-phase-matched nonlinear crystal, and the generated second harmonic is detected by a photomultiplier, as in conventional autocorrelators. In our scheme, however, the photomultiplier output is the input to a high impedance oscilloscope. The time-base of the oscilloscope is triggered by the output of the photodiode PD which is placed between M_2 and M_3 in such a way that it intercepts a portion of the beam before it is incident on M_2. As shall be seen in the next section, the rotation of the parallel pair of mirrors, M_1 and M_2, results in a linear variation of delay with time. Therefore, the oscilloscope directly displays the second order intensity autocorrelation, with background, of the incoming train of pulses. To properly position the autocorrelation trace, one translates mirror M_4 until a peak occurs at the center of the scan range on the oscilloscope screen. The calibration of the oscilloscope in terms of delay is done by measuring the displacement of the autocorrelation peak on the screen for a given translation of M_4.

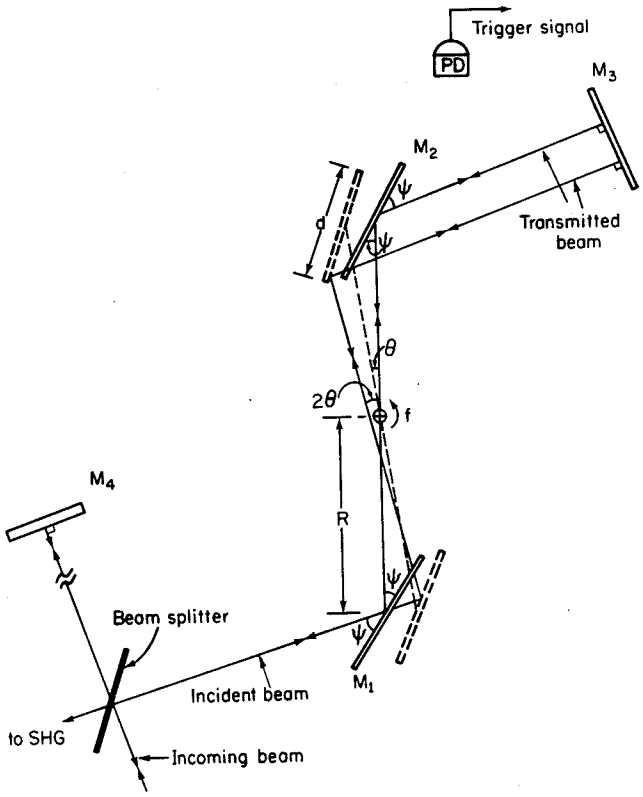

Fig. 16. The rapid-scanning Michelson interferometer part of the SGH autocorrelator. R is the radius of the rotating shaft, d is the mirror diameter, and ψ is the angle of mirror orientation with respect to the incident beam. Dashed lines represent the shaft and mirrors after a rotation by an angle θ. PD is the photodiode used to trigger the oscilloscope.
(XBL 8010-2270)

Figure 17 shows the intensity autocorrelation trace, with background, for a cw train of incompletely mode-locked R6G dye laser pulses, as displayed on an oscilloscope using the above described method. As can be seen from the figure, the coherence spike and the contrast ratio of 3:2:1 are clearly observed.

In principle, the time resolution of this autocorrelator is set by the second harmonic generation process itself. This is true as long as the rise time of the detection and displays parts of the autocorrelator are sufficiently fast.

PLANNED ACTIVITIES FOR FY 1981

Future Directions

In the area of laser photoacoustic and photothermal detection, work will continue in developing ultra-sensitive multiparameter molecular detectors for the characterization of gaseous trace contaminants, particularly those associated with synfuels. Emphasis will be placed on in situ

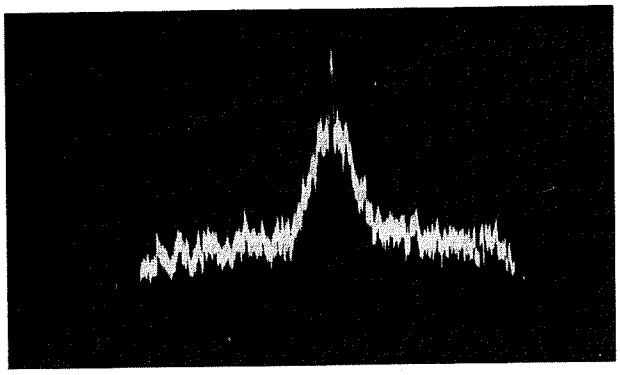

Fig. 17. Rapidly scanned, 2nd-order-intensity, autocorrelation trace of a cw train of ultrashort dye laser pulses. Horizontal scale is 500 μsec/division. Vertical scale is 40 mV/division. (XBL 8011-12725)

and remote sensing schemes. We plan to extend opto-acoustic and photo thermal detection to water pollutants, with specific emphasis on nitrates, sulphates, and photo thermal and organic contaminants. The elemental detection and analysis by tunable laser photoacoustic spectroscopy is planned. In collaboration with the Atmospheric Aerosol Research Group at LBL, we will continue the investigation of optical properties of carbonaceous particulates.

In studying amorphous photovoltaics, our primary effort will continue to center on the physics of those processes governing conversion efficiencies of solar cells made of these amorphous semiconductors. The optical characterization of hydrogenated and flourinated amorphous silicon will continue with particular emphasis placed on the nature of gap states. Experiments, initiated this summer to investigate the mobility of photogenerated carriers, will continue; and time-resolved studies of the de-excitation mechanisms of photoexcited amorphous silicon will be conducted. Other amorphous photovoltaics, e.g., amorphous gallium arsenide, will be studied.

Various potential applications of liquid crystals will continue to be explored. Optimization and comparison of ferro-nematic and ferro-cholesteric dose-integrating magnetometers will resume. Work on gaseous organic detectors will continue to investigate the fundamental mechanism responsible for the observed effect, and sensitizers will be incorporated in the liquid crystal detector to adjust the concentration threshold. In the study of lyotropic monolayers, work will continue on the oil-water interface case, and the emulsification and vesicle formation will be investigated. Finally, the activities in the area of laser development will focus on further narrowing the pulsewidth of our "reciprocal mode-locking" scheme to the subpicosecond regime.

MICROPROCESSOR CONTROLLED ANODIC STRIPPING VOLTAMETER FOR TRACE METALS ANALYSIS IN WATER*

R. Clem, F. Park, F. Kirsten, S. Phillips, and E. Binnall

INTRODUCTION

Trace metals in public drinking water supplies are of special concern because of their potential long-term harmful effects after being ingested.[1,2] Water supply resources for municipalities vary in both the type and concentration of dissolved metals; in untreated water these concentrations are generally significantly lower than the EPA Interim Primary Drinking Water Standards.[3,4] However, chemicals used in water treatment and containing traces of metals as impurities may introduce these metals to water at the treatment plant. Another potential source of metals is corrosion and dissolution of metallic piping or tank interiors through which the treated water passes or is stored prior to ingestion. Thus, there is a need to measure the concentration of dissolved metals at the user tap where the water is actually ingested by a household.[4]

While a number of methods are available for measuring trace metals in drinking water,[1] the method described herein was selected because anodic stripping voltametry (ASV) offers a number of advantages including: (1) capability for simultaneous analyses of more than one metal; (2) sensitivity to concentrations levels less than 1 μg/L; (3) portability of instrumentation; (4) capability for metal speciation at ambient concentrations; (5) ease of automation; and (6) rapid analyses at a relatively low cost.

This report describes the ASV instrument system constructed by LBL; calibration of the instrument with known metal concentrations; and results of analyses of tapwater in Seattle, Washington, and Berkeley, California. Selected background information is given on the anodic stripping electrochemistry of Cd, Pb, and Cu; the ASV method using mercury thin films plated onto graphite electrodes; and the instrumentation electronics.

ANODIC STRIPPNG VOLTAMETRY AT MERCURY FILM ELECTRODES

Anodic stripping is applied to the analysis of mercury soluble metals, such as cadmium and lead, using thin films formed by the deposition of mercury onto carbon electrodes.[5] The Hg is co-deposited with the metals (Cd,Pb,Cu) being analyzed.

The first step involves electroplating during which the metals being determined are concentrated within the Hg film. This deposition step is not exhaustive (non-stoichiometric). The applied potential is stepped to a sufficiently negative value so that the electrodeposition rate is limited only by the rate of mass transfer of the dissolved metals from the bulk of the solution to the electrode surface. The solution is stirred by rotating the cell to enhance mass transfer. The plated metals being analyzed establish a concentration gradient within the Hg film whereby the concentration of metal at the electrode-solution inter-

*This work was supported by Drinking Water Research Division, Municipal Environmental Research Laboratory, Office of Research and Development, U.S. Environmental Protection Agency, under Interagency Contract No. EPA-790-X-0507 and by the U.S. Department of Energy under Contract No. W-7405-ENG-48.

face is larger than that toward the interior of the electrode.

After a set time, such as 5-10 minutes, stirring is stopped, and the solution becomes quiet. During this quiescent period, the concentration gradient within the Hg film is essentially eliminated because deposition is almost negligible, and the plated metals diffuse through the film from regions of high concentrations to lower concentrations.

The third step is anodic stripping of the metals from the amalgam by application of a linearly increasing positive potential. At potentials near the Nernstian value for a particular metal, the metal begins to dissolve (strip) giving rise to typically peak-shaped curves at more positive potentials. A peak is obtained for each metal, thus a charge-voltage curve can consist of more than one peak. Usually, this peak height is measured and related to the metal concentration in the solution via calibration data. Peak areas have also been measured.

INSTRUMENT SYSTEM COMPONENTS

The ASV system constructed here was designed to automate settings for the analytical procedure, to acquire data relating peak height to metal concentration in water samples, and to store data from the analysis of tap water for subsequent calculations. The system is comprised mainly of the following: a rotating cell containing the water sample, electrodes and inlet for the sparge gas; the electronic controller for plating and stripping; and a pen recorder or magnetic tape for data storage and calculation (Fig. 1). The functions of these four major components described in Table 1 are discussed below.

Rotating cell

A cylindrically shaped rotating cell machined from Lucite was used to provide both quick oxygen removal during the sparging step and a high rate of metal preconcentration during the metal deposition. Only 60 seconds is required for effective oxygen removal. Quick oxygen sparging is important in reducing the time required for an analysis.[5] The solution volume used was generally 15 mL.

During oxygen sparging, the cell containing the 15 mL of solution is rotated automatically in a clockwise direction for 0.9 seconds; a counterclockwise pulse is then imparted for a duration of 0.1 seconds. Under these conditions, the dissolved oxygen concentration is lowered until the background current due to oxygen reduction does not interfere with the analysis procedure.

Nitrogen or other inert gas, such as carbon dioxide, is introduced near the bottom of the cell through the bottom of the electrode holder at a rate of ∿5 L/min to effect sparging. At the conclusion of the 60-second sparging period, the microprocessor stops cell rotation, and the solution drains completely to the floor of the cell because a Lucite surface is not wetted by water. Then the agitation (stirring) period is begun; during this time, amalgam is accumulated in the preconcentration step. A low flow rate of nitro-

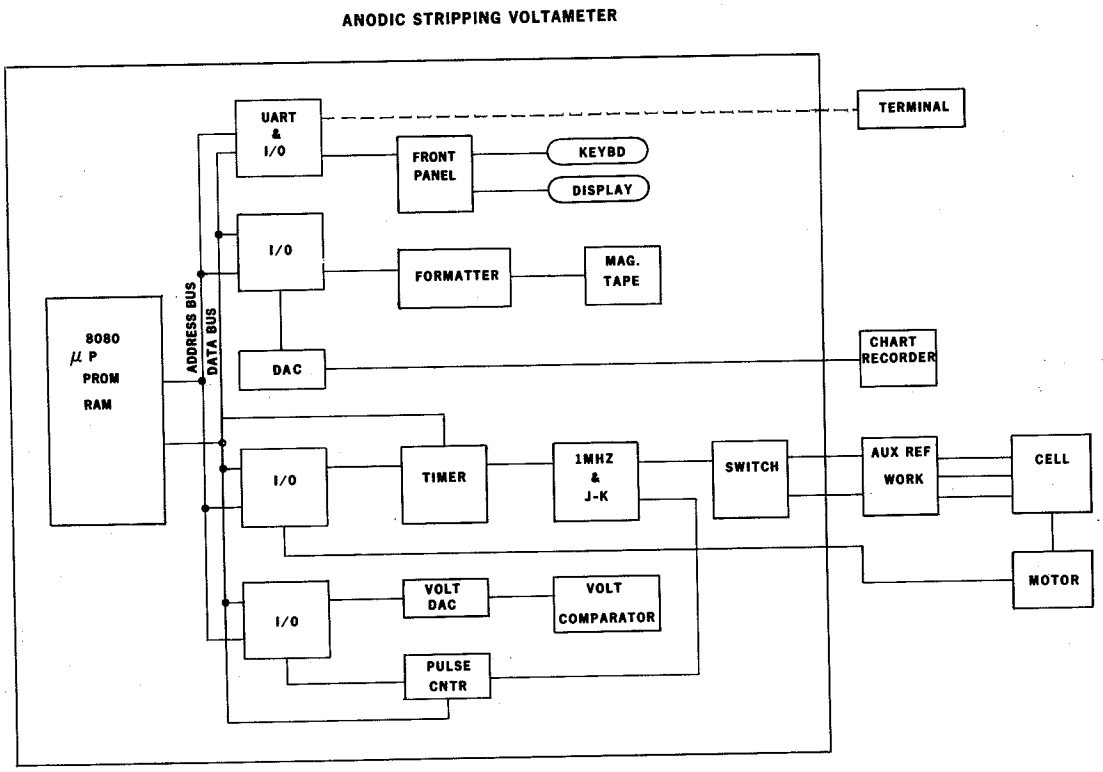

Fig. 1. Block diagram of anodic stripping voltameter. (XBL 794-9252).

Table 1. Major functions of the ASV system components.

Component	Functions
Rotating cell	Contains samples and electrodes, oxygen sparging, preconcentration of trace metals, anodic stripping of amalgams
Digital potentiostat	Applies and maintains plating potential, applies anodic stripping ramp potential, measures stripping peak heights
Microcomputer controller	Start/stop following: cell rotation for sparging, cell rotation for plating, sparge and plating times, anodic stripping ramp, transmits peak height data to cassette and strip chart recorders
Recorder	Strip chart: records background trace, records peak height traces Cassette: Fast rate data storage for later calculation.

gen, e.g., 1-2 L/min., is maintained during the plating step to prevent infusion of oxygen into the cell and thereby maintain a low background current.

Efficient stirring is important for short analysis times such as those used here. Stirring is produced in the rotated cell during plating by controlled periodic reversal of the rotation direction of the cell each second. The graphite working electrode is placed on a radius of the cell and is positioned to face the cell wall. Turning the electrode through 180° until it faces the center of the cell results in a decrease in the rate of amalgam accumulation. This means that the electrode, once positioned and locked into place with the set screw, must not be moved until the analysis is completed.

Digital Potentiostat

The digital potentiostat controls the potential between the working Hg film electrode and the reference electrode by injecting or extracting pulses of charge. The total charge injected is digitized simply by counting the pulses of charge. Advantages of digitization include capability for direct readout on a scaler, and direct computer compatibility.

Microcomputer Controller

In addition to the applied potential, the following functions are also controlled: time for each step, sequencing of each step, storage of the ASV data, output of the data, and a visual indication of the stripping process using a strip chart recorder. Control is provided by a system based on an Intel 8080A 8-bit microprocessor central processing unit. Changes in test parameter variables can be entered by the operator from a 16 button keyboard on the front panel of the instrument. A flow chart detailing the various controlled functions is shown in Figure 2.

The "Power On" or "System Reset" buttons return all parameters to the initial conditions programmed for the plating and stripping parameters. When either of these buttons is pressed, the following preprogrammed values from PROM memories are set into the microprocessor:

Sparge:	60 sec
Start:	1000 mV
Step:	5 mV
Plate:	420 sec
Delay:	1 msec
Count:	400 msec
Day:	0
Test No.:	0
Spike A:	0
Spike B:	0

The MONITOR light will come ON.

Pressing any key will show the value programmed.

To set "SPIKE" press SPIKE and A, or SPIKE and B.

For example, to enter a value for SPIKE B, press SPIKE, press B, press ENTER, press 2, press 5, press ENTER and the change is made. The MONITOR light will go ON. Remember to enter values for Test No. and Day after SYSTEM RESET or Power ON buttons have been pressed.

The software is written in both BASIC and Intel 8080 assembly language. A description of the program is stored on magnetic tapes at LBL and is available on request.

Data Handling

The output signal of analytical interest from the ASV is the stripping peak height as a function of applied potential. For this instrument, the stripping peak heights were measured mainly from the tracing on either a strip chart recorder or an X-Y recorder. Output to the strip chart recorder is the digital-to-analog (DAC) conversion times a scale factor, of the counts accumulated during each 5 millivolt (or other selected step magnitude) step during the stripping cycle. The scale factor (sensitivity) of the strip-chart recording can be chosen by the operator as appropriate for a particular measurement. Data are also recorded on a cartridge digital tape recorder, where they are available for further off-line processing.

Each water analysis is identified by both a test number and run numbers. A complete analysis must have three sequential runs which are performed on: (1) the water sample; (2) the water sample

with spike A added; (3) the same sample with spike B also added. Runs 2 and 3 establish the calibration of the instrument for that analysis. Each run is identified by both test number and run number; a test must have three sequential runs to be valid. If a run is aborted when using the magnetic tape, the test number must be changed before starting a new test. At present, the tape cartridge, which is a 3M DC 300, must be read and analyzed at the LBL Computer Center.

EXAMPLE OF A TAP WATER ANALYSIS

A sample of LBL tap water was obtained by running the water for about 1 - 2 minutes, then collecting 500 mL in a polyethylene bottle which had been cleaned and rinsed with the tap water. Hydrochloric acid was added to pH 1 and the solution permitted to equilibrate for about 48 hours. The sample was then discarded, and an additional 500 mL collected in the same manner. After 48

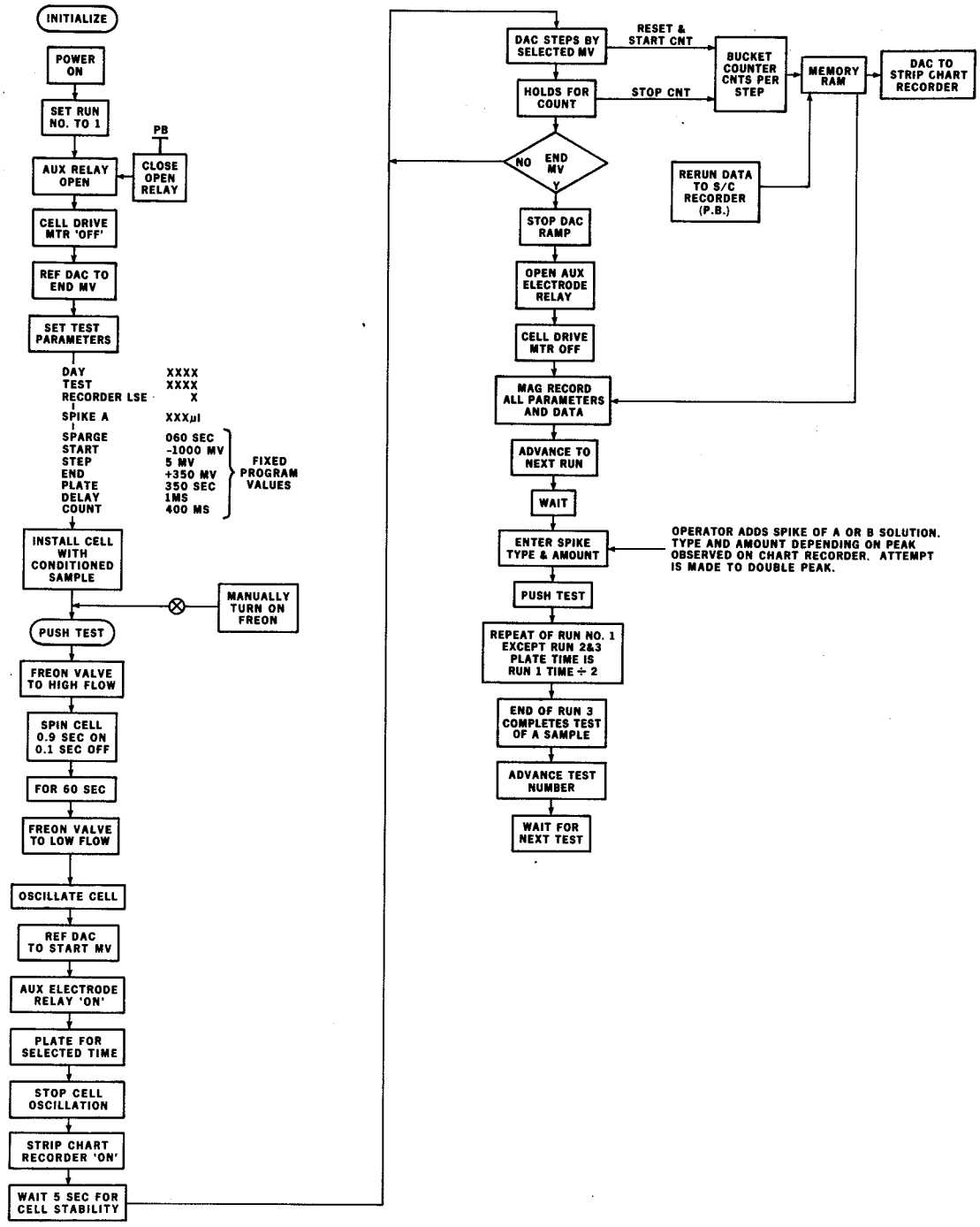

Fig. 2. Flow chart of anodic stripping voltameter. (XBL 794-9471).

hours, 15 mL were added to the rotating cell, and ammonia treated sodium acetate was added to the rotating cell, and ammonia treated sodium acetate was added dropwise to pH 4.7. Then 25 µL of 0.0025 M mercury nitrate solution were pipetted in and background anodic stripping curves obtained. Known µL concentrations of Cd, Cu and Pb standards were pipetted in, and stripping curves again obtained. The peak heights were measured on an X - Y recorder, and the concentrations of the three metals in the tap water were determined by the method of standard additions. Any cadmium in the water was below the limits of detectability of the procedure used, and analysis by atomic absorption did not detect any cadmium. (See Table 2 for LBL and Seattle data.)

PLANNED ACTIVITIES FOR FY 1981

The ASV system is expected to be installed in the EPA mobile laboratory to become part of the water quality monitoring system.

REFERENCES

1. Standard Methods for the Examination of Water and Wastewater, 14th ed., American Public Health Association, Washington, D.C. (1975).

2. J. E. McKee, and H. W. Wolf, Water Quality Criteria, The Resources Agency of California, State Water Resources Control Board, Sacramento, CA (1963).

3. N. I. McClelland and K. H. Mancy, Water Quality Monitoring in Distribution Systems, EPA-600/2-77-074, National Sanitation Foundation, Ann Arbor, MI (1977).

Table 2. Analysis of municipal water samples.

Sample designation	AA values, ppb Cu	AA values, ppb Pb	ASV values, ppb Cu	ASV values, ppb Pb
Seattle, Washington				
NE 24 105NE	1000	10	--	--
7914 NE 26	680	<10	550	1.3
9850 Belfair Rd, Standing	950	<10	1100	N.D.*
9850 Belfair Rd, Running	510	<10	800	N.D.*
Taylor Creek Well 7/4	<6	<10	2.6	N.D.
Taylor Creek Well 7/13	<6	<10	1.4	N.D.
EPA SAMPLES				
Jones Res. Running	--	--	12.4	2.3
Jones Res. Standing	--	--	1800	N.D.*
Park Place Standing, 1st run	--	--	1000	N.D.*
Park Place Standing, 2nd run	--	--	1000	N.D.*
Berkeley, California				
Tap water sample			ASV Values, µg/C	
			Cu 22	Pg 3
				Cd <0.2

N.D. = Not detected.

N.D.* = Non-detection likely due to solid phase amalgam formation.

4. S. Miller, Env. Sci. Technol., vol. 14, p. 1287 (1980).

5. F. Vydra, K. Stalek, and E. Julakova, Electrochemical Stripping Analysis, translated by J. Tyson, John Wiley and Sons, Inc., New York (1976).

THE SURVEY OF INSTRUMENTATION FOR ENVIRONMENTAL MONITORING*

M. Quinby-Hunt, C. Case, R. McLaughlin, G. Morton, D. Murphy, A. Nero, and D. Mack

INTRODUCTION

The ever-increasing demand for energy and the demand for a clean environment have made it essential that pollution levels be monitored and regulated. Only through such monitoring can we define existing levels of pollutants and the value of various control strategies. The identification and quantification of pollutants and the evaluation of their impact on ourselves and our environment has resulted in the development of numerous highly sophisticated techniques and instruments. Monitoring methods have been improved by increasing sensitivity, lessening interference, and simplifying data processing, and incorporating automatic operation. However, choosing an analytical method is difficult because of the large variety of instruments and techniques available, the rapid development of new instrumentation, and the large financial investment required.

For the last decade, the Instrumentation for Environmental Monitoring Group of LBL has been investigating and analyzing analytical techniques and instrumentation resulting in a survey, Instrumentation for Environmental Monitoring, which is an aid for individuals responsible for monitoring or controlling pollutants in the environment. Contents include information on current Federal environmental standards and regulations, sources of conventional and radioactive pollutants and their pathways to humans, pollutant forms and characteristics, sampling and calibration techniques, and descriptions of instruments and techniques for monitoring these pollutants. Lawrence Berkeley Laboratory has sold over 4000 volumes to public and private

*This work was supported by the Assistant Secretary for Environment, Office of Health and Environmental Research, Pollutant Characterization and Safety Research Division of the U.S. Department of Energy under Contract No. W-7405-ENG-48.

laboratories, libraries, institutions conducting environmental studies, scientists, engineers administrators, and other groups concerned with protecting the environment. The survey contains four volumes in seven binders: Air (3 binders), Water (2 binders), Radiation (1 binder), and Biomedical (1 binder). Each volume includes several instrument note sections describing the latest commercial instruments.

ACCOMPLISHMENTS DURING FY 1980

During FY 1980 the Survey Group completed two major updates, started work on two other major revisions and a new section, began selection of a publisher to publish existing and new material in book format, started transferring material to a word processing system, and began work on a new direction for the survey.

1. The completed and published update for the Water Volume includes a section describing sources and environmental impacts of halogens and cyanides, analysis methods using ion-selective electrodes, amperometric titrations, and ion chromatography. Another section describes the source and abatement of coliform bacteria and methods of determination. Other sections include information on the significance and determination of solids in various waters and on asbestos in the air and water. This update also includes a multi-paged table describing commercial ion-selective electrodes.

2. The update for the Radiation Volume includes revised sections on these subjects:

- Particle accelerators
- Sources of X-radiation
- Alpha particle instrumentation
- Beta particle instrumentation
- X and gamma monitoring instrumentation
- Gamma spectroscopy

Also included are instrument notes describing commercial monitoring instruments.

3. The Group has almost finished another revision of the Radiation Volume which will include rewritten material on instrumentation for these specific radionuclides:

- Tritium
- Krypton-85
- Radon-222 and its daughters
- Strontium-90 and 89
- Iodine-131 and 129
- Radium
- Uranium
- Plutonium

This update will include instrument notes describing instruments designed to monitor these specific radionuclides.

4. The new Water Volume material will revise the following sections:

- Pesticides
- Phenols
- Petrochemicals
- Oil and Grease

These revisions will include the effect of pollutants associated with new energy conversion technologies and old chemical waste dumps. The impact of the EPA list of priority pollutants will also be discussed. The material will include information on long term effects of oil spills and instrument notes describing GC and LC instrumentation.

5. A new section for the Water Volume will describe sampling techniques in marine, fresh water, and wastewater environments. Information will include sampling methodologies; logistics such as sampling frequency, site selection, and sampling profile; sources of sample contamination and contamination prevention; sample storage and pretreatment; and sampling techniques for specific energy related pollutants. The section will also include instrument notes.

6. For the last decade, LBL has distributed the survey in loose-leaf binders. We are now selecting a publisher to produce the survey in a more standard textbook format. This publisher will handle advertising, process orders, and maintain an inventory. The effect should be to expand circulation by offering the volumes at lower cost. We plan to revise certain volumes every few years. Instrument notes will probably be published separately.

7. We are investigating a new direction for the survey which will more closely relate the material to certain energy producing technologies such as oil-shale and coal conversion, and to energy related pollutants such as acid-rain. Material in current updates and new sections will reflect this new direction. The survey group is also considering a fifth volume concerning monitoring of energy related pollutants.

8. Finally, the survey group is transferring most of the present material to a text processing system. This will facilitate updating the material, writing new sections, and making changes suggested by reviewers. A phototypesetter will print the material.

PLANNED ACTIVITIES FOR FY 1981

The planned activities for FY 1981 include finishing the Radiation and Water volume updates, selecting a publisher, publishing the Radiation Volume as a book, and preparing the Water Volume for book publication. In addition, the group plans to start a major update on the Air Particulates Section of the Air Volume and to prepare a new section on biomass indicators for the Water Volume. Work will continue on the new direction for the survey and the presentation of material on energy related pollutants.

THE POSSIBLE CHRONDRITIC NATURE OF THE DANISH CRETACEOUS-TERTIARY BOUNDARY*

F. Asaro, H. Michel, L. Alvarez, and W. Alvarez

INTRODUCTION

Our research to date has demonstrated that deep-sea limestones exposed in Italy,[1-3] Denmark,[4] New Zealand,[4] and northern Spain[5] show unusual increases in the abundance of iridium (Ir) above the background level at exactly the time of the Cretaceous-Tertiary (C-T) extinctions, 65 million years ago. As Ir is much depleted on the earth's surface with respect to the average solar system abundance, such an enrichment is not likely to have come from a terrestrial source because extraterrestrial sources contain 3 orders of magnitude more Ir than terrestrial sources and are much more likely to have produced the enrichment. Measurement of the isotopic ratio of the two iridium isotopes in the Italian C-T boundary layer showed that it was identical with that of a terrestrial source.[1] This eliminated a supernova explosion 65 million years ago as a source of the iridium. An interstellar origin for the asteroid, as postulated by Napier and Clube for impacting planetesimals,[6] would only be possible if isotopic ratios (at least for Ir) in our part of the galaxy were nearly constant. Many sources of extraterrestrial material from within the solar system were considered and subjected to three tests. These sources had to be (1) able to deposit the Ir, (2) able to cause the C-T extinctions, and (3) likely to have occurred about 65 million years ago. Only one source survived the tests.

ASTEROID-IMPACT HYPOTHESIS

We have developed an asteroid-impact theory that satisfied these conditions and many others.[1] The theory assumes the following events. An Apollo object, with about a 10 km diameter, struck the earth 65 million years ago. It vaporized as did a much larger mass of terrestrial material. About 20 percent of this combined mass, modeled after the volcanic explosion of Krakatoa, ended up in the stratosphere, encircled the earth, and blocked out nearly all of the direct sunlight. Photosynthesis then stopped. The larger animals, which depended on the plant food chain, died while some smaller animals, needing less food, survived. Some seeds could have survived for several years and then reestablished the plants after the dust cloud sank to earth and direct sunlight reappeared. Mass extinctions of this type have occurred about every 100 million years.

*Later stages of this work were partially supported by the California Space Group and the National Aeronautics and Space Administration Ames Research Center and by the U.S. Department of Energy under Contract No. W-7405-ENG-48.

SUMMARY OF RESEARCH BY OTHER INVESTIGATORS

Dutch geologists, after learning of the Italian Ir data, found a similar Ir anomaly in a rock section from Caravaca (Barranco-del-Gredero) in southeast Spain.[7] We were able to confirm the iridium abundances in a sample supplied by J. Smit and to determine the variation in abundance within a few centimeters of the C-T boundary.[8] Smit and Hertogen[7] also measured the abundances of another platinum group element, osmium, which also exhibited an anomalously high abundance at the C-T boundary near Caravaca. These authors also stated the ratio of two osmium isotopes in the C-T boundary was indistinguishable within 0.1 percent from the terrestrial (i.e., solar system) ratio.

Concern has been expressed[9,10] about the correctness of the stratigraphy upon which the selection[1] of our Italian samples was based. However, very recent work[11] on a deep-sea core from the southeastern Atlantic Ocean near South Africa, supported the Italian stratigraphy.

There have been a number of suggestions in the past that an extraterrestrial object impacting on the earth caused or could cause massive extinctions of life. E. J. Öpik,[12] for example, discussed the lethal effects which could be caused by the heat generated from such objects striking the earth, and H. C. Urey[13] stated specifically that a comet was probably the cause of Cretaceous-Tertiary extinctions.

Events likely to occur if sunlight were temporarily "turned off" have also been discussed.[14] Our deduction, in contrast to others, is based on physical science data (the iridium anomaly) and is the only explanation we found which explained the Ir anomaly, could cause the massive extinction of life and was likely to occur in a period of $\sim$100 million years.

Smit and Hertogen[7] also concluded a large meteorite may have struck the earth and caused the extinctions. K. J. Hsü[15] suggested the extinctions were caused by cyanide poisoning resulting from a cometary impact; and Cesare Emiliani[16] proposed that a sudden heat flash, possibly caused by an asteroid impact, could have caused the C-T extinctions. Ganapathy[17] measured the abundances of Pt group elements (Ru, Pd, Re, Os, Ir, Pt), Au, Co and Ni in the Danish C-T boundary layer and confirmed that it contained a chondritic component. Kyte et al.[18] measured Pt group elements in the Danish boundary layer. They also found Ir in a deep sea core from the Central Pacific (hole 465a) (we have also extensively studied samples from this hole). Kyte et al. believe that an extraterrestrial projectile consisting of a metal sulfide core, interstellar

matter, or structurally weak cometary matter was the source of the platinum group elements. They do not think a chondritic asteroid or a comet could be the source.

REVIEW OF 1980 STUDIES AND RESEARCH

We have observed the Ir anomaly in uplifted marine sediments in five locations in Italy, one in Denmark, three in Spain (besides that found by Smit and Hertogen), and one in New Zealand. Ir has been found in one (hole 465a) of two deep-sea cores. The validity of the asteroid-impact theory would be in doubt if the Ir anomaly is not found wherever the C-T boundary is intact. The deep sea core in which the Ir anomaly was not found (hole 356) was in the South Atlantic; it will be studied further.

Measurements of the abundances of platinum group elements have been made in a C-T boundary layer sample from Denmark. Figure 1 shows the ratio of abundances of different elements to that of Ir in various mantle materials, divided by the same quantities for Cl chondrites.[19] The Pt and Au ratios approach the chondritic abundances as the degree of partial melting of the mantle gets higher. An ultra-basic nodule,[20] which may represent the mantle, has very close to the chondritic ratios for Ir and Pt. Some of our recent measurements of Pt, Au, and non-volatile Os, as well as Ir, in the Danish C-T boundary layer are shown in Figure 1 and Table I. The Pt and Ir data are

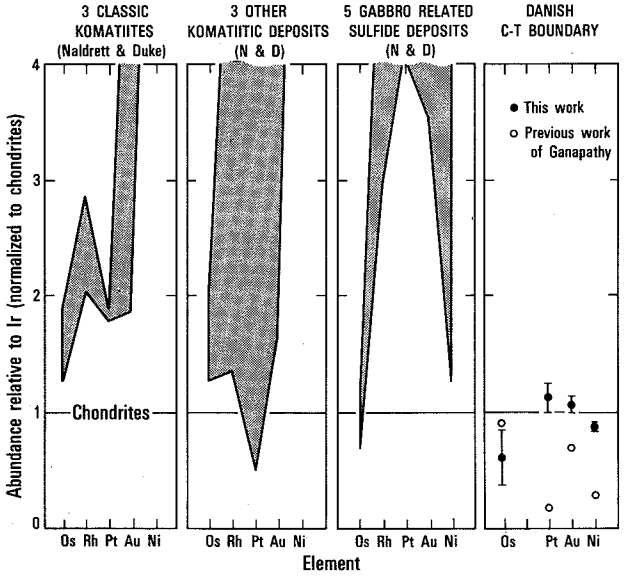

Fig. 1. Relative abundances of some platinum group elements, gold, and nickel with respect to iridium. Each abundance was divided by the abundance of that element, except for Rh, in Type I carbonaceous chondrites. Rh abundances were divided by Rh abundances in other types of chondrites because Cl values were not available. Errors in the LBL measurements reflect one sigma value of the counting errors, except for the Au error which is the root mean square deviation of 6 measurements, as the 6 values were not consistent within counting errors. The Os measurement was on a nitric-acid-insoluble residue which had been fired to 800°C. (XBL 809-1964)

Table 1. Possible chondritic nature of the Danish C-T boundary.[a]

	Ganapathy[b] (Average of 2)	Our Work[c]	Cl Chondrites[d]
Pt/Ir	0.40	2.24 ± 0.23	1.98
Ni/1000 Ir	6.2	16.6 ± 0.5	20
Co/1000 Ir	0.82	2.07 ± 0.03	1.01[e]
Au/Ir	0.21	0.319 ± 0.020	0.296

[a]If the C-T boundary includes an asteroid component with chondritic abundancies, the ratios of the abundances of various elements to Ir should be larger than chondritic because of terrestrial contributions.

[b]Ratios were calculated from abundances given in Ganapathy.[17]

[c]Pt and Au data are from unpublished work of F. Asaro, H.V. Michel, W. Alvarez, and L.W. Alvarez, 1980. Other data are from Ref. 1.

[d]Au and Ir data are from U. Krähenbühl et al.[24] Pt datum is from Ehmann and Gillum.[25]

[e]The Co abundance is a weighted average (507 ppm) of the data given by Moore.[26]

consistent with a chondritic origin, as predicted by the asteroid-impact theory. Part of the data of Ganapathy is also included in Figure 1 and Table I. In addition to measurements of Pt group elements on the Danish and other C-T boundary layers, similar measurements are needed on nearby Cretaceous and Tertiary rock formations. $^{187}Os/^{186}Os$ isotopic ratios[21] might determine if the Os and Re have maintained chondritic relative abundances throughout the predominant part of their existence since coalescence from dispersed materials billions of years ago.

More studies of the clay mineralogy of the C-T boundary layer are needed. These may indicate if the boundary deposition was associated with an extraordinary event.

Rare earth abundances patterns, particularly of the clay fraction, may also help determine the origin of the terrestrial components. Rare earth patterns in clay fractions of sediments tend to inherit the patterns of the rocks from which they originated.[22] Figure 2 shows several examples of the rare earth abundance patterns of nitric-acid-insoluble residues from the Danish boundary layer and the limestones above and below. Such patterns along with the other chemical data may indicate the type of rock from which the boundary layer originated. This may help indicate if the origin was continental, sea floor, rift, or otherwise.

The intensity of the C-T iridium anomaly as a function of geographical location along with the mineralogical and chemical studies of the boundary layers may suggest an impact location when considerably more data are obtained. If the asteroid-impact theory is correct, the extinctions should be repetitive and the Ir anomaly should be observed in other geological stratigraphic levels corresponding to known extinctions. About five other massive extinctions, in addition to the event at the end of the Cretaceous Period, have been noted.[23] These come at the end of the Cambrian (∿500 MY ago), the Ordovician (∿435 MY ago), the Devonian (∿345 MY ago), the Permian

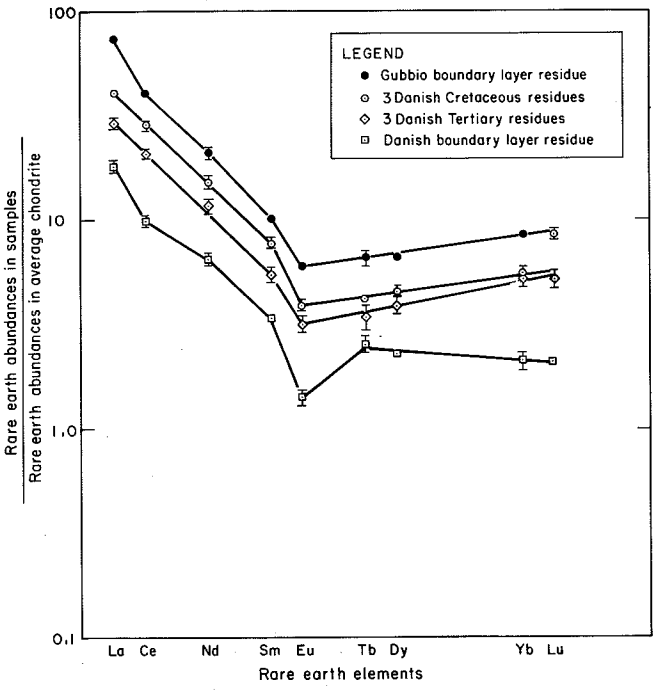

Fig. 2. Rare earth abundance patterns as normalized to the data of Masuda et al. except for Tb, for the Leedy L6 meteorite.[27] The Tb abundance in meteorites is assumed to be 0.059 ppm. Errors for the Danish Cretaceous (3 samples) and Tertiary (2 samples) nitric-acid-insoluble residues are root-mean-square deviations. Errors for the nitric-acid-insoluble residues from the Gubbio and Danish boundary layers are 1 sigma values of the counting errors. (XBL 7911-13249)

(∿230 MY ago) and the Triassic (∿195 MY ago) Periods.

PLANNED FUTURE ACTIVITIES

In the next four years, we plan to: test the concept of world-wide distribution of the Ir anomaly and the premise of an extraordinary extraterrestrial origin of the anomaly; attempt to determine the location of the C-T impact site, and test the repetitive nature of the proposed impact. From the results of these tests and the questions which will develop, the extent to which the theory is correct can be evaluated and the need and direction for future work can be assessed.

REFERENCES

1. L. W. Alvarez, W. Alvarez, H. V. Michel and F. Asaro, "Extraterrestrial Cause for the Cretaceous-Tertiary Extinction," Science, vol. 208, pp. 1095-1108 (1980).

2. W. Alvarez, L. W. Alvarez, F. Asaro and H. V. Michel, "Experimental Evidence in Support of an Extraterrestrial Trigger for the Cretaceous-Tertiary Extinctions," EOS Trans. Am. Geophys. Union, vol. 60, p. 734 (1979).

3. W. Alvarez, L. W. Alvarez, F. Asaro and H. V. Michel, "Anomalous Iridium Levels at the Cretaceous-Tertiary Boundary at Gubbio, Italy: Negative Results of Tests for a Supernova Origin," Geol. Soc. America Abstract, vol. 11, p. 378 (1979).

4. D. Russell, L. W. Alvarez, W. Alvarez, H. V. Michel and F. Asaro, unpublished data (1980) cited in Ref. 1.

5. M. Arthur, L. W. Alvarez, W. Alvarez, H.V. Michel and F. Asaro, unpublished data, 1980.

6. W. M. Napier and S. V. M. Clube, "A Theory of Terrestrial Catastrophism," Nature (London), vol. 282, pp. 455-459 (1979).

7. J. Smit and J. Hertogen, "An Extraterrestrial Event at the Cretaceous-Tertiary Boundary," Nature, vol. 285, pp. 198-200 (1980).

8. L. W. Alvarez, W. Alvarez, H. V. Michel and F. Asaro, unpublished data, 1979. Ir values are plotted in Ref. 7.

9. F. C. Wezel, "The Scaglia Rossa Formation of Central Italy: Results and Problems Emerging from a Regional Study," Ateneo Parmense, Acta Nat., vol. 15, pp. 243-259 (1979).

10. Finn Surlyk, "The Cretaceous-Tertiary Boundary Event," Nature, vol. 285, pp. 187-188 (1980).

11. K. S. Hsü, private communication to Walter Alvarez and News Release NSF PR 80-56 (1980).

12. E. S. Öpik, "On the Catastrophic Effects of Collisions with Celestial Bodies," Irish Astronomical Journal, vol. 5 no. 1, p. 34 (1978).

13. H. C. Urey, "Cometary Collisions and Geological Periods," Nature, vol. 242, p.32 (1973).

14. K-TEC group (P. Beland et al.). "Cretaceous-Tertiary Extinctions and Possible Terrestrial and Extraterrestrial Causes," Proceedings of Workshop, National Museum of Natural Sciences, Ottawa, 16 and 17 November 1976, pp. 144-149 (1976).

15. K. J. Hsü, "Terrestrial Catastrophe Caused by Cometary Impact at the End of the Cretaceous," Nature, vol. 285, pp. 201-203 (1980).

16. Cesare Emiliani, "Death and Renovation at the End of the Mesozoic" EOS, vol. 61, no. 26, pp. 505-506 (1980).

17. R. Ganapathy, "A Major Meteorite Impact on the Earth 65 Million Years Ago. Evidence from the Cretaceous-Tertiary Boundary Clay," Science, vol. 209, pp. 921-923 (1980).

18. F. T. Kyte, Z. Zhou and J. Wasson, Submitted to Nature (Oct. 1980).

19. Data for basic materials was taken from "Platinum Metals in Magnatic Sulfide Ores" by A. J. Naldrett and J. M. Duke, Science, vol. 208, pp. 1417-1424, (1980).

20. L. P. Greenland, D. Gottfried, and R. I. Tilling, "Iridium in Some Calcic and Calc-Alkaline Batholithic Rocks of the Western United States," Chem. Geol., vol. 14, pp. 117-122 (1974); reported in J. H. Crocket, "Platinum-Group Elements and Mafic and Ultramafic Rocks: A Survey," Canadian Mineralogist, vol. 17, pp. 391-402 (1979).

21. C. J. Allègre and J. M. Luck, "Osmium Isotopes as Petrogenetic and Geological Tracers," Earth Planet. Sci. Lett. vol, 48, pp. 148-154 (1980).

22. R. L. Cullers, Long-Tsu Yeh, S. Chaudhuri, and C. V. Guidotti, "Rare Earth Elements in Silurian Peltic Schists from N. W. Maine," Geochim. Cosmochim. Acta, vol. 38, pp. 389-400, (1974).

23. N. D. Newell, "Crises in the History of Life," Scientific American, vol. 208, no. 2, pp. 76-92 (1963).

24. U. Krähenbühl, S. W. Morgan, R. Ganapathy and E. Anders, "Abundance of 17 Trace Elements in Carbonaceous Chondrites," Geochem. Cosmochim. Acta, vol. 37, pp. 1353-1370 (1973).

25. W. D. Ehmann and D. E. Gillum, "Platinum and Gold in Chondritic Meteorites," Chem. Geol., vol. 9, pp. 1-11 (1972).

26. B. Mason, (ed.), Handbook of Elemental Abundances in Meteorites, Gordon and Breach Science Publishers, London (1971).

27. A. Masuda, N. Nakamura and T. Tanaka, "Fine Structures of Mutually Normalized Rare-Earth Patterns of Chondrites," Geochim. Cosmochim. Acta, vol. 37, pp. 239-248 (1973).

IMPROVEMENT OF THE SENSITIVITY AND PRECISION OF NEUTRON ACTIVATION ANALYSIS OF SOME ELEMENTS IN PLANKTON AND PLANKTONIC FISH*

F. Asaro, H. Michel, R. Flegal,† and Quinby-Hunt

The normal LBL method for measuring elemental abundances using neutron activation analysis was designed to maximize the precision for measurements on substances with approximately the composition of the average earth's crust. The standard procedure needs to be modified for materials with an abundance of many trace elements much lower than normally present in the earth's crust and with an abundance of Na of approximately 10 percent.

The sample preparation procedure was modified by pressing the pellets in a die made of Al_2O_3 instead of tool steel.

The neutron irradiation for measuring the short lived elements Al, Cl, Mn, Mg, Cu, Ca, K, Na, Ga, Dy, Ba, and In was reduced from 18 minutes at 11 kw to 3 minutes at 11 kw. The gamma-ray spectrum of each irradiated unknown was counted for 1 minute, approximately 9 minutes after bombardment began (a normal gamma-ray counting procedure). The samples were counted again for 12 minutes each about one hour after irradiation (instead of the normal 6 minutes) and recounted the following day for 2 hours. Table 1 shows the sensitivities and precision obtained with these procedures.

Table 1. Element sensitivities obtained after a 3 min. neutron irradiation (2.7 n/sec-cm^2) in plankton samples containing large amounts of Na and Sr.

Element	Sensitivity (or precision) for a 95% confidence limit
Al[a,b]	0.3%
Ba[c,d]	176 ppm
Ca[a]	2.8%
Cl[a]	32%
Cu[e]	86 ppm
Dy[c]	0.9 ppm
Ga[e]	142 ppm
In[c]	0.7 ppm
K[e]	0.7%
Mg[a]	4.6%
Mn[c]	8 ppm
Na[e]	.09% precision when abundance is 10.3%
Sr[c,d]	.15% precision when abundance is 3.1%
Ti[a,d]	.21%

[a]Data is from the 1.00 min. counts taken ∿9 minutes after the irradiation.

[b]The Al radiation can also result from irradiated Si (from SiO_2). 100% SiO_2 appears as 0.51% Al.

[c]Data is from the 12.00 min. counts taken ∿1 hour after the irradiation.

[d]Better data can be obtained following a long irradiation.

[e]Data is from the 120.00 min. counts taken ∿1 day after the irradiation.

* This work was supported by the Assistant Secretary for Conservation and Solar Energy, Office of Solar Power Application, Ocean Energy Systems Division of the U.S. Department of Energy under contract W-7405-ENG-48.

†Moss Landing Marine Laboratory

A significant improvement in the sensitivity of detection of the longer lived isotopes is gained by using a large 128 cc Ge-Li detector, instead of a 7 cc Ge detector, and counting for longer periods of time.

Table 2 compares the elemental abundance determined normally with the estimated abundance determined with the large Ge-Li detector. Sample P7 is plankton and FD is planktonic fish. In addition to elements already discussed, 16 were measured and 13 were detected in plankton samples.

In the case of marine base-line studies on plankton and fish, where precision and detection of trace elements is critical to the assessment of environmental impact, this improvement in measurement capability is important. The samples were supplied by Dr. Russ Flegal of the Moss Landing Marine Laboratory and Dr. George Knauer of the California Institute of Technology.

Table 2. Estimates[a] of abundances in plankton determined with a 128 cc Ge-Li detector, ppm.

Sample	γ ray detector volume	Elements						
		Co[6]	Cr	Cs	Fe	Hf	Ir	Ni
P7	128cc[c]	.446±.006	1.06±.17	.0066±.008	29.2±1.5	<.010	<.00028	5.84±.11
	7cc[d]	.472±.026	<1.9	.032 ±.018	<84	<.07	<.0018	6.4 ±1.0
FD	128cc[e]	.127±.007	.17±.04	.0503±.0011	34.6±.9	<.0032	<.00009	1.60±.07
	7cc[d]	.111±.018	<1.2	.056 ±.016	<74	<.07	<.0035	<3.2

Sample	γ ray detector volume	Elements					
		Rb(+Sr)[f]	Sb[g]	Ta[g]	Th	Ag	Sr
P7	128cc[c]	3.30±.21	.173 ±.004	.0055±.0005	<.021	.04±.004	-
	7cc[d]	2.0 ±.6	.138 ±.026	<.020	<.08	<.16	-
FD	128cc[e]	6.97±.18	.0154±.0012	.00135±.00018	<.008		576±14
	7cc[c]	7.5 ±.7	<.029	<.024	<.05		460±110

[a]Only estimates were obtained for the measurements made with the 128 cc detecter because flux monitors were used for all elements. Uncertainties of ∿10% are possible due to calibration. The listed errors are 1σ values of the counting error and would be the precision if a multi-element standard were used.

[b]Abundances have been modified to reflect an estimated .03-.04 ppm Co contribution from the Al wrapping foil.

[c]464 minute gamma-ray count about 70 days after the end of the long irradiation.

[d]60 minute gamma-ray count about 24 days after the end of the long irradiation.

[e]754 minute gamma-ray count about 71 days after the end of the long irradiation.

[f]The ^{86}Rb radiation is also produced by the reaction ^{86}Sr (n,p) ^{86}Rb. The Sr contribution has not been removed. Sea water and Sr probably account for all the ^{86}Rb detected in P7 and very little of that detected in FD.

[g]Estimated contaminants from the Al wrapping foil of ∿.001→.004 ppm for Ta and ∿.01 ppm for Sb have not been removed. Accurate abundances of these elements can be obtained by removing the Al foil from each of the pills and measuring its gamma-ray spectrum.

SOURCES OF SOME SECONDARILY WORKED OBSIDIAN ARTIFACTS FROM TIKAL, GUATEMALA*

H. Moholy-Nagy, F. Asaro, and F. Stross

A small series of secondarily-worked obsidian artifacts from Tikal, Guatemala, was analyzed to determine the source of the stone. The results of this analysis shed light upon obsidian procurement at Tikal and also relate to obsidian source studies in general.

Tikal seems to have imported obsidian throughout its history. Although most obsidian found at Tikal is grey or black in color, a small proportion, estimated at about 2 percent of the recorded total, is green. Green obsidian is consistently present after the beginning of the Classic Period, with the highest frequency occurring during the Early Classic. Source analyses carried out on Mesoamerican obsidian since the late 1960s[1] strongly suggest that all green obsidian found in the Maya area comes from quarries in the vicinity of Pachuca, Hidalgo, Central Mexico.

Source analysis by X-ray flourescence (XRF) or neutron activation analysis (NAA)[2] provides a possibility for confirming or dicarding hypotheses about sources suggested by other data, such as differences in artifact forms, color of the obsidian, manufacturing techniques, or archaeological context.

Samples taken from 28 incomplete artifacts were analyzed: 14 point-knives, 4 obsidian eccentrics, 2 incised obsidians, a ground obsidian earspool, 3 prismatic blades, and 2 cortical flakes from Tikal, and 2 flakes from Tetitla, Teotihuacan, Mexico. The secondarily worked point-knives, eccentrics, and incised obsidians were the main focus of the analysis. The ground earspool of grey obsidian was analyzed because of its uniqueness at Tikal. At the time of its discovery, it was felt that the earspool represented additional evidence of influence from Central Mexico. The prismatic blades, two grey and one brown-green, were chosen because of their unusual optical properties. The two small grey cortical flakes seem to be debitage and might therefore support the hypothesis that Highland obsidian arrived in Tikal as core preforms. The two waste flakes from Tetitla, Mexico, were analyzed for comparison with the Tikal materials.

The source of the obsidian was first determined by XRF (Table 1) and then confirmed by an abbreviated NAA on a representative sample from each provenience group (Table 2). Any artifacts still unassigned by the abbreviated NAA were submitted to a more intensive NAA measurement that might involve twenty to thirty elements (Table 3). This procedure was successful in assigning the obsidian used for all artifacts except two point-knives (TIKL-10 and TIKL-11). The detailed analysis of these two opaque black specimens is given in Table 3. The stone used for one specimen, TIKL-11, is similar to obsidian from Zinapecuaro, Michoacan, Mexico.

No transparent or translucent green obsidian point-knives were selected for analysis because it was assumed that the source of the stone was Pachuca, Hidalgo. However, one fragment of an unusual, opaque, silver-green obsidian point-knife was analyzed (45G-11/7, TIKL-6), and this also proved to be from the Pachuca area. Of the 13 other grey and black point-knives, nine were made of Mexican obsidian, seven of these of stone from Otumba. Two point-knives were made of obsidian from the Guatemalan highlands source of Ixtepeque. Two, as noted above, could not be attributed to a source.

Although the size of the sample is small, the results of the analysis generally support the hypothesis that obsidian eccentrics and incised obsidians were locally manufactured from core preforms from the Guatemalan Highlands. The circumstance that these ceremonial artifacts were made of El Chayal obsidian reinforces the relationship between ceremonial use of obsidian at Tikal and the predominantly utilitarian prismatic blade manufacture already suggested by a behavioral typology and previous, less accurate source analyses.

Analysis results also indicate that most of the grey obsidian point-knives found at Tikal are Central Mexican products, not local imitations of Central Mexican types. This finding supports the observations of specialized obsidian workshops in the Basin of Mexico.

Present evidence examined at Mesoamerican quarries indicates that raw obsidian was rarely, if ever, transported any distance. Usually, some preliminary working into core preforms or macroblades took place in workshops near the quarries.[7-10]

The analysis of this sample of secondarily-worked artifacts has confirmed earlier suggestions that Tikal imported most of its obsidian from the Guatemalan highlands, predominantly as core preforms. During the Classic Period, Tikal also received a very small amount of obsidian from Central Mexico, predominantly as finished point-knives and green obsidian prismatic blades. The inception, as well as the high point, of this latter obsidian exchange network coincides with the time of maximum Teotihuacan influence in other aspects of Tikal material culture during the Early Classic period.

Although the presence at Tikal of Central

*This work was supported by Tikal Project, University Museum, University of Pennsylvania, Philadelphia, PA and by the U.S. Department of Energy under Contract No. W-7405-ENG-48.

Table 1. Results of x-ray fluorescence analysis (XRF).

Sample (Number of artifacts)	Ba[a] (ppm)	Ce (ppm)	Rb/Zr	Sr/Zr
Artifacts assigned to El Chayal-La Joya-Cornelia Dome (Guatemala) source				
Mean (8)	897	51.6	1.23	1.33
RMSD[b](8)	21	4.2	0.07	0.04
TIKL-15	896	48 ± 6	0.99	1.25
Reference Group:				
Asaro et al. (1978)	943	47.4	1.24	1.29
Artifacts assigned to Ixtepeque (Jutiapa) source (R. Sidrys' 2-1 source)				
Mean (3)	1010	46	0.56	0.88
RMSD[b](3)	17	4.4	0.03	0.04
Reference Group:				
Asaro et al. (1978)	1030	43.3	0.57	0.90
Artifact assigned to San Martin Jiloteqeque area (Chimaltenango) (Rio Pixcaya type)				
TIKL-22	1051	47 ± 4	0.85 ± 0.05	1.66 ± 0.06
Reference Group:				
Asaro et al. (1978)	1103	47.4	0.95	1.64
Artifact assigned to Ucareo (Michoacán) type				
TIKL-4	159	74 ± 6	1.18 ± 0.07	0.08 ± 0.02
Reference Group:				
Asaro et al. (1975)	138 ± 19	71 ± 2	1.24	0.11
Artifacts assigned to Otumba (Mexico) source				
Mean (9)	751	59	0.83	0.87
RMSD[b](9)	29	6	0.07	0.05
Reference Groups:				
Stross et al. (1976)	880-1000	60-65	~1.0	~1.0
Asaro et al. (1975)	806 ± 26	54.9 ± 0.8		
Artifacts assigned to Pachuca (Hidalgo) source				
Mean (2)	16	102	0.21	<0.008
RMSD[b](2)	10	6	0.01	
Reference Groups:				
Stross et al. (1976)	0-10	110-115	0.25	<0.006
Asaro et al. (1975)		96.4 ± 1.9		
Artifact assigned to Zaragoza (Puebla) source				
TIKL-3	434	82 ± 13	0.67	0.15
Reference Group:				
Stross et al. (1976)	500	70	0.79	0.21
Asaro et al. (1975)	474 ± 21	75.9 ± 9		

[a]Uncertainty in the Ba measurement (except for Pachuca results) is about 4%.

[b]RMSD is the root-mean-square-deviation.

Mexican green obsidian has been known for a number of years, the presence of Mexican grey obsidian was discovered by analyzing point-knives. Therefore, in attempting to trace obsidian procurement networks for any particular site or region,[11] samples should be taken from as many different types of artifacts present as possible. In assessing the qualities of materials, ancient craftsmen made fine distinctions between materials that are now lost to us or that we are just beginning to appreciate.

In this type of study it is of particular interest that recent developments in method permit increased precision in the sourcing of obsidian by XRF and NAA.

Acknowledgments: The authors thank William R. Coe for his generous support, and Payson D. Sheets for his helpful criticism.

REFERENCES

1. F. H. Stross, J. R. Weaver, G. E. A. Wyld, R. F. Heizer, and J. A. Graham, "Analysis of American Obsidian by X-ray Fluorescence and Neutron Activation Analysis," in Contributions of the University of California Archaeological Research Facility, No. 4, pp. 59-79, Berkeley, California (1968).

2. F. Asaro, H. V. Michel, R. Sidrys, and F. Stross, "High-Precision Chemical Characterization of Major Obsidian Sources in Guatemala," American Antiquity, vol. 43, pp. 436-443 (1978).

3. F. H. Stross, T. R. Hester, R. F. Heizer, and R. N. Jack, "Chemical and Archaeological Studies of Meso-American Obsidians," in Advances in Obsidian Glass Studies: Archaeological and Geochemical Perspectives,

Table 2. Neutron activation verification of XRF assignments.

Artifact	Element abundances[a] and errors[b] Mn	Ba	Dy	Na %	K %
TIKL-4	164±2	154±18	3.93±0.08	2.86±0.03	4.43±0.30
Ucareo Reference Group	170±4	162±12	3.82±0.10	2.91±0.03	4.27±0.25
TIKL-12	453±5	1064±28	2.49±0.10	3.08±0.03	4.21±0.32
Ixtepeque Source (Sidrys' 2-1 source)	449±9	1030	2.30±0.11	3.05±0.06	3.61±0.26
TIKL-21	640±6	922±35	2.73±0.12	3.25±0.06	3.83±0.27
TIKL-15	639±6	926±32	2.60±0.11	3.21±0.03	3.58±0.31
El Chayal - La Joya-Cornelia Dome Source	649±13	943	2.66±0.11	3.15±0.06	3.45
TIKL-22	529±5	1130±34	2.18±0.11	2.96±0.03	3.59±0.30
San Martin Jilotepeque Area (Rio Pixcaya Type)	521±10	1036±40	2.10±0.11	2.92±0.06	3.71±0.24
TIKL-24	1132±11	<130	16.63±0.21	3.96±0.04	3.75±.37
Pachuca Type	1132±25	<36	16.46±0.34	3.81±0.13	3.64±0.46
TIKL-1	389±4	811±28	3.54±.10	3.24±.06	3.57±.25
TIKL-5	395±4	758±25	3.61±.10	3.16±.03	3.83±.30
LBL-391 (ppm) Mn Type (very likely) Otumba, Mexico source)	391±6	839±21	3.29±0.14	3.15±0.06	3.64±0.46
TIKL-3	250±5	432±25	5.11±0.10	3.13±0.06	4.17±0.24
LBL-252(ppm)Mn type (very likely Zaragoza, Puebla source)	252±5	488±14	4.93±0.10	3.05±0.06	4.16±0.12

[a]Abundances are given in percent for Na and K and in parts-per-million (ppm) for the other elements.

[b]The errors for the individual artifacts reflect the precision of the measurement. For the reference groups, the error is the standard deviation or root-mean-square-deviation (RMSD).

R. E. Taylor, ed., Noyes Press, Park Ridge, New Jersey, pp. 240-258 (1976).

4. F. Asaro, F. H. Stross, and H. V. Michel, Unpublished data (1975).

5. J. E. Ericson and J. Kimberlin, "Obsidian Sources, Chemical Characterization and Hydration Rates in West Mexico," Archaeometry, vol. 19, no. 2, pp. 157-166 (1977).

6. I. Perlman and F. Asaro, "Pottery Analysis by Neutron Activation," in Science and Archaeology, R. H. Brill, ed., Massachusetts Institute of Technology Press, Cambridge, Massachusetts and London, England, pp. 182-195 (1971).

7. W. H. Holmes, Handbook of Aboriginal American Antiquities, Part 1. Introduction: The Lithic Industries, Bureau of American Ethnology, Bulletin 60, Washington, D. C. (1919). Burt Franklin Reprints, New York (1974).

8. M. W. Spence and J. R. Parson, "Prehistoric Obsidian Mines in Southern Hidalgo," American Antiquity, vol. 32, no. 4, pp. 542-543 (1967).

9. J. A. Graham and R. F. Heizer, "Notes on the Papalhuapa Site, Guatemala," in Contributions of the University of California Archaeological Research Facility, No. 5, pp. 101-125, Berkeley, California (1968).

10. P. D. Sheets, "Behavioral Analysis and the Structure of a Prehistoric Industry," Current Anthropology, vol. 16, no. 3, pp. 369-391 (1975).

11. N. Hammond, "Obsidian Trade Routes in the Mayan Area," Science, vol. 178, p. 1092 (1972).

Table 3. Detailed analysis of two unassigned artifacts. (NAA except where indicated.)

	68I-45/20 (TIKL-10)	77A-17/7 (TIKL-11)	Zinapecuaro (LBL)	Zinapecuaro (Ericson & Kimberlin)
Al%	7.28 ± 0.13[a]	6.51 ± 0.10[a]	6.59 ± 0.15[b]	
Ba	773 ± 18	34 ± 9	74 ± 12	[c]
Ce	60.5 ± 0.7	47.1 ± 0.7	59.4 ± 8.0	51.1[d] ± 1.8
Co	1.16 ± 0.07	0.30 ± 0.05	0.26 ± 0.06	0.21 ± 0.01
Cs	5.58 ± 0.09	10.66 ± 0.15	8.32 ± 0.30	9.9[d] ± 0.8
Dy	4.29 ± 0.10	5.04 ± 0.12	4.23 ± 0.23	
Eu	0.64 ± 0.010	0.097 ± 0.006	0.129 ± 0.010	
Fe%	1.277 ± 0.014	0.733 ± 0.010	0.75 ± 0.03	0.72[d] ± 0.01
Hf	4.92 ± 0.07	4.43 ± 0.07	4.07 ± 0.10	4.11[d] ± 0.18
K%	3.58 ± 0.17	4.00 ± 0.22	3.86 ± 0.30	
La	29.7 ± 0.5	22.3 ± 0.5	29.1 ± 4.6	
Lu	0.362 ± 0.017	0.460 ± 0.020	0.360 ± 0.022	
Mn	276 ± 5	192 ± 4	175 ± 5	
Na%	3.30 ± 0.06	3.10 ± 0.06	2.90 ± 0.05	
Rb	145 ± 5	209 ± 7	186 ± 10	191[d] ± 7
Sb	0.17 ± 0.04	0.60 ± 0.06	0.56 ± 0.07	
Sc	3.39 ± 0.03	3.15 ± 0.03	2.78 ± 0.06	3.41 ± 0.14
Sm	4.58 ± 0.05	4.54 ± 0.05	4.51 ± 0.25	
Sr[e]	171 ± 26	<18 ±	<13 ±	
Ta	0.990 ± 0.010	1.671 ± 0.017	1.310 ± 0.064	1.51[d] ± 0.11
Th	10.54 ± 0.11	18.33 ± 0.18	16.02 ± 0.58	16.9[d] ± 0.9
U	3.21 ± 0.03	5.32 ± 0.04	4.37 ± 0.17	
Yb	2.54 ± .03	3.21 ± 0.04	2.64 ± 0.10	2.92[d] ± 0.28
Zr[e]	256 ± 38	125 ± 19	112 ± 17	[c]

[a]The measurements were calibrated with Standard Pottery whose composition and abundances are given in Ref. 6. The indicated errors are the precision (one standard deviation) of measurement. The accuracies can be deduced from the uncertainties in Standard Pottery given in the reference.

[b]The values in this column are the standard deviations measured in 7 Zinapecuaro obsidian rocks or the experimental error, whichever is larger.

[c]Ba and Zr data from Ref. 5 were not included because of uncertainties in these data.

[d]This value was normalized to the LBL calibration system with Teuchitlan and Etzatlan obsidian data.

[e]Measured by XRF.

OIL SHALE RESEARCH

INTRODUCTION

J. P. Fox

"Why should an oil shale industry be developed when coal is a far more abundant fossil fuel resource?" This is the question probably most often asked during any serious discussion of shale oil as a replacement for petroleum. The question arises from the fact that there is at least twenty times more energy in known U. S. coal reserves than in oil shale. However, there is one basic answer to that question and, surprisingly enough, it is the counter-argument least advocated: The hydrogen content of shale oil, typically 10-12% by weight, is much higher than the hydrogen content of the organic material in coal. To produce liquid fuels that flow easily and behave properly in internal combustion engines, enough hydrogen must be chemically bound into the fuel to approximate the properties of the liquid hydrocarbons found in commercial petroleum. The oil fraction recovered from oil shale is already hydrogenated to nearly this composition. To achieve a comparable degree of hydrogenation starting with coal, heroic chemical engineering must be practiced on a grand scale. By contrast, an oil shale industry could be established without this "heroic" and "grand" effort because the technology required is comparatively simple, economical, and--in some cases--is ready to be scaled up for commercial use. However, both economic and environmental constraints still exist. The Lawrence Berkeley Laboratory (LBL) is investigating these environmental constraints and is seeking economically viable solutions, as appropriate.

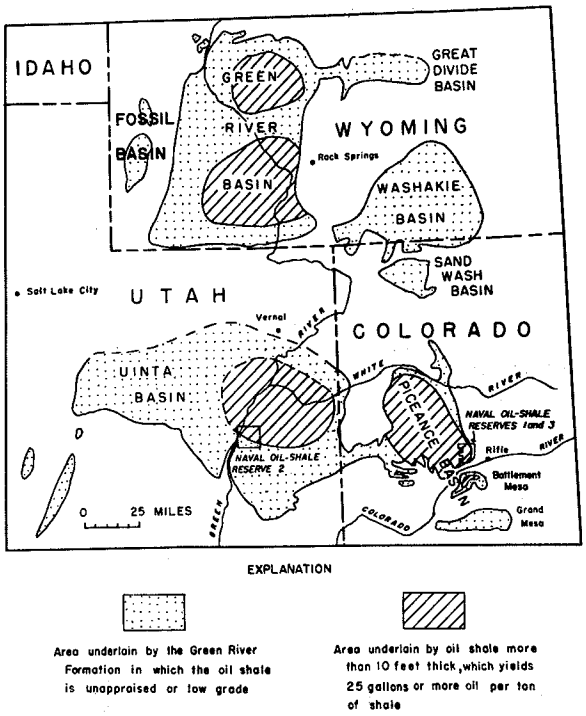

Fig. 1. Oil shale deposits in the Green River Formation of Colorado, Utah, and Wyoming. (XBL 798-10883)

Vast resources of oil shale--in excess of 1.8 trillion barrels (bbl) of oil--exist in the tri-state area of Colorado, Utah, and Wyoming (Fig. 1). Some 80 billion bbl of this oil are recoverable with current technology--more energy than is contained in all of the known oil and gas reserves in the United States. The U. S. Department of the Interior has estimated that, with more advanced technology and under economic conditions different from today's, oil shale deposits in the U. S. might yield as much as 800 billion bbl of oil.

Oil shale is a layered, greyish, sedimentary rock that was deposited eons ago in freshwater lakes. It contains about 20% organic material, primarily kerogen, which originated from algae and other microorganisms and wind-blown or waterborne pollen and spores. The inorganic material is a dense, tough marlstone composed primarily of the two carbonaceous minerals, dolomite and calcite. The shale may exist anywhere from 100-3000 ft beneath the surface, interbedded with varying amounts of tuff, siltstone, sandstone, and claystone and laced with groundwater aquifers.

Oil may be extracted from the shale by heating the rock to break down the kerogen, a high molecular weight polymer, into smaller molecules. This process, termed pyrolysis, may be carried out in a surface retort or in the ground (in-situ processes). The technology for surface retorting is further advanced but is limited by economic and environmental factors. Large volumes of rock must be mined, crushed, transported, and disposed of. The surface technologies are capital intensive and require large volumes of water. In the in-situ processes, the majority of the resource is pyrolyzed in the ground (a small amount, usually about 20%, is removed to create void space). This approach to processing oil shale is presently under intensive study by industry and the U. S. Department of Energy (DOE) as an economical and environmentally superior alternative to surface processing.

The possibility of using oil from shale has been known for centuries. Marine oil shale was used in the 14th century to manufacture Icthyol, a medicinal ointment named after the Greek word for "fish oil." In 1694, the first commercial patent was filed in England for distilling "...oyle from a kind of stone." Oil shale industries flourished in the 19th century in Scotland, France, South Africa, Australia, Russia, Brazil, and the United States. Today, such industries exist in Estonia, China, and Brazil.

Since these early beginnings, the production of and interest in shale oil has fluctuated in response to the availability of U. S. and world petroleum. Shale oil has simply never been economically competitive in a market in which conventional crude was abundant. Even today, economic uncertainties continue to constrain oil shale development by industry. Commercial developers face economic perplexities which include the following: uncertain-

ties about the real costs of oil shale production and about the future price of noncompetitive oil on world markets; the substantial amount of front-end capital required for each project; the large capital risk involved compared to the assets of some companies; and the possibility of long delays which might be caused by environmental and governmental requirements and regulations.

The most basic and serious economic problem, however, is the difficulty of attracting capital for development of an oil shale industry. Investment institutions are reluctant to support this development because of the risks and the uncertainties of present oil shale technology. If early and successful development of a commercial oil shale industry is to be accomplished, government support will probably be required, at least for the pioneer projects. Without this support, industrial development may be much slower than desired because, in some instances, proposed plant investments far exceed the present total assets of some of the companies proposing to enter commercial oil shale production. Consequently, government incentives will probably be required for production of at least 100,000 to 400,000 bbl of oil per day. These incentives might take the form of direct credits, guarantees, outright grants, or governmental equity positions.

Environmental issues are also a serious deterrent to the development of a commercial oil shale industry. Retorting processes produce large quantities of liquid, solid, and gaseous wastes that must be disposed of in a pristine and largely undeveloped environment (Fig. 1). The types and quantities of these material per ton of shale retorted are shown schematically in Figure 2. The surface retorting processes, such as Paraho and Lurgi, are more efficient than the in-situ processes and produce 25-29 gal oil/ton of rock from a 30 gal/ton shale. They also produce considerably less gas and water than the in-situ processes. However, they generate large quantities of spent shale, about 0.8 tons/ton retorted, which must be returned to the mine and/or piled in nearby canyons. The more inefficient in-situ processes may produce only 15-20 gal of oil/ton of rock from the same 30 gal/ton shale. Additionally, they produce larger quantities of gas (due, in part, to the use of steam during retorting) and larger quantities of water (from combustion and groundwater inflow). However, the majority of the spent shale remains underground and only a small fraction (which was mined to create in-situ void space and surface retorted) requires surface handling and disposal. However, initial optimism that in-situ retorting solved the significant solids disposal problem attendant with surface retorting has waned as researchers have discovered that in-situ spent shale may pose an even more serious water contamination problem than spent shale retorted on the surface.

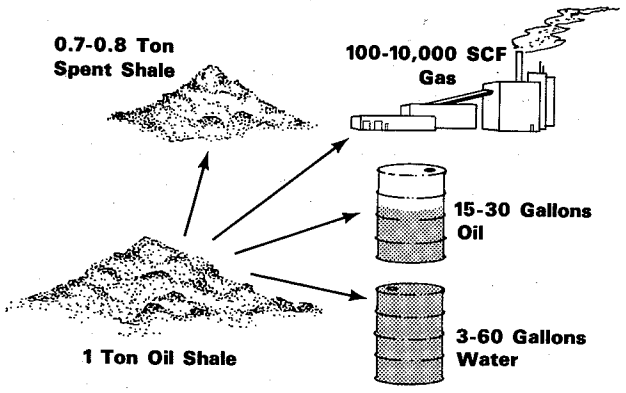

Fig. 2. Schematic showing types and quantities of products and byproducts produced during oil shale conversion. (FXBL 812-269)

The Oil Shale Research Program at the Lawrence Berkeley Laboratory is concerned with the far-reaching environmental consequences of shale oil production: air, solid waste, and water pollution. The program is concerned with the characterization, transport, fate, and control of organic, organometallic, and inorganic compounds synthesized or released during retorting. A number of previously unrecognized or little understood environmental concerns have been identified, such as in-situ leaching, air emission of toxic trace elements, and aqueous effluent disposal. These concerns are being studied at LBL in basic and applied research programs in these areas. The goal of the program is to develop the scientific information necessary to understand and, ultimately, to control environmental problems.

Information on the chemical composition of oil shale and its by-products is being developed by the Characterization Group to assess environmental impacts and to select and develop suitable control strategies. The gases, oils, waters, and solids produced by oil shale retorting are being analyzed for molecular species and major, minor, and trace elements. This work has indicated that the primary elements of environmental concern are As, Se, Cd, Hg, F, and B, and that inorganic and organometallic species, including arsenate and methylarsonic acid, are present in process waters. Methods are being developed to measure organometallic and organic compounds present in aqueous effluents. In-depth geochemical investigations of the Green River Formation in Colorado have been conducted which indicate a remarkable uniformity in most major, minor, and trace element concentrations throughout the formation. Highly variable elements include As, Se, Mo, and Hg. Cores through spent horizontal true in-situ retorts are being studied to determine mineralogical reactions that occur during retorting.

The distribution or partitioning of major, minor, and trace elements during oil shale retorting is being investigated by the Partitioning Group. Elemental mass balances are being performed on pilot-scale and laboratory-scale retorts, and the effect of retort operating conditions on elemental distribution is being studied as well as the kinetics and chemical transformation of select elements. These studies utilize LBL's 6-kg oil shale retort.

A recent focus of the Partitioning Group has been on the trace element content of gases produced

during retorting. Large quantities of low-Btu gas, from 100 to 10,000 scf/ton of shale, are produced during oil shale conversion. The proper use and disposal of this low-Btu gas represents a significant challenge to the oil shale industry. This gas contains a significant fraction of the recoverable energy and is highly corrosive, has a low heating value, and may contain high concentrations of such toxic trace elements as Hg, As, Se, and Cd. Real-time instrumentation is being developed to measure toxic trace elements in oil shale gases and is used to measure As, Se, Cd, and Hg in gases from laboratory, pilot, and field retorts. A Zeeman atomic absorption spectrometer capable of making real-time, in-place measurements has been developed and used to demonstrate that Hg emissions from in-situ retorts may be nonuniform and that the majority of the Hg released occurs as a pulse towards the end of the retorting. Similar work on Cd is in progress.

Large cavities of spent shale remain in the underground environment after oil is extracted from an in-situ retort. These cavities of spent shale, referred to as "abandoned retorts," pose several serious environmental hazards. They may cause groundwater contamination from leaching or they may subside, creating surface disturbance. These problems and potential solutions are being investigated by the Retort Abandonment Group. Several possible control strategies for abandoned retorts have been identified, including filling the retorts with a grout, intentional leaching, and various geohydraulic modifications. These strategies are being investigated in laboratory and modeling studies. A numerical model of the subsidence phenomenon over a large field of retorts has been developed and used to study the effect of retort geometry and grout properties on subsidence. A mass transfer model has been developed for the leaching of organic carbon from in-situ spent shale and is being used to investigate intentional leaching as a control strategy for retort abandonment. A high-strength hydraulic cement has been developed from spent shale that may be used to seal underground retorts or for commercial construction, and studies are in progress to develop a cheaper and lower-cost grout from spent shale and locally available materials, such as fly ash. Pre- and post-abandonment hydrogeology have been investigated using a mathematical model of the retort-aquifer system. These studies have shown that dewatering and reinvasion rates may be much lower than previously believed, due to the saturated-unsaturated flow produced by large-scale dewatering, and that dewatering volumes may be much larger than previously calculated.

Oil shale processing may also produce from 0.1-22 bbl of highly contaminated water/bbl of oil. This water represents a potential resource for the arid oil shale region, if the water can be upgraded. The Wastewater Treatment Group is exploring the use of various physical, chemical, and biological processes to upgrade this water for in-plant use or for discharge. They have conducted laboratory treatability studies on coagulation-flocculation for the removal of oil and grease, on biological oxidation for the removal of organic carbon, and on steam stripping for the removal of dissolved gases. This work has lead to the development of several novel techniques for the treatment of retort water. (The more conventional methods are not satisfactory for retort waters due to fouling, toxicity, and other problems.) These techniques include foam fractionation and raw and spent shale adsorption. Retort waters produce copious amounts of foam when aerated. This property is being used as the basis of a novel separation technique to remove oil and grease from retort water. Spent shale, a solid waste produced during retorting, significantly reduces the organic and inorganic carbon, color, and odor of retort water and gas condensate. Inorganic carbon is removed by the reaction of carbonate species in the waters with hydroxides formed from the hydration of oxides in the spent shale. Organic carbon and its associated properties of color and odor are reduced by adsorption on char. Raw shale behaves in a manner similar to spent shale.

This report summarizes the progress during FY 1980 on these oil shale research efforts.

SPECIATION OF INORGANIC AND ORGANIC ARSENIC COMPOUNDS IN OIL SHALE PROCESS WATERS*

R. H. Fish, J. P. Fox, J. Cantor, P. C. Babbitt, F. E. Brinckman,† and K. L. Jewett†

INTRODUCTION

Oil is recovered from oil shale kerogen by a controlled pyrolysis using surface and in-situ technologies. In addition to oil, these processes produce considerable amounts of process waters which originate from mineral dehydration, combustion, groundwater seepage, and steam and moisture in the input gas. Since the waters are in intimate contact with raw and partially retorted shale and shale oils, they constitute a leachate of these products.

Water derived from in-situ oil shale retorting is heavily contaminated with organic and inorganic constituents. It is generally alkaline (pH 8-9.5) and contains a variety of polar organic species, including carboxylic acids, bases (amines, N-heterocyclics, N-aromatics), and organic oxygen and sulfur compounds (phenols, pyrans, thiophenes). The inorganic content of retort waters is also high, including the following anions: HCO_3, CO_3, F, S_2O_3, SCN, and SO_4. The principal dissolved cations are Na, NH_4, Mg, and Fe. Trace elements of environmental concern include As, Se, Hg, Zn, Mo, and B.

The presence of even very low levels of organometallic forms of the toxic metals, which may enhance their biological uptake and movement through an ecosystem, may multiply their toxic potential to sensitive species by orders of magnitude. The purpose of this program is to identify and quantify the organometallic and inorganic species present in shale oils, process waters, gases, and leachates from oil shale solid wastes and to evaluate the data in an environmental context.

ACCOMPLISHMENTS IN FY 1980

Organic and inorganic arsenic compounds were speciated in seven oil shale process waters, including samples from simulated, true, and modified in-situ processes using a high-performance liquid chromatograph automatically coupled to a graphite furnace atomic absorption detector (HPLC-GFAA). The molecular forms of arsenic at ppm levels in these waters were identified for the first time and shown to include arsenate, methylarsonic acid, and phenylarsonic acid. An arsenic-specific "fingerprint" chromatogram was obtained for each process water.

Seven in-situ oil shale process waters were examined, including three process waters from Occidental Oil Company's Logan Wash modified in-situ process (retort, boiler blowdown, and heater treater waters); one from Geokinetics' horizontal, true in-situ experiment near Books Cliff, Utah (retort water); one from Laramie Energy Technology Center's Rock Springs Site 9 true in-situ experiment (Omega-9 retort water); and one each from two large-scale simulated, modified in-situ retorts: retort water from run L-2 of Lawrence Livermore National Laboratory's 6,000-kg retort and retort water from Laramie Energy Technology Center's 150-ton retort. Additional descriptions of these waters are in the Energy and Environment Division Annual Report 1979.[1] These materials were warmed to room temperature, filtered (0.45 μm, Millipore), appropriately diluted with deionized (18 MΩ-cm) water, and directly injected (100-250 μℓ) into the HPLC-GFAA.

Several available gradient compositions were used for the HPLC speciation of arsenicals in the basic (pH ≃ 9.2) process waters. A very effective combination was a commercial anion-exchange column (Dionex) and an eluent composition recommended by Woolson and Aharonson.[2] Thus, with a step gradient starting at 10 min from 100% water-methanol (80:20 vol%) to 100% 0.02 M $(NH_4)_2CO_3$ in water-methanol (85:15 vol%) at 5$\bar{7}$ min, with a flow rate of 1.2 ml/min, we readily separated mixtures in deionized water of the five arsenic standards employed (Fig. 1), as well as individual authentic spikes of these species in the process waters (Fig. 1). The HPLC eluent was automatically sampled from a specially designed[3] flowthrough teflon cup for periodic graphite furnace atomic absorption (GFAA) detection at 193.7 nm for arsenic. This procedure produces a chromatogram that consists of a series of histogrammic peaks which, in combination, represent an eluting chromatographic peak and permit offline analysis of eluting fractions. Approximately 2-6% of the eluent is consumed by the GFAA detector, depending on flow rate and sample size. Thus, molecular components that cannot be identified using retention times (t_R) of authentic compounds can

* This work was supported by the Assistant Secretary for Fossil Energy, Deputy Assistant Secretary for Oil, Gas, and Shale Technology, Office of Oil Shale of the U.S. Department of Energy under Contract No. W-7405-ENG-48.

† Center for Materials Science, National Bureau of Standards.

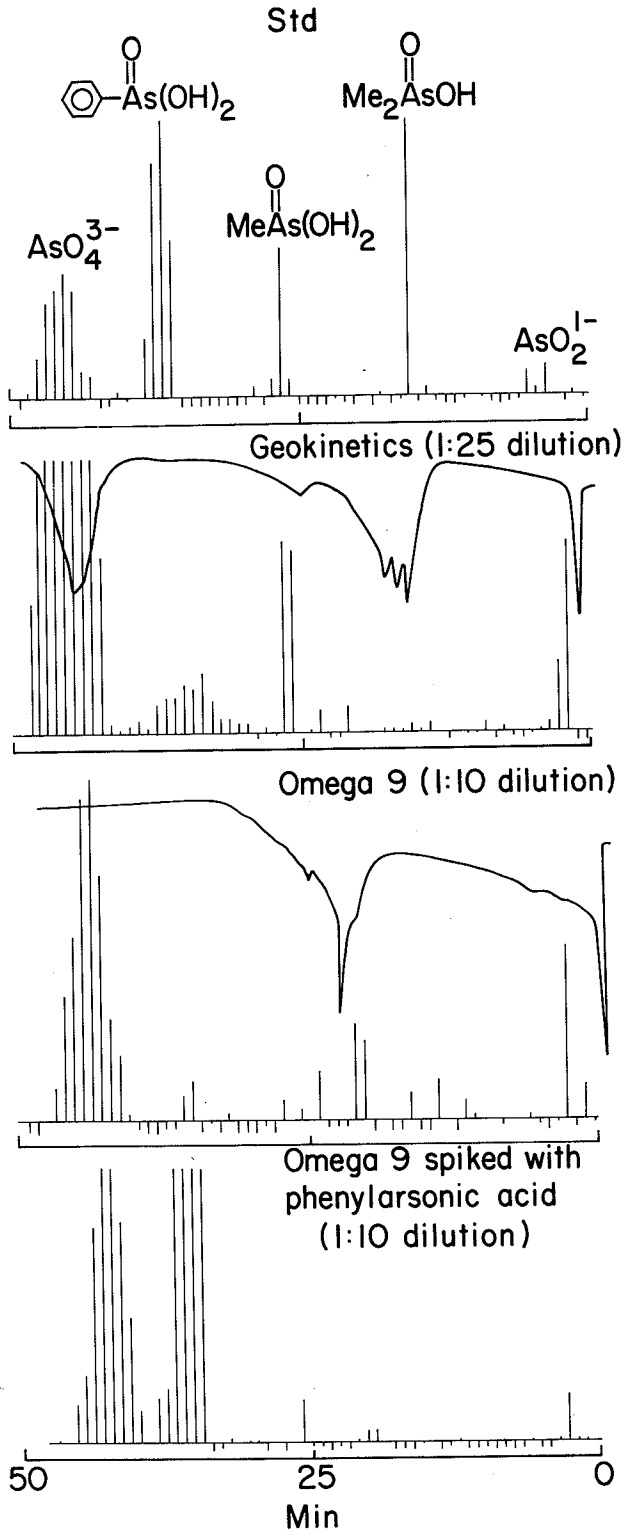

Fig. 1. Element-specific chromatograms (arsenic species fingerprints) obtained by HPLC-GFAA (see bottom of each sample set) and associated ultraviolet detector chromatograms (see continuous trace shown at top of each sample set) compared against authentic arsenic standards for two retort waters from true in-situ processes.
(XBL-10168A)

be isolated and later subjected to alternate, off-line spectroscopic characterization.

A typical result, shown in Figure 1, compares the arsenic-specific GFAA chromatograms obtained for two true in-situ retort waters. Conventional chromatograms, taken with an ultraviolet (254 nm) detector in series with the GFAA detector, are shown superimposed (solid traces) on the arsenic-selective outputs. These clearly reveal the intensity and complexity of the organic matrix and the analytical limitations of nonselective detectors. Each time we ran a sample, we also ran five authentic arsenic standards (as 10 ng As in each peak) combined into one solution, which included sodium arsenite, dimethylarsinic acid, methylarsonic acid, phenylarsonic acid, and sodium arsenate. Each process water had a distinctive "fingerprint" and substantial quantities of arsenate, methylarsonic acid, and phenylarsonic acid are present, while arsenite and dimethylarsinic acid are probably absent or, at best, marginally detected.

Tables 1 and 2 correlate the identified arsenic species and their estimated concentrations with the corresponding process waters. Areas of the chromatographic peaks were obtained from the sums of their component GFAA signals. These were converted to concentration values (μg/ml) by comparison with authentic peaks (at $t_R \pm \sigma$) in the aqueous calibration solutions and by comparison with peak areas of appropriate arsenicals individually spiked at corresponding concentrations in process waters. We regarded each GFAA chromatographic peak as "positively" identified if its retention volume matched that of the mean value of the calibration peak for each As species within two standard deviations (2-5% root-mean-square deviation) (Table 1). "Tentative" assignments were given to those peaks outlying two standard deviations although spiking the samples with authentic arsenic compounds yielded the same (increased) single peak for both positively and tentatively identified species (Fig. 1).

Estimated detection limits and sensitivities for each arsenic species were found to vary, mainly due to the alkaline organic matrix and the fixed GFAA atomization program. Consequently, we compared each sample chromatogram against that of a standard solution of authentic arsenicals in distilled water. Reliable retention times were obtained in this way, as were approximate concentrations of major arsenic species in process waters. In order to more fully assess matrix effects on t_R and concentrations of minor components, we tested authentic arsenicals as spikes in several process waters. For example, in Occidental retort water (diluted 1:10), detection limits at 95% confidence level using additions of 0, 2.5, 5, 10, or 20 ng of analyte were: arsenite, 3.0; dimethylarsinic acid, 20.4; methylarsonic acid, 17.3; phenylarsonic acid, 7.4; and arsenate, 5.2 ng/ml (as As), respectively. Comparable results were obtained with several other process waters. A neutral arsenical(s) eluting just prior to arsenite undoubtedly interfered with estimations of its

Table 1. Tentative identification of inorganic and organic arsenic compounds by HPLC-GFAA in various oil shale process waters.

Sample	Retention Times[a] (min)					
	Sodium Arsenite $NaAsO_2$	Cacodylic Acid $(CH_3)_2As(O)(OH)$	Methylarsonic Acid $CH_3As(O)(OH)_2$	Phenylarsonic Acid ϕ-$As(O)(OH)_2$	Sodium Arsenate Na_2AsO_4H	Unknown
Calibration Solutions[b]	2.1 ± 0.4	16.3 ± 1.8	25.4 ± 0.4	35.7 ± 0.4	44.8 ± 1.1	--
Simulated In-Situ Retorts[c]						
L-2 retort water	--	--	25.2 (+)	35.6 (+)	42.9 (+)	1.0
150-ton retort water	--	--	23.8 (±)	--	43.9 (+)	0.5
Field In-Situ Retorts[c]						
Omega-9 retort water	--	--	25.2 (+)	34.9 (+)	43.7 (+)	1.4 20.4
Geokinetics retort water	--	--	26.0 (+)	33.3 (±)	44.5 (+)	1.1 20.4
Occidental heater-treater water[c]	--	--	25.1 (+)	36.4 (+)	46.8 (+)	1.0 14.6
Occidental boiler blowdown water	--	--	24.9 (+)	34.6 (±)	44.2 (+)	0.8
Occidental retort water	--	--	24.6 (+)	35.9 (+)	44.8 (+)	0.5 15.0

[a] A dash (--) signifies that the species was not detected. A (+) signifies that the species was tentatively identified. The numerical values are the retention times at which the species or unknown peaks were detected.

[b] Mean ± standard deviation of five or more scattered runs.

[c] Positive identification (+) fell within ± 2 σ (2-5% root-mean-square deviation) for calibration runs taken in sequence with unknown runs.

Table 2. Estimation of inorganic and organic arsenic compounds separated and detected by HPLC-GFAA analyses.

Process Water	Compound[a]	µg/ml[b] (ppm)
Occidental retort water	Unknown organoarsenic compound	--
	Methylarsonic acid	0.16
	Phenylarsonic acid	<0.003
	Arsenate	0.46
Occidental heater-treater water	Unknown organoarsenic compound	--
	Methylarsonic acid	<2.0
	Phenylarsonic acid	<0.42
	Arsenate	∿10
Occidental boiler blowdown water	Unknown organoarsenic compound	--
	Methylarsonic acid	0.58
	Phenylarsonic acid	0.15
	Arsenate	0.63
LETC 150-ton retort water	Unknown organoarsenic compound	--
	Methylarsonic acid	<1.5
	Arsenate	<3.0
LLL L-2 water	Unknown organoarsenic compound	--
	Methylarsonic acid	0.63
	Unknown inorganic or organo-arsenic compound	--
	Phenylarsonic acid	0.31
	Arsenate	>2.0
Geokinetics retort water	Unknown organoarsenic compound	--
	Methylarsonic acid	<2.0
	Phenylarsonic acid	<0.38
	Arsenate	>10
LETC Omega-9 water	Unknown organoarsenic compound	--
	Methylarsonic acid	<0.18
	Phenylarsonic acid	<0.02
	Arsenate	<1.6

[a] Determination of identified compounds by retention times with known authentic compounds, Table 1.

[b] Each standard 10 ng as As. Area under each peak estimated by method of summing peak heights digitized with an integrator and compared with calibration solutions in deionized water or method of additions with spikes in sample solutions.

detection limit. We presently place an upper limit on arsenite in the seven waters at <0.06 ± 0.03 ppm and on dimethylarsinic acid, at <0.01 ± 0.02 ppm.

Arsenate is by far the major (0.6-10 ppm) arsenical identified in all of the samples studied, but the variable concentrations of the other species suggest quantitative diagnostics for monitoring widely different production sites. It is interesting to note that Occidental's process waters (Table 1) all contain methylarsonic acid, phenylarsonic acid, arsenate, and one or several neutral or weakly ionized arsenicals, possibly in the molecular R_3As or R_3AsO classes, which elute early.

The two true in-situ process waters, Geokinetics and Omega-9, also display early peaks and contain methyl- and phenylarsonic acids, arsenate, and another unknown ionic arsenic species eluting at 20.4 min. (Fig. 1). Both simulated in-situ process waters are readily distinguished by a significant diagnostic feature involving an absence of detectable (<0.003 ppm) phenylarsonic acid in the 150-ton sample whereas water from trial L-2 contains >0.3 ppm of this species (Table 2). Beyond this, both 150-ton and L-2 samples contain methylarsonic acid, arsenate, and the neutral component which makes them reminiscent of Omega-9. These different fingerprints may reflect differences in operating parameters used in the various

processes. The similarities indicate that basic chemical phenomena are the same in certain laboratory and field retorts.

The origin of these observed organoarsenic compounds is not presently understood. Kerogen, which is biogeochemical in origin and is largely from lipid fractions of ancient algae, forms the ubiquitous oil-source matrix in oil shales. Thus, it is conceivable that these methyl- and phenylarsonic acids occur naturally following original biosynthesis or bioaccumulation and subsequent mineralization in oil shale and are released with little decomposition upon pyrolysis; they could be partitioned into the process water after intimate contact with shale oil. Ample evidence is available for both terrestrial and marine biomethylation of inorganic arsenic(V) by modern microorganisms and marine algae to produce both dimethylarsinate and methylarsonate species; no analogous biophenylation is reported as far as we know. Alternatively, purely abiotic synthesis form methyl- or phenylarsenic bonds in the hot reaction zone of the retort. This last pathway seems quite reasonable for methylarsonic acid because it parallels the long-known Meyer reaction between alkyl halides and arsenite salts. In boiling aqueous solution, both alkylarsonic and dialkylarsinic acids can form, but arylarsonic acids are not similarly obtained. This suggests that the phenylarsonic acid observed may arise from possible free radical reactions that are known to occur under similar pyrolysis conditions. Additionally, biomethylated arsenicals could be introduced with boiler feedwater (Occidental boiler blowdown) or by groundwater seepage into in-situ retorts (Omega-9 and Geokinetics retort waters) and could be converted to the observed arsonic acids under conditions of high temperatures and pH.

This work indicates that potentially toxic organic and inorganic arsenic compounds of appreciable concentrations are either released or synthesized during oil shale retorting processes using present-day technology. These compounds may be bioaccumulated in soils, water, and edible biota at appreciable distances from the retorting site and may thus represent potential health hazards for humans as well as a threat to aquatic species.

PLANNED ACTIVITIES FOR FY 1981

This work will be expanded to include additional samples and elements. Other oil shale wastewaters from additional processes will be characterized. Analyses of organometallic species in shale oils and leachates will be included in future work, and other retorting processes, including Paraho and the Rio Blanco Oil Shale Project process, will be characterized. Methods will be developed to speciate other elements including Se, Hg, and Zn. Experiments will be conducted to determine the origin of the identified organometallic species.

REFERENCES

1. R. H. Fish, J. P. Fox, F. E. Brinckman, and K. L. Jewett, "Speciation of Inorganic and Organic Arsenic Compounds in Oil Shale Process Waters," Energy and Environment Division Annual Report 1979, Lawrence Berkeley Laboratory report LBL-10486, 1980.

2. E. A. Woolson and N. Aharonson, "Separation and Detection of Arsenical Pesticide Residues and Some of Their Metabolites by High Pressure Liquid Chromatography-Graphite Furnace Atomic Absorption Spectrometry," Journal of Association of Official Analytical Chemists, vol. 63, 1980, p. 523.

3. F. E. Brinckman, W. R. Blair, K. L. Jewett, and W. P. Iverson, "Application of a Liquid Chromatograph Coupled with a Flameless Atomic Absorption Detector for Speciation of Trace Organometallic Compounds," Journal of Chromatographic Science, vol. 15, 1977, p. 493.

IDENTIFICATION OF CARBOXYLIC ACIDS IN OIL SHALE PROCESS WATERS*

P. C. Babbitt, R. H. Fish, L. H. Joseph, and A. S. Newton

INTRODUCTION

In-situ oil shale retorting produces a number of aqueous effluents that may reach the environment by accidental spills or discharge to surface and ground waters. These effluents include (1) retort water, (2) gas condensate, (3) heater-treater water, and (4) boiler blowdown (Fig. 1). Retort water and gas condensate, the most voluminous waters, are coproduced with the oil. They originate from combustion, mineral dehydration, steam and moisture in the input gas, and groundwater seepage into in-situ retorts. The retort water is condensed at elevated temperatures while the gas condensate is condensed at lower temperatures, from 15 to -15°C. Blowdown is a concentrated stream produced in the boiler used to make process steam. Heater-treater water is that removed from the shale oil by heat treatment.

* This work was supported by the Assistant Secretary for Fossil Energy, Deputy Assistant Secretary for Oil, Gas, and Shale Technology, Office of Oil Shale of the U.S. Department of Energy under Contract No. W-7405-ENG-48.

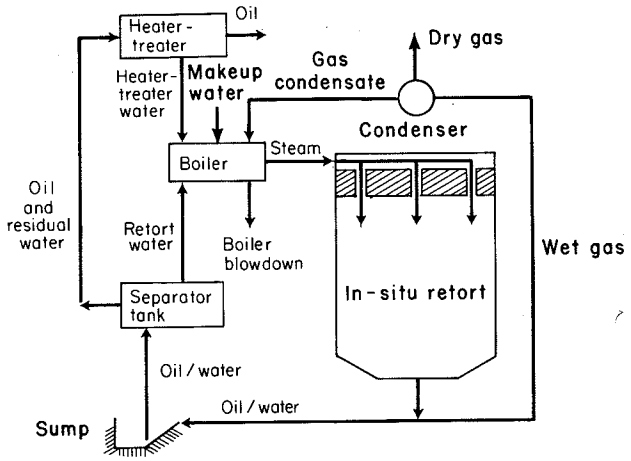

Fig. 1. Schematic of aqueous waste streams associated with the modified in-situ process. (XBL-805-971)

These four types of water may contain a number of toxic trace metals, including As, Se, Zn, B, and Fe, which may be complexed by organic ligands. Earlier work showed that As and Se were concentrated in methylene chloride acid extracts of oil shale process waters.[1] Carboxylic acids are known to occur at high concentrations in retort waters and may be present in other oil shale process waters. Since these acids may act as ligands for these and other metals, their identification will contribute to the characterization of organometallic compounds and complexes present in the waters. Additionally, knowledge of these compounds is important in making a realistic appraisal of the overall toxicity of the waters and their treatability. These organic ligands may increase the mobility of the associated trace elements, increase their biological uptake rate, enhance their toxicity, and interfere with various oil refining and water treatment processes.

The purpose of this work, initiated in August 1979, is to identify and quantitate carboxylic acid ligands that may be associated with trace metals in oil shale process waters using capillary column gas chromatography-mass spectrometry (GC-MS). The original method and early results are described in the Energy and Environment Division Annual Report 1979.[2]

ACCOMPLISHMENTS DURING FY 1980

This year we improved the chromatographic separation and identification procedure for carboxylic acids and elucidated some new low-molecular weight compounds by modifying the derivation procedure. We also initiated work to quantitate identified compounds by capillary GC. This work is described in following sections.

Chromatographic Separations

Early work was done on a 10 m x 0.025 mm test column coated with OV-101 in a Hewlett-Packard 5840A gas chromatograph. In 1980, a new column, 30 m x 0.025 mm and coated with SP 2100, was installed. Using standards of known compounds, the column was tested and the instrument parameters were set. Oven temperatures were programmed from 70°C to 265°C at 3°/min, starting 4.5 min into the run. Area reject and baseline reset functions were added to the time programming to maximize integration accuracy.

These modifications resulted in dramatically improved separation of carboxylic acid methyl esters yielding information on six carboxylic acids not obtained from the preliminary system.[2] Several compounds previously characterized only by number of carbon atoms and/or type of acid were specifically identified. All compounds were first identified by comparison with known standards on the basis of their retention times. Verification was obtained by GC-MS on a Finnigan quadrupole mass spectrometer.

Chemical Modification: Butylation Experiments

Carboxylic fatty acids with more than four carbon atoms are not sufficiently volatile to be directly analyzed on our chromatographic system. Traditionally, experimenters have analyzed the methyl ester derivatives of these compounds because their volatility allows good chromatographic separation. This type of derivation was performed on the process waters prior to our analysis. The method is discussed in the 1979 Annual Report.[2] While this method worked well for most of the carboxylic acids we identified, it produced negative results in the analysis of carboxylic acids with less than four carbon atoms. These derivatives proved to be so volatile on our system that they traveled through the column with the solvent and could not be distinguished. In 1980, we modified these acids by forming butyl ester derivatives which, being less volatile than the methyl ester derivatives, could be separated from the solvent peak.

A summary of both methods of chemical modification is presented in Table 1. This work allowed separation and identification of three low molecular weight carboxylic acids (C_2-C_4) in all of the waters studied. As in our work with methyl ester derivatives, identification was established using retention times and comparison with known compounds. These results were verified using GC-MS. Quantitation of these three compounds was not attempted.

Quantitation

Considerable effort was made to develop the chromatographic system to a state that would allow us to accurately quantitate identified carboxylic acids. While partial success in programming integrator functions on our system allowed us to get "order of magnitude" estimates of the incidence of those acids showing the largest or best separated peaks, the samples proved too complex to yield reproducible quantitative data from our chromatograms. Our main accomplishment in this area was to define some of the problems in getting quantitative data and to perform some preliminary experimentation with our system which indicated how the problem should be approached in future work.

Table 1. Preparation of carboxylic acid ester derivatives in oil shale process waters.

Methyl Ester Derivatives	Butyl Ester Derivatives
Lyophilize 20 ml process water; pH ~ 9.	Lyophilize 20 ml process water; pH ~ 9.
Reflux residue with 20 ml of BF_3/MeOH for 5 h under nitrogen.	Reflux residue with 20 ml of HCl/n-butanol for 5 h.
Add 20 ml water to decompose excess BF_3.	Add 20 ml of water; separate the two phases (aqueous and organic).
Extract the aqueous product mixture with 3 x 10 ml portions of benzene.	Extract the aqueous phase with 3 x 10 ml portions of benzene.
Concentrate the combined benzene extracts to 1 ml or less by fractional distillation.	Add benzene extracts to the organic phase and concentrate to 1 ml or less by fractional distillation.

Experimental Results

The results of the above-described experiments are summarized in Table 2 and Figure 2. Figure 2 shows the chromatograms of the six in-situ process waters studied. (The gas condensate, L-2, was included in the 1979 work[2] but was omitted from the work in 1980 because our methods lacked sufficient sensitivity to distinguish more than one carboxylic acid compound. Work is currently in process to develop a chemical work-up that will allow us to characterize ligands in such dilute waters.) While the same "fingerprinting" patterns as seen in previous work on these waters is evident,[2] additional patterns emerge.

The three Occidental Oil Company process waters have an homologous series of both mono- and dicarboxylic acids. Figure 2 and Table 2 indicate a high incidence of lower molecular weight monocarboxylic acids with carbon atoms numbering 2-13 and a lower but distinct homologous series of dicarboxylic acids with carbon numbers from 8-12. The overwhelming majority of the carboxylic acids in these waters are straight chain mono- and dicarboxylic acids. Since the Occidental waters are sampled from the same retort at different points in the process (Fig. 1), their profiles are nearly identical, with major variations found only in the relative concentrations of fatty acids. In the most concentrated of the Occidental waters, boiler blowdown, the straight chain monocarboxylic acids represent about 78% of the total area of the chromatogram, while the dicarboxylic acids represent about 14% of the area. Only about 8% of the

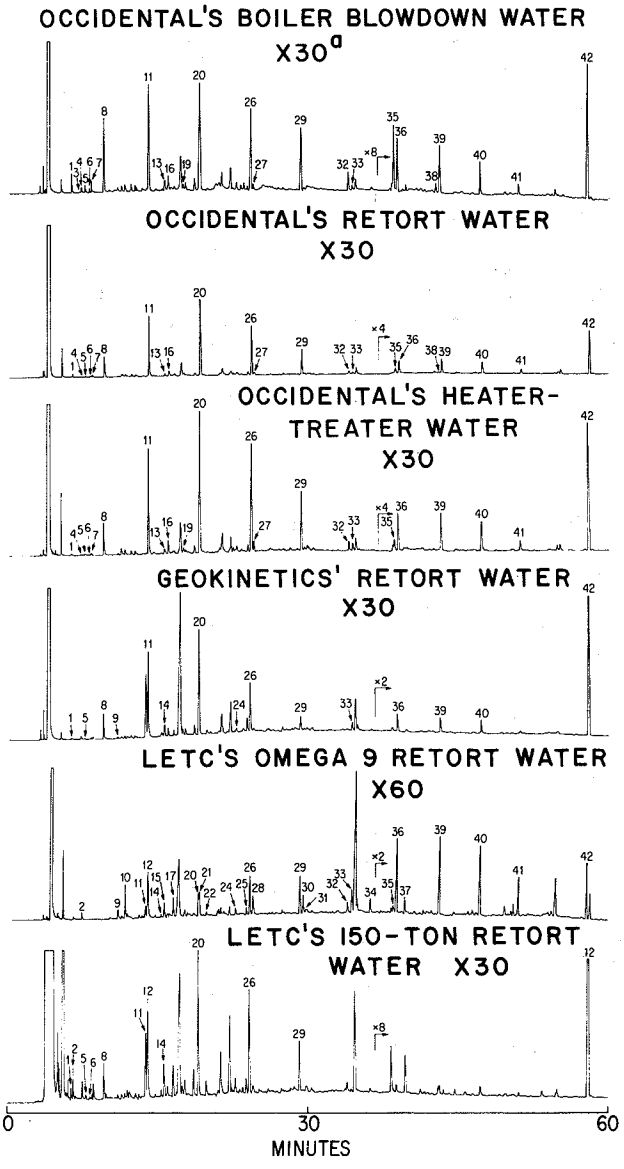

Fig. 2. Carboxylic acid methyl ester profiles of six in-situ oil shale process waters obtained by capillary gas chromatograph (30 m x 0.025 mm SP 2100 column). a = concentration factor; X30 represents concentration from 30 ml benzene extract to 1 ml. (FXBL 807-10684)

Table 2. Identification of carboxylic acids in six in-situ oil shale process waters.

Numbers below refer to Fig. 2*	Chain Length†	Acid Type‡	Carboxylic Acid	Occidental Waters			LETC's	Omega-9	Geokinetics*
				Boiler Blowdown	Heater Treater	Retort (product)	150 ton		
1	C_2	n, mono	ethanoic (acetic)	x	x	x	x	x	x
1	C_3	n, mono	propanoic	x	x	x	x	x	x
1	C_4	n, mono	butanoic	x	x	x	x	x	x
1	C_5	n, mono	pentanoic	x	x	x	x	x	x
2	C_2	n, di	ethanedioic	x	x	x	x	x	x
3	C_6	br, mono	2,3-dimethylbutanoic	o	o	o	x	x	x
4	C_6	br, mono	2-ethylbutanoic	x	o	o	o	o	o
5	C_6	br, mono	2-methylpentanoic	x	o	o	o	o	o
6	C_6	br, mono	3-methylpentanoic	x	o	o	x	o	x
7	C_6	br, mono	unidentified, branched	x	o	o	o	o	o
8	C_6	n, mono	hexanoic	o	o	o	o	o	o
9	C_3	n, di	propanedioic	o	o	o	o	x	x
10	C_5	keto	4-ketopentanoic	o	o	o	o	x	o
11	C_7	n, mono	heptanoic	x	x	x	x	x	x
12	C_4	n, di	butanedioic	o	o	o	x	x	x
13	C_7	cyc, mono	cyclohexanecarboxylic	x	o	o	o	o	o
14	C_5	br, di	methylbutanedioic	o	o	o	x	x	o
15	C_5	br, di	methylbutanedioic (isomer)	o	o	o	x	x	o
16	C_8	br, mono	unidentified, branched	x	x	x	o	o	o
17	C_8	keto subt.	2,3,4-trimethyl cyclopent-2-ene-1-one	o	o	o	o	x	o
19	C_7	ano, mono	benzoic	x	x	x	o	o	x
20	C_8	n, mono	octanoic	x	x	x	x	x	x
21	C_5	n, di	pentanedioic	o	o	o	o	o	o
22			unidentified, di	o	o	o	o	x	o
23									
24	C_8	aro, mono	3-methylbenzoic	o	o	o	o	x	x
25		aro, mono	methyl substituted benzoic	o	x	o	x	x	x
26	C_9	n, mono	nonanoic	x	x	x	x	x	x
28	C_6	n, di	hexanedioic	o	o	o	o	x	o
29	C_{10}	n, di	decanoic	x	x	x	x	x	x
30	C_7	n, di	heptanedioic	o	o	o	o	x	o
31	C_9	aro, mono	3,5-dimethylbenzoic	o	o	o	o	x	o
32	C_{11}	n, mono	undecanoic	x	x	x	o	x	o
33	C_{18}	n, di	octanedioic	x	x	x	o	x	x
34			methyl substituted benzoic	o	x	o	x	x	o
35	C_{12}	n, mono	dodecanoic	x	x	x	o	x	o
36	C_9	n, di	nonanedioic	x	x	x		x	x
37	C_9	aro, di	4-methyl-1,2 benzene dicarboxylic	o	o	o	x	x	o
38	C_{13}	n, mono	tridecanoic	x	x	x	o	x	o
39	C_{10}	n, di	decanedioic	x	x	x	o	x	x
40	C_{11}	n, di	undecanedioic	x	x	x	o	x	x
41	C_{12}		dodecanedioic	x	x	x	o	x	x
42	C_{17}	n, mono	Internal Standard (heptadecanoic)	§	§	§	§	§	§

*Compounds listed in order of their retention times as shown in Fig. 2.

†Number represents the total number of carbon atoms.

‡n = normal (straight chain) acid
br = branched acid
keto = keto acid
cyc = cyclic acid
aro = aromatic acid
mono = monocarboxylic acid
di = dicarboxylic acid

§Indicates no data.

xPositively identified in process water.

oAbsent from process water.

acids in this water are branched, multisubstituted, or aromatic. Similar percentages were obtained for the other Occidental waters.

PLANNED ACTIVITIES FOR FY 1981

This work will be extended to other in-situ process waters and to surface retorting process waters in FY 1981. We will also continue our efforts to quantitate previously separated and identified carboxylic acids.

ACKNOWLEDGEMENT

The authors wish to thank M. J. Kland for her guidance and/or commentary on this work. The described research was initiated by M. J. Kland in 1978 and was subsequently participated in by R. H. Fish during FY 1980.

REFERENCES

1. M. J. Kland, A. S. Newton, and H. L. Eaton, "Trace Contaminants in Oil Shale Retort Water," Energy and Environment Division Annual Report 1979, Lawrence Berkeley Laboratory report LBL-10486, 1980.

2. R. H. Fish, A. S. Newton, L. M. Bowles, and P. C. Babbitt, "Use of Capillary Column Gas Chromatography-Mass Spectroscopy to Identify Organic Ligands of Metals in Oil Shale Process Waters," Energy and Environment Annual Report 1979, Lawrence Berkeley Laboratory report LBL-10486, 1980.

CHARACTERIZATION OF TWO CORES FROM THE NAVAL OIL SHALE RESERVE NUMBER 1*

R. D. Giauque, J. P. Fox, and J. W. Smith†

INTRODUCTION

Interest in mineral and element concentrations in oil shale of the Green River Formation has been augmented recently by geochemical and environmental considerations. Geochemical interest is focused on energy and element balances during retorting and on developing an understanding of the formation of oil shale over geologic time. Environmental interest is directed at mobile elements and minerals having potentially important consequences during and after oil production.

Environmental and geochemical questions continually arise concerning the magnitude and significance of stratigraphic variations. For the geochemist, this stratigraphic distribution provides information on how variable the depositional conditions were and how important this variation was to formation geochemistry. To the environmentalist, this stratigraphic distribution can provide data which can be used to answer questions on the size and significance of the overall consequences of oil shale development and on controls that might be used.

In this program, the stratigraphic distribution of 71 variables has been determined for two cores from the Green River Formation on Colorado's Naval Oil Shale Reserve No. 1, the site of much development testing. Geologic stratigraphy and composited sampling intervals are reported elsewhere.[1] The stratigraphic zones we studied are shown in Figure 1.

ACCOMPLISHMENTS DURING FY 1980

The analysis of mineral phases, elemental concentrations, and of the oil and water content of Fischer Assay products was completed on two cores from Colorado's Naval Reserve No. 1. Table 1 lists the parameters measured and the analytical techniques used. These measurements were carried out at three laboratories: Laramie Energy Technology Center, Lawrence Berkeley Laboratory, and Los Alamos Scientific Laboratory.

We previously reported results for core 25. This year, we completed our analyses of core 15/16. Typical histograms of mineral phases and trace elements for core 15/16 are shown in Figures 2 and 3. The range of results for both cores for 65 of these variables are summarized in Tables 2 and 3. In general, the range of values for each variable is very similar for the two cores. These results generally illustrate the degree of horizontal uniformity across the Green River oil shale deposit. This result is remarkable for a sedimentary deposit where variations of an order of magnitude or more are common.

Individual composited sample results for 48 elements, eight minerals, and oil and water content were entered into a computerized statistical program package. Subsequently, relationships between minerals, elements, oil, and water content were established. Composited samples were treated as individual groups, based on geologic stratigraphic zones in each core.

The principal phases with which the various major, minor, and trace elements are associated are summarized in Table 4. Listed below are specific conclusions established:

- Oil shale from both cores was comprised principally of dolomite, quartz, analcime, calcite, Na-feldspar, K-feldspar, and organic matter. The concentrations of dolomite and quartz were relatively constant. These two minerals typically accounted for an estimated 40% (by weight) of the matrix.

- Over one-half of the elements determined were principally associated with two minerals, Na-feldspar and/or K-feldspar. Most of the elements associated with the feldspars did not vary in concentration by more than a factor of three.

- High Fischer Assay oil yields and elevated Na- and K-feldspar concentrations were concurrent in the oil-rich Mahogany Bed for both cores. This is consistent with other studies.

- The composition of the two cores was very similar for corresponding stratigraphic zones even though core 15/16 and 25 were six miles apart. Thus, these studies agree with previous investigations which revealed that oil shale is remarkably uniform laterally.

- Concentrations of the major organic elements--organic carbon, hydrogen, and nitrogen--varied by an order of magnitude. Similar concentration variations were observed for As, Cd, Hg, Mo, Se, B, and F, all of which are trace elements of potential environmental significance. The first five

* This work was supported by the U.S. Environmental Protection Agency and by the Assistant Secretary for Environment, Office of Environmental Compliance and Overview, Environmental Control Technology Division and by the Assistant Secretary for Fossil Energy, Deputy Assistant Secretary for Oil, Gas, and Shale Technology, Office of Oil Shale of the U.S. Department of Energy under Contract No. W-7405-ENG-48.

† Laramie Energy Technology Center, Laramie, Wyoming.

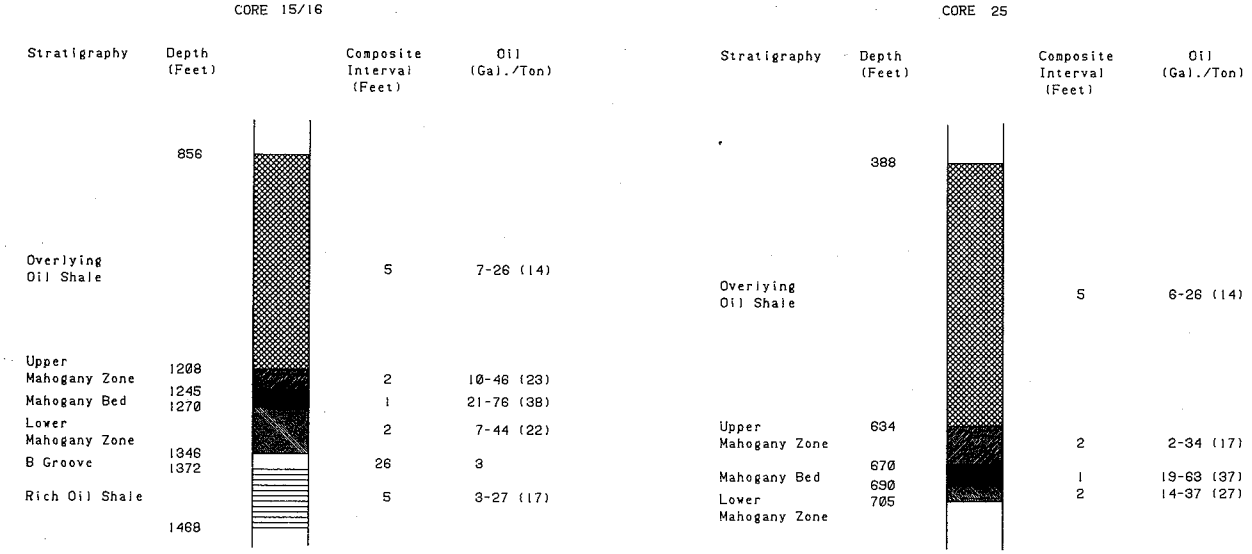

Fig. 1. Stratigraphic zones, depth of zones, and composite sampling intervals for cores 25 and 15/16. (XBL 8012-13548B)

Table 1. List of variables and analytical techniques used to characterize cores 15/6 and 25.

Variable Determined	Analytical Techniques
Dolomite, calcite, aragonite, Mg-siderite, dawsonite, K-feldspar, Na-feldspar, analcime, illite, quartz, pyrite, fluorite	X-ray diffraction
Oil, water	Modified Fischer Assay
Ag, Al, As, Au, Ba, Ca, Ce, Cl, Co, Cr, Cs, Dy, Eu, Fe, Hf, In, Ir, K, La, Lu, Mg, Mn, Mo, Na, Nd, Sb, Sc, Sm, Sn, Ta, Tb, Th, Ti, U, V, W, Yb	Instrumental neutron activation
Br, Cu, Ga, Ge, Ni, Pb, Rb, Se, Sr, Y, Zn, Zr	X-ray fluorescence
Cd, Hg	Zeeman atomic absorption
C_{org}, H, N	Combustion
C_{min}	Gravimetric
B	Optical emission
F	Spectrophotometric

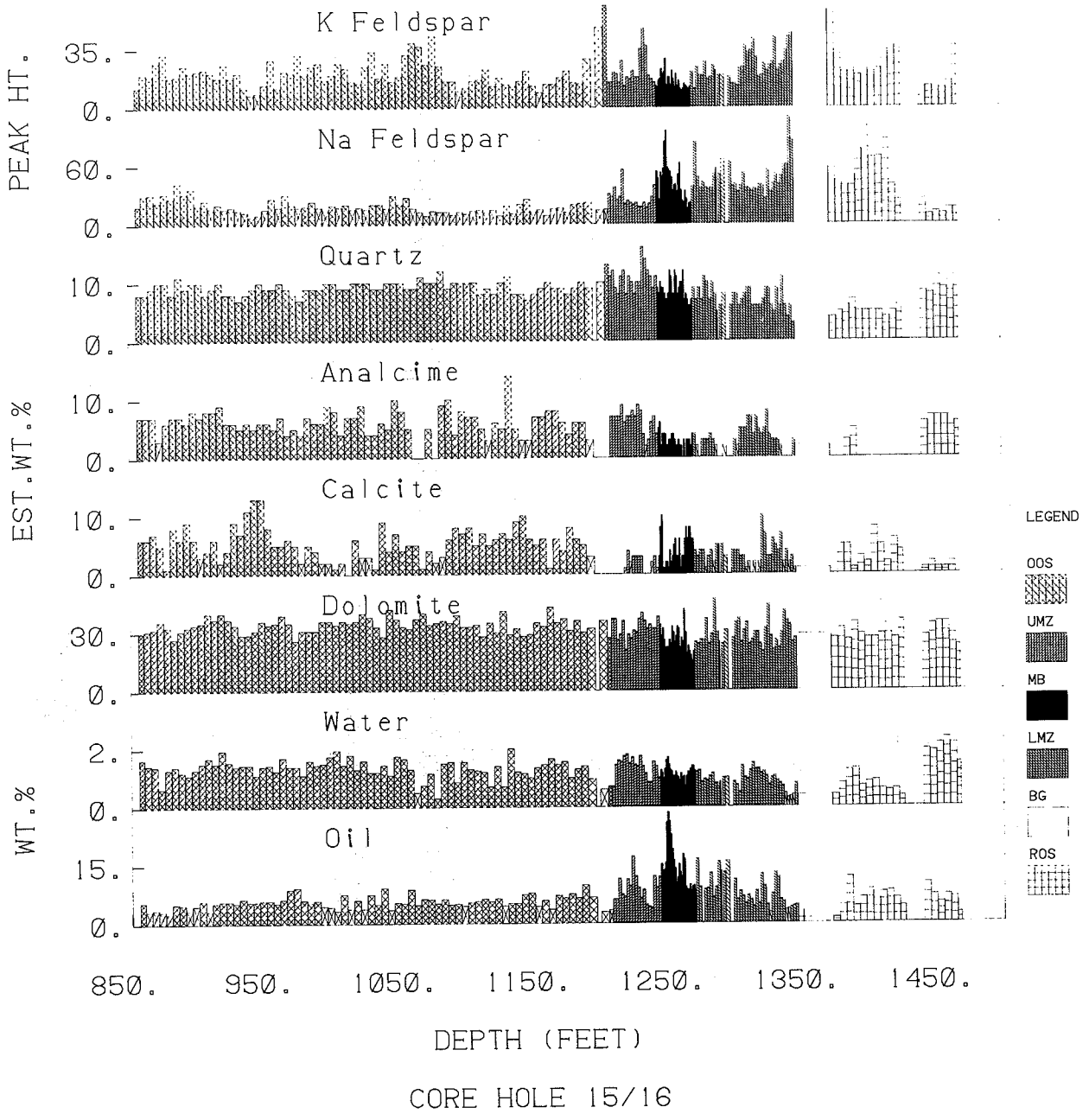

Fig. 2. Vertical variation of mineral phases and Fischer Assay products in core 15/16. (XBL 8010-7313)

of these elements are thought to be associated with the organic fraction of the oil shale matrix.

- Trace elements Co, Cu, Ni, Pb, Sb, and Zn showed consistent association. These elements are probably present in the oil shale principally as sulfides.

- Variation in the assay water yield was strongly associated with variation in analcime content in both cores. This parallels observations reported elsewhere. However, the water in analcime typically accounted for only about one-third of the water content determined by Fischer Assay.

PLANNED ACTIVITIES FOR FY 1981

A program is being initiated to investigate the vertical variability of elements and mineral phases in raw and spent shale cores from a field in-situ retort, Geokinetics Retort No. 16. This field experiment was conducted in the vicinity of Book Cliff, Utah. Four spent shale cores are being composited at approximately one-foot

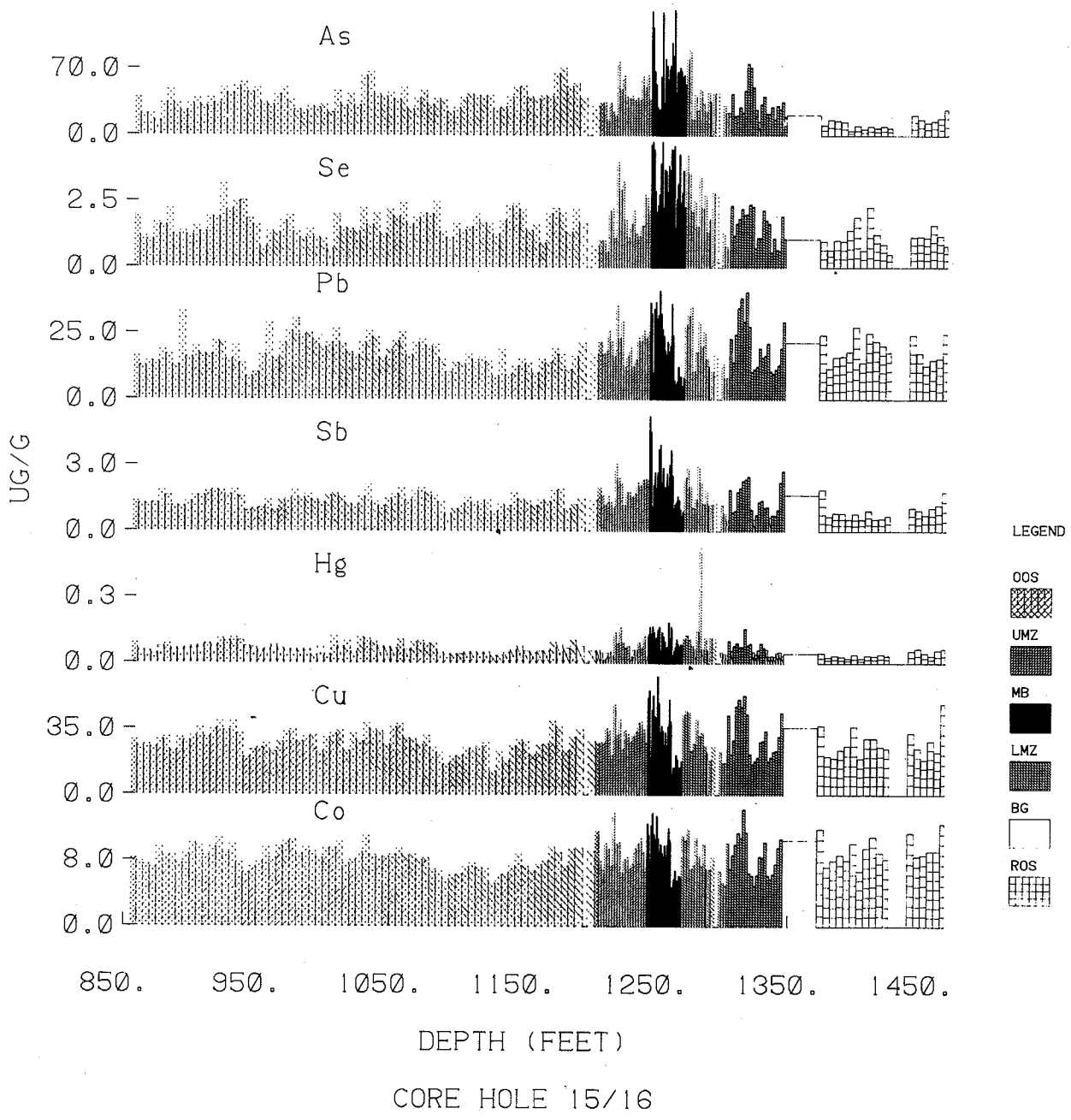

Fig. 3. Vertical variation of As, Se, Pb, Sb, Hg, Cu, and Co in core 15/16. (XBL 8010-7312)

Table 2. Range of Fischer Assay and mineral results for two cores.

	Core 15/16 Concentration Range (%)	Core 25 Concentration Range (%)
Oil	1-29	1-24
Water	0.3-2.4	0.8-3.0
Analcime	0-14	0-14
Quartz	3-16	7-15
Calcite	0-13	0-18
Dolomite	15-47	21-47
	XRD Peak Height*	XRD Peak Height*
Na-feldspar	8-110	8-106
K-feldspar	8-62	9-59

*XRD = x-ray diffraction

Table 3. Elemental concentration ranges for the two cores.*

	Core 15/16	Core 25		Core 15/16	Core 25
Ag	<0.7-1.7	<1.0-1.4	La	10-34	12-32
Al (%)	1.8-6.9	2.0-6.5	Lu	0.08-0.34	0.11-0.36
As	5-134	8-98	Mg (%)	1.8-5.8	1.9-5.9
Au	<0.02-0.4	<0.03-0.14	Mn	190-460	201-440
B	25-250	40-200	Mo	4-54	7-48
Ba	240-1230	270-800	N (%)	0.2-1.2	0.2-1.1
Br	<0.6-1.4	<0.6-0.8	Na (%)	0.4-3.1	0.4-3.1
C_{min} (%)	1.9-7.2	2.1-7.2	Nd	8-30	9-25
C_{org} (%)	3-35	2-29	Ni	11-32	11-30
Ca (%)	5-21	5-19	Pb	8-41	9-39
Cd	†	0.2-1.4	Rb	32-124	47-139
Ce	21-69	25-63	Sb	0.5-5.2	0.8-3.9
Cl (%)	0.05-0.12	0.05-0.09	Sc	3-12	4-10
Co	5-14	4-13	Se	0.5-12.3	0.5-3.7
Cr	18-60	17-54	Sm	1.5-5.0	1.7-5.3
Cs	0.7-14.0	2.0-5.9	Sn	<80-130	<80-130
Cu	11-63	14-58	Sr	260-1440	300-1120
Dy	1.1-3.9	1.3-4.9	Ta	0.24-0.74	0.27-0.77
Eu	0.3-1.1	0.4-1.0	Tb	0.15-0.58	0.20-0.73
F	200-3200	100-2500	Th	3.1-10.6	3.8-9.2
Fe (%)	1.0-3.5	1.1-3.2	Ti (%)	0.03-0.28	0.06-0.27
Ga	3-17	5-16	U	1.8-8.2	2.0-6.1
Ge	<1.1-2.3	<1.1-2.0	V	29-203	45-185
H (%)	0.3-4.5	0.4-3.8	W	<0.8-11.0	<0.9-3.0
Hg	0.01-0.50	0.03-0.21	Y	2-23	4-28
Hf	0.8-2.7	1.1-3.5	Yb	0.6-2.5	0.8-2.6
In	<0.1-0.6	<0.1-0.3	Zn	38-153	41-111
Ir	<0.004-0.008	<0.005-0.009	Zr	13-73	18-219
K (%)	0.6-5.6	0.8-5.7			

*All concentration ranges are in µg/g unless otherwise indicated.

†Concentration range not determined.

Table 4. Principal phases with which the major, minor, and trace elements are associated.

Principal Phases	Trace Elements
K-feldspar, Mg-siderite, Na-feldspar	Al, B, Ce, Co, Cr, Cu, Dy, Eu, Fe, Ga, Hf, La, Mn, Nd, Ni, Pb, Sb, Sc, Sm, Ta, Tb, Th, Ti, V, Y, Yb, Zn, Zr
K-feldspar, Mg-siderite	K, Rb
Na-feldspar, analcime, water	Na
Analcime, water	Cs
Calcite	Ba, C_{min}, Ca, Sr
Dolomite	Mg
C_{org}, oil	As, H, Hg, Mo, N, Se, U
Unknown	Cd, F

sampling intervals. Mineralogical reactions that occur during retorting will be studied, and the environmental importance of trace element distribution in the Geokinetics retort will be assessed.

REFERENCE

1. R. D. Giauque, J. P. Fox, and J. W. Smith, Characterization of Two Core Holes from the Naval Oil Shale Reserve Number 1, Lawrence Berkeley Laboratory report LBL-11450, 1979.

A PARTITIONING MODE FOR Hg IN SIMULATED IN-SITU OIL SHALE RETORTS*

J. P. Fox

INTRODUCTION

Hg is one of the most volatile and toxic elements in an oil shale retorting system.[1,2] Only H and organic C, major constituents of the organic phase of oil shale, are more volatile. About 70% of the Hg originally present in oil shale is partitioned to the offgases and lesser amounts to the oil and water. This Hg may reach the environment by atmospheric or aqueous discharges of retorting byproducts.

Previous work indicated that the amount of Hg volatilized is a function of maximum retorting temperature and that volatilized Hg may adsorb or condense on the cool shale ahead of the reaction zone and be released from the retort as a pulse toward the end of the run. These observations were explored this year from a theoretical standpoint by hypothesizing chemical reactions that take place during retorting and by computing partial pressures of Hg and gaseous species distribution in the four zones of an in-situ oil shale retorting system.

ACCOMPLISHMENTS DURING FY 1980

This year, a theoretical framework for interpreting the partitioning data presented in last year's report[1] was developed. The qualitative model interprets the partitioning of Hg in terms of mineral decomposition, reduction, oxidation, shale-product interactions, and kerogen conversion. Thermochemical calculation procedures were developed within this framework and used to investigate the volatility and stable gas-phase species of Hg. This work is summarized here.

Partitioning Mechanisms

The specific mechanisms that determine the partitioning of a given element are not fully understood and can only be inferred from available data.[2] The types of reactions thought to occur during in-situ retorting are summarized in Figure 1. In general, it is proposed that elements may be volatilized from the shale as a consequence of mineral decomposition (Eqs. 1-4), kerogen conversion (Eq. 5), or reduction by C, CO, and other species (Eqs. 6 and 7). These volatile species may be removed from the gas stream as metal oxides (Eqs. 8 and 9), condensed on the cool shale ahead of the reaction front (Eq. 10), entrapped in the oil-water emulsion (Eqs. 11 and 12), or swept out of the retort in the gas stream as gaseous or condensed species. The water that condenses out of the gas stream in the cool regions ahead of the reaction zone may leach some constituents from the unreacted shale (Eqs. 14 and 15). Interactions may occur between the oil and water, which are in intimate contact as an emulsion (Eq. 13). Finally, raw and spent shale fines may be entrained in the gas stream in the reaction zone or may be picked up as the oil-water emulsion passes over the cool shale and incorporated in the oil and water (Eq. 16).

Partitioning Model

Hg may be partitioned from the raw oil shale to the products--shale oil, retort water, or offgas--because its compounds are volatile under retorting conditions and because its compounds are soluble in, or entrained in, these products. Solubility is determined by the interaction of gas with water and oil (Eqs. 11 and 12) and the interaction of water with oil and shale (Eqs. 13-15). The amount of an element that is partitioned due to volatility can be calculated from standard thermodynamic data, while the amount resulting from dissolution and entrainment can only be roughly estimated. Only the former is considered here.

The volatilization of elements from the mineral matrix and the stable gas-phase species may be estimated using thermodynamic procedures. Equilibrium constants may be computed from free energy of formation values, ΔG_T, for the reactions and conditions of interest. The equilibrium constant, K_p, is calculated from the relationship

$$\ln K = -\frac{\Delta G_T}{RT} \qquad (1)$$

$$R = 1.987 \text{ cal/K·mole}$$

and used to predict relative volatility and stability of various gas-phase chemical species. Free energies of formation are obtained from available tabulations of thermochemical data or are estimated from the expression:

$$\Delta G_T = \Delta H_{298} - TS_{298} \qquad (2)$$

where

* This work was supported by the Assistant Secretary for Fossil Energy, Deputy Assistant Secretary for Oil, Gas, and Shale Technology, Office of Oil Shale of the U.S. Department of Energy under Contract No. W-7405-ENG-48.

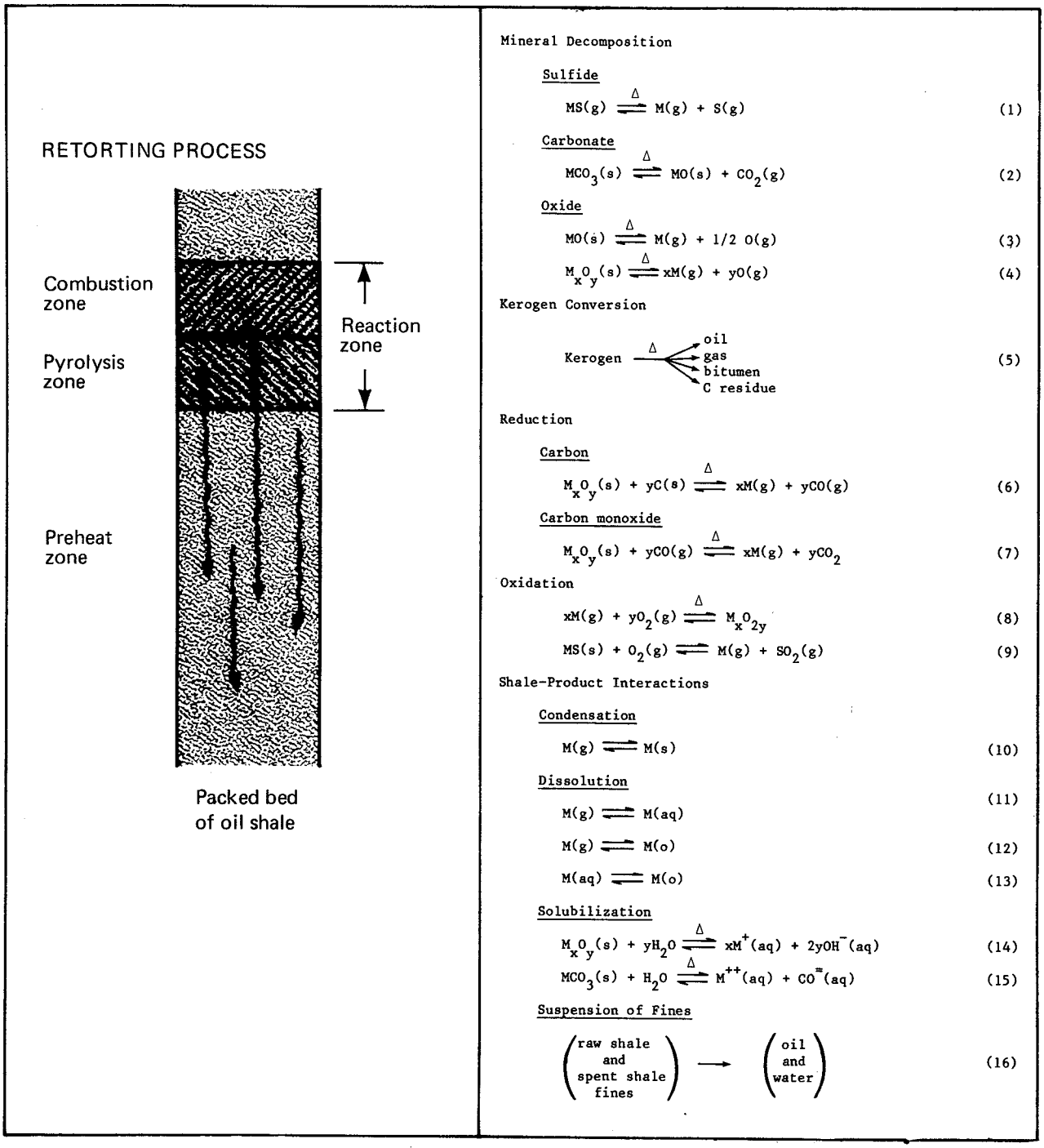

(s) = solid; (g) = gas; (aq) = aqueous; (o) = oil

Fig. 1. Some proposed mechanisms that may lead to the observed elemental partitioning in simulated in-situ retorts. (XBL 791-239)

ΔH_{298} = standard enthalpy in kcal/mole K at 298K,

S_{298} = standard entropy in kcal/mole K at 298K,

T = temperature in K,

using tabulated values of standard enthalpy and entropy.

The retorting system is divided into four zones: combustion, pyrolysis, preheat, and discharge, and Eq. 1 and the Law of Chemical Equilibrium are used to predict volatility and gas-phase species in each zone. The zones are shown schematically on Figure 1. Idealized temperature and gas compositions assumed to exist in each are summarized in Table 1.

Table 1. Estimated gas composition and temperature in combustion, pyrolysis, preheat, and discharge zones (vol %).

	Combustion Zone	Pyrolysis Zone	Preheat Zone	Discharge
Temperature	1300K	800K	400K	298K
Cl	0.1-0.0001[a]	0.1-0.0001[a]	0.1-0.0001[a]	0.1-0.0001[a]
CO	0.001	1.7	1.7	0.9
COS	0.1-0.0001[a]	0.1-0.0001[a]	0.1-0.0001[a]	0.1-0.0001[a]
CO_2	0.04	11.5-34.1	11.5-34.1	5.8-17.1
CS	0.1-0.0001[a]	0.1-0.0001[a]	0.1-0.0001[a]	0.1-0.0001[a]
F	0.1-0.0001[a]	0.1-0.0001[a]	0.1-0.0001[a]	0.1-0.0001[a]
H_2	0.001	5.1	5.1	2.6
H_2O	46.6	0.6	0.6	3.1
H_2S	0.000001	0.003-1.1	0.003-1.1	0.002-0.6
O_2	11.2	0.0	0.0-1.0	11.0
S	0.1-0.0001[a]	0.1-0.0001[a]	0.1-0.0001[a]	0.1-0.0001[a]

[a]Inadequate or no data. Range selected to bracket probable concentration.

Some chemical reactions and corresponding equilibrium constants hypothesized to control the distribution of Hg during oil shale retorting are summarized in Table 2. Other reactions may also occur, particularly with organic radicals, but these are not included due to lack of thermochemical and other experimental data. These equilibrium constants, computed using Equation 1, were used to estimate Hg partial pressures and species distribution in the combustion, pyrolysis, preheat, and discharge zones of a simulated in-situ retort.

Hg may be volatilized by mineral decomposition, by direct vaporization, by reduction of its compounds, or by reaction of its compounds with halides (HgCl) and organic radicals ($HgCH_3$) to form volatile species. The Hg partial pressure in equilibrium with the phases--HgO, HgS, $HgCl_2$, HgF_2--are summarized in Table 3. This table shows that the formation of elemental Hg from mineral decomposition and reduction is thermodynamically favored for most of the conditions considered.

The mercury partial pressures in Table 3 suggest that the thermodynamically most favored volatilization pathways for Hg in the reaction zone are:

Pyrolysis Zone

$$HgS + H_2 \rightleftharpoons Hg(g) + H_2S(g) \quad (3)$$

$$HgS + CO \rightleftharpoons Hg(g) + COS(g) \quad (4)$$

Combustion Zone

$$HgS + O_2 \rightleftharpoons Hg(g) + SO_2 \quad (5)$$

$$HgS + H_2(g) \rightleftharpoons Hg(g) + H_2S(g) \quad (6)$$

$$HgS + C \rightleftharpoons Hg(g) + CS(g) \quad (7)$$

These equations suggest that elemental Hg is formed in the pyrolysis zone by the reduction of HgS by H_2 and CO in the pyrolysis gas. Any Hg not volatilized by reduction in this zone would be released in the combustion zone, which trails the pyrolysis zone, by the formation of HgO and its subsequent decomposition at temperatures greater than 500°C or by reduction of HgS and HgO by char and H_2. The pyrolysis mechanism would occur in the pyrolysis zone of a combustion retort or throughout the reaction zone or an inert gas run, while the combustion mechanism would occur only in the combustion zone.

Note that Equations 3-7 assume that Hg occurs as HgS in oil shale. This is assumed because HgS is the stable form of Hg for the conditions hypothesized to exist during the genesis of oil shale and due to volatility considerations. If Hg existed as HgO or as an organomercury compound, it would

Table 2. Equilibrium constants (log Kp) of selected reactions involving Hg which are hypothesized to participate in Hg partitioning in simulated in-situ retorts.

Reaction	Equilibrium Constant, log Kp			
	Discharge Zone 298K	Preheat Zone 400K	Pyrolysis Zone 800K	Combustion Zone 1300K
Volatilization				
Mineral Decomposition				
$HgO \rightleftharpoons Hg(g) + 1/2\ O_2(g)$	-10.250	-6.206	0.641	4.092[g]
$HgO \rightleftharpoons HgO(g)$	-14.452	-8.560	-0.142	2.780[g]
$HgS \rightleftharpoons Hg(g) + S(g)$	-50.674	-35.601	-12.563	-3.526[g]
Reduction/Oxidation				
$HgO + CO(g) \rightleftharpoons Hg(g) + CO_2(g)$	34.811	26.221	14.561	10.886
$HgO + H_2(g) \rightleftharpoons Hg(g) + H_2O(g)$	29.910	23.117	13.980	11.166
$HgO + C \rightleftharpoons Hg(g) + CO(g)$	13.779	12.902	12.562	13.174
$HgS + CO(g) \rightleftharpoons Hg(g) + COS(g)$	-3.230	-2.043	0.617	1.811
$HgS + H_2(g) \rightleftharpoons Hg(g) + H_2S(g)$	-2.965	-1.313	1.887	3.174
$HgS + C \rightleftharpoons Hg(g) + CS(g)$	-40.106	-27.242	-7.487	0.208
$HgS + O_2(g) \rightleftharpoons Hg(g) + SO_2(g)$	44.774	33.111	18.380	12.841
Gas-Phase Composition				
$Hg(g) \rightleftharpoons 1/2\ Hg_2(g)$	-0.800	-1.426	-2.398	-2.829
$1/2\ Hg_2(g) \rightleftharpoons Hg(\ell)$	11.965	7.144	2.402	2.828
$Hg(g) \rightleftharpoons Hg(\ell)$	0.000	0.000	-1.035	-2.453
$1/2\ H_2(g) + Hg(g) \rightleftharpoons HgH(g)$	-37.696	-27.080	-12.704	-8.276
$H_2(g) + Hg_2(g) \rightleftharpoons 2HgH(g)$	-63.431	-47.016	-23.005	-13.723
$Hg(g) + 1/2\ O_2(g) \rightleftharpoons HgO$	10.250	6.206	-0.641	-4.092
$Hg(g) + 1/2\ O_2(g) \rightleftharpoons HgO(g)$	-4.170	-2.322	-0.758	-1.266
$Hg(g) + CH_3(g) \rightleftharpoons HgCH_3(g)$	--	--	--	--
$Hg(g) + 2CH_3(g) \rightleftharpoons Hg(CH_3)_2(g)$	27.69	17.24	1.95	-3.93
$H_2S(g) + Hg(g) \rightleftharpoons HgS + H_2(g)$	2.967	1.313	-1.887	-3.174
$Hg(g) + Cl(g) \rightleftharpoons HgCl(g)$	8.485	6.547	2.505	-0.209
$Hg(g) + Cl_2(g) \rightleftharpoons HgCl_2$	32.247	22.007	8.226	3.086
$Hg_2(g) + Cl_2(g) \rightleftharpoons Hg_2Cl_2$	48.827	32.222	--	--
$HgCl(g) + S(g) \rightleftharpoons HgS(g) + Cl(g)$	42.188	29.058	10.059	3.735
$HgCl_2 + H_2S(g) \rightleftharpoons HgS + 2HCl(g)$	4.110	4.451	2.876	1.988
$Hg(g) + F(g) \rightleftharpoons HgF(g)$	14.024	10.602	4.381	0.833
$Hg(g) + F_2(g) \rightleftharpoons HgF_2$	65.546	46.724	18.382	8.543
$Hg_2(g) + F_2(g) \rightleftharpoons Hg_2F_2$	86.848	60.408	22.210	--
$HgF(g) + S(g) \rightleftharpoons HgS + F(g)$	36.650	25.003	8.182	2.693
$HgF_2 + H_2S(g) \rightleftharpoons HgS + 2HF(g)$	33.145	26.118	15.778	10.615

probably be 100% volatilized during oil shale retorting. Since experimental data indicate that volatilization is not 100% complete and, in fact, that only about 70% of the Hg is volatilized, it is concluded that Hg may exist in a less volatile form than the oxide or an organic form in oil shale. (Alternatively, Hg may occur in two or more forms, one of which may be volatile at retorting temperatures and the other may not be. Other work reported elsewhere in this annual report[3] suggests that some Hg may be associated with the organic phase of oil shale.)

Once the Hg is volatilized, it may undergo a large number of chemical reactions in all four zones which will alter its gas-phase form or result in its removal from the gas phase by condensation or the formation of less volatile species. Some possibilities are summarized in Table 3 under the heading "gas-phase composition." Additional reactions are possible but there are inadequate data to assess them quantitatively; some of these reactions will be discussed qualitatively below.

The volatilized Hg, which is predominantly elemental Hg, may react with O_2, H_2S, organic radicals, or the halogens F_2 and Cl_2 (both F and Cl exist at about 0.1% in oil shales and are suspected to be volatilized because they occur at high levels in retort waters and oils; Br and I, on the

Table 3. Estimated partial pressure of Hg(g) in shale gas in the combustion, pyrolysis, preheat, and discharge zones of a simulated in-situ retort (in atm.).

REACTION	Combustion Zone 1300 K	Pyrolysis Zone 800 K	Preheat Zone 400 K	Discharge Zone 298 K
Volatilization				
Mineral Decomposition				
$HgO \rightleftharpoons Hg(g) + 1/2\ O_2(g)$	$10^{4.6}$	(b)	$10^{-5.2}$-(b)	$10^{-9.8}$
$HgO \rightleftharpoons HgO(g)$	$10^{2.8}$	$10^{-0.1}$	$10^{-8.6}$	$10^{-14.4}$
$HgS \rightleftharpoons Hg(g) + S(g)$	$10^{-0.5}$-$10^{2.5}$	$10^{-9.6}$-$10^{-6.6}$	$10^{-32.6}$-$10^{-29.6}$	$10^{-47.7}$-$10^{-44.7}$
Reduction/Oxidation				
$HgO + CO(g) \rightleftharpoons Hg(g) + CO_2(g)$	$10^{9.2}$	$10^{13.3}$-$10^{13.7}$	$10^{24.9}$-$10^{25.4}$	$10^{33.5}$-$10^{34.0}$
$HgO + H_2(g) \rightleftharpoons Hg(g) + H_2O(g)$	$10^{-3.6}$	$10^{14.9}$	$10^{24.1}$	$10^{29.8}$
$HgO + C \rightleftharpoons Hg(g) + CO(g)$	$10^{18.2}$	$10^{14.3}$	(a)	(a)
$HgS + CO(g) \rightleftharpoons Hg(g) + COS(g)$	$10^{-0.2}$-$10^{2.8}$	$10^{1.8}$-$10^{4.8}$	$10^{-0.8}$-$10^{2.2}$	$10^{-2.3}$-$10^{0.7}$
$HgS + H_2(g) \rightleftharpoons Hg(g) + H_2S(g)$	$10^{6.2}$	$10^{2.6}$-$10^{5.1}$	$10^{-0.6}$-$10^{1.9}$	$10^{-2.3}$-$10^{0.2}$
$HgS + C \rightleftharpoons Hg(g) + CS(g)$	$10^{4.2}$-$10^{6.2}$	$10^{-4.1}$-$10^{-1.5}$	(a)	(a)
$HgS + O_2(g) \rightleftharpoons Hg(g) + SO_2(g)$	$10^{14.9}$-$10^{17.9}$	(b)	$10^{34.1}$-(b)	$10^{45.8}$-$10^{48.8}$
Gas-Phase Composition				
$2Hg(g) + 1/2\ O_2(g) = Hg_2O$	$10^{3.4}$	(b)	$10^{-2.2}$-(b)	$10^{-4.5}$
$H_2S(g) + Hg(g) \rightleftharpoons HgS + H_2(g)$	$10^{6.2}$	$10^{2.6}$-$10^{5.1}$	$10^{-0.6}$-$10^{1.9}$	$10^{0.2}$-$10^{5.2}$
$Hg(g) + Cl_2(g) \rightleftharpoons HgCl_2$	$10^{-0.1}$-$10^{2.9}$	$10^{-5.2}$-$10^{-2.2}$	$10^{-19.0}$-$10^{-16.0}$	$10^{-29.2}$-$10^{-26.2}$
$Hg(g) + F_2(g) \rightleftharpoons HgF_2$	$10^{-5.5}$-$10^{-2.5}$	$10^{-15.4}$-$10^{-12.4}$	$10^{-43.7}$-$10^{-40.7}$	$10^{-62.6}$-$10^{-59.5}$
$Hg(g) \rightleftharpoons Hg(\ell)$	$10^{-2.4}$	$10^{-1.0}$	10^{0}	10^{0}

[a]There is no char (C) in the preheat and discharge zones. Therefore, this reaction will not proceed.

[b]Oxygen partial pressure is zero.

other hand, occur at 1 to 10 ppm in oil shales and, thus, are not significant for gas-phase calculations). The partial pressures of Hg in Table 3 suggest that elemental Hg may be removed from the gas stream by reacting with H_2S and O_2 to form HgS and HgO, respectively. The oxide HgO is known to form rapidly at temperatures of 300 to 350°C and much more slowly at lower temperatures. Thus, HgO and/or HgS may form in the preheat zone by the following reactions:

$$Hg(g) + 1/2\ O_2 \rightleftharpoons HgO \qquad (8)$$

$$Hg(g) + HgS \rightleftharpoons HgS + H_2(g) \qquad (9)$$

This is in agreement with experimental results.[2]

The stable gas-phase species of Hg were estimated (Table 4) by computing partial pressures or ratios of partial pressure for Hg species from the equilibrium data in Table 2 and gas-phase composition in Table 1. These calculations indicate that the principal gaseous species, in order of magnitude from the largest to the smallest, are: Hg(g), HgO(g), $Hg(CH_3)_2$, and $Hg_2(g)$. (No thermodynamic data are available for $Hg(CH_3)$). Elemental Hg, Hg(g), is the stable and predominant species in all four zones. These results suggest that dimethyl (and probably methyl) Hg may form in the preheat and discharge zones but that they are thermodynamically unstable in the combustion and pyrolysis zones. Hg transport as a volatile halide, HgF or HgCl, is not thermodynamically favored in any of the four zones. The mercuric and mercurous halides react with S to form HgS (see Table 2). These predictions are consistent with experimental measurements.[2]

Table 4. Estimated composition of oil shale gases in the combustion, pyrolysis, preheat, and discharge zones of a simulated in-situ retort. Values in table are partial pressures (in atm.) or ratios of partial pressures.

Gaseous Specie	Combustion Zone 1300K	Pyrolysis Zone 800K	Preheat Zone 400K	Discharge Zone 299K
$Hg/(Hg_2(g))^{1/2}$	$10^{2.8}$	$10^{2.4}$	$10^{1.4}$	$10^{0.8}$
Hg/HgH	$10^{10.8}$	$10^{13.4}$	$10^{27.7}$	$10^{38.5}$
$Hg/HgCH_3$	b	b	b	b
$Hg/Hg(CH_3)_2$	$10^{15.9} - 10^{9.9}$	$10^{10.0} - 10^{4.1}$	$10^{-5.2} - 10^{-11.2}$	$10^{-15.7} - 10^{-21.7}$
Hg/HgO(g)	$10^{1.7}$	a	$10^{3.3}$ - (a)	$10^{4.6}$
HgCl	$10^{-6.7} - 10^{-0.7}$	$10^{-13.1} - 10^{-7.1}$	$10^{-32.1} - 10^{-26.1}$	$10^{-45.2} - 10^{-39.2}$
HgF	$10^{-5.7} - 10^{0.3}$	$10^{-11.2} - 10^{-5.2}$	$10^{-28.0} - 10^{-22.0}$	$10^{-39.7} - 10^{-33.7}$

[a] Oxygen partial pressure is zero.

[b] No data available.

PLANNED ACTIVITIES FOR FY 1981

This work will be extended and verified using experimental data from the LBL oil shale retort.

REFERENCES

1. J. P. Fox, "Mass Balance and Partitioning Studies of Simulated In-situ Retorts," Energy and Environment Division Annual Report 1979, Lawrence Berkeley Laboratory report LBL-10486, 1980.

2. J. P. Fox, "The Partitioning of Major, Minor, and Trace Elements during Simulated In-situ Oil Shale Retorting," Ph.D. dissertation, Department of Engineering, University of California, Berkeley; Lawrence Berkeley Laboratory report LBL-9062, 1980.

3. R. D. Giauque, J. P. Fox, and J. W. Smith, "Characterization of Two Cores from the Naval Oil Shale Reserve Number 1," Energy and Environment Division Annual Report FY 1980, Lawrence Berkeley Laboratory report LBL-11990, 1981.

PARTITIONING OF As, Cd, Hg, Pb, Sb, AND Se DURING SIMULATED IN-SITU OIL SHALE RETORTING*

D. C. Girvin, A. T. Hodgson, G. J. Harris-Winston, and M. J. Pollard

INTRODUCTION

Oil shales from the Green River Formation in Colorado and Utah contain significant quantities of potentially mobile, toxic trace elements such as As, Cd, Hg, Pb, Sb, and Se. These elements could be released to the environment as the result of commercial exploitation of the oil shale resource through disposal of liquid and gaseous by-products, through leaching of solid wastes, and through refining and use of the oil. Concern about toxic trace element mobilization and their potential public health and environmental consequences has led to several recent investigations of elemental distributions in oil shales from the Green River Formation.[1-4] These studies have revealed that As, Mo, Sb, Se, and Zn, which are conventionally sulfide-forming elements, are significantly enriched in the shales while most other elements are no more abundant in the shales than in the earth's crust.[3] Although Cd and Hg, with typical concentrations of 0.1 ppm, are not significantly enriched in oil shales, they are included among the potentially mobile elements because of their high volatilities. No reliable information currently exists for Pb.

Retorting of oil shale results in the production of shale oil, retort offgases, an aqueous

* This work was supported by the U.S. Environmental Protection Agency and by the Assistant Secretary for Fossil Energy, Deputy Assistant Secretary for Oil, Gas, and Shale Technology, Office of Oil Shale of the U.S. Department of Energy under Contract No. W-7405-ENG-48.

effluent known as retort water, and a solid which is referred to as spent shale. The elements initially present in the oil shale are distributed, or partitioned, to these products during the retorting process in a manner which depends on the mineralogy of the oil shale and on the retort operating conditions. The limited information available on trace elemental partitioning during oil shale retorting is summarized in Figure 1. The percentage of each element in the offgas was estimated by measuring the mass of the element in the raw shale and in the spent shale, shale oil, and retort water. The difference between the raw shale and the products is assigned to the offgas stream plus loss.[3] These indirect "mass balance" measurements suggest that significant fractions of the Hg and Cd enter the offgas stream. Although the percentages of As and Se entering the offgas are low, the relatively high concentrations of these elements in the raw shale mean that large quantities of As and Se may enter the offgas and be released to the atmosphere. Based on these estimates, the magnitude of total atmospheric emissions of trace elements could be on the order of tens to hundreds of kilograms per day for a 100,000 barrel per day commercial in-situ oil shale facility.

An accurate appraisal of the extent to which atmospheric emissions of As, Cd, Hg, and Se may constitute a problem depends on reliable, direct measurements of these elements in the offgas stream over the entire time span of the retorting process. The only offgas measurements meeting these criteria have been for Hg and are summarized in Table 1. Direct offgas measurements were made during Laramie Energy Technology Center's (LETC) simulated in-situ retort run, CS-69, by LBL scientists using Zeeman atomic absorption spectroscopy (ZAA). The results showed that more than two-thirds of the Hg originally present entered the offgas.[3,5] This is in substantial agreement with indirect estimates of Hg partitioning into the offgas. Mercury measurements in the other product streams accounted for the remainder of the Hg originally present; thus there was no Hg imbalance.

Direct ZAA measurements of Hg in the offgas produced from the LBL simulated in-situ retort showed a lower fraction of the Hg entering the offgas. However, a significant imbalance was observed and must be resolved before conclusions can be drawn. Discrete, direct measurements of Hg in the Paraho surface retort offgas by a gold-amalgamation

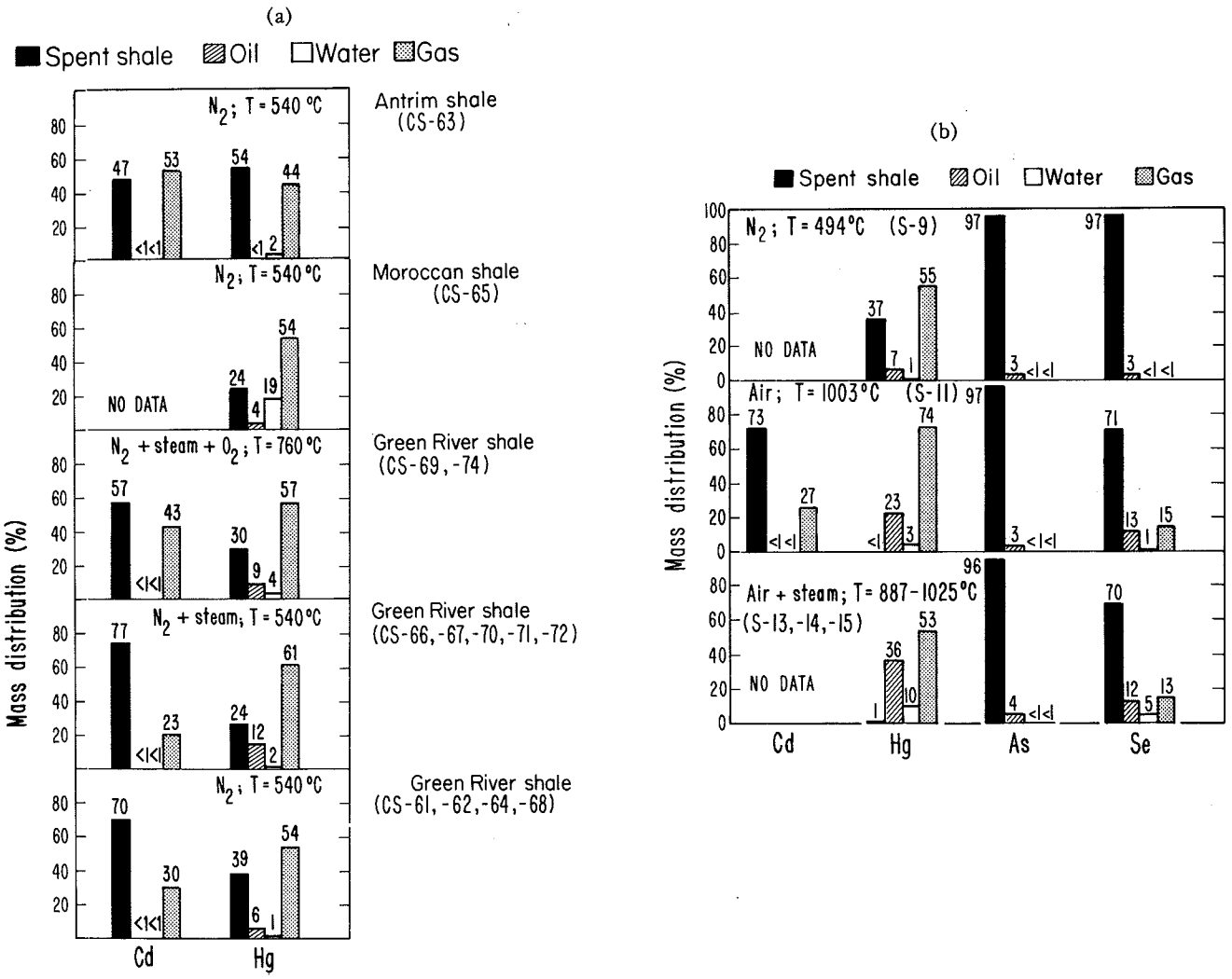

Fig. 1. Summary of available data on the partitioning of As, Se, Cd, and Hg during simulated in-situ oil shale retorting.[3] Figure 1a shows Laramie Energy Technology Center 20-kg controlled-state retort. Figure 1b shows Lawrence Livermore National Laboratory 125-kg simulated in-situ retort.

Table 1. Mercury mass balances obtained by direct measurements of Hg in offgas.

Retort	Percent Distribution				
	Spent shale	Shale oil	Retort water	Offgas	Imbalance
LETC (CS-69)*	13	9	2	76	0
LBL-02,-03,-04	<3	10	1	38	-48
Paraho Surface	33	28	≪1	23	-16

*LETC stands for Laramie Energy Technology Center.

technique, indicate that the partitioning of Hg during this surface retorting process may be significantly different from that observed for in-situ retorting.[6] Discrete, direct measurements of Hg using Au-amalgamation were also made in the offgas during the six-month Occidental Oil Shale modified in-situ retort experiment no. 6 at Logan Wash, Colorado in 1980.[7] However, no attempt was made to determine Hg partitioning due to the enormous difficulty of complete sampling of large-scale retorts.

ACCOMPLISHMENTS DURING FY 1980

Scope

The purpose of this program, which is entering its third year, is to investigate the partitioning of As, Cd, Hg, Pb, Sb, and Se during simulated in-situ oil shale retorting. A six-kg LBL laboratory-scale retort, which was specifically designed and built for the program, is being used to determine the effects of retort operating conditions, such as temperature regime and gas composition, on elemental partitioning. A major goal of the investigation is to make continuous direct measurements of As, Cd, Hg, and Se in oil shale retort offgases. Gas monitoring instrumentation based on ZAA spectroscopy is being developed for this purpose. Conventional analytical methods are being adapted, as necessary, and applied to the measurement of the six elements in shale oils, retort waters, and raw and spent shales.

Retort Experiments

A major achievement during the second year of the program has been the completion of six oil shale retort experiments using the laboratory-scale retort designed and built during the first year. A successful shake-down run was followed by five runs to a maximum temperature of 550°C to study elemental partitioning during low-temperature, inert-gas retorting. During four of these runs, continuous on-line measurements of Hg in the offgas stream were made with the ZAA spectrometer built during the first year. Elemental mass balance data have been obtained for Hg during three runs and for As, Se, and Pb during two runs.

The Colorado raw shale used in these experiments had a Fischer Assay of 35 gal of oil per ton of raw shale and a particle size distribution of -1/4 in. to +30 mesh. Retorting was accomplished with a nitrogen sweep gas flow rate of 2 l/min and a heating rate of 1°C/min. The shale column was uniformly heated as shown in the time-temperature profile for thermocouples located along the center line at the top, middle, and bottom of the column (Fig. 2). The total volume of offgas and the total mass of oil, water, and spent shale were measured to obtain a material balance which was typically 100 ±3%.

The concentration of Hg in the offgas, as measured by the ZAA spectrometer during retort run LBL-02 is shown in Figure 3 as a function of retorting temperature. This Hg offgas profile is typical for all runs conducted with the above retorting parameters. At temperatures less than 177°C and greater than 350°C, Hg concentrations were less than 6 $\mu g/m^3$. The volatilization of Hg from the

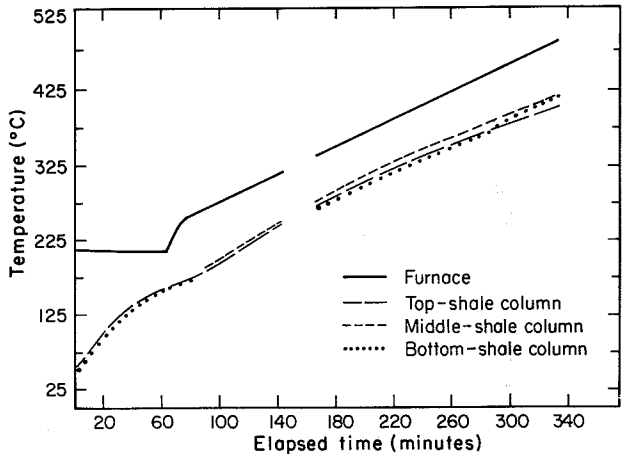

Fig. 2. Furnace and shale column time-temperature profiles for inert gas retort run, LBL-04. (XBL 811-53)

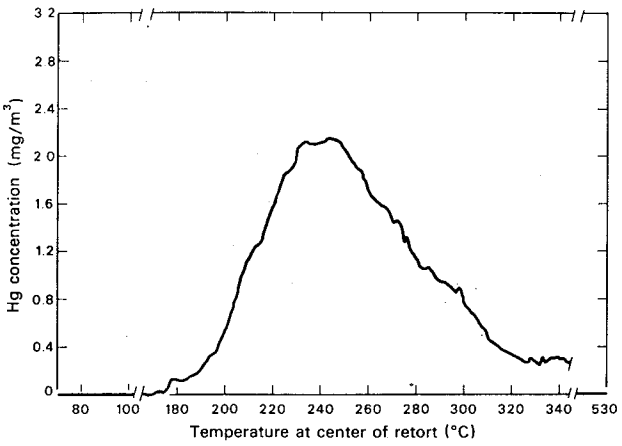

Fig. 3. Mercury concentration in offgas of inert gas retort run, LBL-02. (XBL 802-240)

shale occurred between 200°C and 320°C and peaked around 245°C. These temperatures are substantially lower than one would expect if Hg in the raw shale existed predominantly as an oxide or sulfide: HgO decomposes at 500°C, and HgS sublimes at 584°C. The volatilization of Hg precedes oil production, which occurs between 370°C and 450°C, due to the pyrolytic decomposition of kerogen. The low volatilization temperature of Hg suggests that Hg occurs as organic species associated with the kerogen. This hypothesis is consistent with recent geochemical investigations reported in another article in this report.[8]

Elemental mass balance data for Hg from the LBL retort runs are summarized in Table 1. Both the fractions of Hg entering the offgas and remaining in the spent shale are significantly lower than those observed previously. This is due in part to our inability to account for 48% of the Hg originally present in the raw shale. A major effort is being made to identify the possible causes of this imbalance.

Independent methods have been used to determine Hg concentrations in the offgas and in the oil.[9] Since good agreement between methods has been obtained, incorrect Hg determinations in the offgas and oil are no longer suspected as major contributions to the imbalance. It was also suspected that Hg might be lost to the cool portions of the retort vessel, which is composed of mullite ceramic (75% Al_2O_3 and 25% SiO_2). Two experiments demonstrated that cool mullite surfaces can act as a sink for Hg vapor. Design constraints associated with flanging the mullite tube prohibited the heating of the cool portions of the tube. Consequently, a new retort vessel has been fabricated entirely of stainless steel. This vessel will be held entirely within the heated zone of the retort furnace in an attempt to obtain a complete elemental balance for Hg.

Elemental mass balance data for As, Se, and Pb from the LBL retort runs are summarized in Table 2. Since these were low-temperature experiments, it is not surprising that 94% or more of these elements remained in the spent shale. The As and Se data agree with those shown in Figure 1. No previous partitioning data exist for Pb. Based on the indirect data in Figure 1 and Table 2 and the measured concentrations of each element in the raw shale, we can estimate the concentrations of As, Cd, Pb, and Se which might occur in the offgas stream during future high-temperature, LBL retort runs. Assuming a retort gas flow rate of 2 l/min, a retort heating rate of 2°C/min, and a vaporization temperature profile similar to that of Hg at the 1°C/min heating rate (Fig. 3), concentrations on the order of 7 mg As/m^3, 5 mg Cd/m^3, 5 mg Pb/m^3, and 4 mg Se/m^3 could occur in the offgas. These estimates are the same order of magnitude as the observed Hg concentrations and can easily be detected by ZAA even if they prove to be a factor of 30 too high.

PLANNED ACTIVITIES FOR FY 1981

Direct on-line ZAA measurements of Hg in the offgas and determinations of the partitioning of As, Cd, Hg, Pb, Sb, and Se to spent shale, shale oil, and retort waters for the 550°C retort experiments will be completed. In addition, direct ZAA measurements of Cd in the offgas during 750°C retort experiments will be initiated, and the partitioning of all six elements at this higher temperature will be determined.

Table 2. As, Se, and Pb mass balance data for two LBL inert-gas retort runs; the maximum retorting temperature was 550°C.

Product	As	Se	Pb
Spent shale	94%	99%	98%
Shale oil	5%	1%	--
Water	1%	<1%	--
Offgas	--	--	--

REFERENCES

1. G. A. Desborough, J. K. Pitman, and C. Huffman, Jr., "Concentration and Mineralogical Residence in Elements in Rich Oil Shales of the Green River Formation, Piceance Creek Basin, Colorado, and the Uinta Basin, Utah--A Preliminary Report," Chemical Geology, vol. 17, 1976, pp. 13-26.

2. J. P. Fox, K. K. Mason, and J. J. Duvall, "Partitioning of Major, Minor, and Trace Elements During Simulated In-Situ Oil Shale Retorting in a Controlled-State Retort," Twelfth Oil Shale Symposium Proceedings, Colorado School of Mines, Golden, Colo., 1979.

3. J. P. Fox, The Partitioning of Major, Minor, and Trace Elements During Simulated In-Situ Oil Shale Retorting, Ph.D. dissertation, Department of Engineering, University of California, Berkeley, 1980.

4. R. D. Giauque, J. P. Fox, J. W. Smith, and W. A. Robb, "Geochemical Studies of an Oil Shale Deposit," Energy and Environment Division Annual Report 1979, Lawrence Berkeley Laboratory report LBL-10486, 1980.

5. J. P. Fox, J. J. Duvall, K. K. Mason, R. D. McLaughlin, T. C. Bartke, and R. E. Poulson, "Mercury Emissions from a Simulated In-Situ Oil Shale Retort," Eleventh Oil Shale Symposium Proceedings, Colorado School of Mines, Golden, Colo., 1978.

6. J. S. Fruchter, C. L. Wilkerson, J. C. Evans, R. W. Sanders and K. W. Abel, Source Characterization Studies at the Paraho Semiworks Oil Shale Retort, Battelle Pacific Northwest Laboratory report PNL-2945, 1979.

7. U.S. Department of Energy, "'Environmental Research on a Modified In-Situ Oil Shale Process.' A Progress Report from the Oil Shale Task Force," Department of Energy report DOE/EV-0078, 1980.

8. R. D. Giauque, J. P. Fox, and J. W. Smith, "Characterization of Two Cores from the Naval Oil Shale Reserve Number 1," Energy and Environment Division Annual Report FY 1980, Lawrence Berkeley Laboratory report LBL-11990, 1981.

9. A. T. Hodgson, G. J. Harris-Winston, and R. G. Clem, "Analytical Methods for Trace Elements in Oil Shale and Retorting Products," Energy and Environment Division Annual Report, FY 1980, Lawrence Berkeley Laboratory report, LBL-11990, 1981.

ON-LINE MEASUREMENT OF TRACE ELEMENTS IN OIL SHALE OFFGASES BY ZEEMAN ATOMIC ABSORPTION SPECTROSCOPY*

D. C. Girvin and M. J. Pollard

INTRODUCTION

The recent emphasis on the development of synfuel processes has renewed interest in the vast oil shale deposits of Colorado, Utah, and Wyoming and in the technology needed to utilize this source of domestic oil. The development of economically competitive oil shale recovery processes will cause a number of important environmental consequences. Among these are the mobilization and release to the atmosphere of toxic trace elements. Preliminary mass balance studies of pilot-scale in-situ oil shale retorting processes indicate that significant quantities of the toxic trace elements As, Cd, Hg, and Se, originally present in the raw shale, and volatilized during the retorting (heating) process, are subsequently swept from the retort into the atmosphere in the stream of process offgas.

Assessment of this potential problem and development of the control technology to minimize emissions depend on reliable direct measurements. The lack of data is due to the fact that measurements of As, Cd, Hg, and Se are very difficult to make in a matrix as complex and corrosive as oil shale offgas. No direct on-line offgas measurements of As, Cd, or Se exist; direct on-line Hg measurements have been made however. These preliminary measurements in the offgas of a pilot-scale, in-situ oil shale processing plant were made by LBL scientists[1] using Zeeman atomic absorption spectroscopy (ZAA). This successful use of a prototype ZAA spectrometer demonstrated that the unique background correction capability of ZAA makes it suitable for continuous on-line analysis of trace elements in a highly complex, organic-rich gas matrix.

The purpose of this program, which is entering its third year, is to develop and apply ZAA spectroscopy for direct on-line trace element analysis of gases. The specific objectives are to (1) develop highly stable light sources and accurate calibration techniques for each of these elements; (2) design and build two ZAA spectrometers for analysis of gas streams, one for Hg for field and

*This work was supported by the U.S. Environmental Protection Agency and by the Assistant Secretary for Fossil Energy, Deputy Assistant Secretary for Oil, Gas, and Shale Technology, Office of Oil Shale of the Department of Energy under Contract No. W-7405-ENG-48.

laboratory use and a second for As, Cd and Se for laboratory use; (3) design and build appropriate gas sampling and metering systems; and (4) test these instruments in the offgas streams of laboratory-scale and pilot-scale oil shale retorts.

ACCOMPLISHMENTS DURING FY 1980

Two major changes have been made to the Hg ZAA spectrometer which was built last year. A new Hg light source temperature controller and a new stainless steel furnace have been built, tested, and incorporated into the Hg ZAA spectrometer. This spectrometer has been used this year to measure Hg vapor in the retort offgas stream produced during five of the six LBL oil shale retorting experiments. In addition, the accuracy of the dynamic Hg calibration device, which generates a saturated stream of Hg vapor and is used to calibrate the Hg ZAA, has been examined over a wide range of gas flows. Finally, a new ZAA furnace for continuous on-line analysis of As, Cd, and Se in gas streams has been designed and built and is ready for testing. These accomplishments are described below.

Light Source

The ZAA Hg light source is very sensitive to changes in ambient temperature. This is due to a difference in the self-absorption of the 2537 Å analytical line and the Zeeman split background correction lines inside the Ar plasma of the light source. As the ambient temperature varies, the relative intensity of these lines changes. This effect manifests itself as a change in the instrumental baseline voltage and, thus, is indistinguishable from the signal produced by Hg in the sample gas. The magnitude of this effect is shown in Figure 1. The upper curve shows this change in ppb. If the light source is operated at 25°C, a variation of ±2°C produces a ±5 ppb Hg/m^3 error, which is significant when levels are 80 ppb or lower. This problem has been eliminated by enclosing the light source in a water-jacket assembly and coupling the source to a small thermoelectric constant-temperature, circulating-water bath mounted within the instrument. This unit, fabricated from individual components, maintains a temperature control by driving an induction heater in opposition to a Borg-Warner thermoelectric heat pump (containing a bi-directional P-N semiconductor junction) used in the cooling mode (Fig. 2). A constant current passing through the junction produces a temperature gradient across the junction which is used to cool the flow of circulating water. An induction heater is driven in proportion to the temperature difference between the light source and the desired operating temperature, 25°C. The circulation pump, induction heater, and heat pump can be fitted into a 9 x 9 x 5-inch package. The unit is capable of maintaining the light source temperature at 25°C ± 0.1°C for ambient temperatures between 11°C and 37°C and for temperature transients of up to 20°C/hr (Fig. 3). With this temperature stability, the instrumental baseline drift, shown in Figure 1, is less than ± 1 ppb.

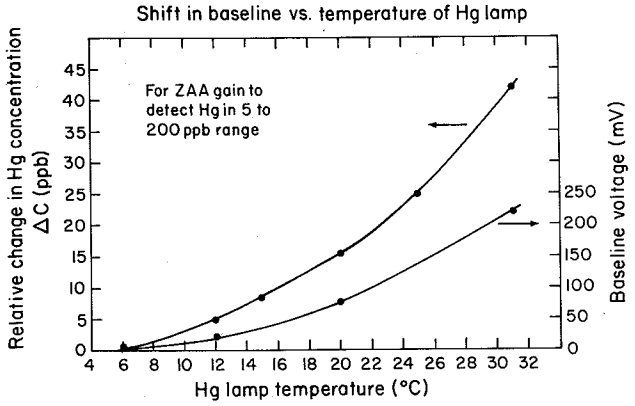

Fig. 1. Change in ZAA output voltage to temperature-induced self-reversal in the absence of Hg in the sample gas. (XBL 793-868)

5-cm Hg Furnace

A new stainless-steel furnace with an optical absorption chamber 5 cm in length was built to extend the concentration range over which the Hg ZAA can be used. This 5-cm furnace is shown in Figure 4. The length of the optical absorption chamber determines the attenuation path length, ℓ, of the analytical and background correction lines in the furnace absorption chamber. The magnitude of this attenuation is exponentially dependent upon the product $\ell \cdot (\rho_{Hg} + \rho_{scat})$, where ρ_{Hg} is the density of mercury atoms in the sample gas and ρ_{scat} is the density of atoms and molecules which scatter just the background correction lines. Thus, as ρ_{Hg} and ρ_{scat} increase, for a given value of ℓ, the slope of the instrumental response curve decreases, eventually becoming zero and finally negative. To cover the wide range of concentrations encountered in this application, furnaces of different lengths are needed.

The 18-cm furnace (described in the 1979 Annual Report[2]) is used to measure low concentrations of Hg. The response of the ZAA is linear up to 170 ppb with this 18-cm furnace. However, above 227 ppb, the instrumental response becomes nonlinear and flattens out around 450 ppb. The 5-cm furnace is linear up to 910 ppb and has a working range between 11 and 1364 ppb. For higher concentrations, a 1-cm furnace of similar design could be used. The 5-cm and 18-cm furnaces have identical mounting brackets and are easily interchangeable. They do differ, however, in the geometry of the gas flow and in that the temperature of the absorption chamber is higher for the 5-cm furnace.

Mercury Calibration System

The dynamic Hg calibration device used to calibrate the ZAA is shown in Figure 5. A metered stream of heated N_2 carrier gas impinging on a pool of Hg at 60°C produces a supersaturated stream of Hg vapor. Excess Hg condenses out in the equilibrium vessels, the temperature of the saturated vapor is measured, and the Hg concentration in the carrier gas is determined for that temperature from equilibrium Hg vapor pressure tables. The Au-amalgamation ZAA method for measuring Hg vapor in gas streams (described in a previous article[3]) was

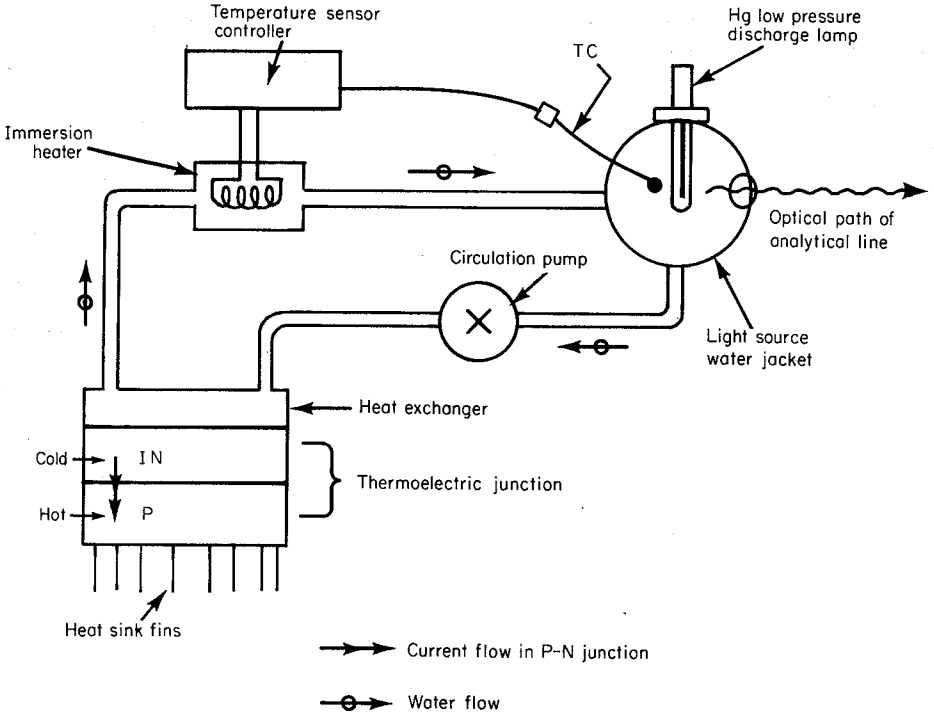

Fig. 2. Thermoelectric constant temperature water bath coupled to Hg light source water jacket. (XBL 811-45)

used to measure the mass of Hg in a given volume of calibration gas leaving the calibration device. N_2 flow rates through the calibration device were varied between 25 and 400 cc/min to determine if Hg saturation in the calibration gas was affected by flow rate. Using Au-amalgamation tubes, discrete gas samples were collected from the calibration gas stream both before and after dilution with another N_2 stream. Calibration curves were prepared using fixed volumes of saturated Hg vapor from a closed 2-liter glass container and by vaporizing aqueous Hg standards, prepared from $HgCl_2$, into a N_2 stream entering the Au-amalgamation tubes. These calibration curves were in good agreement. Measured Hg concentrations in the calibration gas from the dynamic calibration device averaged 102 ± 4% (n=7) of the calculated concentrations. These calculated concentrations were based upon the temperature of the gas exiting the dynamic calibration device up to a throughput flow rate of 400 cc/min.

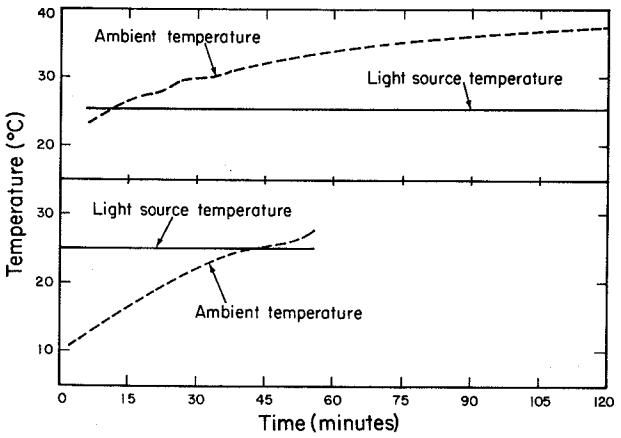

Fig. 3. Hg light source temperature and ambient temperature versus time. Light source was maintained at a constant temperature by temperature control system while ambient temperature varied from 11°C to 37°C. (XBL 811-44)

During the May 1979 field test of the Hg ZAA spectrometer at Lawrence Livermore National Laboratory (LLNL)[2] and during LBL laboratory retort runs, matrix effects have been observed which have necessitated the use of standard additions to quantify Hg levels in the offgas. These matrix effects were not directly related to the broadband UV extinction of the 2537 Å analytical line. The matrix effect manifested itself as a factor-of-two reduction in the slope of the standard addition curves obtained in offgas relative to the slope of the standard addition curves in a stream of N_2 or air. At LLNL, air was used as a sample gas diluent and as a calibration carrier gas. Laboratory experiments have been conducted to determine whether H_2S and thiophene (C_4H_4S), both present in oil shale retort gas, cause matrix suppression. For furnace atomization temperatures of 750°C and 925°C and using both air and N_2 as a carrier gas, tests showed that only in the presence of O_2 did the thiophene and the H_2S produce matrix suppression effects similar to those observed in retort offgas. The

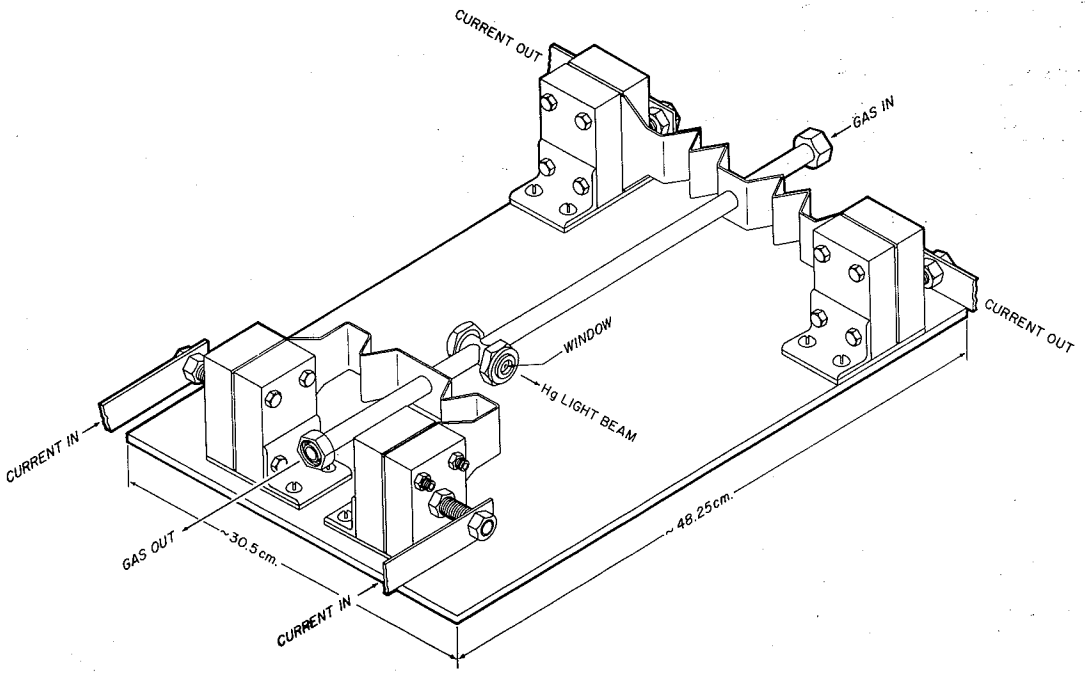

Fig. 4. Five-cm ZAA furnace. The furnace is supported by flexible SS sheet held in position by copper blocks which also act as a power bus. The section of the furnace where the gas enters is filled with ceramic chips. At right angles to this is the absorption chamber through which the Hg light beam passes.
(XBL 812-262)

effect of pyridine was also examined. However, no evidence of matrix suppression was observed.

O_2 is not normally present in the offgas stream, and N_2 rather than air is now used as a sample gas diluent and as a calibration carrier gas. However, when the offgas concentrations of oil and organic vapors are high, O_2 is added to the sample gas to promote combustion of these vapors in the 925°C atomization chamber of the Hg ZAA furnace to reduce broadband UV absorption. Under these circumstances, use of the standard addition technique to quantify Hg is essential.

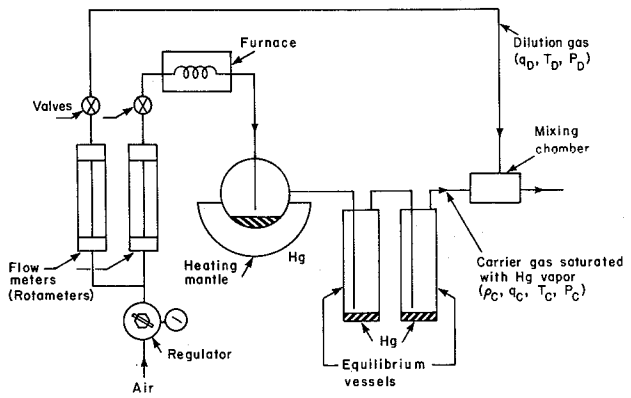

Fig. 5. Schematic of Hg calibration system.
(XBL 793-792)

With a sample gas composition as complex and variable as oil shale offgas, it is our general practice to use the method of standard additions.

High-Temperature ZAA Furnace

Since the atomization temperatures of As, Cd, and Se are all in excess of 2200°C, the ZAA furnace required for continuous analysis of these elements in the offgas must be of the graphite tube design since no other suitable furnace material can withstand these temperatures. Figure 6a shows a typical heated graphite atomizer furnace (HGA) designed for analysis of discrete liquid samples. The optical path in this furnace runs along the longitudinal axis of the graphite tube. We have redesigned the furnace so that the optical path of the analytical lines passes through the hot region of the graphite tube perpendicular to the gas flow along the longitudinal axis as shown in Figure 6b. With this configuration, As, Cd, Se, and also Hg measurements can be made directly in the hottest region of the furnace before chemical recombination of atomized elements can occur. A baffle or series of baffles in the graphite tube increases heating efficiency and insures atomization of the flowing gas sample. Quartz windows isolate the exterior surface of the graphite from atmospheric O_2. Due to the high temperatures, O_2 will probably not need to be added to the sample gas to promote combustion of organic vapors in the offgas. A very low flow of Ar will be introduced into the region between the outer wall of the furnace assembly and the graphite tube to prevent oxidative deterioration of the graphite. Graphite

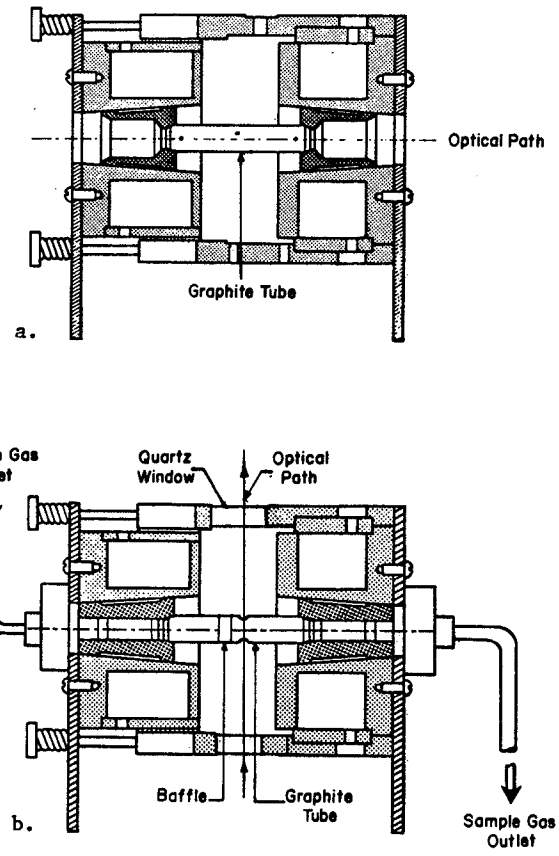

Fig. 6a-b. Standard and modified versions of Perkin Elmer HGA-2000 heated graphite furnace. (XBL 811-7651)

tubes can be used at temperatures in excess of 2600°C for up to an hour in an inert atmosphere without showing signs of failure. This furnace has been built and is ready for preliminary testing.

PLANNED ACTIVITIES FOR FY 1981

The graphite furnace described above for analysis of As, Cd, and Se in gas streams will be tested and any necessary modifications in design will be made. The first tests will be made for the analysis of Hg since a well-characterized calibration device and well-tested stable light source exist for this element. The Cd ZAA spectrometer, built last year, will be fitted with a Hg light source, light source temperature controller, and the graphite furnace to be tested. Using this instrument, measurements of Hg in calibration gas and in offgas will be compared with measurements using the existing Hg ZAA spectrometer. In addition, static and dynamic calibration techniques for the Cd ZAA spectrometer will be developed.

REFERENCES

1. J. P. Fox, J. J. Duvall, K. K. Mason, R. D. McLaughlin, T. C. Bartke, and R. E. Poulson, "Mercury Emissions from a Simulated In-Situ Oil Shale Retort," Eleventh Oil Shale Symposium Proceedings, Colorado School of Mines, Golden, Colo., 1978.

2. D. C. Girvin, A. T. Hodgson, and S. Doyle, "On-Line Measurement of Trace Elements in Oil Shale Offgases by Zeeman Atomic Absorption Spectroscopy," Energy and Environment Division Annual Report 1979, Lawrence Berkeley Laboratory report LBL-10486, 1980.

3. A. T. Hodgson, G. J. Harris-Winston, and R. G. Clem, "Analytical Methods for Trace Elements in Oil Shale and Retorting Products," Energy and Environment Division Annual Report FY 1980, Lawrence Berkeley Laboratory report LBL-11990, 1981.

ANALYTICAL METHODS FOR TRACE ELEMENTS IN OIL SHALE AND RETORTING PRODUCTS*

A. T. Hodgson, G. J. Harris-Winston, and R. G. Clem

INTRODUCTION

The Oil Shale Research group's laboratory and field studies of the partitioning of trace elements during simulated in-situ oil shale retorting require and utilize a wide variety of analytical methods. The elements of primary interest are As, Cd, Hg, Pb, Sb, and Se. The retorting components being analyzed are raw and spent shale, shale oil, retort water, and offgas. Standard techniques are applicable to the analysis of many of the combinations of trace elements and retorting components. Analysis of the remaining combinations requires the adaptation of standard methods and the development of new methods.

The analytical data are being used to determine elemental balances for simulated in-situ retorting. High levels of accuracy and precision are required to account for each element and to calculate how it is partitioned. Consequently,

* This work was supported by the U.S. Environmental Protection Agency and by the Assistant Secretary for Fossil Energy, Deputy Assistant Secretary for Oil, Gas, and Shale Technology, Office of Oil Shale of the U.S. Department of Energy under Contract No. W-7405-ENG-48.

all methods have to be carefully evaluated. This evaluation is accomplished by comparing different methods and by repeated analyses.

ACCOMPLISHMENTS DURING FY 1980

Scope

Analytical methods that we have studied for analyzing the retorting components shale, shale oil, retort water, and offgas are shown in Table 1. During the past year, we have performed graphite furnace atomic absorption spectroscopy (AAS), x-ray fluorescence spectrometry, and neutron activation analyses on shale, oil, and water samples. In addition, we have developed and tested a variety of analytical methods for Hg in all retorting components. Additional analytical development work is required for Cd in shale and oil and for Cd, As, Se, Sb, and Pb in offgas.

Au-Amalgam Method for Gaseous Hg

One of the significant accomplishments during the past year is the development of an alternate analytical method for Hg vapor in offgas and inert gas streams. With this method, we have been able to assess the performance of the dynamic calibration device and the on-line Zeeman Atomic Absorption (ZAA) Hg monitor.[1]

Initially, an attempt was made to use the Environmental Protection Agency (EPA) reference method, designed for determination of particulate and gaseous Hg emissions from stationary sources, as the alternate technique. This method employs an acidic iodine monochloride (ICl) solution for collection of Hg. Although the ICl solution readily removes inorganic Hg from inert gas streams, we experienced great difficulty in reducing and purging the Hg from solution for analysis. We also discovered that the ICl method did not work well in retort offgas streams because organic compounds in the gas used up the oxidation capacity of the solution before sufficient sampling time had elapsed.

A literature review revealed that a number of investigators had successfully used amalgamation on Ag and Au or charcoal absorption to collect Hg in ambient air[2-4] and one reported on the use of the method in oil shale offgas.[5]

We subsequently assembled and tested a system for the collection and analysis of gaseous Hg based on the amalgamation of Hg on Ag-plated quartz wool. The gas stream being sampled was passed through a glass tube containing a section of Ag-plated quartz wool. Flow rate and sampling time were measured. The collected Hg was thermally desorbed from the Ag by heating to 400°C in a stream of helium. The Hg was transferred to a second, cold, analytical tube and then thermally desorbed in the same manner. Detection was by cold vapor atomic absorption spectroscopy (AAS) using either a conventional or Zeeman-effect AAS instrument. This Ag-amalgam method allowed us to clearly demonstrate the accuracy of the dynamic calibration device.

Table 1. Analytical methods for selected trace elements in oil shale retorting components.

Retorting Component	Element					
	Hg	Cd	As	Se	Sb	Pb
Shale	ZAA-batch NAA		XRF NAA	XRF NAA	NAA	XRF
Oil	NAA Au-amalgam		XRF NAA	XRF NAA	NAA	XRF
Water	Au-amalgam Cold vapor AAS	GFAA	GFAA XRF	GFAA XRF	GFAA NAA	GFAA XRF
Gas	ZAA-continuous Au-amalgam		--	--	--	--

AAS = atomic absorption spectroscopy.

GFAA = graphite furnace atomic absorption spectroscopy.

NAA = neutron activation analysis

XRF = x-ray fluorescence spectrometry.

ZAA = Zeeman atomic absorption spectroscopy

We are currently using amalgamation with Au-plated glass beads as an alternate analytical procedure for Hg in Lawrence Berkeley Laboratory (LBL) retort offgas. Samples are collected by amalgamation without prior treatment of the offgas and then thermally desorbed and pyrolyzed in a 1000°C combustion tube. The combustion and analytical procedures are identical to those currently being used for oil samples (see "Hg in Shale Oils").

The Hg concentrations in offgas determined by the Au-amalgam technique have been compared to results obtained with the ZAA Hg monitor. Concentrations for seven of the nine amalgam samples collected during the last retort run were within 30% of corresponding ZAA concentrations. This general agreement of the two methods is considered to be good. Additional comparisons are planned for future laboratory retort runs and field studies in order to further evaluate the relative accuracies of the two methods.

Hg in Shale Oils

Considerable effort has been spent developing an analytical method for Hg in oil produced in the LBL retort. Attempts at direct analysis of this oil in the batch-sample ZAA spectrometer were unsuccessful due to severe matrix suppression. We subsequently attempted to decompose the oil with HNO_3 in high pressure acid digestion bombs but obtained less than 75% recovery of Hg added to samples prior to digestion.

A breakthrough occurred when our search for an alternate analytical procedure for Hg in retort offgas led us to the collection of Hg by amalgamation. A workable method for recovering Hg from oil was developed by coupling this technique with a combustion technique for oil decomposition. In this method's initial form, a small quantity of oil was heated to 500°C in a stream of N_2 which passed through a cupric oxide combustion tube maintained at 500°C. Liberated Hg was collected downstream of the combustion tube by amalgamation. Analysis was the same as for gas samples.

Acceptable results for the analysis of Hg in shale oils from other retorts were obtained with this technique. However, inconsistent results were obtained with fresh oil from the LBL retort due to incomplete combustion and inorganic interferences or both. As a result, the combustion technique was modified. The cupric oxide was replaced with tungsten trioxide (WO_3), and the combustion temperature was raised to 1000°C. The Hg collection procedure also had to be modified. We discovered that acids were forming in the combustion tube outlet vent during decomposition of the oil. To prevent Hg from being scrubbed from the carrier gas by the acids, we packed calcium oxide in the outlet of the combustion tube and shortened the length of external tubing. After exit from the combustion tube, the carrier gas then passed directly through a bubbler containing 1.5 vol% HCl. On completion of the combustion step, sodium borohydride is injected into the bubbler to evolve the trapped Hg for collection on Au-plated glass beads. Analysis is the same as for gas samples.

The above procedure has been used with moderate success on fresh oil from LBL retort runs. The accuracy of the technique was evaluated by comparison with neutron activation analysis (NAA) (Table 2). The combustion-amalgamation-AAS method produced Hg concentrations which were lower than NAA concentrations by 13-20%. In addition, imprecision of the combustion-amalgamation-AAS technique, as measured by the coefficient of variation was as high as 43%. Based on this performance, NAA is the preferred technique for analysis of Hg in shale oil. However, the length of time required for this analysis (more than one month), and the high cost, preclude the use of NAA on a routine basis. We are, therefore, utilizing the combustion-amalgamation-AAS technique for screening of samples and using NAA only for those samples which require the highest accuracy and precision.

Hg in Retort Waters

Retort water samples were originally analyzed for Hg using a commercial cold-vapor generation system. With this system, we determined that Hg was rapidly lost from unpreserved samples. This loss necessitated either immediate sample analysis or adequate sample preservation. Immediate analysis is not always practical, so we conducted a

Table 2. Comparison of methods for determination of Hg in shale oil.

Shale Oil Origin	Hg Concentration ± 1 σ(μg/g)		
	NAA	Combustion-Amalgamation-AAS	Acid Digestion-AAS
Geokinetics	0.152 ± 0.017	0.133 ± 0.023 n = 10, CV = 17%	0.082 ± 0.021 n = 7, CV = 26%
LBL	0.090 ± 0.019	0.072 ± 0.031 n = 33, CV = 43%	

NAA = neutron activation analysis.

CV = coefficient of variation (100 $\sigma/\bar{x}$).

literature review of preservation and storage procedures for water samples intended for subsequent Hg analysis. From the literature, we selected a procedure which employs 5 vol% HNO_3 plus 0.05% potassium dichromate as preservatives and employs glass containers for storage. Periodic analysis of a preserved spiked sample demonstrated that the procedure prevented the loss of Hg for periods of at least a month.

The Au-amalgam procedure developed for offgas and oil samples was adapted for use with retort water samples and produced a level of precision superior to that obtained with the commercial cold-vapor system. A small aliquot of preserved retort water is added to 1.5 vol% HCl in a bubbler. Sodium borohydride is injected into the bubbler, which is then swept with N_2. The liberated Hg is collected by amalgamation. Analysis is the same as for gas samples.

Hg in Raw and Spent Shales

Raw and spent shale are analyzed for Hg with the batch-type ZAA spectrometer. A small quantity of ground shale is introduced directly into a 900°C Ni furnace aligned along the optical path of the instrument with O_2 as the carrier gas. Analyses are performed using calibration curves constructed with aqueous standards and by the method of additions using aqueous standards.

PLANNED ACTIVITIES FOR FY 1981

The Au-amalgam method for gaseous Hg will be tested during the operation of a pilot-scale retort if a sampling opportunity arises in 1981. This test will probably be conducted in conjunction with on-line Hg monitoring using the ZAA instrument. Further refinement of the Au-amalgam method may be warranted, since the method has good potential for monitoring emissions compliance. Major analytical development emphasis in 1981 will be placed on the analysis of Cd in oil shale and retorting products.

REFERENCES

1. D. C. Girvin and M. J. Pollard, "On-Line Measurement of Trace Elements in Oil Shale Offgases by Zeeman Atomic Absorption Spectroscopy," Energy and Environment Division Annual Report FY 1980, Lawrence Berkeley Laboratory report LBL-11990, 1981.

2. R. S. Braman and D. L. Johnson, "Selective Absorption Tubes and Emission Technique for Determination of Ambient Forms of Mercury in Air," Environmental Science and Technology, vol. 8, no. 12, 1974, p. 966.

3. P. E. Trujillo and E. E. Campbell, "Development of a Multistage Air Sampler for Mercury," Analytical Chemistry, vol. 9, no. 47, 1975, p. 1629.

4. W. F. Fitzgerald and Gary A. Gill, "Subnanogram Determination of Mercury by Two-Stage Gold Amalgamation and Gas Phase Detection Applied to Atmospheric Analysis," Analytical Chemistry, vol. 51, no. 11, 1979, p. 1714.

5. C. L. Wilkerson, "Vapor Mercury Levels in the Offgas of Occidental's Modified In-Situ Retort 6," Pacific Northwest Laboratory Annual Report for 1979 to the DOE Assistant Secretary for Environment, part 4, (Richland, Wash: Pacific Northwest Laboratory, 1980), p. 105.

DEVELOPMENT OF LOW COST GROUTS FROM SPENT OIL SHALE*

P. Persoff

INTRODUCTION

In vertical modified in-situ (VMIS) retorting, the resource is processed in the ground. Large chambers of rubblized oil shale are formed by mining out 20 to 40% of the in-place shale and blasting the remainder of the shale into the created void. The mined-out material is brought to the surface and oil is recovered from it by surface retorting. The in-place material is pyrolized to recover oil, leaving large abandoned retort chambers underground.

This type of oil shale processing may result in a number of environmental problems including leaching of chemicals from abandoned in-situ retorts by groundwater and ground subsidence. It may also result in low resource recovery (in that large pillars are needed to support the overburden). These problems may be mitigated by filling abandoned retorts with a grout. This would occupy the void space created by mining and blasting, thus improving the structural stability of the retorts, and it would reduce the retort's permeability to groundwater flow. If the filled area is sufficiently strong, it may be possible to design retorts so that pillars eventually can be retorted for additional resource recovery after the grouting is complete.

Because oil shale is a low-grade hydrocarbon resource (a typical assay considered economic for VMIS development is 25 gal/ton) and because 20 to 40% of this material is removed to create permeability in the VMIS process, the void space to be filled by grout is large--about 9 to 13 ft^3/bbl of oil recovered. Thus, low cost is the first requirement for any candidate grout material. Transportation costs prohibit the importation of materials that are often considered as cheap grouts, such as fly ash or bentonite. However, surface retorting done in conjunction with VMIS retorting will produce large quantities of spent shale on site--about 1.4 ton/bbl of oil recovered by surface retorting. Properties of spent shale vary widely depending on the retorting process used, but in some cases, the spent shale has properties which may commend it as a grout material.[1]

Grouting with spent shale would also accomplish disposal of much of the spent shale.

The purpose of this program, which was started in June 1978, is to evaluate low-cost grouts incorporating spent shale for grouting abandoned in-situ retorts to achieve structural integrity and reduced permeability.

ACCOMPLISHMENTS DURING FY 1980

A series of low-cost grouts was prepared containing only spent shale, sand, water, and less than 10% cement. After curing, these grouts were tested for permeability and uniaxial and triaxial compressive strength. Comparison of the strength tests with model calculations[2] indicate that these grouts do not give enough strength to permit any additional resource recovery by pillar extraction, but the permeabilities observed may be low enough to prevent leaching by groundwater.

Additional work was done to determine post-retorting heat treatments that could improve the performance of spent shale grouts. Spent shale was heated at various temperatures under various atmospheres. The results of this work tentatively indicate that heating spent shale under an autogenous atmosphere or flowing N_2 gas at 800°C 850°C enhances setting.

Samples

The spent shale used in this investigation was Lurgi spent shale, collected in the electrostatic precipitator from Lurgi run no. 9, in 1976. This material was selected because both commercial oil shale ventures, Rio Blanco Oil Shale Project and Occidental Oil Shale-Tenneco, are considering the Lurgi process for surface retorting of mined shale. This spent shale is a fine powder with a median particle size about 3 μm; for more information see last year's report.[1]

Grout Recipe Design

The most important variable in the design of low-cost grouts is the water-to-solids ratio (WSR). A high WSR favors fluidity, enabling the grout to penetrate voids in an abandoned retort, but it can also result in bleeding, that is, separation of a clear supernatant by sedimentation. We wanted a nonbleeding grout that would still be sufficiently fluid. Our criterion for fluidity was that the time of efflux from a standard Corps of Engineers grout flow cone[3] should be 18-22 s. Experience with intrusion grouting of preplaced aggregate has shown this to be reasonable.[4] Grouts of spent shale and water with WSR low enough to be nonbleeding were too thick to measure by the flow cone method. However, we found that replacing of

* This work was supported by the Assistant Secretary for Environment, Office of Environmental Compliance and Overview, Environmental Control Technology Division of the U.S. Department of Energy and by the Assistant Secretary for Fossil Energy, Deputy Assistant Secretary for Oil, Gas, and Shale Technology, Office of Oil Shale of the U.S. Department of Energy under Contract No. W-7405-ENG-48.

the spent shale with -30 +50 mesh sand resulted in slurries which met both criteria.

The recipes of the grouts tested are shown in Table 1. The grouts were prepared by first mixing with minimum water and then adding water incrementally until the flow cone time was 20±2 s. All grouts were tested for bleeding by allowing a 250-ml graduated cylinder full of grout to stand for 4 h. Bleeding was always less than 1%. Specimens were cast in waxed-cardboard cylinder molds because the anticipated strength was so low that metal cylinders could not be removed from the specimens without damaging them. Some specimens were made with coarse aggregate to simulate material in a grouted retort (for strength measurements), while others were made without coarse aggregate (for permeability measurements). The samples were cured at 70±3°F under 100% humidity. After two months, strength and permeability measurements were made.

Compressive Strength Measurements

For triaxial compressive strength measurements, specimens must have flat parallel ends. Usually, these are produced by trimming soil specimens with a knife, or capping rock or concrete specimens with a molten sulfur capping compound, which is then trimmed to the circumference of the sample. Neither technique could be used here. Trimming the sample with a knife would dislodge pieces of aggregate and damage the specimen. The capping compound is stronger than the grout/aggregate; thus trimming the caps would also damage the specimen. Therefore, a novel capping technique was devised. Specimens were placed in a mold with flat parallel end cavities into which hydrostone, a proprietary plaster, was injected. This eliminated the need to trim the end caps. For uniaxial tests, in which the caps need not be trimmed, sulfur capping compound was used. Results of the unconfined (uniaxial) compressive strength tests are shown in Table 1. Triaxial compressive strength tests tentatively indicate that there is no increase in strength with confining pressure; that is, the materials have cohesion but little internal friction. This behavior is typical of clay soils. The low strengths observed indicate that the grout, and not the aggregate, controls the strength.

Permeability Measurements

The permeability of spent shale grout, like that of a saturated soil, depends on its state of stress. To determine the relationship between permeability and the state of stress, permeability was measured by placing the cured grout sample in a triaxial pressure chamber with water inlet and outlet at the specimen ends. With this apparatus, any desired confining pressure can be applied, and de-aired water can be applied to one end of the specimen at any pressure less than the confining pressure. Testing of these specimens is still in progress.

Figure 1 shows results from two specimens each of grouts Q-0 and Q-1. The dependency of permeability upon confining pressure is evident. At high confining pressures, water is squeezed out of the specimen ends, leading to consolidation of the sample. The actual permeability that will exist in a field grouting operation depends on the stress to be experienced by a grouted retort. Cal-

Table 1. Low-cost spent shale grouts.

	Samples				
	Q-0	Q-1	Q-3	Q-4	Q-5
Lurgi spent shale (g)	1500	1500	1500	1500	1500
Sand -30 +50 mesh (g)	750	750	750	750	750
Portland cement (g)	0	56.3	0	0	0
Lurgi spent shale cement (g)[a]	0	0	56.3	112.5	225
Simulated ground water (ml)[b]	1320	1430	1400	1602	2025
Water-solids ratio	0.587	0.620	0.607	0.678	0.818
Flow-cone time (sec)	20.5	19.9	21.4	20.3	22.5
Unconfined compressive strength (psi)	30	81	34	52	90

[a] $CaCO_3$-Lurgi spent shale ratio 0.9, calcined 1 h at 1000°C, 5% gypsum added. This cement had a 28-day strength of 528 psi (American Society for Testing and Materials test C 109); stronger cement can be produced by increasing the $CaCO_3$-spent shale ratio to 1.0.

[b] 0.61 g $NaHCO_3$ and 0.88 g Na_2SO_4 per liter to simulate native groundwater.

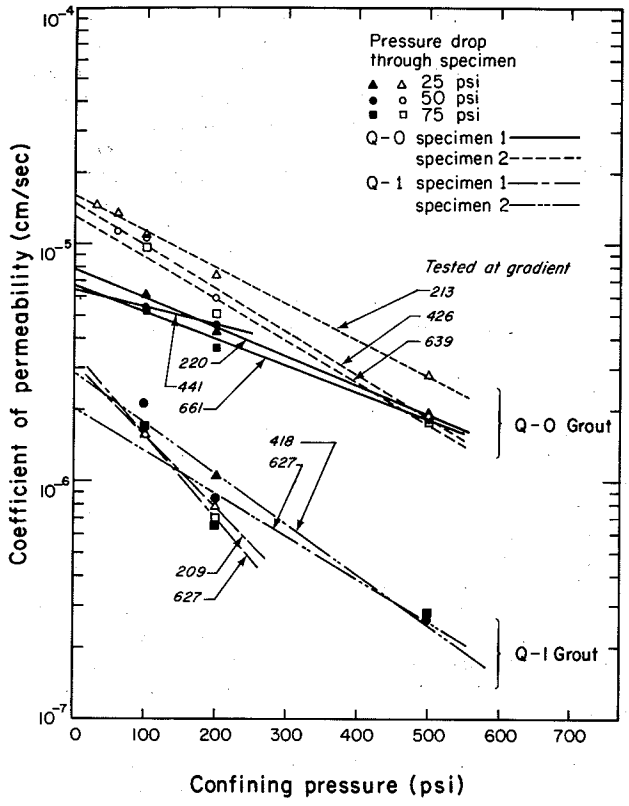

Fig. 1. Variation of permeability with confining pressure and hydraulic gradient during test for grouts Q-0 (no cement) and Q-1 (2-1/2% portland cement.) (FXBL 8012-2556)

culations of the type described in the accompanying paper by Ratigan[2] must be used to determine this stress. A much smaller dependency of permeability on hydraulic gradient is also shown in Figure 1. This was not expected. The explanation may be that after each calibrated increase in the hydraulic gradient, more rapid flow through the specimen dislodges some particles and results in a denser, more stable packing which is less permeable. This effect was more pronounced for Q-0, which contains no cement, than for Q-1, which contains 2-1/2% portland cement. This supports this hypothesis.

Heat Treatment to Improve the Setting Properties of Spent Shale

In addition to testing spent shale as received, work is in progress to determine what treatments can accelerate the setting and hardening properties of this material. Production of a true hydraulic cement, as reported last year,[1] is expensive due to the need to add large quantities of limestone. Thus, alternate mechanisms to accelerate the setting and hardening properties of spent shale were considered. Spent shales produced at retorting temperatures of less than about 700°C contain much of their original calcite and dolomite. Thus, further heating of spent shale will form CaO and MgO which should improve the setting and hardening properties of spent shale. The produced CaO can undergo pozzolanic reactions with silica in the spent shale or can react with atmospheric or aqueous CO_2 to form $CaCO_3$. The MgO, on the other hand, can hydrate to $Mg(OH)_2$, which may also contribute to cementation. These reactions may thus increase the cementing property and decrease the permeability of the spent shale grout by forming crystalline or amorphous precipitates in the pores of the grout.

Accordingly, spent shale was heated under flowing N_2, steam, or under an autogenous atmosphere (primarily evolved CO_2 in this case). The products of heat treatment were analyzed by x-ray diffraction, and were also given a qualitative time of set test.

None of the products developed setting and hardening characteristics except those heated at 800 or 850°C under flowing N_2 or autogenous atmosphere, which showed an initial set in less than two days. Figure 2 shows the x-ray diffraction peak heights after heating under N_2. From this figure, it is apparent that at 800°C, optimum proportions of both CaO and MgO were present, while the noncementing compound åkermanite had not yet formed. This is probably the reason that spent shale heated at this temperature showed some setting and hardening.

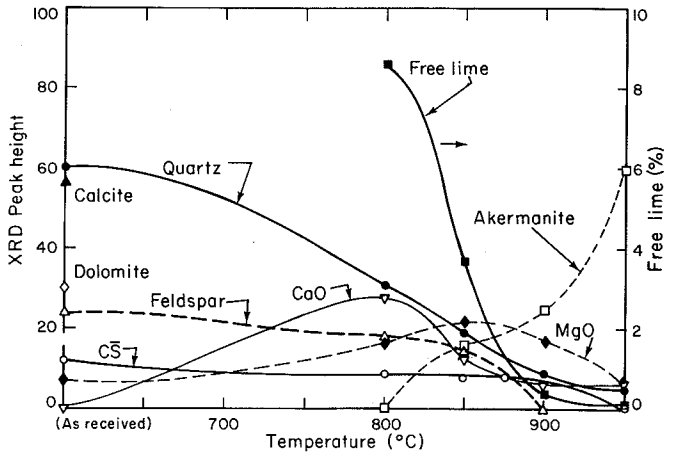

Fig. 2. XRD peak height and free lime of Lurgi spent shale after 1 h heating under flowing N_2. (XBL 811-46)

PLANNED ACTIVITIES FOR FY 1981

Testing on this series of candidate grouts will continue to better define the effect of confining pressure on triaxial compressive strength and on permeability. Additional series of candidate grouts will be prepared and tested, to determine the value of fluidizers (compounds that reduce grout viscosity) and pozzolanic fly ashes as grout ingredients. Samples of spent shales from near-commercial-scale surface retorting activities have been received for these tests.

REFERENCES

1. P. K. Mehta and P. Persoff, "Hydraulic Cement Production from Lurgi Spent Shale," Energy and Environment Division Annual Report 1979, Lawrence Berkeley Laboratory report LBL-10486, 1980.

2. J. L. Ratigan, "Structural Requirements for the Abandonment of In-Situ Retorts," Energy and Environment Division Annual Report 1979, Lawrence Berkeley Laboratory report LBL-10486, 1981.

3. U.S. Army Corps of Engineers Handbook for Cement and Concrete, Standard CRD-C 79, Vicksburg, Miss., 1977.

4. Anonymous, "Preplaced Aggregate Concrete for Structural and Mass Concrete," ACI Journal, October 1969, p. 796.

THE PREDICTION OF THE PENETRATION DISTANCE OF SPENT SHALE IN AN IN-SITU RETORT*

N. A. Thomsen and P. Persoff

INTRODUCTION

Adverse environmental effects of oil shale development by modified in-situ retorting include groundwater degradation due to leaching of in-situ spent shale and subsidence of retort overburden. Low resource recovery is an additional problem because of the need to leave large pillars of intact raw shale in place to support overburden. One possible solution to all three of these problems is backfilling abandoned retorts with a grout containing a large proportion of surface-retorted shale. Development of a low-cost grout based on surface-retorted shale is described elsewhere in this volume.[1]

The distribution of such a grout into an abandoned retort is one of the most technically difficult and potentially costly aspects of retort abandonment. The abandoned retort consists of a packed chamber of retorted shale with a complex void distribution. Voids include spaces between pieces of rubble, which may range from fines to boulders, fractures along the bedding plane in individual pieces of shale, and micropores created by the pyrolysis of kerogen. The introduced grout must uniformly penetrate a majority of these voids to achieve low permeability in the retort. This may be achieved if a sufficiently large number of closely spaced drill holes are used or if the viscosity of the grout is sufficiently low. An economic tradeoff exists between the costs of drill holes and the costs of reducing grout viscosity. Since retorts are deep, 1,000-2,000 ft below the surface, drilling grout injection holes will be costly. However, use of slurry fluidizers to reduce grout viscosity will also be costly.

The purpose of this program is to theoretically and experimentally examine the flow of particulate grouts through porous media. Particulate grouts usually have nonNewtonian fluid properties, and this aspect of the flow problem has been our main concern.

ACCOMPLISHMENTS DURING FY 1980

A report examining the theoretical aspects of grout flow was prepared.[2] The report's main conclusions are summarized in the following paragraphs.

Figure 1 shows typical flow curves for several non-Newtonian fluids. Most particulate grouts behave as Bingham, Casson, or Herschel-Bulkley fluids. The most important characteristic of particulate grouts is that they possess a yield strength, τ_y. If the applied shear stress in the fluid is less than τ_y, then the fluid will not flow. Mathematical models of non-Newtonian fluids with nonzero yield strengths were examined to determine if Darcy's Law, which characterizes Newtonian fluid flow through a porous medium, is applicable to non-Newtonian fluids. It was concluded on the basis of theoretical considerations that Darcy's Law does not apply to non-Newtonian grout flow. This is due to the plug flow phenomena shown in Figure 2. Because the non-Newtonian fluid possesses a nonzero yield strength, a solid plug moving at constant velocity forms in the flowing

* This work was supported by the Assistant Secretary for Environment, Office of Environmental Compliance and Overview, Environmental Control Technology Division of the U.S. Department of Energy and by the Assistant Secretary for Fossil Energy, Deputy Assistant Secretary for Oil, Gas, and Shale Technology, Office of Oil Shale of the U.S. Department of Energy under Contract No. W-7405-ENG-48.

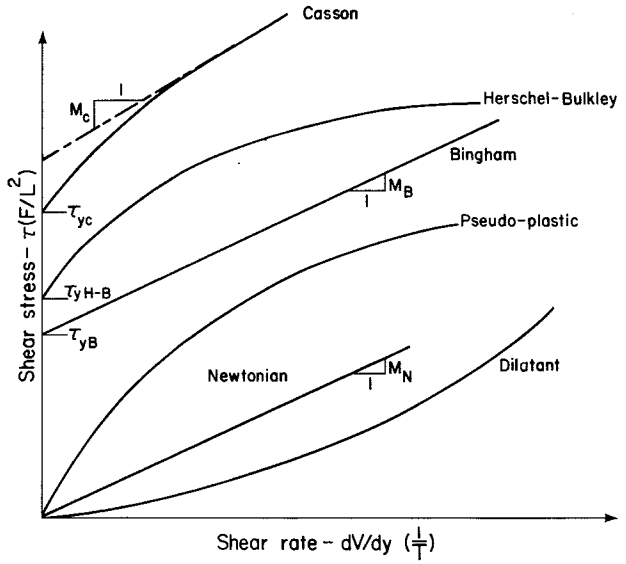

Fig. 1. Flow curves for Newtonian and non-Newtonian fluids. (XBL 8010-2098)

fluid. The radius of the plug, r_p, is a function of the yield strength of the fluid (τ_y) and the pressure gradient (dP/dx), where

$$r_p = \frac{2\tau_y}{dP/dx} \qquad (1)$$

for straight, circular capillaries. When r_p is equal to the radius of the capillary, R, then flow ceases and the fluid does not penetrate any further. Therefore, when grout is injected into a porous medium, fluid will not enter pores smaller than the plug radius, r_p. Since the pressure gradient decreases with increasing distance from the injection point, then, obviously, r_p must increase continuously. As a result, r_p must increase until at some distance, L_{max}, all pores are smaller than r_p and flow ceases. The purpose of our research is to predict the distance of penetration of non-Newtonian grouts based on a knowledge of grout properties, induced pressure gradients, and porous media properties.

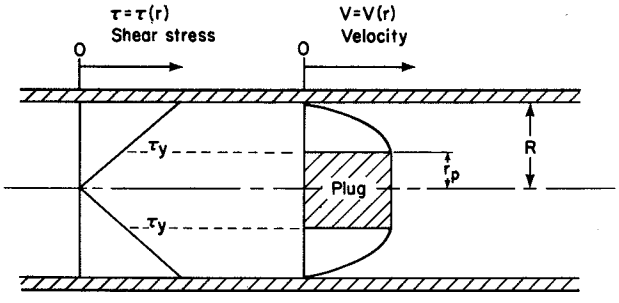

Fig. 2. Fluids with yield strength flow with a central plug, not in shear, carried by an annular cylinder of fluid in shear. (XBL 8010-2108)

For a straight circular capillary, fundamental considerations indicate that the distance of penetration for a grout is given by:

$$L_{max} = \frac{R(H_1-H_2)\gamma_f}{2\tau_y} \qquad (2)$$

where L_{max} = distance of penetration,
R = capillary radius,
H_1 = injection hydraulic head,
H_2 = in-situ hydraulic head,
γ_f = specific weight of fluid,
τ_y = yield strength of grout.

We hypothesize that the maximum distance of grout penetration in a porous medium is given by:

$$L_{max} = \frac{R_H \; Co \; T(H_1-H_2)\gamma_f}{2\,\tau_y} \qquad (3)$$

where R_H = hydraulic radius of media pores,
C_o = pore shape coefficient,
T = tortuosity coefficient.

Other symbols are defined in Equation 2. Therefore, once C_o and T are experimentally determined, we can use the method shown in Figure 3 for predicting distance of penetration if we know how the hydraulic radius varies along the flow path. Figure 4 is a section through a grouted mass showing how different flow paths have different penetration distances depending on variations of R_H along that path.

PLANNED ACTIVITIES FOR FY 1981

The report prepared in 1980[1] contains a proposed experimental program for testing the hypothesized formula for predicting grout penetration distance (Eq. 3). The plans of the experimental program are described in the following paragraphs:

Grout Characterization

A viscometer will be used to determine flow properties of several candidate grouts. The emphasis of the viscometer tests will be on accurately measuring the yield strength (τ_y) of the grouts. Various mixes of cement and spent shale and clay will be tested.

Capillary Flow Experiments

The emphasis of this part of the program will be to verify Equation 2 for straight, circular capillaries and to establish Equation 3 for manufactured sinuous, noncircular capillaries. By testing capillaries of various sinuosity and pore shape, we hope to establish pore shape and tortuosity coefficients (C_o, T) that can be used in tests with porous media.

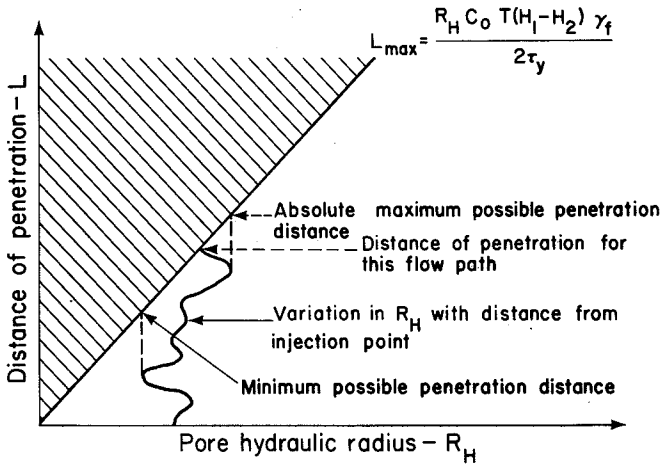

Fig. 3. Hydraulic radius varies along flow path length. Radius of plug increases along flow path length. Limit of penetration is where they are equal. (XBL 8010-2094)

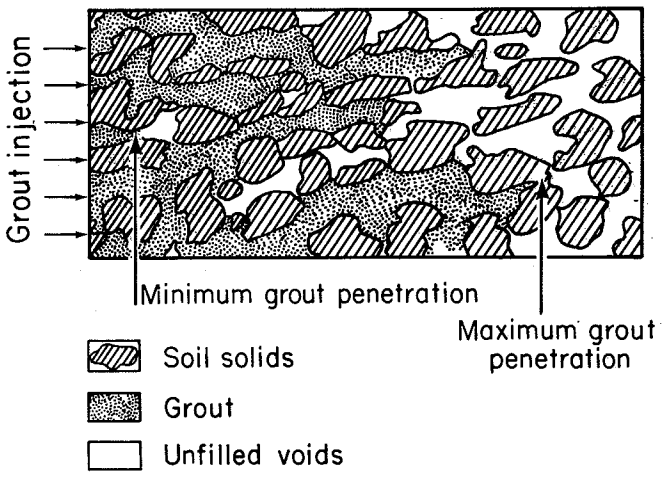

Fig. 4. Sketch of section through a grouted mass in porous medium containing a wide range in pore sizes. (XBL 811-47)

Ideal Porous Media Experiments

Once the relationship expressed in Equation 3 has been established, then we can test our hypothesis by injecting grout into an "ideal" porous medium composed of glass balls of known size, shape, and packing. Geometrical studies will allow us to calculate pore paths and sizes before grout is injected.

Injection of Grout into Models of In-Situ Retorts

After the above experiments have been completed, we should be able to inject spent shale grouts into cylinders filled with retorted rubble similar to that found in in-situ retorts. Pore size analysis of the medium will tell us the pore shape and tortuosity factors appropriate to the material, and we can then predict the distance grout will penetrate based on the hypothetical relationships established in the preceding experiments. Injection into a "real" medium will then provide us with data to verify our predicted values.

REFERENCES

1. P. Persoff, "Development of Low Cost Grouts from Spent Oil Shale," Energy and Environment Division Annual Report 1980, Lawrence Berkeley Laboratory report, LBL-11972, 1981.

2. N. A. Thomsen, The Prediction of the Penetration Distance of NonNewtonian Grouts, Lawrence Berkeley Laboratory report LBL-11442 (to be published), 1981.

STRUCTURAL REQUIREMENTS FOR THE ABANDONMENT OF IN-SITU RETORTS*

J. L. Ratigan and R. E. Goodman†

INTRODUCTION

In virtually all mining and tunneling operations, the elevation of the land surface above the underground openings is decreased due to the compression of the structural support members (usually pillars) in the underground works and the deformation of the overlying strata (overburden). Vertical modified in-situ retorting (VMIS) operations will be no exception and, in fact, present an unprecedented subsidence design problem. This retorting method calls for an underground mining plan which has not yet been employed in other ventures. Thus, no experience is available with regard to the plan's subsidence effects. Therefore, one aim of this study was to model the essential features of the subsidence problem and then apply the model.

The purpose of this study is to provide preliminary estimates of the subsidence potential and to evaluate the decrease in subsidence resulting from use of a structural grout in the retort chambers following pyrolysis. The specific objectives of this study, which was begun in December 1979, are fourfold:

1. Determine the strength and stiffness requirements for grouted retorts to support the overburden and to permit secondary recovery of the pillars.

2. Develop a numerical model incorporating the essential characteristics of oil shale deformation which would allow cost-effective parametric and sensitivity studies of the salient problem variables.

3. Determine the sensitivity of safety factors to variations in extraction ratio, design dimensions, and grouted-retort deformability.

4. Determine pillar and overburden stresses without grouting to provide "baseline" values for evaluating grout efficiency.

ACCOMPLISHMENTS DURING FY 1980

This year we developed a computer model[1] which simulates subsidence around a field of VMIS retorts and which includes the nonlinear stress and strain response of both the oil shale pillars and the grouted retorts as observed in laboratory tests. The overburden, which will undergo significantly lower strains, is modeled with a linear response to load. This model was used to study rock mechanics aspects of VMIS retorting.

The remaining sections of this article will describe the components of the computer model, the constitutive relationships assumed for the geologic materials, implementation of the constitutive relations, and results.

*This work was supported by the Assistant Secretary for Environment, Office of Environmental Compliance and Overview, Environmental Control Technology Division and Assistant Secretary for Fossil Energy, Deputy Assistant Secretary for Oil, Gas, and Shale Technology, Office of Oil Shale Technology of the U.S. Department of Energy under Contract No. W-7405-ENG-48.

†University of California, Berkeley, Calif.

Subsidence Model Elements

The program we developed is a nonlinear, two-dimensional, finite element computer program for evaluating static subsidence in a room-and-pillar or a lane-and-pillar configuration with homogeneous and isotropic overburden and homogeneous and isotropic pillars. The basic structural elements (Fig. 1) within the program are: overburden, pillar, and room elements.

The two-dimensional overburden elements possess six degrees of freedom, horizontal and vertical translation and rotation at both ends. The behavior of these elements is governed by the slope deflection equations of classical beam theory with the inclusion of shear deflections. The shear deflections are assumed to be invariant with respect to depth.

The room elements are similar to the pillar elements. These elements may represent totally excavated cavities by specifying a compressive strength of zero, or they may represent "backfilled" rooms with the appropriate input parameters. Room elements are also considered to be rigidly attached to a foundation at the lower end. Shear deflections for the pillar and room elements are assumed invariant over the width of the room or pillar.

The uniaxial pillar and room elements do not allow for horizontal variations in vertical stress and are only connected structurally via the overburden elements. The response of the pillar and room elements to load is characterized by an initial pore volume decrease and collapse followed by a monotonic strain hardening behavior asymptotically approaching the unconfined compressive strength. Only response to loading in compression is modelled in the program. The pillar and room elements possess infinite stiffness in tension.

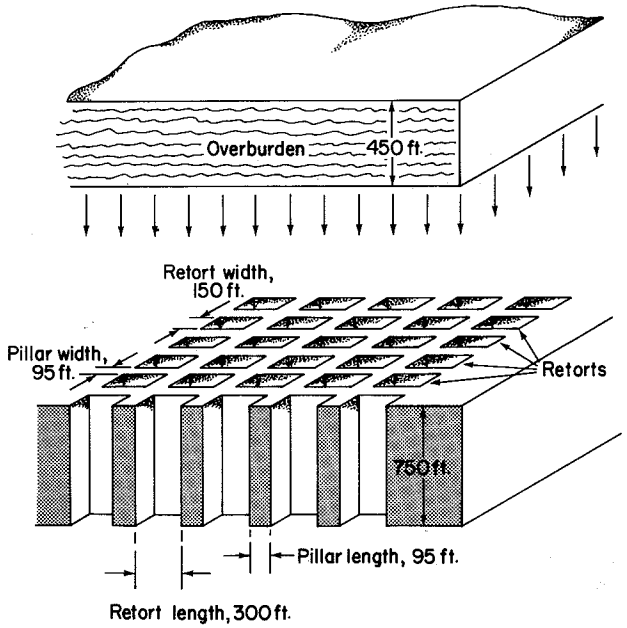

Fig. 1. Retort/pillar geometries used in model calculations. (XBL 801-120)

Constitutive Relationships

The uniaxial stress/strain behavior of the pillar and room elements is illustrated in Figure 2. Region I of the stress/strain curve represents pore volume decrease or microcrack closing, and Region II represents strain hardening of the matrix material. Mathematically:

$$\sigma = k(\varepsilon/\varepsilon^*)^N, \text{ for } \varepsilon \leq \varepsilon^*, \text{ and} \tag{1}$$

$$\sigma = (C_o - k)\left[1 - e^{\lambda - (\varepsilon - \varepsilon^*)}\right] + K, \text{ for } \varepsilon \leq \varepsilon,$$

where σ = uniaxial stress,

ε = uniaxial strain,

C_o = unconfined compressive strength,

ε^*, N, λ = constraints determined from laboratory stress/strain data.

Bending and flexural deformations within the pillar and room elements are considered to be linear with the applied load and represented with the slope deflection equations. The deformation modulus for these modes of loading is taken to be identical to the tangent modulus from the stress/strain curve of Figure 2 at the present vertical compressive strain. The load/deformation response of the overburden elements is taken to be linear and constant. Classical beam theory applies with the addition of shear deformations.

Element Stiffness Matrices

This section describes the form of the element stiffnesses. The general form of the force/displacement relations is:

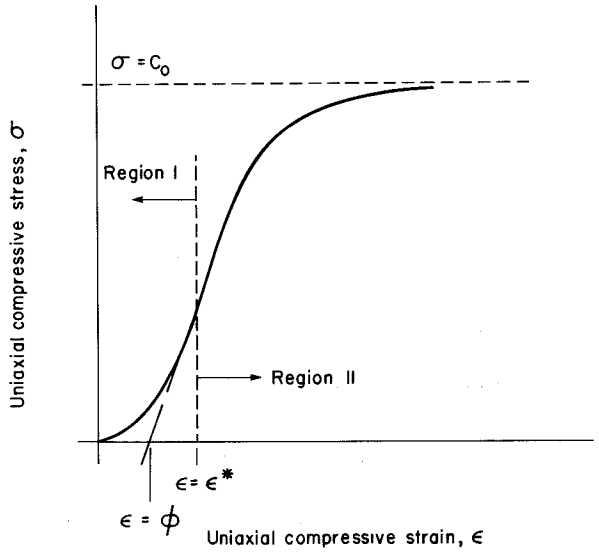

Fig. 2. Uniaxial stress/strain response for pillar and room elements. (XBL 809-1973)

$$[K^e]\ \{U^e\} = \{F^e\} \qquad (2)$$

where $[K^e]$ = the element stiffness matrix,

$\{U^e\}$ = the element displacement vector,

$\{F^e\}$ = element force vector.

Overburden Elements

The forces, displacements, and appropriate sign convention for an overburden element are illustrated in Figure 3. The corresponding form of Equation (2) is:

$$\frac{E_b I_b}{L(1+2\beta_b)}\begin{bmatrix} \frac{A_b(1+2\beta_b)}{I_b} & & & & \text{Symmetric} & \\ 0 & \frac{12}{L^2} & & & & \\ 0 & -\frac{6}{L} & 4+2\beta_b & & & \\ -\frac{A_b(1+2\beta_b)}{I_b} & 0 & 0 & \frac{A_b(1+2\beta_b)}{I_b} & & \\ 0 & -\frac{12}{L^2} & -\frac{6}{L} & 0 & \frac{12}{L^2} & \\ 0 & \frac{6}{L} & 2-2\beta_b & 0 & -\frac{6}{L} & 4+2\beta_b \end{bmatrix}\begin{bmatrix} X_1 \\ Y_1 \\ \theta_1 \\ X_2 \\ Y_2 \\ \theta_2 \end{bmatrix} = \begin{bmatrix} F_{X_1} \\ F_{Y_1} \\ F_{\theta_1} \\ F_{X_2} \\ F_{Y_2} \\ F_{\theta_2} \end{bmatrix}$$

where E_b = Young's modulus of the overburden element,

I_b = moment of inertia of the overburden element about the z axis,

L = length of the overburden element,

A_b = cross-sectional area of the overburden element,

$$\beta_b = 6E_b I_b/L^2\bar{A}_p G_b = 12I_b(1+\nu)/L^2\bar{A}_p),$$

$\bar{A}_p$ = effective area of the overburden element cross section ($5A_b/6$ for a rectangular cross section; see any elementary structures text),

G_b = shear modulus of the overburden element,

ν = Poisson's ratio.

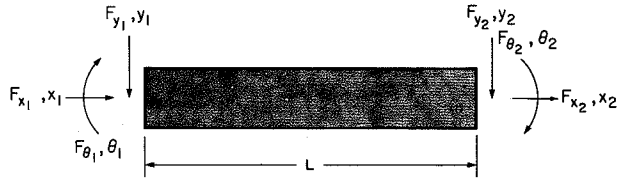

Fig. 3. Overburden element forces, displacements, and positive sign convention.
(XBL 809-1969)

Pillar Elements

The forces, displacements, and appropriate sign convention for a pillar element are illustrated in Figure 4. The force/displacement equations are:

$$F_{X_i} = \frac{12E_pI_p}{H_p^3(1+2\beta_p)} \cdot X_i - \frac{6E_pI_p}{H_p^2(1+2\beta_p)}\left(1 + \frac{H^b}{H_p}\right) \cdot \theta_i$$

$$F_{Y_i} = k\,A_p \left[\frac{Y_i}{H_p\varepsilon^*}\right]^N, \quad \text{for} \quad \frac{Y_i}{H_p} \leq \varepsilon^*$$

$$= A_p(C_o - k)\left\{1 - \exp\left[-\lambda\left(\frac{Y_i}{H_p} - \varepsilon^*\right)\right]\right\} + k\,A_p, \quad \text{for} \quad \frac{Y_i}{H_p} \geq \varepsilon^*$$

$$F_{\theta_i} = -\frac{6E_pI_p}{H_p^2(1+2\beta_p)}\left[1 + \frac{H_b}{H_p}\right] \cdot X_i + \left[\frac{4+2\beta_p}{1+2\beta_p}\right]\frac{E_pI_p}{H_p}\left[1 + \frac{3Hb}{4H_p}\left(2 + \frac{H_b}{H_p}\right)\right] \cdot \theta_i$$

where E_p = tangent modulus of the pillar at Y_p/H_p from Equation (1),

I_p = moment of inertia of the pillar about the z axis,

H_p = height of the pillar,

A_p = cross-sectional area of the pillar,

β_p = shear strain parameter for the pillar.

Equation 1 cannot be written in the form of Equation (2) directly due to the obvious nonlinearity. In other words, the stiffness of the pillar element depends explicitly on the vertical displacement of the pillar element. The solution procedure or numerical algorithm for the nonlinear equations is discussed later in this paper.

Room Element

The forces, displacements, and appropriate sign convention for the room element are illustrated in Figure 5. The force/displacement equations are identical to those of the pillar elements except that the subscript "p" is replaced with a subscript "r" indicating room material properties and geometry.

Numerical Algorithm

If the nonlinearity of Equation 1 did not exist, the element force/displacement relations (Equation 2) for each element in a given problem mesh or structure could be merely assembled by means of the direct stiffness method and the resulting set of equations solved. Mathematically:

$$[K]\ \{U\} = \{F\} \qquad (3)$$

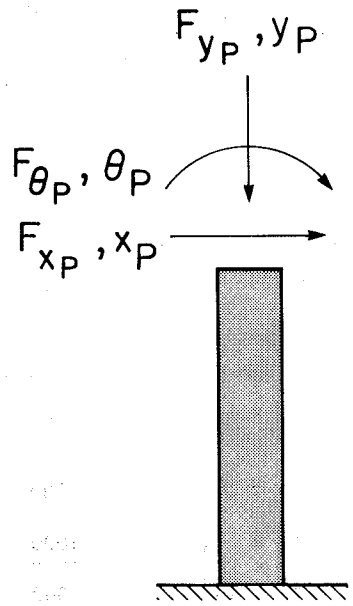

Fig. 4. Pillar element forces, displacements, and positive sign convention. (XBL 809-1978)

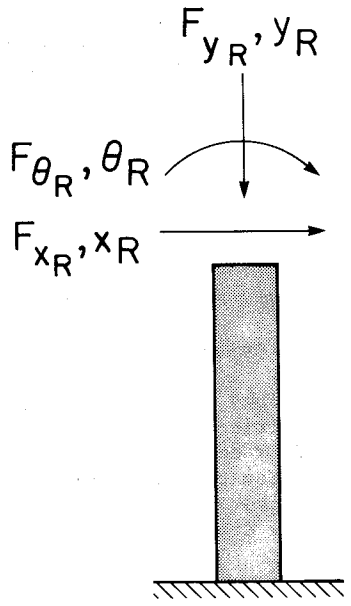

Fig. 5. Room element forces, displacements, and positive sign convention. (XBL 809-1970)

where $[K] = \sum_e [K^e]$,

$\{U\}$ = 1 by 3N vector of displacements at each of the N nodes,

$\{F\}$ = 1 by 3N vector of forces at each of the N nodes (typically gravitational forces vertically or those due to tectonic in-situ stresses horizontally).

However, due to the nonlinear equations, the solution procedure implied by Equation (3) is recast as:

$$[K] \left\{U_i\right\} = \{F\} - \left[K^* (U_{i-1})\right] \left\{U_{i-1}\right\}, \quad (4)$$

where $[K]$ = the stiffness of the structure consisting of the linear portion of the stiffness for all element types,

$\left\{U_i\right\}$ = 1 by 3N vector of displacements at iteration i,

$[K^*]$ = the nonlinear part of the stiffness of the structure evaluated for displacements at the i - 1 iteration.

The linear portion of the pillar and room stiffness is obtained by taking a power series representation of the exponential term of Equation 1. In this manner, the stiffness components for the room and pillar elements in the [K] matrix are calculated with the maximum tangent modulus (modulus at $\varepsilon = \varepsilon^*$). Therefore, the incremental displacement resulting at each iteration ($U_i - U_{i-1}$) is guaranteed to be a monotonically decreasing function of the number of iterations.

The iteration procedure of Equation 4 is repeated until a specified number of iterations has been performed or until a maximum relative tolerance on displacement change has been satisfied at every node. Relative tolerance for this program is defined as:

$$\text{Maximum} \left| \frac{U_i^j - U_{i-1}^j}{U_i^j} \right| \quad j = 1,2,3,\ldots,3N \quad (5)$$

where j = the displacement equation number,

i = the iteration number.

Equation (9) is solved with a direct solver for banded symmetric matrices. Repeated iterations are accomplished by continually reevaluating the right-hand side of Equation (4) and performing the appropriate load vector modification and back-substitution for the new displacements.

Results

The problem in retort design is to maximize the extraction ratio (fraction of land occupied by retorts, not including pillars) without exceeding allowable limits of subsidence, pillar stress, or overburden tensile stress. This year a series of computer model calculations was performed using retort and pillar geometry as shown in Figure 1; laboratory data for the mechanical properties of raw shale pillars; and various assumed properties for backfilled retorts (Table 1) corresponding to various grout formulas. Subsidence and induced tensile and compressive stresses in overburden and pillars were calculated for these cases, and various secondary extraction schemes (e.g., the retorting of pillars between grouted retorts) were modeled. The principal conclusions from these calculations are:

1. A grouted retort stiffness of 500 ksi (tangent modulus at zero strain) and an unconfined compressive strength of 1 ksi would allow total extraction of the resource under a prudent excavation and backfilling sequence. Grouted retorts of less stiffness would allow appropriately lower resource extraction.

2. The amount of resource extraction allowable under the assumed structural criterion is governed by overburden fracturing considerations.

3. Allowable extraction is based on the specific design (pillar width and retort width) used to obtain the extraction.

4. "Webbed" structurally connected pillars significantly reduce the tensile overburden fracturing which would exist if a conventional room-and-pillar mining plan were employed.

The results of some typical calculations are described here. Figure 6 shows the effect of varying grouted retort properties for a constant retort geometry. The effect of grouting to produce a stiffer grouted retort (greater E_R) is that the grouted retort takes more load, the pillars take less load and subsidence is reduced.

Table 1. Material properties used in model calculations.

Region	Modulus (E) (psi)	Compresive Strength (Co) (psi)
Overburden	2.35×10^6	a
Oil Shale Pillars	1.35×10^6	9500
Grouted Retorts	50×10^3	1000
	250×10^3	1000
	750×10^3	1000

[a]Value not used in model.

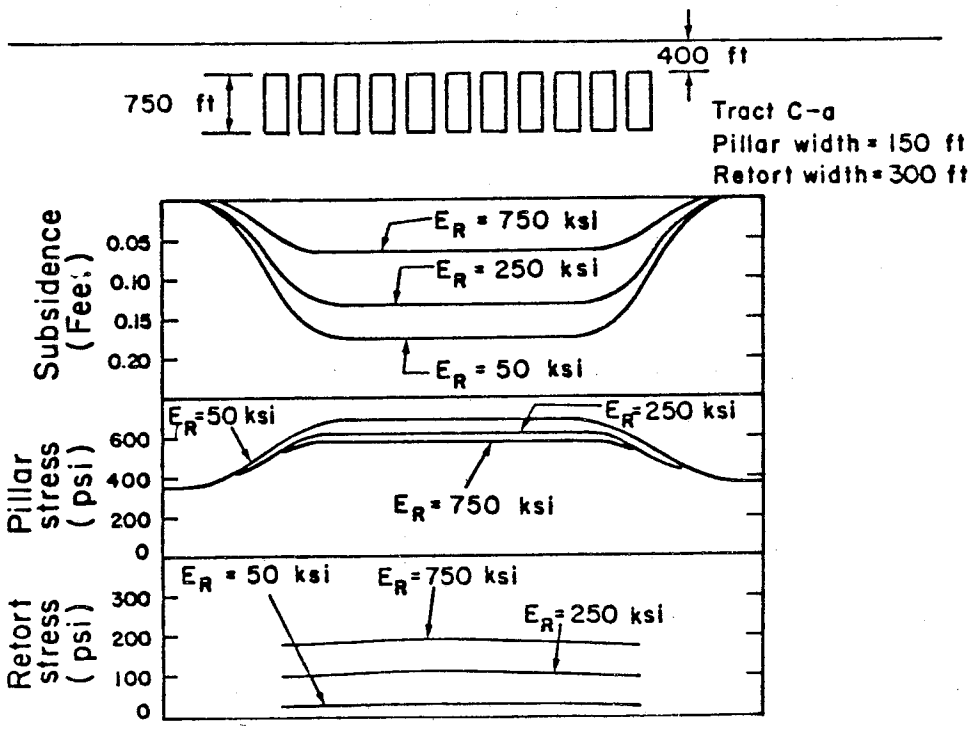

Fig. 6. Subsidence and stress in pillars and retorts for fixed geometry and three different grouted retort stiffnesses. (XBL 801-121)

Figure 7 shows the effect of varying retort dimensions (and thus extraction ratio) and grouted retort stiffness. Either pillar compressive stress or maximum overburden tensile stress can limit extraction. For examples, as shown in Figure 7, with a safety factor of 10 and no grout, pillar compressive stress limits extraction to under 40%. Grouted retorts with a stiffness of 250 ksi increase this to 46%, and grouted retorts with a stiffness of 750 ksi increase it to 74%. In these calculations, it is assumed that the retorts are grouted soon after pyrolysis; actual field calculations must take into account the time sequence of mining, retorting, and grouting.

PLANNED ACTIVITIES FOR FY 1981

Future efforts will consider the influence of the prevailing in-situ state of stress, thermal/structural effects, and the influence of discontinuities and the significance of three-dimensional structural effects.

REFERENCES

1. J. L. Ratigan, User Information Manual: SUBSID--A Non-Linear, Two-Dimensional, Finite Elemental Program for Status Evaluation of Mining Subsidence, Lawrence Berkeley Laboratory report LBL-11356, 1980.

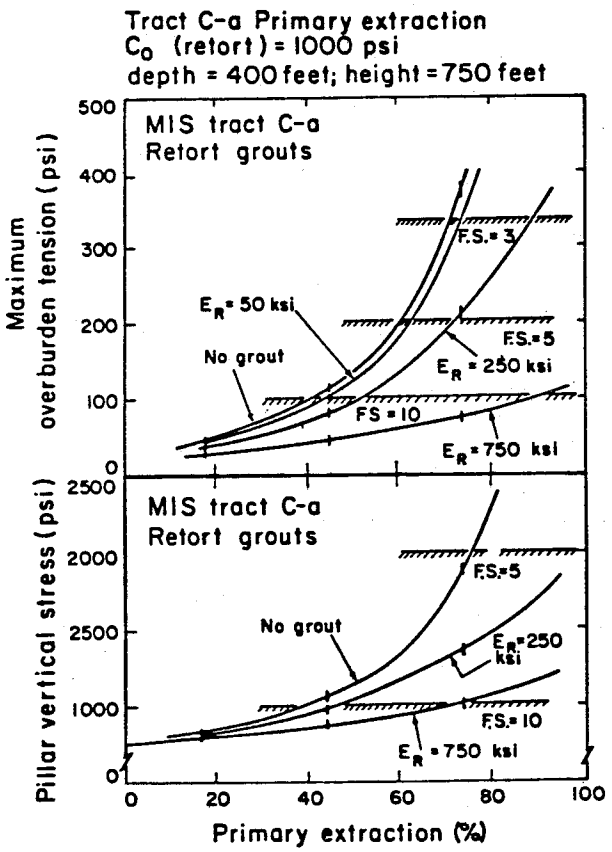

Fig. 7. Effect of factor of safety (FS) and stiffness (E_R) on extraction. Allowable extraction ratio is limited by maximum overburden tension or vertical pillar stress. Greater extraction is possible with stiffer grouted retorts. (XBL 801-119)

AN INVESTIGATION OF DEWATERING FOR THE MODIFIED IN-SITU OIL SHALE RETORTING PROCESS*

M. Mehran, T. N. Narasimhan, and J. P. Fox

INTRODUCTION

The Green River Formation of Colorado, Utah, and Wyoming is the largest and richest oil shale deposit in the world and is estimated to contain in excess of 600 billion barrels of high-grade recoverable oil. The C-a and C-b tracts (Fig. 1) of Colorado's Piceance Creek basin are potential sites for the development of oil shale by the vertical modified in-situ (VMIS) retorting process. This proposed exploitation on these two 5000-acre tracts may eventually require the disturbance of over 3 billion m^3 of oil shale to a depth of about 400 m below ground level. This disturbance, along with removal of water (dewatering), which is required to facilitate the mining operations and underground combustion, will result in the modification of groundwater flows, fluid potentials, and the chemical and thermal regimes of native groundwaters on an unprecedented scale. On retort abandonment, water will reinvade the area, leaching organic and inorganic chemicals from the spent shale into surrounding aquifers and eventually into surface waters. The potential environmental impacts of dewatering and reinvasion accompanying the VMIS process will include mining and depletion of groundwater supplies, reduced stream flows, increased salinity in surface water bodies, and contamination of the total hydrologic system by organic and inorganic pollutants leached from spent shale.

The purpose of this work is to investigate hydrogeological impacts of VMIS retorting using predictive, numerical modeling techniques. The dewatering and reinvasion processes at federal lease tracts C-a and C-b are investigated using an integrated finite difference model that incorporates saturated-unsaturated flow to carry out parametric studies and long-term simulations. This study extends earlier investigations in as comprehensive a manner as data permit. The geologic idealization of the hydrologic system is similar to that used by previous workers. However, we have incorporated greater physical detail in the form of unsaturated flow effects and complete interaction between various layers. The present study also seeks to identify, through a parametric approach, the key variables that are required to characterize systems such as those at the C-a and C-b tracts. This study is intended to provide insight into the relative importance of key hydrogeologic parameters and will eventually lead to the design of carefully controlled field experiments which will provide the critically required field data for long-term predictions.

*This work was supported by the Assistant Secretary for Environment, Office of Environmental Compliance and Overview, Environmental Control Technology Division and the Office of Technology Assessment of the U.S. Department of Energy under Contract No. W-7405-ENG-48.

ACCOMPLISHMENTS DURING FY 1980

The approach, conceptualization, assumptions, and significant findings of previous modeling efforts were reviewed.[1] The dewatering process through internal drainage was simulated by a numerical model that incorporated saturated-unsaturated flow under isothermal conditions. Two broad scenarios, namely, a fixed geometry retort and an expanding retort, were investigated. A sensitivity analysis of mine dewatering in an expanding retort was performed to examine the effects of saturation, hydraulic conductivity, material distribution, porosity, and anisotropy. For purposes of understanding possible long-term consequences, 30- and 60-year simulations of dewatering were carried out for the C-a and C-b tracts taking into account their respective rates of mine expansion. The results were compared with those of previous studies wherever such comparison was possible. The process of reinvasion was also simulated, but in a less comprehensive manner. The results of this study are summarized here. The methods used and a more detailed discussion of the results are presented elsewhere.[1]

Methods

The study area, the C-a and C-b tracts, is shown in Figure 1. The general stratigraphic succession on the tracts consists of the upper aquifer (including the alluvial zone), the confining layer, and the lower aquifer. The thickness of the flow region for the C-a and C-b tracts is taken to be 272 m and 690 m from the bottom of the lower aquifer to the average position of the water table, which is about 34 m and 100 m below the land surface, respectively. The locations of the upper aquifer, the Mahogany Zone, and the lower aquifer, and their thicknesses for the two tracts are given in Figure 2. As an initial condition, the flow region is assumed to be hydrostatic with hydraulic heads of 272 m and 690 m for the C-a and C-b tracts, respectively.

The flow region is idealized as a multilayered system of aquifers separated by aquitards (Fig. 2). Within this system, the expanding mine is represented as a disc-shaped opening which starts at the axis of symmetry of the flow region and extends radially outward (Fig. 3). The flow region is assumed to be bounded by impermeable zones and extends to a distance where no boundary effects are observed during dewatering. Seepage into the retorted region takes place through the upper surface, the lower surface, and the periphery of the disc-shaped volume. Water from the surrounding region drains into the mine at atmospheric pressure. As desaturation proceeds, water table profiles evolve in time and continually move downward.

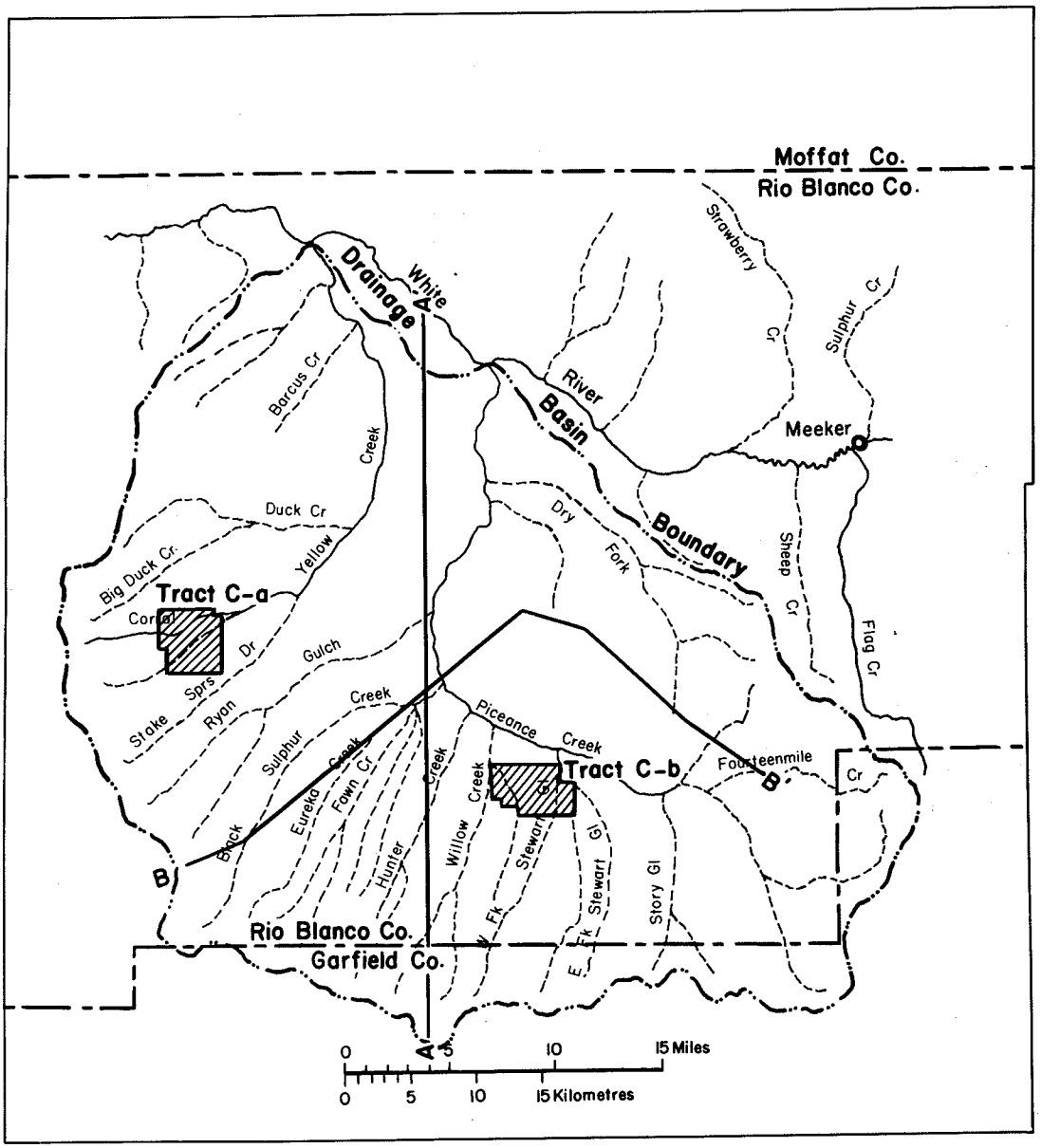

Fig. 1. Location of the Piceance basin and prototype oil-shale lease tracts C-a and C-b (after Weeks et al.[4]). (FXBL 8011-2286)

Simulation of the dewatering and reinvasion processes was carried out by a numerical model called TRUST, which is capable of solving transient saturated-unsaturated isothermal flow in one, two, or three dimensions for simple or complex geometrical configurations under various initial and boundary conditions[2,3]. Anisotropy of the media can be handled by the model by orienting volume elements in such a manner that their boundary surfaces are perpendicular to the principal direction of anisotropy.

Two broad scenarios were considered for the C-b tract. In the first, the retorted region was assumed to have a fixed geometry, while in the second, the geometry of the retorted region was allowed to vary with time. All of the parametric studies and the C-a tract simulations were done with a variable geometry.

Sensitivity Analyses

The cases we studied are summarized in Figure 4. In the first, using fixed geometry, it is assumed that a cavity the size of the area to be retorted is created without disturbing the flow pattern prior to simulation. (This case is not physically realistic and was modeled to facilitate comparison of our results with earlier work.) The inflow rate for a two-year simulation of dewatering in a retort of 500-m radius showed extremely high initial inflow rates which leveled out to less than 0.5 m^3/s after 10 months. The high initial rates were due to very high potential

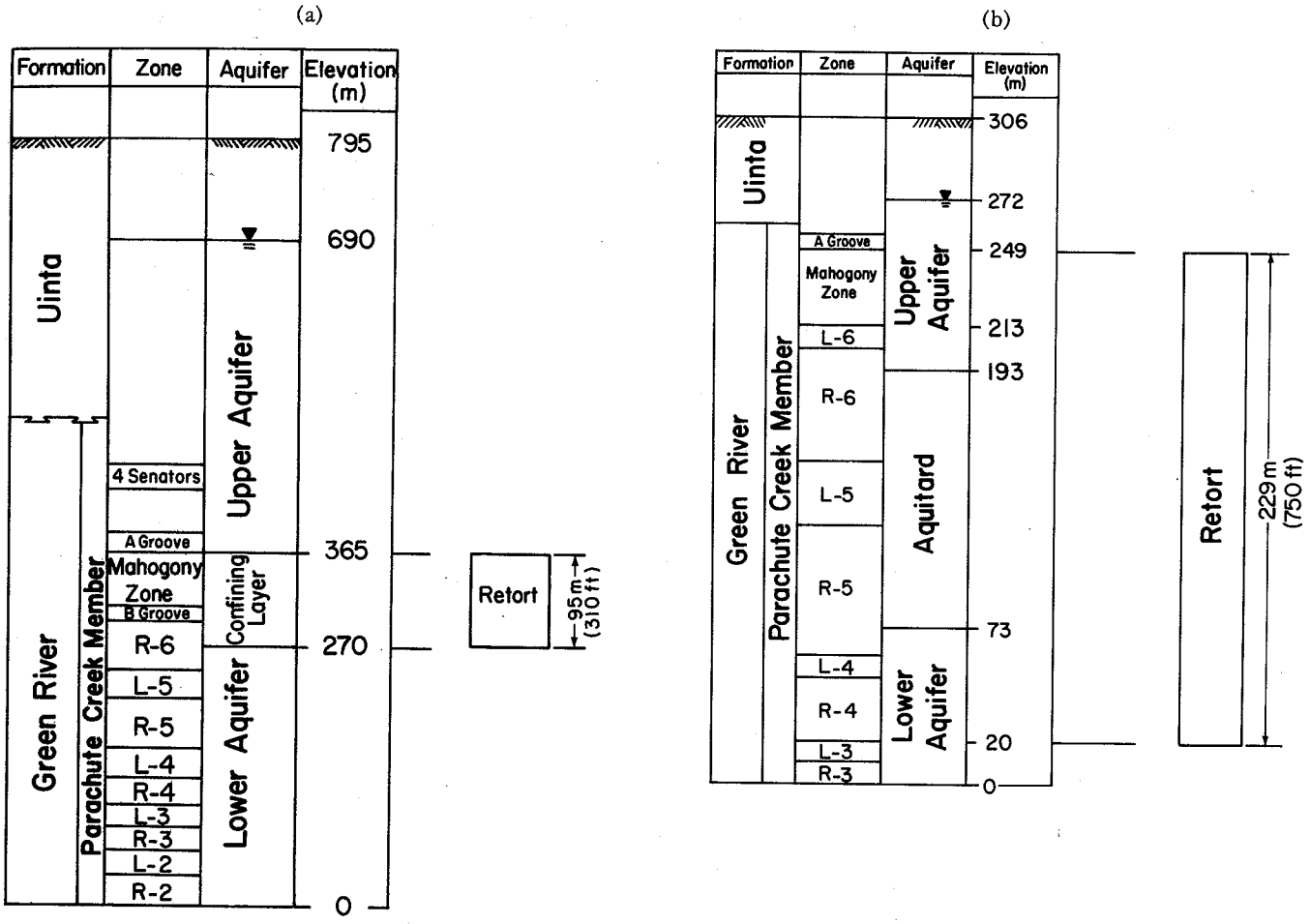

Fig. 2. Stratigraphy of the C-a and C-b tract and location of the mining zone used in model simulations. [(a) FXBL 8011-2306; (b) FXBL 8011-3310]

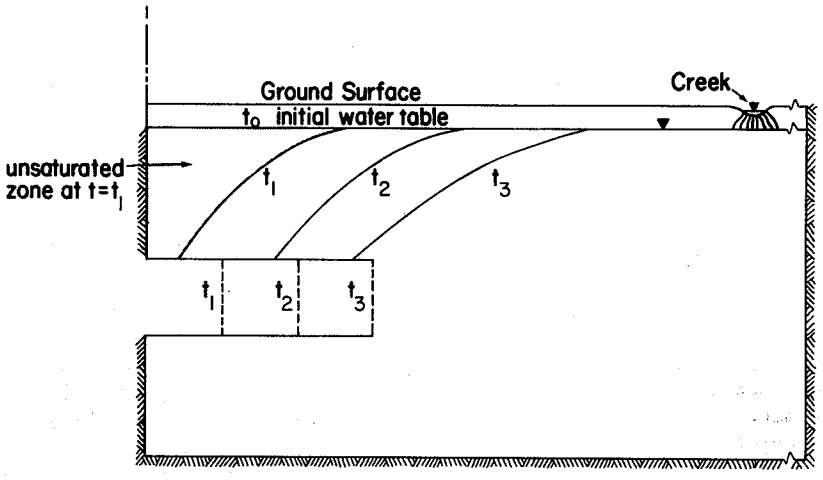

Fig. 3. Schematic diagram of the flow region, expanding retort, and hypothetical water table profiles. (FXBL 8011-2305)

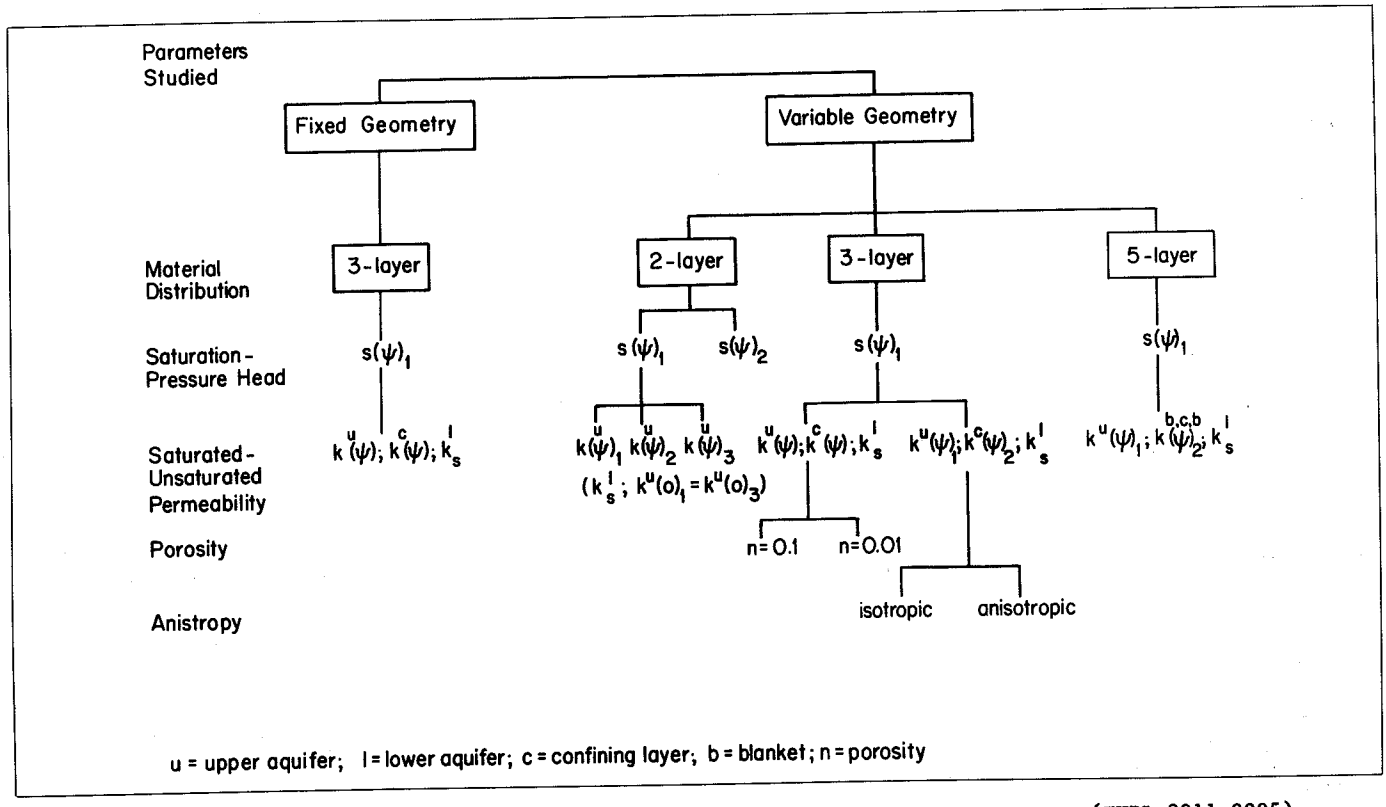

Fig. 4. Dewatering scenarios and cases considered for the C-b tract. (FXBL 8011-2295)

gradients at all boundaries at time zero. Subsequent reduction in inflow rate is due to desaturation of the upper aquifer located above the retorted region.

In the remaining cases, which use time-dependent geometry and are more physically realistic, the sensitivity of flow rates and pressure heads to hydrologic variables was studied. This approach was necessary due to a lack of adequate field and laboratory data to characterize the system. The sensitivity analyses included the examination of various properties and parameters of the flow region as follows: (1) degree of saturation and its pressure head dependency, (2) hydraulic conductivity and its pressure head dependency, (3) material distribution, (4) porosity, and (5) anistropy. These analyses suggest that, in general, higher hydraulic conductivities and isotropy will tend to increase mine inflows. The results of these analyses should help guide field and laboratory programs to better characterize the hydrogeological system.

Long-Term Simulations

For purposes of understanding possible long-term consequences of VMIS retorting, 30- and 60-year simulations were carried out for the C-a and C-b tracts for the expanding retort scenario, respectively. Pertinent input parameters are presented elsewhere.[1]

The C-b Tract

The variation of inflow rate for the 60-year life of the project at the C-b tract is shown in Figure 5. The expansion of the mine is the primary reason for the continuous but gradual increase in mine inflow rate, which peaks at 0.9 m^3/s. Assuming a production level of 50,000 bbl/day and a maximum water consumption of 6.6 bbl/bbl of oil, 0.62 m^3/s of the pumped water will be consumed on site. Therefore, the balance must either be reinjected into the ground, used for stream flow augmentation, or disposed of as waste. Considering the large drawdowns of the water table in the Piceance Creek vicinity (Fig. 6), the options of reinjection or stream flow augmentation appear desirable.

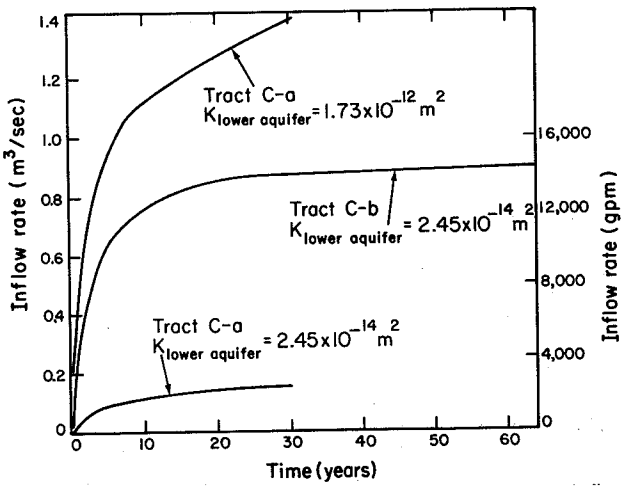

Fig. 5. Results of the long-term simulations at the C-a and C-b tracts in terms of mine inflow (dewatering) rate. (XBL 811-52)

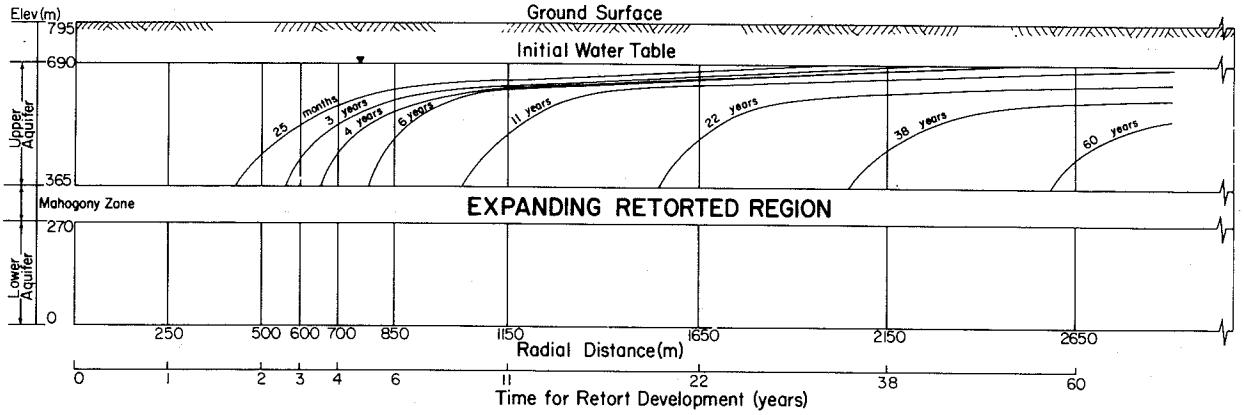

Fig. 6. The position of the phreatic surface for dewatering the C-b tract in an expanding retort scenario. (XBL 8011-2321)

These results show that large quantities of water must be pumped to the surface, which will require large quantities of energy. Assuming an approximate pumping rate of 1 m^3/s from a depth of 400 m, the power requirements at 50% efficiency will be about 8 MW.

As desaturation proceeds, the phreatic surface becomes dynamic and moves downward as shown in Figure 6. The periphery of the retorted region at various times is shown in this figure with corresponding positions of the phreatic surface. This figure demonstrates that almost always, the tail of the phreatic surface intersecting the roof of the retort lags the front of the mined region.

This, perhaps, can give an indication of the proper timing for burning the retorts. The model results show that the contribution of the unsaturated region of the upper aquifer to the overall inflow into the mine is substantial at the C-b tract primarily because of the large thickness of the upper equifer (Fig. 2). For the 60-year simulation, this contribution amounts to approximately 43% of the total flow. It is also shown that the effect of dewatering is reflected at distances far away from the center of the tract. The drawdown of the phreatic surface at 3.5 km from the center of the tract, which is the approximate location of the Piceance Creek, could be as much as 100 m or more after 60 years of dewatering.

The C-a Tract

The variation of inflow rates for a 30-year simulation of dewatering at the C-a tract is shown in Figure 5 using two saturated permeabilities for the lower aquifer. The smaller inflow rate reaches a value of 0.14 m^3/s at the end of 30 years. The larger inflow rate corresponds to the case where the transmissivity of the lower aquifer is assumed to be 87 m^2/day. The inflow rate in this case is about 10 times the previous case, indicating that the lower aquifer has a significant role in the dewatering operation at the C-a tract. This behavior is expected because, while the thickness of the upper aquifer is very small, the aquitard constitutes a large portion of the overall aquifer system. It is clear that since the contribution of the upper aquifer to the total inflow into the mine is small, the effect of porosity and unsaturated properties of the upper aquifer on flow rates would also be less significant.

Water use on the C-a tract during the commercial phase will be 0.0875 m^3/s. The results of this study show that even the lowest estimates of lower aquifer permeability can furnish more than the required water for consumption.

The drawdown of the water table at a radial distance of 5 km from the center of the tract (the approximate location of the waters tributary to Yellow Creek) for the high permeability case after 30 years of dewatering is estimated to be 31 m.

Reinvasion

Due to its environmental implications, the reinvasion of water subsequent to retort abandonment is one of the crucial aspects of the VMIS process. Reinvasion of water into the retorts could result in leaching of soluble chemical species from the spent shale and their transport to surrounding groundwater and surface water supplies. The hydrology of the aquifer system at the time of retort abandonment is further complicated by the thermal regime of the spent shale. Since water is the prime agent of chemical transport, it is essential that the hydrogeologic regime at retort abandonment be known before solute transport is studied. Therefore, understanding the flow behavior at retort abandonment is necessary before one can proceed with the analysis of reinvasion.

In the reinvasion analysis at the C-b tract, we assumed no change in hydraulic properties of the upper and lower aquifers at abandonment even though this is a gross simplification of the actual field conditions. Because of rubblization and oil recovery, it is assumed that the retorted region has a porosity of 30% to a radial distance of 2650 m while the remaining part of the confining layer maintains its original properties. Porosity increase will undoubtedly increase the hydraulic conductivity of the medium by many orders of magnitude. In our analysis, we have assumed that hydraulic conductivity is 10,000 times

greater than that of the confining layer. Furthermore, the retorted region is assumed to be near residual saturation.

The results indicate that reinvasion takes place primarily in the vicinity of the periphery of the retorted region because of the high conductivity of that region. Gradually, the water table rises along the bottom length of the retorted region, starting with the upper surface of the lower aquifer. This behavior prevents the invasion of water into the upper aquifer for decades and perhaps centuries. Therefore, one should expect the reinvasion process to be extremely slow due to the large volume of void spaces that have to be filled and the extremely low hydraulic conductivity due to very low saturation and to the hysteresis effect. Considering the uncertainties in the assumptions made in the reinvasion analysis, further work is required to arrive at realistic field data before we can draw any conclusions regarding the environmental impacts of the reinvasion process.

PLANNED ACTIVITIES FOR FY 1981

This work will be extended in 1981 to include more detailed investigations of the reinvasion process and to evaluate the effect of various control strategies on fluid potentials and pressure heads.

REFERENCES

1. M. Mehran, T. N. Narasimhan, and J. P. Fox, An Investigation of Dewatering for the Modified In-Situ Retorting Process, Piceance Creek Basin, Colorado, Lawrence Berkeley Laboratory report LBL-11819, 1980.

2. T. N. Narasimhan and P. A. Witherspoon, "Numerical Model for Saturated-Unsaturated Flow in Deformable Porous Media: 1. Theory" Water Resources Research, vol. 13, no. 3, 1977 pp. 657-664.

3. T. N. Narasimhan, P. A. Witherspoon, and A. L. Edwards, "Numerical Model for Saturated-Unsaturated Flow in Deformable Porous Media: 2. The Algorithm," Water Resources Research, vol. 14, no. 2, 1978 pp. 255-261.

4. J. B. Weeks, G. H. Leavesley, F. A. Welder, and G. J. Saulnier, Jr., Simulated Effects of Oil Shale Development on the Hydrology of Piceance Basin, Colorado, U.S. Geological Survey Professional Paper 908, 1974.

A MATHEMATICAL MODEL FOR LEACHING OF ORGANIC CARBON FROM IN-SITU RETORTED OIL SHALE

W. G. Hall, R. E. Selleck,[†] and J. F. Thomas[†]

INTRODUCTION

The rich oil shale deposits in Colorado's Piceance Creek Basin are being considered for early commercialization by vertical modified in-situ retorting (VMIS). In this process, large underground chambers of oil shale, several hundred feet in cross section and up to 700 feet in height, are pyrolyzed in place. This type of processing may result in low resource recovery and in several environmental problems, including leaching of retorted shale and subsidence. These problems were described in last year's report.[1]

One of the major environmental concerns is leaching of the retorted shale. Most of the rich oil shale deposits in the Piceance Creek Basin are laced with groundwater aquifers. During in-situ retort preparation and retorting, groundwater levels adjacent to the development site are lowered below the retorts by pumping. After oil recovery is complete, the returning groundwater may pass through the spent underground chambers and leach out soluble organic and inorganic materials. These materials may be transported in surrounding aquifers where they may be withdrawn from wells or discharged to local springs and streams.

Several methods have been proposed to solve these problems.[1] These include grouting, intentional leaching, and various hydrologic modifications. The purpose of this program, initiated in June 1978, is to investigate selective leaching as a means of minimizing the impact of abandoned in-situ retorts on local water quality. In this approach, water would be injected into the retort, collected, and treated in a surface facility. This appears feasible because experimental work revealed that most of the leachable material is readily removed with a few pore volumes of water.

The approach we are using is to first define the kinetics of leaching of inorganic and organic compounds from spent shale by using data collected from batch and column leaching experiments. The

*This work was supported by the Environmental Protection Agency and by the Assistant Secretary for Environment, Office of Environmental Compliance and Overview, Environmental Control Technology Division and Assistant Secretary for Fossil Energy, Deputy Assistant Secretary for Oil, Gas, and Shale Technology, Office of Oil Shale of the U.S. Department of Energy under Contract No. W-7405-ENG-48.

[†]University of California, Berkeley, Calif.

kinetic data is then incorporated into a mathematical model of the leaching and transport processes. This model may then be used to predict the movement of leached organic and inorganic compounds through the in-situ retort and into the surrounding aquifers. The resulting model will be used to predict the number of pore volumes that must be treated to produce a leachate with a sufficiently low concentration of organics and inorganics.

ACCOMPLISHMENTS DURING FY 1980

This year we conducted additional batch and continuous-flow column leaching experiments to develop kinetic constants for use in the leaching and transport model, and we initiated analyses to develop a mathematical model of the leaching process. This work is summarized here.

Mass Transport Equations

Water passing through a bed of spent shale leaches out soluble material and transports it through the pores of the bed. The solute is a complex mixture of organic and inorganic compounds. Since the modeling of multicomponent mass transfer and diffusion is beyond the scope of this study, it is assumed that the organic portion of the solute can be characterized by total organic carbon (TOC) and the inorganic portion by electrical conductivity (EC). Both of these parameters are easily measured.

The leaching and transport of the solute, EC and TOC, can be modeled by a mass transport rate equation:

$$\frac{\partial C}{\partial t} = -u_{pore}\frac{\partial C}{\partial z} + D\frac{\partial^2 C}{\partial z^2} + r_r - \frac{\partial q}{\partial t}\cdot\frac{\rho_B}{\varepsilon} \qquad (1)$$

in which:

C = concentration of solute in the liquid phase

t = time

u_{pore} = velocity of the liquid phase in pores of the media

z = distance along column

D = dispersion coefficient

r_r = rate of chemical reaction

q = concentration of solute in the solid phase

ρ_B = bulk density

ε = porosity of shale bed

The terms on the right side of the equation are the contributions to the net change of the solute concentration with time due to convection, dispersion, chemical reaction, and mass transfer. The chemical reaction term is neglected since it is assumed that TOC and EC are conservative. The mass-transfer term is coupled with an equation describing the transfer of solute between the solid and liquid phases as follows:

$$\frac{\partial q}{\partial t} = KaF(C,q) \qquad (2)$$

in which:

a = interface area between phases

K = mass transfer coefficient

$F(C,q)$ = driving force expressed as a difference between equilibrium and actual solute concentrations in solid or liquid phases.

In the application of Equation 2, we are following the approach of Amy.[2] Mass transfer between phases may be represented by a series of equations similar to Equation 2, each one in the series applicable to the movement of solute in a particular domain. These domains include the solid shale, pores within the solid boundaries, and interfaces between solid and liquid phases. It is likely that the overall mass transfer will be dominated by transfer within a single domain, such as movement through the solid phase. Investigations are directed toward the determination of the dominant domain and the development of an overall mass transfer coefficient applicable to the total movement of solute from the solid to liquid phase.

Leaching Experiments

Batch and column leaching experiments were performed on two types of spent shale. The first, S-55, was produced in the Laramie Energy Technology Center 10-ton simulated in-situ retort in Wyoming. The raw shale was mined at Anvil Points, Colorado, and had an oil content of 26 gal/ton. The maximum temperature reached in the retort was 640°C and the retorting rate was 0.93 m/day under a 67%/33% air/steam atmosphere. The second type, L-2, is from Lawrence Livermore Laboratory's (LLL) 7-ton simulated in-situ retort. The raw shale was mined at Anvil Points, Colorado, and had an oil content of 24 gal/ton. The maximum retorting temperature was 915°C and the retorting rate was 1.8 m/day under a 47% /53% air/steam atmosphere.

Column leaching experiments are being conducted in lucite columns, 11.5 cm in diameter by 1.3 m in length. Distilled water is pumped to a column containing a bed of packed shale. Taps are located at 15-cm intervals so that leachate samples can be withdrawn. A schematic of the column is shown on Figure 1. Twenty-eight runs in these columns have been completed. At the completion of the small column studies, additional runs will be made in steel columns, 30.5 cm in diameter by 3.0 m in length.

The small column experiments are conducted in two parts. In the first part, a column packed with spent shale is filled with water and allowed to set for two hours so that the TOC levels in the leachate reach quasi-equilibrium with the shale. Water is then moved downward through the shale. Downward flow minimizes the effects of

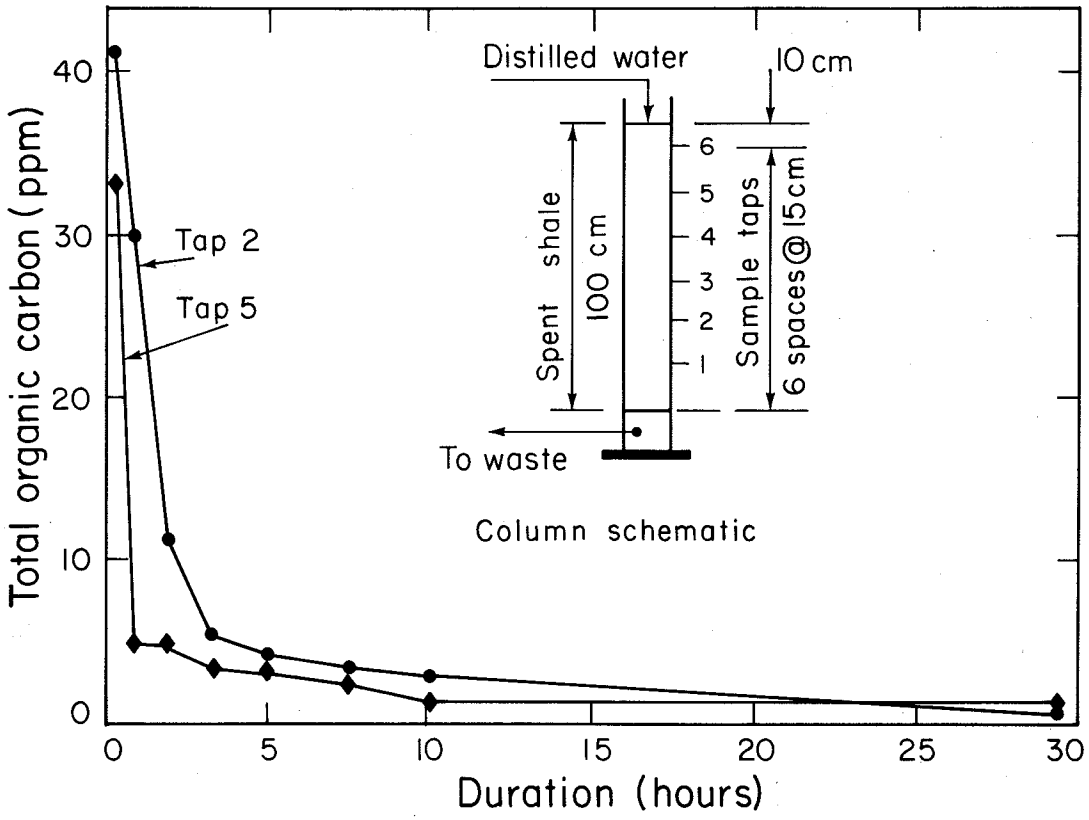

Fig. 1. Results of a typical, small-column leaching experiment. (XBL 811-51)

density currents caused by differential salt concentrations created in the leachate during passage through the bed.[3] Flow is continued until the TOC concentrations in the effluent reach 1 ppm. At this point, the second part of the experiment is started. The flow is stopped and the TOC allowed to build up in the leachate that quiescently remains in the pores.

Typical results from a small column experiment are shown in Figures 1 and 2. This particular column was packed with -1/2 to +1/8 inch S-55 spent shale having a porosity of 58%. A pore velocity of about 13 m/day was maintained. Pore velocities in these investigations ranged between 1.5 and 13 m/day. TOC concentrations versus time are plotted on Figure 1 for two of the six sample taps. Note that tap 5 corresponds to 25 cm of leachate travel and tap 2 corresponds to 70 cm. Effluents from both taps show a rapid decrease of TOC with time. Concentrations at tap 5 decrease more rapidly at first than do those at tap 2. Similar results are observed at other taps, i.e. the shorter distance of leachate travel at any time and the greater the time at any distance, the lower the TOC concentration.

These results appear reasonable. The transfer of mass between the phases is governed by Equation 2. As fresh fluid enters the column, it first comes in contact with the solute on the surface of the particles in the upper portion of the bed. The driving force, F(C,q), is high and the rate of mass transfer is high. As the leachate passes through the bed and the concentration of solute rises, the driving force decreases and the rate of transfer drops. Since the amount of readily leachable TOC on the surface of the shale is limited, there is also a drop of concentration with time at any point along the column length. Results similar to those shown in Figure 1 have been obtained for other pore velocities. The rate of mass transfer between phases, however, varies with the pore velocity as indicated by Equation 1.

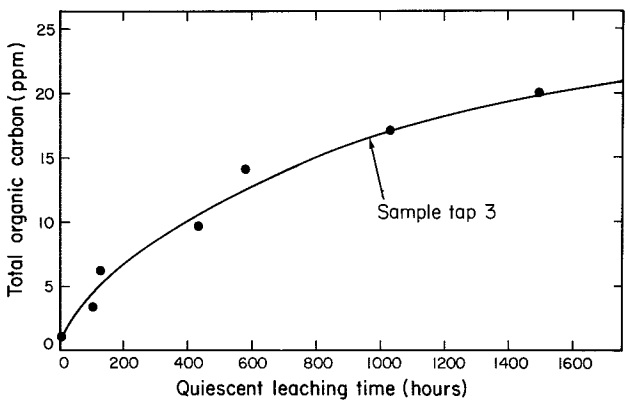

Fig. 2. Results of a quiescent leaching experiment. (XBL 811-48)

Part 2 of the experiment is designed to investigate the movement of solute within the solid boundaries of the solid phase. The leachate in the column pores remains in contact with the spent shale. If one assumes that all of the surface TOC on the particles has been removed by the moving leachate, then any increase in the TOC in the fluid must be due to solute moving to the phase interface from within the solid. A graph of the increase of TOC in the leachate at sample tap 3 is shown in Figure 2. The TOC concentration increases at a slowly decreasing rate toward an equilibrium level slightly above 20 ppm. This equilibrium level is consistent with other experiments in which samples of leached spent S-55 shale and leachate have been stored in flasks for about 18 months. Concentrations in the range of 20 to 25 ppm were measured in leachate samples from these latter experiments.

As Figures 1 and 2 indicate, two separate leaching mechanisms occur over time. First, there is the rapid removal of TOC from the surface of the shale particles (Fig. 1). Second, there is a slow transfer of TOC at the phase interface which has migrated from sites within the particle (Fig. 2). The impact of the latter mechanism on the proposed intentional leaching of abandoned in-situ retorts could be significant. Implicit in the plan to collect and treat leachate from the retort is that a large amount of the leachable material must be removed and treated in a short period of time. The operation of a treatment facility over a long period of time to remove relatively small concentrations of TOC and other pollutants attributable to internal migration from leachates could have a decidedly adverse impact on the proposal's feasibility. Both mechanisms will be incorporated in the leaching and transport model under development.

PLANNED ACTIVITIES FOR FY 1981

Work planned for the next fiscal year includes the completion of the small and large column studies, the incorporation of kinetic data into the transport model, and the completion of the investigation.

REFERENCES

1. P. Persoff and J. P. Fox, "Control Strategies for Abandoned In-Situ Oil Shale Retorts," Energy and Environment Division Annual Report 1979, Lawrence Berkeley Laboratory report LBL-10486, 1980.

2. G. L. Amy, Contamination of Groundwater by Organic Pollutants Leached from In-Situ Spent Shale, Ph.D. dissertation, Department of Civil Engineering, University of California at Berkeley, 1978.

3. W. G. Hall, R. E. Selleck, and F. Thomas, "A Mathematical Model for Leaching of Organic Carbon from In-Situ Retorted Oil Shale," Energy and Environment Division Annual Report 1979, Lawrence Berkeley Laboratory report LBL-10486, 1980.

TREATMENT OF WASTEWATER FROM MODIFIED IN-SITU OIL SHALE RETORTING*

B. M. Jones, R. H. Sakaji, and C. G. Daughton†

INTRODUCTION

Two unique types of wastewater are generated during oil shale retorting (Fig. 1). These wastewaters are produced from combustion, mineral dehydration, steam input, and often, groundwater inflow during retorting. The first kind of wastewater, retort water, is condensed and collected with the oil as an emulsion and is later separated from the oil by heat treatment and decantation. Retort water contains a complex spectrum of organic and inorganic compounds and would require extensive treatment prior to reuse. The second waste stream, gas condensate, results from the condensation of water vapor and inorganic gaseous species (e.g., NH_3, SO_2, H_2S, and CO_2) in a condenser train or in gas-scrubbing systems. Both gas condensate and retort water are produced in large volumes and have proven to be difficult and costly to treat. Successful development of a commercial oil shale industry in a semiarid region of the U.S. may depend on the effective treatment of these wastewaters for industrial reuse.

In a commercial in-situ operation, the retort water and gas condensate will be collected and treated separately because of their different compositions. The relative properties and compositions of each type of water depend on the geographic locale of the shale deposit, gas exit temperature, and product collection system design and operation. Combined production of these two waters is from 0.1 to 22 bbl of water/bbl of oil. A 5×10^5 bbl/day plant (roughly 6% of the 1977 U.S. crude oil production) would generate from 2×10^6 to 500×10^6 gal of these highly contaminated wastewaters per day.

Retort waters are characterized by their odoriferous and intensely colored organoleptic qualities and by high levels of inorganic and organic constituents, which include NH_3, $SO_4^{=}$ carbonates, carboxylic acids, and organonitrogen compounds. The gas condensate, which leaves the retort as steam, contains lower concentrations of most organic and inorganic species and higher concentrations of dissolved gases (e.g., NH_3 and CO_2) than does retort water.

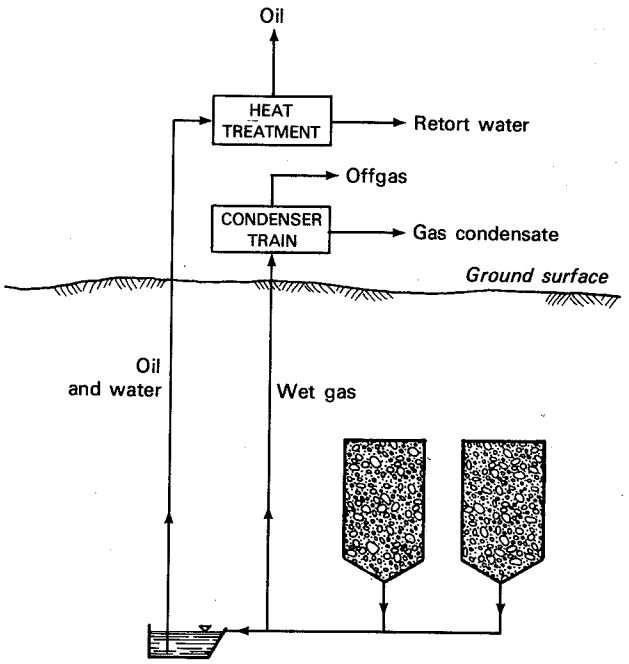

Fig. 1. Schematic showing the production of retort water and gas condensate during in-situ retorting. (XBL 804-739)

The purpose of this program, initiated in June 1978, is to develop treatment systems capable of upgrading gas condensate and retort water for on-site reuse. Emphasis is on the modification of, and novel approaches to, standard treatment technology (physical, chemical, and biological processes) to upgrade the wastewaters by the most economical means. Experimentation has included determining the feasibility of such novel schemes as the use of co-generated solid wastes as treatment agents.

ACCOMPLISHMENTS DURING FY 1980

This year we continued our work to develop a treatment system for retort waters. We further investigated coagulation-flocculation and initiated studies on a novel method, foam fractionation, to remove suspended materials from retort waters. We also investigated the biological oxidation of organic compounds in retort waters. These studies are summarized here.

Coagulation-Flocculation Studies

The objective of coagulation-flocculation in wastewater treatment is to enhance the settling

* This work was supported by the Assistant Secretary for Environment, Office of Environmental Compliance and Overview, Environmental Control Technology Division of the U.S. Department of Energy under Contract No. W-7405-ENG-48.

† Sanitary Engineering Research Laboratory, University of California, Berkeley, California.

characteristics of discrete colloidal particles by promoting their aggregation into larger, tightly packed aggregates with higher sedimentation velocities. Colloidal particles remain in suspension because of their high surface charge. This surface charge must be reduced to bring about particle aggregation or flocculation. This may be done by the addition of electrolytes, polymers, or chemicals that form hydrolyzed metal ions, i.e., alum and ferric hydroxide.

Previous attempts to remove oil and grease using coagulation-flocculation met with limited success. The proper interpretation of these initial results was severely hampered by the lack of accurate methods to quantitate oil and grease and to determine optimum coagulant dosage. This year, we have resolved some of these analytical problems[1] and have continued to investigate the nature of the colloidal system in retort waters. These investigations have led to the development of a method to screen coagulants by measuring the surface charge associated with the colloidal particles.

Colloids in aquatic systems do not exist in isolation but are surrounded by four distinct layers of various ionic compositions. The first layer on the colloid surface is usually negatively charged because of the preferential adsorption of anions. The second, the double layer, is a tightly held layer of counter ions. These ions are drawn to the surface by electrostatic attraction and distributed uniformly over the colloid surface by Brownian motion. The double layer reduces the surface charge of the colloid. This allows the balance of the counter ions required to neutralize the surface charge to be held in a third or diffuse layer. The diffuse layer extends from the double layer to a point where the surface charge of the colloid no longer exerts an electrostatic effect. The bulk solution or fourth layer exists beyond this point.

The region between the tightly held and diffuse portions of the double layer is called the "zone of slippage." Electric potential or Zeta Potential, is a function of the charge of the diffuse double layer and the distance of the diffuse double layer from the colloid surface. The particle velocity or electrophoretic mobility (EM) is a function of the Zeta Potential. By measuring the EM of the colloids, we have shown that the colloids in retort water are negatively charged.

Samples of diluted and undiluted retort water from two simulated in-situ retorts (Laramie Energy Technology Center's 10-ton and 150-ton retorts) and a modified in-situ field experiment (Occidental Retort No. 6) were analyzed with a Zeta Meter. The EM as a function of dilution for Oxy-6 retort water is shown in Figure 2; this curve is similar to those for 10-ton and 150-ton retort waters. These results indicate that in an undiluted system the particles have a negative EM; the absolute value for EM increases with dilution. The decrease in EM at higher dilutions is due to the suppression of the diffuse double layer caused by an influx of counter ions. This is best illustrated by the negative correlation between specific conductance and EM (Fig. 2).

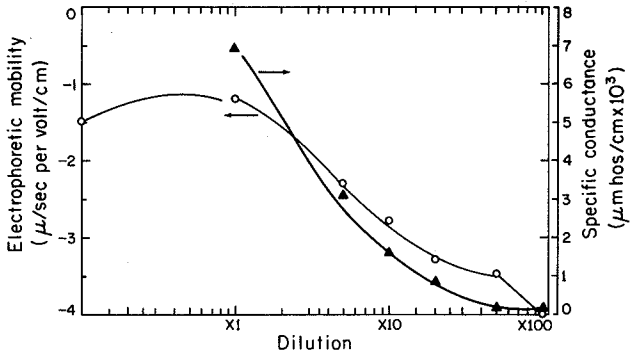

Fig. 2. Electrophoretic mobility of colloids in Occidental retort water at 25° C. (XBL 811-49)

These results indicate that colloids in retort water can be coagulated with a cationic polymer or a metal salt. Addition of a cationic organic polymer to the retort water colloidal suspension will decrease the EM of the particles by sorption of the polymer onto the negatively charged particles. This will allow the particles to floc. Figure 3 shows the decrease of EM with increasing polymer dosage. The EM for this system approached zero for polymer concentrations in the range of 20 to 40 mg/l. At higher polymer dosages, the EM was reversed. Because of analytical problems[1] associated with the oil-and-grease test and the turbidimeter, we could not verify that the point of zero EM corresponded to the optimum coagulant dosage for this system.

The ability to neutralize particle charge may find use in many physical-chemical treatment processes including suspended solids and oil-and-grease removal. The use of coagulants for reducing the surface charge and improving agglomeration may be useful in foam fractionation.

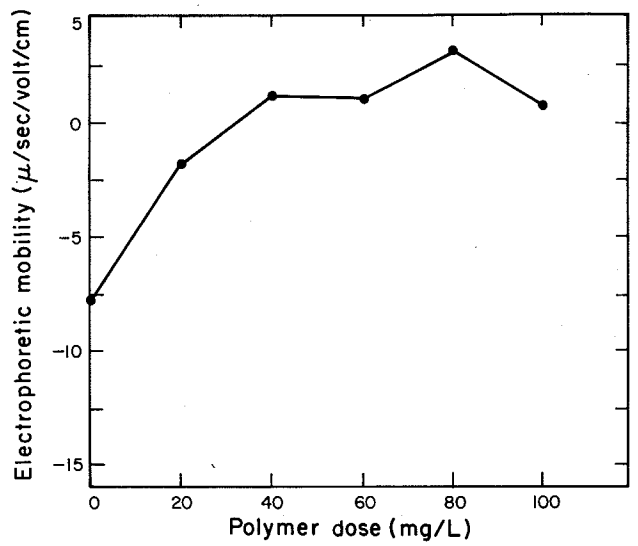

Fig. 3. Reduction of particle electrophoretic mobility of 150-ton retort water by an organic polymer (Tretolite 398). (XBL 811-55)

Foam Fractionation

Surface-active compounds are concentrated at air-water interfaces in accordance with the Gibbs equation, which relates change in surface tension to the interfacial concentration of solute. Surface tension is decreased by concentration of the solute at the phase interface because the solvent has less affinity for the solute molecules than for the solvent molecules themselves. Concentration of solutes at the air-liquid interface results in an overall decrease in the amount of work required to overcome the surface tension of the fluid, i.e., a reduction in surface tension. This reduction facilitates foam production during submersive aeration and therefore increases the surface area of the air-liquid interface.

The retort waters contain large quantities of hydrophobic organic compounds that are amenable to concentration at an air-water interface, and have a great propensity to foam. Submersive aeration easily creates copious quantities of foam which greatly increases the water-air surface area of the retort water. Suspended solids and surface-active organic materials can be removed with the foam by this process which we call "foam fractionation." The overall effect of foam fractionation is to reduce the concentrations of organic solutes and suspended solids in the wastewater by concentrating them in a sidestream of condensed foam (foamate). The reduced volume and elevated solute concentrations in this sidestream may make the treatment and disposal of retort water easier.

An initial batch study was conducted to evaluate the feasibility of this proposal. A 300-ml sample of 150-ton retort water was placed in a gas wash-bottle, and the impinger inlet was connected to a metered humidified air supply. The water was aerated for five minutes, and the foamate and residual liquid volumes were collected, measured, and analyzed for suspended solids, chemical oxygen demand (COD), and ammonia.

Three separate runs at different air-to-liquid ratios show that COD and suspended solids concentrations increased in the foamate by 10 and 22%, respectively. These results are preliminary and the optimum gas-to-liquid ratio has not been determined. These results were encouraging, and future foam fractionation studies will include the evaluation of organic polymers to improve colloid removal.

Biological Treatment

The removal of organic substances is presently the major technical constraint to developing a system to upgrade retort water. This subject has received more study than any other in the treatment arena, and results have been generally disappointing. This is attributed to the unique and complex nature of retort waters. They consist of a complex mixture of hundreds and perhaps thousands of organic compounds including organonitrogen compounds such as pyridines, quinolines, and anilines; carboxylic acids; aliphatic hydrocarbons; and many others. Dissolved organic species are conventionally removed by biological oxidation, solvent extraction, or chemical, wet air, or electrolytic oxidation. Biological treatment is usually the favored process because it is cost effective and reduces organic molecules to benign gases and a cellular mass which can be concentrated and landfilled. Accordingly, a considerable amount of research has been conducted on biological treatment of retort waters.

Exploratory studies[2] of biological oxidation by other investigators have indicated that up to 50% reduction in organic carbon can be achieved with long hydraulic and mean cell residence times, pH adjustment, ammonia removal, and nutrient addition. These removals can be improved somewhat by the addition of powered activated carbon to the aeration basin. Limited organic solute removal and poorly settling floc observed in these studies will limit the commercial application of this process and suggest that system performance is limited by a toxicity problem or by the presence of significant amounts of biorefractory organic compounds.

Preliminary results from experiments we have conducted to evaluate the use of biological oxidation to remove organic compounds from retort waters have largely agreed with those previously reported by other investigators.[2] We have carried our work several steps further than others, however, and are endeavoring to understand the biochemical processes that occur during the biological oxidation of organic compounds in retort water. We are seeking scientific explanations for the previously noted poor performance of biological oxidation. This work has led to the development of a conceptual model of the biological oxidation of organic substrates in retort waters that successfully explains our early preliminary results with this process. Some of our preliminary work is described here.

Problems with biological oxidation could result from several factors including:

1. Osmoregulation. The addition of large amounts of acid, required for control of culture pH, increases the ionic strength of the water and may stress the cellular membrane integrity.

2. Toxicity. The organisms may produce a metabolite that accumulates to toxic concentrations. Certain indigenous solutes may also elicit toxicity of their own.

3. Refractory organic compounds. The residual COD or dissolved organic carbon (DOC) may be recalcitrant to biological oxidation.

4. Nutrient limitation. The growth of microorganisms may be limited by the depletion of essential nutrients or the unavailablity of these nutrients.

We have conducted batch culture experiments to determine which of these factors may limit biological oxidation of retort waters. Accurate analytical methods, described elsewhere in this report,[1] were developed to monitor these cultures.

Protein production was used as a direct measure of biological growth. Turbidity and suspended solids were used as a facile and rapid indication of growth for more routine analyses.

A sample of 150-ton retort water, pretreated with CaO to raise the pH and aerated to reduce the high ammonia concentration, was used as a culture medium. A mixed culture, obtained from soil and activated sludge by enrichment on and acclimation to retort water, was used to inoculate the medium. Substrate concentration, as soluble COD (SCOD), and growth (suspended solids and protein) were monitored for 10 days. The results are plotted as a function of time in Figure 4. Microbial growth, as indicated by an increase in suspended solids concentration, did not begin until the second day of the experiment. This lag phase was a reflection of both the poor detection limit of the suspended solids test and the stationary growth phase of the inoculum. Following lag phase, the suspended solids concentration increased exponentially, reached a brief plateau, and then underwent another exponential increase before reaching a stationary phase.

The SCOD concentration decreased 12% during the first six hours following inoculation. This initial decrease was followed by a steady increase in SCOD for the remainder of lag phase and the first exponential growth phase. During the first brief plateau in growth, a decrease in SCOD was observed, and this decrease continued through the second exponential phase until the SCOD reached a constant value (19% lower than the initial value).

The increase in SCOD above initial levels and the plateau in the growth curve with the concomitant decrease in SCOD were the most interesting results from this study. Microbiological alteration of non-COD yielding compounds in retort water to compounds which yield a COD could explain the observed increases in SCOD. The plateau between the two regions of exponential growth could have many explanations. The growth curve for a mixed culture is not necessarily the simple exponential curve of a pure culture. The growth curve generated by a mixed culture is a summation of different growth curves from all of the populations. Therefore, changes in slope, or multiple plateaus, such as seen here, should not be surprising. These results could be explained by one or several of the following possibilities: (a) Compounds that were recalcitrant to degradation during the initial growth were consumed by a new population of bacteria; (b) Metabolites that were released during the first growth phase were utilizable by a new group of bacteria; (c) The initial populations of bacteria were undergoing diauxic growth.

Substrate removal, as measured by SCOD, did not exceed 20%. As a result, we decided to investigate one of the possibilities for limitation of removal (i.e., toxicity). Two retort waters, 10-ton (S-55) and Oxy-6, were used for these initial studies because their low ammonia concentrations allowed their use without chemical alteration to facilitate ammonia stripping. A group of culture flasks containing serially diluted raw retort water were inoculated with an acclimated mixed microbial community that originated from soil extracts and activated sludge. The flasks were brought to a constant volume (30 ml) with phosphate buffer and supplemented with essential micronutrients. The cultures were incubated at 30°C and then assayed for protein concentration.

The results of this initial study (Fig. 5) showed that the yield of protein (μg of protein per ml of retort water) decreased with increasing concentrations of retort water. The decreasing yields may be the result of toxicity. These studies will continue in order to elucidate the problems associated with degradation of recalcitrant organic species in retort waters.

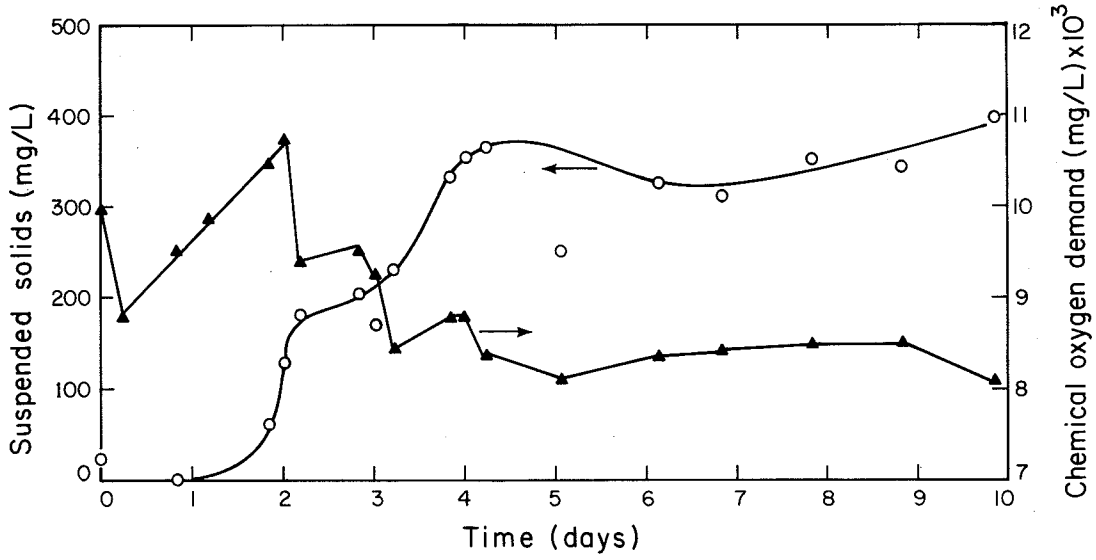

Fig. 4. Microbial oxidation of 150-ton retort water, pretreated with lime and air-stripped to remove ammonia. (XBL 811-57)

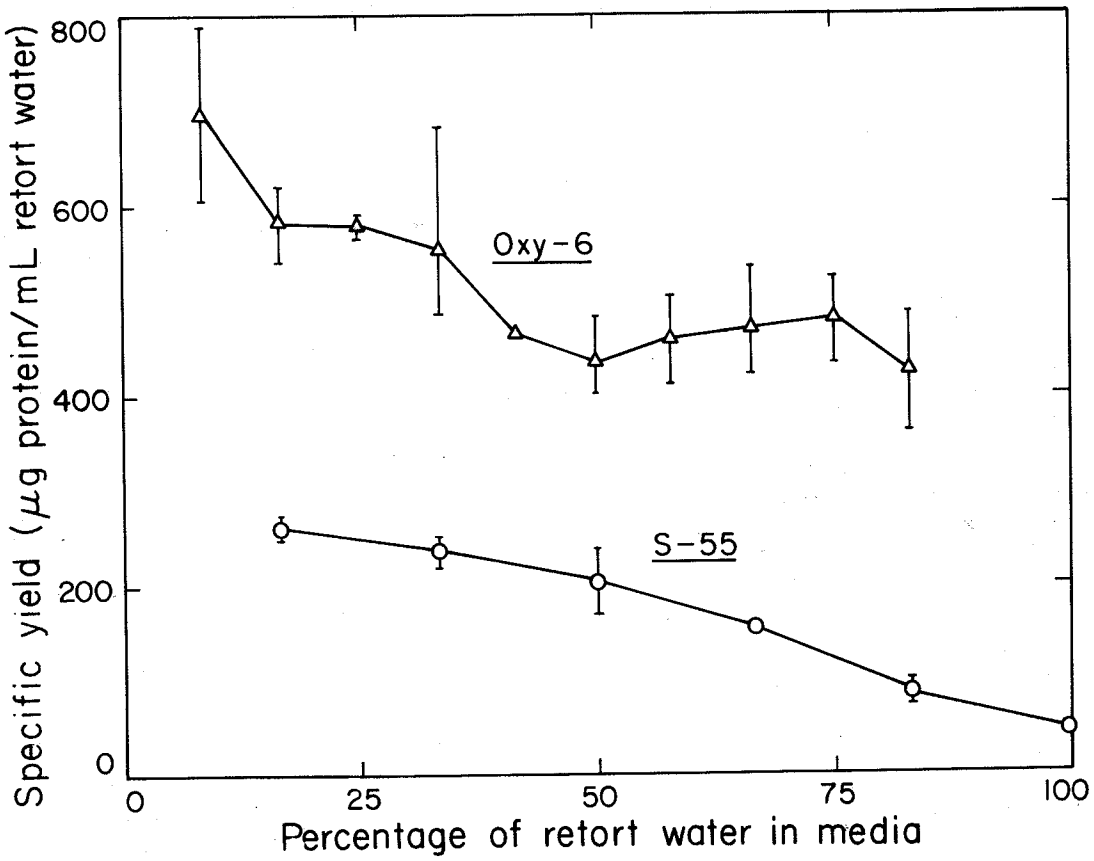

Fig. 5. Protein yield for cultures grown on filtered S-55 and Oxy-6 retort water. (XBL 811-50)

PLANNED ACTIVITIES FOR 1981

When the analytical problems associated with turbidity measurements and the oil-and-grease test are resolved, we will continue to investigate the use of organic polymers and metal salts as coagulant aids. If the use of chemical coagulants appears to be successful, then their application to enhance the foam fractionation process will be studied.

Studies of biological treatment will continue with the use of batch cultures to further elucidate the problems with biological oxidation of organic compounds in retort water.

REFERENCES

1. C. G. Daughton, B. M. Jones, and R. H. Sakaji, "Analytical Problems in Monitoring Retort Water Treatment," Energy and Environment Division Annual Report FY 1980, LBL-11990, 1981.

2. J. P. Fox and T. R. Phillips, "Wastewater Management Strategies, Issues and Research Needs," Proceedings, Oil Shale, the Environmental Challenges, Lawrence Berkeley Laboratory report LBL-11214, 1980.

RAW AND SPENT SHALE FOR THE TREATMENT OF OIL SHALE PROCESS WATERS*

R. H. Sakaji, B. M. Jones, and C. G. Daughton†

INTRODUCTION

Production of synthetic crude from oil shale generates from 0.10 to 22 bbl of wastewater and 11.4 to 45.5 kg of solid waste per bbl of oil, depending on the specific process used. The water, referred to as retort water, originates from combustion, mineral dehydration, input steam, and groundwater intrusion (resulting only from in-situ processes). The organic content of retort water may reach 3%, and inorganic concentrations of as much as 5% are typical. The principal organic constituents are carboxylic acids and nitrogen-containing organic compounds, and the principal inorganic components are NH_4, Na, and HCO_3, with lesser but significant amounts of S_2O_3, Cl, SO_4, and CO_3. The solid waste, referred to as spent shale, is a porous material that contains weight percent concentrations of Na, Ca, Mg, Fe, K, and inorganic C. The spent shale and retort water pose significant disposal problems for the oil shale industry.

The retort water would be a valuable resource for the arid regions in which oil shale deposits are located if effective and economical treatment methods can be found. Past attempts to adapt conventional treatment technologies, such as anaerobic fermentation, activated sludge, and carbon adsorption, to remove organic and inorganic solutes from retort waters indicate that these methods have serious technical and economic limitations. An observation made at LBL during the course of other work suggests, however, that raw and spent shales might be used to economically reduce some organic and inorganic components of retort water.

The purpose of this program, initiated in June 1978, is to determine whether raw and spent shales can be effectively used in the treatment of in-situ process waters. In-situ oil shale retorting processes produce large volumes of water compared to surface processes, and they leave large deposits of spent shale underground. In modified in-situ processing, which is currently under development by industry and by the Department of Energy, 20 to 40% of the in-place shale is mined and processed in surface retorts.

This program is investigating two potential uses of spent shale for treatment of in-situ retort waters. In the first application, the abandoned in-situ retort would be directly used in a treatment system. Water generated in one retort would be circulated through an adjacent spent retort to reduce contaminants in the water and to cool the in-situ spent retort in preparation for grouting. In the second application, spent shale produced in surface retorts would be used in fixed-bed columns. The exhausted spent shale would be disposed with other solid wastes in an on-site solid waste disposal facility.

The effect of raw and spent shales on organic carbon, inorganic carbon, electrical conductivity, and pH is being investigated in batch and column studies. The results of these studies will be used to design a complete treatment system that includes spent shale treatment.

ACCOMPLISHMENTS DURING FY 1980

We successfully operated several continuous-flow columns of either raw or spent shale. These tests are summarized in Table 1. It was difficult to reach a conclusion on the feasibility of using either raw or spent shale for retort water treatment because of the limited availability of samples. Experiments using raw shale demonstrated that for dissolved organic carbon (DOC) and color removal, the effect of shale particle size was more important than surface loading rate. Spent shale was capable of decreasing the dissolved inorganic carbon (DIC) concentration by 98% for a short period of time. Spent shales were also investigated by addition of the spent shale to retort water to create a slurry. Removal of DIC was accomplished, but the quantity of shale required would make liquid-solid separation by conventional means difficult.

Spent Shales Column Studies

Batch studies[1] have demonstrated that spent shales reduce the color, odor, and electrical conductivity of retort water as well as the concentrations of organic and inorganic carbon, but increase the pH of retort waters and gas condensate. The removal of organic materials from retort water could prevent the fouling of ion-exchange resins and filtration equipment, should these be used as downstream treatment processes. The removal of organic compounds may be especially advantageous if these compounds have associated toxicity. If ammonia removal were necessary, the elevation of pH would be beneficial because of the shift in equilibrium to the volatile species (ammonia gas). The removal of inorganic carbon would also prevent carbonate salt deposition in the packing of the stripping tower. Furthermore, the removal of carbonate species, which strongly buffer oil shale process waters, would eliminate the problems of pH control during biological treatment.

We have successfully operated two continuous-flow spent shale columns (Table 1). Graded L-2

* This work was supported by the Assistant Secretary for Environment, Office of Environmental Compliance and Overview, Environmental Control Technology Division of the U.S. Department of Energy under Contract No. W-7405-ENG-48.

† Sanitary Engineering Research Laboratory, University of California, Berkeley, California.

Table 1. Summary of raw and spent shale column studies.

SHALE	RETORT WATER	SURFACE LOADING RATE (gpm/ft^2)	EQUIVALENT PORE VOLUMES TO COLUMN EXHAUSTION[a] DISSOLVED ORGANIC CARBON	DISSOLVED INORGANIC CARBON	ABSORBANCE @ 450 nm	pH
18-25 mesh L-2 spent shale	150-ton	0.1	NS	3.4	–	1.8
18-25 mesh L-2 spent shale	150-ton + Tretolite 398	0.1	NS	3.1	–	3.4
16-25 mesh Colony raw shale	150-ton	0.1	0.4	0.1	2.0	NS
16-25 mesh Colony raw shale	150-ton	0.5	0.6	NS	3.4	NS
60-80 mesh Colony raw shale	150-ton	0.1	0.8	NS	6.4	NS
60-80 mesh Colony raw shale	150-ton	0.5	1.0	NS	8.0	NS

[a] Equivalent pore volume = ml effluent/bed void volume; exhaustion is taken as the point when the effluent concentration is 90% of the influent concentration for organic and inorganic carbon and absorbance; for pH, exhaustion is defined as the point when the pH is 9.3.

Notes: NS = not significant; all columns operated in upflow mode

spent shale (18-25 mesh) was placed in 0.9 m x 2.5 cm ID Lucite columns (Fig. 1). Retort water from a combustion run of the 150-ton retort at Laramie Energy Technology Center was metered with a peristaltic pump upward through the column at a constant loading rate of 0.41 ml/min/cm^2. Figure 2 shows the results for DIC removal and pH elevation as functions of time. The dashed lines show the influent DIC and pH values. An initial effluent DIC reduction of 99% was achieved but was not sustained; after two void volumes had passed through the column, the DIC reduction dropped to 50%. Similarly, elevation of the effluent pH was not sustained; an initial increase in pH from 8.8 to 10.4 was followed by a decrease to 9.4 after two void volumes. Also, the spent shale did not reduce the organic carbon concentration. These findings are consistent with the results of the batch studies[1] which indicated that L-series spent shale is not effective in removing DOC.

The length of the primary reaction zone of this column was calculated. A reaction zone is

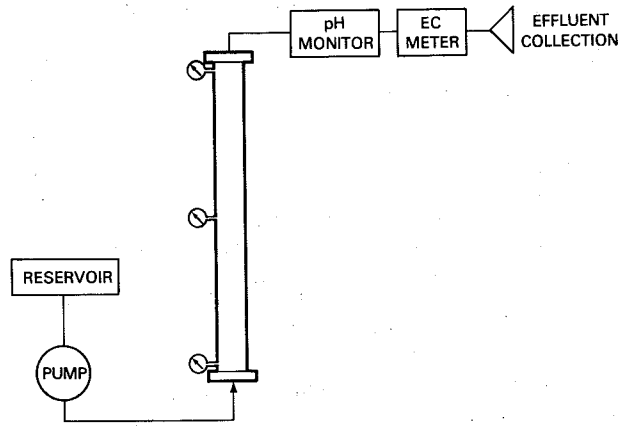

Fig. 1. Upflow column used in raw and spent column studies. (FXBL 812-8164)

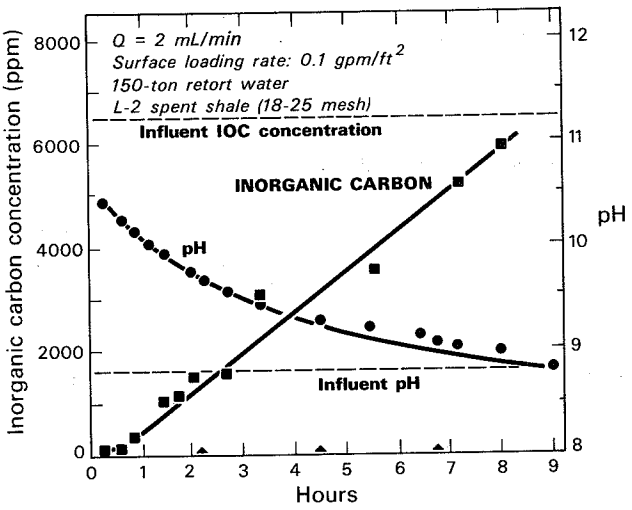

Fig. 2. Inorganic carbon concentration in spent shale column effluent using 18-25 mesh L-2 shale and 150-ton retort water. (XBL 805-1079)

the region of constant column length within which solutes are sorbed; it is advanced immediately in front of a constantly growing solute-saturated zone. The data from this experiment indicate that the theoretical reaction zone was 150 cm, which was longer than the actual column length (91 cm). This simply indicates that the solutes were not efficiently retained by the column. An attempt was made to decrease the reaction-zone length by adding an organic polymer to the influent retort water to coagulate and remove tarry materials that might coat shale particles and prevent the removal of DIC. The data from this experiment showed that the organic polymer had no effect on increasing the operational capacity of the shale. Additional fixed-bed columns using other types of spent shale may give better results. Bed life, primary reaction zone length, head loss, DIC and DOC removal, and pH elevation will vary with the type of spent shale.

Spent Shale Slurry Studies

A series of experiments was conducted to evaluate the use of spent shale in a slurry-contact or dry chemical feed system. Slurry contact was investigated to determine if DOC and DIC removals could be improved by increasing the contact between the process waters and shales and to evaluate an alternative method of application for very fine spent shales produced in some surface retorts. Additionally, industrial developers presently plan to wet spent shale prior to disposal to facilitate compaction, to cool it off, and to control dust. By increasing the water-to-solids ratio required for spent shale disposal, it may be feasible to collect a partially treated water for use elsewhere on site.

Lurgi spent shales are extremely fine (< 230 mesh). Since head loss through a column packed with this fine shale would be excessive, it was decided that this fine spent shale could be best used by addition to the wastewater as a solid. Batch studies conducted using L-2 and Lurgi spent shales showed that these shales elevated pH and removed inorganic carbon (Table 2). They had properties similar to CaO (lime), which is used in wastewater treatment. Lime is slaked and added as a slurry to a wastewater to effect inorganic carbon removal and pH elevation. Solids separation will be a constraining factor for slurry additions because of the necessity to add large quantities of shale to achieve good removals. Measured quantities of shale were added to beakers containing replicate volumes of 150-ton retort water. After one min of vigorous stirring, the rate was decreased. Slow stirring was stopped after 15 min, and the solid and liquid phases were allowed to separate for 60 min. The depth of the solution occupied by the sediment (the interface height) was noted at intervals during the settling process. At the end of the settling period, portions of the supernatant fluid were withdrawn for analysis of pH, DOC, DIC, and ammonia.

The DOC and DIC removals for Lurgi spent shale are presented in Figure 3. The results show that up to 50% of the DIC could be removed by this method for a dose of 85 g per 100 ml of retort water. Lurgi shale did not remove any DOC, in agreement with the results of the batch studies.[1] The pH was elevated only to 9.3 for this same dose.

Spent shale from the L-2 retort was also tested as a slurry with 150-ton retort water (Table 2). The results of using < 230 mesh L-2 spent shale were similar to those of the Lurgi shale. With 100 g of shale per 100 ml of retort water, removal of DIC was 90% and the pH was elevated to 10.1.

The results of the settling studies for Lurgi spent shale are presented in Figure 4. The quality of the supernatant fluid was improved compared to that of the raw water, but because of the large quantity of shale required for DIC removal, the

Table 2. Summary of slurry studies.

SHALE	*DOSE (mg/100 ml)*	*DIC REMOVAL*	*FINAL pH*
L-2 (< 230 m)	100	90	10.1
L-2 (18-25 m)	75	55	9.3
Lurgi (< 230 m)	85	50	9.3

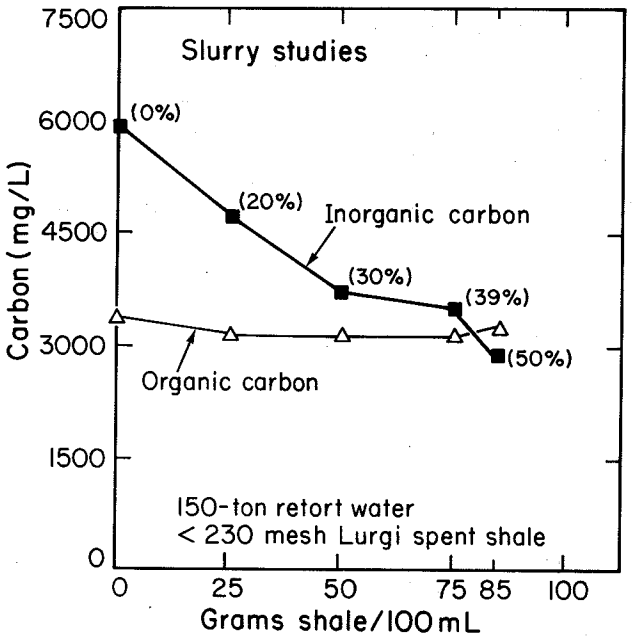

Fig. 3. Effect of slurry addition of Lurgi spent shale (<230 mesh) on dissolved organic and inorganic carbon concentrations in 150-ton retort water. (XBL 811-54)

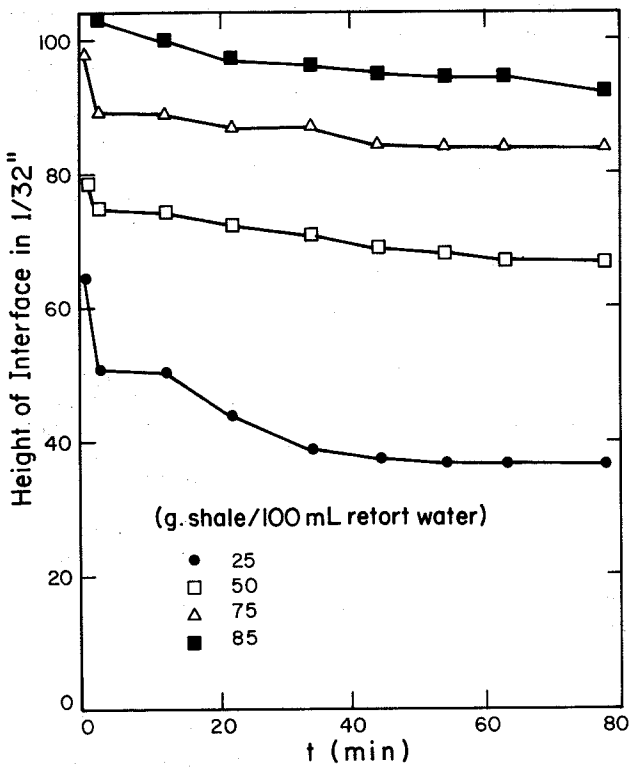

Fig. 4. Settling curves: height of the interface during the settling period. (XBL 812-323)

yield of this fluid was extremely low. The resultant shale sludge compacted poorly. Both the low yield of fluid and the large quantity of sludge were results of the necessarily high shale-to-water ratio. Separation of the fluid and the shale was not accomplished. Since inadequate separation is usually a result of turbulent flow around a given particle, lower dosages of spent shale might result in better settling characteristics. Lower dosages, however, would probably not yield adequate treatment.

These studies suggest that conventional slurry-contact may not be effective due to solids separation problems. Additional investigations and analyses are required to put these studies in context. It may be feasible to use spent shale in combination with lime (conventionally used to remove carbonate alkalinity) to reduce the quantity of spent shale that would be required. Additionally, the use of slurry contact to dispose of spent shale should be assessed. Since industrial developers presently envisage prewetting spent shale destined for surface disposal sites with retort water, it may be feasible to build this operation into a wastewater treatment step. A higher water-to-solids ratio could be used than would be required for wetting and compaction operations, and the residual water could be drained off and reused or further treated.

Raw Shale Studies

Our studies on analytical methodologies[2] have shown that reverse-phase chromatographic packing materials are efficient at partitioning and retaining large quantities of dissolved materials from retort water. The color and odor of the effluent from reverse-phase cartridges (C-18 Sep Pak, Waters Associates) is tremendously reduced compared with untreated retort water. The principle of reverse-phase chromatography may have application in the design of a wastewater treatment process. It has been hypothesized that raw shale could be used in a manner similar to reverse-phase chromatography to achieve the removal of organic solutes from retort water.[3] Commercial reverse-phase material has hydrophobic aliphatic groups covalently bonded to polar surface silanol groups of silica particles. These immobilized aliphatic coatings serve to partition hydrophobic solutes from the retort water. In an analogous manner, raw oil shale is an inorganic matrix that contains an immobilized hydrophobic material (kerogen). Consequently, we tested the ability of raw shale in fixed-bed columns to remove organic solutes from retort water.

Raw shale was obtained from the Anvil Points Mine (Colo.). The raw shale columns (Fig. 1) were operated as described in the previous section. Initial studies showed that the DOC removal was correlated with color removal. Color, therefore, could be monitored as a facile indicator of DOC. We also believe that the biorefractory and toxic organic compounds in retort water are associated with the color. If raw shale were successful in color removal, it perhaps could serve as a pretreatment for biological oxidation. The results reported here represent the first attempt, to our knowledge, to use raw shale as a means of removing (via liquid-solid partitioning) organic compounds from retort water.

Differential absorbance was used to monitor column performance. The wavelength that yielded the maximum differential absorbance between influent and effluent samples was determined from scans of the UV-visible range. This indicated that a wavelength of 450 nm yielded the greatest difference in absorbance values. Column effluent fractions and influent samples were collected, filtered through membrane filters (0.45 μm diameter pores), and subsampled. This ensured that any removal of colored species would not be interpreted as the raw shale acting as a depth filter.

The results of continuous-flow raw shale column tests at two loading rates and with two shale size fractions are summarized in Table 1. A typical absorbance profile at 450 nm as a function of volume treated is shown in Figure 5. These data indicate that the removal of compounds that absorb at 450 nm is a function of the particle size of the raw shale. Comparison of the columns operated at similar surface loading rates, but with different raw shale size ranges, showed that while the initial removals of chromophoric solutes were equivalent, the total removal, as represented by the area above the curve, was greater for the column containing shale of smaller particle size; also, the reduction in color was sustained for a longer period of time. The results also showed that the ability to remove chromophoric compounds was not a function of the surface loading rate.

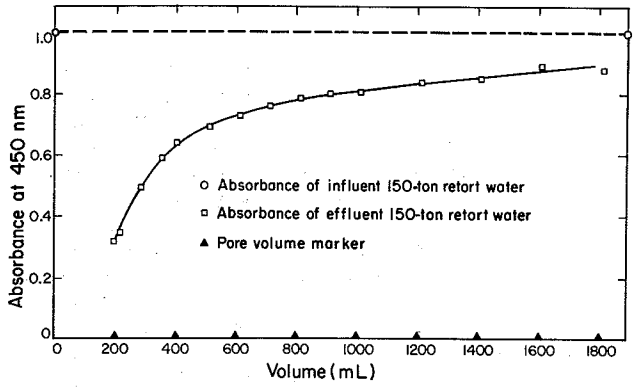

Fig. 5. Absorbance versus volume of effluent from 150-ton retort water and raw shale, 60-80 Anvil Points mesh, surface loading rate = 0.5 gal/min/ft^2 (Q = 10 ml/min). (XBL 812-322)

The overall operation of the columns based on DOC removal was poor; an initial reduction in DOC concentration of only 18-25% was achieved. This reduction lasted only through one pore volume and exponentially decreased in an asymptotic approach to the influent value. The removal of 18-25% of the DOC yielded a 68% reduction in color. Small quantities of organic compounds having relatively high extinction coefficients could have been responsible for the highly colored nature of the water. The possibility of color caused by large quantities of organic materials with low extinction coefficients was thereby eliminated.

PLANNED ACTIVITIES FOR FY 1981

The effect of "activation" of raw shale kerogen on removal of organic solutes from retort water will be studied. Analogous to the activation step in reverse-phase chromatography, kerogen activation could be accomplished by organic solvents that swell and soften the kerogen. This would increase the degree of interaction between the retort water and the hydrophobic kerogen and allow for more effective partitioning of the organic solutes. This phenomenon is very important for retort water, because we have shown that unactivated reverse-phase cartridges (i.e., with no water-miscible organic solvent treatment) do not retain any organic species of retort water.

We will also study additional raw and spent shales in experiments similar to those reported here. We have been able to study only one type of raw shale and our results indicate that it may not be a good sorbent. Raw shales collected from different zones and geographic locales may vary in their sorptive characteristics and capacities. Raw shale collected from outside the Mahogany Zone will contain less kerogen and therefore will possibly have less ability to partition organic compounds. Analogously, we have used only one spent shale in our column studies. We will extend this work to other spent shales.

REFERENCES

1. J. P. Fox, D. E. Jackson, and R. Sakaji, "Spent Shale as a Control Technology for Oil Shale Retort Water," Energy and Environment Division Annual Report 1979, Lawrence Berkeley Laboratory report LBL-10486, 1980.

2. C. G. Daughton, B. M. Jones, and R. H. Sakaji, "Analytical Problems in Monitoring Retort Water Treatment," Energy and Environment Division Annual Report FY 1980, Lawrence Berkeley Laboratory report LBL-11990, 1981.

3. C. G. Daughton, "Method for Purification of Retort Water by Raw Oil Shale," DOE Invention Case #IB-412, 1980.

STEAM STRIPPING OF GAS CONDENSATE AND RETORT WATER*

F. Pearson,† R. Selleck,† V. Diyamandoghi,† Y. Nurdogan,† and S. Wong†

INTRODUCTION

Steam stripping was investigated as a process for removing ammonium carbonate and organics from Occidental Retort No. 6 gas condensate and retort water. Gas condensate contained NH_3 at a concentration of 5,000 mg N/l, ≥25,000 mg $CaCO_3$/l of alkalinity, and 2,000 mg total organic carbon (TOC)/l in carbon form. Corresponding values for retort water were 1,500 mg of NH_3 as N/l, ≥5,000 mg $CaCO_3$/l, and 10,000 mg TOC/l.

Environmental Protection Agency water quality criteria for boiler feed and cooling makeup appear pertinent as treated water quality objectives. These criteria include limits of 500 mg $CaCO_3$/l on alkalinity and 100 mg chemical oxygen demand (COD)/l on organics, the latter being equivalent to perhaps 40 mg TOC/l. NH_3 limits for reuse appear uncertain, although petroleum industry practice in reuse of sour-water stripper effluent may provide a guide. Alkalinity and organics limits prescribe 95% removal of each from gas condensate,

* This work was supported by the Assistant Secretary for Environment, Office of Environmental Compliance and Overview, Environmental Control Technology Division of the U.S. Department of Energy under Contract No. W-7405-ENG-48.

†Sanitary Engineering Research Laboratory, University of California, Berkeley, California.

and 99.6% removal of organics from retort water. Steam stripping alone appears infeasible for attaining 99.6% removal of organics from retort water, so further treatment processes will probably be required. The objective of this investigation, which was initiated in June 1980, was to relate steam stripper performance to process characteristics such as the steam-to-water ratio. This data would permit assessment of the technical and economic feasibility of including steam stripping in an oil shale wastewater renovation process train.

ACCOMPLISHMENTS DURING FY 1980

This year we initiated work to investigate the feasibility of removing NH_3, alkalinity, and organic C from in-situ retort water and gas condensate. We used a batch steam stripper to estimate the minimum steam-to-water ratio for effective removal of these constituents, and we designed and operated a prototype continuous-flow stripper column to develop stripper design criteria. This work is reviewed here.

Bench-Scale Batch Steam Stripping

Since the cost of energy for steam production is the major cost item for steam stripping, information on the minimum steam-to-water ratio for effective removal of contaminants is crucial for analysis of the economic feasibility of the process. Batch steam stripper units were operated to investigate the minimum steam-to-water ratios for removing stated percentages of specified volatile contaminants from gas condensate and retort water.

The batch units were operated to approach equilibration of contaminants between the steam and water phases, thereby attaining near maximum removals of contaminants for the quantity of steam used. Continuous-flow process units may only approach these limiting steam-to-water ratios because equilibrium between the water and the steam phases is limited by mass transfer rates in continuous-flow units to a greater extent than in batch units.

The batch stripping unit shown in Figure 1 consists of a still containing wastewater which is boiled on a hot plate. Untreated water, and periodic samples drawn from the unit were analyzed for NH_3, alkalinity, and organic C. Makeup water or raw wastewater was added to the unit after each sampling to replenish losses due to boiling and sampling.

Figure 2 presents experimental data on the fraction of the original mass of NH_3 and carbonic species remaining in the units, at various stages of treatment, expressed in terms of the ratio of the quantity of steam used to the quantity of water treated. Different symbols represent different experimental trials. Broken lines in Figure 2 represent first order removals of 90% of the NH_3 and 99% of the CO_2 at a steam-to-water ratio of 0.1. These lines essentially envelope the experimental data. The data are scattered due to as-yet unexplained variations in steam generation rates between experiments ostensibly conducted under near-identical conditions.

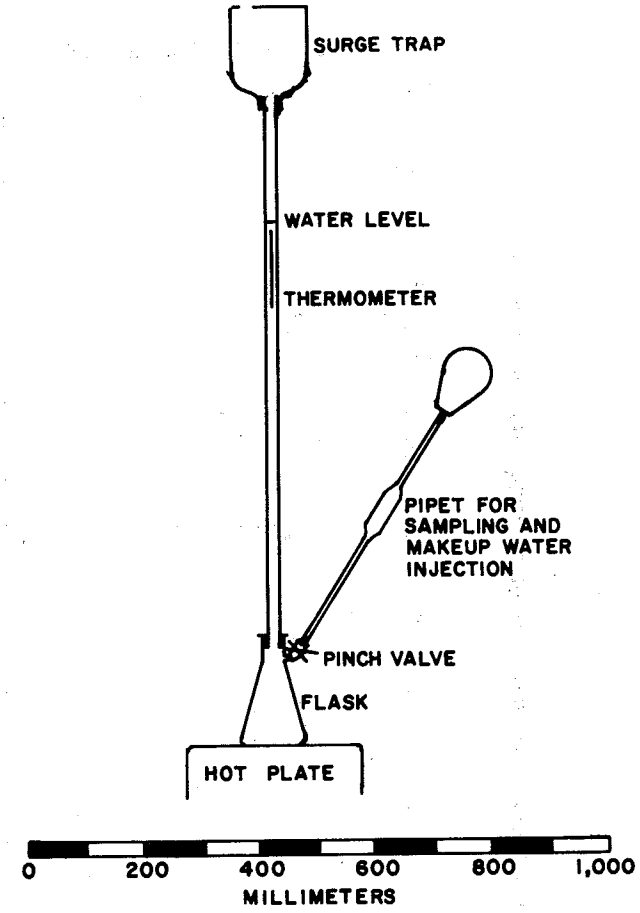

Fig. 1. Apparatus for batch steam stripping. (XBL 8012-13550)

If a steam-to-water ratio as low as 0.1 can be attained in a continuous-flow steam stripper, the energy cost would be approximately $10/1000 gal at a rate of 1¢/1000 BTU for fuel or recovered heat.

Pilot-Scale Continuous Flow-Steam Stripping

A continuous flow pressurized steam stripping unit was designed and fabricated (Fig. 3) and used in several preliminary experiments to investigate the removal of NH_3, alkalinity, and organic C from synthetic and actual process waters.

Steam from a 20-kW generator enters the base of the stripping column packed with 16 mm x 16 mm Raschig rings and passes upward against the downward percolating wastewater, which is injected 450 mm below the top of the column. Packing above the wastewater inlet reduced entrainment of wastewater in rising steam to approximately 2% of the volume of condensed steam (brine). Condensed stripped wastewater and brine outflows were controlled by manipulation of valves discharging to collection vessels. Pressure and temperature in the stripping column were maintained at preset values in the range 5-55 psi (106-147° C) by pressure switch control of the steam generator.

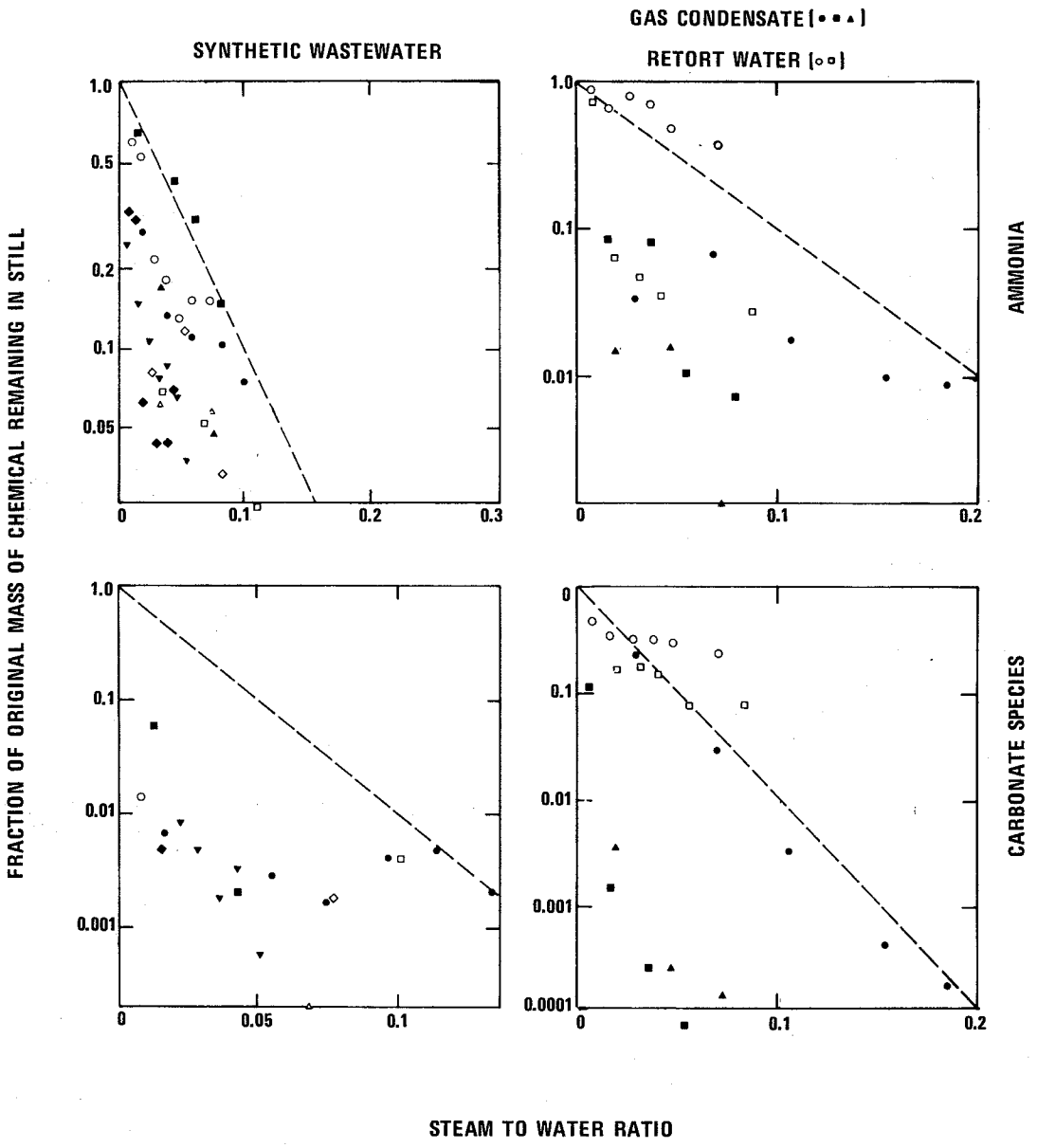

Fig. 2. Depletion of NH_3 and carbonic species from synthetic and actual gas condensate and retort water versus steam-to-water ratio. (XBL 8012-13552)

Figure 4 presents operational data on removals of NH_3 and carbonic acid species from synthetic and actual gas condensate and retort water plotted versus steam-to-water ratio. Steam volume was measured as the volume of brine or the amount by which the volume of brine plus stripped waste exceeded the volume of influent (whichever was greater). Steam volume may have been overestimated in some cases where inadvertent flooding of the stripping column occurred. Figure 4 indicates 90% removals of both NH_3 and carbonic species at steam-to-water ratios ≥ 0.4. Because operational controls of the steam-to-water ratio, and of system pressure were not entirely independent of one another, the effects of steam-to-water ratio on process performance cannot be separated from the effects of stripper pressure and temperature. The stripper is presently being redesigned to improve performance and to separate these effects.

Figure 4 also shows percentage recoveries of NH_3 and carbonic species, computed from the volumes of, and chemical concentration in, influent and brine. Shortfalls in recovered chemicals averaging 25% are due in part to losses resulting from volatilization from effluent and brine collection vessels and residuals retained in the stripping unit at the end of each run. Analytical tolerances probably explain the major part of variations in recovery.

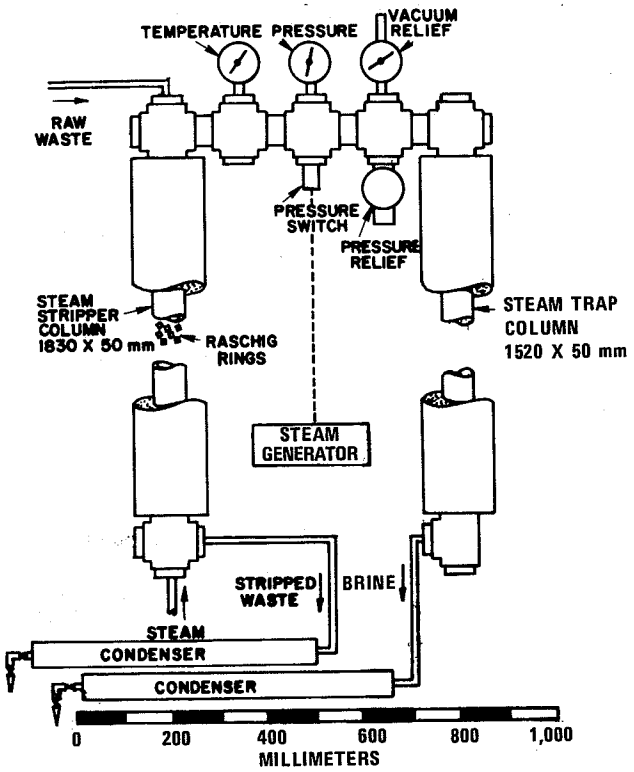

Fig. 3. Pilot pressurized steam stripper, as built. (XBL 8012-13551)

The steam-to-water ratio of 0.4 found necessary for 90% removal of NH_3 and carbonic species in the continuous-flow unit exceeds the ratio of 0.1 tentatively established from batch studies. Mass transfer limitations in the stripping column undoubtedly contribute to the excessive continuous-flow steam consumption. This can probably be reduced by using smaller stripper packing material. Close optimization and control of the steam-stripping process will be required if continuous-flow units are to be designed and operated for a steam-to-water ratio as low as 0.1 at an energy cost of $10/1000 gal.

PLANNED ACTIVITIES FOR FY 1981

The prototype steam stripper designed and operated in 1980 will be modified to correct operational problems and to improve overall performance. The new stainless-steel stripper will be operated at a range of pressures, steam-to-water ratios, and water temperatures to develop design criteria for a commerical-sized stripper. Analytical problems encountered with the measurement of NH_3, alkalinity, and organic C in the complex matrices represented by gas condensate and retort water will be investigated.

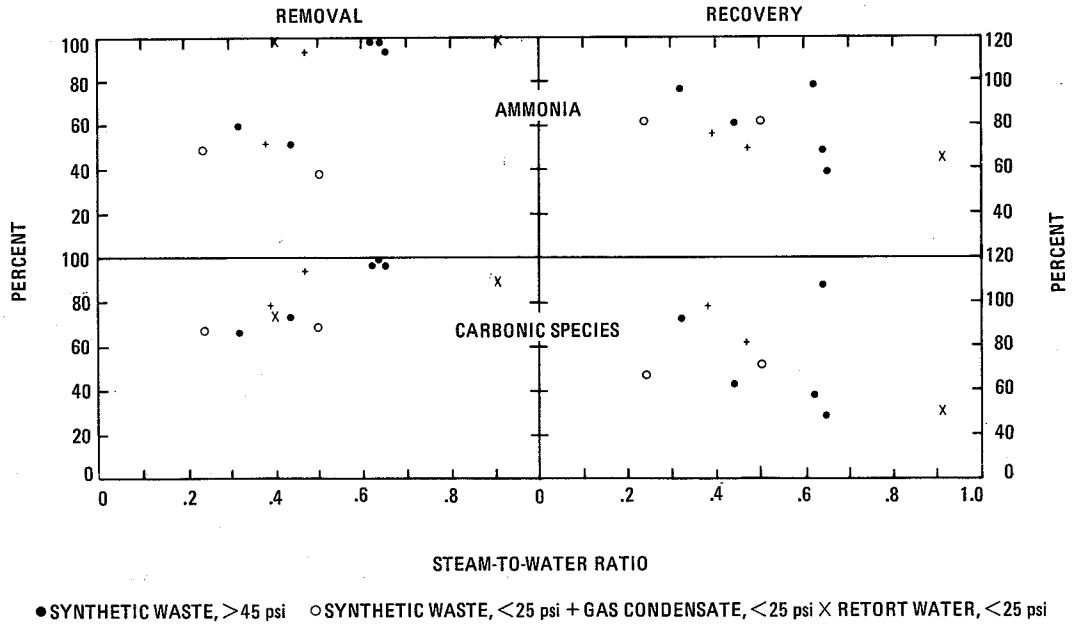

Fig. 4. Removal and recovery of NH_3 and carbonic species from synthetic and Occidental 6 shale oil waste water versus steam-to-water ratio. (XBL 8012-13549)

ANALYTICAL PROBLEMS IN MONITORING RETORT WATER TREATMENT*

C. G. Daughton,† B. M. Jones, and R. H. Sakaji

INTRODUCTION

The development of effective treatment processes for retort water requires reliable analytical methods for the identification of troublesome compounds to be removed and the identification of compounds that may be required for the treatment's success (e.g., trace nutrients for biological treatment). There are two intimately related, yet separate, aspects to the development of these methods. Methods are required for the investigation and development of the bench-scale treatment scheme as well as for the maintenance and monitoring of the resultant commercial process, as mandated by the Environmental Protection Agency. A major difference between the research work and the plant operation and environmental monitoring activities is that of scale. Analyses for research must usually be applicable to smaller samples because of the smaller quantity of material available. Methods that are nondestructive or of "semi-micro" capabilities are frequently needed but are often unavailable. Moreover, many of the individual contaminants or compound classes of interest are hard to measure quantitatively and standard analytical methods yield inaccurate results.

The inability to routinely measure certain characteristics of retort water results from three major causes:

1. The unavailability of a sufficiently simple and reproducible method, e.g., for the quantitation of nitrogenous heterocyclics as a class;

2. The inability to apply an existing method because of sample matrix idiosyncracies (e.g., chemical and physical interferences preclude its use). The colorimetric determination of free inorganic orthophosphate in retort water is an example;

3. The inappropriateness of an existing method. The method can be applied, but its results are uninterpretable; the complexity of the sample exceeds the capacity of the technique to yield meaningful results. For instance, chemical oxygen demand (COD), an estimator of the amount of O_2 that would be consumed in the total theoretical oxidation of solutes in a sample, and not an estimator of organic carbon (OC), yields results for retort water which are difficult to interpret because of interfering solutes and changes in the oxidative states of its many constituents.

Examples of these problems are easily illustrated when one investigates the application of "standardized" analytical techniques to retort water.

ACCOMPLISHMENTS DURING FY 1980

This year, in trying to develop treatment processes for retort water, we looked more carefully at what is required in defining and determining the effectiveness of treatment. Analytical methodology is crucial to the development of any treatment scheme and to the elucidation of the causes of a particular process's shortcomings. Our investigations have concentrated on delineating the possible pitfalls in commonly used methods, such as measuring COD, OC, oil and grease, and suspended solids. New methods and improvements have been instituted for oil-and-grease determination and for cell biomass concentration. Considerable effort has been invested in the validation of the COD test as applied to retort water.

The following sections broadly discuss the results and conclusions of these investigations. Some of the unique sampling and analytical problems encountered with retort waters are described, and solutions developed are presented. The concepts presented here were developed from original investigations into the analytical chemistry of retort waters.

Sampling and Subsampling

The problem of representative sample acquisition and subsampling is a particularly perplexing one with respect to retort water because this waste may contain biotic and abiotic particulates, such as insoluble salts, asphaltic tars, bacterial flocs, and emulsified/suspended oil. Retort waters that are available for study have been collected from the oil-water separators of retorting operations and stored in polyethylene-lined drums for long time periods. The hydrophobic nature of the plastic lining causes the removal of much of the dissolved and suspended hydrophobic material from the waters simply by the process of liquid-solid partitioning. Therefore, homogeneous samples can easily revert to a nonhomogeneous state. This partitioning process can occur at all steps where plastics, silicone, and other rubbers (e.g., tubing, plastic syringes and pipettes, stoppers, and caps) come in contact with the wastewater during storage, subsampling, sample preparation, and experimental treatment. For example, the use of polypropylene packing material in trickling filters or air-strippers, or the use of Tygon tubing in transfer lines, can result in apparent

* This work was supported by the Assistant Secretary for Environment, Office of Environmental Compliance and Overview, Environmental Control Technology Division of the U.S. Department of Energy under Contract No. W-7405-ENG-48.

†Sanitary Engineering Research Laboratory, University of California, Berkeley, California.

treatment efficiences that are artificially high because of the removal of hydrophobic materials by the plastics. When the surfaces of the plastics become saturated, these compounds will then be seen in the effluent.

Retort water has both organic and inorganic abiotic particulates. Particulates are especially troublesome for bench-scale treatability studies because of the difficulty of representative subsampling. These particles cannot simply be subtracted as a constant background during a treatment process study; their amounts can decrease with time from dispersion, dissolution, and degradation, and can increase because of precipitation, coalescence, and biopolymerization.

Fouling of Membranes

Many analytical procedures require paper or membrane filtraton (e.g., suspended solids, dissolved OC, soluble COD) or membranes of selective permeability (e.g., pH, ion-specific, and gas-sensing electrodes). Membranes are easily fouled by retort water. Tarry substances such as asphaltenes will sorb and coat these membranes. This results in the premature failure of the membrane (low filtrate yield, inconsistent results, sluggish response times). This phenomenon can also result in the unintended removal of solutes (i.e., solubilized compounds) from the water during filtration by their partitioning into the immobilized tars or by precipitation of carbonates on the filter paper. Filtration can also remove dissolved compounds (true solutes). Filtrate, therefore, is not necessarily representative of soluble or dissolved material, and likewise, the retentate cannot be considered solely as representative of suspended matter. A further complication is that these filtration phenomena are partially dependent on the membrane or filter type (e.g., glass-fiber, polycarbonate, mixed cellulose esters, Teflon, nylon, etc.). These effects can be responsbile for the great difficulty in collecting sufficient volumes of retort water filtrate.

Oil-and-Grease Determination

An accurate measurement of oil and grease in retort water samples is required to assess the ability of treatment processes, such as dissolved air flotation and foam fractionation, to remove these materials from the waste stream. Oil and grease are conventionally measured gravimetrically following solvent extraction. This method yields erratic and inaccurate results when applied to retort waters. Thus, we have developed a new method that yields reproducible and accurate results in the retort water matrix.

Gravimetric Method

The standard method for quantitating oil and grease, the partition-gravimetric method, is to extract oil and grease from retort water with a highly nonpolar organic solvent (e.g., Freon, 1,1,2-trichloro-2,2,1-trifluoroethane), removing most of the organic solvent in a vacuum, drying the residual at 80-100°C, and weighing the residuum. Every step in this method has difficulties. To minimize emulsification, the partition step requires acidification to pH 2 and addition of large quantities of salt. The high total alkalinity of retort water requires the addition of large amounts of acid for acidification. This leads to CO_2 offgassing, excessive foam production, and protonation of aliphatic carboxylic acids, which will then tend to partition into the organic phase. The large quantity of additional salts will tend to "salt-out" (i.e., decrease their solubilities in the aqueous phase) some of the less hydrophilic solutes, which are not oils. The partitioning process itself is not selective. Polar compounds can be coextracted as organic ligands or ion-pairs, and both polar and nonpolar species can be concentrated at the organic-aqueous interface by surface-active agents, such as carboxylic acids. Compounds are lost continuously during the drying step via volatilization; standardization of the drying time is impossible because the rate of volatilization is substantial and not constant. The gravimetric detection step is notoriously inaccurate and totally nonselective.

Reverse-phase Chromatographic Method

A new approach to the determination of oil and grease (specifically, true oil) in water has been based on reverse-phase chromatography and infrared (IR) spectroscopy. Retort water was passed through a cartridge containing octadecylsilyl-bonded silica (C-18 Sep Paks, Waters Associates). The hydrophobic solutes retained by the cartridge were eluted with organic solvent. The organic eluate was then passed through a normal-phase silica cartridge in which the more hydrophilic compounds were adsorbed. The organic eluate, which contained the oils, was analyzed by IR spectroscopy for absorbance due to carbon-hydrogen stretching (i.e., aliphatic oil).

Cell Biomass

Quantitation of microbial growth on retort water is necessary for studying biological treatment processes and for performing enrichment experiments. Unfortunately, retort water has several characteristics that preclude any facile measurement. The concentration of microbial biomass in a liquid culture is commonly measured by determination of at least one of the following:

- Dry cell mass can be measured by membrane filtration. However, the endogenous levels of filterable nonbiological particulates in retort water give high and nonreproducible background levels.

- Turbidity can be used if it is standardized to a parameter such as cell mass. Nonbiological particulates interfere with turbidity measured by nephelometric or absorbance techniques. Furthermore, the highly chromophoric character of retort water prevents direct absorbance measurements, and the dark color of the particulates and colloidal matter gives a negative interference with scattered light measurements.

- Protein is a good direct measure of biomass. Whole cells can be digested to free

their protein, but the endogenous color of retort water interferes with colorimetric methods. Alternatively, the cells can be separated from the culture medium prior to digestion.

A number of analytical problems are associated with the use of standard methods for cell biomass determinations. Accordingly, we conducted investigations of existing methods, and we developed modified methods that are suitable for the retort water matrix.

Protein Assay

Biological cell material is most easily approximated as "volatile suspended solids." The problems with this determination include:

1. Obtaining a sufficient sample volume for filtration. The volume to be filtered must contain at least several milligrams of dry cell mass for an accurate gravimetric determination. This requirement poses the problems of consuming excessive amounts of experimental treatment samples and of filtering retort water, which is not conducive to membrane filtration.

2. Measuring abiotic particulates and "filterable solutes" indiscriminately as biological material.

We have investigated several standard protein assays and have adapted and modified a commonly used method of protein assay in order to minimize sample size and to obtain a more selective measure of cell material. We considered the five major methods for protein assay: total protein N, biuret, Lowry, amino acid analysis (e.g., ninhydrin), and dye-binding. Total N and amino acid analyses are very time consuming. The Lowry method is very sensitive, but prone to many interferences. The biuret and dye-binding procedures have relatively high detection limits, but they are simple to perform. We studied the latter three methods and adopted a modified version of the Lowry method.

The Folin-Ciocalteu reagent, as adapted by Lowry et al.[1], is used for a colorimetric determination of soluble protein. The method has a low detection limit, which allows for sample sizes generally smaller than 1 ml. This does create the problem, however, of obtaining representative subsamples. Experimental batch cultures can therefore be sampled repetitively for time-course studies with minimum volume disruption. The whole cells were harvested by filtration onto a Teflon membrane and immediately washed with methanol to remove sorbed tarry materials. This concentrated the cells, but more importantly, separated the cells from the many compounds in retort water that could interfere with the assay. The membrane and retained cells were then subjected to alkaline digestion in order to solubilize the cellular constituents. The solubilized protein could then be determined colorimetrically with the "reducing phenol" method.

Turbidity

Experimental design often requires facile nondestructive determination of cell concentration. Turbidity, a measure of the light-scattering properties of a solution, is commonly used as a measure of suspended solids. This is very useful for determining cell biomass and for quantitating the effectiveness of chemical flocculants. Retort water is highly colored. Some of the suspended particulates are inherently dark and others, such as bacterial cells, become dark because they sorb and concentrate color on their surfaces. This precludes the measurement of turbidity as "optical density" (i.e., by measuring pseudoabsorbance or transmitted light) unless every sample is referenced to its own membrane-filtrate. Nephelometric measurements are invalid because much of the scattered light is subsequently absorbed by the chromogenic particulates and fluid. The amount of both scattered and transmitted light is affected by particle shape and size (e.g., bacterial species and growth phase). Turbidimetric measurements of a flocculated mixed bacterial culture can be difficult and inaccurate. Nevertheless, turbidity is the most facile and least destructive measure of biomass for samples that require reuse.

We have developed an alternative approach to nephelometric measurements. Our procedure uses an instrument which determines ratios of intensities of transmitted light to two values of scattered light measured at 90°. This eliminates the problems associated with chromophoric solutes and colored suspended solids. Correction curves need to be calculated because the nephelometric idiosyncracy of higher sensitivity at higher turbidity due to secondary scattering will give overestimations of cell biomass. Work is still under way on development of this method.

Chemical Oxygen Demand and Organic Carbon

An accurate measure of OC is required to assess the performance of physical-chemical processes which seek to remove these substances from a waste stream. Additionally, investigations into the biological oxidation of retort waters and the design of a commerical process require knowledge of the oxidation state of the waste stream during treatment. The classical methods for determining COD and OC may not be well suited for retort water. Thus, we have initiated investigations into the suitability of these conventional parameters for characterizing the OC content and oxidation state of retort waters.

Chemical Oxygen Demand

COD is often interpreted as a measure of OC concentration. Soluble COD (SCOD, determined as COD of membrane filtrate) is used as a measure of materials that are available as growth substrates for microorganisms. COD, however, gives a distorted reflection of organic compound concentration for four major reasons:

1. Inorganic species such as thiocyanates, thiosulfates, and Cl yield COD values;

2. Certain classes of organic compounds yield COD values that are much lower than theoretical values because these compounds are not easily oxidized by dichromate. These include aliphatic molecules and nitrogenous heterocycles. Ag catalyst addition does not fully solve this incomplete oxidation problem, and the high concentrations of Cl^- in retort water can precipitate the Ag ion; larger amounts of Hg^{++} must be added in order to complex the excess Cl^-. If nitrogenous heterocycles remain after oxidation, they possibly can form ligands with ferrous ion during titration, thereby artificially increasing the final COD value;

3. Equally important, but not generally recognized, is the fact that COD is not a measure of organic compound concentration, but a measure of both the quantity and oxidative state of carbon. CH_4 and CHOOH represent two extremes which have equivalent carbon contents but different COD values. The measurement of COD gives no information as to either the oxidative state or the concentration of carbon in a heterogeneous system unless the carbon concentration is determined independently;

4. Certain solutes in retort water may impede the oxidation of compounds that would normally be easily oxidized. This possibility was investigated by using the method of "standard additions." The fortification of retort water with compounds, such as phthalic acid, yielded COD values that were often inconsistent with parallel standards.

Organic Carbon

Dissolved organic carbon (DOC; i.e., OC values of membrane filtrate) gives a more meaningful estimate of the quantity of substrate available for microbial uptake. However, the characteristics of retort water cause several procedural difficulties. The carbon analyzers that use a high-temperature O_2 combustion furnace seem to operate best, but retort water's high concentration of inorganic salts causes deposition of solid material on combustion catalysts. The extraordinarily high carbonate alkalinity causes tremendous offgassing when the samples are acidified for the necessary purging step for direct DOC analysis. This problem can only be avoided by indirect determination of OC by the difference between total carbon (TC) and inorganic carbon (IC). This offgassing is further complicated by surfactants in retort water which cause foaming. These problems require that samples be diluted many fold prior to analysis, which exacerbates the problem of cumulative errors due to subsampling.

The most perplexing question concerning OC determinations is that of verifying the efficiency of "recovery" of carbon from a complex sample matrix. If the same chemical classes that resist oxidation in the COD test are only partially oxidized by high temperature O_2, then there is no method to verify the accuracy of the analysis. The aqueous condensate from the combustion furnace may give information concerning combustion efficiency. Preliminary results indicated that this condensate is colored and contains organic carbon. Brown tarry materials have also been seen deposited on the outlet end of the combustion furnace.

SCOD:DOC Ratio Studies

The concepts of SCOD and DOC require particular attention as to the meaning of their respective values. DOC is a strict measure of carbon concentration. It gives absolutely no information about the type or "quality" of the organic species present. SCOD by itself is only a reflection of the amount of dichromate that can be reduced by these same constituents, i.e., an indicator of the amount of O_2 that would be consumed; it is neither a measure of the quantity nor quality of the species present. SCOD values depend on the ease with which a substance can be oxidized by dichromate, on the oxidation state of the carbon, and on the concentrations of the compounds. Relating the two measures, COD and OC, by ratio yields a considerable amount of information about the types of chemicals that are present in such a heterogeneous matrix as retort water. The amount of COD yielded per unit of organic carbon can be viewed as "specific COD." The higher the reductive state of the compound the higher will be the ratio of COD to OC. The two extremes for this concept are CH_4 and CHOOH, having theoretical specific COD's of 5.33 and 1.33, respectively.

For an unknown mixture of compounds, such as retort water, this concept is complicated by the possibility that some organic compounds present may not yield COD values (i.e., they are recalcitrant to dichromate oxidation). Reverse-phase chromatography separates compounds partially on the basis of their hydrophobicity, which is a reflection of the reductive state of the molecule. Carbon species that are more fully reduced yield higher COD values and also should have greater affinity for the stationary phase in reverse-phase separations. Consequently, the specific COD of a reverse-phase separation should increase with increasing retention time of the eluted compounds. We have obtained exactly this result for one retort water. For another water, we have seen the opposite result of decreasing specific COD with increasing retention time. We have been able to interpret this latter result as proof that many of the compounds that should yield high specific COD's actually give very low or no COD.

PLANNED ACTIVITIES FOR FY 1981

Our work has shown that the use of standard analytical methodology to measure certain aspects of the complex chemical matrix of retort water may be unjustified. Past problems in assessing retort water treatment have resulted from the use

of standard methods without sufficient validation of the accuracy, reproducibility, or appropriateness of the methods. The work initiated in the past fiscal year will continue in an attempt to develop valid and appropriate analytical techniques for application to retort water.

REFERENCE

1. O. H. Lowry, N. J. Rosebrough, A. L. Farr, and R. J. Randall, "Protein Measurement with the Folin Phenol Reagent," Journal of Biological Chemistry, vol. 193, 1951, pp. 265-275.

COAL RESEARCH

ORGANIC COMPOUNDS IN COAL SLURRY PIPELINE WATER*

A. S. Newton, H. M. Villarreal, W. E. Walker, and J. P. Fox

INTRODUCTION

The use of coal is increasing rapidly as it represents the easiest short-term solution to our energy demands. Because of the problem of SO_2 pollution and acid rains in the Northeast, the increase in coal produced will be, to an increasing extent, low-sulfur western coals. The transportation of large amounts of coal between fixed points can be done most economically and with least environmental impact by slurry transport.[1] Such pipelines are capital intensive, but once built, are relatively immune to inflation as little labor is required to keep the pipe line operating. The Black Mesa Pipeline from Kayenta, Ariz., to the Mohave Power Plant on the Colorado River is the only operating coal slurry pipeline at the present time. Several more are near the construction stage, and it is expected that soon as much as 100 million tons of coal per year will be transported by slurry pipeline. At a 50 wt% slurry, this will require 100 million tons of water/yr (some 73,000 acre-ft/yr) and most of this must be disposed at the receiving terminal. This is not a tremendous amount of water, but will represent several thousand acre-ft of water to be disposed at each receiving facility. To facilitate disposal, this water must not be contaminated with toxic or noxious material.

Several studies have been made in which metals have been determined in coal slurry water.[2,3,4] However, little attention has been given to organic impurities. When coal is ground with water in a rod mill, considerable hydrogen gas is evolved. The nascent hydrogen may react with the coal surface to form various organic compounds which will be partitioned to the water. In our preliminary work, a laboratory-sized rod mill produced 6.25 mmol of H_2 gas/h. This is sufficient to be a possible source of contamination at the ppm level.

The purpose of this program, initiated in June 1979, is to identify and quantitate the organic compounds in coal slurry waters, to assess their environmental significance, and to interpret the resulting data in terms of coal technology requirements.

ACCOMPLISHMENTS DURING FY 1980

This year we designed and built a laboratory-scale rod mill to simulate the preparation of coal for slurry transport at the head end of the pipeline (Fig. 1 and 2) and, we used the rod mill to generate coal slurries. We also developed and applied gas chromatography-mass spectrometry (GC-MS) methods for the analysis of phenols and other compounds in the resulting slurries. This work is described here.

Experimental Apparatus

An industrial rod mill for the preparation of coal slurries is ∿4 m in diameter and 5.5 m in length. The average residence time of coal in a continuous mill is only a few minutes. We designed and constructed a laboratory batch mill which duplicates some of these conditions (Fig. 1 and 2). It is made from a 9-in. length of 8 in. O.D. seamless steel pipe. Inside are welded 1/2 in. x 1/2 in. steel bars to carry the rods and provide a good grinding action. Five 1-in. diameter steel rods are adequate. The cover is sealed with an "O" ring, and it also contains a flush valve through which gas samples can be removed from the rod mill. The net volume of the mill for coal, water, and gas space is 5278 ml. The mill is driven on a jar mill drive, Fisher Scientific Co., Model 753 RM. The drive was modified to reduce the speed by adding an additional 4:1 reduction pulley system. With the modified drive, the rod mill is rotated at 28 rpm. The free volume is 5,700 ml, and 5,000 ml of slurry can be processed.

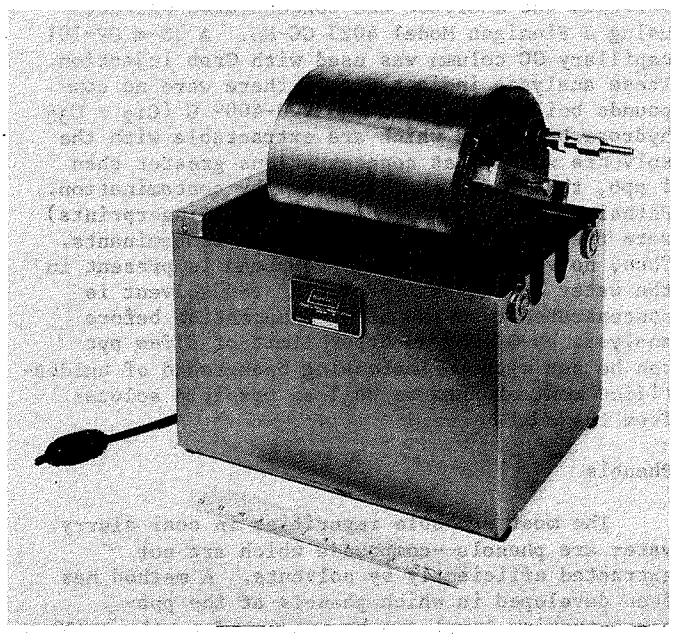

Fig. 1. Assembled rod mill. (XBB 7910-15385)

* This work was supported by the Assistant Secretary for Environment, Office of Environmental Compliance and Overview, Environmental Control Technology Division of the U.S. Department of Energy under Contract No. W-7405-ENG-48.

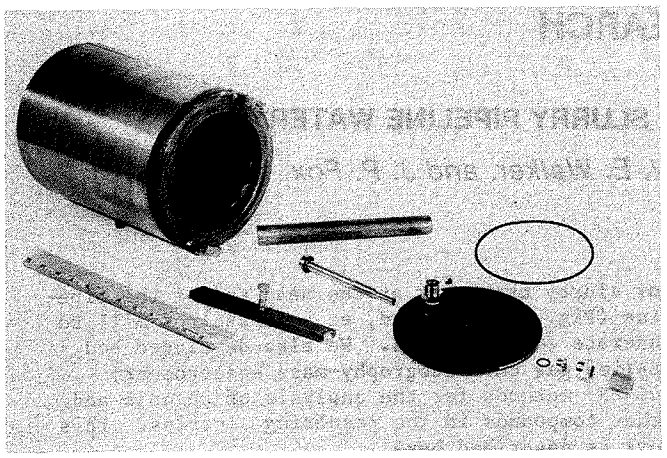

Fig. 2. Exploded view of rod mill.
(XBB 7910-15386)

Research Procedures

We are studying three different coals, since differences occur between coals from various geographic locations. Wyodak coal from Gillette, Wyo., and Black Mesa coal from the Peabody mine at Kayenta, Ariz., are subbituminous coals. Illinois No. 6 is a standard reference bituminous coal. We are investigating slurries prepared from de-ionized water and each of these three coals. The laboratory rod mill is used to slurry the coal and water, and the water is separated by centrifugation. The resulting waters are analyzed for organic compounds using gas chromatography-mass spectrometry (GC-MS), following appropriate chemical modifications.

Volatile Nonpolar Hydrocarbons

In preliminary experiments, we exhaustively extracted the waters with hexane or other suitable solvents and analyzed the concentrated extracts using a Finnigan Model 4023 GC-MS. A 30-m OV-101 capillary GC column was used with Grob injection. These analyses indicated that there were no compounds boiling in the range 200-400° C (C_{12} - C_{30} hydrocarbons) and which are extractable with the solvents we used at concentrations greater than 1 ppb, that cannot be explained by contamination. Phthalate esters and squalene (from fingerprints) were the most obvious and abundant contaminants. Thus, no volatile nonpolar compound is present in the water at the ppb level. If the solvent is concentrated to a few µl by evaporation before analysis by GC-MS, an upper limit of a few ppt can be set with an increasing background of unidentified contaminants as well as possible solutes from the coal.

Phenols

The most probable impurities in coal slurry water are phenols--compounds which are not extracted efficiently by solvents. A method has been developed in which phenols at the ppb-concentration level can be converted to the methoxy derivatives by methylation with methyl sulfate in 0.1 N NaOH. The best procedure is to add about 10 ppb of perdeutero phenol (C_6D_5OD) to the slurry water, add NaOH to 0.1 N, cool the solution to about 2°C in an ice bath, add 50 ml of dimethyl sulfate, and stir overnight. It is important that the dimethyl sulfate hydrolyze as slowly as possible since the methyl ether formation is a second-order reaction while the hydrolysis is pseudo-first order. The methylated phenyl ethers are then extracted with hexane and the extract reduced to a fixed volume. The extract is analyzed with a Finnigan GC-MS model 4023 using a 30-m OV-101 capillary column temperature programmed from 40° to 270° C. The data system using mass chromatograms at M/z = 108 and M/z = 113 can readily separate the ordinary anisole from the 2,3,4,5,6 pentadeutero anisole formed from the perdeutero phenol internal standard. The methyl ethers of other phenols are shown on the mass chromatograms at their respective parent ion masses.

As noted previously, differences occur between coals. This is demonstrated by the failure of this methylation procedure with the slurry water from Illinois No. 6 coal. This water contains some material which catalyzes the hydrolysis of dimethyl sulfate, and the reagent disappears before it has a chance to methylate the phenols present in low concentration. Phenols in this water can be methylated with fair success if the alkaline solution, spiked with deutero phenol internal standard, is pre-extracted with methylene chloride and hexane before the dimethyl sulfate is added.

Absorption Studies

Because coal is an organic material with absorptive properties, the absorption of phenols, polynuclear aromatics (PNAs), and nitrogenous compounds was studied by adding one or more of these compound types to the water before slurrying with coal.

Results and Discussion

The distributions of phenol between various coals and water is shown in Table 1. The distribution has been approached from both sides. The Wyodak coal slurry water has a phenol content of near 10 ppb whether or not phenol is added to the water before the slurry is made. The 10 ppb represents the distribution of phenol between Wyodak coal and water. Both Black Mesa coal and Illinois No. 6 coal absorb phenol, but with these two coals, the solution rate is slower and a steady-state distribution between coal and water has not been achieved.

The absorption of various phenolic compounds from water by each of the three types of coal is shown in Table 2. Both Wyodak and Illinois No. 6 coals absorb more than 99% of the heavier phenols, but Black Mesa coal acts differently and the absorption of O-cresol, dimethyl phenol, and resorcinol are less complete. Naphthol and 4-phenylphenol are more than 99.9% absorbed by each coal.

The absorption of the nitrogenous compounds listed in Table 3 is virtually complete by each of the coals. Absorption of more than 99.9% of each of the nitrogenous compounds occurs on each

Table 1. Phenol in coal slurry water made with and without added phenol before slurry preparation.

Coal Type	ppb Phenol in Slurry Water by Extraction[a]	ppb Phenol in Slurry Water by Absorption[b]
Wyodak	9.0 ± 2	11.0 ± 3
Illinois No. 6	<2.0	4.5
Black Mesa	1.2	12.9

[a]Nothing added to the water before slurry formation.

[b]100 ppb phenol added to the water before slurry formation.

of the coals with the possible exception of the absorption of quinoline by Wyodak coal. A small amount of quinoline is present in the slurry water from Wyodak coal when the nitrogenous compounds are added to the starting water.

PNA's are absorbed from water by Wyodak and Illinois No. 6 coals as shown in Table 4. These compounds are reduced well below a concentration of 0.1 ppb during slurry preparation with these two coals. Black Mesa coal appears to be less active in absorbing PNA's from water. All values found are well below the Environmental Protection Agency's limit of 1 ppb.

It does not appear that low molecular weight compounds of the types described above will constitute a serious environmental contamination problem with coal slurry water. Phenol may represent a slight hazard in chlorination systems owing to the ease of chlorination to trichloro or even pentachloro phenol.

The slurry waters contain up to 20 ppm of organic C which is not accounted for by extraction and GC/MS analysis. Humic or fulvic acids are possible contributors to this organic C, and these must be investigated separately.

Table 2. The absorption of phenolic compounds from water during coal slurry formation.

Compound[a]	ppb Compound in Coal Slurry Water From: Wyodak Coal	Illinois No. 6	Black Mesa
phenol	11	4.5	12.9
O-cresol	0.5	0.02	7.4
2,6 dimethyl phenol	<0.5	<0.01	14.5
resorcinol	<0.5	<0.005	23.8
1-naphthol	<0.5	<0.005	<0.1
4-phenyl phenol	<0.5	<0.005	<0.1

[a]The initial concentration of each compound was 100 ppb.

Table 3. The absorption of nitrogenous compounds from water during coal slurry preparation.

Compound[a]	ppb of Compound in Coal Slurry Water From: Wyodak Coal	Illinois No. 6	Black Mesa
pyroll	<0.01	<0.01	<0.01
pyridine	<0.01	<0.1	<0.1
aniline	<0.01	<0.1	<0.1
quinoline	0.08	<0.1	<0.1
diphenylamine	<0.05	<0.1	<0.1

[a]The initial concentration of each compound was 100 ppb.

Table 4. The absorption of PNA'a from water during coal slurry preparation.

Compound[a]	ppb of Compound in Coal Slurry Water From: Wyodak Coal	Illinois No. 6	Black Mesa
acenaphthene-D_{10}	0.009	0.04	0.27
phenanthrene-D_{10}	<0.005	0.01	0.21
pyrene-D_{10}	<0.003	<0.01	0.13
1,2 benzanthrene-D_{12}	<0.003	<0.01	0.15
chrysene-D_{12}	<0.003	<0.01	0.14
p-terphenyl-D_{14}	0.003	<0.01	0.12
perylene-D_{12}	<0.008	<0.01	0.10

[a]Deuterated compounds were used to avoid possible interferences with contaminants. Each compound was added as a 100 ppm solution in alcohol to give a 100 ppb solution in water.

PLANNED ACTIVITIES FOR FY 1981

Work will continue to identify organic compounds in coal slurry waters. Only a small fraction of the total organic C in these waters has been molecularly characterized. Thus, other compounds potentially present, such as coal humic acids and organonitrogen compounds, will be characterized.

REFERENCES

1. W. Banks, "Slurry Pipeline Economics and Political Issues; a Review," Proceedings of the Fourth International Technical Conference on Slurry Transportation, Las Vegas, Nev., March 28-30, 1979, pp. 19-27.

2. J. W. Moore, "Water Quality Aspects of Coal Transportation by Slurry Pipeline," ibid, pp. 140-152.

3. J. W. Moore, "Quality Characteristics of Slurry Wastewater Resulting from the Slurry Pipelining of Eastern Coal," Proceedings of the Fifth International Technical Conference on Slurry Transportation, Lake Tahoe, Nev., March 26-28, 1980, pp. 242-251.

4. J. Godwin and S. E. Manahan, "Interchange of Metals and Organic Matter between Water and Subbituminous Coal or Lignite under Simulated Coal Slurry Pipeline Conditions," Environmental Science and Technology, vol. 13, 1979, pp. 1100-1104.

WATER QUALITY AND HYDROLOGIC EFFECTS OF COAL MINING*

J. P. Fox, M. J. Kland, F. H. Pearson,† and P. Persoff

INTRODUCTION

Spiralling oil prices, a revolution in Iran, and the long gasoline lines of the summer of 1979 have provided needed incentives to reduce U.S. dependence on foreign oil. Since coal is one of our nation's most abundant fuel resources, it is a logical candidate for expanded production. This conclusion is reinforced by the National Energy Plan (NEP) of 1977 and by renewed interest in coal conversion to liquid and gaseous hydrocarbons. Production of coal has already begun to grow. It reached 650 million tons in 1975, exceeding the 400-600 million tons/yr production rates that had persisted since World War II. And most experts now predict that coal use will double or possibly even triple before the turn of the century.

Under NEP, the major increase in coal production will occur in the West, primarily in the Missouri and Upper Colorado River basins. Mining of low-sulfur coals in these areas is projected to increase by more than 500% within the next 10 yr. This will make the West a major coal producing region in the U.S., accounting for 46% of the total national production compared with only 17% of the total in 1975.

Since there are a number of environmental problems associated with coal production, many still poorly understood and largely unsolved, these accelerated production rates may lead to severe environmental impacts and high control-technology costs. Further, inability to comply with federal legislation may impede the needed expansion in coal production.

The greatest problems are liable to occur in the West where the major increase in coal production will occur. The western coal areas are water-short and relatively pristine. Accelerated coal mining in these areas will deplete local water supplies (by consumptive use and water table drawdown during dewatering) and will contaminate water resources (by mine drainage and surface runoff). However, problems are also anticipated in the East where deep mining is projected to increase to 62% of the total. Here, high population densities could exacerbate existing public health problems in heavily industrialized areas.

Widespread public realization of the potential for serious harm from a program of intensive exploitation of our vast coal resources led to passage of the Surface Mining Control and Reclamation Act of 1977 (PL 95-87). However, scientific knowledge and engineering knowhow are currently inadequate to guarantee compliance with this Act. The projected rapid expansion in coal production will result in new environmental problems and will exacerbate other well known ones (e.g., acid mine drainage) for which there are still no solutions.

The purpose of this program, begun in July 1980, is to investigate the hydrologic and water-quality impacts of expanded coal mining. Scientific information necessary to understand some of the anticipated environmental problems will be developed and used to delineate engineering solutions to these problems.

ACCOMPLISHMENTS IN FY 1980

This year, we reviewed the literature on hydrologic and water-quality impacts of coal mining and developed a research plan which will serve

* This work was supported by the Assistant Secretary for Fossil Energy, Deputy Assistant Secretary for Coal Technology, Office of Coal Mining of the U.S. Department of Energy under Contract No. W-7405-ENG-48.

† University of California, Berkeley, Calif.

as a basis of our future laboratory investigations. These were the specific objectives of that work: (1) Identify and discuss pertinent federal legislation regulating the hydrologic and water-quality impacts of coal mining; (2) Survey and review the hydrologic and water-quality impacts resulting from coal mining; (3) Survey and review the state of knowledge in control technology for hydrologic and water-quality impacts of coal mining and analyze the ability of these existing methods to assure coal industry compliance with federal legislation; and (4) Identify unresolved technical issues and areas requiring research and development. This work was published in Reference 1. Some pertinent conclusions from that survey are summarized here.

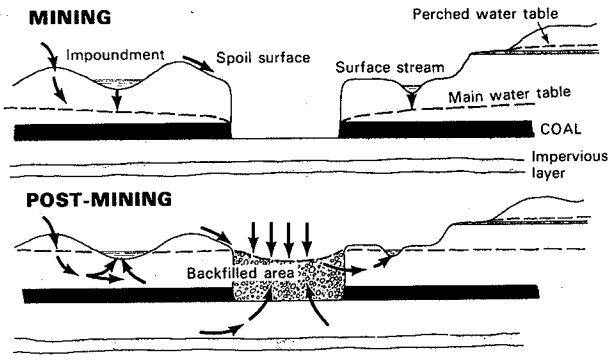

Fig. 1. Schematic of generalized effects of coal mining on hydrology. (FXBL 8010-2155)

Regulatory Framework

Federal acts have been passed in recent years regulating hydrologic and water-quality impacts of coal mining. Compliance with these acts will require the development, demonstration, and use of control technology to mitigate acid and alkaline mine drainage, hydrologic impacts, and erosion.

The Surface Mining Control and Reclamation Act of 1977 (PL 95-87), the most comprehensive and far-reaching such legislation, sets forth provisions for the control of environmental impacts of surface coal mining and surface effects of underground coal mining. The environmental protection performance standards that mines will have to meet are outlined in Title V, sections 515-516 of the Act and include the protection of the hydrologic system, the safe disposal of solid wastes, and the implementation of control strategies and technologies.

In addition to PL 95-87, other recent federal acts regulate the environmental impacts of coal mining. The Federal Water Pollution Control Act (PL 92-500) sets uniform water-quality standards on receiving waters and effluent limitations on discharges from coal mines and coal preparation plants, while the Safe Drinking Water Act (PL 93-523) protects from degradation those underground aquifers that meet drinking water standards. Finally, the Resource Conservation and Recovery Act (PL 94-580) protects surface waters and groundwater from contamination by solid wastes.

Hydrologic and Water Quality Impacts

Principal hydrologic effects of coal mining are the reduction in surface water and groundwater supplies resulting from mine dewatering and reclamation activities and the sum total of local hydrologic effects attributable to the surface plant, mine wastes and workings. Figure 1 depicts principal mining and post-mining effects schematically. The nature and severity of these impacts are dependent on a large number of variables. Prominent among these are climate, the amount and location of surface water and groundwater, the type of terrain, and the mining methods used.

Groundwater

The major hydrologic impacts on groundwater, alteration of fluid potentials, groundwater velocity and elevation of the phreatic surface, occur during active mine operations. These impacts are due to site dewatering and to the physical location of the mine in the hydrologic system. If hydraulic properties have not been altered appreciably by blasting, subsidence, or changes in hydraulic conductivity as a consequence of backfilling, the post-mining groundwater flow pattern will eventually be reestablished with minimal hydrologic impact.

Dewatering, the removal of considerable quantities of water during surface and underground mining, may disrupt aquifers located in overburden or in coal seams. The degree and kinds of disturbance depend on factors mentioned earlier in this section. If an aquifer is intercepted during mining and the site is dewatered, water may be lost from adjacent wells and from surface waters replenished by these groundwaters. The mine's location, whether at a point of recharge or discharge within the hydrologic system, or somewhere in between, is an important factor in the hydrologic impact, as is the location of the coal seam within, above, or below an aquifer, or sandwiched between two aquifers (Fig. 2). Thus, two previously separated aquifers may be joined by mining a seam, and aquifers drained as a result of the fracture of strata which confined them. "Perched" water bodies may develop (Fig. 1) or water recharge, discharge, or transmission areas may be truncated, thereby affecting the flow far from the mine itself.

The effects of coal mining on groundwater hydrology for three different hydrogeologic conditions are shown in Figure 2. Where unconfined aquifers exist (top two rows) above or within a coal seam, groundwater flow into the voids will result in a lowered phreatic surface. This effect may extend to local wells, streams, or springs for a considerable distance beyond the mine site. Where a coal seam confines an underlying aquifer (third row, Fig. 2), water will flow upward into the mined void and will have a negligible impact on local water supplies.

Surface Water

Surface and underground coal mining may affect the hydraulic characteristics and contours of surface soils, which, in turn, alters the hydrologic

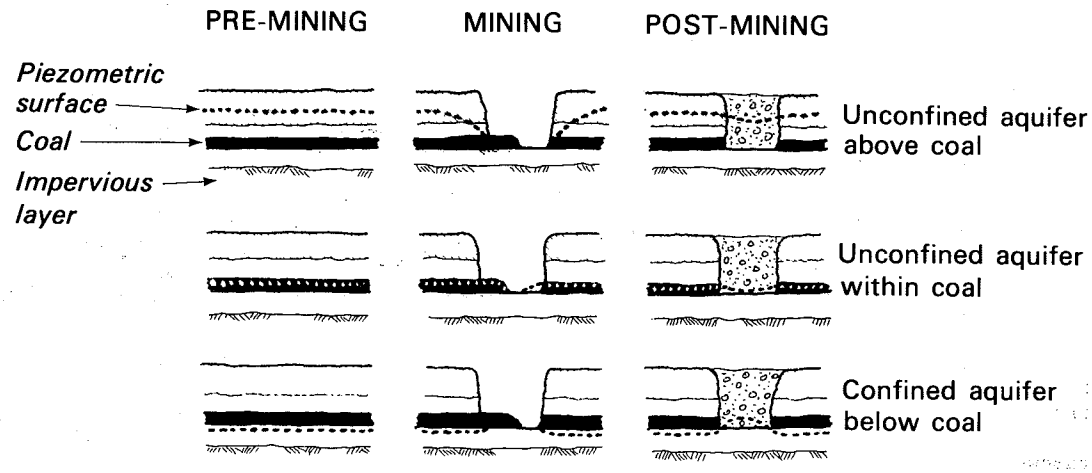

Fig. 2. Schematics showing the effect of coal mining on groundwater hydrology prior to, during, and following mining. (FXBL 8010-12452)

properties of local or regional springs, rivers, and lakes. Resultant changes in flow rate and volume can be harmful to flow-dependent aquatic organisms and can affect patterns of water distribution. Additionally, where a coal seam is located below a water table (Fig. 2) and dewatering is required to prevent water inflow to the mine, the cone of depression may extend beyond the mine confines, affecting hydraulically connected local bodies of water (Fig. 1). During dry periods when runoff is absent, springs and streams with reduced volumes may dry completely. In the water-short West, loss of surface water in this manner may adversely impact downstream users.

Surface mining methods will probably have more impact on surface water hydrology than underground mining methods since the former disturb large surface areas by removal of overlying strata, topsoil, and vegetation. The removal of vegetation reduces infiltration rates and reduces peak stream flow. Backfilled mined areas are generally more porous and frequently more permeable than original ground cover. Consequently, they have greater water retention capacities and higher infiltration rates. This favors reduced peak flows and enhances sustained base flows.

Water Quality Effects

Coal mining may affect local and regional water quality by the discharge of mine drainage and sediment into surface water and groundwater. The magnitude of these effects depends on local geology, hydrogeology, and topography. Acid mine drainage is more prevalent in eastern coal fields while alkaline mine drainage is more common in western fields. Erosion, however, is greater in the hilly Appalachian coal fields that are exposed to high precipitation.

Mine Drainage

Mine drainage may form from the interaction of surface and subsurface waters and air with coal and associated minerals present in gob piles, spoil banks, refuse piles, underground mines, and surface mines.

In coal mining, large quantities of geologic material are disturbed, exposing it to air and water and greatly accelerating natural leaching processes. These materials contain pyrite and other minerals which are oxidized and leached when exposed to air and water during and following mining. The resulting leachate is referred to as acid or alkaline mine drainage depending on its composition. The volumes and composition of the leachate depend on mining methods as well as on local geology and hydrology (Table 1). Although acid mine drainage is one of the most intensely investigated problems related to coal mining, its chemistry is obscure. The chemical mechanisms and kinetics for the formation of mine drainage are still poorly understood. Stoichiometry of initial reactants and final products is understood, and there is general agreement that the basic chemical changes proceed as follows:

Oxidation of sulfide to sulfate--

$$2FeS_2 + 2H_2O + 7O_2 \rightarrow 2FeSO_4 + 2H_2SO_4,$$

Oxidation of ferrous iron to ferric iron--

$$4FeSO_4 + 2H_2SO_4 + O_2 \rightarrow 2Fe_2(SO_4)_3 + 2H_2O,$$

Hydrolysis and precipitation of ferric hydroxide--

$$Fe_2(SO_4)_3 + 6H_2O \rightarrow 2Fe(OH)_3 + 3H_2SO_4.$$

Alkaline mine drainage, on the other hand, was largely ignored until 1977, and the basic stoichiometry is unknown, although the following mechanisms have been proposed:

Oxidation of sulfide to sulfate--

$$2FeS_2 + 7O_2 + 2H_2O \rightarrow 2FeSO_4 + 2H_2SO_4,$$

Neutralization--

$$Ca(HCO_3)_2 + H_2SO_4 \rightarrow CaSO_4 + CO_2 + H_2O,$$

$$2CaCO_3 + H_2SO_4 \rightarrow Ca(HCO_3)_2 + CaSO_4.$$

In surface mining, overburden is removed to expose the coal by one of several techniques, such as area or contour stripping. This exposes large quantities of disaggregated overburden and freshly exposed coal surfaces to air and precipitation. Precipitation may run off or percolate through this material and form mine drainage which may contaminate surface water and groundwater. When coal extraction is complete, the mine is backfilled with spoil. Precipitation and subsurface waters moving through the reclaimed area may continue to form mine drainage long after the site is abandoned. If the mine is located within an aquifer, interaction of subsurface flows with freshly exposed coal surfaces may also form mine drainage. Discharges from surface mines are often intermittent and generally occur during and immediately following periods of precipitation.

Mine drainage may also result from underground mining, either by in-mine formation or leaching of gob piles. Generally, acid mind drainage from underground mines has a lower acidity than that from surface mines (Table 1). In underground mining, overburden material is removed from mine entrances (shafts, adits) and stockpiled on the surface (gob piles). Since the quantity of material available for leaching is considerably less than for surface mines, leaching of surface wastes is less of a problem. However, underground mines develop large cavities or voids which induce flow torward the mine if located in an aquifer. The resulting mine inflow leaches coal exposed to air and forms mine drainage which must be removed during mining. On abandonment, these mines may be partially or completely flooded and drainage may discharge from mine entrances into seeps, springs and streams around the mine perimeter.

Research Needs and Recommendations

Most mining research to date is focused on stream water quality and theoretical and laboratory-scale assessments of control technologies. The coal mining industry will find it hard to fulfill the stringent environmental constraints imposed by PL 95-87, PL 94-580, and other relevant air, water, and health legislation. Our literature review[1] revealed a dearth of information on the hydrologic effects of coal mining in general and alkaline mine drainage in particular. Hydrologic and water-quality considerations associated with groundwaters have not been adequately addressed, nor have the presence, control, and/or removal of the toxic trace elements and organic compounds from mine waters. The lack of information is most acute for western coal mining, which is projected to undergo the greatest expansion.

The rate-controlling steps in acid mine drainage are as yet uncertain, impeding the a priori prediction of hydrologic and water-quality impacts required by law. Even more obscure are the precise environmental determinants of pyritic oxidation and the extent to which this process is purely oxygen-dependent. Absence of a firm theoretical foundation for both the pyritic oxidation process and for alkaline mine drainage is an impediment to strict compliance with the Surface Mining Control and Reclamation Act requirement for prior hydrologic and water-quality impact assessments. It also makes drainage control at the source more difficult and haphazard.

Also lacking is comparative hydrologic and water-quality information needed to establish the effects of mining and reclamation procedures on surface water and groundwater, particularly with respect to underground mining and some more recent mining methods, e.g. mountaintop removal. The acquisition and careful analyses of data from premining, mining, and postmining field studies and their use in developing valid predictive methods, and in validating models, is essential.

PLANNED ACTIVITIES FOR 1981

The "Research Needs and Recommendations" summarized in the previous section and described in detail in Reference 1 will form the basis for the LBL research program in future years. In 1981,

Table 1. Estimated 30-day average effluent concentration in active mine drainage (mg/l).

Parameter	Underground Mines		Surface Mines	
	Acid	Alakaline	Acid	Alkaline
Total suspended solids	230	26	550	96
Total dissolved solids	4750	2700	4060	2870
Alkalinity (as $CaCO_3$)	60	470	5	315
Total iron	350	1.5	52	0.8
Zinc	1.5	0.06	1.7	0.1
Nickel	0.7	0.01	0.7	0.02
Manganese	7.3	0.08	45	0.6
Ammonia	12	0.9	6.5	4.2

we plan to investigate hydrologic impacts of various surface and underground mining configurations using numerical modeling techniques and to study the mechanisms and kinetics of mine drainage formation and treatment.

REFERENCES

1. J. P. Fox, F. H. Pearson, M. J. Kland, and P. Persoff, Hydrologic and Water Quality Effects and Controls for Surface and Underground Coal Mining--State of Knowledge, Issues, and Research Needs, Lawrence Berkeley Laboratory report LBL-11775, 1981.

APPENDIX

ENERGY AND ENVIRONMENT DIVISION PERSONNEL LISTING

ENERGY ANALYSIS PERSONNEL

Grace Afong
Vincent Berg
Carl Blumstein
Peter Chan
Tim Chapman
Ray Coover
Karl Dake
Lynn Danielson
Bill Dapkus
Peter Deibler
Mohamed El-Gasseir
Henry Estrada
Robert Feinbaum
Sandra French
Andre Ghirardi
David Goldstein
Eric Gray
Kendall Haven
Mark Henriquez
Horace Herring
Kathleen Hudson
John Ingersoll
Reid Judd
Ed Kahn
Andrea Ketoff
Mark Levine
Jim McMahon
James Mass
Matt Milukas
Paul Podvin
Suzan Rainey
Lisa Rau
Fred Reid
Ron Ritschard
Henry Ruderman
Jayant Sathaye
Lee Schipper
Robert Schladale
Nancy Schorn
Rich Sextro
William Siri
Renee Slonek
Aram Sogomonian
Kwok Tsang
Karen Tsao
Issac Turiel
Tony Usibelli
Gleb Verzhbinsky
Ed Vine
Winifred Yen
Carl York

SOLAR ENERGY PROGRAM PERSONNEL

Michael Wahlig, Program Leader
Claire Amkraut
Brandt Andersson
Cynthia Ashley
Ridgway Banks
Fred Bauman
Paul Berdahl
Jean Marc Bouchez
Barbara Boyce
Chanoch Carmeli
Bill Carroll
Charles Case
Eduardo Ceballos
Hannah Clark
Craig Conner
M. Benay Curtis
Kim Dao
Don Elmer
David Evans
Nina Friedman
Richard Fromberg
Peter Fuller
Ashod Gadgil
Ron Glas
Donald Grether
Michael Harms
Mary Hart
Al Heitz
Jeffrey Herz
William Hubert
Patricia Hull
Arlon Hunt
Ron Kammerud
Stephen Kanzler
N. Karro
Josh Kay
Jeff Kessel
Mark Kruskopf
Janet Linse
Bart Lucarelli
Marlo Martin
Atila Mertol
Ashraf Mesbahi
Sophia Mitina
Jack Mitchell
Ed Molishever
Peter Moy
Mark Nansteel
Dave Nawrocki
Lester Packer
Sherwood Peters
Albert Pfeiffhofer
Wayne Place
Cindy Polansky
Nancy Pope
Alexandre Quintanilha
John Randolph
Joseph Rasson
Stephen Roberts
Gerald Sadler
Fateh Sakkal
Fenwick Salter
Laurie Sampietro
Peter Scherrer
Steven Schiller
Charlotte Standish
Gerald Stoker
P. Sullivan
Mehdi Tavana
John Thornton
John Tichy
S. Tristram
Christian Vilmer
Mashuri Warren
Christopher Weaver
Tom Webster
Kevin Whitley

CHEMICAL PROCESS RESEARCH AND DEVELOPMENT PROGRAM PERSONNEL

Robert Antonoplis
Myra Baker
Harvey Blanch
David Brink
Patricia Bronnenberg
Elton Cairns
Gregg Cremer
Hubert Davis
Thomas Delfino
Robert Demyanovich
George Dove
Sabri Ergun
Mark Featherstone
Carlos Figueroa
Alan Foss
Raymond Gansley
Edward Grens
Donald Hanson
Neil Hendy
Richard Hix
Cihan Karatas
Marc Katz
Cary J. King III
Dieter Kloden
Philip Lessner
Nen-Hua Lin
Billy Long
Scott Lynn
John MacGlashan
Patricia MacKenzie
Frank McLarnon
Brian Maiorella
Anthony Mancuso
Kenneth Miller
Donald Mohr
Curtis Munson
Thomas Murphy
Stuart Naftel
James Nichols
Steven Oblath
Stephan Orichowskyj
William Oswald
Javier Perez
Steven Rosenberg
Larry Schaleger
Aldo Sciamanna
Linda Sindelar
Rodney Thompson
Theodore Vermeulen
Bruce Vickroy
Dale Wiley
Charles Wilke
Harry Wong
Nasser Yaghoubzadeh
Suen-Man Yu
Rafael Zamora

ENERGY EFFICIENT BUILDINGS PROGRAM PERSONNEL

Administration

Howard Beckman
Pamela Bostelmann
Michael Charney
Peter Cleary
Laurel Cook
Theodore Edlin
Jeffrey Harris
Carol Henderson
Kathryn Hendricks
Jeana McCreary
Arthur Rosenfeld
Dorothy Turner
Maureen Westmoreland

Energy Performance of Buildings

Jim Adams
David Anderson
Richard Beerman
Ake Blomsterberg
William Carroll
Paul Condon
Richard Diamond
Darryl Dickerhoff
John Dickinson
David Grimsrud
Michael Kennedy
David Krinkel
Clayton Ma
Mark Modera
Max Sherman
Brian Smith
Robert Sonderegger
Carol Stoker

Building Ventilation and Indoor Air Quality

Helen Adamson
Ken Alder
Michael Apte
Doug Anthon
Keith Archer
Mark Barnes
James Berk
Thomas Berk
Rakefet Bitton
Mary Boegel
Pipon Boonchanta
Taras Boyan
Steve Brown
Frank D'Amato
Lloyd Davis
Badia El-Adawy
Arnold Falick
Leah Fanning
William Fisk
Kristin Geisling
John Girman
Ron Haynes
Thomas Hernandez
Craig Hollowell
John Ingersoll
Linda Jenks
Irving Ko
Buck Koonce
Amey Lee
Susan Lepman
Ruth Marsh
Vera Martin
Robert Miksch
William Nazaroff
Anthony Nero
Francis Offermann
Maria Ossa
James Pepper
Nils Peterson
Renee Ramos

ENERGY EFFICIENT BUILDINGS PROGRAM PERSONNEL (CONTINUED)

Kenneth Revzan
Alan Robb
Gary Roseme
Nick Rosenlicht
John Rudy
Heidi Schmidt
Philip Strong
Miles Tashima
Andy Toth-Fejel
Greg Traynor
Isaac Turiel
Dora Wolosin
Rodger Young
Geordie Zapalac

Building Energy Analysis Group

Fred Buhl
Steven Choi
Richard Curtis
Kathy Ellington
Ender Erdem
Hideaki Hayashi
James Hirsch
Metin Lokmanhekim
Karen Olson
Tom Wagner
Frederick Winkelmann

Energy Efficient Windows & Lighting

Pam Balch
Vladimir Bazjanac
Sam Berman
Robert Clear
Bruce Dexter
Dennis DiBartolomeo
Kreg Eacret
Margaret Endersby
Jean Ferrari
Richard Johnson
Mahmut Karayel
Jeff Kessel
Joseph Klems
Craig Kletzing
Doug Kosty
Carl Lampert
Clifford Lee
David MacGowan
Moya Melody
Harry Miller
Eli Naor
Mojtaba Navvab
Jeannie Nelson
Joyce Popendorf
George Rand
Mike Rubin
Francis Rubinstein
Joel Ryan
Stephen Selkowitz
Lynne Sherman
Sheelah Sigel
Paul Stuart
Rudy Verderber
Michael Wilde
Ruth Williams
Cecile Wolf

Building Energy Data Compilation, Analysis and Demonstration

Haldun Arin
Peter Cleary
Joseph Costello
Bruce Dickenson
David Goldstein
Jeff Harris
Alan Meier
Steve Meyers
Brian O'Regan
Leon Schipper
Barbara Shohl
Jan Wright

ENVIRONMENTAL POLLUTANT STUDIES PERSONNEL

Atmospheric Aerosol Research Group

Tihomir Novakov, Group Leader
William Benner
Richard Brodzinsky
Shih-Ger Chang
Mark Clemenson
Sidney Cohen
Ray Dod
Sergei Gomiscek*
Lara Gundel
Anthony Hansen
Samuel Markowitz
Michael McKinney
Steven Oblath
Hal Rosen
Richard Schmidt
Reza Toossi
Linda Wroth

Lake Ecotoxicology Group

John Harte, Group Leader
Michael Dudzik
Don Levy
Gregory Lockett
Joan Oldfather
John Rees
Ellen Saegebarth
Richard Schneider
Kathy Tonnessen

Membrane Bioenergetics Group

Lester Packer, Group Leader
Anne Lewis
John Maguire
Rolf Mehlhorn
Alex Quintanilha
Brenda Soares

*On leave from the University of Ljubljana, Yugoslavia.

COMBUSTION RESEARCH PERSONNEL

Abdel Abdel-Hafez †
Mary Jane Alpaugh *
Robert Bill *
Thierry Brault
M. Quinn Brewster *
Nancy Brown
John Brunetto
Minna Chan
Daih-Yeou Chen
Robert Cheng
Alexandra Chorin *
Andre Colpart
Enrique Cuellar
John Daily
Fred Fisher *
Ahmed Ghoniem *
Cecile Grant
Ralph Greif
Hasan Heperkan
Kenneth Hom
Frank Hurlbut
Bruce Ingraham
Claire Johnson *
Thomas Kokoska
Terry Ling
Donald Lucas
John Metcalf
Kenneth Metchette
Michelle Milan *
M. Mohtasheni *
Janice Miyamoto-Mills *
Izak Namer
Terry Ng
Antoni Oppenheim
Rebecca Palmer
Gary Parsons
John Pennucci
Richard Peterson
William Pitz
Ola Rashed
Frank Robben
Robert Sawyer
Robert Schefer
Pauline Sherman †
Gautam Shiralkar
Horton Stewart *
Lawrence Talbot
Chang Tien
Timothy Tong
Steve Vosen
R. Brady Williamson
Joan Woodard †

---

* University of California Berkeley employee
† Guest

LASER SPECTROSCOPY AND TRACE ELEMENT ANALYSIS PERSONNEL

Luis Alvarez
Nabil Amer
Frank Asaro
Neil Bergstrom
Charles Case
Ray Clem
Robert Gerlach
Robert Giauque
Warren Jackson
Ralph Johnson
Stanley Kohn
Ralph McLaughlin
Helen Michel
Anthony Nero
Marjorie Olmstead
Sidney Phillips
Mary Quinby-Hunt
Douglas Wake
Zafer Yasa

OIL SHALE AND COAL RESEARCH PERSONNEL

Jess Albino
Patricia Babbitt
Lisa Bowles
Barbara Branstetter
Jeremy Cantor
Eric Courtney
Christian Daughton
Vasil Diyamandoghi
Suzanne Doyle
Joshua Duberman
Elahe Ensani
Alice Filmer
Dick Fish
Phyllis Fox
Bob Giauque
Gloria Gill
Don Girvin
Dick Goodman*
Tetsuo Hadeishi
Bill Hall
Gloria Harris-Winston
Al Hodgson
David Jenkins*
Bonnie Jones
Laura Joseph
Mathilde Kland
Eric Ko
Bruce Koball
Gregg Langlois
Stephen Lubic
Mohsen Mehran
Kumar Mehta*
Carl Meyer
T. N. Narasimhan
Amos Newton
Yakup Nurdogan
Steve Onysko
Lucy Pacas
Frank Pearson*
Peter Persoff
Martin Pollard
Joe Ratigan
Peter Russell
Rick Sakaji
Kathy Salisbury
Bob Selleck*
Irene Stachura
Jerry Thomas*
Neil Thomsen
Louise Tom
Linda Veneziano
Hector Villarreal
Skip Walker
Steve Wong
Karen Yu

*Associated with the University of California; Berkeley faculty and research associates.

GPO 587-122/4

This report was done with support from the Department of Energy. Any conclusions or opinions expressed in this report represent solely those of the author(s) and not necessarily those of The Regents of the University of California, the Lawrence Berkeley Laboratory or the Department of Energy.

Reference to a company or product name does not imply approval or recommendation of the product by the University of California or the U.S. Department of Energy to the exclusion of others that may be suitable.

TECHNICAL INFORMATION DEPARTMENT
LAWRENCE BERKELEY LABORATORY
UNIVERSITY OF CALIFORNIA
BERKELEY, CALIFORNIA 94720